NUCLEAR PHYSICS

JOURNAL DEVOTED TO THE EXPERIMENTAL AND THEORETICAL STUDY OF THE FUNDAMENTAL CONSTITUENTS OF MATTER AND THEIR INTERACTIONS

EDITOR: L. ROSENFELD - COPENHAGEN
ASSOCIATE EDITOR: O. NATHAN - COPENHAGEN

VOLUME XI

NORTH-HOLLAND PUBLISHING COMPANY - AMSTERDAM

NUCLEAR PHYSICS

EDITORIAL BOARD

AUSTRALIA & NEW ZEALAND:	H. Messel (Sydney), M. L. Oliphant (Canberra)
AUSTRIA:	B. Karlik, (Vienna), H. Thirring (Vienna)
BELGIUM:	M. de Hemptinne (Louvain), J. Verhaeghe (Ghent)
CANADA:	G. Volkoff (Vancouver)
DENMARK:	C. Møller (Copenhagen), S. Rozental (Copenhagen)
FINLAND:	L. Simons (Helsinki)
FRANCE:	A. Berthelot (Saclay), S. Gorodetzky (Strasbourg)
GERMANY (DEM. REP.):	G. Hertz (Leipzig)
GERMANY (FED. REP.):	W. Gentner (Freiburg i. B.), J. H. D. Jensen (Heidelberg)
GREAT BRITAIN:	S. Devons (Manchester), T. H. R. Skyrme (Harwell)
HUNGARY:	L. Janossy (Budapest)
INDIA:	H. Bhabha (Bombay), B. Peters (Bombay), R. Ramanna (Trombay)
IRISH REPUBLIC:	J. McConnell (Maynooth)
ISRAEL:	G. Racah (Jerusalem)
ITALY:	E. Amaldi (Rome)
JAPAN:	S. Kikuchi (Tokyo), S. Tomonaga (Tokyo)
MEXICO:	M. Moshinsky (Mexico)
NETHERLANDS:	H. Brinkman (Groningen), S. R. de Groot (Leiden)
NORWAY:	E. Hylleraas (Oslo), A. Lundby (Oslo), H. Wergeland (Trondheim)
POLAND:	L. Infeld (Warsaw)
PORTUGAL:	J. M. Araújo (Porto), J. R. de Almeida Santos (Coimbra)
SOUTH AMERICA:	G. Beck (São Paulo), J. Leite Lopes (Rio de Janeiro)
SPAIN:	J. M. Otero (Madrid), C. Sanchez del Rio (Madrid)
SWEDEN:	O. Klein (Stockholm), K. Siegbahn (Uppsala), I. Waller (Uppsala)
SWITZERLAND:	P. Huber (Basel), P. Scherrer (Zürich)
U.A.R. & ARAB COUNTRIES:	F. El Bedewi (Alexandria), M. G. Nooh (Cairo)
U.S.A.:	H. H. Barschall (Madison, Wisconsin), V. Weisskopf (Cambridge, Mass.)
U.S.S.R.:	M. A. Markov (Moscow), I. S. Shapiro (Moscow), D. V. Skobeltzyn (Moscow)
YUGOSLAVIA:	I. Supek (Zagreb)

NUCLEAR PHYSICS

JOURNAL DEVOTED TO THE EXPERIMENTAL AND THEORETICAL STUDY OF THE FUNDAMENTAL CONSTITUENTS OF MATTER AND THEIR INTERACTIONS

EDITOR: L. ROSENFELD · COPENHAGEN

VOLUME XI

MAY 1959—JUNE 1959

NORTH-HOLLAND PUBLISHING COMPANY-AMSTERDAM

PRINTED IN THE NETHERLANDS

1.E.1:
6.D

Nuclear Physics **11** (1959) 1—340; © *North-Holland Publishing Co., Amsterdam*
Not to be reproduced by photoprint or microfilm without written permission from the publisher

ENERGY LEVELS OF LIGHT NUCLEI. VI

F. AJZENBERG-SELOVE
Haverford College, Haverford, Pennsylvania †

and

T. LAURITSEN
California Institute of Technology, Pasadena, California

Received 23 December 1958—11 January 1959

Introduction

The present article is the sixth of a series of compilations [1]) summarizing experimental information on the energy levels of the nuclei from He^5 to Ne^{24}. In form and arrangement, it follows the plan of previous versions, with only slight modifications made necessary by the increasing amount of information to be presented. Each nucleus is represented by a diagram and a table in which the known energy levels are indicated, together with the nuclear reactions in which they are involved. The listings are supported by a brief text for each reaction, mainly intended as an annotated bibliography, but abstracting as far as possible the most relevant information. A number of numerical tables have been included, listing what appear to be "best" values for the various level parameters. Although the present summary is intended to be self-sufficient, in the sense that each diagram or table entry finds a defense somewhere in the cited literature, considerations of space have dictated that much important information contained in the earlier versions be omitted here. For a more detailed discussion of certain reactions, and for a more complete bibliography, the reader may wish to refer to the earlier summaries [1]). A comprehensive exposition of theory and experiment as applied to the reactions and spectra of light nuclei has been published by W. E. Burcham [2]). The experimental data on nuclei with Z from 11 to 20 have been summarized by Endt and Braams [3]).

ARRANGEMENT OF THE MATERIAL

The diagrams and their accompanying tables contain, in addition to a representation of the energy levels and their characteristic parameters, an indication in each case of the experiments in which particular levels have been

† This work has been supported in part by the joint program of the Office of Naval Research and the U. S. Atomic Energy Commission, and by the National Science Foundation.

studied. Such experiments generally fall within one of two categories: those in which the given nucleide occurs as the intermediate stage in a reaction, and those in which it represents the final stage. In a few instances, for example in "pick-up" reactions, the interest may centre on the target nucleus. Where a compound nucleus is formed, the excitation function may yield rather detailed information about the energy levels of the intermediate system. To illustrate the general nature of this information, particularly as regards the breadths, relative intensities of excitation, and preferred modes of decay of the various levels, the thin-target excitation functions are shown on the level diagrams, with approximate relative yields plotted horizontally against bombarding energy in a vertical direction. To permit direct association with the levels, the vertical scale is adjusted to centre-of-mass energies, with values of bombarding energy indicated in laboratory coordinates. The cross section scales are arbitrary, different for various products, and in some instances rather strongly distorted to exhibit weak resonances. All definitely established resonances are indicated by leaders, and where space permits, with the (laboratory) energy corresponding to the peak cross section. Where no resonances appear in an excitation function, or where there is reason to believe that the reaction proceeds without formation of a compound nucleus, a brace within the level diagram indicates what products are observed.

Reactions in which the nucleide of interest occurs as the residual nucleus are indicated on the diagrams by the notation X+a−b, where X, a and b are the target nucleus, bombarding particle, and ejected particle respectively. Horizontal lines with this notation are located on the drawings at a height above the origin equal to the reaction Q-value, as calculated from the mass table. The highest bombarding energy at which observations have been made is shown by a vertical arrow, drawn to scale unless otherwise indicated. The levels actually observed are listed in the text for each such reaction, usually in tabular form. Conversely, for each level, the master table lists all the reactions in which the level has been observed.

The nature of decay of the various excited states is shown on the diagrams by arrows, or where excitation functions are plotted, by notations on the curves. Gamma decays are exhibited by vertical arrows. For certain nucleides, separate γ-decay diagrams are presented to permit inclusion of detailed branching ratio information.

On each level in the diagram and in the master table corresponding to a given nucleus, a value of the excitation energy is quoted. This value represents the weighted mean derived from all relevant experiments. It is of course not always certain that the different experiments refer to the same level, but we have assumed that they do so wherever the probable errors overlap and where there appears to be no obvious inconsistency in such an interpretation.

Levels, particle groups, or γ-transitions whose existence is uncertain are represented by dashed lines; uncertain numbers are enclosed in parentheses. In some cases, where a level is particularly broad, this fact has been indicated by cross hatching. Among the lighter nuclei, where the level spacing is large, the breadth of the cross hatching indicates the estimated half-width.

The discussion of reactions in the text is divided in the same way as on the diagrams. Features of the reactions such as cross sections, excitation functions, and alternate modes of decay, which relate primarily to the compound nucleus, will be found discussed under that nucleus; particle-group spectra, γ-transitions, and Q-values are entered under the residual nucleus. Angular distribution data are entered in one or the other category, depending upon which seems the more appropriate to the case in hand.

Since the emphasis in this summary is on experimental results, no attempt has been made to treat theoretical papers in any systematic way or to maintain a complete bibliography of such papers. A partial list of relevant theoretical papers is given under the heading "Theory" at the beginning of each section. A detailed account of the shell-model interpretation of the energy levels of light nuclei has been presented by A. M. Lane [4]).

MASSES AND Q-VALUES

The mass values used in the present compilation are listed at the end of the article. Almost all of these have been taken from the tables of Wapstra [5]). For masses not included in these tables — and in a few instances where significant changes have occurred — we have estimated the masses from the available experimental data; details of the estimates will be found in the text. For each reaction, the Q-value calculated from the masses, designated Q_m, is listed with the reaction heading, as is the binding energy of the bombarding particle in the compound nucleus, E_b. Both quantities are in MeV. Although the mass values generally are assigned probable errors of five to ten keV, the Q-values are often more accurate. Some recently reported Q-values are included in the text; comprehensive listings have been published by Van Patter and Whaling [6]).

CONVENTIONS

Within the limitations imposed by the requirement of brevity, we have endeavored to avoid the use of unfamiliar conventions and abbreviations. We set forth here some of the symbols which we have used, together with their definitions:

E Energy in MeV, laboratory coordinates unless otherwise specified. Subscripts p, d, t, etc., refer to protons, deuterons, tritons, etc.

θ Angle of observation, in laboratory coordinates unless otherwise specified.

E_{res} General: the bombarding energy at which resonance occurs; specific: the bombarding energy at which the resonant part of the phase shift of the partial wave in question reaches 90°.

Γ Observed width of a resonance, in keV; laboratory coordinates unless otherwise specified.

E_λ "Characteristic" energy of a level as determined by certain conditions on the logarithmic derivative of the wave function at the nuclear surface.

$\omega\Gamma_x$ Statistical weight factor times partial width of particle x.

γ_λ^2 "Partial" width, after removal of barrier penetration factors, evaluated at E_λ.

θ_x^2 "Reduced" partial width, $\gamma_{\lambda x}^2 \times 2\mu R^2/3\hbar^2$.

J Total angular momentum.

π Parity

T, T_z Isobaric spin quantum numbers: $T_z = \frac{1}{2}(N-Z)$.

We have made much use of the several collections of experimental data which have become available in recent years. Of these, the most important in the present connection has been the "Nuclear Data Sheets," published monthly by the National Academy of Sciences — National Research Council [7]). We have also derived great benefit and have extracted much material from the compilations of "Neutron Cross Sections," by Hughes and Schwartz[8]), and "Charged Particle Cross Sections," by Jarmie and Seagrave[9]).

As always, we owe a particular debt to our many colleagues who have criticized the draft manuscript and who have been kind enough to supply material in advance of publication. The active help and advice of C. C. Lauritsen, W. A. Fowler, R. F. Christy and W. Selove is gratefully acknowledged. We are also much indebted to Miss Barbara Zimmerman and to Mrs. Jan Rasmussen for their invaluable assistance in preparing the manuscript.

References

(to Introduction)

1) W. F. Hornyak and T. Lauritsen, Revs. Mod. Phys. **20** (1948) 191;
T. Lauritsen, N. R. C. Preliminary Report No. 5 (1949);
Hornyak, Lauritsen, Morrison and Fowler, Revs. Mod. Phys. **22** (1950) 291;
F. Ajzenberg and T. Lauritsen, Revs. Mod. Phys. **24** (1952) 321;
F. Ajzenberg and T. Lauritsen, Revs. Mod. Phys. **27** (1955) 77

2) W. E. Burcham, "Nuclear Reactions, Levels, and Spectra of Light Nuclei", Encyclopedia of Physics **40**, Editor Flügge (Springer, 1958)

3) P. M. Endt and C. M. Braams, Revs. Mod. Phys. **29** (1957) 683

4) A. M. Lane, Revs. Mod. Phys., to be published

5) A. H. Wapstra, Physica **21** (1955) 367

6) D. M. Van Patter and W. Whaling, Revs. Mod. Phys. **29** (1957) 757

7) McGinnis, Anderson, Fuller, Marion, Way and Yamada, "Nuclear Data Sheets", (National Research Council, Washington D. C.)
8) D. J. Hughes and R. B. Schwartz, "Neutron Cross Sections", Brookhaven National Laboratory Report BNL 325 (July 1, 1958) (U. S. Govt. Printing Office, Washington, D. C.)
9) N. Jarmie and J. D. Seagrave, "Charged particle Cross Sections", Los Alamos Scientific Laboratory Report LA 2014 (Feb. 1, 1957)

Atomic Mass Excesses ($M-A$) in MeV

n	8.3675 ± 0.0014	N^{12}	21.00 ± 0.06[a]
		N^{13}	9.185 ± 0.005
H^1	7.5845 ± 0.0014	N^{14}	7.002 ± 0.003
H^2	13.7256 ± 0.0026	N^{15}	4.528 ± 0.005
H^3	15.358 ± 0.005	N^{16}	10.402 ± 0.012
H^5	32.2 ± 2[a]	N^{17}	12.93 ± 0.06[a]
He^3	15.817 ± 0.005	O^{14}	12.149 ± 0.007[a]
He^4	3.6073 ± 0.0024	O^{15}	7.287 ± 0.005[a]
He^5	12.932 ± 0.030	O^{16}	0
He^6	19.398 ± 0.029	O^{17}	4.222 ± 0.005
He^7	31.5 ± 2[a]	O^{18}	4.521 ± 0.007
		O^{19}	8.931 ± 0.012
Li^5	12.988 ± 0.200	O^{20}	13.3 ± 2[a]
Li^6	15.862 ± 0.005		
Li^7	16.977 ± 0.006	F^{15}	22.0 ± 1[a]
Li^8	23.310 ± 0.005	F^{16}	15.63 ± 0.02[a]
Li^9	28.1 ± 1[a]	F^{17}	6.989 ± 0.004
		F^{18}	6.188 ± 0.008
Be^6	20.3 ± 0.2[a]	F^{19}	4.142 ± 0.007
Be^7	17.840 ± 0.005	F^{20}	5.904 ± 0.010
Be^8	7.309 ± 0.005	F^{21}	6.193 ± 0.030[a]
Be^9	14.010 ± 0.006		
Be^{10}	15.566 ± 0.007	Ne^{18}	10.415 ± 0.200
Be^{11}	23.39 ± 0.15[a]	Ne^{19}	7.398 ± 0.008
		Ne^{20}	−1.146 ± 0.008
B^8	25.287 ± 0.008[a]	Ne^{21}	0.465 ± 0.009
B^9	15.081 ± 0.006	Ne^{22}	−1.533 ± 0.011
B^{10}	15.010 ± 0.006	Ne^{23}	1.643 ± 0.011
B^{11}	11.914 ± 0.006	Ne^{24}	1.113 ± 0.040[a]
B^{12}	16.917 ± 0.006		
B^{13}	20.40 ± 0.05[a]	Na^{20}	14.187 ± 0.200
		Na^{21}	3.987 ± 0.033
C^9	32.3 ± 2[a]	Na^{22}	1.307 ± 0.013
C^{10}	18.79 ± 0.09[a]	Na^{23}	−2.744 ± 0.010
C^{11}	13.895 ± 0.007	Na^{24}	−1.336 ± 0.013
C^{12}	3.541 ± 0.005		
C^{13}	6.963 ± 0.005	Mg^{24}	−6.853 ± 0.014
C^{14}	7.157 ± 0.003	Mg^{25}	−5.818 ± 0.014
C^{15}	14.305 ± 0.005[a]	Mg^{26}	−8.569 ± 0.021

The masses excesses are taken from A. H. Wapstra, Physica 21 (1955) 367 except for those marked (a) which are derived from data reviewed in the present article and in (Aj 55).

H^5

(Not illustrated)

The possible existence of a particle-stable H^5 is discussed by (Bl 57b) † who point out that a $T = \frac{3}{2}$ level of He^5—Li^5 might plausibly be formed by combination of H^3 or He^3 and a deuteron in the singlet ($T = 1$) state at an energy ≈ 2.3 MeV higher than the known 16.7—16.8 MeV level. If such a level exists, calculation of Coulomb corrections and n—H^1 mass difference suggests a mass excess of 32.22 MeV for H^5, which would be 0.35 MeV stable against H^3+2n. Presumably H^5 would then decay by β-emission ($\approx$ 19 MeV) followed by neutron emission (Bl 57b). A search for delayed neutrons from $Li^7(\gamma, 2p)H^5$ with 320-MeV bremsstrahlung yielded no evidence of formation of H^5 (Ta 58c). It is concluded that less than 1 % of the expected yield of $Li^7(\gamma, 2p)H^5$ leads to a particle-stable product (Ta 58c); see also (Ce 58). A reaction yielding H^5 might be $H^3(t, p)H^5$ with $Q \approx -8.1$ MeV, assuming the mass of H^5 given by (Bl 57b).

He^5

(Fig. 1, p. 7) ††

I. $H^3(d, \gamma)He^5$ $\quad Q_m = 16.629$

At $E_d = 160$ keV, the capture cross section is less than 0.5 mb. This limit is not inconsistent with $\Gamma_\gamma \approx 11$ eV as estimated from the mirror reaction $He^3(d, \gamma)Li^5$ (Sa 55b).

TABLE 5.1

Energy levels of He^5

E_x in He^5 (MeV)	J^π	Γ (MeV)	Decay	Reactions
0	$\frac{3}{2}^-$	0.55±0.03	n, α	V, VI, VIII, IX, X, XI, XII, XIII, XIV, XVI, XVII
3—6	$\frac{1}{2}^-$	3—5	n, α	VIII, XIV
16.69	$\frac{1}{2}^+$	0.08	n, d, t, α	II, VIII
(≈ 20)		> 1	n, d, t, α	II

II. (a) $H^3(d, n)He^4$ $\quad Q_m = 17.586$ $\quad E_b = 16.629$

(b) $H^3(d, 2n)He^3$ $\quad Q_m = -2.991$

(c) $H^3(d, pn)H^3$ $\quad Q_m = -2.226$

$Q_0 = 17.580 \pm 0.025$ (Ma 57f).

Excitation curves and angular distributions for reaction (a) from $E_d = 8$ keV to 10 MeV are summarized by (Ja 57, Fo 56a). Additional data

† References are collected at the end of the article.

†† For level scheme of Li^5, see fig. 2, p. 13.

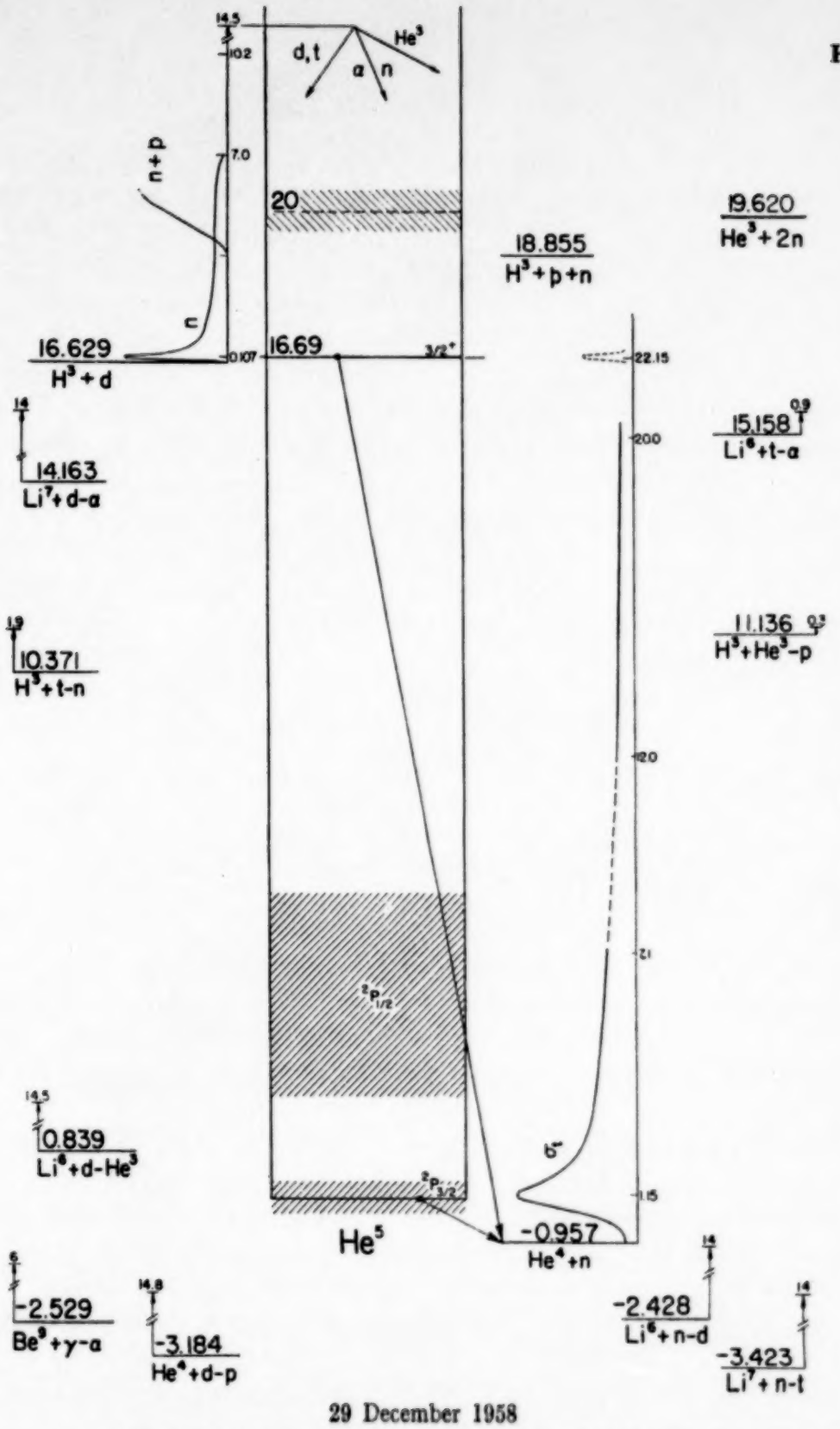

29 December 1958

Fig. 1. Energy levels of He^5. In these diagrams, energy values are plotted vertically in MeV, based on the ground state as zero. Uncertain levels or transitions are indicated by dashed lines; levels which are known to be particularly broad are cross-hatched. Values of total angular momentum J, parity, and isobaric spin T which appear to be reasonably well established are indicated on the levels; less certain assignments are enclosed in parentheses. For reactions in which He^5 is the compound nucleus, thin-target excitation functions are shown schematically (where known), with the yield plotted horizontally and the bombarding energy vertically. Bombarding energies are indicated in laboratory coordinates and plotted to scale in centre-of-mass coordinates. Excited states of the residual nuclei involved in these reactions have generally not been shown; where transitions to such excited states are known to occur, a brace has been used to suggest reference to another diagram.

For reactions in which the present nucleus occurs as a residual product, excitation functions have not been shown; a vertical arrow with a number indicating some bombarding energy, usually the highest, at which the reaction has been studied, is used instead.

Further information on the levels illustrated, including a listing of the reactions in which each has been observed, is contained in the master table, entitled "Energy Levels of He^5".

are given for $E_d = 0.04$ to 0.73 MeV by (Ba 57o, Ba 57p), for $E_d = 1.0$ to 5.8 MeV by (Ga 56) and for $E_d = 0.25$ to 7.0 MeV by (Ba 57h). Below $E_d = 100$ keV, the cross section follows the Gamow function, $\sigma = (A/E) \exp(-44.40\, E^{-\frac{1}{2}})$ (Ja 53d, Ar 54). A strong resonance, σ(peak) = 5.0 b, appears at $E_d = 107$ keV. A precision measurement ($\pm$ 5 %) of the cross section at $E_t = 1.50$ MeV gives 20.0 and 19.6 mb/sr (c.m.) at 30° and 60° (lab), respectively (Al 58b). There is some question as to whether a broad maximum exists between 4 and 8 MeV (Ga 56, Ba 57h).

In the region $E_d = 10$ to 500 keV, the cross section is closely fitted with the assumption of s-wave formation of a $J = \frac{3}{2}^+$ state, with the parameters given in table 5.2. For a given interaction radius, two sets of parameters are

TABLE 5.2

Resonance parameters for H^3(d, n)He^4 and He^3(d, p)He^4

E_r (keV)	Γ_{lab} (keV)	l_d	J^π	$l_{n,p}$	R ($\times 10^{-13}$cm)	E_λ (keV)	γ_d^2 [c] (keV)	$\gamma^2_{n,p}$ [c] (keV)	θ_d^2 [c]	$\theta^2_{n,p}$ [c]	E_x (MeV)
107[a]	135	0	$\frac{3}{2}^+$	2	5.0	−464	2000	56	1.0	0.018	16.69
					7.0	−126	715	17	0.7	0.011	
430[b]	≈450	0	$\frac{3}{2}^+$	2	5.0	−391	2930	42	1.4	0.013	16.81
					7.0	129	780	12	0.7	0.008	

[a] H^3(d, n)He^3: (Co 52f, Ar 52d, Ku 55). See also (Ba 57o, Ba 57p).
[b] He^3(d, p)He^4: (Ku 55).
[c] Units of $3\hbar^2/2MR^2$.

obtained, depending upon whether Γ_n/Γ_d is assumed > 1 or < 1 (Ar 52d, Co 52f). Agreement with the mirror reaction, He^3(d, p)He^4, is obtained with the second choice (Ku 55). The fact that the proton width is relatively small suggests that this level arises from excitation of the He^4 core. See also (Fl 51), (Jo 54b), (Jo 55b), (Le 58c), (Ha 55e; theo.) and (Da 57a).

The angular distribution of neutrons is isotropic at and below resonance, and shows increasing forward peaking at higher energies (Ja 57). Angular distributions at $E_d = 6$ MeV are almost identical to those of H^3(d, p)He^4 (Br 57e). At $E_d = 10$ MeV, the distribution is dominated by the stripping process, with $l_p = 0$ (Bu 51i). Again, close correspondence is found with the mirror reaction. See also (He 55a, Ba 56). See also (Pa 58b, Le 58c).

At $E_d = 12$ to 14 MeV, reactions (b) and (c) are observed (Bo 56g, Br 58b). The He^3 distributions from (b) show no evidence for a bound dineutron or for a well-defined virtual state, although some interaction between the neutrons does appear to occur. Absolute differential cross sections are reported (Br 58b).

For $E_d > 3.71$ MeV, deuteron breakup (reaction c) is energetically possible. The cross section for this process has been studied for $E_d = 3.8$ to 6.0 MeV by (He 55d). At $E_d = 14$ MeV, the number of low-energy (4 to 10 MeV)

neutrons is about three times as large as observed in the corresponding reaction He^3(d, pn)He^3. The difference may indicate formation of a $T = 0$, 22-MeV excited state of He^4 via H^3(d, n)He^{4*} (Bo 56g, Bo 56l, Bo 56m; see, however, Br 58b). See also (Ba 55t), (Co 54j), (Be 55j), (La 55e; theo.), (Bl 56d; theo.), (Fo 56a), (Bl 57b), (Po 58; theo.).

III. H^3(d, p)H^4

Assuming the atomic mass excess of $H^4 = 26$ MeV (if first $T = 1$ state in He^4 has $E_x = 22$ MeV), Q_m for this reaction would be -4 MeV. This reaction has not been observed (Mc 51a). An attempt has also been made by (Re 55f) to observe the β-decay of H^4 formed in the 300-MeV proton bombardment of C^{12}. The results are negative: if $\tau_{\frac{1}{2}} = (2 \text{ to } 4) \times 10^{-3}$ sec, $\sigma < 1\ \mu$b; if $\tau_{\frac{1}{2}} = (4 \text{ to } 10) \times 10^{-3}$ sec, $\sigma < 10\mu$b. See also (No 57a: $B^{10}(Li^7, H^4)N^{13}$).

IV. H^3(d, d)H^3 $E_b = 16.629$

Differential cross sections for $E_d = 0.96$ to 3.2 MeV are tabulated by (St 52e) and for $E_d = 10$ MeV by (Al 52b); see also (Br 57e, Ja 57). The distributions are closely similar to those for He^3(d, d)He^3. See also (Ba 58n).

V. H^3(t, n)He^5 $Q_m = 10.371$

The ground state of He^5 has been observed at $E_t = 1.48$ MeV (Ba 57e) and 1.9 MeV (Ja 56d). The neutron spectrum contains an excess of medium-energy neutrons, attributed to direct 3-body reaction or to a broad excited state of He^5. An earlier reported peak corresponding to a 2.6-MeV excited state (Le 51a) is not confirmed (Ba 57e). The alphas show a double peaking, reflecting the influence of the $P_{\frac{3}{2}}$ ground state, superposed on a distribution arising from the $P_{\frac{1}{2}}$ state and direct 3-body disintegration (Ja 58); see He^6.

VI. $H^3(He^3, p)He^5$ $Q_m = 11.136$

$Q_0 = 11.18 \pm 0.07$ (Al 53a).

$Q_0 = 11.13 \pm 0.07$ (Mo 53d).

The spectrum shows a well-defined proton peak corresponding to the ground state, superposed on a background attributed to the three-body breakup (Al 53a, Mo 53d). See also (Go 54c).

VII. $H^3(\alpha, d)He^5$ $Q_m = -7.215$

Not observed.

VIII. He^4(n, n)He^4 $E_b = -0.957$

Total cross sections for $E_n = 0.0004$ eV to 20 MeV are given in (Hu 55c, Hu 57, Hu 58); angular distributions of (Ad 52)and (Se 53) are given in (Hu 56): additional data for $E_n = 2.6$ to 4.1 MeV are given by (St 57c), for $E_n = 14$ MeV by (Sm 54, Sh 55) and at $E_n = 15.7$ MeV by (Al 54c). The

current experimental and theoretical situation is surveyed by (Ho 58a). The total cross section has a peak of 7.4 b at $E_n = 1.15 \pm 0.05$ MeV, $E_{c.m.} = 0.95$, with a width of ≈ 1.7 MeV (Ba 51a), $\Gamma_{c.m.} = 1.4 \pm 0.2$ MeV (Hu 58). The thermal cross section is 0.78b (Hi 51), 0.71 ± 0.1 b (Mc 51d), 0.74 ± 0.04 b (So 55a).

Both the total cross sections and the angular distributions are well accounted for by the phase shifts determined by (Cr 49a, Do 52b) for $He^4(p, p)He^4$ with a shift in E_λ of about 1 MeV: see also (Cl 55a; theo.). Earlier discrepancies in the range 3 to 4 MeV (Hu 52c) appear to have been resolved by (St 57c). In a polarization measurement, (Le 57b, Le 57d) find $\delta(P_{\frac{3}{2}}) = 12 \pm 1°$ at $E_n = 2.45$ MeV, in disagreement with the value $\delta = 20°$ derived from $He^4(p, p)He^4$, but agreeing with a low cross section point at $E_n = 2.61$ MeV reported by (Se 53). The s-wave phase shift decreases monotonically with increasing energy, and can be accounted for by hard-sphere scattering, with $R = 2.9 \times 10^{-13}$ cm (Ad 52, Do 52b; see, however, Br 54a, Ho 54g, Ho 55j, Va 56a). The $P_{\frac{3}{2}}$ shift shows strong resonance behaviour near 1 MeV, while the $P_{\frac{1}{2}}$ shift changes more slowly, possibly indicating a broad $P_{\frac{1}{2}}$ level at several-MeV excitation (Do 52b). At $E_n = 15.7$ MeV the angular distribution is best accounted for with $\delta(D_{\frac{3}{2}}) = -14°$, $\delta(D_{\frac{5}{2}}) = -7°$, the latter being somewhat less than the hard-sphere value, suggesting a higher resonance (Al 54c). Theory: see Li^5. (For present purposes, the ground state of He^5 is assumed to correspond to the maximum in the total cross section; $E_{c.m.} = 0.95$ MeV).

A resonance is reported at $E_n = 22.15 \pm 0.13$ MeV, $\Gamma \leqq 120$ keV, corresponding to the 16.7-MeV level (see $H^3(d, n)He^3$) (Bo 57e). See also (In 57).

Polarization of neutrons scattered in He has been discussed by (Ad 52, Si 53, Wh 57a, Se 53, Le 55b, Le 56d, Le 57b, Le 57d, Pa 58b) and others.

IX. (a) $He^4(d, p)He^5$ $\quad Q_m = -3.184$

(b) $He^4(d, pn)He^4$ $\quad Q_m = -2.226$

Q for reaction (a) $= -3.10 \pm 0.05$ (Fr 54h).

The proton spectrum observed at $E_d = 14.8$ MeV, $\theta = 19.5°$, shows a prominent peak, of width $\Gamma_{c.m.} = 550 \pm 30$ keV, and a monotonic continuum of lower energy protons, attributed to reaction (b). There is no evidence of structure corresponding to possible sharp excited states of He^5. Cross sections for the ground state group are $d\sigma/d\Omega = 25 \pm 5$ mb/sr at $\theta_{c.m.} = 18°$ and 15 ± 4 mb/sr at $\theta_{c.m.} = 24°$. The dimensionless reduced width of the ground-state group, analyzed by stripping theory is $\theta^2 = 0.05$, more than a factor of 10 smaller than is indicated by $He^4(n, n)He^4$ (see Li^5: $He^4(p, p)He^4$) (Wa 56e, Wa 57). For reaction (b), see Li^6.

X. $Li^6(\gamma, p)He^5$ $\quad Q_m = -4.655$

The threshold is $E_\gamma = 4.64 \pm 0.08$ MeV (Ry 58); see Li^6.

XI. $Li^6(n, d)He^5$ $Q_m = -2.428$

At $E_n = 14$ MeV, a well-defined ground state group ($\Gamma_{c.m.} = 0.8$ MeV) is observed, as is a continuum extending to $E_x \approx 4$ MeV in He^5. Angular distributions of the ground state group and of the continuum indicate $l_p = 1$ for the ground state transition and are not inconsistent with $l_p = 1$ for the continuum (Fr 54b): see Li^6, Li^7: $Li^6(n, d)He^5$.

XII. $Li^6(d, He^3)He^5$ $Q_m = 0.839$

At $E_d = 14.5$ MeV, the ground state group is observed: $Q_0 = 0.91 \pm 0.09$ MeV, $\Gamma_{c.m.} = 0.69 \pm 0.2$ MeV (Le 55).

XIII. $Li^6(t, \alpha)He^5$ $Q_m = 15.158$

$Q_0 = 15.15 \pm 0.04$ (Cr 56d).

The width of the ground state $\Gamma_{c.m.} = 0.7 \pm 0.2$ MeV (Cr 56d). See also (Al 54e, Ba 56f, Ma 56k).

XIV. $Li^7(n, t)He^5$ $Q_m = -3.423$

The angular distribution exhibits a forward maximum at $E_n = 14$ MeV. The total cross section is 55 ± 8 mb (Fr 54b). At $E_n = 14$ MeV, events corresponding to transitions to the ground state and possibly to a level at 2.4 ± 0.6 MeV are observed in Li-loaded photoplates; the latter group may actually be due to a level at 9.25 MeV in Li^7 (Al 54b): see $Li^7(n, n')Li^{7*}$.

XV. $Li^7(p, He^3)He^5$ $Q_m = -4.188$

Not reported

XVI. $Li^7(d, \alpha)He^5$ $Q_m = 14.163$

$Q_0 = 14.26 \pm 0.09$ (Le 55a)

$Q_0 = 13.719 \pm 0.02$ (Kh 55, Kh 55a)

$Q_0 = 14.15 \pm 0.22$ (Fa 57a)

$Q_0 = 14.11 \pm 0.08$ (We 58)

The angular correlation of ground state alpha particles and those resulting from the break up of He^5 is $W(\theta) = 1 + 1.2 \sin^2\theta$, excluding a $J = \frac{1}{2}$ assignment, but consistent with $J = \frac{3}{2}$ (Fr 51b). (Ri 56d) reports $W(\theta) = \sin^2\theta$, also consistent with $J = \frac{3}{2}^-$. The (α—n) correlation observed at $E_d = 0.16$ MeV, yields $W(\theta) = 1 + (0.75 \pm 0.05) \sin^2\theta$ and is again consistent with the assignment $J = \frac{3}{2}^-$ for the ground state of He^5 (Fa 57a). The coincidence α-spectrum agrees in shape with a computed spectrum based on the $He^4(n, n)He^4$ cross sections (Ri 56d).

The width of the ground state of He^5 is 0.3 ± 0.1 MeV (Cu 53a), 0.66 ± 0.2 MeV (Le 55). The work of (Cu 53a, Ju 56f) at $E_d = 0.6$ to 1.5 MeV appears to indicate an excited state at $E_x = 2.5 \pm 0.2$ MeV, $\Gamma \approx 1.5 \pm 0.3$ MeV. High-resolution magnetic spectra, observed for $E_d = 1.0$ to 2.2 MeV show

only the ground state peak, superposed on a continuous distribution, with no evidence of an excited-state group. The shape of the ground-state peak is well accounted for with the parameters $\gamma^2 = 17.6\times10^{-13}$ MeV-cm, $R = 2.9\times10^{-13}$ cm, taken from (n, α) scattering data (We 58a).

XVII. $Be^9(\gamma, \alpha)He^5$ $Q_m = -2.529$

See Be^9.

Li^5

(Fig. 2, p. 13) †

I. $H^3(He^3, n)Li^5$ $Q_m = 10.297$

Not reported.

II. $He^3(d, \gamma)Li^5$ $Q_m = 16.555$

The excitation curve measured from $E_d = 0.2$ to 2.85 MeV shows a broad maximum at $E_d = 0.45\pm0.04$ MeV ($E_\gamma = 16.6\pm0.2$, $\sigma = 50\pm10$ μb, $\Gamma_\gamma = 11\pm2$ eV). Above this maximum, nonresonant capture is indicated by a slow rise of the cross section. The radiation appears to be isotropic to ±10 per cent at $E_d = 0.58$ MeV, consistent with s-wave capture (Bl 54). See also (Ku 55b), (Ba 55t; theo.).

TABLE 5.3
Energy levels of Li^5

E_x (MeV)	J^π	Γ (MeV)	Decay	Reactions
0	$\frac{3}{2}^-$	≈ 1.5	p, α	II, V, VI, IX, X XI, XII, XIII
5–10	$\frac{1}{2}^-$	3–5	p, α	VI
16.81	$\frac{3}{2}^+$	≈ 0.3	d, He^3, p, α, γ	II, III, IV

III. (a) $He^3(d, p)He^4$ $Q_m = 18.351$ $E_b = 16.555$

(b) $He^3(d, np)He^3$ $Q_m = -2.226$

Cross sections and angular distributions for reaction (a) from $E_d = 35$ keV to 10 MeV are given in (Ja 57); see also (Fi 57, Bo 57g). Below 100 keV the cross section follows the simple Gamow form: $\sigma = (18.2\times10^3/E)\exp(-91\,E^{-\frac{1}{2}})$ b (E in keV) (Ar 54, Ja 53d). A pronounced resonance occurs at $E_d = 430$ keV, of about 450-keV width. The peak cross section is given as 0.695±0.014 b by (Ku 55, Bo 52a) and 0.92±0.07 b by (Ya 53, Fr 54a). The resonance is closely fitted with the one-level dispersion formula, using the parameters listed in table 5.2 (see $H^3(d, n)He^4$). See also (Kl 56b, Ha 55e, Jo 55b, Ba 55t), (Po 58; theo.).

The angular distribution of protons is isotropic near resonance and shows forward peaking at higher energies; the similarity to $H^3(d, n)He^4$ is very close. See also (Br 57e, Ku 55b, Bo 57g).

† For level scheme of He^5, see fig. 1, p. 7.

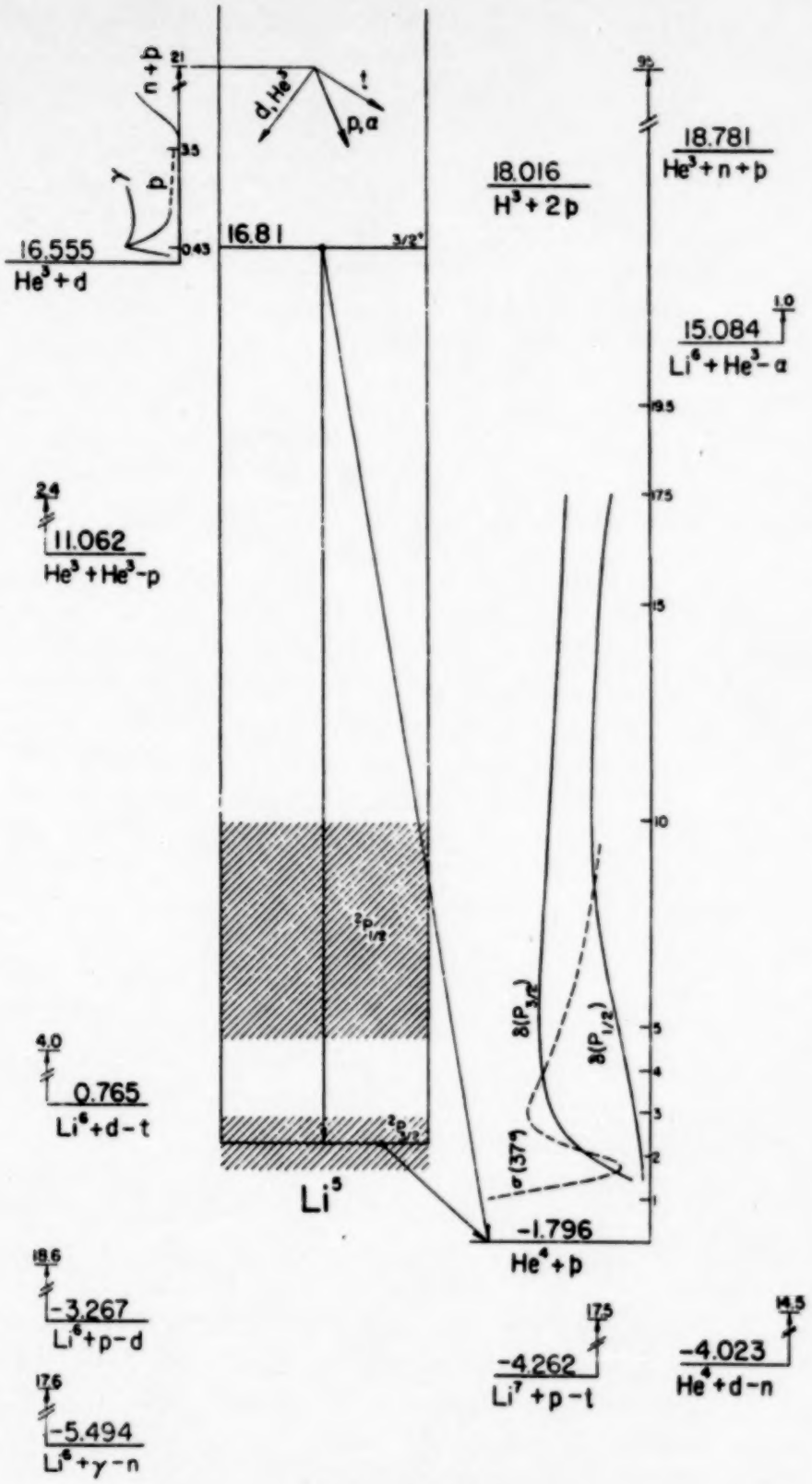

20 December 1958

Fig. 2. Energy levels of Li^5: for notation, see fig. 1, p. 7.

Above $E_d = 3.71$ MeV, deuteron breakup (reaction b) is observed (He 55d).

IV. $He^3(d, d)He^3$ $E_b = 16.555$

Differential cross sections for $E_d = 0.4$ to 3 MeV are plotted in (Ja 57); see also (Al 52b, Br 57e, Fi 57). In the range $E_d = 380$ to 570 keV, $\theta_{c.m.} = 65°$, the scattering cross section is considerably below Rutherford scattering and is consistent with s-wave formation of a $J = \frac{3}{2}^+$ state. Above $E_d = 2$ MeV, the distributions are quite similar to those observed in $H^3(d, d)H^3$ (Br 54b, Br 57e, Al 52b).

V. $He^3(He^3, p)Li^5$ $Q_m = 11.062$

The proton spectrum at $E(He^3) = 360$ keV shows an unresolved ground-state group superposed on a broad continuum. No evidence is found for well-defined proton groups of lower energy than the ground state group (Go 54c). See also (Al 53a), (Br 57) and Be^6.

VI. $He^4(p, p)He^4$ $E_b = -1.796$

Differential elastic scattering cross sections have been measured at numerous energies from 0.95 to 95 MeV, as indicated in table 5.4; curves at several energies are given by (Ja 57) and (Br 57k). Phase shifts derived from the experimental data are listed in the table. At $E_p = 40$ MeV, the differential cross section shows "diffraction" maxima and minima characteristic of the optical model (Br 57b: see also Bu 56j, Ho 57d, Gi 57, Ga 58). Recent surveys of the experimental and theoretical situation are reported by (Ho 58a, Ga 58, Mi 58a).

Even at low energies, the phase shift analysis clearly requires a splitting of $P_{\frac{1}{2}}$ and $P_{\frac{3}{2}}$ levels, generally attributed to spin-orbit effect. Either order of the P-doublet can be used to fit the cross section data (Cr 49a, Do 52b): that the $P_{\frac{3}{2}}$ state is the lower is established by measurement of the polarization of scattered protons (He 52a, Sc 55b, Ju 56a, Sc 58). The tabulated phase shifts apply to this case.

The $P_{\frac{3}{2}}$ phase shift shows a pronounced resonance effect, passing through 90° at $E_p = 2.8$ MeV (Cr 49a), while the $P_{\frac{1}{2}}$ changes only slowly over a range of several MeV. Analysis by (Do 52b), based on resonance theory, yields for the $P_{\frac{3}{2}}$ level (ground state of Li^5) E_λ(c.m.) $= -4.1$ MeV, $\gamma_\lambda^2 = 25\times10^{-13}$ MeV-cm and for the $P_{\frac{1}{2}}$, E_λ(c.m.) $= 3.4$ MeV, $\gamma_\lambda^2 = 105\times10^{-13}$ MeV-cm (see also Ad 52). (These widths correspond to $\theta_p^2 = 0.9$ and 3.9 times the sum-rule limit, respectively, using $R = 2.9\times10^{-13}$ cm.) It thus appears that the $P_{\frac{1}{2}}$ state, if resonance theory is at all appropriate here, is extremely broad and located 5—10 MeV above the ground state. A new analysis of all data < 18 MeV yields E_{res} (lab) $= 2.6$ MeV, $\gamma_p^2 = 12\times10^{-13}$ MeV-cm, $\theta_p^2 = 0.40$ for the ground state and E_{res} (lab) $= 10.8$ MeV, $\gamma_p^2 = 30\times10^{-13}$

TABLE 5.4

Phase shifts in $He^4(p, p)He^4$ [a]

E_p (lab) (MeV)	$S_{\frac{1}{2}}$ (deg)	$P_{\frac{1}{2}}$ (deg)	$P_{\frac{3}{2}}$ (deg)	$D_{\frac{3}{2}}$ (deg)	$D_{\frac{5}{2}}$ (deg)	Reference
0.95	−12.0	3.3	3.3	0	0	Cr 49a, Fr 49c
1.49	−18.1	4.1	20.4			Cr 49a, Fr 49c
1.70	−17.6	4.2	31.1			Cr 49a, Fr 49c
2.02	−24.6	8.1	47.8			Cr 49a, Fr 49c
2.22	−26.7	9.4	60.6			Cr 49a, Fr 49c
2.53	−28.2	13.1	78.8			Cr 49a, Fr 49c
3.03	−27.3	10.3	99.3	0.7	0.1	Mi 58a
3.04	−32.0	15.7	96.6			Cr 49a, Fr 49c
3.51	−30.9	18.8	107.6	1.3	−1.1	Mi 58a
3.58	−35.2	20.3	105.4			Cr 49a, Fr 49c
4.02	−32.9	23.6	112.4	2.1	−1.7	Mi 58a
4.50	−43.1	29.1	111.6	−3.1	−0.5	Mi 58a
5.00	−51.8	35.5	109.9	−4.7	0.1	Mi 58a
5.1	(no analysis)					Br 51h
5.78	−47.9	38.7	112.9	−1.3	−0.49	Kr 54, Do 52b, Lu 55a
7.50	−57.95	52.51	112.1	−1.87	+0.44	Pu 56a
9.48	−65.36	54.72	109.2	−5.73	−3.21	Pu 52a, Pu 56a
9.55	(optical model)					Fr 54h, Gi 57: see Wi 55c, Ho 57d
9.76	(no analysis)					Wi 55c
9.8	(no analysis)					Co 54g
12.0	−66.9	60.1	108.7			Br 57k [b]
14.0	−76.7	50.2	92.7			Br 57k [b]
16.0	−81.1	49.1	89.5			Br 57k [b]
17.0 [c]				(−14)	(−17)	Al 54c
17.45	−85.7	53.2	94.8			Br 56a, Br 57k
18	−85.8	46.4	85.4			Br 56a, Br 57k
19.4	(no analysis)					Va 56b, Va 57b
27.9	(no analysis)					Wi 57f
31.6	(no analysis)					Co 53l
39.85	(optical model)					Br 57b
95	(no analysis)					Te 55

[a] Phase shifts for $E_p = 1$ to 18 MeV are plotted by (Mi 58a); extrapolated values from 10 to 40 MeV are tabulated by (Ga 58).

[b] (Br 57k) also tabulates values for $E_p = 13$, 15 and 17 MeV; D-wave $< 8°$.

[c] From $He^4(n, n)He^4$.

MeV-cm, $\theta_p^2 = 1.0$ for the excited state, using $R = 2.6 \times 10^{-13}$ cm (Mi 58a). The s-wave phase shifts are will accounted for by hard-sphere scattering, with $R = 2.9 \times 10^{-13}$ cm (Ad 52, Do 52b; see, however, Va 56a), $R = 2.0 \times 10^{-13}$ cm (Mi 58a). Semi-empirical phase shifts and polarizations for $E_p = 10$ to 40 MeV are given by (Ga 58).

Proton and neutron scattering in helium are discussed in terms of a central potential with spin-orbit interaction by (Sa 54, Ja 54a, Br 54a, Ho 54g, Ho 55j, Ga 58). (Ho 55j) obtain a good account of the s- and p-wave interactions with a gaussian potential and Serber exchange force. The effect of

tensor forces is discussed by (Fe 56). See also (Ab 56, Le 56e, Ho 58a).

Polarization of the scattered protons is discussed by (Cr 49a, Ad 52, Do 52b, He 52a, Sc 55b, Br 56g, Ju 56a, Se 57a, Sc 57a, Sc 58, Sc 58a, Br 58f, Ro 57c) and others.

For α-scattering in hydrogen: see (Ru 54, Ju 54a, Ro 57c). See also (Ei 56, Ty 57a).

VII. (a) $He^4(p, d)He^3$ $Q_m = -18.351$ $E_b = -1.796$
(b) $He^4(p, pn)He^3$ $Q_m = -20.577$

Angular distributions are reported at $E_p = 27.9$ MeV (Wi 57f), 31.6 MeV (Be 52a) and 95 MeV (Te 55) for reaction (a). The cross section at $E_p = 40$ MeV, $\theta = 30°$, is 10 ± 1 mb/sr (Ei 56). For reaction (b), see (Wi 57f) and (Ei 56).

VIII. $He^4(p, 2p)H^3$ $Q_m = -19.812$ $E_b = -1.796$

See (Wi 57f) and (Ei 56).

IX. $He^4(d, n)Li^5$ $Q_m = -4.023$

At $E_d = 13$ MeV, a broad, asymmetric neutron group corresponding to the ground state is observed. There is no evidence for structure corresponding to the $P_{\frac{1}{2}}$ excited state (Bo 56l, Bo 56m).

X. $Li^6(\gamma, n)Li^5$ $Q_m = -5.494$

The photoneutron threshold is 5.4 ± 0.2 MeV (Ti 51), 5.35 ± 0.2 MeV (Sh 51d), 5.6 ± 0.1 MeV (Ti 55a), 5.73 ± 0.05 MeV (Ry 58). An earlier reported higher state is not confirmed (Ti 55a).

XI. $Li^6(p, d)Li^5$ $Q_m = -3.267$
Q_0 -3.0 ± 0.15 (Li 55).

At E_p 18.6 MeV, the ground state group appears as a broad, asymmetric peak (Γ 1.8 MeV) which tails off to a low continuum at lower energies. The angular distribution of the ground state group has a maximum at 15° (c.m.) and, at small angles, conforms with stripping theory ($l_n = 1$) (Li 55).

XII. $Li^6(d, t)Li^5$ $Q_m = 0.765$
Q_0 0.80 ± 0.15 (Fr 58a).

At E_d 1 MeV a broad ground state triton group is observed ($\Gamma_{c.m.} = 1.5$ MeV). The distribution of protons from the Li^5 breakup indicates a pronounced forward distribution (Fr 58a). See also Be^8.

XIII. $Li^6(He^3, \alpha)Li^5$ $Q_m = 15.084$

See (Al 55b) and (Ku 53b).

XIV. $Li^7(p, t)Li^5$ $Q_m = -4.262$

This reaction has been observed at $E_p = 17.5$ MeV (Ma 57c).

He^6

(Fig. 3, p. 19)

SPIN OF He^6

In a Stern-Gerlach experiment, (Co 58h) find $\mu(He^6) < 0.16$ nuclear magnetons if J is taken as 1; it is concluded that $J(He^6) = 0$.

THEORY

See (Ba 55s, Sk 58).

I. $He^6(\beta^-)Li^6$ $\quad Q_m = 3.536$

The β-spectrum is simple, with an end point $E_\beta(\max) = 3.50 \pm 0.05$ (Wu 52), 3.50 ± 0.02 MeV (Sc 56i). Recently reported half-lives are 0.852 ± 0.01 sec (Ve 56), 0.83 ± 0.02 sec (He 58c), 0.85 ± 0.03 sec (Ru 55). The weighted mean of half-lives cited here and in (Ho 50b, Aj 55) is 0.813 ± 0.007 sec. Using Q_m, log ft is 2.92.

The electron-neutrino correlation is found to be $W(\theta) = 1 + \alpha\,(p/W)\cos\theta$, with $\alpha = -(0.39 \pm 0.02)$, in good agreement with the value $\alpha = -\frac{1}{3}$ for pure axial vector interaction (He 58c, He 59, Pl 59). An earlier report by (Ru 55) appears to have been in error: see (Wu 58, Al 58a). See also (Ba 55s, Le 57f, La 55a; theo.).

II. (a) $H^3(t, n)He^5$ $\quad Q_m = 10.371$ $\quad E_b = 12.272$

(b) $H^3(t, \alpha)2n$ $\quad Q_m = 11.328$

(c) $H^3(t, \alpha)n^2$

At $E_t = 1.9$ MeV, the α-spectrum, observed at 30°, extends from 1 to 7 MeV, with peaks at $E_\alpha = 2$ and 5 MeV. The same general shape is observed at other angles and for $E_t = 0.95$ to 2.1 MeV. These peaks are attributed to a two-stage process involving formation and breakup of He^5 in the $P_{\frac{3}{2}}$ and $P_{\frac{1}{2}}$ states and are superposed on the 3-body spectrum, reaction (b). Structure observed near the end point may indicate a correlation between the two neutrons (Ja 58). At $E_t = 1.48$ MeV, the neutron spectrum shows a continuum from 0 to 12 MeV with a broad peak at 11.3 MeV, corresponding to formation of He^5 in the ground state (Ba 57e).

The cross section for neutron production rises monotonically from 0.1 to to 2.2 MeV (Ag 51, Ja 57, Ja 58). At $E_t = 1.90$ MeV, the total cross section for production of α-particles is 106 ± 5 mb (Ja 58).

III. $H^3(t, t)H^3$ $\quad E_b = 12.272$

Differential scattering cross sections have been measured at $E_t = 1.58$ to 2.01 MeV by (Ho 56a). At $E_t = 1.90$ MeV, θ (lab) = 30°, $\sigma(\theta) = 286$ mb/sr (± 5 %) (Al 58b). A phase-shift analysis shows that the distributions at $E_t = 1.80$ and 2.01 MeV are adequately accounted for by a ^1S phase shift corresponding to a hard sphere of radius 2.35×10^{-13} cm. There is no evidence of p-waves or of resonance in this region (Fr 55e).

IV. $H^3(\alpha, p)He^6$ $Q_m = -7.540$
Not reported.

V. $Li^6(n, p)He^6$ $Q_m = -2.753$
See Li^7.

VI. $Li^6(t, He^3)He^6$ $Q_m = -3.518$
Not reported.

VII. $Li^7(\gamma, p)He^6$ $Q_m = -10.006$

A γ-emitting level at $E_x = 1.6 \pm 0.2$ MeV is reported by (Ti 54a). This evidence, based on the colinearity of p and He^6 tracks in photoplates, appears to conflict with other indications that this state decays predominantly to He^4+2n (Al 54e; see, however, Ma 56o). See $Li^7(t, \alpha)He^6$.

TABLE 6.1
Energy levels of He^6

E_x in He^6 (MeV)	J^π	Γ (MeV)	Decay	Reactions
0	0^+	$\tau_{\frac{1}{2}} = 0.813 \pm 0.007$ sec	β^-	I, V, VII, VIII, IX, X, XI, XII
1.71 ± 0.01	(2^+)	$\lesssim 0.1$	α, n, (γ)	VII, X, XI
(3.4)		($\lesssim 0.3$)		XI
(6.0 $\pm$0.9)				XI
(9.3 $\pm$0.7)			α, n	XI

VIII. $Li^7(n, d)He^6$ $Q_m = -7.779$
See Li^8.

IX. $Li^7(p, 2p)He^6$ $Q_m = -10.006$

The summed proton spectrum at $E_p = 185$ MeV shows two peaks, attributed to formation of He^6(g.s.) by removal of a p-proton from Li^7 and $He^{6*} \approx 15$ MeV, formed by removal of an s-proton (Ty 57c, Ty 58b, Ma 58h).

X. $Li^7(d, He^3)He^6$ $Q_m = -4.512$.

At $E_d = 14.5$ MeV, the ground state and the 1.71-MeV level are observed. The angular distributions analyzed by pick-up theory indicate even parity for both states. Peak differential cross sections are 8.0 mb/sr at $\theta_{c.m.} = 17°$ and 2.0 mb/sr at $\theta_{c.m.} = 16.5°$ for the ground and 1.7-MeV states respectively (Le 55); $\theta^2 = 0.055$ and 0.017 (Fr 57).

XI. $Li^7(t, \alpha)He^6$ $Q_m = 9.807$
$Q_0 = 9.79 \pm 0.03$ (Al 54e)
$Q_0 = 9.79 \pm 0.14$ (Ma 56k)

The energy of the first excited state is 1.71 ± 0.01 MeV, $\Gamma \lesssim 100$ keV (Al 54e, Al 55a). Preliminary results may indicate a state at 3.4 MeV,

$\Gamma < 0.3$ MeV (Al 54e, Al 55a). (Ma 56o) report evidence for a state at (6.0±0.9 MeV) and for one or more states at 9.3±0.7 MeV (3.8-MeV tritons from Be^9(d, t)Be^8 were used). Angular distributions at $E_t = 240$ keV are

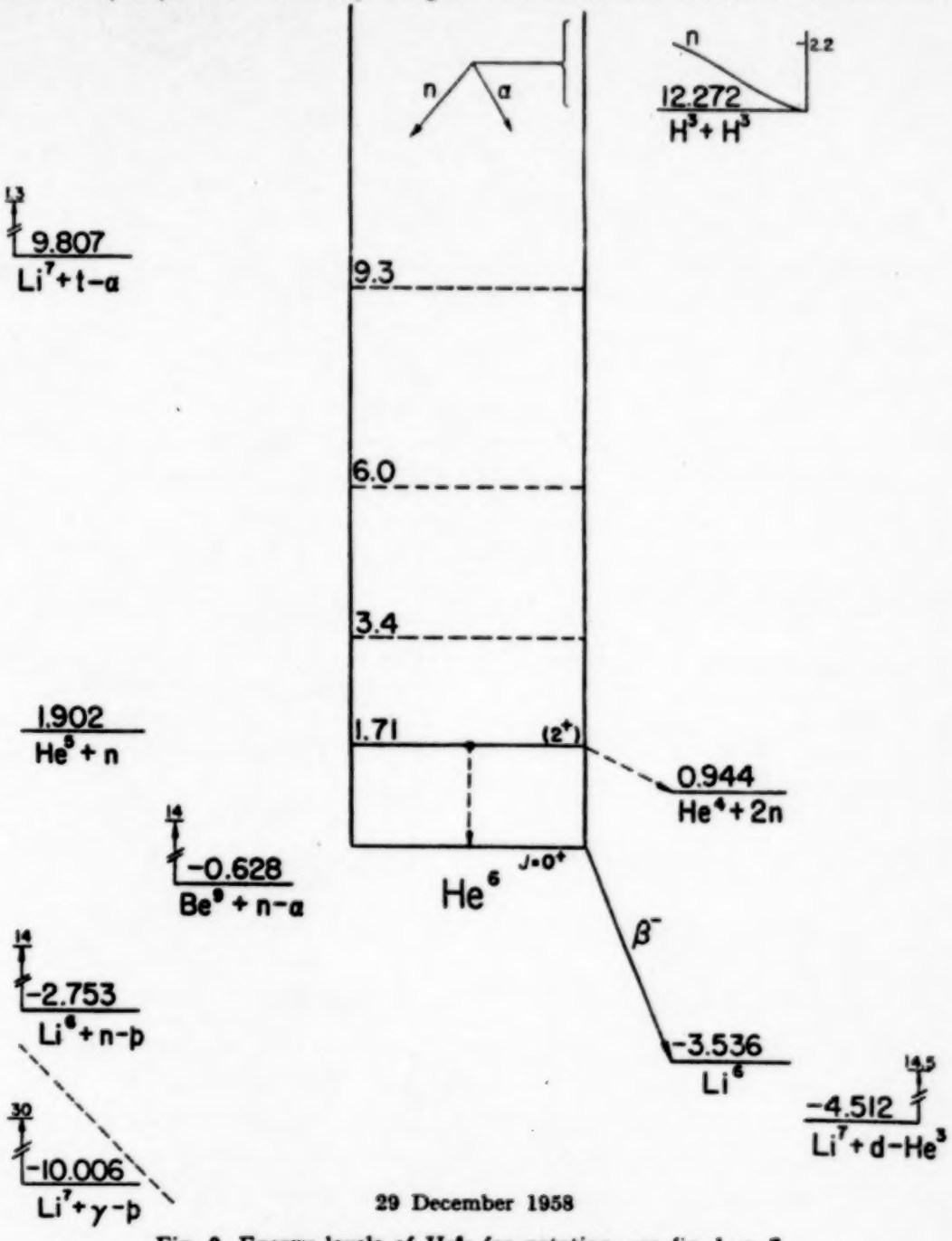

29 December 1958

Fig. 3. Energy levels of He^6: for notation, see fig. 1, p. 7.

consistent with $J = 0$ and 2 for the ground state and the 1.7-MeV level respectively (Al 54d: see Be^{10}). At $E_t = 0.84$ MeV, $\theta = 90°$, the cross sections for formation of He^6(0) and He^6(1.7) are 16 and 26 mb/sr, respectively (Ma 56k).

The absence of He^6 recoils corresponding to the 1.7-MeV state implies that this state decays predominantly into He^4+2n (Al 54e). See also (Cu 55b), (Ba 56f), and (Aj 52c).

XII. $Be^9(n, \alpha)He^6$ $\quad Q_m = -0.628$

See Be^{10}.

Li^6

(Fig. 4, p. 21)

THEORY

See (Ad 55), (Au 55), (Ba 55s), (Fe 56), (Fr 57), (Ir 55), (La 55), (Le 57f), (Ly 57), (Pi 58), (Me 56), (Mo 54f), (Ne 56d), (Ot 55), (Sk 58), (So 57), (Ta 57).

TABLE 6.2

Energy levels of Li^6

E_x in Li^6 (MeV)	J^π; T	Γ (keV)	Decay	Reactions
0	1^+; 0		Stable	IV, VI, XI, XII, XIII, XIV, XV, XVI, XVII, XVIII, XIX, XX, XXII, XXIII
2.184 ±0.003	3^+; 0	21	α, d	IV, XI, XII, XIII, XIV, XVIII, XIX, XX, XXII, XXIV
3.560 ±0.006	0^+; 1	< 5	γ	XII, XVIII, XX, XXII
4.52 ±0.08	2^+; 0	≈ 600	α, d	IV, XII, XIII, XIV, XIX, XX
5.35 ±0.07	; (1)	< 100		XX
5.5 ±0.4	1^+; 0	≈ 1000	α, d	IV, XX
6.63 ±0.08	; (1)	< 200		XX
7.40 ±0.10	; (0)	≈ 500	α, d, p, n	XIII, XIX, XX
(8.37 ±0.08)	; (1)	(< 200)		XX
(9.3 ±0.2)		(≈ 500)		XX

I. (a) $H^3(He^3, d)He^4$ $\quad Q_m = 14.319$ $\quad E_b = 15.790$

(b) $H^3(He^3, p)He^5$ $\quad Q_m = 11.136$

(c) $H^3(He^3, p)He^4+n$ $\quad Q_m = 12.093$

The relative intensities (43 ± 2, 6 ± 2, 51 ± 2) of reactions (a), (b) and (c), do not vary for $E(He^3) = 225$ to 600 keV. The deuterons are isotropic (c.m.) at $E_t = 360$ keV. The total cross section, reported for $E(He^3) = 100$ to 800 keV, varies from 0.5 mb to 0.18 b, without showing resonance behaviour, the main variation being accounted for by the Coulomb barrier effect (Mo 53d). See also (Al 53a) and (Ja 57).

II. $He^3(\alpha, p)Li^6$ $\quad Q_m = -4.004$

See (Ch 58d).

III. $He^4(d, \gamma)Li^6$ $\quad Q_m = 1.471$

An upper limit for capture radiation at $E_d = 1.055$ MeV (2.18-MeV state)

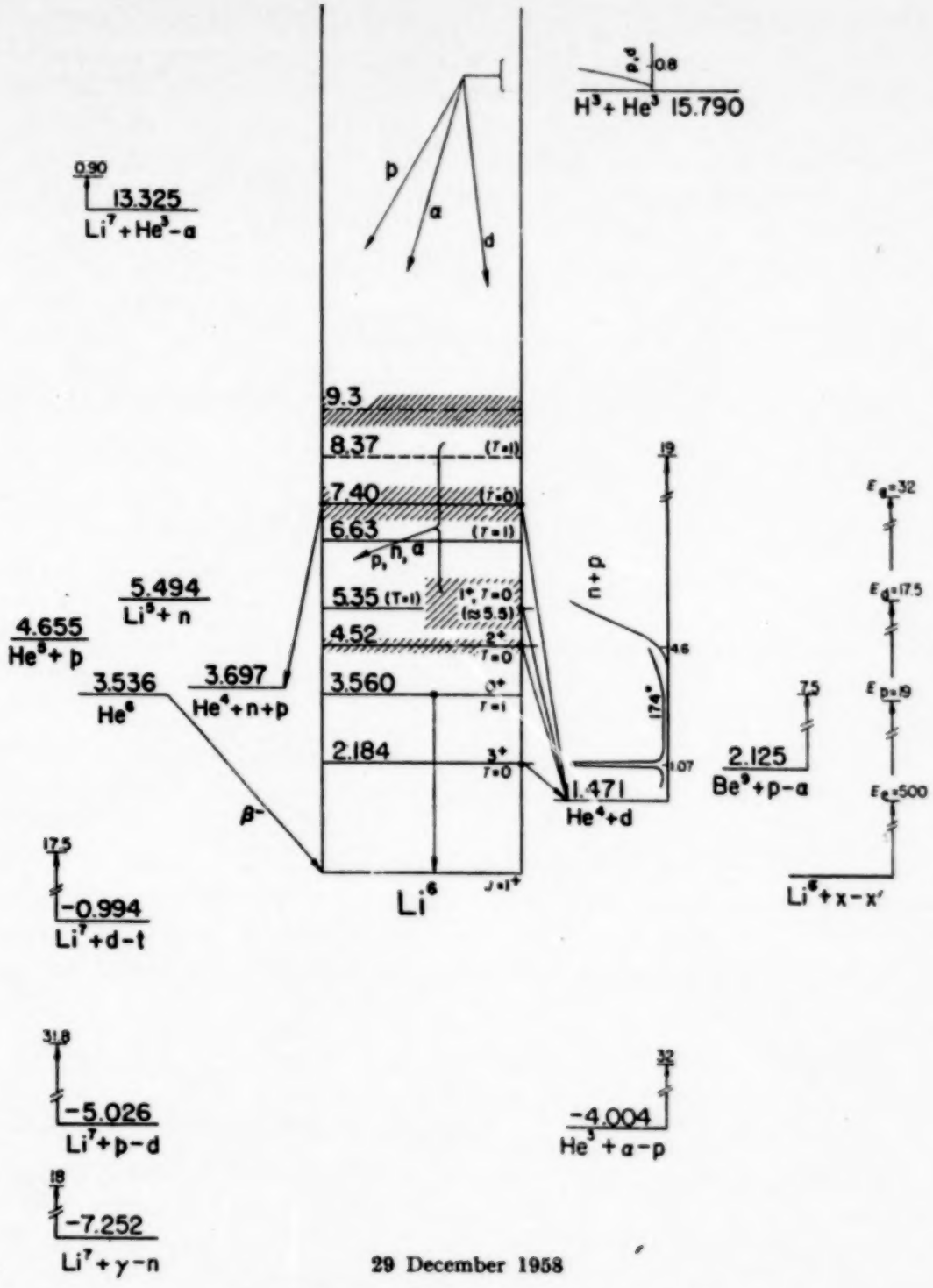

Fig. 4. Energy levels of Li^6: for notation, see fig. 1, p. 7.

is 0.1 mb (Si 54). A search for resonant capture radiation at $E_d = 3.1$ MeV ($Li^{6*} = 3.56$) yields $\Gamma_{d\alpha} < 0.2$ eV. It is concluded that the intensity of parity non-conserving parts of the wave functions, $F^2 \lesssim 10^{-7}$ (Wi 58b).

IV. $He^4(d, d)He^4$ $E_b = 1.471$

Differential cross sections have been measured for $E_d = 0.88$ to 3.51 MeV (Bl 49), $E_d = 1.0$ to 1.2 MeV (La 53), $E_d = 0.28$ to 4.62 MeV (Ga 55), $E_d = 6.5$ MeV (Gu 47), $E_d = 7.94$ MeV (Bu 51h), $E_d = 10.3$ MeV (Al 51l), $E_d = 13.7$ and 19.0 MeV (Fr 54h): see (Ja 57).

At $E_d = 1.07$ MeV, a strong resonance is observed (see table 6.3) attributed to d-wave formation of a $J = 3^+$ state. The best fit is obtained with the p-wave phase shift set equal to zero. If an interaction radius of $R = 3.5 \times 10^{-13}$ cm is used, the s-wave phase shift requires a contribution from the ground state, whose width is thus determined to be $\theta^2 = 0.51$; for a radius $R = 5.0 \times 10^{-13}$ cm, hard-sphere scattering alone suffices (Ga·55a).

The anomaly in the region 3.5 to 4.5 MeV requires two levels, $J = 1^+$ and 2^+ (see table 6.3) formed by d-waves. Again the p-wave phase shift differs from the hard sphere value, suggesting an odd parity state at higher energy. There is no indication of the 3.56-MeV Li^6 level, consistent with its assumed $J = 0^+$, $T = 1$ character. The three states found here are presumed to be the components of a ^3D term; their spacings indicate a coupling rather close to the L-S limit (Ga 55a: see In 53).

TABLE 6.3

Levels of Li^6 from $He^4(d, d)He^4$ (Ga 55a)
(interaction radius = 3.5×10^{-13} cm)

E_{res} (MeV)	Γ (keV)	E_x (MeV)	l_d	J^π	E_λ[a] (MeV)	θ_d^2[a]
		0	0	1^+	−2.26	0.51
1.070 ± 0.003	35 ± 5	2.183	2	3^+	2.333	0.80
4.57 ± 0.08	900	4.52	2	2^+	7.05	1.0
5.1 −6.5	1000	4.9−5.8	2	1^+	5.5−9.7	0.2−1.0

[a] Measured from Li^6 ground state.

V. (a) $He^4(d, p)He^5$ $Q_m = -3.184$ $E_b = 1.471$
(b) $He^4(d, n)Li^5$ $Q_m = -4.023$
(c) $He^4(d, pn)He^4$ $Q_m = -2.226$

Ground-state protons from reaction (a) and ground-state neutrons from (b) have been studied by (Wa 57; $E_d = 14.8$ MeV) and by (Bo 56l, Bo 56m; $E_d = 13.5$ MeV) respectively; see He^5, Li^5. The cross section for (a) is 25 ± 5 mb/sr at $\theta = 18°$ (c.m.) and 15 ± 5 mb/sr at 24° (c.m.) (Wa 57).

Cross sections for production of low-energy neutrons have been measured in the range $E_d = 3$ to 6 MeV by (He 55d). It is argued that reaction (c) probably involves production of the ^1S state of the deuteron and hence is isobaric spin forbidden in the present case: the low energy neutrons are therefore attributed to reaction (a) (He 55d). See also (Bu 51h, Al 51l, Ja 57).

VI. $He^6(\beta^-)Li^6$ $Q_m = 3.536$

See He^6.

VII. $Li^6(\gamma, n)Li^5$ $Q_m = -5.494$

The cross section is 0.3 ± 0.2 mb at $E_\gamma = 6.2$ MeV (Ed 56a) and 0.5 ± 0.2 mb for $E_\gamma = 14.8$ to 17.6 MeV (Ti 51). See also (Ba 57, Fo 57c, Pr 58, Be 58c, Ry 58).

VIII. $Li^6(\gamma, p)He^5$ $Q_m = -4.655$

This reaction has been observed with photoplates for $E_\gamma(\max) = 30$ to 80 MeV. The angular distribution is of the form $a+b\sin^2\theta(1+\cos\theta)^2$ (Kl 56a). For 17.5-MeV bremsstrahlung, no n—p correlation is observed; this result argues against a (He^4+d) model for Li^6(Pr 58). See also (Ti 55a, Ry 58).

IX. $Li^6(\gamma, d)He^4$ $Q_m = -1.471$

The cross section is $\lesssim 5$ μb in the range $E_\gamma = 2.6$ to 17 MeV (Je 53b, Gl 52a, Ti 52, Ti 54b, Ti 55a). Electric dipole absorption is forbidden by isobaric spin selection rules (Ge 53a); the relative weakness of both electric and magnetic interaction may be made plausible on a simple (He^4+d) model for Li^6 (Je 53b: see also Va 54c, Da 55, Da 55c, Pr 58).

X. $Li^6(\gamma, t)He^3$ $Q_m = -15.790$

The cross section is < 10 μb at $E_\gamma = 17.6$ MeV (Ti 54b).

XI. (a) $Li^6(e, e')Li^6$

(b) $Li^6(e, p)He^5$ $Q_m = -4.655$

(c) $Li^6(e, d)He^4$ $Q_m = -1.471$

Elastic scattering of 187-MeV electrons yields an r.m.s. radius of 2.78×10^{-13} cm ± 2 per cent: for the uniform model, $R_0 = 1.98 \times 10^{-13}$ cm (St 55e, Ho 56e). At $E_e = 426$ MeV, the data are fitted by an r.m.s. radius of $(2.2 \pm 0.2) \times 10^{-13}$ cm. Inelastic scattering has been observed to the 2.18-MeV state and to higher states (Ho 57f, Ho 57g). See also (Me 57c, Eh 57).

Reactions (b) and (c) have been observed and angular distributions measured at $E_e = 500$ MeV (Ke 57b).

XII. $Li^6(p, p')Li^{6*}$

At $E_p = 7.0$ to 7.5 MeV, and three angles, proton groups are observed corresponding to the ground state, to a state at 2.188 MeV ($\Gamma_{c.m.} = 25$ keV) and to a state at 3.559 MeV ($\Gamma < 5$ keV): (see table 6.4). No other sharp levels ($\Gamma < 100$ keV) are seen below $E_x = 5$ MeV: the intensity limit of groups corresponding to such states is 3 % of the intensity of the group corresponding to the 2.18-MeV state. A group of ≈ 1 MeV breadth would have escaped detection unless its intensity were ≈ 3 times that of the

TABLE 6.4

Levels of Li^6 from $Li^6(p, p')Li^6$, $Li^6(d, d')Li^6$, $Li^7(d, t)Li^6$ and $Be^9(p, \alpha)Li^6$ (Br 57a)

	Reaction	E_x (MeV)	$\Gamma_{c.m.}$ (keV)
	$Li^6(p, p')Li^6$	2.188	25.4
	$Li^6(p, p')Li^6$	3.559	< 5
	$Li^6(d, d')Li^6$	2.186	24.5
	$Li^7(d, t)Li^6$	(2.18)	<27
	$Be^9(p, \alpha)Li^6$	2.192	29
	$Be^9(p, \alpha)Li^6$	3.561	
Mean:		2.188 ±0.006	24
		3.560 ±0.006	< 5

2.18-MeV state group (Br 57a). At $E_p = 14.8$ and 19.0 MeV, the angular distributions of the protons to the 2.18-MeV state peak at $\approx 40°$. The protons from the 3.56-MeV state appear weakly, if at all, on the side of the broad group from the 4.5-MeV level ($\Gamma \approx 1.8$ MeV) (Sh 56f). For a theoretical discussion of the data see (Le 57f). See also (Fr 52, Aj 52c, Ch 58).

XIII. $Li^6(d, d')Li^{6*}$

At $E_d = 7.0$ and 7.5 MeV ($\theta = 60°$ and 90°), deuteron groups are observed corresponding to the ground state and to a level at 2.186 MeV ($\Gamma_{c.m.} = 24$ keV; see table 6.4). At $E_d = 7.5$ MeV, $\theta = 60°$, an upper limit of 0.9 % of the intensity of the 2.18-MeV group is given for a group corresponding to the 3.56-MeV state. The fact that the 2.18-MeV state was observed in this experiment but that the 3.56-MeV state was not is consistent with the assignments $T = 0$ and $T = 1$, respectively, for these states. No other sharp groups with $E_x < 5$ MeV were observed: their intensity limits are 1 per cent of the intensity of the 2.18-MeV state. A 1-MeV broad group would have escaped detection unless its intensity were > 2 times that of the 2.18-MeV state group (Br 57a). At $E_d = 15$ MeV, the angular distribution of the deuterons to the 2.18-MeV state has been measured by (Ha 56c). Comparison is made with predictions based on nuclear and electric interactions (Ha 56c).

Excitation of Li^6 states at 2.2, ≈ 4.5, and 7.6 ± 0.3 MeV is observed in deuteron bombardment, $E_d(\text{max}) = 13.8$ MeV, of Li-loaded emulsions. Observed stars are reported to correspond to $d+\alpha$ decay of the first two states and decay into $\alpha+p+n$ of the last (So 56). At $E_d = 17.5 \pm 0.25$ MeV, these three states and two additional states at 5.9 and 8.3 MeV are reported (So 56a).

XIV. $Li^6(\alpha, \alpha')Li^6$

Angular distributions of elastic and inelastic scattering have been studied at $E_\alpha = 31.5$ MeV by (Wa 56f). Inelastic groups corresponding to the 2.18 and 4.52-MeV levels are observed; the isobaric spin-forbidden group corresponding to the 3.56-MeV level is < 4 per cent as intense. The angular distributions of the inelastic groups are well described by the direct interaction theory of (Au 53) with $R = 6.6$ and 5.8×10^{-13} cm respectively (Wa 56f).

XV. $Li^6(p, He^3)He^4$ $\quad Q_m = 4.022$

Angular distributions observed at $E_p = 15$ and 18.5 MeV indicate a deuteron pickup process. An analysis based on Born approximation theory leads to deuteron reduced widths for the ground state of Li^6 of $\theta_d^2 = 0.30$ and 0.45 (Li 56b). See also Be^7.

XVI. (a) $Li^6(n, t)He^4$ $\quad Q_m = 4.787$

(b) $Li^6(n, d)He^5$ $\quad Q_m = -2.428$

Angular distributions at $E_n = 1.5$ and 2.0 MeV reported by (We 54) and $E_n = 14$ MeV by (Fr 54b) are analyzed by (Da 55, Da 55a, Da 55c, Sa 55i) in terms of pickup theory in Born approximation, using an (He^4+d), two-body model for Li^6. (Li 56b) calculate $\theta^2 = 0.5$ from the data of (Fr 54b) on reaction (a). See also Li^7.

XVII. $Li^7(\gamma, n)Li^6$ $\quad Q_m = -7.252$

See Li^7 and (Ti 55a, Ti 58).

XVIII. $Li^7(p, d)Li^6$ $\quad Q_m = -5.026$

At $E_p = 17.5$ MeV, angular distributions of the deuterons to the ground state and the 2.18-MeV level, analyzed by pickup theory, indicate $l_n = 1$ and hence even parity, $J \leqq 3$ for both states. The absolute differential cross section (at $\approx 20°$ c.m.) for the formation of the ground state is 17 ± 4 mb/sr, in good agreement with the value computed from the observed cross section for the inverse reaction. The cross section for the formation of the excited state is about half that for the ground state. The derived reduced widths (Li^7) are $\theta_n^2 = 0.05$ and $\theta_n^2 = 0.035$ for $Li^{6*}(0)$ and (2.2), respectively. The ratio is in good agreement with that calculated from shell theory in intermediate coupling with $1.4 \leqq a/K \leqq 2.1$, near the L-S limit (Re 56). See also (Si 57a). At $E_p = 18$ and 31.8 MeV, a deuteron group has also been observed leading to the 3.56-MeV state (Fr 52, Si 57a). See also (Hi 55c, Ma 57c, El 58a).

XIX. $Li^7(d, t)Li^6$ $\quad Q_m = -0.994$

At $E_d = 14.5$ MeV, the angular distributions of the tritons analyzed by pickup theory, indicate $l_n = 1$, and hence even parity, for the ground state

and the 2.18-MeV state. Peak cross sections are 32.4 and 16.0 mb/sr at $\theta_{c.m.} = 11°$ and 16° respectively (Le 55). The corresponding reduced widths are $\theta^2 = 0.11$ and 0.061 (Fr 57: compare $Li^7(p, d)Li^6$). See also (Ho 53c, Ha 56c, Br 57a, El 58a). At $E_d(max) = 13.8$ MeV, stars are observed in Li-loaded emulsions corresponding to excitation of Li^6 states at 2.2, ≈ 4.5 and 7.5 MeV with subsequent disintegrations into (α+d) (So 56). At $E_d = 17.5$ MeV, the decay of additional states at 5.2, 5.9, 6.7, 8.3, 9.5 and 10.1 MeV is also reported (So 56a). A search in the region $E_x = 4.4$ to 8.5 MeV has revealed only the 5.4-MeV level; no other level appears with $\Gamma < 80$ keV (Ha 58a).

XX. $Li^7(He^3, \alpha)Li^6$ $\quad Q_m = 13.325$

Alpha-particle groups observed at $E(He^3) = 700$ to 900 keV are listed in table 6.5. Li^6-recoils corresponding to the 3.56-MeV state are observed,

TABLE 6.5

States in Li^6 from $Li^7(He^3, \alpha)Li^6$ (Al 55a)

E_x in Li^6 (MeV)	Γ (keV)	T
0		
2.19	<100	
3.56±0.06	<100	
4.3 ±0.2		
5.35±0.07	<100	($T = 1$)
(5.6 ±0.2)	(≈2000)	($T = 0$)
6.63±0.08	<200	($T = 1$)
7.40±0.10	≈600	($T = 0$)
(8.37±0.08)	(<200)	($T = 1$)
(9.3 ±0.2)	(≈600)	

indicating that the state decays by γ-emission. The states at 2.2, 4.3 and (5.6) MeV are presumably those observed in $He^4(d, d)He^4$. The small width of the 5.35 and (8.37)-MeV states suggests that they have $T = 1$ (Al 55a).

XXI. $Be^9(\gamma, t)Li^6$ $\quad Q_m = -17.687$

See (Aj 55).

XXII. $Be^9(p, \alpha)Li^6$ $\quad Q_m = 2.125$

At $E_p = 7.2$ to 7.5 MeV ($\theta = 30°$ and 60°), alpha-particle groups are observed to the ground state and to levels at 2.188 ($\Gamma_{c.m.} = 24$ keV) and 3.560-MeV (see table 6.4). No other sharp levels with $E_x < 5$ MeV are seen with an intensity greater than 5 per cent of the intensity of the groups to the 2.18 and 3.56-MeV states (Br 57a). The 3.56-MeV state is observed to decay by γ-radiation: $E_\gamma = 3.572 \pm 0.012$ MeV. The internal pair spectrum is consistent with an M1 transition (Ma 54b). Both the γ-ray angular distribu-

tion and the $(\alpha-\gamma)$ correlation are isotropic at $E_p = 2.56$ MeV, consistent with $J = 0$ for $Li^6(3.56)$ (St 56d). Determination of the Doppler shift establishes that the lifetime is $< 3\times10^{-14}$ sec (Ro 57d), $< 3.3\times10^{-14}$ sec (Le 57e; see Wa 58c), consistent with M1 radiation but not with E2. The fact that the ground-state and 2.18-MeV state α-particles do not show resonance at $E_p = 2.56$ MeV is consistent with the assumption that the first two levels have $T = 0$: see B^{10} (Ma 54g). See also (Ra 56a).

XXIII. $B^{10}(\gamma, \alpha)Li^6$ $Q_m = -4.459$
See B^{10}.

XXIV. $B^{10}(n, dn' 2\alpha)$ $Q_m = -5.930$

At $E_n = 12.2$ to 19.5 MeV, this reaction proceeds partly through the 2.18-MeV state of Li^6 (Fr 56a).

Be^6

(Not illustrated)

MASS OF Be^6

From the Q-value of the $Li^6(p, n)Be^6$ reaction (Bo 57i), and using the Wapstra masses (Wa 55c) for Li^6, H^1 and n, the mass excess $(M-A)$ of Be^6 is 20.3 ± 0.2 MeV (see also Aj 55).

I. (a) $He^3(He^3, 2p)He^4$ $Q_m = 12.858$ $E_b = 10.4$
(b) $He^3(He^3, p)Li^5$ $Q_m = 11.062$

The total cross section shows a monotonic increase for $E(He^3) = 100$ to 800 keV. At $E(He^3) = 200$ keV, it is at least 2.5 μb. Below $E(He^3) = 350$ keV, the cross section fits the simple Gamow exponential form. At higher energies, partial waves of $l \geqq 2$ appear to be required (Go 54c). See also (Al 53a).

II. (a) $He^3(\alpha, n)Be^6$ $Q_m = -9.2$
(b) $He^4(He^3, n)Be^6$ $Q_m = -9.2$
Not observed.

III. $Li^6(p, n)Be^6$ $Q_m = -5.2$

At $E_p = 9$ MeV, a neutron group is observed with $Q = -5.2\pm0.2$ MeV; the reported ground-state width is < 300 keV (Bo 57i).

IV. $Li^6(He^3, t)Be^6$ $Q_m = -4.5$
Not observed.

He^7

(Not illustrated)

Not observed: see (Aj 55).

Li^7

(Fig. 5, p. 29) †

THEORY

See (Ab 56), (Au 55), (Da 55), (Fe 56), (Fr 57), (Ku 56), (La 55a), (Me 56), (Ma 57e), (So 57), (Fe 57c), (Le 57f), (Ma 57j), (Sk 58), (Ha 58d).

I. $H^3(\alpha, \gamma)Li^7$ $Q_m = 2.465$

For $E_\alpha = 0.5$ to 1.9 MeV, capture radiation is observed to Li^{7*}(g.s.) and (0.48), with intensity ratio 5 : 2. The smooth rise of the cross section suggests a direct capture process. The angular distribution is not isotropic, indicating

TABLE 7.1

Energy levels of Li^7

E_x in Li^7 (MeV)	J^π	τ_m or Γ (sec) (keV)	Decay	Reactions
0	$\frac{3}{2}^-$		Stable	I, III, IV, IX, X, XVII XIX, XX, XXI, XXII, XXIII, XXIV, XXV, XXVI, XXVII, XXVIII, XXX, XXXI
0.4780 ±0.003	$\frac{1}{2}^-$	$\tau_m = (0.9 \pm 0.1) \times 10^{-13}$	γ	I, III, IV, IX, X, XVI, XVII, XIX, XXIII, XXIV, XXV, XXVIII, XXX, XXXI
4.630 ±0.01	$(\leq\frac{7}{2}^-)$	93 ± 8	t, α	IX, XVIII, XIX, XXIII, XXX, XXXI
6.54 ±0.02	$(\frac{1}{2}^+, \frac{3}{2}^+)$	broad	t, α	(V), IX, XVIII, XIX
7.47 ±0.01	$\frac{5}{2}^-$	141 ±20	n, α, t	V, VI, IX, XVIII, XIX, XXX
(9.6)			γ, n, t, α	XII, XV, XVIII, XIX
(10.8)			γ, n, t, α	XII, XV
12.4			γ, n	XII
14.0			γ, n	XII
16.2			γ, t, α	XV
17.5			γ, n	XII, XIX
(21.5)			γ, t, α	XV, XIX
(23.5)			γ, t, α	XV

$l > 0$ (Ri 58b); see also (Li 58a). In the range $E_\alpha = 0.48$ to 1.13 MeV, the cross section increases from 0.6 to 1.2 μb (Ho 59).

II. $He^4(t, t)He^4$ $E_b = 2.465$

Differential cross sections have been measured for $E_t = 1.2$ to 2.2 MeV (He 56). At $E_t = 1.677$ MeV, $\theta = 30°$, $d\sigma/d\Omega$ (lab) = 875 mb/sr (Al 58b).

III. $He^4(\alpha, p)Li^7$ $Q_m = -17.347$

At $E_\alpha = 38.5$ MeV, two groups of protons are observed, corresponding to the ground and 0.48-MeV states of Li^7. Absolute c.m. differential cross

† For level scheme of Be^7, see fig. 6, p. 37.

sections are given as $(1.53\pm0.09)+(1.93\pm0.15)\cos^2\theta$ and $(1.32\pm0.07)+(0.66\pm0.23)\cos^2\theta$ mb/sr for the ground state and excited state groups

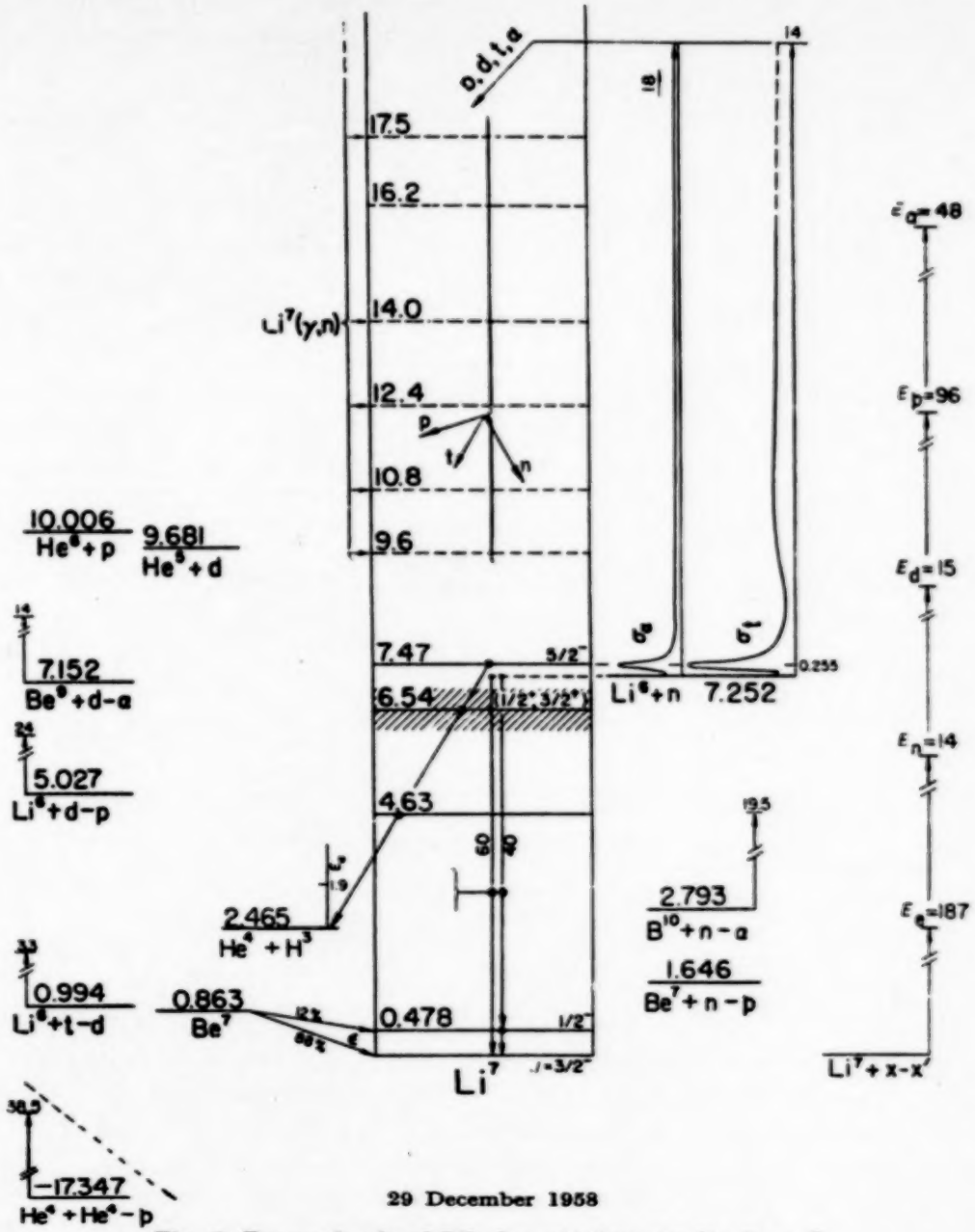

29 December 1958

Fig. 5. Energy levels of Li^7: for notation, see fig. 1, p. 7.

respectively. The cross sections are in fair agreement with those calculated from $Li^7(p,\alpha)He^4$ by the principle of detailed balancing. The partial inelastic cross sections are estimated to be 11 ± 1 mb for s-waves, 33 ± 3 mb for d-waves (Bu 58).

IV. $Li^6(n, \gamma)Li^7$ $Q_m = 7.252$

Two γ-rays with $E_\gamma = 7.26 \pm 0.03$ and 6.78 ± 0.05 MeV, and relative intensities 10 and 7.5 ± 2.0, corresponding to transitions to the first two states of Li^7 are observed. The total radiative capture cross section is 28 ± 8 mb (Ba 57m).

V. $Li^6(n, n)Li^6$ $E_b = 7.252$

The total cross section has been measured from $E_n = 4$ eV to 10 MeV (Hu 55c, Hu 57, Hu 58, Go 56m, Jo 54f, Ka 57b, Ne 54c), from $E_n = 7$ to 14 MeV by (Br 58h) and at 14 MeV by (Co 52 h, Ka 57b). A pronounced resonance occurs at $E_n = 255$ keV (see table 7.2) with a peak cross section of

TABLE 7.2

Resonance parameters for 7.2—7.5 MeV level in Li^7—Be^7

	$Li^6(n, n)Li^6$, $Li^6(n, \alpha)He^3$				$Li^6(p, \alpha)H^3$	
	(Ba 51e)	(Jo 54f)	(Wi 56a)	(Ma 56l)	(Ba 51e)	(Ma 56l)
E_r(keV, lab) [d]	250	255	255		1820	1850
Γ (keV, lab)	100	100	100		500	
E_λ(keV above gnd)	7540	7700	6640 [b]	7680	7310	7800
$\Gamma_{n,p}(E_r)$(keV, c.m.)	50	114	82	114	400	670
radius (n, p) in 10^{-13} cm	4.0	2.54	3.94	4.08	4.0	4.08
$\gamma^2_{n,p}(10^{-13}$ MeV-cm)	2.4	11.8	3.5 [b]	4.6	2.6	4.2
$\theta^2_{n,p}$	[0.13]	0.42	0.19 [b]	0.26	[0.14]	0.24
$\Gamma_\alpha(E_r)$(keV, c.m.)	36	60	43	64	30	50
radius (α) in 10^{-13} cm		3.5		4.39		4.39
$\gamma_\alpha{}^2(10^{-13}$ MeV-cm)		0.4 [a]	0.12 [b]	0.14		0.79
$\theta_\alpha{}^2$		[0.04]	0.014 [b]	0.017 [c]		0.095 [c]

[a] $\gamma_n{}^2/\gamma_\alpha{}^2 = 30$; see (Ma 56l, footnote p. 1406).

[b] With same convention as other references, $E_\lambda = 7580$ (H. B. Willard, private communication).

[c] Corrected value: see (Ma 57e).

[d] $E_r = 265$ keV, $\sigma = 9.5 \pm 0.2$ b (Go 56m); see also (Ba 59, Hu 58).

10.3 b (Jo 54f). Angular distributions for $E_n = 0.2$ to 0.4 MeV have been studied by (Wi 56a): all observations are consistent with p-wave formation of a $J = \frac{5}{2}^-$ level, $Li^{7*}(7.47)$. The s-wave potential scattering has a statistical channel spin mixture with negative phase shift (Wi 56a). Resonance parameters are compared with those of the mirror level (Be^{7*}) in table 7.2. The 7.47-MeV level has been assumed to be the upper member of the $^2F_{\frac{7}{2},\frac{5}{2}}$ doublet of which $Li^{7*}(4.6)$ is the lower. It is pointed out by (Me 56, Ma 57e and So 57) that it may in fact be a component of the ^4P multiplet and that the $F_{\frac{5}{2}}$ is to be found at a lower energy. This assumption would explain the large values of $\theta_p{}^2$ and $\theta_n{}^2$ and would make the large difference of $\theta_\alpha{}^2$ for the mirror levels less disturbing (Ma 57e). See also (La 54a, Da 56a, Ha 58d: theo.).

No other clearly defined resonance is observed, although the cross section exhibits a broad maximum near $E_n = 5$ MeV (Jo 54f, Hu 57, Hu 58).

The large coherent thermal scattering length suggests the existence of at least one bound s-level (La 54a).

VI. $Li^6(n, \alpha)H^3$ $Q_m = 4.787$ $E_b = 7.252$

The isotopic thermal capture cross section is 945 b (Hu 58); up to $E_n \approx 70$ eV, the cross section varies as $1/v$. Cross sections and angular distributions are summarized in (Hu 55c, Hu 56, Hu 57, Hu 58, Ho 58c). A strong resonance is observed at $E_n = 0.25$ MeV with a peak cross section of 2.9 b, attributed to p-wave formation of a $J = \frac{5}{2}^-$ level (see $Li^6(n, n)Li^6$ and table 7.2). In the range $E_n = 9$ to 90 keV the cross section is higher than the $1/v$ law would indicate (Go 56n, Ba 59). Above the resonance, the cross section appears to exhibit a broad hump, $\sigma \approx 250$ mb, at $E_n = 1.5$ to 2 MeV, and then decreases smoothly to 26 mb at 14 MeV. The decrease at 2 MeV is attributed to competing reactions (Ri 56b, Mu 58; see, however, Ho 58c). (Ke 58a) find an almost linear decrease from 34.3 mb at $E_n = 12.5$ MeV to 17.5 mb at $E_n = 18.3$ MeV. For $E_n \gtrsim 2$ MeV the reaction appears to proceed by a pickup process. See Li^6: $Li^6(n, t)He^4$. See also (Da 56a, Pe 55, Be 57e, El 57c, Ko 57a) and (Ba 59).

VII. $Li^6(n, p)He^6$ $Q_m = -2.753$ $E_b = 7.252$

The cross section at $E_n = 14$ MeV is 6.7 mb (Ba 53, Fr 54b).

VIII. $Li^6(n, d)He^5$ $Q_m = -2.429$ $E_b = 7.252$

The total cross section is about 200 mb at $E_n = 5.5$, 6.5 and 14 MeV (Ri 56b). For the He^5 ground-state peak, $\sigma = 89$ mb for the continuum, $\sigma = 77$ mb at $E_n = 14$ MeV (Fr 54b). The reaction appears to proceed by pickup: see Li^6: $Li^6(n, d)He^5$.

IX. $Li^6(d, p)Li^7$ $Q_m = 5.027$

The weighted mean value of the excitation energy of the first excited state is 477 ± 2 keV (see Aj 55). Levels are also observed at $E_x = 4.630$ MeV, $\Gamma = 93 \pm 8$ keV (Br 57j), 4.61 ± 0.02 MeV (Ge 52), 4.46 ± 0.02 MeV (Kh 55a) and $E_x = 6.54 \pm 0.02$ MeV (Kh 55, Kh 55a), 6.56 MeV (Le 55; see, however, Ha 58e) and $E_x = 7.457$ MeV, $\Gamma = 91 \pm 8$ keV (Br 57j). A search for a level at 5.5 MeV was unsuccessful at $\theta = 30°$, 70° and 90°, $E_d = 7.0$ and 7.5 MeV (Br 57j). Angular distributions of the protons to the ground state and the 0.48-MeV level, at $E_d = 8$ MeV (Ho 53c) and $E_d = 14.5$ MeV (Le 55), analyzed by stripping theory, show odd parity, $J \leqq \frac{5}{2}$ for both states: see also (Ni 54). The ratio of reduced widths $\theta^2(\text{g.s.})/\theta^2(0.48) = 0.69$ and 0.66 from these two experiments (Re 56); $\theta^2(\text{g.s.}) \approx 0.060$ (Fr 57). The angular correlation between the protons and the 0.48-MeV γ-rays is isotropic

(see Aj 55) indicating $J = \frac{1}{2}$ for Li^{7*}. The mean life of this state as determined in the present reaction and in Be^9(d, α)Li^7 is $(7.7 \pm 0.8) \times 10^{-14}$ sec (Bu 56b). At $E_d = 15$ MeV, the angular distribution of the protons to the 4.6-MeV state has been measured for $\theta = 30°$ to 100° and can be reasonably accounted for by stripping theory with $l_n = 2$, $J \leqq \frac{7}{2}^-$ (Ha 56c); on the other hand, (Ha 58e) report the distribution nearly isotropic at $E_d = 15$ MeV. At $E_d = 24$ MeV the distribution is in poor agreement with stripping theory (Co 57g). For the 7.5-MeV level, the proton distribution at $E_d = 15$ MeV indicates $l_n = 1$ and a reduced width equal to that of the ground state (Ha 58e). A search for 4.1 MeV γ-rays from a possible (4.6 → 0.48) transition was unsuccessful: at $E_d = 1.8$ MeV, $I_{4.1} < 0.1$ ($I_{0.48}$) (Wi 57). See also Be^8, (Au 55, La 55a, Fr 57, theo.) and (Aj 52c).

X. Li^6(t, d)Li^7 $\quad Q_m = 0.994$

$Q_0 = 0.986 \pm 0.007$ (Al 54e)

At $E_t = 240$ keV, the reaction has been observed to the ground state and to the 0.48-MeV level (Al 54e). See also (Cu 55b).

XI. Li^6(α, He^3)Li^7 $\quad Q_m = -13.325$

Not reported.

XII. Li^7(γ, n)Li^6 $\quad Q_m = -7.252$

The total cross section for neutron production (including the γ, np and γ, 2n processes) has a broad maximum ($\sigma = 2.3$ mb) at $E_\gamma = 16.8$ MeV, $\Gamma = 9.3$ MeV (Ry 58: natural Li). For the (γ, n) process alone, the peak cross section is estimated as ≈ 2.7 mb at $E_\gamma \approx 14$ MeV (Go 54b). Discontinuities reported in the integral yield curve are listed in table 7.3.

TABLE 7.3

Levels of Li^7(in MeV) from Li^7(γ, t)He^4 and Li^7(γ, n)Li^6

γ, t				γ, n
Ti 53b	St 53a	St 54h	Mi 55b	Go 54f
		4.7		
	5.25	5.5		
		6.8		
	7.25		7.6	
			8.6	
9.3	(9.25)		9.6	9.6[a]
			11.7	10.8
				12.4
			(13.5)	14.0
(16.7)			16.2	
				17.5
(21.5)				
(23.5)				

[a] 9.66 ± 0.04 MeV (Ry 58).

Integrated cross sections are tabulated by (Go 54f). See also (Mo 53c, He 55c, Ti 58, Be 58c) and (Pe 53c, Ba 57; theo.). (It is to be noted that the total cross section in $Li^6(n, n)Li^6$ exhibits no evidence of sharp structure in the region $E_x = 9$ to 12 MeV: see (Jo 54f, Hu 57, Hu 58).)

XIII. $Li^7(\gamma, p)He^6$ $Q_m = -10.005$

According to (Ti 53b) and (Ti 54a), the cross section in the range $E_\gamma = 12$ to 20 MeV exhibits a single broad maximum at ≈ 15.6 MeV with a width of ≈ 4 MeV. At $E_\gamma = 14.8$ MeV the cross section is 2.2 ± 0.25 mb; according to (Ha 55a), the integrated cross section is 11 MeV-mb. There appears to be some disagreement on the shape of this excitation function. It is suggested that a γ-emitting state of He^6 at ≈ 1.6 MeV could account for the discrepancy between the Canberra and Saskatoon results (Ti 55a, Ti 54a). Some evidence for fine structure is reported by (Ha 55a). See also (Tu 53, Tu 54, Ru 54a, St 58a, Ti 58, Sm 58a, Wh 58).

XIV. $Li^7(\gamma, d)He^5$ $Q_m = -9.681$

See (Ba 58f, Wh 58, Ti 58, Pa 58).

XV. $Li^7(\gamma, t)He^4$ $Q_m = -2.465$

Reported peaks in the excitation function are listed in table 7.3. Observations are made in nuclear emulsions, mainly under continuous-spectrum irradiation. It is pointed out by (Pe 53c) that $T = \frac{3}{2}$ levels of Li^7 will not be observed in the present reaction in the region 0 to 15 MeV above threshold: compare $Li^7(\gamma, n)Li^6$. See also (Ti 55a, Ti 58, Tu 53, Tu 54, Er 54, Na 52b, Ti 53) and (Cz 55, Cz 56b, theo.).

XVI. $Li^7(\gamma, \gamma')Li^{7*}$

Measurement of resonance scattering and absorption in Li yield $\tau(\text{mean}) = (1.1 \pm 0.3) \times 10^{-13}$ sec (Be 58), $(1.15 \pm 0.14) \times 10^{-13}$ sec (Sw 58, Sw 59) for the 0.48-MeV state.

XVII. $Li^7(e, e)Li^7$

Elastic and inelastic (0.47-MeV state) scattering have been studied at $E_e = 187$ MeV by (St 55e). Elastic scattering results indicate an r.m.s. radius of about 2.1×10^{-13} cm (Ho 57g: see also Ho 56e, Me 57c).

XVIII. $Li^7(n, n')Li^{7*} \rightarrow H^3 + He^4$ $Q_m = -2.465$

At $E_n = 14$ MeV, there is evidence for Li^7 states at 4.6 ± 0.25, $\approx 6.5 \pm 0.25$, 7.5 ± 0.25 and 9.25 (?) MeV (Al 54b: Li-loaded photoplates). See also (Fr 54b).

XIX. $Li^7(p, p')Li^{7*}$

Elastic scattering at $E_p > 10$ MeV is characterized by direct interaction processes: see (Ki 56, Hi 57a). Inelastic proton groups corresponding to the

states at 0.48, 4.63, 6.54 and 7.46 MeV have been observed at bombarding energies up to 18.3 MeV: see (Aj 52c). A careful check on the isotropy of the 477-keV radiation from the $J = \frac{1}{2}^-$ level yields $W(\theta) = 1+\alpha \cos\theta$, with $\alpha = (2.9\pm6.2)\times10^{-4}$; the result implies an upper limit for the intensity of a parity non-conserving part of the wave function $F^2 < 1\times10^{-4}$ (Wi 58d).

At $E_p = 12$ MeV, the angular distribution of the protons leaving Li^7 in the 4.63-MeV state can be accounted for by a mixture of direct interaction with $l = 0$, and compound nucleus formation, indicating $J = \frac{1}{2}^-, \frac{3}{2}^-$, or $\frac{5}{2}^-$. It is also possible to fit the data under the assumption of compound nucleus formation with s, p, and d-waves, permitting $J = \frac{7}{2}^-$ (Co 57). Angular distributions at $E_p = 17.5$ MeV are reported by (Ma 57c). The relative intensities observed in this work for protons leading to the 4.6, 6.6, and 7.5-MeV states are consistent with assignments $^{22}F_{\frac{7}{2}}$, $^{22}F_{\frac{5}{2}}$, $^{24}P_{\frac{3}{2}}$; it is presumed that the 6.6-MeV state in question here is not the broad even-parity state at 6.54 MeV (Le 57f). At 31.8 MeV, angular distributions of protons leading to the 4.6-MeV and 6.6-MeV levels fit the direct interaction theory with $l = 1$ ($J = \frac{1}{2}^+, \frac{3}{2}^+, \frac{5}{2}^+, \frac{7}{2}^+$). A weak group to a 9.6-MeV level is also reported (Si 57a). Levels at 18 ± 1.4 (?) and 22 ± 1.4 (?) MeV are observed with 96-MeV protons (St 56c). See also (Ch 58, Ty 58, Ty 57c, Ty 58b, Ma 58h).

XX. $Li^7(p, d)Li^6$ $\quad Q_m = -5.026$

The ground-state reduced width $\theta_n^2 = 0.05$ and 0.035 for Li^{6*} (g.s.) and (2.2), respectively: see Li^6.

XXI. $Li^7(d, t)Li^6$ $\quad Q_m = -0.994$

$\theta_n^2 = 0.11$ and 0.061 for Li^{6*}(g.s.) and (2.2), respectively: see Li^6.

XXII. $Li^7(d, He^3)He^6$ $\quad Q_m = -4.512$

$\theta_p^2 = 0.055$ and 0.017 for He^{6*}(g.s.) and (1.7), respectively: see He^6.

XXIII. $Li^7(d, d')Li^{7*}$

Inelastic deuteron groups have been observed to the states at 0.48 and 4.6 MeV: see (Aj 52c) and (Kh 55, Kh 55a). (Le 55) report $Q = -4.62\pm0.04$, $\Gamma = 0.3\pm0.1$ MeV, for the latter state; $\theta_\alpha^2 = 0.5\pm0.2$ (Ma 57e). At $E_d = 14.4$ MeV, the angular distribution of the deuterons corresponding to the 0.48-MeV state is moderately well accounted for by the theory of (Hu 52l), with $l = 2$ (Le 55). Some discrepancies appear to exist between reported angular distributions of deuterons corresponding to the 4.6-MeV level at $E_d = 14$ to 15 MeV: compare (Le 55), (Ha 56c). See also (So 56), (So 56a).

XXIV. $Li^7(\alpha, \alpha')Li^{7*}$

Li^7 states at 0.48 and 4.6 MeV have been observed at various energies up to 48 MeV: see (Aj 55). At $E_\alpha = 31.8$ and 48 MeV, the angular distribution

of the α-particles to the 4.6-MeV state exhibits a prominent peak in the forward direction, suggesting a direct interaction process (Si 57a, Co 56h). (Zh 54) finds $E_\gamma = 478 \pm 2$ keV and a lifetime for the first excited state $< 1.3 \times 10^{-13}$ sec (see also Li^6(d, p)Li^7 and Be^9(d, α)Li^7). At $E_\alpha = 1.9$ MeV, the angular distribution of the 0.48-MeV radiation is isotropic within 10 per cent (Li 54). See also (Br 55), (Ne 57b).

XXV. $Be^7(\varepsilon)Li^7$ † $Q_m = 0.863$

The decay proceeds to the ground and 0.48-MeV states. The fraction to the excited state is 0.115 ± 0.01 (see Aj 55). The γ-ray energy is 477.8 ± 0.3 keV (weighted mean of values quoted in Aj 55, including the value 477.3 ± 0.4 reported by (Du 57b)). The weighted mean value of the half-life is 53.37 ± 0.11 days (Se 49, Kr 53c, Bo 56i, Wr 57), log $ft = 3.25$ for the ground state transition and 3.44 for the excited state. Both transitions are super-allowed (Ma 54h, Ch 56). A measurement of the internal conversion coefficient for the 0.48-MeV γ-radiation indicates that the radiation is 55 % to 100 % M1 (Le 58). See also (La 55a; theo.).

XXVI. Be^7(n, p)Li^7 $Q_m = 1.646$
See Be^8.

XXVII. (a) Be^9(γ, d)Li^7 $Q_m = -16.693$
(b) Be^9(γ, np)Li^7 $Q_m = -18.919$
See (Aj 55) and Be^9.

XXVIII. Be^9(n, t)Li^7 $Q_m = -10.435$
See (Va 57a, Sc 57c) and Be^{10}.

XXIX. Be^9(p, He^3)Li^7 $Q_m = -11.200$
Not observed.

XXX. Be^9(d, α)Li^7 $Q_m = 7.152$

A number of α-groups have been observed with deuteron energies of up to 14 MeV. These correspond to levels at 480 ± 2 keV (Bu 48c, Co 53), 4.62 ± 0.02 MeV (Ge 53; see also As 52, Go 51a, Ju 56e), and 7.5 ± 0.17 (?) MeV (Go 51a). There is no evidence in this reaction of a state at 5.5 MeV suggested in Li^7(γ, t)He^4 (see Aj 55): at $E_d = 0.5$ and 0.7 MeV ($\theta = 70°$), the intensity of a group leading to such a state is less than 5 per cent of the intensity of the ground-state alpha group (Ge 56e; see also Cu 55, Ju 56e). Observation of the continuous distribution of alpha-particles and tritons indicates production and breakup of Li^7 levels at 4.6 and 6.6 MeV (Cu 55, Ju 56e).

The (α, γ) angular correlation has been observed for $E_d = 0.40$ and 0.84 MeV (Ue 53, Co 54e). There is no significant departure from isotropy, in agreement with $J = \frac{1}{2}$ for the 0.48-MeV level. The mean life of this state is $(7.7 \pm 0.8) \times 10^{-14}$ sec (Bu 56b; Doppler shift; mean of observations in this

† The symbol (ε) denotes orbital electron capture.

reaction and in $Li^6(d, p)Li^7$); compare $Li^7(\gamma, \gamma)Li^7$. This value is considerably shorter than that given by a shell-model calculation (La 55a). See also Be^7: $B^{10}(p, \alpha)Be^7$.

See also (Tu 56), (Gr 56b) and B^{11}.

XXXI. $B^{10}(n, \alpha)Li^7$ $Q_m = 2.793$

With thermal neutrons, two groups of α-particles are observed, corresponding to Li^{7*} (0 and 0.48); the fraction of transitions leading to the ground state is about 6 per cent; see (Aj 52c, De 54, Bu 58a, and B^{11}). The γ-ray energy is 478.5 ± 1.5 keV (El 48), 478 ± 4 keV (Da 56d); the mean life is $(7.5 \pm 2.5) \times 10^{-14}$ sec (El 49). The $(\alpha—\gamma)$ correlation is isotropic (Ro 50: pile neutrons). See also (Ja 55e).

For neutrons in the range $E_n = 5.6$ to 19.5 MeV, the reaction appears to proceed mainly through the 4.6-MeV level or through direct 3-body disintegration (Fr 56a). See also (Aj 55).

XXXII. $B^{11}(\gamma, \alpha)Li^7$ $Q_m = -8.670$

Not reported.

Be^7

(Fig. 6, p. 37) †

THEORY

See (Fr 57, Ma 57e, Sk 58).

I. $Be^7(\varepsilon)Li^7$ $Q_m = 0.863$

The decay is complex; see Li^7.

II. $He^4(He^3, \gamma)Be^7$ $Q_m = 1.584$

TABLE 7.4

Energy levels of Be^7

E_x in Be^7 (MeV)	J^π	τ or Γ (keV)	Decay	Reactions
0	$\leq \frac{3}{2}^-$	$\tau_{\frac{1}{2}} = 53.37 \pm 0.11$d	ε	I, V, IX, XIII, XVI, XVIII
0.431 ± 0.002	$\frac{1}{2}^-$	$\tau_m = (2.7 \pm 1.0) \times 10^{-13}$ sec	γ	V, IX, XIII, XVIII
4.53 ± 0.02	$\frac{7}{2}^-$	102	He^3, α	III, XIII, XVIII
6.35 ± 0.1	$(\frac{5}{2}^+)$	≈ 1000	p, He^3, $\alpha(\gamma)$	V, VII, IX, XVIII
7.18 ± 0.06	$(\frac{5}{2}^-)$	575	p, He^3, α	VII, IX, XIII, XVIII
(14.6 ± 0.3)				XVIII

In the range $E(He^3) = 0.48$ to 1.32 MeV, the capture cross section increases from 0.04 to 1.2 μb. At $E(He^3) = 1.32$ MeV, about 50 per cent of the transitions involve the 0.43-MeV state (Ho 59). See also (Ba 58h,

† For level scheme of Li^7, see fig. 5, p. 29.

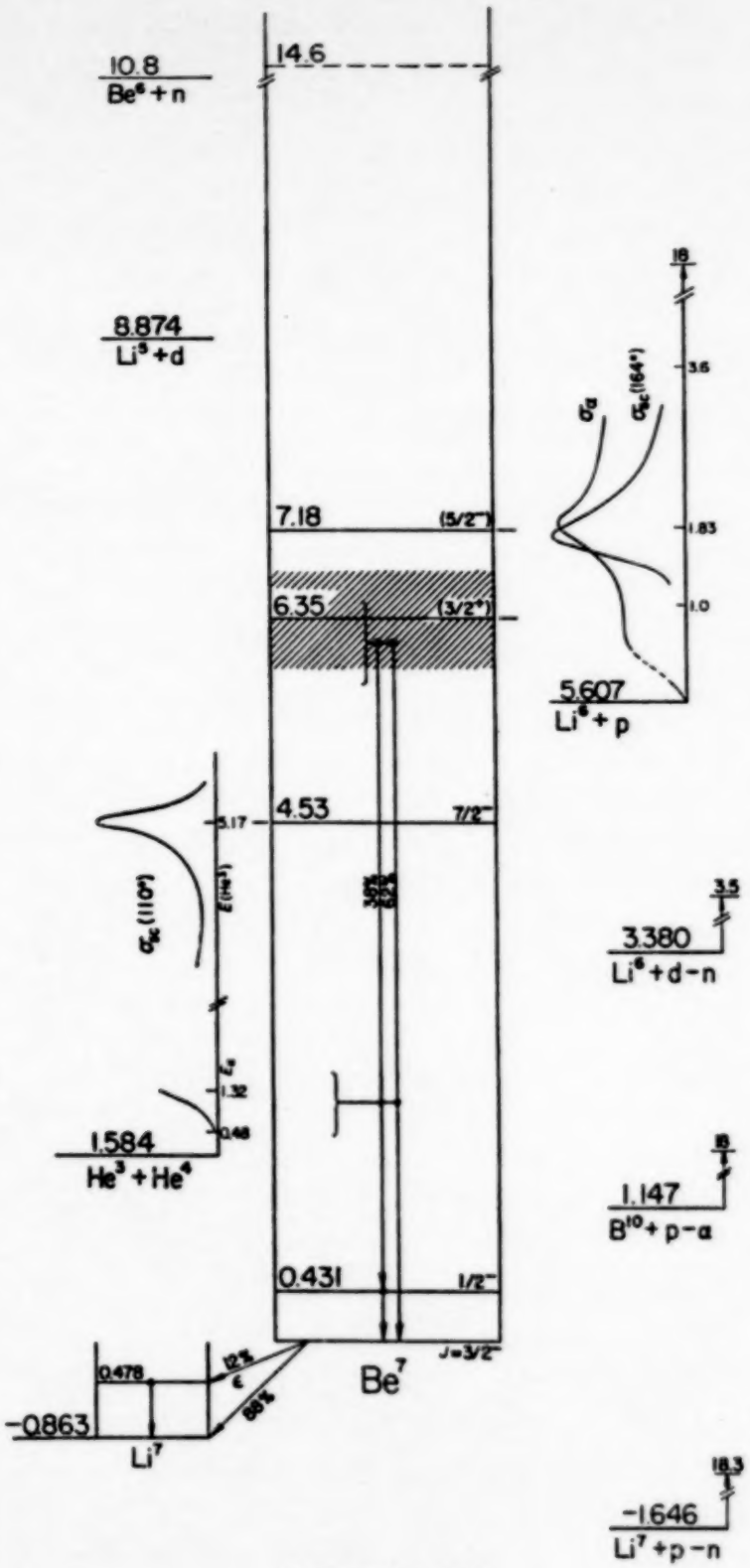

2 December 1958

Fig. 6. Energy levels of Be^7: for notation, see fig. 1, p. 7.

He 58a). The significance of this reaction for energy generation in stars is discussed by (Fo 58a, Ca 58b).

III. $He^4(He^3, He^3)He^4$ $E_b = 1.584$

Elastic scattering studies for $E(He^3) = 3$ to 5.5 MeV ($\theta = 54°$ to 126°) indicate a prominent resonance at $E(He^3) = 5.17$ MeV, $\Gamma = 0.180$ MeV ($Be^{7*} = 4.53$ MeV, $\Gamma_{c.m.} = 0.102$ MeV). Phase-shift analysis indicates that the state is $F_{\frac{7}{2}}$, with $\gamma_\alpha^2 = 3.0\times10^{-13}$ MeV-cm, $\theta_\alpha^2 = 0.36$, $R = 4.4\times10^{-13}$ cm. The behaviour of the p-wave phase shifts suggests that the ground state, and possibly $Li^{7*}(0.48)$, have widths which approach $\theta_\alpha^2 = 1$. The s-wave phase shift is consistent with hard-sphere scattering, with $R = 2.8\times10^{-13}$ cm (Mi 58b). See also (Ch 58d).

IV. $He^4(\alpha, n)Be^7$ $Q_m = -18.993$

A search for this reaction at $E_\alpha = 39$ MeV, 0.5 MeV (c.m.) above threshold, led to a negative result; the cross section is < 0.7 mb. This result is consistent with the assumption that Be^7 has negative parity (Wa 52c).

V. $Li^6(p, \gamma)Be^7$ $Q_m = 5.607$

$Q_0 = 5.66\pm0.05$ (Wa 56a).

Gamma transitions to the ground state and to the 0.43-MeV state are observed. The yield shows no evidence of resonance for $E_p = 0.4$ to 1.0 MeV, and the branching ratio remains approximately constant at 62 ± 5 per cent, (65 per cent: Ba 55d) to the ground state, 38 per cent to the 0.43-MeV state, (< 4 per cent to the 4.6-MeV state: Ba 55d). The 90°-differential cross section at 750 keV is 0.02 μb/sr (Wa 56a). (Ba 55d) estimate 0.2 μb/sr from observation of (430 ± 20)-keV radiation. (Because of the extremely low cross section of the present reaction, small amounts of contaminants may have a strong influence; in particular, earlier reports of a resonance at $E_p \approx 1.6$–1.8 MeV may be due to $B^{10}(p, \alpha)Be^7$: see (Wa 56a).)

The angular distribution of both γ-rays (to the ground state and the 0.43-MeV level) is the same at $E_p = 750$ keV, $W(\theta) = 1+(1.05\pm0.15)\cos^2\theta$. Neither s- or d-wave capture yields such a distribution, and p-wave, $J = \frac{3}{2}^-$, is indicated; a direct non-resonant capture process seems also possible (Wa 56a).

VI. $Li^6(p, n)Be^6$ $Q_m = -5.2$ $E_b = 5.607$

At $E_p = 9$ MeV, the cross section for production of ground state neutrons is $d\sigma/d\Omega = 0.19+0.23\cos\theta+0.70\cos^2\theta$ mb/sr; $\sigma = 5\pm1$ mb (Bo 57i).

VII. (a) $Li^6(p, \alpha)He^3$ $Q_m = 4.022$ $E_b = 5.607$

(b) $Li^6(p, p)Li^6$

The excitation function follows the Gamow function from $E_p = 19$ to 250 keV (Sa 53b, Ja 57). The total cross section exhibits two resonances, one at ≈ 1 MeV (broad) and one at 1.83 MeV (Ba 51e, Ma 56l). (There is some

discrepancy in the reported absolute cross sections.) In the range $E_p = 1.3$ to 3.1 MeV, the elastically scattered protons, $\theta = 164°$, exhibit a single maximum at $E_p = 1.75$ MeV, with $\Gamma = 0.5$ MeV (Ba 51e): see table 7.2. Preliminary results of a study at $\theta = 156°$ for $E_p = 0.45$ to 1.8 MeV clearly show the 1.75-MeV anomaly, but no marked effect near 1 MeV (Mc 58e). Analysis of α-particle angular distributions in the range $0.6 \leqq E_p \leqq 2.5$ MeV is consistent with $J = \frac{3}{2}^+, \frac{5}{2}^-$ for the two states at 6.35 and 7.18 MeV. A large, non-resonant background may indicate other states or some direct interaction (Ma 56l): see also $Li^6(p, \gamma)Be^7$. At $E_p = 15$ and 18 MeV, the angular distributions of He^3-particles are sharply peaked forward (Li 56b: see Li^8). See also (Sa 55i; theo.).

VIII. $Li^6(p, d)Li^5$ $Q_m = -3.269$
See Li^5.

IX. (a) $Li^6(d, n)Be^7$ $Q_m = 3.380$
(b) $Li^6(d, n)He^3+He^4$ $Q_m = 1.796$

Two neutron groups are reported, corresponding to the ground- and 0.43-MeV states. The γ-ray energy is given as 428.9 ± 2 keV (corrected for Doppler shift): the Li^{7*}—Be^{7*} difference is 48.5 ± 1.0 keV (Th 52). At $E_d = 3.5$ MeV, the angular distributions of the neutron groups, analyzed by stripping theory indicate $l_p = 1$, $J \leqq \frac{5}{2}^-$ for both states. Reaction (b) is also observed (Aj 52). Pronounced stripping patterns for neutrons leading to the 0.43-MeV state, observed at $E_d = 0.6$ to 1.5 MeV, also indicate $l_p = 1$. Neutron-gamma correlations, with the neutron counter at a fixed angle, are isotropic; taken together with the stripping results, this observation indicates $J = \frac{1}{2}^-$ for the excited state (Ne 56b, Ne 58a, Sa 58); see also (Th 51f, Th 53). A search for neutron groups leading to levels of Be^7 in the range 0.3 to 2.0 MeV revealed no others with intensities > 10 per cent of the main group (Ne 56b).

Broad maxima observed in the ratio of low energy to high-energy neutrons at $E_d = 4.2$ and 5.1 MeV are attributed to Be^7 states at 6.5 MeV ($\Gamma = 1.2$ MeV, c.m.) and 7.2 MeV ($\Gamma = 0.5$ MeV, c.m.). The 4.6-MeV state produces no such effect, presumably because of the high angular momentum of the neutrons (Sl 57): see $He^4(He^3, He^3)He^4$. At $E_d = 1.8$ MeV, a search for 4.2-MeV γ-rays (from the $4.58 \rightarrow 0.43$ transition) was unsuccessful: I(4.2-MeV γ) $< 0.1\ I$(0.4-MeV γ) (Wi 57). See also (Ca 55d).

X. $Li^6(He^3, d)Be^7$ $Q_m = 0.113$
Not observed.

XI. $Li^6(\alpha, t)Be^7$ $Q_m = -14.206$
Not observed.

XII. $Li^6(Li^6, n\alpha)Be^7$ $Q_m = 1.909$
See (No 57a).

XIII. $Li^7(p, n)Be^7$ $Q_m = -1.646$

A weighted mean of measurements of the ground state threshold gives 1.8811 ± 0.0005 MeV (Jo 54d). Using a two-meter absolute electrostatic analyzer, (Bo 58e) obtain E(thresh.) $= 1.8812 \pm 0.0009$ keV.

The weighted mean value of five independent observations for the energy of the excited state is 431 ± 5 keV; see table II (7) in (Aj 52c). A neutron threshold determination gives 434 ± 4 keV (Ma 55k). At $E_p = 9$ MeV, neutrons corresponding to $Be^{7*}(4.6)$ are reported by (Bo 57i). At $E_p = 18.3$ MeV, Be^7 levels are observed at 4.6 ± 0.2 and 7.1 ± 0.2 MeV (Th 52d).

XIV. $Li^7(He^3, t)Be^7$ $Q_m = -0.881$

Not observed.

XV. $Be^9(\gamma, 2n)Be^7$ $Q_m = -20.565$

See Be^9.

XVI. $Be^9(p, t)Be^7$ $Q_m = -12.081$

See (Co 54b) and (Be 56a).

XVII. $Be^9(d, tn)Be^7$ $Q_m = -14.307$

See (He 55e) and B^{11}.

XVIII. $B^{10}(p, \alpha)Be^7$ $Q_m = 1.147$

The weighted mean of five determinations of the energy of the first excited state gives 430.3 ± 2 keV: see table III (7) in (Aj 52c), and (Cr 52c); $E_\gamma = 432 \pm 3$ keV (Da 54). The mean life-time of this state is $(2.7 \pm 1.0) \times 10^{-13}$ sec (Bu 56b; Doppler shift). This value agrees with a shell model calculation by (La 55a).

At $E_p = 18$ MeV, α-groups are reported corresponding to $Be^{7*} = 0$, 0.49 ± 0.10, 4.72 ± 0.08, 6.27 ± 0.10, 7.21 ± 0.10 and 14.6 ± 0.3 MeV. The last group is ten times as intense as any of the others. It is not completely excluded that it may be due to $B^{10}(p, He^3)Be^8$ (Re 55a).

Li^8

(Fig. 7, p. 41) †

THEORY

See (La 55a, Ku 56, Ku 57, Fr 57).

I. $Li^8(\beta^-)Be^8$ $Q_m = 16.001$

TABLE 8.1

Energy levels of Li^8

E_x in Li^8 (MeV)	J^π	$\tau_{\frac{1}{2}}$ or Γ (keV)	Decay	Reactions
0	2^+	$\tau_{\frac{1}{2}} = 0.848 \pm 0.004$ sec	β^-	I, II, III, IX, XII, XIV, XVIII
0.975 ± 0.012	$\leqq 3^+$		(γ)	II, IX, XVIII
2.260 ± 0.005	3^+	28	n	IV, IX
3.22	$1^{(+)}$	≈ 1000	n	V

† For level scheme of B^8, see fig. 9, p. 59.

The weighted mean of half-lives reported in (Aj 55) is 0.848 ±0.004sec. A value of 0.873±0.013 sec is given by (Ve 58a). See also (Im 58). The decay is complex: see Be⁸.

II. $Li^6(t, p)Li^8$ $Q_m = 0.803$

$Q_0 = 0.790 \pm 0.011$ (Al 54e).

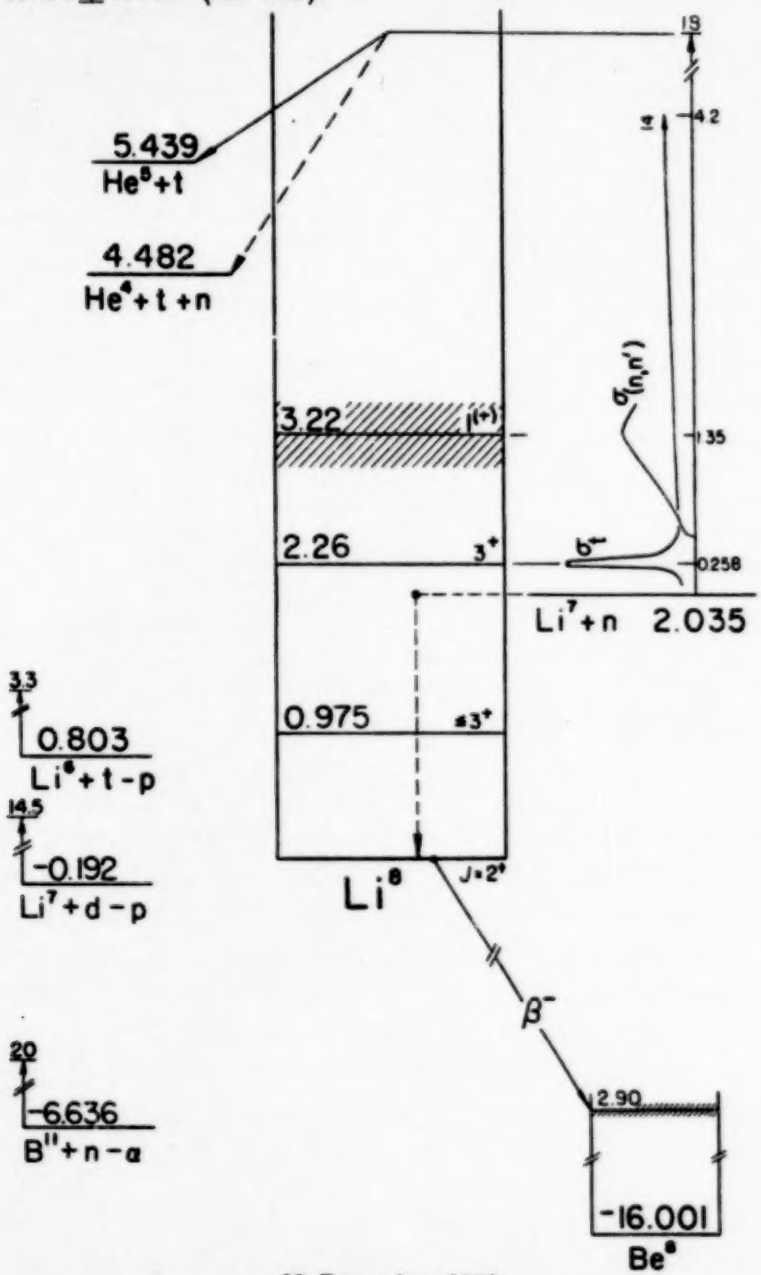

29 December 1958

Fig. 7. Energy levels of Li⁸: for notation, see fig. 1, p. 7.

The ground state reaction has been observed by (Pe 52, Mo 52, Al 54e, Cu 55b). (Cu 55b) also reports one event corresponding to the transition to an excited state at 0.7±0.2 MeV.

III. $Li^7(n, \gamma)Li^8$ $Q_m = 2.035$

The thermal capture cross section is 33 ± 5 mb (Hu 47a), 42 ± 10 mb (Ko 56e). At $E_n = 275$ keV, neutron capture is not observed: $\sigma < 0.25$ mb (Ko 56e). Polarization of Li^8 produced by polarized thermal neutrons has been detected by (Bu 57). See also (Ku 57, Sh 58, Im 58).

IV. $Li^7(n, n)Li^7$ $E_b = 2.035$

Cross sections for Li metal and for Li^7 are reported in (Hu 58; see also Go 56m, Ka 57b, Br 58h). The thermal cross section is 1.07 ± 0.04 b (C. Hibdon: see Th 56 and Hu 55c).

A pronounced resonance occurs at $E_n = 258$ keV (see table 8.2). Total

TABLE 8.2

$Li^7(n, n)Li^7$ resonance parameters [a]

	(Wi 56a)	(Th 56, Hu 58)
E_{res} (keV)	256	258 ± 3 [b]
Γ (keV)	32	32 [c]
$\Gamma_n(E_r)$ (keV)	35.8	
γ_n^2 (keV)	351	307
E_λ (keV)	−49	−43
radius (in 10^{-13} cm)	4.08	4.0
σ_{max} (b)		12.0

[a] Energies in the laboratory system.
[b] $E_{res} = 275$ keV, $\sigma_{max} = 7.0 \pm 0.2$ b (Go 56m).
[c] 35 ± 5 keV (Hu 58).

cross sections and angular distributions establish that the state has $J = 3^+$, formed by p-waves (Wi 56a). A further, broad peak centering at $E_n \approx 5$ MeV may indicate a broad level of Li^8 at ≈ 6.5 MeV (see Hu 58; see also Go 56m).

Data on coherent scattering and total cross section for zero-energy neutrons permit two solutions for the two s-wave scattering lengths corresponding to anti-parallel ($J = 1^-$) and parallel ($J = 2^-$) interactions; for the first solution, the interaction is essentially pure $J = 1^-$, for the other, pure $J = 2^-$. Measurement of the interference between the s-wave background and the p-wave (channel spin 2) resonance indicate that the second solution is the correct one, and it is concluded that the splitting between parallel and anti-parallel interactions is about 1.5 MeV (Th 56). (Wi 56a) find, on the other hand, that the observed asymmetries in the angular distributions indicate a nearly statistical ($\frac{5}{3}$) mixture of $J = 1^-$ and 2^- background. Use of scattering in Li^7 as a polarization analyzer is discussed by (Wi 56b).

See also (Be 56c, Kh 57a).

V. $Li^7(n, n')Li^{7*}$ $E_b = 2.035$

The excitation function for 0.48-MeV γ-rays shows an abrupt rise from threshold (indicating s-wave formation and emission) and a broad maximum ($\Gamma \approx 1$ MeV) at $E_n = 1.35$ MeV. The rise above threshold indicates the existence of a $J = 1^-$ level, which may be identified with the 1.35-MeV resonance (if a strong d-wave contribution is included). On the other hand, the latter resonance appears to be better described as a $J = 1^+$ level, formed by p-waves. Under this assumption, $E_r = 1.45$ MeV (lab), $\Gamma = 1.14$ MeV, with the sum of reduced widths $\theta^2_{in}+\theta^2_{out} \approx 0.5(\times 3\hbar^2/2Mr^2)$. The ratio $\theta^2_{in}/\theta^2_{out} = 0.1$ to 0.4 or 1.6 to 3.0 (Fr 55a).

VI. $Li^7(n, p)He^7$ $Q_m = -14$ $E_b = 2.035$
Not observed: see He^7.

VII. $Li^7(n, d)He^6$ $Q_m = -7.779$ $E_b = 2.035$

At $E_n = 14$ MeV, the cross section is 9.8 ± 1.1 mb (Ba 53). See also (Fr 54b).

VIII. (a) $Li^7(n, t)He^5$ $Q_m = -3.423$ $E_b = 2.035$
(b) $Li^7(n, t)He^4+n$ $Q_m = -2.466$

The cross section for reaction (a) is 55 ± 8 mb at $E_n = 14$ MeV (Fr 54b). See also (Ma 54f) and (Ba 54).

IX. $Li^7(d, p)Li^8$ $Q_m = -0.192$
$Q_0 = -0.183\pm0.02$ (Kh 55).

Three proton groups are observed, corresponding to the ground-state and to levels at 0.974 ± 0.015 (Le 55), 0.977 ± 0.02 MeV (Kh 55, Kh 55a) and 2.28 MeV (Le 55). A search for further levels in the range $E_x = 2.28$ to 8 MeV revealed no levels with $\Gamma < 80$ keV (Ha 58a). At $E_d = 14$ MeV, the angular distributions of the protons, analyzed by stripping theory, indicate $l_n = 1$ and therefore even parity, $J \leqq 3$, for the ground state and the 0.98-MeV level (Le 55). On the assumption that $J = 2^+$ and 1^+ for the ground state and 0.98-MeV level, respectively, (Fr 57) calculate $\theta^2 = 0.054$ and 0.028 from the data of (Le 55). These two levels are presumed to arise from a ^3P term, with a third component of $J = 0^+$ expected at higher energy (Fr 57). See also (Gi 55).

X. $Li^7(t, d)Li^8$ $Q_m = -4.224$
Not observed.

XI. $Li^7(\alpha, He^3)Li^8$ $Q_m = -18.543$
Not observed.

XII. $Be^9(\gamma, p)Li^8$ $Q_m = -16.885$
See Be^9 and (Ch 58c).

XIII. $Be^9(n, d)Li^8$ $Q_m = -14.658$
Not observed.

XIV. $Be^9(p, 2p)Li^8$ $Q_m = -16.885$

Production of Li^8 at $E_p = 20$ MeV is reported by (Le 56g). At $E_p = 185$ MeV, the summed proton spectrum shows two peaks, corresponding to pickup of protons with binding energies of ≈ 18 and ≈ 26 MeV, respectively. There is some indication of α-particle structure (Ty 58b, Ma 58h).

XV. $Be^9(d, He^3)Li^8$ $Q_m = -11.409$
See (Wi 54f).

XVI. $Be^9(t, \alpha)Li^8$ $Q_m = 2.928$
Not observed.

XVII. $B^{10}(n, He^3)Li^8$ $Q_m = -15.771$
Not observed.

XVIII. $B^{11}(n, \alpha)Li^8$ $Q_m = -6.636$
See B^{12}.

TABLE 8.3
Energy levels of Be^8

E_x in Be^8 (MeV)	J^π; T	τ_m or Γ	Decay	Reactions
0	0⁺; 0	2.5±1 eV	α	I, III, XII, XIII, XIV, XXI, XXII, XXIV, XXVI, XXIX, XXX, XXXI, XXXII, XXXIII, XXXIV, XXXV, XXXVI, XXXVII, XXXVIII, XXXIX, XL, XLI, XLII
2.90 †	2⁺; 0	1.2±0.3 MeV ††	α	III, XII, XIV, XXI, XXVI, XXVII, XXVIII, XXIX, XXX, XXXI, XXXII, XXXIII, XXXV, XXXVI, XXXVII, XXXVIII, XXXIL, XL
11.7	4⁺; 0	≈6.7 MeV	α	III, XII, XXI, XXVII, XXVIII
16.08		0.31 MeV	(α)	XXI, XXXIX, XLI
16.67	(2⁺; 1)	0.19 MeV	α	XXI, XXXIX, XLI
(17.6)	(2⁺; 1)	(<0.3 MeV)	(α)	XXXIX
17.64	1⁺; (1)	10.7±0.5 keV	γ, p	XIV, XVI, XXI
18.15	1⁺; (0)	147 keV	γ, p	XIV, XVI, XVII, XXI
18.9	(2⁻; 0)	>0.5 MeV	n, p	XV, XVI, XVII, XXV
19.1	(3⁻)	0.4 MeV	γ, p	XIV, XV, XVI
19.22	3⁺; (1)	0.19 MeV	n, p	XV, XVI
19.9	(2⁺)	≈0.9 MeV	(n), α, p	XV, XX
21.6		≈0.8 MeV	n, p	XV
22.6	(⁺)	≈0.35 MeV	d, n, α, p, γ	V, VI, X, XIV

† A number of additional states from $E_x = 2$ to 15 MeV have been reported by various observers: see, e.g. $Li^7(d, n)Be^8$, $B^{10}(d, \alpha)Be^8$, $B^{11}(p, \alpha)Be^8$, $C^{13}(\gamma, \alpha)Be^8$ and (Ti 54).
†† See table 8.4.

Be^8

(Fig. 8, p. 45)

THEORY

See (He 55f, Bi 57f, Ku 56, Pe 56a, Fr 57, Wi 58g).

I. $Be^8 \rightarrow 2He^4$ $\quad Q_m = 0.094$

Recent Q-values are 93.7 ± 0.9 keV (Co 57d: $Be^9(p, d)Be^8$), 90 ± 5 keV

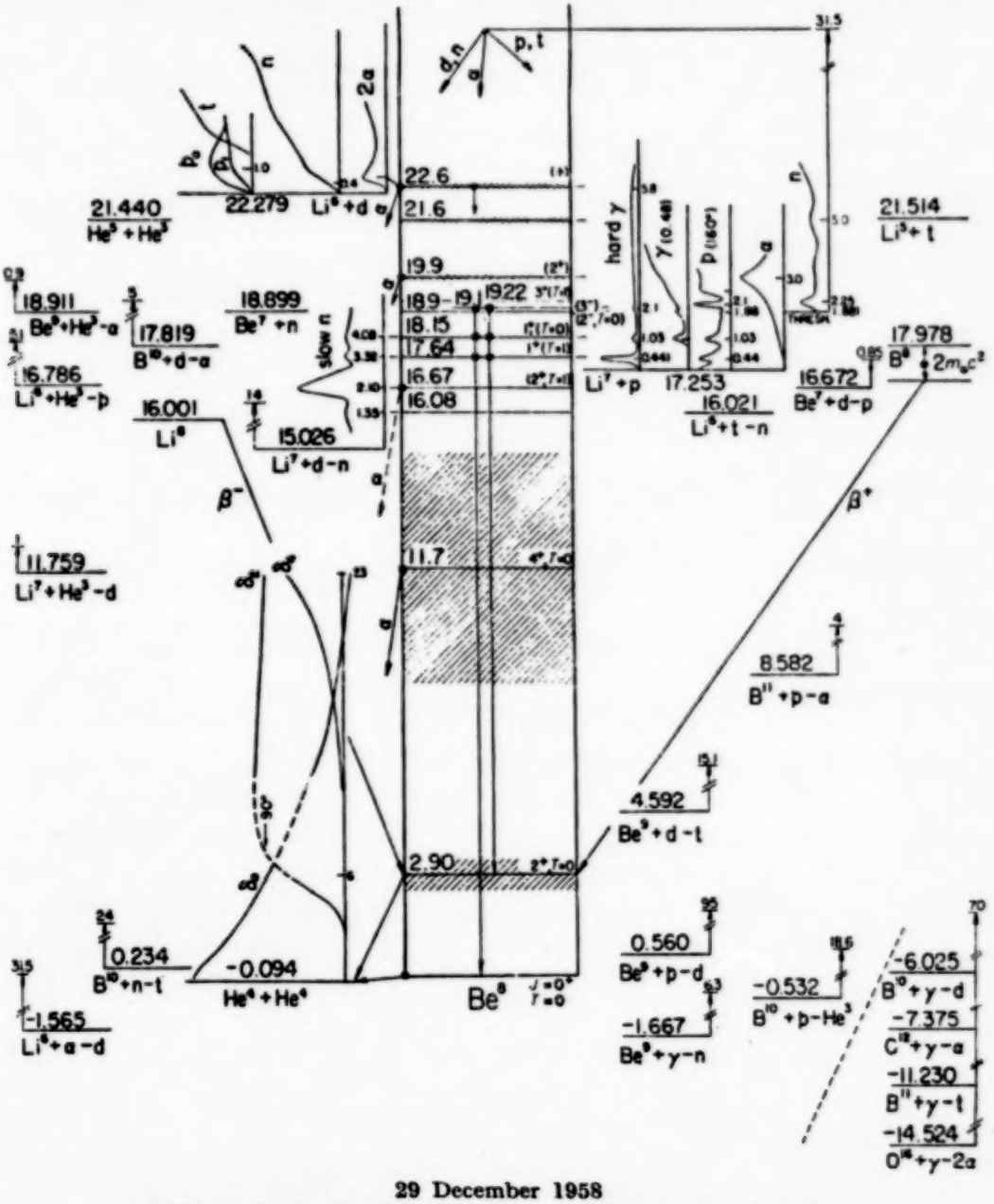

29 December 1958

Fig. 8. Energy levels of Be^8: for notation, see fig. 1, p. 7.

(Tr 55: $B^{11}(p, \alpha)Be^8$): the weighted mean of all measurements is 94.1 ± 0.7 keV (Va 57). The width of the ground state is 4.5 ± 3 eV (Ru 56a; 15 per cent of Wigner limit), $\leqq 3.5$ eV (He 56b). The second value leads to $\tau_m \geqq 2 \times 10^{-16}$

sec. (Combination of these values places the mean life in the range $\tau_m = 2$ to 4.5×10^{-16} sec.) An upper limit to the mean life is 6×10^{-15} sec (Tr 55). See also (Aj 55).

II. $He^4(\alpha, p)Li^7$ $\quad Q_m = -17.347 \quad E_b = -0.094$

See Li^7.

III. $He^4(\alpha, \alpha)He^4$ $\quad E_b = -0.094$

Absolute differential cross sections are reported by: (He 56b): $E_\alpha = 0.15$ to 3.0 MeV, (Ru 56a): $E_\alpha = 3.0$ to 5. 9 MeV, (St 53): $E_\alpha = 12.9$ to 21.6 MeV,

TABLE 8.4
Energy and width of first excited state of Be^8

E_x (MeV)	Γ (MeV)	Reaction	Reference
2.9	2.0	$He^4(\alpha, \alpha)He^4$	(Ru 56a)
	1.9	$Li^7(p, \gamma)Be^8$	(Me 58a)
2.95	1.6 $\pm$0.4	$Be^7(d, p)Be^8$	(Sp 58a)
3.0 $\pm$0.1	1.0 $\pm$0.2	$Li^8(\beta^-)Be^8$	(Aj 55) [a]
2.8 $\pm$0.1	0.8	$Be^9(d, t)Be^8$	(Cu 55)
2.87$\pm$0.06	0.9 $\pm$0.2 [b]	$B^{10}(d, \alpha)Be^8$	(Aj 55) [a]
2.94$\pm$0.06	0.84	$B^{11}(p, \alpha)Be^8$	(Aj 55) [a]
3.06	0.9	$C^{13}(\gamma, \alpha)Be^8$	(Go 55b)

[a] See also text below.
[b] $\theta^2 \approx 2$ (Tr 53).

(Ni 56a): $E_\alpha = 12.3$ to 22.9 MeV, (Ma 51a, Br 51i): $E_\alpha = 20$ and 20.4 MeV, (Gr 51, Gr 52): $E_\alpha = 30$ MeV, (Bu 57b): $E_\alpha = 38.5$ MeV, and (Co 57f): $E_\alpha = 44.7$ MeV. See also (Ch 58d).

Phase shifts summarizing the work of (He 56b), (Ru 56a) and (Ni 56a) are presented in (Ru 56a) and (Ni 58). These three sets of data appear to join smoothly, but do not appear to fit well with the data of (St 53). For $E_\alpha < 3$ MeV, only the s-wave phase shift is important. A careful survey in the range 146—202 keV reveals no effect of the ground state and places an upper limit of $\Gamma \leqq 3.5$ eV on this state (He 56b): see table 8.5. Analysis of

TABLE 8.5
Levels of Be^8 from $He^4(\alpha, \alpha)He^4$ [a]

E_x (MeV)	J^π	$\Gamma_{c.m.}$	R (10^{-13} cm)	θ^2 ($3\hbar^2/2MR^2$)
0	0^+	2.5$\pm$1 eV	5.7	0.15
			4.44	0.75
2.9	2^+	2.0 MeV	5.0	0.7
			3.5	0.4
11.8	4^+	6.7 MeV	4.44	1.3

[a] From (He 56b, Ru 56a, Ni 58). Double entries indicate alternative solutions.

the 0 to 6 MeV data by effective range theory leads to a value $\Gamma = 4.5 \pm 3$ eV for the ground-state width; $\theta^2 \approx 0.15$ of the Wigner limit (with $R = 5.7 \times 10^{-13}$ cm). Some evidence of shape-dependence is found in this analysis (Ru 56a). According to (Ni 58) a good account of the s-wave phase shift below 6 MeV is given by hard-sphere scattering plus resonance scattering from the ground state with a width $\theta^2 = 0.75$ ($R = 4.44 \times 10^{-13}$ cm). There is no indication of other S-states below $E_x = 11.5$ MeV (Ni 58).

The d-wave phase shift first becomes appreciable near $E_\alpha = 2.5$ MeV (He 56b) and appears to pass through resonance at 6.0 MeV (Ru 56a). The g-wave shift rises continuously from $E_\alpha = 11$ to 23 MeV; a broad Be^8 level is indicated at $E_x = 11.7$ MeV (Ni 56a, Ni 58). The course of the phase shifts appears to be consistent with a simple two-body interaction with an attractive potential near $R \approx 5 \times 10^{-13}$ cm and a repulsive core at a smaller radius; some dependence of the well shape on l is required (He 56a, Ru 56a, Ha 51e, Ni 58, Va 58c). A detailed comparison with the model of (Ha 51e) is made by (Ni 58). At 38.5 MeV, the s and d phase shifts are large, while the δ_4, δ_6 and δ_8 phase shifts are small. These results are consistent with 0^+ and 2^+ states near 19 MeV (see $Li^7(p, \alpha)He^4$) and are not inconsistent with a 4^+ state at ≈ 11 MeV (Bu 57b). See also (Aj 55), (Ha 56g, Mc 58b: theo.) and (Sn 54).

IV. $Li^6(d, \gamma)Be^8$ $\quad Q_m = 22.279$

Not observed: see (Sa 53b) and (Si 54).

V. (a) $Li^6(d, n)Be^7$ $\quad Q_m = 3.380$ $\quad E_b = 22.279$

(b) $Li^6(d, n)He^4 + He^3$ $\quad Q_m = 1.796$

The excitation curve has been measured for $E_d = 0.06$ to 5.5 MeV (Ba 52, Hi 54b, Ne 56b, Sl 57). A broad s-wave resonance is indicated at $E_d = 0.41$ MeV, $\Gamma = 0.45$ MeV (Ba 52, Ne 56b). At this energy the neutron yield to the 0.43-MeV state of Be^7 is isotropic, while at $E_d = 600$ keV and above, the angular distributions indicate a strong admixture of stripping process (Ne 56b). A sharp resonance at $E_d = 2.12$ MeV is reported by (Ba 52). However, (Sl 57) find that the forward cross section rises from ≈ 22 mb/sr at $E_d = 1.1$ MeV to ≈ 57 mb/sr at 5.5 MeV without sharp resonances. This is confirmed by (Bu 54c) who reports no appreciable change in slope at $E_d \approx 1.8$ MeV and suggests that the increase in neutron yield observed by (Ba 52) might have been due to oxygen contamination.

The ratio of 430-keV γ-radiation from this reaction and 477-keV γ-radiation from the mirror reaction, $Li^6(d, p)Li^7$, has been measured for $E_d = 0.2$ to 1.8 MeV. This ratio, which measures Γ_n/Γ_p, rises from 1.1 to about 1.13 at $E_d = 0.45$ MeV, falling to 0.98 at $E_d = 1.8$ MeV. The theoretical ratio, assuming charge symmetry, rises from 0.96 at low energy to 0.98 at E_d

= 1.8 MeV. It is concluded that the predictions of charge independence are borne out within 15 per cent, and that the slight deviation observed may be connected with the resonance near $E_d = 0.45$ MeV (Wi 57). See also (Hi 54b).

VI. (a) $Li^6(d, p)Li^7$ $Q_m = 5.027$ $E_b = 22.279$
(b) $Li^6(d, p)He^4+He^3$ $Q_m = 2.561$

Cross sections and angular distributions have been measured for $E_d = 30$ keV to 3 MeV by (Kr 50, Sa 53b: see Ja 57, Wh 50d, Ni 54). A broad maximum near $E_d = 1.0$ MeV is interpreted by (Wh 50d) as indicating a level at $E_d = 0.4$ MeV, $\Gamma \approx 0.5$ MeV. The angular distributions at $E_d > 1$ MeV indicate stripping effects, with $l_n = 1$ (Ni 54). See also the discussion of the work of (Wi 57) in the preceding section. See also (Aj 55).

VII. $Li^6(d, d)Li^6$ $E_b = 22.279$
See Li^6.

VIII. $Li^6(d, t)Li^5$ $Q_m = 0.765$ $E_b = 22.279$

The cross section for tritium production rises rapidly to 190 mb at 1 MeV, then more slowly to 290 mb near 4 MeV. There is evidence of deviation from isotropy near 0.4 MeV (Ma 55d). See also Li^5.

IX. $Li^6(d, He^3)He^5$ $Q_m = 0.839$ $E_b = 22.279$
See He^5.

X. $Li^6(d, \alpha)He^4$ $Q_m = 22.373$ $E_b = 22.279$

Cross sections have been measured for $E_d = 30$ keV to 1.6 MeV (Sa 53b, see Ja 57; Hi 54b, Wh 50d). A broad maximum is observed at $E_d = 0.6$ MeV which is interpreted in terms of a resonance at $E_d = 0.35$ MeV ($\Gamma \approx 0.5$ MeV) [(Wh 50d); see, however, (Hi 54b)]. See also (Po 56), (Sa 56; theo.) and (Aj 52c).

XI. $Li^6(t, n)He^4+He^4$ $Q_m = 16.115$
See (Cu 52a).

XII. $Li^6(He^3, p)Be^8$ $Q_m = 16.786$

At $E(He^3) = 1.25$ MeV, proton groups are observed to the ground state, the 2.9-MeV state and possibly to a state at ≈ 12.3 MeV ($\Gamma \approx 2$ MeV, intensity ≈ 6 per cent of 2.9-MeV transition). It is suggested that the 12.3-MeV state may be that observed in $He^4(\alpha, \alpha)He^4$. No other states are observed with $E_x \lesssim 14$ MeV. The upper limits on the intensities of groups leading to such states are 1 per cent (of 2.9-MeV transition) for sharp states and 3 per cent for levels 1 MeV wide (Mo 56a). These results are confirmed by (Sc 56f) at $E(He^3) = 1.5$ and 2 MeV: no group of width $\lesssim 1$ MeV appears for $E_x < 14$ MeV with an intensity as much as 2 per cent of the $Be^8(2.9)$ group. See also (Ku 53b), (Al 55b).

XIII. $Li^6(\alpha, d)Be^8$ $Q_m = -1.565$

This reaction has been observed at $E_\alpha = 31.5$ MeV (Wa 56f).

XIV. $Li^7(p, \gamma)Be^8$ $E_b = 17.253$

The cross section has been studied from $E_p = 30$ keV (see Ja 57) to 7.7 MeV. Resonances are observed at $E_p = 0.44$, 1.03, and 2.1 MeV: see table 8.6.

TABLE 8.6[b]

Resonances in $Li^7(p, \gamma)Be^8$

E_r (keV)	Γ_{lab} (keV)	Be^{8*} (MeV)	References
441.4±0.5	12	17.64	(Fo 49b, Bo 48c)
441.5±0.5	12.2±0.5		(Hu 52f)
441.2±0.6	12 ±1		(Bu 55f, Bu 56e)
1030 ±5[a]	168[a]	18.15	(Kr 54a)
2000			(Pr 54b)
2100	400		(Sw 55)
2130	400	19.1	(Ne 57a)

[a] From $Li^7(p, p)Li^7$ (Fo 49b).

[b] See also table 8.7.

There is no further structure up to 5 MeV (Ba 52a). The radiation comprises two components, one from the ground-state transition, with $E_\gamma = 17.2 + \frac{7}{8} E_p$ and the other from the transition to the 2.9-MeV broad excited state, with $E_\gamma \approx 14.3 + \frac{7}{8} E_p$. Both are resonant at the 0.44-MeV resonance, but only the lower energy transition shows the 2.1-MeV resonance (Ne 57a). The intensity ratio of the higher to the lower-energy radiation increases from 0.5 at $E_p = 0.2$ MeV to 1.7 at $E_p = 0.44$ MeV and falls to 1.0 at $E_p = 0.6$ MeV (Ca 56f, $\theta = 90°$). Between $E_p = 1.0$ and 3.5 MeV the ratio is constant within 30 per cent at $\frac{2}{3}$ (Wi 55g, Ne 57a). Evidence for a component at ≈ 12 MeV is discussed by (Ti 53a; see also Ca 55b). A broad resonance appears near $E_p = 5.8$ MeV probably corresponding to the "giant" (γ, p) resonance, $E_x = 22.3$ MeV (Ge 59a).

The angular distributions of both γ-rays show small deviations from isotropy at the $E_p = 0.44$ MeV resonance and exhibit strong interference effects nearby. The observed distribution of the 17.6-MeV radiation at resonance is consistent with p-wave formation if the channel spin ratio $\chi \equiv \sigma(1)/\sigma(2) = \frac{1}{4}$: this ratio implies an intermediate coupling with $a/K = 2$ to 3 (Ne 58: see also De 50a, Fr 57). Angular distributions in the range $E_p = 0.9$ to 1.2 MeV are reported by (Kr 54a) and 0°/90° cross sections for $E_p = 1.5$ to 3.5 MeV by (Ne 57a). The latter observations indicate that some process other than direct s-wave capture is responsible for the background between resonances (Ne 57a, Wi 54a).

A study of (γ—α) coincidences at $E_p = 0.45$ MeV yields an angular correlation which rules out the assignment $J = 0^+$ to the 2.9-MeV Be^8 level and indicates that the 14.7-MeV γ-radiation contains a mixture of E2 and M1 radiation (Bo 56c: see also De 54b). The alpha spectra, taken singly (La 56c) and in coincidence with γ-rays (Me 58a) show no evidence of weakly excited levels reported by (In 54: see also Ti 55). In the work of (Me 58a), the 2.9-MeV level appears to have a width of 1.9 MeV; compare (Bu 50h). There is some evidence for a broad level near $E_x = 10$ MeV (La 56c).

See also (Ri 55b), (Po 56), (Ku 57a, Fr 57; theo.).

TABLE 8.7

Levels in Be^8 from Li^7+p

E_{res} (keV)	Be^{8*} (MeV)	Γ_{lab} (keV)	l_p	$J^\pi; T$	θ_p^2	$Li^7(p,\gamma)Be^7$	
						σ_{res} (mb)	$\omega\Gamma_\gamma$ (eV)
441.5	17.64	12.2	1	1^+; 1	0.064	6.0	9.4
1030	18.15	168	1	1^+; (0)		res.	2
1900	18.94	>500	0	2^-		non res.	
2100	19.1	400	2(1)	(3^-)		res.	
2250	19.22	220	1	3^+; (1)	0.04	(non res.)	
(≈3000)	(19.9)	>1000	(1)	(1^+)			
≈3000	19.9[a]	≈1000	(1)	(2^+)			
5000	21.6	≈900					

[a] $Li^7(p,\alpha)He^4$.

XV. $Li^7(p,n)Be^7$ $\quad Q_m = -1.646$ $\quad E_b = 17.253$

The cross section has been studied from the threshold at $E_p = 1.8811$ MeV (see Be^7) to 10 MeV (see Ja 57, Ka 57a, Bo 57i; see also Ta 58a). Resonances are indicated at $E_p = 1.93$, 2.25, (3.0), and 5.0 MeV (see table 8.7). Absolute cross sections are given by (Ta 48) and (Ma 58b): see also (Ma 59, footnote 14). Angular distributions in the range $E_p = 2.0$ to 2.5 MeV show strong ($\cos\theta$) terms, suggesting interference of states of opposite parity (Ta 48, Br 48a). (Ad 54) has shown that the behaviour in this region can be accounted for by ascribing the 2.25-MeV resonance to p-wave formation, with $J = 3^+$ and $\gamma_p^2 = \gamma_n^2 = 0.8\times10^{-13}$ MeV-cm (presumably the $T = 1$ analogue of $Li^8(2.28)$), and assuming a background due to s-wave, $J = 1^-$ and 2^-, levels of undetermined location. According to (Ne 57a), a better account of the cross section below 2.4 MeV is obtained with the $J = 3^+$ level assumed to have $\gamma_n^2/\gamma_p^2 = 5.5$ and a single s-wave $J = 2^-$ level at $E_p = 1.9$ MeV, with $\gamma_n^2/\gamma_p^2 = 5.5$. With this large ratio the low energy cross section can be acounted for in detail and can be made to agree with that derived from the inverse reaction $Be^7(n,p)Li^7$ (Ne 57a, Ma 58b; see also Ha 55c). [It is of interest to note that a similar apparent deviation from charge independence

occurs in $B^{10}(\alpha, n)N^{13}$ and $B^{10}(\alpha, p)C^{13}$ (see N^{14}). On the other hand, see $Li^6(d, p)Li^7$ and $Li^7(d, n)Be^7$.] Using the stacked-foil method, (Ka 57a) report structure in the excitation function corresponding to Be^8 levels at 21.5, 22.5, 23.85, (24.9) and (25.6) MeV. At $E_p = 10$ MeV, the cross section for production of Be^7 is 120 ± 20 mb (Ka 57a), 100 ± 20 mb (Bo 57i).

The relative intensity of the low-energy neutrons (to Be^{7*} (0.43)) to the high-energy (ground state) neutrons varies with energy: see table 8.8. In the range $E_p = 2.5$ to 2.9 MeV, the low-energy neutrons are practically isotropic (c.m. system). From the shape of the excitation function, (Ba 55o) conclude that the reaction to Be^{7*} proceeds by s-wave protons in and s-wave neutrons out.

$Li^7(p, n)Be^7$			$Li^7(p, p')Li^{7*}$	References
l_n	γ_n^2/γ_p^2	θ_n^2	$\Gamma_{p'}$ (keV)	
			0	(Fo 49b, Hu 52f)
			≈6	(Fo 49b, Br 51a, Mo 54a, Kr 54a)
0	4.5 [b]	>0.3	res.	(Ne 57a, Ma 58b)
		small	small	(Ne 57a)
1	5.5 [c]	[0.2]	small	(Ne 57a) [d]
		(res.)		(Ne 57a, Ma 58b) [d]
		res. [e]		(Ba 52a, Bl 51a, Gi 59)

[b] 5.2 ± 0.3 (Ma 58b); $\Gamma_n = \Gamma_p$ at $E_p = 1.93$ to 1.97 MeV.
[c] 5.2; $\gamma_n^2 = 2.9\times10^{-13}$ MeV-cm (Ma 58b), $\Gamma_n = \Gamma_p$.
[d] See also (Ma 55k).
[e] (Gi 59) find $E_{res} \approx 5.0\pm0.5$ MeV, $\Gamma \approx 0.9$ MeV, $\sigma \approx 140$ mb, $J \geq 3$ (if single resonance).

It is pointed out by (Ad 54) that the existence of the $J = 3^+$ level, apparently well separated from the other components $J = 1^+$ and 2^+ which can be formed with channel spin 2, indicates a strong spin-orbit interaction,

TABLE 8.8

Relative yield of neutrons to Be^{7*} (0.43) and Be^7(g.s.)

E_p (MeV)	θ(lab)	$I_{0.43}/I_0$ (per cent)	References
2.40	all	0.18 ± 0.06	(Ma 55k)
2.5	all	2.5 [a]	(Ba 55n, Ba 55o)
2.75	30°	$9\ \pm1.5$	(Jo 50b)
2.89	30°	$10.5\ \pm1$	(Jo 50b)
3.0		8 [a]	(Ba 55n, Ba 55o)
3.66	30°	$12\ \pm1$	(Jo 50b)
3.9 —5.4		≈10	(Cr 54a)
5.0	20°—90°	52.5	(Gr 50)

[a] See curve in (Ba 55n).

which should lead to polarization of the neutrons and scattered protons. Polarization measurements are reported by (Ad 54, Wi 54c, Wi 56b, Ok 55, St 58, Cr 58, Cl 58). See also (Gi 58, Ro 57a).

XVI. $Li^7(p, p)Li^7$ $E_b = 17.253$

Absolute differential scattering cross sections are reported for $E_p = 0.4$ to 1.4 MeV by (Wa 53), for $E_p = 1.4$ to 3.0 MeV by (Ma 56), and for $E_p = 14.5$, 20.0 and 31.5 MeV by (Ki 56). Anomalies appear at $E_p = 0.44$, 1.03, 1.88, 2.1, and 2.5 MeV (see table 8.7). Both the 0.44- and the 1.03-MeV resonances are ascribed to p-waves, $J = 1^+$, with channel spins 1 and 2 in a ratio of 1 to 5 (Li 53a, Ch 53d, Li 55b: compare $Li^7(p, \gamma)Be^8$).

The anomaly at $E_p = 1.88$ MeV coincides with the $Li^7(p, n)$ Be^7 threshold and is ascribed to the abrupt change in total width of a broad (2^-?) resonance when neutron emission becomes possible (Ma 56, Ne 57a). The observed structure at 2.0—2.25 MeV may reflect interference of the p-wave 2.25-MeV ($J = 3^+$) resonance with one at $E_p = 2.1$ MeV, also formed by p-waves (Ma 56). Preliminary results of a phase shift analysis suggest, on the other hand, interference between a $J = 3^-$ level at $E_p = 2.1$ MeV with a 2^- level at $E_p = 1.9$ MeV, and interference of the 3^+ level at $E_p = 2.25$ MeV with a broad 1^+ level near 3 MeV (J. Olness, quoted in Ne 57a).

XVII. $Li^7(p, p')Li^{7*}$ $E_b = 17.253$
$Li^7(p, p'\gamma)Li^7$

A pronounced resonance appears in the yield of inelastically scattered protons (Br 51a and Mo 54a) and 0.48-MeV γ-rays (Kr 54a) at $E_p = 1.030 \pm 0.005$ MeV, $\Gamma = 168$ keV. The angular distribution of the protons is approximately isotropic at resonance, $\sigma = 42$ mb, and asymmetric above it, consistent with an s- or p-wave resonance interfering with a non-resonant wave of opposite parity (Mo 54a: see also Li 55b).

The yield of 480-keV radiation rises smoothly from $E_p = 1.5$ to 3.0 MeV except for a pronounced cusp at 1.881 MeV (Ne 57a, Ha 55c). Analysis of the excitation function suggests that the inelastic process is enhanced by the $J = 2^-$ level at 1930 keV and that the cusp results from the sudden increase in the total width when neutron emission becomes possible (Ne 57a). See also (Ba 51e).

XVIII. $Li^7(p, d)Li^6$ $Q_m = -5.026$ $E_b = 17.253$
See Li^6.

XIX. $Li^7(p, t)Li^5$ $Q_m = -4.261$ $E_b = 17.253$
See Li^5.

XX. $Li^7(p, \alpha)He^4$ $Q_m = 17.347$ $E_b = 17.253$

The cross section, which has been measured to 3.8 MeV, exhibits a broad

maximum at $E_p = 3$ MeV which is interpreted in terms of a level ≈ 1 MeV wide, with $J = 2^+$, at $E_p \approx 3$ MeV, and a several-MeV broad level of $J = 0^+$, underlying the region: see (Sa 53b, Ja 57, He 48e, He 48g, In 48). Absolute differential cross sections are reported by (Fr 58) for $E_p = 1.0$ to 1.5 MeV: at 1.01 MeV, $d\sigma/d\omega$ lab (90°) = 0.67 mb/sr [see also (Ma 56)]. Differential cross sections have also been measured at $E_p = 15.0$ and 18.5 MeV; there are indications of a triton pickup process at these energies (Ma 57a). See also $He^4(\alpha, p)Li^7$, (Ri 55b, Cr 56d, Ba 56f, Bu 58, Aj 55).

XXI. $Li^7(d, n)Be^8$ $Q_m = 15.026$

A careful study of the neutron spectrum at $E_d = 2$ MeV at several angles reveals only two distinct groups, corresponding to $Be^8(0)$ and $Be^8(2.9)$. No other levels below $E_x = 10$ MeV appear in this work: upper limits for groups leading to levels near $E_x = 4$ to 5 MeV and $E_x = 7.5$ MeV are 10 per cent and 20 per cent, respectively, of the ground state group. Angular distributions of the ground state and 3-MeV state neutrons exhibit $l_p = 1$ stripping patterns at forward angles (Tr 54b, Tr 55a). Other workers have reported neutron groups corresponding to levels at 2.2, 2.9, 4.1, 5.1 and 7.6 MeV — see for instance, (Tr 53a, Re 54b, Ih 55, Ih 55a, Gi 55a, Be 55b) — as well as states at 10 MeV (Ri 41), 11.1 and 14.7 MeV (Wh 50c).

Thresholds for slow neutron production indicate Be^8 levels at 16.08, 16.67, 17.61, and 18.20 MeV (Bo 54c, Sl 57) (see table 8.9). It is suggested

TABLE 8.9

Slow neutron thresholds in $Li^7(d, n)Be^8$ (Sl 57)

E_d (MeV)	$\Gamma_{c.m.}$ (MeV)	Be^{8*} (MeV)
1.35	0.31	16.08
2.10	0.19	16.67
3.32	<0.02	17.61
4.08	0.23	18.20

that the 16.67-MeV level is the lowest $T = 1$ level of Be^8, and that the levels at 17.61 and 18.20 MeV correspond to those seen in (Li^7+p) at $E_p = 0.44$ and 1.03 MeV (Bo 54c). A search for nuclear pairs from possible pair-emitting states of Be^8 yielded an upper limit of 2×10^{-5} mb at $E_d = 0.33$ MeV for excitation of such states in the range $E_x = 5.0$ to 8.5 MeV (Be 55a). See also (Ca 55d, Bo 56l, Bo 56m, Ca 55e, Ca 56h, Ca 57i, Pe 55e, Ri 56d).

XXII. $Li^7(He^3, d)Be^8$ $Q_m = 11.759$

See (Mo 54d) and (Al 55b).

XXIII. $Li^7(\alpha, t)Be^8$ $Q_m = -2.560$

Not observed.

XXIV. $Li^7(Li^7, He^6)Be^8$ $Q_m = 7.247$

See (No 57a).

XXV. $Be^7(n, p)Li^7$ $Q_m = 1.646$ $E_b = 18.899$

$Be^7(n, \alpha)He^4$ $Q_m = 18.993$

At thermal energies, the (n, p) cross section is $(5.1 \pm 0.6) \times 10^4$ b (Ha 55c) while the (n, α) cross section is < 25 mb (Se 58). These observations are consistent with the odd parity of Be^7. Less than 10 per cent of transitions involve $Li^7(0.48)$. Comparison of the (n, p) cross section with the cross section for $Li^7(p, n)Be^7$ gives evidence for an $l = 0$ level in Be^8 within 20 keV below the neutron threshold, with $\Gamma < 30$ keV (Ha 55c). See, however, (Ma 58b, Ne 57a), and see also (Ad 54). Comparison of the thermal cross section with the (p, n) cross section observed in the inverse reaction supports the assignment $J = \frac{3}{2}$ for Be^7 (g.s.) (Ne 57a).

XXVI. $Be^7(d, p)Be^8$ $Q_m = 16.672$

At $E_d = 0.85$ MeV, $\theta = 30°$, 90° and 270°, proton groups are observed corresponding to Be^8 g.s. and the broad level, $E_x = 2.95$ MeV, $\Gamma = 1.6 \pm 0.4$ MeV. No other prominent groups appear for $E_x < 5.8$ MeV (Sp 58a).

XXVII. $Li^8(\beta^-)Be^8$ $Q_m = 16.001$

$Q_0 = 15.94 \pm 0.08$ (Ve 58a).

The observed β-spectrum closely matches the mean of reported α-spectra (see Fr 55b) for $E_\beta > 3$ MeV and is consistent with 89 % branching via $Be^{8*}(2.9)$, with log $ft = 5.67$ and 11 % to higher states, possibly $Be^{8*}(11.7)$, log $ft = 4.6$. Less than 1 % of transitions involve Be^8(g.s.): log $ft > 8$ (Ve 58a: see also Aj 55). Upper limits to transitions to sharp states in Be^8 with $E_x = 2$, 4 and 6 MeV are, respectively, 2.5, 1 and 0.5 per cent (Fr 55b: see also Ar 56).

The α—β angular correlation is isotropic within a few per cent for all β-energies: see (Aj 55). It is pointed out by (Mo 55b) that a small, ≈ 0.5 %, anisotropy may be expected at high β-energies because of the increased importance of $l = 1$ and 2 emission, even in an allowed transition. Anisotropy in the β-decay from partially oriented Li^8 nuclei is reported by (Bu 57: see also Sh 58). The distribution of recoil momenta and the neutrino-recoil correlation establish that the decay is at least 90 % Gamow-Teller and that the Gamow-Teller portion is at least 90 % axial vector in character. The observations also require $J = 2^+$ for the Li^8 ground state (Ba 58i, La 58, La 58b; see also Mo 58d). An upper limit of 0.2 ± 0.1 per cent is reported by

(Ta 56c) on the number of disintegrations leading to 4.9-MeV γ-radiation: see also (Bu 53a). See also (Gi 55) and (La 55a, Ja 55d; theo.).

XXVIII. $B^8(\beta^+)Be^8$ $Q_m = 17.978$

The observed positon spectrum matches the Li^8—B^8 α-spectra for $E_{\beta^+} > 6$ MeV. About 80 % of transitions involve $Be^{8*}(2.9)$, $\log ft = 5.72$, with $\approx 19\%$ to higher states, possibly $Be^{8*}(11.7)$, $\log ft = 4.6$. Less than 5 % go to Be^8(g.s.), $\log ft > 7.3$ (Ve 58a). See (Al 50g, Ki 52, Gi 54). See also (Gi 55).

XXIX. (a) $Be^9(\gamma, n)Be^8$ $Q_m = -1.667$
(b) $Be^9(n, 2n)Be^8$ $Q_m = -1.667$
$Q_0 = -1.664 \pm 0.004$ (Co 56e)

At $E_\gamma = 6$ MeV, most of the transitions are to the 2.9-MeV state (Ca 54e). See also Be^9, and (Co 56e). For reaction (b), see Be^9 and Be^{10}.

XXX. $Be^9(p, d)Be^8$ $Q_m = 0.560$

Angular distributions of ground-state deuterons are remarkably similar for $E_p = 5$, 10, 16.5 and 22 MeV and show strong contributions from the pickup process (Ha 51a, Co 53e, Ra 56a, Su 55a, Su 56b, Su 58a, Re 56). The significance of this result, which is not consistent with the simple Butler theory, is discussed by (Gl 56, Da 55b; see also Da 55d, Da 56e, Sa 55h, Ko 56d, Gr 57e). At $E_p = 16.5$ MeV, the distribution is consistent with $l_n = 1$, $R_0 = 3.0 \times 10^{-13}$ cm, and $\theta^2 = 0.024$ for $Be^8(0)+n$ (Re 56). At higher energies, the distributions appear to be affected by pickup from within the nuclear volume (Be 56a, Se 56a). For $E_p = 31$ and 95 MeV, unresolved Be^8 states near 17 MeV appear, possibly representing pickup of a 1s neutron in Be^9 (Be 56a, Se 56a: see Be^9).

At $E_p = 7.4$ MeV, a search for Be^8 levels revealed only the ground-state and the 2.9-MeV state in the range $E_x = 0$ to 6.5 MeV (Ca 56i). See also (Fi 54d, Gi 55, St 56c, Be 57b) and (La 55; theo.).

XXXI. (a) $Be^9(d, t)Be^8$ $Q_m = 4.592$
(b) $Be^9(d, t)He^4+He^4$ $Q_m = 4.686$

At $E_d \approx 1.2$ and 3.5 MeV, the ground and first excited states are observed: see (Cu 52, Cu 53, Ge 53, Ge 56e, Ju 56e). For the first excited state, (Cu 55) finds $E_x = 2.8 \pm 0.1$ MeV, $\Gamma = 0.8$ MeV. At $E_d = 0.5$ MeV ($\theta = 60°$ and 90°), there is no evidence for excited states of Be^8 with $E_x = 3.4$ to 4.8 MeV: the upper limit to the intensity of the corresponding groups is 2 per cent of the 2.9-MeV group (Ge 56e). At $E_d = 14.8$ MeV ($\theta = 15°$), there is no evidence for states with $E_x = 7.1$ to 15.4 MeV (Ca 56i).

Recent studies of the angular distribution of ground-state tritons for $E_d = 0.1$ to 15 MeV have been reported by (Sm 57a, Ju 55, Ju 55b, Ha 56c: see also Aj 55). Below $E_d \approx 0.5$ MeV, the tritons show strong backward

peaking, suggestive of interference of compound nucleus states of opposite parity (Sm 57a: see B^{11}). At high energies, the reaction proceeds mainly by pickup, with $l_n = 1$ (Ha 56c). See also (Da 55d; theo.), (Ha 57h) and Be^9.

XXXII. $Be^9(He^3, \alpha)Be^8$ $Q_m = 18.911$

At $E(He^3) = 0.90$ MeV, the ground (weak) and 2.9-MeV (strong) states are observed: see (Aj 55).

XXXIII. $B^{10}(\gamma, d)Be^8$ $Q_m = -6.025$

Be^8 states up to $E_x = 10$ MeV are reported to be involved in this reaction: (see Ti 54, Ti 55a, Aj 55).

XXXIV. $B^{10}(n, t)Be^8$ $Q_m = 0.234$

See (Fr 56a, Ti 57, Ja 55e, Pe 51b, Ri 54a) and B^{11}.

XXXV. $B^{10}(p, He^3)Be^8$ $Q_m = -0.532$

See (Re 55a, Cr 52c).

XXXVI. (a) $B^{10}(d, \alpha)Be^8$ $Q_m = 17.819$

(b) $B^{10}(d, \alpha)He^4+He^4$ $Q_m = 17.913$

All observers agree that transitions occur to the ground state and to a state at $E_x \approx 2.87 \pm 0.06$ MeV, $\Gamma = 0.93 \pm 0.15$ MeV, (weighted mean of (Wh 51b, Tr 53, Cu 53b)). However, there is conflicting evidence on whether other states with $E_x < 15$ MeV are involved in this reaction. (Cu 54) report additional states at (4), 5.1, and 7.5 MeV (see also Aj 55). However, (Tr 53; $E_d = 0.6$ to 1.07 MeV) reports no other low lying states; (Bo 56k; $E_d = 5$ MeV, $\theta = 50°$ and 90°) have not observed any other states below $E_x = 9$ MeV; (Ho 55f; $E_d = 1.4$ to 3.2 MeV, several angles) find no evidence for excited states other than the 2.9-MeV level below $E_x \approx 10$ MeV; and (Ka 56, Ka 58a; $E_d = 1.7$ MeV) finds no groups corresponding to Be^8 states with $E_x = 9.8$ to 14.8 MeV above the continuum attributed to $B^{10}(d, \alpha)He^4+He^4$.

The observed α-spectrum corresponding to the 2.9-MeV level may be reasonably well accounted for by the Breit-Wigner formula with $l_\alpha = 2$, $E_\lambda = 5.29$ MeV, $\gamma_\alpha^2 = 13.4 \times 10^{-13}$ MeV-cm, $R = 4.48 \times 10^{-13}$ cm [$\theta^2 \approx 2$] (Tr 53).

XXXVII. (a) $B^{11}(\gamma, t)Be^8$ $Q_m = -11.230$

(b) $B^{11}(\gamma, t)He^4+He^4$ $Q_m = -11.136$

These reactions have been observed in boron-loaded photoplates. Six states of Be^8 below $E_x = 5$ MeV are reported to be involved in reaction (a) (Er 53). See also (Ti 55a).

XXXVIII. $B^{11}(p, \alpha)Be^8$ $Q_m = 8.582$

Alpha-particle groups corresponding to the ground state and to the

2.9-MeV state are reported; $E_x = 2.94 \pm 0.06$ MeV, $\Gamma = 0.84$ MeV (Li 51, Be 53: see Aj 55). Excitation of several additional levels is reported by (Gl 53); however, a careful search by (Ho 55f) reveals no evidence for any levels with $E_x < 7$ MeV except the ground state and that at 2.9 MeV.

The alpha particles leading to the ground state are strongly anisotropic at the $E_p = 163$-keV resonance ($C^{12*} = 16.11$, $J = 2^+$, $T = 1$); it is thus unlikely that $J = 2$ (Th 52c). The directional correlation of successively emitted α-particles at $E_p = 163$ keV indicates isotropic breakup of $Be^8(0)$ and hence $J = 0$, with $J = 2$ excluded. From the angle between the α-particles resulting from the breakup, $Q = 90 \pm 5$ keV is obtained; the half-life is $< 4 \times 10^{-15}$ sec (Tr 55). The angular correlation of alpha particles leading to the 2.9-MeV state with those resulting from the subsequent breakup is consistent with $J = 2^+$ for the 2.9-MeV state (Ge 55c). Certain peculiarities in the relative yields of ground state and 2.9-MeV excited state α-particles suggest that the latter level may have a significant $T = 1$ admixture: see (Be 53, Ho 55f).

Nuclear pairs have been reported with $E(\pi) = 7$ MeV (Ph 51b); see, however, (Be 55a). See also (Ti 55).

XXXIX. $C^{12}(\gamma, \alpha)Be^8$ $\quad Q_m = -7.375$

For $E_\gamma < 40$ MeV, the reaction involves mainly states of Be^8 at 0, 2.9, (4.1) (16.5 ± 0.2; $\Gamma < 0.4$), 16.8 ± 0.2 ($\Gamma < 0.3$), 17.6 ± 0.2 ($\Gamma < 0.3$) MeV, with indications of further states near 6, 10, and 15 MeV. There is no evidence for three-body reactions in this work (Go 55b). Evidence for levels at 3.2, 4.0, (7.5) and 9.0 MeV is reported by (Gl 55: see also Ti 54). The ground state decay energy is given as 87 ± 8 keV; for the first excited state, $E_x = 3.06$ MeV, $\Gamma = 0.9$ MeV (Go 55b). The excitation function is characterized by a number of resonances, suggesting that the process takes place via definite energy levels of C^{12} (see C^{12}); the principal types of levels involved being $J = 1^-$, $T = 1$, (E1 absorption) and $J = 2^+$, $T = 0, 1$ (E2) (Go 55b; see also Ti 55a, Ge 53a, Mu 57c). For $E_\gamma < 25$ MeV, the reaction proceeds mainly to $Be^8(0)$ and $Be^8(2.9)$; angular correlations indicate $J = 0$ and $J = 2$, respectively for these states. Wide variations in the branching ratio with energy are attributed to differences in isobaric spin impurities, estimated as 0.05×10^{-3} for the ground state, and $\geqq 10^{-3}$ for $Be^8(2.9)$.

For $E_\gamma > 26$ MeV the reaction changes radically, now involving the 17 to 18 MeV states of Be^8, with E1 absorption. The fact that these levels are so strongly excited in this manner suggests that they have $T = 1$. Angular distributions indicate $J = 2$ for $Be^8(16.8)$ and $J = 2$ (or possibly 0) for $Be^8(17.6)$. It is noted that the latter level cannot be identified with the well-known 17.63-MeV, $J = 1^+$ level (see $Li^7 + p$) (Go 55b; see, however, Wa 53). Excitation of proton-emitting levels near $E_x = 18$ and 22 MeV is reported by (Li 56). See also (Ti 56a, Ha 55g, Gu 53a).

XL. (a) $C^{12}(n, n')3He^4$ $Q_m = -7.281$

(b) $C^{12}(p, p')3He^4$ $Q_m = -7.281$

Reaction (a) has been studied for $E_n = 12.3$ to 20.1 MeV by (Fr 55i) who find evidence for transitions through the ground state and the 2.9-MeV level. See also (Aj 55) and C^{12}.

Reaction (b) at $E_p = 29$ MeV appears to proceed predominantly through the ground state and the 2.9-MeV level. It is not clear whether higher levels in Be^8 are involved (Ne 55c). See also (Sa 56e, Sa 56f, Cu 55a, Ja 57b).

XLI. $O^{16}(\gamma, \alpha)C^{12*} \rightarrow Be^8 + He^4$ $Q_m = -14.524$

At $E_\gamma \approx 22$ MeV, the reaction appears to proceed mainly via the 9.6 and 10.8-MeV states of C^{12} to the ground state of Be^8. For $E_\gamma > 24$ MeV, transitions through the 15(?) and 16-MeV $T = 1$ state(s) of C^{12}, to the 2.9-MeV state of Be^8 appear to dominate: see (Aj 55) and (Da 56c, Ha 55g, Ti 55a).

XLII. $O^{16}(p, p')4He^4$ $Q_m = -10.822$

At $E_p = 29$ MeV, more than half the transitions are through the ground state of Be^8; there is no evidence for participation of any excited states of Be^8(Ko 55). See also (Ja 57b).

B^8

(Fig. 9, p. 59) †

MASS OF B^8

The mass excess of B^8 is 25.287 ± 0.008 MeV, from the threshold energy of the $Li^6(He^3, n)B^8$ reaction.

I. $B^8(\beta^+)Be^8$ $Q_m = 17.978$

$Q_0 = 17.91 \pm 0.12$ MeV (Ve 58a).

The half-life of B^8 is 0.78 ± 0.01 sec (Du 58), 0.61 ± 0.11 sec (Sh 52), 0.65 ± 0.1 sec (Al 50g), 0.75 ± 0.02 sec (Ve 58a). The decay proceeds mainly to the 2.9-MeV state of Be^8, $\log ft = 5.72$ (Ve 58a). See also (Du 58) and Be^8.

TABLE 8.10
Energy levels of B^8

E_x in B^8 (MeV)	J^π	Γ or $\tau_{\frac{1}{2}}$ (MeV)	Decay	Reactions
0	$(2^+, 3^+)$	$\tau_{\frac{1}{2}} = 0.77 \pm 0.01$ sec	β^+	I, II, III, IV
(0.6 ± 0.1) ††		0.15 ± 0.1		II
(0.80 ± 0.05) ††		0.05 ± 0.03		II

II. $Li^6(He^3, n)B^8$ $Q_m = -1.976$

The threshold has been observed, both in production of slow neutrons and of B^8 positon activity, at $E(He^3) = 2.9661 \pm 0.0017$ MeV, yielding a mass

† For level scheme of Li^8, see fig. 7, p. 41.

†† *Note added in proof:* See, however, (Fa 59a).

excess of 25.287 ± 0.008 MeV. B^8 is then stable with respect to $Be^7 + H^1$ by 138 ± 9 keV. Two additional thresholds † for slow neutron production are reported, in the range $E(He^3) = 2.9$ to 6.0 MeV, at 3.9 ± 0.1 and 4.16 ± 0.05 MeV which may correspond to excited states of B^8 at $E_x = 0.6 \pm 0.1$ MeV ($\Gamma = 0.2 \pm 0.1$ MeV) and 0.80 ± 0.05 MeV ($\Gamma = 0.07 \pm 0.04$ MeV). It is pointed out that the existence of two low-lying levels in B^8 would be rather surprising in view of the level structure of Li^8(Du 58).

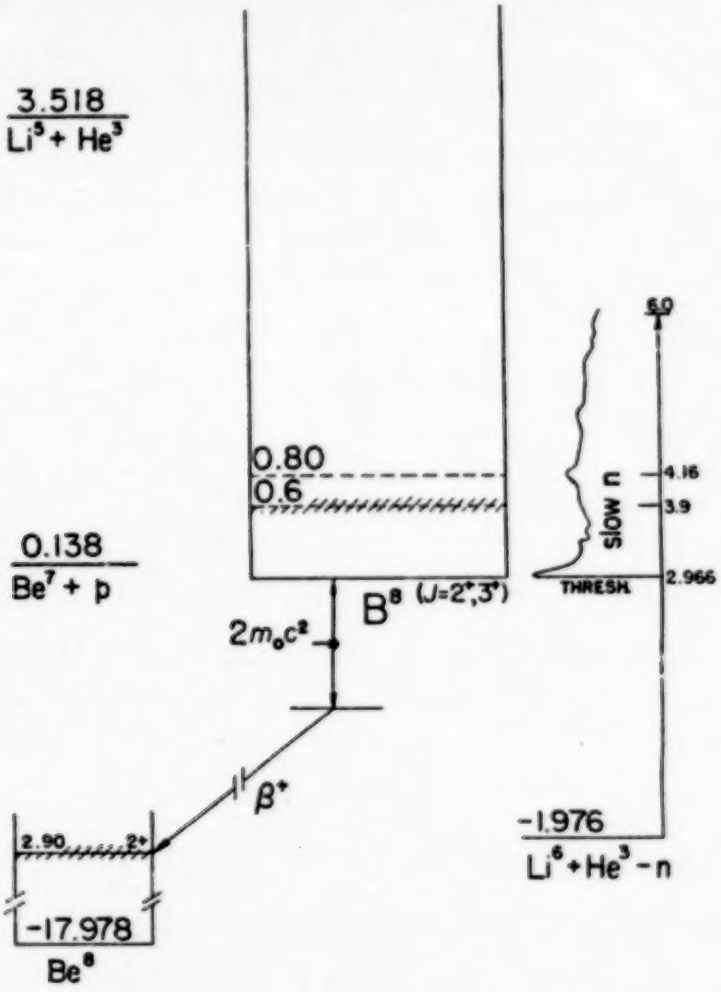

29 December 1958

Fig. 9. Energy levels of B^8: for notation, see fig. 1, p. 7.

III. (a) $B^{10}(p, t)B^8$ $\quad Q_m = -18.528$

(b) $Be^9(p, 2n)B^8$ $\quad Q_m = -20.418$

(c) $C^{12}(p, n\alpha)B^8$ $\quad Q_m = -26.136$

See (Al 50g).

† *Note added in proof:* See, however, (Fa 59a).

IV. (a) $B^{10}(\gamma, 2n)B^8$ $Q_m = -27.002$
(b) $B^{11}(\gamma, 3n)B^8$ $Q_m = -38.456$
(c) $C^{12}(\gamma, p3n)B^8$ $Q_m = -54.423$

See (Sh 52).

Li^9

(Not illustrated)

MASS OF Li^9

From the threshold for $Be^9(d, 2p)Li^9$, $E_d = 19 \pm 1$ MeV (Ga 51c), the mass excess of Li^9 is determined as $M-A = 28.1 \pm 1$ MeV.

I. $Li^9(\beta^-)Be^{9*} \rightarrow Be^8+n$ $Q_m = 12.4$

Li^9 decays to excited states of Be^9 which decay by neutron emission. The mean of the reported half-lives is 0.169 ± 0.003 sec (Ga 51c, Ho 52b). See also (Sh 52, Fr 53a, Be 55d, Ta 58b, Fl 56).

II. $Be^9(d, 2p)Li^9$ $Q_m = -15.5$

The threshold is 19 ± 1 MeV (Ga 51c).

III. $B^{11}(\gamma, 2p)Li^9$ $Q_m = -31.4$

See (Sh 52, Ta 58b).

IV. $C^{12}(\gamma, 3p)Li^9$ $Q_m = -47.3$

See (Re 53, Ta 58b).

The following reactions are not reported: $Li^7(t, p)Li^9$ ($Q_m = -2.9$), $Be^9(n, p)Li^9$ ($Q_m = -13.3$), $Be^9(t, He^3)Li^9$ ($Q_m = -14.1$) and $B^{11}(n, He^3)Li^9$ ($Q_m = -23.6$).

Be^9

(Fig. 10, p. 63) †

THEORY

See (Bl 56a, Da 55d, De 56, Fr 55h, Ku 56, Ba 57, Ku 58b, Pa 57a).

I. (a) $Li^6(t, d)Li^7$ $Q_m = 0.994$ $E_b = 17.687$
(b) $Li^6(t, p)Li^8$ $Q_m = 0.803$
(c) $Li^6(t, n)Be^8$ $Q_m = 16.021$
(d) $Li^6(t, \alpha)He^5$ $Q_m = 15.158$
(e) $Li^6(t, n)He^4+He^4$ $Q_m = 16.115$

The differential cross section at 90° for reaction (a) rises steeply from 8.8 mb/sr at $E_t = 0.72$ MeV to 19 mb at 0.90 MeV, and then more slowly to 21 mb at $E_t = 1.15$ MeV. For reaction (d), the differential cross section at 90° rises from 0.75 mb/sr at 0.62 MeV to 5.7 mb/sr at 1.8 MeV and

† For level scheme of B^9, see fig. 11, p. 71.

then decreases slowly to 5.3 mb/sr at 2.2 MeV (R. W. Crews, quoted in Ja 57).

See also (Pe 52), He^5, Li^7, Li^8 and Be^8.

II. $Li^6(\alpha, p)Be^9$ $Q_m = -2.125$

See (Wa 56f).

III. $Li^7(d, p)Li^8$ $Q_m = -0.192$ $E_b = 16.693$

Cross sections have been measured for $E_d = 0.4$ to 1.8 MeV by (Ba 52), and for $E_d = 0.7$ to 3.3 MeV by (Ba 54a); see (Ja 57). The yield for $E_d = 1.1$ to 4.0 MeV has been measured by (Be 56g). Resonances are observed at 0.80 and 1.04 MeV (Ba 52, Ba 54a), 1.4 MeV (Ba 52; see, however, Ba 54a), 2.0, 2.5, and 3.7 MeV (Be 56g; see, however, Ba 54a). See also (Aj 55).

IV. (a) $Li^7(d, n)Be^8$ $Q_m = 15.026$ $E_b = 16.693$

(b) $Li^7(d, \alpha)He^5$ $Q_m = 14.163$

(c) $Li^7(d, n)He^4+He^4$ $Q_m = 15.121$

The cross section for (a) has been measured for $E_d = 70$ to 110 keV by (Ra 55) and that for (b) has been measured for $E_d = 30$ to 250 keV by (Sa 53b). Resonances for neutron production occur, in the range $E_d = 0.2$ to 4.8 MeV, at $E_d = 0.68$ ($\Gamma = 250$ keV), 0.98 ($\Gamma = 60$ keV) and 1.8 MeV ($\Gamma = 400$ keV) (Ba 52, Sl 57). At $E_d = 0.90$ MeV, the α-particles in reaction (b) are isotropic to within 2 per cent, consistent with formation by s-wave deuterons. No evidence is found for direct interaction effects at this energy (Ri 57b). The angular correlation of ground-state α-particles with those resulting from breakup of He^5 indicate $J = \frac{5}{2}^-$ (Ri 56d), $J = \frac{3}{2}^-$ (Fa 57a), for the Be^9 level mainly responsible for this reaction at $E_d = 0.9$ MeV. Reactions (a) and (c) account for less than 10 per cent of the disintegrations at this energy (Ri 56d). See also He^5, Be^8 and (Ca 56h).

V. (a) $Li^7(d, d)Li^7$ $E_b = 16.693$

(b) $Li^7(d, t)Li^6$ $Q_m = -0.994$

(c) $Li^7(d, He^3)He^6$ $Q_m = -4.512$

The cross section for reaction (b) rises steeply from threshold to 95 mb at $E_d = 2.4$ MeV, and then more slowly to about 165 mb at $E_d = 4.1$ MeV (Ma 55d). See also He^6 and Li^7.

VI. $Li^7(t, n)Be^9$ $Q_m = 10.435$

Not observed.

VII. $Li^7(He^3, p)Be^9$ $Q_m = 11.200$

At $E_d = 0.7$ and 1 MeV, proton groups are observed corresponding to excited states of Be^9 at 1.83 ± 0.04 MeV ($\Gamma < 0.4$ MeV), 2.39 ± 0.08 MeV

($\Gamma < 0.2$ MeV), 3.10±0.04 MeV ($\Gamma < 0.3$ MeV), 4.74±0.08 MeV ($\Gamma = 1.25 \pm 0.25$ MeV) and (9.1 ±0.2 MeV) ($\Gamma = 1.2$ MeV) (Al 55b, Mo 54d, Mo 58f). The 1.8-MeV level admits a description in terms of an s-wave n—Be⁸ interaction with a scattering length $a = 23 \times 10^{-13}$ cm (Mo 58f: see $B^{11}(d, \alpha)Be^9$).

VIII. $Li^7(\alpha, d)Be^9$ $\quad Q_m = -7.151$

Not observed.

IX. $Li^9(\beta^-)Be^{9*} \rightarrow Be^8 + n$ $\quad Q_m = 12.4$

See Li⁹.

TABLE 9.1

Energy levels of Be⁹

E_x in Be⁹ (MeV)	$J^\pi; T$	Γ (keV)	Decay	Reactions
0	$\frac{3}{2}^-$		stable	II, VII, XIII, XIV, XV, XVI, XVII, XVIII, XIX, XX, XXII, XXV, XXVI, XXVII
1.75 ±0.02	$\frac{1}{2}^{(+)}$	150	n, γ	VII, X, XIV, XV, XVI, XVII, XXV
2.430±0.002	$(\frac{5}{2}^-)$	<1	(n), α	VII, XIII, XIV, XV, XVI, XVII, XX, XXII, XXV, XXVI
3.04 ±0.016	$(\leq\frac{5}{2})$	161±15		VII, XV, XVI, XVII, XXII, XXV
(4.74 ±0.08)		1250		VII, XV, XVI
6.76 ±0.06				XIII, XV, XVI, XVII
(7.94 ±0.08)				XV
(9.1 ±0.2)		1200		VII
(11.3 ±0.2)			n, γ	X, XV, XVII
(13.3)			n, γ	X
(14.5)				XV
17.28		200	(d, p, n)	III, IV
17.48		50	(d, p, n)	III, IV, XV
(18.1)		(300)	(d, p, n)	III, IV
(18.6)			(d, p)	III
19.6			(d, p)	III, XV
(21.7 ±0.1)			p, γ, n	XI, XV

X. (a) $Be^9(\gamma, n)Be^8$ $\quad Q_m = -1.667$

(b) $Be^9(\gamma, \alpha)He^5$ $\quad Q_m = -2.529$

(c) $Be^9(\gamma, n)He^4 + He^4$ $\quad Q_m = -1.572$

(d) $Be^9(\gamma, 2n)Be^7$ $\quad Q_m = -20.565$

The photo-neutron cross section has been studied from threshold ($E_\gamma = 1.664 \pm 0.004$ MeV: Co 56e) to 320 MeV: see table 9.2. A sharp peak, $\Gamma < 50$ keV, $\sigma \approx 100$ mb, occurs at $E_\gamma = 1.70$ MeV (Co 56e). A further broad maximum appears at $E_\gamma \approx 10$ MeV, followed by the giant resonance at 20—22 MeV (Na 53a, Jo 53f: see Co 56d). Measurements from 6 to 18 MeV show pronounced peaks at 11.3 and 13.3 MeV and a broad, low peak at

16 MeV, immediately preceding the giant resonance (Sp 59). At $E_\gamma = 6.1$ MeV the main processes appear to involve $Be^9(\gamma, n)Be^{8*}$ (2.9) and $Be^9(\gamma, \alpha)He^5$ (Ca 54e). Angular distributions for $E_\gamma = 1.7$ and 1.8 MeV are spheri-

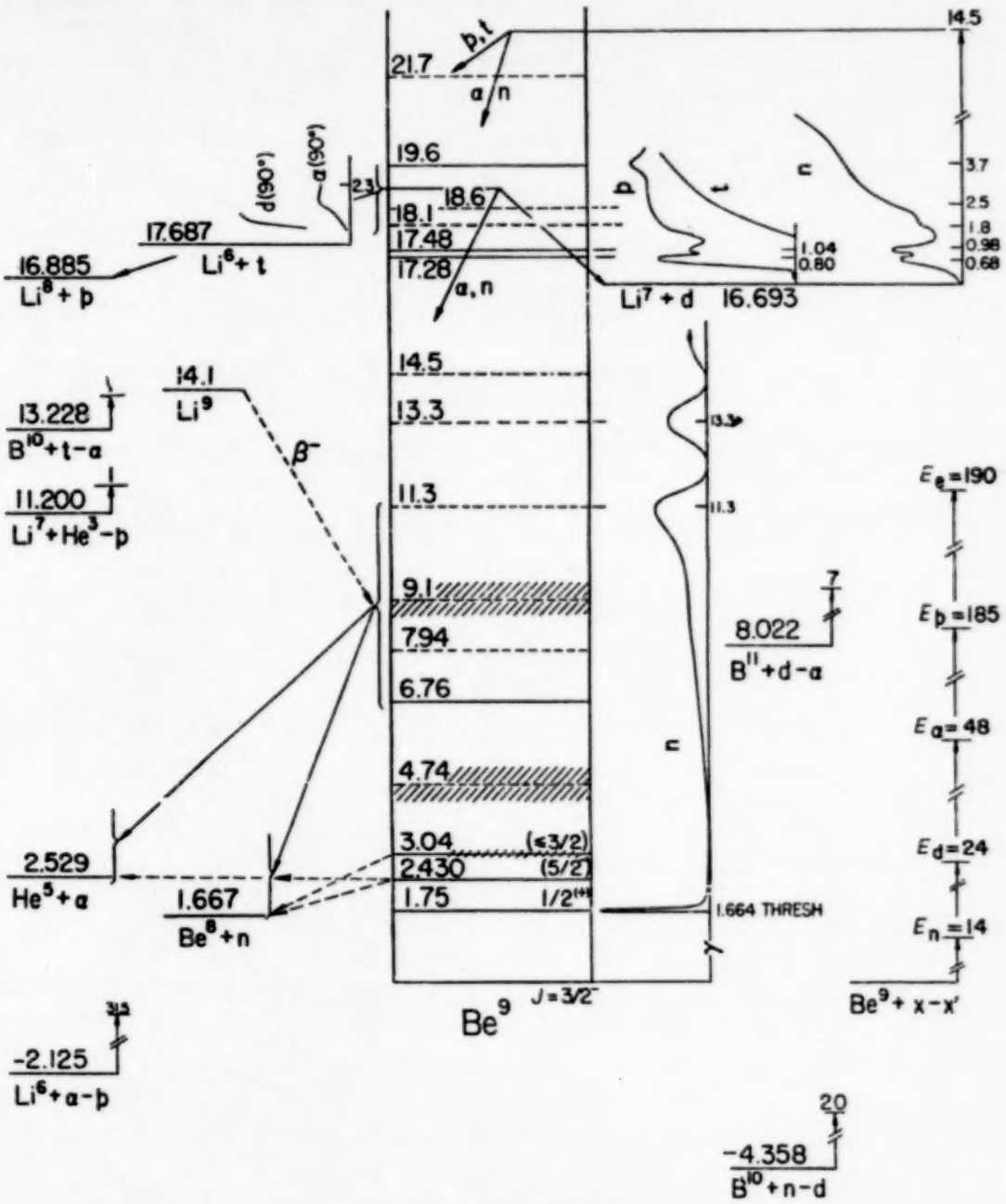

7 January 1959

Fig. 10. Energy levels of Be^9: for notation, see fig. 1, p. 7.

cally symmetric; at $E_\gamma = 2.76$ MeV, $W(\theta) = 1.2+\sin^2\theta$ (Ha 49j: see also Ni 54a, Fa 56a).

Calculations of (Gu 49a) and (Ma 56g) envisage E1 transitions to p^4s

and p^4d configurations, with levels at ≈ 1.8 and ≈ 5 MeV (assuming a fixed well depth). The angular distributions and general trend of the cross section are well accounted for, as is the ratio of $\sigma(\gamma, n)/\sigma(e, e'n)$ (Ba 56l: 6 to 17 MeV). (Co 56e) state, on the other hand, that the 1.70-MeV peak is to be attributed to an M1 transition.

See also (Er 54d, Jo 55f, Ch 58c, Ba 58l) and (Cz 56, Cz 56a, De 56, Ko 57b; theo.).

The cross section for reaction (c) is < 1 mb at $E_\gamma = 1.63$ MeV (Al 52a). For reaction (d) see (Lo 57).

TABLE 9.2

Photoneutron cross section of Be^9

E_γ (MeV)	σ (mb)	Reference
1.69 (Sb^{124})	1.262 ± 0.069	Gi 59a
1.70 (brems.) [a]	100	Co 56e
1.77 (Mn^{56})	0.6	Ru 48: see Ha 53b, Ed 56
1.85 (Y^{88})	0.654 ± 0.031	Gi 59a
2.185 (Pr^{144})	0.39	Ha 53b
2.5 (La^{140})	0.5	Ru 48: see Ha 53b
2.61 (ThC″)	0.39 ± 0.02	Ed 56
2.76 (Na^{24})	0.7	Ru 48: see Ha 53b
	0.674 ± 0.05	Sn 50e
4.4 ($N^{15}(p, \alpha)C^{12}$)	0.186 ± 0.32	Ed 56
6.2 ($F^{19}(p, \alpha)O^{16}$)	1.13 ± 0.16	Ed 56
8.1 ($C^{13}(p, \gamma)N^{14}$)	1.38 ± 0.16	Ed 56
10 [b] (brems.)	1.6	Na 53a
11.3 (brems.)	4.2	Sp 59
12 (brems.)	0.1	Sp 59
13.3 (brems.)	3.0	Sp 59
14.2 (brems.)	0.1	Sp 59
15 (brems.)	0.9	Sp 59
17 (brems.)	0.8	Na 53a
22 [c] (brems.)	3.0	Na 53a
25—320 (brems.)	3—2	Jo 53f

[a] Resonance width < 50 keV.
[b] Broad resonance: $\Gamma \approx 8$ MeV.
[c] Giant resonance.

XI. (a) $Be^9(\gamma, p)Li^8$ $\quad Q_m = -16.885$
(b) $Be^9(\gamma, np)Li^7$ $\quad Q_m = -18.919$

The yield has a broad maximum, $\Gamma = 4.7$ MeV, at $E_\gamma = 22.2$ MeV where $\sigma = 2.72$ mb (Ha 53). The angular and energy distributions of photoprotons produced by bremsstrahlung with $E_{max} = 25$ to 80 MeV has been studied by (Kl 56a, Co 56d). The angular distributions can be accounted for by the direct interaction of γ-rays with individual nucleons (Kl 56a). The energy distributions indicate that transitions to levels in the residual nucleus play

an important part in the direct photoeffect (Kl 56a). (Co 56d) suggest, on the other hand, that the relatively large proportion of low-energy protons indicates predominance of a (γ, n) process, followed by proton emission from Be^8 levels at high excitation. See also (Na 53a, Pa 58, Wh 58, He 53a, Ch 57b, Ch 58c, St 58a).

XII. (a) $Be^9(\gamma, d)Li^7$ $Q_m = -16.693$
(b) $Be^9(\gamma, t)Li^6$ $Q_m = -17.687$
(c) $Be^9(\gamma, \alpha)He^5$ $Q_m = -2.529$

See (Aj 55), (Co 56d, Wh 58) and $Be^9(\gamma, n)Be^8$.

XIII. $Be^9(e, e')Be^{9*}$

Elastic scattering has been studied at $E_e = 125$, 150 and 190 MeV (Ho 53e, Mc 54a). An r.m.s. radius of $2.2 \pm 0.2 \times 10^{-13}$ cm is obtained (Ho 57g: see also Ho 56e). Inelastic peaks corresponding to levels at 2.54 and 6.96 MeV are reported by (Mc 54a). Comparison of $\sigma(\gamma, n)$ and $\sigma(e, e'n)$ for $E_e = 6$ to 17 MeV indicates that the transitions are mainly E1 (Ba 58l). See also Eh 57, Eh 58).

XIV. (a) $Be^9(n, n)Be^9$
(b) $Be^9(n, 2n)Be^8$ $Q_m = -1.667$

The neutron spectrum observed when Be^9 is bombarded with 3.7-MeV neutrons exhibits a structure which is consistent with the excitation of the known states at 0, 1.5, 2.4 and 3.1 MeV, with subsequent neutron emission from the latter two. It is concluded that the (n, 2n) process at this energy proceeds mainly via discrete states of Be^9(Hu 57c, Wa 58b). At the same bombarding energy (Fo 55a) observe two discrete groups in coincidence, suggesting the process $Be^9(n, n')Be^{9*}(2.43) \rightarrow n + Be^8$: see, however, (Bo 57f: $Be^9(\alpha, \alpha')Be^{9*}$). Using monochromatic neutrons with $E_n = 2.6$ to 3.25 MeV, (Fi 57a) finds a sharp threshold for (n, 2n) at $E_n = 2.7$ MeV, corresponding to excitation of $Be^{9*}(2.43)$. On the other hand, (Ma 58f) find evidence for (n, 2n) at $E_n = 2.6$ MeV, below the threshold for (n, n'); at $E_n = 5$ to 6 MeV, the spectra show neutrons from the direct (n, 2n) process. At $E_n = 14$ MeV, the cross section for production of Be^{9*} is 170 ± 30 mb; comparison with $\sigma(n, 2n) = 530 \pm 40$ mb indicates that about $\frac{1}{3}$ of the (n, 2n) processes proceed via $Be^{9*}(2.4)$ (An 58). See also (Ro 57b) and (Be 58d; theo.).

A search for γ-transitions from the 1.8 and 2.4-MeV levels yields upper limits of 0.3 and 0.2 mb, respectively, for $E_n = 2.56$ MeV and 1.8 and 0.3 mb for $E_n = 2.74$ MeV (Da 56d).

Elastic and inelastic neutron angular distributions show forward peaking at $E_n = 14$ MeV (Na 58, An 58): see Be^{10}, (To 58, Re 58c).

XV. $Be^9(p, p)Be^9$

Elastic scattering has been studied at $E_p = 14.5$, 20, and 31.5 MeV by (Ki 56), at 10 MeV by (Ra 56a), at 12 MeV by (Su 58a), at 17 MeV by (Da 56b), at 31 MeV by (Wr 53a, Be 56a, Fi 54d): see also B^{10}. All angular distributions show pronounced diffraction maxima characteristic of the optical model. Analysis in terms of the diffuse-surface optical model is discussed by (Me 57b). See also (Sh 56b, Kl 56).

Inelastic scattering is observed corresponding to levels at (1.8), 2.43, 3.1, 5.0, 6.8, 7.9, 11.3, (14.5), (17.5), (19.9) and (21.7) MeV: see table 9.3. It is

TABLE 9.3

Levels of Be^9 from $Be^9(p, p')$, (d, d') and (α, α')

E_x (MeV)	Γ (keV)	J^π
0		
(1.8)	150 [a]	$(\frac{1}{2}^+)$ [a]
2.433 ±0.003	≦1 [a]	$\frac{1}{2}^-$, $\frac{3}{2}^-$
3.03	>280 [e]	≦$\frac{1}{2}$
5.0 [b] ±0.3		
6.76 [c] ±0.06		$\frac{1}{2}^-$, $\frac{3}{2}^-$, $\frac{5}{2}^-$
7.94 [b] ±0.08		$\frac{1}{2}^+$, $\frac{3}{2}^+$, $\frac{5}{2}^+$, $\frac{7}{2}^+$
11.3 [d] ±0.2		
(14.5) [b]		
(17.5) [b]		
19.9 [b] ±0.1		$\frac{1}{2}^-$, $\frac{3}{2}^-$, $\frac{5}{2}^-$
21.7 [b] ±0.1		$\frac{1}{2}^-$, $\frac{3}{2}^-$, $\frac{5}{2}^-$ or $\frac{1}{2}^+$, $\frac{3}{2}^+$, $\frac{5}{2}^+$

[a] (Go 55e, Su 58a, Bo 57f).
[b] (Be 56a).
[c] This level may be double: see (Br 52c, Be 56a, St 56c, Su 58a, Ty 58).
[d] (Br 52c, Be 56a, St 56c).
[e] See $B^{11}(d, \alpha)Be^9$ (Ka 58a).

not clear whether the structure observed near 1.8 MeV is properly to be attributed to a level at this energy or to a three-body breakup, modified by the proximity of the neutron threshold. If the former is correct, the level width is 0.15 MeV and $J = \frac{1}{2}^+$ (Go 55e, Su 58a). If a three-body breakup is involved, some interaction between the neutron and the Be^8 must be invoked: (Bo 56f) find a satisfactory fit to the observed shape with an s-wave scattering length of 20×10^{-13} cm; see also (Mi 58) and $B^{11}(d, \alpha)Be^9$. It is suggested by (Su 56, Su 58a) that the observed structure is to be understood in terms of a heavy particle stripping process and it is conjectured that the 4.8-MeV level may reflect the same effect, involving $Be^{8*}(2.9)$; see, however, (Mi 58).

A continuous distribution of neutrons, observed for $E_p > 4.5$ MeV is

attributed to formation of $Be^{9*}(2.4)$ with subsequent breakup into $n+Be^{8*}$ (2.9) (Ma 59). Breakup into (Be^8+n) occurs in 12 ± 5 % of transitions (J. B. Marion, private communication).

The energy of the 2.4-MeV level is given as 2433 ± 5 (Br 51f), 2434 ± 5 (Bo 56f), 2432 ± 4 keV (Go 55e); the width is $\leqq 1$ keV (Go 55e). Analysis of angular distributions at $E_p = 12$ MeV in terms of direct interaction plus compound nucleus formation indicate $J = \frac{1}{2}^-$ or $\frac{5}{2}^-$ (Su 58a). At $E_p = 31$ MeV, analysis indicates $J = \frac{1}{2}^+$, $\frac{3}{2}^+$ or $\frac{5}{2}^+$ (Be 56a: see, however, Su 58a). Results at $E_p = 10$ MeV are consistent with odd parity (Ra 56a). See also B^{10}(n, d)Be^9 and (Da 52b).

The 3.03 ± 0.03 MeV level has a width > 0.28 MeV; the Wigner limit then restricts l_n to 0 or 1, $J \leqq \frac{3}{2}$ (Bo 56f; see, however, B^{11}(d, α)Be^9). Angular distributions for the higher levels have been studied by (Be 56a); the resulting spin assignments are given in table 9.3. See also (Fi 54d, Gr 55a, Ty 58), (Bl 56a; theo.).

XVI. Be^9(d, d')Be^{9*}

Elastic scattering angular distributions have been studied at $E_d = 24$ MeV by (Su 58a). See also (Gu 47, El 52) and B^{11}.

Inelastic groups are reported corresponding to levels at (1.7), 2.4, 3.01 ± 0.1 ($\Gamma \approx 0.3$), 4.8, and 6.8 MeV (Ra 55b, Gr 56b, Mi 58, Su 58a). The structure at $Q = -1.7$ MeV may be accounted for as a three-body breakup with an s-wave (n—Be^8) interaction characterized by a scattering length of 20×10^{-13} cm, or by a resonance of about single-particle width. In either case a $J = \frac{1}{2}^+$ level of Be^9 is indicated near the binding energy (Mi 58, Ra 55b: see also B^{11}(d, α)Be^9). The angular distribution of the $Q = -2.43$-MeV group has been studied at $E_d = 15$ MeV (Ha 56c) and $E_d = 24$ MeV (Su 58a). Analysis by direct interaction theory yields $l = 2$, $J = \frac{1}{2}^-$, $\frac{5}{2}^-$ or $\frac{7}{2}^-$ (Su 58a: see, however, Ha 56c). See also (Su 56b).

XVII. $Be^9(\alpha, \alpha')Be^{9*}$

Elastic scattering has been studied at $E_\alpha = 48$ MeV by (Su 58a).

Inelastic groups are observed corresponding to Be^{9*} = (1.8), 2.4, (3.1), 6.8 and 11.3 MeV (Ra 55b, Fa 56, Su 58a). The group corresponding to the 1.8-MeV "level" has a peak at $Q = -1.83\pm0.03$ MeV, $\Gamma \approx 200$ keV. It is suggested, however, that just such a structure would be expected from a heavy particle stripping process in which the proton also escapes, preferentially with the maximum possible energy. In this case, the 4.8-MeV "level" might arise from a similar process, in which the final nucleus is now $Be^{8*}(2.9)$. The angular distribution of the $Q = -2.4$ MeV group at $E_\alpha = 48$ MeV indicates $l = 2$, $J = \frac{1}{2}^-$, $\frac{5}{2}^-$ or $\frac{7}{2}^-$ (Su 58a). Measurement of the momentum and angular distributions of α-particles from the breakup of $Be^{9*}(2.4)$ indicate that the decay proceeds mainly via He^4+He^5, or by direct three-

body breakup. Gamma decay is < 1 per cent, neutron emission to $Be^8(0)$ is < 10 per cent (Bo 57f). See also (Bl 56a, Pi 58a; theo.).

XVIII. (a) $Be^9(p, d)Be^8$ $Q_m = 0.560$
(b) $Be^9(d, t)Be^8$ $Q_m = 4.592$

At $E_p = 95$ MeV, two groups of deuterons are observed from reaction (a), corresponding to Be^8(g.s.) and to states near 17 MeV. It is suggested that these reflect the "snatching" of the loosely bound neutron or of one of the tightly bound "alpha-particle" neutrons, respectively. Angular distributions lend some support to the α-particle model of Be^9; the occurrence of high momenta for the tightly bound neutrons indicates the operation of strong short-range two-body forces (Se 56a).

Angular distributions at $E_p = 6.5$ and 22 MeV, and at $E_d = 7.7$ MeV are analyzed in terms of pickup theory, using a square-well (n—Be^8) interaction to represent the ground state of Be^9 (Da 55b, Da 55d). See also B^{10}, B^{11}.

XIX. (a) $B^{10}(\gamma, p)Be^9$ $Q_m = -6.585$
(b) $B^{10}(\gamma, p)Be^8+n$ $Q_m = -8.251$

For reaction (a) see (Go 56k, Go 56l). For reaction (b) see Be^8 and B^{10}.

XX. $B^{10}(n, d)Be^9$ $Q_m = -4.358$

At $E_n = 14$ MeV, the ground state and the level at 2.43 MeV are observed. No other deuteron groups were detected below $E_x \approx 5.5$ MeV. The angular distribution of the deuterons, analyzed by pickup theory, indicate odd parity, $\frac{1}{2} < J \leqq \frac{9}{2}$ for both states (Ri 54a). See also (Fr 56a), (Fr 55h; theo.) and B^{11}.

XXI. $B^{10}(d, He^3)Be^9$ $Q_m = -1.091$
Not observed.

XXII. $B^{10}(t, \alpha)Be^9$ $Q_m = 13.228$

At $E_t = 1$ MeV, α-groups are observed corresponding to Be^9 levels at 2.39 and 3.06 MeV (Al 55b).

XXIII. $B^{11}(n, t)Be^9$ $Q_m = -9.564$
Not observed.

XXIV. $B^{11}(p, He^3)Be^9$ $Q_m = -10.329$
Not observed.

XXV. $B^{11}(d, \alpha)Be^9$ $Q_m = 8.022$
$Q_0 = 8.015 \pm 0.010$ MeV (Bo 56f).

Alpha-particle groups are reported to states at (1.75), 2.4 and 3.0 MeV. The structure corresponding to the 1.75-MeV state can be explained in

terms of an (n—Be⁸) interaction with a scattering length a of 20×10^{-13} cm or in terms of a resonance near threshold, with $\theta^2 \approx 1$ (Bo 56f, Mi 58). (Ka 58a) find, on the other hand, that a value of $a \geqq 80\times10^{-13}$ cm is required to fit their distribution and suggest that the (n—Be⁸) interaction must be very near resonance on this model. The energy of the 2.4-MeV state is given as 2422±5 keV by (Va 51), 2431±6 keV (El 54), 2424±5 keV (Bo 56f). The next state is located at 3.02±0.03 (Le 55d), 3.05±0.03 MeV (Bo 56f). The width is ≈ 0.3 MeV (Bo 56f), $\Gamma_{c.m.} = 161\pm15$ keV (Ka 58a). See also (Ho 55f).

XXVI. $C^{12}(n, \alpha)Be^9$ $Q_m = -5.709$

At $E_n = 14$ MeV, the cross section to the ground state of Be⁹ is 80±20 mb; that to the 2.43-MeV level, $\sigma_{2.43}$, is $10 \leqq \sigma_{2.43} \leqq 210$ mb (Gr 55b).

XXVII. $C^{13}(\gamma, \alpha)Be^9$ $Q_m = -10.654$

See (Mi 53c).

B⁹

(Fig. 11, p. 71) †

I. $Li^6(He^3, p)Be^8$ $Q_m = 16.786$ $E_b = 16.598$

The excitation functions for protons leading to the ground and 2.9-MeV excited states of Be⁸ have been measured for $E(He^3) = 0.9$ to 5.1 MeV ($\theta = 0°$ and 150°, lab.). Resonances are observed at $E(He^3) = 1.6$ MeV ($\Gamma = 0.25$ MeV, $B^{9*} = 17.6$ MeV) and 3.0 MeV ($\Gamma = 1.5$ MeV, $B^{9*} = 18.6$ MeV) (Sc 56f). However, J. W. Butler (private communication) suggests that the decrease in the yield for $E(He^3) \gtrsim 3$ MeV can be accounted for by competition from the $Li^6(He^3, n)B^8$ reaction with a threshold at 2.966 MeV. Angular distributions, taken at 6 energies, are isotropic at ≈ 1 MeV and become increasingly asymmetric at higher energies. In particular, the ground state protons exhibit strong backward peaking for $E(He^3) \gtrsim 3$ MeV (Sc 56f).

II. $Li^6(\alpha, n)B^9$ $Q_m = -3.979$

See (Ro 56).

III. $Li^7(He^3, n)B^9$ $Q_m = 9.346$

Not reported.

IV. $Be^9(p, n)B^9$ $Q_m = -1.854$

The width of the ground state is < 2 keV (St 51e). At $E_p = 6.59$ MeV, a neutron group is observed corresponding to a level at 2.37±0.04 MeV. A continuous distribution of neutrons, attributed to the (p, p'n) reaction, is also observed (Aj 53, Ma 59: see also Jo 50a and Be⁹). For $E_p = 2$ to 5.8 MeV,

† For level scheme of Be⁹, see fig. 10, p. 63.

two neutron thresholds have been observed at $E_p = 2.060 \pm 0.003$ and 4.645 ± 0.005 MeV ($B^{9*} = 2.326 \pm 0.006$ MeV$+\frac{1}{2}\Gamma$). The continued slow neutron yield above threshold suggests $l = 1$ neutron emission (Ma 55k). A broad threshold reported at $E_p = 3.6$ MeV appears to have been due to variation in counter sensitivity. It is possible, however, that part of the continuum neutron spectrum arises from a B^9 level expected near 1.4 MeV (Ma 59). See also (Bo 58, Ki 57a).

V. $Be^9(He^3, t)B^9$ $\quad Q_m = -1.089$

The ground state angular distributions are peaked in the forward direction at $E(He^3) = 5.7$ MeV (S. Hinds and R. Middleton) and 21 MeV (We 58c).

VI. $B^{10}(\gamma, n)B^9$ $\quad Q_m = -8.439$

See (Sh 51d).

TABLE 9.4

Energy levels of B^9

E_x in B^9 (MeV)	J^π	Γ (keV)	Decay	Reactions
0	$>\frac{1}{2}^-$	<2	(p, α)	IV, V, VI, VII, VIII, IX, XI
2.37 ± 0.02	$>\frac{1}{2}^-$	80	(p, α)	IV, VII, IX, XI
2.83 ± 0.03		300		IX
(7.0)				XI[g]
17.6		170	p, He^3, α	I
(18.6)		1000	p, He^3, α	I

VII. $B^{10}(p, d)B^9$ $\quad Q_m = -6.212$

At $E_p = 18.9$ MeV, deuteron groups are observed corresponding to the ground state of B^9 and to an excited state at 2.40 ± 0.15 MeV. The angular distributions to both states, analyzed by pickup theory, show an $l = 1$ transfer, indicating odd parity, $\frac{1}{2} < J \leqq \frac{9}{2}$, for these states (Re 56). The ratio of cross sections is in good agreement with an intermediate-coupling calculation (Fr 55h).

VIII. $B^{10}(d, t)B^9$ $\quad Q_m = -2.180$

$Q_0 = -2.187 \pm 0.010$ (Bo 56f).

IX. $B^{10}(He^3, \alpha)B^9$ $\quad Q_m = 12.139$

At $E(He^3) = 1$ MeV, alpha-particle groups have been observed corresponding to the ground state of B^9 and to an excited state at 2.58 ± 0.13 MeV (Al 55b). At $E(He^3) = 2$ to 3 MeV, groups are observed corresponding to the ground state and to levels at $E_x = 2.37 \pm 0.02$ MeV and

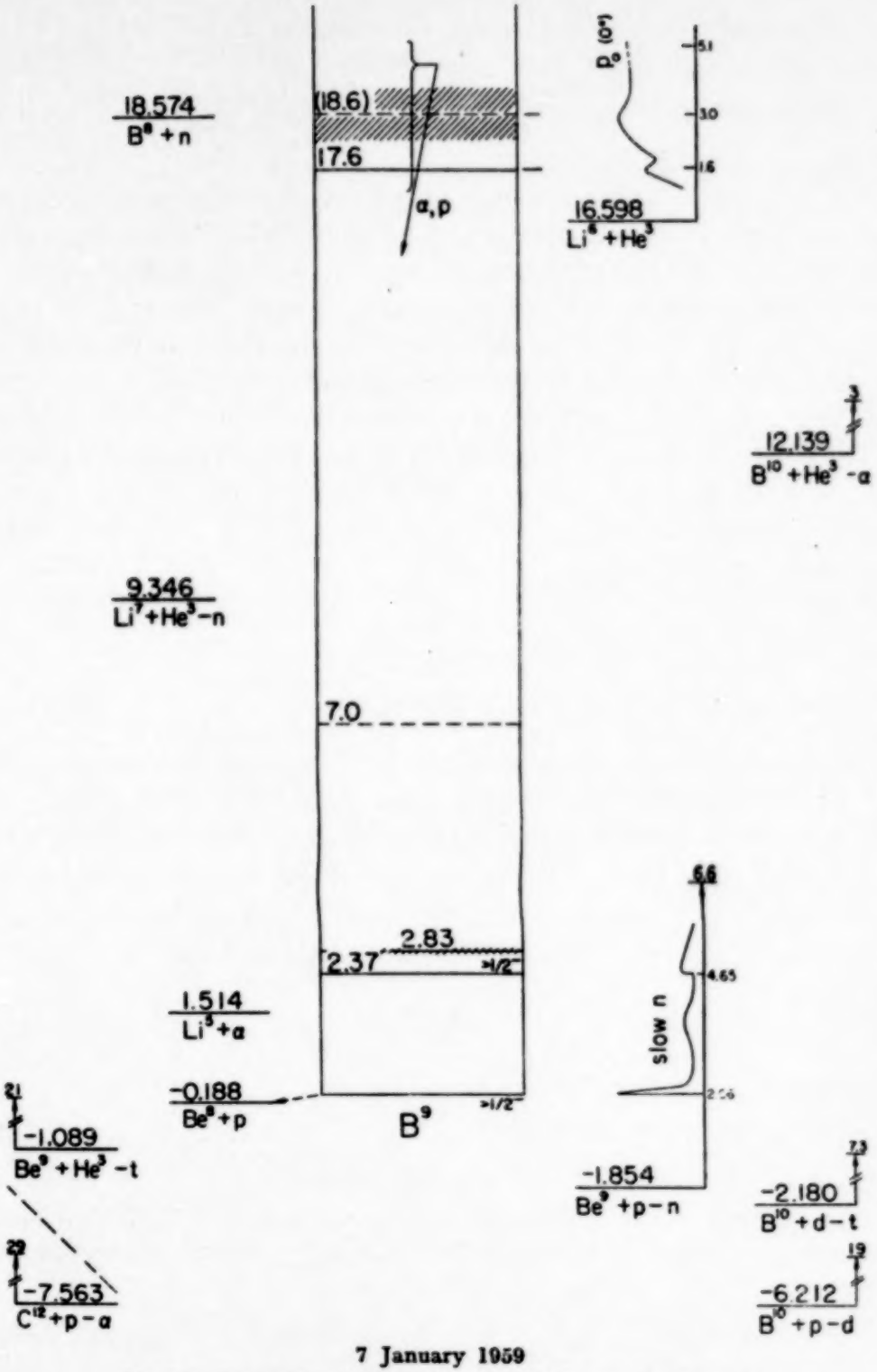

7 January 1959

Fig. 11. Energy levels of B^9: for notation, see fig. 1, p. 7.

2.83±0.03 MeV. The widths are 80 keV and 300 keV for B^{9*}(2.37) and (2.83) respectively. There is no evidence of a well-defined state corresponding to Be^{9*}(1.75) (Po 58a, Po 59). See also (Sp 59a).

X. $B^{11}(p, t)B^9$ $Q_m = -11.418$

Not observed.

XI. $C^{12}(p, \alpha)B^9$ $Q_m = -7.563$

$Q_0 = -7.58 \pm 0.1$ (Re 55a).

At $E_p = 18.8$ MeV, alpha-particle groups have been observed to the ground state of B^9 and to an excited state at 2.39 ± 0.08 MeV. The two α-groups are superimposed on a background possibly due to $C^{12}(p, p')C^{12*} \rightarrow 3\alpha$. The average differential cross section for the ground state group at $E_p \approx 18$ MeV is 3 ± 1 mb/sr. No other groups were observed up to $E_x \approx 7.9$ MeV (Re 55a). The angular distribution of the ground state group at $E_p = 15.6$ to 18.6 MeV is consistent with triton pickup or knock-on theories, except for discrepancies at low angles (Ma 58i). At $E_p = 29$ MeV, the reaction appears to go to the ground state and to a level at 3.2 ± 1.0 MeV (Ne 55c: stars in a cloud chamber; $C^{12} + p \rightarrow \alpha + B^9 \rightarrow 3\alpha + p$). At $E_p = 32$ MeV, groups corresponding to B^{9*}(g.s.), (2.4) and a new level at 7.0 MeV are observed (Kn 58).

C^9

(Not illustrated)

Comparison with the mass of Li^9 leads to an estimated mass excess of 32.3 ± 2 MeV (Aj 55). Analysis of a single star attributed to β-decay of C^9 and subsequent breakup into $p + 2\alpha$ yields $Q > 15.4$ MeV, mass excess > 30.2 MeV (Sw 56a). Stability against $B^8 + p$ requires a mass excess < 32.9 MeV. Two reactions leading to C^9 which have not been reported are $Be^7(He^3, n)C^9$ ($Q_m = -7$) and $C^{12}(\gamma, 3n)C^9$ ($Q_m = -54$).

Be^{10}

(Fig. 12, p. 75) †

THEORY

See (Ku 56, Fr 57, Fr 58b).

I. $Be^{10}(\beta^-)B^{10}$ $Q_m = 0.556$

The weighted mean end-point energy is 0.556 ± 0.003 MeV (Li 51a). The mean half-life is $(2.7 \pm 0.4) \times 10^6$ y (Ku 49a): $\log ft = 13.65$ (Fe 51b). The spectrum is of the D_2 type (Wu 50).

II. (a) $Li^7(t, \alpha)He^6$ $Q_m = 9.807$ $E_b = 17.246$

(b) $Li^7(t, 2n)Be^8$ $Q_m = 8.768$

(c) $Li^7(t, n)Be^9$ $Q_m = 10.435$

(d) $Li^7(t, n)He^5 + He^4$ $Q_m = 7.905$

The neutron yield (elemental Li) at 0° exhibits two broad resonances,

† For level scheme of C^{10}, see fig. 15, p. 92.

at $E_t = 0.84$ and 1.70 MeV. The angular distributions are not isotropic (Cr 51b). The cross section for reaction (a) has been measured for $E_t = 0.6$ to 2.3 MeV ($\theta = 90°$ and 165°): both the yield of $He^6(0)$ and $He^{6*}(1.71)$ α-particles show a broad resonance at $E_t \approx 1.7$ MeV. At $E_t = 1.8$ MeV, $\theta = 90°$, the differential cross section is 2.6 mb/sr for $He^6(0)$ and 8 mb/sr for $He^{6*}(1.71)$ (Ja 57).

At $E_t = 0.24$ MeV the ground state α-particles are distributed as $W(\theta_{c.m.}) = 1-(0.66\pm0.06)\cos^2\theta$, while those corresponding to the 1.7-MeV state of He^6 are isotropic within 8 per cent. The formation of the 1.7-MeV state is 8 times more probable than the formation of the ground state. These results indicate p-wave formation of the 0.84-MeV resonance and $J = 2^+$ for the 17.83-MeV state (De 52, Ch 53d and Al 54d). See also He^6 and (Ma 56k).

III. $Li^7(\alpha, p)Be^{10}$ $\qquad Q_m = -2.566$

At $E_\alpha = 31.5$ MeV, proton groups are observed leading to the ground and first excited state of Be^{10} (Wa 56f).

IV. $Be^9(n, \gamma)Be^{10}$ $\qquad Q_m = 6.812$

The thermal capture cross section is 10 ± 1 mb (Hu 58). In addition to the ground-state transition, a 3.41 ± 0.06-MeV γ-ray is observed, attributed to a cascade through the 3.4-MeV state. The intensity of the cascade transition is ≈ 0.25 photon/capture (Ba 53d), 0.27 photon/capture (Gr 55g). See also (Wi 53f).

V. $Be^9(n, n)Be^9$ $\qquad E_b = 6.812$

The total cross section is constant at 6.04 ± 0.03 b from 0.1 eV to 100 keV (Hu 58): the spin dependent scattering is < 0.003 b (Pa 52).

In the region $E_n = 0$ to 18 MeV, three resonances are reported at 0.62, 0.81 and 2.73 MeV. The parameters of these resonances are exhibited in table 10.2.

Angular distributions have been measured for $E_n = 0.54$ to 0.70 MeV by (Wi 55d). The patterns are symmetric about 90° in this range, indicating absence of interference between resonance and potential scattering waves of opposite parity. The 0.62-MeV resonance has $J = 3$; a satisfactory fit to the angular distribution is obtained with the assumption of p-wave formation in channel spin 2, with s-wave potential scattering all in channel spin 1. It is observed that the assumption of spin-dependent potential scattering is at variance with observation at thermal energies (see also La 56b). The possibility of d-wave formation is not excluded. The cross section at the 0.81-MeV resonance is consistent with $J = 2$ (Wi 55d). A comparison of reduced widths suggests a close correspondence between $Be^{10*}(7.37)$, (7.54) and the two B^{10} levels at 8.89 MeV (Ma 56h).

Differential elastic scattering cross sections have been measured in the

non-resonant regions from $E_n = 0.7$ to 3.0 MeV (Fo 57, Fo 58b) and analyzed in terms of phase shifts (Fo 57). For $E_n = 1.0$ to 2.0 MeV, an appreciable p-wave contribution is observed (Fo 58b).

TABLE 10.1
Energy levels of Be^{10}

E_x in Be^{10} (MeV)	J^π	Γ or τ (keV)	Decay	Reactions
0	0^+	$\tau_{\frac{1}{2}} = (2.7\pm0.4)\times10^6$ y	β^-	I, III, IV, IX, XII, XVIII
3.368 ± 0.009	2^+	$\tau_m < 3.0\times10^{-13}$ sec	γ	III, IV, IX
5.959 ± 0.009	1^-	sharp	γ	IX
6.178 ± 0.009		sharp		IX
6.262 ± 0.009	2^-	sharp	(γ)	IX
$7.37\ \pm0.01$	$3(^+)$	25 ± 4	n	V, IX
$7.54\ \pm0.01$	2	8 ± 3	n	V, IX
9.27	$(^-)$	≈100	n	V, IX
(9.4)	(2^+)	broad	(n)	V, (VIII)
17.83	(2^+)		n, t, α	II
18.43			n, t, α	II

The shape of the 2.73-MeV structure suggests that there may actually be two levels involved, at $E_p = 2.73$ MeV, $\Gamma \approx 0.1$ MeV, and a broad state at $E_p = 2.85$ MeV (Bo 51c; see, however, the similar situation in B^{10}(Ma 59)).

The elastic scattering in this region changes from being nearly symmetric at 2.4 MeV to being peaked forward at 2.9 MeV. This evidence also suggests two resonances and, together, with the $Be^9(n,\alpha)He^6$ results of (St 57d) probably identifies the broad 2.9-MeV resonance as formed by p-wave

TABLE 10.2
Resonances in $Be^9(n,n)Be^9$

E_{res} (MeV)	Be^{10*} (MeV)	J^π	l	Γ (keV)	σ (b)	θ_n^2 (per cent)	References
0.62 ± 0.01	7.37	3		30	3.7[a]	1.7[d]	Bo 51c
		$3^{(+)}$	1, (2)	25 ± 4	4.35[a]		Wi 55d,
					7.75[b]		Hu 55c, Hu 58
0.81 ± 0.01	7.54	>0	≥1	≤11	≈1.3[a]		Bo 51c, Hu 55c
		2	1, 2	8 ± 3	5.25[b]	0.34[e]	Wi 55d, Hu 58
2.73[c]	9.27	$(^-)$[f]		100	≈4[b]		Bo 51c
(2.85)	(9.4)	(2^+)[f]	(1)	(≈400)			Bo 51c

[a] Cross section above background.
[b] Includes background.
[c] The large cross section, peak asymmetry and angular distributions suggest two resonances, a sharp one at 2.73 MeV and a much broader one at $\approx$ 2.85 MeV (Bo 51c, Fo 58b).
[d] Assuming $l = 1$, $R = 4.3\times10^{-13}$ cm.
[e] (Ma 56h), assuming $l = 1$.
[f] (Fo 58b).

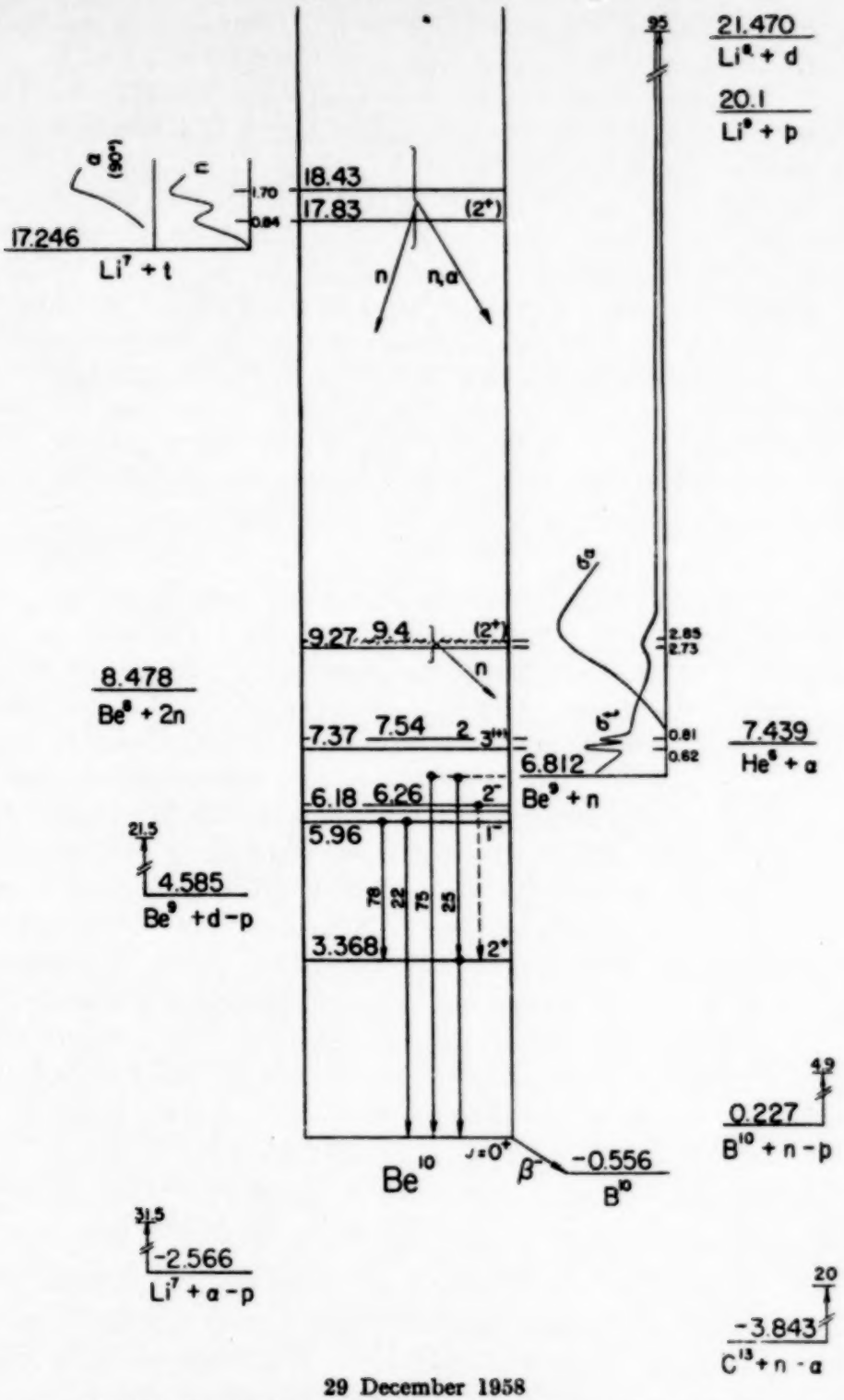

29 December 1958

Fig. 12. Energy levels of Be^{10}: for notation, see fig. 1, p. 7.

neutrons with $J = 2^+$ for $Be^{10*}(9.4)$ (Fo 58b). Polarization measurements at $E_p = 3.1$ MeV indicate interference between a broad $d_{\frac{3}{2}}$ resonance and $s_{\frac{1}{2}}$

hard-sphere scattering (Mc 57). Other measurements of differential cross sections from $E_n = 0.06$ to 1.80 MeV are reported by (La 57c, La 56b), from 2.30 to 3.66 MeV by (Me 53), at 4.1 MeV by (Wa 55a), 7.0 MeV by (Be 56e), and 14.2 MeV by (An 57) and (Na 58). At the higher energies, the neutrons show strong optical-model effects.

The total cross section decreases from 2.14 b at 3.8 MeV to 1.7 b at 8.7 MeV (Bo 57a, Be 56c, Wa 55a, Ma 58f, Br 58h); see also (Hu 58). At $E_n = 12.7$ MeV, $\sigma_t = 1.60$ b (Ne 53a, Ta 55, Br 58h) and at $E_n = 14.1$ MeV, $\sigma_t = 1.55$ b (Ta 55), 1.49 ± 0.02 b (Co 54f), 1.53 ± 0.03 b (Co 52h), 1.46 ± 0.03 b (Kh 57a), 1.51 ± 0.02 b (Br 58h). The cross section then decreases monotonically to 1.38 ± 0.03 b at $E_n = 18.0$ MeV (Co 54f). Non-elastic cross sections are given by (Wa 55a, Be 55f, Be 55b, Ma 55n, Fl 56a, Ma 58f, Ma 58j, Ro 57b, Be 56e, Ta 55, Mc 58c, Ba 58g). See also (Hu 57), $Be^9(n, n')Be^{9*}$, $Be^9(n, 2n)Be^8$ and $Be^9(n,\alpha)He^6$. See also (La 56d, Za 57, He 56d, St 57e).

VI. (a) $Be^9(n, 2n)Be^8$ $Q_m = -1.666$ $E_b = 6.812$
(b) $Be^9(n, n')Be^{9*}$

The cross section for reaction (a) has been measured for $E_n = 2.6$ to 3.2 MeV. A sharp increase is reported at $E_n = 2.70$ MeV, threshold for process (b): $Be^9(n, n')Be^{9*}(2.4) \rightarrow n + Be^8$; the resonance at $E_p = 2.73$ MeV (see $Be^9(n, n)Be^9$) does not appear (Fi 57a: see, however, Ed 56a). It is suggested that the (n, 2n) reaction mainly proceeds via process (b) in this energy region (Fo 55a, Fi 57a). On the other hand (Ma 58f) report evidence from energy spectra that the direct (n, 2n) process occurs for $E_n = 2.6$ to 6 MeV. See Be^9. The absolute cross section $\sigma(n, 2n)$ rises linearly from 0.1 b at 2.8 MeV to 0.7 b at 3.25 MeV (Fi 57a). The 90° differential cross section at $E_n = 3.7$ MeV is 39 ± 8 mb/sr (Hu 57c, Wa 58b), 27 ± 6 mb/sr (Fo 55a: quoted in Hu 57c). The cross section for Ra-Be and Po-Be neutrons is 0.37 ± 0.06 b (Ed 56a). The average cross section for $E_n = 2$ to 11 MeV is 0.20 ± 0.12 b (Va 57a). At $E_n = 14$ MeV, the cross section is 0.42 ± 0.07 b (Ro 57b, St 57), in agreement with predictions of (Sa 56a) but not of (Ma 53j). (As 58) finds $\sigma = 0.54 \pm 0.04$ b at $E_n = 14.1$ MeV. See also (Ho 50b, Ag 52, Be 58d, Du 57a, Ho 58c, An 58).

VII. $Be^9(n, t)Li^7$ $Q_m = -10.435$ $E_b = 6.812$

At $E_n = 14$ MeV, $\sigma(n, t) = 18 \pm 1.5$ mb (Wy 58a). See also (Va 57a).

VIII. $Be^9(n, \alpha)He^6$ $Q_m = -0.628$ $E_b = 6.812$

The cross section for production of He^6 has been measured for $E_n = 0.7$ to 4.4 MeV by (St 57d), for $E_n = 1$ to 6 MeV by (Va 57c) and for $E_n = 3.3$ to 6.1 MeV by (Sa 55c). (St 57d) find only a smooth rise to a broad maximum of 104 ± 7 mb at 3.0 MeV, followed by a gradual decrease to 70 mb at 4.4 MeV, possibly to be attributed to competition by $Be^9(n, 2n)Be^8$. No indication of resonance is found at $E_n = 2.7$ MeV. Weak resonances are reported at

$E_n = 3.73$ and 4.27 MeV by (Sa 55c). The cross section at $E_n = 14$ MeV is 10 ± 1 mb (Ba 53). See also (Al 47b, Va 57a).

IX. $Be^9(d, p)Be^{10}$ $\quad Q_m = 4.585$

Levels reported by (Ju 54, Ju 54b, Gr 56b, Ca 58a) are listed in table 10.3.

TABLE 10.3
Levels of Be^{10} from $Be^9(d, p)Be^{10}$

Be^{10} [a] (MeV)	Γ [a] (keV)	l_n [c]	l_n [b]	J^π	θ_n^2 [d] (per cent)
0		1	1	0^+	5–9
3.368 ± 0.009		1	1	2^+	1
5.959 ± 0.009		0	0(1)	1^-, (2^-)	15
6.178 ± 0.009					(0.5)
6.262 ± 0.009		0	0(1)	(1^-), 2^-	8
7.37	≈ 25	1		(2^+), 3^+	1.2–1.4
			2	$0^-, 1^-, 2^-, 3^-, 4^-$	
7.54	< 10				0.34
9.27 [b]					

[a] (Ju 54, Ju 54b).
[b] (Ca 58a: $E_d = 14.9$ MeV).
[c] (Gr 56b: $E_d = 9.0$ MeV).
[d] Computed by (Me 58b) from data of (Fu 54, Gr 56b, Bo 51c, Ma 56h, and others). See also (Fr 57).

At $E_d = 7$ MeV the group corresponding to $Be^{10*}(6.18)$ is only 5 per cent as intense as that corresponding to $Be^{10*}(6.26)$. The upper limit to the intensity of other groups is 3 per cent (Ju 54: $\theta = 90°$, $E_d = 5.4$—7.4 MeV).

Angular distributions of the protons to Be^{10}(g.s.) and (3.37) have been studied at many energies from $E_d = 1$ to 14.9 MeV: see (Eb 54, Va 56c, Ju 55, Ju 55b, Ju 56g, Ju 57, Ze 56, Mi 58a, Sm 57a, Gr 56b, Co 57a, Ca 58a, Aj 52c, Aj 55). Except at the lowest energies, the stripping process appears to dominate. At $E_d = 9$ MeV, the ratio of the maximum differential cross sections of the $Be^9(d, p)Be^{10}$(g.s.) and $Be^9(d, n)B^{10*}(1.74)$ reactions is 1.64 ± 0.25; $\gamma_n^2/\gamma_p^2 = 2.16$ (calculated from stripping theory; predicted value = 2) (Ca 56b). See also B^{11} and (Gr 56g; theo.).

The 3.37-MeV level has $J = 2^+$, established by the (p, γ) correlation ($J \geqq 2$), the stripping pattern ($J \leqq 3^+$) and the internal pair formation coefficient (E1, M1 or E2): see (Aj 55, Ch 58b). Detailed study of the (p, γ) correlation at $E_d = 2.5$ to 3.9 MeV confirms this assignment and fixes the channel spin mixture (for capture of $l = 1$ neutrons) as 10 per cent $J_c = 1$, 90 per cent $J_c = 2$. This mixture is just that expected in pure L-S coupling for a $^3P_2$ state (Co 57a). Similar results are reported at $E_d = 7.7$ MeV by (Pa 58d). The gamma-ray energy is 3351 ± 27 (Ma 53e), 3400 ± 30 (Mc 57a), 3360 ± 30 keV (Me 58b). Comparison of the γ-energy at $E_d = 3.2$ MeV with recoils in vacuum and recoils stopped in Ta reveals no

effect on the Doppler shift and sets an upper limit of 3.0×10^{-13} sec on the mean lifetime. A value of 0.4 to 1.0×10^{-12} sec is expected for a single-particle E2 transition (Ko 59). It thus appears that shifts of some 20—30 keV should be subtracted from the observed γ-energies.

From the stripping pattern, the 5.96-MeV level is assigned $J = 1^-$ or 2^-(table 10.3). A gamma ray of energy 5.98 ± 0.04 (Ma 53e), 6.035 ± 0.04 (Mc 57a, Be 55g), 6.01 ± 0.06 MeV (Me 58b) is assigned to this level, as is another, of energy 2.54 ± 0.04 MeV (Me 58b: Be^{10*} 5.96 → 3.37). The fact that the cascade and direct transitions are roughly comparable in intensity fixes $J = 1^-$ (Me 58b).

The 6.26-MeV level ($J = 1^-$ or 2^-) appears to decay only to the 3.37-MeV level: the absence of the ground state transition indicates $J = 2^-$ (Me 58b). The 7.37-MeV level presents some difficulty. From stripping results $l_n = 1$, $J = 2^+, 3^+$ (see, however Ca 58a); from Be^9(n, n), $J = 3$ and $l_n = 1$, possibly 2. The reduced width appears to be nearly the same as that of the 3.37-MeV level and $J = 2^+$ is suggested. Shell-model calculations indicate a vanishing width if $J = 3^+$ (Gr 56b, Fr 57). The polarization of ground-state protons has been studied by (Hi 58a). See also (Ge 56e, Ha 57h, Tu 56).

X. Be^9(t, d)Be^{10} $Q_m = 0.553$
Not reported.

XI. Be^9(α, He^3)Be^{10} $Q_m = -13.766$
Not reported.

XII. B^{10}(n, p)Be^{10} $Q_m = 0.227$
See (Ja 55e, Eg 48).

XIII. B^{10}(α, He^3)Be^{10} $Q_m = -0.538$
Not reported.

XIV. B^{11}(n, d)Be^{10} $Q_m = -9.010$
Not reported.

XV. B^{11}(p,2p)Be^{10} $Q_m = -11.237$
See (Ty 58b, Ma 58h).

XVI. B^{11}(d, He^3)Be^{10} $Q_m = -5.743$
Not reported.

XVII. B^{11}(t, α)Be^{10} $Q_m = 8.576$
Not reported.

XVIII. C^{13}(n, α)Be^{10} $Q_m = -3.843$
See C^{14}.

B^{10}

(Fig. 13, p. 81)

THEORY

See (Fr 55h, Ku 56, Fr 57, Ku 57a, Ku 58a, Gr 57d, Fr 58b, Wa 59).

I. $Li^6(\alpha, \gamma)B^{10}$ $Q_m = 4.459$

Five resonances are observed in the range $E_\alpha = 0.5$ to 2.6 MeV, corresponding to B^{10*}(4.76 to 6.06 MeV): see table 10.5. No other resonances appear for $E_\alpha < 3.8$ MeV ($B^{10*} = 6.74$) (Me 57d).

The 4.76-MeV state decays mainly to B^{10*}(0.7). The angular distribution of γ-rays indicates $J = 2^+$, with a ratio E2/M1 = 1.8 (Me 57d), E2/M1 = 0.68; $J = 3^+$ is possible, but unlikely (Wa 57d). The strength of the E2 radiation is ≈ 0.01 eV, several times the single-particle value (Me 57d). The relative weakness of the M1 transition may reflect the predicted inhibition of such transitions for $T_z = 0$, $\Delta T = 0$ transitions (Mo 58). The weakness of the ground-state radiation is puzzling (Wi 53h). Observation of γ-decay in Be^9(d, n)B^{10} suggests $\Gamma_\gamma \approx \Gamma_\alpha$(Me 58b).

The 5.11-MeV level was not observed by (Jo 54e) who estimated $\omega\Gamma_s < 0.02$ eV ($\Gamma_s = \Gamma_\alpha\Gamma_\gamma/\Gamma_\alpha+\Gamma_\gamma$). According to (Me 57d), $\omega\Gamma_s = 0.1$ eV. The angular distribution admits $J = 2^+$ and 4^- as possible assignments; $J = 3^+$ is possible but unlikely. The earlier suggested assignment $J = 2^-$ appears to be excluded. On the other hand, (Me 58b) observe that the angular distribution can be accounted for by $J = 2^-$ if E1 radiation is strongly inhibited, i.e. if $T = 0$. See Be^9(d, n)B^{10} and Be^9(p, γ)B^{10}.

Angular distributions of gamma radiation from the 5.16-MeV level admit $J = 1^+$ or 2^+; 1^- and 2^- are possible, but unlikely (Me 57d). Observation of a γ-decay in Be^9(d, n)B^{10} strongly supports the suggestion that $\Gamma_\alpha \approx \Gamma_\gamma$ and that the reported width is largely experimental (Me 58b). In this case, the assignment $T = 1$ is indicated (Jo 54e, Wa 59). See also (Ku 57a; theo.).

For the 5.92-MeV level, $J = 2^\pm$, 3^+ and 4^+ are possible. Only $J = 4^+$ gives a satisfactory account of the angular distribution from the 6.02-MeV level. The ratio E2/M1 = 9.0 (Me 57d).

II. (a) $Li^6(\alpha, p)Be^9$ $Q_m = -2.125$ $E_b = 4.459$

(b) $Li^6(\alpha, d)Be^8$ $Q_m = -1.565$

See (Wa 56f).

III. (a) $Li^7(He^3, p)Be^9$ $Q_m = 11.200$ $E_b = 17.784$

(b) $Li^7(He^3, d)Be^8$ $Q_m = 11.759$

(c) $Li^7(He^3, \alpha)Li^6$ $Q_m = 13.325$

See Li^6, Be^8 and Be^9.

IV. $Li^7(\alpha, n)B^{10}$ $Q_m = -2.793$

$Q_0 = -2.788 \pm 0.004$ (Bi 57b; neutron threshold).

Thresholds for production of slow neutrons are observed at $E_\alpha = 4.379 \pm 0.006$ MeV (B^{10} g.s.) and $E_\alpha = 5.51$ MeV (B^{10*} 0.71) (Bi 57b). Thresholds at $E_\alpha = 4.45$, 5.64, 6.49 and 7.15 MeV are reported by (Ro 56): $B^{10*} = 0$, 0.76, 1.30 and 1.72 MeV. At $E_\alpha = 8.16$ MeV, neutron groups corresponding

TABLE 10.4
Energy levels of B^{10}

E_x in B^{10} (MeV)	J^π; T	Γ or τ_m (keV)	Decay	Reactions
0	3^+; 0	stable	–	IV, X, XIII, XVI, XVII, XX, XXI, XXIII
0.7174 ±0.001	1^+; 0	$(9.6 \pm 0.6) \times 10^{-10}$ sec	γ	IV, V, X, XI, XV, XVI, XVII, XVIII, XIX, XXIII
1.739 ±0.005	0^+; 1		γ	IV, V, X, XI, XVI, XIX
2.152 ±0.005	1^+; 0		γ	V, X, XI, XV, XVI, XVII, XXIII
3.583 ±0.005	2^+; 0		γ	V, X, XVI, XVII
4.771 ±0.005	(2^+); 0	<10	α, γ	I, X, XVI
5.105 ±0.007	$(2^-; 0)$	1.2	α, γ	I, X, XVI
5.159 ±0.007	$(1^+, 2^+; 1)$	<0.5	α, γ	I, X, XVI
(5.37 ±0.04)				X
5.58 ±0.04				X
5.92 ±0.02	$(2^\pm, 3^+, 4^+)$	12±3	α, γ	I, X
6.02 ±0.01	4^+	<1	α, γ	I, X
6.16 ±0.02		<20		X
6.40 ±0.03		<100		X
6.57 ±0.02		≈30		X
(6.77 ±0.04)				X
6.88 ±0.01	1^-; 0	145	p, γ, d, α	V, VII, IX
(7.01)			p, d	IX
(7.20)			p, d, α	IX
7.47	2^+	≈80	p	VII
7.48 ±0.01	2^-; 1	80±3	p, γ, d, α	V, VII, (IX)
7.56 ±0.01	0^+; (1)	3.5±0.5	p, γ	V, VII
7.78	2^-	≈360	p, (γ), d, α	V, VII, IX
(8.07)		≈350	p, d	IX
(8.66)		≈220	p, d	IX
8.89 ±0.01	2^+; 1	36±2	p, γ, α_2	V, VII, IX
8.89 ±0.01	$(3^+; 1)$	84±6	p, n	VI, VII
9.7	; (1)	≈650	p, n, α_2	VI, IX
10.7	$(^+; 1)$	≈450	p, γ, n, α_2	V, VI, IX

to $B^{10*} = 0$, 0.72, 1.32 and 1.71 MeV are reported. It is noted that the 1.3-MeV level is not observed in any other reaction (Ro 56). See also (Ne 57b).

V. $Be^9(p, \gamma)B^{10}$ $\qquad Q_m = 6.585$

Observed resonances are listed in table 10.6. An earlier reported resonance at 0.49 MeV is not confirmed (Lo 55, Cl 56). Cross sections from $E_p = 30$ to 250 keV are reported by (Sa 53b: see Ja 57).

The $E_p = 0.33$-MeV resonance ($B^{10*} = 6.89$ MeV) has been the object of

considerable study. The proton width indicates s-wave formation (Wi 56g); the isotropy of the radiation is consistent with this assignment (Cl 56, Ca 55).

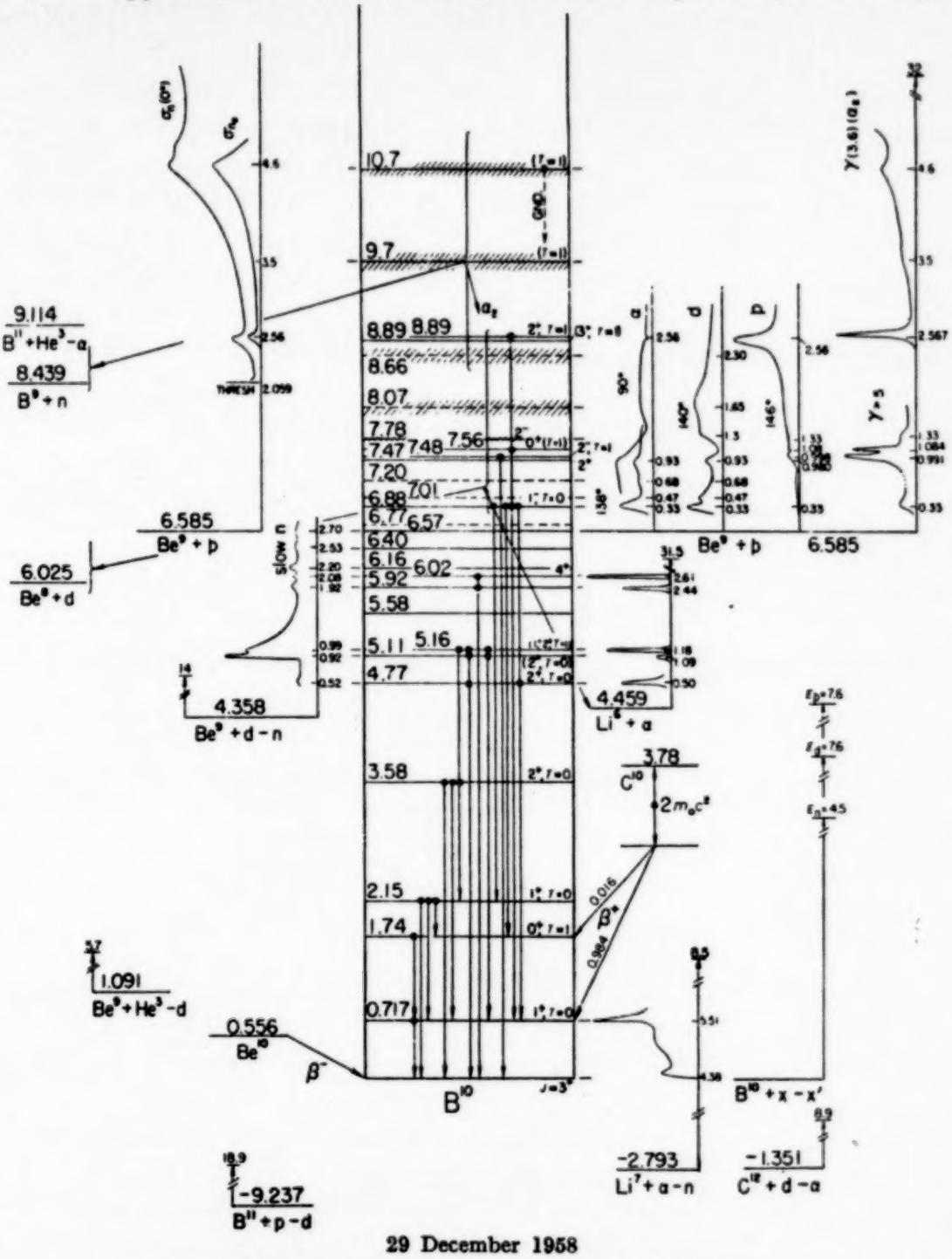

29 December 1958

Fig. 13. Energy levels of B^{10}: for notation, see fig. 1, p. 7.

Of the possibilities $J = 1^-$ or 2^-, the latter appears to be excluded by the strength of the transition to $B^{10*}(1.74,\ J = 0^+,\ T = 1)$ (Wi 56g). The angular correlation in the cascade $B^{10*}(6.89 \rightarrow 0.7 \rightarrow \text{g.s.})$ is consistent with $J = 1^-$ (E1)1^+(E2)3^+ (Bi 57e). The strong E1 transition to $B^{10*}(1.74)$ and

the large deuteron width indicate $T = 0$ for the 6.89-MeV level. On the other hand, the transitions to B^{10*}(0.7 and 2.1) are nearly as strong, and would appear to require a $T = 1$ admixture of the order of 20 per cent. Such a large admixture might be ascribed to a neighboring $J = 1^-$, $T = 1$ state of the same parentage (Be^9+s-wave proton) (see, however, Ba 57b). The strong M1 transition to B^{10*} (5.11) and the absence of the E1 transition to B^{10*}(5.16) present some difficulty (Wi 56g). According to (Me 59) however, the observed transition is not to B^{10*}(5.11) but rather to B^{10*}(5.16); also this transition is not strongly resonant in this region. The 6.2, 5.2 and 4.7-MeV γ-rays all show the same resonance, excluding the possibility that two states may be involved. The ground-state transition shows only a monotonic rise, attributable partly to direct capture and partly to the tail of

TABLE 10.5

Levels of B^{10} from $Li^6(\alpha, \gamma)B^{10}$ (Me 57d)

E_{res} (keV)	E_x (MeV)	Γ_{lab} (keV)	E_γ[a] (MeV)	(Per cent)	$\omega\Gamma_\gamma$[b] (eV)	J^π
500±25[c]	4.759		4.76	8[d]		2^+, (3^+)
			4.05	92	0.05[e]	
1085	5.110	2[f]	5.1	96	0.10	(2^+), (4^-), (2^-)
			4.4	4	0.005	
1175[g]	5.164	<0.8[f]	5.16	7	0.04	1^+, 2^+
			4.44	29	0.15	
			3.01	64	0.32	
2435	5.920	20	5.9	100		$2^\pm$, 3^+, 4^+
2605	6.022	<1.5[f]	6.0	100		4^+

[a] Primary radiation: see fig. 14.
[b] $\Gamma_\gamma \equiv \Gamma_\alpha\Gamma_\gamma/(\Gamma_\alpha+\Gamma_\gamma)$.
[c] (Wi 53h, Jo 54e).
[d] (Me 57d); (Wa 57d) finds <3 per cent.
[e] (Wa 57d).
[f] S. S. Hanna, Private communication: see (Me 58b).
[g] (Jo 54e) give 1183±5, $\omega\Gamma_\gamma \approx 1$ eV, $J = 2^+$, $T = 1$; (Wi 53h) give branching fractions 5 : 25 : 70.

the 993-keV resonance (Ed 58a). The angular correlation of 1.0 and 0.7-MeV γ-rays is consistent with $J = 1^+$ or 2^+ for B^{10*}(0.7) (Ca 55).

For $E_p = 380$ to 460 keV (thick target), a 2—4 per cent anisotropy is observed in the high energy radiation ($E_\gamma > 3$ MeV). At $E_p = 600$ keV, (thick target), the cascade $B^{10*}(6.9 \rightarrow 3.58 \rightarrow 0.7 \rightarrow$ g.s.) is observed, with an intensity of 0.35 that of the $(6.9 \rightarrow 1.74)$ cascade. It is suggested that the intensity of this transition implies a strong $T = 1$ admixture in B^{10*}(3.58) (Bi 57e).

The broad resonance at 0.99 MeV ($E_x = 7.48$ MeV) is also believed to be formed by s-waves. The angular distribution of the γ-radiation suggests dominant s-wave formation with some d-wave contribution (De 49d and

Pa 53d); see, however, (Mo 56d). The resonance is located at 993±2 (Ho 53b; $\Gamma = 88\pm3$ keV), 989.5±1.4 keV (Hu 56b; $\Gamma = 91\pm5$ keV). Assuming $J = 2$, $\Gamma_\gamma = 23$ eV (Ho 53b). The strength of the transition to the ground state indicates E1, $T = 1$ (Wi 53a): again, as in the 6.89-MeV level, a considerable contamination is required, since Be^9(p, d)Be^8 and Be^9(p, α)Li^6 are also resonant. Study of the angular correlation of internal conversion pairs indicates about equal contributions of E1 and E3 or M2 transitions (De 54b). It is suggested by (Mo 56d) that the observed transitions actually arise from two levels at 980 keV, ($J = 2^+$) and 993 keV, with ($J = 2^-$): see Be^9(p,p)Be^9.

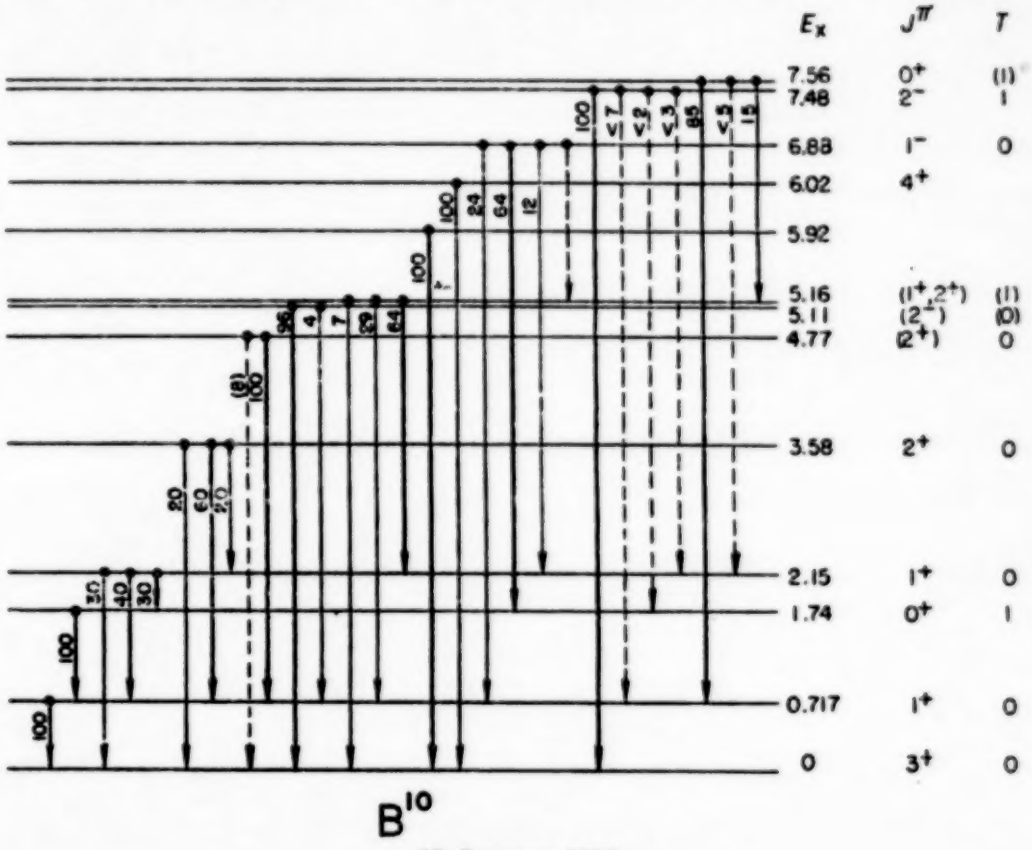

13 January 1959

Fig. 14. Gamma-ray transitions in B^{10}. The horizontal lines indicate the pertinent levels of B^{10}, identified on the right by the level energies, and where known, the total angular momentum J, parity, and isobaric spin T. Solid vertical lines indicate observed transitions, while dashed lines indicate transitions whose assignmentis not well established. Numbers on the vertical lines give the (estimated) percentage branching from each level; figures in parentheses are least certain.

The narrow 7.56-MeV level [$E_p = 1085\pm2$ keV (Ho 53b), 1083.7 ±0.7 keV, $\Gamma = 3.8\pm0.5$ keV (Hu 56b)] decays mainly to the 0.7-MeV state ($\Gamma_\gamma = 6.0$ eV assuming $J = 0$: Ho 53b). The angular distributions of these γ-rays and the subsequent 0.7-MeV γ-rays are isotropic, consistent with $J = 0$ (Pa 53d). From $E_p = 1.1$ MeV to the neutron threshold at 2.06 MeV, no further structure is observed except a possible broad level tailing off from 1.15 to 1.55 MeV (Ki 55d): see Be^9(p, d)Be^8 and Be^9(p, p)Be^9.

TABLE 10.6

Resonances in Be^9+p^r

E_p (keV)	E_x (MeV)	Γ_{lab} (keV)	l_p	Product [a]	E_γ (MeV)	Final State	Γ_γ (eV)	J^π; T
330 [b]	6.88	160	0	γ, α, d, p	(6.9)	g.s.	0 [d]	1^-; 0
					6.2	0.7	1.0	
					5.2	1.7	2.6	
					4.7	2.1	0.52	
					(1.7)	(5.1)	(0.61) [c]	
(470) [e]	(7.01)			d, p				
(680) [e]	(7.20)			α, d, p				
980 [f] $\pm$10	7.467	90	1	p				2^+;
991 $\pm$1.4 [g]	7.477	89 $\pm$3 [g]	0	γ, α, d, p	7.5	g.s.	23 [i]	2^-; 1
					(6.8)	0.7	$\leqq$1.7	
					(5.8)	1.7	$\leqq$0.4	
					(5.4)	2.1	$\leqq$0.7	
1083.7 $\pm$0.7 [j]	7.561	3.8 $\pm$0.5	1 [h]	γ, p	6.9	0.7	6.0 [i]	0^+; (1) [h,p]
					5.4	2.1	$\leqq$0.3	
					(2.5)	5.1	$\approx$0.9 [a]	
1330 [k]	7.78	$\approx$400 [h]	0	p, (γ), d, α				2^-;
1650 [q]	8.07	$\approx$400		p, d				
2300 [q]	8.66	$\approx$250		p, d				
2567 $\pm$2 [j]	8.895	40 $\pm$2	1	p, α_2, γ (α_0n)	(8.1) [l]	0.7		2^+; 1
2567 $\pm$3	8.895	93 $\pm$7 [n]	(1)	p, n				(3+; 1) [a]
(3500) [n]	9.7	$\approx$700		p, n, α_2				(; 1)
4600 [n]	10.7	$\approx$500		p, n, γ, α_2				(+; 1)

[a] "α_2" to Li^{8*}(3.58), $J = 0^+$, $T = 1$.

[b] Removal of s-wave penetration factor gives $E_{res} = 307$ keV, $\Gamma = 160$ keV (Lo 55).

[c] (Wi 56g). (Mo 56d) finds 48/0.5, 47/0.4, 62/0.05 with a factor of 2 uncertainty.

[d] (Cl 56). (Ca 55) report relative intensities 15 : 40 : 100 : 45 for the first four and $\Gamma_\gamma = 5$ eV for the 5.1-MeV radiation; however, the ground-state transition appears to be non-resonant (Lo 55, Cl 56, Ed 58a). See also (Bi 57e).

[e] (Ne 51, Th 49).

[f] (Mo 56d, De 56c).

[g] (Ho 53b, Hu 55).

[h] (Mo 56d).

[i] (Ho 53b).

The excitation curve for $E_\gamma > 6$ MeV shows a pronounced resonance at $E_p = 2.567 \pm 0.003$ MeV, and another, ≈ 0.5 MeV wide, superimposed on a general rise, at $E_p = 4.72 \pm 0.01$ MeV. At the 2.6-MeV resonance, the capture radiation appears to proceed predominantly to the 0.7-MeV state (Ma 53e). It would appear from the width that this resonance corresponds to the $Be^9(p, \alpha\gamma)Li^6$ resonance, $J = 2^+$, and not to the $Be^9(p, n)B^9$ resonance, $J = 3^+$, at the same energy (see Ma 56h).

VI. $Be^9(p, n)B^9$ $\quad Q_m = -1.854$ $\quad E_b = 6.585$

Resonances in the neutron yield occur at $E_p = 2.56$, 4.70 and (4.90) MeV (Ha 52e, Ma 55k, Ma 56h, Ma 59, Gi 59); see (Ja 57) and table 10.6). A

TABLE 10.6 (continued)

E_p (keV)	Γ_p (keV) / θ_p^2	Γ_d (keV) / θ_d^2	Γ_α (keV) / θ_α^2	Γ_{α_2} (keV) [a] / $\theta^2_{\alpha_2}$	Γ_n (keV) / θ_n^2
330 [b]	25 [c] / 0.15	59 / 0.12	57 / 0.013	0	0
(470) [o]				0	0
(680) [o]				0	0
980 [f] ±10	80 [h] / 0.07	≦10 [r] / ≦0.02	≦10 [r] / <0.005	0	0
991 ±1.4 [g]	60 [h] / 0.06	≈15 [r] / 0.008	≈15 [r] / 0.004	0	0
1083.7±0.7 [j]	3.8 [h]			0	0
1330 [k]	260 [h] / 0.15	≦70 [r] / ≦0.03	≦70 [r] / ≦0.016	0	0
1650 [q]					
2300 [q]					
2567 ±3 [j]	[16] [l] / 0.0016	<13.5 [m] / $<5\times10^{-3}$	0.08−4.0 [m] / $10^{-5}-10^{-3}$	[20] [l] / 0.33	[4] [l] / 0.0016
2567 ±3	0.013			(0)	0.013
(3500) [n]					
460(					

[j] (Hu 56b, Ha 52e).
[k] (Mo 56d, Ki 55d, We 56c).
[l] (Ma 53e, Ma 54b).
[m] (We 56c): based on $\Gamma_p = 7$ keV.
[n] (Ma 56h, Ma 59, Gi 59).
[o] (Me 59) find that this transition proceeds to the 5.16-MeV level, and is mainly non-resonant.
[p] (Wa 59).
[q] (We 56c): see (Me 58b).
[r] See a similar table in (Me 58b).
[s] Meyerhof and Tanner (Me 59) find this transition is resonant and proceeds mainly to B^{10*} (5.16). The large width suggests E1 or M1 radiation.

broad maximum ($\theta = 90°$) near $E_p = 3.5$ MeV suggests an additional B^{10} state at 9.7 MeV with $\Gamma \approx 0.7$ MeV (Ma 56h, Ma 59). Angular distributions are nearly isotropic near $E_p = 2.56$ MeV but show marked structure at higher energies (Ma 56h). The excitation function for ground-state neutrons (n_0) does not show the resonance at 4.9 MeV. If this peak represents neutrons leading to $B^{9*}(2.3)$, it may arise from the tail of the $E_p = 3.5$-MeV resonance rather than from a new level. A continuous distribution of neutrons, observed for $E_p > 4.5$ MeV, is attributed to excitation of $Be^{9*}(2.4)$ followed by break-up via $Be^{8*}(2.9)$ (Ma 59).

The 2.56-MeV resonance is believed to be distinct from the resonance observed at the same energy in $Be^9(p, \alpha\gamma)Li^6$, because of its greater width

(93 keV vs. 38 keV). Estimates of the reduced proton and neutron widths agree well with the known parameters of the 7.37 MeV, $J = 3^+$, $T = 1$ state of Be^{10}. Assignment of $J = 3^+$ to the B^{10} state accounts for the absence of Be^9 $(p, \alpha\gamma)Li^6$ γ-rays at this resonance (Ma 56h). See also (Ta 58a, Ma 58a, St 57e).

VII. $Be^9(p, p)Be^9$ $E_b = 6.585$

For $E_p = 0.22$ to 0.78 MeV, the elastic scattering is adequately described by s-wave formation of a broad level at $E_p = 330$ keV, $J = 1^-$ or 2^-. For $J = 1^-$, $\Gamma_p/\Gamma = 0.30$ (Mo 56d).

In the range $E_p = 0.8$ to 1.6 MeV, attempts to fit the scattering data with s-waves are only moderately successful. That the major contribution at the 980-keV state is s-wave is indicated by the existence of interference minima at all angles near $E_p = 1$ MeV. Inclusion of d-waves, $J = 2^-$, does not improve the fit. The best account of the behaviour of the cross section in this region is obtained with the assumption of two s-wave resonances, $J = 2^-$, at $E_{res} = 998$ and 1330 keV, $\Gamma_p/\Gamma = 0.65 \pm 0.15$, $\Gamma(998) = 150 \pm 50$ keV, $\Gamma(1330) = 400 \pm 100$ keV, $\theta_p^2 \approx 0.006$ and 0.15, respectively, superposed on a p-wave, $J = 2^+$ resonance at 980 keV (see below). There is also some hint of a higher s-wave, $J = 1^-$, resonance (Mo 56d). (De 56c) also finds that the $E_p = 998$ keV level is formed by s-waves, with $\Gamma = 90$ keV, $\Gamma_p/\Gamma = 0.7$ The scattering near 1.1 MeV requires a broad p-wave resonance at 1.1 MeV, $\Gamma = 200$ keV, Γ_p/Γ small (De 56c).

At the 1084-keV resonance ($B^{10*} = 7.56$ MeV), the smallness of the scattering anomaly indicates $J = 0$. Absence of interference at $\theta = 90°$ suggests $l = 1$, hence $J = 0^+$. A satisfactory fit is obtained with the inclusion of a p-wave, 2^+, state in the background. The 2^+ state appears to be formed with channel spin 1, $\Gamma_p/\Gamma \approx 0.9$ and to be located within a few hundred keV below 1084 keV. A fit to the data near 1 MeV gives $E_{res} = 980 \pm 10$ keV, $\Gamma = 90$ keV, $\theta_p^2 \approx 0.07$ (Mo 56d). A scattering anomaly has also been observed at $E_p \approx 2.56$ MeV. This anomaly increases in the backward direction indicating p-wave formation of a level at 8.89 MeV with $J \geqq 2$, Γ_p large (De 56c).

Recent work on differential cross sections has been done in the range $E_p = 5.4$ to 31.5 MeV by (Wr 53a, Br 52c, Kl 56, Ra 56a, Da 56b, Ki 56). See also (Gr 55a, Hi 55b, Br 58f) and Be^9.

VIII. $Be^9(p, t)Be^7$ $Q_m = -12.081$ $E_b = 6.585$
See (Co 54b).

IX. $Be^9(p, d)Be^8$ $Q_m = 0.560$ $E_b = 6.585$
$Be^9(p, \alpha)Li^6$ $Q_m = 2.125$

Excitation functions and angular distributions have been studied for $E_p = 0.3$ to 1.3 MeV by (Th 49, Ne 51, Mo 56d) and for $E_p = 0.8$ to 3.0 MeV by (We 56c). Observed resonances are listed in table 10.6. Angular distributions at the 330-keV resonance are isotropic, consistent with s-wave forma-

tion (Mo 56d). Proton and deuteron reduced widths for this resonance are evidently quite large, while the α-width is some 10 times smaller (Mo 56d, Wi 56g). For $E_p > 500$ keV, the distributions show strong interference terms, implying contributions from states of both parities (Ne 51, We 56c). It is noted by (Mo 56d) that the states appearing in $Be^9(p, p)Be^9$ are not sufficient to account for this interference, and an additional p-wave state near $E_p \approx 700$ keV offers a plausible solution; see also (Me 58b). Above $E_p = 1.8$ MeV, pronounced pickup is evident in the (p, d) reaction (We 56c).

A pronounced maximum occurs in the integrated cross section for both reactions at $E_p = 930$ keV, $\Gamma = 130 \pm 30$ keV, presumably due to the $J = 2^-$, $T = 1$ resonance seen in $Be^9(p, \gamma)B^{10}$ and $Be^9(p, p)Be^9$ at $E_p = 991$ keV. The reason for the energy shift is not clear. An appreciable $T = 0$ contamination is required; this may be due to the 1330-keV, $J = 2^-$, resonance which appears in the (p, d), (p, α), (p, p) and possibly (p, γ) yields (We 56c).

The 7.56-MeV state is not resonant for (p, α) or (p, d); this observation is consistent with its $J = 0^+$ character. Broad, weak maxima occur in the total (p, d) cross section at $E_p = 1.25$, 1.64 and 2.3 MeV; the 90°(p, α) cross section shows maxima at $E_p = 1.25$, and ≈ 2.0 MeV with a small anomaly at $E_p = 2.56$ MeV, $\Gamma = 40 \pm 10$ keV. The $E_p = 1.25$-MeV structure is probably associated with the $E_p = 1.33$-MeV resonance in $Be^9(p,p)Be^9$, while the 2.56-MeV anomaly is clearly connected with the strong resonance at that energy seen in $Be^9(p, \alpha\gamma)Li^6$ ($J = 2^+$, $T = 1$). An upper limit to the deuteron width at this resonance is $\Gamma_d = 13.5$ keV, $\theta^2 = 4.5 \times 10^{-3}$. For α_0 particles, $0.08 < \Gamma_\alpha < 4.0$ keV, $2.2 \times 10^{-5} < \theta_\alpha^2 < 1.1 \times 10^{-3}$ (We 56c). For the (p, $\alpha_2\gamma$) reaction, the resonance occurs at 2.562 ± 0.006 MeV, $\Gamma = 38 \pm 3$ keV, $\theta_\alpha^2 + \theta_p^2 = 0.0032$ (Ma 56h, Ma 54g: $\Gamma = 41 \pm 2$ keV). From the fact that this state ($B^{10*} = 8.89$ MeV) decays primarily to the $T = 1$, $J = 0^+$ state of Li^6(3.58 MeV) it is concluded that it has $T = 1$ (Ma 54g, Ma 54b). The observed cross section requires $J \geqq 2$, while the width requires $J \leqq 2$. For $J = 2$, $\theta_{\alpha 2}^2 = 0.19$ or 0.33, $\theta_n^2 = 0.0016$ (Ma 54b). This resonance is presumed to be distinct from the $Be^9(p, n)B^9$ resonance which occurs at the same energy (Ma 56h). A further resonance for 3.6 MeV (Li^{6*}) γ-rays appears at $E_p = 4.49$ MeV, and a broad rise near $E_p = 3.5$ MeV, observed in $Be^9(p, n)B^9$, seem also to be found here. It is suggested that these states have $T = 1$ and correspond to $Be^{10*} = 9.27$ and 9.4 MeV (Ma 59).

X. $Be^9(d, n)B^{10}$ $\quad Q_m = 4.358$

Neutron groups are observed corresponding to B^{10} states listed in table 10.7: see (Aj 51, Pr 52a, Pr 53, Ge 55d, Gr 55f, Mu 57, Ne 57, Sh 57a, Ne 58a, Ge 58c). Thresholds for slow neutron production corresponding to B^{10} states from 4.77 to 6.57 MeV are reported by (Bo 54c). Indications of a state at 2.8 MeV are reported by (Dy 53, Re 54b, Ge 58c). Angular distributions to

TABLE 10.7
Levels of B^{10} from $Be^9(d, n)B^{10}$ [a], $B^{10}(p, p')B^{10*}$ [h] and $B^{10}(d, d')B^{10*}$ [h]

B^{10*} (MeV)	l_p [a]	J^π	θ_p^2 [a] (per cent)	Γ_γ (eV) to final state at E_x [d]			
				0	0.7	1.7	2.1
0	1	3^+	≈1.7				
0.717 [h]	1	1^+	≈3.5	$[10^{-4}]$ [e]			
1.739	1	0^+	≈2.5	<7 % [f]	100 %		
2.152	1	1^+		30 % [g]	[40 %]	30 %	
3.583	1	2^+	≈0.7	20 % [g]	60 %	0	(20 %)
4.771 [c]	(1)	2^+	≈0.3	(0.005) [d]	(0.055)		
5.105 [b,c]	(0)	(2^-)	≈1.3	0.06 [d]	0.003		≦0.012
5.159 [b,c]	(1)	(2^+)	(0.5)	(0.04) [d]	(0.18)		(0.39)
(5.37)							
5.58							
(5.72)							
5.93 [c]	(1)	(3^+)	≈0.5	100 %			
6.06 [b,c]		4^+		100 %			
6.16 [b,c]							
6.43 [c]							
6.57 [c]							
(6.77)							

[a] (Me 58b, Aj 52b).
[b] Not resolved in neutron groups.
[c] Observed as slow neutron thresholds (Bo 54c).
[d] (Me 58b): see also table 10.5. ($Li^6(\alpha, \gamma)B^{10}$).
[e] (Th 53a, Se 56c).
[f] (Mc 57a).
[g] (Ra 49b, Sh 54a, Mc 57a).
[h] Energies of first 7 excited states are from (Bo 53, Br 53i); probable errors are ±5 keV for first 5, and ±7 keV for the 5.11 and 5.16-MeV states. For more precise values for the 0.7-MeV state, see text.

the low states have been studied at many energies from $E_d = 0.5$ to 3.4 MeV: see (Aj 52b, Pr 52a, Pr 53, Ge 55d, Gr 55f, Ne 57, Sh 57a). The data show evidence both for stripping and compound nucleus formation with more evidence of the former in the higher energy work: the ground state and the first four excited states have $J \leqq 3$ and even parity, and one or both of the 5·1-MeV levels have $J = 1^-$ or 2^- (Aj 52b). It is of interest that the 3.6-MeV state shows a well developed stripping pattern even at the lowest bombarding energies. According to (Sa 58, Ne 59), however, the character changes drastically at $E_d = 1.5$ to 2 MeV, suggesting some contribution of "heavy particle" stripping. The group leading to the 0.72-MeV state also shows this effect. See also (Ma 56s; theo.). Absolute reduced widths for several levels have been estimated by (Me 58b) using published cross section data: see table 10.7.

The mean lifetime of the 0.72-MeV state is $(7\pm2)\times10^{-10}$ sec (Th 53a), $(8.5\pm2.0)\times10^{-10}$ sec (Se 56c), $(11.8\pm3.3)\times10^{-10}$ sec (Kn 58a, Go 58f), $(9.6\pm1.0)\times10^{-10}$ sec (Da 58c); compare with $B^{10}(p, p')B^{10*}$. The γ-ray energy is 716.6±1 keV (Ra 49b). The 1.74-MeV state ($J = 0^+$; $T = 1$)

decays via the 0.7-MeV state: $E_\gamma = 1022 \pm 2$ keV (Ra 49b). The ground-state transition is < 10 per cent (Al 51i). See also (Sh 54a).

The 2.1-MeV state decays directly to the ground state and via cascades through the 0.72 and 1.74-MeV levels; $E_\gamma = 2151 \pm 16$, 1433 ± 5, 413.5 ± 1 keV; the intensities are in ratio 1.2 : 2.5 : 1.2 (Ra 49b). The relative contribution of the 1400-keV γ-ray is uncertain since this radiation also arises from the transition 3.58 → 2.1 (Sh 54a). The relative strength of the low energy, 2.1 → 1.7 MeV, transition is attributed to a strong inhibition of the M1, $\Delta T = 0$ transition from B^{10*}(2.1 to 0.7) (Mo 58; see also Ku 57a). For the 3.58-MeV level, the ground state transition is about $\frac{1}{3}$ as intense as that to the 0.7-MeV state (Ra 49a: see also Mc 57a, Ch 58b). The transition (3.58 → 2.1) also occurs (Sh 54a). The angular correlation (2.86 → 0.7) is consistent with $J = 1^+$ or 2^+ for the 3.6-MeV level; $J = 0$, 3 are excluded. For $J = 2^+$, acceptable schemes are 2 (0.93 M1+0.07 E2)1(E2)3 or 2(E2)1 (E2)3 (Sh 56e). A spin 1^+ assignment would permit a strong M1 transition to the $T = 0$, $J = 0^+$ state at 1.74 MeV (Mo 58).

The fact that gamma radiation is observed in competition with α-decay from the 4.77 and 5.16-MeV levels suggests that $\Gamma_\gamma \approx \Gamma_\alpha$ for these two states. No radiation is observed from the 5.11, 5.93, or 6.06-MeV levels in Be^9(d, n)B^{10} (Me 58b; see also Ne 59). No gamma rays of energy 6.5 to 8.0 MeV are observed with intensity > 5 per cent of the 6.0-MeV, Be^{10} radiation (Be 55g: $E_d = 3.85$ MeV). The ratio of 5.16 → g.s. to 5.16 → 0.7 radiation is 1 : 2 (Be 55g; see, however, Mc 57a).

At $E_d = 9$ MeV, the ratio of the maximum differential cross sections of the Be^9(d, p)Be^{10} and Be^9(d, n)B^{10} reactions to the first $T = 1$ states leads to a ratio of reduced widths of 2.16 (calculated from stripping theory; predicted value from charge independence: 2) (Ca 56b). See also (Be 58f, De 56d, Ba 56m, Bo 56l, Bo 56m, Go 56, Gr 57b).

XI. $Be^9(He^3, d)B^{10}$ $\quad Q_m = 1.091$

At $E(He^3) = 2.1$ MeV, gamma-rays from the 0.72-MeV state have been observed (Fe 57a). At $E(He^3) = 5.7$ MeV, deuteron groups are observed to the ground state of B^{10} and to levels at 0.724 ± 0.010, 1.751 ± 0.010, and 2.163 ± 0.010 MeV (S. Hinds and R. Middleton, private communication). The angular distributions follow quite closely the $l_p = 1$ stripping patterns.

XII. $Be^9(\alpha, t)B^{10}$ $\quad Q_m = -13.228$

Not reported.

XIII. $Be^{10}(\beta^-)B^{10}$ $\quad Q_m = 0.556$

See Be^{10}.

XIV. (a) $B^{10}(\gamma, d)He^4 + He^4$ $\quad Q_m = -5.930$

(b) $B^{10}(\gamma, \alpha)Li^6$ $\quad Q_m = -4.459$

(c) $B^{10}(\gamma, np)He^4 + He^4$ $\quad Q_m = -8.157$

(d) $B^{10}(\gamma, p)Be^9$ $Q_m = -6.585$

In the range $E_\gamma = 10$ to 30 MeV, reaction (a) proceeds almost entirely through excited states of Be^8: transitions via (α+d)-emitting states of Li^6 apparently do not occur. Reaction (b) is said to proceed via the ground state and γ-emitting states of Li^6 at 1.1 and 2.2 MeV (Er 53) (there is no evidence for a state at 1.1 MeV in any other reaction: see (Aj 52c) and (Aj 55)). For reaction (d) see (Go 56k, Ba 57, Go 56l).

XV. $B^{10}(n, n')B^{10*}$

At $E_n = 2.56$ MeV, a 717 ± 7 keV γ-ray is observed (Da 56d).

XVI. $B^{10}(p, p')B^{10*}$

The first seven excited states have been accurately located by inelastic scattering: see table 10.7 (Bo 53, Br 53i). The energy of the first state is given as 717 ± 5 keV (Bo 53), 719 ± 1.6 keV (Cr 52c) and 718 ± 5 keV (Da 54: γ-radiation). The mean life of this state is $(10.5 \pm 1.0) \times 10^{-10}$ sec (Bl 57a), $(9.0 \pm 1) \times 10^{-10}$ sec (Ho 58b). This lifetime is about a factor of 10 shorter than that calculated on the shell model with reasonable values of the radius and intermediate coupling parameter (Bl 57a: see, however, Fr 57, Ku 57a; see also $Be^9(d, n)B^{10}$).

At $E_p > 3$ MeV, gamma rays of energy 710 ± 15, 1023 ± 5, 1438 ± 5, and 2120 ± 60 keV are observed (Mc 57a, Hu 57b). An upper limit of 7 per cent is found for direct transitions from $B^{10*}(1.74 \rightarrow \text{g.s.})$ (Mc 57a). At $E_p > 4.5$ MeV, additional radiations at 2860 ± 10 and 3560 ± 50 keV (Doppler corrected) are observed, with intensity ratio 2.9. Shell model calculations would predict a ratio of 0.67 to 0.5 (Mc 57a: see also Ku 57a).

XVII. $B^{10}(d, d')B^{10*}$

Deuteron groups corresponding to the ground state and to states at 0.7, 2.1, and 3.6 MeV are reported by (Bo 53): see table 10.7. The absence of deuteron groups corresponding to the 1.74-MeV state is strong evidence of its $T = 1$ character.

XVIII. $B^{10}(\alpha, \alpha')B^{10*}$

See (Bo 56a).

XIX. $C^{10}(\beta^+)B^{10}$ $Q_m = 3.78$

The half-life is 19.1 ± 0.8 sec (Sh 49); $E_{\beta^+}(\text{max}) = 2.10 \pm 0.1$ MeV. The β^+-decay is to the first two excited states of B^{10}: relative transition probabilities to the 0.72-, 1.74- and 2.15-MeV levels are $98.4/1.65 \pm 0.2/< 0.1$ (Sh 53a): log ft using $E_\beta(\text{max}) = 2.04$ and 1.02 MeV (from Q_m above) are 3.7 and 3.2. The gamma decay of the first two excited states of B^{10} is observed: $E_\gamma = 723 \pm 15$ and 1033 ± 30 keV (Sh 53a). See also (Ko 53), (Ge 58) and (Fr 57).

XX. $B^{11}(\gamma, n)B^{10}$ $Q_m = -11.464$

See (Sh 51d).

XXI. $B^{11}(p, d)B^{10}$ $Q_m = -9.237$

At $E_p = 18.9$ MeV, the ground state deuteron angular distributions indicate $l_n = 1$ (Re 56).

XXII. (a) $B^{11}(d, t)B^{10}$ $Q_m = -5.205$
(b) $B^{11}(He^3, \alpha)B^{10}$ $Q_m = 9.114$
(c) $C^{12}(n, t)B^{10}$ $Q_m = -18.937$
(d) $C^{12}(p, He^3)B^{10}$ $Q_m = -19.702$

These reactions have not been reported.

XXIII. $C^{12}(d, \alpha)B^{10}$ $Q_m = -1.351$
$Q_0 = -1.39 \pm 0.02$ (El 57a).

At $E_d = 8.9$ MeV, α-groups have been observed corresponding to the ground state of B^{10} and to excited states at 0.72 ± 0.02 and 2.14 ± 0.02 MeV. No α-group was observed to the $T = 1$, 1.74-MeV state (El 57a). See also (As 51) and (Sp 53c).

XXIV. $C^{13}(p, \alpha)B^{10}$ $Q_m = -4.070$
Not reported.

XXV. $N^{14}(\gamma, \alpha)B^{10}$ $Q_m = -11.615$
See (Mi 53c), (Co 54i) and (Li '56).

Arguments supporting the J^π assignments for the first five excited states of B^{10} are presented on p. 105—106 of (Aj 55). The assignment of the 4.77-MeV state now appears to be $J = 2^+$ (see $Li^6(\alpha, \gamma)B^{10}$).

C^{10}

(Fig. 15, p. 92) †

MASS OF C^{10}

The mass difference $C^{10}-B^{10}$ is given as 3.84 ± 0.1 MeV from β-end-point measurements (Sh 53a), and as 3.57 ± 0.2 MeV (Aj 54b) from the $B^{10}(p, n)C^{10}$ Q-value. The weighted mean of these two results yields a mass excess for C^{10} of 18.79 ± 0.09 MeV, using the Wapstra (Wa 55c) value for the mass of B^{10}.

I. $C^{10}(\beta^+)B^{10}$ $Q_m = 3.78$

The decay is complex. See B^{10}.

II. $B^{10}(p, n)C^{10}$ $Q_m = -4.56$

At $E_p = 17.2$ MeV, neutron groups are observed corresponding to the ground state ($Q_0 = -4.35 \pm 0.2$ MeV), to an excited state at 3.34 ± 0.2 MeV, and possibly to wide or unresolved levels at $E_x \approx 5.1$ MeV (Aj 54b). The slow neutron threshold for the ground state of C^{10} has not been observed up to $E_p = 6$ MeV in preliminary measurements by (Ba 55f). The neutron

† For level scheme of Be^{10}, see fig. 12, p. 75.

threshold measurement reported in (Aj 55) has been withdrawn: (T. W. Bonner, private communication).

TABLE 10.8
Energy levels of C^{10}

E_x in C^{10} (MeV)	J^π	$\tau_{\frac{1}{2}}$ or Γ	Decay	Reactions
0	(0^+)	19.1 ± 0.8 sec	β^+	I, II
3.34 ± 0.2				II
(5.1)		broad or unresolved		II

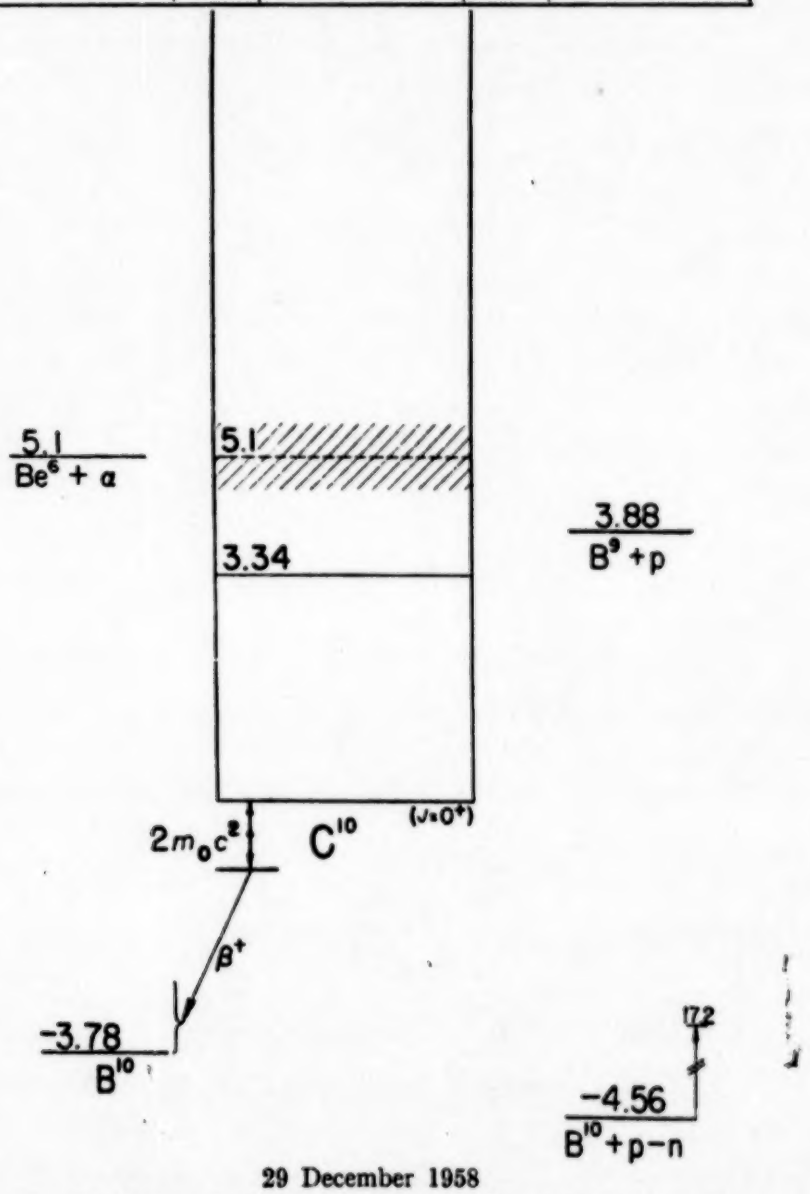

29 December 1958

Fig. 15. Energy levels of C^{10}: for notation, see fig. 1, p. 7.

Two other reactions leading to C^{10} have not been observed: $B^{10}(He^3, t)C^{10}$ ($Q_m = -3.80$) and $C^{12}(p, t)C^{10}$ ($Q_m = -23.50$).

Be^{11}

(Not illustrated)

MASS OF Be^{11}

From the decay energy, $Be^{11}(\beta^-)B^{11}$, and using the Wapstra mass (Wa 55c) for B^{11}, the mass excess of Be^{11}, $M-A = 23.39\pm0.15$ MeV (Wi 59). The binding energies of a neutron, deuteron and triton in Be^{11} are, respectively, 0.54, 18.4 and 15.76 MeV.

I. $Be^{11}(\beta^-)B^{11}$ $\quad Q_m = 11.48$

The decay proceeds to B^{11}(g.s.) and to several excited states. For the ground-state transition, $E_\beta(\max) = 11.48\pm0.15$ MeV $\tau_{\frac{1}{2}} = 13.57\pm0.15$ sec, $\log ft = 6.77$ (Al 58e, Wi 59); see B^{11}.

II. $Be^9(t, p)Be^{11}$ $\quad Q_m = -1.13$

Not reported.

III. $B^{11}(n, p)Be^{11}$ $\quad Q_m = -10.69$

At $E_n = 14.8$ MeV, an activity with a 14.1 ± 0.3 sec half-life is observed which is attributed to the β-decay of Be^{11} formed in this reaction (Nu 58).

B^{11}

(Fig. 16, p. 95) †

THEORY

(See (Ku 56, Ku 57a, Fr 58b).

I. $Li^7(\alpha, \gamma)B^{11}$ $\quad Q_m = 8.670$

Three resonances are reported below $E_\alpha = 2.5$ MeV (Be 51, He 54b): see table 11.2. Study of α—γ and γ—γ angular correlations, taken together with the relative γ-intensities, leads to the following assignments: 9.28-MeV level, $J = \frac{5}{2}^+$; 9.19-MeV, $J = \frac{5}{2}^-$; 8.93-MeV, $J = \frac{3}{2}$ or $\frac{5}{2}$; 6.81-MeV, $J = \frac{3}{2}^-$; 4.46-MeV, $J = \frac{5}{2}^-$ (Jo 52d and D. H. Wilkinson, private communication). The strength of the transition (8.92 → g.s.) implies E1 radiation (Bi 58). Angular distributions of several gamma rays at each resonance are tabulated by (Me 57); no terms higher than $\cos^2\theta$ are indicated. The absence of the transition (9.28 → 2.14) speaks for $J = \frac{1}{2}^-$ for the latter (Wi 57c). Angular distributions of γ-rays from the 9.28-MeV level have been measured by (Fe 58c). The results are in agreement with assignments $J = \frac{5}{2}^+$ and $\frac{5}{2}^-$ for B^{11*}(9.28) and (4.46), respectively. The angular distribution of the transition 9.28 → 6.76 strongly favors $J = \frac{7}{2}^-$ for the latter. See also (Me 58c): $B^{11}(\gamma,\alpha)Li^7$, and $B^{10}(d, p)B^{11}$.

† For level scheme of C^{11}, see fig. 18, p. 107.

II. $Li^7(\alpha, n)B^{10}$ $Q_m = -2.793$ $E_b = 8.670$

For $E_\alpha < 5.8$ MeV, two resonances are observed; at $E_\alpha = 4.7$ MeV (broad), and 5.15 ± 0.08 MeV ($\Gamma = 0.22$ MeV) corresponding to $B^{11*} = 11.68 \pm 0.10$ and 11.95 ± 0.08 MeV (Bi 57b). A further resonance at $E_\alpha = 7.15$ MeV, $B^{11*} = 13.22$ MeV, is reported by (Ma 58g, Gi 59). Calculation of $\sigma(B^{10}(n, \alpha)Li^7)$ from the observed yield of $Li^7(\alpha, n)B^{10}$ gives good agreement for $E_n = 0$ to 0.8 MeV. The 5.15-MeV resonance corresponds to that reported in $\sigma(n, \alpha)$ at 0.52 MeV: $E_x = 11.95$ MeV. It is concluded that the resonance is formed by s or p-wave neutrons, $J = \frac{5}{2}^+$ or $\frac{3}{2}^-$, $\Gamma_n \approx 20$ keV and $\Gamma_\alpha \approx 300$ keV (Gi 59). See also (Ho 50b).

TABLE 11.1

Energy levels in B^{11}

E_x in B^{11} MeV ± keV	J^π	τ_m or Γ (sec) (keV)	Decay	Reactions
0	$\frac{3}{2}^-$	stable	–	I, X, XI, XII, XIX, XXII, XXIX, XXX, XXXI, XXXIV, XXXVI, XXXVIII
2.127 ± 6	$\frac{1}{2}^-$	$\tau_m = (4.6 \pm 0.6) \times 10^{-15}$ sec	γ	X, XI, XIX, XXII, XXIII, XXVII, XXVIII, XXXVI, XXXVIII
4.459 ± 8	$(\frac{5}{2}^-)$	$\tau_m = (1.17 \pm 0.17) \times 10^{-15}$ sec	γ	I, X, XII, XIII, XIX, XXIII, XXVIII, XXXVI, XXXVIII
5.035 ± 8	$(\frac{3}{2}^-)$	< 13	γ	I, X, XIX, XXXVIII
6.758 ± 7	$(\frac{7}{2}^-)$	< 13	γ	X, (XII), XIII, XIX, XXII, XXVIII, XXXVIII
6.808 ± 7	$(\frac{1}{2})^-$	< 13	γ	I, X, (XII), XIX, XXII, XXXVI
7.298 ± 6	$(\frac{1}{2}^-)$	< 13	γ	I, X, XIX, XXXVIII
7.987 ± 9		< 8	γ	X, XIX, XXII, XXVIII, XXXVIII
8.568 ± 5	$(\frac{1}{2}^+, \frac{3}{2}^+)$	< 8	γ	X, XIX, XXVIII, XXXVIII
8.927 ± 5	$(\frac{5}{2}^+)$	< 0.7	γ, α	I, X, XII, XIII, XIX, XXXVIII
9.191 ± 5	$(\frac{7}{2}^+)$	< 0.1	γ, α	I, X, XIII, XIX, XXVI
9.276 ± 5	$(\frac{3}{2}^+)$	5	γ, α	I, X, XIX
9.88 ± 20	$(\leqq\frac{5}{2})$	160	α	IV, X
10.26	$(\leqq\frac{7}{2})$	220	α	IV
10.32 ± 20		45 ± 14		XIX
10.62		100	α	IV
11.0		670	α	IV
11.46		70	α, (n)	IV, XVIII
11.68 ± 100	$(\frac{1}{2}^+, \frac{7}{2}^+)$	140	α, n	II, IV, XII, XVIII
11.95 ± 80	$(\frac{3}{2}^-, \frac{5}{2}^+)$	320	α, n	II, IV, XIII, XVIII, XXXVIII
13.16		450	α, n	II, XIII, XVIII
14.0		300	α, n	XIII, XVIII
15.1		500	α, n	XIII, XVIII
16.77		60	d, (n), p, t	VI, VII, VIII, XVIII
16.93		100	d, p, t	VII, VIII
17.5			d, p	VIII

III. $Li^7(\alpha, p)Be^{10}$ $Q_m = -2.566$ $E_b = 8.670$

See (Ec 37).

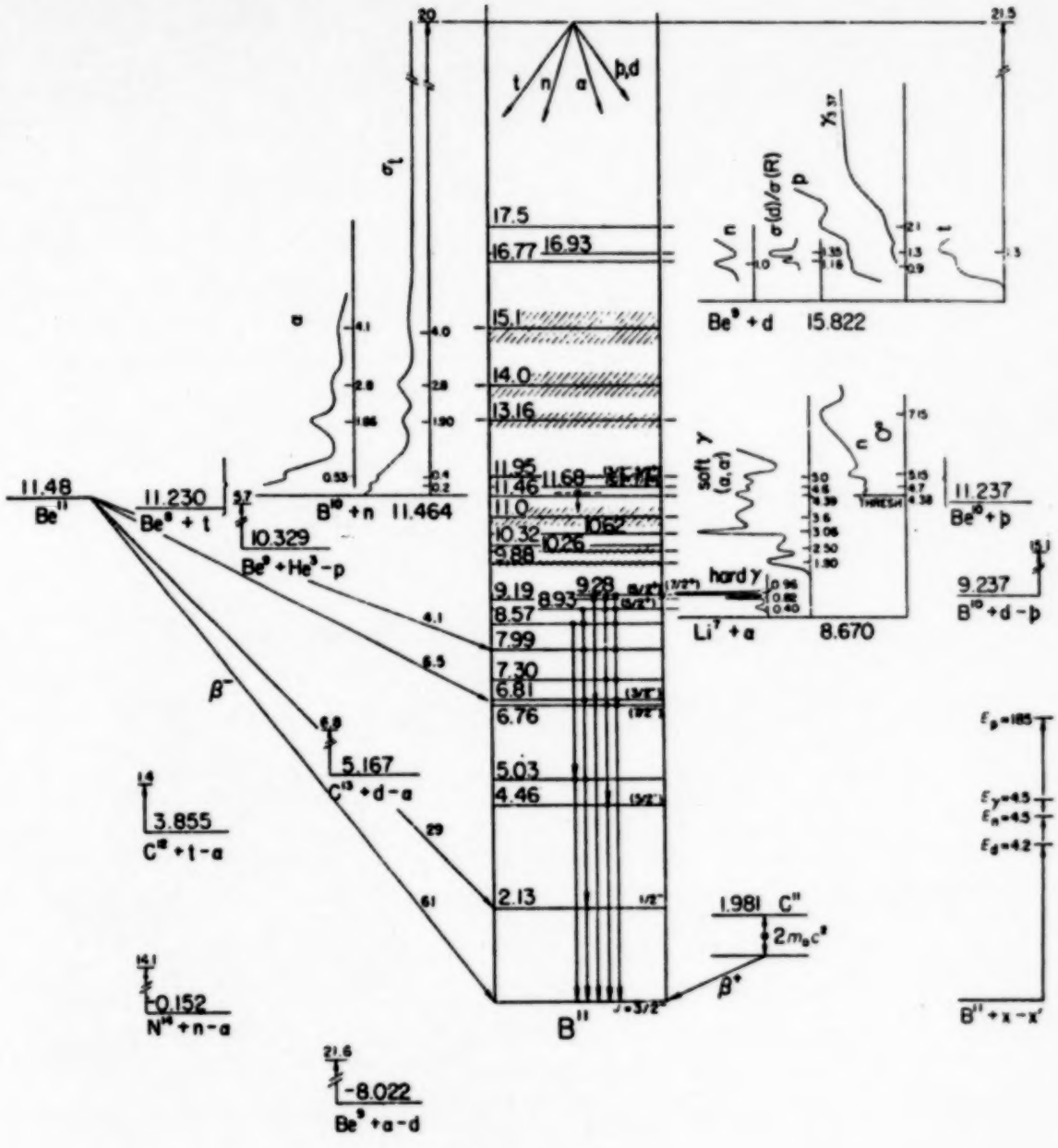

31 December 1958

Fig. 16. Energy levels of B^{11}: for notation, see fig. I, p. 7.

IV. $Li^7(\alpha, \alpha')Li^{7*}$ $E_b = 8.670$

Observed resonances in the yield of 0.48-MeV γ-radiation are exhibited in table 11.3 (Bi 57b, He 54b, Li 54). Sum rule limits give $J \leqq \frac{5}{2}$ for the 9.88-MeV level and $J \leqq \frac{7}{2}$ for the 10.26-MeV level (Li 54).

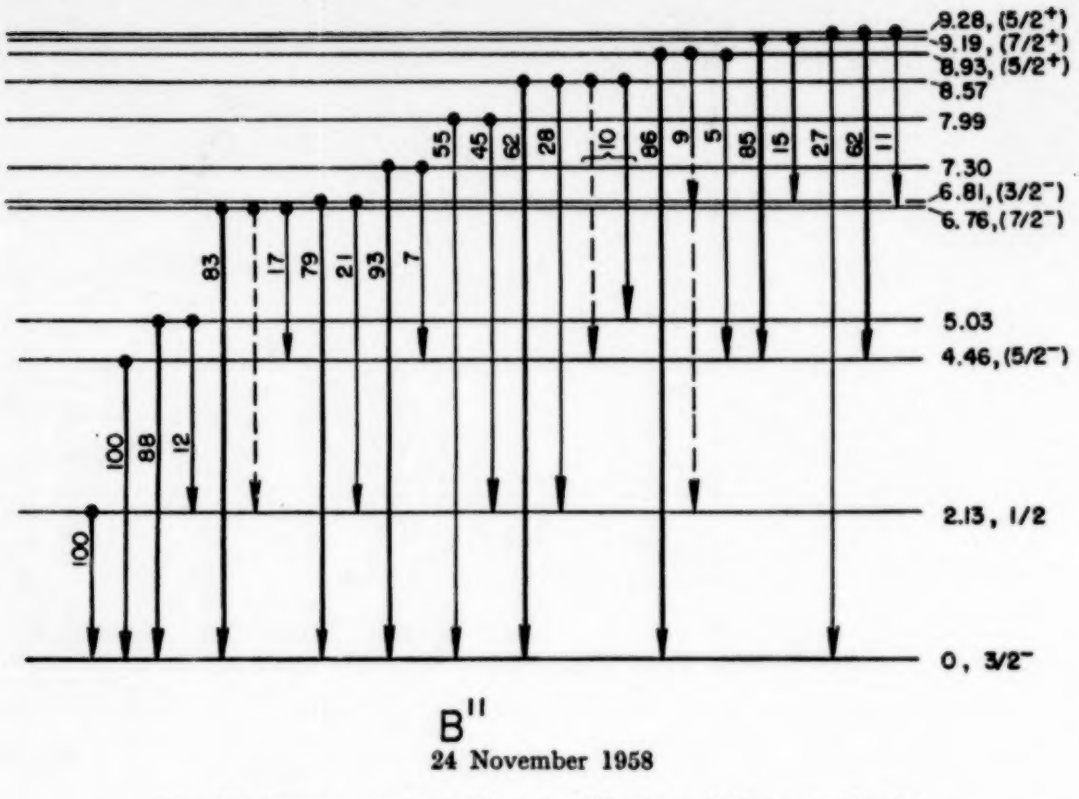

Fig. 17. Gamma-ray transitions in B^{11}: for notation, see fig. 14.

TABLE 11.2

Resonances in $Li^7(\alpha, \gamma)B^{11}$

E_r [a] (MeV ± keV)	Γ_{lab} [a] (keV)	B^{11*} (MeV)	Partial widths [b], $\omega\Gamma_\gamma$(eV) to states of B^{11} at				
			0	2.14	4.46	5.03	6.81 [d]
0.401	<1	8.925	0.15 [c]	<0.003	<0.003	≈0.005	<0.003
0.819 ± 1	≈4	9.191	<0.05	<0.02	2.0	<0.1	≈0.35
0.958 ± 1 [d]	7	9.280	3.5 [e]	<0.17	8.1	<0.4	2.4

[a] (Be 51). See also (He 54b).

[b] (Jo 52d) and D. H. Wilkinson, private communication: compare $Be^9(He^3, p)B^{11}$ and fig. 17. (Be 51) report total gamma widths of 0.04, 0.6 and 4.7 eV for the three resonances.

[c] (Wa 57d) finds $\omega\Gamma = 9 \times 10^{-3}$ eV for the 8.9-MeV state.

[d] (Br 57) find 957.2 ± 2 keV. According to (Fe 58c) the transition from B^{11*}(9.28) is to the 6.76-MeV level and not that at 6.81 MeV.

[e] (Me 58c) report $\omega\Gamma = 0.8$ eV: see $B^{11}(\gamma, \alpha)Li^7$.

V. $Be^9(d, \gamma)B^{11}$ $\quad Q_m = 15.822$

This reaction has not been observed: at $E_d = 0.9$ MeV, $\sigma < 1.8$ μb; at $E_d = 1.5$ MeV, $\sigma < 20$ μb (Al 55c).

VI. $Be^9(d, n)B^{10}$ $\quad Q_m = 4.358$ $\quad E_b = 15.822$

The cross section follows the Gamow function for $E_d = 70$ to 110 keV (Ra 55). The fast neutron and γ-ray yield rise smoothly to $E_d = 1.8$ MeV

TABLE 11.3

Resonances in $Li^7(\alpha, \alpha'\gamma)Li^7$ [a]

E_α (MeV)	B^{11*} (MeV)	$\Gamma_{(c.m.)}$ (MeV)
1.90 ± 0.01 [b]	9.88	0.16 [d]
2.50 ± 0.03 [b]	10.26	0.22 [d]
3.06 ± 0.03 [c]	10.62	0.10
3.6 ± 0.1	11.0	0.67
4.39 ± 0.01	11.46	0.07
4.6 ± 0.1	11.6	0.14
5.0 ± 0.1	11.9	0.17

[a] (Bi 57b): no correction for barrier penetration effects.
[b] (Li 54) and (Bi 57b). See also (He 54b).
[c] (He 54b) and (Bi 57b).
[d] (Li 54) find $\Gamma_{c.m.} = 125 \pm 10$ and $\approx$ 155 keV for the first two levels.

except for a broad resonance at $E_d = 1$ MeV (Sh 57a, Ev 49, Bo 55e). This resonance is observed in the total neutron yield and in the yield of the fast neutrons to each of the first five states of B^{10}. Angular distributions change markedly through the resonance except for that corresponding to $B^{10*}(3.58)$, which is dominated by stripping throughout (Sh 57a). On the other hand, (Ne 58a, Ne 59) have obtained integrated cross sections for three separate neutron groups from $E_d = 0.5$ to 2.0 MeV and find no evidence of a resonance near 1 MeV. See also B^{10}.

VII. $Be^9(d, d)Be^9$ $E_b = 15.822$

In the range $E_d = 1.02$ to 1.44 MeV, two resonance anomalies are reported by (Ju 56d) at $E_d = 1.162$ and 1.348 MeV corresponding to $B^{11*} = 16.77$ and 16.93 MeV ($\Gamma \approx 70$ and 120 keV, respectively). See also Be^9.

VIII. (a) $Be^9(d, p)Be^{10}$ $Q_m = 4.585$ $E_b = 15.822$
(b) $Be^9(d, \alpha)Li^7$ $Q_m = 7.152$
(c) $Be^9(d, t)Be^8$ $Q_m = 4.592$
(d) $Be^9(d, 2\alpha)H^3$ $Q_m = 4.686$
(e) $Be^9(d, tn)Be^7$ $Q_m = -14.307$

Reaction (a) exhibits a simple Gamow dependence to 250 keV (Sa 53b). Angular distributions for $E_d < 1.5$ MeV are reported by (De 52b, Ju 55, Ju 55b, Ju 58a, Sm 57a and Hy 57). The distributions of long-range protons for $E_d = 0.1$ to 0.2 MeV are analyzed in terms of two B^{11} states with $J = \frac{1}{2}^-$ and $\frac{1}{2}^+$ or $J = \frac{3}{2}^-$ and $\frac{1}{2}^+$ (Sm 57a). (Ca 52) reports broad maxima in the 90° yield of ground-state protons at $E_d \approx 0.9$, (1.3) and 2.1 MeV. (Mc 57a) observe broad resonances at 1.3 and possibly at 1.8 MeV in the yield of 3.37-MeV γ-rays, in the range $E_d = 1.0$ to 5.6 MeV. No resonances are observed in the yield of 6-MeV γ-rays for $E_d = 2.0$ to 5.6 MeV. The

cross section for production of Be^{10} (reaction a) rises to a peak value of ≈ 0.34 b at ≈ 4 MeV and then falls almost linearly to ≈ 0.08 b at ≈ 21.5 MeV (He 55e). See also (Co 57a).

The cross section for reaction (b) shows a simple Gamow rise to $E_d = 250$ keV (Sa 53b). Angular distributions have been measured for $E_d = 0.3$ to 0.7 MeV by (Re 51a): see also Li^7. The cross section for reaction (c) has been measured for $E_d = 0.15$ to 0.62 MeV by (De 52b), for $E_d = 0.6$ to 1.5 MeV by (Ju 55, Ju 55b), and at several energies in the range $E_d = 3$ to 19 MeV by (He 55e). The forward yield of tritons shows a peak at $E_d = 1.38$ MeV (Ju 55, Ju 55b). There seems also the possibility of a resonance at $E_d = 0.87$ MeV (Ju 58a). Triton angular distributions for $E_d = 0.1$ to 0.2 MeV are analyzed in terms of two B^{11} states with $J = \frac{5}{2}^-$ and $\frac{3}{2}^+$. (Sm 57a). See also (Hy 57) and Be^8.

Relative yields for the various groups from reactions (a), (b) and (c) are given by (Ge 53). See also (Ja 57).

The direct three-body reaction (d) does not appear to occur (Ge 53). The cross section for reaction (e) has been measured from threshold to $E_d \approx 21.5$ MeV ($\sigma \approx 80$ μb) (He 55e).

IX. $Be^9(t, n)B^{11}$ $\quad Q_m = 9.564$

Not reported.

X. $Be^9(He^3, p)B^{11}$ $\quad Q_m = 10.329$

Angular distributions of the protons to the ground state and several excited states of B^{11} have been determined at various bombarding energies from 2 to 6 MeV: see C^{12}. See also (Wo 56, Ho 56d, Jo 57b).

Gamma rays from the first nine excited states have been observed at $E(He^3) = 2.1$ MeV in coincidence with proton groups. The direct ground state gamma-transition is observed for all the levels. In addition the cascade through the 2.14-MeV state is observed from the 5.03, 6.81, 7.99 and 8.57-MeV states and, possibly, from the 6.76- and 8.92-MeV states, generally with an intensity comparable with that of the corresponding ground state transition. The gamma-ray width, Γ_γ, of the 8.92-MeV level is found to be comparable with its Γ_α. The decay scheme derived from this work is shown in fig. 17 (Fe 57a, Fe 58c). The branching of the 5.03 and 7.30-MeV levels agrees with the shell-model assignments $\frac{3}{2}^-$ and $\frac{5}{2}^-$ (Fe 58c, Ku 57a). At $E(He^3) = 5.7$ MeV, proton groups are reported to levels at 2.126 ± 0.010, 4.459 ± 0.010, 5.037 ± 0.010, 6.756 ± 0.010, 6.807 ± 0.010, 7.296 ± 0.010, 7.987 ± 0.010, 8.569 ± 0.010, 8.927 ± 0.010, 9.191 ± 0.010, 9.278 ± 0.010 and 9.87 ± 0.02 MeV. The 9.87-MeV state is broad, $\Gamma \approx 150$ keV (S. Hinds and R. Middleton, private communication). See also (Mo 54b, Sw 58a, Br 58e) and $Li^7(\alpha, \gamma)B^{11}$.

XI. $Be^9(\alpha, d)B^{11}$ $Q_m = -8.022$

Deuteron groups have been observed at $E_\alpha = 21.6$ MeV to the ground and 2.14-MeV states of B^{11}. A search in the region $E_x = 0.4$ to 1.0 MeV showed no deuteron groups with intensity greater than 0.1 of the intensity of the two observed groups (Ra 55b).

XII. $B^{10}(n, \gamma)B^{11}$ $Q_m = 11.464$

The thermal neutron capture cross section is 0.5 ± 0.2 b. Observed capture γ-rays are listed in table 11.4. The relative weakness of the ground state transition suggests $J = \frac{7}{2}^+$ for the capturing level.

TABLE 11.4

Capture γ-rays in $B^{10}(n, \gamma)B^{11}$ (Ba 57 m)

E_γ [a] (MeV)	Intensity [b] (%)	Γ_γ (eV)	Assignment [c]
11.43 ± 0.04	0.8	0.01	C → 0
8.91 ± 0.03	6		8.93 → 0
6.98 ± 0.03	18	0.2	C → 4.46
6.74 ± 0.03	10		6.76 → 0
4.73 ± 0.03	30	0.1	C → 6.76 9.19 → 4.46?
4.47 ± 0.02	80		4.46 → 0

[a] Corrected for recoil.
[b] γ-rays per 100 radiative captures (Ba 58k).
$\sigma_{n,\gamma}$ (total) $= 0.5 \pm 0.2$ b.
[c] "C" = capturing level: $Q_m = 11.464$.

XIII. $B^{10}(n, n)B^{10}$ $E_b = 11.464$

The epithermal scattering cross section (free) is 3.6 ± 0.2 b (Hu 58). Broad maxima appear in the total cross section at $E_n = 1.9$ and 2.8 MeV (Bo 51c) and at 4 MeV (Hu 57); additional peaks near 0.2 and 0.4 MeV may be indicated (Bo 51c). Differential cross sections have been measured at $E_n = 0.55$, 1.00 and 1.50 MeV: derived phase shifts are $\delta_0 = -53.5°$ at $E_n = 0.55$ MeV, $\delta_0 = -60.7°$, $\delta_1 = -4.0°$ at $E_n = 1.00$ MeV, and $\delta_0 = -66.9°$, $\delta_1 = -10.3°$, $\delta_2 = -2.9°$ at $E_n = 1.50$ MeV (Wi 55d). The total cross section decreases from ≈ 1.9 b at 4.4 MeV to 1.6 b at 5.6 MeV and then remains approximately constant at ≈ 1.5 b from 6 to 9.7 MeV (Be 56c, Ne 54c). At $E_n = 14$ MeV it is 1.47 ± 0.03 b (Co 52h) and it remains nearly constant to 18 MeV (Co 54f: $\sigma = 1.45 \pm 0.02$ b). See (Hu 57).

XIV. $B^{10}(n, n')B^{10*}$ $E_b = 11.464$

See (Ph 52b) and (Da 56d).

XV. $B^{10}(n, p)Be^{10}$ $Q_m = 0.227$ $E_b = 11.464$

The thermal cross section is < 0.2 b (Hu 58); the cross section for fast pile neutrons is 3 mb (Eg 48).

XVI. $B^{10}(n, d)Be^{9}$ $Q_m = -4.358$ $E_b = 11.464$

At $E_n = 14$ MeV, the integrated cross sections (0° to 90°, c.m.) for the transitions to the ground and the 2.4-MeV states of Be^9 are 21 ± 3 m band 16 ± 2 mb, respectively (Ri 54a). See also (Fr 56a).

XVII. $B^{10}(n, t)Be^{8}$ $Q_m = 0.234$ $E_b = 11.464$

For $E_n = 5.20$ MeV, production of tritons appears to be mainly via $B^{10}(n, \alpha)Li^{7*}(4.7)$ and direct 3-body breakup (Fr 56a). Cross sections at $E_n = 4$, 5.6, 9.6 and 14.1 MeV are 95 ± 10, 230 ± 25, 125 ± 15 and 85 ± 6 mb, respectively (Wy 58a).

XVIII. $B^{10}(n, \alpha)Li^{7}$ $Q_m = 2.793$ $E_b = 11.464$

Recent values for the thermal neutron absorption cross section in natural boron are 749 ± 4 b (Ca 53c), 755 ± 3 b (Ha 53g), 744 ± 20 b (Sc 54b), 764 ± 3 b (Da 54b) and 760 ± 3 b (Co 56c). (Hu 58) give 755 ± 2 b for the thermal absorption cross section in "U. S. standard" boron and 3813 b for the thermal isotopic cross section; see also (Hu 57). The cross section follows the $1/v$ law from 7×10^{-4} eV to 100 keV (Bi 57b, Hu 55c). (Bi 57) report $\sigma_{tot} = 642/\sqrt{E_n} + 2.45$ b for $E_n = 3$ to 70 keV. The data from $E_n = 0$ to 250 keV can be satisfactorily interpreted in terms of the B^{11} levels at 11.46 and 11.68 MeV ($E_n = 0$ and 140 keV) observed in $Li^7(\alpha\ \alpha')Li^{7*}$ (Bi 57b). (Be 57e) find, on the other hand, that deviations from the $1/v$ law for $E_n < 1$ MeV indicate a single broad level at $E_n \approx 250$ keV with $J = \frac{5}{2}^+$ or $\frac{7}{2}^+$, $\Gamma_\alpha \approx 400$ keV, $\Gamma_n \approx 200$ keV. A pronounced resonance is observed at $E_n = 1.86$ MeV: $\Gamma_{c.m.} = 0.45$ MeV ((Bi 57b) and (Pe 51c); see also (St 50d) and (Bi 52)). There are indications of less pronounced resonances at 0.53, 2.8 and 4.1 MeV (with $\Gamma_{c.m.} = 0.10$, 0.3 and 0.5 MeV) in the energy range to $E_n = 4.8$ MeV (Bi 57b). The ratio of ground-state to excited state transitions varies strongly with energy: see (Aj 52c, De 54, Bu 58a).

Cross sections for production of $2\alpha + t$ either through the 4.6-MeV level of Li^7 or via three-body breakup have been determined for $E_n = 4$ to 19.5 MeV. A strong maximum near $E_n = 5.6$ MeV may indicate a resonance near $B^{11*} = 16.6$ MeV (Fr 56a, Wy 58). See also (Aj 55).

XIX. $B^{10}(d, p)B^{11}$ $Q_m = 9.237$

Proton groups reported by (Va 51a) and (El 53) are listed in table 11.5. No other levels are observed below $E_x = 11.46$ MeV: the known levels observed in $Li^7(\alpha, \alpha')Li^7$ are presumably too wide to be seen here. See also (Kh 54, Kh 55a).

TABLE 11.5

Proton groups from $B^{10}(d, p)B^{11}$

B^{11}* [a] (MeV ± keV)	Γ (keV)	$\frac{d\sigma}{d\Omega}$ [b] (mb/sr)	l_n	J^π	A_n [h]
0 ±11		2	1 [e]	$\frac{3}{2}^-$	5.0
2.138 ± 9	<15	0.4	1 [d]	$\frac{1}{2}^-$ [d]	0.9
4.459 ± 8	<15	1.2	1 [e]	$\frac{3}{2}^-$, $\frac{5}{2}^-$ [g]	1.6
5.034 ± 8	<15	1.0	1 [e]		0.5
6.758 ± 7	<15	2	1 [f]	$\frac{3}{2}^-$, $\frac{7}{2}^-$ [g]	5.7
6.808 ± 7	<15	0.2			weak [f]
7.298 ± 6	<15	1.2			weak [f]
7.987 ± 9	<10				weak [f]
8.568 ± 5	<10	0.3	(2) [f]	$(\frac{1}{2}^+, \frac{3}{2}^+)$	weak [f]
8.927 ± 5	< 4	5	2, 0 [f]	$\frac{3}{2}^+$, $(\frac{7}{2}^+)$	
9.191 ± 5	<10	8	0 [f]	$(\frac{1}{2}^+)$, $\frac{7}{2}^+$	
9.276 ± 5	<10	4	0 [f]	$\frac{3}{2}^+$, $(\frac{7}{2}^+)$	
10.32 ±20	54 ± 17 [c]				

[a] (Va 51a, El 53): stated errors refer to Q-values.
[b] Approximate differential cross sections in mb/sr at $\theta = 90°$, $E_d = 1.51$ MeV (Va 51a).
[c] The width of this state suggests that it is not to be identified with that observed at 10.26 MeV in $Li^7(\alpha, \alpha')Li^7$.
[d] See text.
[e] (Ev 54; $E_d = 7.7$ MeV).
[f] (Bi 58).
[g] From $p-\gamma$ correlation (Co 57a).
[h] Relative neutron capture probability (Ev 54: $E_d = 7.7$ MeV).

The angular distribution of protons leading to the ground state ($J = \frac{3}{2}^-$) shows a well-developed $l_n = 1$ stripping pattern at all energies $\gtrsim 2.0$ MeV (Ev 54, Ev 58: 7.7 MeV), (Ho 53c: 8 MeV), (Ze 56: 10 MeV), (Le 57: 15.1 MeV), (Ma 56j: 1.0 to 3.0 MeV); see, however, (Co 57a). Even below $E_d = 1$ MeV, stripping appears to play an important role in formation of this level (Pa 54a, Bu 54, Ha 57i). The relatively large neutron capture probability suggests a single-particle character (Ev 54, Ho 53c). See also (Ha 57i, Co 57a). The polarization has been studied by (Hi 58a, He 58b).

For the 2.1-MeV state, the evidence is not so clear: the pattern though generally of an $l_n = 1$ shape (see, however, Pa 54a, Le 57) shows strong variations with energy (Ev 54, Ev 58, Ze 56, Le 57, Ma 56j, Co 57a). An $l_n = 1$ formation implies $\frac{3}{2}^- \leqq J \leqq \frac{9}{2}^-$, in contradiction to the shell-model expectation that the state should have $J = \frac{1}{2}^-$; however to form such a state requires $l_n = 3$, involving rearrangement of several nucleons and hence a low probability (Ma 56j, Ev 58). The more probable mode of formation would appear to involve a nucleon exchange (Ev 58) or a spin reversal of the outgoing proton (Wi 57c). The observation that the polarization of protons for this state is opposite to those corresponding to the ground state

is consistent with either point of view, and permits $\frac{1}{2}^- \leqq J \leqq \frac{11}{2}^-$ (He 58b). Support for the assignment $J = \frac{1}{2}$ is found in the observed isotropy of the p—γ correlation (see below): see also $B^{11}(p, p')B^{11*}$, (Wi 57c, Bo 58f).

The 4.46-, 5.03- and 6.76-MeV states are also formed by $l_n = 1$. The large neutron capture probability for the 6.76-MeV state indicates that it has a single-particle character (Bi 58, Ev 54). See also (Co 57a, Sj 57). The next four states appear only weakly and probably arise from configuration mixing (Bi 58).

For the 8.92-MeV state, $l_n = 2$ with a small admixture of $l_n = 0$ is indicated; $J = \frac{5}{2}^+, \frac{7}{2}^+$. The large γ-width suggests $J = \frac{5}{2}^+$. The 9.19 and 9.28-MeV states are formed with $l_n = 0$, $J = \frac{5}{2}^+$ or $\frac{7}{2}^+$; the intensity ratio is consistent with $J(9.19) = \frac{7}{2}^+$, $J(9.28) = \frac{5}{2}^+$. Again, the high relative intensities suggest that these three are single-particle states, formed by direct capture into the 1d, 2s shell (Bi 58); see also $Li^7(\alpha, \gamma)B^{11}$.

Gamma rays reported by (Be 55g) and (Sa 55f) are listed in table 11.6.

TABLE 11.6

γ-rays from $B^{10}(d, p)B^{11}$

E_γ [a] (MeV)	Total σ [b] (mb)	E_γ [c] (MeV)	$I_{(rel)}$ [d]	Assignment B^{11*}
4.49±0.05	5.0	4.46±0.04	14	4.46 → 0
5.03±0.03	3.0	5.03±0.09	6	5.03 → 0
6.75±0.03	5.4	6.78±0.07	6	6.76 → 0
7.30±0.03	6.0	7.29±0.04	5	7.30 → 0
		8.27±0.09	4	
8.57±0.04	1.8			8.57 → 0
8.93±0.04	8.1	8.87±0.02	11	8.93 → 0
4.73±0.03	6.3	4.75±0.03	6	9.19 → 4.46

[a] (Be 55g): Doppler corrected.
[b] Average value $E_d = 0$ to 2.0 MeV (Be 55g).
[c] (Sa 55f): no Doppler correction.
[d] Relative intensity (Sa 55f): ($E_d = 1.4$ MeV).

The p—γ angular correlation through the 2.14-MeV state is isotropic to ≈ 4 per cent, consistent with $J = \frac{1}{2}$: see (Th 53, Ga 57a, Go 55i, Go 56h, Go 56f). The angular correlation through the 4.46-MeV state is consistent with $J = \frac{3}{2}^-$ or $\frac{5}{2}^-$; that through the 6.76-MeV state rules out $J = \frac{3}{2}$ and suggests $J = \frac{9}{2}^-$ is unlikely for that state (Co 57a). See also (Va 56c).

XX. $B^{10}(t, d)B^{11}$ $\quad Q_m = 5.205$

Not reported.

XXI. $B^{10}(\alpha, He^3)B^{11}$ $\quad Q_m = -9.114$

Not reported.

XXII. $Be^{11}(\beta^-)B^{11}$ $\quad Q_m = 11.48$

The decay properties of Be^{11} are exhibited in table 11.7. The transition energy to the ground state is $E_\beta(\max) = 11.48 \pm 0.15$ MeV; $\tau_{\frac{1}{2}} = 13.57 \pm 0.15$ sec, log $ft = 6.77$ (Al 58e, Wi 59), $\tau_{\frac{1}{2}} = 14.1 \pm 0.3$ sec (Nu 58). The transition probabilities to B^{11}(g.s.), $J = \frac{3}{2}^-$, and $B^{11*}(2.1)$, $J = \frac{1}{2}^-$, suggest $J = \frac{1}{2}^-$ for Be^{11}, but it is not clear why the transition should be so much inhibited as compared with other allowed transitions (Wi 59).

TABLE 11.7

Beta decay of Be^{11}(Al 58e, Wi 59)

B^{11*} (MeV)	J^π	% betas	log ft	E_γ (MeV $\pm$ keV)	% gammas [a]
0	$\frac{3}{2}^-$	61	6.77		
2.138	$\frac{1}{2}^-$	29	6.63	2.121 $\pm$ 10	32
4.459	$(\frac{1}{2}^-)$	$\leqq$0.2	$\geqq$8.2		
5.034		$\leqq$0.2	$\geqq$8.2		
6.758		6.5	5.93	6.76 $\pm$30	4.4
6.808				4.64 $\pm$20	2.1
7.298		$\leqq$1.5	$\geqq$6.4		
7.987		4.1	5.53	7.97 $\pm$30	1.7
				5.86 $\pm$40	2.4
8.568		$\leqq$0.3	$\geqq$6.3		
8.927		$\leqq$0.15	$\geqq$6.3		

[a] Relative to all β-transitions.

XXIII. $B^{11}(\gamma, \gamma)B^{11}$

The mean life of the 4.46-MeV level, determined by resonance absorption and scattering is $\tau_m = 1.17 \pm 0.17 \times 10^{-15}$ sec, assuming $J = \frac{5}{2}$. On the same assumption, the intensity ratio of quadrupole to dipole transitions is $\leqq 0.2$ (Ra 58a). A mean life of $\approx 1.5 \times 10^{-15}$ sec is calculated by (Ku 57a).

A similar experiment yields $\tau_m = (4.6 \pm 0.6) \times 10^{-15}$ sec for the 2.1-MeV state, assuming $J = \frac{1}{2}$. The result does not distinguish $J = \frac{1}{2}^-$ from $J = \frac{1}{2}^+$, but the shortness of the lifetime excludes $J > \frac{1}{2}$(Me 58): see (Wi 57c: $B^{11}(p, p')B^{11*}$). A calculation in intermediate coupling, assuming an M1 transition yields $\tau_m = (2.5$ to $5) \times 10^{-15}$ sec (Ku 57a). See also (Mc 58).

XXIV. $B^{11}(\gamma, n)B^{10}$ $\quad Q_m = -11.464$

See (Sh 51d) and (Ti 55a).

XXV. $B^{11}(\gamma, t)He^4 + He^4$ $\quad Q_m = -11.136$

See (Aj 55).

XXVI. $B^{11}(\gamma, \alpha)Li^7$ $\quad Q_m = -8.670$

Resonance absorption of 9.19-MeV radiation yields $\Gamma < 100$ eV, $(2J+1)\Gamma_\gamma \approx 0.8$ eV for $B^{11*}(9.19)$ (Me 58c).

XXVII. $B^{11}(n, n')B^{11*}$

At $E_n = 4.5$ MeV, a 2.2-MeV γ-ray is reported (Gr 55d, Da 56). See also (Sc 54c).

XXVIII. $B^{11}(p, p')B^{11*}$

At $E_p = 3.58$ MeV, a 2.134 ± 0.005-MeV γ-ray is observed (Mc 57a); see also (Hu 53). The mean lifetime of the 2.14-MeV state has been determined by a Doppler shift measurement to be $< 4 \times 10^{-14}$ sec (Wi 57c): see $B^{11}(\gamma, \gamma)B^{11}$. It is pointed out that the observed isotropy in $B^{10}(d, p\gamma)B^{11}$ requires a nearly pure E2 transition if $J = \frac{3}{2}^-$ and the present lifetime value excludes E2. On the other hand, the lifetime is quite consistent with M1 (Wi 57c). The 2.14-MeV γ-ray exhibits $< 2.0 \times 10^{-3}$ part of circular polarization; this observation places an upper limit of $F^2 \lesssim 1 \times 10^{-7}$ for the intensity of the parity non-conserving part of the wave function (Wi 58c).

At $E_p = 185$ MeV, inelastic groups with $Q = -4.7$, -6.6 and -8.5 MeV are observed; the latter shows strong forward peaking and is attributed to a spin flip of a target nucleon, indicating $J = \frac{1}{2}^-$, $\frac{3}{2}^-$ or $\frac{5}{2}^-$ (Ty 58). See also (St 56, Aj 55) and C^{12}.

XIX. $B^{11}(d, d')B^{11*}$

Ground state deuterons have been observed at $E_d = 4.2$ MeV (Kh 55a).

XXX. $C^{11}(\beta^+)B^{11}$ $\quad Q_m = 1.981$

See C^{11}.

XXXI. $C^{12}(\gamma, p)B^{11}$ $\quad Q_m = -15.958$

See C^{12}.

XXXII. $C^{12}(p, 2p)B^{11}$ $\quad Q_m = -15.958$

At $E_p = 185$ MeV, the summed proton spectrum shows peaks attributed to removal of p- and s-protons (Ty 58b, Ma 58h).

XXXIII. (a) $C^{12}(n, d)B^{11}$ $\quad Q_m = -13.731$

(b) $C^{12}(d, He^3)B^{11}$ $\quad Q_m = -10.465$

These reactions have not been reported.

XXXIV. $C^{12}(t, \alpha)B^{11}$ $\quad Q_m = 3.855$

This reaction has been observed at $E_t = 1.4$ MeV (Cu 55b). See also (Ja 58).

XXXV. (a) $C^{13}(n, t)B^{11}$ $\quad Q_m = -12.419$

(b) $C^{13}(p, He^3)B^{11}$ $\quad Q_m = -13.184$

These reactions have not been reported.

XXXVI. $C^{13}(d, \alpha)B^{11}$ $Q_m = 5.167$

Alpha-particle groups have been observed corresponding to $B^{11*} = 2.107 \pm 0.017$ MeV (Li 51b) and 4.45 and 6.83 MeV (Sp 53c). A 4.46-MeV γ-ray observed by (Be 55a) in (C^{13}+d) is definitely assigned to the present reaction by (Ra 58b). See also (Aj 55).

XXXVII. $C^{14}(p, \alpha)B^{11}$ $Q_m = -0.780$

Not reported.

XXXVIII. $N^{14}(n, \alpha)B^{11}$ $Q_m = -0.152$

Q_0-values of -0.12 ± 0.06 and -0.18 ± 0.05 MeV are reported by (Do 58a). See also (Li 52).

C^{11}

(Fig. 18, pag. 107) †

THEORY

See (Ku 56, Ku 57a, Fr 58b).

I. $C^{11}(\beta^+)B^{11}$ $Q_m = 1.981$

The spectrum is simple; $E_{\beta^+}(\max) = 968 \pm 8$ keV (Wo 54a). The mean of half-lives reported in (Aj 55) is 20.44 ± 0.04 min. Recent values of the half-lives are 20.26 ± 0.1 min (Ba 55e), 20.8 ± 0.2 min (Pr 57b) and 20.11 ± 0.13 min (Ar 58); log $ft = 3.62$ (Wo 54a). The ratio of K-capture to positon emission is 0.19 ± 0.03 per cent (Sc 57). See also (Br 57, Ka 57a).

II. (a) $Li^6(Li^6, n)C^{11}$ $Q_m = 9.462$

(b) $Li^7(Li^6, 2n)C^{11}$ $Q_m = 2.209$

See (No 57a).

III. $Be^9(He^3, n)C^{11}$ $Q_m = 7.565$

See (Po 52b, Ku 53a, Mo 54b).

IV. $B^{10}(p, \gamma)C^{11}$ $Q_m = 8.700$

For $E_p = 0.7$ to 3 MeV, the main capture radiation is to the ground state. Weaker radiations, ≈ 5 per cent, with $E_\gamma \approx 4.2$ and 5.8 MeV suggest a cascade through the 4.23-MeV level (Hu 57b, Ch 56a). Two broad resonances are reported at 1.14 and ≈ 4 MeV: see table 11.9 (Da 54, Ch 56a, Ha 55, Hu 57b, Ba 55f). The angular distribution at the first resonance is $1+0.5 \cos^2 \theta$. Using $\sigma_a = 16$ mb/sr, (Ch 56a) find $\omega\Gamma_p \approx 40$ keV, $\Gamma_a \approx 500$ keV, $\omega\Gamma_\gamma = 10$ eV, consistent with M1 radiation. The angular distribution and the gamma-ray width appear to rule out all $J \leqq \frac{7}{2}$ except $J = \frac{5}{2}^-$(Ch 56a); see, however, $B^{10}(p, \alpha)Be^7$ (Cr 56a). The cross section increases rapidly in the range $E_p = 2.2$ to 2.7 MeV, but there is no indication of a previously reported

† For level scheme of B^{11}, see fig. 16, p. 95

2.4-MeV resonance (see (Da 54)) (Hu 57b, Ba 55f). See also (Wi 55i), (Aj 55), and (Ja 57).

V. $B^{10}(p, n)C^{10}$ $Q_m = -4.56$ $E_b = 8.700$

The cross section is $\leqq 1.4$ mb at $E_p = 5.35$ MeV, $\leqq 2$ mb at $E_p = 5.51$ MeV (Gi 59). See (Ma 58a, Ta 58a) and C^{10}.

TABLE 11.8

Energy levels of C^{11}

E_x in C^{11} (MeV)	J^π	$\tau_{\frac{1}{2}}$ or Γ (min) (keV)	Decay	Reactions
0	$(\frac{3}{2}^-)$	$\tau_{\frac{1}{2}} = 20.45 \pm 0.06$ min	β^+	I, II, III, IV, XI, XIV, XV, XVII, XVIII, XIX, XX, XXI, XXIII, XXIV
1.99 ±0.02	$(\frac{1}{2}^- \rightarrow \frac{3}{2}^-)$		γ	XI, XII, XV, XXI
4.26 ±0.03	$(\frac{1}{2}^- \rightarrow \frac{3}{2}^-)$		γ	IV, XI
4.75 ±0.03	$(\frac{1}{2}^- \rightarrow \frac{3}{2}^-)$		γ	XI
6.50 ±0.02			γ	XI
6.77 ±0.04			(γ)	XI
7.40 ±0.04			γ	XI
8.108±0.008				XI
8.431±0.008				XI
8.661±0.008				XI
8.98 ±0.03				XI
(9.13 ±0.02)				XI
(9.28 ±0.03)				XI
9.74 ±0.01	$(\frac{1}{2}^-)$	450	γ, p, α	IV, VI, X, XI
10.09 ±0.01	$(\frac{7}{2}^+)$	200	p, α	VI, X, XI
(10.69±0.02)				XI
10.89 ±0.02				XI
(11.26 ±0.02)				XI
(11.52±0.02)				XI
12.3		≈500	γ, p, α	IV, X
13.8 ±0.2			p, α	X
(15.7 ±0.2)			(p, α)	X

VI. $B^{10}(p, p)B^{10}$ $E_b = 8.700$

The elastic scattering cross section at $\theta = 138°$ rises from nearly the Rutherford value for $E_p < 0.9$ MeV to 4 times Rutherford at $E_p = 1.6$ MeV. Anomalies are observed at $E_p = 1.15$ and 1.5 MeV (Br 51a). See table 11.9.

VII. $B^{10}(p, p')B^{10*}$ $E_b = 8.700$

The yield of 0.71-MeV radiation, from the first excited state of B^{10}, rises monotonically from $E_p = 1.5$ to 2.7 MeV (Da 52, Da 54, Hu 57b). At $E_p = 2.7$ MeV the cross section is 11 ± 5 mb (Hu 57b). Above $E_p = 2.4$ MeV, weak (≈ 1 per cent) γ-rays of 1.00 ± 0.04 MeV ($1.74 \rightarrow 0.71$ transition in B^{10}) and 2.12 ± 0.06 MeV ($2.14 \rightarrow$ ground transition) are observed (Hu 57b). See also (Cr 52c), (Ch 56a) and (Ja 57).

VIII. $B^{10}(p, d)B^{9}$ $Q_m = -6.212$ $E_b = 8.700$

See B^{9}.

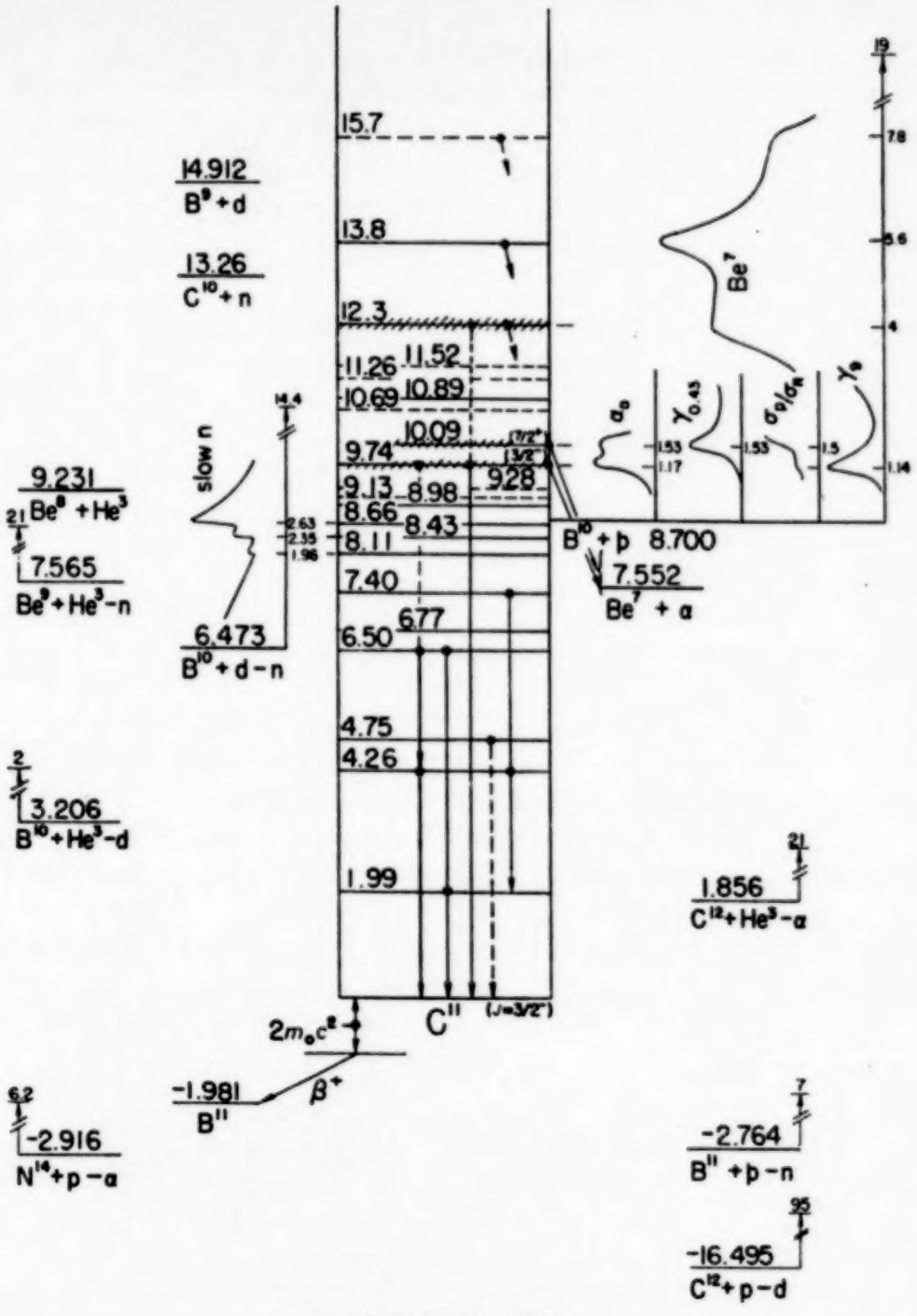

29 December 1958

Fig. 18. Energy levels of C^{11}: for notation, see fig. 1.

IX. $B^{10}(p, He^{3})Be^{8}$ $Q_m = -0.532$ $E_b = 8.700$

See Be^{8}.

TABLE 11.9

Resonances in $B^{10}(p, \gamma)C^{11}$, $B^{10}(p, p)B^{10}$, $B^{10}(p, \alpha_0)Be^7$ and $B^{10}(p, \alpha_1\gamma)Be^7$

Reaction	E_{res} (MeV)	Γ_{lab} (keV)	σ	E_x (MeV)	J^π	Refs.
$B^{10}(p, \gamma)C^{11}$	1.146±0.005	414±20	5.5±2.8 μb	9.74		(Hu 57b)
$B^{10}(p, \gamma)C^{11}$	1.135±0.015	540±40	3.5±1.0 μb		$(\frac{1}{2}^-)$	(Ch 56a)
$B^{10}(p, \gamma)C^{11}$	1.21		7.5±3.8 μb			(Da 54)
$B^{10}(p, \gamma)C^{11}$	1.18 ±0.04	570±20				(Ha 55)
$B^{10}(p, \alpha_0)Be^7$	1.15		205 ±40 mb			(Br 51a)
$B^{10}(p, p)B^{10}$	(1.15)					(Br 51a)
$B^{10}(p, \alpha_0)Be^7$	1.1	>330			$(\frac{1}{2}^+)$	(Al 56c)
$B^{10}(p, \alpha_0)Be^7$	1.17	300	210 ±40 mb		$\frac{1}{2}^-$	(Cr 56a)
$B^{10}(p, \alpha_1\gamma)Be^7$	1.533±0.005	220	80 ±40 mb	10.09		(Hu 57b)
$B^{10}(p, \alpha_1\gamma)Be^7$	1.5	250	100 ±20 mb		$\frac{3}{2}^+$	(Cr 56a)
$B^{10}(p, \alpha_0)Be^7$	1.5	250	230 ±40 mb		$\frac{3}{2}^+$	(Cr 56a)
$B^{10}(p, \alpha_1\gamma)Be^7$	1.52	250	140 ±30 mb			(Br 51a,
			210 ±70 mb			Da 54)
$B^{10}(p, \alpha_0)Be^7$	1.5		140 ±30 mb			(Br 51a)
$B^{10}(p, p)B^{10}$	(1.5)					(Br 51a)
$B^{10}(p, \alpha_1\gamma)Be^7$	1.53		210 ±50 mb			(Ch 56a)
$B^{10}(p, \alpha_0)Be^7$	1.5	≈230			$(\frac{1}{2}^-)$	(Al 56c)
$B^{10}(p, \gamma)C^{11}$	≈4	≈500		12.3		(Ba 55f)
$B^{10}(p, \alpha)Be^7$	≈4					(Ka 57a)
$B^{10}(p, \alpha)Be^7$	5.6			13.8		(Ka 57a)
$B^{10}(p, \alpha)Be^7$	(7.8)			(15.7)		(Ka 57a)

X. $B^{10}(p, \alpha)Be^7$ $\quad Q_m = 1.147$ $\quad E_b = 8.700$

The excitation function is a smooth exponential from $E_p = 60$ to 200 keV (Ba 55m). Excitation functions have been studied up to 3 MeV (see Ja 57). Using the stacked foil method, (Ka 57a) report structure in the excitation function corresponding to C^{11} levels at 12.3, 13.8±0.2 and 15.7±0.2 MeV. The ground state α-particles (α_0) exhibit broad resonances at $E_p = 1.17$ and 1.53 MeV superposed on a continuous isotropic background (Cr 56a, Br 51a, Al 56c). Alpha particles to the 0.43-MeV Be^7 state (α_1) and 0.43-MeV γ-rays show only the resonance at $E_p = 1.53$ MeV (Hu 57b, Cr 56a, Br 51a, Da 54,

TABLE 11.10

Resonance parameters for $B^{10}(p, \alpha)Be^7$ (Cr 56a)

E_{res} (MeV)	J^π	Γ (keV)	Γ_p (keV)	Γ_{α_0} (keV)	Γ_{α_1} (keV)	θ_p^2 (%)	$\theta_{\alpha_0}^2$ (%)	$\theta_{\alpha_1}^2$ (%)
1.17	$\frac{1}{2}^-$	300	75 [a,c]	225	non res	0.8	8	
			225 [a]	75		2.5	2.7	
1.53 [b]	$\frac{3}{2}^+$	250	160 [a]	56	34	13	15.7	20.3
			90 [a]	100	60	9	32	42

[a] Alternative solutions.

[b] (Hu 57b).

[c] Compare $B^{10}(p, \gamma)C^{11}$.

Ch 56a). A summary of the evidence on the (B^{10}+p) resonances is given in tables 11.9 and 11.10.

The reaction cross section for α_0 at the $E_p = 1.17$-MeV resonance requires $J \geqq \frac{3}{2}$. The angular distribution is isotropic, except for small terms attributed to interference, restricting the choice to $\frac{5}{2}^+$, $\frac{7}{2}^+$, $\frac{3}{2}^-$. The absence of α_1 suggests $\frac{3}{2}^-$, $\frac{5}{2}^+$ as most likely; $\frac{3}{2}^-$ would agree with the mirror level in B^{11} (Cr 56a: see table 11.10).

At the $E_p = 1.5$-MeV resonance. the angular distribution of α_0 has the form $1-0.53\cos^2\theta$. Between resonances, coefficients of odd order Legendre polynomials show a sharp peak, indicating that the two levels have opposite parity. The α_1 distribution at $E_p = 1.5$ MeV also shows interference effects. From the reaction cross section at $E_p = 1.5$ MeV, $J \geqq \frac{5}{2}$. The most satisfactory account of the α_0 and α_1 angular distributions is given with the assumption of $J = \frac{7}{2}^+$, formed by s- and d-waves. The assumption $J = \frac{5}{2}^+$, $\frac{5}{2}^-$ for the 1.17 and 1.5-MeV resonances is excluded (Cr 56a: see table 11.10).

At $E_p = 1.2$ MeV the (non-resonant) 430-keV γ-rays are isotropic ± 2 per cent (Ch 56a). See also (Wi 55i).

XI. B^{10}(d, n)C^{11} $Q_m = 6.473$

Level information derived from studies of the neutron groups is displayed in table 11.11 (Jo 52a, Pa 54b, Gr 56f, Ma 56p, Ce 56, Gr 57a, Mc 58f, Ne 59). See also (Bu 54, Bo 56l, Gi 53). A search for possible doublet structure at $E_x = 6.50$ MeV revealed no other level in this neighborhood. A group with relative intensity $\frac{1}{10}$ would have been seen if the separation were as much as 40 keV (Ne 59: $E_d = 1.5$ MeV, $\theta = 60°$).

Neutron threshold measurements indicate levels in C^{11} at 8.108, 8.431, and 8.661 MeV (Ma 55j; ± 0.008 MeV). Gamma-ray measurements indicate lines with $E_\gamma = 4.75 \pm 0.03$ MeV (Sa 55f), 5.35 ± 0.05 MeV (Sa 55f; from $C^{11*}(7.4 \rightarrow 2.0)$), and 6.50 ± 0.03 (Be 55g; Doppler corrected), 6.52 ± 0.05 MeV (Sa 55f). Gamma rays of energy 6.5, 4.3 and ≈ 2.0 MeV are observed in coincidence with neutrons leading to C^{11*}(6.50). In coincidence with neutrons to C^{11*}(4.26 and 4.75, unresolved) are $E_\gamma = 4.28$, ≈ 2.3, ≈ 2.0 MeV (Mc 58f). See also (Bi 57c).

XII. B^{10}(He^3, d)C^{11} $Q_m = 3.206$

At $E(He^3) = 2$ MeV, deuterons have been observed in coincidence with a 2.0 ± 0.1 MeV γ-ray (Go 57b).

XIII. $B^{10}(\alpha, t)C^{11}$ $Q_m = -11.113$

Not reported.

XIV. B^{10}(Li^6, He^5)C^{11} $Q_m = 4.045$

See (No 57a).

TABLE 11.11
Levels of C^{11} from $B^{10}(d, n)C^{11}$

E_x (MeV ± keV)	l_p	J^π	References
0	1	$\frac{3}{2}^- \rightarrow \frac{3}{2}^-$ [c]	Ma 56p, Pa 54b, Ce 56
1.94 ±50	1	$\frac{3}{2}^- \rightarrow \frac{3}{2}^-$ [a,c]	Jo 52a, Gr 56f, Ce 56, Ma 56p, Pa 54b
4.26 ±30	1	$\frac{3}{2}^- \rightarrow \frac{1}{2}^-$	Jo 52a, Pa 54b, Gr 56f, Ce 56, Ne 59, Mc 58f
4.75 ±30	1	$\frac{3}{2}^- \rightarrow \frac{1}{2}^-$	Jo 52a, Gr 56f, Ce 56, Sa 55f, Ne 59
6.50 ±20	b		Jo 52a, Ce 56, Be 55g, Sa 55f, Ne 59, Mc 58f
6.77 ±40	b		Jo 52a, Ce 56
7.40 ±40			Jo 52a, Ce 56
8.108 ± 8			Ma 55j, Jo 52a, Ce 56
8.431 ±10	d		Ma 55j, Jo 52a, Ce 56
8.661 ±10	d		Ma 55j, Jo 52a, Ce 56
8.97 ±20			Jo 52a, Ce 56, Gr 57a
(9.13 ±20)			Jo 52a
(9.28 ±30)			Ce 56
9.69 ±30			Ce 56
10.09 ±20			Ce 56, Gr 57a
(10.69 ±20)			Ce 56, Gr 57a
10.89 ±20 [e]			Ce 56, Gr 57a

[a] J probably $\frac{1}{2}^-$: see $B^{10}(d, p)B^{11}$.
[b] $l_p = 1$ for unresolved groups at $E_x \approx 6.6$ MeV (Ma 56p).
[c] $(2J+1)\gamma^2 = 2.1 \times 10^{-13}$ and 0.8×10^{-13} erg · cm for $B^{11}(0)$ and (2.1), respectively (Ma 56p): $\theta_n^2 = 0.02$ and 0.016.
[d] $l_p = 1$ for unresolved groups at $E_x \approx 8.5$ MeV (Ma 56p). (Gr 57a) reports $l_n = 0$.
[e] Neutron groups are also reported to $E_x = (11.26 \pm 0.02)$ and (11.52 ± 0.02) MeV (Ce 56).

XV. $B^{11}(p, n)C^{11}$ $\quad Q_m = -2.764$
$Q_0 = -2.83\ ^{+0.06}_{-0.05}$(Aj 56).

At $E_p = 7.03$ MeV, groups are observed corresponding to the ground state and to a state at 2.01 ± 0.06 MeV. The intensity of the ground-state group is ≈ 2.5 times that of the $C^{11*}(2.0)$ group at the four angles studied; $I(0°)/I(20°) \approx 2.5$ for both groups. An appreciable number of low-energy (< 1.5 MeV) neutrons of undetermined origin is reported (Aj 56). See also (Ma 55k, Go 58g).

XVI. $B^{11}(He^3, t)C^{11}$ $\quad Q_m = -1.999$
Not reported.

XVII. $C^{12}(n, 2n)C^{11}$ $\quad Q_m = -18.722$
See C^{13}.

XVIII. $C^{12}(\gamma, n)C^{11}$ $\quad Q_m = -18.722$
See C^{12}.

XIX. $C^{12}(p, d)C^{11}$ $Q_m = -16.495$

See (Br 52c, Gr 56e, We 56a).

XX. $C^{12}(d, t)C^{11}$ $Q_m = -12.463$

See (We 56a) and N^{14}.

XXI. $C^{12}(He^3, \alpha)C^{11}$ $Q_m = 1.856$

At $E(He^3) = 1.3$ and 2.0 MeV, no 1.9-MeV γ-radiation (from $C^{11*}(2.0)$) is observed by (Br 57). The energy of the first excited state is 1.990 ± 0.010 MeV (Po 59). See also (Fr 52e, Po 52b, Ku 53a, We 58c).

XXII. $C^{12}(p, t)C^{11}$ $Q_m = -15.183$

Not reported.

XXIII. $N^{14}(p, \alpha)C^{11}$ $Q_m = -2.916$

See O^{15}.

XXIV. $O^{16}(\gamma, n\alpha)C^{11}$ $Q_m = -25.870$

See (Aj 55).

B^{12}

(Fig. 19, p. 113) †

THEORY

See (Ku 56, Fr 58b).

I. $B^{12}(\beta^-)C^{12}$ $Q_m = 13.376$

The spectrum is complex: see C^{12}. The transition to C^{12}(g.s.) is allowed; hence $J(B^{12}) = 1^+$.

II. $Li^6(Li^7, p)B^{12}$ $Q_m = 8.338$

Three groups of protons are reported, corresponding to the ground state and to the excited states at 0.95 and 1.67 MeV. At $E(Li^7) = 2.0$ MeV, $\theta = 90°$ (lab), the relative intensities are 1: 1.1 : 0.8 (No 57). See also (No 57a).

III. $Li^7(Li^7, d)B^{12}$. $Q_m = 3.311$

See C^{14}.

IV. $Be^9(\alpha, p)B^{12}$ $Q_m = -6.884$

At $E_\alpha = 21.7$ MeV, proton groups are observed corresponding to $B^{12}(0)$ and to B^{12*} at 0.95, 1.65, 3.38 and 3.82 MeV (Mc 51b, Ra 55b).

V. $Be^9(Li^7, \alpha)B^{12}$ $Q_m = 10.463$

See (No 57a).

VI. $B^{10}(t, p)B^{12}$ $Q_m = 6.344$

At $E_t = 0.90$ MeV, proton groups are observed corresponding to B^{12}

† For level scheme of N^{12}, see fig. 21, p. 137.

levels at 0.94, 1.65, 2.61, 3.37, 3.75, and 4.46 MeV (Bi 55;$\pm \approx 0.1$ MeV).

VII. $B^{11}(n, \gamma)B^{12}$ $Q_m = 3.365$

$\sigma_{th} < 50$ mb (Hu 58). See also (Wi 53f).

VIII. $B^{11}(n, n)B^{11}$ $E_b = 3.365$

The parameters of observed resonances at $E_n = 0.43$, 1.28, 1.78, 2.45 and 2.58 MeV are exhibited in table 12.2. The rise of the cross section at low energies may indicate a broad level formed by s-wave neutrons (Bo 51c). The angular distributions of elastically scattered neutrons have been studied for $E_n = 0.43$ to 1.50 MeV by (Wi 55d). It is found that the 0.43-MeV resonance has $J = 2^+$, formed by p-waves, either all in channel spin 1 or all in channel spin 2. The 1.28-MeV resonance has $J = 3^-$, formed by d-waves,

TABLE 12.1

Energy levels of B^{12}

E_x in B^{12} (MeV)	J^π	$\tau_{\frac{1}{2}}$ or Γ (keV)	Decay	Reactions
0	1^+	$\tau_{\frac{1}{2}} = (20.34 \pm 0.5) \times 10^{-3}$ sec	β^-	I, II, III, IV, V, X, XIII, XV, XX, XXII
0.947 ± 0.005	$\leqq 3^+$	< 10	γ	II, IV, VI, X
1.674 ± 0.011	$1^-, 2^-$	< 10	γ	II, IV, VI, X
2.618 ± 0.011		< 10		VI, X
2.723 ± 0.011		< 10		X
3.383 ± 0.009	$\leqq 3^+$	< 10		IV, VI, X
3.76 ± 0.01	2^+	40 ± 5	n	IV, VI, VIII, X
4.54 ± 0.02	3^-	140 ± 20	n	VI, VIII, X
5.00 ± 0.02	1	60 ± 20	n	VIII
5.61 ± 0.02	2	120 ± 40	n	VIII
5.73 ± 0.02	3	60 ± 20	n	VIII

with the level width of channel spin 2 about 10 times that of channel spin 1. Potential scattering at $E_n = 1.5$ MeV is nearly all s-wave: $\delta_0 = -90°$ (Wi 55d).

The total cross section for natural boron shows no sharp discontinuities for $E_n = 4.4$ to 5.6 MeV ($\sigma \approx 1.6$ b) and for $E_n = 7.8$ to 8.6 MeV ($\sigma \approx 1.4$ b) (Be 56c). The total cross section has also been measured for $E_n = 6$ to 9.7 MeV (Ne 54c) and from $E_n = 14.1$ to 18.0 MeV by (Co 52h, Co 54f); see (Hu 55c). See also (Hi 55, Hu 58, La 56d, La 57c). At $E_n = 14.5$ MeV the non-elastic cross section for natural boron is 0.64 ± 0.04 b (Fl 56a).

IX. (a) $B^{11}(n, d)Be^{10}$ $Q_m = -9.010$ $E_b = 3.365$

(b) $B^{11}(n, t)Be^{9}$ $Q_m = -9.564$

(c) $B^{11}(n, \alpha)Li^{8}$ $Q_m = -6.636$

(d) $B^{11}(n, p)Be^{11}$ $Q_m = -10.69$

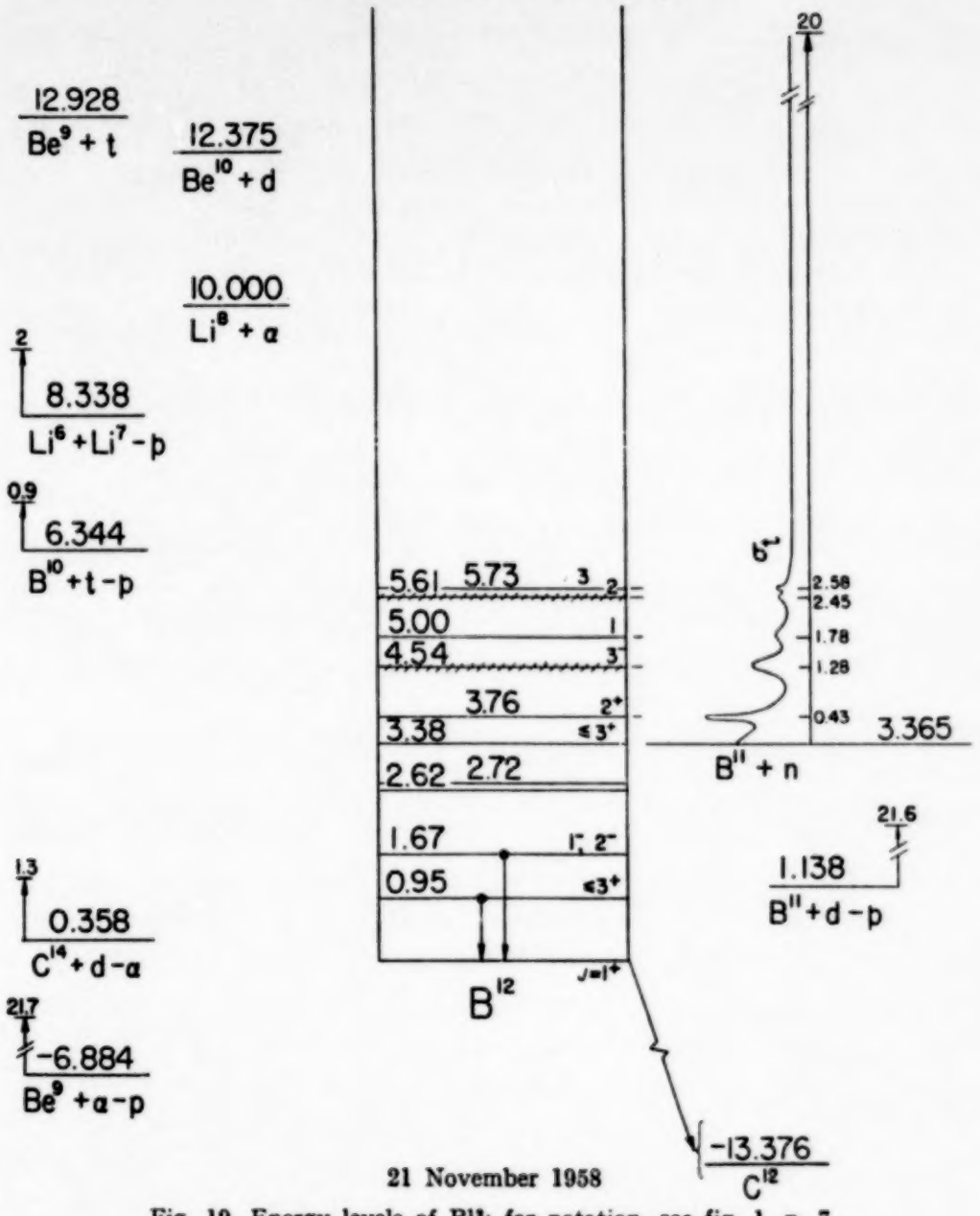

21 November 1958

Fig. 19. Energy levels of B^{12}: for notation, see fig. 1, p. 7.

TABLE 12.2

Resonances in $B^{11}(n, n)B^{11}$

E_n [a] (MeV)	$\sigma_{max}-\sigma_{pot}$ [b] (b)	Γ_n [a] (keV)	B^{12*} (MeV)	l [c]	θ_n^2 [b]	J^π
0.43±0.01	2.9	40± 5	3.76	1	0.036	2⁺
1.28±0.02	2	140±20	4.54	2	0.28	3
1.78±0.02	0.4	60±20	5.00	1	0.012	1
				2	0.056	
2.45±0.02	0.5	120±40	5.61	1	0.017	2
				2	0.053	
2.58±0.02	0.6	60±20	5.73	1	0.008	3
				2	0.025	

[a] (Hu 58, Bo 51c).

[b] (Bo 51c): $R = 4.5\times10^{-13}$ cm.

[c] (Bo 51c, Wi 55d, Hu 58).

The cross section for reaction (c) decreases from 27 mb at $E_n = 12.6$ MeV to 16 mb at $E_n = 20.0$ MeV (Ar 56). At $E_n = 14.1$ MeV, the cross section for reaction (b) is 15 ± 5 mb (Wy 58a). Reaction (a) has not been reported. See also (He 54c). For reaction (d) see Be^{11}.

X. $B^{11}(d, p)B^{12}$ $\quad Q_m = 1.138$

Proton groups observed at $E_d = 4.0$ to 8.5 MeV are listed in table 12.3.

TABLE 12.3

B^{12} levels from $B^{11}(d, p)B^{12}$

B^{12} [a] (MeV)	l_n	J^π	$\frac{\Lambda^2}{2J+1}$
0	1	1^+ [c]	3.4
0.947 ± 0.005	1	$3^+, 2^+, 1^+, (0^+)$	1.5, 2.1, 3.5, (10)
1.674 ± 0.011	0	$2^-, (1^-)$	3.5, (5.8)
2.618 ± 0.011			
2.723 ± 0.011			
3.383 ± 0.009	1	$3^+, 2^+, 1^+, (0^+)$	1.6, 2.2, 3.7, (11)
3.76 [b]			
4.53 [b]	2	3^- [d]	3.8

[a] (El 53, Bu 50d).
[b] (Ho 53c).
[c] From $B^{12}(\beta^-)C^{12}$.
[d] From $B^{11}(n, n)B^{11}$.
[e] Neutron capture probability; proportional to reduced width; values greater than 4 are regarded as improbable (Ho 53c).

No other groups are observed for $E_x = 0$ to 3.15 MeV with an intensity greater than 4 per cent of the ground-state group, or from 3.15- to 3.5-MeV excitation with an intensity greater than 8 per cent (El 53). See also (Kh 54, Kh 55a). Angular distributions and absolute cross sections have been determined at $E_d = 8$ MeV. Analysis by stripping theory leads to the assignments indicated in table 12.3. Neutron capture probabilities are compared with expected single-particle values to eliminate certain spin possibilities (Ho 53c). At $E_d = 1.05$ MeV, γ-rays with energy 0.94 and 1.64 MeV are observed with an intensity ratio of 2 : 1 (Th 54d). See also (Ra 55b, Ka 56, Ta 56c, Co 57d, Ch 57a).

XI. $B^{11}(t, d)B^{12}$ $\quad Q_m = -2.894$

Not reported.

XII. $B^{11}(\alpha, He^3)B^{12}$ $\quad Q_m = -17.213$

Not reported.

XIII. $C^{12}(n, p)B^{12}$ $\quad Q_m = -12.593$

See (Je 48c).

XIV. $C^{12}(t, He^3)B^{12}$ $Q_m = -13.358$
Not reported.

XV. $C^{13}(\gamma, p)B^{12}$ $Q_m = -17.539$
See C^{13}.

XVI. $C^{13}(d, He^3)B^{12}$ $Q_m = -12.045$
Not reported.

XVII. $C^{13}(t, \alpha)B^{12}$ $Q_m = 2.274$
Not reported.

XVIII. $C^{14}(n, t)B^{12}$ $Q_m = -17.228$
Not reported.

XIX. $C^{14}(p, He^3)B^{12}$ $Q_m = -17.993$
Not reported.

XX. $C^{14}(d, \alpha)B^{12}$ $Q_m = 0.358$
$Q_0 = 0.362 \pm 0.0015$ (Do 56c).
See also (Hu 50e).

XXI. $N^{14}(n, He^3)B^{12}$ $Q_m = -17.365$
Not reported.

XXII. $N^{15}(n, \alpha)B^{12}$ $Q_m = -7.629$
See (Je 48c).

C^{12}

(Fig. 20, p. 117)

THEORY

See (Fe 55a, He 55f, Mo 56, Wi 56k, Na 56b, Re 57, Pa 57a, Sa 57c, Bi 57f, Gl 56a, Re 56b, El 56, Pe 56a, He 57b, Ku 56, Ku 57a, Ba 57, Ha 56g, Ha 56h, Ca 56e, Ca 58c, Fr 58b).

I. $Li^7(Li^6, n)C^{12}$ $Q_m = 20.931$
See (No 57a).

II. (a) $Be^9(He^3, n)C^{11}$ $Q_m = 7.565$ $E_b = 26.286$
(b) $Be^9(He^3, p)B^{11}$ $Q_m = 10.329$
(c) $Be^9(He^3, \alpha)Be^8$ $Q_m = 18.911$
(d) $Be^9(He^3, d)B^{10}$ $Q_m = 1.093$

The yields and angular distributions of protons leading to the ground state and several excited states of B^{11} have been investigated by (Al 56b: $E(He^3)$ up to 2.7 MeV), by (Ho 55i, Ho 56d: $E(He^3) = 2.0$ MeV), by (Wo 56, Wo 56b, Jo 57b, and E. Wolicki, private communication: 2 to 4.5 MeV) and

TABLE 12.4

Energy levels of C^{12}

E_x in C^{12} (MeV)	$J^\pi; T$	Γ (keV)	Decay	Reactions
0	$0^+; 0$	—[a]	stable	I, III, X, XI, XVI, XVII, XIX, XX, XXIV, XXV, XXVI, XXVII, XXVIII, XXIX, XXX, XXXI, XXXII, XXXIII, XXXIV, XXXVII, XXXIX, XL, XLI, XLII
4.433 ± 0.005	$2^+; 0$	$0.01-0.02$ eV[b]	γ	III, X, XVI, XIX, XX, XXIV, XXV, XXVI, XXVII, XXIX, XXX, XXXIV, XXXIX, XLI
7.656 ± 0.007	$0^+; 0$	<25	α, (γ)	III, X, XVI, XIX, XXIV, XXV, XXVI, XXIX, XXX, XXXIX
9.63 ± 0.014	$(1^-); 0$	30 ± 8[a]	α	X, XVI, XXIV, XXV, XXVI, XXVII, XXIX, XXXIX, XLII
10.1 ± 0.2	$0^+; 0$	≈ 2000	α	XIX, XXV, XLII
10.84 ± 0.05				X, XVI, XXVI
11.1 ± 0.1				XVI
11.81 ± 0.05				X, XVI
12.73 ± 0.05	$(1^+); 0$		(α), γ	X, XVI, XXVI, XXIX, XXX
(13.21 ± 0.05)				XVI
13.30 ± 0.05				X, XVI
14.05 ± 0.06				X, XVI
15.11 ± 0.01	$1^+; 1$	0.069	(α), γ	III, X, XVI, XX, XXIII, XXV, XXVI, XXXIV, XXXIX
15.62 ± 0.06				X, XVI
16.11 ± 0.002	$2^+; 1$	6	α, p, γ	X, XII, XIV, XVI, XXIII
16.58 ± 0.015	$2^-; (1)$	295	α, p, γ	X, XII, XXIII
17.23	$1^-; (1)$	1160	α, p, γ	XII, XIV, XXII, XXIII
17.77	(0^+)	140	α, p	XII
18.37	(2^+)	280	γ, p, α	XII, XXIII
18.40		46	p, p′	XIV
18.85		90	γ, n, p	XII, XIII, XIV
19.26		450	γ, n, p	XII, XIII, XIV, XXI
19.42		45	p	XIV
19.67		180	n, p, (γ)	XIII, XXI
19.88		90	p, p′	XIV
20.27		180	n, p, (γ)	XIII, XIV, XXI
20.49		180	γ, (n), p	XII, XXI
20.65		180	γ, n, p	XII, XIII, XIV, XXI, XXII, XXVI
21.34			n, p, (γ)	XII, XIII, XXI, XXII
21.80			n, (α), p, (γ)	XII, XIII, XXI, XXIII, XXII
22.55 ± 0.1		≈ 4000	n, p, γ	XII, XIII, XX, XXI, XXII, XXIII

[a] For reduced width, see $B^{11}(d, n)C^{12}$, table 12.8, p. 124.

[b] III, XX, XXIV.

TABLE 12.4 (continued)

E_x in C^{12} (MeV)	$J^\pi; T$	Γ (keV)	Decay	Reactions
(22.8)			(n), (α), (p), (γ)	XXI, XXII
(24.3)			n, (α), (γ)	XIII, XXIII
(25.4)			n, p, d	VI, XIII
(26.0)			(p), n, α, d, (γ)	V, VI, VIII, XXII
(26.4)			p, (α), d	VI, VIII
(26.8)			p, α, d	VI, VIII
(27.0)			p, d	VI
(27.2)			p, d	VI
(27.4)			p, d	VI
(29.4)			(α), (γ)	XXIII

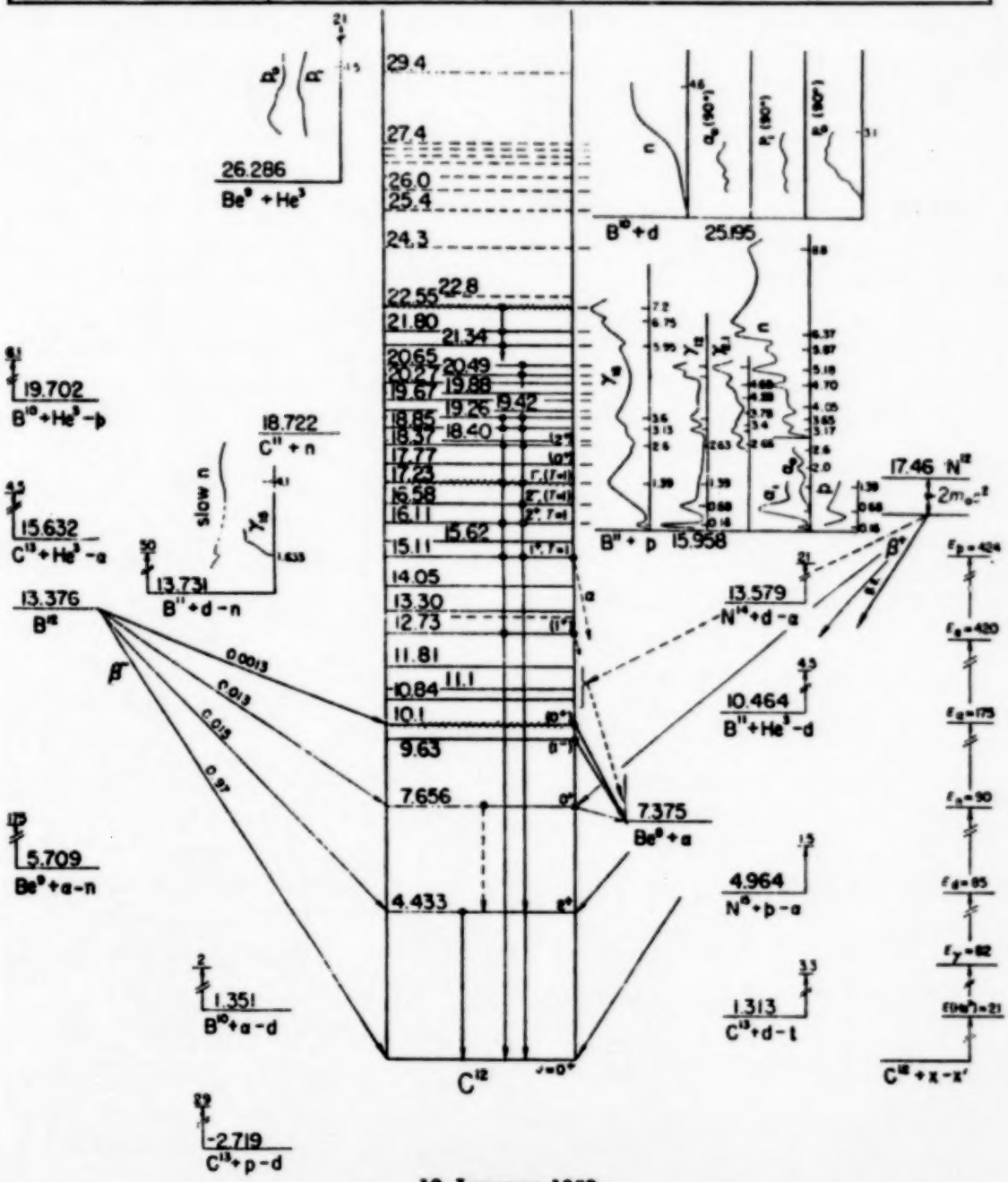

12 January 1959

Fig. 20. Energy levels of C^{12}: for notation, see fig. 1, p. 7.

by (D. R. Sweetman, private communication: 6.05 MeV). The yield rises rapidly to $E(He^3)=1.8$ MeV and remains approximately constant to 4.5 MeV, with no indication of resonance. Angular distributions show fore and aft asymmetry and vary only slowly with energy. At $E(He^3) = 2$ MeV, it appears that both direct interaction and compound nucleus formation, involving interfering resonances with $l \leqq 3$, may be taking place. At higher energies the forward peaking suggestive of direct interaction becomes more obvious. See also B^{11}. For reactions (a), (c) and (d), see C^{11}, Be^8 and B^{10}.

III. $Be^9(\alpha, n)C^{12}$ $\qquad Q_m = 5.709$

Neutron groups corresponding to states of C^{12} at 0, 4.4, and 7.6 MeV have been observed with E_α up to 5.3 MeV. At $E_\alpha = 5.3$ MeV the forward yield of the group leading to the 7.6-MeV state is about $\frac{1}{8}$ of that leading to the 4.4-MeV state: see (Gu 52, St 55b, Me 56a, Ri 57); see also (Di 57).

The energy of the γ-ray from the first excited state is 4.425 ± 0.020 (Mi 54d), 4.48 ± 0.06 MeV (Be 55h) (both values corrected for Doppler shift). The internal pair conversion coefficient indicates an E2 transition (Mi 54d); the angular correlation of pairs admits M1 or E2, favoring the latter (Ha 54a, Go 56g, Go 56d, Ar 58a). The angular distribution of γ-rays observed at several bombarding energies is consistent with $J = 2^+$ (Pr 56, Ta 55b). The n—γ correlation at $E_\alpha = 5.3$ MeV (thick target) is isotropic within 6.5 per cent (St 56b: see also Ta 58d). The mean lifetime of the 4.4-MeV level is $(2.6\pm0.9)\times10^{-14}$ sec, about one-eighth of the single-particle value for an E2 transition (De 56a).

The 7.7-MeV state appears to decay predominantly into $Be^8+\alpha$ (see $B^{12}(\beta^-)C^{12}$ and $C^{12}(\alpha, \alpha')C^{12*}$). A gamma ray of energy 3.1 MeV has been reported by (Be 53c, Ue 54, St 56b, St 56f, and St 57g), but (Be 55h, Go 57d and Kr 57) find no evidence of the 7.7-MeV nuclear pairs which should accompany the decay to the ground state. (Be 55h) estimate that at least 96 per cent of the decays proceed to $Be^8+\alpha$; (Kr 57, Kr 58b) find $< 1.6 \times 10^{-5}$ 7-MeV pairs per 4.4-MeV γ-ray; assuming a population ratio of 1 : 8, this result yields $\Gamma_n/\Gamma < 1.3\times10^{-4}$. An upper limit of $\frac{1}{600}$ for the ratio of 7.6/4.4 MeV pairs is reported by (Go 57d). (Di 54) find no n—γ coincidences other than those associated with the 4.4-MeV level. See also (Ro 57f).

At $E_\alpha = 21.7$ and 175 MeV, γ-radiation from the 15-MeV, $J = 1^+$, $T = 1$ state (see $C^{12}(p, p')C^{12*}$) is reported (Ra 54a, Wa 57b). At the higher energy, the ratio of 15-MeV to 4.4-MeV radiation is 1.2×10^{-2} (Wa 57e). See also (Br 55, El 54b, Ha 55b, Go 56j, Br 57h) and (Ma 55i; theo.).

IV. $B^{10}(d, \gamma)C^{12}$ $\qquad Q_m = 25.195$

At $E_d = 0.95$ MeV, the upper limit to the capture cross section is 0.1 μb (Sa 55f).

V. $B^{10}(d, n)C^{11}$ $Q_m = 6.473$ $E_b = 25.195$

The thin-target excitation function in the forward direction in the range $E_d = 0.3$ to 4.6 MeV shows some indication of a broad resonance near $E_d = 0.9$ MeV. Above $E_d = 2.4$ MeV, the cross section increases rapidly to 210 mb/sr at 3.8 MeV, and then remains constant to 4.6 MeV (Ma 55j, Bu 54). Angular distributions seem to be dominated by the stripping process: see C^{11}. The yield of 6.5-MeV γ-rays has been measured at four bombarding energies between 0.8 and 2.2 MeV (Sa 55f). See also C^{11}.

VI. $B^{10}(d, p)B^{11}$ $Q_m = 9.237$ $E_b = 25.195$

Absolute yields and angular distributions are reported for various proton groups by (Pa 54a, En 52, Va 56c, Bu 54 and Ma 56j) for $E_d = 0.18$ to 3.1 MeV. Although the excitation functions show several broad peaks, no clear resonances can be identified, and it must be assumed that many overlapping resonances are involved (Ma 56j). Angular distributions indicate both stripping and compound nucleus processes even at low bombarding energies (Pa 54c). However, the p_1 group, leading to $B^{11*}(2.1)$, shows no stripping even at $E_d = 3$ MeV; it is suggested that an orbital angular momentum selection rule is operative here (Ma 56j; see B^{11}). Absolute cross sections reported by (Bu 54, Pa 54a, and Ma 56j) differ rather greatly.

The yields of 6.8 and 7.3-MeV γ-rays have been measured at four bombarding energies between 0.8 and 2.2 MeV (Sa 55f). At $E_d = 1.70$ MeV, θ(lab) = 58°, the cross section for protons leading to the 6.76-MeV state is 6.1($\pm$15 per cent) mb/sr (Ka 56).

VII. $B^{10}(d, d)B^{10}$ $E_b = 25.195$

See B^{10}.

VIII. $B^{10}(d, \alpha)Be^8$ $Q_m = 17.819$ $E_b = 25.195$

Excitation curves for ground state α-particles have been measured for $E_d = 0.9$ to 2.6 MeV at 45°, 90° and 150°. Broad maxima are observed at 1.0, (1.4) and 2.0 MeV. At $E_d = 0.91$ MeV, the angular distribution of α_0 particles shows a peaking in the forward direction (Ma 56j). See also Be^8.

IX. $B^{10}(t, n)C^{12}$ $Q_m = 18.937$

Not reported.

X. $B^{10}(He^3, p)C^{12}$ $Q_m = 19.702$

Proton groups reported by (Bi 55) and (Mo 58f) are listed in table 12.5. A careful search, at $E(He^3) = 1.25$ MeV, reveals no other level in the range

$E_x = 4.4$ to 7.7 MeV (Mo 58f: region at $E_x = 6.4$ MeV obscured). At $E(He^3) = 2.0$ MeV, the proton group leading to the 15.11-MeV level was found to be in coincidence with a 15.10-MeV γ-ray: Γ_γ/Γ for this level is 0.77 ± 0.20. The ratio of the width for γ-emission to the 4.4-MeV level to the

TABLE 12.5

C^{13} states from $B^{10}(He^3, p)C^{13}$

A		B	
E_x (MeV)	Γ_γ/Γ	E_x (MeV $\pm$ keV)	Γ_γ/Γ
4.43	1	4.43	1
7.77		7.65	<0.009
9.61		9.61	
10.75		10.90 $\pm$ 60	
11.83		11.84 $\pm$ 60	
12.76	0.02	12.69 $\pm$ 60	0.03 $\pm$0.01
13.31		13.30 $\pm$ 60	
13.97		14.05 $\pm$ 60	
15.10	0.77 $\pm$ 0.20	14.97 $\pm$ 60	0.50 $\pm$0.25
		15.62 $\pm$ 60	
16.04		16.10	
16.57		16.57 $\pm$ 60	

A: (Bi 55, Go 57b): $E(He^3) = 0.9$ and 2.0 MeV, values ± 0.1 MeV.
B: (Mo 58f): $E(He^3) = 1.25$ MeV.

ground state Γ_γ is ≈ 0.03. The 12.76-MeV level also emits γ-rays: $\Gamma_\gamma/\Gamma \approx 0.02$, suggested $J^\pi = 1^+$ (Go 57b and H. E. Gove, private communication). Coincidence studies by (Mo 58f) lead to $\Gamma_\gamma/\Gamma < 0.9$ % for the 7.7-MeV level, $\Gamma_\gamma/\Gamma = 3 \pm 1$ % for the 12.76-MeV level, and 50 ± 25 % for the 15-MeV level. See also $B^{11}(d, n)C^{12}$, (Sw 58a, Br 58e) and N^{13}.

XI. $B^{10}(\alpha, d)C^{12}$ $\quad Q_m = 1.351$

$Q_0 = 1.341 \pm 0.002$ (Do 56c)

$Q_0 = 1.36 \pm 0.09$ (Pi 56)

$Q_0 = 1.39 \pm 0.01$ (Sh 53b)

See also N^{14}.

XII. (a) $B^{11}(p, \gamma)C^{12}$ $\quad Q_m = 15.958$

(b) $B^{11}(p, \alpha)Be^8$ $\quad Q_m = 8.582$ $\quad E_b = 15.958$

In the range $E_p = 0$ to 3 MeV, five principal resonances occur, at $E_p = 0.16$, 0.67, 1.4, 2.0 and 2.6 MeV (see table 12.6). All except the second and fourth exhibit resonance for α_0, α_1, γ_0 and γ_1 (to $Be^8(0)$ and (2.9), $C^{12}(0)$ and (4.4)); at $E_p = 0.67$ MeV, only α_1, γ_1 are resonant. It follows from angular momentum selection rules that resonances for α_0 must have the character $J^\pi = 0^+, 1^-, 2^+, 3^- \ldots$; $J = 0^+$ is excluded by observation of γ_0.

The $E_p = 0.16$-MeV resonance ($C^{12*} = 16.11$ MeV) is well established as $J = 2^+$, probably the $T = 1$ analogue of $B^{12*}(0.95)$. The angular distribution of α_0 particles is strongly anisotropic at resonance and shows a $(\cos\theta)$ term varying with energy near resonance. The assumption $J = 2^+$, $l_p = 1$, with interference from an s-wave state at higher energy gives a good account of the observed angular distributions from $E_p = 0.13$ to 0.3 MeV. The channel spin ratio $\chi = 0.42 \pm 0.02$; the relative amplitude of the interfering $J = 1^-$ state is 0.022 ± 0.002 (Th 52c). The angular correlation of α_1 and the subsequent breakup of $Be^{8*}(2.9)$ also requires $J = 2^+$, with the ratio of reduced matrix elements for outgoing d to s-waves, $B = 0.80$, phase difference $\cos\beta = 0.60$ (Ge 55c). The angular distribution of γ_1 and of the following 4.4-MeV radiation is consistent with the scheme $2^+(M1)2^+(E2)0^+$ with the channel spin ratio $\chi = 0.42$ (Gr 54a); (Cr 56c) obtain $\chi = 0.51 \pm 0.03$. Angular distributions of the 16-MeV radiation, γ_0, require $J = 2^+$, with interference from a $J = 1^-$ level at $E_p = 1.4$ MeV (Gr 54a, Cr 56c). (γ_0 is not resonant at $E_p = 0.67$ MeV, so this state cannot be involved here.) The resonant energy is 163.1 ± 0.2 keV; $\Gamma_{lab} = 6.5 \pm 0.6$ keV (see Aj 55) The very small α-width suggests $T = 1$ (Be 53).

For the $E_p = 1.4$-MeV state ($C^{12*} = 17.23$ MeV), the possible assignments are 1^- (s-wave), 2^+ (p-wave), 1^- or 3^- (d-wave); d-wave formation would seem to be excluded by the observed width. As indicated above, $J = 1^-$ appears to be required to account for the interference at lower energies in α_0 and γ_0; known higher resonances are probably too narrow to produce the observed effects. (De 57a) find that the α_0-distributions for $E_p = 0.6$ to 1.4 MeV are well accounted for by the assumption of s-wave formation of $J = 1^-$ through channel spin 1 ($\chi = 0$) with a relative d-wave amplitude $A = 0.5$, and interference by the 2.6-MeV, $J = 2^+$, state, with relative amplitude $C = 0.25$. A qualitative fit to the behaviour of α_1 can be obtained with the same assumptions (De 57a). Angular distributions of γ_0 at $E_p = 1.4$ MeV admit either $J = 2^+$ or 1^-; for the latter, however, formation in channel spin 2 ($\chi = \infty$, d-waves) is required (Go 55). The angular correlation of internal pairs indicates E1 for γ_0 (Go 56j, Go 56g, Ar 58a). The large E1 width suggests $T = 1$ for this state (Be 53).

The $E_p = 0.67$-MeV state ($C^{12*} = 16.58$ MeV) may be formed by s- or p-waves; d-waves are excluded by the width (Be 53). The angular distribution of α_1 at $E_p = 0.64$ and 0.93 MeV indicates s-wave formation: if $J = 2^-$ is

assumed, the d-wave admixture is < 10 per cent. The correlation of α_1 with the subsequent $Be^8(2.9)$ breakup is consistent with $J = 2^-$ and excludes 1^-; an appreciable f-wave admixture in outgoing α_1-particles is indicated (De 57a). Correlation results at $E_p = 270$ keV can be accounted for by $J = 2^-$ with interference from the 1^-, $E_p = 1.4$-MeV state (Ge 55c, De 57a). The angular distribution of γ_1 is reported to require $J = 2^+$, with interference

TABLE 12.6

Resonances in B^{11} (p, γ)C^{12} and B^{11}(p, α)Be^8

E_p (MeV)	$\Gamma_{(lab)}$ (keV)	$\sigma(\gamma_{16})$ [a] (μb)	$\sigma(\gamma_{12})$ [a] (μb)	$\sigma(\alpha_0)$ [e] (mb)	$\sigma(\alpha_1)$ [e] (mb)
0.163	7	5.5	152	0.2	10
0.675 [b]	322	(<2.3) [g]	48	(<0.2) [g]	600
1.388 [b]	1270	35	18	6	150
1.98 [c,d]	150	non-res.	non-res.	[8] [f]	[39] [f]
2.63 [c,d]	300	weak	res.	[16] [f]	[180] [f]
3.13 [d]	100	weak	res.		
3.55 [d]	500	res.	res.		
4.94 [d]	200	non-res.	res.		
5.12 [d]	200	non-res.	res.		

[a] (Hu 53); ratio $\sigma(\gamma_{16})/\sigma(\gamma_{12}) = 3.3\pm1$ per cent at $E_p = 0.16$ MeV (Cr 56c).
[b] (Hu 53).
[c] (Ho 55f).
[d] (Ba 55f).
[e] (Be 53).

from the 1^-, $E_p = 1.4$ MeV state (Gr 54): according to (De 57a), however, the distributions observed by (Gr 54a and Go 55) can equally well be ascribed to $J = 2^-$, with interference from a broad, even parity state, possibly at $E_p = 2.0$ or 2.6 MeV (see, however, Gi 54c). The angular correlation of internal pairs indicates E1 for the γ_1 radiation (Go 56j, Go 56g, Ar 57). The relatively large E1 width suggests $T = 1$ for this state (Be 53).

The $E_p = 2.0$-MeV level is reported to be resonant for α_0 and α_1; the relative weakness of α_1 suggests $J = 0^+$ (Pa 53b). There seems to be no clear indication of resonance for γ_0 or γ_1 at this energy (Go 55, see also Hu 53). At $E_p = 2.65$ MeV, resonance occurs for α_0, α_1 (Pa 53b) and, weakly, for γ_0, γ_1 (Go 55, Ba 55f). A large P_2 coefficient in the angular distribution of γ_0 suggests $J = 2^+$ (Go 55). (Ho 55f) find $E_p = 1.98$ and 2.61 MeV for the resonant energies for α_0. Additional resonances for γ_0 and γ_1, reported by (Ba 55f) are listed in table 12.6. (Ge 59a) have examined the excitation function for ground-state transitions from $E_p = 4$ to 7.7 MeV. The experiment locates the maximum of the C^{12} giant resonance at $E_x = 22.55\pm0.1$ MeV but does not resolve individual levels. Two additional peaks, at $E_x = 21.4$ and 22.1 MeV are suggested. The maximum value of $\sigma(\gamma, p)$ is calculated to be 29 ± 5 mb.

An upper limit for the total cross section (average value, $E_p = 1.7$ to 4.0 MeV) for the production of nuclear pairs with $E_\pi = 6.5$ to 9.5 MeV is 0.03 μb (Be 55a). See also (Aj 55), (Si 57b; theo.), (Ma 56r) and Be^8.

XIII. $B^{11}(p, n)C^{11}$ $\quad Q_m = -2.764$ $\quad E_b = 15.958$

Observed maxima in the (p, n) cross section are listed in table 12.7

$\Gamma_{\gamma_{10}}$ [a] (eV)	$\Gamma_{\gamma_{11}}$ [a] (eV)	Γ_{α_0} [a] (keV)	Γ_{α_1} [a] (keV)	Γ_p [a] (keV)	C^{12*} (MeV)	J^π; T
$\lesssim 3$	70	0.1	5	0.005	16.11	2^+; 1
$\lesssim 0.5$	15	$\lesssim 0.05$	150	150	16.58	2^-; (1)
40	20	7	200	1000 [b]	17.23	1^-; (1)
					17.77	(0^+)
					18.37	(2^+)
					18.83	
					19.21	
					20.49	
					20.65	

[a] (Pa 53b): normalized at $E_p = 1.4$ MeV. See also (Ho 55f).
[a] Non-resonant.
[b] According to (De 57a), $\Gamma_p \approx 50$ keV: see $B^{11}(p, p)B^{11}$. If this value is used, α-widths should be increased by a factor of 6, and γ-widths by a factor of 20.

(Bl 51a, Ba 55f, Gi 59, Ka 57a). The region covered is characterized by considerable overlapping of resonances (Gi 59). See also (Ko 56, Ma 58a, Ta 58a).

XIV. $B^{11}(p, p)B^{11}$ $\quad E_b = 15.958$
$B^{11}(p, p')B^{11*}$

Absolute elastic scattering cross sections are reported for one angle for $E_p = 0.6$ to 2.0 MeV by (Ta 56a), for four angles for $E_p = 0.3$ to 1.0 MeV by (De 57a). A pronounced anomaly is observed near $E_p = 0.67$ MeV at all angles; the level is therefore formed by s-waves. The 0.3 to 1.0 MeV results are well accounted for by two resonances: $E_p = 0.67$ MeV, s-wave, $J = 2^-$, $\Gamma = 0.33$ MeV, $\Gamma_p/\Gamma = 0.5$, d-wave < 10 per cent, and $E_p = 1.4$ MeV, s-wave, $J = 1^-$, $\Gamma = 1.27$ MeV, $\Gamma_p/\Gamma = 0.05$ (De 57a). (The reported Γ_p/Γ for the 1.4-MeV resonance appears to be inconsistent with the values 0.8 or 0.2 derived by (Be 53) from (p, γ) and (p, α) cross sections.) (Ta 56a) find no rapid variation in cross section near $E_p = 2.0$ MeV. The absence of a detectable anomaly near $E_p = 0.16$ MeV confirms the small value of Γ_p assumed for this resonance; $\Gamma_p < 200$ eV (J. C. Overley, private communication). See also (Ki 56).

TABLE 12.7

Maxima in yields of $B^{11}(p, n)C^{11}$ and $B^{11}(p, p')B^{11*}$

A	B		C	D		E		C^{12*}
E_p (MeV)	E_p (MeV)	Γ (keV)	E_p (MeV)	E_p (MeV)	σ (mb)	E_p (MeV)	Γ (keV)	(MeV)
						2.664	48	18.40
	3.17	100		3.18	25	3.15	100	18.87
3.7	3.65	500		3.67	62	3.4	500	19.31
						3.78	50	19.42
	4.05	200						19.67
						4.28	100	19.88
	4.70	200	≈4.5	4.70	55	4.68	200	20.27
5.18				5.10	105	5.13	200	20.63
5.87								21.34
6.37								21.81
			6.6					22.0
			8.8					24.0
			10.1					25.3

A: (p, n) (Bl 51a): stacked foils.
B: (p, n) (Ba 55f): $\theta = 0-15°$.
C: (p, n) (Ka 57a): stacked foils.
D: (p, n) (Gi 59): total cross section (estimated from curve).
E: (p, p′) (Ba 55f).

TABLE 12.8

Energy levels of C^{12} from $B^{11}(d, n)C^{12}$

C^{12*} [a] (MeV)	l_p	$(2J+1)\gamma^2$ (10^{-13} MeV-cm)	$(2J+1)\theta^2$
0	1 [e]	1.6 [e]	0.11
4.38±0.07	1 [c,e]	2.0 [e]	0.14
7.57±0.11	d		
9.6 ±0.1	2 [c,e]	1.9 [e]	0.13
10.8 ±0.1			
11.1 ±0.1			
11.74±0.08			
12.76±0.08			
13.21±0.05 [b]			
13.36±0.05 [b]			
(14.16±0.05)			
15.09±0.03			
(15.52±0.03)			
16.07±0.03			

[a] (Jo 52a, Gr 54b, Bi 57c).
[b] May represent a single level at 13.3 MeV (Jo 52a).
[c] (Gr 54b).
[d] Angular distribution shows peaking forward and backward: (see Bi 57c, Gr 54b).
[e] (Ma 56p: $E_d = 9$ MeV).

Maxima in the yield of 2.1-MeV γ-radiation from $B^{11*}(2.1)$ are observed at $E_p = 2.664$ MeV, $\Gamma = 48$ keV: (Hu 53, Ba 55f) and at $E_p = 3.15$, 3.4, 3.78, 4.28, 4.68 and 5.13 MeV (Ba 55f: see table 12.7). (Judging from the width, the 2.66-MeV resonance is not that observed, e.g., in $B^{11}(p, \gamma)C^{12}$.)

XV. $B^{11}(p, d)B^{10}$ $\quad Q_m = -9.237$ $\quad E_b = 15.958$

See B^{10}.

XVI. $B^{11}(d, n)C^{12}$ $\quad Q_m = 13.731$

$Q_0 = 13.63 \pm 0.05$ (Bi 57c).

Reported neutron groups are listed in table 12.8. The group corresponding to the 7.6-MeV state is weak, relative to neighboring groups, at all bombarding energies investigated, and the stripping pattern is poorly developed. The relative weakness of the 7.6-MeV state in this reaction and in the $C^{12}(e, e')C^{12*}$ and $C^{12}(p, p')C^{12*}$ reactions is attributed to lack of parentage overlap with the ground state of C^{12} (La 55). At $E_d = 0.92$ MeV, there is no indication of a state in the range $E_x = 5.1$—6.6 MeV: the upper limit of the intensity of the corresponding neutron group is $\lesssim 1$ per cent of the intensity of the group corresponding to the 4.4-MeV state (Bi 57c). For $E_d = 1.1$ to 2.0 MeV only the groups corresponding to $C^{12*} = 4.4$ and 12.76 MeV are accompanied by γ-radiation; an upper limit for (n, γ) coincidences from $C^{12*}(7.6)$ is 0.2 per cent of $C^{12*}(4.4)$ (Ne 58a, Da 58c, Ne 59).

Angular distributions of the neutrons to the first four states of C^{12} have been reported for a number of energies in the range $E_d = 0.5$ to 10 MeV. At the higher energies, the distributions are understood in terms of simple stripping theory (except for the 7.6-MeV state). At the lower energies, $E_d = 0.5$ to 5 MeV, a good account of the angular distributions of ground-state neutrons is obtained with the theory of (Ow 57) which includes not only stripping of the deuteron but also the possibility of stripping a neutron from B^{11}, and the interference between the two processes. The relative probability of the exchange stripping increases with energy until the Coulomb barrier is surmounted. The exchange process seems to involve s-wave deuteron capture by a B^{10} core with $J = 1^+$ (Ow 57, Pr 56a, Am 57a; see also Ne 59). Angular distributions at $E_d = 9$ MeV indicate odd parity for the 9.6-MeV state (Ma 56p; see also Gr 54b and table 12.8). For other work on angular distributions, see (Am 57a, Am 58; $E_d = 0.50$ to 1.15 MeV), (Wa 55e: $E_d = 0.6$ MeV), (Ih 55a; $E_d = 0.69$ MeV), (Gr 54b: $E_d = 0.85$ MeV), (Bi 57c: $E_d = 0.92$ MeV), (Pr 56a: $E_d = 1.5$ to 5 MeV), (Gi 53: $E_d = 8.1$ MeV), and (Ze 57: $E_d = 10$ MeV). See also (Bu 54, Ko 56a, Bo 56l, Bo 56m, Ra 57a) and (Ma 55i, Ed 58: theo.).

In the range $E_d = 1.0$ to 5.5 MeV, two slow neutron thresholds are observed at 1.627 ± 0.004 MeV ($E_x = 15.11 \pm 0.01$ MeV) and near 4.1 MeV (broad; $E_x = 17.23$ MeV) (Ma 55j). Gamma rays are observed with E_γ

$= 4.44 \pm 0.05$ (Ru 51a) and 12.8 ± 0.3 MeV (Ka 58a). If the latter γ-ray is properly attributed to decay of the 12.8-MeV level, it is not clear why the level should so decay in view of its instability with respect to Be^8 and $Be^{8*}(2.9)$ (Ka 58a; see also $B^{10}(He^3, p)C^{12}$). A 15.1-MeV γ-ray is observed with a threshold of $E_d = 1633 \pm 3$ keV, attributed to the first $T = 1$ state of C^{12} at 15.11 MeV. The observed width is < 2 keV. A search for α-particles to Be^8 and Be^{8*} gives $\Gamma_\alpha/\Gamma_\gamma < 1.5$. At $E_d = 2.96$ MeV the cross section for production of the 16.1-MeV $T = 1$ state is < 1 mb/sr (Ka 58a). See also (Aj 55) and (Wa 57b).

XVII. $B^{11}(He^3, d)C^{12}$ $\quad Q_m = 10.464$

At $E(He^3) = 4.5$ MeV, the ground state deuteron group is strongly peaked in the forward direction (Ho 57b).

XVIII. $B^{11}(\alpha, t)C^{12}$ $\quad Q_m = -3.855$

Not reported.

XIX. $B^{12}(\beta^-)C^{12}$ $\quad Q_m = 13.376$

The half-life is 20.34 ± 0.5 msec (weighted mean of Aj 55, Ve 58a, No 56b, Co 57b, Kr 58, excluding Je 48c). $E_\beta(\max) = 13.40 \pm 0.05$ MeV (Ve 58a). Branches are observed leading to C^{12}(g.s.), (4.4), (7.65) and (10.1): see table 12.9.

TABLE 12.9 Branching in B^{12} $(\beta^-)C^{12}$ (Co 58a)

C^{12*} (MeV)	J^π	Branching fraction (per cent)	log ft [a]
0	0^+	97	4.1 ± 0.1
4.43	2^+	1.5 ± 0.3 [b]	5.1 ± 0.2
7.653 ± 0.008	0^+	1.3 ± 0.4	4.2 ± 0.3
10.1 ± 0.2 [c]	0^+	0.13 ± 0.04	4.1 ± 0.4

[a] Based on $\tau_{\frac{1}{2}} = 20.6$ msec.
[b] (Ka 58a): 1.4 ± 0.4 per cent. (Ta 56c): 1.7 ± 0.4 per cent. (Ve 58a): 6 ± 3 per cent.
[c] $\Gamma = 2.5$ MeV, $\theta_\alpha^2 = 1.5$.

The fact that the transition to the 0^+ ground state is allowed establishes $J = 1^+$ for B^{12}. This assignment is confirmed by the allowed character of the transition to $C^{12*}(4.4)$, $J = 2^+$. The 7.7-MeV level decays mainly by α-emission to Be^8(g.s.) with $Q = 278 \pm 4$ keV; $E_x = 7.653 \pm 0.008$ MeV (Co 57d). Gamma transitions with $E_\gamma > 6$ MeV accompany $< 10^{-4}$ of all β-decays (Ka 56, Ka 58a); an upper limit of 3×10^{-5} is obtained in a search for β—γ (7.6) coincidences (Ka 58). Upper limits for (3.2+4.4) MeV cascades are given as $(0.4 \pm 2) \times 10^{-3}$ and 10^{-5} of all decays by (Ta 56c) and (Ka 58) respectively. It follows that the relative partial width of the 7.6-MeV level

is $< 3 \times 10^{-3}$ for 7.6-MeV γ-rays and $< 10^{-3}$ for 3.2-MeV γ-rays (see also $Be^9(\alpha, n)C^{12}$). Since the β-transition is allowed, the 7.7-MeV state has $J = 0^+$, 1^+ or 2^+; $J = 1^+$ is ruled out by the α-decay. The preponderance of α-decay over γ-decay speaks for $J = 0^+$ (Co 57d).

The 10.1-MeV level decays mainly via α-emission to Be^8(g.s.); transitions to $Be^{8*}(2.9)$ amount to < 4 per cent. The c.m. width is about 2.5 MeV (after removing the E_β^5 factor): the best account of the observed α-spectrum is obtained with $J = 0^+$, $E_\lambda = 10.4$ MeV, $\theta_\alpha^2 = 1.5$, $R = 5.21 \times 10^{-13}$ cm (Co 58a).

The β-spectrum has been reported by (Ho 50, Ve 58a). (Ge 58b) discusses a possible distortion of high-energy β-spectra in axial-vector coupling due to a "weak-magnetic" interaction.

See also (Ch 57a), (Ja 55d, Fe 57b, Sc 59: theo.).

XX. $C^{12}(\gamma, \gamma')C^{12*}$

The lifetime of the 4.4-MeV state has been determined by resonance scattering and resonant absorption (of γ-radiation from $N^{15}(p, \alpha)C^{12*}$) as $\tau_{mean} = (6.5 \pm 1.2) \times 10^{-14}$ sec (Ra 58a).

Excitation of the 15.1-MeV level by bremsstrahlung is reported by (Ha 57e, Ga 57b, Ga 58a). From measurement of the yield of resonance scattered radiation and of the self-absorption coefficient, the integrated scattering cross section $\int \sigma_s dE$, and the peak absorption cross section σ_n^0 are deduced. The resulting values for partial widths are given in table 12.10. It is noted

TABLE 12.10

Parameters of the 15.1-MeV C^{12} level from $C^{12}(\gamma, \gamma')C^{12*}$

	Ha 57e	Ga 58a
peak absorption, σ_n^0 (b)	22.2 ± 2.2	29.7 ± 1.1
integrated scattering, $\int \sigma_s dE$ (MeV · mb)	1.90 ± 0.27	2.33 ± 0.19
Γ (total) (eV)	79 ±16	64.5 ±10.4
$\Gamma_\gamma(15 \to$ g.s.) eV	54.5 ± 9.3	59.2 ± 9.7
$\Gamma_\gamma(15 \to 4.4)$ eV	< 5.5	3.2 ± 2.5
Γ_α(eV)	18 −25 [a]	2.1 ± 3.2

[a] $\Gamma_\alpha/\Gamma < 1.5$ from $B^{11}(d, n)C^{12}$ (Ka 58a).

that the γ-ray width for the ground state transition is near the single-particle M1 value of 65 eV, and that the very small α-width strongly suggests $T = 1$ for this level (Ha 57e). The scattering angular distribution indicates dipole radiation (Le 56a, Ga 57b, Ga 58a). The strength of the M1 radiation also indicates $T = 1$: see (Mo 58). Inelastic scattering in the giant-resonance region has been studied by (Ga 58a). See also (Ax 58, Mc 58, Go 57j).

XXI. $C^{12}(\gamma, n)C^{11}$ $Q_m = -18.722$

The cross section for production of C^{11} exhibits a broad peak at $E_\gamma = 22.5$ MeV, $\Gamma \approx 4$ MeV, $\sigma_{max} = 8.3$ mb (Ba 55e). Other reported values for σ_{max} are summarized by (Co 57b: note a 10 per cent correction in this work). See also (Ca 57f). At high energies, the cross section exhibits a long tail, falling off approximately as E_γ^{-3}. The integrated cross section to $E_\gamma = 250$ MeV is 80 MeV-mb, accounting for about $\frac{1}{3}$ of the sum-rule limit for all absorption processes. It is noted that the relative prominence of the high-energy tail is not a general feature of (γ, n) reactions in heavy elements (Ba 55e, Co 57b). Comparison of (γ, n) and (e, n) cross sections for 28 to 145 MeV are consistent with the assumption that the transitions are predominantly E1 (Ba 58l). The angular distribution of photoneutrons at the giant resonance is $W(\theta) = 1+(1.35\pm0.88)\sin^2\theta$, indicating considerable emission of neutrons with $l > 0$ (Fa 56a). See $C^{12}(\gamma, p)B^{11}$ and (Ba 57d, Te 54c, Mo 55a; theo.).

Discontinuities in the yield function are reported to indicate levels at 19.3, 19.8, 20.1, 20.5, 20.7, 21.1, 21.6, 22.4, and 22.8 MeV (Ka 54a, Go 54f). The first two are given as 19.09 ± 0.05 and 19.55 ± 0.05 MeV by (Sp 55a). Eighteen discontinuities observed between $E_\gamma = 18.90$ and 22.88 MeV are tabulated by (Ka 58b). A search for resonance absorption near $E_\gamma = 22.8$ MeV indicates a width $\Gamma > 580$ keV, in apparent contradiction of the activation results (Tz 56). (Wo 58a), using monochromatic gamma rays, find no evidence of fine structure in the total cross section from $E_\gamma = 20.3$ to 20.8 MeV. The upper limit is, however, not in conflict with the recent report of (Ka 58b). See also (Sa 55j, Jo 55f, Ba 58b, Sm 58a).

XXII. $C^{12}(\gamma, p)B^{11}$ $Q_m = -15.958$

The cross section exhibits a giant resonance at $E_\gamma = 21.5\pm0.5$ MeV, $\Gamma = 1.7\pm0.5$ MeV (Ha 51f). The peak cross section is 22 mb, and the integrated cross section to 24 MeV is 56 MeV-mb (Co 56d): compare $B^{11}(p, \gamma)C^{12}$ (Ge 59a). The photoproton spectrum shows the general features of the inverse reaction, $B^{11}(p, \gamma)C^{12}$, and suggests resonances at $E_\gamma = 17.3$, (20.8), 22.6, and (23.1) MeV (Co 56d; see, however, Wo 58a). (Li 57c) finds indications of peaks at $E_\gamma = 21.8$, 22.6, 23.3 and 25.8 MeV. An absolute measurement, based on $\sigma(C^{12}(\gamma, 3\alpha))$ for $E_\gamma = 17.6$ MeV yields $\sigma(\gamma, p) = 1.19\pm0.21$ mb, in good agreement with the value 1.09 ± 0.16 mb calculated from the inverse reaction (Ma 56r). See also (Go 56l, Ch 58c, Pe 58, Wh 58).

Angular distributions of photoprotons show a pronounced 90° peaking, somewhat skewed in the forward direction (Ha 52g, He 53a, Jo 55f, Mi 57b, Do 57, Kl 56a, Li 57c). Such distributions are inconsistent with s-wave proton emission from $J = 1^-$ C^{12} compound states formed by E1 absorption and suggest a direct interaction involving independent-particle states:

L-S coupling seems to be favoured (Ma 55e). The angular distributions of $C^{12}(\gamma, n)$ and (γ, p) are evidently quite similar, as expected on the assumption of charge independence; the difference of about a factor of 2 in total cross section is ascribed to a 1 per cent $T = 0$ admixture in the intermediate state (Ba 57d). See also (He 53a, Ch 57b, Sm 58a, Pa 58, Pe 58a, Ba 58a) and (Si 57b, Mo 55a; theo.).

XXIII. $C^{12}(\gamma, 3\alpha)$ $\quad Q_m = -7.281$

Maxima in the yield of 3-prong stars are reported at $E_\gamma = 17.3$, 18.3, 21.9, 24.3 and 29.4 MeV; some evidence of fine structure is also found. The integrated cross section is 1.21 ± 0.16 MeV-mb for $E_\gamma < 20.5$ MeV, 2.8 ± 0.4 MeV-mb for $20.5 \leqq E_\gamma < 42$ MeV, and < 0.2 MeV-mb for $42 \leqq E_\gamma < 60$ MeV (Go 53f, Go 55b). (Ca 55b) summarize cross section measurements for the $Li^7(p, \gamma)$ radiation and find evidence for a resonance near $E_\gamma = 12.3$ MeV and possibly others at 15 and 16 MeV. According to (Jo 55), peaks occur at $E_\gamma = 14.7$, 15.8, 16.6, 18.3, 24.3, and > 29 MeV, in fair agreement with (Go 53f). Absolute cross sections are reported for $E_\gamma = 13$ to 30 MeV, and integrated cross sections agree well with (Go 53f) (Jo 55). See also (Da 53d, Mi 53c, Ha 55g, Gu 53a). According to (Go 55b), the three-body reaction is not involved for $E_\gamma < 40$ MeV (see, however, Mi 53c, Ch 54e). The reaction $C^{12}(\gamma, \alpha)Be^{8*}(p)Li^7$ is reported by (Li 56).

Studies of angular distributions indicate that for $E_\gamma = 12$ to 15.6 MeV, the reaction involves mainly E2 absorption (C^{12*} $J = 2^+$, $T = 0$); from 15.6 to 20 MeV both E1 ($J = 1^-$, $T = 1$) and E2 ($J = 2^+$, $T = 1$), and for $E_\gamma > 20$ MeV, mainly E1 ($J = 1^-$, $T = 1$). Significant E2 absorption ($J = 2^+$, $T = 0$) also occurs for $E_\gamma = 20$ to 25 MeV (Go 55b: see, however, Ge 53a, Te 51b). See also (Li 53b, Gr 54, Co 55, So 55, Ti 55a, Mu 57c, Ma 56r).

XXIV. $C^{12}(e, e')C^{12}$

Both elastic and inelastic scattering angular distributions have been studied at $E_e = 80$, 150 and 187 MeV by (Fr 55, Fr 56d) and at 420 MeV by (Eh 58a). The elastic data are well accounted for by a modified Gaussian charge distribution of r.m.s. radius 2.50×10^{-13} cm, derived from a harmonic well with a characteristic length parameter of 1.68×10^{-13} cm (Fr 56d, Eh 58a). See also (Ho 53e, Fe 56d, Ho 56e, Eh 58, Ho 57g, Ra 58e).

Inelastic peaks corresponding to C^{12} levels at 4.4, 7.7, and 9.6 MeV are observed, in addition to some unresolved structure near 11 MeV. There is no indication of the 15.1-MeV level. The observed angular distributions agree well with shell-model calculations of (Ra 55c, Mo 56c, Ta 56d, Ta 57c) with a harmonic well of r.m.s. radius 2.40×10^{-13} cm. Predicted absolute cross sections are low by a factor of 2 in L-S coupling, 6 in j-j coupling; it is presumed that some collective modes of excitation are involved.

Excitation of the 4.4-MeV level is electric; a width of $12.5\pm2.5\times10^{-3}$ eV, $\tau_m = (0.53\pm0.11)\times10^{-13}$ sec, is obtained (He 56e). The 7.7 and 9.6-MeV levels are also electrically excited; the angular distributions indicate either monopole or quadrupole transitions, $J = 0^+, 2^+$. The matrix element for the 7.7-MeV E0 transition is 50 mb, in good agreement with that observed for the O^{16} monopole transition (Fr 56d, Sc 55a). A shell model calculation in intermediate coupling indicates that configuration mixing is required to give a non-zero matrix element for the 0^+-0^+ transition and suggests that a semi-collective model is indicated (Sh 56d, Sc 55a, Ta 57c, see also La 55). According to (El 56), satisfactory agreement is obtained with a 50 per cent admixture of $1s^3 1p^8 2s$ and $1s^4 1p^7 2p$. (Re 56b) also finds reasonable agreement using the $1s^{-1}2s$ configuration and suggests that such a "core" excitation might appear quite generally in the light nuclei (see O^{16}, C^{14} and Ch 54d). Calculations using an independent-particle approach to a collective description give a good account of the form factors for both the 4.4 and 7.7-MeV excitations. The form factor for the 9.6-MeV level is consistent with $J = 1^-$ (Fe 56d: see also Pa 57c). See also (El 58; theo.).

Neutron production with $E_e = 35$ to 150 MeV has been studied by (Ge 56d). Comparison of $\sigma(\gamma, n)$ and $\sigma(e, e'n)$ for $E_e = 24$ to 145 MeV indicates that the transitions are largely E1 (Ba 58l).

XXV. (a) $C^{12}(n, n)C^{12}$
(b) $C^{12}(n, n')C^{12*}$
(c) $C^{12}(n, n')3He^4$ $\quad Q_m = -7.281$

For $E_n \gtrsim 14$ MeV, elastic scattering angular distributions show pronounced optical-model effects: see (Na 58, Cu 56, Bu 56j) and C^{13}.

A gamma ray of energy 4.42 ± 0.03 MeV is observed at $E_n = 6.58$ MeV (Da 56d: see also Th 54b, Be 55i, Ba 55c). Production of 15.1-MeV γ-rays is observed at $E_n = 90$ MeV (Wa 57e, Wa 57b). At $E_n = 14$ MeV, inelastic neutron groups corresponding to $C^{12*} = 4.4$ and 9.6 MeV are reported by (Wo 56a; see also Wh 53, Ca 56, Be 56b, An 58). The angular distributions for neutrons corresponding to $C^{12*}(4.4)$ agree well with (p, p') distributions and with direct interaction theory (An 58: $E_n = 14$ MeV).

Inelastic excitation leading to α-particle stars has been studied by (Fr 55i); levels of C^{12} at 7.7 and 9.6 MeV are involved. (Ja 53) find that for $E_n < 20$ MeV, most events proceed through a level at 10 ± 0.8 MeV, $\Gamma_{obs} = 1.6$ MeV, to Be^8(g.s.) (See Fr 55i, $B^{12}(\beta^-)C^{12}$). See also C^{13}, (Li 53b) and (La 56e; theo.).

XXVI. (a) $C^{12}(p, p')C^{12*}$
(b) $C^{12}(p, p')3He^4$ $\quad Q_m = -7.281$

Elastic scattering differential cross sections have been determined by (Bu 53b, Gi 57, Gr 57f; $E_p = 9.4$ to 9.6 MeV), (Fi 54b: $E_p = 10$ MeV),

(Sh 56b: $E_p = .12$ MeV), (Pe 57a: $E_p = 14$ to 19.4 MeV), (Da 56b: $E_p = 17.0$ MeV, c.m.), (Ki 55b, Ki 56: $E_p = 14.5$, 20 and 31.5 MeV), (Br 52c, Wr 53a: $E_p = 30.6$ MeV), (Hi 57: 40 MeV) and (Ge 57: 96 MeV). Calculations based on the diffuse-surface optical model give a good account of the data at higher energies (Me 57b, Gl 57, Gl 58). At $E_p = 9.5$ MeV, some evidence for compound elastic scattering is seen in the marked energy variation at back angles (Gi 57). See also N^{13}. Polarization of elastic and inelastic protons has been studied by (Br 58f) for $E_p = 16$ to 18 MeV. Polarization of elastic protons for $E_p = 5$—7 MeV is reported by (Wa 58a, Wa 58d). See also (Ko 58b, Le 57h, Sq 58; theo.). Polarization studies at high energies are discussed by (Ni 56b, Ni 58b, Ni 58c, Er 56a, Ty 57, He 57c, Al 57b, Hi 57b).

Excitation of the 4.4-MeV level is commonly observed for all energies above $E_p \approx 5$ MeV: see (Aj 55) and (Re 56c: $E_p = 5$ to 6 MeV), (Ho 57c, Gi 57: 9.5 MeV), (Co 57: 12 MeV), (Pe 57a: 14 to 19 MeV), (Br 52c: 31.5 MeV), (Ch 58: 40 MeV), (St 56a: 96 MeV), (Di 57a: 95 and 135 MeV) and (Ma 57b, Ma 58h, Ty 57b, Ty 58b, Al 57c: 182 MeV). $E_x = 4431 \pm 8$ keV (Bu 57c). The 7.7 and 9.6-MeV levels are reported by (Co 57, Pe 57a, Ho 57c, Ch 58, Ma 57b). Levels at 12.6, 15.0, and $\approx$ 20 MeV are also reported by (Ma 57b, Ty 57b); the last appears strongly in the work of (St 56a) ($E_x = 20.8$ MeV) and is there associated with the giant resonance seen in $C^{12}(\gamma, n)$ and $C^{12}(\gamma, p)$.

For $E_p \lesssim 30$ MeV, the angular distribution of the proton group corresponding to the 4.4-MeV level exhibits a minimum near 90°—100° (c.m.) and a definite fore-and-aft asymmetry. Neither the compound nucleus model nor the direct interaction theory appears to give a satisfactory account of these distributions (Pe 57a, Co 57, Gi 57). A direct interaction calculation, using distorted waves, does reproduce the general features of the distributions and also fits the observed (p′—γ) correlation of (Sh 56) (Le 58a). See also (Bu 57a, Be56 f, Ma 57i, Ch 58, Br 58c, Ba 57k, Mo 58c).

The angular distribution of protons corresponding to the 7.7-MeV state depends strongly on energy in the range $E_p = 14$ to 19 MeV, but consistently shows a strong forward peak, indicative of $l = 0$ and hence $J = 0^+$ (Pe 57a). See also (La 55). An attempt to observe γ-decay of this level yields an upper limit of 3 per cent for $\Gamma_\gamma/\Gamma_\alpha$ (Ho 56c). The angular distribution of protons leading to the 9.6-MeV level is consistent with $l = 1$, $J = 0^-, 1^-, 2^-$ (Pe 57a).

The angular distribution of pick-up deuterons at $E_p = 95$ MeV indicates significant contributions of high momentum components in the bound, 1p neutron wave function, suggesting strong interactions, ($\approx$ 200 MeV), for close distances, $R \approx 1 \times 10^{-13}$ cm (Se 55c, Se 56a). See also (Gr 56e).

Emission of (15.1 ± 0.2) MeV γ-radiation, ascribed to the first $T = 1$ level, has been studied in the range $E_p = 15$ to 340 MeV by (Wa 57b, Wa 57e). The general shape of the excitation function indicates direct nucleon-nucleon interaction for the higher energies; near threshold, emission of s-wave protons

is indicated. Estimates of the α-particle width, and comparison with isobaric spin forbidden reactions (e.g. $C^{12}(\alpha, \alpha')C^{12*}$, $C^{12}(d, d')C^{12*}$) indicate a $T = 0$ admixture $a^2 \approx 10^{-3}$. At 31 MeV, $\theta_{lab} = 80°$, γ-rays of energy 15.1, 12.8 and 10.7 MeV are observed, with relative intensities $1/0.090 \pm 0.015/0.095 \pm 0.014$. The 12.8-MeV radiation is ascribed to excitation of a C^{12} level of that energy, while the 10.7-MeV radiation represents a cascade from $C^{12*}(15.1)$ to $C^{12*}(4.4)$ (Wa 57e: see also $B^{10}(He^3, p)C^{12}$).

A study of reaction (c) at an energy of 29 MeV shows no indication of direct 4-body decay of N^{13*}; $\frac{1}{4}$ of the events proceed via $Be^8(0)$, and $> \frac{1}{2}$ via $Be^8(2.9)$. Evidence is found for the participation of C^{12*} at 9.6, ≈ 12, 16, 20 and 25 MeV (Ne 55c). See also (Re 55a), (Ja 57b) and (Sa 56e, Sa 56f, Cu 55a).

See also (St 56c, Al 57c, Go 57f) and (El 58, Ka 57; theo.).

XXVII. $C^{12}(d, d')C^{12*}$

The angular distribution of elastic scattering has been studied at $E_d = 19$ MeV by (Fr 54e); several diffraction peaks appear. See also (Wa 58e).

Inelastic groups corresponding to levels at 4.4 and 9.6 MeV are reported by (Ke 51b, Fr 54e, Ha 56c, Gr 56b; see also Ca 56k). The 7.7-MeV level has not been observed. The angular distribution of the $Q = -4.4$-MeV group at $E_d = 15$ MeV has been analyzed in terms of direct nuclear interaction theory and in terms of electric interaction theory by (Ha 56c); neither appears to give a satisfactory account of the observations.

A search for 15-MeV γ-radiation at $E_d = 85$ MeV yielded a negative result; a $T = 0$ admixture of $< 4 \times 10^{-2}$ is indicated (Wa 57b, Wa 57e).

See also (Kh 55, Kh 55a).

XXVIII. $C^{12}(He^3, He^{3'})C^{12*}$

See (We 58c).

XXIX. (a) $C^{12}(\alpha, \alpha')C^{12*}$

(b) $C^{12}(\alpha, \alpha n)C^{11}$ $\quad Q_m = -18.722$

Elastic scattering has been studied at $E_\alpha = 19$ MeV by (Pr 58a), at 31.5 MeV by (Wa 56f), at 40 MeV by (We 56, Ig 56, Ig 57) and at 48 MeV by (Va 55b). The angular distributions show strong diffraction effects indicative of a direct interaction. Inelastic groups corresponding to levels at 4.4, 7.64 ± 0.07, 9.6 and possibly, 12.7 MeV are observed. C^{12} recoils corresponding to the ground- and 4.4-MeV states are also reported; the absence of recoils corresponding to the 7.7-MeV state is taken to indicate that this state disintegrates primarily (> 80 per cent) by α-emission (Ra 55a: see $B^{11}(d, n)C^{12}$). From a similar experiment, (Ec 58) find that the chance is less than 0.1 for $\Gamma_\gamma/\Gamma > 10^{-3}$.

Angular distribution of the $Q = -4.4$ MeV inelastic group at $E_\alpha = 31.5$

MeV are consistent with the direct surface interaction theory of (Au 53). A similar analysis of the $Q = -7.7$ MeV group gives good agreement for $J = 0^+$ (Wa 56f). At $E_\alpha = 42$ MeV, the angular distribution of this group is well matched by the $j_0^2(kr)$ or $j_2^2(kr)$ functions, indicating $J^\pi = 0^+$ or 2^+. The former is preferred in view of the small γ-width (Ec 58). See also (We 56, Fi 57b, Pr 58a, Sh 58a).

A search for γ-radiation from the de-excitation of the 15-MeV, $T = 1$ level at $E_\alpha = 48$ and 175 MeV gives an upper limit of $\approx 10^{-3}$ for the $T = 0$ admixture (Wa 57b, Wa 57e).

See also (Ju 54a). For reaction (b), see (Li 53c).

XXX. $N^{12}(\beta^+)C^{12}$ $Q_m = 17.46$

The decay is mainly to the ground state via an allowed transition. Transitions to $C^{12*}(4.4)$ and (7.65) also are allowed. Branching ratios are 100/15/3; $\log ft = 4.17$, 4.4 and 4.4, respectively (Ve 58a). Delayed α-particles with a total energy of ≈ 4 MeV are also observed, suggesting that a state of C^{12} in the region 11 to 12 MeV is involved (Al 50g). See N^{12}.

XXXI. $C^{13}(\gamma, n)C^{12}$ $Q_m = -4.946$

See C^{13}.

XXXII. $C^{13}(p, d)C^{12}$ $Q_m = -2.719$

$Q_0 = -2.720 \pm 0.007$ (Bu 57c)

See (Be 57b) and (Ne 55c).

XXXIII. $C^{13}(d, t)C^{12}$ $Q_m = 1.313$

Angular distributions of the ground state tritons have been measured at $E_d = 2.2$ and 3.3 MeV (Ho 54c).

XXXIV. $C^{13}(He^3, \alpha)C^{12}$ $Q_m = 15.632$

Angular distributions of the α-particle groups to the ground and 4.4-MeV states have been obtained at $E(He^3) = 2$ MeV (Ho 57) and 4.5 MeV (Ho 57a). Some direct interaction appears to be involved at both energies. At $E(He^3) = 2$ MeV, a 15.1-MeV γ-ray is observed (Go 57b, Br 57, Br 58e).

XXXV. $C^{14}(p, t)C^{12}$ $Q_m = -4.635$

Not observed.

XXXVI. $N^{14}(\gamma, d)C^{12}$ $Q_m = -10.265$

Not observed.

XXXVII. $N^{14}(n, t)C^{12}$ $Q_m = -4.007$

See N^{15} and (Li 52).

XXXVIII. $N^{14}(p, He^3)C^{12}$ $Q_m = -4.772$

Not observed.

XXXIX. $N^{14}(d, \alpha)C^{12}$ $Q_m = 13.579$

Four α-groups have been observed corresponding to the ground state of C^{12} and to the levels at 4.4, 7.7 and 9.6 MeV: see table 12.11 and (Ho 57c).

TABLE 12.11

C^{12} states from $N^{14}(d, \alpha)C^{12}$

A		B	C	D	E	F	G
Q (MeV $\pm$ keV)	σ (mb)	Q (MeV $\pm$ keV)	Q (MeV $\pm$ keV)	Q (MeV $\pm$ keV)	Q (MeV $\pm$ keV)	Q (MeV $\pm$ keV)	C^{12*} (MeV)
13.39 $\pm$ 80	1	13.575 $\pm$ 12					0
9.02 $\pm$ 70	3	9.137 $\pm$ 6					4.442
5.77 $\pm$ 70	0.3		5.89 $\pm$ 30	5.910 $\pm$ 15	5.912 $\pm$ 13		7.664
		3.955 $\pm$ 3				3.933 $\pm$ 14	9.63

A: $E_\alpha = 1.01$ MeV, $\theta = 90°$ (Ho 40).
B: (Ma 51).
C: Based on $Q_1 = 9.137$ for the second group (Du 53). At $E_\alpha = 0.62$ MeV, $\theta = 90°$, this group has 6 % the intensity of the first.
D: (Pa 55a).
E: (Ah 56).
F: (Do 56c): it is suggested that a systematic error exists in Ma 51's value for this state.
G: Based on $Q_0 = 13.579$.

Alpha-gamma correlations give $J = 2^+$ for the 4.4-MeV state (St 54f) while γ—γ correlations give $J = 0$ or > 2 for the 7.7-MeV state (Se 55: see, however $B^{12}(\beta^-)C^{12}$). The width of the 7.7-MeV state is < 25 keV (Du 53, Ah 56) and that of the 9.6-MeV state is 30 ± 8 keV (c.m.). The J^π values for the 9.6-MeV state are limited to 0^+, 1^-, 2^+, 3^-, 4^+ (Do 56c). Angular distributions of the α-particles to the ground, 4.4 and 9.6 MeV states have been measured at $E_d = 20.9$ MeV (Fi 57b). See also (Gi 52, Bo 58a, Bo 58c). A small yield of 15-MeV γ-radiation is observed at $E_d = 10.8$ MeV, presumably due to excitation of the 15.1-MeV, $T = 1$ state (Ra 54a). See also (Ra 58b, Gr 56b) and O^{16}.

XL. $N^{14}(He^3, p\alpha)C^{12}$ $Q_m = 8.086$

See O^{16}.

XLI. $N^{15}(p, \alpha)C^{12}$ $Q_m = 4.964$

Alpha particles have been observed to a state of C^{12} at 4.432 ± 0.010 MeV (Sc 52). The γ-ray energy after Doppler correction of 20 keV is 4.443 ± 0.020 MeV. The necessity for the correction implies a lifetime $< 3 \times 10^{-13}$ sec (Th 52); see $C^{12}(\gamma, \gamma')C^{12*}$. The angular distributions of short-range alpha

particles and 4.4-MeV γ-radiation indicate that the 4.4-MeV state has $J = 2^+$ or > 4 (Kr 53; see also Go 57h). See also O^{16} and (Ra 58a).

XLII. (a) $O^{16}(\gamma, \alpha)C^{12}$ $Q_m = -7.148$

(b) $O^{16}(\gamma, 4\alpha)$ $Q_m = -14.429$

There is evidence of the involvement of C^{12} states at 9.6 and $\approx$ 11 MeV, which decay to the ground state of Be^8, a state at 12—13 MeV, decaying mainly to the 2.9-MeV state of Be^8, and $T = 1$ states at $\approx$ 16 and 18—19 MeV, again leading mainly to the 2.9-MeV Be^8 state. The 4.4- and 7.7-MeV states of C^{12} seem to occur rarely, if at all (see O^{16}).

XLIII. $F^{19}(p, 2\alpha\gamma)C^{12}$ $Q_m = 0.971$

See (Za 57).

N^{12}

(Fig. 21, p. 137)†

MASS OF N^{12}

From the Q of the $B^{10}(He^3, n)N^{12}$ reaction, 1.46 ± 0.06 MeV, and the Wapstra (Wa 55c) atomic masses for B^{10}, He^3 and n, the mass excess of N^{12} is 21.00 ± 0.06 MeV.

I. $N^{12}(\beta^+)C^{12}$ $Q_m = 17.46$

The half life is 12.5 ± 1 msec; $E_\beta(\max) = 16.6 \pm 0.2$ MeV (Al 49a), $\tau_{\frac{1}{2}} = 11.43 \pm 0.05$ msec; $E_\beta(\max) = 16.37 \pm 0.06$ MeV (Ve 58a). The decay is complex; N^{12} decays to the ground state of C^{12} and to $C^{12*}(4.4)$ and (7.6): see C^{12}. Log $ft = 4.17$ for the ground state transition (Ve 58a). See also (Sc 59; theo.).

II. $B^{10}(He^3, n)N^{12}$ $Q_m = 1.46$

$Q_0 = 1.46 \pm 0.06$ (Aj 57a).

The neutron spectrum has been studied at $E(He^3) = 2.54$ and 3.60 MeV. Seven neutron groups are observed, corresponding to the ground state and to excited states at 1.06 ± 0.08, 1.56 ± 0.08, (1.97 ± 0.10), 2.35 ± 0.08, 3.18 ± 0.15 and 3.46 ± 0.15 MeV, in good agreement with the levels of the mirror nucleus, B^{12}. At the lower energy, the (c.m.) angular distribution of the ground state neutrons is isotropic within $\approx$ 15 per cent statistics; at the higher energy, the distribution is peaked forward (Aj 57a).

III. $C^{12}(p, n)N^{12}$ $Q_m = -18.24$

$E_{\text{thresh}} = 20.0 \pm 0.1$ MeV (Al 49a). See also (Gr 57, Ca 57g) and N^{13}.

IV. $C^{12}(He^3, t)N^{12}$ $Q_m = -17.48$

Not reported.

V. $N^{14}(\gamma, 2n)N^{12}$ $Q_m = -30.73$

See N^{14}.

† For level scheme of B^{12}, see fig. 19, p. 113.

VI. $N^{14}(p, t)N^{12}$ $Q_m = -22.25$

Not reported.

TABLE 12.12
Energy levels of N^{12}

E_x in N^{12} (MeV)	J^π	$\tau_{\frac{1}{2}}$	Decay	Reactions
0	1^+	$(11.43 \pm 0.05) \times 10^{-3}$ sec	β^+	I, II, III, V
1.06 ± 0.08				II
1.56 ± 0.08				II
(1.97 ± 0.10)				(II)
2.35 ± 0.08				II
3.18 ± 0.15				II
3.46 ± 0.15				II

B^{13}

(Not illustrated)

MASS OF B^{13}

The mass excess of B^{13} is 20.40 ± 0.05 MeV from the Q of the reaction $Li^7(Li^7, p)B^{13}$ (No 57), and Wapstra's masses (Wa 55c) for Li^7 and H^1. B^{13} is then stable by 4.88 MeV to decay into $B^{12}+n$, by 11.00 MeV to decay into $Be^{10}+t$ and by 11.3 MeV to decay into $Li^9+\alpha$.

TABLE 13.1
Energy levels of B^{13}

E_x in B^{13} (MeV)	J^π; T	$\tau_{\frac{1}{2}}$ (sec)	Decay	Reactions
0	$(\frac{3}{2}^-)$; $\frac{1}{2}$	$(35 \pm 15) \times 10^{-3}$	β^-	I, II

I. $B^{13}(\beta^-)C^{13}$ $Q_m = 13.44$

The half-life of B^{13} is $(35 \pm 15) \times 10^{-3}$ sec (No 56b). Attempts to observe delayed neutrons from the decay of neutron-unstable statesof C^{13} have been unsuccessful (Hu 53a, No 56b). It is pointed out by (No 57) that transitions to such states are unlikely if B^{13} has the expected $J = \frac{3}{2}^-$. See also (Sh 52, Sn 48).

II. $Li^7(Li^7, p)B^{13}$ $Q_m = 5.97$

$Q_0 = 5.97 \pm 0.05$ (No 57)

This reaction has been observed for $E(Li^7) = 1.4$ to 2.0 MeV (Al 56, No 57, Li 58c). At $E(Li^7) = 2$ MeV, no proton groups have been observed

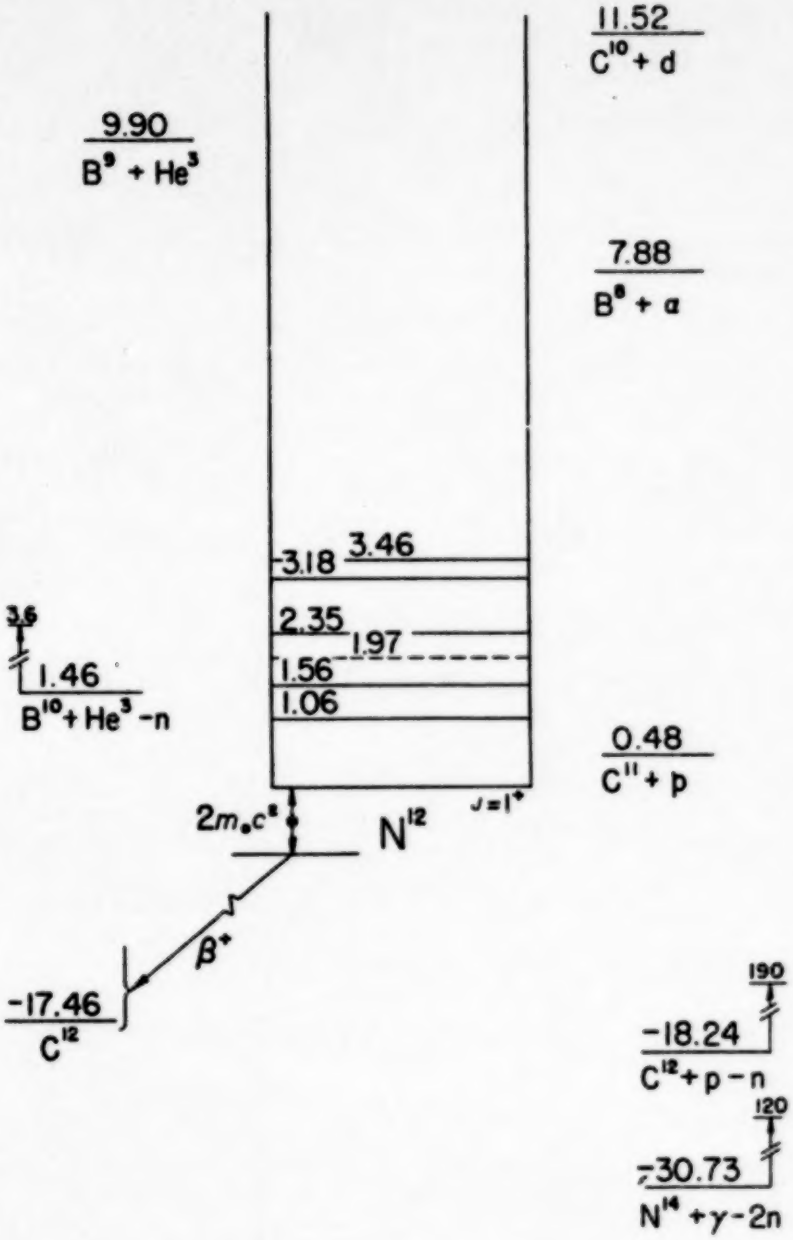

21 November 1958

Fig. 21. Energy levels of N^{12}: for notation, see fig. 1, p. 7.

corresponding to excited states of B^{13} below $E_x = 2.9$ MeV (Li 58c). See also C^{14}.

III. $B^{11}(t, p)B^{13}$ $\quad Q_m = 0.24$

Not reported.

C^{13}

(Fig. 22, p. 139)†

THEORY

See (Au 55, La 55b, Da 56g, De 56, Ku 56, Ba 57, Sk 58, Fr 58b).

TABLE 13.2

Energy levels of C^{13}

E_x in C^{13} (MeV)	J^π	Γ(keV) or τ_m	Decay	Reactions
0	$\frac{1}{2}^-$	—	stable	II, IX, XV, XVII, XXIII, XXIX, XXX, XXXII, XXXIV, XXXV, XXXVII, XL, XLI
3.085±0.005	$\frac{1}{2}^+$	$\tau_m < 3\times10^{-13}$ sec	γ	IX, XV, XVIII, XXIII, XXIX, XXXII, XL
3.680±0.007	$\frac{3}{2}^-$	$\tau_m < 3\times10^{-13}$ sec	γ	IX, XV, XVII, XXIII, XXIX, XXXII, XXXIV, XL
3.850±0.010	$\frac{5}{2}^+$	$\tau_m > 3\times10^{-13}$ sec	γ	IX, XV, XXIII, XXXII, XL
5.51 ±0.05				XV
6.10±0.05				XV
6.86 ±0.01	$\frac{5}{2}^+$	6	n	XV, XVIII, XXIII, XL
7.470±0.02				XXIII, XL
7.533±0.02				XV, XXIII, XL
7.641±0.02	$\frac{3}{2}^+$	55± 15	n	XVIII, XXIII, XL
8.33 ±0.1	$\frac{3}{2}^+$	1000±250	n	XVIII, XXIII, XXXV
8.82 ±0.04			n	XV, XVIII, XL
9.50 ±0.02			n	XV, XVIII, XXIII, XL
9.90 ±0.02	>0		n	XV, XVIII, XXIII, XL
10.76 ±0.02			n	XVIII, XIX, XXIII
10.94 ±0.1			n	XV, XVIII, XIX
11.02 ±0.03	$(\frac{1}{2}^+)$	50	α, n	IV, XV
11.08 ±0.03		sharp	α, n	IV, XV
11.97 ±0.015	$(\frac{7}{2}^-)$	70	α, n	IV, XV, XVIII, XIX
12.21 ±0.03		≈140	α, n	IV, XV, XVIII, XIX
12.44 ±0.03	$(\frac{1}{2}^-)$	≈140	α, n	IV, XIX
12.81 ±0.1				XV
13.41 ±0.03		50	α, n	IV
13.77 ±0.03		≈280	α, n	IV
14.1 ±0.1		≈210	α, n	IV
14.64 ±0.03			α, n	IV
16.1 ±0.1			α, n	IV
20.52 ±0.02		115± 10	d, n	X
21.28 ±0.02		160± 15	d, n	X

I. (a) $Li^6(Li^7, p)B^{12}$ $Q_m = 8.338$ $E_b = 25.876$

(b) $Li^6(Li^7, n)C^{12}$ $Q_m = 20.931$

(c) $Li^6(Li^7, 2n)C^{11}$ $Q_m = 2.209$

See (No 57a).

II. $Li^7(Li^7, n)C^{13}$ $Q_m = 18.624$

See (No 57a).

† For level scheme of N^{13}, see fig. 24, p. 151.

III. $Be^9(\alpha, \gamma)C^{13}$ $Q_m = 10.654$

At $E_\alpha = 1.60$ MeV, the capture cross section is less than 30 μb (Al 55c).

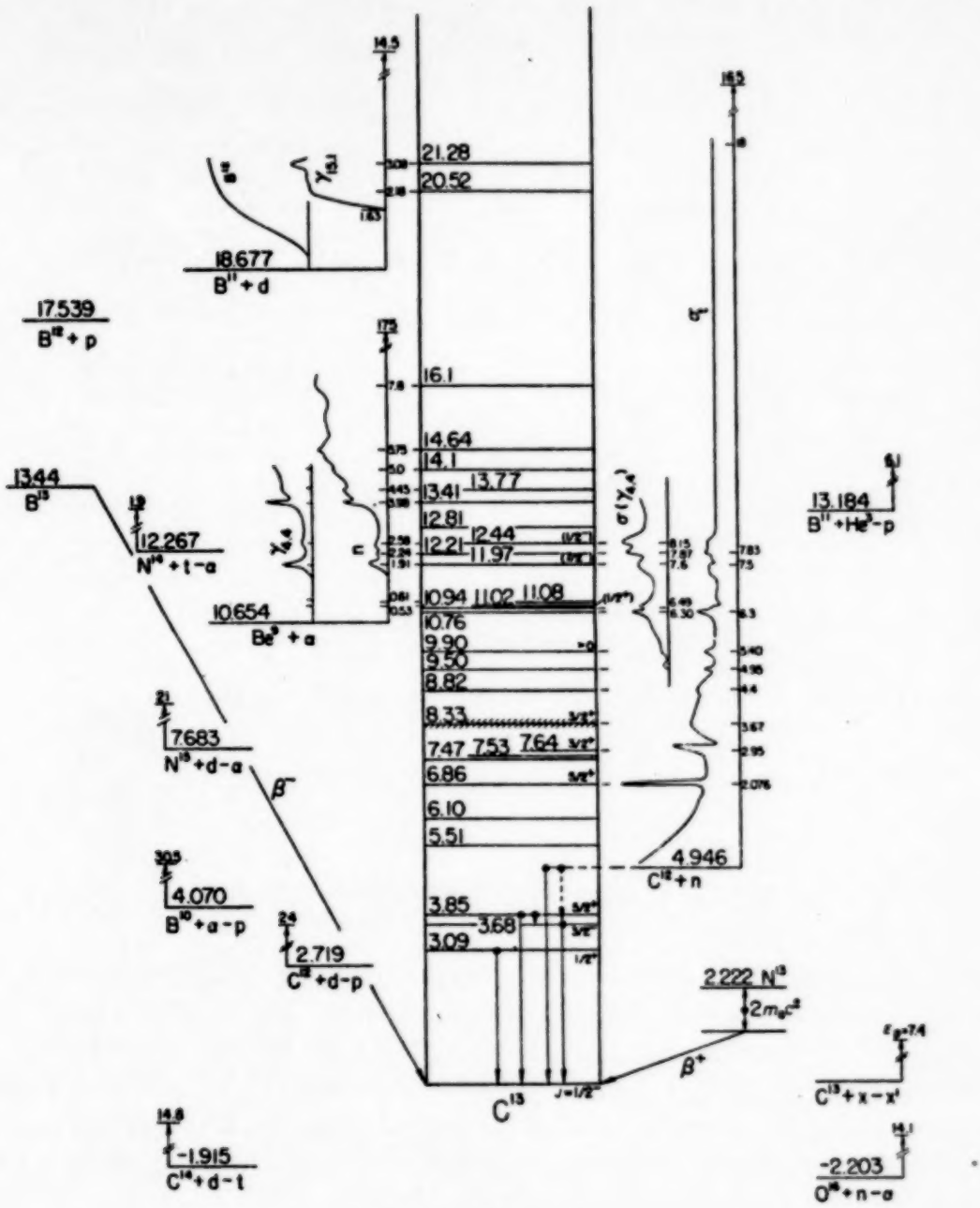

31 December 1958

Fig. 22. Energy levels of C^{13}: for notation, see fig. 1, p. 7.

IV. $Be^9(\alpha, n)C^{12}$ $Q_m = 5.709$ $E_b = 10.654$

Resonances for neutrons and for γ-rays from $C^{12*}(4.4)$ are given in table 13.3. Absolute cross sections for several resonances are reported by (Bo 56d, Gi 59). For the prominent 1.9-MeV resonance, $d\sigma/d\Omega(90°)$ for 4.4-MeV

γ-rays is given as 12 mb/sr (lab) by (Bo 56d) and as 26 mb/sr by (Ta 55b). For $E_\alpha = 2.5$ to 8.2 MeV, absolute neutron yields have been measured by (Ma 58g, Gi 59).

TABLE 13.3

Resonances in $Be^9(\alpha, n)C^{13}$

E_α [a] (MeV)	E_α [b] (MeV)	Γ (keV)	J^π	C^{13*} (MeV)	Ref.
0.53	0.53	70	$(\frac{1}{2}^+)$ [j]	11.02	c
0.61	0.61	sharp		11.08	c
1.9	1.905	180	$(\frac{7}{2}^-)$ [j]	11.97 [k]	d
2.24		≈200		12.21 [k]	e
2.58	2.6	≈200	$(\frac{1}{2}^-)$ [j]	12.44 [k]	f
4.00	3.98	70		13.41	h, i
(4.2)		(≈300)		(13.6)	g
4.50	4.4	≈400		13.77 [k]	h, i
5.0	5.0	≈300		14.1 [k]	h
5.75				14.64	i
7.8				16.1	i

[a] Resonances in neutron yield.
[b] Resonances for 4.4-MeV γ-rays.
[c] (Be 54).
[d] (Ta 53, Be 54, Tr 54, Ta 55b, Bo 56d), $\Gamma_n/\Gamma_\alpha > 12$ (Ta 55b).
[e] (Tr 54, Bo 56d).
[f] (Ta 53, Tr 54, Bo 56d, Ma 58g).
[g] (Ri 57).
[h] (Bo 56d).
[i] (Ma 58g, Gi 59).
[j] (Ja 56a).
[k] Not corrected for effects of Coulomb barrier penetration.

Separate excitation curves (at 0°) for ground state neutrons (n_0) and for neutrons to the 4.4-MeV state (n_1) are reported by (Ri 57) in the range $E_\alpha = 1.7$ to 4.8 MeV (n_0) and 3.1 to 4.8 MeV (n_1). The n_0 yield curves show broad maxima at $E_\alpha = 1.9$, 2.0, 2.6, 4.2 and 4.5 MeV. The sharp 3.98-MeV resonance is strong for n_1, but quite weak for n_0. Angular distributions of ground-state neutrons suggest two broad resonances in the region $E_\alpha = 3.9$ to 4.6 MeV, probably $J = \frac{3}{2}^+$ and $\frac{5}{2}^+$ (Ri 57).

Extensive angular distribution studies have been made for $E_\alpha < 2$ MeV by (Ja 56a, Ta 55b). According to (Ja 56a), the best fit to the distributions in the range $E_\alpha = 0.4$ to 1.3 MeV is obtained from the assignments $J = \frac{1}{2}^+$, $\frac{7}{2}^-$, $\frac{1}{2}^-$ for the 0.5, 1.9 and 2.6 (?) MeV resonances (see also Ta 55b). The angular correlation of neutrons and 4.4-MeV gamma-rays is isotropic at $E_\alpha = 1.2$ and 2.8 MeV, indicating that stripping plays only a minor role at these energies (Ta 58d). See also (Ma 55i; theo.) and (Be 56c).

V. $Be^9(\alpha, p)B^{12}$ $Q_m = -6.884$ $E_b = 10.654$

See B^{12}.

VI. $Be^9(\alpha, d)B^{11}$ $Q_m = -8.022$ $E_b = 10.654$

See B^{11}.

VII. (a) $Be^9(\alpha, \alpha')Be^{9*}$ $E_b = 10.654$

(b) $Be^9(\alpha, \alpha' n)Be^8$ $Q_m = -1.667$

(c) $Be^9(\alpha, n)3He^4$ $Q_m = -1.572$

For reaction (a) see Be^9 and (Ta 55b). For reactions (b) and (c), see (Aj 52c).

VIII. $B^{10}(t, \alpha)Be^9$ $Q_m = 13.210$ $E_b = 23.882$

See Be^9.

IX. $B^{10}(\alpha, p)C^{13}$ $Q_m = 4.070$

$Q_0 = 4.064 \pm 0.012$ (W. J. Fader, quoted in Va 57).

$Q_0 = 4.08 \pm 0.03$ (Pi 56)

$Q_0 = 4.10 \pm 0.03$ (Pa 56b)

Four proton groups are observed, corresponding to the C^{13} levels at 0, 3.09, 3.68 and 3.85 MeV (Sh 53b, Fa 54a, Fa 54d, Pi 56). Additional groups are reported by (Ro 57e). The relative intensities depend strongly on bombarding energy (see N^{14}, Sh 53b). See also (Aj 55).

A study of gamma rays from this reaction and from C^{12}(d, p)C^{13} shows three lines with $E_\gamma = 0.1695 \pm 0.0004$, 3.844 ± 0.015 and 3.69 ± 0.02 MeV. The 3.85-MeV γ-ray exhibits no Doppler shift and therefore has a lifetime greater than 3×10^{-13} sec; the 3.69-MeV line shows approximately the maximum possible Doppler shift ($\tau < 3 \times 10^{-13}$ sec). The 170-keV line is due to the cascade transition between the 3.84 and 3.68-MeV states; the internal conversion coefficient is consistent with E1, although M1 cannot be excluded. The probability of this cascade decay of the 3.84-MeV state is 0.24 ± 0.05. Cascade transitions to the 3.1-MeV excited state have not been observed. Their intensities are less than 3 per cent of the ground state transitions (Ma 56f): see fig. 23. (For earlier work see (Sh 53b) and (St 54c)). The angular distributions and p—γ correlations for the 3.8-MeV radiation contain terms in $(\cos^4\theta)$, indicating $J = \frac{5}{2}^+$ for the 3.84-MeV state (St 54c: see C^{12}(d, p)C^{13}). If the 170-keV line is due to an E1 transition, the J^π of the 3.68-MeV state is then $\frac{3}{2}^-$ ($J^\pi = \frac{1}{2}^-, \frac{3}{2}^-$ follows from C^{12}(d, p)C^{13}); the angular distribution of the 3.7-MeV radiation is consistent with M1 (St 54c).

Angular distributions of the ground state protons are reported at $E_\alpha = 4.9$, 6.0, 7.0 and 8.1 MeV (Vo 57) and at $E_\alpha = 30.5$ MeV (Hu 57a): in both cases direct interaction appears to be involved. See also (Ba 57d) and (Br 55).

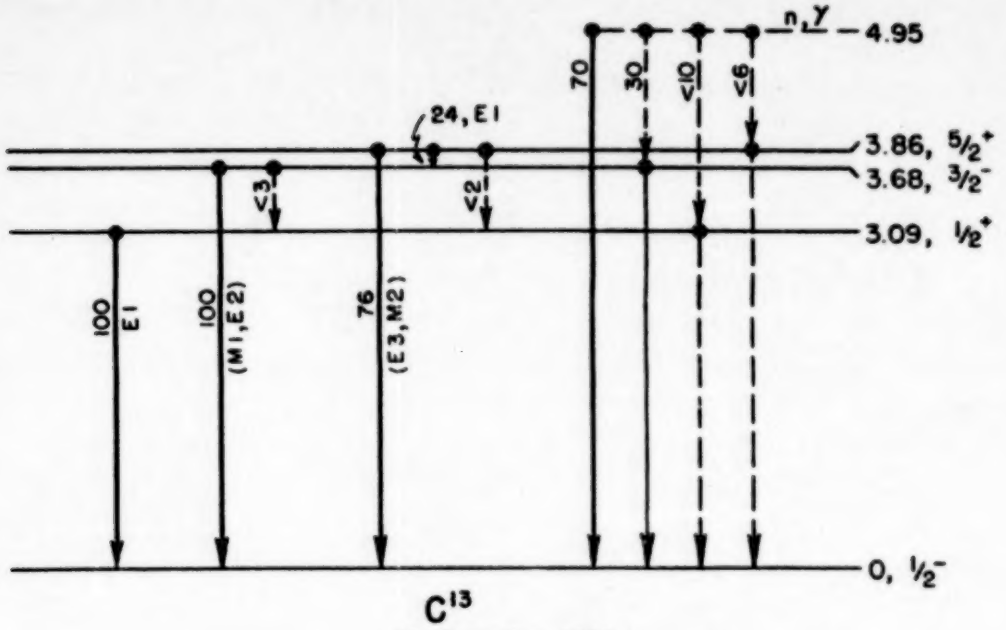

Fig. 23. Gamma-ray transitions in C^{13}: for notation, see fig. 14, p. 83.

X. $B^{11}(d, n)C^{12}$ $Q_m = 13.731$ $E_b = 18.677$

The yield of neutrons has been measured for $E_d = 0.2$ to 5.4 MeV. The total cross section for ground state neutrons in the 0.5 to 1.15-MeV range rises from 0.5 to 30 mb; both direct and exchange stripping processes seem to be involved (Am 57a, Pa 56a). The yield of the excited-state group, $C^{12*}(4.4)$ rises smoothly from $E_d = 0.5$ to 1.1 MeV and is essentially flat from $E_d = 1.1$ to 2.0 MeV (Ne 59). At $E_d = 600$ keV, angular distributions indicate that stripping is important for the ground-state group. For the excited-state group ($C^{12*}(4.4)$), the interpretation is less clear; the observed distribution can be accounted for by p-wave formation of a $J = \frac{7}{2}^+$ level in C^{13} (Wa 55e). (Ne 59) find evidence of strong "heavy-particle" stripping for this group in the range $E_d = 0.5$ to 2.0 MeV. The cross section for emission of neutrons in the forward direction is ≈ 270 mb/sr at $E_d = 5.4$ MeV (Ma 55j). For $E_d = 1.6$ to 3.2 MeV, the yield of 15.1-MeV γ-rays shows resonances at $E_d = 2.180 \pm 0.010$ and 3.080 ± 0.015 MeV, corresponding to $C^{13*} = 20.52$ and 21.28 MeV with $\Gamma_{(c.m.)} = 115 \pm 10$ and 160 ± 15 keV, respectively; the cross section at $E_d = 2.2$ MeV is 29 ± 7 mb (Ka 58a). See also (Bu 54, Ri 55) and C^{12}.

XI. $B^{11}(d, p)B^{12}$ $Q_m = 1.138$ $E_b = 18.677$

The thin-target yield rises smoothly from $E_d = 0.3$ to 3.1 MeV with no evidence of resonances (Hu 49j, Ka 58a). At $E_d = 1.5$ MeV, $\sigma \approx 0.38$ b (Ka 58a; see, however, Hu 49j). See also B^{12} and (Ja 57).

XII. $B^{11}(d, d)B^{11}$ $E_b = 18.677$

See B^{11}.

XIII. $B^{11}(d, \alpha)Be^9$ $Q_m = 8.022$ $E_b = 18.677$

Some absolute cross sections are given by (Ka 58a). See also Be^9.

XIV. $B^{11}(t, n)C^{13}$ $Q_m = 12.419$

Not reported.

XV. $B^{11}(He^3, p)C^{13}$ $Q_m = 13.184$

Levels derived from reported proton groups are listed in table 13.4. The

TABLE 13.4

Levels of C^{13} from $B^{11}(He^3, p)C^{13}$

E_x[a] (MeV ± keV)	E_x[b] (MeV)
0	0
3.09	3.08
3.68	3.77
3.86	
5.51 ± 50	
6.10 ± 50	
6.87	6.89
7.55 ± 40	7.63
8.87 ± 50	8.96
9.52 ± 60	
9.91 ± 50	10.00
10.9 ± 150[c]	10.99
11.1 ± 150[c]	
	11.67
12.08 ± 100[c]	
12.81 ± 100[c]	

[a] (Mo 58f): $E(He^3) = 1.23$ MeV.
[b] (Bi 55): $E(He^3) = 0.9$ MeV; values are ± 100 keV.
[c] (Ga 57): $E(He^3) = 1.25$ MeV.

levels at 5.5 and 6.1 MeV have not been observed in any other reaction. From the fact that they do not appear in $C^{12}(n, n)C^{12}$, an upper limit of $\Gamma = 10$ keV is estimated; the mirror levels in N^{13} must be assumed to have $\theta_p^2 < 0.02$ (Mo 58f).

Angular distributions have been measured for the p_0, p_1 and (p_2+p_3) groups at $E(He^3) = 4.5$ MeV. The p_0 group appears to be peaked in both the forward and the backward direction. The other groups do not exhibit a strong angular variation (Ho 57b). At $E(He^3) = 6.05$ MeV the p_0 group is strongly peaked forward (Sw 58a, and D. R. Sweetman, private communication).

XVI. $B^{11}(\alpha, d)C^{13}$ $Q_m = -5.167$

Not reported.

XVII. $C^{12}(n, \gamma)C^{13}$ $Q_m = 4.946$

The thermal capture cross section is 3.3 ± 0.2 mb (Hu 58). In addition to the 4.95-MeV ground state transition ($E_\gamma = 4948 \pm 8$ keV), a γ-ray is reported with an energy of 3.68 ± 0.05 MeV and an intensity of 0.3 γ/capture. If 3.1- and 3.9-MeV γ-rays occur, their intensities are less than 0.10 and 0.06 γ/capture, respectively (Ba 53d).

XVIII. $C^{12}(n, n)C^{12}$ $E_b = 4.946$

The cross section is approximately constant to 160 keV, then decreases monotonically to $E_n = 2$ MeV. There follows a region of resonances to 8.5 MeV, followed by a smooth variation of the cross section to $E_n = 100$ MeV (Hu 58). (Co 58b) finds a minimum of 1.3 b at $E_n = 14$ MeV, followed by a rise to 1.5 b at $E_n = 15.5$ MeV: see also $C^{12}(n, p)B^{12}$. The average total cross section in the range $E_n = 14$ to 10 000 eV is 4.69 ± 0.10 b (Br 56e).

The parameters of observed resonances are displayed in table 13.5.

TABLE 13.5

Resonances in $C^{12}(n, n)C^{12}$

E_{res} (MeV)	Γ_{lab} (keV)	C^{13*} (MeV)	l_n	J^π	θ^2
2.076 ± 0.008 [a]	7 [a]	6.862	2 [a]	$\frac{5}{2}^+$ [a]	0.006 [a]
2.95 [b]	90 [g]	7.67	2 [h]	$\frac{3}{2}^+$ [h]	0.038 [a]
3.67 [b]	1690 [g]	8.33	2 [h]	$\frac{3}{2}^+$ [h]	0.51 [a]
4.4 [c]		9.0			
4.95 [d]		9.51			
5.40 [d]		9.93	>0 [d]	$>\frac{1}{2}$ [d]	
6.3 [e]		10.8			
7.5 [f]		11.9			
7.83 [f]		12.17			

[a] (Wi 58): see also (Bo 51c).
[b] (See (Ri 50d, Bo 51c, Ri 51c, Ri 51e, Wi 58).
[c] (Fr 50b).
[d] (Be 56c).
[e] See (Ne 53a, Bo 57a, Hu 58).
[f] (Ha 56a).
[g] (Wi 58): (Me 54) report 60 and 1200 keV.
[h] See (Ri 50d, Bo 51c, Ri 51c, Ri 51e, Me 54, Bu 55c, Wi 58).

A careful search for resonances in the region $E_n = 20$ to 1360 keV with 10 and 22-keV resolution revealed no deviation > 5 per cent from a smooth monotonic decrease in σ_t (Mi 50c) (see, however, $B^{11}(He^3, p)C^{13}$). The course of the cross section in this region can be accounted for by the broad $s_{\frac{1}{2}}$ state at $C^{13*}(3.09)$ (Th 52b). A similar search, with 5-keV resolution, in the range

$E_n = 2.73$ to 2.80 MeV revealed no deviations > 0.2 b from a smooth function (Wi 58a: see C^{12}(d, p)C^{13}).

Below $E_n = 4.0$ MeV, three d-wave resonances occur, at 2.08, 2.95, and 3.67 MeV. The total cross section and angular distributions establish the first as $D_{\frac{3}{2}}$ (Wi 58); phase shift analyses of angular distributions yield $D_{\frac{3}{2}}$ for the other two. The s-wave phase shift is everywhere negative and decreases slowly with energy: the behaviour for $E_n = 0$ to 4 MeV can be accurately reproduced by a static potential well with a diffuse boundary (Wi 58). See also (Hu 54c). The $p_{\frac{1}{2}}$ and $p_{\frac{3}{2}}$ phase shifts are negative and small, not inconsistent with hard-sphere scattering (Me 54, Bu 55c, Wi 58). Polarization of scattered neutrons is discussed in these three papers and in (Mc 56b, Mc 57). Other angular distribution studies in this range are reported by (La 57c: $E_n = 0.06$ to 1.8 MeV), (Wi 55d: $E_n = 0.55$ to 1.5 MeV), (Mu 56a: $E_n = 1.66$ MeV), (Li 55a: $E_n = 2.7$ MeV), (Wa 55a: $E_n = 4.1$ MeV).

For $E_n = 4$ to 8 MeV, several additional resonances are reported by (Fr 50b, Be 56c, Bo 57a, Ha 56a): see table 13.5 and (Hu 58). The structure above $E_n = 7$ MeV is undoubtedly quite complex: see $Be^9(\alpha, n)C^{12}$ and $C^{12}(n, n')C^{12*}$. Further angular distribution measurements are reported by (Je 55: 4.4 MeV), (Hi 58: 5 MeV), (Br 58g: 5.6 MeV), (Be 56e: 7 MeV), Do 56d, Na 58: 14 MeV), (Co 58e: 14.5 MeV) and (Kh 57b: 14.8 MeV): see also (Hu 56). Optical model effects become apparent at the higher energies; see (Cu 56; theo.).

In the region beyond the resolved resonances, recent measurements of the total cross section have been made by (Br 58h; $E_n = 7$ to 14 MeV), (Co 58b; $E_n = 13.1$ to 15.6 MeV), (Ve 58; $E_n = 13.6$ to 14.75 MeV) and (Kh 57a; $E_n = 14.8$ MeV). For a review of the earlier work, see (Aj 55) and (Hu 57). Non-elastic cross section measurements are reported by (Be 56e; $E_n = 7$ MeV), (Ba 58g; $E_n = 7$ to 14 MeV), (Ta 55; $E_n = 12.7$ and 14.1 MeV), (St 57f, Gr 55b, Fl 56a; $E_n = 14$ MeV) and (Ma 58j; $E_n = 21$, 26 and 29 MeV): see also (Hu 47, Za 57, Ma 55n). See also (La 56d) and (Ka 56b; theo.).

XIX. (a) $C^{12}(n, n')C^{12*}$ $E_b = 4.946$

(b) $C^{12}(n, n')3He^4$ $Q_m = -7.281$

In the range $E_n = 4.4$ to 8 MeV, four resonances are observed in the yield of 4.4-MeV γ-rays, at $E_n = 6.30$, 6.49, 7.6, 7.87 and 8.15 MeV, corresponding to $C^{13*} = 10.76$, 10.94, 12.0, 12.21 and 12.47 MeV. The differential cross section at 90° reaches a maximum of 60 mb/sr at 7.87 MeV (Ha 56a, Hu 58). At $E_n = 6.58$ MeV, the cross section for production of 4.4-MeV γ-rays is 353 ± 59 mb (Da 56d); at 14 MeV, it is 245 ± 35 mb (Ba 55c). (Gr 55b) estimate 160 mb for the inelastic cross section at $E_n = 14$ MeV to C^{12} levels at 9.6 to $\approx$ 13 MeV and 100 to 300 mb as the cross section to the C^{12} states at

4.4 and 7.6 MeV. See $C^{13}(n, n)C^{13}$ above, for further references on non-elastic cross sections.

Reaction (b) has been studied for $E_n = 12.3$ to 20.1 MeV. The cross section is 190 ± 50 mb at 12.9 MeV. It goes through a broad maximum of $\approx 300\pm60$ mb at ≈ 16.5 MeV and then decreases to 240 ± 50 mb at $E_n=20.1$ MeV (Fr 55i). See also (Be 55b, Be 55f, Va 58d), (Sa 56a; theo.) and (Aj 55).

XX. $C^{12}(n, 2n)C^{11}$ $Q_m = -18.722$ $E_b = 4.946$

See (Br 52e, As 58).

XXI. $C^{12}(n, p)B^{12}$ $Q_m = -12.593$ $E_b = 4.946$

The cross section has been measured from threshold to $E_n=17.5$ MeV. At $E_n=17.5$ MeV, the cross section is 29.1 ± 4 mb (Kr 58). See also (Kr 56, Kr 56a).

XXII. $C^{12}(n, \alpha)Be^{9}$ $Q_m = -5.709$ $E_b = 4.946$

See (Gr 55b) and Be^{9}.

XXIII. $C^{12}(d, p)C^{13}$ $Q_m = 2.719$

$Q_0 = 2.721\pm0.002$ (Va 57).

Measurements on the proton groups are summarized in table 13.6. The level assignments were obtained by analysis of angular distributions (with

TABLE 13.6

Levels of C^{13} from $C^{12}(d, p)C^{13}$

C^{13a} (MeV)					l_n	J^π	$\sigma(\theta)$ [c] mb/sr	θ_n^2 [b] (%)
(St 51, Va 51a)	(Sp 54e)	(Do 56c)	(Kh 53, Kh 55a)[a]	(Mc 55c)				
0	0		0	0	1 [c]	$\frac{1}{2}^-$, $\frac{3}{2}^-$ [c]	26	7
3.086 ± 0.006	3.090 ± 0.010		3.107	3.09 [b]	0 [c]	$\frac{1}{2}^+$ [c]	103	25
3.686 ± 0.011	3.684 ± 0.010	[3.681 ± 0.003]	3.699	3.68 [b]	1 [c]	$\frac{1}{2}^-$, $\frac{3}{2}^-$ [c]	16	2
	3.855 ± 0.007	[3.851 ± 0.003]	3.869	3.84 [b]	2 [c]	$\frac{3}{2}^+$, $\frac{5}{2}^+$ [c]	152	10
				6.87 [b]	(0), (2) [d]	($\leqq \frac{5}{2}^+$) [d]	36	
				7.470 ± 0.02			$\approx$0.8	
				7.533 ± 0.02			9.6	
				7.641 ± 0.02 [f]			7.5	
				8.4 ±0.30 [g]			100	
				9.500 ± 0.02			1.6	
				9.897 ± 0.02			2.2	
				10.759 ± 0.02			4.5	

[a] ±10 to 50 keV.

[b] Energies given for identification only.

[c] (Ro 51j, Ro 51k, Bl 52, Ca 53f, Mc 55c, Ca 56b, Co 57g, Fr 54e, Gr 56b).

[d] (Mc 55c).

[e] (Mc 55c); differential cross sections at the first maximum or in the forward direction; ± 25 per cent.

[f] $\Gamma = 70\pm15$ keV.

[g] $\Gamma = 1.1\pm0.3$ MeV.

[h] (Mc 58d, Gr 56b, El 56a).

deuterons of energies up to 24 MeV) in terms of direct interaction theories. A careful search with $E_d = 5$ to 8.5 MeV ($\theta = 90°$) reveals no further proton groups corresponding to levels in the range 0 to 4.9 MeV with intensity greater than 0.5 per cent of the ground state group (Sp 54e). At $E_d = 14.8$ MeV, all groups show pronounced stripping distributions except that corresponding to C^{13*}(9.50), for which the distribution is roughly isotropic. The proton spectrum exhibits a conspicuous broad structure attributed to a C^{13} level at $E_x = 8.4$ MeV, $\Gamma = 1.1 \pm 0.3$ MeV. (It seems probable that this level is to be identified with the $D_{\frac{3}{2}}$ level of similar width observed in C^{12}(n, n)C^{12} at $E_x = 8.33$ MeV: see table 13.5.) Only one other level has a measurable width: $E_x = 7.64$ MeV, $\Gamma_{lab} = 70 \pm 15$ keV (compare table 13.5) (Mc 55c). It is of interest that the 7.47 and 7.53-MeV levels do not appear in C^{12}(n, n)C^{12} (Wi 58a).

Angular distributions at low energies have been studied by (Ta 54c; $E_d = 0.52$ to 0.84 MeV), by (Ju 56b, Ju 56g, Ju 57; $E_d = 0.60$ to 1.45 MeV), by (Al 55e, Al 55f; $E_d = 1.4$ to 2.0 MeV), by (Mc 56a, Be 56; $E_d = 1.86$ to 2.86 MeV for the p_0 group — on and off resonances — and $E_d = 2.74$ and 2.89 MeV for the p_1 group), by (Bo 56, Ho 54c; $E_d = 3.2$ to 4.4 MeV) and by (Ko 56f, Va 56c; $E_d = 0.26$ to 0.59 MeV). In the range $E_d = 1$ to 6 MeV, the (C^{12}+d) reactions are characterized by numerous strong, overlapping resonances (see N^{14}); the angular distributions show evidence of both stripping and compound nucleus formation, even below 1 MeV (Ju 56g, Ju 57, Ko 56f, Va 56c). From $E_d = 2$ to 6 MeV, angular distributions of the p_0 group (to C^{13} g.s.) generally show a stripping maximum near 25°, as expected for an $l = 1$ transfer; several of the "resonances" appear most conspicuously at this angle. The p_1-group, C^{13*}(3.09), shows even stronger stripping effects, with a pronounced forward maximum (Bo 56, Mc 56a, Mc 58d). A detailed comparison of distributions for C^{12}(d, p)C^{13} and C^{12}(d, n)N^{13} at $E_d = 2.68$ and 3.26 MeV indicates equality of the ground-state reduced widths (Be 56, Mc 58d). At $E_d = 9$ MeV, a similar comparison yields $\gamma^2(C^{13})/\gamma^2(N^{13}) = 0.86$ (Ca 56b). See also (Wi 55h).

Observed gamma rays are listed in table 13.7. No γ-rays are observed with $E_\gamma = 3.9$ to 5.8 MeV with intensity > 10 per cent of the 3.85 MeV γ-ray (Be 55a). An upper limit of 3 per cent is placed on the fraction of cascade transitions from the 3.67- and 3.84-MeV levels via the 3.1-MeV level. The internal conversion coefficient of the 170-keV radiation indicates E1, though M1 is not excluded (Ma 56f). The internal pair formation coefficient for the 3.09-MeV level indicates an E1 transition (Th 52); the angular correlation of internal pairs also indicates E1 (Go 55a, Go 56g, Ar 58a). Polarization of protons accompanying the formation of C^{13} (g.s.) and C^{13*}(3.1) has been studied by (Hi 56b, Ju 58, Bo 58d, He 58b, Hi 58a, Bo 58d, Ju 58b). The sense of polarization is correlated with the coupling of l_n and s_n: $P = \pm$ when

TABLE 13.7

Gamma radiation from $C^{13}(d, p)C^{13}$

E_γ [a] (MeV)	E_γ [b] (MeV)	Reference
3.86 ±0.02	(3.84 ±0.03) [c]	(Be 55a)
3.844 ±0.015		(Ma 56f)
0.1695±0.0004 [f]		(Ma 56f)
(3.76 ±0.02) [c]	3.74 ±0.03	(Be 55a)
(3.69 ±0.02) [c]	3.675±0.015 [d]	(Ma 56f)
(3.097 ±0.005) [e]	3.082±0.007	(Th 52)

[a] Uncorrected for Doppler shift.
[b] Corrected for Doppler shift.
[c] Doppler shift correction is not required for the 3.86-MeV radiation, but is required for the 3.67-MeV radiation (Ma 56f): see $B^{10}(\alpha, p)C^{13}$.
[d] Value obtained by subtraction: 3.844—0.170 (Ma 56f).
[e] Doppler shift required (Th 52).
[f] From the proton groups, ΔE = 170±3 keV (Sp 54e), and 170±1.5 keV (Do 56c).

$j = l \mp \frac{1}{2}$ (He 58b). See (Ch 54f, Sa 57a; theo.). See also (Ca 52a, Ca 54i, Ca 56j, Se 57d, Kh 55), (Da 57; theo.) and N^{14}.

XXIV. $C^{12}(t, d)C^{13}$ $Q_m = -1.313$

Not reported.

XXV. $C^{12}(\alpha, He^3)C^{13}$ $Q_m = -15.632$

Not reported.

XXVI. $C^{13}(\gamma, n)C^{12}$ $Q_m = -4.946$

The cross section for neutron production has been determined to 38 MeV. The (γ, n) cross section exhibits two peaks at 13.3±1 MeV (Γ = 5±1 MeV, σ = 3.3 mb) and at ≈ 22 MeV ($\sigma \approx 6$ mb, $\Gamma \approx 7$ MeV). The total absorption cross section, $\sigma(\gamma, xn)+\sigma(\gamma, p)$ shows maxima at E_γ = 13.5 and 25 MeV. The lower resonance is much too large to be explained on a single-particle model (Co 57b). See also (Co 56f, Se 49a, Go 53f).

XXVII. $C^{13}(\gamma, p)B^{12}$ $Q_m = -17.539$

The yield of β-particles from the B^{12} decay has been determined to 45 MeV. The cross section shows a broad maximum of 8.8 mb near 25.5 MeV (Co 57b, Co 56f).

XXVIII. $C^{13}(\gamma, \alpha)Be^9$ $Q_m = -10.654$

See (Mi 53c).

XXIX. $C^{13}(p, p')C^{13*}$

Angular distributions of the 3.09-MeV γ-rays are isotropic for E_p = 3.7 to 4.2 MeV, consistent with the assignment $J = \frac{1}{2}$ to C^{13*} (3.09). Angular

distributions of the 3.68-MeV radiation have also been studied near the $E_p = 4.5$-MeV resonance (Ba 57q). See also (Co 52g).

XXX. $N^{13}(\beta^+)C^{13}$ $Q_m = 2.222$

See N^{13}.

XXXI. $C^{14}(p, d)C^{13}$ $Q_m = -5.947$

Not reported.

XXXII. $C^{14}(d, t)C^{13}$ $Q_m = -1.915$

At $E_d = 14.8$ MeV, triton groups have been observed leading to the C^{13} states at 0, 3.09, 3.68 and 3.85 MeV (Mo 58e). See C^{14}.

XXXIII. $C^{14}(He^3, \alpha)C^{13}$ $Q_m = 12.404$

Not reported.

XXXIV. $N^{14}(n, d)C^{13}$ $Q_m = -5.319$

At 14 MeV, deuteron groups to the 0 and 3.68-MeV (but not to the 3.09 and 3.84-MeV) states of C^{13} have been observed (Ca 57e). See also (Li 52) and N^{14}.

XXXV. $N^{14}(p, 2p)C^{13}$ $Q_m = -7.546$

At $E_p = 185$ MeV, the summed proton spectrum shows two peaks, corresponding to ejection of $p_{\frac{1}{2}}$ and $p_{\frac{3}{2}}$ protons, with binding energies of ≈ 7 and ≈ 15 MeV, $C^{12*} = 0$ and ≈ 8 MeV (Ty 58b, Ma 58h).

XXXVI. $N^{14}(d, He^3)C^{13}$ $Q_m = -2.052$

Not reported.

XXXVII. $N^{14}(t, \alpha)C^{13}$ $Q_m = 12.267$

This reaction has been observed at $E_t = 1.9$ MeV (Ja 58).

XXXVIII. $N^{15}(n, t)C^{13}$ $Q_m = -9.903$

Not reported.

XXXIX. $N^{15}(p, He^3)C^{13}$ $Q_m = -10.668$

Not reported.

XL. $N^{15}(d, \alpha)C^{13}$ $Q_m = 7.683$

Observed alpha particle groups are displayed in table 13.8 (Ma 51, Wa 57). The broad level at 8.4 MeV observed in $C^{12}(d, p)C^{13}$ does not appear in the present reaction; it is suggested that the direct (d, α) transition is forbidden by the nature of the configurations involved (Wa 57). The angular distribution of the ground-state alpha particles at $E_d = 21$ MeV shows a maximum at 70° (c.m.) (Fi 58).

TABLE 13.8

C^{13} states from $N^{13}(d, \alpha)C^{13}$

(Ma 51) C^{13*} (MeV)	(Wa 57)	
	C^{13*} (MeV) [a]	$d\sigma/d\Omega$ ($\theta = 12.6°$, lab) mb/sr
0	0	0.85±0.09
3.083±0.005	3.09	0.18±0.03
3.677±0.005	3.68	2.4 ±0.3
	3.85	<0.3
	6.87	1.3 ±0.2 [c]
	7.47, 7.53, 7.64 [b]	1.1 ±0.2
	8.80±0.04	0.56±0.11
	9.5	0.15±0.04
	9.9	0.26±0.06

[a] Level energies for identification purposes only except for $C^{13*} = 8.80$ MeV.
[b] Not resolved.
[c] Measured at $\theta = 18°$.

XLI. $O^{16}(n, \alpha)C^{13}$ $Q_m = -2.203$

See (Hu 51f, Li 52) and O^{17}.

N^{13}

(Fig. 24, p. 151) †

THEORY

See (La 55b, Da 56g, Sk 58, Fr 58b, Ha 58d).

I. $N^{13}(\beta^+)C^{13}$ $Q_m = 2.222$

Recent determinations of the half-life give 10.05±0.03 min (Ch 53c),

TABLE 13.9

Energy levels of N^{13}

E_x in N^{13} (MeV)	J^π	$\tau_{\frac{1}{2}}$ or Γ (keV)	Decay	Reactions
0	$(\frac{1}{2})^-$	$\tau_{\frac{1}{2}}$ = 10.02±0.02 min	β^+	I, II, VII, IX, XV, XVI, XVIII, XIX, XX, XXI, XXII
2.365±0.003	$\frac{1}{2}^+$	32±2	p, γ	VII, IX, XII, XV, XXII
3.507±0.007	$\frac{3}{2}^-$	63±6	p, γ	VII, IX, XII, XV, XXII
3.555±0.01	$\frac{5}{2}^+$	61	p	XII, XV, XXII
6.379±0.01	$\frac{5}{2}^+$	11	p	XII
6.908±0.01	$\frac{3}{2}^+$	115	p	XII
7.415±0.01	$(\frac{1}{2}^+)$	≈ 85	p	XII
(8.08)	$(\frac{3}{2}^+)$	(350)	p	XII
22.7 ±0.3		≈ 1400	p	XII
23.2		400	p, He^3	IV
24.5		550	p, He^3	IV
24.8		90	p, He^3	IV
25.2		120	p, He^3	IV

† For level scheme of C^{13}, see fig. 22, p. 139.

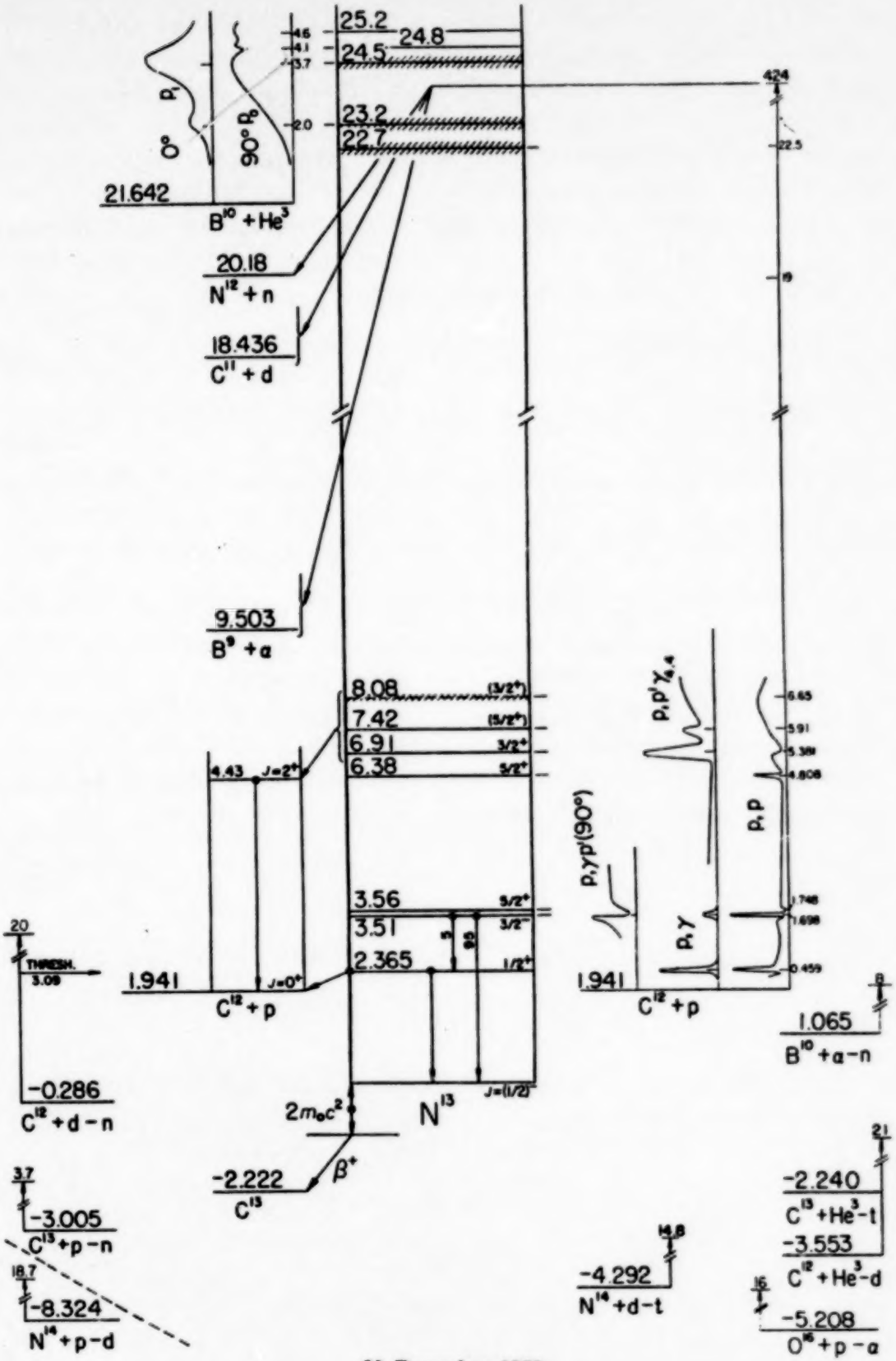

31 December 1958

Fig. 24. Energy levels of N^{13}: for notation, see fig. 1, p. 7.

10.08±0.04 min (Wi 55h), 10.07±0.06 min (No 57a), 9.96±0.03 min (Ar 58), 9.96±0.03 min (Da 58e); see also (De 57). $E_\beta(\max) = 1.202\pm0.005$ MeV (Ho 50), 1.185±0.025 MeV (Gr 54c), 1.190±0.003 MeV (Da 58e). The positon spectrum shows no deviation from the allowed shape; it is concluded that the Fierz coefficient in the Fermi interaction is $< 11\,\%$. Log $ft = 3.66$ (Da 58e, Da 57b). The positon polarization has been studied by (Ha 57g, Bo 57h). The results indicate that the positons are completely polarized and hence that Fermi transitions as well as G-T transitions exhibit the maximum effect of parity nonconservation.

II. $Be^9(Li^6, 2n)N^{13}$ $Q_m = 3.952$

See (No 57a).

III. $B^{10}(He^3, n)N^{12}$ $Q_m = 1.46$ $E_b = 21.642$

At $E(He^3) = 2.54$ MeV, the cross section for formation of the ground state is $5.2^{+2.1}_{-1.6}$ mb. At $E(He^3) = 3.60$ MeV, the differential cross section for formation of the ground state at $\theta = 0°$ is 0.73±0.30 mb/sr (Aj 57a).

IV. $B^{10}(He^3, p)C^{12}$ $Q_m = 19.702$ $E_b = 21.642$

The yields of the protons to the ground and 4.4-MeV excited states of C^{12} have been measured for $E(He^3) = 1.3$ to 5 MeV. Resonances are observed at 2.0, 3.7, 4.1 and 4.6 MeV, with widths of 0.5, 0.7, 0.12 and 0.15 MeV, respectively, corresponding to $N^{13*} = 23.2$, 24.5, 24.8 and 25.2 MeV. Angular distributions taken at six energies in the above range tend to be more asymmetric at the higher energies (Sc 56f). See also (Jo 56a).

V. $B^{10}(He^3, d)C^{11}$ $Q_m = 3.206$ $E_b = 21.642$

See C^{11}.

VI. $B^{10}(He^3, \alpha)B^9$ $Q_m = 12.139$ $E_b = 21.642$

See B^9.

VII. $B^{10}(\alpha, n)N^{13}$ $Q_m = 1.065$

Measurements at $E_\alpha = 8$ MeV with a proton recoil telescope and a neutron threshold detector are reported to indicate N^{13} states at 2.4±0.3, 3.6±0.3, (4.3±0.3) and 5.0±0.3 MeV (Qu 56). See also (Ba 57d) and N^{14}.

VIII. $B^{11}(He^3, n)N^{13}$ $Q_m = 10.179$

Not reported.

IX. (a) $C^{12}(p, \gamma)N^{13}$ $Q_m = 1.941$

(b) $C^{12}(p, \gamma p')C^{12}$

Two resonances for capture radiation are reported, at $E_p = 0.46$ and 1.70 MeV (table 13.10). The resonance at $E_p = 1.75$ MeV observed in

$C^{12}(p, p)C^{12}$ does not appear in the γ-excitation curve (Se 51e). The displacement of the lower level ($N^{13*} = 2.37$ MeV, $J = \frac{1}{2}^+$) from its mirror in C^{13}(3.09) is ascribed to the large reduced width (Th 52b, Eh 51). The angular distribution of the ground-state radiation from the upper resonance ($N^{13*} = 3.51$ MeV, $J = \frac{3}{2}^-$) has the form $W(\theta) = 1 - 0.52\cos^2\theta$ (Da 51, Da 51b).

TABLE 13.10

Resonances in $C^{12}(p, \gamma)N^{13}$

E_p (keV)	Γ_{lab} (keV)	σ_{res} (mb)	$\omega\Gamma_\gamma$ (eV)	N^{13*} (MeV)	Ref.
456.8±0.5	39.5±1.0			2.363	a
456 ±2	35				b
450	35	127	0.67		c
1697 ±12	74 ± 9			3.507	d
1698 ± 5	70 ±10	35	1.39		c

[a] (Hu 53d).
[b] (Fo 49b).
[c] (Se 51c, Se 51e).
[d] (Va 49).

The capture cross section at low energy is of interest in connection with stellar energy generation. Measurements have been reported in the range $E_p = 80$ to 360 keV by (Ba 50, Ha 50, La 57b, De 57). At 80 keV, $\sigma = (1.4 \pm 0.4) \times 10^{-5}$ μb; from 80 to 126 keV, the course of the cross section is reasonably well accounted for by extrapolation of the $E_p = 0.46$-MeV resonance (La 57b: see also De 57).

From $E_p = 5$ to 11 MeV, the cross section for formation of N^{13} changes only from 2.5 to 1.8 mb; this small change strongly indicates the predominance of direct capture in this region (Co 55c). According to (Re 56c), however, the 90-degree differential cross section for formation of N^{13} is < 1 μb/sr at $E_p = 4.8$ MeV. See also (Ch 56c).

In the range $E_p = 1.2$ to 2.5 MeV, reaction (b) is observed, involving a γ-transition to the 2.37-MeV state. Excitation functions at $\theta = 0°$ and 90° indicate interference between p-wave resonant capture at $E_p = 1.70$ MeV, with $\Gamma_\gamma = 0.04$ eV, and direct p-wave capture (Wo 54). The angular distributions at $E_p = 1.37$ and 1.58 MeV have the form $W(\theta) = (0.02 \pm 0.02) + \sin^2\theta$(He 55).

X. $C^{12}(p, n)N^{12}$ $\quad Q_m = -18.24$ $\quad E_b = 1.941$

See (Ta 58a, St 57e), and N^{12}.

XI. $C^{12}(p, pn)C^{11}$ $\quad Q_m = -18.722$ $\quad E_b = 1.941$

See (Ch 47c, Mc 48, Wh 58a).

XII. $C^{12}(p, p)C^{12}$ $E_b = 1.941$
$C^{12}(p, p')C^{12*}$

Elastic scattering studies indicate a number of pronounced resonances in the range $E_p = 0$ to 6 MeV: see table 13.11. The first five excited states

TABLE 13.11

N^{13} levels from $C^{12}(p, p)C^{12}$ and $C^{12}(p, p')C^{12*}$

E_{res} (MeV ± keV)	N^{13*} (MeV)	$\Gamma_{c.m.}$ (keV)	l_p	J^π	θ_p^2
0.461 [a] ± 3	2.367	31	0	$\frac{1}{2}^+$	0.54
1.698 [b]	3.508	55	1	$\frac{3}{2}^-$	0.031
1.748 [b]	3.555	61	2	$\frac{5}{2}^+$	0.21
4.808 [c]	6.379	11	2	$\frac{5}{2}^+$	0.0031
(5.05) [e]		(75)	(0)	$(\frac{1}{2}^+)$	(0.014)
5.381 [d] ± 7	6.908	115	2	$\frac{5}{2}^+$	0.012
5.930 [f] ± 7	7.415	≈ 85	2	$\frac{5}{2}^+$	
(6.65) [g]	(8.08)	(350)	(2)	$(\frac{5}{2}^+)$	(0.11)

[a] (Ja 53b). (Mi 54) finds $E_r = 0.462$ MeV, $\Gamma = 32$ keV.
[b] (Ja 53b).
[c] (Re 56c).
[d] (Re 56c): parameters estimated from elastic scattering; $\theta_{p'}^2 = 0.2$. E_{res} from $C^{12}(p, p')C^{12*}$ (Li 57). See also (Sc 56d).
[e] (Sc 56d): $E_p = 4.8$ MeV, $J = \frac{5}{2}^+$ level not observed.
[f] $C^{12}(p, p')C^{12*}$ (Li 57). (Br 56d) finds $E_{res} = 5.891$ MeV, $\Gamma_{lab} = 59$ keV. See also (Sc 56d).
[g] (Sc 56d). See, however, (Br 56d).

correspond in character and approximately in reduced width to those of C^{13}: see $C^{12}(d, p)C^{13}$ and $C^{12}(n, n)C^{12}$. The relatively large reduced widths of the first and third ($s_{\frac{1}{2}}$ and $d_{\frac{5}{2}}$) excited states indicate a single-particle character (Ja 53b). The small and roughly equal widths of $N^{13*}(6.4)$ and (6.9) suggest that they may comprise a doublet, built upon $C^{12*}(4.4)+p$ (Re 56c. see also Ma 53h, Bl 53a, Sc 56d). Angular distribution measurements above $E_p = 10$ MeV generally show direct interaction effects: see C^{12}. Some form of resonance structure may exist near 23 MeV (Ki 55b). See also (Kl 56).

The yields of 4.4-MeV gamma rays and inelastic protons from $C^{12*}(4.4)$ show resonances at $E_p = 5.39$ and 5.93 MeV (Ma 53h, Br 56d, Li 57). Angular distributions of inelastic protons at $E_p = 6.1$ to 6.9 MeV do not fit direct interaction theory and suggest the effects of still higher compound nucleus levels (Br 56d).

Polarization studies for $E_p < 6$ MeV are reported by (Ga 56a, So 56b, Wa 58a): see also C^{12}. See also (Ni 56b, Er 56a, Gl 57, To 55c; theo.) and (Go 57f).

XIII. $C^{12}(p, d)C^{11}$ $Q_m = -16.495$ $E_b = 1.941$
See C^{11}.

XIV. $C^{12}(p, \alpha)B^9$ $Q_m = -7.563$ $E_b = 1.941$

See B^9.

XV. $C^{12}(d, n)N^{13}$ $Q_m = -0.286$

Neutron groups have been observed corresponding to excited states of N^{13} at 2.29 ± 0.12 (Gr 49a), 2.38 ± 0.05 MeV (Mi 53) and 3.48 ± 0.12 (Gr 49a), 3.74 ± 0.05 (Gr 57b), 3.53 ± 0.05 MeV (Mi 53). The angular distributions of the ground state group and the groups corresponding to the 2.37 and (3.51+3.56) MeV states at $E_d = 9.0$ MeV are consistent with $l_p = 1, 0$ and 2. The dimensionless reduced widths of the ground and (3.56) MeV states are respectively 0.056 and 0.19 (Ca 57a; see also Mi 53). (Mc 58d) finds that the reduced widths of the ground states of C^{13} and N^{13} are the same, 0.09 ± 0.035 (see also Ca 56b, Be 56, Ka 58d and $C^{12}(d, p)C^{13}$). In the range $E_d = 2.8$ to 3.7 MeV, a single neutron threshold is observed, at $E_d = 3.09 \pm 0.02$ MeV, corresponding to $N^{13*} = 2.36 \pm 0.02$ MeV; the slow rise above threshold is attributed to p-wave neutron emission (Ma 55j).

Polarization of neutrons has been studied for $E_d = 2.5$ to 3.6 MeV by (Ha 57c). See also (De 56d, Bo 56l, Bo 56m).

XVI. $C^{12}(He^3, d)N^{13}$ $Q_m = -3.553$

See (Fr 52e, We 58c).

XVII. $C^{12}(\alpha, t)N^{13}$ $Q_m = -17.872$

Not reported.

XVIII. $C^{13}(p, n)N^{13}$ $Q_m = -3.005$

$E_{thresh} = 3.2372 \pm 0.0016$ (Bo 58e)

See also (Ri 50e, Ma 55k, Bi 58a) and N^{14}.

XIX. $C^{13}(He^3, t)N^{13}$ $Q_m = -2.240$

See (Fr 52e).

XX. $N^{14}(\gamma, n)N^{13}$ $Q_m = -10.551$

See N^{14}.

XXI. $N^{14}(p, d)N^{13}$ $Q_m = -8.324$

See N^{14}.

XXII. $N^{14}(d, t)N^{13}$ $Q_m = -4.292$

At $E_d = 14.8$ MeV, triton groups are observed corresponding to the states at 0, 2.37 and (3.51+3.56) MeV. The cross section for the transition to the 2.37-MeV state is two orders of magnitude smaller than that for the ground state transition. Transitions to $N^{13*}(2.37)$ and (3.56) are shell-model forbidden (Wa 57).

XXIII. $N^{14}(He^3, \alpha)N^{13}$ $Q_m = 10.027$
Not reported.

XXIV. $N^{15}(p, t)N^{13}$ $Q_m = -12.908$
Not reported.

XXV. $O^{16}(p, \alpha)N^{13}$ $Q_m = -5.208$
See (Wh 58a).

C^{14}

(Fig. 25, p. 157) †

THEORY

See (El 56b, Ca 57d, Go 57a, Go 56a, Su 58, Sh 57b, Vi 57, Sh 55d, Ja 54a, St 56, Ba 58e).

I. $C^{14}(\beta^-)N^{14}$ $Q_m = 0.155$

The mean of reported end points is 156±1 keV (Li 57d). The weighted mean half-life is 5568±30 years (Li 55c: see St 58b): log ft = 9.03. The spectrum does not deviate from the allowed shape down to 3 keV (Mo 54e); see also (Po 55), (Fo 54c).

TABLE 14.1
Energy levels of C^{14}

E_x in C^{14} (MeV)	J^π; T	τ or Γ	Decay	Reactions
0	0^+; 1	$\tau_{\frac{1}{2}}$ = 5568±30 y	β^-	I, III, IV, V, VI, IX, XII, XIII, XV, XVI, XVIII
6.091±0.015	1^-	$\tau_m < 3\times10^{-13}$ sec	γ	III, V, IX
6.589±0.02	$(1^-, 2^\pm, 3^-)$	sharp		III, IX
6.723±0.015	$(3^-, 2^-)$	$\tau_m > 3\times10^{-13}$ sec	γ	III, IX
6.894±0.015	$0^{(-)}$	$\tau_m < 3\times10^{-13}$ sec	γ	III, IX
7.346±0.02	$(2^-, 3^-)$	sharp	γ	III, IX
8.321±0.02		sharp		III, IX
9.800±0.02		Γ = 24 keV	n	VII, IX
10.433±0.02		Γ = 14 keV	n	VII, IX
10.505±0.02		Γ = 14 keV	n	VII, IX
11.9 ±0.30		Γ = 950 keV		IX
12.601±0.02		Γ = 110 keV		IX
12.854±0.02		sharp		IX
12.958±0.02		sharp		IX

It appears that the long lifetime of C^{14} may be due to chance cancellation in the matrix element for the decay, brought about by a small tensor force (Vi 57, Sh 55d, Ja 54a, St 56); see, however, (Ba 58e). See also (St 57b, Sm 55).

II. (a) $Li^7(Li^7, p)B^{13}$ $Q_m = 5.97$ $E_b = 26.797$
(b) $Li^7(Li^7, d)B^{12}$ $Q_m = 3.311$
(c) $Li^7(Li^7, Be^8)He^6$ $Q_m = 7.247$

† The level scheme of O^{14} is not illustrated (see p. 176)

These reactions have been studied for $E(Li^7) \approx 1.3$ to 2.0 MeV: see (No 57, No 57a).

III. $Be^9(Li^6, p)C^{14}$ $Q_m = 15.130$

At $E(Li^6) = 2$ MeV, the ground state proton group, and proton groups corresponding to the known levels between $E_x = 6.1$ and 8.5 MeV have been observed (Li 58c).

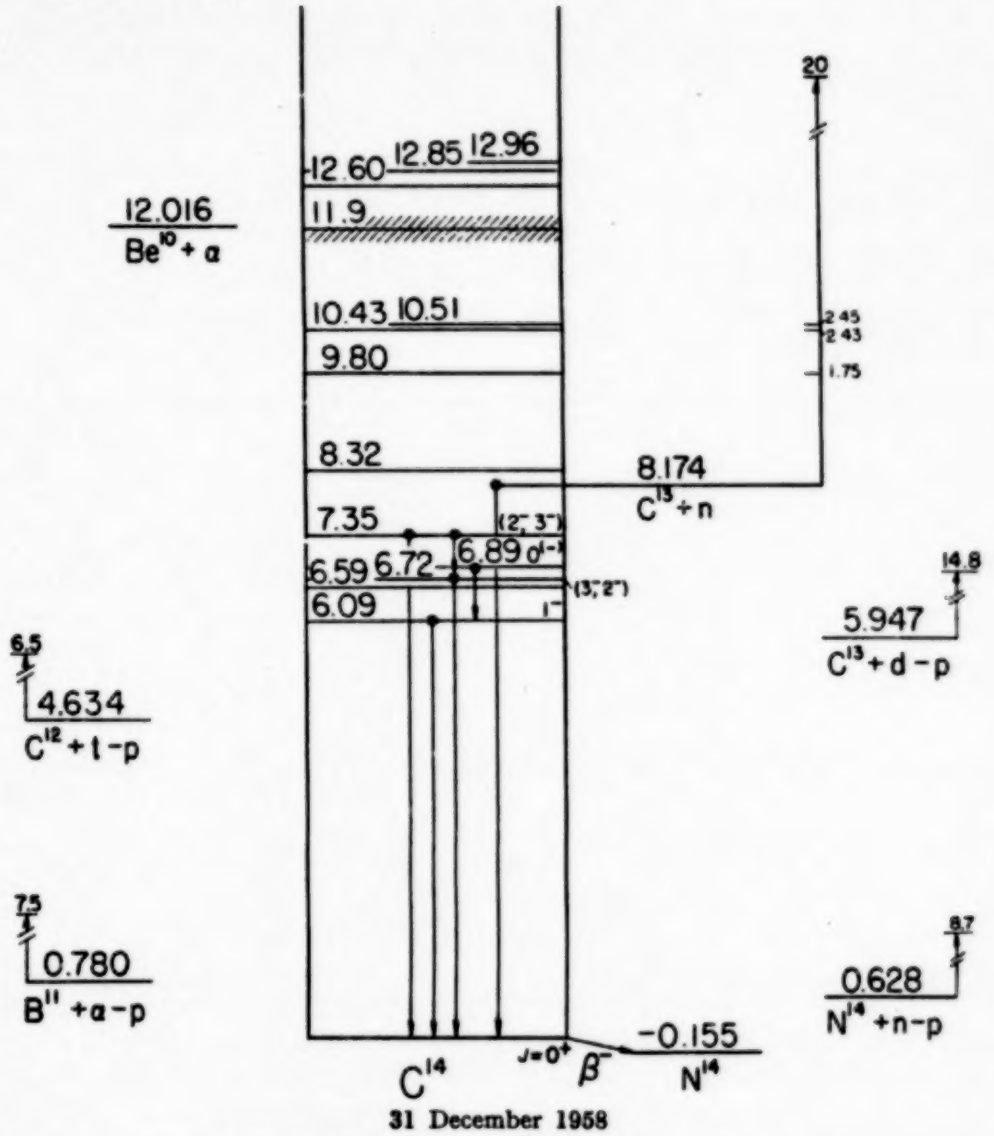

31 December 1958

Fig. 25. Energy levels of C^{14}: for notation, see fig. 1, p. 7.

IV. $B^{11}(\alpha, p)C^{14}$ $Q_m = 0.780$

$Q_0 = 0.788 \pm 0.017$ (W. J. Fader, quoted in Va 57).

See (Fr 51c), (Ma 53f) and N^{15}.

V. $C^{12}(t, p)C^{14}$ $Q_m = 4.634$

See (Po 51, Cu 55b, Ma 56k, Ba 56f, Ja 56e).

VI. $C^{13}(n, \gamma)C^{14}$ $Q_m = 8.174$

The thermal capture cross section is 0.5 ± 0.2 mb, 0.9 ± 0.3 mb (Hu 55c).

VII. $C^{13}(n, n)C^{13}$ $E_b = 8.174$

The thermal scattering cross section is 4.7 ± 0.09 b (Hu 55c: free atoms); see also (Ko 52). In the range $E_n = 0.2$ to 3 MeV, resonances are observed at $E_n = 1.75$ MeV ($\Gamma = 25$ keV), 2.43 and 2.45 MeV. The latter levels, whose widths are of the order of 15 keV, interfere strongly. The non-resonant cross section decreases smoothly from about 3 b at 0.2 MeV to 1 b at 3 MeV (Wi 58a).

VIII. $C^{13}(n, \alpha)Be^{10}$ $Q_m = -3.843$ $E_b = 8.174$

See (Sa 54a) and (Hu 47).

IX. $C^{13}(d, p)C^{14}$ $Q_m = 5.947$

The weighted mean of seven Q-values is 5.943 ± 0.003 MeV (Va 57; see also Sp 54e, Ah 54d).

Proton groups reported by (Sp 54e) and (Mc 55c) are displayed in table

TABLE 14.2

Proton groups from $C^{13}(d, p)C^{14}$

(Sp 54e)	(Mc 55c)				(Wa 58)	
E_x (MeV)	E_x (MeV)	$d\sigma/d\Omega$ [b] (mb/sr)	l_n [c]	J^π	J^π	θ_n^2 [b]
0	0	10	1	$0^+, 1^+, 2^+$	0^+	0.10 ($J = 0^+$)
6.091 ± 0.010	6.09	62	0 [g]	$0^-, 1^-$	1^-	0.40 ($J = 1^-$)
	6.589 ± 0.02	1.6	1, 2, 3 [d]	$(1^-, 2^\pm, 3^-)$		$\lesssim 0.01$
6.723 ± 0.010 [a]	6.72	74	2	$1^-, 2^-, 3^-$	$3^-, (2^-)$	0.11 ($J = 3^-$)
6.894 ± 0.010 [a]	6.89	22	0, 1 [d]	$0^\pm, 1^\pm, 2^+$	0^- [d]	0.39 ($J = 0^-$)
	7.346 ± 0.02	56	2	$1^-, 2^-, 3^-$	$2^-, 3^-$	0.11 ($J = 2^-$)
	8.321 ± 0.02	2.2				
	9.800 ± 0.02	7.1				
	10.433 ± 0.02	≈ 1.9				
	10.505 ± 0.02	≈ 1.4				
	11.9 ± 0.30 [e]	90				
	12.601 ± 0.02 [f]	6.3				
	12.854 ± 0.02	1.0				
	12.958 ± 0.02	1.9				

[a] The spacing of these two levels is 171 ± 3 keV (Sp 54e).

[b] Differential cross section at the first maximum or in the forward direction, $\pm$ 25 per cent (Mc 55c: $E_d = 14.8$ MeV).

[c] See also (Br 52, Be 53d, El 56a).

[d] See footnotes 18 and 31 in (Wa 58).

[e] $\Gamma_{lab} = 1.10 \pm 0.30$ MeV.

[f] $\Gamma_{lab} = 0.130 \pm 0.020$ MeV.

[g] With $J = 1^-$, $\theta^2 = 0.32$ (El 56a).

[h] E. Baranger, private communication: see (Wa 59a).

14.2. No other groups have been observed for $E_x = 0$ to 8.1 MeV with an intensity greater than 0.2 of the group corresponding to the 6.1-MeV state (Sp 54e: $\theta = 90°$). See also (El 56a, Ko 53a, Va 56c, Ko 56f).

Observed γ-radiation assigned to C^{14} is exhibited in table 14.3. The inter-

TABLE 14.3

Gamma rays from $C^{13}(d, p)C^{14}$

(Ma 55a)	(Be 55a)		(Ra 58b)		(Wa 58)
E_γ (MeV)	E_γ (MeV)	Total σ [d] (mb)	E_γ (MeV)	Total σ [e] (mb)	E_γ (MeV)
6.090 ± 0.025 [a]	6.11 ± 0.030 [a,b]	52	6.090 ± 0.020 [a]	131	6.09
6.730 ± 0.040 [f]	6.720 ± 0.030 [f,b]	26	6.738 ± 0.025 [f]	68	6.72
	(7.30 ± 0.05) [b]		7.323 ± 0.025 [a]	12	7.35
0.811 ± 0.003 [c]					0.813 ± 0.008 [c]
(6.89 →6.09)					(6.89 →6.09)
					0.621 ± 0.007
					(7.35 →6.72)

[a] Corrected for Doppler shift: see (Wa 58).
[b] Average of values at $E_d = 2.0$ and 4.0 MeV.
[c] A Doppler shift of 0.5—1.0 % applies (Wa 58).
[d] Average value, $E_d = 3.4$ to 4.0 MeV.
[e] $E_d = 4.5$ MeV.
[f] No Doppler shift: $\tau > 3 \times 10^{-13}$ sec (Wa 58). See also (Be 55a).

nally-formed positon distribution suggests that the 6.1-MeV line is E1 and hence that the level has $J = 1^-$ and is the analog to the 8.06-MeV level of N^{14} (Th 52, Ch 58b, Go 58h). The 0.81-MeV cascade transition from the 6.89-MeV state shows a Doppler shift ($\tau_m < 3 \times 10^{-13}$ sec) and hence is predominantly dipole. The angular correlation of 6.1 and 0.8-MeV γ-rays is consistent with $J = 0$ and excludes $J = 1$ or 2. $J = 0$ is also suggested by the absence of the direct ground state transition for the 6.89-MeV level (Wa 58). The 6.89-MeV level is probably the analog of the $J = 0^-$ level of N^{14} at 8.71 MeV. Assuming that the 6.1-MeV radiation is E1, the relative intensities of external and internal pairs for the 6.1 and 6.7-MeV γ-rays are consistent with E2, E1, M1 or E3 for the 6.7-MeV transition (Be 55h). The mean lifetime of the 6.72-MeV state is greater than 3×10^{-13} sec, suggesting E3 or M2 (Wa 58). The 0.61-MeV γ-ray is in coincidence with the 6.7-MeV γ-ray and has an intensity roughly equal to that of the 7.35-MeV γ-ray (within a factor of 5). The strength of the cascade then suggests $J = 2^-$ or 3^- for the 7.35-MeV state (Wa 58): see also (Au 55; theo.). Comparison of reduced widths and calculation of level shifts suggests the following associations of C^{14} and N^{14} levels: 6.09—8.06, 6.72—8.91, 6.89—8.71 and 7.35—9.50 (Wa 59a).

X. $C^{13}(t, d)C^{14}$ $Q_m = 1.915$

Not observed.

XI. $C^{13}(\alpha, He^3)C^{14}$ $Q_m = -12.404$

Not observed.

XII. $C^{14}(d, t)C^{13}$ $Q_m = -1.915$

Reduced widths derived from pick-up angular distributions at $E_d = 14.8$ MeV are listed in table 14.4 (Mo 58e). The observation of strong contributions

TABLE 14.4

C^{14} ground-state widths from $C^{14}(d, t)C^{13}$ (Mo 58e)

C^{13} [a] (MeV)	l_n	J^π [a]	θ^2 [b]
0	1	$\frac{1}{2}^-$	1
3.08	0	$\frac{1}{2}^+$	0.03
3.68	1	$\frac{3}{2}^-$	0.5
3.86	2	$\frac{5}{2}^+$	0.19

[a] See C^{13}.

[b] Relative to ground state value.

from C^{13} excited states indicates considerable configuration mixing in the ground state of C^{14}. An admixture of $2s^2$ and $2d^2$ consistent with these results also permits a satisfactory account of the cancellation in the C^{14}—N^{14} beta decay matrix element without recourse to tensor forces (Ba 58e). See also $C^{14}(\beta^-)N^{14}$.

XIII. $N^{14}(n, p)C^{14}$ $Q_m = 0.628$

The weighted mean of five Q-value determinations is 0.626 ± 0.001 MeV (Va 57). See also (St 51b, Li 52, Do 58a) and N^{15}.

XIV. $N^{14}(t, He^3)C^{14}$ $Q_m \triangleq -0.137$

Not observed.

XV. $N^{15}(\gamma, p)C^{14}$ $Q_m = -10.214$

See N^{15}.

XVI. $N^{15}(n, d)C^{14}$ $Q_m = -7.987$

See (Fr 56b).

XVII. (a) $N^{15}(d, He^3)C^{14}$ $Q_m = -4.720$

(b) $N^{15}(t, \alpha)C^{14}$ $Q_m = 9.581$

(c) $O^{16}(n, He^3)C^{14}$ $Q_m = -14.607$

Not observed.

XVIII. $O^{17}(n, \alpha)C^{14}$ $Q_m = 1.825$

See O^{18}.

N^{14}

(Fig. 26, p. 163)

THEORY

See (Ad 55, Ot 55a, El 56b, Fr 56b, Ba 57, Gr 57d, Vi 57, Fa 58, Ma 58c, Mo 58, Sk 58, Wa 59).

I. $Be^{9}(Li^{6}, n)N^{14}$ $Q_m = 14.503$

See (No 57a).

II. $B^{10}(\alpha, n)N^{13}$ $Q_m = 1.065$ $E_b = 11.615$

Resonances are reported at $E_\alpha = 1.51$, 1.64, 2.16, 2.26, 2.95, 4.53, 4.85 and 5.36 MeV: see table 14.6 (Sh 53b, Sh 55c, Bo 56d, Ma 58g, Gi 59). Angular distributions have been measured at $E_\alpha = 1.51$ and 2.16 MeV (Sh 55c).

III. $B^{10}(\alpha, p)C^{13}$ $Q_m = 4.070$ $E_b = 11.615$

Observed resonances in the yields of γ-rays (from C^{13*}) and of various proton groups are given in table 14.6. Studies of the angular distributions of protons (Sh 53b), γ-ray angular distributions, and (p—γ) correlations (St 54c) lead to the J^π assignments given in the table. Angular distributions of the protons at the $E_\alpha = 1.51$ and 2.16 MeV resonances are identical with those of the neutrons at the same resonances. However, the reduced neutron width at $E_\alpha = 1.51$ MeV is 5.7 ± 0.5 times the proton width, while at $E_\alpha = 2.16$ MeV the ratio is near unity. It is suggested that strong isobaric

TABLE 14.5

Energy levels of N^{14}

E_x in N^{14} (MeV $\pm$ keV)	J^π; T	τ_m or Γ (keV)	Decay	Reactions
0	1^+; 0	—	Stable	I, VI, XIII, XV, XVIII, XXI, XXII, XXIV, XXV, XXVI, XXVII, XXVIII, XXIX, XXX, XXXI, XXXVI
2.312 $\pm$ 1.2	0^+; 1	$< 2 \times 10^{-13}$ sec	γ	VI, XIII, XV, XVIII, XXII, XXV, XXVIII, XXIX, XXX, XXXI, XXXVI
3.945 $\pm$ 5	1^+; 0		γ	VI, XIII, XV, XVIII, XXVIII, XXIX, XXXVI
4.910 $\pm$ 9	(0^-); 0		γ	VI, XIII, XV, XVIII, XXVIII
5.104 $\pm$ 10	2; 0	$> 3 \times 10^{-13}$ sec	γ	XIII, XV, XXVIII, XXIX, XXXVI
5.685 $\pm$ 7	1; 0		γ	XV, XVIII, XXVIII
5.832 $\pm$ 12	$3(^-)$	$0.5 < \tau < 6.5 \times 10^{-13}$ sec	γ	XV, XVIII, XXVIII, XXIX

TABLE 14.5 (continued)

E_x in N^{14} (MeV±keV)	J^π; T	τ_m or Γ (keV)	Decay	Reactions
(5.98)				XVIII, XXVIII
6.23 ±20	1(−); 0		γ	XV, XVIII, XXVIII
6.44 ±30	(3); 0		γ	XV, XVIII, XXVIII, XXIX
(6.60 ±40)				XXVIII
7.03 ±30	(2); 0		γ	XVIII, XXVIII, XXIX
7.40 ±50			(γ)	XVIII, XXVIII
7.60 ±20				XVIII, XXVIII
7.962±10	; (0)		p, γ	XV, XXIX
8.060±6	1−; 1	30 ± 1	p, γ	XV, XVI, XVIII, XXIV
(8.45)	; (0)			XXIX
8.62	0+; 1	5.5± 2	p, γ	XV, XVI
8.71	0−; 1	460	p, γ	XV, XVI
8.903± 6	3−; (1)	15 ± 2	p, γ	XV, XVI
8.99	(1+)	7	p, γ	XV, XVI
9.17 ±10	2+, 1+; 1	0.075	p, γ	XV, XXIV
9.40 ±20	1−	≈20	p	XVI
9.504± 6	2−; 1	41 ± 2	p, γ	XV, XVI
9.71 ±20	1+	14 ± 3	p, γ	XVI, XXIV
(10.05 ±70)	; (0)			XXIX
10.24 ±40		75 ±30	p	XVI
10.43 ±10	2; 1	28 ± 3	p, γ	XV, XVI
(10.57)			d, p	VIII
11.07	1+; 0	120	d, p, n	VIII, XVI, XVII
11.23	; 1	25	d, p, n	VIII, XVII
11.26	2−; 0	200	d, p, (n)	VIII
11.38	3+; 0	55	d, p, n	VIII, XVI, XVII
11.50	3+	13	d, p	VIII
11.66		17	d, p	VIII
11.73		130	p, n	XVI, XVII
11.95			p, n	XVII
12.05			p, n	XVII
12.20			p, n,	XVII
12.29			p, α	III
12.41 ±10	4−	41 ± 3	p, α, d	III, VIII, IX
12.51 ±10		36 ± 5	p, α, d	III, VIII
12.61 ±10	3+	48 ± 3	p, α, d	III, VIII, IX
12.69 ±10	3−	16 ± 4	n, p, α, d	II, III, IV, VIII, IX
12.80 ±10	4+	15 ± 4	n, p, α, d	II, III, IV, VIII, IX
12.82 ±10	4−	7 ± 3	p, α, d, n	III, IV, VIII, IX
12.93 ±10	4+	22 ± 4	p, α, d	III, IV, VIII, IX
13.16 ±10	0−, 1−	35 ±15	n, p, α, d	II, III, VIII; IX
13.23		140	n, p, α	II, III, XVII
13.71	3	135	n, p, α, d	II, III, VIII
14.22		290	p, α, d	III, VIII
14.43		≈140	p, α, d	III, VIII
14.84		≈140	n, p, α, d	II, III, VIII
15.09		≈35	n, p, α, d	II, III, VIII
15.44		≈70	n, p, α	II, III

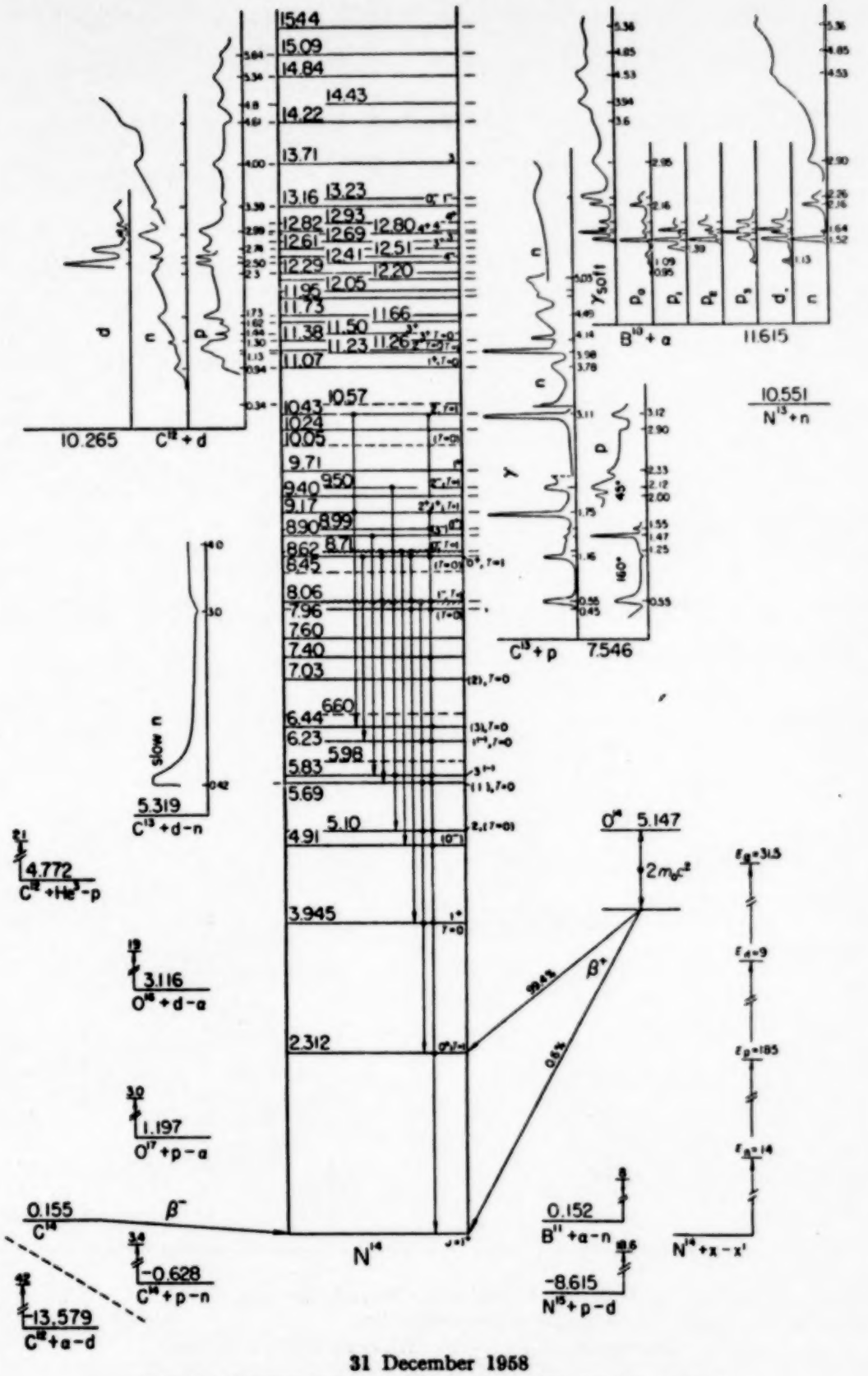

31 December 1958

Fig. 28. Energy levels of N^{14}: for notation, see fig. 1, p. 7.

spin mixing must occur for the $E_\alpha = 1.51$-MeV state: $N^{14*}(12.70)$ (Sh 55c: see also Ba 57d, Mc 58d).

TABLE 14.6

Resonances in $B^{10}+\alpha$

E_α (MeV)	$\Gamma_{c.m.}$ (keV)	Outgoing[a] particle (x)	σ_x (mb)	Γ_x (keV)	θ_x^2	N^{14*} (MeV)	J^{π}[b]	References
0.95		p_0				12.29		Ma 53f
1.09		p_0						Ma 53f
1.13 ±0.01	43±4	p_0, p_2, d				12.42	4^-	Sh 53b, St 54c
1.20		p_0						Ma 53f
1.24 ±0.01	36±5	p_0				12.50		Sh 53b
1.39 ±0.01	50±5	p_1, p_2				12.61		Sh 53b
1.518±0.004	14±4	α		1.7	6.0	12.70	3^-	Sh 53b, St 54c Ta 53, Br 57
		p_0	4.7	0.62	0.012			
		p_1	1.3	0.17	0.29			
		p_2	5.3	0.70	0.31			
		p_3	42	5.6	0.47			
		d	7.0	0.93	0.26			
		n	32	4.3	0.19			
1.64 ±0.01	14±4	α		1.0	8.2	12.79	4^+	Sh 53b, St 54c Ta 53
		p_0	0.98	0.18	0.012			
		p_1	0.46	0.085	2.7			
		p_2	2.4	0.44	3.0			
		p_3	52	9.6	4.9			
		d	11	2.0	3.9			
		n	3.2	0.59	0.16			
1.68 ±0.01	5±2	p_1, p_2, p_3, d				12.82	4^-	St 54c, Ta 53, Sh 53b
1.83 ±0.01	21±4	p_0, p_1, p_2, p_3, d				12.92	4^+	Ta 53, Sh 53b, St 54c
2.16	20	p_0, γ, n				13.16		Ta 53, Sh 55c
2.26	140	p_0, γ, n				13.23		Ta 53, Sh 55c
2.95	≈100	p_0, γ, n				13.72		Ta 53, Bo 56d, Ma 58g, Gi 59
3.6	290	γ				14.2		Bo 56d, Gi 59
3.94	≈140	γ				14.43		Bo 56d
4.53	140	n, γ				14.85		Bo 56d, Ma 58g, Gi 59
4.85	≈ 35	n, γ				15.08		Bo 56d, Ma 58g, Gi 59
5.36	≈70	n, γ				15.44		Bo 56d

[a] p_0, p_1, p_2, p_3 correspond respectively to the ground state and the 3.1, 3.7 and 3.9-MeV states of C^{13}; γ-rays are presumably also from C^{13*}.

[b] From angular distributions and (p—γ) correlations (Sh 53b, St 54c).

IV. $B^{10}(\alpha, d)C^{12}$ $Q_m = 1.351$ $E_b = 11.615$

Observed resonances are exhibited in table 14.6 (Sh 53b).

V. $B^{10}(\alpha, \alpha)B^{10}$ $E_b = 11.615$

See B^{10}.

VI. $B^{11}(\alpha, n)N^{14}$ $Q_m = 0.152$

Evidence is reported for levels of N^{14} at 0, 2.0, 3.15, 3.85 and 4.8 MeV (± 0.3 MeV) (Qu 56). See also (Pe 44, Br 55 and Aj 55).

VII. $C^{12}(d, \gamma)N^{14}$ $Q_m = 10.265$

At $E_d = 1.50$ MeV, the cross section is less than 1 μb (Al 55c).

VIII. (a) $C^{12}(d, n)N^{13}$ $Q_m = -0.286$ $E_b = 10.265$

(b) $C^{12}(d, p)C^{13}$ $Q_m = 2.719$

Resonances in the yields of protons and neutrons are displayed in table

TABLE 14.7

Resonances in $C^{13}+d$ [e]

E_d (MeV)	$\Gamma_{c.m.}$ (keV)	Particle out [a]	N^{14*} (MeV)	J^π; T	References
0.335		p	10.57		Va 56c, Ko 56f
0.94	140	p_0, n	11.07	1^+; 0	Sa 57, Ph 50b, Ba 48
1.13	33	p_0	11.23	; 1	Sa 57, Ph 50b, Ba 48
1.16	200	p_0, n	11.26	2^-; 0	Sa 57, Ph 50b, Ba 48
1.30	55	p_0, n	11.38	3^+; 0	Sa 57, Ph 50b, Ba 48
1.435	13	p_0, p_1	11.50	3^+	Sa 57, Ph 50b, Ba 48
1.62	17	p	11.66		Ph 50b
1.73	170	p, n	11.76		Ph 50b, Ba 48
2.3		p, n			Ba 48
2.502 $\pm$ 0.007 [d]	40 $\pm$ 3	p_0, p_1, d, n	12.41	4^- [b]	Mc 56a, Bo 56, Ba 48 Mc 58d
2.62 $\pm$0.012	22 $\pm$ 15	p_0, p_1, n	12.51		Mc 58d, Bo56, Ba 48, Mc 56a
2.735 $\pm$ 0.006	47 $\pm$ 3	p_0, p_1, d	12.61	3^+ [b]	Mc 56a, Bo 56
2.81 $\pm$0.010	22 $\pm$ 7	d	12.67		Mc 56a
2.954 $\pm$ 0.007	17 $\pm$ 8	d	12.80		Mc 56a
2.986 $\pm$ 0.006	11 $\pm$ 3	p, n, d	12.82		Mc 56a, Bo 56
3.123 $\pm$ 0.0065	28 $\pm$ 10	p, d	12.94		Mc 56a
3.39 $\pm$0.012	47 $\pm$ 15	d, p, n	13.17	0^-, 1^- [c]	Mc 56a, Bo 56
4.004	130	p, n	13.70	3	Bo 56
4.61		p, n	14.22		Bo 56
4.8		p	14.4		Bo 56
5.336		p	14.84		Bo 56
5.635	300	p	15.10		Bo 56

[a] p_0 and p_1 correspond, respectively to the ground- and first excited states of C^{13}.
[b] (Mc 58d).
[c] (Ma 55j).
[d] There is some discrepancy between the energy scales of (Bo 56) and (Mc 56a).
[e] See (Bo 56, Mc 56a, Ja 57).

14.7: See (Va 56c, Ko 56f, Sa 57, Mc 56a, Bo 56, Ma 55j, Mc 58d, Ja 57). See also (De 57, Ba 48, Bo 49a, Ph 50b).

Angular distributions of protons for $E_d < 1$ MeV are reported to be strongly influenced by stripping effects (Ju 56g, Ju 57, Ko 56f, Va 56c); the same influence is seen for $E_d > 2$ MeV (Mc 56a: see C^{13}). In the region $E_d = 0.8$ to 1.7 MeV, however, (Sa 57) find no stripping contribution and analyze the observed distributions in terms of 5 resonances: see table 14.7. Although the J^π assignments listed are determined in part by choosing $\gamma_n^2 \approx \gamma_p^2$, neutron reduced widths seem generally to be nearly a factor of 10 low (Sa 57). A detailed analysis for the region $E_d = 2.5$ to 3 MeV has been made by (Mc 58d). Both stripping and compound nucleus formation are involved. See also (Al 55e, Al 55f).

For $E_d = 5$ to 30 MeV, the course of the cross section indicates predominance of stripping over compound nucleus effects (Wi 55h).

IX. $C^{12}(d, d)C^{12}$ $E_b = 10.265$

Reported resonances are given in table 14.7 (Mc 56a, Mc 58d). A detailed analysis of the resonances at $E_d = 2.502$ and 2.735 MeV has been made by (Mc 58d). See also (Ca 54j, Ca 56g, Aj 55).

X. $C^{12}(d, t)C^{11}$ $Q_m = -12.463$ $E_b = 10.265$

The cross section rises from ≈ 0.1 mb at $E_d = 16$ MeV to ≈ 10 mb at 20 MeV. The magnitude of the cross section is indicative of the pick-up character of the reaction (Wi 55h).

XI. $C^{12}(d, \alpha)B^{10}$ $Q_m = -1.351$ $E_b = 10.265$

See B^{10}.

XII. $C^{12}(t, n)N^{14}$ $Q_m = 4.007$

Not reported.

XIII. $C^{12}(He^3, p)N^{14}$ $Q_m = 4.772$

Proton groups have been observed corresponding to the first five states of N^{14}. Angular distributions of the various proton groups have been measured for $E(He^3) = 1.30$ to 21 MeV (Br 57: 1.30 to 2.66 MeV; p_0, p_1, p_2), (Jo 58: 2.0 to 5.0 MeV; p_0, p_1, p_2), (Sw 58a: 6.05 MeV; p_0, p_1, p_2, p_{3+4}), and (We 58c: 21 MeV). At the lower energies, the distributions show both compound nucleus and direct interaction effects. At the higher energies, the forward peaking increases, and at 6.05 MeV the direct interaction character is well developed.

The de-excitation of the 3.95-MeV state has been studied; the direct ground-state decay is (3.7 ± 0.6) per cent of the total (Br 57, Go 56e); see also (Mo 58) and $C^{13}(p, \gamma)N^{14}$. The angular distribution of the 2.31-MeV γ-rays is

spherically symmetric while that of the 1.64-MeV γ-ray (from the 3.95 → 2.31 cascade transition) involves a 22 per cent $P_2(\cos\theta)$ term, consistent with $J = 0^+$ and 1^+ for the 2.31 and 3.95-MeV states respectively (Go 56e, Br 57). The polarization of the 1.64-MeV γ-ray also indicates that the parity of these two states is the same (Li 58b). Since the J^π assignments permit M1 transitions for both the ground state and cascade transitions from the 3.95-MeV level, the ground state transition would be expected to dominate by a large factor. However, the M1 matrix element effectively cancels for $\Delta T = 0$, $T_z = 0$ (Mo 58, Vi 57, Wa 59). The E2 transition is estimated to be 0.9 per cent: the observed value of 3.7 per cent must be ascribed to collective enhancement (Vi 57, El 56b). See also $C^{14}(\beta^-)N^{14}$ and O^{15}.

XIV. $C^{12}(\alpha, d)N^{14}$ $\qquad Q_m = -13.579$

This reaction has been observed at $E_\alpha = 42$ MeV. The deuteron angular distribution is similar to the α-particle distribution in the $N^{14}(d, \alpha)C^{12}$ reaction at $E_d = 20$ MeV (Bo 58c).

XV. $C^{13}(p, \gamma)N^{14}$ $\qquad Q_m = 7.546$

Resonances are observed at $E_p = 0.45$, 0.55, 1.16, 1.25, 1.47, 1.55, 1.75, 2.10 and 3.11 MeV; their parameters are displayed in table 14.8; see also (Ja 57). The decay schemes of various levels of N^{14}, as derived from the γ-spectra in this and other reactions are exhibited in fig. 27 (Wo 53c, Cl 53a, Le 56h, Wi 57b, Br 57i and D. Hebbard, private communication). At $E_p = 114$ and 126 keV, the capture cross sections are, respectively, $(5.1 \pm 2.0) \times 10^{-3}$ μb and $(8.2 \pm 2.5) \times 10^{-3}$ μb (La 57b). The 0.45-MeV resonance involves both ground state decay and ≈ 4 MeV cascade radiation with about equal radiative widths (D. Hebbard).

The width of the $E_p = 0.55$-MeV resonance ($E_x = 8.06$ MeV) indicates s-wave formation ($J = 0^-, 1^-$) (Wo 53c). The observed isotropy of the radiation supports this assignment (De 49d). The level is established as $J = 1^-$ from $C^{13}(p, p)C^{13}$. (Br 57i) find a 1 per cent anisotropy, indicating a d-wave admixture of ≈ 6 per cent, $\theta_p^2(d) = 0.45$; see, however, (Wa 59a). The γ-width for the ground-state radiation indicates an uninhibited E1 transition, and hence $T = 1$ for $N^{14*}(8.06)$ (Cl 53a). The relative strength of the T-forbidden transition to $N^{14*}(2.3)$ is about 2 per cent (Pi 56a, Le 56h, Wi 57b, Br 57f), indicating a strong $T = 0$ admixture in $N^{14*}(8.06)$. The fact that the 6.23-MeV state, $J = (1^-)$, $T = 0$ (see below) shows a similar contamination, suggests that these two states have a common parentage and contaminate each other (Wi 57b): See, however, (Br 57f, Br 57i, Wa 59a). The strength of the transition 8.06 → 5.69, $\Gamma_\gamma \approx 0.7$ eV, suggests E1 radiation and hence $J = 0^+, 1^+, 2^+, T = 0$, for $N^{14*}(5.69)$. The further transition 5.69 → 2.3 rules out $J = 0^+$. $J = 2^+$ is excluded by the strength of 8.62

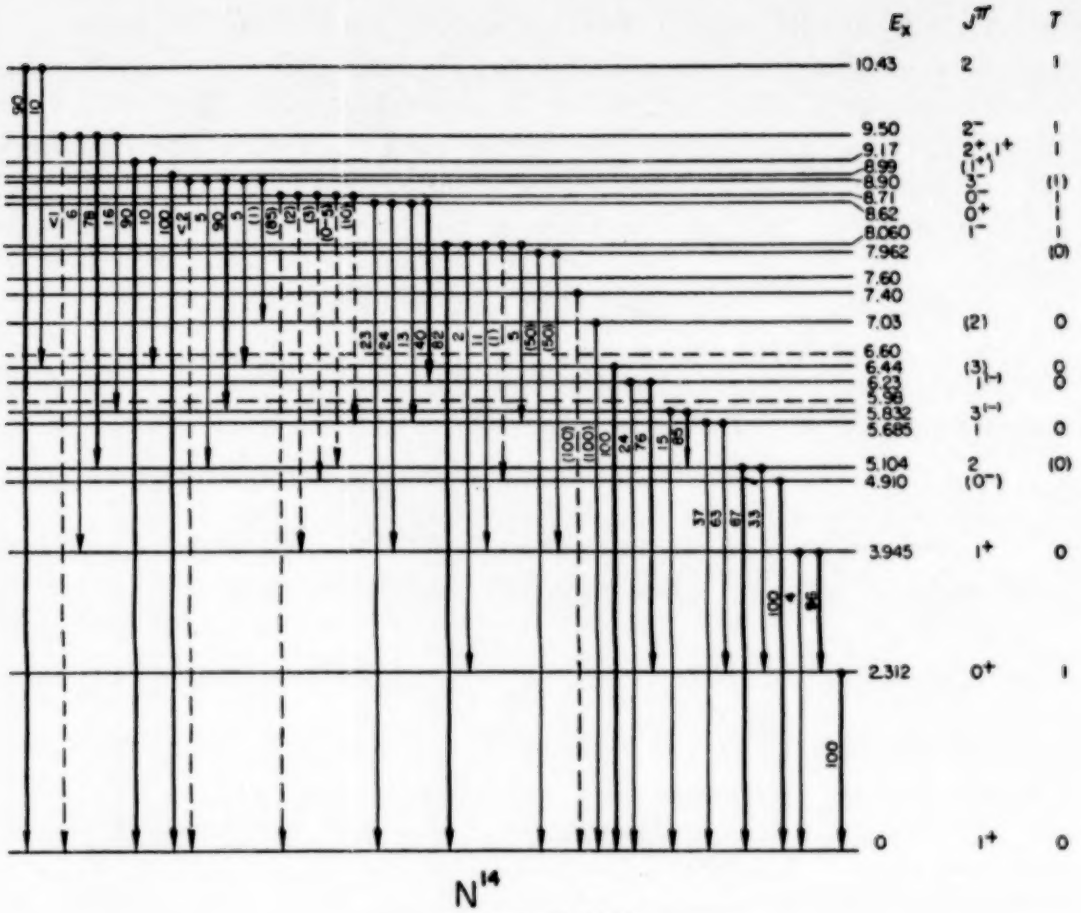

8 January 1959

Fig. 27. Gamma-ray transitions in N^{14}: for notation, see fig. 14, p. 83.

TABLE 14.8

Levels of N^{14} from $C^{13}(p, \gamma)N^{14}$ and $C^{13}(p, p)C^{13}$

E_p (MeV ± keV)	Γ_{lab} (keV)	l_p	θ_p^2	σ_γ (mb)	$\omega\Gamma_\gamma$ (eV)	J^π; T	N^{14*} (MeV)	Ref.
0.448 ± 1				res	0.008		7.962	a
0.554 ± 2	32.5 ± 1	0	0.13	1.44	8.6	1^-; 1	8.060	b
1.16	6 ± 2	1	0.013	0.56	1.3	0^+; 1	8.62	b
1.25	500	0	0.23	0.062	12.8	0^-; 1	8.71	b
1.466 ± 6	16 ± 2	2	0.17	0.074	0.72	3^-; (1)	8.903	b, g
1.55	7	1	0.005	0.037	0.13	(1^+)	8.99	b
1.7473 ± 0.8	0.075			[340]	14.8	$2^+, 1^+$; 1	9.17	c
2.00 ±20	≈20	2	0.08			1^+	9.40	d
2.112 ± 6	44 ± 2	2	0.14	0.20	6.2	2^-; 1	9.504	e
2.33 ±20	15 ± 3	1	0.005			1^+	9.71	d
2.90 ±40	80 ±30						10.24	d
3.11 ±10	30 ± 3		0.02	0.70	17	2; 1	10.43	f
3.12 ±30	80 ±10						10.44	d

[a] D. Hebbard, private communication.

[b] (Se 52, Wo 53c, Mi 54).

[c] (Se 52, Wo 53c, Ma 56n, Pa 58c, Bo 58e); $(2J+1)\Gamma_\gamma = 29$ eV from inverse reaction (Ha 57k). Parity is even, according to (St 58c).

[d] (Zi 57, Zi 58).

[e] (Zi 57, Zi 58, Se 52, Wo 53c, Wa 59a).

[f] (Wi 57e): (possibly same as next entry).

[g] (Wa 59a).

$\rightarrow$ 5.69, $\Gamma_\gamma = 0.7$ eV (Wi 57b, Le 56h); see, however, (Br 57i). According to (Wa 59a), the transition strength of 8.06 $\rightarrow$ 5.69 also admits M1, $\Delta T = 1$, and hence $J = 1^-$, $T = 0$ for $N^{14*} = 5.69$ MeV. The transition $N^{14*}(3.95) \rightarrow$ g.s. is 5.5 ± 1.0 per cent of the cascade, 3.95 $\rightarrow$ 2.3 (Pi 56a, Le 56h). See also (Hi 54e, Gr 56a), $C^{12}(He^3, p)N^{14}$.

The narrow $E_p = 1.16$-MeV resonance, $N^{14*} = 8.62$ MeV, $J = 0^+$ (from $C^{13}(p, p)C^{13}$) shows strong transitions to the ground state and to $N^{14*}(3.95)$ and (5.69): hence $T = 1$ (Wa 59). The strength of transition to $N^{14*}(6.23)$ indicates E1 radiation, $J = 1^-$, $T = 0$ for the 6.23-MeV state (Wi 57b). However, the angular correlation in the cascade 8.62 $\rightarrow$ 6.23 $\rightarrow$ g.s. favours $J = 1^+$ or 2^+ for $N^{14*}(6.23)$ (Go 56f, Go 57e, Ga 57a). In this case, the transition strength still requires $J = 1$, $T = 0$ for $N^{14*}(6.23)$. The strong transition 8.62 $\rightarrow$ 3.95 requires dipole radiation and hence $J = 1$ for the latter (Wa 59a).

The $E_p = 1.25$-MeV resonance ($E_x = 8.71$ MeV, $J = 0^-$ from $C^{13}(p, p)C^{13}$) is established as due to s-waves by its width (Wo 53c). Again the large γ-width is consistent with E1 radiation and $T = 1$ (Wi 53c). The γ-spectrum has been studied by (Br 57i) at $E_p = 0.9$ and 1.0 MeV, where the main effects should be due to the $E_p = 1.25$-MeV resonance: see, however, (Ja 57, Wa 59a). The results indicate relatively strong transitions to both the 4.9 and 5.7-MeV levels (see fig. 27) and would appear to exclude the assignments $J = 0^-, 1^-$ respectively for these levels. An assignment $J = 1^+$ to $N^{14*}(5.10)$ is suggested. At $E_p = 1.4$ MeV, (Wa 59a) finds no evidence of transitions to the 5.10-MeV state. It is pointed out that some of the reported transitions may derive from the background or from other resonances.

The angular distribution of ground-state γ-rays at the $E_p = 1.75$-MeV resonance ($N^{14*} = 9.17$ MeV) indicates $J = 1^+, 2^+$ or 2^-; the relatively large γ-width, 13.3 eV, suggests an uninhibited E1 transition, $J = 2^-$, $T = 1$ (Da 51, Da 51b, Wo 53c, Ma 56n). However, the polarization is consistent with M1 or E2 but not E1 (St 58c); see also (Wa 59). The total width is < 400 eV (Ma 56n), < 150 eV (Pa 58c), 75 ± 50 eV (Bo 58e). The resonant energy is 1746.9 ± 0.8 (Ma 56n), 1747.6 ± 0.9 keV (Bo 58e). If the transition 9.17 $\rightarrow$ 6.44 is dipole ($\omega\Gamma_\gamma = 1.3$ eV), and if $J(9.17)$ is 2, the angular distribution requires $J(6.44) = 3$ (Wo 53c) and $T = 0$ (Wa 59). See also (Me 58c).

From elastic scattering work (see $C^{13}(p, p)C^{13}$), the $E_p = 1.47$-MeV resonance, $N^{14*} = 8.90$ MeV, has $J = 2^-$, with 3^- and 1^- possible. The resonance at $E_p = 2.11$ MeV, $N^{14*} = 9.50$ MeV has $J = 3^-$, with 2^- and 1^- possible. A study of the gamma decay scheme and angular distributions confirms the assignments $J = 2^-$ ($T = 1$) and $J = 3^-$, $T = 1$ for these two levels. For the latter, the channel spin mixture is $(56 \pm 14)\% J_c = 0$. Levels at $N^{14*} = 5.83$ and 5.10 MeV are $J = 3^{(-)}$ and $J = 2$. The

mean lives for these two levels, determined by Doppler shift, are $0.5 < \tau < 6.5 \times 10^{-13}$ sec, and $\tau > 3 \times 10^{-13}$ sec, respectively. The 7.02-MeV level probably has $J = 2$, while the 6.44-MeV level has $J = 2$, 3 or 4. Shell-model assignments and the correlation with the levels of C^{14} are discussed in some detail (Wa 59a). See also (Wi 56e).

At the $E_p = 3.11$-MeV resonance ($E_x = 10.43$ MeV), the angular distribution of ground-state γ-rays is $1-(0.40\pm0.02)\,P_2(\cos\theta)$, indicating $J = 2^-$, formed by d-waves with channel spin mixture $\sigma(J_c = 0)/\sigma(J_c = 1) = \frac{3}{2}$, followed by E1 radiation, or $J = 2^+$, f-wave formation, $J_c = 1$, M1 radiation. The relatively large gamma width, 17eV, suggests E1 radiation and $T = 1$ (Wi 57e). According to (Wa 59), however, the assignment $J = 2^+$ (p or f) is equally satisfactory. The integrated cross section is 0.033 MeV-mb, in good agreement with the corresponding value for $N^{14}(\gamma, p)C^{13}$ (Wi 57e).

XVI. (a) $C^{13}(p, p)C^{13}$ $E_b = 7.546$
(b) $C^{13}(p, p')C^{13*}$

The elastic scattering has been studied for $E_p = 0.15$ to 0.75 MeV by (He 57f), for $E_p = 0.45$ to 1.60 MeV by (Mi 54) and for $E_p = 1.5$ to 3.4 MeV by (Zi 57, Zi 58): see table 14.8. Assignments and level parameters for $E_p < 2$ MeV are based in part on a qualitative analysis of the elastic scattering and in part on $C^{13}(p, \gamma)N^{14}$ (Mi 54, Wo 53c, Se 52). Near the 0.55-MeV resonance, the cross sections of (He 57f) are about 10 per cent lower than those of (Mi 54). A close fit to the theory is obtained from $E_p = 0.12$ to 0.65 MeV when the energy variation of Γ and E_0 are taken into account (He 57f: see also Ch 56b). Above $E_p = 2$ MeV, the non-resonant background requires s, p and d waves. At the 9.51-MeV level, the channel spin mixture $\sigma(1)/\sigma(0) = \frac{2}{3}$ corresponds to $(\frac{5}{2}, \frac{1}{2})$ in j-j coupling (Zi 57, Zi 58): compare $N^{14*}(10.43)$ in $C^{13}(p, \gamma)$.

The yield of γ-rays in reaction (b) has been measured for $E_p = 3.6$ to 5.0 MeV: the 3.1-MeV γ-yield shows broad resonances at $E_p = 3.80$, 4.1, and 4.14 MeV, while the 3.7-MeV γ-yield shows one strong resonance at $E_p = 4.52$ MeV ($N^{14*} = 11.1$, 11.36, 11.39 and 11.7 MeV) (Co 57h, Ba 57q).

XVII. $C^{13}(p, n)N^{13}$ $Q_m = -3.005$ $E_b = 7.546$

Observed resonances are exhibited in table 14.9 (Ba 53e, Bl 51a, Ad 50b, Ba 57q). Absolute cross sections have been determined from threshold to 5 MeV by (Ma 58a, Gi 59). The behaviour at threshold appears to reflect the effect of a bound level, possibly that at $E_p = 3.11$ MeV. See also (Bl 58b).

XVIII. $C^{13}(d, n)N^{14}$ $Q_m = 5.319$

$Q_0 = 5.325\pm0.040$ (Bi 55a).
$Q_0 = 5.41\ \pm0.06$ (Gr 55f).

Observed neutron groups are exhibited in table 14.10 (Be 53d, Br 52, Gr 55f, Bi 55a). At $E_d = 0.86$-MeV the third excited state shows a strong,

TABLE 14.9

Resonances in $C^{13}(p, n)N^{13}$

E_p [a] (MeV)	Γ [a] (keV)	E_p [b] (MeV)	Γ [b] (keV)	E_x (MeV)
3.78	100	3.77	110	11.06
3.99	15	3.98	25	11.25 [c]
(4.1)	150			(11.35)
4.14	30	4.14	50	11.39
4.49	150	4.51	140	11.73
4.8	100	4.74		11.95
		4.85		12.05
		5.03		12.20
6.20				13.30

[a] (Ba 53e, Bl 51a, Ad 50b, Ba 57q).
[b] (Gi 59).
[c] Corresponds to $N^{14*} = 11.23$ in table 14.7.

TABLE 14.10

Neutron groups from $C^{13}(d, n)N^{14}$

N^{14*} (MeV) (Be 53d) [a]	N^{14*} (MeV) (Bi 55a) [b]	N^{14*} (MeV) (Gr 55f) [c]	l_p	J^π
0	0	0	1 [d]	0^+, 1^+, 2^+
2.23 ± 0.10	2.30 ± 0.05	2.34 ± 0.07	1 [e]	0^+, 1^+, 2^+
3.85 ± 0.08	3.95 ± 0.03	4.02 ± 0.07	1 [e]	0^+, 1^+, 2^+
4.80 ± 0.07	4.95 ± 0.02 [f]	5.02 ± 0.07	0 [e]	0^-, 1^-
4.97 ± 0.07		5.20 ± 0.07		
(5.5 ± 0.1)				
5.76 ± 0.05				
(6.1 ± 0.1)				
6.23 ± 0.05				
6.43 ± 0.04				
7.00 ± 0.04				
(7.50 ± 0.04)				
7.72 ± 0.04				
8.08 ± 0.06				

[a] $E_d = 3.89$ MeV.
[b] $E_d = 0.92$ MeV.
[c] $E_d = 0.86$ MeV.
[d] (Br 52).
[e] (Be 53d).
[f] May be due to more than one level.

$l = 0$ stripping pattern (Gr 55f; see also Bi 55a). In the range $E_d = 0.4$ to 4.2 MeV, a single strong neutron threshold occurs at $E_d = 0.422 \pm 0.005$ MeV ($N^{14*} = 5.685 \pm 0.007$ MeV). The outgoing neutrons are likely to be p-wave, and the incident deuterons s-wave (because of their low energy): the results are consistent with $J = 1^+$ (Ma 55j); see, however, (Wa 59a). Observed γ-rays attributed to transitions in N^{14} are shown in table 14.11 (Th 52, Be 55a, Ma 55a, Ra 58b). A study of the angular correlation of internal pairs indicates that the transition $N^{14*}(5.69) \rightarrow$ g.s. is M1 or E2; of the two transitions $(4.91 \rightarrow \text{g.s.})$ and $(5.10 \rightarrow \text{g.s.})$, one is E1 and the other is E2 or M1 (Ch 58b). See also (Go 58h). See also (El 56b, Au 55; theo.).

TABLE 14.11

Gamma rays from $C^{13}(d, n)N^{14}$

(Th 52) [a] E_γ [d] (keV)	(Be 55a) [b] E_γ [e] (keV)	(Ma 55a) [c] E_γ [d] (keV)	(Ra 58b) [f] E_γ [e] (keV)	Assignment N^{14*}
725 ± 4		729 ± 3		5.83→5.10
1638 ± 8				3.95→2.31
2310 ± 12				2.31
3381 ± 13	3410 ± 40			5.69→2.31
	3920 ± 70 [g]	3910 ± 50		3.95
	4940 ± 40	4930 ± 40	4897 ± 25	4.91
5052 ± 25	5100 ± 50	5130 ± 30	5102 ± 25	5.10
5690 ± 50	5720 ± 40	5730 ± 30	5669 ± 25	5.69
			5833 ± 30 [d]	5.83
	6490 ± 60	6450 ± 50	6419 ± 30	6.43
	7050 ± 40		7012 ± 25	7.02
	7300 ± 50 [g]			7.40

[a] $E_d = 1.2$, 1.6 MeV.
[b] $E_d = 2$, 4 MeV.
[c] $E_d = 1.4$ MeV.
[d] Not corrected for Doppler shift.
[e] Includes ≈ 0.5 per cent Doppler correction.
[f] $E_d = 4.5$ MeV.
[g] Assignment not certain.

XIX. $C^{13}(He^3, d)N^{14}$ $Q_m = 2.052$

Not observed.

XX. $C^{13}(\alpha, t)N^{14}$ $Q_m = -12.267$

Not observed.

XXI. $C^{14}(\beta^-)N^{14}$ $Q_m = 0.155$

See C^{14}.

XXII. $C^{14}(p, n)N^{14}$ $Q_m = -0.628$
$Q_0 = -626.4 \pm 0.5$ keV (Sa 56d).

Neutron thresholds have been observed at $E_p = 671.5 \pm 0.5$ and 3149.6 ± 1.1 keV, corresponding to the ground state of N^{14} and to an excited state at 2.3119 ± 0.0012 MeV (Sa 56d). See also N^{15}.

XXIII. $C^{14}(He^3, t)N^{14}$ $Q_m = 0.137$

Not observed.

XXIV. (a) $N^{14}(\gamma, n)N^{13}$ $Q_m = -10.551$
(b) $N^{14}(\gamma, p)C^{13}$ $Q_m = -7.546$
(c) $N^{14}(\gamma, np)C^{12}$ $Q_m = -12.491$
(d) $N^{14}(\gamma, \alpha)B^{10}$ $Q_m = -11.615$

The cross section for neutron production, reactions (a) and (c), exhibits a maximum at $E_\gamma = 22.5$ MeV, $\Gamma = 3.2$ MeV, $\sigma = 15.3$ mb (Fe 54; see also Jo 51b, Li 57c). Below this maximum, there are less intense peaks in the cross section of reaction (a) at (≈ 10.8), ≈ 11.5 and ≈ 12.7 MeV. The latter two have widths of ≈ 0.3 and ≈ 1 MeV, respectively (Ch 55b). At E_γ(max) $= 23$ MeV, proton + recoil energies (reaction b) of 0.51, 1.63, and 2.92 MeV are observed, corresponding to the 8.06, 9.18 and 10.43-MeV levels of N^{14}. Integrated cross sections of 0.6, 0.8 and 1.2 MeV-mb respectively, are found, in good agreement with those obtained from the inverse reaction $C^{13}(p, \gamma)N^{14}$ (Wr 56). In a resonance absorption experiment, using γ-radiation from $C^{13}(p, \gamma)N^{14}$ at $E_p = 1.76$ MeV, (Ha 57k and private communication) find for the 9.17 MeV level of N^{14}, $\Gamma = 0.07 \pm 0.02$ keV, $\sigma_{res} \approx 6$ b, $(2J+1)\Gamma_\gamma \approx 48$ eV. For the 8.06-MeV level, (Gr 56a, Gr 58) finds $\Gamma_\gamma = 10.5 \pm 6$ eV (compare $C^{13}(p, \gamma)N^{14}$).

At E_γ(max) $= 70$ MeV, reaction (d) appears to proceed via a level at 8.2 MeV in B^{10} (which then decays by proton emission) (Li 56). See also (Co 55, Ti 55a, Go 561, Jo 56f, Jo 58a, Rh 58a, Sa 55j, Be 57a, Bi 54, Co 58g, Ho 50b and Aj 55).

XXV. $N^{14}(n, n')N^{14*}$

Elastic scattering of 14-MeV neutrons has been studied by (Sm 54, Co 52h, Bu 56j). At $E_n = 3.95$ MeV, a 2.30 ± 0.05 MeV γ-ray is observed (Da 56d). See also N^{15}.

XXVI. $N^{14}(n, d)C^{13}$ $Q_m = -5.319$

At $E_n = 14$ MeV, deuteron groups are observed leading to $C^{13}(0)$ and $C^{13*}(3.7)$. The reduced width of N^{14}(g.s.) for separation into $p+C^{13}(0)$ is $\theta^2_{p_0} = 0.025$; for separation into $p+C^{13*}(3.7)$, $\theta^2_{p_1} = 0.06$. The ratio is consistent with N^{14}(g.s.) $= {}^3S_1$ but not with pure ${}^3D_1$. On the other hand, the value of $\theta^2_{p_0}$, when suitably corrected, is consistent with a large amount of D

character for N^{14}(g.s). Upper limits for decomposition into C^{13*}(3.09) or C^{13*}(3.86) are $\theta^2_{p_1} < 0.003$ and $\theta^2_{p_2} < 0.03$ (Ca 57e): see also N^{14}(p, d)N^{13}.

XXVII. N^{14}(p, d)N^{13} $Q_m = -8.324$

Angular distributions measurements for ground-state deuterons at $E_p = 18$ MeV indicate $l_n = 1$. The peak cross section (18°, c.m.) is 5.0 ± 0.6 mb/sr, yielding a reduced width $\theta^2 = 0.021$ for N^{14}(g.s.). With appropriate correction, the reduced width is in qualitative agreement with that calculated from the independent-particle model and the result suggests that the N^{14} ground state is largely D. Upper limits of 0.1 to 0.4 mb/sr are quoted for the transition to the first excited state of N^{13} and are taken to indicate admixtures of p^8s^2 or p^8sd in N^{14} of a few per cent or less (St 56, St 54a). See also N^{14}(n, d)C^{13}.

XXVIII. (a) N^{14}(p, p′)N^{14*}
(b) N^{14}(d, d′)N^{14*}

Elastic proton scattering has been studied at $E_p = 9.5$ MeV (Fr 54f, Gi 57), $E_p = 9.8$ MeV (Hi 57a), 19.4 MeV (Va 56b, Va 57b) and 20 MeV (Ch 55). Analysis in terms of the optical model is not entirely satisfactory (Bu 56j, Hi 57a). Elastic deuteron scattering has been studied at $E_d = 8$ MeV by (Gi 52).

Observed inelastic proton and deuteron groups are shown in table 14.12

TABLE 14.12

N^{14} levels from N^{14}(p, p′)N^{14*} and N^{14}(d, d′)N^{14*}

N^{14*} (p, p′) [a]	N^{14*} (p, p′) [b]	N^{14*} (p, p′) [c]	N^{14*} (d, d′) [c]
2.32±0.02	[f]	2.313±0.005	[d]
3.96±0.02	[f]	3.945±0.005	3.95
	[f]	4.910±0.010	[e]
5.09±0.02	[f]	5.104±0.010	[e]
	5.69±0.03		
	5.83±0.03		
	(5.95)		
	6.23±0.02		
	6.46±0.02		
	(6.60±0.04)		
	7.03±0.02		
	7.40±0.02		
	7.60±0.02		

[a] (Ar 52e; $E_p = 8$ MeV).
[b] (Bu 56h; $E_p = 9.5$ MeV).
[c] (Bo 53; $E = 7$ and 7.6 MeV).
[d] Intensity <0.5 per cent of d_0 group at $E_d = 7.0$ MeV, $\theta = 90°$.
[e] No attempt to observe.
[f] Also observed.

(Ar 52e, Bo 53, Bu 56h). At $E_p = 9.5$ MeV, the p_1 group (to the 2.3-MeV, first excited state) is surprisingly weak: $< \frac{1}{6}$ of p_2 (Fr 54f). At $E_p = 6.98$ MeV, $\theta = 90°$, the ratio of the intensities of the p_1 and p_2 groups to the p_0 (elastic group) is 5 and 10 per cent, respectively. For deuterons, the ratio for the d_2 group is 10 per cent, while an upper limit of about 0.5 per cent is set for the d_1 group corresponding to the $T = 1$, 2.31-MeV state, as expected from the T selection rule (Bo 53). Angular distributions of the p_0 and p_2 groups have been studied at $E_p = 9.5$ MeV (Fr 54f). See also (Ba 56b; theo.). At $E_p = 96$ and 185 MeV, inelastic groups with $Q = -9.2$, -17 and -21.5 MeV are reported (Ty 58; see also St 56c). See also (Ty 58b, Ma 58h). Inelastic scattering of deuterons is also reported at $E_d = 9$ MeV by (Gr 56b): the d_2, d_3 and d_4 groups are observed.

For $E_p = 3.9$ to 4.9 MeV, the 2.3-MeV γ-radiation is isotropic, confirming the $J = 0$ assignment to the first excited state (Ba 56i). The Doppler shift is very nearly the maximum possible, indicating a half-life less than 3.5×10^{-13} sec (Sh 55d), $< 2 \times 10^{-13}$ sec (Th 55b). See also O^{15}.

XXIX. $N^{14}(\alpha, \alpha')N^{14*}$

At $E_\alpha = 21.5$ MeV, inelastic alpha groups are reported to N^{14} states at 3.95 ± 0.04, 5.12 ± 0.07, 5.79 ± 0.07, 6.47 ± 0.09, 7.02 ± 0.06, 7.94 ± 0.07, 8.45 ± 0.07 and 10.05 ± 0.07 MeV. Except for the 7.94-MeV level, which has recently been observed in $C^{13}(p, \gamma)N^{14}$, the last three have not been reported in other reactions. The absence of the $Q = -2.3$ and $Q = -8.06$-MeV groups is consistent with their $T = 1$ assignment (Mi 56: see also Wa 56f). At $E_\alpha = 31.5$ MeV, the upper limit for the α_1 group, corresponding to $N^{14*}(2.3)$, $T = 1$, is 6 per cent of the α_2 group (Wa 56f).

XXX. $O^{14}(\beta^+)N^{14}$ $\quad Q_m = 5.147$

The decay proceeds almost entirely to the $J = 0^+$, $T = 1$ state of N^{14} at 2.3 MeV: see O^{14}.

XXXI. $N^{15}(p, d)N^{14}$ $\quad Q_m = -8.615$

At $E_p = 18.6$ MeV, the transitions to the ground and first excited states of N^{14} have been observed. The angular distributions of both groups are fitted by $l_n = 1$ pickup curves. The peak cross section for the ground state is about 7 times greater than that for the 2.31-MeV state (Be 57b, Sh 57b). See also (Fr 56b; theo.).

XXXII. $N^{15}(d, t)N^{14}$ $\quad Q_m = -4.583$

Not reported.

XXXIII. $N^{15}(He^3, \alpha)N^{14}$ $\quad Q_m = 9.736$

Not reported.

XXXIV. $O^{16}(n, t)N^{14}$ $Q_m = -14.470$

Not reported.

XXXV. $O^{16}(p, He^3)N^{14}$ $Q_m = -15.235$

Not reported.

XXXVI. $O^{16}(d, \alpha)N^{14}$ $Q_m = 3.116$

$Q_0 = 3.108$ (Br 55c: see also Va 54).

Alpha-particle groups leading to N^{14} levels at 0, 3.95, 5.01 and 5.70 MeV are reported by (As 51); 0, 3.98±0.04, 5.06±0.05 MeV by (Bu 51f); 0, 3.9 and ≳ 5 MeV by (Fr 53e); 0, 3.949 MeV by (Br 55c). The group leading to $N^{14*}(2.3)$, $T = 1$, is ordinarily not observed; however, careful studies in the range $E_d = 5.5$ to 7.5 MeV (Br 56f) and $E_d = 6.8$ to 8.9 MeV (Da 58b) show a weak α_1-group whose intensity shows marked resonance effects. The observed intensity is consistent with the expected isobaric spin impurity of the O^{16}, F^{18*}, and N^{14*} states involved (Br 56f): see F^{18}. Angular distributions of α-groups have been measured at $E_d = 7.0$ MeV (Br 56f; $\alpha_0, \alpha_1, \alpha_2$), 6.8 and 8.9 MeV (Da 58b; α_0, α_2) and at 19 MeV (Fr 53e; α_0). See also (El 57; theo.) and (Gr 56b, Sp 53c).

XXXVII. $O^{17}(p, \alpha)N^{14}$ $Q_m = 1.197$

See F^{18}.

O^{14}

(Not illustrated) †

MASS OF O^{14}

The mass excess of O^{14} is 12.149±0.007 MeV, based on the threshold energy of the $C^{12}(He^3, n)O^{14}$ reaction (Br 57) and on the Wapstra masses (Wa 55c) for C^{12}, He^3 and n. The binding energies of a proton, alpha particle, He^3-particle and deuteron in O^{14} are, respectively, 4.621, 10.25, 17.563 and 22.58 MeV. In terms of the Mattauch masses (Ma 56m), the mass excess obtained by (Br 57) is 12.146±0.0065 MeV.

TABLE 14.13

Energy levels of O^{14}

E_x in O^{14} (MeV)	J^π	$\tau_{\frac{1}{2}}$ or Γ	Decay	Reactions
0	0^+	72.1±0.4 sec	β^+	I, II, III, IV
≈6.2		broad or unresolved		IV
≈7.5		broad or unresolved		IV
≈9.3		broad or unresolved		IV

† For level scheme of C^{14}, see fig. 25, p. 157.

I. $O^{14}(\beta^+)N^{14}$ $Q_m = 5.147$

The decay proceeds primarily (99.4 ± 0.1 %) (Sh 55d) to the $J = 0^+$, $T = 1$ first excited state of N^{14}: $E_{\beta^+}(\text{max}) = 1.835\pm0.008$ (Ge 54); 1.830 ± 0.030 MeV (Pe 54a); $E_\gamma = 2.30\pm0.03$ MeV (Sh 53a). Using Q for $C^{12}(He^3, n)O^{14} = 1.1585$, $N^{14*} = 2.313\pm0.005$, and mass excess of (Ma 56m), (Br 57) calculate $E_{\beta^+}(\text{max}) = 1.8097\pm0.0078$. The positon spectrum has an allowed shape (Ge 54). The half-life is 72.1 ± 0.4 sec (Ge 54), $ft = 3088\pm56$ sec (Br 57); see also (Ge 58). The direct ground state transition occurs in (0.60 ± 0.10) % of the cases: $ft = (2.0\pm0.3)\times10^7$ sec. The corresponding matrix element is about 50 times larger than that for $C^{14}(\beta^-)N^{14}$. Explicit wave functions for O^{14}, N^{14}, and C^{14} are derived (Sh 55d: see also Ja 54a, El 56b, Vi 57). A slight deviation from linearity in the Kurie plot is predicted by (Vi 57, Go 58c). The polarization of the positons has been studied by (Ge 58d). See also (Ma 58c, Su 58, Be 58e, Sh 57b, Ge 58b; theo.).

II. $B^{10}(Li^6, 2n)O^{14}$ $Q_m = 1.988$

See (No 57a).

III. $C^{12}(He^3, n)O^{14}$ $Q_m = -1.159$

$E_{\text{thresh}} = 1.4496\pm0.0028$ MeV;

$Q_0 = -1.1585\pm0.003$ MeV (Br 57).

This reaction has been studied from threshold to $E(He^3) = 2.7$ MeV (Br 57: see O^{15}). (Bu 56a) report a tentative threshold value of $E(He^3) = 1.435$ MeV; $Q = -1.148\pm0.004$ (Wa 58c).

IV. $N^{14}(p, n)O^{14}$ $Q_m = -5.930$

At $E_p = 17.3$ MeV, neutron groups are observed to the ground state and to broad or unresolved states of O^{14} at ≈ 6.2, 7.5 and 9.3 MeV (Aj 54). See also (Bo 58).

C^{15}

(Fig. 28, p. 179)

MASS OF C^{15}

From the Q of the $C^{14}(d, p)C^{15}$ reaction given by (Do 56c) ($Q_0 = -1.007\pm0.001$ MeV), and using the Wapstra masses for C^{14}, d and H^1, the mass excess of C^{15} is 14.305 ± 0.005 MeV. Application of Coulomb corrections indicates an excitation of 11.72 to 11.87 MeV for the first $T = \frac{3}{2}$ state of N^{15} (Ba 56a, Do 56b, Mu 57a).

I. $C^{15}(\beta^-)N^{15}$ $Q_m = 9.777$

The half-life is 2.25 ± 0.05 sec. The β-spectrum is complex, with 32 ± 2 per cent of transitions ($\log ft = 6.0$) to the N^{15} ground state ($E_\beta(\text{max}) = 9.82\pm0.04$ MeV) and 68 per cent ($\log ft = 4.1$) to the upper of the 5.3-MeV levels of N^{15}. A 5.299 ± 0.006-MeV γ-ray is observed (Al 59): no other γ-rays with $E_\gamma > 5.3$ MeV are observed with intensities > 5 per cent, and the intensity

of a 1.9-MeV γ-ray (expected if the N^{15} 7.16-MeV level were involved) is < 10 per cent (Do 56b). The internal pair conversion coefficient of the 5.30-MeV γ-ray is consistent with E1. All data are consistent with $J = \frac{1}{2}^+$ for the 5.305-MeV state in N^{15} and $J = \frac{1}{2}^+$ for C^{15} (Al 59). See also (Ba 56a, Do 56b, Aj 55).

II. $Be^9(Li^7, p)C^{15}$ $\quad Q_m = 9.098$

At $E(Li^7) = 2.0$ MeV ($\theta = 90°$) proton groups are observed corresponding to the ground state of C^{15} and to excited states at 0.62 ± 0.06, 2.48 ± 0.05, 3.08 ± 0.04, 4.26 ± 0.04, 5.93 ± 0.04, 6.58 ± 0.04 and 8.16 ± 0.06 MeV. The ground state Q is 9.04 ± 0.05 MeV (Mu 57a). In an earlier experiment, (No 57) found $Q_0 = 9.05 \pm 0.05$ and $Q_1 = 8.35 \pm 0.05$ MeV ($E_x = 0.70 \pm 0.05$ MeV). Calculation of Coulomb and ($n - H^1$) energy difference places the analogue state of N^{15} at 11.72 to 11.87 MeV. Identification with the known $T = \frac{3}{2}$, $J = \frac{1}{2}^+$ level of N^{15} at 11.61 MeV supports $J = \frac{1}{2}^+$ for C^{15}(g.s.) (Ba 56a, Mu 57a, No 57).

TABLE 15.1

Energy levels of C^{15}

E_x in C^{15} (MeV $\pm$ keV)	J^π	$\tau_{\frac{1}{2}}$	Decay	Reactions
0	$(\frac{1}{2}^+, \frac{1}{2}^+)$	2.25 ± 0.05 sec	β^-	I, II, III
0.66 ± 50				II, III
2.48 ± 50				II
3.08 ± 40				II
4.26 ± 40				II
5.93 ± 40				II
(6.2 ±150)				III
6.58 ± 40				II
8.16 ± 60				II

III. $C^{14}(d, p)C^{15}$ $\quad Q_m = -1.007$

$Q_0 = -1.007 \pm 0.001$ (Do 56c).

Identification of C^{15}(g.s.) with $N^{15*}(11.61)$, $T = \frac{3}{2}$, $J = \frac{1}{2}^+$, is suggested by (Ba 56a). Proton groups corresponding to the ground state and to levels at 0.7[illegible].1 and 6.2 ± 0.15 MeV are reported by (Mo 58a). The weak activity previously reported at $E_d < 1.3$ MeV, indicating a $Q \approx 0.1$ MeV (see Aj 55), is now attributed to contamination (Bo 56b). See also N^{16}.

IV. $C^{14}(n, \gamma)C^{15}$ $\quad Q_m = 1.220$

The capture cross section is < 1 μb (Ya 51, Hu 55c, Hu 58).

The following reactions leading to C^{15} are not reported: $C^{13}(t, p)C^{15}$ ($Q_m = 0.909$), $C^{14}(t, d)C^{15}$ ($Q_m = -5.039$), $C^{14}(\alpha, He^3)C^{15}$ ($Q_m = -19.358$), $N^{15}(n, p)C^{15}$ ($Q_m = -8.994$), $O^{18}(n, \alpha)C^{15}$ ($Q_m = -5.024$).

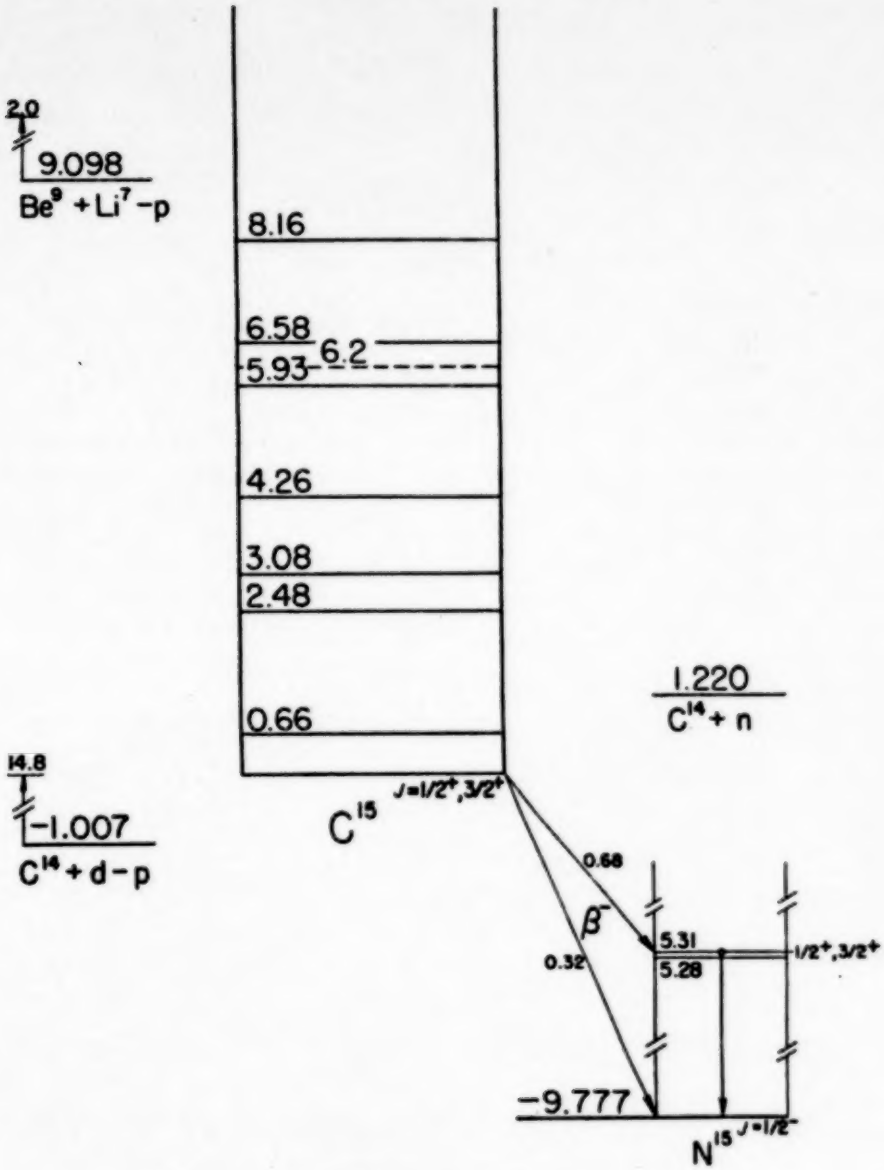

15 December 1958

Fig. 28. Energy levels of C^{15}: for notation, see fig. 1, p. 7.

N^{15}

(Fig. 29, p. 181) †

THEORY

See (Ka 56c, Ha 57b, Pe 57b, Fe 57c, Fr 58b).

I. $Be^9(Li^7, n)N^{15}$ $Q_m = 18.092$

See (No 57a).

II. $B^{11}(\alpha, n)N^{14}$ $Q_m = 0.152$ $E_b = 10.993$

Reported resonances are listed in table 15.3 (Be 54, Sh 55c, Tr 54, Bo 56d,

† For level scheme of O^{15}, see fig. 30, p. 195.

TABLE 15.2
Energy levels of N^{15}

E_x in N^{15} (MeV ± keV)	J^π	Γ (keV)	Decay	Reactions
0	$\frac{1}{2}^-$	—	stable	I, V, XI, XVI, XIX, XX, XXVII, XXVIII, XXXI, XXXII, XXXIII, XXXIV, XXXVI, XXXVII, XXXVIII
5.276 ± 6	$\leq\frac{7}{2}^+$		γ	V, XI, XVI, XIX, XX, XXVII, XXXII
5.305 ± 6	$\frac{1}{2}^+$, $\frac{3}{2}^+$		γ	V, XI, XVI, XIX, XX, XXVII, XXXII
6.328 ± 6	$\leq\frac{5}{2}^-$		γ	V, XI, XVI, XX, XXVII, XXXII, XXXIV
7.164 ± 6	$\leq\frac{7}{2}^+$		γ	XIII, XX, XXVII
7.309 ± 6	$\frac{1}{2}^+$, $\frac{3}{2}^+$		γ	XVI, XX, XXVII
7.572 ± 8	$\leq\frac{7}{2}^+$		(γ)	XVI, XXVII
8.316 ± 6	$\frac{1}{2}^+$, $\frac{3}{2}^+$		γ	XX, XXVII
8.575 ± 8	$\leq\frac{7}{2}^+$		γ	XX, XXVII
9.062 ± 10	$\frac{1}{2}^+$, $\frac{3}{2}^+$		γ	XX, XXVII
9.165 ± 10			γ	XX, XXVII
9.834 ± 10			(γ)	XXVII
10.069 ± 10	$\leq\frac{5}{2}^-$		γ	XXVII
10.458 ± 10			γ	XIII, XXVII
10.548 ± 10	$\frac{5}{2}$, $\frac{7}{2}$		γ	XIII, XXVII
10.710 ± 10	$\frac{3}{2}^+$		γ	XIII, XIV, XXVII
10.815 ± 10	$\frac{3}{2}^-$		γ	XIII, XXVII
11.243 ± 10	$>\frac{1}{2}^-$	3.3	n	XXI, XXVII
11.299 ± 10	$\frac{1}{2}^-$	5.5 ± 1	γ, n, p	XIII, XV, XXI, XXIII
11.438 ± 10	$\frac{1}{2}^+$	40 ± 3	γ, n, p, α	II, XIII, XV, XXI, XXIII
11.61	$\frac{1}{2}^+$ [a]	450	γ, n, p	XIII, XV, XXX
11.773 ± 10	$\frac{3}{2}^+$	39 ± 3	n, p, α	II, XV, XXI, XXIII
11.885 ± 10	$\frac{3}{2}^-$	20 ± 2	n, p, α	II, XV, XXI
11.950 ± 10	$>\frac{1}{2}$	≤ 3	n, α	II, XXI
11.972 ± 10	$\frac{1}{2}^-$	16	n, p, α	XV, XXI
12.103 ± 10	$\frac{5}{2}$	19 ± 5	n, p, α	II, III, XV, XXI
12.152 ± 10	$\frac{3}{2}$	49	n, p, α	II, III, XV, XXI, XXIII, XXIV
12.333 ± 10	$\frac{5}{2}$	21 ± 3	n, p, α	XV, XXI
12.502 ± 10	$\frac{5}{2}^+$	28	n, p, α	II, III, XV, XXI, XXIV
12.928 ± 10	$\frac{3}{2}^-$	60	n, p, α	III, XV, XXI
12.93	$\frac{7}{2}^-$	30	p, α	III
13.15		<2	n, p, α	II, III
13.18		6	n, p, α	II, III
13.36	$\frac{3}{2}^-$	20	n, α	II, III
13.41	$\frac{5}{2}^+$	30	p, α	III
13.61	$(\frac{5}{2}^-)$	15	n, α	II, III
13.71		30	n, α	II
13.85		50	n, α	II
14.08		≈ 7	n, α	II
14.17		25	n, α	II
14.63		53	n, α	II
14.90			n, α	II
15.01			n, α	II
15.08			n, α	II
15.29			n, α	II
15.37			n, α	II

[a] $T = \frac{3}{2}$.

TABLE 15.2 (continued)

E_x in N^{15} (MeV±keV)	J^π	Γ (keV)	Decay	Reactions
15.61			n, α	II
15.92			n, α	II
15.93			n, α	II
15.99			n, α	II
16.04			n, α	II
16.47			p	VII
16.72		≈90	n, p, d	VI, VII
16.90		≈350	n, d	VI
17.11		broad	d, α	IX
17.24		≈170	t, d	VIII
17.37		≈350	p, α, t, d, n	VI, VII, VIII, IX
17.58		≈170	t, d	VIII
17.70		≈500	d, n, α	VI, IX
17.72		48 ± 9	p, α, d, t	VII, VIII, IX
18.07		19 ± 4	α, d	IX
18.09		≈45	p, d, t	VII, VIII
18.28		230 ±60	n, p, α, d	VI, VII, IX
19.16		≈130	n, d	VI

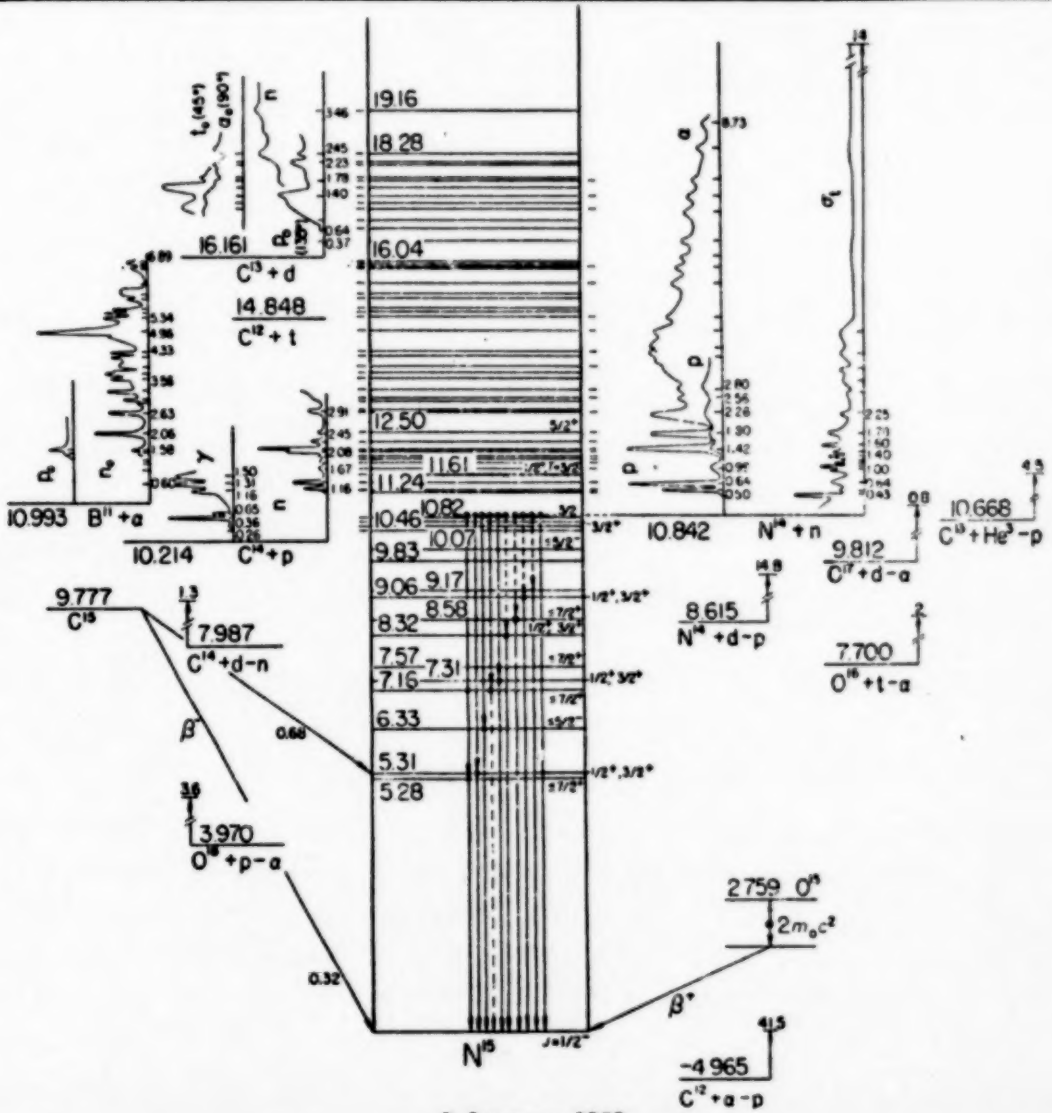

8 January 1959

Fig. 29. Energy levels of N^{15}: for notation, see fig. 1, p. 7.

TABLE 15.3

Resonances in $B^{11}+\alpha$

E_α (MeV)	Γ_{lab} (keV)	Particle Out	E_x (MeV)	J^π	Ref.
0.60		n	11.43		a
1.03		n	11.75		a
1.18		n	11.86		a
1.30		n	11.95		a
1.51		n, p	12.10		b
1.58		n, p	12.15		b
2.06	66	n_0, p_0	12.50	$\frac{5}{2}^+$	c
2.63	80	n_0, p_0	12.92	$\frac{3}{2}^-$	d
2.64	40	p_0	12.93	$\frac{7}{2}^-$	e
2.94	<3	n_0, p_0	13.15		d
2.99	8	n_0, p_0	13.18		d
3.23	29	n_0, p	13.36	$\frac{3}{2}^-$	d
3.30	40	p	13.41	$\frac{5}{2}^+$	e
3.56	20	n_0, p	13.61	$(\frac{1}{2}^-)$	d
3.71	40	n_0	13.71		f
3.90	70	n_0, (n_1)	13.85		f
4.21	≈10	n_0, n_1	14.08		f
4.33	35	n_0	14.17		f
4.96	72	n_0	14.63		f
5.34		n_0	14.90		g
5.49		n_0	15.01		g
5.58		n_0	15.08		g
5.86		n_0	15.29		g
5.98		n_0, n_2	15.37		g
6.30		n_0, (n_2)	15.61		g
6.72		n_0, (n_2)	15.92		g
6.74		n_0, n_2	15.93		g
6.82		n_0, n_2	15.99		g
6.89			16.04		g

[a] (Be 54, and private communication).
[b] (Sh 55c).
[c] (Sh 55c, Bo 56d, Ha 58c, Le 58b, Le 59).
[d] (Le 58b, Le 59, Bo 56d, Ha 58c).
[e] (Le 59).
[f] (Bo 56d, Ha 58c).
[g] (Ha 58c).

Ha 58c: see also Ho 50b). Some absolute cross sections are given by (Bo 56d). See also N^{14}.

III. $B^{11}(\alpha, p)C^{14}$ $\quad Q_m = 0.780$ $\quad E_b = 10.993$

Reported resonances are listed in table 15.3 (Sh 55c, Le 58b, Le 59). Angular distributions of the ground state protons have been measured at 150 energies in the range $E_\alpha = 2$ to 4 MeV. The assignment $J = \frac{5}{2}^+$ to $N^{15*}(12.50)$ agrees with an independent determination in $N^{14}(n, n)N^{14}$ (Le 58b). Partial widths for several resonances are listed by (Le 59). See also C^{14}.

IV. $C^{12}(t, p)C^{14}$ $Q_m = 4.634$ $E_b = 14.848$

See (Po 51).

V. $C^{12}(\alpha, p)N^{15}$ $Q_m = -4.965$

Proton groups have been observed corresponding to the ground state of N^{15} and to $N^{15*}(5.4)$, (6.5) and to other unresolved excited states up to $E_x \approx 13.5$ MeV (Sh 57, Bu 51, Bu 51c). Angular distributions have been studied at $E_\alpha = 30.5$ MeV (Hu 57a) and 41.5 MeV (Sh 57). They all show strong anisotropic structure typical of direct interaction. The ground state angular distribution is qualitatively similar to that of the inverse reaction. An excellent fit is obtained to the data $> 30°$ under the assumption l (triton) $= 1$, $R = 5.10 \times 10^{-13}$ cm (Sh 57, Sh 57b: see also Bu 57a).

VI. $C^{13}(d, n)N^{14}$ $Q_m = 5.319$ $E_b = 16.161$

Observed resonances are displayed in table 15.4 (Ri 50c, Ma 55j). Absolute cross sections are given by (Ma 55j). See also N^{14} and (Ja 57).

TABLE 15.4

Resonances in $C^{13}+d$

E_d (MeV)	Emitted particles	Γ (keV)	N^{15*} (MeV)	References
0.37	p		16.47	Va 56c
0.64	n, p_0	≈ 100	16.72	Ri 50c, Ko 53a, Ma 56c, Cu 50, Va 56c
0.85	n	≈ 400	16.90	Ri 50c
1.10	α_0	broad	17.11	Ma 56d
1.24 ± 0.04	t_0	≈ 200	17.24	Ma 56d
1.40 ± 0.04	p_0, α_0, t_0	≈ 400	17.37	Ma 56c, Ma 56d
1.55[a]	n	≈ 100		Ri 50c, Be 41
1.64 ± 0.04	t_0	≈ 200	17.58	Ma 56d
1.78 ± 0.05	n, α_0	≈ 600	17.70	Ri 50c, Ma 55j, Ma 56d
1.80 ± 0.01	(p_0), α_1, t_0	55 ± 10	17.72	Ma 56c, Ma 56d
2.20 ± 0.01	α_0, α_1	22 ± 4	18.07	Ma 56d
2.23 ± 0.02	p_0, t	≈ 50	18.09	Ma 56c, Ma 56d
2.45 ± 0.03	n, p_0, α_0	270 ± 70	18.28	Ma 55j, Ma 56c, Ma 56d
3.46 ± 0.03	n	≈ 150	19.16	Ma 55j

[a] Possibly to be identified with 1.40-MeV resonance (Ma 56d).

VII. $C^{13}(d, p)C^{14}$ $Q_m = 5.947$ $E_b = 16.161$

Observed resonances are displayed in table 15.4 (Ma 56c, Ko 53a, Cu 50, Be 41). Angular distributions have been measured at a number of energies in the range $E_d = 0.3$ to 2.8 MeV (Ko 53a, Ko 56f, Va 56c, Ma 56c). At most energies some stripping contribution is observed, although compound nucleus formation appears to be quite important for $E_d < 3$ MeV (Ma 56c). There is

some disagreement on absolute cross sections; see (Ko 53a, Va 56c, Ma 56c, Ho 57). See also C^{14}.

TABLE 15.5

Low-energy $C^{14}(p, \gamma)N^{15}$ resonances [a]

E_p (keV)	N^{15*} (MeV)	$\omega\Gamma_p$ (eV)	$\omega\Gamma_{\gamma_0}$ (eV)	$\omega\Gamma_{\gamma_5}$ (eV)	$\omega\Gamma_{\gamma_{5,4}}$ (eV)	l_p	J^π
261	10.458	$\approx 5\times10^{-4}$ [b]	$\approx 1\times10^{-4}$	$\approx 4\times10^{-4}$	$\approx 1\times10^{-4}$	$\leqq 4$	
351	10.542	$\geqq 0.04$	$\leqq 3\times10^{-4}$	0.018 [d]	0.025 [e]	$\leqq 3$	$(\frac{1}{2}^\pm, \frac{3}{2}^-)$
527	10.706	≈ 200 [c]	0.36	0.18		2	$\frac{3}{2}^+$
634	10.806	≈ 0.4 [b]	0.11	0.04			

[a] (He 57f, He 58f, He 59a); see also table 15.6.
[b] Estimated from γ-intensities in $N^{14}(d, p)N^{15}$: see (Ra 58b).
[c] $\theta_p^2 \approx 0.2$ (He 57f, He 59a).
[d] to $N^{15*}(5.28)$.
[e] to $N^{15*}(7.16)$. The ground state transition $(7.16 \rightarrow 0)$ is 3 times as strong as $(7.16 \rightarrow 5.28)$(He 59a)

TABLE

Resonances in $C^{14}(p, \gamma_0)N^{15}$

E_p [a] (keV)	Yields [b] 10^{-11} γ/p	Yields [b] 10^{-8} n/p	Γ [b] (keV)	Γ_n [b] (keV)	Γ_p [b] (keV)	Γ_α [a] (keV)
361	0.01					
537	5.7					
646	0.49					
1163±2	3.1	20	12	1.6	10.4	0
1312±3	7.9	120	43±5 [d]	24.4	15.0	0
1500	49	88	520 [d]	18.4	506	
1668±3		17	37	36.5	0.5	0
1788±3		1.5	24.5	24.5	0.03	0.05
1884±3		5.6	21.5	21.2	0.3	0.26
2025±4		40	18	17.2	0.8	0.6
2079±4		290	53	38	15	2.2
2272±4		10	22	21.7	0.3	0.1
2450±4			34±4	28	0.3	5.5
2908±4			71±5			

[a] (Sa 56d).
[b] (Ba 55l): see comparable values in (Sa 56d, Ro 51h).
[c] θ^2 as defined by (Ba 55l).
[d] (Fe 56a).

VIII. $C^{13}(d, t)C^{12}$ $Q_m = 1.313$ $E_b = 16.161$

Observed resonances are listed in table 15.4. Angular distributions and absolute cross sections are reported (Ma 56d). See also C^{12}.

IX. $C^{13}(d, \alpha)B^{11}$ $Q_m = 5.167$ $E_b = 16.161$

Observed resonances are listed in table 15.4. Angular distributions and

absolute cross sections are reported. Analysis of the narrow $E_\alpha = 2.2$-MeV resonance suggests that it is formed by $l_d = 3$ or 4 (Ma 56d). See also B^{11}.

X. $C^{13}(t, n)N^{15}$ $Q_m = 9.903$

Not reported.

XI. $C^{13}(He^3, p)N^{15}$ $Q_m = 10.668$

Proton groups have been observed corresponding to the ground state of N^{15} and to the levels at 5.3 MeV (unresolved) and 6.3 MeV; $E(He^3)$ to 4.5 MeV. Angular distributions show strong forward and backward peaking, roughly symmetric about 90°, and may indicate either compound nucleus formation or exchange stripping (Il 57, Jo 57b, Sc 56f). See also (Br 57) and O^{16}.

XII. $C^{13}(\alpha, d)N^{15}$ $Q_m = -7.683$

Not observed.

15.6
and $C^{14}(p, n)N^{14}$

Γ_{γ_0} [b] (eV)	J^π [b]	l_n	θ_n^2 [c]	l_p	θ_p^2 [c]	E_x (MeV)
(<0.004) [h]						10.551
(0.12) [h]	$(\frac{3}{2}^-)$ [h]					10.715
(0.010) [h]	$(\frac{5}{2}^-)$					10.817
0.29	$\frac{1}{2}^-$ [e]	1	0.002	1	0.04	11.299
2.4	$\frac{1}{2}^+$ [f]	0	0.01	0	0.007	11.438
26.3	$\frac{1}{2}^+$ [g]	0	0.001	0	1.0	11.61
	$\frac{3}{2}^+$	0	0.01	2	0.004	11.771
	$\frac{3}{2}^-$, $(\frac{5}{2}^-)$	1	0.01	3	0.003	11.883
	$\frac{1}{2}^-$	1	0.009	1	0.0004	11.972
	$\frac{3}{2}(^-)$ [e]	1	0.007	3	0.05	12.104
	$\frac{3}{2}(^+)$ [e]	0	0.008	2	0.06	12.154
	$\frac{5}{2}(^+)$	2	0.007	2	0.0009	12.335
	$(\frac{5}{2})$					12.501
						12.928

[e] See also (Ka 53).
[f] Assignment from $N^{14}(n, n)N^{14}$: see also (Ka 53).
[g] $T = \frac{1}{2}$.
[h] Compare table 15.5.

XIII. $C^{14}(p, \gamma)N^{15}$ $Q_m = 10.214$

Resonances for capture γ-radiation are listed in tables 15.5 and 15.6. The energies of the first four resonances (table 15.5) agree well with level energies derived from $N^{14}(d, p)N^{15}$ (He 58f, He 59a); corresponding values given by (Ba 55l) are 8 to 10 keV higher. Quoted limits on l_p in table 15.5 are based on estimates of Γ_p. The assignment $\frac{3}{2}^+$ to $N^{15*}(10.71)$ is based on

$C^{14}(p, p)C^{14}$ (He 58f, He 59a); the assignment $\frac{3}{2}^-$ gives a more satisfactory account of the p, γ_0 angular distribution both for this level and for $N^{15*}(10.81)$ (Ba 55l); $J = \frac{3}{2}^+$ is, however, not excluded for either (Ba 57m). Combination of N^{15*} (10.81) and (9.84) permits a good account of the low energy (n, n) and (n, γ) cross sections (He 59a). The thermal (n, p) cross section can be ascribed to the E_p=1.5 MeV resonance (N^{15*}=11.61) (Ba 55l: see also $N^{14}(n, \gamma)N^{15}$).

Strong interference effects in the (p, γ) yield curve indicate that the $E_p = 1.31$ and 1.59-MeV states have the same J^π (the former is given as $\frac{1}{2}^+$ from $N^{14}(n, n)N^{14}$) and that the $E_p = 1.16$-MeV state has opposite (odd) parity: $J = \frac{1}{2}^-, \frac{3}{2}^-$; $J = \frac{1}{2}^-$ is favored by $\sigma(n, n)$.

The $E_p = 1.66$-MeV state has even parity. Assignments for these four levels indicated in table 15.6 are consistent with the $C^{14}(p, n)N^{14}$ results (Ba 55l: see also Ka 53). The state at $E_p = 1.50$ MeV probably has $T = \frac{3}{2}$ and corresponds to C^{15}(g.s.) (Ba 55l, Ba 56a: see $C^{14}(p, n)N^{14}$). See also (Fe 56a, Sp 54).

XIV. $C^{14}(p, p)C^{14}$ $E_b = 10.214$

Elastic scattering has been studied for $E_p = 340$ to 690 keV. At the $E_p = 527$-keV resonance (see table 15.5), the scattering is consistent with d-wave formation of a $J = \frac{3}{2}^+$ state, $\Gamma_p = 0.2$ keV. No anomalies are observed at $E_p = 351$ or 635 keV (He 58f, He 59a).

XV. $C^{14}(p, n)N^{14}$ $Q_m = -0.628$ $E_b = 10.214$

Resonances reported by (Ba 55l, Sa 56d, Ba 54f, Ro 51h, Ka 53) are listed in table 15.6: see also (Gi 59). Neutron distributions are essentially isotropic at the $E_p = 1.16$, 1.31 and 1.50-MeV resonances and agree with the assignments derived from $C^{14}(p, \gamma)N^{15}$ and $N^{14}(n, n)N^{14}$; the distribution at $E_p = 1.67$ MeV favors $J = \frac{3}{2}$. At $E_p = 1.79$ MeV, the distributions favor $\frac{5}{2}^-$, but $\frac{3}{2}^-$ is not excluded (Ba 55l: see also Ka 53); a computation of the cross section favors $J = \frac{3}{2}$ (Sa 56d). At $E_p = 1.88$ MeV, the angular distribution is consistent with the $J = \frac{1}{2}^-$ assignment from $N^{14}(n, n)N^{14}$ and at $E_p = 2.02$ MeV the appearance of a $P_4(\cos\theta)$ term supports the assignment $J = \frac{5}{2}$, excluding $J = \frac{5}{2}^+$ (Ba 55l: compare table 15.7). Parities of this and the next two states disagree with $N^{14}(n, n)N^{14}$ results. The $E_p = 2.27$-MeV state has $J = \frac{3}{2}$ or $\frac{5}{2}$; the σ_{nn} clearly indicates the latter (Ba 55l, Sa 56d).

For $N^{15*}(11.61)$ ($E_p = 1.50$ MeV), the proton reduced width indicates a single-particle level, while the neutron reduced width is only 10^{-3}. This behaviour is taken to indicate that the level has $T = \frac{3}{2}$ and corresponds to C^{15}(g.s.); the predicted energy from $M(C^{15})$ is $N^{15*} = 11.7$ to 11.9 MeV (Ba 55l, Ba 56a).

XVI. $C^{14}(d, n)N^{15}$ $Q_m = 7.987$

Neutron groups have been observed corresponding to levels in N^{15} at 5.34, 6.32 and 7.46 MeV (Hu 50e). See also (Fr 56b; theo.).

XVII. $C^{14}(He^3, d)N^{15}$ $Q_m = 4.720$

Not reported.

XVIII. $C^{14}(\alpha, t)N^{15}$ $Q_m = -9.599$

Not reported.

XIX. $C^{15}(\beta^-)N^{15}$ $Q_m = 9.777$

See C^{15}.

XX. $N^{14}(n, \gamma)N^{15}$ $Q_m = 10.842$

$Q_0 = 10.833 \pm 0.008$ (Ba 57m).

The thermal cross section is 80 ± 20 mb (Ba 57m). Observed γ-rays are given in table 15.7 together with the N^{15} levels with which they are presumed

TABLE 15.7

Gamma radiation from $N^{14}(n, \gamma)N^{15}$ (Ba 57m, Ba 58k)

E_γ (MeV)	γ rays/100 captures [a]	Assignment [b]
10.833 ± 0.008	11	C→0
>9.152	≦0.3	
9.152 ± 0.010	1	9.16→0
9.03 ± 0.03	0.2	9.06→0
8.54 ± 0.04	0.2	8.57→0
8.313 ± 0.013	4	8.32→0
7.305 ± 0.012	9	7.31→0
(7.164)	≦0.8	
6.323 ± 0.008	17	6.33→0
5.559 ± 0.005	14	C→5.28
5.530 ± 0.008	18	C→5.31
5.293 ± 0.007	35	5.31→0
5.263 ± 0.010	22	5.28→0
4.497 ± 0.011	16	C→6.33
3.669 ± 0.016	17	C→7.16 [c]
3.520 ± 0.016	15	C→7.31
(3.267)	≦6	

[a] The intensity of the 7.57→0 transition is ≦0.7.

[b] C = capturing state.

[c] The direct ground state decay is ≦0.8.

to be associated. The decay scheme is in good accord with that derived from $N^{14}(d, p)N^{15}$ (Ba 57m). It does not appear that any of the known levels in this region can account for the large thermal cross section. The $T = \frac{3}{2}$, $J = \frac{1}{2}^+$ level at $N^{15*} = 11.61$ MeV gives the same capture radiation spectrum and accounts very well for the thermal $N^{14}(n, p)C^{14}$ cross section, but contributes only 0.4 mb to $\sigma_{n\gamma}$. The required level is presumably to be found below the neutron threshold, $N^{15*} = 10.2$ to 10.7 MeV, and should have a large

neutron and a small proton width, $J = \frac{1}{2}^+$ or $\frac{3}{2}^+$, and $\Gamma_{\gamma_0} = 1$ eV (Ba 55l): compare C^{14} (p, γ) (He 59a). See also (Ra 58b).

XXI. $N^{14}(n, n)N^{14}$ $E_b = 10.842$

The coherent scattering cross section is 11.0 ± 0.5 b; the total scattering cross section is 11.4 ± 0.5 b (bound atoms, epithermal neutrons: Hu 58). The large thermal scattering reflects a nearby bound level (Me 49b). The approximate equality of the two values indicates that the scattering has little spin-dependence (Fo 55). See (He 59a).

Resonances in the range $E_n = 0.4$ to 2.3 MeV are listed in table 15.8

TABLE

Resonances

E_n (keV)	Γ_{lab} (keV)	Γ_n (keV)	Γ_p (keV)	Γ_α (keV)	l_n	J^π
430± 5	3.5	<3	<0.01		≧1	≧$\frac{1}{2}$
495± 5	7.5	<3	<10		(1)	$\frac{1}{2}^-$ [c]
639± 5	43	34	9		0	$\frac{1}{2}^+$
998± 5	46	45	0.8		0	$\frac{1}{2}^+$
1120± 6	19	19	0.20	d	1	$\frac{3}{2}^-$
1188± 6	≦3.2	<2	<0.1		≧1	≧$\frac{1}{2}$
1211± 7	13	12	0.4	d	1	$\frac{3}{2}^-$
1350± 7	22	21	1.0	d	(2)	$\frac{5}{2}^{(+)}$
1401± 8	54	42	10	2	1	$\frac{3}{2}^{(-)}$
1595± 8	22	21	0.4	0.2	(1)	$\frac{3}{2}^{(-)}$
1779±10	24	18	6	0.2	2	$(\frac{5}{2}^+)$
2250		0.48Γ			1	$(\frac{3}{2}^-)$

[a] θ^2 as defined by (Hi 52).
[b] See (Hu 58).

(Jo 51a, Hi 52, Fo 55, Hu 55c, Hu 57, Hu 58). Angular distributions at and between these resonances have been studied by (Ba 50g, Fo 55). The potential s-wave phase shift approximately fits hard-sphere scattering ($R = 3.7 \times 10^{-13}$ cm) for $E_n < 1.3$ MeV: from 1.3 to 1.7 MeV, an abrupt increase (negative) appears, which may be associated with a shape resonance. The p-wave phase shift is somewhat smaller than the hard-sphere value; the d-wave shift is $< 3°$ (Fo 55: $E_n < 2.0$ MeV).

The narrow $E_n = 430$-keV resonance is formed by $l_n \geqq 1$; the proton width is very small, and the level has not been detected in C^{14}+p. The $E_n = 495$-keV resonance appears strongly in $N^{14}(n, p)C^{14}$ and $C^{14}(p, n)N^{14}$, but not in elastic scattering. The two resonances at $E_n = 639$ and 998 keV are s-wave, assigned $J = \frac{1}{2}^+$ and $\frac{3}{2}^+$ respectively from $\sigma_{max} - \sigma_{min}$ (Jo 51a, Hi 52). According to (Fe 56a) an additional broad $J = \frac{1}{2}^+$ level is located in this region ($C^{14}(p, n)N^{14}$; $E_p = 1.5$ MeV: $N^{14*} = 11.61$ MeV), presumably the first $T = \frac{3}{2}$ state. This level has not appeared in $N^{14}(n, n)N^{14}$; see e.g.

(Fo 55). The $E_n = 1120$-keV resonance is given as $J = \frac{3}{2}$ or $\frac{5}{2}$ from cross sections; the angular distributions favor $\frac{3}{2}^-$ (Fo 55). The narrow 1188-keV resonance does not appear in (C^{14}+p) (Sa 56d). Aside from the $J = \frac{1}{2}^-$ resonance at $E_n = 1211$ keV, the remaining J^π assignments disagree with those derived from C^{14}+p (compare (Fo 55) and (Ba 55l)). For the $E_n = 2250$-keV resonance, (Fo 55) find $J = \frac{3}{2}^-$, while (Me 53a) report $J = \frac{1}{2}^-$. From $E_n = 1.8$ to 4.0 MeV, there is evidence for considerable structure in the cross section curve, but little agreement as to the exact location of the levels involved. (Me 53a) list 14 maxima in the total cross section for $E_n = 1.9$ to 3.6 MeV. Angular distributions have been studied by (Hu 54b)

15.8
in N^{14}+n

θ_n[a] (%)	θ_p[a] (%)	θ_α[a] (%)	N^{15*} (MeV)	References[b]
			11.243	(Jo 51a, Hi 52)
(0.1)	(1.8)		11.301	(Hi 52)
0.9	0.4		11.439	(Jo 51a, Hi 52)
1.0	0.6		11.774	(Jo 51a, Hi 52)
0.8	0.08		11.887	(Jo 51a, Hi 52, Fo 55)
			11.950	(Hi 52)
0.5	0.02		11.972	(Hi 52)
6	0.7		12.102	(Jo 51a, Hi 52, Fo 55)
1.5	0.7	5	12.150	(Jo 51a, Hi 52, Fo 55)
0.7	3.0		12.331	(Hi 52, Fo 55)
3.0	0.07	14	12.503	(Hi 52, Fo 55)
			12.94	(Fo 55, Hu 57, Me 53a)

[a] Assignments by (Sa 56d), based on quoted σ_{nn}, $\sigma_{n\alpha}$, σ_{np}.
[b] See table 15.6.

for energies between 3.2 and 3.9 MeV. The observed distributions can be accounted for by seven levels in the range 2.5 to 4.4 MeV with $J = \frac{3}{2}^+$ to $\frac{7}{2}^+$ (Sp 54c, Sp 54d). See also (Aj 55, Be 56c, Fl 56a, Hu 57).

XXII. $N^{14}(n, 2n)N^{13}$ $\quad Q_m = -10.551$ $\quad E_b = 10.842$

At $E_n = 14.3$ MeV, the cross section is 4.5 ± 0.8 mb (Hu 55c), 19 ± 10 mb (As 58), 8.5 mb (Ra 58g). See also (Sm 55a).

XXIII. $N^{14}(n, p)C^{14}$ $\quad Q_m = 0.628$ $\quad E_b = 10.842$

The thermal cross section is 1.75 ± 0.05 b (Hu 58) A major portion of this cross section can be ascribed to $N^{15*}(11.61)$ (Ba 55l). Resonances reported by (Jo 50b) occur at $E_n = 495$, 640, (993), and 1415 keV; parameters are listed in table 15.8 (Hu 55c, Hu 58). Many additional levels have been reported through analysis of particle groups induced by continuous neutron spectra: see (Gi 53a, Aj 52c, Be 57e).

XXIV. $N^{14}(n, \alpha)B^{11}$ $Q_m = -0.152$ $E_b = 10.842$

(Jo 50b) report resonances at $E_p = 1415$ and 1800 keV: see table 15.8 (Hu 55c). See also $N^{14}(n, p)C^{14}$ above.

XXV. $N^{14}(n, d)C^{13}$ $Q_m = -5.319$ $E_b = 10.842$

See (Li 52, Ca 57e, Za 57), N^{14} and C^{13}.

XXVI. (a) $N^{14}(n, t)C^{12}$ $Q_m = -4.007$ $E_b = 10.842$

(b) $N^{14}(n, t)3He^4$ $Q_m = -11.287$

For reaction (a), see (Fi 53). For reaction (b), see (Fr 56a).

XXVII. $N^{14}(d, p)N^{15}$ $Q_m = 8.615$

Proton groups corresponding to levels of N^{15} are listed in table 15.9. The J^π assignments are based on stripping analysis of angular distributions

TABLE 15.9

N^{15} levels from $N^{14}(d, p)N^{15}$

A	E_x (in MeV) B	C	l_n	$(2J+1)\theta^2$ [j]	J^π
0			1 [a]	0.097	$\frac{1}{2}^-$, $\frac{3}{2}^-$, $\frac{5}{2}^-$
5.276±0.006	5.280±0.010		2 [b]	0.03	$\leq\frac{7}{2}^+$
5.305±0.006			X [bc]		
6.328±0.006	6.330±0.010		1 [d]	0.035	$\frac{1}{2}^-$, $\frac{3}{2}^-$, $\frac{5}{2}^-$
7.164±0.006	7.165±0.010		2 [e]	0.32	$\leq\frac{7}{2}^+$
7.309±0.006	7.314±0.010	7.307±0.008	0 [e]	0.45	$\frac{1}{2}^+$, $\frac{3}{2}^+$
	7.575±0.010	7.570±0.008	2 [f]	0.41	$\leq\frac{7}{2}^+$
8.315±0.006	8.316±0.010	8.319±0.008	0 [d]	0.40	$\frac{1}{2}^+$, $\frac{3}{2}^+$
	8.571±0.010	8.577±0.008	0+2 [g]	0.03	$\leq\frac{7}{2}^+$
	9.062±0.010		0 [h]		$\frac{1}{2}^+$, $\frac{3}{2}^+$
	9.165±0.010		X [ch]		
	9.834±0.010				
	10.069±0.010		1 [e]	0.14	$\frac{1}{2}^-$, $\frac{3}{2}^-$, $\frac{5}{2}^-$
	10.458±0.010		X [ch]		
	10.544±0.010		X [ch]		
	10.705±0.010		X [ch]		
	10.811±0.010		X [ch]		
	11.2		1 [i]	0.24	$\frac{1}{2}^-$, $\frac{3}{2}^-$, $\frac{5}{2}^-$

A (Ma 50i); $E_d = 1.4$ MeV, $\theta = 90°$.

B (Sp 54e); $E_d = 5$ to 8.5 MeV; $\theta = 90°$. Accurate level separations are also given.

C (Do 56c); E_x based on Q_m; Q's given by (Do 56c) are given to ±1 or 1.5 keV.

[a] (Gi 52, Wa 57).

[b] (Sh 55b; see Wa 58c).

[c] Isotropic: no clear stripping pattern.

[d] (Gi 52, Gr 56b, Sh 55b, Wa 57).

[e] (Sh 55b, Gr 56b).

[f] (Gr 56b): (Wa 57) find a possible $l = 0$ component.

[g] (Sh 55b, Wa 57).

[h] Sharp, Buechner and Sperduto, to be published.

[i] (Gr 56b).

[j] (Gr 56b, Wa 57, Ha 57b).

(Ma 50i, Sp 54e, Do 56c, Gi 52, Sh 55b, Wa 57, Gr 56b). A detailed comparison of the experimental observations with shell-model calculations is made by (Ha 57b; see also Wa 57). Angular distributions have also been studied by (Jo 54c, Eb 54, Va 56c, Bo 58a). The ratio of the reduced widths of the ground states of N^{15} and O^{15} is 1.71 (Ca 56b; $E_d = 9$ MeV).

Observed gamma rays are listed in table 15.10 (Be 55g, Ra 58b). The observation of a 10.81-MeV γ-ray indicates a small proton width for the

TABLE 15.10

Gamma rays from $N^{14}(d, p)N^{15}$ [a]

E_γ (MeV) [b]	Relative gamma intensity [c]
5.26 ±0.04	47 [d]
6.33 ±0.05	10
7.31 ±0.04	33
8.321±0.020	10
9.07 ±0.04	3.0
10.03 ±0.04	3.6
10.81 ±0.04	0.8

[a] (Be 55g, Ra 58b).

[b] Doppler corrected.

[c] The ground state decay of a number of known levels of N^{15} (see table 15.9) has not been observed; the upper limit to the relative gamma intensity is given in parenthesis following the energy of the level: 7.17 (2.0), 7.58 (1.4), 8.57 (0.7), 9.17 (1.5), 9.83 (1.1), 10.46 (<0.4), 10.54 (0.3). See also $N^{14}(n, \gamma)N^{15}$.

[d] Includes some contribution from $N^{14}(d, n)O^{15*}$.

N^{15} level; it is suggested that this level may account for the large (n, γ) cross section (Ra 58b). According to (Ba 55l, He 58f), however, the γ-spectra are quite different: see tables 15.5, 15.7. A 1.88-MeV γ-ray is reported by (Th 54d), attributed to N^{15*} 7.16 → 5.2. A p—γ correlation experiment suggests that the 5.3-MeV radiation is dipole (St 54f). The relative intensities of the 7.31-MeV γ-ray and of the O^{15} 6.81-MeV radiation have been determined at several energies by (Be 55h). See (Sh 57b, El 56b, Ha 57b, Fr 56b: theo.).

XXVIII. $N^{14}(t, pn)N^{15}$ $Q_m = 2.357$

See (Cu 52a).

XXIX. $N^{14}(\alpha, He^3)N^{15}$ $Q_m = -9.736$

Not reported.

XXX. $N^{15}(\gamma, p)C^{14}$ $Q_m = -10.214$

With bremsstrahlung of $E_{max} = 18.7$ and 24.6-MeV, photoprotons corresponding to the ground state and excited states of C^{14} are observed. Peaks in the yield appear at $E_\gamma = 11.6$, ≈ 15, ≈ 18.6 MeV, in addition to the giant resonance at ≈ 20 MeV. The first peak corresponds to excitation of N^{15*} ($J = \frac{1}{2}^+$, $T = \frac{3}{2}$): the angular distribution is consistent with isotropic

emission. At 15 MeV, the distribution indicates dipole absorption, while the giant resonance shows a predominently $\sin^2\theta$ distribution (Rh 58a, Rh 58b).

XXXI. $O^{15}(\beta^+)N^{15}$ $Q_m = 2.759$

See O^{15}.

XXXII. $O^{16}(\gamma, p)N^{15}$ $Q_m = -12.113$

Transitions have been observed to the 5.3 and 6.3-MeV levels of N^{15} (St 55a, Sv 57). See also O^{16}.

XXXIII. $O^{16}(n, d)N^{15}$ $Q_m = -9.884$

See (Li 52).

XXXIV. $O^{16}(p, 2p)N^{15}$ $Q_m = -12.113$

At $E_p = 185$ MeV, the summed proton spectrum shows two peaks, corresponding to ejection of $p_{\frac{1}{2}}$ and $p_{\frac{3}{2}}$ protons with binding energies of ≈ 12 and ≈ 19 MeV, respectively. The separation is consistent with the interpretation of $N^{15*}(6.3)$ as a state with a hole in the $p_{\frac{1}{2}}$ shell (Ty 58b, Ma 58h).

XXXV. $O^{16}(d, He^3)N^{15}$ $Q_m = -6.619$

Not reported.

XXXVI. $O^{16}(t, \alpha)N^{15}$ $Q_m = 7.700$

See (Ja 56e, Ba 56f, Ma 56k).

XXXVII. $O^{17}(d, \alpha)N^{15}$ $Q_m = 9.812$

$Q_0 = 9.807 \pm 0.012$ (Pa 54).

XXXVIII. $O^{18}(p, \alpha)N^{15}$ $Q_m = 3.970$

$Q_0 = 3.961 \pm 0.009$ (Mi 54a).

See (Aj 52c, Ri 55b) and F^{19}.

O^{15}

(Fig. 30, p. 195) †

THEORY

See (Ta 57a, Fr 58b).

MASS OF O^{15}

The most precise determination of the mass difference $O^{15}-N^{15}$ comes from $N^{15}(p, n)O^{15}$, where (Jo 58c) find $E_{thresh} = 3.7808 \pm 0.0011$ MeV: this value, with $(n-H^1) = 0.783$ MeV leads to $O^{15}-N^{15} = 2.7595$. Including the (p, n) value of (Ki 55c) and the two $O^{15}(\beta^+)N^{15}$ values of (Ki 57), one obtains a weighted mean of $O^{15}-N^{15} = 2.7586 \pm 0.0012$, or O^{15} (mass excess) $= 7.287 \pm 0.005$ MeV, 54 keV higher than the value of (Wa 55c).

† For level scheme of N^{15}, see fig. 29, p. 181.

I. $O^{15}(\beta^+)N^{15}$ $Q_m = 2.759$

The maximum positon energy is 1.723 ± 0.005 MeV, 1.736 ± 0.010 MeV; the mean of these and two values from $N^{15}(p, n)O^{15}$ is 1.733 ± 0.005 MeV (Ki 57); an earlier report by (Br 50d) appears to be in error. The half-life is 123.4 ± 1.3 sec (Kl 54), 121 ± 3 sec (Ba 55g), 120 ± 2 sec (Ki 57), 123.95 ± 0.50 sec (Pe 57): mean $= 123.6 \pm 0.45$ sec. Log $ft = 3.64$. See also (Be 58e; theo.).

II. $Li^7(N^{14}, He^6)O^{15}$ $Q_m = -2.706$

See (Al 58d).

III. (a) $B^{10}(Li^6, n)O^{15}$ $Q_m = 15.218$
(b) $B^{10}(Li^7, 2n)O^{15}$ $Q_m = 7.965$

See (No 57a).

IV. (a) $C^{12}(He^3, p)N^{14}$ $Q_m = 4.772$ $E_b = 12.071$
(b) $C^{12}(He^3, n)O^{14}$ $Q_m = -1.159$
(c) $C^{12}(He^3, \alpha)C^{11}$ $Q_m = 1.856$
(d) $C^{12}(He^3, d)N^{13}$ $Q_m = -3.553$

Resonances in the yields of reactions (a) and (b) are displayed in table 15.12 (Br 57, Jo 58). Differential cross sections and angular distributions have been determined to $E(He^3) = 5$ MeV for the p_0, p_1 and p_2 groups. At low energies, the distributions tend to be symmetric; at the higher energies they become more complex; they seem to conform neither to compound nucleus or stripping theory, and it must be concluded that features of both processes are present (Br 57, Jo 58). Consideration of the relative yields of the first four resonances lead to the tentative J^π assignments given in the table (Br 57). Neutron angular distributions have been determined in the range $E(He^3) = 1.89$ to 2.51 MeV: they are asymmetric at the higher energies. The ratio of the cross sections of the (He^3, n) and (He^3, p_1) reactions (both to the first $T = 1$ states of the $A = 14$ triad) has been determined at a number of energies for $E(He^3) = 1.8$ to 2.6 MeV. The ratio approaches the theoretically predicted value of 2 at the higher energies. The ratio of the (He^3, α_0) to the (He^3, n_0) cross sections has been determined at two energies; the large cross section for the former suggests a direct interaction (Br 57). The yields of C^{11} and N^{13} have been determined for $E(He^3) = 13$ to 21 MeV by (Co 58d). See also C^{11}, N^{14} and O^{14}.

V. $C^{12}(\alpha, n)O^{15}$ $Q_m = -8.507$

See (Ki 57, Ki 39).

VI. $C^{13}(He^3, n)O^{15}$ $Q_m = 7.126$

Not reported.

VII. $N^{14}(p, \gamma)O^{15}$ $Q_m = 7.300$

Observed resonances are listed in table 15.13 (Du 51, Ba 55g, Ov 56, Pi 57a). The cross section increases from $(8.5 \pm 3.7) \times 10^{-12}$ b at 100 keV to $(140 \pm 30) \times 10^{-12}$ b at 135 keV (La 57f). Extrapolation of the 278-keV resonant yield

TABLE 15.11

Energy levels of O^{15}

E_x in O^{15} (MeV ± keV)	J^π	$\tau_{\frac{1}{2}}$ or Γ (sec) (keV)	Decay	Reactions
0	$(\frac{1}{2})^-$	$\tau_{\frac{1}{2}} = 123.6 \pm 0.45$	β^+	I, II, III, V, XII, XV, XXI, XVIII
5.195 ± 10			γ	VII, XII, XXI
5.247 ± 10				
6.15 ± 30	$(\leq \frac{1}{2}^-)$		γ	VII, XII
6.792 ± 9	$\frac{1}{2}^+, \frac{3}{2}^+$		γ	VII, XII
6.860 ± 9				
7.560 ± 2	$\frac{1}{2}^+$	1.5 ± 0.5	p, γ	VII, IX, XII
8.291 ± 4	$\frac{3}{2}^+$	3 ± 1	p, γ	VII, IX, XII
8.747 ± 7	$\frac{1}{2}^+$	32	p, γ	VII, IX
8.928 ± 5	$(\leq \frac{3}{2})$	4 ± 1	p, γ	VII, IX
8.988 ± 6	$\frac{1}{2}^-, \frac{3}{2}^-$	4 ± 1	p, γ	VII, IX, XII
9.47	$\frac{1}{2}$	510	p, γ	VII, IX
9.497 ± 12		13 ± 4	p, γ	VII, IX
9.619 ± 12		10 ± 3	p, γ	VII, IX
9.666 ± 4		< 8	p	IX
10.29 ± 80			p	IX
10.47			p	IX
10.949 ± 8	$\geq \frac{1}{2}$	77 ± 14	p	IX
11.030 ± 10		< 14	p	IX
11.780 ± 20		75	p	IX
11.864 ± 15		65	p, α	IX, XI
12.3		broad	p, α	XI
12.5		broad	p, α	XI
13.04 ± 20	$(\frac{1}{2}^-)$		He^3, p, α	IV, XI
13.1			He^3, p	IV
13.79	$(> \frac{1}{2})$		He^3, p, n	IV
14.09	$(\frac{1}{2}^+)$		He^3, p, n	IV
14.2			He^3, p, n	IV
14.5			He^3, p	IV
15.0			He^3, p	IV
15.6			He^3, p	IV
15.9			He^3, p	IV

and s-wave background from the broad 2600-keV resonance yields cross section values in good agreement with those of (La 57f). Judging from N^{15}, one level near 7 MeV in O^{15} remains undiscovered (Pi 57a); see $N^{14}(p, p)N^{14}$.

At the 277-keV resonance ($E_x = 7.56$ MeV), capture gamma rays resulting from cascades through O^{15} states at 5.2, 6.1 and 6.7 MeV are observed, with partial radiative widths of 0.003 eV, 0.008 eV and 0.002 eV, respectively (± 25 per cent). The direct ground-state transition has not been observed:

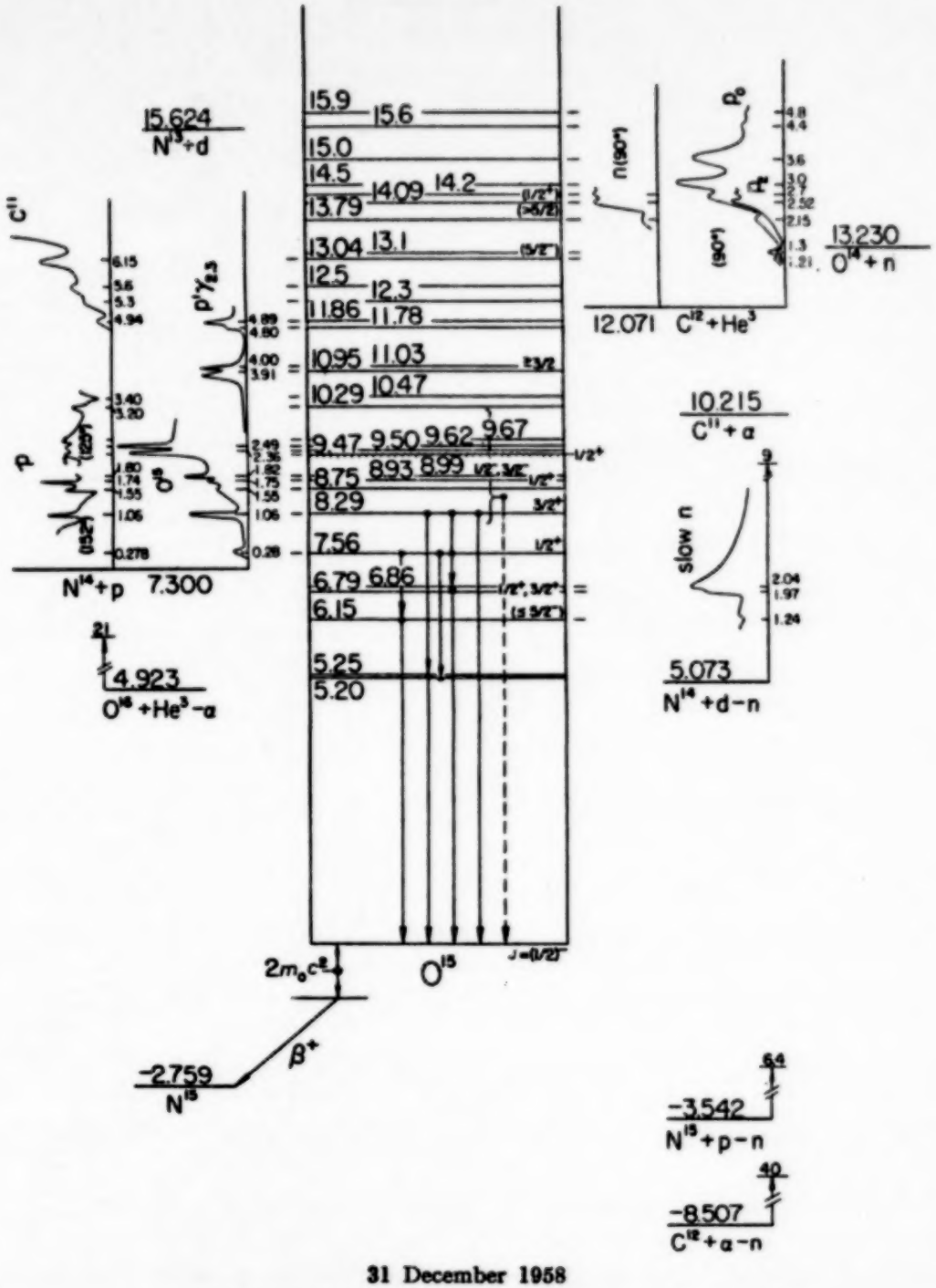

31 December 1958

Fig. 30. Energy levels of O^{15}: for notation, see fig. 1, p. 7.

the relative intensity is less than 5 per cent of the 6.10-MeV line (Ba 55g; see also Jo 52b). Asymmetry (7 ± 3 per cent) in the ratio of 6.1 and 5.2-MeV γ-rays indicates that the 7.56-MeV state is not formed by s-waves. It is suggested that $J = \frac{5}{2}$ (Ba 55g). (Ov 56, Pi 57a) find, on the other hand, that

TABLE 15.12

Resonances in $C^{12}+He^3$

$E(He^3)$ [a] (MeV)	Resonant for:	E_x (MeV)	J^π
1.21	p_0, p_2	13.04	$(\frac{1}{2}^-)$
1.3	p_0, p_1, p_2, p_2	13.1	
2.15	p_0, n	13.79	$(>\frac{1}{2})$
2.52	p_0, p_1, p_2, p_2, n	14.09	$(\frac{1}{2}^+)$
2.7	p_1, p_2, n	14.2	
3.0	p_0, p_1, p_2	14.5	
3.6	p_0, p_1, p_2	15.0	
4.4	p_0, p_1, p_2	15.6	
4.8	p_0, p_1, p_2	15.9	

[a] The first five resonances are primarily from (Br 57), the last four from (Jo 58).

TABLE 15.13

Resonances from $N^{14}(p, \gamma)O^{15}$ (Du 51)

E_p [e] (keV)	Γ [e] (keV)	$\omega\Gamma_\gamma$ [e] (eV)	J^π	O^{15*} [e] (MeV)
277	1.9± 0.5 [c]	0.013 [b]	$(\frac{1}{2})$ [b], $(\frac{1}{2}^+)$ [c]	7.559
1064± 2	4.8± 1	0.63	$\frac{3}{2}$ [d]	8.293
1550±20	50 ±20	0.16	$\frac{1}{2}^+$ [a]	8.747
1748± 5	11 ± 3	0.21		8.931
1815± 4	7 ± 1.5	0.52		8.994
2356± 8	14 ± 4	2.4		9.499
2489± 7	11 ± 3	3.3		9.623
2600±50 [f]	1270 ±50	46	$(\frac{1}{2}^+, \frac{3}{2}^+)$	9.73

[a] From $N^{14}(p, p)N^{14}$.
[b] (Ba 55g).
[c] (Ov 56, Pi 57a).
[d] (Ga 57a, Go 57h, Go 57i).
[e] See also table 15.14 ($N^{14}(p, p)N^{14}$).
[f] Presumably to be identified with O^{15*}(9.465), table 15.14 (Fe 59b).

the 0.75 and 1.35-MeV γ-rays are isotropic and conclude that $J = \frac{1}{2}^+$: see $N^{14}(p, p)N^{14}$. The transition (7.56 → 5.2) appears to involve O^{15*}(5.20) and not (5.25) (B. Povh and D. Hebbard, priv. comm.). (It is not clear why the ground state decay (E1) should not occur.) The structure formerly attributed to a broad resonance at $E_p = 0.7$ MeV (Du 51) is probably due to direct capture (see Ha 57). At the 1.06-MeV resonance ($E_x = 8.28$ MeV), transitions are observed through the 5.2 and 6.8—6.9-MeV states in addition to the direct ground state transition (Li 53). A p—γ correlation study indicates $J = \frac{3}{2}$ for the 8.28-MeV state (Go 57h, Go 57i, Ga 57a, Go 58d).

VIII. $N^{14}(p, n)O^{14}$ $Q_m = -5.930$ $E_b = 7.300$

See (Ta 58a) and O^{14}.

IX. (a) $N^{14}(p, p)N^{14}$ $E_b = 7.300$

(b) $N^{14}(p, p')N^{14*}$

The yield of elastic protons, of inelastic protons and of 2.3-MeV γ-rays has been examined to $E_p = 5.1$ MeV: see table 15.14. The scattering

TABLE 15.14

Anomalies in $N^{14}(p, p)N^{14}$ and $N^{14}(p, p'\gamma)N^{14}$

E_p (keV)	Γ (keV)	$\omega\Gamma_\gamma$ [e] (eV)	θ_p^2 [e] (%)	J^π	E_x (MeV)	Ref.
278.1 ± 0.4	1.5 ± 0.5			$\frac{1}{2}^-$	7.560	a
1058 ± 3	3 ± 1	0.40	0.29 [b]	$\frac{3}{2}^+$	8.288	e, h, g
1550 ± 6	34	0.11	1.6 [b]	$\frac{1}{2}^+$	8.747	e, f, h, g
1740 ± 4	4 ± 1	0.076	0.13 [b]	$(\leq \frac{1}{2})$	8.924	e, f, h, g
			1.7 [c]			
1801 ± 5	4 ± 1	0.30	0.28 [d]	$(\frac{1}{2}^-, \frac{3}{2}^-)$	8.981	e, f, h, g
2320	550			$\frac{1}{2}^+$	9.465	f, i
2350 ±10					9.494	f, g
2480 ±10					9.614	f, g
2535 ± 3	<8				9.666	j
3200 ±10					10.29	f, k
3400 ±10					10.47	f
3910 ± 8	82 ±15			$\geq \frac{1}{2}$	10.949	l, m, n, j
4000 ± 8	<15				11.033	l, m, j
4800 ±20	80				11.780	l
4890 ±10	70				11.864	l, m

[a] (Ov 56, Pi 57a).
[b] Assuming s-waves.
[c] Assuming d-waves.
[d] Assuming p-waves.
[e] (Ha 57).
[f] (Bo 57b).
[g] (Fe 56c, Fe 59a).
[h] (Ta 56a).
[i] (Fe 58, Fe 59a, Fe 59b).
[j] (Ol 57).
[k] (Ba 56c).
[l] (Ba 56i): $N^{14}(p, p'\gamma)N^{14}$.
[m] (Th 55b).
[n] (Do 58).

anomalies are superposed on a background which decreases less rapidly than the Rutherford cross section; for $E_p < 2.3$ MeV, the background is largely s-wave, with some p-wave contribution above $E_p = 1.5$ MeV (see Ha 57, Ta 56a, Ba 56c, Fe 58, Fe 59a, Bo 57b). (Fe 59b) finds that two s-wave and one p-wave phase shifts are required to fit the non-resonant angular distributions above $E_p = 1$ MeV.

Data taken near the 277-keV resonance, $O^{15*} = 7.56$ MeV, at three angles, are consistent only with s-wave formation. The magnitude of the anomaly indicates $J = \frac{1}{2}^+$, $\Gamma = 1.5$ keV (Ov 56, Pi 57a). The 1054-keV resonance, $O^{15*} = 8.28$ MeV, is also formed by s-waves, but the anomaly indicates $J = \frac{3}{2}^+$ (Ha 57: see, however, Ta 56a). Calculation of level shifts suggests identification of these two states with $N^{15*}(8.32)$ and (8.57). The mirror of $O^{15*}(6.79)$ is probably $N^{15*}(7.31)$; $O^{15*}(6.86)$ may correspond either to $N^{15*}(7.16)$ or (7.57). In either case, one O^{15} level remains to be discovered in this region (Pi 57a: see also Ha 57). The 1544-keV resonance is again s-wave, $J = \frac{1}{2}^+$. Assignments for the $E_p = 1737$ and 1799-keV resonances are not certain (Ha 57). The broad resonance at $E_p = 2.3$ MeV, $O^{15*}(9.465)$, is s-wave, $J = \frac{1}{2}^+$ (Fe 58, Fe 59b). It is suggested that the apparent breadth of this level reported in $N^{14}(p, \gamma)$ may reflect some contribution from direct capture (Fe 59b).

Elastic scattering has also been studied at $E_p = 9.8$ MeV (Hi 57a), at 14.5, 20 and 31.5 MeV (Ki 56) and at 20.0 MeV (Ch 57). See also (Ja 57b) and N^{14}.

X. $N^{14}(p, d)N^{13}$ $\quad Q_m = -8.324$ $\quad E_b = 7.300$

See N^{13} and N^{14}.

XI. $N^{14}(p, \alpha)C^{11}$ $\quad Q_m = -2.916$ $\quad E_b = 7.300$

Broad resonances in the yield of C^{11} are observed at $E_p = 4.94$, 5.3, 5.6 and 6.15 MeV, corresponding to $O^{15*} = 11.91$, 12.3, 12.5 and 13.04 MeV (Bl 52a: stacked foil method).

XII. $N^{14}(d, n)O^{15}$ $\quad Q_m = 5.073$

$Q_0 = 5.15 \pm 0.16$ (Ev 53).

$Q_0 = 5.13 \pm 0.05$ (No 57b).

Neutron groups are listed in table 15.15, together with J^π assignments obtained from stripping analysis of the angular distributions. Except for the ground state and the level (s) at 6.8 MeV, the fits to the theoretical distributions are not completely satisfactory, and the assignments must be treated with some reserve (Ev 53). See also (No 56, No 57b). At $E_d = 9$ MeV, the ratio of the ground state reduced widths of N^{15} and O^{15} (from the maximum cross sections of the (d, p) and (d, n) reactions) is 1.71 (Ca 56b). Neutron thresholds have been observed at $E_d = 1.24 \pm 0.02$, 1.967 ± 0.004 and 2.044 ± 0.004 MeV, corresponding to $O^{15*} = 6.15 \pm 0.03$, 6.792 ± 0.009 and 6.860 ± 0.009 MeV (Ma 55m).

At $E_d = 4.0$ MeV, γ-radiation has been observed with $E_\gamma = 6.81 \pm 0.04$, 6.12 ± 0.06 and 5.26 ± 0.04 MeV (the latter probably includes $N^{14}(d, p)N^{15}$) (Be 55g; corrected for Doppler shift). Relative cross sections for the N^{14}(d,

p)N^{15*}(7.31) and N^{14}(d, n)O^{15*} (6.81) γ-rays are given by (Be 55h) for three energies. See also (Fr 56b; theo.) and O^{16}.

TABLE 15.15

O^{15} levels from N^{14}(d, n)O^{15}

O^{15*} (MeV)	l_p	$\leq J^\pi$
0	1 [b]	$\leq \frac{1}{2}^-$
5.29 ±0.17 [a]	2	$(\leq \frac{3}{2}^+)$
6.15 ±0.03 [c]	1	$(\leq \frac{1}{2}^-)$
6.792±0.009 [c]	0	$\frac{1}{2}^+, \frac{3}{2}^+$
6.860±0.009		
7.48 ±0.16 [a]	1	$(\leq \frac{1}{2}^-)$
8.42 ±0.16 [a]	1	$(\leq \frac{1}{2}^-)$
9.06 ±0.16 [a]	1	$(\leq \frac{1}{2}^-)$

[a] (Ev 53): $E_d = 7.7$ MeV.
[b] (Ev 53) and (No 56, No 57b: $E_d = 1.9$ MeV).
[c] From slow neutron thresholds (Ma 55m).

XIII. $N^{14}(He^3, d)O^{15}$ $Q_m = 1.806$

Not reported.

XIV. $N^{14}(\alpha, t)O^{15}$ $Q_m = -12.513$

Not reported.

XV. $N^{15}(p, n)O^{15}$ $Q_m = -3.542$

$E_{thresh} = 3.776 \pm 0.008$; $Q_0 = -3.539 \pm 0.008$ (Ki 55c)

$E_{thresh} = 3.7808 \pm 0.0011$; $[Q_0 = -3.5425 \pm 0.0011]$ (Jo 58c).

XVI. $N^{15}(He^3, t)O^{15}$ $Q_m = -2.777$

Not reported.

XVII. $O^{16}(\gamma, n)O^{15}$ $Q_m = -15.655$

See (Sv 57).

XVIII. $O^{16}(n, 2n)O^{15}$ $Q_m = -15.655$

See (Aj 55).

XIX. $O^{16}(p, d)O^{15}$ $Q_m = -13.428$

Not reported.

XX. $O^{16}(d, t)O^{15}$ $Q_m = -9.396$

Not reported.

XXI. $O^{16}(He^3, \alpha)O^{15}$ $Q_m = 4.923$

At E (He^3) = 3 MeV, α-groups are observed corresponding to levels at $E_x = 5.195 \pm 0.01$ and 5.247 ± 0.01 MeV. The separation is 52 ± 5 keV (Po 59). From a similar experiment, excitations of 5.185 and 5.244 MeV are reported (K. W. Allen, R. Middleton and S. Hinds, private communication). See also (Po 52b, Ku 53a).

XXII. $O^{17}(p, t)O^{15}$ $Q_m = -11.316$

Not reported.

F^{15}

(Not illustrated)

MASS OF F^{15}

Calculation of Coulomb and ($n-H^1$) mass differences from C^{15} indicates that F^{15} should be unstable to proton emission by 2.3 MeV (Mu 57a): the mass excess of F^{15} is 22.0 ± 1 MeV.

N^{16}

(Fig. 31, p. 201)†

THEORY

See (Fl 54a, Ka 56c, El 57b).

I. $N^{16}(\beta^-)O^{16}$ $Q_m = 10.402$

From the character of the beta decay, it is concluded that $N^{16}(0)$ has $J = 2^-$. See O^{16}.

TABLE 16.1

Energy levels of N^{16}

E_x (MeV ± keV)	J^π	$\tau_{\frac{1}{2}}$ or Γ (keV)	Decay	Reactions
0	2^-	$\tau_{\frac{1}{2}} = 7.37 \pm 0.04$ sec	β^-	I, II, V, XII, XIII, XVI, XIX, XXIV
0.120 ± 1	0^-	$\tau_{\frac{1}{2}} = 5.7$ μsec	γ	XVI, XXIV
0.295 ± 4	3^-		γ	XVI, XXIV, XXV
0.392 ± 3	1^-		γ	XVI, XXIV, XXV
(3.53 ± 30)		sharp		XVI
3.980 ± 20		sharp		XVI
4.80 ± 50		230 ± 40		XVI
(5.01 ± 50)				XVI
5.25 ± 50	$2^-, 3^\pm$	200	n	XIV, XVI
12.2		270	d, p	VII
12.62		190	d, p	VII
12.8		165	d, p	VII

II. $Li^7(N^{14}, Li^5)N^{16}$ $Q_m = 0.589$

See (Al 58d).

† The level scheme of F^{16} is not illustrated (see p. 220).

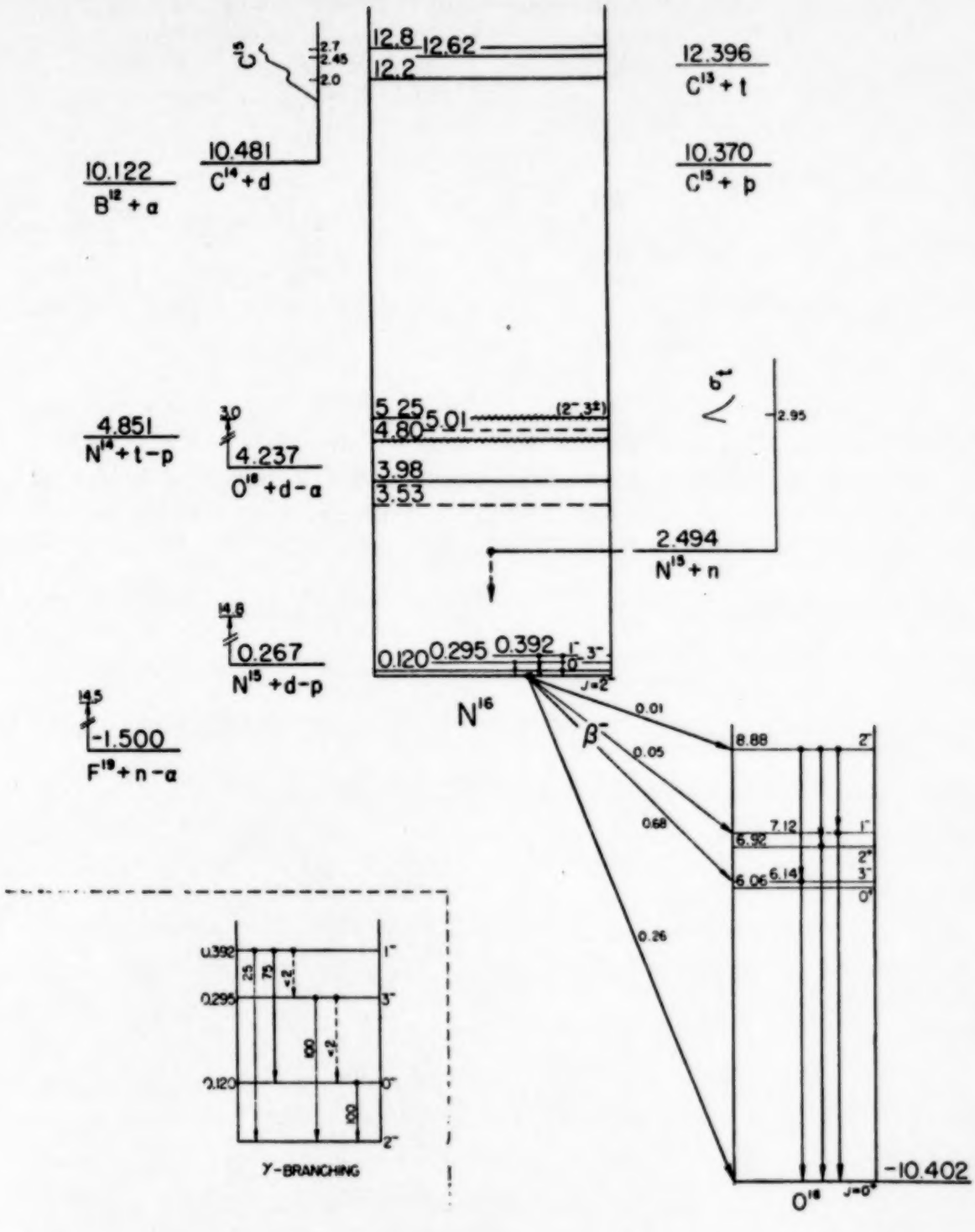

9 January 1959

Fig. 31. Energy levels of N^{16}: for notation, see fig. 1, p. 7.

III. $Be^9(Li^7, Li^8)Be^8$ $Q_m = 0.368$ $E_b = 20.585$

The cross section for this reaction has been measured from $E(Li^7) = 1.1$ to 2.0 MeV. At the higher energy it is approximately 1 mb (No 57a).

IV. $C^{13}(\alpha, p)N^{16}$ $Q_m = -7.416$

Not reported.

V. $C^{14}(d, \gamma)N^{16}$ $Q_m = 10.481$

At $E_d = 1.16$ MeV, the cross section is $\lesssim 0.1$ mb (Bo 57d). At $E_d = 2.0$ MeV, $\sigma \leqq 0.6$ mb (Do 56b).

VI. $C^{14}(d, n)N^{15}$ $Q_m = 7.987$ $E_b = 10.481$

See (Hu 50e) and N^{15}.

VII. $C^{14}(d, p)C^{15}$ $Q_m = -1.007$ $E_b = 10.481$

The excitation function has been studied from $E_d = 0.6$ to 3.0 MeV (Ri 54b, Do 56b). Resonances are observed at 2.0, 2.45 and 2.7 MeV, with c.m. widths of 270, 190 and 165 keV respectively, corresponding to N^{16*} = 12.2, 12.62 and 12.8 MeV (Do 56b). See also (Ri 54b, Hu 50e) and C^{15}.

VIII. $C^{14}(d, \alpha)B^{12}$ $Q_m = 0.358$ $E_b = 10.481$

See (Hu 50e).

IX. $C^{14}(t, n)N^{16}$ $Q_m = 4.223$

Not reported.

X. $C^{14}(He^3, p)N^{16}$ $Q_m = 4.988$

Not reported.

XI. $C^{14}(\alpha, d)N^{16}$ $Q_m = -13.363$

Not reported.

XII. $N^{14}(t, p)N^{16}$ $Q_m = 4.851$

See (Cu 53c).

XIII. $N^{15}(n, \gamma)N^{16}$ $Q_m = 2.494$

The thermal cross section is 24 ± 8 μb (Hu 58), 80 ± 30 μb (Fe 52).

XIV. $N^{15}(n, n)N^{15}$ $E_b = 2.494$

The total cross section has been measured for $E_n = 2.8$ to 3.3 MeV: a resonance is observed at $E_n \approx 2.95$ MeV. $\sigma_{max} = 4$ b, $\Gamma = 140 \pm 40$ keV, corresponding to $E_x \approx 5.26$ MeV, $J = 2^-$ or $3^\pm$ (Ba 56j).

XV. $N^{15}(n, \alpha)B^{12}$ $Q_m = -7.629$ $E_b = 2.494$

See (Je 48c).

XVI. $N^{15}(d, p)N^{16}$ $Q_m = 0.267$

$Q_0 = 0.286$ (Va 57)

$Q_0 = 0.269 \pm 0.010$ (Wa 57)

Levels derived from observed proton groups and γ-rays are listed in table 16.2. Gamma transitions are shown in the inset of fig. 31. Even at

TABLE 16.2

Levels of N^{16} from $N^{15}(d, p)N^{16}$

E_x [a] (keV)	$\Gamma_{(c.m.)}$ (keV)	l_n [b]	J^π [b]	θ^2 [c]
0	sharp	2	2^-	0.05
120 ± 1	sharp	0	0^-	0.19
294 ± 5	sharp	2	3^-	0.05
392 ± 3	sharp	0	1^-	0.18
(3530 ± 30)	sharp			
3980 ± 20	sharp			
4800 ± 50	230 ± 40			
(5010 ± 50)				
5250 ± 50	290 ± 50			

[a] (Wa 57; $E_d = 14.8$ MeV). No other proton groups are observed corresponding to $N^{16*} < 9$ MeV. Energies of first three excited states are from γ-ray measurements (Fr 57b, Wi 57d).

[b] (Wa 57) and (Zi 56a; $E_d = 2.75$ MeV); J assignments from stripping and gamma decay data: see text.

[c] (Wa 57).

$E_d = 2.7$ MeV, the stripping angular distribution patterns to the low-lying states are well-developed, and the theory yields quite good fits (Zi 56a, Wa 57). Shell-model theory in intermediate coupling predicts a close group of 4 levels within about 700 keV, with $J = 0, 1, 2, 3$, odd parity (order uncertain), arising from the configurations $p_{\frac{1}{2}}^{-1}\, s_{\frac{1}{2}}$ and $p_{\frac{1}{2}}^{-1}\, d_{\frac{3}{2}}$. Levels from $p_{\frac{1}{2}}^{-1}\, d_{\frac{3}{2}}$ should lie several MeV higher (In 53, El 57b). These results are strikingly confirmed by the experimental evidence. The ground state is assigned $J = 2^-$ on the basis of the β-decay (see $N^{16}(\beta^-)O^{16}$). The first excited state may have $J = 0^-$ or 1^- from the stripping pattern; however, the half-life $\tau_{\frac{1}{2}} = 6.7 \pm 0.5$ μs (Fr 57b), 5.43 ± 0.22 μs (Zi 59) is much too long for dipole radiation, and $J = 0^-$ is indicated (Wi 57d). The third excited state ($E_x = 392$ keV), again limited to $J = 0^-$ or 1^- by the stripping pattern, decays to both $N^{16*}(0)$ and $N^{16*}(0.12)$; $J = 0^-$ is therefore excluded and $J = 1^-$ indicated. Of the possibilities $J = 1^-, 2^-, 3^-$ for the second excited state, $N^{16*}(0.285)$, $J = 1^-$ is rendered unlikely by the low intensity of γ-decay to the second excited state and by the absence of an $l_n = 0$ component in the stripping pattern (Zi 56a, Wi 57d, Wa 57). The assignment $J = 3^-$ is strongly favored by the (p—γ) angular correlation (Fr 57b).

The observed γ-branching of $N^{16*}(0.395)$ is in accord with the theory,

which predicts lifetimes in the range 1 to 7×10^{-11} sec. A considerable enhancement through collective excitation is required to account for the lifetime of the first excited state. The reduced neutron widths are expected to be of the order of the single-particle limit. Calculation of level shifts and comparison of observed reduced widths suggests that the O^{16*} analogues to the first four states of N^{16} are O^{16*} = 12.95, 12.78, 13.24, and 13.09 MeV (El 57b): see also (Wi 57d), N^{15}(p, p)N^{15}.

XVII. N^{15}(t, d)N^{16} $Q_m = -3.765$

Not reported.

XVIII. $N^{15}(\alpha, He^3)N^{16}$ $Q_m = 18.084$

Not reported.

XIX. O^{16}(n, p)N^{16} $Q_m = -9.619$

The possibility that N^{16} might have a long-lived ($\approx$ sec) isomeric state has been examined, with negative result (To 56b). See also (Li 52), O^{17}.

XX. $O^{16}(t, He^3)N^{16}$ $Q_m = -10.384$

Not reported.

XXI. $O^{17}(d, He^3)N^{16}$ $Q_m = -8.271$

Not reported.

XXII. O^{18}(n, t)N^{16} $Q_m = -13.349$

Not reported.

XXIII. $O^{18}(p, He^3)N^{16}$ $Q_m = -14.114$

Not reported.

XXIV. $O^{18}(d, \alpha)N^{16}$ $Q_m = 4.237$

$Q_0 = 4.237\pm0.009$ (Pa 55a).

Alpha groups are observed at $E_d = 0.85$ MeV corresponding to N^{16*} = 0, 116 ± 6, 300 ± 12 and 391 ± 12 keV. No other states are observed below $E_x = 1.24$ MeV (Pa 55a). See also (Bo 57d) and F^{20}.

XXV. $F^{19}(n, \alpha)N^{16}$ $Q_m = -1.500$

At $E_n = 4.87$ MeV, an α-group has been observed with $Q = -1.77\pm0.15$ MeV, probably corresponding to a transition to one or more excited states of N^{16} (Ja 55e). See also (To 56b) and F^{20}.

O^{16}

(Fig. 32, p. 207)

THEORY

See (De 54c, Fl 54a, Wi 55f, Ja 55a, Ma 55f, Ma 55o, Sc 55a, Wi 56c, Ja 56c, Ka 56a, Fe 56b, Re 56b, El 56, Mo 56, He 55f, Pe 56a, He 57b, El 57b, Ta 57a, Re 57, To 57a, Gr 57c, Fe 57d, Fe 58a, Fe 58b, Ca 58c, Da 58a Ha 58b, Mo 58, Um 58, Wi 58g, Da 58d, Ra 58f).

I. $C^{12}(\alpha, \gamma)O^{16}$ $Q_m = 7.148$

Resonant capture radiation to O^{16}(g.s.) is observed at $E_\alpha \approx 3.24$ MeV, corresponding to the known $J = 1^-$ state at 9.58 MeV: see $C^{12}(\alpha, \alpha)C^{12}$. The radiative width of 6×10^{-3} eV implies a $T = 1$ admixture of the order of 3×10^{-4}, an amount slightly lower than usual for O^{16} states. It is suggested that the $T = 1$ admixture may derive from O^{16*}(13.09), $J = 1^-$, $T = 1$ (Bl 57): see also (Wi 56c, Jo 53e). This state does not arise in any natural way from $p^{-1}s$, or $p^{-1}d$ (El 57b). The integrated capture cross section to $E_\alpha = 1.60$ MeV is < 30 μb-MeV (Al 55c). See also (Ph 58). The relevance of the capture of alpha particles by C^{12} to the buildup of the elements in stars is discussed by (Ca 56e, Ha 56g, Ha 56h, Bu 57f, Sa 57c).

II. $C^{12}(\alpha, n)O^{15}$ $Q_m = -8.452$ $E_b = 7.148$
See (Ki 39).

III. $C^{12}(\alpha, \alpha n)C^{11}$ $Q_m = -18.722$ $E_b = 7.148$
See (Li 53c).

IV. $C^{12}(\alpha, p)N^{15}$ $Q_m = -4.965$ $E_b = 7.148$
See N^{15}.

V. $C^{12}(\alpha, d)N^{14}$ $Q_m = -13.579$ $E_b = 7.148$

The angular distribution at $E_\alpha = 42$ MeV shows three peaks and three valleys in the range $\theta_{c.m.} = 40°$ to $150°$. The location of peaks and the absolute cross sections agree closely with those obtained in the inverse reaction at $E_d = 20$ MeV. The experiment provides a test of the hypothesis of invariance under time reversal and places an upper limit of a few per cent on possible T-R odd forces (Bo 58c).

VI. $C^{12}(\alpha, \alpha)C^{12}$ $E_b = 7.148$

Resonances derived from a phase-shift analysis of the elastic scattering are exhibited in table 16.4 (Hi 53a, Bi 54a). At the upper limit of these experiments ($O^{16*} = 12.5$ MeV), the existence of higher $J = 0^+$ and 2^+ levels is indicated by a pronounced increase in the $l = 0$ and $l = 2$ phase shifts (Hi 53a, Bi 54a). The inelastic scattering for $E_\alpha = 20.4$ to 22.6 MeV indicates a resonance at $E_\alpha = 21.85 \pm 0.1$ MeV, $\Gamma \approx 0.4$ MeV ($O^{16*} = 23.54$ MeV). The asymmetry of the angular distribution is said to indicate at least

TABLE 16.3

Energy levels of O^{16}

E_x (MeV)	$J^\pi; T$	Γ(keV) or τ_m	Decay	Reactions
0	$0^+; 0$	—	Stable	I, XVIII, XXIV, XXVII, XXXIV, XXXVI, XXXVII, XXXVIII, XLIII
6.056 ± 0.010	$0^+; 0$	$\tau_m = (7.2 \pm 0.7) \times 10^{-11}$ sec	π	IX, XVIII, XXXV, XXVI, XXXVIII, XLIII
6.135 ± 0.010	$3^-; 0$	$\tau_m = (1.2 \pm 0.6) \times 10^{-11}$ sec	γ	XVIII, XXIV, XXVII, XXXV, XXXVI, XXXVIII, XLIII
6.923 ± 0.010	$2^+; 0$	$\tau_m = (1.2 \pm 0.3) \times 10^{-14}$ sec	γ	XVIII, XXXIII, XXXVI XXXVIII, XLIII
7.121 ± 0.010	$1^-; 0$	$\tau_m = (1.0 \pm 0.3) \times 10^{-14}$ sec	γ	XVIII, XXIV, XXVII, XXXIII, XXXVI, XXXVIII, XLIII
8.875 ± 0.010	$2^-; 0$		γ	XVIII, XXIV, XXVII, XXXVI, XXXVIII, XLIII
9.58	$1^-; 0$	650	α, γ	I, VI
9.843 ± 0.012	$2^+; 0$	0.8	α	VI, XXXVI, XLIII
10.363 ± 0.014	$4^+; 0$	27	α	VI, XXXVI, XLIII
(10.804)				(XLIII)
10.937 ± 0.010	$0^-; 0$		γ	(XVIII), XXIV, (XLIII)
11.070 ± 0.010	$3^+; (0)$		γ	(VI), XVIII, XXIV, XXXVI, XLIII
11.25	$0^+; 0$	2500	α	VI
11.51 ± 0.03	$2^+; 0$	80	α	VI, XXXVI
11.62	$3^-; 0$	1200	α	VI
12.02 ± 0.03			(γ)	XXXVI
(12.29)		40	γ	XX
12.43 ± 0.01	$1^-; 0$	89	α, γ, p	VI, XX, XXII
12.52 ± 0.01	2^-	0.8	p, γ, α	XX, XXII, XXXVI
12.78 ± 0.01	$0^-; 1$	38	p, γ	XX, XXI
12.96 ± 0.01	$2^-; 1$	2 ± 0.2	p, α	XXI, XXII
13.09 ± 0.01	$1^-; 1$	130 ± 10	p, γ, α	XX, XXI, XXII, XXXVI
13.25 ± 0.01	$3^-; 1$	21 ± 1	p, α	XXI, XXII
13.65 ± 0.01	$1^+; 0$	64 ± 3	p, α	XXI, XXII
13.97 ± 0.01	2^-	22 ± 2	p, α	XXI, XXII
14.93 ± 0.04	4^+	43 ± 10	p, α	XXII
15.21 ± 0.04	$2^-, 3^+$	72 ± 15	p, α	XXII
15.25 ± 0.06	2^+	720 ± 100	p, α	XXII
15.41 ± 0.05		96 ± 25	p, α	XXII
15.79		30	p, α	XXII
16.21	1^+	23	p, n	XXIII
16.3	0^-	250	p, n	XXIII
16.44		24	p, α	XXII
(16.82)			p, α	XXII
(16.93)			p, α	XXII
17.0		≈ 200	p, n	XXIII
17.12		41	p, n	XXIII
17.29		84	p, n	XXIII
17.5		≈ 250	p, n	XXIII
17.63		66	p, n	XXIII

TABLE 16.3 (continued)

E_x (MeV)	$J^\pi; T$	Γ(keV) or τ_m	Decay	Reactions
17.85		100	p, n	XXIII
17.96		49	p, n	XXIII
18.05		38	p, n	XXIII
22.05		broad	d, n	XI
23.05		broad	d, n	XI
23.54		300	α	VI
24.38		broad	d, n	XI
(25.7)			He^3, p, α	VII, VIII
(26.4)			He^3, p	VII

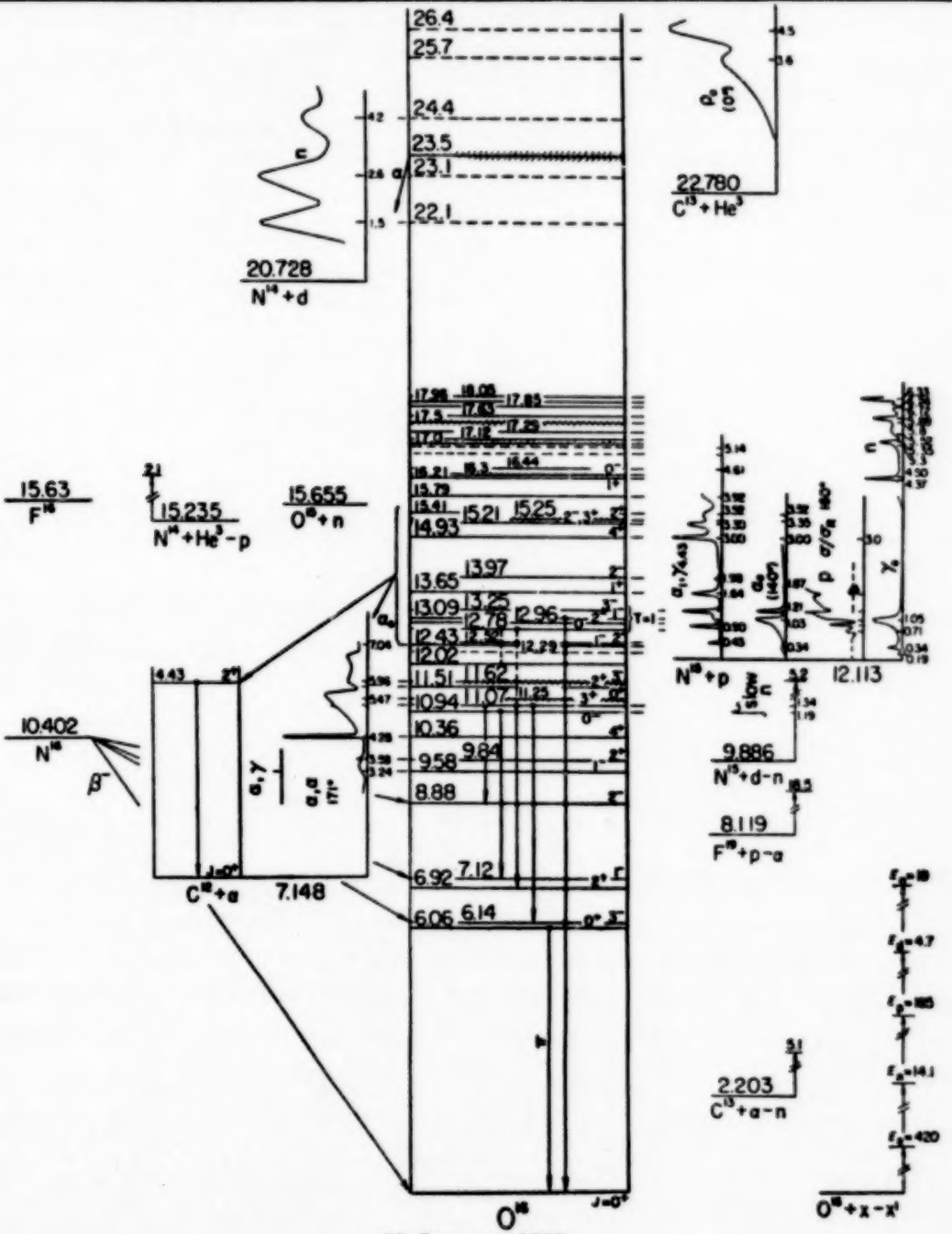

13 January 1959

Fig. 32. Energy levels of O^{16}: for notation, see fig. 1.

one other level, of opposite parity (Ra 55a) See also (De 54c; theo.) and C^{12}.

VII. $C^{13}(He^3, p)N^{15}$ $Q_m = 10.668$ $E_b = 22.780$

The yields of ground state protons have been studied at several angles in the region $E(He^3) = 1.4$ to 4.8 MeV. There are indications of resonances at $E(He^3) \approx 3.6$ and 4.5 MeV ($O^{16*} = 25.7$ and 26.4 MeV) (Sc 56f, Il 57). See also N^{15}.

TABLE 16.4

Resonances in $C^{12}(\alpha, \alpha)C^{12}$

E_α (MeV)	Γ_{lab} (keV)	θ_α^2	O^{16*} (MeV)	J^π
3.24 [a]	860	0.85	9.58	1^-
3.582 [a]	1	0.0015	9.835	2^+
4.28 [b]	36	0.26	10.36	4^+
5.27 [b]	10		(11.10) [d]	
5.47 [b]	3300	0.76	11.25	0^+
5.82 [b]	106	0.03	11.51	2^+
5.96 [b]	1600	0.73	11.62	3^-
7.04 [b]	230	0.04	12.43	1^-
21.85 [c]	400		23.54	

[a] (Hi 53a).
[b] (Bi 54a).
[c] (Ra 55a).
[d] Assignment to present reaction not certain.

VIII. $C^{13}(He^3, \alpha)C^{12}$ $Q_m = 15.632$ $E_b = 22.780$

The ground state α-group shows a broad weak resonance at $E(He^3) \approx 3.6$ MeV (Wo 56b). See also C^{12}.

IX. $C^{13}(\alpha, n)O^{16}$ $Q_m = 2.203$

A threshold for $O^{16*} = 6.05$ MeV is observed at $E_\alpha = 5.05$ MeV (Bo 56d). See also (Jo 51d) and O^{17}.

X. $C^{14}(He^3, n)O^{16}$ $Q_m = 14.607$

Not reported.

XI. $N^{14}(d, n)O^{15}$ $Q_m = 5.073$ $E_b = 20.728$

Excitation functions have been measured for $E_d = 0.6$ to 4.5 MeV (Ma 55m, Jo 56c, Jo 57a, No 57b, Mo 58g, We 58d). The yield of ground-state neutrons shows broad but well-defined peaks at $E_d = 1.52$, 2.62 and 4.19 MeV; $E_x = 22.05$, 23.05 and 24.38 MeV. It is not clear whether the structure is to be attributed to resonances or to surface interaction (We 58d). See also O^{15}.

XII. $N^{14}(d, p)N^{15}$ $Q_m = 8.615$ $E_b = 20.728$

Excitation functions and angular distributions are reported by (Jo 54c:

$E_d = 0.4$ to 0.6 MeV) (Va 56c, Ko 56f: $E_d = 0.2$ to 0.7 MeV), and (Bo 58a: $E_d = 0.6$ to 1.0 MeV): see also (Ja 57). At the lower energies, both stripping and compound nucleus effects are reported, although the distributions for $E_d = 0.6$ to 1.0 MeV (Bo 58a) appear to be explicable entirely on the basis of overlapping resonance levels. See also N^{15} and (St 54f).

XIII. $N^{14}(d, d)N^{14}$ $E_b = 20.728$

See N^{14}.

XIV. $N^{14}(d, t)N^{13}$ $Q_m = -4.292$ $E_b = 20.728$

See (Bo 42).

XV. $N^{14}(d, \alpha)C^{12}$ $Q_m = 13.579$ $E_b = 20.728$

The cross section rises gradually from $E_d = 0.45$ to 0.90 MeV (Ca 54d). Angular distributions for $E_d = 0.6$ to 1.0 MeV indicate that the stripping contribution is small in this range (Bo 58a). The angular distribution at $E_d = 20$ MeV agrees closely with that of the inverse reaction at $E_\alpha = 42$ MeV (Bo 58c): see $C^{12}(d, \alpha)N^{14}$, (Fi 57b) and C^{12}.

XVI. $N^{14}(d, 4\alpha)$ $Q_m = 6.298$ $E_b = 20.728$

See (Fo 47b).

XVII. $N^{14}(t, n)O^{16}$ $Q_m = 14.470$

Not reported.

XVIII. $N^{14}(He^3, p)O^{16}$ $Q_m = 15.235$

At $E(He^3) = 2.1$ MeV, proton groups corresponding to O^{16} levels up to $E_x = 13.6$ MeV have been identified. In the region $E_x \approx 11$ MeV, four groups are resolved, corresponding to $O^{16*} = 10.94$, 11.087 ± 0.020, 11.25 and 11.51 MeV. The first two are presumably those observed in $N^{15}(d, n)O^{16}$ at 10.937 and 11.063 MeV. The gamma decay of O^{16*}(8.88, 10.94 and 11.07) has been studied with coincidence techniques: branching ratios are given in fig. 33. From the observed transition intensities and from (p—γ) and (γ—γ) correlations, the assignment $J = 2^-$ for O^{16*}(8.88) is confirmed, and assignments of $J = 0^-$ and 3^+ are fixed for O^{16*}(10.94) and (11.07), respectively. For the 10.94-MeV state, $\Gamma_\alpha/\Gamma_\gamma < 0.2$, indicating an upper limit for the intensity of possible opposite-parity admixture of $\approx 2 \times 10^{-9}$ (Br 59, Ku 59). See also (Li 57a, Br 57c, Br 58e).

XIX. $N^{14}(\alpha, d)O^{16}$ $Q_m = -3.116$

Not reported.

XX. $N^{15}(p, \gamma)O^{16}$ $Q_m = 12.113$

Ground-state capture radiation resonances occur at $E_p = 190$, 338 keV

(He 58g) and 1050 keV (Sc 52, Ha 57d, He 58g): see table 16.5. The large radiative width, $\Gamma_\gamma = 150$ eV, of the latter indicates E1 radiation and $J = 1^-$, $T = 1$ for O^{16*}(13.09); on the other hand, the large α-width speaks for a

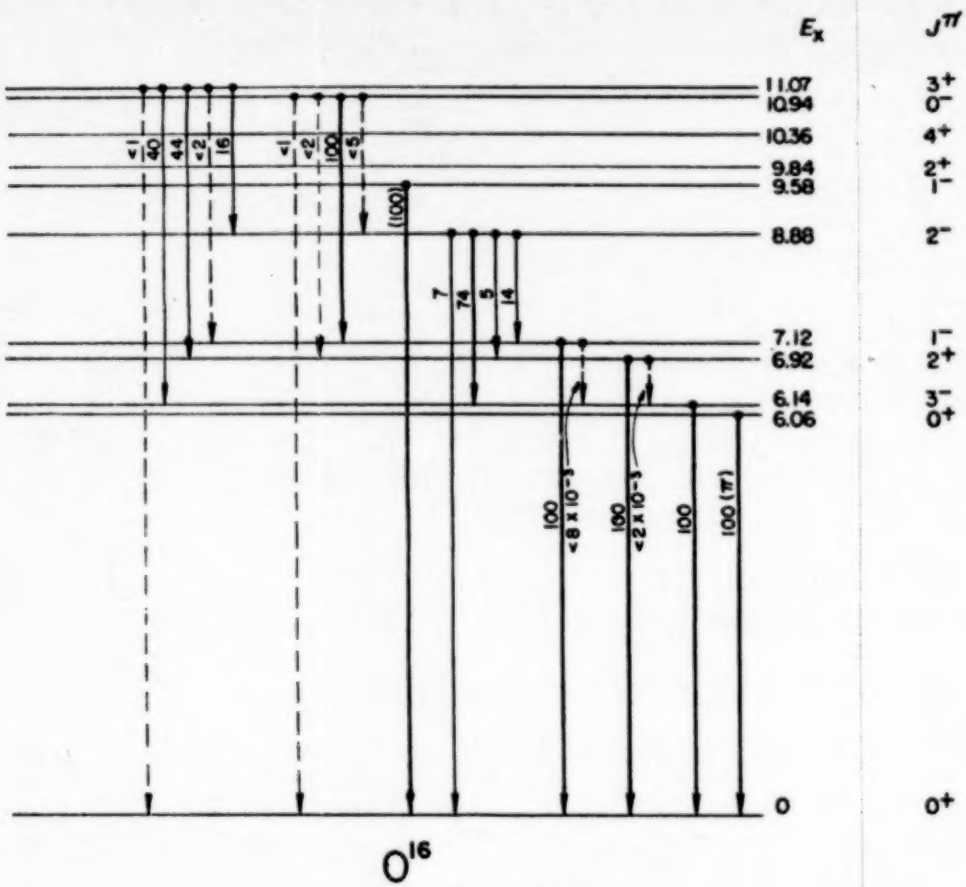

13 January 1959

Fig. 33. Gamma-ray transitions in O^{16}: for notation, see fig. 14, p. 83.

strong admixture of $T = 0$ (Wi 53a, Wi 56c, see also Ba 57l). The 338-keV resonance is relatively weak, $\Gamma_\gamma = 8$ eV. The Breit-Wigner formula with destructive interference between these two $J = 1^-$ states gives a good account of the γ_0 yield from $E_p = 200$ to 1200 keV (He 58g). Cascade radiation, via O^{16*}(6 and 7), is weakly resonant at $E_p = 340$ keV (He 58g): at the higher resonance, the relative amount of cascade radiation is $< 1.3 \times 10^{-3}$ (Go 54h, De 53d). No further resonances for ground-state radiation appear for $E_p < 3.3$ MeV with intensity > 2 per cent of that at $E_p = 1050$ keV (Ba 57l). Within a few microbarns, the cross section for $E_p < 3$ MeV is completely accounted for by the 13.09-MeV state; a small rise from $E_p = 3$ to 4 MeV may reflect higher resonances. This result is in disagreement with that of (Sp 55) on the inverse reaction in which a level at $O^{16*} = 14.7$ MeV ($E_p = 2.8$ MeV) is reported. The isotropy of the radiation over the entire

TABLE 16.5

Levels of O^{16} from $N^{15}(p, p)N^{15}$, $N^{15}(p, \gamma)O^{16}$ and $N^{15}(p, \alpha)C^{13}$

E_p (keV)	Γ_{lab} (keV)	Γ_p (keV)	$\sigma(\alpha_0)$ (mb)	$\sigma(\alpha_1)$ (mb)	$\sigma(\gamma_0)$ (μb)	$\sigma(\gamma_1)$ (μb)	θ_p^2 (%)	J^π; T	E_x (MeV)
(190)	40				res[f]				12.29
338[a]	94	0.8[a,f]	75[a,f]	0.03[f]	7[f]	0.4[f]	4[f,c]	1^- 0[c]	12.430
429± 1[a]	0.9	0.020[f]	n.r.[g]	200[a,f]		1300[f]	4[b]	2^-	12.515
710± 7[b]	40 ± 4	40[b]	n.r.	n.r.	n.r.	res.	11	0^-; 1[b]	12.779
898± 1[a]	2.2± 0.2	1.2	n.r.	800			8.8	2^-; 1	12.955
1028±10[b]	140 ± 10	110	500[i]	15	1000[a]	<1.3[h]	10	1^-; 1	13.088
1210± 3[a]	22.5± 1	4.1	600[i]	425[d]			7.4	3^-; 1	13.247
1640± 3[c]	68 ± 3	10	n.r.[d]	340			0.8	1^+; 0	13.651
1979± 3	23 ± 2	0.5[c]	n.r.	35				2^-[d]	13.968
3000±30[d]	45 ± 10		50	600				4^+	14.93
3300±35	75 ± 15		n.r	270				2^-, 3^+	15.21
3350±50	750 ±100		50	205				2^+	15.25
3520±40	100 ± 25		100	80					15.41
3920[e]	30			res[e]					15.79
4610	25			res					16.44
(5020)				(res)					(16.82)
(5140)				(res)					(16.93)

[a] (Sc 52); values for 338-keV resonance corrected for s-wave penetration: observed E_{max} = 360 keV, σ_{α_0} (max) = 90 mb.
[b] (Ha 57d).
[c] (Ha 57f).
[d] (Ba 57l).
[e] (Li 56a). see also table 16.6, p. 213.
[f] (He 58g).
[g] n.r. = non-resonant.
[h] (Go 54h).
[i] (Sc 52): (Ha 57f) find 340 and 300 mb respectively.

range from E_p = 1 to 4 MeV places an upper limit of 3 per cent on the relative intensity of p^{-1} d in the 13.09-MeV state (Wi 57a); see also (El 57b).

At E_p = 429 keV (He 58g) and 710 keV (Ha 57d), resonances for cascade radiation are found; neither produces any detectable ground state radiation. See also (Ca 58).

XXI. $N^{15}(p, p)N^{15}$ E_b = 12.113

Elastic scattering studies are reported for E_p = 600 to 1800 keV by (Ha 57d) and for E_p = 950 to 3960 keV by (Ba 56c); see table 16.5. The E_p = 710 keV state, (O^{16*} = 12.78 MeV) having $J = 0^-$, does not appear in the (p, α) reaction or in the ground-state capture: see $N^{15}(p, \gamma)O^{16}$. The assignment $J = 3^-$ to the state at E_p = 1210 keV (O^{16*} = 13.25 MeV) is in disagreement with the observed angular distribution in $N^{15}(p, \alpha_1)C^{12*}$ but is confirmed by the $\alpha_1-\gamma$ correlation. The reason for this discrepancy is not known (Ha 57d).

By comparison of J, π assignments and reduced widths, it is concluded that the O^{16} levels formed at $E_p = 898, 710, 1210$ and 1028 keV are the analogues of the first four states of N^{16} (Ha 57d, Wi 56d, Wi 56e, El 57b). It is pointed out that the $E_p = 340$ and 429-keV states are also possible candidates, and that in any case appreciable isobaric spin mixing is to be expected (Ha 57d). See also (Wi 56c).

Elastic scattering at $\theta = 132°$ shows structure at $E_p = 3000$ keV and a large peak of undetermined origin at $E_p = 3920 \pm 40$ keV (Ba 56c). See also (Ca 58).

XXII. $N^{15}(p, \alpha)C^{12}$ $Q_m = 4.964$ $E_b = 12.113$

Two groups of α-particles occur, to $C^{12}(0)$ (α_0) and to C^{12} (4.43, $J = 2^+$) (α_1, γ). Observed resonances are exhibited in table 16.5. The cross section for (p, α_0) is 5×10^{-7} b at $E_p = 100$ keV (Sc 50: see also Sc 52, Ba 57l). See (Ja 57).

Angular distributions $(p—\alpha_0)$ have been studied in the range $E_p = 230$ to 960 keV by (Co 53k), $E_p = 500$ to 1000 keV by (Ne 53b), $E_p = 920$ to 1260 keV by (Ha 57f). At and below the 338-keV resonance, the distribution is isotropic. Strong $\cos \theta$ terms develop for $E_p > 400$ keV, with $\cos^2 \theta$ terms gradually increasing above 700 keV, and higher-order terms above 1 MeV. The terms in $\cos \theta$ indicate interference between states of opposite parity. Analysis of this effect led (Co 53k) to the conclusion that the resonances in question were $E_p = 338$ keV, assigned $J = 0^+$, and $E_p = 1028$ keV, $J = 1^-$. Subsequent work has shown, however, that the lower state is $J = 1^-$, formed by s-wave protons: evidently the interfering even parity state or states remain to be identified; see also $C^{12}(\alpha, \alpha)C^{12}$. The 1028-keV resonance has a large width both for α-particles and E1 radiation and appears to have a mixed character as regards isobaric spin (Wi 53a, Wi 53c, Ha 57d, Wi 56c).

Analysis of the $(p—\alpha_0)$ distribution at the $E_p = 1210$-keV resonance indicates $J = 3^-$, although $J = 4^+$ is not clearly excluded (Ha 57f). Angular distributions of (p, α_1) and the 4.4-MeV γ-ray have been studied at the $E_p = 429, 898$ and 1210-keV resonances by (Kr 53, Se 52a and Ba 52g). Channel-spin ratios have been interpreted in terms of L-S and j-j coupling models by (Ch 53d). The α_1-distribution at $E_p = 1210$ keV appears to require $J = 4^+$ (Kr 53, Ha 57d), but the $(\alpha_1—\gamma)$ correlation requires $J = 3^-$, in agreement with elastic scattering results; the reason for this discrepancy is not clear (Ha 57d). Angular distributions of the 4.4-MeV γ-rays are reported for $E_p = 1050$ and 1640 keV by (Kr 54b) and for various energies from $E_p = 1210$ to 3900 keV by (Ba 57l). See also (Ca 58).

A pronounced anomaly appears at $E_p = 1.87$ MeV in the (p, α_0) excitation curve which is faintly reproduced in (p, α_1) but not in (p, p) (Ha 57f).

XXIII. $N^{15}(p, n)O^{15}$ $Q_m = -3.542$ $E_b = 12.113$

The excitation function has been measured from threshold to 6.4 MeV, and angular distributions have been studied at several energies: see table 16.6.

TABLE 16.6
Resonances in $N^{15}(p, n)O^{15}$ (Jo 58c)

E_p (MeV)	Γ_{lab} (keV)	J^π	E_x in O^{16} (MeV)
4.372	24	1^+	16.21
≈4.5	≈250	0^-	16.3
≈5.3	≈200		17.0
5.35	44		17.12
5.52	90		17.29
≈5.8	≈250		17.5
5.88	70		17.63
6.12	105		17.85
6.24	52		17.96
6.33	40		18.05

Only four levels are found with $\Gamma \lesssim 40$ keV, as contrasted with the ten or more reported in $O^{16}(\gamma, n)O^{15}$ (Jo 58c).

XXIV. $N^{15}(d, n)O^{16}$ $Q_m = 9.886$

Slow neutron thresholds have been observed at $E_d = 1.192$ and 1.335 MeV, corresponding to $O^{16*} = 10.937 \pm 0.010$ and 11.063 ± 0.015 MeV (We 57b). At $E_d = 5.1$ MeV, in this reaction, and at $E_p = 5.77$ MeV in $F^{19}(p, \alpha)O^{16}$, four γ-ray lines are observed which are assigned to O^{16}: $E_\gamma = 2.73$ $(8.87 \rightarrow 6.14)$, 3.86 ± 0.04 $(10.94 \rightarrow 7.12)$, $6.14 (6.14 \rightarrow 0)$ and 7.1 MeV $(6.9 + 7.1 \rightarrow 0)$. The 10.94-MeV state is not observed to decay in any way other than through the $J = 1^-$ state at 7.12 MeV; upper limits to transitions to $O^{16*} = 0$, 6.06, 6.14, 6.92 and 8.87 MeV are, respectively, 5, 1, 6, 20 and 40 per cent of the observed cascade. The strong transition to $O^{16*}(7.1)$, $J = 1^-$, suggests $J = 0^-$ for $O^{16*}(10.94)$, although $J = 1^+$ is not ruled out. The γ—γ correlation strongly favours $J = 0^-$. It is suggested that this γ-emitting state is to be identified with the first neutron threshold: $O^{16*}(10.94)$, above, and is distinct from either the (doubtful) O^{16*} (11.1) reported in $C^{12}(\alpha, \alpha)C^{12}$ or the $O^{16*}(11.08)$ reported in $O^{16}(p, p')O^{16*}$. Possibly both $O^{16*}(10.94)$ and (11.08) are involved in $N^{14}(He^3, p)O^{16}$ (Be 57f). It is noted that the $F^{19}(p, \alpha)O^{16}$ spectrum of (Sq 56) shows three groups in this range, of which one is definitely attributed to $O^{16*}(11.085)$ (We 57b). The 8.87-MeV state has a 7 ± 2 per cent direct transition to O^{16} (g.s.) (Be 57f). Angular distributions of ground-state neutrons for $E_d = 1.1$ to 5.2 MeV are well accounted for by the exchange stripping theory of (Ow 57) (We 58d: see O^{17}). See also (Aj 55) and (El 57b; theo.).

XXV. $N^{15}(He^3, d)O^{16}$ $Q_m = 6.619$

Not reported.

XXVI. $N^{15}(\alpha, t)O^{16}$ $Q_{rn} = -7.700$

Not reported.

XXVII. $N^{16}(\beta^-)O^{16}$ $Q_m = 10.402$

N^{16} decays to several states of O^{16}: reported branching fractions are listed in table 16.7. The ground-state transition, with $E_\beta(\max) = 10.33 \pm 0.08$ MeV

TABLE 16.7

Beta-decay of N^{16}

Final State		A		B		C		D
O^{16*} (MeV)	J^π	Branch (%)	log f_0t	Branch (%)	log f_0t	Branch (%)	log f_0t	
0	0^+	26 ± 2	6.7	28	6.67 [a]	24 ± 2	8.2 [b]	
6.06	0^+	$\leqq 0.015$	$\geqq 8.2$					
6.14	3^-	68	4.5	54	4.6	55 ± 4	4.5	14 ± 1
6.92	2^+							
7.12	1^-	4.9	5.1	18	4.6	21 ± 4	4.4	1
8.88	2^-	1.1	4.4					

A: (Wi 56, Al 58c, Al 59): includes data of B, C, D.
B: (Br 58a).
C: (Mo 57b).
D: γ-rays (Mi 51a, To 56b, Bo 57d).
[a] log $(f_1t) = 8.0$.
[b] log (f_1t).

(Mo 57b), 10.40 ± 0.05 MeV (Br 58a), has the unique first-forbidden shape corresponding to $\Delta J = 2$, yes, fixing J^π of N^{16} as 2^- (Mo 57b, Br 58a, Al 59). This assignment is also indicated by the fact that the transitions to $O^{16*}(6.1)$ and (7.1) are both allowed (Mi 51a). There appears to be some discrepancy between the branching ratios to $O^{16*}(6.1)$ and (7.1) as determined by decomposition of the β-spectrum (Br 58a) and by comparison of the γ-ray intensities (Mi 51a, Bo 57d: see, however, Al 59). The low ft-value for $O^{16*}(7.1)$ presents some difficulty for the theory (El 57b). Transitions to the nuclear pair emitting state are $< 1.5 \times 10^{-4}$: log $ft > 8.2$ (Al 58c: see also El 56, El 57b). A 1.1 per cent branch leads to $O^{16*}(8.87)$ which decays via the 7.1, 6.9 and 6.1-MeV levels in the ratio 3 : 1 : 30. Since the β-transition is allowed, J^π of $O^{16}(8.8)$ is 1^-, 2^- or 3^-; the first and last would permit α-decay, so $J^\pi = 2^-$. The γ-branching and the γ—γ correlation (8.88 → 6.1 → g.s.) are consistent with this assignment (Wi 56).

The half-life is 7.35 ± 0.05 sec (Bl 47), 7.38 ± 0.05 sec (Ma 54d). (To 56b) finds no evidence for β-decay of excited states of N^{16}.

XXVIII. $O^{16}(\gamma, n)O^{15}$ $Q_m = -15.655$

$E_{thresh} = 15.60 \pm 0.05$ (Ba 57n: see also Ba 55k).

The cross section exhibits a slow rise for ≈ 3 MeV above threshold followed by the usual giant resonance. Characteristics of the giant resonance are: $E_\gamma = 24$ MeV, $\Gamma = 3.5$ MeV, $\sigma_{max} = 10$ mb; $\int \sigma dE = 40$ MeV-mb (Fe 54, Mo 53c, Jo 51b, Ca 57f).

Discontinuities in the activation curve are said to indicate absorption into discrete levels of O^{16}: see table 16.8 (Pe 55d, Ka 58b, Ba 55k, Ba 57n, Co 55a, Be 58g). From the cross section it would appear that a substantial fraction of the absorption takes place through discrete levels (Ka 54a, Pe 55d). However, in a measurement of the absorption in water for $E_\gamma = 15$ to 25 MeV, using various detectors including O^{16}, (Si 58a) conclude that the absorption is generally continuous, with only a small contribution from

TABLE 16.8

Levels in O^{16} from $O^{16}(\gamma, n)O^{15}$

E_γ (MeV)			
(Pe 55d)	(Ka 54a)	(Ba 55k, Ba 57n)	(Co 55a, Be 58g)
15.85	15.9 [a]	(15.8)	15.93 [b]
16.03		16.03	16.17 [b]
16.47	16.4	16.50	16.37 [c]
16.75	16.7	(16.7)	
16.95	16.9	16.82	16.84 [c]
17.02		17.04	
17.13	17.1		
17.18			
17.55			
17.68			
17.84			
18.04			
18.70			
19.01	18.9		
19.18	19.3		
20.33			
20.58			
20.79	20.7		
20.93			
21.21			
21.52	21.54 ± 0.05		
	21.96 ± 0.05		
22.37			
22.54			
22.76			
23.02			

[a] See also (Ka 58b).
[b] (Be 58g).
[c] (Co 55a).

discrete, narrow levels. See also (Ca 55g, Bi 54, Sa 55j, Sv 57, Sp 57, Wo 58, Li 58), (Mo 55, Wi 56c, Ba 57, El 57b, Fe 58a, Fe 58b, Wi 58g; theo.) and (Aj 55).

XXIX. $O^{16}(\gamma, p)N^{15}$ $Q_m = -12.113$

Resonances are observed at $E_\gamma = 19.6$, 20.6, 22.4 MeV; $\int \sigma dE = 2$, 2, and 20 MeV-mb for ground-state protons (Co 56d), $E_\gamma = 20.7$, 21.9, 24.0 MeV (Li 56c). See also (Jo 55c). The 22-MeV resonance appears to be the giant resonance. Proton angular distributions have been measured by (Co 56d, Li 56c, Mi 57c). A resonance reported at $E_\gamma = 14.7$ MeV (Sp 55; see also Co 56d) does not appear in the inverse reaction $N^{15}(p, \gamma)O^{16}$ (Wi 57a, Wi 55f). (Si 58a) find that the absorption in the range $E_\gamma = 15$ to 25 MeV is generally continuous, with only small contributions from narrow resonances: see also $O^{16}(\gamma, n)O^{15}$. See also (St 55a, Jo 56f, Sv 57, Mi 57a, Mi 58c, Br 57l, Pe 58, Li 58) and (Go 56l, Wi 57g, Ba 57d, Mo 55a; theo.).

XXX. $O^{16}(\gamma, \alpha)C^{12}$ $Q_m = -7.148$

The cross section for production of C^{12} exhibits a maximum near 17.5 MeV ($\Gamma \approx 5$ MeV), $\sigma(\max) \approx 50\,\mu$b (Mi 53c). Evidence is also reported for excited states of O^{16} at (14.2), 16.75, 17.3, 22.6, (23.15) and 24.6 MeV with $J = 2^+$, $T = 0$ (St 54h). See also (Ti 55a, Da 56c, Ha 55g) and (Aj 55).

XXXI. $O^{16}(\gamma, 4\alpha)$ $Q_m = -14.429$

The cross section for production of 4-pronged stars shows a number of maxima: see table 16.9 (Go 52, Da 56c, Co 54i). An appreciable fraction of

TABLE 16.9

Maxima in $O^{16}(\gamma, 4\alpha)$ [a]

E_γ (MeV)		
(Go 52)	(Da 56c)	(Co 54i)
22.6	22.5	23.2
25.8	(26.0)	24.7
	(27.5)	27.2
29.5	(29.5)	29.2
	32.5	
	(35.2)	

[a] Maxima in number of 4-pronged stars.

the stars appear to involve excited states of C^{12} and Be^8 (Da 56c, Aj 55; see, however, Mi 53c). See also (Ha 55g, Co 55) and (Aj 55).

XXXII. (a) $O^{16}(\gamma, n\alpha)C^{11}$ $Q_m = -25.870$

(b) $O^{16}(\gamma, t)N^{13}$ $Q_m = -25.020$

See (Er 57, Sc 55).

XXXIII. $O^{16}(\gamma, \gamma')O^{16*}$

Measurement of the resonance scattering cross section for 6.9 and 7.1-MeV γ-rays from $F^{19}(p, \alpha)O^{16}$ yields mean lifetimes of $(1.2\pm0.3)\times10^{-14}$ and $(1.0\pm0.3)\times10^{-14}$ sec for O^{16*}(6.92) and (7.12) respectively. Values obtained from self absorption measurements are consistent with these. The observed life of the 7.1 → g.s., E1 transition is consistent with an isobaric spin inhibition of the order of 300 (see Ma 55f). The lifetime of the 6.9-MeV state is longer than that expected from a collective model but can be accounted for by one version of the α-particle model (Sw 57a). See also (Gr 57c, Ka 56a; theo.) and $F^{19}(p, \alpha)O^{16}$.

XXXIV. $O^{16}(e, e')O^{16*}$

Elastic scattering angular distributions at $E_e = 240$, 360 and 420 MeV strongly favor a shell-model charge distribution based on a harmonic well with a length parameter $a = 1.76\pm0.02\times10^{-13}$ cm. The rms radius of the charge distribution is 2.70×10^{-13} cm (Eh 58a); see also (Ho 57g, Ra 58e, Fe 56d, Fe 58b).

XXXV. $O^{16}(n, n')O^{16*}$

At $E_n = 7.06$ MeV, a 6.094 ± 0.06 MeV γ-ray is observed with a cross section of 104 ± 25 mb (Da 56d). See also (Th 54b, Be 55i).

XXXVI. $O^{16}(p, p')O^{16*}$

At $E_p = 19$ MeV, proton groups are observed corresponding to O^{16} states at 6.14, 7.02, 8.87, 9.85, 10.34, 11.08, 11.51, 12.02, 12.53, 13.06 and (13.39) MeV (±30 keV). Of these, three have not been reported elsewhere: O^{16*}(11.08, 12.02, 13.39). The level at 11.08 MeV decays via cascade through the 6 to 7 MeV states; it is presumably not to be identified with the (doubtful) 11.10 MeV state reported by (Bi 54a) in $C^{12}(\alpha, \alpha)C^{12}$ since the 10 keV-width of the latter would preclude observation of the γ-decay. If it is a pure γ-emitting state, $J = 2^-$ is favored. The 12.02-MeV state appears to give weak γ-radiation; the state at 12.53 MeV yields 4.4-MeV γ-rays via $O^{16}(p, p'\alpha)C^{12*}$ as expected from its behaviour in N^{15}+p. The 8.87-MeV state cascades 80 per cent via O^{16*}(6.1) and 20 per cent via O^{16*}(6.9—7.1) (Ho 55g).

At higher bombarding energies, evidence is reported for the excitation of states at 6 to 7, 12.5 and $\approx$ 20 MeV (St 56c, Ty 57b; $E_p = 96$ and 177 MeV). The elastic scattering at high energies is generally characterized by direct interaction and may be described in terms of the optical model: see (Bu 53b, Ki 55b, Fu 55, Ki 56, Bu 56j, Ch 57, Va 57b, Gi 57). Polarization of scattered protons has been studied at $E_p = 173$ MeV by (Hi 57b, Al 57c, Ma 57i). See also (Ma 58h, Ty 58b, Ja 57b, Ko 55).

XXXVII. $O^{16}(d, d)O^{16}$

See F^{18}.

XXXVIII. $O^{16}(\alpha, \alpha')O^{16*}$

Both elastic and inelastic scattering distributions ($O^{16*} = 6$--7, 8.8 MeV) have been studied at $E_\alpha = 19$ MeV by (Co 57c, Co 58c). The elastic scattering shows strong diffraction effects.

XXXIX. $O^{17}(p, d)O^{16}$ $Q_m = -1.919$

Not reported.

XL. $O^{17}(d, t)O^{16}$ $Q_m = 2.113$

Not reported.

XLI. $O^{17}(He^3, \alpha)O^{16}$ $Q_m = 16.432$

Not reported.

XLII. $O^{18}(p, t)O^{16}$ $Q_m = -3.730$

Not reported.

XLIII. $F^{19}(p, \alpha)O^{16}$ $Q_m = 8.119$

$Q_0 = 8.110 \pm 0.010$ (Sq 56).

Levels derived from observed α-particle groups are listed in table 16.10

TABLE 16.10

O^{16} levels from $F^{19}(p, \alpha)O^{16}$

A		B		
E_x (MeV)	Γ (keV)	E_x (MeV)	$\frac{d\sigma}{d\Omega}$ [a]	J^π
0	<20	0		0^+
6.051±0.010	<20	6.058±0.017	0.1	0^+
6.131±0.010	<20	6.138±0.011	0.8	3^-
6.920±0.010	<20	6.926±0.011	1	2^+
7.120±0.010	<20	7.122±0.011	2	1^-
8.874±0.012	<20	8.882±0.011	0.6	2^-
9.852±0.012	<20			
10.363±0.014	≈25—30			
11.085±0.014	≈25—30			

A: (Sq 56): $E_p = 7$ MeV.

B: (Yo 57a): $E_p = 5.2$ MeV; E_x calculated from reported Q-values and Q_m.

[a] Cross sections in mb/sr at $\theta = 180°$.

(Sq 56, Yo 57a: see also Aj 52c). There is some evidence for a broad level near 9.58 MeV (compare $C^{12}(\alpha, \alpha)C^{12}$) and for two additional unidentified groups which may represent levels near 11 MeV (see $N^{15}(d, n)O^{16}$); no other groups

appear with intensity > 5 per cent of that corresponding to $O^{16*}(8.87)$ (Sq 56). (Yo 57a) find no other groups corresponding to $O^{16*} = 6$ to 9 MeV with $d\sigma/d\Omega > 0.4$ mb/sr. The indicated assignments for the first five states derive from a variety of evidence; see (Aj 55).

6.06-MeV state

$W_\pi = 6.065 \pm 0.009$ MeV (Al 56f). The angular correlation of the monopole pairs is given by $W(\theta) = 1 + (0.955 \pm 0.007) \cos\theta$, consistent with $J = 0^+ \rightarrow 0^+$ (Ar 58a, Go 55f; see also De 54a). The mean life is $(7.2 \pm 0.7) \times 10^{-11}$ sec, considerably longer than is given by the α-model (De 54a). Calculations on various models are summarized by (Gr 57c); see also (Fe 57d, El 56, El 57b).

6.14-MeV state

The mean life is $(1.2 \pm 0.6) \times 10^{-11}$ sec (Ko 58), 0.5 to 1×10^{-11} sec (De 55). This transition rate is somewhat faster than that predicted on the α-particle model (Ka 56a) and is an order of magnitude faster than indicated by shell-model calculations (El 57b). It accounts for about one third of the total E3 width to the ground state from $T = 0$ states (Ko 58). See also (Kn 58a).

6.92-MeV state

$E_\gamma = 6.97 \pm 0.05$ MeV (Be 55a; Doppler corrected). The mean life is $\leqq 2.5 \times 10^{-14}$ sec (De 56a; see also De 55). Compare $O^{16}(\gamma, \gamma')O^{16*}$: (Sw 57a).

7.12-MeV state

The mean life is $\leqq 1.2 \times 10^{-14}$ sec (De 55); compare $O^{16}(\gamma, \gamma')O^{16*}$: (Sw 57a). A search for circular polarization of the γ-ray yields an upper limit of 2.0×10^{-3} indicating a maximum of $F^2 = 3 \times 10^{-8}$ for the intensity of any parity non-conserving part of the wave function (Wi 58c).

8.87-MeV state

The direct ground state transition is 7 ± 2 per cent (Be 57f), 9 ± 4 per cent (Mc 57a), 0.6 per cent (Wa 57f) of the cascade decays. The cascade decays take place via the 6.14, 6.92 and 7.12-MeV states with relative intensities 27 : 1 : 3. The three γ-rays have energies 2.75 ± 0.02, 1.90 ± 0.03 and 1.72 ± 0.03 MeV, fixing the energy of the state as 8.87 ± 0.02 MeV. The observed branching ratios, together with the absence of α-decay fix the assignment as $J^\pi = 2^-$ (Wi 56, Mc 57a). The separation of this state from the nearest 2^+ state ($O^{16*} = 9.85$ MeV) is too large to be accounted for in the α-model of (De 54c) (Wi 56: see also Ka 56a).

10.94-MeV state

At $E_p = 5.77$ MeV, a γ-ray of energy 3.86 ± 0.03 MeV is observed in coincidence with the 7.1-MeV radiation, indicating a level energy of 10.98

± 0.04 MeV. It is presumed that this level is to be identified with one of the unassigned groups observed by (Sq 56), (Be 57f). The direct ground state decay is < 5 per cent and cascades via $O^{16*} = 6.0$, 6.1, 6.9 and 8.9 MeV are less than 1, 6, 20 and 40 per cent respectively. The strong branch to $O^{16}(7.1)$, $J = 1^-$, and the weakness of other branches suggests $J(10.94) = 0^-$, although 1^+ is not excluded. The γ—γ correlation favours $J = 0^-$ (Be 57f: see also N^{15}(d, n)O^{16}). (Wa 57f find the γ-ray energy to be 3.86 ± 0.02 MeV and report a weak 4.9 MeV γ-ray). A search for possible nuclear pairs from the $0^- \rightarrow 0^+$ ground-state transition yielded an upper limit of $< 2 \times 10^{-5}$ for the pair branch (Ek 58). The importance of a definitive assignment of J^π for this state is stressed by (El 57b).

The influence of isobaric spin selection rules on cascade decays in O^{16} has been discussed by (Wi 53, Wi 56c: see also Ma 55f, Ma 55o). At $E_p = 18.5$ MeV, the α_0 angular distribution has been studied by (Li 56b): see F^{19}.

The reaction exhibits a large number of resonances: see Ne^{20}. See also (Mo 57c, Mo 58b, Bi 57e, Is 56).

F^{16}

(Not illustrated) †

MASS OF F^{16}

From the threshold of the $N^{14}(He^3, n)F^{16}$ reaction and the Wapstra (Wa 55c) masses for N^{14}, He^3 and n, the mass excess of F^{16} is 15.63 ± 0.02 MeV. A semi-empirical computation of the level shifts of the low $T = 1$ levels of N^{16} and O^{16} suggests that the ground state of F^{16} should have $J = 0^-$, and be unstable to proton emission by about 1 MeV (El 57b). Using the $(M-A)$ stated above, F^{16} is unstable with respect to proton emission by 0.81 MeV. The binding energies of a deuteron, a He^3-particle, and an α-particle in F^{16} are, respectively, 10.24, 9.37 and 8.98 MeV.

I. $N^{14}(He^3, n)F^{16}$ $\qquad Q_m = -1.18$

A slow neutron threshold has been observed at $E(He^3) = 1.434 \pm 0.015$ MeV corresponding to the ground state of F^{16}($Q_0 = -1.18 \pm 0.01$ MeV). There is some indication of another threshold corresponding to an excited state at ≈ 60 keV. The lifetime of F^{16} for decay into O^{15}+p is computed to be $\approx 10^{-19}$ sec (H. Bichsel, private communication). See also (Bu 56a).

II. $O^{16}(p, n)F^{16}$ $\qquad Q_m = -16.41$

See F^{17}.

III. $O^{16}(He^3, t)F^{16}$ $\qquad Q_m = -15.61$

Not reported.

† For level scheme of N^{16}, see fig. 31, p. 201.

N^{17}

(Fig. 34, p. 223)

MASS OF N^{17}

From the Q_0 of the $B^{11}(Li^7, p)N^{17}$ reaction and the Wapstra masses (Wa 55c) for B^{11}, Li^7 and H^1, the mass excess $(M-A)$ of N^{17} is 12.93 ± 0.06 MeV.

I. $N^{17}(\beta^-)O^{17*} \rightarrow O^{16}+n$ $\quad Q_m = 4.57$

The decay is complex. See O^{17}.

II. $B^{11}(Li^7, p)N^{17}$ $\quad Q_m = 8.38$

$Q_0 = 8.38\pm0.06$ (C. Littlejohn, private communication).

At $E(Li^7) = 2$ MeV, proton groups are observed corresponding to the ground state of N^{17} and to excited states at 1.32 ± 0.08, 1.89 ± 0.08, 2.50 ± 0.08, 2.82 ± 0.08, 3.27 ± 0.09, 3.57 ± 0.09, 3.86 ± 0.09 and 4.18 ± 0.09 MeV. The data on the four highest levels are preliminary (C. Littlejohn, private communication).

III. $C^{14}(\alpha, p)N^{17}$ $\quad Q_m = -9.75$

See O^{18}.

IV. $N^{15}(t, p)N^{17}$ $\quad Q_m = -0.15$

See (Sh 56a).

V. $O^{17}(n, p)N^{17}$ $\quad Q_m = -7.93$

See (Fa 57b).

VI. $O^{18}(\gamma, p)N^{17}$ $\quad Q_m = -15.99$

See (Re 55e).

VII. $O^{18}(n, d)N^{17}$ $\quad Q_m = -13.77$

Not reported.

VIII. $O^{18}(d, He^3)N^{17}$ $\quad Q_m = -10.50$

Not reported.

IX. $O^{18}(t, \alpha)N^{17}$ $\quad Q_m = 3.82$

See (Sh 56a).

X. $F^{19}(n, He^3)N^{17}$ $\quad Q_m = -16.24$

Not reported.

XI. Photospallation reactions.

A number of spallation reactions yielding N^{17} have been observed by (Re 55e) and (Ch 55c). See also (Ba 58l).

TABLE 17.1
Energy levels of N^{17}

E_x (MeV)	J^π; T	$\tau_{\frac{1}{2}}$ (sec)	Decay	Reactions
0	; $\frac{1}{2}$	4.14±0.04	β	I, II, III, IV, V, VI, IX, XI
1.32±0.08				II
1.89±0.08				II
2.50±0.08				II
2.82±0.08				II
(3.27±0.09)				II
(3.57±0.09)				II
(3.86±0.09)				II
(4.18±0.09)				II

O^{17}

(Fig. 35, p. 225) †

THEORY

See (Am 57b, Am 57c, Ra 57b, Pe 57b, Ba 56e, Ta 57a, Ka 56c, Ni 58a, Le 56e, Ki 56b, Ba 58c, Sc 56h, Fe 57c, Vi 56, Fa 57).

I. $C^{13}(\alpha, n)O^{16}$ $Q_m = 2.203$ $E_b = 6.348$

Observed resonances for $E_\alpha = 1$ to 5 MeV are listed in table 17.3 (Bo 56d, Wa 57c, Jo 53e, Tr 54, Be 56c, Ru 56c), together with those observed in $O^{16}(n, \alpha)C^{13}$. The observed cross section of $C^{13}(\alpha, n)O^{16}$ is closely matched by that calculated from the inverse reaction, for $E_\alpha = 4.0$ to 5.2 MeV (Wa 57c). Assignments for J^π in the range $O^{16*} = 7.1$ to 9.0 MeV are derived from angular distributions (Sc 56g, Wa 57c). The existence of additional broad states underlying this region is indicated by the analysis (Wa 57c, Ru 56c). Reduced widths have been tabulated for a number of levels by (Wa 57c); it is of interest that θ_n^2 and θ_α^2 generally differ by less than one order of magnitude (Wa 57c). The implications of the present reaction for element synthesis in stars is discussed by (Fo 55b, Sa 57c, Bu 57f). See also (Na 54a, Ba 56g).

II. $C^{14}(\alpha, n)O^{17}$ $Q_m = -1.825$

$Q_0 = -1.820 \pm 0.002$ (Sa 56d).

III. $N^{14}(\alpha, p)O^{17}$ $Q_m = -1.197$

Proton groups have been observed to the ground and first excited states of O^{17} (Ro 51g, Hj 53, Hj 53a).

IV. $N^{15}(d, n)O^{16}$ $Q_m = 9.886$ $E_b = 14.032$

The excitation function has been measured from 0.5 to 5.3 MeV. Above $E_d = 1.0$ MeV pronounced peaks are observed, presumably to be ascribed to

† For level scheme of F^{17}, see fig. 36, p. 233.

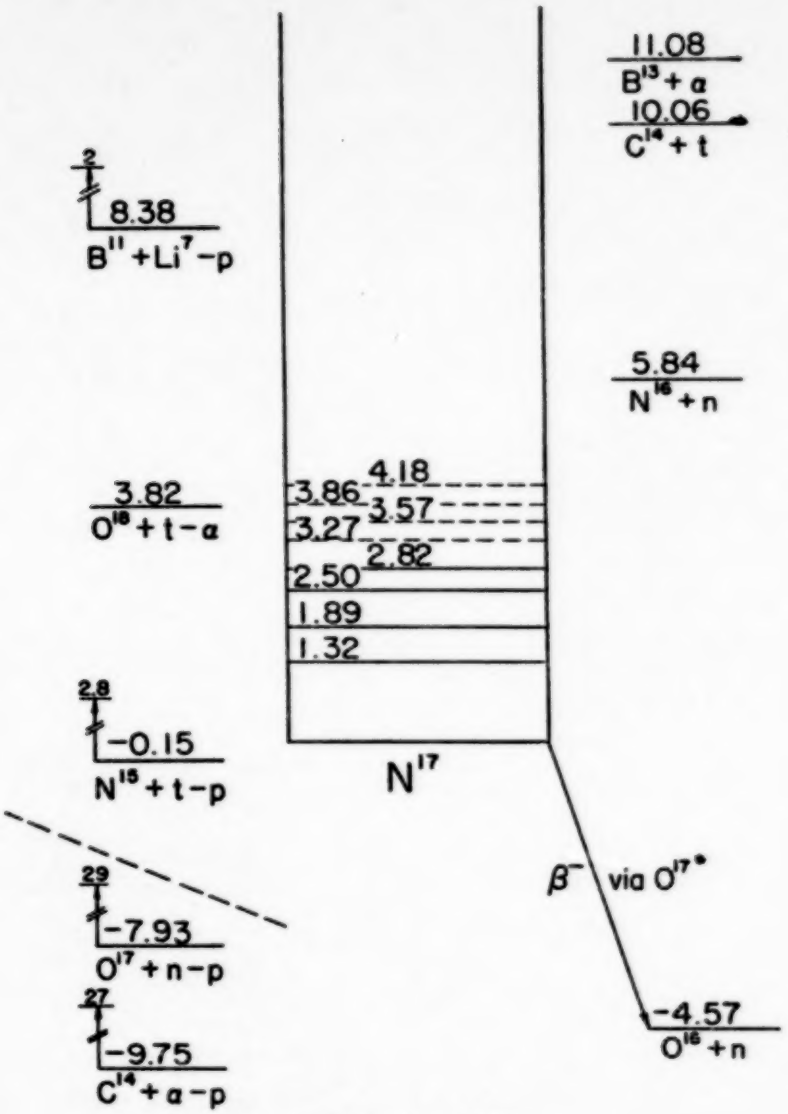

11 December 1958

Fig. 34. Energy levels of N^{17}: for notation, see fig. 1, p. 7.

numerous overlapping resonances. Angular distributions are generally well accounted for by the exchange stripping theory of (Ow 57), with an admixture of heavy-particle stripping which is almost constant for $E_d > 1$ MeV (We 58d).

V. $N^{15}(d, p)N^{16}$ $\quad Q_m = 0.267$ $\quad E_b = 14.032$

The excitation curve has been obtained for $E_d = 0.3$ to 2.7 MeV. There is some resonance structure at $E_d = 1.3$ and 1.9 MeV corresponding to $O^{17*} = 15.2$ and 15.8 MeV (Bo 57d). See also N^{16}.

TABLE 17.2
Energy Levels of O^{17}

E_x in O^{17} (MeV ± keV)	J^π	τ_m or Γ (keV)	Decay	Reactions
0	$\frac{5}{2}^+$		Stable	II, III, XVII, XXI, XXII, XXIII, XXVIII, XXIX
0.871 ± 4	$\frac{1}{2}^+$	$(2.5\pm1)\times10^{-10}$ sec	γ	III, XVII, XXVIII, XXIX
3.058 ± 6	$(\frac{1}{2}^-)$		γ	XVII, XXVIII
3.846 ± 5	$(\frac{7}{2}^-)$		γ	XVII, XXVIII
4.555 ± 5	$\frac{3}{2}^-$	40 ± 3	n	XI, XVII, XXVIII
5.083 ± 5	$\frac{3}{2}^+$	90 ± 5	n	XI, XVII, XXVIII
5.217 ± 5		< 8		XVII, XXVIII
5.378 ± 7	$\frac{3}{2}^-$	31 ± 4	n	XI, XVII, XXVIII
5.697 ± 4	$\frac{7}{2}^-$	≦ 7	n	XI, XVII
5.729 ± 5		< 8		XVII, XXVIII
5.866 ± 5	≧ $\frac{3}{2}$	≦ 8	n	XI, XVII, XXVIII
5.940 ± 10	$\frac{1}{2}^-$	26 ± 5	n	XI, XVII, XXVIII
6.24 ± 20				XVII, XXVIII
6.38 ± 30	$\frac{1}{2}^+$	130	n	XI
6.87 ± 20				XVII, XXVIII
(6.99 ± 20)				XXVIII
7.161 ± 6	$\frac{5}{2}$	2.7 ± 1	n, α	I
7.28 ± 30	$\frac{3}{2}^+$	210	n	XI
7.373 ± 6	$\frac{5}{2}$	≦ 2	n, α	I, XXVIII
7.560 ± 10	≧ $\frac{7}{2}$	≦ 4	n, α	I, XVII, XXVIII
7.676 ± 7	≧ $\frac{5}{2}$	22	n, α	I
(7.72 ± 80)	$(\frac{3}{2}^-)$	750	n	XI
7.94 ± 20	$\frac{1}{2}$	90	n, α	I, XVI
8.07 ± 20	$\frac{3}{2}$	75	n, α	I, XI, XVI
8.20 ± 20	$\frac{3}{2}$	60	n, α	I, XI, XVI
8.27 ± 40				XXVIII
8.340 ± 7	$\frac{1}{2}$	≦ 5	n, α	I, XI, XVI, XXVIII
8.390 ± 7	$\frac{5}{2}$	8	n, α	I, XI, XVI
8.460 ± 7	$\frac{7}{2}$	9	n, α	I, XI, XVI
8.493 ± 7	$(\frac{3}{2})$	≦ 6	n, α	I, XI, XVI
(8.59 ± 40)				XXVIII
8.70 ± 20	$\frac{3}{2}$	70	n, α	I, XI, XVI
8.89 ± 20	$\frac{3}{2}$	110	n, α	I, XI, XVI
8.96 ± 20	$\frac{7}{2}$	30	n, α	I, XI, XVI
9.06 ± 40				XXVIII
9.15 ± 20		≦ 6	n, α	I, XI
9.20	$\frac{5}{2}$	≦ 4	n, α	I
9.50	$\frac{7}{2}$	11	n, α	I, XI
9.73	$\frac{7}{2}$	19	n, α	I, XI
9.78		55	n, α	I
9.89	$\frac{5}{2}$	12	n, α	I
9.98	$(\frac{5}{2}, \frac{7}{2})$	150	n, α	I
10.21		50	n, α	I, XI
10.5			n	XI, XII
10.9			n	XI, XII
11.5			n	XI, XII
12.1			n	XI, XII
15.2			d, p	V
15.8			d, p	V

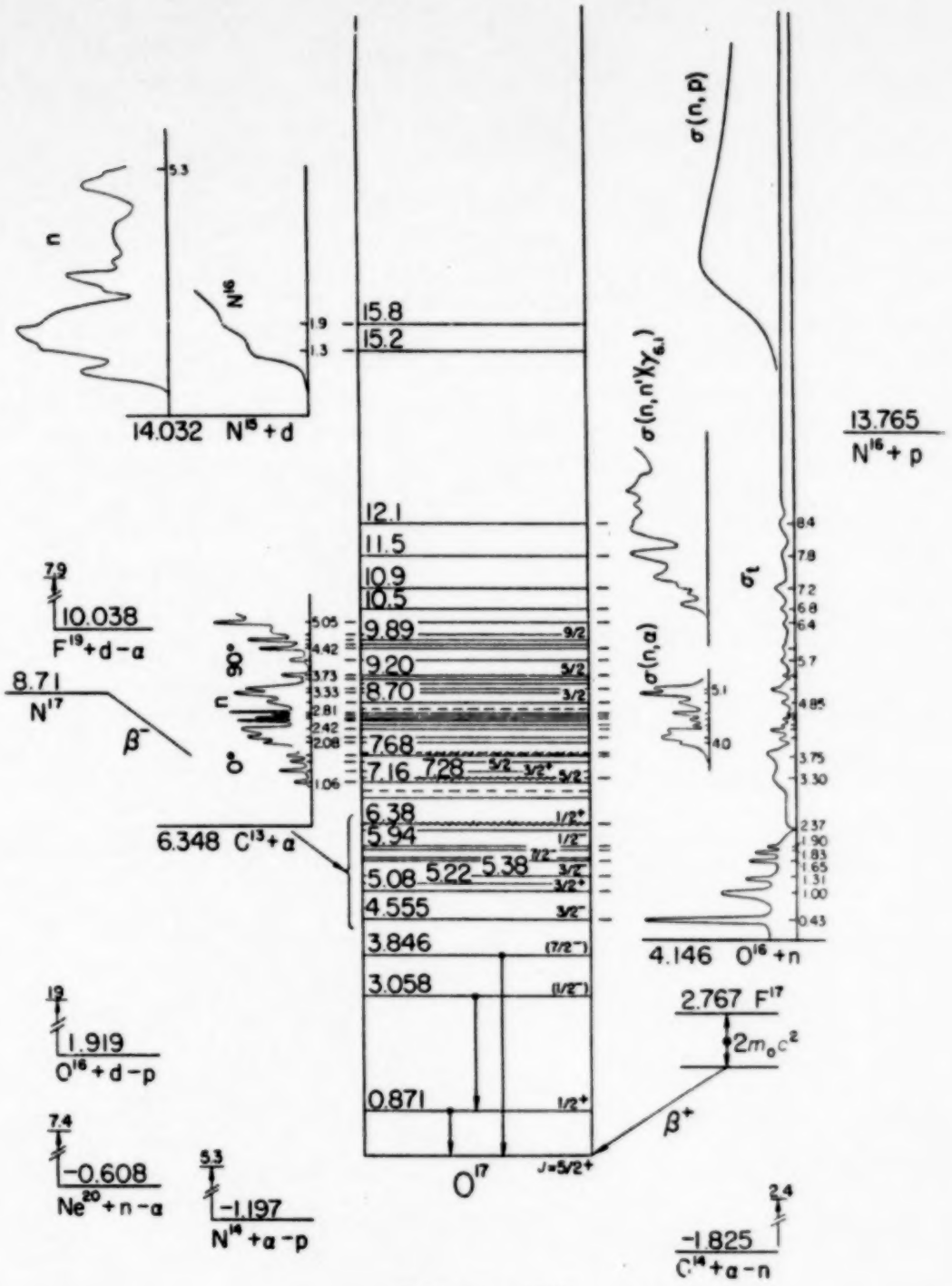

8 January 1959

Fig. 35. Energy levels of O^{17}: for notation, see fig. 1, p. 7.

VI. $N^{15}(d, \alpha)C^{13}$ $Q_m = 7.683$ $E_b = 14.032$

See (Ho 40).

VII. $N^{15}(t, n)O^{17}$ $Q_m = 7.774$

Not reported.

TABLE 17.3

Resonances in $C^{13}(\alpha, n)O^{16}$ and $O^{16}(n, \alpha)C^{13}$

E_α MeV ± keV	E_n	$\Gamma_{c.m.}$ (keV)	l_α	l_n	J^π	$E_x(O^{17})$ (MeV)	Refs.
1.063 ± 4		2.7 ± 1	3,2	2,3	$\frac{1}{2}^+$	7.161	a
1.340 ± 4		≦2	3,2	2,3	$\frac{5}{2}^+$	7.373	a
1.585 ± 7		≦4			$\frac{7}{2}^-$ or $\frac{9}{2}^-$	7.560	b
1.736 ± 5		22			$\frac{3}{2}^-$ or $\frac{9}{2}^-$	7.676	b
2.080 ± 20	4.0	90	1,0		$\frac{1}{2}^\pm$	7.94	c
2.250 ± 20	4.15	75	2,1		$\frac{3}{2}^\mp$	8.07	d
2.420 ± 20	4.25	60	1,2	2,1	$\frac{1}{2}^\pm$	8.20	d
2.603 ± 5	4.46	≦5	1,0		$\frac{1}{2}^-$	8.34	e
2.675 ± 5	4.53	8	3,2		$\frac{5}{2}^+$	8.39	f
2.760 ± 5	4.59	9	3,4		$\frac{7}{2}^\pm$	8.46	f
2.805 ± 5	4.62	≦6	1,2		$(\frac{3}{2}^\mp)$	8.493	g
3.08 ± 15	4.85	70	1,2		$\frac{3}{2}^\pm$	8.70	g
3.33 ± 15	5.05	110	2,1		$\frac{3}{2}^\mp$	8.89	f
3.42 ± 15	5.13	30	3,4		$\frac{7}{2}^\pm$	8.96	f
3.67 ± 15		≦6				9.15	h
3.73		≦4			$\frac{5}{2}^+$	9.20	i
4.125		11			$\frac{7}{2}^-$	9.502	i
4.42		19			$\frac{7}{2}^-$	9.73	i
(4.50)		55				9.78	i
4.63		12			$\frac{9}{2}^+$	9.89	i
4.75		150			$\frac{5}{2}^+$, $\frac{7}{2}^-$	9.98	i
5.05		50				10.21	i

[a] (Jo 53e, Ru 56c, Wa 57c).
[b] (Ru 56c, Wa 57c).
[c] (Se 55a, Bo 56d, Sc 56g, Ru 56c, Wa 57c).
[d] (Tr 54, Se 55a, Bo 56d, Sc 56g, Ru 56c, Be 56c, Wa 57c).
[e] (Bo 56d, Sc 56g, Be 56c, Wa 57c).
[f] (Tr 54, Bo 56d, Sc 56g, Be 56c, Wa 57c).
[g] (Bo 56d, Sc 56g, Be 56c, Wa 57c).
[h] (Bo 56d).
[i] (Bo 56d, Sc 56g).

VIII. $N^{15}(He^3, p)O^{17}$ $Q_m = 8.539$

Not reported.

IX. $N^{15}(\alpha, d)O^{17}$ $Q_m = -9.812$

Not reported.

X. $O^{16}(n, \gamma)O^{17}$ $Q_m = 4.146$

$\sigma_{capt} < 0.2$ mb (Hu 55c).

XI. $O^{16}(n, n)O^{16}$ $E_b = 4.146$

The cross section is almost constant at 3.76 b from thermal energies to $E_n = 0.3$ MeV (Hu 58). Observed resonances are indicated in table 17.4 (Ba 52b, Ok 55, Be 56c, Wa 57c, Hu 58, La 58c, St 58). (Fo 58) have measur-

ed angular distributions at six energies in the range $E_n = 0.7$ to 2.2 MeV and have derived the phase shifts up to 2.4 MeV. From measurements in the range $E_n = 0.1$ to 1.7 MeV, (La 58c) find that the $E_n = 1.65$-MeV resonance

TABLE 17.4

Resonances in $O^{16}(n, n)O^{16}$

E_n (MeV ± keV)	Γ_{lab} (keV)	l_n	J^π	$E_x(O^{17})$ (MeV)	Refs.
0.433 ± 4	41 ± 3	1	$\frac{3}{2}^-$	4.554	a, b
0.998 ± 8	96 ± 5	2	$\frac{5}{2}^+$	5.085	a, c, d
1.310 ± 8	33 ± 4	1	$\frac{3}{2}^-$	5.379	a, c
1.651 ± 6	≦7	≧1	$\frac{7}{2}^-$	5.700	a, d
1.830 ± 6	≦8	≧1	≧$\frac{3}{2}$	5.868	a
1.903 ± 11	28 ± 5	1	$\frac{1}{2}^-$	5.937	a, e
2.370 ± 20	140	0	$\frac{1}{2}^+$	6.377	a, e
3.330 ± 30	220	2	$\frac{5}{2}^+$	7.28	a, e
3.750 ± 20	<100			7.68	a, g
(3.800)	800	1	$(\frac{3}{2}^-)$	(7.72)	a, e
4.190 ± 20	<100			8.09	a, g
4.320 ± 20	<100			8.21	a, e, g
4.440 ± 20	<100			8.32	a, f, g
4.53			≧$\frac{3}{2}$	8.41	f
4.59				8.47	f
4.62			≧$\frac{3}{2}$	8.49	f
4.85				8.71	f
5.08				8.93	f
5.13				8.97	f
5.37				9.20	f
5.7				9.5	a
5.9				9.7	a
6.4				10.2	a
6.8				10.5	a
7.2				10.9	a
7.8				11.5	a, f
8.4				12.1	a, f

a (Hu 58).
b (Ok 55).
c (St 58).
d (La 58c).
e (La 52b).
f (Be 56c).
g (Wa 57c).

is due to a $\frac{7}{2}^-$ state. Phase shifts for $E_n = 0.2$ to 1.4 MeV derived by (St 58) from total cross section measurements are in good agreement with those of (Fo 58) except for a 5° discrepancy in $\delta_{\frac{1}{2}+}$ at $E_n = 0.73$ MeV. According to (St 58), the s-wave shifts from 0.2 to 2.3 MeV fit hard-sphere scattering with $R = 5.6 \times 10^{-13}$ cm. (Fo 58) find that the s- and d-wave phase shifts and the locations of O^{17}(g.s. : $d_{\frac{5}{2}}$), O^{17*}(0.87 : $s_{\frac{1}{2}}$) and O^{17*}(5.08 : $d_{\frac{3}{2}}$) can be ade-

quately described by a potential well 40—45 MeV deep, with a diffuse boundary. See also (Vi 56).

The angular distribution has also been measured at $E_n = 5$ MeV (Hi 58). Polarization studies have been carried out for $E_n = 0.25$ to 0.6 MeV by (Wi 54c, Ok 55) and for $E_n = 0.7$ to 1.4 MeV by (St 58). Cross sections at $E_n = 14$ MeV are tabulated by (Hu 58). See also (Fl 56a, Ba 56g, Mc 57) and (Aj 55).

XII $O^{16}(n, n')O^{16*}$ $E_b = 4.146$

The yield of γ-rays shows marked structure in the range $E_n = 7$—10 MeV (See Hu 58). At $E_n = 14.1$ MeV, the inelastic scattering cross section is 0.5 b (Co 53b).

XIII. $O^{16}(n, 2n)O^{15}$ $Q_m = -15.655$ $E_b = 4.146$

See (Aj 55).

XIV. $O^{16}(n, p)N^{16}$ $Q_m = -9.619$ $E_b = 4.146$

The cross section rises from threshold to a peak of 89 ± 30 mb at $E_n = 14$ MeV, falling to ≈ 60 mb at 18 MeV (Ma 54d). See also (Aj 55) and (Ki 53c, Fa 57b, Hu 58).

XV. $O^{16}(n, d)N^{15}$ $Q_m = -9.884$ $E_b = 4.146$

See (Hu 55c, Ki 53c).

XVI. $O^{16}(n, \alpha)C^{13}$ $Q_m = -2.203$ $E_b = 4.146$

The cross section has been measured from threshold to 4.2 MeV by (Se 55a) and from 4.0 to 5.2 MeV by (Wa 57c). All of the O^{16} levels observed in $C^{13}(\alpha, n)O^{17}$ from $O^{17*} = 7.92$ to 8.96 MeV are also observed in this reaction, with good agreement in level position: see table 17.3. Observed cross sections correspond closely to those calculated from the inverse reaction (Wa 57c). At higher energies, using continuous fast neutrons, (Ki 56a) report 18 levels in O^{17} in the range $E_x = 6.8$ to 9.7 MeV, and (Gi 53a) reports 32 levels in the range $E_x = 6.8$ to 12.8 MeV. See also (Ki 53c, Hu 55c, Hu 55d, Ba 56g).

XVII. $O^{16}(d, p)O^{17}$ $Q_m = 1.919$

$O_0 = 1.918 \pm 0.004$ (Br 57g).

$Q_0 = 1.915 \pm 0.010$ (Sp 54e).

$Q_0 = 1.885$ (Kh 55a).

O^{17} levels derived from observed proton groups are listed in table 17.5 (Bu 51f, Br 57g; see also Sp 54e, Kh 55a, Kh 53), together with those from the α-groups from $F^{19}(d, \alpha)O^{17}$. The J^π assignments are derived from stripping analysis: see (Aj 55, Gr 56b, Ri 58c). It is noted that the relatively large capture probabilities corresponding to O^{17*}(g.s.), (0.87), (3.8) and (5.08) are consistent with the assumption that these are relatively pure single

particle states formed from an O^{16} core with 1d, 2s, 1f and 1d neutrons, respectively. The states at $E_x = 3.06$ and 4.55 MeV must be presumed to arise from more complicated configurations (Gr 56b).

TABLE 17.5

States of O^{17} from $O^{16}(d, p)O^{17}$ and $F^{19}(d, \alpha)O^{17}$

E_x [a] (MeV ± keV)	$\Gamma_{c.m.}$ [a] (keV)	l_n [b]	J^π [b]	A [c] / $2J+1$	E_x [d] (MeV ± keV)	E_x [e] (MeV ± keV)
0	<8	2	$\frac{5}{2}^+$	72	0	0
0.871 ± 4	<8	0	$\frac{1}{2}^+$	68	0.870 ± 20	0.883 ± 11
3.055 ± 4	<8	iso.	$(\frac{1}{2}^-)$		3.060 ± 30	3.069 ± 10
3.846 ± 5	<8	3	$(\frac{7}{2}^-)$	15	3.850 ± 30	3.856 ± 11
4.553 ± 6	40 ± 5	1	$\frac{3}{2}^-$	2.2	4.580 ± 20	4.567 ± 14
5.083 ± 10	95 ± 5	2	$\frac{3}{2}^+$	25	5.070 ± 20	
5.215 ± 5	<8					5.229 ± 13
5.378 ± 7	28 ± 7				5.310 ± 20	5.397 ± 14
5.695 ± 5	<8					
5.731 ± 5	<8				5.760 ± 20	5.723 ± 14
5.866 ± 5	<8					5.875 ± 15
5.940 ± 15	23 ± 10					5.947 ± 15
					6.240 ± 20	
					6.890 ± 30	6.869 ± 14
						(6.986 ± 15)
						(7.371 ± 15)
					7.510 ± 30	
					8.270 ± 40	
					(8.590 ± 40)	
					9.060 ± 40	

[a] $O^{16}(d, p)O^{17}$: (Br 57g); $E_d = 6.5$ to 7.5 MeV. No other proton groups appear with intensities greater than 0.1 of 4.55-MeV group.
[b] $O^{16}(d, p)O^{17}$: (Gr 56b); $E_d = 9$ MeV.
[c] (Gr 56b); relative capture probabilities.
[d] $O^{16}(d, p)O^{17}$ and $F^{19}(d, \alpha)O^{17}$: (Bu 51f); $E_d = 7.9$ MeV.
[e] $F^{19}(d, \alpha)O^{17}$: (Wa 52b); $E_d = 1.8$ MeV.

An earlier report that the 871-keV level might be a close doublet (Do 56c) is not confirmed by (Mo 57, Br 57g, Ma 57f). Q for this level is 1049.0 ± 2.2 keV (Mo 57), 1048 ± 2 keV (Do 56c), 1047 ± 4 keV (Br 57g). The γ-ray energy is 870.5 ± 2.0 keV (Th 52), 869 ± 3 keV (Ma 55a); the internal conversion coefficient is consistent with E2 (Th 52). The lifetime is $\tau_m = (2.5 \pm 1) \times 10^{-10}$ sec (Th 53a): this value indicates a considerable enhancement of the single particle transition rate. Possible models are discussed by (Ka 56a, Ba 56e, Ba 58c, Am 57b, Am 57c, Ra 57b, Sc 56h, Fa 57).

Observed widths and shapes of $O^{17*} = 4.55$ and 5.08 MeV are in good accord with $O^{16}(n, n)O^{16}$ results (Br 57g). The ratio of ground state reduced widths is 1.30 (Ca 56b). See also (Al 55e, Kh 55, El 56a, Aj 55), (Iv 56; theo.) and F^{18}.

XVIII. $O^{16}(t, d)O^{17}$ $Q_m = -2.113$

Not reported.

XIX. $O^{16}(\alpha, He^3)O^{17}$ $Q_m = -16.436$

Not reported.

XX. $N^{17}(\beta^-)O^{17*} \rightarrow O^{16}+n$ $Q_m = 4.57$

The half-life is 4.14 ± 0.04 sec (Kn 48), 4.15 ± 0.1 sec (St 51a), 4.16 ± 0.15 sec (Fa 57b). $E_\beta(\max) = 3.7\pm0.2$ MeV (Al 49c): $\log ft = 3.8$. The β-decay proceeds to an excited state or states of O^{17} which in turn decay to O^{16} by neutron emission: the neutron spectrum has a maximum at 0.92 ± 0.07 MeV (Al 49c, Ha 49c) and a half-width < 0.5 MeV. See also (Jo 57c; theo.).

XXI. $O^{17}(p, p')O^{17*}$

See (Wa 54).

XXII. $F^{17}(\beta^+)O^{17}$ $Q_m = 2.767$

See F^{17}.

XXIII. $O^{18}(p, d)O^{17}$ $Q_m = -5.842$

See (Ts 56).

XXIV. $O^{18}(d, t)O^{17}$ $Q_m = -1.810$

Not reported.

XXV. $O^{18}(He^3, \alpha)O^{17}$ $Q_m = 12.509$

Not reported.

XXVI. $F^{19}(n, t)O^{17}$ $Q_m = -7.548$

Not reported.

XXVII. $F^{19}(p, He^3)O^{17}$ $Q_m = -8.313$

Not reported.

XXVIII. $F^{19}(d, \alpha)O^{17}$ $Q_m = 10.038$

Observed alpha groups are displayed in table 17.5 (Bu 51f, Wa 52b). At $E_d = 1.2$ MeV, two γ-rays are observed with $E_\gamma = 2.2$ MeV ($3.06 \rightarrow 0.87$) and 3.81 MeV. The absence of the direct ground state decay of the 3.06-MeV state is consistent with $J = \frac{1}{2}$ (Go 56i, Mu 57b).

XXIX. $Ne^{20}(n, \alpha)O^{17}$ $Q_m = -0.608$

See Ne^{21}.

F^{17}

(Fig. 36, p. 233) †

THEORY

See (Ka 56c, Ba 58c).

I. $F^{17}(\beta^+)O^{17}$ $Q_m = 2.767$

The decay proceeds to the ground state of O^{17}: $E_{\beta^+}(\max) = 1.748 \pm 0.006$ MeV. The spectrum has the allowed shape down to 570 keV, and an upper limit of one per cent is placed on possible transitions to the 875-keV state of O^{17} (Wo 54a). The weighted mean value of the half-life from the determinations of (Br 49, La 51d, Wo 54a, Wa 54, Ko 54, Ar 58) is 66.0 ± 0.3 sec. Log $ft = 3.38$. See also (Be 58e; theo.).

II. $N^{14}(\alpha, n)F^{17}$ $Q_m = -4.747$

$Q_0 = -4.76 \pm 0.07$ (Do 56a)

Slow neutron threshold and proton recoil measurements indicate an excited state at 0.53 ± 0.04 MeV (Do 56a).

III. $N^{15}(He^3, n)F^{17}$ $Q_m = 4.989$

Not observed.

IV. $O^{16}(p, \gamma)F^{17}$ $Q_m = 0.596$

Nonresonant capture has been studied for $E_p = 0.8$ to 2.1 MeV. This work indicates, in addition to the direct ground-state transition (γ_1), a transition (γ_2) to a state of F^{17} at 487 ± 10 keV which then radiates (γ_3) to the ground state. The ratio of γ_2 to γ_1 is ≈ 10 over the energy region studied. The γ_1 and γ_3 radiations are approximately isotropic, while γ_2 has an almost pure ($\sin^2\theta$) distribution ($E_p = 1.0$ to 1.9 MeV). At $E_p = 1.35$ MeV, the cross section for production of γ_2 radiation is 6 ± 3 μb. The fact that most transitions involve the 0.50-MeV state (γ_2) indicates that the non-resonant yield is not to be attributed to this state; it is suggested that direct, one-stage capture is involved (Wa 54).

The relative F^{17} activity has been measured from $E_p = 1.1$ to 4.1 MeV by (La 51d). The cross section increases almost linearly with proton energy from 1.1 to 3.75 MeV, except for a sharp resonance at 3.47 MeV. There is some indication of a broad resonance at 3.99 MeV (La 51d, La 51e).

For $E_p = 140$ to 170 keV, the cross section varies from 0.46 to 2.34×10^{-10} b (He 58h). At $E_p = 616$ keV, $\sigma = 0.29 \pm 0.03 \times 10^{-6}$ b; both the magnitude of the cross section and the character of the excitation function from $E_p = 275$ to 616 keV are consistent with a direct capture process (Ta 59). See also (Wi 53c, Li 58a, Bu 57f, Ch 59).

The excitation energy of the first level of F^{17} is 495 ± 15 keV (Ho 58b), 505 ± 10 keV (Le 57g). The lifetime of $F^{17*}(0.5)$ is $\tau_m = (2.5 \pm 0.7) \times 10^{-10}$ sec (Le 57g), $(3.5 \pm 1.5) \times 10^{-10}$ sec (Ho 58b). Using the weighted mean, $2.9 \times$

† For level scheme of O^{17}, see fig. 37, p. 225.

10^{-10} sec, the ratio $\tau_m F^{17*}(0.5)/\tau_m O^{17*}(0.87) = 1.2$ (Ho 58b): see $O^{16}(d,p)O^{17}$ and (Ba 58c).

V. $O^{16}(p, n)F^{16}$ $Q_m = -16.41$ $E_b = 0.596$

See (Ta 58a).

TABLE 17.6

Energy Levels of F^{17}

E_x (MeV)	J^π	τ or Γ (keV)	Decay	Reactions
0	$(\frac{5}{2}^+)$	$\tau_{\frac{1}{2}} = 66.0 \pm 0.3$ sec	β^+	I, II, IV, VIII, XIII
0.500 ± 0.003	$\frac{1}{2}^+$	$\tau_m = (2.9 \pm 0.7) \times 10^{-10}$ sec	γ	II, IV, VIII
3.10	$\frac{1}{2}^-$	18.7	p	VI, VIII
3.86	$\frac{3}{2}^-$	<3.3	p, γ	IV, VI
4.4	$(\frac{3}{2}^-)$	≈ 400	p	VI
4.7	$(\frac{5}{2}^+)$	(300)	p	VI, VIII
(5.1)	$(\frac{1}{2}^+)$	190	p	VI
5.45		≈ 40	p	VI
5.66		≈ 40	p	VI
5.83		≈ 40	p	VI
(6.15)		<25	p	VI
(6.6)	$(\frac{1}{2}^+)$	140	p	VI
(6.75)		<25	p	VI
(6.90)		<25	p	VI

VI. $O^{16}(p, p)O^{16}$ $E_b = 0.596$

Observed anomalies in the scattering are exhibited in table 17.7. The low energy scattering data require a large s-wave phase shift, probably reflecting the bound level at $F^{17*} = 0.55$ MeV, and a relatively large d-wave shift (La 51e, Ep 53). A study of proton polarization for $E_p = 2.5$ to 3.0 MeV confirms the assignment $J = \frac{1}{2}^-$ to $F^{17*}(3.10)$ and excludes $\frac{1}{2}^+$, $\frac{3}{2}^-$ (So 57a). A phase shift analysis for $E_p = 3$ to 7 MeV requires four broad resonances corresponding to $F^{17*} = 4.5$ ($P_{\frac{3}{2}}$), 4.6 ($D_{\frac{3}{2}}$), 5.15 ($S_{\frac{1}{2}}$) and 6.65 MeV ($S_{\frac{1}{2}}$). Eight additional sharp resonances are found in this region (Se 54a: see table 17.7): however, the curves of (He 56a) show no evidence of fine structure from $E_p = 2.5$ to 5.5 MeV beyond that indicated in column A of table 17.7. See also $O^{16}(d, n)F^{17}$.

Scattering at $E_p > 10$ MeV appears to be dominated by optical model effects: see O^{16}.

VII. $O^{16}(p, \alpha)N^{13}$ $Q_m = -5.208$ $E_b = 0.596$

See (Wh 58a).

VIII. $O^{16}(d, n)F^{17}$ $Q_m = -1.631$

$E_{thresh} = 1.830 \pm 0.004$; $Q_0 = -1.626 \pm 0.004$ (Ma 55m)

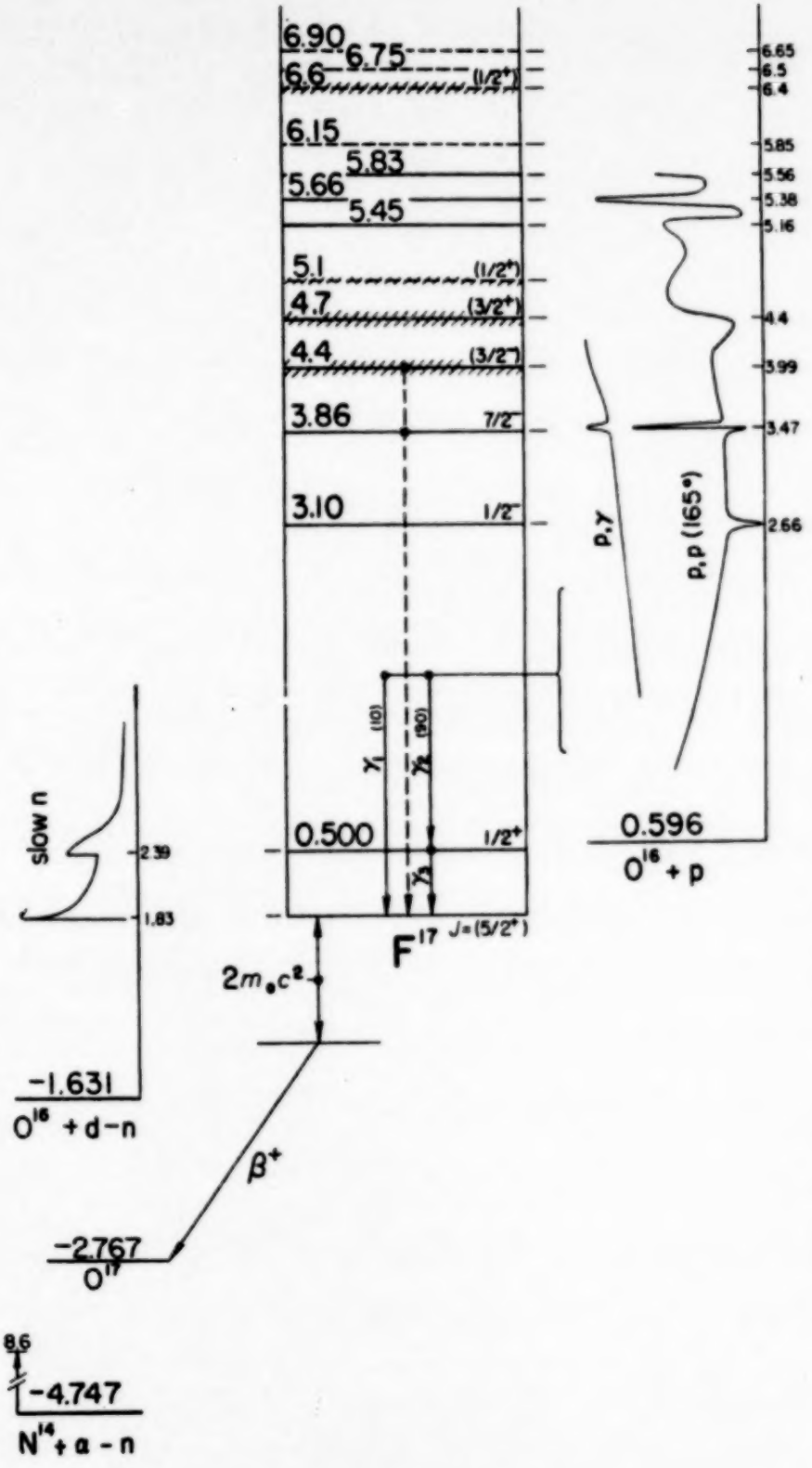

29 December 1958

Fig. 36. Energy levels of F^{17}: for notation, see fig. 1, p. 7.

Neutron groups have been observed corresponding to $F^{17*} = 0$, 0.536 $\pm$0.010 (Aj 51b), 0.53$\pm$0.06 MeV (El 51a, Mi 53), 3.03$\pm$0.06 MeV and 4.74$\pm$0.07 MeV (Gr 57b). Angular distributions of the n_0 and n_1 groups, analyzed by stripping theory, indicate $J = \frac{3}{2}^+$ or $\frac{5}{2}^+$ for the ground state and

TABLE 17.7
Levels of F^{17} from $O^{16}(p, p)O^{16}$

A			B				
E_p (MeV)	Γ (keV)	J^π	E_p (MeV)	Γ (keV)	J^π	$\theta_p{}^2$ (%)	F^{17*} (MeV)
2.66	19.9	$\frac{1}{2}^-$					3.10
3.47	<3.5	$\frac{3}{2}^-$	3.50	<25			3.86
(3.99)	≈500	$(\frac{3}{2}^+)$	4.1	400	$\frac{3}{2}^-$	20	4.4
(4.39)	240	$(\frac{1}{2}^-)$	4.2	350	$\frac{1}{2}^+$	32	4.7
			4.70	<25			(5.05)
			4.8	200	$\frac{1}{2}^+$	5.5	5.1
			4.95	<25			(5.30)
5.16	60		5.20	<25			5.45
5.38	50		5.40	<25			5.66
5.56	60		5.60	<25			5.83
			5.85	<25			(6.15)
			6.50	<25			(6.75)
			6.4	150	$\frac{1}{2}^+$	3.7	(6.6)
			6.65	<25			(6.90)

A: (La 51d, La 51e, Ep 53, He 56a).
B: (Se 54, Se 54a).

$J = \frac{1}{2}^+$ for the first excited state (El 51a, Mi 53, Aj 51b). The ratio of the reduced widths of the F^{17} and O^{17} ground states is 1.30 (Ca 56b). The width of the neutron group corresponding to $F^{17*}(4.74)$ is < 90 keV, considerably smaller than is reported in $O^{16}(p, p)O^{16}$ (Gr 57b).

Slow neutron thresholds have been observed corresponding to the ground and first excited states of F^{17}: $Q_1 = -2.125\pm0.004$ MeV corresponding to $F^{17*} = 499\pm3$ keV (Ma 55m). See also (Be 58f, Go 58g)

IX $O^{16}(He^3, d)F^{17}$ $Q_m = -4.898$

Not reported.

X. $O^{16}(\alpha, t)F^{17}$ $Q_m = -19.217$

Not reported.

XI. $O^{17}(p, n)F^{17}$ $Q_m = -3.550$

Not reported.

XII. $O^{17}(He^3, t)F^{17}$ $Q_m = -2.785$

Not reported.

XIII. $F^{19}(\gamma, 2n)F^{17}$ $Q_m = -19.582$

See F^{19}.

XIV. $F^{19}(p, t)F^{17}$ $Q_m = -11.098$

Not reported.

XV. $Ne^{20}(p, \alpha)F^{17}$ $Q_m = -4.158$

Not reported.

O^{18}

(Fig. 37, p. 237)

THEORY

See (El 55a, Re 55b, Th 56a, Ra 57, Re 58).

I. $C^{14}(\alpha, \gamma)O^{18}$ $Q_m = 6.243$

Three resonances are reported, at $E_\alpha = 1.13$, 1.79, and 2.33 MeV (Go 58b, Ph 58): see table 18.2. Angular distribution measurements of the capture radiation at the resonances permit the assignments $J = 0^+$, 2^+, 4^+ for the first three states of O^{18} and $J = 4^+$, 1^- and 1^- to the resonance levels, $O^{18*} = 7.12$, 7.64 and 8.06 MeV (Ph 58, Go 58b). The branching ratios for the upper two levels do not agree with values estimated from a simple collective model (Ph 58). The ground state transition from $O^{18*}(3.55)$ is less than 3 per cent of the transition $3.55 \rightarrow 1.98$ (Go 58b).

II. $C^{14}(\alpha, n)O^{17}$ $Q_m = -1.825$ $E_b = 6.243$

$E_{thresh} = 2.340 \pm 0.003$, $Q_0 = -1.820 \pm 0.002$ (Sa 56d).

Observed resonances in the 0^0 yield curve for $E_\alpha = 2.3$ to 3.6 MeV are shown in table 18.3. The angular distribution of the neutrons at the 2.64-MeV resonance indicates $J = 1^-$ or 3^- for the 8.29-MeV state of O^{18} (Sa 56d).

III. $C^{14}(\alpha, \alpha)C^{14}$ $E_b = 6.243$

Observed anomalies in the scattering for $E_\alpha = 2$ to 3.9 MeV are shown in table 18.3. The resonances at $E_\alpha = (2.8)$, 3.3, and 3.5 MeV appear to have $\Gamma_n \gg \Gamma_\alpha$ (We 58).

IV. $C^{14}(\alpha, p)N^{17}$ $Q_m = -9.75$ $E_b = 6.238$

See (Su 51b).

V. $N^{15}(t, p)N^{17}$ $Q_m = -0.15$ $E_b = 15.842$

See (Sh 56a).

VI. $N^{15}(\alpha, p)O^{18}$ $Q_m = -3.971$

Not observed.

VII. $O^{16}(t, p)O^{18}$ $Q_m = 3.730$

See (Cu 53c).

TABLE 18.1
Energy levels of O^{18}

E_x in O^{18} (MeV±keV)	J^π	Γ (keV)	Decay	Reactions
0	0^+		Stable	I, VII, X, XII, XIII, XIV, XV, XVI, XVIII
1.982± 4	2^+		γ	I, X, XII, XIII, XVI, XVIII
3.55 ±20	4^+		γ	I, X, XIII, XVIII
3.929±40				XVIII
5.007±40				XVIII
5.170±40				XVIII
5.311±40				XVIII
5.456±40				XVIII
6.190±40				XVIII
6.328±40				XVIII
7.12	4^+		γ, α	I
7.638±15	1^-	<3	γ, α	I
8.057±15	1^-	<3	γ, α	I, III
8.229±15	2^+	1.3± 0.8	α, n	II, III
8.302±15	3^-	8 ± 1	α, n	II, III
8.42 ±20)		17 ± 8	α, n	II
8.84 ±20		80 ±16	α, n	II
8.971±15	$\geq 2^+$	42 ± 2	α, n	II, III
9.0 – 9.2 (two levels)	$2^+, 3^-$ or $4^+, 3^-$	>150	α	III

VIII. $O^{17}(n, p)N^{17}$ $Q_m = -7.93$ $E_b = 8.069$

See (Ch 49d).

IX. $O^{17}(n, \alpha)C^{14}$ $Q_m = 1.825$ $E_b = 8.069$

The thermal neutron cross section is 0.4±0.1 b (Hu 58).

X. $O^{17}(d, p)O^{18}$ $Q_m = 5.842$

$Q_0 = 5.821 \pm 0.010$ (Ah 54d, Ah 54e).

Proton groups have been observed, corresponding to excited states at 1.986±0.013 (Ah 54d, Ah 54e; based on Q_0), 1.981±0.02 MeV, at 2.449±0.02

TABLE 18.2
Resonances in $C^{14}(\alpha, \gamma)O^{18}$ (Go 58b, Ph 58)

E_{res} (MeV±keV)	Γ keV)	E_x in O^{18} (MeV)	J^π	Γ_α[a] (eV)			
				(g.s.)	(1.98)	(3.55)	(3.93)
1.13		7.12	4^+		0.01		
1.794±6	<3	7.638	1^-	0.12	0.24	<0.02	<0.02
2.334±6	<3	8.058	1^-	0.09	0.23	<0.05	<0.05

[a] $\Gamma_\alpha\Gamma_\gamma/\Gamma$ for γ-transitions leading to the states indicated.

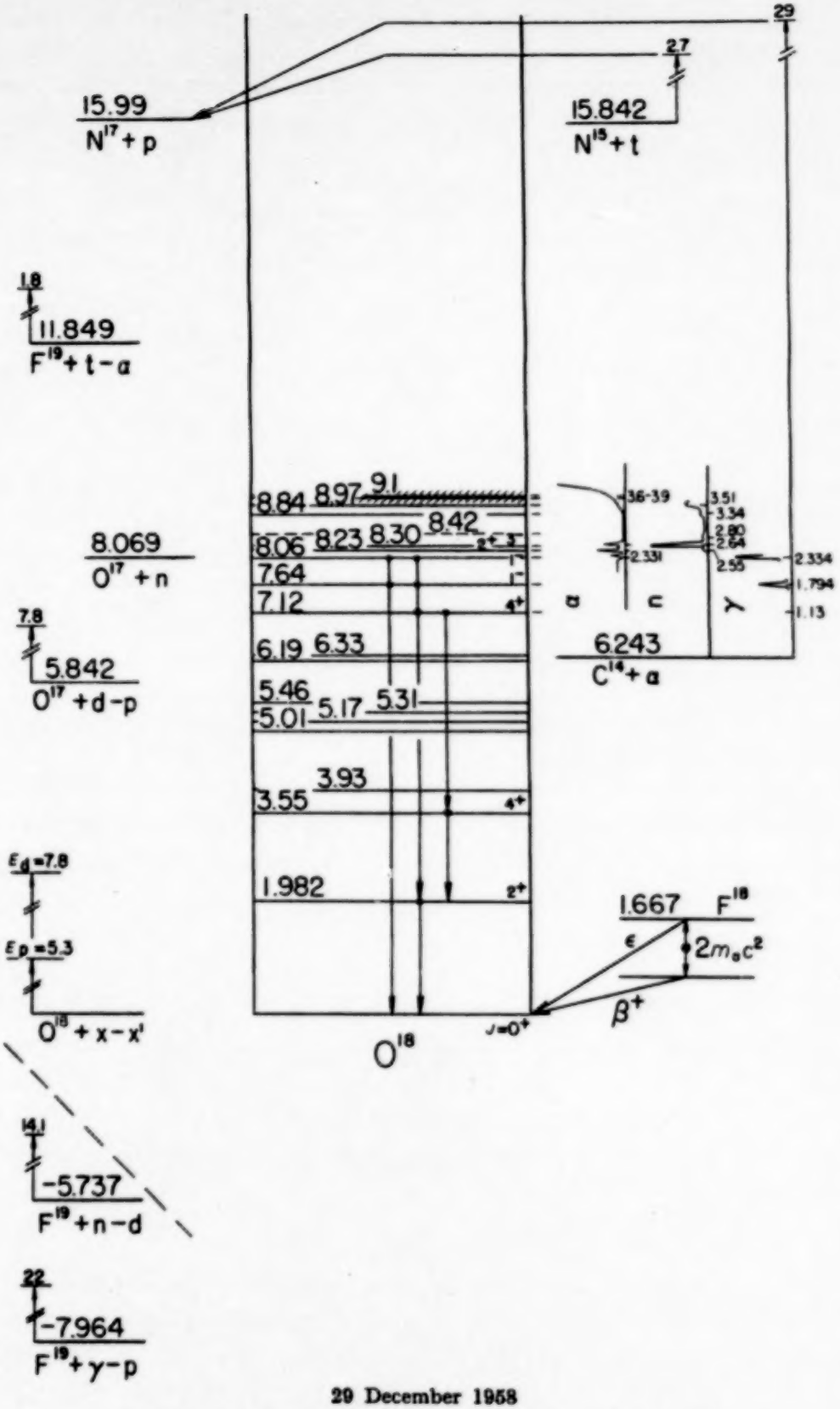

29 December 1958

Fig. 37. Energy levels of O¹⁸: for notation, see fig. 1, p. 7.

MeV (Ho 55c; based on Q_m) and at 3.56 ± 0.02 MeV (Ba 56d; based on Q_0). The reported level at 2.45 MeV is not found by (Ba 56d): an upper limit of 0.2—0.3 is given for the relative intensity of groups leading to states in the range $E_x = 2$ to 3.5 MeV compared to the ground-state group; see also

TABLE 18.3

Resonances in $C^{14}(\alpha, n)O^{17}$ and $C^{14}(\alpha, \alpha)C^{14}$

E_{res} (MeV ± keV)	Γ_{lab} (total) (keV)	θ_α^2 (%)	θ_n^2 (%)	E_x (MeV)	J^π [c]
2.331 ± 5 [a]	<6 ± 3 [a,d]	<2.8		8.056	0^+, 1^- [d]
2.553 ± 4 [a,b]	1.6 ± 1 [b]	0.90	6.2×10^{-4}	8.229	2^+
2.642 ± 3 [a,b]	10 ± 1 [b]	20	0.16	8.302	3^-
(2.798 ± 11) [b]	22 ± 10 [b]			(8.419)	
3.335 ± 15 [a,b]	100 ± 20 [b]			8.837	
3.508 ± 4 [a,b]	54 ± 3 [b]			8.971	$\geq 2^+$
3.6 to 3.9 [a]	>200 [a]			9.0 to 9.2 (two levels)	2^+, 3^- or 4^+, 3^-

[a] (We 58): $C^{14}(\alpha, \alpha)C^{14}$; measurements at several back angles.
[b] (Sa 56d): $C^{14}(\alpha, n)O^{17}$; 0°.
[c] From analysis of (α, α) and (α, n) data (We 58).
[d] Compare $C^{14}(\alpha, \gamma)O^{18}$.

$O^{18}(p, p')O^{18*}$ and $F^{19}(t, \alpha)O^{18}$. At $E_d = 7.77$ MeV, angular distributions of protons to the first three states of O^{18} are fitted by $l_n = 2$, 0 and 2, respectively. Assignments of $J^\pi = 0^+$, 2^+, 4^+ are indicated for $O^{18*} = 0$, 1.98 and 3.56 MeV. Derived coefficients for the first excited state wave function are in good agreement with the theories of (El 55a and Re 54c) (Bi 57d).

XI. $O^{18}(\gamma, p)N^{17}$ $\qquad Q_m = -15.99$

See (Aj 55) and (Re 55e).

XII. $O^{18}(p, p')O^{18*}$

At $E_p = 4.6$ to 5.3 MeV, a group is reported corresponding to $O^{18*} = 1.981 \pm 0.004$ MeV. No evidence is found for a level at 2.45 MeV reported in $O^{17}(d, p)O^{18}$: intensity less than 0.1 of 1.98-MeV group (Yo 57a). A 1.9-MeV γ-ray is reported by (Na 56a), presumably arising from the decay of the first excited state.

XIII. $O^{18}(d, d')O^{18*}$

At $E_d = 7.8$ MeV, deuteron groups are reported to states at 0, 1.98 and 3.551 ± 0.019 MeV. Upper limits of 3 to 8 per cent are given for other possible groups in the range $E_x = 2$ to 3.5 MeV (Ba 56d). At $E_d = 4.98$ MeV, the $Q = -1.98$ MeV group is < 3 per cent of the ground-state group (Yo 57a).

XIV. $F^{18}(\beta^+)O^{18}$ $Q_m = 1.667$

See F^{18}.

XV. $F^{19}(\gamma, p)O^{18}$ $Q_m = -7.964$

See F^{19}.

XVI. $F^{19}(n, d)O^{18}$ $Q_m = -5.737$

$Q_0 = -5.79 \pm 0.08$ (Ri 57a).

At $E_n = 14.1$ MeV, deuteron groups are observed to the ground state, to an excited state at 1.9 ± 0.1 MeV and, possibly, to others near 3 to 4 MeV. Angular distributions indicate $l_p = 0$ for the ground state transition, consistent with $J = 0^+$ or 1^+, and most probably $l_p = 2$ for the 1.9-MeV state ($J = 1^+, 2^+, 3^+$). The ratio of reduced widths $\theta_p^2(1.9)/\theta_p^2(0) = 0.87$, in good agreement with shell model calculations of (El 55a) (Ri 57a).

XVII. $F^{19}(d, He^3)O^{18}$ $Q_m = -2.470$

Not observed.

XVIII. $F^{19}(t, \alpha)O^{18}$ $Q_m = 11.849$

At $E_t = 1.8$ MeV, α-groups are reported to levels at 1.989 ± 0.024, 3.504 ± 0.034, 3.929 ± 0.040, 5.007 ± 0.040, 5.170 ± 0.040, 5.311 ± 0.040, 5.456 ± 0.040, 6.190 ± 0.040 and 6.328 ± 0.040 MeV. No other states below $E_x = 6.8$ MeV are observed (Ja 56e).

XIX. $Ne^{21}(n, \alpha)O^{18}$ $Q_m = 0.704$

Not observed.

F^{18}

(Fig. 38, p. 240)

THEORY

See (Re 54c, El 55, El 55a, Ne 56d, Gr 57d, Wa 59).

I. $F^{18}(\beta^+)O^{18}$ $Q_m = 1.677$

The positon end point is 635 ± 15 (Bl 49a), 649 ± 9 keV (Ru 51). The spectrum is simple (see (Dr 56a)). The half-life is 112 ± 1 min (Bl 49a), 111 ± 1 min (Ja 55), 110 ± 1 min (Be 58g): log $ft = 3.62$. The fact that the β transition to the ground state of O^{18} is allowed indicates $J = 1^+$ for F^{18} (assumed $T = 0$) (Mo 54). The ratio $\varepsilon_K/\beta^+ = 0.030 \pm 0.002$ (Dr 56a). See also (Dz 56) and (Re 58; theo.).

II. $C^{12}(Li^7, n)F^{18}$ $Q_m = 5.963$

See (No 57a).

III. $N^{14}(\alpha, \gamma)F^{18}$ $Q_m = 4.421$

Resonances have been observed at $E_\alpha = 1.53$, 1.62, 2.35 and 2.88 MeV,

corresponding to $F^{18*} = 5.61$, 5.68, 6.25 and 6.651 MeV (Pr 55, Ph 58, Al 58, Br 58): see table 18.5.

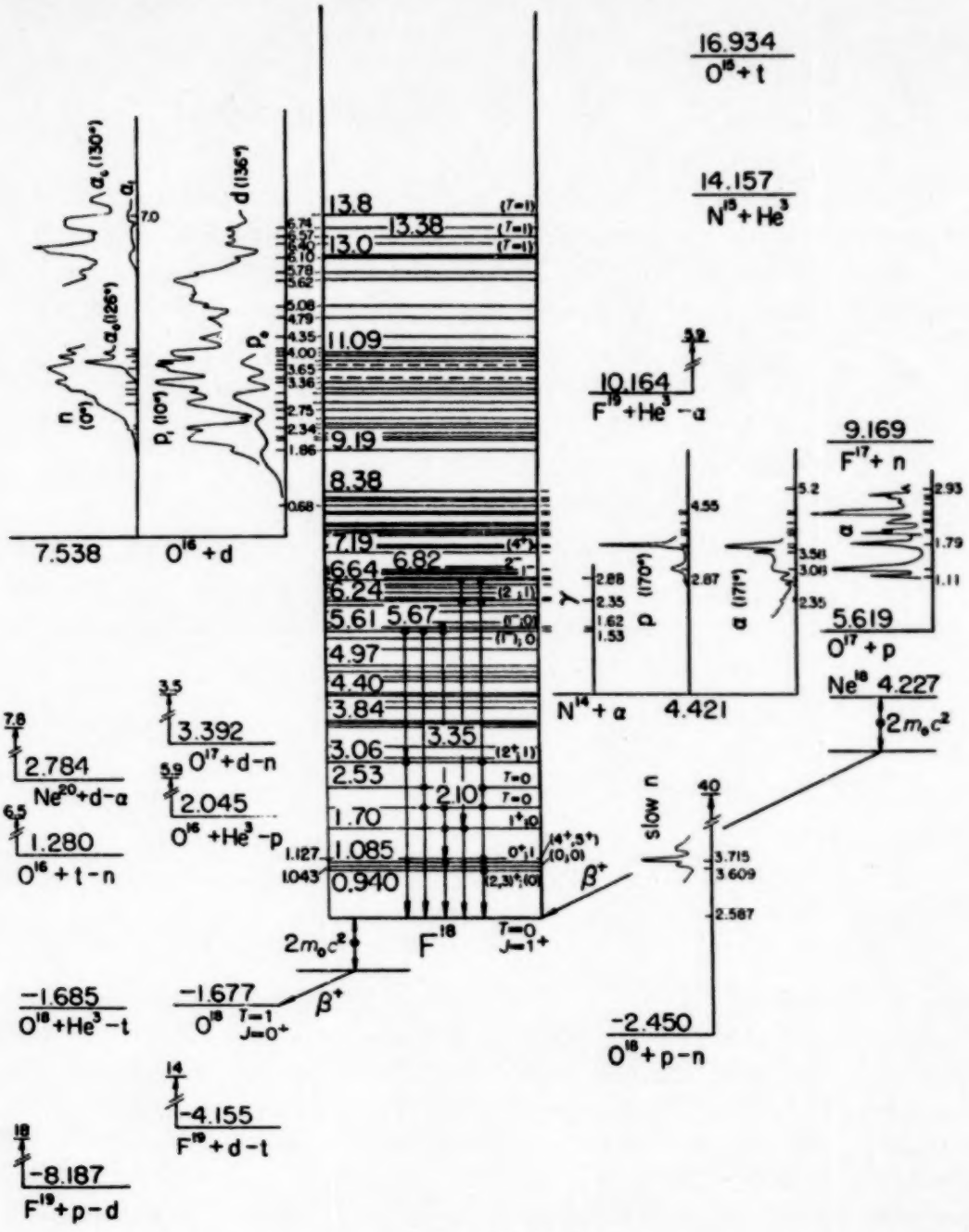

8 January 1959

Fig. 38. Energy levels of F^{18}: for notation, see fig. 1, p. 7.

The 5.61-MeV state decays to the F^{18} ground state (16 per cent), and to states at 1.08 MeV (41 per cent) and 3.06 MeV (45 per cent). Gamma rays

TABLE 18.4

Energy levels of F^{18}

E_x in F^{18} (MeV ± keV)	J^π; T	$\tau_{\frac{1}{2}}$ or Γ (keV)	Decay	Reactions
0	1^+; 0	$\tau_{\frac{1}{2}} = 111 \pm 1$ min	β^+	I, II, III, VIII, XIII, XIV, XV, XVI, XVII, XIX, XXII, XXIII, XXIV, XXV, XXVI, XXVII, XXVIII, XXIX, XXXII, XXXIV
0.940 ± 10	$(2^+, 3^+; 0)$	$\tau_m \leq 5 \times 10^{-9}$ sec	γ	III, XIV, XXII, XXVII, XXVIII, XXIX
1.043 ± 10	(0; 0)			III, XIV, XXII, XXIX, XXXII
1.085 ± 10	0^+; 1	$\tau_m < 3 \times 10^{-13}$ sec	γ	III, XIV, XXVII, XXVIII, XXIX
1.127 ± 10	$(4^+, 5^+)$			XIV, (XXII), XXIX
1.700 ± 10	1^+; 0		γ	III, XIV, XXVII, XXIX, XXXII
2.104 ± 10	(1, 2); 0		γ	XIV, XXIX, XXXII
2.525 ± 10	(1, 2, 3); 0		γ	XIV, XXIX, XXXIII
3.063 ± 10	$(2^+; 1)$		γ	III, XIV, XXIX
3.133 ± 10				XIV, XXIX, XXXIII
3.354 ± 10				XIV, XXVII, XXIX, XXXIII
3.725 ± 10				XIV, XXIX
3.790 ± 10				XIV, XXIX
3.839 ± 10				XIV, XXVII, XXIX, XXXII
4.115 ± 10				XIV, XXVII, XXIX, XXXII
4.226 ± 10				XIV, XXIX
4.360 ± 10				XIV, XXIX
4.400 ± 10				XXIX, XXXII
4.649 ± 10				XXIX
4.741 ± 10				XXIX
4.840 ± 10				XXIX
4.965 ± 13				XXIX, XXXII
5.292 ± 10				XXIX
5.500 ± 10				XXIX
5.608 ± 15	(1^-); 0	< 1.5	α, γ	III, XXIX
5.670 ± 10	$(1^-; 0)$	< 1.0	α, γ	III, XXIX
5.785 ± 10				XXIX
6.093 ± 10				XXIX
6.137 ± 10				XXIX
6.240 ± 10	$(2^\pm; 1)$	< 1.0	α, γ	III, VI, XXIX
6.264 ± 10	(1^+)	< 3	α	VI, XXIX
6.374 ± 10				XXIX
6.470 ± 10				XXIX
6.560 ± 10	$(3^+, 4^+, 5^+)$	< 0.8	α	VI, XXIX
6.640 ± 10		< 2.0	p, α, γ	III, VI, XVIII, XXIX
6.653 ± 10	1^-	93 ± 5	α	V, VI
6.765 ± 10				XXIX

TABLE 18.4 (continued)

E_x in F^{18} (MeV±keV)	J^π; T	τ_γ or Γ (keV)	Decay	Reactions
6.790±10				XXIX
6.817±10	2^-	101 ±5	α, p	V, VI, XVIII
6.857±10				XXIX
7.190±10	(4^+)	<4	α, p	VI, XXIX
7.29 ±20	(1^+)	45	α, p	V, VI, XVIII
7.313±10	(3^-)	53	α, p	V, VI, XVIII, XXIX
7.50 ±20	(3^-)	25	α, p	V, VI, XVIII, XXIX
7.56 ±20		75	α, p	V, VI, XVIII
7.62 ±20		40	α, p	V, VI
7.71 ±20		11	α, p	XVIII
7.74 ±20		110	α, p	V, VI, XVIII
7.91 ±20	(2^-)	≈25	α, p	V, VI, XVIII
7.96 ±20	(1^+)	70	α, p	V, VI
8.10 ±20		≈40	d, p, α	X, XVIII
8.22 ±20		≈15	α, p	XVIII
8.24 ±20		≈10	α, p	XVIII
8.38 ±20		≈50	α, p	VI, XVIII
9.19 ↓ 13.8	29 levels reported in O^{16}+d: see table 18.6, p. 245.			

TABLE 18.5

Resonances in N^{14}+α

E_α (keV)	Particle Out	$\Gamma_{c.m.}$ (keV)	J^π; T	θ_α^2	E_x (MeV)	References
1530 ±3	γ	<1.5	(1^-); 0		5.611	Ph 58, Pr 55, Al 58
1617 ±3	γ	<1.0	$(1^-; 0)$		5.679	Ph 58, Pr 55, Wa 59
2351 ±3	γ, α	<1.0	$2^\pm$; 1		6.250	Ph 58, He 58d, He 58e, Wa 59
2370 ±4	α	<3	(1^+)	<0.033	6.264	He 58d, He 58e
2767 ±4	α	(<0.8)	$(3^+, 4^+, 5^+)$		6.573	He 58d, He 58e
2868 ±4	γ, p_0	<2.0			6.651	He 58d, He 58e, Ph 58
2870 ±6	α	93± 5	1^-	0.715	6.653	He 58d, He 58e, Ka 58c
3080 ±6	α, p_0	101± 5	2^-	0.50	6.817	He 58d, He 58e, He 53, Ka 58c
3576 ±4	α	<4	(4^+)		7.202	He 58d, He 58e, Ka 58c
3.67	α	45±10	(1^+)		7.28	He 58d, He 58e, Ka 58c
3.72	α, p_0	53± 6	(3^-)		7.32	He 58d, He 58e, Ka 58c
4.00	α, p_0	35	(3^-)		7.53	Ka 58c
4.05	α, p_0	60			7.57	Ka 58c
4.11	α, p_0	40			7.62	Ka 58c
4.28	α, p_0	120			7.75	Ka 58c
4.50	α, p_0	30	(2^-)		7.92	Ka 58c
4.55	α, p_0	70	(1^+)		7.96	Ka 58c
5.2	α				8.5	De 39a, Br 39

with $E_\gamma = 2.12$ and 0.94 MeV are also observed (Al 58): see fig. 39. The radiative widths $\omega\Gamma_0$ to the ground state and $F^{18*}(1.08)$ are 0.7 and 2.2 eV respectively; all others amount to 3 eV (Pr 55). The branching ratios favor $J = 1^-$, $T = 0$ for $F^{18*}(5.61)$ and $T = 1$ for $F^{18}(1.08)$ and (3.06). Angular

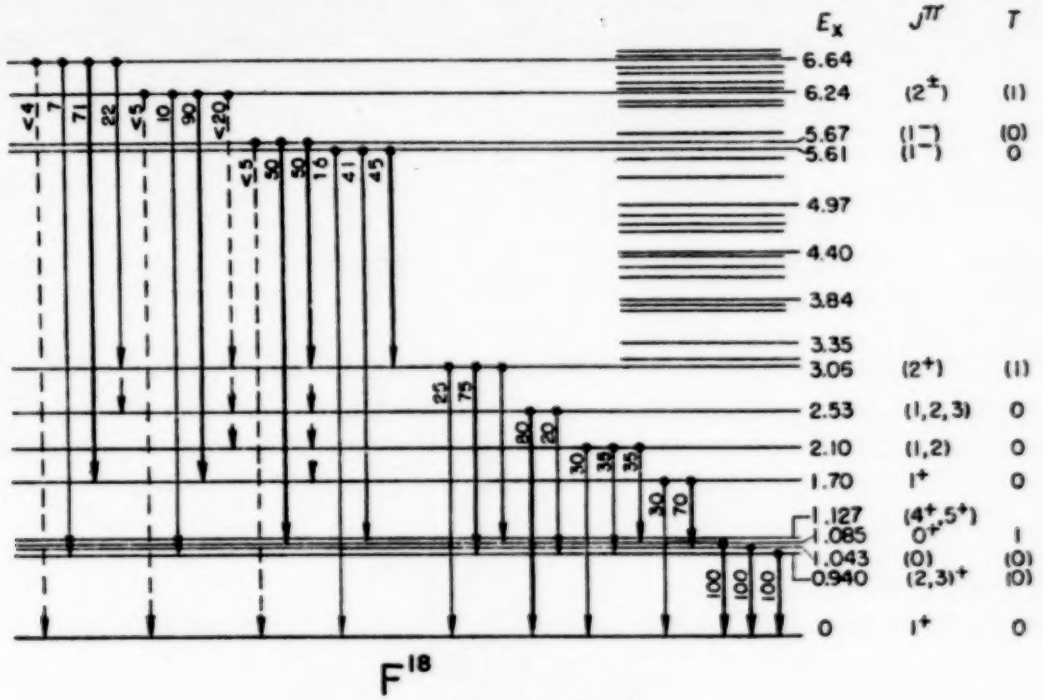

8 January 1959

Fig. 39. Gamma-ray transitions in F^{18}: for notation, see fig. 14, p. 83.

distributions of the cascade γ-rays are consistent with $J = 0^+$ and 2^+ for the states at 1.08 and 3.06 MeV. Angular correlations rule out $J = 0$ for the 0.94-MeV state. The 3.06 MeV state shows a 25 per cent ground-state branch and a 75 per cent cascade through the 0.94-MeV level (Al 58; see also Ku 58c). Delayed coincidence measurements on the γ-decay of the 0.94-MeV state show $\tau \leqq 5\times10^{-9}$ sec. This implies $1 \leqq J \leqq 3$ when taken together with the results of the $O^{16}(He^3, p\gamma)F^{18}$ reaction (Br 58).

The 5.68-MeV state decays to the 1.08-MeV state (1.075 ± 0.010 MeV) with $\omega\Gamma_\gamma = 2.2\pm0.3$ eV. The ground-state transition is < 0.2 eV; others amount to about 2 eV (Pr 55). The strength of the transition $5.68 \rightarrow 1.08$ suggests dipole radiation, J (5.68) $= 1$, $T = 0$ (Wa 59).

The 6.25-MeV state decays mainly to $F^{18*}(1.7)$: $E_\gamma = 4.45\pm0.05$ MeV ($\omega\Gamma_\gamma = 7.9\pm1.0$ eV), and $F^{18*}(0.94)$: $E_\gamma = 5.30\pm0.10$ MeV ($\omega\Gamma_\gamma = 0.8 \pm0.15$ eV). Transitions to the ground state and to levels at ≈ 3 MeV have upper limits of 5 per cent and 20 per cent. The 1.7-MeV state decays through $F^{18*}(1.05)$. The $(6.25 \rightarrow 1.7)$ and $(1.05 \rightarrow 0)$ γ—γ correlation is isotropic within 10 per cent, consistent with $J = 0^+$ for the 1.05-MeV state. The

1.7-MeV state is most likely to be $1^{\pm}$ or (2^+), and is assumed to be $T = 0$ from the O^{18} level structure (compare Ne^{20} (d, α) F^{18}). The 6.25-MeV state is then $2^{\pm}$ or 3^- (Ph 58). If the 1.7-MeV state is 1^+, $J(6.25)$ is 2^+ or 2^-; the strength of the transition (6.25 → 1.7) indicates $T = 1$ for $F^{18*}(6.25)$ (Wa 59).

The 6.65-MeV state decays with $E_\gamma = 5.80 \pm 0.10$ (7 per cent), $\omega\Gamma_\gamma = 0.25$ eV and 4.90 ± 0.05 MeV (70 per cent), $\omega\Gamma_\gamma = 2.1$ eV to the 0.94 and 1.70-MeV states respectively. Transitions with relative intensity ≈ 23 per cent are also reported to states with $E_x \approx 3$ MeV (Ph 58). See also (Ba 58h, Br 58e, He 58a) and $O^{16}(He^3, p)F^{18}$.

IV. $N^{14}(\alpha, n)F^{17}$ $Q_m = -4.747$ $E_b = 4.421$

See (Fu 38).

V. $N^{14}(\alpha, p)O^{17}$ $Q_m = -1.197$ $E_b = 4.421$

Observed resonances are displayed in table 18.5 (He 58d, Ka 58c, He 53). Absolute cross sections are given by (He 58d) for $E_\alpha = 2.7$ to 3.6 MeV. The yield of protons to $O^{17*}(0.7)$ is at least a factor of 10 smaller than the ground-state yield. See also (Gr 55, Ma 54 m) and (Aj 52c).

VI. $N^{14}(\alpha, \alpha)N^{14}$ $E_b = 4.421$

Observed anomalies in the elastic scattering are exhibited in table 18.5 (He 58d, He 58e, Ka 58c, He 53, De 39a, Br 39). The indicated assignments to the narrow resonances at $E_\alpha = 2.35$, 2.37, 2.77, 2.88, and 3.58 MeV are obtained from qualitative analysis of the excitation functions. The two broad resonances at $E_\alpha = 2.870$ and 3.080 MeV have been analyzed in detail: both are formed with p-waves, $J = 1^-$ and 2^- respectively. For the former, $\Gamma_\alpha/\Gamma = 0.85$. See also (Ka 58c). A broad anomaly at $E_\alpha = 3.7$ MeV requires two levels, and possible admixture of higher l-values (He 58e, Ka 58c).

VII. $N^{15}(\alpha, n)F^{18}$ $Q_m = -6.420$

Not reported.

VIII. $O^{16}(d, \gamma)F^{18}$ $Q_m = 7.538$

At $E_d = 1.7$ MeV, the capture cross section is ≈ 10 μb (Bu 55a). See also (Si 54).

IX. $O^{16}(d, n)F^{17}$ $Q_m = -1.631$ $E_b = 7.538$

Observed resonances in the forward yield of neutrons are displayed in table 18.6 (Ma 55m). See also (Aj 52c) and (Bu 55a).

X. $O^{16}(d, p)O^{17}$ $Q_m = 1.919$ $E_b = 7.538$

The yield shows strong variations with energy, suggesting compound nucleus formation (Ro 56a, Be 55e, Va 56c, St 55c, He 48a): see table 18.6.

On the other hand, angular distribution measurements show strong stripping peaks for both p_0 and p_1, for $E_d = 0.5$ to 4.1 MeV (Ko 56f, Ju 55a, Ju 56c, Ju 57, Be 55e, Al 55f, Gr 56, St 55c, Ba 57f). See also O^{17}.

TABLE 18.6

Maxima in the yield of (O^{16}+d) reactions

E_d (MeV)	Particle Out	E_x in F^{18} (MeV)	References
(0.68)	p_0	(8.14)	Va 56c
1.86	p_0, p_1	9.19	He 48a, Ro 56a, Be 55c
2.06	p_1	9.37	Ro 56a, Be 55c
2.14	p_1	9.44	Ro 56a
2.22	n	9.51	Ma 55m
2.34	n, p_1	9.62	Ro 56a, Ma 55m
2.42 [a]	n	9.69	Ma 55m
2.55	p_1	9.81	Ro 56a, St 55c
2.75	p_1	9.98	Ro 56a
2.92	n, p_0, p_1	10.13	He 48a, Ro 56a, St 55c, Ma 55m
3.10	n, p_1	10.29	Ro 56a, Ma 55m
3.22	n	10.40	Ma 55m
3.36	n, p_0, p_1	10.53	Ro 56a, St 55c, Ma 55m
(3.43)	p_1	(10.59)	Ro 56a
3.65	n, p_0, p_1	10.78	Ro 56a, Ma 55m, St 55c
(3.75)	p_1	(10.87)	Ro 56a
3.84 [b]	p_1, α_0	10.95	Ro 56a, Ba 57f
3.94	n, p_1	11.04	Ro 56a, Ma 55m
4.00 [c]	p_1, α_0	11.09	Ro 56a, Ba 57f
4.10	n, p_1	11.18	Ro 56a, Ma 55m
4.35	p_1	11.41	Ro 56a
4.79	d_0	11.80	Be 56d
5.08	d_0	12.05	Be 56d
5.617	d_0	12.53	Be 56d
5.78	d_0	12.68	Be 56d
6.10	d_0	12.96	Be 56d
6.2 [d]	α_1	13.0	Br 56f
6.40	d_0	13.23	Be 56d
6.57 [d]	d_0, α_1	13.38	Be 56d, Br 56f
6.74	d_0	13.53	Be 56d
7.0 [d]	α_1	13.8	Br 56f

[a] $J^\pi = 2^+$ or 3^+.
[b] $\Gamma \approx 100$ keV (Ba 57f).
[c] $\Gamma \approx 35$ keV (Ba 57f).
[d] ($T = 1$).

XI. O^{16}(d, d)O^{16} $E_b = 7.538$

Observed maxima in the $\theta = 135°$ and 97° cross section are listed in table 18.6 (Be 56d). Structure in the yield of elastically scattered deuterons is also reported by (Ba 57f). See also (Kh 55, Kh 55a).

XII. $O^{16}(d, \alpha)N^{14}$ $Q_m = 3.116$ $E_b = 7.538$

Two resonances are reported for ground-state α-particles at $E_d = 3.85$ MeV, $\Gamma = 35$ keV, and 4.0 MeV, $\Gamma = 100$ keV (Ba 57f): see table 18.6. Yield curves of the α_0, α_1 and α_2 groups are reported for $E_d = 5.5$ to 7.5 MeV by (Br 56f). The α_1-group, leading to the $T = 1$, 2.31-MeV state of N^{14}, is greatly inhibited: the average intensity is only a few per cent of the average yield of the α_0 group. Broad resonances are observed in the yields of all three α groups. The resonances in the α_1-yield occur at ≈ 6.2, 6.6 and 7.0 MeV; they are presumably due to predominantly $T = 1$ states at $E_x \approx 13.0$, 13.4, and 13.8 MeV (Br 56f). At $E_d = 7.2$ MeV, the intensity ratio α_1/α_0 is 16 per cent ($\theta = 35°$), at 6.8 and 7.1 MeV, $\alpha_1/\alpha_0 < 6$ per cent, and at 8.9 MeV, < 2 per cent (Da 58b). The observations are consistent with expected isobaric spin impurities in the states involved (Br 56f). Angular distributions for α_0, α_2 may give evidence of compound nucleus effects (Da 58b): see also N^{14}.

XIII. $O^{16}(t, n)F^{18}$ $Q_m = 1.280$

See (Po 51, Ba 55i, Sh 56a).

XIV. $O^{16}(He^3, p)F^{18}$ $Q_m = 2.045$

$Q_0 = 2.052 \pm 0.015$ (Hi 59).

Seventeen proton groups corresponding to excited states of F^{18} from 0 to $E_x = 4.36$ MeV are reported by (Hi 59: $E(He^3) = 5.7$ to 5.9 MeV): see table 18.7. See also (Ku 58c). Angular distributions for the first five states, analyzed by direct interaction theory, indicate $J = 1^+$, 2^+ or 3^+, 0^+, (?), and 4^+ or 5^+ for F^{18*}(g.s., 0.94, 1.04, 1.08 and 1.13) respectively (Hi 59: tentative assignments). Gamma transitions to F^{18}(g.s.) have been observed from the levels at 0.94, 1.04 and 1.08 MeV; the decay of the 1.13-MeV level has not been detected (Ku 58c). Proton-gamma coincidence techniques have been used to determine branching ratios and angular correlations involving F^{18} states at 0.94, 1.08, 1.7, 2.1, 2.5 and 3.07 MeV (Ku 58: see also Bu 56): see fig. 39. All of these states show at least one anisotropic radiation except for F^{18*}(1.04) and (1.08), excluding $J = 0$ for all but these two (Ku 58 and E. Almqvist, private communication).

The mean life of the 0.94-MeV state is $\leqq 5 \times 10^{-9}$ sec, indicating $J \leqq 3$ (Br 58). The polarization of the γ-radiation indicates positive parity for the state (Li 58b). The strong transition from F^{18*}(3.07: $T = 1$) suggests $T = 0$. For the 1.04-MeV state, $J = 0^+$ is indicated by the proton angular distributions (Hi 59); $J = 0^-$, $T = 0$ is suggested by the γ-branching (E. Almqvist, private communication). The 1.08-MeV state appears to have $J = 0^+$, $T = 1$ (see $N^{14}(\alpha, \gamma)F^{18}$). The absence of the ground-state transition from F^{18*}(1.12) is consistent with its expected $J = 5^+$ character. The 1.7-MeV

TABLE 18.7

Energy levels of F^{18} from $O^{16}(He^3p)F^{18}$, $F^{19}(He^3, \alpha)F^{18}$ and $Ne^{20}(d, \alpha)F^{18}$

(Hi 59) [a]		(Ku 58c) [b]	(Mi 51d) [c]	Assignment [d]	
(He^3, p) (MeV)	(He^3, α) (MeV)	(He^3, p) (MeV)	(d, α) (MeV $\pm$ keV)	l_p	J^π; T
0	0	0	0	0+2	1^+; 0
0.941	0.940	0.940		2	2^+, 3^+; (0)
1.044	1.042	1.045	1.05 $\pm$ 30	0	0(+) [e]; (0)
1.084	1.087	1.080 [g]			0^+; 1 [h]
1.126	1.129	1.125		(4)	(4^+, 5^+)
1.704	1.699		1.83 $\pm$ 30		1^+; 0
2.104	2.105		2.20 $\pm$ 60		1, 2; 0
2.525	2.525		2.61 $\pm$ 50		1, 2, 3; 0
3.064	3.063				2^+; 1
3.135	3.131		3.23 $\pm$ 80		
3.357	3.352				
3.723	3.727				
3.791	3.790				
3.837	3.841				
4.115	4.116		3.92 $\pm$ 40		
4.226	4.227				
4.361	4.358				
	4.400		4.42 $\pm$ 100		
	4.649				
	4.741				
	4.840				
	4.965 [f]		5.01 $\pm$ 90		
	5.292				
	5.500				
	5.603 [f]		5.61 $\pm$ 100		
	5.666				
	5.785				
	6.093				
	6.137				
	6.232				
	6.264 [f]				
	6.374				
	6.470				
	6.551				
	6.633				
	6.765				
	6.790				
	6.857				
	7.183				
	7.313				
	7.495				

[a] $E(He^3)$ = 5.7 and 5.9 MeV: energies $\pm$ 10 keV.
[b] $E(He^3)$ = 2.4 to 2.9 MeV.
[c] E_d = 7.8 MeV.
[d] l_p from proton distributions (Hi 59).
[e] $J = 0^-$, $T = 0$ suggested by γ-branching.
[f] $\pm$13 keV.
[g] $\pm$10 keV.
[h] Assignment from γ-branching; proton group weak but suggests odd parity (Hi 59).

state is fixed as $J = 1^+$ from the present reaction and $F^{19}(p, d)F^{18}$. For $F^{18*} = 2.1$ and 2.54 MeV assignments of $J = 1, 2$ and $1, 2, 3$ are indicated by the branching ratios (E. Almqvist, private communication). See also (Br 58d, Br 58e).

XV. $O^{16}(\alpha, pn)F^{18}$ $Q_m = -18.533$

See (Te 47).

XVI. $O^{16}(Li^6, \alpha)F^{18}$ $Q_m = 6.067$

See (No 57a).

XVII. $O^{17}(p, \gamma)F^{18}$ $Q_m = 5.619$

A resonance in the capture cross section may be indicated near 1.24 MeV ($E_x = 6.79$ MeV), $\sigma \approx 1$ mb (Ni 56).

XVIII. $O^{17}(p, \alpha)N^{14}$ $Q_m = 1.197$ $E_b = 5.619$

Resonances in the yield of ground state α-particles are displayed in table 18.8 (Ah 57).

TABLE 18.8

Resonances in $O^{17}(p, \alpha_0)N^{14}$(Ah 57)

E_p (MeV)	$\Gamma_{c.m.}$ (keV)	E_x (MeV)
1.110	9	6.667
1.273	90	6.821
1.786	≈65	7.306
2.021	11	7.528
2.048	90	7.553
2.218	11	7.714
2.235	100	7.730
2.406	≈25	7.891
2.435	≈25	7.919
2.623	≈40	8.096
2.753	≈15	8.219
2.775	≈10	8.240
2.928	≈50	8.384

XIX. $O^{17}(d, n)F^{18}$ $Q_m = 3.392$

See F^{19}

XX. $O^{17}(He^3, d)F^{18}$ $Q_m = 0.125$

Not reported.

XXI. $O^{17}(\alpha, t)F^{18}$ $Q_m = -14.194$

Not reported.

XXII. $O^{18}(p, n)F^{18}$ $Q_m = -2.450$

$E_{thresh} = 2.590 \pm 0.004$ (Ri 50e).

$E_{thresh} = 2.584 \pm 0.010$ (Ma 56e).

$E_{thresh} = 2.577 \pm 0.008$ (Hi 56c).

Slow neutron thresholds are reported corresponding to $E_x = 960 \pm 10$, 1065 ± 15, and, possibly, 1245 ± 10 keV; no others appear with $E_x < 1.65$ MeV (Na 56). Gamma rays are observed with $E_\gamma = 940 \pm 20$ and 1040 ± 20 keV at $E_p = 4.3$ and 4.4 MeV: the 1040 keV γ-ray exhibits a Doppler shift ($\tau < 3 \times 10^{-13}$ sec, consistent with $J = 0^+$), the 940 keV γ-ray does not, which is consistent with $J = 3^+, 5^+$. No γ-ray is observed from the 1245-keV state (Na 56a, Ro 56b). See also $O^{16}(He^3, p)F^{18}$ and F^{19}.

XXIII. $O^{18}(He^3, t)F^{18}$ $Q_m = -1.685$

See (Ku 53a).

XXIV. $Ne^{18}(\beta^+)F^{18}$ $Q_m = 4.227$

See Ne^{18}.

XXV. $F^{19}(\gamma, n)F^{18}$ $Q_m = -10.414$

See F^{19}.

XXVI. $F^{19}(n, 2n)F^{18}$ $Q_m = -10.414$

See F^{20}.

XXVII. $F^{19}(p, d)F^{18}$ $Q_m = -8.187$

$Q_0 = -8.12 \pm 0.2$ (Re 56).

At $E_p = 18$ MeV, angular distributions have been measured to the ground state of F^{18} (Re 56, Be 58a) and to levels at 0.94, 1.05, 1.7, 3.4 and 4.1 MeV (Be 58a). The results indicate $J = 0^+$ or 1^+ for the ground state (Re 56), even parity for the 0.94, 1.04, 1.7 and 4.1-MeV states; probable assignments are stated to be 3^+, 0^+, 0^+ and 2^+ respectively, and odd parity, $J \leqq 2$ for the 3.4-MeV state (Be 58a). The reduced width for the ground state reaction is $\theta^2 = 0.009$ (Re 56). According to (Wa 59), the distributions permit $J = 0^+$ or 1^+ for $F^{18}(1.7)$; $J = 0$ is excluded by the observed γ-decay to $F^{18*}(1.04)$. See also F^{19} and (El 58a; theo.).

XXVIII. $F^{19}(d, t)F^{18}$ $Q_m = -4.155$

$Q_0 = -4.17 \pm 0.02$ (El 57a)

At $E_d = 8.9$ MeV proton groups are observed to the ground state and to states at 0.94 ± 0.02 and 1.07 ± 0.02 MeV. The angular distributions are consistent with $l_n = 0$, 1 and 0, respectively (El 57a). The $l_n = 1$, odd parity assignment for the 0.94-MeV state is not in accord with other experiments (see, e.g., $O^{16}(He^3, p)F^{18}$ and $F^{19}(p, d)F^{18}$). See also (Bo 50d, Sh 51a).

XXIX. $F^{19}(He^3, \alpha)F^{18}$ $Q_m = 10.164$

$Q_0 = 10.162 \pm 0.015$ (Hi 59).

At $E(He^3) = 5.9$ MeV, 41 α-particle groups have been observed, corresponding to the ground state of F^{18} and to excited states with $E_x < 7.5$ MeV (Hi 59): see table 18.7.

XXX. $Ne^{20}(n, t)F^{18}$ $Q_m = -14.802$
Not reported.

XXXI. $Ne^{20}(p, He^3)F^{18}$ $Q_m = -15.567$
Not reported.

XXXII. $Ne^{20}(d, \alpha)F^{18}$ $Q_m = 2.784$
$Q_0 = 2.791 \pm 0.009$ (Mi 54b).
Observed alpha-particle groups are listed in table 18.7 (Mi 51d).

XXXIII. $Ne^{21}(p, \alpha)F^{18}$ $Q_m = -1.746$
Not reported.

XXXIV. $Mg^{25}(p, 2\alpha)F^{18}$ $Q_m = -11.636$
See (Co 54h).

Ne^{18}

(Not illustrated)

THEORY

See (Ra 57).

I. $Ne^{18}(\beta^+)F^{18}$ $Q_m = 4.227$
The maximum energy of the positons is 3.2 ± 0.2 MeV, the half-life is 1.6 ± 0.2 sec: $\log ft = 2.9 \pm 0.2$ (Go 54d). See also (Dz 56).

II. $O^{16}(He^3, n)Ne^{18}$ $Q_m = -2.966$
See (Ku 53a).

III. $F^{19}(p, 2n)Ne^{18}$ $Q_m = -15.424$
See (Go 54d).

IV. $Ne^{20}(p, t)Ne^{18}$ $Q_m = -19.812$
Not reported.

O^{19}

(Fig. 40, p. 251)

THEORY

See (El 55, El 55a, Re 55, Re 55b, Re 58, Ra 57).

TABLE 19.1
Energy levels of O^{19}

E_x (MeV $\pm$ keV)	J^π	τ	Decay	Reactions
0	$\frac{1}{2}^+$, ($\frac{3}{2}^+$)	$\tau_{\frac{1}{2}} = 29$ sec	β^-	I, III, IV, VII
0.096 $\pm$ 11	$\frac{3}{2}^\pm$, $\frac{5}{2}^+$	$\tau_m = (1.75 \pm 0.3) \times 10^{-9}$ sec	γ	IV
1.469 $\pm$ 11	$\frac{1}{2}^+$		γ	IV

I. $O^{19}(\beta^-)F^{19}$ $Q_m = 4.789$

The decay is complex: see F^{19}, (St 58b).

II. $O^{17}(t, p)O^{19}$ $Q_m = 3.542$

Not reported.

III. $O^{18}(n, \gamma)O^{19}$ $Q_m = 3.958$

The thermal cross section is 0.21 ± 0.04 mb (Hu 58).

IV. $O^{18}(d, p)O^{19}$ $Q_m = 1.731$

Observed proton groups are exhibited in table 19.2. Angular distributions of p_0, p_1 have been measured at $E_d = 0.8$ MeV by (Ah 56b: see Po 56b), of p_2 at $E_d = 3.0$ MeV by (St 55c) and of p_0, p_1, p_2 at $E_d = 1.2$ to 2.5 MeV by (Zi 59a). The p_0 and p_2 groups show clear stripping distributions (Zi 59a, St 55c), corresponding to $l_n = 2$ and 0, respectively: $J_0 = \frac{3}{2}^+$ or $\frac{5}{2}^+$ and

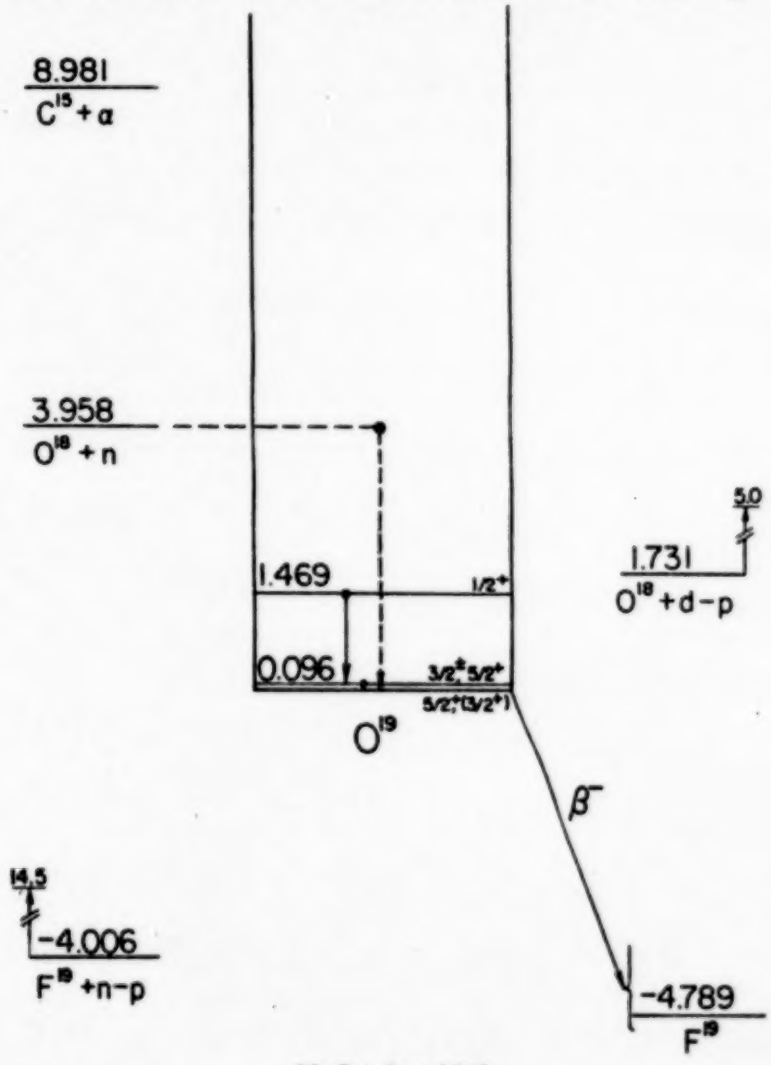

10 October 1958

Fig. 40. Energy levels of O^{19}: for notation, see fig. 1, p. 7.

$J_2 = \frac{1}{2}^+$. The p_1 group is almost isotropic at $E_d = 2.5$ MeV, indicating a small reduced width (Zi 59a).

TABLE 19.2

Proton groups from $O^{18}(d, p)O^{19}$

Q (in keV)				E_x	l_n	J^π
(Ah 54b, Mi 54e)	(Th 54a)	(Ho 55c)	(Ah 57a)	(in keV)		
1730±8	1732± 8	1735± 8	1734± 5	0	2[a]	$\frac{3}{2}^+$, $\frac{5}{2}^+$
1636±8	1632± 8	1641± 8		96±11		$\frac{3}{2}^\pm$, $\frac{5}{2}^+$
262±6	263±10	264±13		1469±11	0[b]	$\frac{1}{2}^+$

[a] (Zi 59a).
[b] (St 55c, Zi 59a).

The 1.47-MeV state decays almost entirely to $O^{19*}(0.096)$ in preference to the ground state, suggesting $J = \frac{1}{2}^\pm, \frac{3}{2}^\pm$ for $O^{19*}(0.096)$, with $\frac{5}{2}^+$ a less likely possibility. The lifetime of $O^{19*}(0.096)$ is $\tau_m = (1.75 \pm 0.3) \times 10^{-9}$ sec, consistent with a slow E1 or M1 transition. If the ground state is $\frac{5}{2}^+$, the 0.096-MeV state is $\frac{3}{2}^\pm$ or $\frac{5}{2}^+$ (Zi 59a). No other proton groups are observed at $E_d = 2.18$ MeV, $\theta = 140°$, corresponding to states in O^{19} below 2.4 MeV (Th 54a).

V. $O^{18}(t, d)O^{19}$ $Q_m = -2.301$
Not reported.

VI. $O^{18}(\alpha, He^3)O^{19}$ $Q_m = -16.620$
Not reported.

VII. $F^{19}(n, p)O^{19}$ $Q_m = -4.006$
See F^{20} and (Je 50d, Ri 55a, Jo 56d, Ph 56).

VIII. $F^{19}(t, He^3)O^{19}$ $Q_m = -4.771$
Not reported.

IX. $Ne^{21}(n, He^3)O^{19}$ $Q_m = -15.916$
Not reported.

X. $Ne^{22}(n, \alpha)O^{19}$ $Q_m = -5.704$
Not reported.

F^{19}

(Fig. 41, p. 255) †

THEORY

See (Re 55, El 55, El 55a, Re 55b, Ba 56e, Pa 56a, Pa 57, Ra 57, Ab 58, Re 58, Ku 58a).

† For level scheme of Ne^{19}, see fig. 43, p. 263.

I. $Be^{9}(N^{14}, \alpha)F^{19}$ $Q_m = 13.263$

See (Go 58e).

II. $N^{15}(\alpha, \gamma)F^{19}$ $Q_m = 3.993$

Three resonances are observed (Pr 57a): see table 19.4. The γ-transition strengths indicate that all three yield dipole or E2 radiation. The indicated assignments are derived from branching ratios and angular distributions. Neither the 1.34 or the 2.8-MeV level may have $J = \frac{1}{2}$ (Pr 57a).

III. $N^{15}(\alpha, \alpha)N^{15}$ $E_b = 3.993$

Differential cross sections for elastic scattering at several angles have been measured for $E_\alpha = 1.7$ to 5.4 MeV. Over twenty resonances have been observed: below $E_x = 7$ MeV the levels are narrow ($\approx$ 10 keV); above this energy they are much broader (Sm 58; see Bu 58b).

IV. $O^{16}(t, n)F^{18}$ $Q_m = 1.280$ $E_b = 11.693$

The excitation function has been measured for $E_t = 0.68$ to 2.13 MeV; at the latter energy the cross section is 100 ± 20 mb (Ja 55). See also (Ho 50b).

V. $O^{16}(\alpha, p)F^{19}$ $Q_m = -8.119$

At $E_\alpha = 20.6$ MeV, proton groups are observed corresponding to excited states at 1.36 ± 0.05, 2.67 ± 0.05 and 3.92 ± 0.05 MeV (Bu 51c).

VI. $O^{17}(d, n)F^{18}$ $Q_m = 3.392$ $E_b = 13.806$

See (Bu 55a) and (Ho 50b).

VII. $O^{17}(d, p)O^{18}$ $Q_m = 5.842$ $E_b = 13.806$

See O^{18}.

VIII. $O^{17}(d, \alpha)N^{15}$ $Q_m = 9.812$ $E_b = 13.806$

See N^{15}.

IX. $O^{17}(t, n)F^{19}$ $Q_m = 7.548$

Not reported.

X. $O^{17}(He^{3}, p)F^{19}$ $Q_m = 8.313$

Not reported.

XI. $O^{17}(\alpha, d)F^{19}$ $Q_m = -10.038$

Not reported.

XII. $O^{18}(p, \gamma)F^{19}$ $Q_m = 7.964$

Resonances for capture radiation observed for $E_p = 0.3$ to 2.6 MeV are displayed in table 19.5 (Bu 55b, Hu 55b, Hi 56c). The 9.07-MeV level ($E_p = 1.169$ MeV) decays preferentially through the 2.8-MeV level. Its

TABLE 19.3

Energy levels of F^{19}

E_x (MeV ± keV)	J^π	τ_m or Γ (keV)	Decay	Reactions
0	$\frac{1}{2}^+$	—	Stable	I, II, V, XVII, XX, XXVI, XXVII, XXVIII, XXIX, XXX, XXXI, XXXVII
0.10987 ± 0.04	$\frac{1}{2}^-$	$\tau_m = (1.0 \pm 0.25) \times 10^{-9}$ sec	γ	II, XX, XXVI, XXVII, XXIX, XXX, XXXVII
0.198 ± 1	$\frac{3}{2}^+$	$\tau_m = (1.25 \pm 0.025) \times 10^{-7}$ sec	γ	II, XVII, XX, XXVI, XXVII, XXIX, XXX, XXXVII
1.347 ± 3	$\frac{3}{2}$, ($\frac{5}{2}$)		γ	II, V, XVII, XXVI, XXVII
1.460 ± 3	$\frac{1}{2}$, $\frac{3}{2}$		γ	XVII, XXVI, XXVII
1.556 ± 3	$\frac{3}{2}^+$		γ	XVII, XX, XXVI, XXVII, XXVIII
2.784 ± 8	($\frac{7}{2}$, $\frac{9}{2}$)		γ	II, V, XII, XVII, XXVI, XXVII, XXVIII
3.912 ±10				V, XVII, XXVII
4.002 ±10				XXVII
4.036 ±10				XXVII
(4.41)				XXVII
(4.48)				XVII, XXVII
4.57 ±20				XXVII
4.76 ±50				XVII, XXVII
(4.95 ±20)				XXVII
5.320 ±10	$\frac{1}{2}$, ($\frac{3}{2}^-$)		α, γ	II, XVII, XXVII
5.455 ±10	$> \frac{1}{2}$		α, γ	II, XVII, (XXVII)
5.480 ±10	($\frac{3}{2}^+$)		α, γ	II, XV, (XXVII)
6.048 ±14			γ	XVII
(6.07 ±20)				XVII, XXVII
6.210 ±14	($\frac{1}{2}^+$, $\frac{3}{2}^+$)		γ	XVII
6.262 ±15			γ	XVII
(6.50 ±90)				XXVII
7.40 ±50	($T = \frac{3}{2}$)		γ	XVII
7.67 ±50			γ	XVII
8.11 ±50			γ	XVII
8.49 ±15			p, α, γ	XII, XVI, XVII
8.564 ±10	$\frac{3}{2}$	2.5	p, α, γ, n, d	XII, XVI, XVII
↓	Thirty nine levels observed in O^{18} + p: see table 19.5			
14.28			p, n	XVI
15.3			γ, n	XXI
22.2		5600	γ, n	XXI

small width and the absence of α-decay may indicate a $T = \frac{3}{2}$ character; the position is close to that expected for the analogue of the 1.47-MeV state of O^{19}(Bu 55b).

XIII. $O^{18}(p, n)F^{18}$ $\quad Q_m = -2.450$ $\quad E_b = 7.964$

Observed resonances in the neutron yield are listed in table 19.5 (Ma 56e,

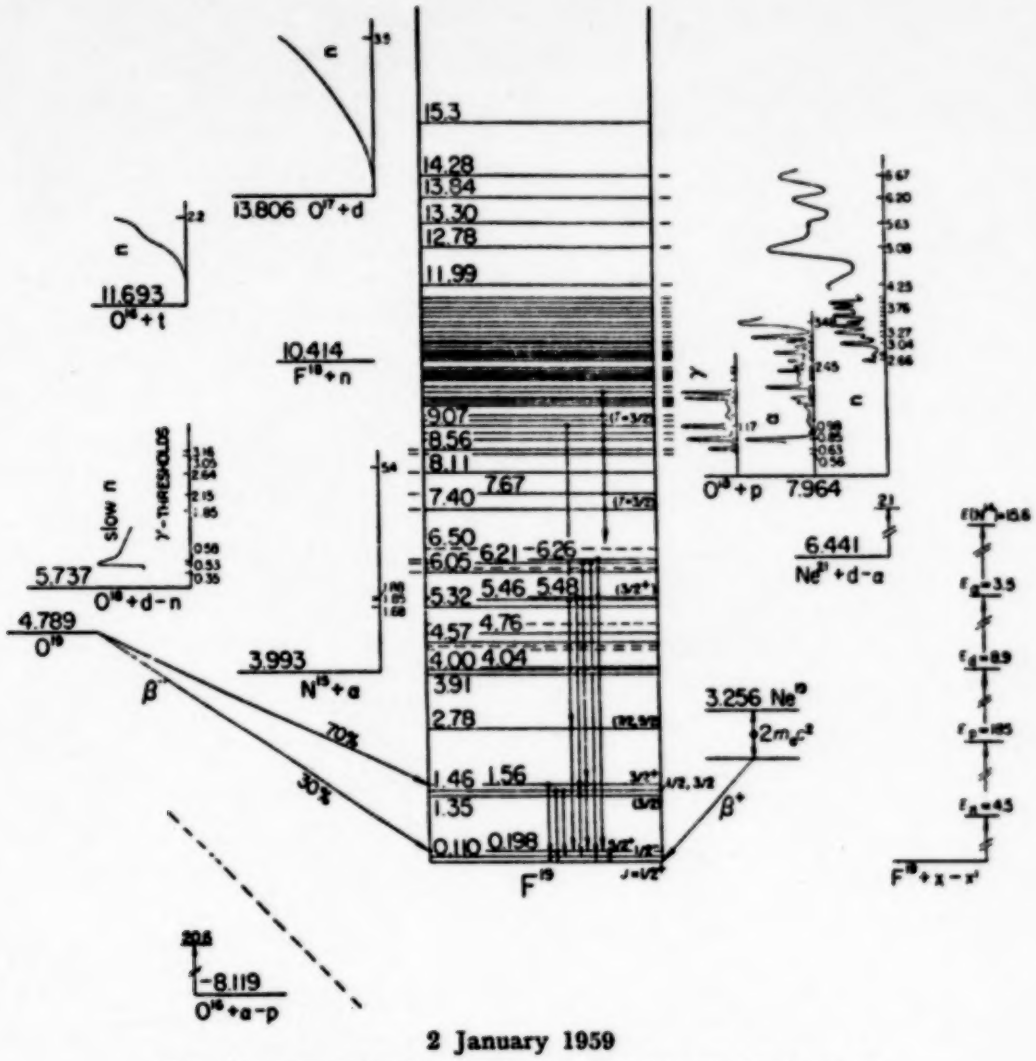

2 January 1959

Fig. 41. Energy levels of F^{19}: for notation, see fig. 1, p. 7.

TABLE 19.4

Resonances in $N^{15}(\alpha, \gamma)F^{19}$ (Pr 57a)

E_α (keV)	Γ (keV)	E_x (MeV)	E_γ (keV)	$\omega\Gamma_\alpha$ [a] (eV)	J^π
1681±5	<2	5.320	5.2 0.11	6.6	$\frac{1}{2}$, $(\frac{1}{2}^-)$
1852±3	<1	5.455	4.0 2.6 1.3 0.20 0.11	3.8 7.0	$\frac{3}{2}$, $\frac{5}{2}$, $\frac{7}{2}$ $(>\frac{7}{2})$
1883±3	4±1	5.480	5.2 4.0 1.3 0.19 0.11	5.2 3.3	$\frac{3}{2}^+$, $(\frac{3}{2}^-, \frac{5}{2}^+, \frac{7}{2})$

[a] $(2J+1)\Gamma_\gamma\Gamma_\alpha/\Gamma$.

TABLE 19.5

Resonances in $O^{18}(p, \gamma)F^{19}$, $O^{18}(p, n)F^{18}$ and $O^{18}(p, \alpha)N^{15}$

E_p (keV)	Γ (keV)	Particle out	J^π	E_x (MeV)	References
560		γ, α		8.495	Co 53h, Hu 55b
633 ± 4	2.6	γ, α	$\frac{3}{2}^+$	8.564	Bu 55b, Se 51b, Co 53h
846 ± 5	40	γ, α	$\frac{1}{2}^+$	8.765	Bu 55b, Se 51b, Hu 55b, Co 53h, Hi 56c
980 ± 4		α		8.892	Hi 56c
1169 ± 2[a]	<0.9	γ		9.071	Bu 55b
1271 ± 10		α		9.168	Hi 56c
1403 ± 4	<15	γ, α		9.292	Bu 55b, Hi 56c
1621 ± 4		α		9.500	Hi 56c
1687 ± 4	<15	γ, α		9.562	Bu 55b, Hi 56c
1736 ± 5		α		9.609	Hi 56c
1765 ± 3	4.0	γ, α		9.636	Bu 55b, Hi 56c, Hu 55b
1932 ± 2	1.5	γ, α		9.794	Bu 55b, Hi 56c, Hu 55b
2007 ± 4		α		9.865	Hi 56c
2175 ± 4		α, γ'		10.025	Hi 56c, Hu 55b
2232 ± 5		α		10.079	Hi 56c
2258 ± 5		α		10.103	Hi 56c
2291 ± 5		α, γ		10.134	Hi 56c, Hu 55b
2378 ± 5		α, γ		10.217	Hi 56c, Hu 55b
2450 ± 5		α, γ		10.285	Hi 56c, Hu 55b
2635 ± 5		α		10.460	Hi 56c
2655 ± 5	10 ± 3	n		10.479	Hi 56c, Na 56, Ma 56e, Ri 50e
2712 ± 5		α		10.533	Hi 56c
2729 ± 5		n		10.549	Hi 56c, Na 56, Ma 56e
2773 ± 5	<20	n, α		10.591	Hi 56c, Na 56, Ma 56e, Ri 50e
2798 ± 6		α		10.615	Hi 56c
2929 ± 5		α		10.739	Hi 56c
3037 ± 7	33 ± 3	n, α	$\frac{3}{2}^+$	10.841	Ma 56e, Ri 50e, Na 56, Hi 56c
3064 ± 6		α		10.867	Hi 56c
3165 ± 5		n, α	$(\frac{1}{2}^+)$	10.962	Ma 56e, Na 56, Hi 56c
3266 ± 4	29 ± 3	n, α	$\frac{3}{2}^+$	11.058	Ma 56e, Ri 50e, Na 56, Hi 56c, Sz 57
3386 ± 4	15 ± 3	n	$(\frac{1}{2}^+)$	11.172	Ma 56e, Ri 50e, Na 56, Hi 56c, Sz 57
3483 ± 6		n, α		11.264	Ma 56e, Ri 50e, Na 56, Hi 56c
3600 ± 20	85 ± 20	n		11.38	Ma 56e
3685		n, α		11.46	Na 56, Sz 57
3755 ± 20[a]		n(α)		11.52	Ma 56e, Na 56, Sz 57
3901		n, α		11.66	Na 56, Sz 57
4018		n		11.77	Na 56
4250		n		11.99	Bl 51a
5080		n		12.78	Bl 51a
5630		n		13.30	Bl 51a
6200		n		13.84	Bl 51a
6670		n		14.28	Bl 51a

[a] ($T = \frac{3}{2}$).

Hi 56c, Na 56, Ri 50e, Bl 51a). The relative weakness of (p, α) at $E_p = 3.8$ MeV suggests $T = \frac{3}{2}$ for $F^{19*} = 11.5$ MeV (Sz 57). See also (Ts 56).

XIV. $O^{18}(p, p)O^{18}$ $E_b = 7.964$

See O^{18}.

XV. $O^{18}(p, d)O^{17}$ $Q_m = -5.842$ $E_b = 7.964$

See (Ts 56).

XVI. $O^{18}(p, \alpha)N^{15}$ $Q_m = 3.970$ $E_b = 7.964$

Observed resonances are exhibited in table 19.5 (Hi 56c, Se 51b, Co 53h, Sz 57). The sharp resonances at $E_p = 633$ and 846 keV are superposed on what may be one or more broad resonances: see (Co 53h).

XVII. $O^{18}(d, n)F^{19}$ $Q_m = 5.737$

Neutron groups corresponding to 12 levels of F^{19} are reported by (Se 53c). Two thresholds for slow neutron production are observed (Ha 56): see table 19.6. Both are quite sharp, suggesting s-wave neutron emission; the lower is

TABLE 19.6

Thresholds in the $O^{18}(d, n)F^{19}$ reaction

E_d (keV)		E_x (MeV)	Gamma decay to F^{19} states at (MeV)
(Ha 56) [a]	(Bu 58b, Bu 59) [b]		
	346 ± 8	6.048 ± 0.014	0, 1.57
	(370)	(6.07)	
497 ± 15	525 ± 8	6.210 ± 0.014	0, 1.57
	584 ± 10	6.262 ± 0.015	0.20
	1850 ± 50	7.40 [c]	
	2150 ± 50	7.67	
	2640 ± 50	8.11	
3050 ± 20		8.48 ± 0.02	
	3160 ± 30	8.58	

[a] Slow neutron thresholds.
[b] Thresholds for γ-rays.
[c] ($T = \frac{3}{2}$).

probably formed by s-wave deuterons, $J = \frac{1}{2}^+, \frac{3}{2}^+$ (Ha 56). Seven thresholds for γ-ray production are reported. Of these one, at $E_d = 1.85$ MeV ($F^{19*} = 7.40$ MeV), does not appear in $N^{15}(\alpha, \alpha)N^{15}$; it is suggested that this may be the first $T = \frac{3}{2}$ level of F^{19}. Gamma-spectra are reported for several levels (Bu 58b, Bu 59).

XVIII. $O^{18}(He^3, d)F^{19}$ $Q_m = 2.470$

Not reported.

XIX. $O^{18}(\alpha, t)F^{19}$ $Q_m = -11.849$

Not reported.

XX. $O^{19}(\beta^-)F^{19}$ $\quad Q_m = 4.789$

The decay branches 30 ± 10 per cent to the 198-keV state ($E_\beta = 4.5\pm0.3$ MeV) and 70 per cent to a state at 1.57 MeV ($E_\beta = 2.9\pm0.3$ MeV) (Bl 47a, Jo 54g). With a half-life of 29 sec (See St 58b, Ah 54b, Mi 54e), log $ft = 5.55$ and 4.33 respectively (Fe 51b). Gamma rays of energy $\gamma_1 = 1366\pm8$ keV, $\gamma_2 = 199.6\pm1.5$ keV, and $\gamma_3 = 111.5\pm1.5$ keV with relative intensities 0.67 : 1.00 : 0.04 are reported, as is the transition, γ_4, from the 1570-keV level to the 0.110-keV level. The $\gamma_1-\gamma_2$ coincidences indicate that γ_1 arises from the transition 1570 → 197: see fig. 42. The transition 197 → 110 has an

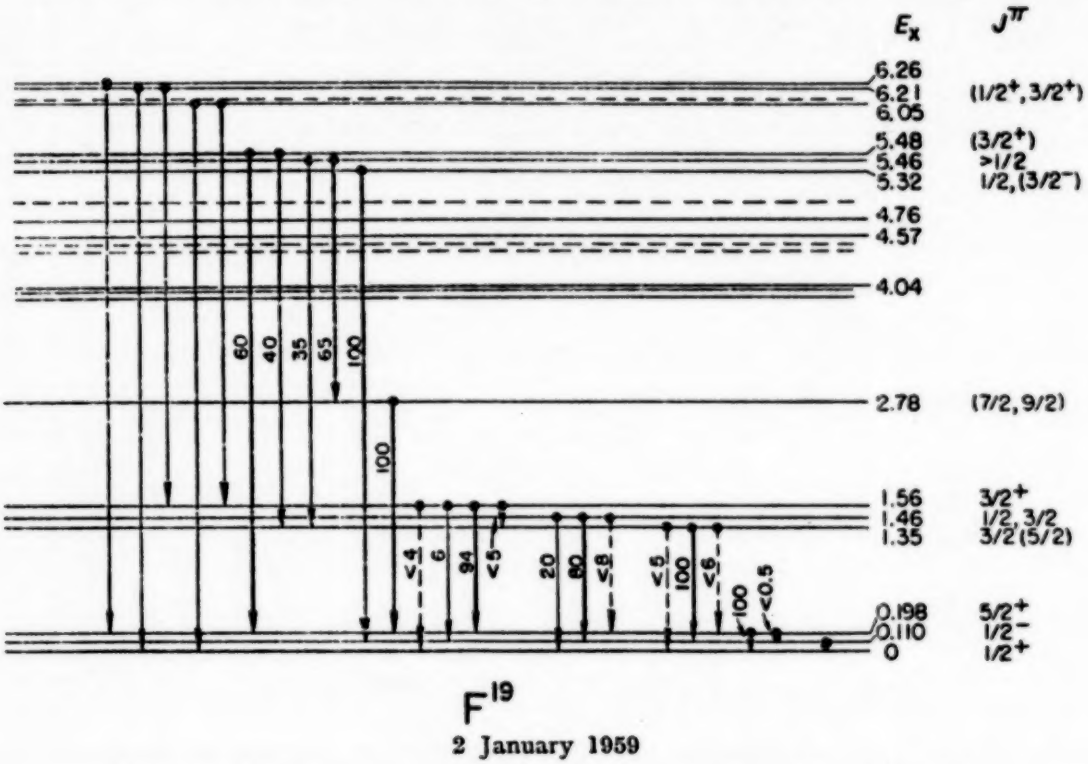

Fig. 42. Gamma-ray transitions in F^{19}: for notation, see fig. 14, p. 83.

intensity < 0.5 per cent and the transitions 1570 → ground state and 1570 → 1350 are $\leqq 3$ and $\leqq 4$ per cent respectively. The mean lifetime of the 197-keV state is $(1.0\pm0.2)\times10^{-7}$ sec (Jo 54g), $(1.25\pm0.025)\times10^{-7}$ sec (Jo 56d) while that of the 110-keV state is $\ll 10^{-6}$ sec (compare $F^{19}(p, p')F^{19*}$) (Jo 54g). The magnetic moment of the 197-keV state is 3.50 ± 0.24 nuclear magnetons (Ph 56) (compare $F^{19}(p, p')F^{19*}$). Lower limits on log ft for β transitions to the ground state and those at 110 and 1350 keV are 6.5, 7.3, and 5.3 (Jo 54g).

The present observations, together with Coulomb excitation data ($F^{19}(\alpha, \alpha')F^{19*}$) require $J = \frac{1}{2}^-$ and $\frac{5}{2}^+$ for the 110-keV and 197-keV levels (see also $F^{19}(p, p')F^{19*}$). The assignment $J = \frac{3}{2}^+$ for the 1570-keV state is obtained from the O^{19} beta decay, from the $\gamma_1-\gamma_2$ angular correlation, and a study of

γ_4. If the beta transitions to the 1570- and 197-keV states are allowed and that to the ground state is forbidden, it follows that O^{19} has $J = \frac{5}{2}^+$ (Jo 54g). See also (To 56), (Ra 57, Re 58; theo.).

XXI. $F^{19}(\gamma, n)F^{18}$ $\quad Q_m = -10.414$

Discontinuities in the activation curve are reported at 70±20 keV above threshold (Be 58g) and at 10.6, 11.0, 11.2, 11.5, 11.9, 12.2 and 15.3 MeV (Go 54f, Ta 54). The "giant" resonance appears at $E_\gamma = 22.2$ MeV, $\Gamma = 5.6$ MeV (Fe 54; see also Ho 52a). See also (Aj 55).

XXII. $F^{19}(\gamma, 2n)F^{17}$ $\quad Q_m = -19.582$

See (Ho 52a, Ma 58d).

XXIII. $F^{19}(\gamma, p)O^{18}$ $\quad Q_m = -7.964$

See (La 55h, Wh 56, Jo 58a).

XXIV. $F^{19}(p, d)F^{18}$ $\quad Q_m = -8.187$

At $E_p = 18$ MeV, the ground-state reduced width, $\theta_n^2 = 0.009$ (Re 56).

XXV. $F^{19}(p, \alpha)O^{16}$ $\quad Q_m = 8.119$

At $E_p = 18.5$ MeV, the angular distribution shows strong maxima and minima, indicative of triton pickup. The triton reduced width for F^{19}(g.s.) is $\theta^2 = 0.1$–0.15 (Li 56b).

XXVI. $F^{19}(n, n')F^{19*}$

At $E_n = 540$ keV, only two γ-ray lines appear, at $E_\gamma = 111 \pm 1.5$ keV and 196 ± 2 keV. At $E_n = 1.50$ MeV, a threshold occurs for a further line, at $E_\gamma = 1.24$ MeV. At $E_n = 1.6$ MeV, lines with $E_\gamma = 1.24$, 1.36, and 1.47 MeV are observed: see table 19.7 and fig. 42. The level assignments indicated in

TABLE 19.7

Gamma rays from $F^{19}(n, n'\gamma)F^{19}$

A		B	
E_γ (keV)	σ mb	E_γ (keV)	Assignment
110± 1	193	111± 1.5	111→g.s.
197± 2	537	196± 2	196→g.s.
1234±20	50	1236±12	1346→111
1358±30	307	1358±12	1466→111 1557→197
1460±30	57	1472±16	1466→g.s
(1560±30)	21		
		2594±15	2791→197

A: (Da 56d); $E_n = 2.6$ MeV.

B: (Fr. 55f, Fr 56c, Fr 57a): $E_n = 0.5$ to 3.7 MeV.

the table derive from coincidence studies. Upper limits on other γ-lines are about 10 per cent (Fr 56c). At $E_n = 3.7$ MeV, a line at $E_\gamma = 2.594$ MeV is observed, attributed to a level at 2.791 MeV (cascade to $F^{19*} = 0.197$ MeV). The excitation function suggests $J = \frac{7}{2}$ or $\frac{9}{2}$ (Fr 57a). (Va 56) find the threshold for 1.37-MeV radiation at $E_n = 1.55 \pm 0.2$ MeV. (Da 56d) reports the relative intensity of the cascade $F^{19*}(0.197 \rightarrow 0.111)$ as $< 6 \times 10^{-3}$ of $(0.197 \rightarrow \text{g.s.})$. See also (Cr 56b, Gr 55d, Va 55a, Fr 55f).

XXVII. $F^{19}(p, p')F^{19*}$

Observed proton groups are listed in table 19.8 (Sq 56, Ho 57e, Ar 52e,

TABLE 19.8

Proton groups from $F^{19}(p, p')F^{19*}$

Level energies (MeV ± keV)					
A	B	C	D	E	F
0.111 ± 2			0.1104 ± 0.8	0.1088 ± 0.8	
0.197 ± 2			0.1978 ± 1.2	0.1960 ± 1.4	
1.350 ± 5	1.37	1.36 ± 20			1.344 ± 5
1.462 ± 5					1.458 ± 5
1.558 ± 5	1.59	1.55 ± 10			1.554 ± 5
2.784 ± 8	2.82	2.83 ± 20			
3.912 ± 10	3.94	3.92 ± 40			
4.002 ± 10					
4.036 ± 10	4.06	4.06 ± 50			
	4.41				
	4.48				
	4.59	4.57 ± 20			
	4.76	4.76 ± 50			
		(4.95 ± 20)			
		5.27 ± 20			
		5.53 ± 30			
		6.07 ± 20			
		(6.50 ± 90)			

A: (Sq 56: $E_p = 7.0$ to 7.3 MeV).
B: (Ar 52e: $E_p = 8$ MeV).
C: (Ho 57e: $E_p = 9.5$ MeV).
D: (Go 55c: $E_p = 2.1$ to 4.5 MeV).
E: (Pe 54d: $E_p = 0.3$ to 1.5 MeV).
F: (Yo 57a: $E_p = 5.2$ MeV).

Pe 54d, Go 55c, Yo 57a). At $E_p = 7.3$ MeV, no other groups appear for $E_x < 4.05$ MeV with intensity > 2 per cent of the $Q = -1.558$ MeV group (Sq 56).

The energy of the first excited state is given as 109.87 ± 0.04 keV from the energy of the γ-decay (Ch 58a; see also table III (19) in Aj 55). The lifetime of the state is $(1.0 \pm 0.25) \times 10^{-9}$ sec (Th 54). The internal conversion coefficient indicates E1 and therefore $J = \frac{1}{2}^-$ or $\frac{3}{2}^-$ for the 0.11-MeV state

(Mi 55e). Since the cascade transition from the 0.2 ($J = \frac{5}{2}^+$) to the 0.1 MeV state is not observed, $J = \frac{1}{2}^-$ is indicated (Ba 55, Sh 54e).

The lifetime of the 198-keV state is 0.8×10^{-7} sec (Th 54), $(1.23 \pm 0.07) \times 10^{-7}$ sec (Fi 55, Le 56c): see also $O^{19}(\beta^-)F^{19}$. The lifetime requires E2 or faster radiation; the internal conversion coefficient indicates E2 (Mi 55e). Angular distributions at various $J = 2^-$ resonances in Ne^{20*} confirm the assignment $J^\pi = \frac{5}{2}^+$ for $F^{19*} = 0.197$ (Sh 54e, Pe 54d, Ch 54b, Ba 55). The Coulomb excitation also requires an E2 transition (Te 56). The magnetic moment is 3.70 ± 0.45 nuclear magnetons (Le 56c, Le 56f, Le 55a), 3.0 ± 0.7 n.m. (Su 56a), 4.5 ± 1.0 n.m. (Tr 56, Tr 56b), 3.5 ± 0.5 n.m. (Ma 58l): the value predicted by (El 55a)is 3.3 n.m.; compare $O^{19}(\beta^-)F^{19}$. The static electric quadrupole moment is 0.13×10^{-24} cm^2 (K. Sugimoto, to be published). See also (Tr 57, Tr 57a, Ra 57, Ba 56e).

The γ-decay of higher excited states has been studied by (To 56; $E_p = 2.4$ to 4.1 MeV): see fig. 42. Gamma rays with $E_\gamma = 1.238 \pm 0.010$, 1.350 ± 0.010 and 1.449 ± 0.010 MeV are observed in addition to the two low energy γ's. The 1.24 and 1.35-MeV γ-rays are in prompt coincidence with 0.11-MeV radiation, indicating cascade decay of states at 1.342 ± 0.010 MeV and 1.452 ± 0.010 MeV through the 0.11-MeV state. A (1.354 ± 0.010)-MeV γ-ray is found to be in delayed coincidence with 197-keV radiation, indicating the cascade decay of a level at 1.551 ± 0.010 MeV through the $J = \frac{5}{2}^+$ second excited state. The 1.34-MeV state does not appear to decay to the 0.198-MeV state (< 8 per cent); it decays almost entirely to the $J = \frac{1}{2}^-$ first excited state. This observation suggests $J = \frac{1}{2}$ or $\frac{3}{2}$, with $J = \frac{5}{2}$ not excluded; the observed anisotropy excludes $J = \frac{1}{2}$. Similarly, the γ-decay of the 1.46-MeV state suggests $J = \frac{1}{2}$ or $\frac{3}{2}$. The assignment $J = \frac{3}{2}^+$ for $F^{19*} = 1.56$ MeV follows from $O^{19}(\beta^-)F^{19}$ (To 56). (Ra 58h) find gamma-ray energies of 1236 ± 10, 1358 ± 8 and 1460 ± 30 keV, not corrected for Doppler shift. Relative intensities for $E_p = 3.2$ to 4.7 MeV are given. See also (Ra 58c) and $F^{19}(n, n')F^{19*}$.

For elastic and inelastic scattering at high energies, see (Da 56b, Bu 56j, Kl 56, Gi 57, Ty 58a, St 56c).

XXVIII. $F^{19}(d, d')F^{19*}$

At $E_d = 8.9$ MeV, deuteron groups are observed to states at 1.60 ± 0.02 and 2.83 ± 0.02 MeV (El 56a). See also (Th 54d).

XXIX. $F^{19}(\alpha, \alpha')F^{19*}$

Gamma radiation of energy 110 keV and 197 keV (See table III (19) of Aj 55) is observed for $E_\alpha = 0.6$ to 3.5 MeV. The shape of the rise, the absolute cross sections at low energies, and the γ-ray angular distributions agree well with E1 and E2 Coulomb excitation, respectively, of the first two excited states (see He 54b, Sh 54e, Jo 54, Te 54b, Te 56).

XXX. $F^{19}(N^{14}, N^{14'}\gamma)F^{19}$

At $E(N^{14}) = 15.6$ MeV, γ-rays are observed from the Coulomb excitation of the first two excited states (Al 56h).

XXXI. $Ne^{19}(\beta^+)F^{19}$ $Q_m = 3.256$
See Ne^{19}.

XXXII. $Ne^{20}(n, d)F^{19}$ $Q_m = -10.646$
Not reported.

XXXIII. $Ne^{20}(d, He^3)F^{19}$ $Q_m = -7.379$
Not reported.

XXXIV. $Ne^{20}(t, \alpha)F^{19}$ $Q_m = 6.940$
Not reported.

XXXV. $Ne^{21}(n, t)F^{19}$ $Q_m = -11.145$
Not reported.

XXXVI. $Ne^{21}(p, He^3)F^{19}$ $Q_m = -11.910$
Not reported.

XXXVII. $Ne^{21}(d, \alpha)F^{19}$ $Q_m = 6.441$

At $E_d = 2.1$ MeV, α-particle groups are observed to $F^{19*} = 0, 113\pm8$ and 192 ± 12 keV (Mi 52).

XXXVIII. $Ne^{22}(p, \alpha)F^{19}$ $Q_m = -1.698$
Not reported.

Ne^{19}

(Fig. 43, p. 263) †

THEORY

See (El 55a, Re 55, Re 55b, Re 58, Ra 57).

TABLE 19.9
Energy levels of Ne^{19}

E_x (MeV $\pm$ keV)	J^π	$\tau_{\frac{1}{2}}$ or τ_m	Decay	Reactions
0	$\frac{1}{2}^+$	$\tau_{\frac{1}{2}} = 17.8\pm0.1$ sec	β^+	I, V, VII
0.241 ± 4	$(\frac{3}{2}^+)$	$\tau_m = (1.8\pm0.2)\times10^{-9}$ sec	γ	V
0.280 ± 4	$(\frac{1}{2}^-)$	$\tau_m < 5\times10^{-9}$ sec	γ	V
≈10.48			p, α, He^3	III

I. $Ne^{19}(\beta^+)F^{19}$ $Q_m = 3.256$

The positon end point is 2.18 ± 0.03 (Sc 52a), 2.23 ± 0.05 (Al 57), 2.24 ± 0.01 MeV (We 58b). The half-life is 17.4 ± 0.2 sec (He 59), 17.7 ± 0.1 (Pe 57),

† For level scheme of F^{19}, see fig. 41, p. 253.

18.3±0.5 (Al 57), 18.5±0.5 (Sc 52a), 19±1 (Na 54b), 19.5±1.0 (We 58b), 20.3±0.5 sec (Wh 39). The absence of low-energy γ-rays (see F^{19}) indicates that the transition takes place to the ground state, $J = \frac{1}{2}^+$, of F^{19}: log

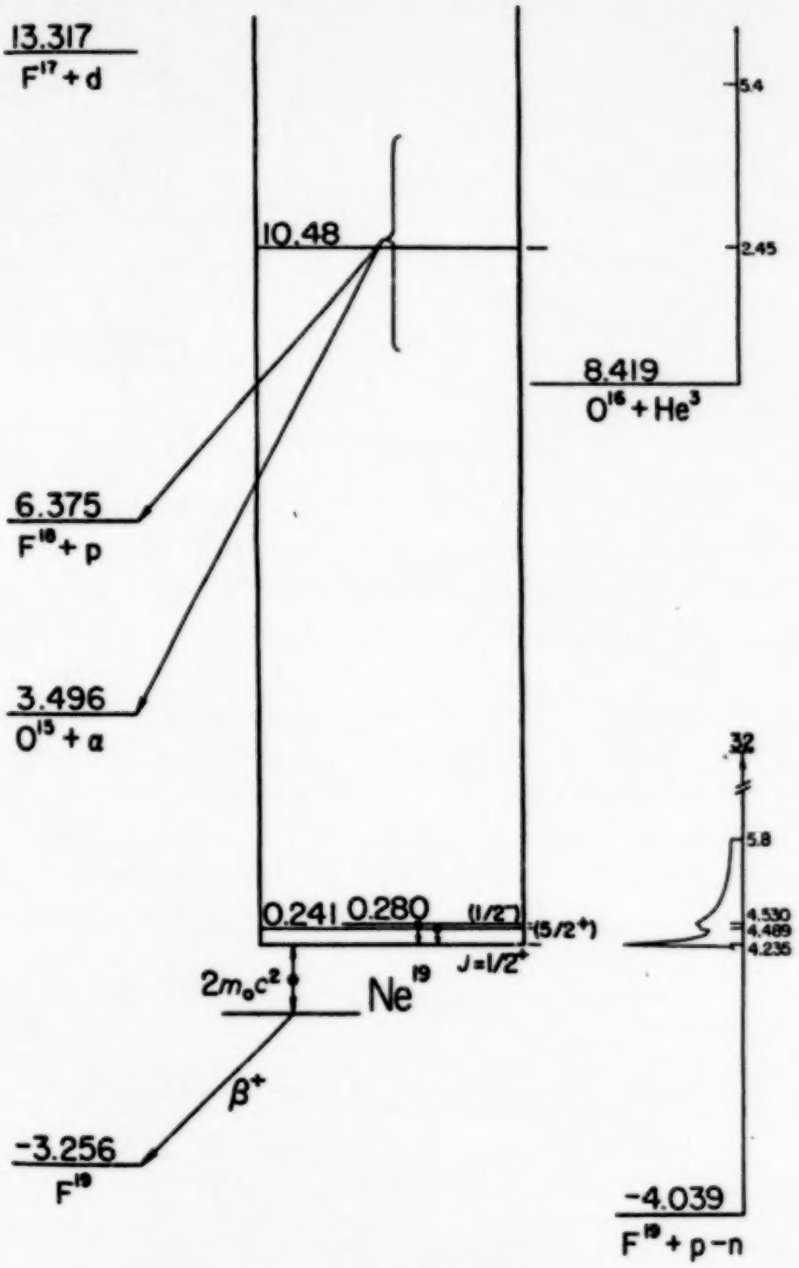

29 December 1958

Fig. 43. Energy levels of Ne^{19}: for notation, see fig. 1, p. 7.

$ft = 3.30$, log ft for a transition to the 0.11-MeV, $J = \frac{1}{2}^-$, state of F^{19} is $\geqq 6.0$; log ft to the 0.20-MeV, $J = \frac{5}{2}^+$, state is $\geqq 5.5$. It follows that the ground state of Ne^{19} is $J = \frac{1}{2}^+$ (Jo 54g). The Kurie plot is linear from the end point to 0.7 MeV (Al 57).

The electron-neutrino angular correlation has been studied by (Ma 55c, Al 57, Go 57, He 58, He 59). See also (Al 54, La 59) and (Re 58; theo.).

II. $O^{16}(\alpha, n)Ne^{19}$ $Q_m = -12.158$

See (Te 47).

III. (a) $O^{16}(He^3, p)F^{18}$ $Q_m = 2.045$ $E_b = 8.419$

(b) $O^{16}(He^3, \alpha)O^{15}$ $Q_m = 4.923$

Yield curves for the ground-state alpha-particle group and for proton groups to the first six states of F^{18} have been obtained for $E(He^3) = 2.0$ to 5.4 MeV. All curves show pronounced resonance structure; in particular, all groups appear to be resonant at $E(He^3) \approx 2.45$ MeV, corresponding to $Ne^{19*} \approx 10.48$ MeV. Angular distributions have also been measured at several energies (Br 58d).

IV. $O^{17}(He^3, n)Ne^{19}$ $Q_m = 4.274$

Not reported.

V. $F^{19}(p, n)Ne^{19}$ $Q_m = -4.039$

The ground-state threshold is $E_p = 4240 \pm 8$ keV (Ki 55c), 4235 ± 5 keV (Ma 55k). Two additional thresholds are observed, corresponding to excited states of Ne^{19} at 241 ± 4 and 280 ± 4 keV. No other excited states appear with $E_x < 1.5$ MeV (Ma 55k). The two excited states radiate to the ground state with $E_\gamma = 242 \pm 5$ and 281 ± 8 keV and with lifetimes of $(1.8 \pm 0.2) \times 10^{-8}$ sec and $< 5 \times 10^{-9}$ sec (Ba 57g). It appears from these results that the position of the first two excited states in the $A = 19$ pair is reversed in F^{19} and Ne^{19}: the sequence in F^{19} is $\frac{1}{2}^+$, $\frac{1}{2}^-$, $\frac{5}{2}^+$, in Ne^{19} it appears from the lifetimes to be $\frac{1}{2}^+$, $\frac{5}{2}^+$, $\frac{1}{2}^-$. See also (Bi 58a).

VI. $F^{19}(He^3, t)Ne^{19}$ $Q_m = -3.274$

Not reported.

VII. $Ne^{20}(\gamma, n)Ne^{19}$ $Q_m = -16.912$

See Ne^{20}.

VIII. $Ne^{20}(p, d)Ne^{19}$ $Q_m = -14.685$

Not reported.

IX. $Ne^{20}(d, t)Ne^{19}$ $Q_m = -10.653$

Not reported.

X. $Ne^{20}(He^3, \alpha)Ne^{19}$ $Q_m = 3.666$

Not reported.

XI. $Ne^{21}(p, t)Ne^{19}$ $Q_m = -15.184$

Not reported.

O^{20}

(Not illustrated)

MASS OF O^{20}

The mass excess of O^{20} is estimated as 13.3 ± 2 MeV by extrapolation from heavier $A = 4n$ isobars (see Sh 54d, Aj 55). O^{20} is then stable to neutron emission by ≈ 4 MeV.

O^{20} has not been observed. A recent attempt to detect its β-decay was unsuccessful: (Ka 56d) bombarded O^{18} with 40-MeV α-particles ($O^{18}(\alpha, 2p)O^{20}$, $Q_m = -20.3$) and found that $\tau_{\frac{1}{2}}$ is not in the range 10 min to 150 years. If $\tau_{\frac{1}{2}}$ is between 1 sec and 10 min, the cross section for the $(\alpha, 2p)$ reaction is less than a few milibarns.

Two possible reactions leading to O^{20} are $O^{18}(t, p)O^{20}$ ($Q_m = -0.5$) and $Ne^{22}(n, He^3)O^{20}$ ($Q_m = -22$).

F^{20}

(Fig. 44, p. 266)

THEORY

See (Ra 57).

I. $F^{20}(\beta^-)Ne^{20}$ $Q_m = 7.050$
See Ne^{20}.

II. $O^{17}(\alpha, p)F^{20}$ $Q_m = -5.659$
Not observed.

III. $O^{18}(d, n)F^{19}$ $Q_m = 5.737$ $E_b = 12.343$
See F^{19}.

IV. $O^{18}(d, p)O^{19}$ $Q_m = 1.731$ $E_b = 12.343$

The proton yield has been measured from $E_d = 0.79$ to 0.88 MeV (Ah 56b). See also (Zi 59a), O^{19}.

V. $O^{18}(d, \alpha)N^{16}$ $Q_m = 4.237$ $E_b = 12.343$

The cross section has been measured for $E_d = 0.5$ to 3.0 MeV. Resonances are observed at $E_d = 1.40$, 1.75, 2.15 and 2.90 MeV, with widths of 500, 400, 300 and 600 keV, respectively, corresponding to $F^{20*} = 13.60$, 13.92, 14.28 and 14.95 MeV (Bo 57d). See also N^{16}.

VI. $O^{18}(t, n)F^{20}$ $Q_m = 6.085$
See (Sh 56a).

VII. $O^{18}(He^3, p)F^{20}$ $Q_m = 6.850$
Not reported.

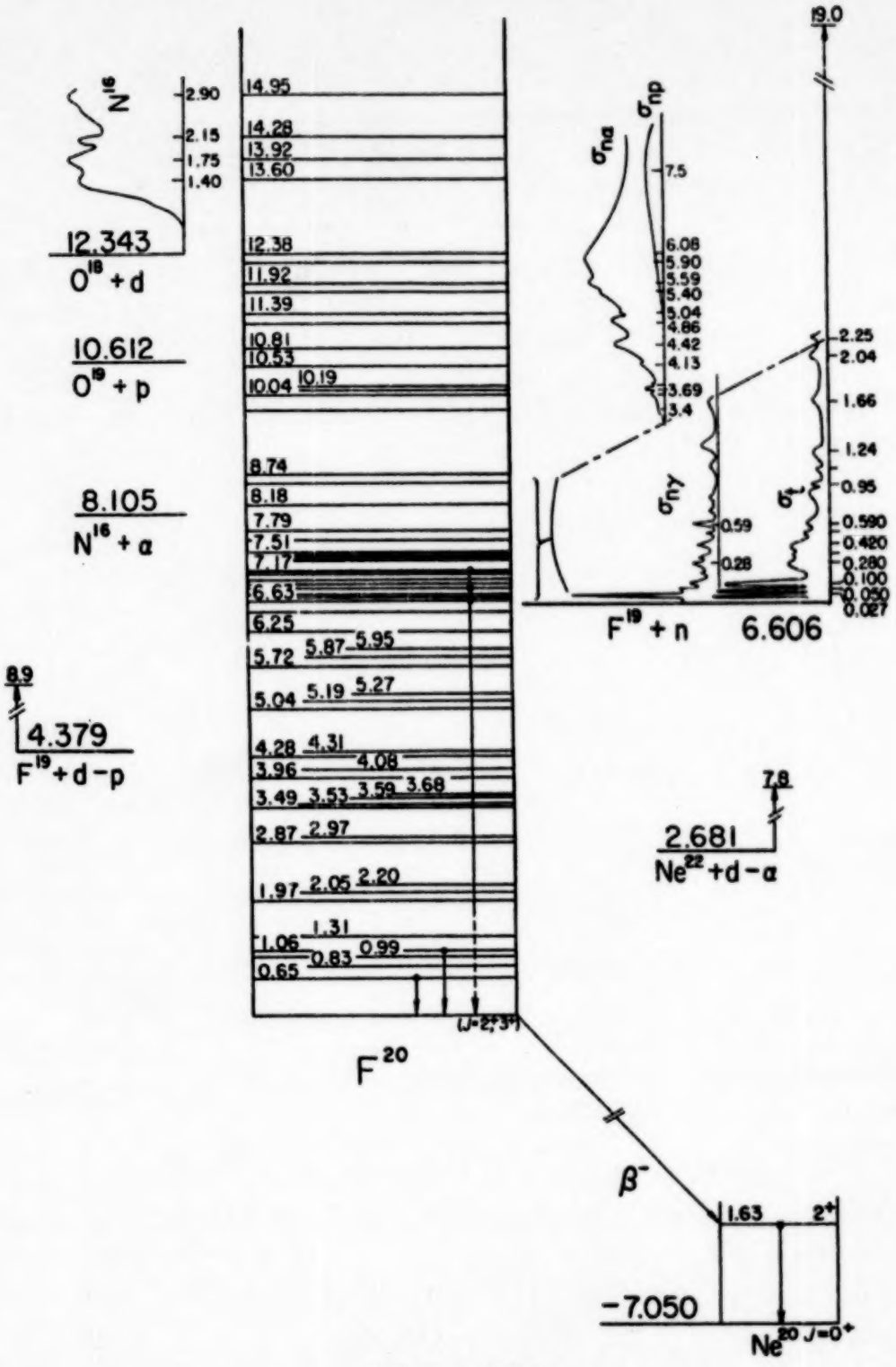

8 January 1959

Fig. 44. Energy levels of F^{20}: for notation, see fig. 1, p. 7.

VIII. $O^{18}(\alpha, d)F^{20}$ $\quad Q_m = -11.501$

Not reported.

TABLE 20.1

Energy levels of F^{20}

E_x (MeV ± keV)	J^π	$\tau_{\frac{1}{2}}$ or Γ (keV)	Decay	Reactions
0	$2^+, 3^+$	$\tau_{\frac{1}{2}} = 11.4 \pm 1$ sec	β^-	I, VI, IX, XV, XXIII, XXIV
0.652 ± 8	$1^+, 2^+, 3^+$		γ	XV, XXIII
0.828 ± 8	$1^+, 2^+, 3^+$			XV
0.988 ± 8	$1^+, 2^+, 3^+$			XV
1.059 ± 8	$0^+, 1^+$		γ	XV
1.309 ± 8				XV
1.970 ± 8				XV
2.048 ± 8	$1^+, 2^+, 3^+$			XV
2.195 ± 8	$1^+, 2^+, 3^+$			XV
2.870 ± 8	$2^-, 3^-, 4^-$			XV
2.966 ± 8	$0^-, 1^-, 2^-$			XV
3.491 ± 8	$0^+, 1^+$			XV
3.528 ± 8	$0^+, 1^+$			XV
3.586 ± 8				XV
3.681 ± 8				XV
3.961 ± 9				XV
4.079 ± 9	$0^+, 1^+$			XV
4.275 ± 9				XV
4.310 ± 9	$0^+, 1^+$			XV
5.04 ± 20	$0^-, 1^-, 2^-$			XV
5.19 ± 20	$0^-, 1^-, 2^-$			XV
5.27 ± 20	$0^-, 1^-, 2^-$			XV
5.72 ± 20				XV
5.87 ± 20	$0^-, 1^-, 2^-$			XV
5.95 ± 20	$0^-, 1^-, 2^-$			XV
6.25 ± 20				XV
6.52 ± 20	$0^-, 1^-, 2^-$			XV
6.63 ± 10	2^-	0.36 ± 0.08	n, γ	IX, X, XV
6.65 ± 10	1^-	1.4	n, γ	IX, X
6.70 ± 10	1^-	11 ± 2	n, γ	IX, X
6.87 ± 15		24 ± 10	n, γ	IX, X, XI
6.93 ± 25		190 ± 95	n, (γ)	IX, X
7.01 ± 15		24 ± 14	n, (γ)	IX, X, XI
7.09 ± 15		24 ± 14	n, γ	IX, X, XI
7.17 ± 15		24 ± 10	n, γ	IX, X, XV
7.35			n, (γ)	IX, XI
7.39			n	XI
7.44			n, (γ)	IX, XI
7.51 ± 20			n, (γ)	IX, X, XI
7.65 ± 20			n, (γ)	IX, X
7.79 ± 20			n, γ	IX, X
8.18 ± 20			n, γ	IX, X
8.55 ± 20			n	X
8.74 ± 20			n	X
9.8 ± 100			n, α	XIV
10.04 ± 50			n, α	XIV
10.11 ± 50			n, α	XIV
10.19 ± 50			n, α	XIV

TABLE 20.1 (continued)

E_x (MeV $\pm$ keV)	J^π	$\tau_{\frac{1}{2}}$ or Γ (keV)	Decay	Reactions
10.53 $\pm$ 50			n, α	XIV
10.81 $\pm$ 50			n, α	XIV
11.22 $\pm$ 50			n, α	XIV
11.39			n, α	XIV
11.74			n, α	XIV
11.92			n, α	XIV
12.21 $\pm$100			n, α	XIV
12.38			n, α	XIV
13.60		450	d, α	V
13.92		360	d, α	V
14.28		270	d, α	V
14.95		540	d, α	V

IX. $F^{19}(n, \gamma)F^{20}$ $Q_m = 6.606$.

The thermal capture cross section is 9.4 ± 2 mb (Se 47). The γ-spectrum has been measured by (Ca 57h) who find transitions with E_γ (corrected for recoil) of 6.600 ± 0.011, 6.019 ± 0.011, 5.54 ± 0.02, 5.28 ± 0.02 and 5.10 ± 0.02 MeV, with intensities of 30, 16, 24, 27 and 14 photons per 100 captures respectively. The 6.60-MeV line is the ground state transition; the other transitions are not uniquely determined. Upper limits for transitions to F^{20*} (0.65, 0.83, and 0.99 MeV) are 1, 3 and 7 photons per capture, respectively. The γ-rays of energy 5.54 and 5.28 MeV may result from transitions to F^{20*} (1.06 and 1.31) (Ca 57h). Two resonances for F^{20} production are observed at $E_n = 280$ and 590 keV, with widths ≈ 20 keV and peak cross sections of 1.2 and 1.3 mb, respectively; $\omega\Gamma_\gamma \approx 15$ eV (He 50b). A number of additional resonances appear in the range $E_n = 25$ to 2000 keV: see (Hu 58). See also (Ki 51a).

X. $F^{19}(n, n)F^{19}$ $E_b = 6.606$

The coherent scattering cross section is 3.8 ± 0.3 b; the total cross section (epithermal, bound) is 4.0 ± 0.1 b (Hu 58). The cross section is approximately constant at ≈ 3.7 b from 0.02 eV to 20 keV (Hu 58). Resonances in the total cross section are listed in table 20.2. The J^π assignments indicated for the first three levels (p-wave) are based on elastic scattering distributions and total cross sections (Bl 58).

Total cross sections have been measured to $E_n = 5$ MeV by (Wi 58), from $E_n = 3$ to 14 MeV by (Ne 54b), from $E_n = 3.8$ to 8.1 MeV by (Bo 57a), from $E_n = 4.4$ to 5.6 MeV by (Be 56c) and from $E_n = 7$ to 14 MeV by (Br 58h). The cross section shows structure at least as high as $E_n \approx 7.5$ MeV: see (Wi 58, Be 56c, Bo 57a). For the presentation of the data as a whole, see (Hu 58). Angular distributions have been measured and phase

shifts determined at five energies in the range $E_n = 0.66$ to 2.92 MeV by (Wi 58). See also (Pa 55, La 57c) and (Ne 56a; theo.).

TABLE 20.2

Resonances in $F^{19}(n, n)F^{19}$

E_n (keV)	Γ_{lab} (keV)	σ_{max} (b)	F^{20*} (MeV)	J^π
27 [a]	0.38 ± 0.08 [a]	23.7 [e]	6.63	2⁻ [e]
49.5 [b]	1.4 [e]	22.7	6.65	1⁻ [e]
99.5 [b]	11 ± 2 [b,e]	22.7	6.70	1⁻ [e]
280 ±10 [c]	25 ± 10	10.0	6.87	
340 ±20 [c]	200 ±100	8.0	6.93	
420 ±10 [c]	25 ± 15	8.8	7.01	
510 ±10 [c]	25 ± 15	5.7	7.09	
590 ±10 [c]	25 ± 10	6.0	7.17	
950 [d]		4.0	7.51	
1100 [d]		3.5	7.65	
1240 [d]		4.2	7.79	
1660 [d]		3.6	8.18	
2040 [d]		3.3	8.55	
2250 [d]		3.0	8.74	

[a] Hu 58.
[b] Hi 55, Hu 58.
[c] Bo 50f, Hu 58.
[d] Wi 51, Wi 58.
[e] Bl 58, Cr 57, Me 57e.

XI. $F^{19}(n, n')F^{19*}$ $E_b = 6.606$

Observed resonances in the yield of 0.1 and 0.2-MeV γ-radiation (see F^{19}) for $E_n < 1$ MeV are exhibited in table 20.3. A satisfactory fit to the excitation

TABLE 20.3

Resonances in $F^{19}(n, n'\gamma)F^{19}$ (Fr 55f)

E_n (0.1) (keV)	σ [a] (0.1-MeV γ) (b)	E_n (0.2) (keV)	σ [a] (0.2-MeV γ) (b)	F^{20*} (MeV)
(100)				(6.70)
270	4.6	(300)	0.8	6.87
(390)	1.4	420	2.1	(7.01)
(500)	1.1			(7.08)
(780)	0.6	780	0.8	7.35
830	0.9			7.39
880	0.8			7.44
950	0.7	950	1.3	7.51

[a] Cross sections ±40 per cent.

function for $E_n < 300$ keV is obtained on the assumption of p-wave resonances at $E_n = 100$ and 260 keV. The excitation functions for 0.1-, 0.2-,

1.24- and 1.37-MeV γ-rays have been measured to $E_n = 2.2$ MeV (Fr 55f).

The cross section for excitation of F^{19*} (2.79) has been studied from $E_n = 3$ to 3.6 MeV. The very slow rise for the first 300 keV above threshold suggests a large spin difference between the 2.79-MeV level and the ground state (Fr 57a). See also (Aj 55, Va 56).

XII. $F^{19}(n, 2n)F^{18}$ $Q_m = -10.414$ $E_b = 6.606$

The cross section at $E_n = 14.1$ MeV is 62 mb (As 58); at $E_n = 14.5$ MeV it is 60 mb (Pa 53a). See also (Ra 58d, Aj 52c).

XIII. $F^{19}(n, p)O^{19}$ $Q_m = -4.066$ $E_b = 6.606$

The excitation function has been measured from $E_n = 4.7$ to 8.0 MeV; it shows a single broad maximum at 7.5 MeV. For $E_n < 8$ MeV, the (n, α) cross section is at least twice as large as the (n, p) cross section (Ma 55l). At $E_n = 14.5$ MeV, $\sigma(n, \alpha)/\sigma(n, p) = 1.2 \pm 0.4$ (Ko 58a); $\sigma(n, p) = 135$ mb (Pa 53a). See (Hu 58).

XIV. $F^{19}(n, \alpha)N^{16}$ $Q_m = -1.500$ $E_b = 6.606$

Observed resonances are listed in table 20.4 (Ma 55l, Bo 55a; see graph in Hu 58). See also (Wi 37e, Bo 55d, Gr 55d, Ko 58a).

TABLE 20.4

Resonances in $F^{19}(n, \alpha)N^{16}$

E_n [a] (MeV)	E_n [b] (MeV)	σ_{max} [a] (mb)	σ_{max} [c] (mb)	F^{20*} (MeV)
3.4				9.8
3.61 ± 0.05		48		10.04
3.69 ± 0.05		55		10.11
3.77 ± 0.05		44		10.19
4.11 ± 0.05	4.17	90	11.1	10.53
4.42 ± 0.05		167		10.81
	4.68		11.7	
4.86 ± 0.05		186		11.22
	5.04		12.2	11.39
	5.40		12.3	11.74
	5.59		11.9	11.92
5.9 ± 0.1	5.90	268	11.4	12.21
	6.08		10.6	12.38

[a] (Ma 55l): $\sigma \pm 40$ per cent.
[b] (Bo 55a).
[c] (Bo 55a, Wa 58c).

XV. $F^{19}(d, p)F^{20}$ $Q_m = 4.379$

$Q_0 = 4.383 \pm 0.015$ (Kh 57).

$Q_0 = 4.38 \pm 0.03$ (El 56a).

Energy levels of F^{20} derived from the proton groups are listed in table 20.5

(Wa 52b, El 56a, Kh 57). The J^π assignments given in the table result from analysis of angular distributions by stripping theory. The angular distribu-

TABLE 20.5

Proton groups from $F^{19}(d, p)F^{20}$

E_x (MeV ± keV) (Wa 52b)	E_x (MeV) (Kh 57) [a]	E_x (MeV) (El 56a) [b]	$(2J+1)\theta^2$ (per cent) (El 56a)	l_n (El 56a)	J^π
0					
0.652 ± 8	0.66		8.0	2 [c]	$1^+, 2^+, 3^+$
0.828 ± 8	0.81		0.5	2	$1^+, 2^+, 3^+$
0.988 ± 8			0.5	2	$1^+, 2^+, 3^+$
1.059 ± 8	1.08		0.1	0	$0^+, 1^+$
1.309 ± 8	1.34			iso.	
1.970 ± 8					
2.048 ± 8			8.1	2	$1^+, 2^+, 3^+$
2.195 ± 8	2.15		2.8	2	$1^+, 2^+, 3^+$
2.870 ± 8			5.7	3	$2^-, 3^-, 4^-$
2.966 ± 8			0.6	1	$0^-, 1^-, 2^-$
	3.11				
3.491 ± 8			7.1	0	$0^+, 1^+$
3.528 ± 8			7.1	0	$0^+, 1^+$
3.586 ± 8	3.58				
3.681 ± 8	3.77				
3.961 ± 9					
4.079 ± 9	4.09		2.1	0	$0^+, 1^+$
4.275 ± 9					
4.310 ± 9	4.37		3.6	0	$0^+, 1^+$
	(4.73)				
(5.062 ± 11)	4.86	5.04	0.7	1	$0^-, 1^-, 2^-$
	5.16	5.19	1.0	1	$0^-, 1^-, 2^-$
		5.27	1.8	1	$0^-, 1^-, 2^-$
	5.41				
	5.54				
		5.72			
		5.87	4.4	1	$0^-, 1^-, 2^-$
		5.95	9	1	$0^-, 1^-, 2^-$
	6.07				
	6.17	6.25			
	6.36				
	6.47	6.52	9	1	$0^-, 1^-, 2^-$
	6.65	6.63	5	1	$0^-, 1^-, 2^-$
	6.74				
		6.81	7	1	$0^-, 1^-, 2^-$
		6.98			
		7.20	4	1	$0^-, 1^-, 2^-$

(Wa 52b): $E_d = 1.8$ MeV.
(El 56a): $E_d = 8.9$ MeV.

[a] $E_d = 3.3$ to 4.0 MeV; errors ±20-25 keV (Kh 57).

[b] Levels 1-19 of (Wa 52b) identified, but not measured; errors on remaining levels ± 20 keV (El 56a).

[c] See also (Se 57b, Ta 56, On 57).

tion of the ground state protons has been studied at a number of energies (Va 56c, Ta 56, On 57, Br 53c, Se 57b). The pattern varies strongly with energy, suggesting compound nucleus interaction rather than stripping: it is concluded that an earlier assignment of $J = 1^+$ (Br 53c) is not supported (Se 57b). See also (To 56a, Ok 56; theo.). At $E_d = 1.05$ MeV, γ rays are observed with $E_\gamma = 0.64$ and 1.06 MeV (Th 54d).

It is of interest to note that among the levels of F^{20} there occur seven groups with equal spacings of $165n$ keV, where n is an integer for each group (Wa 52b, El 56a). Above $E_x = 5$ MeV, only odd parity levels appear; below this value, even parities predominate. The levels appear in groups of the same parity, separated by ≈ 0.6 MeV (El 56a).

XVI. $Ne^{20}(n, p)F^{20}$ $Q_m = -6.267$
Not observed.

XVII. $Ne^{20}(t, He^3)F^{20}$ $Q_m = -7.032$
Not observed.

XVIII. $Ne^{21}(n, d)F^{20}$ $Q_m = -10.797$
Not observed.

XIX. $Ne^{21}(d, He^3)F^{20}$ $Q_m = -7.530$
Not observed.

XX. $Ne^{21}(t, \alpha)F^{20}$ $Q_m = 6.789$
Not observed.

XXI. $Ne^{22}(n, t)F^{20}$ $Q_m = -14.905$
Not observed.

XXII. $Ne^{22}(p, He^3)F^{20}$ $Q_m = -15.670$
Not observed.

XXIII. $Ne^{22}(d, \alpha)F^{20}$ $Q_m = 2.681$

Alpha particle groups have been observed at $E_d = 7.8$ MeV corresponding to the ground state and to a level at 0.57 ± 0.13 MeV (Mi 51d).

XXIV. $Na^{23}(n, \alpha)F^{20}$ $Q_m = -3.888$
See (Je 50d).

Ne^{20}

(Fig. 45, p. 275)

THEORY

See (Ga 55b, He 55f, Mo 56, Ba 57, Ra 57).

I. $Be^9(N^{14}, t)Ne^{20}$ $Q_m = 6.323$
See (Go 58e).

TABLE 20.6

Energy levels of Ne^{20}

E_x (MeV ± keV)	J^π; T	τ_m or Γ (keV)	Decay	Reactions
0	0^+; 0	—	Stable	I, XIII, IX, XX, XXI, XXII, XXV
1.632 ± 4	2^+; 0	$\tau_m = (7.6 \pm 3.3) \times 10^{-13}$ sec	γ	IX, XIII, XVI, XX, XXI, XXII, XXV
4.248 ± 6	; 0		γ	XIII, XX, XXII, XXV
4.969 ± 6	$\geqq 1$; 0		γ	IX, XX, XXII, XXV
5.631 ± 6	; 0			XIII, XX, XXII, XXV
6.745 ± 10	0^+; 0	19	α	VI
7.189 ± 10	3^-; 0	8	α	VI, XIII, XXII
7.225 ± 10	0^+; 0	4	α	VI, XIII, XX
7.457 ± 10	2^+; 0	8	α	VI, XX
7.861 ± 10	2^+; 0	2	α	VI, XIII, XX
≈8.6	0^+; 0	≈1300	α	VI
8.76	1^-; 0	4	α	VI
≈8.8	2^+; 0	≈1200	α	VI
8.84	(5^-); 0	≦4	α	VI
8.91	1^-; 0	20	α	VI
9.11	4^+; 0	8	α	VI, XIII, XX
9.34 ± 100	$(\leqq 2^-)$		γ	XIII, XX
9.97 ± 100	; (1)		(γ), (α)	XIII, XX
(10.61 ± 100)	; (1)		(γ)	XIII
11.11			γ	XIII
11.19			γ	XIII
11.33			γ	XIII
11.42			γ	XIII
11.69			γ	XIII
11.87	; (1)		(γ), α	XIII
12.27			γ	XIII
12.51			γ	XIII
13.086 ± 8		1.0	p, α	XI
13.196 ± 8	1^+	3.1 ± 0.2	p, α	XI
13.253	1^-	100	p, α	XI
13.253	0^+	100	p, α	XI
13.332 ± 8		0.9	p, α	XI
13.440 ± 8	(2^-)	28 ± 3	p, α	XI
13.491	1^-	190	p, α	XI
13.511 ± 8	1^+	5.8 ± 0.7	p, α, γ	IX, X, XI
13.548 ± 10	1^-	33	p, α	XI
13.569 ± 10	2^+	63	p, α	XI
13.613 ± 10	2^+	≈10	p, α	X, XI
13.667 ± 8		6.2 ± 1	p, α	X, XI
13.673 ± 10	0^+, 2^+	20	p, α	X, XI
13.690 ± 10	1^-	110	p, α	XI
13.703 ± 8	2^-	5.1 ± 0.3	p, α, γ	IX, X, XI
13.730 ± 8		4.8 ± 1	p, α	X, XI
13.757 ± 10	0^+	≈170	p, α	XI
13.761 ± 8	1^+	8.2 ± 0.5	p, α, γ	IX, X, XI
13.80			p, γ	IX
13.899 ± 10	1^-	≈200	p, α	XI

TABLE 20.6 (continued)

E_x (MeV ± keV)	J^π; T	τ_m or Γ (keV)	Decay	Reactions
13.909 ± 8		0.7 ± 0.3	p, α, γ	IX, X, XI
13.932 ± 10	2+	45	p, α	XI
13.956 ± 8		3	p, α	X, XI
13.975 ± 10	0+	≈70	p, α	XI
14.003 ± 8		100 ± 20	p, α	XI
14.046 ± 10	1−	≈60	p, α	XI
14.061 ± 10	2+	≈100	p, α	X, XI
14.092 ± 8	(3+)	17.5 ± 1	p, α, γ	IX, X, XI
14.13		3.8	p, γ	IX
14.154 ± 8	2−	5.2 ± 0.5	p, α, γ	IX, X, XI
14.167 ± 10	2+	40	p, α	XI
14.179 ± 8	2−	10.5 ± 1	p, α, γ	IX, X, XI
14.224 ± 10	1+	14 ± 1	p, γ	IX, X
14.380 ± 8		5.7 ± 1	p, α	X, XI
14.436 ± 60		55	p, α	X, XI
14.482 ± 8		33 ± 3	p, α	X, XI
14.497 ± 10	0+	130 ± 5	p, α	XI
14.633 ± 10	1−	125 ± 5	p, α	XI
14.725 ± 8	0+, 1+	38 ± 10	p, α	X, XI
14.802 ± 8		110 ± 20	p, α	XI
14.91	(4+)	70 ± 25	p, α	XI
15.07	(2+)	75 ± 25	p, α	XI
15.08		80	p, α	XI
15.26		27	p, α	XI
15.34	(0+)	285 ± 25	p, α	XI
15.37		85	p, α	XI
15.42		75	p, α	XI
15.53		55	p, α	XI
15.55		120	p, α	XI
15.67			p, α	XI
15.74		28	p, α	XI
15.84		150	p, α	XI
15.90		78	p, α	XI
16.05		100	p, α	XI
16.19		38	p, α	XI
(16.20)		(75)	p, α	XI
(16.28)		(110)	p, α	XI
16.37		(100)	p, α	XI
16.54			p, α	XI
16.60		28	p, α	XI
16.61		190	p, α	XI
16.65		130	p, α	XI
16.67		105	p, α	XI
16.80		95	p, α	XI
16.95		45	p, α, n	XI, XII
17.02		95	p, α	XI
17.11		85	p, α, n	XI, XII
17.14		25	p, α, n	XI, XII
17.22		25	p, α, n	XI, XII
17.26		57	p, n	XII

TABLE 20.6 (continued)

E_x (MeV ± keV)	J^π; T	τ_m or Γ (keV)	Decay	Reactions
17.33		60	p, α	XI
17.35		25	p, α, n	XI, XII
17.41		35	p, α, n	XI, XII
17.53		85	p, α	XI
17.61		35	p, α	XI
17.61		19	p, α, n	XI, XII
17.69		30	p, α, n	XI, XII
17.79		210	p, α	XI
17.81		67	p, α	XI
17.86		67	p, n	XI, XII
18.01			p, n	XII
18.34			p, n	XII
18.66			p, n	XII
19.02			p, n	XII

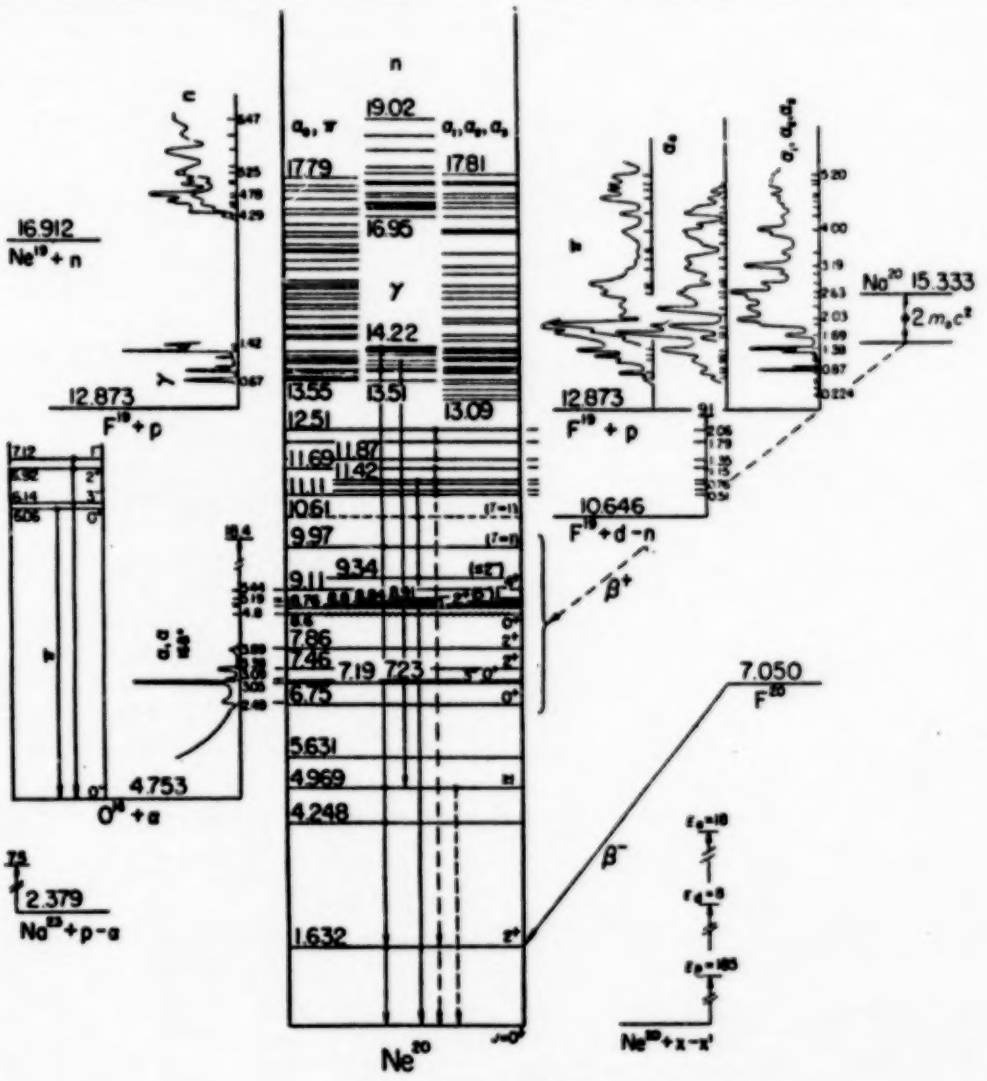

8 January 1959

Fig. 45. Energy levels of Ne^{20}: for notation, see fig. 1, p. 7.

II. $O^{16}(\alpha, \gamma)Ne^{20}$ $Q_m = 4.753$

An unsuccessful attempt has been made to observe the isobaric spin-forbidden transition between the $T = 0$ states at 7.19 MeV ($J = 3^-$) and 1.63 MeV ($J = 2^+$). The radiative width is $< 6\times10^{-3}$ eV, indicating an admixture of $T = 1$ of $< 1.3\times10^{-3}$ in Ne^{20*}(7.19) (To 57). The relevance of alpha capture in O^{16} to element synthesis has been discussed by (Ca 56e, Ha 56g, Ha 56h, Bu 57f, Li 57c, Sa 57c).

III. $O^{16}(\alpha, n)Ne^{19}$ $Q_m = -12.158$ $E_b = 4.753$

See (Te 47).

IV. $O^{16}(\alpha, p)F^{19}$ $Q_m = -8.119$ $E_b = 4.753$

See F^{19}.

V. $O^{16}(\alpha, pn)F^{18}$ $Q_m = -18.533$ $E_b = 4.753$

See (Te 47).

VI. $O^{16}(\alpha, \alpha)O^{16}$ $E_b = 4.753$

The elastic scattering has been studied in the range $E_\alpha = 0.9$ to 4.0 MeV by (Ca 53b) and from $E_\alpha = 3.9$ to 5.5 MeV by (Mc 58a): see table 20.7. See also (Co 57c, Co 58c, Fe 40) and O^{16}.

TABLE 20.7

Resonances in $O^{16}(\alpha, \alpha)O^{16}$

E_α (MeV)	$\Gamma_{(c.m.)}$ (keV)	θ^2 (per cent)	J^π	Ne^{20*} (MeV)	Refs.
2.490	19	22	0^+	6.745	(Ca 53b)
3.045	8	36	3^-	7.189	(Ca 53b)
3.090	4	1.1	0^+	7.225	(Ca 53b)
3.380	8	4.7	2^+	7.457	(Ca 53b)
3.885	2	0.6	2^+	7.861	(Ca 53b)
≈4.8	≈1300	≈70	0^+	≈8.6	(Mc 58a) [a]
5.01	4	0.23	1^-	8.76	(Mc 58a) [a]
≈5.1	≈1200	≈95	2^+	≈8.8	(Mc 58a) [a]
5.11	≦4		(5^-)	8.84	(Mc 58a) [a]
5.19	20	1.0	1^-	8.91	(Mc 58a) [a]
5.44	8	3.9	4^+	9.11	(Mc 58a) [a]
5.6			(1^-)	9.2	(Fe 40)
6.7			(1^-)	10.1	(Fe 40)

[a] Preliminary results.

VII. $O^{17}(\alpha, n)Ne^{20}$ $Q_m = 0.608$

Not observed.

VIII. $O^{18}(He^3, n)Ne^{20}$ $Q_m = 13.117$

Not observed.

IX. $F^{19}(p, \gamma)Ne^{20}$ $Q_m = 12.873$

Resonances for capture radiation are listed in table 20.8 (Si 54, Fa 55). The level formed at $E_p = 0.67$ MeV decays predominantly to the 1.63-MeV

TABLE 20.8

Resonances in $F^{19}(p, \gamma)Ne^{20}$

E_p (keV)	Γ (keV)	Yield [a] (per cent)	Ne^{20*} (MeV)
669 [b,c]	7.5	1.80 ± 0.36	13.511 [f]
874 [c]		0.03 ± 0.01 [e]	13.703 [f]
935 [c]		0.03 ± 0.01	13.761 [f]
980 [c]		0.22 ± 0.04 [d]	13.80
1091 [b,c]	< 1.2	0.34 ± 0.07	13.909 [f]
1280 [c]		0.06 ± 0.01	14.092 [f]
1320 [b,c]	4.0	0.90 ± 0.18 [d]	14.13
1350 [c]		0.12 ± 0.02	14.154 [f]
1370 [c]		0.08 ± 0.02	14.179 [f]
1420 [b,c]	15.7	0.35 ± 0.07 [d]	14.224 [g]

[a] Relative to $F^{19}(p, \alpha\gamma)O^{16}$.
[b] (Si 54; resonances for $E_\gamma = 12$ MeV).
[c] (Fa 55; resonances for $E_\gamma > 8$ MeV).
[d] Resonance not observed for $F^{19}(p, \alpha\gamma)O^{16}$.
[e] $\Gamma_\gamma < 2$ eV (Wi 53g).
[f] Excitation energies from $F^{19}(p, \alpha\gamma)$: table 20.13, p. 238.
[g] Excitation energy from $F^{19}(p, p')$: table 20.10 p. 279.

state: $\Gamma_\gamma = 2.2$ eV (Ca 51a, Cl 55, Jo 52e). The angular distribution of the hard radiation is isotropic within two per cent (Fa 55). The γ—γ angular correlation shows that the transition to the 1.63-MeV state is predominantly M1. The direct ground state transition is < 0.02 eV which implies different nucleon configurations for the ground and first excited states of Ne^{20}(Cl 55). At $E_p = 0.67$ and 1.09 MeV, cascades through the 4.97-MeV state have been observed. The 4.97-MeV level decays with > 95 per cent probability through the 1.63-MeV state. Triple γ-correlations ($C \to 4.97 \to 1.63 \to 0$) show $J \neq 0$ for the 4.97 MeV state. Since a cascade takes place to it from the $J = 1^+$ state at the 0.67-MeV resonance, $J \leqq 3$ (Go 58a). See also (Wi 53g, Wa 57f, Br 58e).

X. (a) $F^{19}(p, p)F^{19}$ $E_b = 12.873$
(b) $F^{19}(p, p')F^{19*}$

The elastic scattering has been studied in the range $E_p = 500$ to 2000 keV by (Pe 54b, De 54d, De 56c, We 55, Ba 55a). Parameters for the observed resonances are exhibited in table 20.9, taken mainly from (Ba 55a); values given by (De 56c) are in good agreement with these. Orbital angular momentum assignments derive from angular distributions; J^π from the anomaly

shape, and Γ_p/Γ from $\sigma(p, p)$, $\sigma(p, p')$ and $\sigma(p, \alpha)$ cross sections. At $E_p = 340$ keV, 480 keV (We 55), and 598 keV (De 56c), the elastic scattering anomaly is too small to be detected: it is concluded that Γ_p/Γ is small for these resonances. Some unresolved structure is observed at $E_p = 900$, 1092 and 1137

TABLE 20.9

Levels of Ne^{20} from $F^{19}(p, p)F^{19}$ (Ba 55a).

E_p (keV)	Γ_{lab} (keV)	l	J^π	Γ_p/Γ	θ_p^2 (per cent)	Ne^{20*} (MeV)
340	2.9	0	1^+ [b]	0.016	3.8	13.196
598	37	1	2^- [b]	0.0012	0.38	13.441
669	7.5	0	1^+	0.98	9.6	13.509
843	23	0	0^+	0.996	10.8	13.674
873	5.2	1	2^- [a]	0.21	1.5	13.702
935	8.0	0	1^+	0.17	0.44	13.761
1346	4.5	1	2^- [a]	0.067	0.07	14.152
1372	15	1	2^- [a]	0.17	0.52	14.176
1422	14.6	0	1^+	0.85	0.92	14.224
1694 [c]						14.482
1940 [c]		(0)	$(0^+, 1^+)$			14.716
2030 [c]						14.802

[a] 1^- not excluded by elastic scattering alone.
[b] not determined by (p, p): see $F^{19}(p, \alpha)O^{16}$.
[c] (De 56c).

keV, in addition to a broad structure near $E_p = 1700$ keV (We 55). It is of interest to note that two of the resonances, at $E_p = 669$ and 843 keV have comparatively large proton reduced widths (Ba 55a). For high-energy scattering, see F^{19}.

Resonances for inelastic scattering involving the 110-keV, $J = \frac{1}{2}^-$ and 197-keV, $J = \frac{5}{2}^+$, states of F^{19} are listed in table 20.10 (Ba 55). Resonance structure in the yield of 109, 197, 1240 and 1360-keV γ-radiation is reported by (Ra 58c) up to $E_p = 4.5$ MeV. In general, the resonances observed are identical with those reported from other F^{19}+p reactions, although the relative intensities differ greatly. The nonresonant yield of the 197-keV radiation appears to be mainly due to Coulomb excitation, while that of the 110-keV radiation suggests contributions from broad, unresolved s-wave resonances (Ba 55, Pe 54b). See also (Pe 54d) and F^{19}.

XI. $F^{19}(p, \alpha)O^{16}$ $\quad Q_m = 8.119$ $\quad E_b = 12.873$

For $E_p \approx 1$ to 3 MeV, five α-particle groups are reported. All show resonance effects with relative intensities varying greatly with bombarding energy. The long-range group (α_0) leaves O^{16} in the ground state ($J = 0^+$); the next longest (α_π) results in the formation of the $J = 0^+$ nuclear pair-emitting state at 6.06 MeV, while the three remaining groups ($\alpha_1, \alpha_2, \alpha_3$) lead

to γ-ray emitting states at 6.14 ($J = 3^-$), 6.91 ($J = 2^+$) and 7.12 MeV ($J = 1^-$). At $E_p > 3$ MeV, excitation of higher O^{16} levels occurs: see O^{16}. Resonances for α_0 and α_π (tables 20.11 and 20.12) are generally identical and different from those for α_1, α_2, α_3 (table 20.13). The resonances for α_0 and α_π

TABLE 20.10

Resonances in $F^{19}(p, p')F^{19*}$ (Ba 55)

E_p (keV)	J^π	Γ_{lab} (keV)	Γ_{p_1} (eV)	Γ_{p_2} (eV)	$\theta_{p_1}^{2a}$ (per cent)	$\theta_{p_2}^{2a}$ (per cent)	E_x in Ne^{20} (MeV)
340	1^+	2.9	<0.5	<0.1	<15		13.196
483		2.2	<1.5	<1.5			13.332
598	2^-	37	<500	<500	<28	<145	13.441
669	1^+	7.5	46	<0.5	0.6	<0.4	13.509
720		≈ 30	<10000	<10000			13.557
780[b]		≈ 10	<400	≈ 9000			13.614
831		8.3	<6	≈ 2300			13.662
845	0^+	23	≈ 50	<10	≈ 0.14	<0.92	13.676
873	2^-	5.2	<2	570	<0.07	2.7	13.702
900		4.8	<30	≈ 2200			13.728
935	1^+	8.0	3000	<20	5.0	<0.8	13.761
1092		<1.2					13.910
1137[c]		3.7	<40	≈ 2100			13.953
≈ 1250		≈ 80	≈ 70000	<4000			14.061
1290		19	<600	≈ 900			14.099
1346	2^-	4.5	300	600	0.92	0.24	14.152
1372	2^-	15	700	1400	1.93	0.56	14.176
1422	1^+	14.6 ± 1	2200	$\leqq 35$	0.56	$\leqq 0.11$	14.224
1610		≈ 5					14.403
1660							14.450
1700							14.488

[a] (Ba 55a)

[b] (Hu 55a) find $E_p = 780.3 \pm 0.8$ keV, $\Gamma = 7.6 \pm 1.0$ keV but assignment to this reaction is uncertain.

[c] (Hu 55a) find 1123 ± 2.0 keV, $\Gamma = 22 \pm 5$ keV, but assignment is uncertain.

are required to have even J, even π or odd J, odd π, while the α_1, α_2, α_3 resonances, insofar as their assignments are known, are all odd-even or even-odd.

Studies of the α_0 yield and angular distributions have been made by (Cl 57, Ra 58c, Is 58, Is 58a, Fr 58, Ta 57b, Br 58j): see table 20.11. Assignments of (Is 58a) and (Cl 57) are based on detailed analysis of angular distributions. It is of interest that the reduced widths of these levels, where known, are generally less than a few per cent of the single-particle limit. There is some disagreement on the assignment of the prominent $E_p = 843$-keV resonance (compare $F^{19}(p, p)F^{19}$). The 1358-keV resonance reported here appears to be distinct from the $E_p = 1372$-keV ($J = 2^-$) resonance seen in $F^{19}(p, p)F^{19}$ and $F^{19}(p, \alpha\gamma)O^{16}$. (Br 58j) find from angular distribution

studies that the 720-keV resonance has $J = 2^+$, and is formed in channel spin 0. Near $E_p = 400$ keV, two resonances are required, with $J^\pi = 1^-$ and

TABLE 20.11

Resonances for ground state α-particles (α_0) in $F^{19}(p, \alpha_0)O^{16}$

E_p (keV)	Γ_{lab} (keV)	σ (mb)	t [f]	θ_{α^2} [a] (per cent)	J^π	Ne^{20*} (MeV)
400 [g]	100	0.04	0		1^-	13.253
400	100	0.005	0		0^+	13.253
650	200	0.2	∞		1^-	13.491
710 [a, g]	35	<0.5		0.6	(1^-)	13.548
733	66	1.4	0.2	1.0	2^+	13.569
778	≈ 10	>0.5	1.6	0.02	2^+	13.612
843	23	3.7	1.38	0.16	2^+ [e]	13.674
≈ 860	120	1.0	10.6	2.1	1^-	13.690
≈ 930	≈ 180	0.5		2.9	0^+	13.757
≈ 1080	≈ 200	3.4	5.1	3.4	1^-	13.899
1115	50	2.4	2.2	0.55	2^+	13.932
1160	≈ 70	5.1		1.1	0^+	13.975
1235 [a, b]	≈ 70	5.2	0.11	1.2	1^-	14.046
≈ 1250 [a]	≈ 150	0.26	0.6	2.7	2^+	14.061
1358 [a, b, c]	54	43 [d]	2.6	0.49	2^+	14.163
1640 [b]	<115					14.431
1709 [b, c]	140	53	0		0^+	14.497
1853 [b, c]	132	76	0.4		1^-	14.633
2110 [b, c]	75	9			(4^+)	14.878
2310 [b, c]	80	29			(2^+)	15.067
(2530) [b]						(15.28)
2590 [b, c]	300	51 ± 10			(0^+)	15.33
2680 [b]	80					15.42
(2820)						(15.55)
2940						15.67
3120	170					15.84
3340	105					16.05
3680	(100)					16.37
3860						16.54
3980	135					16.65
4130	100					16.80
4360	100					17.02
4460	95					17.11
4690	65					17.33
4900	90					17.53
4990	40					17.62

[a] (Is 58, Is 58a): quoted cross sections in these references are resonant cross sections, derived from analysis of angular distributions.

[b] (Ra 58c).

[c] (Cl 57).

[d] See also (Fr 58).

[e] $J = 0^+$ from $F^{19}(p, p)F^{19}$; possibly $T = 1$ (Ba 55, Ba 55a).

[f] $t = \Gamma(J_c = 1)/\Gamma(J_c = 0)$.

[g] (Br 58j).

0^+, both with $\Gamma \approx 100$ keV, $J_c = 0$. A third resonance occurs at $E_p = 650$ keV, with $J = 1^-$, $\Gamma = 200$ keV (Br 58j).

A special study has been made to detect a possible resonance for $F^{19}(p, \alpha_0)O^{16}$ at the $E_p = 340$-keV, $J = 1^+$, resonance. An upper limit of 2 per cent

TABLE 20.12

Nuclear pair resonances (α_π) in $F^{19}(p, \alpha_\pi)O^{16}$

E_p (keV)	Γ (keV)	σ[c] (mb)	θ_α^2[c] (per cent)	J^π	Ne^{20*} (MeV)
710[a]	35	$\approx$ 0.2	2	1^-	13.548
780	$\approx$10	$\approx$ 0.2	0.15	2^+	13.614
842	23	3.4	0.27	2^+	13.673
1115	50	1.5	3.6	2^+	13.932
1236[a,b]	$\approx$70	3	1.0	1^-	14.047
1367[a,b]	30	6.0	0.29	2^+	14.172
1630[b]	60				14.42
1720	95	$\approx$18			14.51
1880	170				14.66
2170	95				14.94
2330	$\approx$100				15.09
2600	100				15.34
2680	100				15.42
2820	125				15.55
3120	145				15.84
3340	100				16.05
(3500)	(80)				(16.20)
(3590)	(115)				(16.28)
3960	200				16.64
4360	95				17.02
4690	$<$150				17.33
4900	115				17.53
4990	40				17.61
5170	220				17.79

[a] (Ch 50, Ph 51a, De 54a, Is 58a).

[b] (Ra 58c).

[c] (Is 58a): resonant cross sections derived from analysis; see also (Ch 50).

resonant/nonresonant yield is found, indicating a maximum admixture of 2×10^{-4} of odd-parity component in the wave functions involved (Ta 57b: see also Wi 58c).

Resonances in the $F^{19}(p, \alpha_\pi)O^{16}$ yield have been investigated by (Ch 50, Ph 51a, De 54a, Is 55, Is 56, Is 58a, Ra 58c): see table 20.12. Resonance locations and absolute reduced widths appear to correspond closely to those for (p, α_0), although some exceptions occur. In the work of (Ra 58c) only 6 of 23 (p, α_0) resonances have no clear counterpart in $\sigma(p, \alpha_\pi)$. For resonances at $E_p = 1.35$, 1.72, 1.88 and 2.33 MeV, $\theta^2_{\alpha_0} = \theta^2_{\alpha_\pi}$ within about 10 per cent; at $E_p = 2.17$ MeV, a large difference occurs, possibly to be ascribed to super-

TABLE 20.13

Resonances for 6-7 MeV γ-rays ($\alpha_1, \alpha_2, \alpha_3$) in $F^{19}(p, \alpha)O^{16}$

E_p (keV)	Γ (keV)	σ[g] (mb)	Γ_{α_1}[j] (eV)	Γ_{α_2}[j] (eV)	Γ_{α_3}[j] (eV)	J^π	Ne^{20*} (MeV)
224.4[d]	1.0	>0.2					13.086
340.5±0.3[a]	3.3± 0.2	160	2800	16	75	1+[h]	13.196
483.6[d]	0.9± 0.1	>32	≈1700	≈30	≈450		13.332
596.8±1.0[b]	30.0± 3	7.1	37000	<100	<100	(2−)[i]	13.440
671.6±0.7[b]	6.0± 0.7	57	110	0.4	25	1+	13.511
834.8±0.9[b]	6.5± 1.0	19	total ≈ 5400				13.667
874.0±1.0[c]	5.0± 0.3	540	2400	850	300	2−	13.703
902.3±0.9[b]	5.1± 1.0	23	≈2500	<130			13.730
935.1±0.9[b]	8.6± 0.5	180	2800	100	780	1+	13.761
1090 ±1.0[b]	0.7± 0.3	>13					13.909
(1123 ±2.0)[b]	22 ± 5						(13.94)
1140 ±1.0[b]	2.5± 5	15	total ≈ 1600				13.956
1189 ±7.0[b]	110 ±20	19					14.003
1283 ±1.4[b]	18.6± 1.0	29	≈13000	≈1300	≈3200	(3+)	14.092
1348 ±1.3[b,e]	5.6±0.5	89	1800	450	1050	2−	14.154
1375 ±1.4[b,e]	11.0± 1.0	300	9100	840	520	2−	14.179
(1607 ±1.6)[b]	6.0± 1.0						14.380
1694 ±1.7[b,f]	35.0± 3.0						14.482
1949 ±2.5[b,f]	40 ±10						14.725
2030 ±3.0[b,f]	120 ±20						14.802
2320[f]	85						15.08
2510	30						15.26
2630	90						15.37
2800	60						15.53
3020	30						15.74
3190	80						15.90
3490	40						16.19
3920	30						16.60
4000	110						16.67
4290	50						16.95
4490	30						17.14
4570	30						17.22
4710	30						17.35
4780	35						17.41
4990	20						17.61
5070	35						17.69
5200	70						17.81

[a] (Bu 55f, Bu 56e): See also (Hu 52f, Mo 49a). (Bo 58e find $\Gamma = 2.4 \pm 0.3$ keV).
[b] (Hu 55a; assignment to this reaction probable but not certain).
[c] Observed values are 872.5±1.8 (Fa 53), 871.3±0.4 (Bu 55f, Bu 56a), 873.5±0.8 (He 49), 872.4±0.4 keV (Bo 58e), 874.5±0.9 keV (Hu 55a).
[d] (Bo 58e, Hu 52f, Hu 53d).
[e] (Ki 55c).
[f] (Wi 52a); these values should be reduced by about 0.2 per cent: see (Ki 55c).
[g] (Ch 50): see also (Bo 48c).
[h] (Ch 50a, Ar 50, Ba 50f).
[i] (Ch 50a, Wi 53g).
[j] (Ba 55).

position of several resonances (Ra 58c). Below $E_p = 1.3$ MeV, several fairly large differences occur (Is 58a).

Resonances in the yield of 6—7 MeV γ-rays have been studied by (Ch 50, Ch 50a, Ar 50, Ba 50f, Wi 52a, Wi 53g, Hu 52f, Hu 53d, He 49, Ki 55c, Hu 55a, Fa 53, Bu 55f, Bu 56e, Bo 48c): see table 20.13.

At $E_p = 224$ keV, the angular distribution of 6-MeV radiation is anisotropic (Ne 54d). The 6—7 MeV radiation produced at the $E_p = 340$, 483, 669 and 935-keV resonances is isotropic or nearly so (De 49d, Da 51b, Sa 52, Sa 53c, Go 57h, Ga 57a). (Re 58b) finds a 3.5 per cent anistropy at $E_p = 340$ keV, indicating a 1 per cent admixture of d-waves: $\theta_d^2 \approx \theta_s^2$. At $E_p = 340$, 669 and 935 keV, the α_1—γ correlations establish that $J = 1^+$ for the corresponding Ne^{20} levels (Ar 50, Ba 50f, Se 52b, Ma 57g): this assignment is confirmed for the 935-keV resonance by the α_1 angular distribution (Pe 54d). Correlations and angular distributions at the $E_p = 874$ keV resonance establish $J = 2^-$ for this level (Se 52b, Pe 54d, Ma 57g), and the observed polarization of the γ rays is consistent with this assignment (Fa 53a). The level corresponding to $E_p = 598$ keV is assigned $J = 2^-$ by (Ch 50a) on the basis of γ-ray angular distributions: $W(\theta) = 1+0.17 \cos^2 \theta$ (Re 58b): (see also Wi 53g). Levels corresponding to resonances at $E_p = 1283$ and 1348 keV are assigned $J = 3^+$ by (Ch 50a). Angular distributions of the α groups at $E_p = 1283$ keV are not inconsistent with $J = 3^+$, but lead to $J = 2^-$ for the 1348-keV resonance (Pe 54d). Gamma-ray angular distributions at $E_p = 1375$ keV indicate a pronounced anisotropy and are consistent with $J = 2^-$ (Sa 53c: see also F^{19}(p, p)F^{19}). This is evidently not the same as the 1.36-MeV α_0 resonance. (α_1—γ_1) angular correlations have been studied by (Ma 57g) at $E_p = 873$, 935, 1250, 1280, 1346 and 1372 keV. For the $J = 2^-$ resonances at $E_p = 873$, 1346 and 1372 keV, the p-wave and f-wave proton reduced widths are comparable in magnitude: for the first and last, g-wave α_1-emission has a surprisingly large probability.

An analysis of certain Ne^{20} levels into partial widths, based on information from F^{19}(p, p), (p, p'), (p, γ) and (p, α) is given by (Ba 55, Ba 55a, Is 58a): see table 20.14. It is noted that a number of $T = 1$ levels may be expected in this region (compare F^{20}).

XII. F^{19}(p, n)Ne^{19} $\quad Q_m = -4.039$ $\quad E_b = 12.873$

Observed resonances are listed in table 20.15 (Wi 52a, Ma 55k, Bl 51a). See also (Ta 58a, Gi 59).

XIII. F^{19}(d, n)Ne^{20} $\quad Q_m = 10.646$

Levels of Ne^{20} derived from reported neutron groups are listed in table 20.16: see also (Ba 56m, To 56a). The earlier reported 2.2-MeV state appears to be spurious. The g.s. and 1.6-MeV groups show a clear stripping pattern,

with $l_p = 0$ and 2 respectively. No clear evidence is found for the 4.2 and 5.4-MeV levels at $E_d = 9$ MeV (Ca 55c). Levels at $E_x = 9.7$ MeV (Fr 50d) (9.97?), and $E_x = 11.85$ MeV (Wa 52b) decay by α-particle emission.

TABLE 20.14

Resonance parameters in $F^{19}+p$ [c] (Ba 55a)

E_r (keV)	J^π	θ^2 [a] (per cent)					
		p_0	p_1	p_2	α_1	α_2	α_3
340	1^+	3.8	<15		18.8	1.0	7.2
598	2^-	0.38	<28	<145	31	<0.5	<5.1
669	1^+	9.6	0.6	<0.4	0.26	0.005	0.27
843	0^+	10.8	≈0.14	<0.92			
873	2^-	1.5	<0.07	2.7	1.05 [b]	1.45 [b]	3.4
935	1^+	0.44	5.0	<0.8	3.3	0.34	2.3
1260	3^+						
1346	2^-	0.07 [b]	0.92	0.24	0.36	0.21 [b]	2.1
1372	2^-	0.52 [b]	1.93	0.56	1.7 [b]	0.34 [b]	0.86
1422	1^+	0.92	0.56	<0.11	Total <0.034		

[a] p_0, p_1, p_2 represent transitions to F^{19}(0), (0.1), (0.2). α_1, α_2, α_3 represent transitions to O^{16}(6.1), (6.9), (7.1).

[b] Assuming lowest possible values of l: see (Ma 57g).

[c] See also (Is 58a).

TABLE 20.15

Resonances in F^{19}(p, n)Ne^{19}

E_p (MeV)	Γ (keV)	Ne^{20*} (MeV)
4.29 [a]	45	16.95
4.46 [a]	80	17.11
4.49 [a]	20	17.14
4.57 [a]	20	17.21
4.62 [a]	60	17.26
4.71 [a]	25	17.35
4.78 [a]	45	17.41
4.99 [a]	20	17.61
5.07 [a]	30	17.69
5.25 [a,b]	70	17.86
5.41 [b,c]		18.01
5.75 [b,c]		18.34
6.09 [c]		18.66
6.47 [c]		19.02

[a] (Wi 52a); these values should be decreased by about 0.2 per cent: see (Ki 55c).

[b] (Ma 55k).

[c] (Bl 51a): broad resonances, stacked-foil method.

Thresholds for production of γ radiation with $E_\gamma \approx 10$—12 MeV, are listed in table 20.17 (Bu 55, Bu 58b). Observed γ-ray energies are exhibited in

TABLE 20.16.
Neutron groups from $F^{19}(d, n)Ne^{20}$

E_x [a] (MeV)	E_x [b] (MeV)	l_p	J^π	$\frac{A}{2J+1}$ [d]
0	0	0	$0^+, 1^+$	0.07
1.5	1.6	2	$1^+, 2^+, 3^+$	0.44
4.2				
5.4				
7.3	7.3 [c]	(0)	$(0^+, 1^+)$	0.039
		(2)	$(1^+, 2^+, 3^+)$	1.0
9.0	9.2	1	$0^-, 1^-, 2^-$	0.054
10.1				

[a] (Bo 40b).
[b] (Ca 55c; $E_d = 9$ MeV).
[c] Unresolved levels; the angular distribution shows a composite of $l_p = 0$ and 2.
[d] Proton capture probability, in c.g.s. units, $\times 10^{28}$.

TABLE 20.17
Levels of Ne^{20} from $F^{19}(d, n)Ne^{20}$ thresholds (Bu 55, ABu 58b)

E_{thresh} (keV)	Ne^{20} (MeV)
510	11.11
600	11.19
760	11.33
850	11.42
1150	11.69
1350	11.87
1790	12.27
2060	12.51

TABLE 20.18
Gamma radiation from $F^{19}(d, n)Ne^{20}$

E_γ (MeV)			Assignment
A	B	C	C
6.7 ± 0.3			
	7.2		
8.1 ± 0.4	8.4		9.97→1.6
9.3 ± 0.3	9.4	9.34 ± 0.1	9.34→g.s.
	10.1	9.97 ± 0.1	9.97→g.s.
	10.6	10.61 ± 0.1	10.61→g.s. or 12.2 →1.6
11.5 ± 0.4		11.51 ± 0.2	11.4 →g.s. or 11.7 →g.s.

A. (Te 51a); $E_d = 1.56$ MeV.
B. (Kr 57a).
C. (Be 55g); $E_d = 3.6$ MeV. Corrected for Doppler shift.

table 20.18 (Te 51a, Kr 57a, Be 55g) †. It is noted that levels yielding appreciable γ-radiation must be presumed not to decay by α-emission. The 9.97 and 10.61-MeV levels may be the $T = 1$ levels corresponding to F^{20} (g.s.) and (0.65). The 10.6-MeV level has not been reported in any other reaction.

XIV. $F^{19}(He^3, d)Ne^{20}$ $Q_m = 7.379$

Not reported.

XV. $F^{19}(\alpha, t)Ne^{20}$ $Q_m = -6.940$

Not reported.

XVI. $F^{20}(\beta^-)Ne^{20}$ $Q_m = 7.050$

The decay is to the 1.6-MeV state of Ne^{20}: $E_\beta(\max) = 5.413 \pm 0.013$ MeV. The energy of the subsequent γ-ray is 1.629 ± 0.005 MeV (Wo 54b, Al 52a). The relative intensity of the ground-state transition is $< 3.2 \times 10^{-4}$ (Wo 54b). The Fermi plot is straight from the end point to $E_\beta = 1$ MeV. With a half-life of 11.4 sec, log ft (1.63 MeV state) = 4.99, log ft (ground state) $\gtrsim 9$ (Wo 54b). A search for γ—γ coincidences from the cascade decay of the 4.97-MeV state was unsuccessful: log $ft > 6.5$ (Ka 58). The (β—γ) angular correlation has the form $W(\theta) = 1 + a \cos^2 \theta$, where $a = (0.94 \pm 0.28) \times 10^{-2}$. The anisotropy is attributed to a "weak magnetic" interaction associated with the anomalous nucleon moments. The sign of a indicates $J = 2^+$ for F^{20}(Bo 58b, Ge 58b).

XVII. $Ne^{20}(\gamma, n)Ne^{19}$ $Q_m = -16.912$

A giant resonance is observed at $E_\gamma = 21.5$ MeV with $\Gamma = 6.6$ MeV and $\sigma(\max) = 7.3$ mb (Fe 54). See also (Ba 57; theo.).

XVIII. $Ne^{20}(\gamma, p)F^{19}$ $Q_m = -12.873$

See (At 56, Wa 57a, Ko 57).

XIX. $Ne^{20}(\gamma, \alpha)O^{16}$ $Q_m = -4.753$

See (At 56, Wa 57a, Ko 57, Er 53a).

XX. $Ne^{20}(p, p')Ne^{20*}$

Ne^{20} levels derived from observations of proton groups are listed in table 20.19 (Fr 54g, Sc 56). A 2.6-MeV γ-ray has been observed in coincidence with the p_2 group (4.2-MeV state) at $E_p = 5.85$ MeV (Kr 57a). At $E_p = 185$ MeV, inelastic peaks corresponding to levels near 5 and 20 MeV are observed (Ty 58c).

Elastic scattering angular distributions have been studied in the range $E_p = 1.8$ to 4.3 MeV by (Ha 55d), for $E_p = 4.7$ to 5.5 MeV by (Ko 58d), at 9.5 MeV by (Fr 54g, Bu 56j, Gi 57). Angular distributions of inelastic

† *Note added in proof:* Recent studies of the γ-spectra at $E_d = 3.6$ MeV confirm the work of (Be 55g) and are not consistent with the fine structure reported in table 20.17 (T. W. Bonner, private communication).

groups are reported by (Ko 58d, Fr 54g, Gi 57, Sc 56). See also (Bu 57a; theo.)

XXI. $Ne^{20}(d, d')Ne^{20*}$

At $E_d = 7.8$ MeV, an inelastic deuteron group is observed corresponding to a state at 1.66 ± 0.02 MeV (Mi 51d). The angular distribution, analyzed by

TABLE 20.19

Levels of Ne^{20} from $Ne^{20}(p, p')Ne^{20*}$, $Ne^{20}(\alpha, \alpha')Ne^{20*}$ and $Na^{23}(p, \alpha)Ne^{20}$

E_x [a] (MeV ± keV)	E_x [b] (MeV)	E_x [c] (MeV)	E_x [d] (MeV ± keV)
0	0	0	0
1.58 ± 10	1.63	1.63	1.635 ± 6 [e]
4.20 ± 10	4.26	4.25	4.248 ± 6
4.95 ± 20	4.97	4.97	4.969 ± 6
5.62 ± 20	5.81	5.81	5.631 ± 6
		7.2	
	7.45		
	7.85		
	9.2		
	10.0		

[a] $Ne^{20}(p, p')$: (Fr 54g), $E_p = 9.5$ MeV.
[b] $Ne^{20}(p, p')$: (Sc 56), $E_p = 18$ MeV; energies for identification only.
[c] $Ne^{20}(\alpha, \alpha')$: (Se 58a), $E_\alpha = 18$ MeV; energies for identification only.
[d] $Na^{23}(p, \alpha)$: (Bu 57c), $E_p = 7.0$ to 7.5 MeV.
[e] 1.634 ± 4 (Do 53).

the direct interaction theory (of Hu 52l), indicates $l = 2$, $J = 1, 2, 3^+$; the observed distributions can also be ascribed to electric excitation, but the required moments are about two orders of magnitude too large (Va 58). See also (Mi 52c).

XXII. $Ne^{20}(\alpha, \alpha')Ne^{20*}$

At $E_\alpha = 18.0$ MeV, inelastic groups are observed to Ne^{20} states at 1.63, 4.25, 4.97, 5.81 and 7.2 MeV: see table 20.19. Angular distributions for α_0(g.s.) and α_1 show sharp diffractions maxima characteristic of direct interaction (Se 58a). See also (Mo 57a; theo.) and (En 57a).

XXIII. $Ne^{22}(p, t)Ne^{20}$ $\quad Q_m = -8.638$

Not reported.

XXIV. $Na^{20}(\beta^+)Ne^{20}$ $\quad Q_m = 15.333$

The decay proceeds to excited states of Ne^{20} between 6.8 and 10.8 MeV which decay by α-particle emission (Al 50g). The half-life is 0.23 ± 0.08 sec (Sh 51c), 0.385 ± 0.01 sec (Ho 53a). See also (En 57a).

XXV. $Na^{23}(p, \alpha)Ne^{20}$ $Q_m = 2.379$

$Q_0 = 2.370 \pm 0.008$ (Bu 57c)

$Q_0 = 2.379 \pm 0.003$ (Do 53)

$Q_0 = 2.372 \pm 0.008$ (Va 52)

At $E_p = 7.04$ to 7.45 MeV, five α-groups are observed, corresponding to the ground state and to levels at 1.635, 4.248, 4.969 and 5.631 MeV (Bu 57c, Do 53): see table 20.19. The first excited state decays with a mean life of $(7.6 \pm 3.3) \times 10^{-13}$ sec (De 56a), emitting a γ-ray with $E_\gamma = 1.63 \pm 0.02$ (St 54e), 1.629 ± 0.008 MeV (Ne 54e, Ne 55a). Over 90 per cent of the decays of the 4.25 and 4.97-MeV states are by cascades through the 1.63-MeV state (Kr 57a; see also Kr 58a). At a resonance located at $E_p = 1.255$ MeV, the α—γ correlation permits the unique assignment of $J = 1^+$ to the Mg^{24} state and $J = 2^+$ to the 1.63-MeV state of Ne^{20} (Se 53b). See also (Ru 55a, St 54j, Sq 56, En 57a).

F^{21}

(Fig. 46, p. 289)

THEORY

See (Ra 57).

MASS OF F^{21}

From the Q-value of the $F^{19}(t, p)F^{21}$ reaction ($Q_0 = 6.200 \pm 0.025$ MeV: Ja 56e), and taking the Wapstra values (Wa 55c) for the masses of F^{19}, H^3 and H^1, one obtains for the mass excess of F^{21}: 6.193 ± 0.030 MeV.

TABLE 21.1

Energy levels of F^{21}

E_x (MeV)	J^π	Γ or τ	Decay	Reactions
0			(β^-)	I, II
0.27 ± 0.04				II
1.09 ± 0.04				II
1.69 ± 0.04				II
2.04 ± 0.04				II
(3.34 ± 0.1)				II
(4.01 ± 0.1)				II

I. $F^{21}(\beta^-)Ne^{21}$ $Q_m = 5.728$

It is not clear whether the decay of F^{21} has been observed: see (Ca 53g).

II. $F^{19}(t, p)F^{21}$ $Q_m = 6.200$

$(M-A) = 6.37 \pm 0.1$ (Bi 55).

$Q_0 = 6.200 \pm 0.025$ (Ja 56e).

Proton groups observed in this reaction are displayed in table 21.2 (Bi 55, Ja 56e, Ja 55c). An upper limit for groups corresponding to levels

other than those found by (Ja 56e) for $E_x < 2.14$ MeV, $\theta = 90°$, is 1 μb/ster except for $E_x = 1.80$ to 1.87 MeV which was obscured. The β-decay

TABLE 21.2

Levels of F^{21} from $F^{19}(t, p)F^{21}$

E_x [a] (MeV ± keV)	E_x [b] (MeV ± keV)
0	0
0.269 ± 40	
1.087 ± 40	0.89 ± 80
1.694 ± 40	
2.036 ± 40	
	(3.34 ± 100)
	(4.01 ± 100)

[a] (Ja 56e): $E_t = 1.80$ MeV.
[b] (Bi 55): $E_t = 0.90$ MeV.

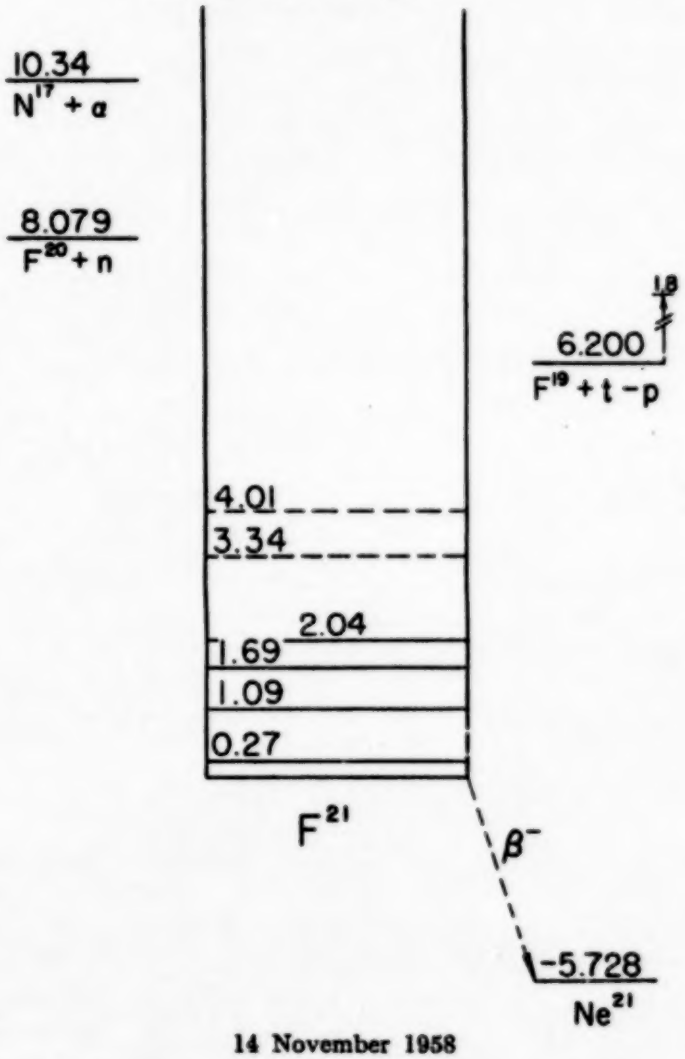

14 November 1958

Fig. 46. Energy levels of F^{21}: for notation, see fig. 1, p. 7.

energy should be about 5.73 MeV, and the first $T = \frac{3}{2}$ state of Ne^{21} should be near 9.25 MeV (Ja 56e).

Reactions not reported are: $O^{18}(\alpha, p)F^{21}$ ($Q_m = -5.649$), $Ne^{21}(n, p)F^{21}$ ($Q_m = -4.945$), $Ne^{21}(t, He^3)F^{21}$ ($Q_m = -5.710$), $Ne^{22}(n, d)F^{21}$ ($Q_m = -13.084$), $Ne^{22}(d, He^3)F^{21}$ ($Q_m = -9.817$), $Ne^{22}(t, \alpha)F^{21}$ ($Q_m = 4.502$) and $Na^{23}(n, He^3)F^{21}$ ($Q_m = -16.387$).

Ne^{21}

(Fig. 47, p. 291)

THEORY

See (Ra 57).

The spin of Ne^{21} is $\frac{3}{2}$ (Hu 56a). The first $T = \frac{3}{2}$ state should be near $E_x = 9.25$ MeV (Ja 56e).

TABLE 21.3

Energy levels of Ne^{21}

E_x (MeV ± keV)	J^π	Γ (keV)	Decay	Reactions
0	$\frac{3}{2}^+$		Stable	I, XI, (XV), XVI, XXI
0.350 ± 5	$\frac{1}{2}^+$, $\frac{5}{2}^+$		γ	I, XI, XXI
1.735 ± 16			γ	XI, XXI
2.79 ± 20	$\frac{1}{2}^+$		γ	XI, XXI
(3.73 ± 60)				XI
4.64 ± 50	$\frac{3}{2}^+$, $\frac{5}{2}^+$			XI
4.81 ± 50	$\frac{1}{2}^-$, $\frac{3}{2}^-$			XI
5.43 ± 60	$\frac{3}{2}^+$, $\frac{5}{2}^+$			XI
5.63 ± 60	$\frac{3}{2}^+$, $\frac{5}{2}^+$			XI
5.78 ± 60	$\frac{1}{2}^-$, $\frac{3}{2}^-$			XI
5.89 ± 80				XI
6.10 ± 80				XI
6.72 ± 60	$\frac{3}{2}^+$, $\frac{5}{2}^+$			XI
(7.23)	$(\frac{1}{2}^+)$			(IX)
7.30 ± 60				(IX), XI
7.62 ± 15	$\frac{3}{2}^-$	13	n	IX
7.97	$\frac{3}{2}^-$	6	n	IX
8.00 ± 15	$\frac{1}{2}^-$	30	n	IX
8.06 ± 15	$\frac{3}{2}^+$	8	n	IX
8.30 ± 15	$\frac{3}{2}^-$	28	n	IX, XI
8.36 ± 15	$\frac{3}{2}^+$	10	n	IX
(8.52)			(n)	IX
8.60	$\frac{3}{2}^+$	19 ± 10	n	IX
8.66	$\frac{3}{2}^-$	48 ± 10	n	IX
8.78	$(\frac{3}{2}^+ + \frac{3}{2}^-)$		n, α	IX, X, XI
9.09			n, α	IX, X, XI
9.23			n, α	IX, X, XI
9.36			n, α	IX, X, XI
9.50			n, α	IX, X, XI
9.88			n, α	IX, X, XI
9.97			n	IX, XI

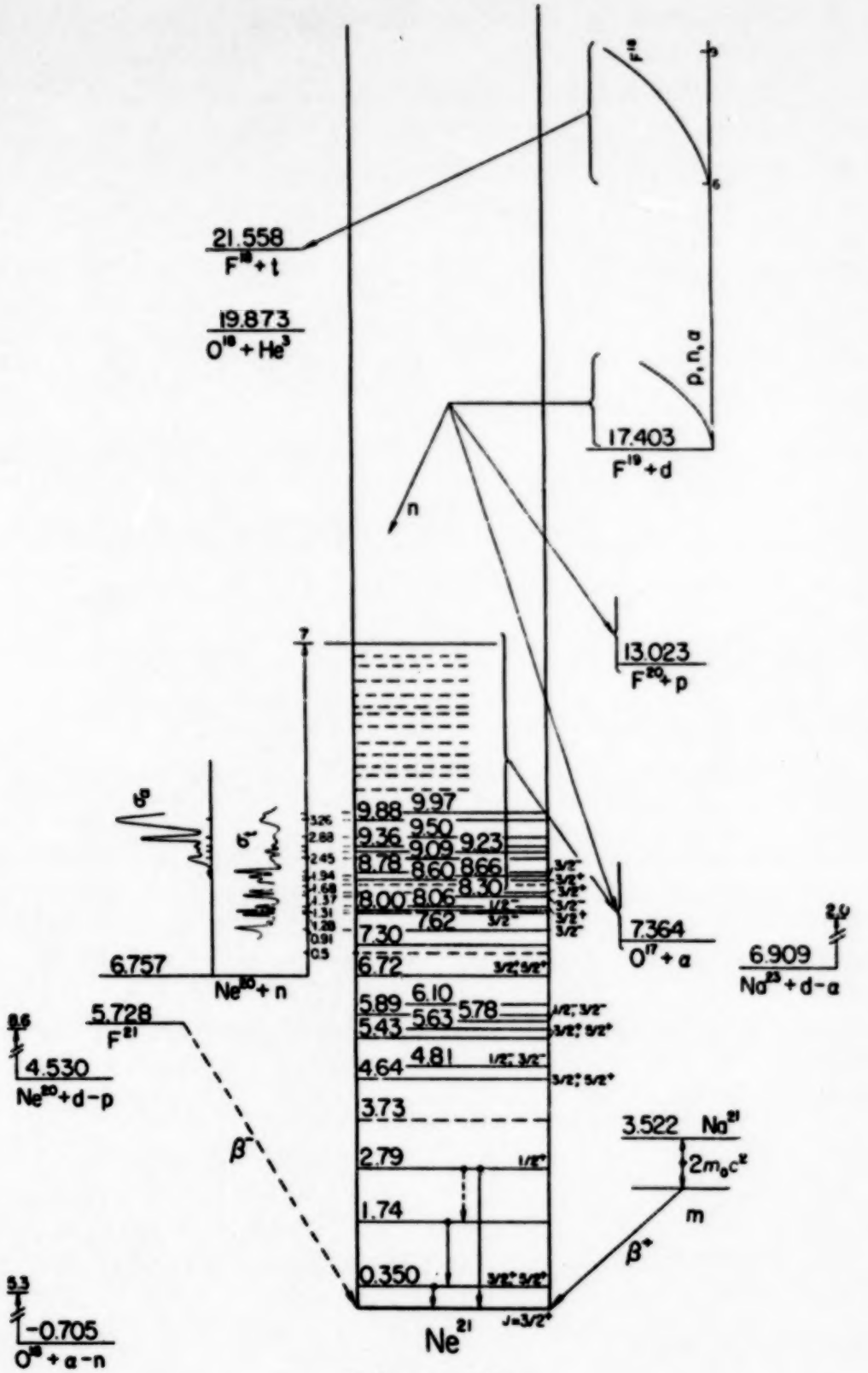

9 January 1959

Fig. 47. Energy levels of Ne^{21}: for notation, see fig. 1, p. 7.

I. $O^{18}(\alpha, n)Ne^{21}$ $Q_m = -0.705$

At $E_\alpha = 5.3$ MeV, a (360 ± 10) keV γ-ray is observed; this occurs in 70 per cent of the transitions, with the direct ground state reaction taking place in ≈ 30 per cent (Se 57c). See also (Ro 55a, We 54b) and Ne^{22}.

II. $F^{19}(d, n)Ne^{20}$ $Q_m = 10.646$ $E_b = 17.403$

See (Bu 52c) and Ne^{20}.

III. $F^{19}(d, p)F^{20}$ $Q_m = 4.379$ $E_b = 17.403$

See (Sn 50a) and F^{20}.

IV. $F^{19}(d, t)F^{18}$ $Q_m = -4.155$ $E_b = 17.403$

See (Kr 41) and F^{18}.

V. $F^{19}(d, \alpha)O^{17}$ $Q_m = 10.038$ $E_b = 17.403$

See (Bu 38) and O^{17}.

VI. $F^{19}(t, n)Ne^{21}$ $Q_m = 11.145$

Not reported.

VII. $F^{19}(He^3, p)Ne^{21}$ $Q_m = 11.910$

Not reported.

VIII. $F^{19}(\alpha, d)Ne^{21}$ $Q_m = -6.441$

Not reported.

IX. $Ne^{20}(n, n)Ne^{20}$ $E_b = 6.757$

The total cross section for thermal neutrons is 2.79 ± 0.14 b (Ca 41); the scattering cross section is 2.4 ± 0.2 b (Ha 50f). See also (Hu 58).

Observed resonances are displayed in table 21.4 (Co 55g, Co 58, Co 59, Si 57, Hu 58). Angular distributions have been studied by (Fo 57d, Co 56a, Co 59: $E_n = 0.8$ to 1.8 MeV) and (Si 57: $E_n = 1.9$ to 2.5 MeV). Above $E_n = 2.0$ MeV, the resonances show strong overlapping and the observed peaks may not correspond to level locations (Si 57). See also (Fo 56c, Hu 56, Va 58a).

X. $Ne^{20}(n, \alpha)O^{17}$ $Q_m = -0.608$ $E_b = 6.757$

An excitation function from $E_n = 1.8$ to 3.3 MeV indicates resonances at $E_n = 2.12$, 2.45, 2.62, 2.72, 2.87 and 3.26 MeV (Jo 51e): see table 21.4. Numerous additional resonances, extending to $E_n = 7$ MeV, are reported by (Gi 54b) and (Fl 53). See also (Si 50).

XI. $Ne^{20}(d, p)Ne^{21}$ $Q_m = 4.530$

Levels derived from observed proton groups are displayed in table 21.5 (Ah 54, Ah 55, Mi 51d, Bu 56d). The absence of stripping to the ground state

is consistent with the assignment $J = \frac{3}{2}^+$ (Bu 56d). At $E_d = 1.13$ MeV, γ-rays are observed with $E_\gamma = 0.35$, 1.05, 1.42 and 2.78 MeV (± 0.03 MeV) (Go 56c, Mu 57b). See also (Go 55d, Go 55g), (Fr 55d, Ra 56b; theo.) and (En 57a).

TABLE 21.4

Resonances in $Ne^{20}(n, n)Ne^{20}$ and $Ne^{20}(n, \alpha)O^{17}$

E_n [a] (MeV $\pm$ keV)	J^π	Γ (keV)	θ_n^2 (%)	E_n [b] (MeV)	E_x in Ne^{21} (MeV)
0.91 $\pm$10	$\frac{3}{2}^-$	14 $\pm$ 4	0.6		7.62
1.28	$\frac{3}{2}^-$	6 $\pm$ 2	0.2		7.98
1.310 $\pm$10	$\frac{1}{2}^-$	32 $\pm$ 6	1.1		8.00
1.370 $\pm$10	$(\frac{3}{2})^+$	(9) $\pm$3	1.0		8.06
1.620 $\pm$10	$\frac{3}{2}^-$	27 $\pm$ 5	0.8		8.30
1.680 $\pm$10	$\frac{1}{2}^+$	10 $\pm$ 3	0.8		8.36
(1.85)					(8.52)
1.94	$\frac{1}{2}^+$	20 $\pm$10	1.3		8.60
2.00	$\frac{3}{2}^-$	50 $\pm$10	1.3		8.66
2.11	$(\frac{1}{2}^+ + \frac{3}{2}^-)$			2.12	8.78
(2.45)				2.45	9.09
2.57				2.62	9.23
2.73				2.72	9.36
2.88				2.87	9.50
3.28				3.26	9.88
3.37					9.97

[a] $Ne^{20}(n, n)$. The first seven entries are from (Co 55g, Co 58, Co 59, Hu 58); the remainder are from (Si 57). An additional resonance at $E_n = 0.5$ MeV, $J = \frac{1}{2}^+$, is reported by (Va 58a).

[b] $Ne^{20}(n, \alpha)O^{17}$ (Jo 51e).

XII. $Ne^{20}(t, d)Ne^{21}$ $Q_m = 0.498$

Not reported.

XIII. $Ne^{20}(\alpha, He^3)Ne^{21}$ $Q_m = -13.821$

Not reported.

XIV. $Ne^{22}(p, d)Ne^{21}$ $Q_m = -8.139$

Not reported.

XV. $F^{21}(\beta^-)Ne^{21}$ $Q_m = 5.728$

See F^{21}.

XVI. $Na^{21}(\beta^+)Ne^{21}$ $Q_m = 3.522$

The positon end point is 2.50 ± 0.03 MeV; no γ-radiation with $E_\gamma > 0.51$ MeV is observed (Sc 52a). The half-life is 23.0 ± 0.2 sec (Ar 58), 22.8 ± 0.5 sec (Sc 52a), 22.9 ± 0.4 sec (Ph 53a). Based on the value of (Sc 52a), $\log ft = 3.56$. See also (Ma 57) and (En 57a).

TABLE 21.5

Levels of Ne^{21} from $Ne^{20}(d, p)Ne^{21}$

E_x (MeV) (Ah 54, Ah 55) [a]	E_x (MeV) (Mi 51d) [b]	E_x (MeV)	l_n [d]	J^π	A
		(Bu 56d) [c]			
0	0	0	(iso.)		
0.349±0.006	0.33±0.05	0.35±0.10	2	$\frac{1}{2}^+$, $\frac{3}{2}^+$	128
	1.68±0.07	1.73±0.1			
2.788±0.012 [e]	2.79±0.05	2.78±0.05	0	$\frac{1}{2}^+$	68
	3.73±0.06				
	4.71±0.05	4.58±0.05	2	$\frac{3}{2}^+$, $\frac{5}{2}^+$	50
		4.81±0.05	1	$\frac{1}{2}^-$, $\frac{3}{2}^-$	98
	5.44±0.05	5.43±0.06	2	$\frac{3}{2}^+$, $\frac{5}{2}^+$	53
		5.63±0.06	2	$\frac{3}{2}^+$, $\frac{5}{2}^+$	49
	5.74±0.05	5.78±0.06	1	$\frac{1}{2}^-$, $\frac{3}{2}^-$	21
		5.89±0.08			
		6.10±0.08			
	(6.66±0.09)	6.72±0.06	2	$\frac{3}{2}^+$, $\frac{5}{2}^+$	46
	7.30±0.06				
	8.28±0.06				
	8.91±0.06				

[a] E_d = 0.86 MeV.
[b] E_d = 7.8 MeV.
[c] E_d = 8.6 MeV; A = relative capture probability.
[d] See also (Mi 52c).
[e] Q = 1738±8 keV.

XVII. $Ne^{22}(d, t)Ne^{21}$ $Q_m = -4.107$

Not reported.

XVIII. $Ne^{22}(He^3, \alpha)Ne^{21}$ $Q_m = 10.212$

Not reported.

XIX. $Na^{23}(n, t)Ne^{21}$ $Q_m = -10.677$

Not reported.

XX. $Na^{23}(p, He^3)Ne^{21}$ $Q_m = 11.442$

Not reported.

XXI. $Na^{23}(d, \alpha)Ne^{21}$ $Q_m = 6.909$

Alpha particles are observed corresponding to levels of Ne^{21} at 0.343 ±0.010, 1.735±0.016 and 2.852±0.021 MeV (Sp 51a); see also (Fr 51d).

Ne^{22}

(Fig. 48, p. 297)

THEORY

See (Ra 57).

I. $Be^{9}(N^{14}, p)Ne^{22}$ $Q_m = 14.961$

Transitions to the ground and to excited states of Ne^{22} are observed at $E(N^{14}) = 25$ and 27 MeV (Ne 56, Go 58, Go 58e). The level density has been compared with that observed in $F^{19}(\alpha, p)Ne^{22}$. From $E_x = 14$ to 22 MeV, the two results agree; below $E_x = 14$ MeV, transitions in the (α, p) reaction are enhanced (Go 58).

II. $O^{18}(\alpha, n)Ne^{21}$ $Q_m = -0.705$ $E_b = 9.661$

The excitation function at 0°—30° has been measured for $E_\alpha = 1.9$ to 4.9 MeV: observed resonances are displayed in table 22.2 (Bo 56d). See also (Ro 55a).

III. $F^{19}(t, \alpha)O^{18}$ $Q_m = 11.849$ $E_b = 21.510$

Excitation functions have been measured at 90° in the range $E_t = 1.0$ to 2.1 MeV for the α_0 and α_1 groups. Broad resonances observed at $E_t \approx 1.4$ and 1.8 MeV in the α_0-yield and at 1.8 MeV in the α_1-yield, correspond to Ne^{22} levels at 22.7 and 23.1 MeV. The differential cross section (lab) at $\theta = 90°$ for production of α_1 is 0.07 mb/sr at $E_t = 1.8$ MeV (Ja 56e).

IV. $F^{19}(\alpha, p)Ne^{22}$ $Q_m = 1.698$

$Q_0 = 1.673 \pm 0.011$ (W. J. Fader; see Va 57).

Proton groups have been observed corresponding to levels of Ne^{22} at 1.27 and 3.35 MeV (Fa 54d; see also Fo 54). Angular distributions of the p_0 and p_1 groups and (p, γ) angular correlations measured by (Pi 58b) in the range $E_\alpha = 6.0$ to 6.6 MeV show the influence of both direct interaction and compound nucleus mechanisms. Gamma radiation from the 1.28-MeV state has been observed by (He 54b, Sh 54e, Fo 54, Br 55, Pi 58b) and from levels at 3.3 and 4.9 MeV by (Fo 54). The radiation from the 3.3-MeV level to the 1.28-MeV, $J = 2^+$, state is three times as probable as the ground state transition, suggesting $J = 2^+$ for the 3.35-MeV state; $J = 1^\pm$ is not excluded (Fo 54). See also $Be^{9}(N^{14}, p)\ Ne^{20}$: (Go 58).

V. $Ne^{20}(t, p)Ne^{22}$ $Q_m = 8.638$

Not reported.

VI. $Ne^{21}(d, p)Ne^{22}$ $Q_m = 8.139$

Proton groups have been observed corresponding to the ground and first excited states of Ne^{22} (Mi 52, Am 50, Zu 50a). See also (Ra 56b).

VII. $Ne^{21}(t, d)Ne^{22}$ $Q_m = 4.107$

Not reported.

VIII. $Ne^{21}(\alpha, He^3)Ne^{22}$ $Q_m = -10.212$

Not reported.

IX. $Ne^{22}(\gamma, n)Ne^{21}$ $Q_m = -10.366$

See (Fe 54).

TABLE 22.1
Energy levels of Ne^{22}

E_x (MeV)	J^π	Γ (keV)	Decay	Reactions
0	0		Stable	I, IV, VI, XIII, XIV
1.277±0.004	2^+		γ	IV, VI, XI, XIII, XIV
3.35	$(1^\pm, 2^+)$		γ	IV, XII, XIV
4.9			γ	IV, XII
(5.4)				XIV
(5.7)				XIV
11.47				
↓	(Thirteen levels: see table 22.2)			II
13.60				
(22.7)		broad	α, t	III
(23.1)		broad	α, t	III

X. $Ne^{22}(\gamma, \alpha)O^{18}$ $Q_m = -9.661$

See (Wa 57a).

XI. $Ne^{22}(p, p')Ne^{22*}$

A 1.28-MeV γ-ray has been observed for $E_p = 1.35$ to 4.4 MeV (Co 54).

TABLE 22.2
Resonances in $O^{18}(\alpha, n)Ne^{21}$ (Bo 56d)

E_α (MeV)	Γ_{lab} (keV)	$d\sigma/d\Omega$ [a] (mb/sr)	E_x in Ne^{22} (MeV)
2.21	30	0.3	11.47
2.47	<15	0.9	11.68
2.56	25	2.3	11.75
2.72	<15	2.6	11.89
2.94	≈40	5.2	12.07
3.24	≈70	9.2	12.31
3.63	≈200	16	12.63
3.91	≈40	13	12.86
4.12	≈40	16	13.03
4.22	≈40	29	13.11
4.33	≈100	42	13.20
4.52	≈70	27	13.35
4.82	≈40	31	13.60

[a] Laboratory cross sections, $\theta = 0$—30°, averaged over 130—90 keV thick target, ±50 per cent.

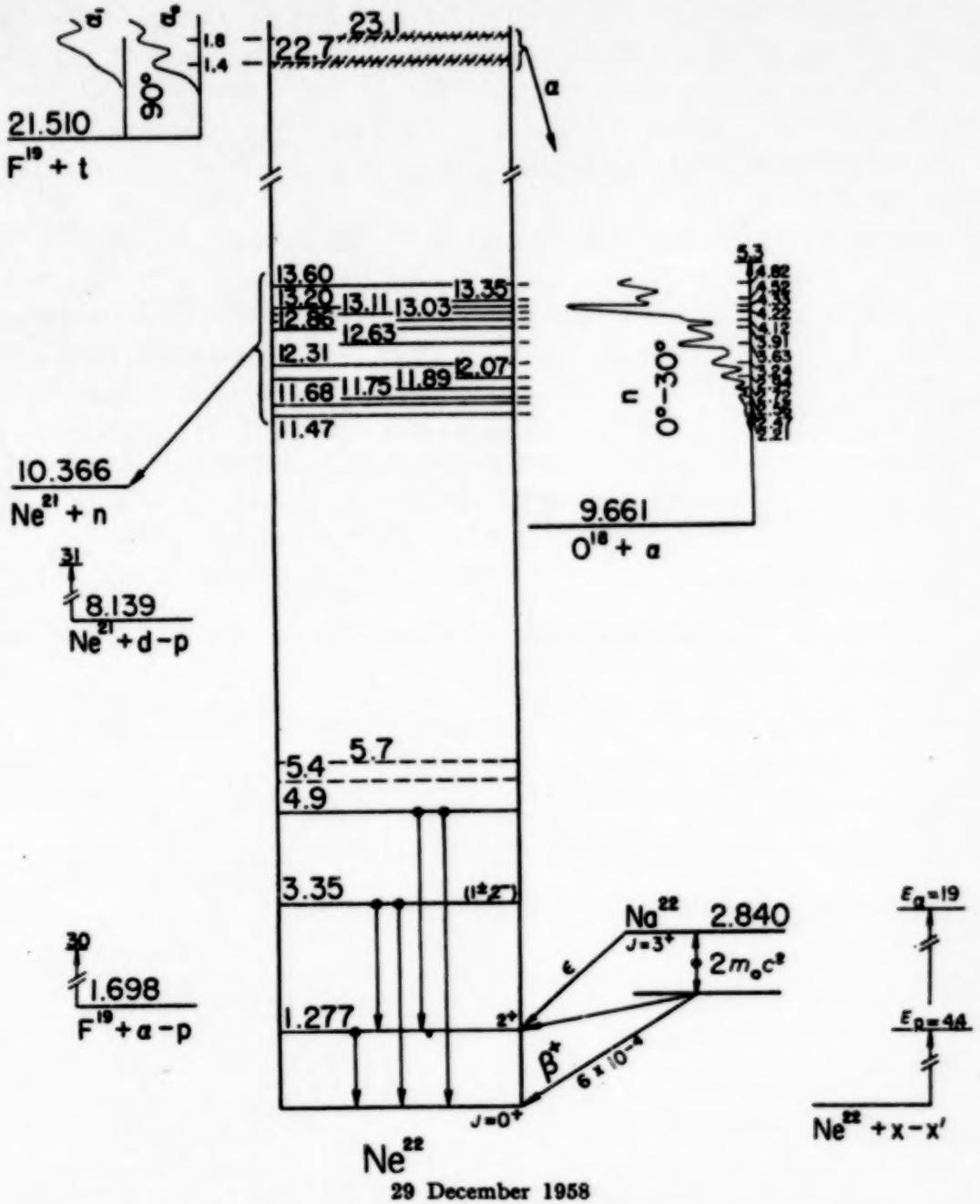

29 December 1958

Fig. 48. Energy levels of Ne^{22}: for notation, see fig. 1, p. 7.

XII. $Ne^{22}(\alpha, \alpha')Ne^{22*}$

At $E_\alpha = 19$ MeV, inelastic groups are observed corresponding to the 3.35 and 4.9-MeV levels of Ne^{22} (Se 56).

XIII. $Na^{22}(\beta^+)Ne^{22}$ $\quad Q_m = 2.840$

The decay proceeds almost entirely to the 1.28-MeV state of Ne^{22}: the half-life is 2.60 years (La 49a), 2.58 ± 0.03 years (Me 57a). E_{β^+}(max)

= 542±5 keV (Ma 50a), 540±5 keV (Wr 53). The γ-ray energy is 1277±4 keV (Al 49d). Electron capture occurs in about 10 per cent of the disintegrations: 9.9±0.6 per cent (Sh 54b), 11.0±0.9 per cent (Kr 54c), 9±5 per cent (Se 54c), 7.1±2.0 per cent (Ho 53b), 10.9±0.9 per cent (Al 55d). Log ft for the β^+-decay = 7.39; for K+L capture, log ft = 7.27 (Ma 54h). See also (Ch 55e).

The internal conversion coefficient indicates that the γ-transition is probably E2 and hence that the 1.28-MeV state has $J = 2^+$ (Le 54a). Since Na^{22} has $J = 3$, and presumably even parity, the beta transition should be allowed. The spectrum follows the allowed shape down to 25 keV (Ma 50a) and the β—γ correlation is isotropic (St 51h). The capture ratio appears to exclude l-forbiddeness as an explanation of the large ft-value (Sh 54b). The direct ground-state transition has been observed; log $ft \approx 13$. The shape is consistent with the D_2 spectrum (Wr 53). See also (Ha 58, Pa 57b, We 54b, Br 55, Ch 55e, Sc 57b), (En 57a) and (Ho 50b).

XIV. $Na^{23}(\gamma, p)Ne^{22}$ $Q_m = -8.796$

With E_γ = 17.6 MeV, transitions are reported to Ne^{22*} = 0, 1.3, 3.3, 4.4, 5.4 and 5.7 MeV (Op 58).

XV. $Na^{23}(n, d)Ne^{22}$ $Q_m = -6.569$
Not reported.

XVI. $Na^{23}(d, He^3)Ne^{22}$ $Q_m = -3.302$
Not observed: See (Vo 58).

XVII. $Na^{23}(t, \alpha)Ne^{22}$ $Q_m = 11.017$
Not reported.

XVIII. $Mg^{24}(n, He^3)Ne^{22}$ $Q_m = -12.770$
Not reported.

XIX. $Mg^{25}(n, \alpha)Ne^{22}$ $Q_m = 0.475$
Not reported.

Ne^{23}

(Fig. 49, p. 301)

THEORY

See (Ra 57).

I. $Ne^{23}(\beta^-)Na^{23}$ $Q_m = 4.387$

The β-decay is allowed to both Na^{23}(g.s.), $J = \frac{3}{2}^+$, and Na^{23*}(0.44), $J = \frac{5}{2}^+$; hence Ne^{23}(g.s.) is $\frac{3}{2}^+$ or $\frac{5}{2}^+$: see (Pe 57, En 57a). The half-life is 37.6±0.1 sec (Pe 57: see also St 58b). The β—γ angular correlation has been studied by (Ri 58a): if the decay is Gamow-Teller, the ratio of axial vector to

tensor coupling lies in the range 0.85 to 1.62. On the other hand, (He 59) find a correlation consistent with pure axial vector interaction. See also (Ge 55e, Ge 56).

II. $Ne^{21}(t, p)Ne^{23}$ $Q_m = 7.073$

Not reported.

III. $Ne^{22}(n, \gamma)Ne^{23}$ $Q_m = 5.192$

The thermal cross section is 36 ± 15 mb (Fe 52).

IV. $Ne^{22}(n, n)Ne^{23}$ $E_b = 5.192$

Observed resonances in the total cross section are displayed in table 23.2. Angular distributions have been measured at a number of energies in the range $E_n = 1.9$ to 3.5 MeV: it appears that the resonances cannot easily be fitted in terms of single levels. The analysis is also complicated by the occurrence of inelastic scattering (Si 58).

V. $Ne^{22}(d, p)Ne^{23}$ $Q_m = 2.965$

Proton groups are reported corresponding to the ground state and to excited states at 0.98 and 1.75 MeV (Zu 50a), 1.79 and (3.0) MeV (Mi 51d). At $E_d = 8.6$ MeV, the angular distribution of p_0 and p_1, analyzed by stripping theory, indicates $l_n = 2$ and 0, respectively, and therefore $J = \frac{3}{2}^+, \frac{5}{2}^+$ for the ground state of Ne^{23} and $\frac{1}{2}^+$ for the 0.98-MeV state. The neutron capture probabilities are in the ratio 102 : 84 (Bu 56d). See also (Ra 56b; theo.), (El 47) and (Aj 55).

VI. $Ne^{22}(t, d)Ne^{23}$ $Q_m = -1.067$

Not reported.

VII. $Ne^{22}(\alpha, He^3)Ne^{23}$ $Q_m = -15.386$

Not reported.

VIII. $Na^{23}(n, p)Ne^{23}$ $Q_m = -3.604$

Cross sections have been measured from threshold to 8.2 MeV. At this energy, the cross section is 12 ± 6 mb; a number of resonances are reported (Wi 58f). At $E_n = 14.3$ MeV, the cross section is 34 ± 15 mb (Hu 55c). See (En 57a).

IX. $Na^{23}(t, He^3)Ne^{23}$ $Q_m = -4.369$

Not reported.

X. $Mg^{25}(n, He^3)Ne^{23}$ $Q_m = -14.911$

Not reported.

XI. $Mg^{26}(n, \alpha)Ne^{23}$ $Q_m = -5.451$

See (Ho 50b).

TABLE 23.1

Energy levels of Ne^{23}

E_x (MeV)	J^π	$\tau_{\frac{1}{2}}$ or Γ (keV)	Decay	Reactions
0	$\frac{5}{2}^+$, $\frac{3}{2}^+$	$\tau_{\frac{1}{2}} = 37.6 \pm 0.1$ sec	β^-	I, III, V, VIII, XI
0.98 ± 0.1	$\frac{1}{2}^+$			V
1.77 ± 0.1				V
(3.0)				V
7.11		<20	n	IV
7.24			n	IV
7.28			n	IV
7.41	($\frac{3}{2}^-$, $\frac{5}{2}^+$)	150	n	IV
7.61		≦30	n	IV
7.79		85	n	IV
7.94			n	IV
8.16			n	IV
8.25			n	IV
8.47			n	IV

TABLE 23.2

Resonances in the total cross section of Ne^{23}+n (Si 58)

E_n (MeV)	Γ (keV)	J^π (MeV)	E_x of Ne^{23} (MeV)
2.01	<20		7.11
2.14			7.24
2.19			7.28
2.32	160	($\frac{3}{2}^-$)	7.41
	160	($\frac{5}{2}^+$)	7.41
2.53	≦30		7.61
2.72	90		7.79
2.87			7.94
3.10			8.16
3.20			8.25
3.43			8.47

Ne^{24}

(Not illustrated)

THEORY:

See (Ra 57).

MASS OF Ne^{24}

From the measurement of the Ne^{24}—Na^{24} mass difference (Dr 56: 2.449 ±0.035 MeV) and the Wapstra mass for Na^{24}, $(M-A)$ for Ne^{24} is 1.113± 0.040 MeV.

I. $Ne^{24}(\beta^-)Na^{24}$ $\qquad Q_m = 2.449$

The β^- decay takes place with a half-life of 3.38±0.02 min to excited

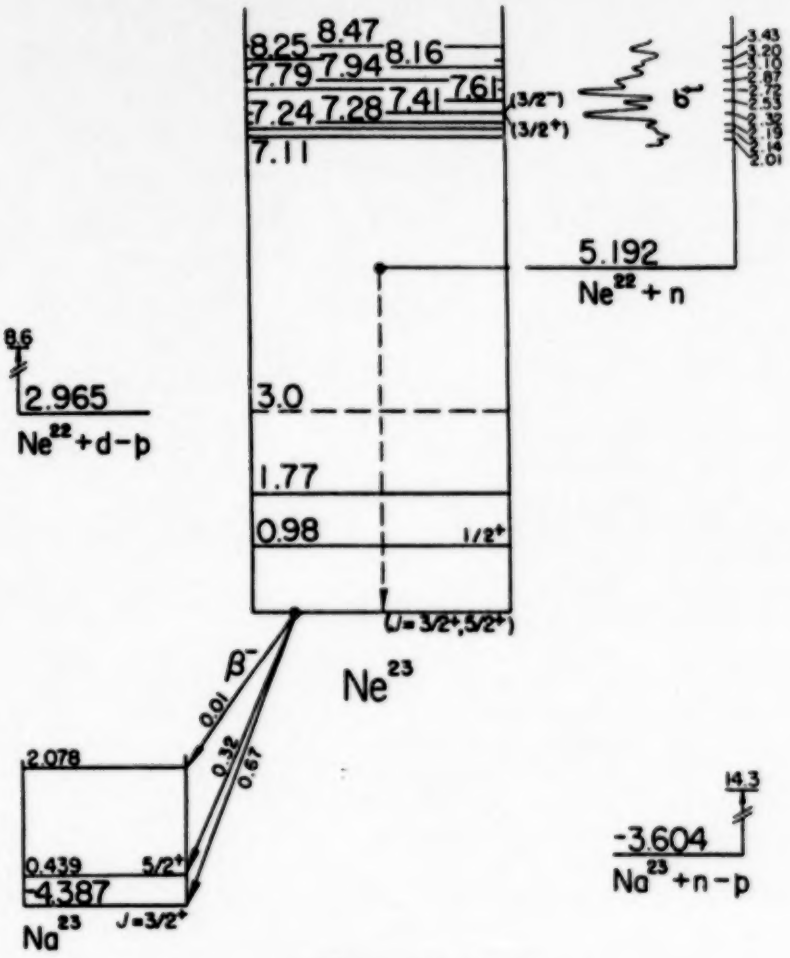

23 December 1958

Fig. 49. Energy levels of Ne^{23}: for notation, see fig. 1, p. 7.

states of Na^{24} at 0.472 ($J = 1^+$) and 1.350 MeV ($J = 1^+$). The corresponding β^- groups have $E_\beta(\max) = 1.98 \pm 0.05$ MeV (92 ± 2 per cent) and 1.10 ± 0.05 MeV (8 ± 2 per cent); log ft for either transition = 4.4. The absence of the direct decay to the ground state of Na^{24} is ascribed to the 4^+ character of Na^{24}(g.s.) (Ne^{24} is even-even, presumably $J = 0^+$): see (Dr 56, En 57a).

II. $Ne^{22}(t, p)Ne^{24}$ $\qquad Q_m = 5.605$

This reaction has been observed at $E_t = 1.5$ MeV (Dr 56).

Another reaction, not reported, leading to Ne^{24} is $Mg^{26}(n, He^3)Ne^{24}$ ($Q_m = -17.132$).

References

(Closed December 1, 1958)

(References are arranged and designated by first two letters of first-mentioned author's name, and year. Otherwise duplicate designations are distinguished by postscript letter.)

Ab 56 Abraham, Nuclear Physics **1** (1956) 415
Ab 58 Abraham and Warke, Nuclear Physics **8** (1958) 69
Ad 50b Adamson, Buechner, Preston, Goodman and Van Patter, Phys. Rev. **80** (1950) 985
Ad 52 Adair, Phys. Rev. **86** (1952) 155
Ad 53 Adair, Phys. Rev. **92** (1953) 1491
Ad 54 Adair, Phys. Rev. **96** (1954) 709
Ad 55 Adkins and Brennan, Phys. Rev. **99** (1955) 706
Ag 51 Agnew, Leland, Argo, Crews, Hemmendinger, Scott and Taschek, Phys. Rev. **84** (1951) 862
Ag 52 Agnew, Los Alamos Report 1371 (1952)
Ah 54 Ahnlund, Arkiv f. Fysik **7** (1954) 155
Ah 54b Ahnlund and Mileikowsky, Arkiv f. Fysik **8** (1954) 161
Ah 54c Ahnlund, Phys. Rev. **96** (1954) 999
Ah 54d Ahnlund, Thulin and Pauli, Arkiv f. Fysik **8** (1954) 489
Ah 55 Ahnlund, Arkiv f. Fysik **9** (1955) 39
Ah 56 Ahnlund, Arkiv f. Fysik **10** (1956) 369
Ah 56b Ahnlund, Arkiv f. Fysik **10** (1956) 425
Ah 57 Ahnlund, Phys. Rev. **106** (1957) 124
Ah 57a Ahnlund, Arkiv f. Fysik **11** (1957) 379
Aj 51 Ajzenberg, Phys. Rev. **82** (1951) 43
Aj 51b Ajzenberg, Phys. Rev. **83** (1951) 693
Aj 52 Ajzenberg, Phys. Rev. **87** (1952) 205A
Aj 52b Ajzenberg, Phys. Rev. **88** (1952) 298
Aj 52c Ajzenberg and Lauritsen, Revs. Mod. Phys. **24** (1952) 321
Aj 53 Ajzenberg and Buechner, Phys. Rev. **91** (1953) 674
Aj 54 Ajzenberg and Franzen, Phys. Rev. **94** (1954) 409
Aj 54b Ajzenberg and Franzen, Phys. Rev. **95** (1954) 153]
Aj 55 Ajzenberg and Lauritsen, Revs. Mod. Phys. **27** (1955) 77
Aj 56 Ajzenberg-Selove, Johnson, Rubin and Mazari, Phys. Rev. **103** (1956) 356
Aj 57a Ajzenberg-Selove, Bullock and Almqvist, Phys. Rev. **108** (1957) 1284
Al 47b Allen, Burcham and Wilkinson, Proc. Royal Soc. A **192** (1947) 114
Al 49a Alvarez, Phys. Rev. **75** (1949) 1815
Al 49c Alvarez, Phys. Rev. **75** (1949) 1127
Al 49d Alburger, Phys. Rev. **76** (1949) 435
Al 50g Alvarez, Phys. Rev. **80** (1950) 519
Al 51i Alburger, Phys. Rev. **83** (1951) 184
Al 51l Allred, Froman, Hudson and Rosen, Phys. Rev. **82** (1951) 786
Al 52a Alburger, Physica **18** (1952) 1034; Phys. Rev. **88** (1952) 1257
Al 52b Allred, Armstrong, Hudson, Potter, Robinson, Rosen and Stovall, Phys. Rev. **88** (1952) 425
Al 53a Almqvist, Allen, Dewan and Pepper, Phys. Rev. **91** (1953) 1022
Al 54 Alford and Hamilton, Phys. Rev. **95** (1954) 1351
Al 54b Allan, Nature **174** (1954) 267
Al 54c Alston, Crewe, Evans, Green and Willmott, Proc. Phys. Soc. A **67** (1954) 657
Al 54d Almqvist, Pepper and Lorrain, Canadian J. Phys. **32** (1954) 621

Al 54e Allen, Almqvist, Dewan and Pepper, Phys. Rev. **96** (1954) 684
Al 55a Allen, Almqvist and Bigham, Phys. Rev. **99** (1955) 631A
Al 55b Almqvist, Allen and Bigham, Phys. Rev. **99** (1955) 631A
Al 55c Allan and Sarma, Proc. Phys. Soc. A **68** (1955) 535
Al 55d Allen, Burcham, Chackett, Munday and Reasbeck, Proc. Phys. Soc. A **68** (1955) 681
Al 55e Alba, Fernandez, Mazari, Serment and Vazquez, Revista Mexicana de Fisica **4** (1955) 207
Al 55f Alba, Brody, Fernandez, Mazari, Serment and Vazquez, An. del Instituto de Fisica, Universidad Nacional Autonoma de Mexico **1** (1955) 1
Al 56 Allison, Murphy and Norbeck, Phys. Rev. **102** (1956) 1182
Al 56b Almqvist, Bromley, Gove, Litherland and Paul, Bull. Amer. Phys. Soc. **1** (1956) 195
Al 56c Allan, Govindjee and Sarma, Proc. Phys. Soc. A **69** (1956) 350
Al 56d Allen, Atomics **7** (1956) 103
Al 56f Alburger, Revs. Sci. Instr. **27** (1956) 991
Al 56h Alkhazov, Andreyev, Greenberg and Lemberg, Nuclear Physics **2** (1956) 65; Physica **22** (1956) 1129A; Zh. Eksp. Teor. Fiz. **30** (1956) 809
Al 57 Alford and Hamilton, Phys. Rev. **105** (1957) 673
Al 57b Alphonce, Johansson and Tibell, Nuclear Physics **3** (1957) 185
Al 57c Alphonce, Johansson and Tibell, Nuclear Physics **4** (1957) 672
Al 58 Almqvist, Bromley and Kuehner, Bull. Amer. Phys. Soc. **3** (1958) 27
Al 58a Allen, Bull. Amer. Phys. Soc. **3** (1958) 52
Al 58b Allen and Jarmie, Phys. Rev. **111** (1958) 1129
Al 58c Alburger, Phys. Rev. **111** (1958) 1586
Al 58d Alkhazov, Gangrskii and Lemberg, Zh. Eksp. Teor. Fiz. ("Soviet Physics") **6** (1958) 892
Al 58e Alburger and Wilkinson, Phil. Mag. **3** (1958) 1332
Al 59 Alburger, Wilkinson and Gallmann, Bull. Amer. Phys. Soc. **4** (1959) 56
Am 50 Ambrosen and Bisgaard, Nature **165** (1950) 888
Am 57a Ames, Owen and Swartz, Phys. Rev. **106** (1957) 775
Am 57b Amado and Blin-Stoyle, Proc. Phys. Soc. A **70** (1957) 532
Am 57c Amado, Phys. Rev. **108** (1957) 1462
Am 58 Ames and Owen, Phys. Rev. **109** (1958) 1639
An 57 Anderson, Gardner, Nakada and Wong, Bull. Amer. Phys. Soc. **2** (1957) 233
An 58 Anderson, Gardner, McClure, Nakada and Wong, Phys. Rev. **111** (1958) 572
Ar 50 Arnold, Phys. Rev. **79** (1950) 170; **80** (1950) 34
Ar 52d Argo, Taschek, Agnew, Hemmendinger and Leland, Phys. Rev. **87** (1952) 612
Ar 52e Arthur, Allen, Bender, Hausman and McDole, Phys. Rev. **88** (1952) 1291
Ar 54 Arnold, Phillips, Sawyer, Stovall and Tuck, Phys. Rev. **93** (1954) 483
Ar 56 Armstrong and Frye, Phys. Rev. **103** (1956) 335
Ar 58 Arnell, Dubois and Almén, Nuclear Physics **6** (1958) 196
Ar 58a Armbruster, Annales de Physique **3** (1958) 88
As 51 Ashmore and Raffle, Proc. Phys. Soc. A **64** (1951) 754
As 52 Ashmore and Raffle, Proc. Phys. Soc. A **65** (1952) 296
As 58 Ashby, Catron, Newkirk and Taylor, Phys. Rev. **111** (1958) 616
At 56 Atkinson, Crawford, Morisson, Preston and Wright, Physica **22** (1956) 1145A
Au 53 Austern, Butler and McManus, Phys. Rev. **92** (1953) 350
Au 55 Auerbach and French, Phys. Rev. **98** (1955) 1276
Ax 58 Axel, Conference on Photonuclear Reactions, National Bureau of Standards (1958)

Ba 48 Bailey, Freier and Williams, Phys. Rev. **73** (1948) 274
Ba 50 Bailey and Stratton, Phys. Rev. **77** (1950) 194
Ba 50f Barnes, French and Devons, Nature **166** (1950) 145
Ba 50g Baldinger, Huber, Ricamo and Zünti, Helv. Phys. Acta **23** (1950) 503
Ba 51a Bashkin, Mooring and Petree, Phys. Rev. **82** (1951) 378
Ba 51e Bashkin and Richards, Phys. Rev. **84** (1951) 1124

Ba 52 Baggett and Bame, Phys. Rev. **85** (1952) 434
Ba 52a Bair, Willard, Snyder, Hahn, Kingston and Green, Phys. Rev. **85** (1952) 946
Ba 52b Baldinger, Huber and Proctor, Helv. Phys. Acta **25** (1952) 142
Ba 52g Barnes, James and Neilson, Can. J. Phys. **30** (1952) 717
Ba 53 Battat and Ribe, Phys. Rev. **89** (1953) 80
Ba 53d Bartholomew and Kinsey, Canadian J. Phys. **31** (1953) 49
Ba 53e Bair, Kington and Willard, Phys. Rev. **90** (1953) 575
Ba 54 Banta and Macklin, Phys. Rev. **94** (1954) 807A
Ba 54a Bashkin, Phys. Rev. **95** (1954) 1012
Ba 54f Bartholomew, Brown, Gove, Litherland and Paul, Phys. Rev. **96** (1954) 1154
Ba 55 Barnes, Phys. Rev. **97** (1955) 1226
Ba 55a Baranger, Phys. Rev. **99** (1955) 145
Ba 55c Battat and Graves, Phys. Rev. **97** (1955) 1266
Ba 55d Bashkin and Carlson, Phys. Rev. **97** (1955) 1245
Ba 55e Barber, George and Reagan, Phys. Rev **98** (1955) 73
Ba 55f Bair, Kington and Willard, Phys. Rev. **100** (1955) 21
Ba 55g Bashkin, Carlson and Nelson, Phys. Rev. **99** (1955) 107
Ba 55i Banks, Nucleonics **13** (12) (1955) 62
Ba 55k Basile and Schuhl, C. Rendus **240** (1955) 2399
Ba 55l Bartholomew, Brown, Gove, Litherland and Paul, Canadian J. Phys. **33** (1955) 441
Ba 55m Bach and Livesey, Phil. Mag. **46** (1955) 824
Ba 55n Batchelor, Proc. Phys. Soc. A **68** (1955) 452
Ba 55o Batchelor and Morrison, Proc. Phys. Soc. A **68** (1955) 1081
Ba 55s Baz', Iszv. Akad. Nauk **19** (1955) 363
Ba 55t Baz', Iszv. Akad. Nauk **19** (1955) 360
Ba 56 Bame and Perry, Bull. Amer. Phys. Soc. **1** (1956) 93
Ba 56a Bartholomew, Litherland, Paul and Gove, Canadian J. Phys. **34** (1956) 147
Ba 56b Banerjee, Levinson, Albright and Tobocman, Bull. Amer. Phys. Soc. **1** (1956) 194
Ba 56c Bashkin, Carlson and Jacobs, Bull. Amer. Phys. Soc. **1** (1956) 212; Physica **22** (1956) 1124A
Ba 56d Bach and Hough, Phys. Rev. **102** (1956) 1341
Ba 56e Barker, Phil. Mag. **1** (1956) 329
Ba 56f Barjon, Magnac-Valette and Schmouker, C. Rendus **242** (1956) 896
Ba 56g Barschall, Helv. Phys. Acta **29** (1956) 145
Ba 56i Bair, Cohn, Kington and Willard, Phys. Rev. **104** (1956) 1595
Ba 56j Baumgartner, Franzen, Huber, Schellenberg and Seiler, Helv. Phys. Acta **29** (1956) 255
Ba 56m Banta, Gibbons, Good and Neiler, ORNL 2076 (1956)
Ba 57 Barker, Phil. Mag. **2** (1957) 780
Ba 57b Barker, Phil. Mag. **2** (1957) 286
Ba 57d Barker and Mann, Phil. Mag. **2** (1957) 5
Ba 57e Bame and Leland, Phys. Rev. **106** (1957) 1257
Ba 57f Baumgartner and Fulbright, Phys. Rev. **107** (1957) 219
Ba 57g Barloutaud, Lehmann, Leveque, Phillips and Quidort, C. Rendus **245** (1957) 422
Ba 57h Bame and Perry, Phys. Rev. **107** (1957) 1616
Ba 57k Banerjee and Levinson, Annals of Physics **2** (1957) 499
Ba 57l Bashkin and Carlson, Phys. Rev. **106** (1957)261
Ba 57m Bartholomew and Campion, Canadian J. Phys. **35** (1957) 1347
Ba 57n Basile, Annals of Physics (Paris) **2** (1957) 267
Ba 57o Balabanov, Barit, Katsaurov, Frank and Stranikh, Soviet J. of Atomic Energy, Suppt. **5** (1957) 37
Ba 57p Balabanov, Barit, Katsaurov, Frank and Stranikh, Soviet J. of Atomic Energy Suppt. **5** (1957) 43
Ba 57q Bair, Cohn and Willard, ORNL 2430 (1957)
Ba 58a Barber, Dodge and Vanhuyse, Conference on Photonuclear Reactions, National Bureau of Standards (1958), Bull. Amer. Phys. Soc. **3** (1958) 173

Ba 58b Baranov, Gol'danskii and Roganov, Phys. Rev. **109** (1958) 1801
Ba 58c Barton, Nuclear Physics **6** (1958) 100
Ba 58e Baranger and Meshkov, Phys. Rev. Lett. **1** (1958) 30
Ba 58f Barton and Smith, Phys. Rev. **110** (1958) 1143
Ba 58g Ball, MacGregor and Booth, Phys. Rev. **110** (1958) 1392
Ba 58h Ball, Fairhall and Halpern, Bull. Amer. Phys. Soc. **3** (1958) 322
Ba 58i Barnes, Fowler, Greenstein, Lauritsen and Nordberg, Bull. Amer. Phys. Soc. **3** (1958) 328
Ba 58j Baranov, Gol'danskii and Roganov, Zh. Eksp. Teor. Fiz. ("Soviet Physics") **6** (1958) 865
Ba 58k Bartholomew and Higgs, AECL 669 (1958)
Ba 58l Barber, Phys. Rev. **111** (1958) 1642
Ba 58m Basile and Gusakow, C. Rendus **246** (1958) 588
Ba 58n Balashko and Barit, Soviet Physics (JETP) **7** (1958) 715
Ba 59 Bame and Cubitt, Phys. Rev. (1959)
Be 41 Bennett, Bonner, Hudspeth, Richards and Watt, Phys. Rev. **59** (1941) 781
Be 51 Bennett, Roys and Toppel, Phys. Rev. **82** (1951) 20
Be 52a Benveniste, Thesis, UCRL 1689 (1952)
Be 53 Beckman, Huus and Zupančič, Phys. Rev. **91** (1953) 606
Be 53c Beghian, Halban, Husain and Sanders, Phys. Rev. **90** (1953) 1129
Be 53d Benenson, Phys. Rev. **90** (1953) 420
Be 54 Bennett, Roys and Toppel, Phys. Rev. **93** (1954) 924A
Be 55a Bent, Bonner and Sippel, Phys. Rev. **98** (1955) 1237
Be 55b Beyster, Henkel and Nobles, Phys. Rev. **97** (1955) 563
Be 55d Bendt and Scott, Phys. Rev. **97** (1955) 744
Be 55e Berthelot, Cohen, Cotton, Faraggi, Grjebine, Leveque, Naggiar, Roclawski-Conjeaud and Steinsznaider, J. Phys. Rad. **16** (1955) 241
Be 55f Beyster, Henkel, Nobles and Kister, Phys. Rev. **98** (1955) 1216
Be 55g Bent, Bonner, McCrary, Ranken and Sippel, Phys. Rev. **99** (1955) 710
Be 55h Bent, Bonner, McCrary and Ranken, Phys. Rev. **100** (1955) 771
Be 55i Beghian, Hicks and Milman, Phil. Mag. **46** (1955) 924
Be 55j Benveniste and Zenger, UCRL 4266 (1955)
Be 56 Benenson, Jones and McEllistrem, Phys. Rev. **101** (1956) 308
Be 56a Benveniste, Finke and Martinelli, Phys. Rev. **101** (1956) 655
Be 56b Benveniste, Gardner, Nakada and Wong, Bull. Amer. Phys. Soc. **1** (1956) 175
Be 56c Becker and Barschall, Phys. Rev. **102** (1956) 1384
Be 56d Berger and Loper, Phys. Rev. **104** (1956) 1603
Be 56e Beyster, Walt and Salmi, Phys. Rev. **104** (1956) 1319
Be 56f Benoist, Marty and Meyer, Physica **22** (1956) 1173A
Be 56g Bezrukov, Panov and Timoshuk, Soviet J. of Nuclear Energy **4** (1956) 609
Be 57b Bennett, Bull. Amer. Phys. Soc. II, **2** (1957) 208
Be 57e Bergman, Isakov, Popov and Shapiro, Zh. Eksp. Teor. Fiz. **33** (1957) 9
Zh. Eksp. Teor. Fiz. ("Soviet Physics") **6** (1958) 6
Be 57f Bent and Kruse, Phys. Rev. **108** (1957) 802
Be 58 Beckman and Sandstrom, Nuclear Physics **5** (1958) 595
Be 58a Bennett, Bull. Amer. Phys. Soc. **3** (1958) 26
Be 58c Benade, Conference on Photonuclear Reactions, National Bureau of Standards (1958)
Be 58d Berlin and Owen, Nuclear Physics **5** (1958) 669
Be 58e Bell and Blin-Stoyle, Nuclear Physics **6** (1958) 87
Be 58f Benenson and Shurman, Revs. Sci. Instr. **29** (1958) 1
Be 58g Bendel, McElhinney and Tobin, Phys. Rev. **111** (1958) 1297
Bi 52 Bichsel, Hälg, Huber and Stebler, Helv. Phys. Acta **25** (1952) 119
Bi 54 Birnbaum, Phys. Rev. **93** (1954) 146
Bi 54a Bittner and Moffat, Phys. Rev. **96** (1954) 374
Bi 55 Bigham, Allen and Almqvist, Phys. Rev. **99** (1955) 631A
Bi 55a Bird, Australian J. Phys. **8** (1955) 314

Bi 55b Bird and Spear, Australian J. Phys. **8** (1955) 567
Bi 57 Bilpuch, Weston, Newson, Rohrer and Jones, Bull. Amer. Phys. Soc. **2** (1957) 218
Bi 57b Bichsel and Bonner, Phys. Rev. **108** (1957) 1025
Bi 57c Bird and Spear, Australian J. Phys. **10** (1957) 268
Bi 57d Bilaniuk and Hough, Phys. Rev. **108** (1957) 305
Bi 57e Bishop and Bizot, J. Phys. Rad. **18** (1957) 434
Bi 57f Biel, Phil. Mag. A **70** (1957) 866
Bi 58 Bilianuk and Hensel, Bull. Amer. Phys. Soc. **3** (1958) 188; U. of Michigan, Cyclotron Report (July 1958)
Bi 58a Bichsel, Phys. Rev. Lett. **1** (1958) 384
Bl 47 Bleuler, Scherrer, Walter and Zünti, Helv. Phys. Acta **20** (1947) 96
Bl 47a Bleuler and Zünti, Helv. Phys. Acta **20** (1947) 195A
Bl 49 Blair, Freier, Lampi and Sleator, Phys. Rev. **75** (1949) 1678
Bl 49a Blaser, Boehm and Marmier, Phys. Rev. **75** (1949) 1953
Bl 51a Blaser, Boehm, Marmier and Scherrer, Helv. Phys. Acta **24** (1951) 465
Bl 52 Black, Phys. Rev. **87** (1952) 205A
Bl 52a Blaser, Marmier and Sempert, Helv. Phys. Acta **25** (1952) 442
Bl 53a Bleuler, Helv. Phys. Acta **26** (1953) 597
Bl 54 Blair, Hintz and Van Patter, Phys. Rev. **96** (1954) 1023
Bl 56a Blair and Henley, Bull. Amer. Phys. Soc. **1** (1956) 20; Physica **22** (1956) 1126A
Bl 56d Blumberg and Schlesinger, AECU 3118 (1956)
Bl 57 Bloom, Toppel and Wilkinson, Phil. Mag. **2** (1957) 57
Bl 57a Bloom, Turner and Wilkinson, Phys. Rev. **105** (1957) 232
Bl 57b Blanchard and Winter, Phys. Rev. **107** (1957) 774
Bl 58 Block, Haeberli and Newson, Phys. Rev. **109** (1958) 1620
Bl 58b Bloom, Lemmon and Moszkowski, Bull. Amer. Phys. Soc. **3** (1958) 418
Bo 40b Bonner, Proc. Royal Soc. A **174** (1940) 339
Bo 42 Borst, Phys. Rev. **61** (1942) 106A
Bo 48c Bonner and Evans, Phys. Rev. **73** (1948) 666
Bo 49a Bonner, Evans, Harris and Phillips, Phys. Rev. **75** (1949) 1401
Bo 50d Boyer, M.I.T. Prog. Rept. (LNSE), July (1950)
Bo 50f Bockelman, Phys. Rev. **80** (1950) 1011
Bo 51c Bockelman, Miller, Adair and Barschall, Phys. Rev. **84** (1951) 69
Bo 52a Bonner, Conner and Lillie, Phys. Rev. **88** (1952) 473
Bo 53 Bockelman, Browne, Buechner and Sperduto, Phys. Rev. **92** (1953) 665
Bo 54c Bonner and Cook, Phys. Rev. **96** (1954) 122
Bo 55a Bostrom, Hudspeth and Morgan, Phys. Rev. **99** (1955) 643A
Bo 55d Bostrom, Hudspeth and Morgan, Phys. Rev. **100** (1955) 973A
Bo 55e Boreli and Lalovic, Nature **176** (1955) 1021
Bo 56 Bonner, Eisinger, Kraus and Marion, Phys. Rev. **101** (1956) 209
Bo 56a Bonner, Kraus, Marion and Schiffer, Bull. Amer. Phys. Soc. **1** (1956) 94
Bo 56b Bostrom, Hudspeth and Morgan, Bull. Amer. Phys. Soc. **1** (1956) 94
Bo 56c Boyle, Nuclear Physics **1** (1956) 581
Bo 56d Bonner, Kraus, Marion and Schiffer, Phys. Rev. **102** (1956) 1348
Bo 56f Bockelman, Leveque and Buechner, Phys. Rev. **104** (1956) 456
Bo 56g Bogdanov, Vlasov, Kalinin, Rybakov and Sidorov, Zh. Eksp. Teor. Fiz. ("Soviet Physics") **3** (1956) 113; Zh. Eksp. Teor. Fiz. **30** (1956) 185
Bo 56i Bouchez, Tobailem, Robert, Muxart, Mellet, Daudel and Daudel, J. Phys. Rad. **17** (1956) 363
Bo 56k Bockelman and Leveque, J. Phys. Rad. **17** (1956) 557
Bo 56l Bogdanov, Vlasov, Kalinin, Rybakov and Sidorov, Physica **22** (1956) 1150
Bo 56m Bogdanov, Vlasov, Kalinin, Rybakov and Sidorov, Zh. Eksp. Teor. Fiz. **30** (1956) 981; Soviet Physics **3** (1956) 793
Bo 57a Bondelid, Dunning and Talbott, Phys. Rev. **105** (1957) 193
Bo 57b Bolmgren, Freier, Likely and Famularo, Phys. Rev. **105** (1957) 210
Bo 57d Bostrom, Hudspeth and Morgan, Phys. Rev. **105** (1957) 1545

Bo 57e Bonner, Prosser and Slattery, Bull. Amer. Phys. Soc. **2** (1957) 180
Bo 57f Bodansky, Eccles and Halpern, Phys. Rev. **108** (1957) 1019
Bo 57g Booth, Hill, Price and Roaf, Proc. Phys. Soc. A **70** (1957) 863
Bo 57h Boehm, Novey, Barnes and Stech, Phys. Rev. **108** (1957) 1497
Bo 57i Bogdanov, Vlasov, Kalinin, Rybakov and Sidorov, Soviet J. of Atomic Energy **3** (1957) 987
Bo 58 Bostick, Adelson, Moyer and Waddell, Bull. Amer. Phys. Soc. **3** (1958) 189
Bo 58a Booth, Price, Roaf and Salmon, Proc. Phys. Soc. A **71** (1958) 325
Bo 58b Boehm, Soergel and Stech, Phys. Rev. Lett. **1** (1958) 77
Bo 58c Bodansky, Eccles, Farwell, Rickey and Robison, Bull. Amer. Phys. Soc. **3** (1958) 327
Bo 58d Bokhari, Cookson, Hird and Weesakul, Proc. Phys. Soc. A **72** (1958) 88
Bo 58e Bondelid and Kennedy, NRL Report 5083 (1958)
Bo 58f Bowcock, Phys. Rev. **112** (1958) 923
Br 39 Brubaker, Phys. Rev. **56** (1939) 1181
Br 48a Breit and Bloch, Phys. Rev. **74** (1948) 397
Br 49 Brown and Perez-Mendez, Phys. Rev. **75** (1949) 1286
Br 50c Brown and Perez-Mendez, Phys. Rev. **78** (1950) 812
Br 50d Brown and Perez-Mendez, Phys. Rev. **78** (1950) 649
Br 51a Brown, Snyder, Fowler and Lauritsen, Phys. Rev. **82** (1951) 159
Br 51f Browne, Williamson, Craig and Donahue, Phys. Rev. **83** (1951) 179
Br 51g Brinkworth and Titterton, Phil. Mag. **42** (1951) 952
Br 51h Braden, Phys. Rev. **84** (1951) 762
Br 51i Braden, Carter and Ford, Phys. Rev. **84** (1951) 837
Br 52 Bromley and Goldman, Phys. Rev. **86** (1952) 790
Br 52c Britten, Phys. Rev. **88** (1952) 283
Br 52e Brolley, Fowler and Schlacks, Phys. Rev. **88** (1952) 618
Br 53c Bromley, Bruner and Fulbright, Phys. Rev. **89** (1953) 396
Br 53i Browne and Bockelman, M.I.T. Progress Report, (May 1953)
Br 54a Bransden and McKee, Phil. Mag. **45** (1954) 869
Br 54b Brown, Famularo, Holmgren, Rankin and Stratton, Phys. Rev. **96** (1954) 80
Br 55 Breen and Hertz, Phys. Rev. **98** (1955) 599
Br 55c Browne, M.I.T. Progress Report L.N.S.E. (May 1955)
Br 56a Brockman, Phys. Rev. **102** (1956) 391
Br 56d Browne and Lamarsh, Phys. Rev. **104** (1956) 1099
Br 56e Brugger, Evans, Joki and Shankland, Phys. Rev. **104** (1956) 1054
Br 56f Browne, Phys. Rev. **104** (1956) 1598
Br 56g Brinkworth and Rose, Nuovo Cimento **3** (1956) 195
Br 57 Bromley, Almqvist, Gove, Litherland, Paul and Ferguson, Phys. Rev. **105** (1957) 957
Br 57a Browne and Bockelman, Phys. Rev. **105** (1957) 1301
Br 57b Brussel and Williams, Phys. Rev. **106** (1957) 286
Br 57c Bromley, Ferguson, Gove, Litherland and Almqvist, Bull. Amer. Phys. Soc. **2** (1957) 51
Br 57e Brolley, Hall and Rosen, Bull. Amer. Phys. Soc. **2** (1957) 207
Br 57f Broude, Green, Singh and Willmott, Phil. Mag. **2** (1957) 499
Br 57g Browne, Phys. Rev. **108** (1957) 1007
Br 57h Breen, Hertz and Wright, Bull. Amer. Phys. Soc. **2** (1957) 357
Br 57i Broude, Green, Singh and Willmott, Phil. Mag. **2** (1957) 1006
Br 57j Browne, Bull. Amer. Phys. Soc. **2** (1957) 350
Br 57k Brockman, Phys. Rev. **108** (1957) 1000
Br 57l Brix and Maschke, Zeits. für Natur. **12a** (1957) 1013
Br 58 Bromley, Kuehner and Almqvist, Bull. Amer. Phys. Soc. **3** (1958) 27
Br 58a Brunhart, Kenney and Kern, Phys. Rev. **110** (1958) 924
Br 58b Brolley, Hall, Rosen and Stewart, Phys. Rev. **109** (1958) 1277
Br 58c Braid and Yntema, Bull. Amer. Phys. Soc. **3** (1958) 188

Br 58d Bromley, Kuehner and Almqvist, Bull. Amer. Phys. Soc. **3** (1958) 199
Br 58e Bromley, Proc. of the Rehovoth Conference (North-Holland Publishing Co., Amsterdam, 1958)
Br 58f Brockman, Phys. Rev. **110** (1958) 163
Br 58g Braley and Cook, Bull. Amer. Phys. Soc. **3** (1958) 267
Br 58h Bratenahl, Peterson and Stoering, Phys. Rev. **110** (1958) 927
Br 58j Breuer and Neuert, private communication (1958),
Br 59 Bromley, Gove, Kuehner, Litherland and Almqvist, Phys. Rev. (1959)
Bu 38 Burcham and Smith, Proc. Royal Soc. A **168** (1938) 176
Bu 48c Buechner, Strait, Stergiopoulos and Sperduto, Phys. Rev. **74** (1948) 1569
Bu 50d Buechner, Van Patter, Strait and Sperduto, Phys. Rev. **79** (1950) 262
Bu 50h Burcham and Freeman, Phil. Mag. **41** (1950) 921
Bu 51 Bullock, McMinn, Rasmussen and Sampson, Phys. Rev. **83** (1951) 212A
Bu 51c Bullock and Sampson, Phys. Rev. **84** (1951) 967
Bu 51f Burrows, Powell and Rotblat, Proc. Royal Soc. A **209** (1951) 478
Bu 51h Burge, Burrows, Gibson and Rotblat, Proc. Royal Soc. A **210** (1951) 534
Bu 51i Butler and Symonds, Phys. Rev. **83** (1951) 858
Bu 52c Butler, Phys. Rev. **85** (1952) 743
Bu 53a Bunbury, Phys. Rev. **90** (1953) 1121; **91** (1953) 1580
Bu 53b Burcham, Gibson, Hossain and Rotblat, Phys. Rev. **92** (1953) 1266
Bu 54 Burke, Risser and Phillips, Phys. Rev. **93** (1954) 188
Bu 54c Butler, NRL Quarterly on Nuclear Science and Technology (Progress Report, July-September, 1954)
Bu 55 Butler, Phys. Rev. **98** (1955) 241A
Bu 55a Butler, Phys. Rev. **99** (1955) 643A
Bu 55b Butler and Holmgren, Phys. Rev. **99** (1955) 1649A; Physica **22** (1956) 1140A
Bu 55c Budde and Huber, Helv. Phys. Acta **28** (1955) 49
Bu 55f Bumiller, Ph. D. Thesis, U. Zurich (1955)
Bu 56 Butler, Holmgren and Kunz, Bull. Amer. Phys. Soc. **1** (1956) 29
Bu 56a Butler, Bull. Amer. Phys. Soc. **1** (1956) 94
Bu 56b Bunbury, Devons, Manning and Towle, Proc. Phys. Soc. A **69** (1956) 165
Bu 56d Burrows, Green, Hinds and Middleton, Proc. Phys. Soc. A **69** (1956) 310
Bu 56e Bumiller, Staub and Weaver, Helv. Phys. Acta **29** (1956) 83
Bu 56h Burge and Prowse, Phil. Mag. **1** (1956) 912
Bu 56j Burge, Fujimoto and Hossain, Phil. Mag. **1** (1956) 19
Bu 57 Burgy, Davidon, Novey, Perlow and Ringo, Bull. Amer. Phys. Soc. **2** (1957) 206
Bu 57a Butler, Phys. Rev. **106** (1957) 272
Bu 57b Burcham, Gibson, Prowse and Rotblat, Nuclear Physics **3** (1957) 217
Bu 57c Buechner and Sperduto, Phys. Rev. **106** (1957) 1008
Bu 57f Burbidge, Burbidge, Fowler and Hoyle, Revs. Mod. Phys. **29** (1957) 547
Bu 58 Burcham, McCauley, Bredin, Gibson, Prowse and Rotblat, Nuclear Physics **5** (1958) 141
Bu 58a Bujdosó, Nuclear Physics **6** (1958) 107
Bu 58b Butler and Holmgren, Phys. Rev. **112** (1958) 461
Bu 59 Butler, Fagg and Holmgren, Phys. Rev. **113** (1959) 268

Ca 41 Carroll, Phys. Rev. **60** (1941) 702
Ca 51a Carver and Wilkinson, Proc. Phys. Soc. A **64** (1951) 199
Ca 52 Canavan, Phys. Rev. **87** (1952) 136
Ca 52a Català, Senent and Aguilar, An. Real. Soc. Españ. Fis. y Quim. **48A** (1952) 73; Physics Abstracts **57** (1954) 1709
Ca 53b Cameron, Phys. Rev. **90** (1953) 839
Ca 53f Català, Senent and Casanova, An. Real. Soc. Españ. Fis. y Quim. **49A** (1953) 91; Nuclear Science Abstracts (1953)
Ca 53g Campbell and Strain, ORNL 1496 (1953)
Ca 54d Cartwright, Green and Willmott, Phil. Mag. **45** (1954) 742

Ca 54e Carver, Kondaiah and McDaniel, Phil. Mag. **45** (1954) 948
Ca 54i Català and Senent, An. Real. Soc. Españ. Fis. y Quim. **50** (1954) 55
Ca 54j Català, Senent and Casanova, An. Real. Soc. Españ. Fis. y Quim. **50A** (1954) 145
Ca 55 Carlson and Nelson, Phys. Rev. **98** (1955) 1310
Ca 55b Carver, Hay and Titterton, Phil. Mag. **46** (1955) 841
Ca 55c Calvert, Jaffe and Maslin, Proc. Phys. Soc. A **68** (1955) 1017
Ca 55d Català, Aguilar and Senent, An. Real. Soc. Españ. Fis. y Quim. **51A** (1955) 173
Ca 55e Català, Senent, Aguilar and Font, An. Real. Soc. Españ. Fis. y Quim. **51A** (1955) 127
Ca 55g Campbell, Australian J. Phys. **8** (1955) 449
Ca 56 Casson, Bull. Amer. Phys. Soc. **1** (1956) 56
Ca 56b Calvert, Jaffe and Maslin, Phys. Rev. **101** (1956) 501
Ca 56e Cameron, Bull. Amer. Phys. Soc. **1** (1956) 191
Ca 56f Campbell, Australian J. Phys. **9** (1956) 156
Ca 56g Català, Senent and Aguilar, An. Real. Soc. Españ. Fis. y Quim. **52A** (1956) 27
Ca 56h Català, Aguilar, Senent and Font, An. Real. Soc. Españ. Fis. y Quim. **52A** (1956) 33
Ca 56i Cameron, Bull. Amer. Phys. Soc. **1** (1956) 324
Ca 56j Català, Villar, Bonet and Miralles, An. Real. Soc. Españ. Fis. y Quim. **A52** (1956) 85
Ca 56k Català, Villar and Bonet, An. Real. Soc. Españ. Fis. y Quim. **A52** (1956) 93
Ca 57a Calvert, Jaffe and Maslin, Proc. Phys. Soc. A **70** (1957) 78
Ca 57d Carlson and Henton, Bull. Amer. Phys. Soc. **2** (1957) 358
Ca 57e Carlson, Phys. Rev. **107** (1957) 1094
Ca 57f Carver and Lokan, Australian J. Phys. **10** (1957) 312
Ca 57g Carpenter and Wilson, Bull. Amer. Phys. Soc. **2** (1957) 382
Ca 57h Campion and Bartholomew, Canadian J. Phys. **35** (1957) 1361
Ca 57i Català, Font, Aguilar, Senent and de la Cuadra, An. Real. Soc. Españ. Fis. Quim. **53A** (1957) 229
Ca 58 Carlson, Douglas, Bashkin and Broude, Bull. Amer. Phys. Soc. **3** (1958) 199
Ca 58a Cameron, Bull. Amer. Phys. Soc. **3** (1958) 187
Ca 58b Cameron, Bull. Amer. Phys. Soc. **3** (1958) 227
Ca 58c Cameron, Bull. Amer. Phys. Soc. **3** (1958) 269
Ce 56 Cerineo, Nuclear Physics **2** (1956) 113; Physica **22** (1956) 1154A
Ce 58 Cence, Moyer and Waddell, Conference on Photonuclear Reactions, National Bureau of Standards (1958)
Ch 47b Champion and Roy, Proc. Royal Soc. **191** (1947) 269
Ch 47c Chupp and McMillan, Phys. Rev. **72** (1947) 873
Ch 49d Charpie, Sun, Jennings and Nechaj, Phys. Rev. **76** (1949) 1255
Ch 50 Chao, Tollestrup, Fowler and Lauritsen, Phys. Rev. **79** (1950) 108
Ch 50a Chao, Phys. Rev. **80** (1950) 1035
Ch 53c Churchill, Jones and Hunt, Nature **172** (1953) 460
Ch 53d Christy, Phys. Rev. **89** (1953) 839
Ch 54b Christy, Phys. Rev. **94** (1954) 1077
Ch 54d Christy and Fowler, Phys. Rev. **96** (1954) 851A
Ch 54e Chastel, J. Phys. Rad. **15** (1954) 240
Ch 54f Cheston, Phys. Rev. **96** (1954) 1590
Ch 55b Chidley and Katz, Phys. Rev. **99** (1955) 1646A
Ch 55c Chupp, UCRL 2955 (1955)
Ch 55e Charpak, J. Phys. Rad. **16** (1955) 62
Ch 56 Cheng, Revs. Mod. Phys. **28** (1956) 45
Ch 56a Chadwick, Alexander and Warren, Canadian J. Phys. **34** (1956) 381
Ch 56b Christy, Physica **22** (1956) 1009
Ch 56c Chick, Evans, Hancock, Hunt and Pope, Proc. Phys. Soc. A **69** (1956) 624
Ch 57 Chow and Wright, Canadian J. Phys. **35** (1957) 184
Ch 57a Chase and Igo, Bull. Amer. Phys. Soc. **2** (1957) 381
Ch 57b Chuvilo and Shevchenko, Zh. Eksp. Teor. Fiz. **32** (1957) 1335
Ch 58 Chen, Bull. Amer. Phys. Soc. **3** (1958) 189

Ch 58a Chupp, DuMond, Gordon, Jopson and Mark, Phys. Rev. **112** (1958) 532
Ch 58b Chevallier, Ph. D. Thesis, U. of Strasbourg (1958)
Ch 58c Chuvilo and Shevchenko, Soviet Physics (JETP) **7** (1958) 410
Ch 58d Chiba, Conzett, Morinaga, Mutsuro, Shoda and Kimura, Bull. Amer. Phys. Soc. **3** (1958) 419
Ch 59 Christy and Duck, (1959)
Cl 53a Clegg and Wilkinson, Phil. Mag. **44** (1953) 1269
Cl 55 Clegg, Jones and Wilkinson, Proc. Phys. Soc. A **68** (1955) 538
Cl 55a Clementel and Villi, Nuovo Cimento **2** (1955) 1121
Cl 56 Clegg, Phil. Mag. **1** (1956) 1116
Cl 57 Clarke and Paul, Canadian J. Phys. **35** (1957) 155
Cl 58 Clement, Boreli, Darden, Haeberli and Striebel, Nuclear Physics **6** (1958) 177
Co 52f Conner, Bonner and Smith, Phys. Rev. **88** (1952) 468
Co 52g Cowie, Heydenburg and Phillips, Phys. Rev. **87** (1952) 304
Co 52h Coon, Graves and Barschall, Phys. Rev. **88** (1952) 562
Co 53 Collins, MacKenzie and Ramm, Proc. Royal Soc. **216** (1953) 242
Co 53b Conner, Phys. Rev. **89** (1953) 712
Co 53e Cohen, Newman, Handley and Timnick, Phys. Rev. **90** (1953) 323
Co 53h Cohen, Phil. Mag. **44** (1953) 583
Co 53k Cohen and French, Phil. Mag. **44** (1953) 1259
Co 53l Cork, Phys. Rev. **89** (1953) 78
Co 54 Cox, Van Loef and Lind, Phys. Rev. **93** (1954) 925A
Co 54b Cohen and Handley, Phys. Rev. **93** (1954) 514
Co 54e Cohen, Hanna and Class, Phys. Rev. **94** (1954) 419
Co 54f Cook and Bonner, Phys. Rev. **94** (1954) 651
Co 54g Cork and Hartsough, Phys. Rev. **96** (1954) 1267; UCRL 2590 (1954)
Co 54h Cohen, Reynolds and Zucker, Phys. Rev. **96** (1954) 1617
Co 54j Cooper, AECU 3204 (1954)
Co 55 Cooper and Zaffarano, Phys. Rev. **98** (1955) 1199A
Co 55a Collie, Proc. of the Glasgow Conference (Pergamon Press, 1955)
Co 55c Cohen, Phys. Rev. **100** (1955) 206
Co 55g Cohen and Fowler, Phys. Rev. **99** (1955) 1625A
Co 56a Cohn and Fowler, Bull. Amer. Phys. Soc. **1** (1956) 175
Co 56c Collie, Meads and Lockett, Proc. Phys. Soc. A **69** (1956) 464
Co 56d Cohen, Mann, Patton, Reibel, Stephens and Winhold, Phys. Rev. **104** (1956) 108
Co 56e Connors and Miller, Bull. Amer. Phys. Soc. **1** (1956) 340
Co 56f Cook, Penfold and Telegdi, Phys. Rev. **104** (1956) 554
Co 56h Conzett and Silver, Bull. Amer. Phys. Soc. **1** (1956) 388
Co 57 Conzett, Phys. Rev. **105** (1957) 1324
Co 57a Cox and Williamson, Phys. Rev. **105** (1957) 1799
Co 57b Cook, Phys. Rev. **106** (1957) 300
Co 57c Corelli, Bleuler and Tendam, Bull. Amer. Phys. Soc. **2** (1957) 34
Co 57d Cook, Fowler, Lauritsen and Lauritsen, Phys. Rev. **107** (1957) 508
Co 57f Conzett, Igo, Shaw and Slobodrian, Bull. Amer. Phys. Soc. **2** (1957) 305
Co 57g Conzett and Hoffman, Bull. Amer. Phys. Soc. **2** (1957) 382
Co 57h Cohn, Bair and Willard, ORNL 2204 (1957)
Co 58 Cohn and Fowler, Bull. Amer. Phys. Soc. **3** (1958) 18
Co 58a Cook, Fowler, Lauritsen and Lauritsen, Phys. Rev. **111**, (1958) 567
Co 58b Conner, Phys. Rev. **109** (1958) 1268
Co 58c Corelli, Bleuler and Tendam, Bull. Amer. Phys. Soc. **3** (1958) 200
Co 58d Cochran and Knight, Bull. Amer. Phys. Soc. **3** (1958) 323
Co 58e Coon, Davis, Felthauser and Nicodemus, Phys. Rev. **111** (1958) 250
Co 58g Cortini, Milone, Rinzivillo and Tribuno, Nuovo Cimento **9** (1958) 188
Co 58h Commins and Kusch, Phys. Rev. Lett. **1** (1958) 208
Co 59 Cohn and Fowler, (1959)
Cr 49a Critchfield and Dodder, Phys. Rev. **76** (1949) 602

Cr 51b Crews, Phys. Rev. **82** (1951) 100
Cr 52c Craig, Donahue and Jones, Phys. Rev. **88** (1952) 808
Cr 54a Cranberg, Moffatt and Smith, Los Alamos Report 1654 (1954)
Cr 56a Cronin, Phys. Rev. **101** (1956) 298
Cr 56b Cranberg and Levin, Phys. Rev. **103** (1956) 343
Cr 56c Craig, Cross and Jarvis, Phys. Rev. **103** (1956) 1414
Cr 56d Craig, Cross and Jarvis, Phys. Rev. **103** (1956) 1427
Cr 57 Crutchfield, Haeberli and Newson, Bull. Amer. Phys. Soc. **2** (1957) 33
Cr 58 Cranberg, Bull. Amer. Phys. Soc. **3** (1958) 365
Cu 50 Curling and Newton, Nature **165** (1950) 609
Cu 52 Cüer and Jung, C. Rendus **234** (1952) 204
Cu 52a Cüer and Magnac-Valette, C. Rendus **234** (1952) 1049
Cu 53 Cüer and Jung, Phys. Rev. **89** (1953) 1151
Cu 53a Cüer and Jung, C. Rendus **236** (1953) 1252
Cu 53b Cüer and Jung, C. Rendus **236** (1953) 2401
Cu 53c Cüer and Magnac-Valette, J. Phys. Rad. **14** (1953) 15S
Cu 54 Cüer, Jung and Bilwes, C. Rendus **238** (1954) 1405
Cu 55 Cüer and Jung, J. Phys. Rad. **16** (1955) 385
Cu 55a Cüer, Samman and Combe, C. Rendus **240** (1955) 1527
Cu 55b Cüer, Magnac-Valette and Baumann, C. Rendus **240** (1955) 1880
Cu 56 Culler, Fernbach and Sherman, Phys. Rev. **101** (1956) 1047
Cz 55 Czyż, Bull. Acad. Polon. Sci. **3** (1955) 365
Cz 56 Czyż, Phys. Rev. **102** (1956) 1185
Cz 56a Czyż and Sawicki, Nuovo Cimento **3** (1956) 864; Physica **22** (1956) 1182A
Cz 56b Czyż, Acta Phys. Polon. **15** (1956) 129

Da 51 Day and Perry, Phys. Rev. **81** (1951) 662
Da 51b Day, Ph. D. Thesis, California Institute of Technology (1951)
Da 52 Day and Walker, Phys. Rev. **85** (1952) 582
Da 52b Davis, Phys. Rev. **86** (1952) 976
Da 53d Dawson and Bigham, Canadian J. Phys. **31** (1953) 167
Da 54 Day and Huus, Phys. Rev. **95** (1954) 1003
Da 54b von Dardel and Sjöstrand, Phys. Rev. **96** (1954) 1566
Da 55 Dabrowski and Sawicki, Phys. Rev. **97** (1955) 1002
Da 55a Dabrowski and Sawicki, Bull. Acad. Polon. Sci. **3** (1955) 91
Da 55b Dabrowski and Sawicki, Acta Phys. Polon. **14** (1955) 143
Da 55c Dabrowski and Sawicki, Acta Phys. Polon. **14** (1955) 323
Da 55d Dabrowski and Sawicki, Acta Phys. Polon. **14** (1955) 407; Acta Phys. Polon. **15** (1956) 431
Da 56 Day, Johnsrud and Lind, Bull. Amer. Phys. Soc. **1** (1956) 56
Da 56a Davaney, Los Alamos Report 1960 (1956)
Da 56b Dayton and Schrank, Phys. Rev. **101** (1956) 1358
Da 56c Dawson and Livesey, Canadian J. Phys. **34** (1956) 241
Da 56d Day, Phys. Rev. **102** (1956) 767
Da 56e Dabrowski and Sawicki, Acta Phys. Polon. **15** (1956) 3
Da 56g Davidson and Giambiagi, Centro Brasileiro de Pesquisas Fisicas, Notas de Fisica Vol. II, No. 12 (1956)
Da 57 Dabrowski and Tulczyjew, Acta Phys. Polon. **16** (1957) 231
Da 57a Davidenko, Pogrebov and Saukov, Soviet J. of Atomic Energy **2** (1957) 474
Da 57b Daniel and Schmidt-Rohr, Zeits. für Natur. **12a** (1957) 750
Da 58 Davis and Hauser, Nucleonics **16** (3) (1958) 87
Da 58a Dabrowski, Proc. Phys. Soc. A **71** (1958) 658
Da 58b Dalton, Hinds and Parry, Proc. Phys. Soc A **71** (1958) 252
Da 58c Dawson, Neilson and Sample, Bull. Amer. Phys. Soc. **3** (1958) 323
Da 58d Dabrowski, Proc. Phys. Soc. A **72** (1958) 499
Da 58e Daniel and Schmidt-Rohr, Nuclear Physics **7** (1958) 516

De 39a Devons, Proc. Royal Soc. A **172** (1939) 127
De 49d Devons and Hine, Proc. Royal Soc. A **199** (1949) 56, 73
De 50a Devons and Lindsey, Proc. Phys. Soc. A **63** (1950) 1202
De 52 Dewan, Pepper, Allen and Almqvist, Phys. Rev. **86** (1952) 416
De 52b De Jong, Endt and Simons, Physica **18** (1952) 676
De 53d Devons, Report of the Birmingham Conference on Nuclear Physics (1953)
De 54 De Juren and Rosenwasser, Phys. Rev. **93** (1954) 831
De 54a Devons, Goldring and Lindsey, Proc. Phys. Soc. A **67** (1954) 134
De 54b Devons and Goldring, Proc. Phys. Soc. A **67** (1954) 413
De 54c Dennison, Phys. Rev. **96** (1954) 378
De 54d Dearnaley, Phil. Mag. **45** (1954) 1213
De 55 Devons, Manning and Bunbury, Proc. Phys. Soc. A **68** (1955) 18
De 56 De Saussure and Guth, Bull. Amer. Phys. Soc. **1** (1956) 21
De 56a Devons, Manning and Towle, Proc. Phys. Soc. A **69** (1956) 173
De 56c Dearnaley, Phil. Mag. **1** (1956) 821
De 56d De Pangher, HW-47284 (1956)
De 57 Deineko, Taranov and Val'ter, Zh. Eksp. Teor. Fiz. **32** (1957) 251; Zh. Eksp. Teor. Fiz. ("Soviet Physics") **5** (1957) 201
De 57a Dearnaley, Dissanaike, French and Jones, Phys. Rev. **108** (1957) 743
Di 54 Diller and Crouch, Phys. Rev. **93** (1954) 362A
Di 57 Dixon, Bielesch and Geiger, Canadian J. Phys. **35** (1957) 699
Di 57a Dickson and Salter, Nuovo Cimento **6** (1957) 235
Do 52b Dodder and Gammel, Phys. Rev. **88** (1952) 520
Do 53 Donahue, Jones, McEllistrem and Richards, Phys. Rev. **89** (1953) 824
Do 56a Doyle and Robbins, Phys. Rev. **101** (1956) 1056
Do 56b Douglas, Gasten and Mukerji, Canadian J. Phys. **34** (1956) 1097
Do 56c Douglas, Broer, Chiba, Herring and Silverstein, Phys. Rev. **104** (1956) 1059
Do 56d Dolan, Fincher, Kenny, Berko and Whitehead, Bull. Amer. Phys. Soc. **1** (1956) 339
Do 57 Dodge and Barber, Bull. Amer. Phys. Soc. **2** (1957) 377
Do 58 Douglas, Carlson, Bashkin and Broude, Bull. Amer. Phys. Soc. **3** (1958) 198
Do 58a Doke, Suzuki and Ogawa, J. Phys. Soc. Japan **13** (1958) 656
Dr 56 Dropesky and Schardt, Phys. Rev. **102** (1956) 426
Dr 56a Drever, Moljk and Scobie, Phil. Mag. **1** (1956) 942
Du 51 Duncan and Perry, Phys. Rev. **82** (1951) 809
Du 53 Dunbar Pixley, Wenzel and Whaling, Phys. Rev. **92** (1953) 649
Du 57a Dubovsky, Kamaev and Makarov, Soviet J. of Atomic Energy **2** (1957) 340
Du 57b DuMond, Annals of Phys. **2** (1957) 283
Du 58 Dunning, Butler and Bondelid, Phys. Rev. **110** (1958) 1076
Dy 53 Dyer and Bird, Australian J. Phys. **6** (1953) 45
Dz 56 Dzhelepov and Peker, Soviet Physics (Doklady) **1** (1956) 71

Eb 54 Eby, Phys. Rev. **96** (1954) 1355
Ec 37 Eckardt, Ann. Physik **29** (1937) 497
Ec 58 Eccles and Bodansky, Bull. Amer. Phys. Soc. **3** (1958) 188; and to be published
Ed 56 Edge, Nuclear Physics **2** (1956) 485
Ed 56a Edge, Australian J. Phys. **9** (1956) 429
Ed 58 Edwards, Owen and Madansky, Bull. Amer. Phys. Soc. **3** (1958) 268
Ed 58a Edge and Gemmell, Proc. Phys. Soc. A **71** (1958) 925
Eg 48 Eggler, Hughes and Huddleston, Phys. Rev. **74** (1948) 1238
Eh 51 Ehrman, Phys. Rev. **81** (1951) 412
Eh 57 Ehrenberg, Meyer-Berkhout, Hofstadter, Ravenhall and Sobottka, Bull. Amer. Phys. Soc. **2** (1957) 390
Eh 58 Ehrenberg and Hofstadter, HEPL 129 (1958)
Eh 58a Ehrenberg, Hofstadter, Meyer-Berkhout, Ravenhall and Sobottka, HEPL 149 (1908)
Ei 56 Eisberg, Phys. Rev. **102** (1956) 1104
Ek 58 Eklund and Bent, Phys. Rev. **112** (1958) 488

El 47 Elder, Motz and Davidson, Phys. Rev. **71** (1947) 917
El 48 Elliott and Bell, Phys. Rev. **74** (1948) 1869
El 49 Elliott and Bell, Phys. Rev. **76** (1949) 168
El 51a El-Bedewi, Middleton and Tai, Proc. Phys. Soc. A **64** (1951) 757
El 52 El-Bedewi, Proc. Phys. Soc. A **65** (1952) 64
El 53 Elkind, Phys. Rev. **92** (1953) 127
El 54 Elliott and Livesey, Proc. Royal Soc. A **224** (1954) 129
El 54b Elliot, McGarry and Faust, Phys. Rev. **93** (1954) 1348
El 55 Elliot and Flowers, Proc. of the Glasgow Conference (Pergamon Press, 1955)
El 55a Elliott and Flowers, Proc. Royal Soc. A **229** (1955) 536
El 56 Elliott, Phys. Rev. **101** (1956) 1212
El 56a El-Bedewi, Proc. Phys. Soc. A **69** (1956) 221
El 56b Elliott, Phil. Mag. **1** (1956) 503
El 56c Elliott, Physica **22** (1956) 1156A
El 57 El Nadi, Proc. Phys. Soc. A **70** (1957) 62
El 57a El-Bedewi and Hussein, Proc. Phys. Soc. A **70** (1957) 233
El 57b Elliott and Flowers, Proc. Royal Soc. A **242** (1957) 57
El 57c Elpidinskii, Shapiro and Stranikh, Soviet J. of Atomic Energy, Suppt. 5 (1957) 56
El 58 Elton, Nuclear Physics **5** (1958) 173
El 58a El Nadi and Hadid, Nuclear Physics **8** (1958) 51
En 52 Endt, Paris, Jongerius and Valckx, Physica **18** (1952) 423
En 57a Endt and Braams, Revs. Mod. Phys. **29** (1957) 683
Ep 53 Eppling, Cameron, Davis, Divatia, Galonsky, Goldberg and Hill, Phys. Rev. **91** (1953) 438A
Er 53 Erdös, Scherrer and Stoll, Helv. Phys. Acta **26** (1953) 207
Er 53a Erdman and Barnes, Proc. Royal Soc. Canada **47** (1953) 131A
Er 54 Erdös, Stoll, Wächter and Wataghin, Nuovo Cimento **12** (1954) 639
Er 54d Eriksen and Zaleski, J. Rad. Phys. **15** (1954) 492
Er 56a Eriksson, Nuclear Physics **2** (1956) 91
Er 57 Erdös, Scherrer and Stoll, Helv. Phys. Acta **30** (1957) 639
Ev 49 Evans, Malich and Risser, Phys. Rev. **75** (1949) 1161
Ev 53 Evans, Green and Middleton, Proc. Phys. Soc. A **66** (1953) 108
Ev 54 Evans and Parkinson, Proc. Phys. Soc. A **67** (1954) 684
Ev 58 Evans and French, Phys. Rev. **109** (1958) 1272

Fa 53 Famularo and Phillips, Phys. Rev. **91** (1953) 1195
Fa 53a Fagg and Hanna, Phys. Rev. **92** (1953) 372
Fa 54a Fader and Sperduto, Phys. Rev. **94** (1954) 748A
Fa 54d Fader, M.I.T. Progress Report, May (1954)
Fa 55 Farney, Givin, Kern and Hahn, Phys. Rev. **97** (1955) 720
Fa 56 Farwell and Kerlee, Bull. Amer. Phys. Soc. **1** (1956) 20
Fa 56a Fabricand, Allison and Halpern, Phys. Rev. **103** (1956) 1755
Fa 57 Fallieros and Ferrell, Bull. Amer. Phys. Soc. **2** (1957) 26
Fa 57a Farley and White, Nuclear Physics **3** (1957) 561, 692
Fa 57b Faull, AERE R/R 1919 (1956); Physics Abstracts 7393 (1956)
Fa 58 Fallieros and Ferrell, Bull. Amer. Phys. Soc. **3** (1958) 49
Fa 59a Farmer and Class. Bull. Amer. Phys. Soc. **4** (1959) 95
Fe 40 Ferguson and Walker, Phys. Rev. **58** (1940) 666
Fe 51b Feingold, Revs. Mod. Phys. **23** (1951) 10
Fe 52 Ferguson and Montague, Phys. Rev. **87** (1952) 215A
Fe 54 Ferguson, Halpern, Nathans and Yergin, Phys. Rev. **95** (1954) 776
Fe 55a Ferrell and Visscher, Phys. Rev. **100** (1955) 1796A
Fe 56 Feingold, Phys. Rev. **101** (1956) 258
Fe 56a Ferguson and Gove, Bull. Amer. Phys. Soc. **1** (1956) 180
Fe 56b Ferrell and Visscher, Phys. Rev. **102** (1956) 450
Fe 56c Ferguson, Clarke, Gove and Sample, PD-261 (1956)

Fe 56d Ferrell and Visscher, Phys. Rev. **104** (1956) 475
Fe 57a Ferguson, Gove, Litherland, Almqvist and Bromley, Bull. Amer. Phys. Soc. **2** (1957) 51
Fe 57b Feingold, Phys. Rev. **105** (1957) 944
Fe 57c Feingold, Bull. Amer. Phys. Soc. **2** (1957) 392
Fe 57d Ferrell, Phys. Rev. **107** (1957) 1631
Fe 58 Ferguson, Bull. Amer. Phys. Soc. **3** (1958) 26
Fe 58a Ferrell, Bull. Amer. Phys. Soc. **3** (1958) 49
Fe 58b Ferrell, Conference on Photonuclear Reactions, National Bureau of Standards (1958)
Fe 58c Ferguson, Gove, Kuehner, Litherland, Almqvist and Bromley, Phys. Rev. Lett. **1** (1958) 414
Fe 59a Ferguson, Clarke and Gove, Phys. Rev. (1959)
Fe 59b Ferguson, Phys. Rev. (1959)
Fi 53 Fireman, Phys. Rev. **91** (1953) 922
Fi 54b Fischer, UCRL 2546 (1954)
Fi 54d Finke, UCRL 2789 (1954)
Fi 55 Fiehrer, Lehmann, Leveque and Pick, C. Rendus **241** (1955) 1746
Fi 57 Fischer, Bull. Amer. Phys. Soc. **2** (1957) 28
Fi 57a Fischer, Phys. Rev. **108** (1957) 99
Fi 57b Fischer and Fischer, Bull. Amer. Phys. Soc. **2** (1957) 182
Fi 58 Fischer and Fischer, Bull. Amer. Phys. Soc. **3** (1958) 199
Fl 51 Flowers, Proc. Royal Soc. A **204** (1951) 503
Fl 53 Flack and Warren, Proc. Royal Soc. Canada **47** (1953) 131A
Fl 54a Florian, Urban and Wildermuth, Zeits. für Natur. **9a** (1954) 748
Fl 56 Flynn, Glendenin and Steinberg, Phys. Rev. **101** (1956) 1492
Fl 56a Flerov and Talyzin, Soviet J. of Nuclear Energy **4** (1956) 617
Fo 47b Fowler, Burrows and Curry, Nature **159** (1947) 569
Fo 49b Fowler and Lauritsen, Phys. Rev. **76** (1949) 314
Fo 54 Foster, Stanford and Lee, Phys. Rev. **93** (1954) 1069
Fo 54c Forster and Oswald, Phys. Rev. **96** (1954) 1030
Fo 55 Fowler and Johnson, Phys. Rev. **98** (1955) 728
Fo 55a Fowler, Hanna and Owen, Phys. Rev. **98** (1955) 249A
Fo 55b Fowler, Burbidge and Burbidge, Astro. J. **122** (1955) 271
Fo 56a Fowler and Brolley, Revs. Mod. Phys. **28** (1956) 103
Fo 56c Fowler and Cohn, ORNL-2076 (1956)
Fo 57 Fowler and Cohn, Bull. Amer. Phys. Soc. **2** (1957) 32; ORNL 2430 (1957)
Fo 57c Foldy, Phys. Rev. **107** (1957) 1303
Fo 57d Fowler and Cohn, ORNL 2430 (1957)
Fo 58 Fowler and Cohn, Phys. Rev. **109** (1958) 89
Fo 58a Fowler, Astrophysical J. **127** (1958) 551
Fo 58b Fowler and Cohn, Bull. Amer. Phys. Soc. **3** (1958) 305
Fr 49c Freier, Lampi, Sleator and Williams, Phys. Rev. **75** (1949) 1345
Fr 50b Freier, Fulk, Lampi and Williams, Phys. Rev. **78** (1950) 508
Fr 50d French, Meyer and Treacy, Proc. Phys. Soc. A **63** (1950) 666
Fr 51b French and Treacy, Proc. Phys. Soc. A **64** (1951) 452
Fr 51c Frye and Wiedenbeck, Phys. Rev. **82** (1951) 960
Fr 51d French and Thomson, Proc. Phys. Soc. A **64** (1951) 203
Fr 52 Franzen and Likely, Phys. Rev. **87** (1952) 667
Fr 52e Fremlin, Proc. Phys. Soc. A **65** (1952) 762
Fr 53a Fry, Phys. Rev. **89** (1953) 325
Fr 53e Freemantle, Gibson, Prowse and Rotblat, Phys. Rev. **92** (1953) 1268
Fr 54a Freier and Holmgren, Phys. Rev. **93** (1954) 825
Fr 54b Frye, Phys. Rev. **93** (1954) 1086
Fr 54e Freemantle, Gibson and Rotblat, Phil. Mag. **45** (1954) 1200
Fr 54f Freemantle, Prowse and Rotblat, Phys. Rev. **96** (1954) 1268
Fr 54g Freemantle, Prowse, Hossain and Rotblat, Phys. Rev. **96** (1954) 1270

Fr 54h Freemantle, Grotdal, Gibson, McKeague, Prowse and Rotblat, Phil. Mag. **45** (1954) 1090
Fr 55 Fregeau and Hofstadter, Phys. Rev. **99** (1955) 1503
Fr 55a Freeman, Lane and Rose, Phil. Mag. **46** (1955) 17
Fr 55b Frost and Hanna, Phys. Rev. **99** (1955) 8
Fr 55d French and Raz, Phys. Rev. **98** (1955) 1523
Fr 55e Frank and Gammel, Phys. Rev. **100** (1955) 973A
Fr 55f Freeman, Phys. Rev. **99** (1955) 1446
Fr 55h French, Halbert and Pandya, Phys. Rev. **99** (1955) 1387
Fr 55i Frye, Rosen and Stewart, Phys. Rev. **99** (1955) 1375
Fr 56a Frye and Gammel, Phys. Rev. **103** (1956) 328
Fr 56b French, Phys. Rev. **103** (1956) 1391
Fr 56c Freeman, Phil. Mag. **1** (1956) 591; Physica **22** (1956) 1135A
Fr 56d Fregeau, Phys. Rev. **104** (1956) 225
Fr 56g Freeman, Prog. Nucl. Phys. **5** (1956) 38
Fr 57 French and Fujii, Phys. Rev. **105** (1957) 652
Fr 57a Freeman, Phil. Mag. **2** (1957) 628
Fr 57b Freeman and Hanna, Nuclear Physics **4** (1957) 599
Fr 58 Freeman, Hanna and Montague, Nuclear Physics **5** (1958) 148
Fr 58a Frost and Hanna, Phys. Rev. **110** (1958) 939
Fr 58b French, Tech. Report **9**, U. of Pittsburgh (1958)
Fu 38 Fünfer, Ann. Physik **32** (1938) 313
Fu 54 Fujimoto, Kikuchi and Yoshida, Prog. in Theo. Phys. **11** (1954) 264
Fu 55 Fujimoto and Hossain, Phil. Mag. **46** (1955) 542

Ga 51c Gardner, Knable and Moyer, Phys. Rev. **83** (1951) 1054
Ga 55 Galonsky, Douglas, Haeberli, McEllistrem and Richards, Phys. Rev. **98** (1955) 586
Ga 55a Galonsky and McEllistrem, Phys. Rev. **98** (1955) 590
Ga 55b Gamba and Moncassoli, Nuovo Cimento **2** (1955) 1119
Ga 56 Galonsky and Johnson, Phys. Rev. **104** (1956) 421
Ga 56a Gavrilovskii, Golovnya, Karadzhev, Klyucharev and Man'ko, Dokl. Akad. Nauk SSSR **111** (1956) 59
Ga 57 Galonsky, Moak, Traughber and Jones, Bull. Amer. Phys. Soc. **2** (1957) 51
Ga 57a Gallmann, Ph. D. Thesis, U. of Strasbourg (1957)
Ga 58 Gammel and Thaler, Phys. Rev. **109** (1958) 2041
Ga 58a Garwin, Phys. Rev. (1958)
Ge 52 Gelinas and Hanna, Phys. Rev. **86** (1952) 253
Ge 53 Gelinas and Hanna, Phys. Rev. **89** (1953) 483
Ge 53a Gell-Mann and Telegdi, Phys. Rev. **91** (1953) 169
Ge 54 Gerhart, Phys. Rev. **95** (1954) 288
Ge 55c Geer, Nelson and Wolicki, Phys. Rev. **100** (1955) 215
Ge 55d Génin, C. Rendus **240** (1955) 2514
Ge 55e Gerber, Garcia Muñoz and Maeder, Helv. Phys. Acta **28** (1955) 478
Ge 56 Gerber, Garcia Muñoz and Maeder, Phys. Rev. **101** (1956) 774
Ge 56d George, Bull. Amer. Phys. Soc. **1** (1956) 387
Ge 56e Gelinas and Hanna, Phys. Rev. **104** (1956) 1681
Ge 57 Gerstein, Niederer and Strauch, Phys. Rev. **108** (1957) 427
Ge 58 Gerhart, Phys. Rev. **109** (1958) 897
Ge 58b Gell-Mann, Phys. Rev. **111** (1958) 362
Ge 58c Génin, C. Rendus **246** (1958) 1028
Ge 58d Gerhart, Schmidt, Bichsel and Hopkins, Bull. Amer. Phys. Soc. **3** (1958) 406
Ge 59a Gemmell, Morton and Titterton, (1959)
Gi 52 Gibson and Thomas, Proc. Royal Soc. A **210** (1952) 543
Gi 53 Gibson, Phil. Mag. **44** (1953) 297
Gi 53a v. Gierke, Zeits. für Natur. **8a** (1953) 567
Gi 54 Gilbert, Phys. Rev. **93** (1954) 499

Gi 54b v. Gierke, Zeits. für Natur. **9a** (1954) 164
Gi 54c Givin, Farney, Hahn and Kern, Phys. Rev. **96** (1954) 1337
Gi 55 Gilbert, Phys. Rev. **98** (1955) 275A
Gi 55a Gibson and Prowse, Phil. Mag. **46** (1955) 807
Gi 57 Gibson, Prowse and Rotblat, Proc. Roy. Soc. **243** (1957) 237
Gi 58 Gibbons and Macklin, Bull. Amer. Phys. Soc. **3** (1958) 26
Gi 59 Gibbons and Macklin, Phys. Rev. (1959)
Gi 59a Gibbons, Macklin, Marion and Schmitt, Phys. Rev. (1959)
Gl 52a Glenn, Phys. Rev. **88** (1952) 418
Gl 53 Glättli and Stoll, Helv. Phys. Acta **26** (1953) 428
Gl 55 Glättli, Loepfe and Stoll, Helv. Phys. Acta **28** (1955) 366
Gl 56 Glashow and Selove, Phys. Rev. **102** (1956) 200
Gl 56a Glassgold and Galonsky, Phys. Rev. **103** (1956) 701
Gl 57 Glassgold and Kellogg, Phys. Rev. **107** (1957) 1372
Gl 58 Glassgold and French, Phys. Rev. **109** (1958) 1291
Go 51a Gove and Harvey, Phys. Rev. **82** (1951) 658
Go 52 Goward and Wilkins, Proc. Phys. Soc. A **65** (1952) 671
Go 53f Goward and Wilkins, Proc. Royal Soc. A **217** (1953) 357
Go 54b Goldemberg and Katz, Canadian J. Phys. **32** (1954) 49
Go 54c Good, Kunz and Moak, Phys. Rev. **94** (1954) 87
Go 54d Gow and Alvarez, Phys. Rev. **94** (1954) 365
Go 54f Goldemberg and Katz, Phys. Rev. **95** (1954) 471
Go 54h Goldring, Proc. Phys. Soc. A **67** (1954) 930
Go 55 Gove and Paul, Phys. Rev. **97** (1955) 104
Go 55a Gorodetzky, Armbruster, Chevallier and Gallmann, C. Rendus **239** (1954) 1623
Go 55b Goward and Wilkins, Proc. Royal Soc. **228** (1955) 376
Go 55c Gossett, Phillips and Eisinger, Phys. Rev. **98** (1955) 724
Go 55d Gorodetzky, Muller and Port, C. Rendus **240** (1955) 2224
Go 55e Gossett, Phillips, Schiffer and Windham, Phys. Rev. **100** (1955) 203
Go 55f Gorodetzky, Armbruster, Chevallier, Gallman and Manquenouille, C. Rendus **241** (1955) 482, 698; J. Phys. Rad. **16** (1955) 594
Go 55g Gorodetzky, Muller and Port, C. Rendus **240** (1955) 1704
Go 55i Gorodetzky, Gallman, Croissiaux and Armbruster, C. Rendus **241** (1955) 1743
Go 56 Good, Neiler and Gibbons, Bull. Amer. Phys. Soc. **1** (1956) 71
Go 56a Goldman, Visscher and Ferrell, Bull. Amer. Phys. Soc. **1** (1956) 17
Go 56c Gorodetzky, Muller and Port, C. Rendus **242** (1956) 1281; J. Phys. Rad. **17** (1956) 549
Go 56d Gorodetzky, Armbruster, Chevallier and Gallman, C. Rendus **242** (1956) 898
Go 56e Gove, Litherland, Almqvist and Bromley, Phys. Rev. **103** (1956) 835
Go 56f Gorodetzky, Gallman and Croissiaux, J. Phys. Rad. **17** (1956) 550; Physica **22** (1956) 1160A
Go 56g Gorodetzky, Armbruster, Chevallier and Gallmann, J. Phys. Rad. **17** (1956) 548
Go 56h Gorodetzky, Gallmann, Croissiaux and Armbruster, C. Rendus **242** (1956) 2545
Go 56i Gorodetzky, Muller and Port, Physica **22** (1956) 1159A
Go 56j Gorodetzky, Armbruster and Chevallier, Physica **22** (1956) 1159A
Go 56k Gol'danskii, Physica **22** (1956) 1143A
Go 56l Gol'danskii, Zh. Eksp. Teor. Fiz. **30** (1956) 969; Soviet Physics **3** (1956) 791
Go 56m Gorlov, Gokhberg, Morozov and Otroshchenko, Dokl. Akad. Nauk **110** (1956) 963; Soviet Physics "Doklady" (1956) 598
Go 56n Gorlov, Gokhberg, Morozov and Otroshchenko, Dokl. Akad. Nauk **111** (1956) 791
Go 57 Good and Lauer, Phys. Rev. **105** (1957) 213
Go 57a Goldman and Ferrell, Bull. Amer. Phys. Soc. **2** (1957) 27
Go 57b Gove, Litherland, Almqvist, Bromley and Ferguson, Bull. Amer. Phys. Soc. **2** (1957) 51
Go 57d Goldring, Wolfson and Wiener, Phys. Rev. **107** (1957) 1667

Go 57e Gorodetzky, Gallmann, Croissiaux and Armbruster, C. Rendus **244** (1957) 62
Go 57f Gooding, Bull. Amer. Phys. Soc. **2** (1957) 350
Go 57h Gorodetzky, Gallmann, Croissiaux and Armbruster, Nuclear Physics **4** (1957) 112
Go 57i Gorodetzky, Gallmann, Croissiaux and Armbruster, C. Rendus **244** (1957) 1759
Go 57j Goldemberg, An. Acad. Bras. Cienc. **29** (1957) 23
Go 58 Goodman and Lee, Bull. Amer. Phys. Soc. **3** (1958) 37
Go 58a Gove, Litherland and Ferguson, Bull. Amer. Phys. Soc. **3** (1958) 36
Go 58b Gove and Litherland, Bull. Amer. Phys. Soc. **3** (1958) 199
Go 58c Goldman and Ferrell, Bull. Amer. Phys. Soc. **3** (1958) 206
Go 58d Gorodetzky, Gallmann, Croissiaux and Armbruster, Nuclear Physics **6** (1958) 517; J. Phys. Rad. **19** (1958) 16
Go 58e Goodman and Need, Phys. Rev. **110** (1958) 676
Go 58f Gorodetzky and Knipper, J. Phys. Rad. **19** (1958) 83
Go 58g Gove, Kuehner, Litherland, Almqvist, Bromley, Ferguson, Rose, Bastide, Brooks and Connor, Phys. Rev. Lett. **1** (1958) 251
Go 58h Gorodetzky, Chevallier, Armbruster, Sutter and Gallmann, Nuclear Physics **8** (1958) 412
Gr 49a Grosskreutz, Phys. Rev. **76** (1949) 482
Gr 50 Grosskreutz and Mather, Phys. Rev. **77** (1950) 580
Gr 51 Graves, Phys. Rev. **84** (1951) 1250
Gr 52 Graves, Phys. Rev. **85** (1952) 703A
Gr 54 Greenberg, Taylor and Haslam, Phys. Rev. **95** (1954) 1540
Gr 54a Grant, Flack, Rutherglen and Deuchars, Proc. Phys. Soc. A **67** (1954) 751
Gr 54b Graue, Phil. Mag. **45** (1954) 1205
Gr 54c Grabowsky and Natanson, Bull. Ac. Pol. Sci. **2** (1954) 379
Gr 55 Graetzer and Pollard, Phys. Rev. **98** (1955) 1184A
Gr 55a Greenlees, Proc. Phys. Soc. A **68** (1955) 97
Gr 55b Graves and Davis, Phys. Rev. **97** (1955) 1205
Gr 55d Griffith, Phys. Rev. **98** (1955) 579
Gr 55f Green, Scanlon and Willmott, Proc. Phys. Soc. A **68** (1955) 386
Gr 55g Groshev, Adyasevich and Demidov, U.N. A/Conf. 8/P/651 (1955)
Gr 56 Grosskreutz, Phys. Rev. **101** (1956) 706
Gr 56a Griffiths, Canadian J. Phys. **34** (1956) 339
Gr 56b Green and Middleton, Proc. Phys. Soc. A **69** (1956) 28
Gr 56e Greider, Bull. Amer. Phys. Soc. **1** (1956) 376
Gr 56f Graue, Phil. Mag. **1** (1956) 1027
Gr 56g Grechukhin, Zh. Eksp. Teor. Fiz. **31** (1956) 895; Soviet Physics **4** (1957) 759
Gr 57 Gross, Bull. Amer. Phys. Soc. **2** (1957) 14
Gr 57a Graue and Trumpy, Phil. Mag. **2** (1957) 138
Gr 57b Grismore and Parkinson, Revs. Sci. Instr. **28** (1957) 245
Gr 57c Griffin, Phys. Rev. **108** (1957) 328
Gr 57d Groshev and Demidov, Soviet J. of Atomic Energy **3** (1957) 853
Gr 57e Grechukhin, Zh. Eksp. Teor. Fiz. **32** (1957) 1460
Gr 57f Greenlees, Kuo and Petravić, Proc. Roy. Soc. **243** (1957) 206
Gr 58 Griffiths, Proc. Phys. Soc. A **72** (1958) 337
Gu 47 Guggenheimer, Heitler and Powell, Proc. Royal Soc. A **190** (1947) 196
Gu 49a Guth and Mullin, Phys. Rev. **76** (1949) 234
Gu 52 Guier, Bertini and Roberts, Phys. Rev. **85** (1952) 426
Gu 53a Gurewitsch, Diss. E.T.H. Zürich, Paper 2205 (1953); Physics abstracts **3103** (1955)

Ha 59c Hayward, Phys. Rev. **75** (1949) 917
Ha 49j Hamermesh, Hamermesh and Wattenberg, Phys. Rev. **76** (1949) 611
Ha 50 Hall and Fowler, Phys. Rev. **77** (1950) 197
Ha 50f Harris, Phys. Rev. **80** (1950) 20
Ha 51a Harvey, Phys. Rev. **82** (1951) 298;

M.I.T. Progress Report (LNSE), January (1951)
Ha 51e Haefner, Revs. Mod. Phys. **23** (1951) 228
Ha 51f Halpern and Mann, Phys. Rev. **83** (1951) 370
Ha 52e Hahn, Snyder, Willard, Bair, Klema, Kington and Green, Phys. Rev. **85** (1952) 934
Ha 52g Halpern, Mann and Rothman, Phys. Rev. **87** (1952) 164
Ha 53 Haslam, Katz, Crosby, Summers-Gill and Cameron, Canadian J. Phys. **31** (1953) 210
Ha 53b Hamermesh and Kimball, Phys. Rev. **90** (1953) 1063
Ha 53g Hamermesh, Ringo and Wexler, Phys. Rev. **90** (1953) 603
Ha 54a Harries, Proc. Phys. Soc. A **67** (1954) 153
Ha 54f Haslam, Physics in Canada **10** (1954) 1, 52
Ha 55 Hahn, Kern and Farney, Phys. Rev. **98** (1955) 1183A
Ha 55b Harding, Proc. Phys. Soc. A **68** (1955) 52
Ha 55c Hanna, Phil. Mag. **46** (1955) 381
Ha 55d Haeberli, Phys. Rev. **99** (1955) 640A
Ha 55e Hale and Present, Phys. Rev. **99** (1955) 1366
Ha 55g Havliček and Dobovišek, Phys. Rev. **100** (1955) 1355
Ha 56 Harlow, Marion, Chapman and Bonner, Phys. Rev. **101** (1956) 214
Ha 56a Hall and Bonner, Bull. Amer. Phys. Soc. **1** (1956) 96
Ha 56c Haffner, Phys. Rev. **103** (1956) 1398
Ha 56g Hayakawa, Hayashi, Imoto and Kikuchi, Prog. in Theo. Phys. **16** (1956) 507
Ha 56h Hayashi and Nishida, Prog. in Theo. Phys. **16** (1956) 613
Ha 57 Hagedorn, Mozer, Webb, Fowler and Lauritsen, Phys. Rev. **105** (1957) 219
Ha 57b Halbert and French, Phys. Rev. **105** (1957) 1563
Ha 57c Haeberli and Rolland, Bull. Amer. Phys. Soc. **2** (1957) 234
Ha 57d Hagedorn, Phys. Rev. **108** (1957) 735
Ha 57e Hayward and Fuller, Phys. Rev. **106** (1957) 991
Ha 57f Hagedorn and Marion, Phys. Rev. **108** (1957) 1015
Ha 57g Hanna and Preston, Phys. Rev. **108** (1957) 160
Ha 57h Harmon and Curtis, Bull. Amer. Phys. Soc. **2** (1957) 350
Ha 57i Harrison and Curtis, Bull. Amer. Phys. Soc. **2** (1957) 350
Ha 57k Hanna and Meyer-Schützmeister, Phys. Rev. **108** (1957) 1644
Ha 58 Hamilton, Langer and Smith, Phys. Rev. **112** (1958) 2010
Ha 58a Hamburger and Hamburger, Bull. Amer. Phys. Soc. **3** (1958) 187, 222
Ha 58b Hall and Eden, Nuclear Physics **6** (1958) 157
Ha 58c Haddad, Perry and Smith, private communication (1958)
Ha 58d Haig, Nuclear Physics **7** (1958) 429
Ha 58e Hamburger and Cameron, Bull. Amer. Phys. Soc. **3** (1958) 381
He 48a Heydenburg and Inglis, Phys. Rev. **73** (1948) 230
He 48e Heydenburg, Hudson, Inglis and Whitehead, Phys. Rev. **74** (1948) 405
He 48g Heydenburg, Hudson, Inglis and Whitehead, Phys. Rev. **73** (1948) 241
He 49 Herb, Snowden and Sala, Phys. Rev. **75** (1949) 246
He 50b Henkel and Barschall, Phys. Rev. **80** (1950) 145
He 52a Heusinkveld and Freier, Phys. Rev. **85** (1952) 80
He 53 Heydenburg and Temmer, Phys. Rev. **92** (1953) 89
He 53a Hendel, Zeits. f. Phys. **135** (1953) 168
He 54b Heydenburg and Temmer, Phys. Rev. **94** (1954) 1252
He 54c Heiberg, Phys. Rev. **96** (1954) 856A
He 55 Heiberg, James and Alexander, Canadian J. Phys. **33** (1955) 34
He 55a Hemmendinger and Argo, Phys. Rev. **98** (1955) 70
He 55c Heinrich and Rubin, Helv. Phys. Acta **28** (1955) 185
He 55d Henkel, Perry and Smith, Phys. Rev. **99** (1955) 1050
He 55e Heft and Libby, Phys. Rev. **100** (1955) 799
He 55f Herzenberg, Nuovo Cimento **1** (1955) 986, 1008
He 56 Hemmendinger, Bull. Amer. Phys. Soc. **1** (1956) 96
He 56a Henry, Phillips, Reich and Russell, Bull. Amer. Phys. Soc. **1** (1956) 96
He 56b Heydenburg and Temmer, Phys. Rev. **104** (1956) 123

He 56d Hereford, McCormac, Steuer and Bond, Bull. Amer. Phys. Soc. **1** (1956) 339
He 56e Helm, Phys. Rev. **104** (1956) 1466
He 57b Herzenberg, Nuclear Physics **3** (1957) 1
He 57c Heiberg, Phys. Rev. **106** (1957) 1271
He 57f Hebbard, Ph. D. Thesis, U. of Melbourne (1957)
He 58 Herrmannsfeldt, Stahelin and Allen, Bull. Amer. Phys. Soc. **3** (1958) 52
He 58a Henley, Conference on Photonuclear Reactions, National Bureau of Standards (1958)
He 58b Hensel and Parkinson, Phys. Rev. **110** (1958) 128
He 58c Herrmannsfeldt, Burman, Stahelin, Allen and Braid, Phys. Rev. Lett. **1** (1958) 61
He 58d Herring, Chiba, Gasten and Richards, Phys. Rev. **112** (1958) 1210
He 58e Herring, Phys. Rev. **112** (1958) 1217
He 58f Hebbard and Dunbar, Bull. Amer. Phys. Soc. **3** (1958) 322
He 58g Hebbard, Bull. Amer. Phys. Soc. **3** (1958) 406
He 58h Hester, Pixley and Lamb. Phys. Rev. **111** (1958) 1604
He 59 Herrmannsfeldt, Burman, Stahelin, Allen and Braid, Bull. Amer. Phys. Soc. **4** (1959) 77
He 59a Hebbard and Dunbar, Phys. Rev. (1959)
Hi 51 Hibdon and Muehlhause, A.N.L. 4680 (September, 1951)
Hi 52 Hinchey, Stelson and Preston, Phys. Rev. **86** (1952) 483
Hi 53a Hill, Phys. Rev. **90** (1953) 845
Hi 54b Hirst, Johnstone and Poole, Phil. Mag. **45** (1954) 762
Hi 54e Hird, Whitehead, Butler and Collie, Phys. Rev. **96** (1954) 702
Hi 55 Hibdon and Langsdorf, Phys. Rev. **98** (1955) 223A
Hi 55a Hill and Blair, Phys. Rev. **100** (1955) 961A
Hi 55b Hintz, Phys. Rev. **100** (1955) 1794A
Hi 55c Hittmair, Zeits. f. Phys. **143** (1955) 465
Hi 56a Hittmair, Zeits. f. Phys. **144** (1956) 449
Hi 56b Hillman, Phys. Rev. **104** (1956) 176
Hi 56c Hill and Blair, Phys. Rev. **104** (1956) 198
Hi 57 Hintz, Bull. Amer. Phys. Soc. **2** (1957) 14
Hi 57a Hintz, Phys. Rev. **106** (1957) 1201
Hi 57b Hillman, Johansson and Tyrén, Nuclear Physics **4** (1957) 648
Hi 58 Hill, Phys. Rev. **109** (1958) 2105
Hi 58a Hird, Cookson and Bokhari, Proc. Phys. Soc. A **72** (1958) 489
Hi 59 Hinds and Middleton, Proc. Phys. Soc. (1959)
Hj 53 Hjalmar and Slätis, Phys. Rev. **89** (1953) 1151
Hj 53a Hjalmar and Slätis, Ark. F. fysik **6** (1953) 451
Ho 40 Holloway and Moore, Phys. Rev. **58** (1940) 847
Ho 50 Hornyak and Lauritsen, Phys. Rev. **77** (1950) 160
Ho 50b Hornyak, Lauritsen, Morrison and Fowler, Revs. Mod. Phys. **22** (1950) 291
Ho 52a Horsley, Haslam and Johns, Phys. Rev. **87** (1952) 756
Ho 52b Holt, Thorn and Waniek, Phys. Rev. **87** (1952) 378
Ho 52f Hodgson, Gallagher and Bowe, Proc. Phys. Soc. A **65** (1952) 992
Ho 53a Hollander, Perlman and Seaborg, Revs. Mod. Phys. **25** (1953) 469
Ho 53b Hornyak and Coor, Phys. Rev. **92** (1953) 675
Ho 53c Holt and Marsham, Proc. Phys. Soc. A **66** (1953) 1032
Ho 53e Hofstadter, Fechter and McIntyre, Phys. Rev. **92** (1953) 978
Ho 54c Holmgren, Blair, Simmons, Stratton and Stuart, Phys. Rev. **95** (1954) 1544
Ho 54g Hochberg, Massey and Underhill, Proc. Phys. Soc. A **67** (1954) 957
Ho 55c Holmgren, Hanscome and Willett, Phys. Rev. **98** (1955) 241A
Ho 55f Holland, Inglis, Malm and Mooring, Phys. Rev. **99** (1955) 92
Ho 55g Hornyak and Sherr, Phys. Rev. **100** (1955) 1409
Ho 55i Holmgren, Bullock and Kunz, Phys. Rev. **100** (1955) 436
Ho 55j Hochberg, Massey, Robertson and Underhill, Proc. Phys. Soc. A **68** (1955) 746
Ho 56a Holm and Argo, Phys. Rev. **101** (1956) 1772

Ho 56c Hornyak, Bull. Amer. Phys. Soc. **1** (1956) 197
Ho 56d Holmgren, Bullock and Kunz, Phys. Rev. **104** (1956) 1446
Ho 56e Hofstadter, Revs. Mod. Phys. **28** (1956) 214
Ho 56g Holmgren, Johnston, Geer and Wolicki, Physica **22** (1956) 1156A
Ho 57 Holmgren, Phys. Rev. **106** (1957) 100
Ho 57a Holmgren, Geer, Johnston and Wolicki, Phys. Rev. **106** (1957) 102
Ho 57b Holmgren, Wolicki and Johnston, Bull. Amer. Phys. Soc. **2** (1957) 181
Ho 57c Hossain and Prowse, Nuovo Cimento **5** (1957) 973
Ho 57d Hossain and Syeduzzaman, Nuclear Physics **4** (1957) 88
Ho 57e Hossain and Kamal, Phys. Rev. **108** (1957) 390
Ho 57f Hofstadter and Burleson, Bull. Amer. Phys. Soc. **2** (1957) 390
Ho 57g Hofstadter, Annual Review of Nuclear Science, Vol. **7** (1957)
Ho 58a Hodgson, Advances in Phys. **7** (1958) 1
Ho 58b Holland, Lynch and Hanna, Phys. Rev. **112** (1958) 903
Ho 58c Howerton, UCRL 5226 (1958)
Ho 59 Holmgren and Johnston, (1959)
Hu 47 Hughes, Eggler and Huddleston, Phys. Rev. **71** (1947) 269
Hu 47a Hughes, Hall, Eggler and Goldfarb, Phys. Rev. **72** (1947) 646
Hu 49j Hudspeth and Swann, Phys. Rev. **76** (1949) 1150
Hu 50e Hudspeth, Swann and Heydenburg, Phys. Rev. **80** (1950) 643
Hu 51f Huber, Baldinger and Proctor, Helv. Phys. Acta **24** (1951) 302
Hu 52c Huber and Baldinger, Helv. Phys. Acta **25** (1952) 435
Hu 52e Hughes *et al.* AECU 2040 and Suppt. 1 (1952)
Hu 52f Hunt, Proc. Phys. Soc. A **65** (1952) 982
Hu 52l Huby and Newns, Phil. Mag. **42** (1952) 1442
Hu 53 Huus and Day, Phys. Rev. **91** (1953) 599
Hu 53a Hubbard, Ruby and Stebbins, Phys. Rev. **92** (1953) 1494
Hu 53d Hunt and Jones, Phys. Rev. **89** (1953) 1283
Hu 54a Hughes *et al.*, AECU 2040, Suppt. **3** (1954)
Hu 54b Huber and Striebel, Helv. Phys. Acta **27** (1954) 157
Hu 54c Huber and Budde, Helv. Phys. Acta **27** (1954) 512
Hu 55a Hunt and Firth, Phys. Rev. **99** (1955) 786
Hu 55b Hudspeth, Morgan and Peoples, Phys. Rev. **99** (1955) 643A
Hu 55c Hughes and Harvey, BNL 325 (1955)
Hu 55d Huber and Seitz, U.N. A/Conf. 8/P/1033 (1955)
Hu 56 Hughes and Carter, BNL 400 (1956)
Hu 56a Hubbs and Grosof, Phys. Rev. **104** (1956) 715
Hu 56b Hunt, Petrie, Firth and Trott, Proc. Inst. Elec. Engrs. **103** (1955) 146
Hu 57 Hughes and Schwartz, BNL 325, Suppt. 1 (1957)
Hu 57a Hunting and Wall, Bull. Amer. Phys. Soc. **2** (1957) 181
Hu 57b Hunt, Pope and Evans, Phys. Rev. **106** (1957) 1012
Hu 57c Huber and Wagner, Helv. Phys. Acta **30** (1957) 257
Hu 58 Hughes and Schwartz, BNL 325, Second Edition (1958)
Hy 57 Hyder, Harmon and Curtis, Bull. Amer. Phys. Soc. **2** (1957) 267

Ig 56 Igo, Wegner and Eisberg, Phys. Rev. **101** (1956) 1508
Ig 57 Igo and Thaler, Phys. Rev. **106** (1957) 126
Ih 55 Ihsan, Phys. Rev. **98** (1955) 689
Ih 55a Ihsan, Proc. Phys. Soc A **68** (1955) 393
Il 57 Illsley, Holmgren, Johnston and Wolicki, Phys. Rev. **107** (1957) 538
Im 58 Imhof, Johnson, Vaughn and Walt, Bull. Amer. Phys. Soc. **3** (1958) 322
In 48 Inglis, Phys. Rev. **74** (1948) 21
In 53 Inglis, Revs. Mod. Phys. **25** (1953) 390
In 54 Inall, Phil. Mag. **45** (1954) 768
In 57 Innes, UCRL 8040 (1957)
Ir 55 Irving and Schonland, Phys. Rev. **97** (1955) 446

Is 55 Isoya, Goto and Momota, J. Phys. Soc. Japan **10** (1955) 1022
Is 56 Isoya, Goto and Momota, J. Phys. Soc. Japan **11** (1956) 899
Is 58 Isoya, Ohmura and Momota, Nuclear Physics **7** (1958) 116
Is 58a Isoya, Nuclear Physics **7** (1958) 126
Iv 56 Ivash, Bull. Amer. Phys. Soc. **1** (1956) 84

Ja 53 Jackson and Wanklyn, Phys. Rev. **90** (1953) 381A
Ja 53b Jackson and Galonsky, Phys. Rev. **89** (1953) 370
Ja 53d Jarvis and Roaf, Proc. Royal Soc. **218** (1953) 432
Ja 54a Jancovici and Talmi, Phys. Rev. **95** (1954) 289
Ja 55 Jarmie, Phys. Rev. **98** (1955) 41
Ja 55a Jancovici, C. Rendus **240** (1955) 1608
Ja 55c Jarmie, Phys. Rev. **99** (1955) 1043
Ja 55d Jancovici, Nuovo Cimento **1** (1955) 840
Ja 55e James, Kubelka, Heiberg and Warren, Canadian J. Phys. **33** (1955) 219
Ja 56a James, Jones and Wilkinson, Phil. Mag. **1** (1956) 949
Ja 56c Jancovici, C. Rendus **242** (1956) 883
Ja 56e Jarmie, Phys. Rev. **104** (1956) 1683
Ja 57 Jarmie, Seagrave *et al.*, Los Alamos Report 2014 (1957)
Ja 57b Jannelli and Mezzanares, Nuovo Cimento **5** (1957) 1047
Ja 58 Jarmie and Allen, Phys. Rev. **111** (1958) 121
Je 48c Jelley and Paul, Proc. Cambridge Phil. Soc. **44** (1948) 133
Je 50d Jelley and Paul, Proc. Phys. Soc. A **63** (1950) 112
Je 53b Jensen and Gis, Zeits. für Natur. **8a** (1953) 137
Je 55 Jennings, Weddell, Alexeff and Hellens, Phys. Rev. **98** (1955) 582
Jo 50a Johnson, Ajzenberg and Laubenstein, Phys. Rev. **79** (1950) 187
Jo 50b Johnson and Barschall, Phys. Rev. **80** (1950) 818
Jo 51a Johnson, Petree and Adair, Phys. Rev. **84** (1951) 775
Jo 51b Johns, Horsley, Haslam and Quinton, Phys. Rev. **84** (1951) 856
Jo 51d Jones and Wilkinson, Proc. Phys. Soc. A **64** (1951) 756
Jo 51e Johnson, Bockelman and Barschall, Phys. Rev. **82** (1951) 117
Jo 52a Johnson, Phys. Rev. **86** (1952) 302
Jo 52b Johnson, Robinson and Moak, Phys. Rev. **85** (1952) 931
Jo 52d Jones and Wilkinson, Phys. Rev. **88** (1952) 423
Jo 52e Jones and Wilkinson, Proc. Phys. Soc. A **65** (1952) 1055
Jo 53e Jones and Wilkinson, Proc. Phys. Soc. A **66** (1953) 1176
Jo 53f Jones and Terwilliger, Phys. Rev. **91** (1953) 699
Jo 54 Jones and Wilkinson, Phil. Mag. **45** (1954) 230
Jo 54b Johnson and Jones, Phys. Rev. **93** (1954) 1286
Jo 54c Jongerius, Valckx and Endt, Physica **20** (1954) 29
Jo 54d Jones Douglas, McEllistrem and Richards, Phys. Rev. **94** (1954) 947
Jo 54e Jones and Wilkinson, Phil. Mag. **45** (1954) 703
Jo 54f Johnson, Willard and Bair, Phys. Rev. **96** (1954) 985
Jo 54g Jones, Phillips, Johnson and Wilkinson, Phys. Rev. **96** (1954) 547
Jo 55 Jones, Proc. of the Glasgow Conference (Pergamon Press, 1955)
Jo 55b Johnson and Porter, Phys. Rev. **99** (1955) 630A
Jo 55c Johansson and Forkman, Phys. Rev. **99** (1955) 1031
Jo 55f Johansson, Phys. Rev. **97** (1955) 434
Jo 56 Johnston and Holmgren, Bull. Amer. Phys. Soc. **1** (1956) 21
Jo 56a Johnston and Holmgren, Bull. Amer. Phys. Soc. **1** (1956) 134
Jo 56c Johnston, Wolicki, Geer and Holmgren, Bull. Amer. Phys. Soc. **1** (1956) 197
Jo 56d Johnson, Phil. Mag. **1** (1956) 573
Jo 56e Jones, Weil, Kruse, Baicker and Lidofsky, Bull. Amer. Phys. Soc. **1** (1956) 326
Jo 56f Johansson, Physica **22** (1956) 1144A
Jo 57a Johnston and Bostrom, Bull. Amer. Phys. Soc. **2** (1957) 104
Jo 57b Johnston, Holmgren and Wolicki, Bull. Amer. Phys. Soc. **2** (1957) 181

Jo 57c Jones and Mandl, Nuclear Physics **4** (1957) 690
Jo 58 Johnston, Holmgren, Wolicki and Illsley, Phys. Rev. **109** (1958) 884
Jo 58a Johansson, Conference on Photonuclear Reactions, National Bureau of Standards (1958)
Jo 58c Jones, Lidofsky and Weil, Phys. Rev. **112** (1958) 1252
Ju 54 Jung and Bockelman, Phys. Rev. **96** (1954) 1353
Ju 54a Jurić, Atomics and Atomic Technology **5** (1954) 333
Ju 54b Jung, Bockelman and Buechner, J. Phys. Rad. **15** (1954) 50S
Ju 55 Jurić, Phys. Rev. **98** (1955) 85
Ju 55a Jurić and Petrovič, Bull. Inst. N. Sciences "Boris Kidrich" **5** (1955) 1
Ju 55b Jurić, Bull. Inst. N. Sciences "Boris Kidrich" **5** (1955) 7
Ju 56a Juveland and Jentschke, Zeits. f. Physik **144** (1956) 521
Ju 56b Jurić, Bull. Inst. N. Sciences "Boris Kidrich" **6** (1956) 35
Ju 56c Jurić, Bull. Inst. N. Sciences "Boris Kidrich" **6** (1956) 41
Ju 56d Jurić and Ćirilov, Bull. Inst. N. Sciences "Boris Kidrich" **6** (1956) 45
Ju 56e Jung and Cüer, J. Phys. Rad. **17** (1956) 555
Ju 56f Jung and Cüer, Physica **22** (1956) 1159A
Ju 56g Jurić, Physica **22** (1956) 1154A
Ju 57 Jurić, Bull. Inst. N. Sciences "Boris Kidrich" **7** (1957) 1
Ju 58 Juveland and Jentschke, Phys. Rev. **110** (1958) 456
Ju 58a Jurić and Zarubica, Bull. Inst. N. Sciences "Boris Kidrich" **8** (1958) 17
Ju 58b Jurić and Ćirilov, Phys. Rev. **112** (1958) 1224

Ka 52a Kavadiniz, Rev. Faculté Sci. Univ. Istanbul A **17** (1952) 1;
Nucl. Sci. Abs. 6—5192
Ka 53 Kay, Mark and Goodman, Phys. Rev. **91** (1953) 472A
Ka 54a Katz, Haslam, Horsley, Cameron and Montalbetti, Phys. Rev. **95** (1954) 464
Ka 56 Kavanagh, Ph. D. Thesis, California Institute of Technology (1956)
Ka 56a Kameny, Phys. Rev. **103** (1956) 358
Ka 56b Kalos and Goldstein, NDA 12—16 (1956)
Ka 56c Kassecker and Urban, Acta Phys. Austriaca **10** (1956) 95
Ka 56d Katcoff and Hudis, J. Inorganic Nuclear Chem. **3** (1956) 253
Ka 57 Kajikawa and Watari, Prog. in Theo. Phys. **18** (1957) 103
Ka 57a Kalinin, Ogloblin and Petrov, Soviet J. of Atomic Energy **2** (1957) 193
Ka 57b Katsaurov, Musaelian and Popov, Soviet J. of Atomic Energy, Suppt. **5** (1957) 67
Ka 58 Kavanagh, Bull. Amer. Phys. Soc. **3** (1958) 316
Ka 58a Kavanagh and Barnes, Phys. Rev. **112** (1958) 503
Ka 58b Katz, Conference on Photonuclear Reactions, National Bureau of Standards (1958)
Ka 58c Kashy, Miller and Risser, Phys. Rev. **112** (1958) 547
Ka 58d Kane, Elwyn, Ofer and Wilkinson, Bull. Amer. Phys. Soc. **3** (1958) 381
Ke 51b Keller, Niedner, Wang and Shull, Phys. Rev. **81** (1951) 481
Ke 57b Kendall and Meyer-Berkhout, Bull. Amer. Phys. Soc. **2** (1957) 378
Ke 58 Kern and Kreger, Bull. Amer. Phys. Soc. **3** (1958) 187
Ke 58a Kern and Kreger, Phys. Rev. **112** (1958) 926
Kh 53 Khromchenko, Dokl. Akad. Nauk. USSR, **93** (1953) 451
Kh 54 Khromchenko, Dokl. Akad. Nauk **94** (1954) 1037
Kh 55 Khromchenko and Blinov, Zh. Eksp. Teor. Fiz. **28** (1955) 741
Zh. Eksp. Teor. Fiz. ("Soviet Physics") **1** (1955) 596
Kh 55a Khromchenko, Iszv. Akad. Nauk **19** (1955) 277
Kh 57 Khromchenko, Zh. Eksp. Teor. Fiz. **32** (1957) 194
Zh. Eksp. Teor. Fiz. ("Soviet Physics") **5** (1957) 231
Kh 57a Khaletskii, Dokl. Akad. Nauk **113** (1957) 305;
Soviet Physics "Doklady" **2** (1958) 129
Kh 57b Khaletskii, Dokl. Akad. Nauk **113** (1957) 553;
Soviet Physics "Doklady" **2** (1958) 152
Ki 39 King, Henderson and Risser, Phys. Rev. **55** (1939) 1118

Ki 51 Kinsey, Bartholomew and Walker, Canadian J. Phys. **29** (1951) 1
Ki 51a Kinsey, Bartholomew and Walker, Phys. Rev. **83** (1951) 519
Ki 52 King, Dismuke and Way, ORNL 1450 (1952)
Ki 53b Kinsey and Bartholomew, Canadian J. Phys. **31** (1953) 537
Ki 53c Kimura, Ishiwara, Sakisaka, Kumabe, Yamashita and Miyake, Bull. Inst. Chem. Res. Kyoto U. **31** (1953) 204
Ki 55b Kinsey, Phys. Rev. **99** (1955) 332
Ki 55c Kington, Bair, Cohn and Willard, Phys. Rev. **99** (1955) 1393
Ki 55d Kington, Bair, Cohn and Willard, ORNL 1975 (1955)
Ki 56 Kinsey and Stone, Phys. Rev. **103** (1956) 975
Ki 56a ura, Kumabe, Miyake, Ogata and Miyasita, J. Phys. Soc. Japan **11** (1956) 1211
Ki 56b slinger, Phys. Rev. **104** (1956) 1077
Ki 57 Kistner, Schwarzschild, Rustad and Alburger, Phys. Rev. **105** (1957) 1339
Ki 57a Kiselev and Fliagin, Zh. Eksp. Teor. Fiz. **32** (1957) 962; Zh. Eksp. Teor. Fiz. ("Soviet Physics") **5** (1957) 786
Kl 54 Kline and Zaffarano, Phys. Rev. **96** (1954) 1620
Kl 56 Kliucharev, Bolotin and Lutsik, Zh. Eksp. Teor. Fiz. ("Soviet Physics") **3** (1956) 463; Zh. Eksp. Teor. Fiz. **30** (1956) 573
Kl 56a Kliger, Riabinkin, Chuvilo and Shevchenko, Physica **22** (1956) 1142A
Kl 56b Kliucharev, Esel'son and Val'ter, Dokl. Akad. Nauk SSSR **109** (1956) 737
Kn 48 Knable, Lawrence, Leith, Moyer and Thornton, Phys. Rev. **74** (1948) 1217A
Kn 58 Knowles, Bull. Amer. Phys. Soc. **3** (1958) 330
Kn 58a Knipper, Ph. D. Thesis, U. of Strasbourg (1958)
Ko 52 Koehler and Wollan, Phys. Rev. **85** (1952) 491
Ko 53 Kofoed-Hansen, Phys. Rev. **92** (1953) 1075
Ko 53a Koudijs, Valkcx and Endt, Physica **19** (1953) 1133
Ko 54 Korsunskii, Usp. Fiz. Nauk **52** (1954) 3
Ko 55 Kolar, UCRL 3012 (1955)
Ko 56 Koch and Turkevich, Bull. Amer. Phys. Soc. **1** (1956) 94
Ko 56a Kondaiah, Proc. Indian Acad. of Sciences **43A** (1956) 130
Ko 56d Kopaleishvili, Zh. Eksp. Teor. Fiz. **30** (1956) 1145; Soviet Physics **3** (1957) 973
Ko 56e Koltypin and Morozov, Dokl. Akad. Nauk SSSR **111** (1956) 331
Ko 56f Koudijs, Ph. D. Thesis, U. of Utrecht (1956)
Ko 57 Komar and Iavor, Zh. Eksp. Teor. Fiz. **32** (1957) 614
Ko 57a Kopaleishvili, Zh. Eksp. Teor. Fiz. **33** (1957) 788; Zh. Eksp. Teor. Fiz. ("Soviet Physics") **6** (1958) 606
Ko 57b Kopaleishvili, Zh. Eksp. Teor. Fiz. **32** (1957) 1249; Zh. Eksp. Teor. Fiz. ("Soviet Physics") **5** (1957) 1018
Ko 58 Kohler and Hilton, Phys. Rev. **110** (1958) 1094
Ko 58a Kondaiah, Iyengar and Badrinathan, Nuclear Physics **5** (1958) 346
Ko 58b Kohler, Nuclear Physics **6** (1958) 161
Ko 58d Kondo and Yamazaki, J. Phys. Soc. Japan **13** (1958) 771
Ko 59 Kohler, Ph. D. Thesis, California Institute of Technology (1959)
Kr 41 Krishnan, Nature **148** (1941) 407
Kr 50 Krone, Hanna and Inglis, Phys. Rev. **80** (1950) 603
Kr 53 Kraus, French, Fowler and Lauritsen, Phys. Rev. **89** (1953) 299
Kr 53c Kraushaar, Wilson and Bainbridge, Phys. Rev. **90** (1953) 610
Kr 54 Kravtsov, Usp. Fiz. Nauk **54** (1954) 3
Kr 54a Kraus, Phys. Rev. **93** (1954) 1308
Kr 54b Kraus, Phys. Rev. **94** (1954) 975
Kr 54c Kreger, Phys. Rev. **96** (1954) 1554
Kr 56 Kreger, Bolotin and Edelsack, USNRDL TR 81 (1956)
Kr 56a Kreger, Bolotin and Edelsack, Bull. Amer. Phys. Soc. **1** (1956) 325
Kr 57 Kruse, Bent and Eklund, Bull. Amer. Phys. Soc. **2** (1957) 29
Kr 57a Kruse, Bent and Lidofsky, Bull. Amer. Phys. Soc. **2** (1957) 351

Kr 58 Kreger and Kern, Bull. Amer. Phys. Soc. **3** (1958) 188; and Phys. Rev. (1958)
Kr 58a Kruse, Bent and Lidofsky, Bull. Amer. Phys. Soc. **3** (1958) 200
Kr 58b Kruse and Bent, Phys. Rev. **112** (1958) 931
Ku 49a Kusch, Phys. Rev. **75** (1949) 887; **76** (1949) 138
Ku 53a Kundu, Donaven, Pool and Long, Phys. Rev. **89** (1953) 1200
Ku 53b Kunz, Moak and Good, Phys. Rev. **91** (1953) 676
Ku 55 Kunz, Phys. Rev. **97** (1955) 456
Ku 55b Kunz, Butler and Holmgren, Phys. Rev. **100** (1955) 1252A
Ku 56 Kurath, Phys. Rev. **101** (1956) 216
Ku 57 Kurath, Bull. Amer. Phys. Soc. **2** (1957) 206
Ku 57a Kurath, Phys. Rev. **106** (1957) 975
Ku 58 Kuehner, Almqvist and Bromley, Bull. Amer. Phys. Soc. **3** (1958) 27
Ku 58a Kurath, Proc. of the Rehovoth Conf. (North-Holland Publishing Co., Amsterdam, 1958)
Ku 58b Kunz and Henley, Bull. Amer. Phys. Soc. **3** (1958) 323
Ku 58c Kuehner, Almqvist and Bromley, Phys. Rev. Lett. **1** (1958) 260
Ku 59 Kuehner, Litherland, Almqvist, Bromley and Gove, Phys. Rev. (1959)

La 49a Laslett, Phys. Rev. **76** (1949) 858
La 51d Laubenstein, Laubenstein, Koester and Mobley, Phys. Rev. **84** (1951) 12
La 51e Laubenstein and Laubenstein, Phys. Rev. **84** (1951) 18
La 53 Lauritsen, Huus and Nilsson, Phys. Rev. **92** (1953) 1501
La 54a Lane, AERE T/R 1289 (1954)
La 55 Lane and Wilkinson, Phys. Rev. **97** (1955) 1199
La 55a Lane, Proc. Phys. Soc. A **68** (1955) 189
La 55b Lane, Proc. Phys. Soc. A **68** (1955) 197
La 55e Larsson, Arkiv f. Fysik **9** (1955) 293
La 55h Lasich, Muirhead and Shute, Australian J. Phys. **8** (1955) 456
La 56b Lane and Monahan, Bull. Amer. Phys. Soc. **1** (1956) 187
La 56c LaVier, Hanna and Gelinas, Phys. Rev. **103** (1956) 143
La 56d Langsdorf, Lane and Monahan, ANL 5567 (1956)
La 56e Lamarsh and Feshbach, Phys. Rev. **104** (1956) 1633
La 57b Lamb and Hester, Phys. Rev. **107** (1957) 550
La 57c Langsdorf, Lane and Monahan, Phys. Rev. **107** (1957) 1077
La 57f Lamb and Hester, Phys. Rev. **108** (1957) 1304
La 58 Lauterjung, Schimmer and Maier-Leibnitz, Zeits. f. Physik **150** (1958) 657
La 58b Lauritsen, Barnes, Fowler and Lauritsen, Phys. Rev. Lett. **1** (1958) 326
La 58c Lane and Monahan, Bull. Amer. Phys. Soc. **3** (1958) 364
La 59 Lambe, Reynolds, Jovanovich and Pond, Bull. Amer. Phys. Soc. **4** (1959) 77
Le 51a Leland and Agnew, Phys. Rev. **82** (1951) 559
Le 54a Leamer and Hinman, Phys. Rev. **96** (1954) 1607
Le 55 Levine, Bender and McGruer, Phys. Rev. **97** (1955) 1249
Le 55a Lehmann, Leveque and Fiehrer, C. Rendus **241** (1955) 700
Le 55b Levintov, Miller and Šamšev, Dokl. Akad. Nauk **104** (1955) 803
Le 55d Lee and Inglis, Phys. Rev. **99** (1955) 96
Le 56a Leiss and Wyckoff, Bull. Amer. Phys. Soc. **1** (1956) 197
Le 56c Lehmann, Leveque and Pick, Phys. Rev. **103** (1956) 411; Physica **22** (1956) 1126A
Le 56d Levintov, Miller, Shamshev and Tarumov, Physica **22** (1956) 1181A
Le 56e Levintov, Zh. Eksp. Teor. Fiz. **30** (1956) 987; Soviet Physics **3** (1956) 796
Le 56f Lehmann, Leveque, Fiehrer and Pick, J. Phys. Rad. **17** (1956) 560
Le 56g Leipunskii, Miller, Morozov and Iampol'skii, Dokl. Akad. Nauk SSSR **109** (1956) 935
Le 56h Lehmann, Leveque and Pick, C. Rendus **243** (1956) 743
Le 57 Lee and Wall, Bull. Amer. Phys. Soc. **2** (1957) 208
Le 57b Levintov, Miller and Shamshev, Nuclear Physics **3** (1957) 221

Le 57d Levintov, Miller and Shamsev, Zh. Eskp. Teor. Fiz. **32** (1957) 274; Zh. Eksp. Teor. Fiz. ("Soviet Physics") **5** (1957) 258

Le 57e Levesque and Shafroth, Bull. Amer. Phys. Soc. **2** (1957) 303

Le 57f Levinson and Banerjee, Annals of Physics **2** (1957) 471

Le 57g Lehmann, Leveque, Grjebine, Picou and Barloutaud, C. Rendus **245** (1957) 2259

Le 57h Leksin, Joint Institute for Nuclear Research, Lab. of Nuclear Problems, USSR (1957)

Le 58 Leamer, Bull. Amer. Phys. Soc. **3** (1958) 61

Le 58a Levinson and Banerjee, Annals of Physics **3** (1958) 67

Le 58b Lee and Schiffer, Bull. Amer. Phys. Soc. **3** (1958) 188

Le 58c Levintov, Miller and Shamshev, Soviet Physics (JETP) **7** (1958) 712

Le 59 Lee and Schiffer, Phys. Rev. (1959)

Li 37 Livingston and Bethe, Revs. Mod. Phys. **9** (1937) 245

Li 51 Li and Whaling, Phys. Rev. **81** (1951) 661

Li 51a Li, Whaling, Fowler and Lauritsen, Phys. Rev. **83** (1951) 512

Li 51b Li and Whaling, Phys. Rev. **82** (1951) 122

Li 52 Lillie, Phys. Rev. **87** (1952) 716

Li 53 Li, Phys. Rev. **92** (1953) 1084A

Li 53a Liberman and Christy, Phys. Rev. **92** (1953) 1085A

Li 53b Livesey and Smith, Proc. Phys. Soc. A **66** (1953) 689

Li 53c Lindner and Osborne, Phys. Rev. **91** (1953) 1501

Li 54 Li and Sherr, Phys. Rev. **96** (1954) 389

Li 55 Likely, Phys. Rev. **98** (1955) 1538A

Li 55a Little, Leonard, Prud'homme and Vincent, Phys. Rev. **98** (1955) 634

Li 55b Liberman, Ph. D. Thesis, California Institute of Technology (1955)

Li 55c Libby, "Radio Carbon Dating", 2nd Edition (U. Chicago Press, 1955)

Li 56 Livesey, Canadian J. Phys. **34** (1956) 216

Li 56a Lidofsky, Jones, Bent, Weil, Kruse, Bardon and Havens, Bull. Amer. Phys. Soc. **1** (1956) 212

Li 56b Likely and Brady, Phys. Rev. **104** (1956) 118

Li 56c Livesey, Canadian J. Phys. **34** (1956) 1022

Li 57 Lidofsky, Weil, Bent and Jones, Bull. Amer. Phys. Soc. **2** (1957) 29

Li 57a Litherland, Almqvist, Bromley, Gove and Ferguson, Bull. Amer. Phys. Soc. **2** (1957) 51

Li 57c Livesey, Canadian J. Phys. **35** (1957) 987

Li 57d Lidofsky, Revs. Mod. Phys. **29** (1957) 773

Li 58 Lindenberger, Conference on Photonuclear Reactions, National Bureau of Standards (1958)

Li 58a Livesey, Conference on Photonuclear Reactions, National Bureau of Standards (1958)

Li 58b Litherland and Gove, Bull. Amer. Phys. Soc. **3** (1958) 200

Li 58c Littlejohn and Morrison, Bull. Amer. Phys. Soc. **3** (1958) 227

Lo 55 Lönsjö, Os and Tangen, Phys. Rev. **98** (1955) 727

Lo 57 Lokan, Proc. Phys. Soc. A **70** (1957) 836

Lu 55a Lustig and Blatt, Phys. Rev. **100** (1955) 777

Ly 57 Lyons, Phys. Rev. **105** (1957) 936

Ma 50a Macklin, Lidofsky and Wu, Phys. Rev. **78** (1950) 318

Ma 50i Malm and Buechner, Phys. Rev. **80** (1950) 771

Ma 51 Malm and Buechner, Phys. Rev. **81** (1951) 519

Ma 51a Mather, Phys. Rev. **82** (1951) 126

Ma 53e Mackin, Ph. D. Thesis, California Institute of Technology (1953)

Ma 53f Manning and Singh, Proc. Phys. Soc. A **66** (1953) 842

Ma 53h Martin, Schneider and Sempert, Helv. Phys. Acta **26** (1953) 595

Ma 53i Manov, NRC Publication 270 (1953)

Ma 53j Mamasakhlisov, Zh. Eksp. Teor. Fiz. **25** (1953) 36

Ma 54b Mackin, Phys. Rev. **94** (1954) 648
Ma 54d Martin, Phys. Rev. **93** (1954) 498
Ma 54f Macklin and Banta, Science **119** (1954) 350
Ma 54g Malm and Inglis, Phys. Rev. **95** (1954) 993
Ma 54h Major and Biedenharn, Revs. Mod. Phys. **26** (1954) 321
Ma 54m Mani and Pandhi, Proc. Indian Acad. of Sci. **40** (1954) 61
Ma 54o Maeder, Müller and Wintersteiger, Helvetica Physica Acta **27** (1954) 3
Ma 55a Mackin, Mims and Mills, Phys. Rev. **98** (1955) 43
Ma 55c Maxson, Allen and Jentschke, Phys. Rev. **97** (1955) 109
Ma 55d Macklin and Banta, Phys. Rev. **97** (1955) 753
Ma 55e Mann, Stephens and Wilkinson, Phys. Rev. **97** (1955) 1184
Ma 55f MacDonald, Phys. Rev. **98** (1955) 60
Ma 55i Madansky and Owen, Phys. Rev. **99** (1955) 1608
Ma 55j Marion, Bonner and Cook, Phys. Rev. **100** (1955) 847
Ma 55k Marion, Bonner and Cook, Phys. Rev. **100** (1955) 91
Ma 55l Marion and Brugger, Phys. Rev. **100** (1955) 69
Ma 55m Marion, Brugger and Bonner, Phys. Rev. **100** (1955) 46
Ma 55n MacGregor, Ball and Booth, Phys. Rev. **100** (1955) 1793A
Ma 55o MacDonald, Phys. Rev. **100** (1955) 51
Ma 56 Malmberg, Phys. Rev. **101** (1956) 114
Ma 56c Marion and Weber, Phys. Rev. **103** (1956) 167
Ma 56d Marion and Weber, Phys. Rev. **102** (1956) 1355; **103** (1956) 1906
Ma 56e Mark and Goodman, Phys. Rev. **101** (1956) 768
Ma 56f Mackin, Mills and Thirion, Phys. Rev. **102** (1956) 802;
J. Phys. Rad. **17** (1956) 551
Ma 56g Mast and Mullin, Bull. Amer. Phys. Soc. **1** (1956) 180
Ma 56h Marion, Phys. Rev. **103** (1956) 713
Ma 56j Marion and Weber, Phys. Rev. **103** (1956) 1408
Ma 56k Magnac-Valette, C. Rendus **242** (1956) 760
Ma 56l Marion, Weber and Mozer, Phys. Rev. **104** (1956) 1402
Ma 56m Mattauch, Waldman, Bieri and Everling, Zeits. für Natur. **11a** (1956) 525
Ma 56n Marion and Hagedorn, Phys. Rev. **104** (1956) 1028
Ma 56o Magnac-Valette and Cüer, J. Phys. Rad. **17** (1956) 553;
Physica **22** (1956) 1156A
Ma 56p Maslin, Calvert and Jaffe, Proc. Phys. Soc. A **69** (1956) 754
Ma 56r Mann and Titterton, Proc. Phys. Soc. A **69** (1956) 917
Ma 56s Mamasakhlisov, Zh. Eksp. Teor. Fiz. **31** (1956) 652
Ma 57 Marion and Fowler, Astro. J. **125** (1957) 221
Ma 57a Maxson and Horie, Bull. Amer. Phys. Soc. **2** (1957) 29
Ma 57b Maris and Tyrén, Nuclear Physics **3** (1957) 52
Ma 57c Maxson and Bennett, Bull. Amer. Phys. Soc. **2** (1957) 180
Ma 57e Marion, Nuclear Physics **4** (1957) 282
Ma 57f Mazari, Castro, Alba and Vazquez, Rev. Mex. Fis. **6** (1957) 9
Ma 57g Martin, Fowler, Lauritsen and Lauritsen, Phys. Rev. **106** (1957) 1260
Ma 57i Maris and Tyrén, Nuclear Physics **4** (1957) 662
Ma 57j Mamasakhlisov and Chilashvili, Zh. Eksp. Teor. Fiz. **32** (1957) 806;
Zh. Eksp. Teor. Fiz. ("Soviet Physics") **5** (1957) 661
Ma 58a Macklin and Gibbons, Bull. Amer. Phys. Soc. **3** (1958) 26
Ma 58b Macklin and Gibbons, Phys. Rev. **109** (1958) 105
Ma 58c MacDonald, Phys. Rev. **110** (1958) 1420
Ma 58d Malvano, Conference on Photonuclear Reactions, National Bureau of Standards (1958)
Ma 58f Marion, Levin and Cranberg, Bull. Amer. Phys. Soc. **3** (1958) 165
Ma 58g Macklin and Gibbons, Bull. Amer. Phys. Soc. **3** (1958) 187
Ma 58h Maris, Hillman and Tyrén, Nuclear Physics **7** (1958) 1
Ma 58i Maxson and Terrell, Bull. Amer. Phys. Soc. **3** (1958) 381

Ma 58j MacGregor, Ball and Booth, Phys. Rev. **111** (1958) 1155
Ma 58k MacGregor and Booth, Phys. Rev. **112** (1958) 486
Ma 58l Martin, Szostak and Marmier, Helv. Phys. Acta **31** (1958) 481
Ma 59 Marion and Levin, Phys. Rev. (1959)
Mc 48 McMillan and Miller, Phys. Rev. **73** (1948) 80
Mc 51a McNeill and Rall, Phys. Rev. **83** (1951) 1244
Mc 51b McMinn, Sampson and Rasmussen, Phys. Rev. **84** (1951) 963
Mc 51d McReynolds, Phys. Rev. **84** (1951) 969
Mc 54a McIntyre, Hahn and Hofstadter, Phys. Rev. **94** (1954) 1084
Mc 55c McGruer, Warburton and Bender, Phys. Rev. **100** (1955) 235
Mc 56a McEllistrem, Jones, Chiba, Douglas, Herring and Silverstein, Phys. Rev. **104** (1956) 1008
Mc 56b McCormac, Steuer, Bond and Hereford, Phys. Rev. **104** (1956) 718
Mc 57 McCormac, Steuer, Bond and Hereford, Phys. Rev. **108** (1957) 116
Mc 57a McCrary, Bonner and Ranken, Phys. Rev. **108** (1957) 392
Mc 58 McElhinney, Conference on Photonuclear Reactions, National Bureau of Standards (1958)
Mc 58a McDermott, Jones, Smotrich and Benenson, Bull. Amer. Phys. Soc. **3** (1958) 199
Mc 58b McDaniels, Blair and Henley, Bull. Amer. Phys. Soc. **3** (1958) 330
Mc 58d McEllistrem, Phys. Rev. **111** (1958) 596
Mc 58e McCray, Bull. Amer. Phys. Soc. **3** (1958) 418
Mc 58f McDonell and Sargood, private communication (1958)
Me 49b Melkonian, Phys. Rev. **76** (1949) 1750
Me 53 Meier and Ricamo, Helv. Phys. Acta **26** (1953) 430
Me 53a Meier, Ricamo, Scherrer and Zünti, Helv. Phys. Acta **26** (1953) 451
Me 54 Meier, Scherrer and Trumpy, Helv. Phys. Acta **27** (1954) 577
Me 56 Meshkov and Ufford, Phys. Rev. **101** (1956) 734
Me 56a Medveczky, Acta Phys. Hungar. **6** (1956) 261; Phys. Abs. 4703 (1957)
Me 57 Meyer-Schützmeister and Hanna, Bull. Amer. Phys. Soc. **2** (1957) 28
Me 57a Merritt, Campion and Hawkings, Canadian J. Phys. **35** (1957) 16
Me 57b Melkanoff, Nodvik, Saxon and Woods, Phys. Rev. **106** (1957) 793
Me 57c Meyer-Berkhout and Hofstadter, Bull. Amer. Phys. Soc. **2** (1957) 390
Me 57d Meyer-Schützmeister and Hanna, Phys. Rev. **108** (1957) 1506
Me 57e Merzbacher, Newson and Crutchfield, Bull. Amer. Phys. Soc. **2** (1957) 33
Me 58 Metzger, Swann and Rasmussen, Phys. Rev. **110** (1958) 906
Me 58a Meyer and Staub, Helv. Phys. Acta **31** (1958) 205
Me 58b Meyerhof and Chase, Phys. Rev. **111** (1958) 1348
Me 58c Meyer-Schützmeister and Hanna, Bull. Amer. Phys. Soc. **3** (1958) 188
Me 59 Meyerhof and Tanner, (1959)
Mi 50c Miller, Phys. Rev. **78** (1950) 806
Mi 51a Millar, Bartholomew and Kinsey, Phys. Rev. **81** (1951) 150
Mi 51d Middleton and Tai, Proc. Phys. Soc. A **64** (1951) 801
Mi 52 Mileikowsky and Whaling, Phys. Rev. **88** (1952) 1254
Mi 52c Middleton and Tai, Proc. Phys. Soc. A **65** (1952) 752
Mi 53 Middleton, El Bedewi and Tai, Proc. Phys. Soc. A **66** (1953) 95
Mi 53c Millar and Cameron, Canadian J. Phys. **31** (1953) 723
Mi 54 Milne, Phys. Rev. **93** (1954) 762
Mi 54a Mileikowsky, Arkiv f. Fysik **7** (1954) 89
Mi 54b Mileikowsky, Arkiv f. Fysik **7** (1954) 117
Mi 54d Mills and Mackin, Phys. Rev. **95** (1954) 1206
Mi 54e Mileikowsky and Ahnlund, Phys. Rev. **96** (1954) 996
Mi 55b Miwa, J. Phys. Soc. Japan **10** (1955) 173
Mi 55e Mills, Hilton and Barnes, Phys. Rev. **100** (1955) 1794A
Mi 56 Miller, Carmichael, Gupta, Rasmussen and Sampson, Phys. Rev. **101** (1956) 740
Mi 57a Milone, Ricamo and Rinzivillo, Nuovo Cimento **5** (1957) 532
Mi 57b Milone, Ricamo and Rubbino, Nuovo Cimento **5** (1957) 528

Mi 57c Milone and Ricamo, Nuovo Cimento **5** (1957) 1338
Mi 58 Miller, Phys. Rev. **109** (1958) 1669
Mi 58a Miller and Phillips, Phys. Rev. **112** (1958) 2043
Mi 58b Miller and Phillips, Phys. Rev. **112** (1958) 2048
Mi 58c Milone, Milone-Tamburino, Rinzivillo, Rubbino and Tribuno, Nuovo Cimento **7** (1958) 729
Mo 49a Morrish, Phys. Rev. **76** (1949) 1651
Mo 52 Moak, Good and Kunz, Phys. Rev. **85** (1952) 928
Mo 53c Montalbetti, Katz and Goldemberg, Phys. Rev. **91** (1953) 659
Mo 53d Moak, Phys. Rev. **92** (1953) 383
Mo 54a Mozer, Fowler and Lauritsen, Phys. Rev. **93** (1954) 829
Mo 54b Moak, Good and Kunz, Phys. Rev. **95** (1954) 641A
Mo 54d Moak, Good and Kunz, Phys. Rev. **96** (1954) 1363
Mo 54e Moljk and Curran, Phys. Rev. **96** (1954) 395
Mo 54f Morita and Tamura, Prog. in Theo. Phys. **12** (1954) 653; **13** (1955) 225
Mo 55 Morinaga, Phys. Rev. **97** (1955) 444
Mo 55a Morinaga, Phys. Rev. **97** (1955) 1185
Mo 55b Morita and Yamada, Prog. in Theo. Phys. **13** (1955) 114, 225
Mo 56 Morinaga, Phys. Rev. **101** (1956) 254
Mo 56a Moak and Wisseman, Phys. Rev. **101** (1956) 1326
Mo 56c Morpurgo, Nuovo Cimento **3** (1956) 430
Mo 56d Mozer, Phys. Rev. **104** (1956) 1386
Mo 57 Mozer and Hagedorn, Phys. Rev. **105** (1957) 1270
Mo 57a Morinaga and Peaslee, Nuclear Physics **3** (1957) 115
Mo 57b Morton and Lewis, Bull. Amer. Phys. Soc. **2** (1957) 286
Mo 58 Morpurgo, Phys. Rev. **110** (1958) 721
Mo 58a Moore and McGruer, Bull. Amer. Phys. Soc. **3** (1958) 198
Mo 58b Morinaga and Johansson, Proc. of the Rehovoth Conf. (North-Holland Publishing Co., Amsterdam, 1958)
Mo 58c Mohr, Proc. Phys. Soc. A **71** (1958) 717
Mo 58d Morita, Phys. Rev. Lett. **1** (1958) 112
Mo 58e Moore, McGruer and Hamburger, Phys. Rev. Lett. **1** (1958) 29
Mo 58f Moak, Galonsky, Traughber and Jones, Phys. Rev. **110** (1958) 1369
Mo 58g Morita, J. Phys. Soc. Japan **13** (1958) 126
Mu 56a Muehlhause, Bloom, Wegner and Glasoe, Phys. Rev. **103** (1956) 720
Mu 57 Murray, Bull. Amer. Phys. Soc. **2** (1957) 267
Mu 57a Murphy, Phys. Rev. **108** (1957) 421
Mu 57b Muller, Ph. D. Thesis, U. of Strasbourg (1957)
Mu 57c Muto, Takekoshi, Nakamura, Imamura and Tsuneoka, J. Phys. Soc. Japan **12** (1957) 109
Mu 58 Murray and Schmitt, Bull. Amer. Phys. Soc. **3** (1958) 381

Na 52b Nabholz, Stoll and Wäffler, Helv. Phys. Acta **25** (1952) 701
Na 53a Nathans and Halpern, Phys. Rev. **92** (1953) 940
Na 54a Nahmias and Savel, C. Rendus **239** (1954) 761
Na 54b Nahmias, J. Phys. Rad. **15** (1954) 677, 775
Na 56 Naggiar, Roclawski-Conjeaud, Szteinsznaider and Thirion, C. Rendus **242** (1956) 1443
Na 56a Naggiar, Roclawski-Conjeaud, Szteinsznaider and Thirion, J. Phys. Rad. **17** (1956) 561
Na 56b Nakagawa, Ohmura, Takebe and Obi, Prog. in Theo. Phys. **16** (1956) 389
Na 58 Nakada, Anderson, Gardner and Wong, Phys. Rev. **110** (1958) 1439
Ne 51 Neuendorffer, Inglis and Hanna, Phys. Rev. **82** (1951) 75
Ne 53a Nereson and Darden, Phys. Rev. **89** (1953) 775
Ne 53b Neilson, James and Barnes, Phys. Rev. **92** (1953) 1084A
Ne 54b Nereson and Darden, Phys. Rev. **94** (1954) 1678

Ne 54c Nereson *et al.*, LA 1655 (1954)
Ne 54d Nelson, Lawrence and Carlson, Phys. Rev. **96** (1954) 825A
Ne 54e Newton, Phys. Rev. **96** (1954) 241
Ne 55a Newton, Proc. of the Glasgow Conference (Pergamon Press, 1955)
Ne 55c Need, Phys. Rev. **99** (1955) 1356
Ne 56 Need and Goodman, Bull. Amer. Phys. Soc. **1** (1956) 193
Ne 56a Newton, Canadian J. Phys. **34** (1956) 804
Ne 56b Neilson and Warren, Phys. Rev. **103** (1956) 1758
Ne 56d Neudachin, Zh. Eksp. Teor. Fiz. **31** (1956) 892; Soviet Physics **4** (1957) 756
Ne 57 Neiler, Gibbons and Good, Bull. Amer. Phys. Soc. **2** (1957) 286
Ne 57a Newson, Williamson, Jones, Gibbons and Marshak, Phys. Rev. **108** (1957) 1294
Ne 57b Nemilov and Pisarevskii, Zh. Eksp. Teor. Fiz. **32** (1957) 139; Zh. Eksp. Teor. Fiz. ("Soviet Physics") **5** (1957) 115
Ne 57c Neiler, Good and Gibbons, ORNL 2302 (1957)
Ne 58 Neuert and Retz-Schmidt, Zeits. für Natur. **13a** (1958) 829
Ne 58a Neilson, Dawson and Sample, Bull. Amer. Phys. Soc. **3** (1958) 323
Ne 59 Neilson, Dawson and Sample, (1959)
Ni 54 Nickell, Phys. Rev. **95** (1954) 426
Ni 54a Niewodniczanski and Wielowiejska, Bull. Acad. Polon. Sci. **2** (1954) 25
Ni 56 Nikolič, Povh and Župančič, Bull. Inst. Nucl. Sci. "Boris Kidrich" **6** (1956) 51
Ni 56a Nilson, Kerman, Briggs and Jentschke, Phys. Rev. **104** (1956) 1673
Ni 56b Nishimura and Ruderman, Bull. Amer. Phys. Soc. **1** (1956) 383
Ni 58 Nilson, Jentschke, Briggs, Kerman and Snyder, Phys. Rev. **109** (1958) 850
Ni 58a Nigam and Sundaresan, Canadian J. Phys. **36** (1958) 571
Ni 58b Nishimura, Phys. Rev. **110** (1958) 1166
Ni 58c Nishimura, Nuclear Physics **7** (1958) 425
No 56 Nonaka, Morita, Kawai, Ishimatsu, Suematsu, Takeshita, Nakajima and Wakuda, J. Phys. Soc. Japan **11** (1956) 1
No 56b Norbeck, Bull. Amer. Phys. Soc. **1** (1956) 329
No 57 Norbeck, Phys. Rev. **105** (1957) 204
No 57a Norbeck and Littlejohn, Phys. Rev. **108** (1957) 754
No 57b Nonaka, Morita, Kawai, Ishimatsu, Takeshita, Nakajima and Takano, J. Phys. Soc. Japan **12** (1957) 841
Nu 58 Nurmia and Fink, Phys. Rev. Lett. **1** (1958) 23

Ok 55 Okazaki, Phys. Rev. **99** (1955) 55
Ok 56 Okai and Sano, Prog. in Theo. Phys. **15** (1956) 203
Ol 57 Olness, Vorona and Lewis, Bull. Amer. Phys. Soc. **2** (1957) 51
On 57 Ono, Shimada, Kuroda and Tanaka, J. Phys. Soc. Japan **12** (1957) 745
Op 58 Ophel and Wright, Proc. Phys. Soc. A **71** (1958) 389
Ot 55 Otsuki, Sawada and Suekane, Prog. in Theo. Phys. **13** (1955) 79
Ot 55a Otsuki, Sawada and Suekane, Prog. in Theo. Phys. **14** (1955) 606
Ov 56 Overley, Pixley and Whaling, Bull. Amer. Phys. Soc. **1** (1956) 387
Ow 57 Owen and Madansky, Phys. Rev. **105** (1957) 1766; **108** (1957) 1647

Pa 52 Palevsky and Smith, Phys. Rev. **86** (1952) 604A
Pa 53a Paul and Clarke, Canadian J. Phys. **31** (1953) 267
Pa 53b Paul and Clarke, Phys. Rev. **91** (1953) 463A
Pa 53d Paul and Gove, Proc. Roy. Soc. Canada **47** (1953) 145A
Pa 54 Pauli, Ahnlund and Mileikowsky, Arkiv f. Fysik **8** (1954) 213
Pa 54a Paris, Valckx and Endt, Physica **20** (1954) 573
Pa 54b Paris and Endt, Physica **20** (1954) 585
Pa 54c Pauli, Arkiv f. Fysik **8** (1954) 16A
Pa 54d Paul, Phys. Rev. **96** (1954) 1563
Pa 55 Patterson, Newson and Merzbacher, Phys. Rev. **99** (1955) 1625A
Pa 55a Pauli, Arkiv f. Fysik **9** (1955) 571

Pa 56a Paul, Physica **22** (1956) 1140A
Pa 56b Papkow, Zeits. für Natur. **11a** (1956) 776
Pa 57 Paul, Phil. Mag. **2** (1957) 311
Pa 57a Pal and Mukherjee, Phys. Rev. **106** (1957) 811
Pa 57b Page and Heinberg, Phys. Rev. **106** (1957) 1220
Pa 57c Pal and Nagarajan, Phys. Rev. **108** (1957) 1577
Pa 58 Palfrey and Tautfest, Bull. Amer. Phys. Soc. **3** (1958) 173
Pa 58b Pasma, Nuclear Physics **6** (1958) 141
Pa 58c Parks, Newson and Williamson, Revs. Sci. Instr. **29** (1958) 834
Pa 58d Parkinson and Hough, U. of Michigan Cyclotron, Prog. Rept. (July, 1958)
Pe 44 Perlman, Richards and Williams, Los Alamos Report 66 (1944)
Pe 51b Perkin, Phys. Rev. **81** (1951) 892
Pe 51c Petree, Johnson and Miller, Phys. Rev. **83** (1951) 1148
Pe 52 Pepper, Allen, Almqvist and Dewan, Phys. Rev. **85** (1952) 155
Pe 53c Peaslee and Telegdi, Phys. Rev. **92** (1953) 126
Pe 54a Penning and Schmidt, Phys. Rev. **94** (1954) 779A
Pe 54b Peterson, Barnes, Fowler and Lauritsen, Phys. Rev. **94** (1954) 1075
Pe 54d Peterson, Fowler and Lauritsen, Phys. Rev. **96** (1954) 1250
Pe 55 Peshkin, Roberts and Telegdi, Phys. Rev. **98** (1955) 1204A
Pe 55d Penfold and Spicer, Phys. Rev. **100** (1955) 1377
Pe 55e Pérez Ferreira and Waloschek, U.N. A/Conf. 8/P/1076 (1955)
Pe 56a Perring and Skyrme, Proc. Phys. Soc. A **69** (1956) 600
Pe 57 Penning and Schmidt, Phys. Rev. **105** (1957) 647
Pe 57a Peelle, Phys. Rev. **105** (1957) 1311
Pe 57b Pearse, Phys. Rev. **106** (1957) 544
Pe 58 Penner and Leiss, Bull. Amer. Phys. Soc. **3** (1958) 56
Pe 58a Penner and Leiss, See Koch in Conference on Photonuclear Reactions, National Bureau of Standards (1958)
Ph 50b Phillips, Phys. Rev. **80** (1950) 164
Ph 51a Phillips and Heydenburg, Phys. Rev. **83** (1951) 184
Ph 51b Phillips, Cowie and Heydenburg, Phys. Rev. **83** (1951) 1049
Ph 52 Phillips, Heydenburg and Cowie, Phys. Rev. **85** (1952) 742
Ph 52b Phillips, Davis and Graves, Phys. Rev. **88** (1952) 600
Ph 53a Phipps and Zaffarano, ISC 443 (1953)
Ph 56 Phillips and Jones, Phil. Mag. **1** (1956) 576
Ph 58 Phillips, Phys. Rev. **110** (1958) 1408
Pi 56 Pieper and Stanford, Phys. Rev. **101** (1956) 672
Pi 56a Pick, Leveque and Lehmann, Physica **22** (1956) 1140A
Pi 57a Pixley, Ph. D. Thesis, California Institute of Technology (1957)
Pi 58 Pinkston and Brennan, Phys. Rev. **109** (1958) 499
Pi 58a Pinkston, Bull. Amer. Phys. Soc. II, **3** (1958) 223
Pi 58b Pieper and Heydenburg, Phys. Rev. **111** (1958) 264
Pl 59 Pleasanton, Johnson and Snell, Bull. Am. Phys. Soc. **4** (1959) 78
Po 42 Powell, Proc. Royal Soc. A **181** (1942) 344
Po 51 Pool, Kundu, Weiler and Donaven, Phys. Rev. **82** (1951) 305
Po 52b Pool, Physica **18** (1952) 1304
Po 55 Pohm, Waddell, Powers and Jensen, Phys. Rev. **97** (1955) 432
Po 56 Post, Revs. Mod. Phys. **28** (1956) 338
Po 56b Popič, Nuovo Cimento **4** (1956) 1597
Po 58 Porter, Roth and Johnson, Phys. Rev. **111** (1958) 1578
Po 58a Povh, Bull. Amer. Phys. Soc. **3** (1958) 406
Po 59 Povh, Phys. Rev. (1959)
Pr 52a Pruitt, Hanna and Swartz, Phys. Rev. **87** (1952) 534
Pr 53 Pruitt, Hanna and Swartz, Phys. Rev. **92** (1953) 1456
Pr 54b Price, Proc. Phys. Soc. A **67** (1954) 849
Pr 55 Price, Proc. Phys. Soc. A **68** (1955) 553

Pr 56 Prosser, Kraus and Schiffer, Bull. Amer. Phys. Soc. **1** (1956) 94
Pr 56a Price, Class and Risser, Bull. Amer. Phys. Soc. **1** (1956) 94
Pr 57a Price, Proc. Phys. Soc. A **70** (1957) 661
Pr 57b Prokoshkin and Tiapkin, Zh. Eksp. Teor. Fiz. **32** (1957) 177; Zh. Eksp. Teor. Fiz. ("Soviet Physics") **5** (1957) 148
Pr 58 Proctor and Voelker, Bull. Amer. Phys. Soc. **3** (1958) 173
Pr 58a Priest, Corelli, Bleuler and Tendam, Bull. Amer. Phys. Soc. **3** (1958) 199
Pr 58b Pradal and Vénéroni, C. Rendus **246** (1958) 2461
Pu 52a Putnam, Phys. Rev. **87** (1952) 932
Pu 56a Putnam, Brolley and Rosen, Phys. Rev. **104** (1956) 1303

Qu 56 Quinton and Doyle, Phys. Rev. **101** (1956) 669

Ra 49a Rasmussen, Lauritsen and Lauritsen, Phys. Rev. **75** (1949) 199
Ra 49b Rasmussen, Hornyak and Lauritsen, Phys. Rev. **76** (1949) 581
Ra 54a Rasmussen, Rees, Sampson and Wall, Phys. Rev. **96** (1954) 812
Ra 55 Ralph and Dunnam, Phys. Rev. **98** (1955) 249A
Ra 55a Rasmussen, Miller and Sampson, Phys. Rev. **100** (1955) 181
Ra 55b Rasmussen, Miller, Sampson and Gupta, Phys. Rev. **100** (1955) 851
Ra 55c Ravenhall, Phys. Rev. **100** (1955) 1797A
Ra 56a Rasmussen, Phys. Rev. **103** (1956) 186
Ra 56b Raz, Bull. Amer. Phys. Soc. **1** (1956) 336
Ra 57 Rakavy, Nuclear Physics **4** (1957) 375
Ra 57a Rask, Ames, Edwards, Madansky and Owen, Bull. Amer. Phys. Soc. **2** (1957) 351
Ra 57b Raz, Phys. Rev. **107** (1957) 1201
Ra 58a Rasmussen, Metzger and Swann, Phys. Rev. **110** (1958) 154
Ra 58b Ranken, Bonner, McCrary and Rabson, Phys. Rev. **109** (1958) 917
Ra 58c Ranken, Bonner and McCrary, Phys. Rev. **109** (1958) 1646
Ra 58d Rayburn, Bull. Amer. Phys. Soc. **3** (1958) 337
Ra 58e Ravenhall, Revs. Mod. Phys. **30** (1958) 430
Ra 58f Rapoport and Butusov, Soviet Physics (JETP) **6** (1958) 1163
Ra 58g Rayburn, Bull. Amer. Phys. Soc. **3** (1958) 365
Ra 58h Ranken, Bonner, Castillo-Bahena, Harlow and Rabson, Phys. Rev. **112** (1958) 239
Re 51a Resnick and Hanna, Phys. Rev. **82** (1951) 463
Re 53 Reagan, Phys. Rev. **92** (1953) 651
Re 54b Reid, Proc. Phys. Soc. A **67** (1954) 466
Re 54c Redlich, Phys. Rev. **95** (1954) 448
Re 55 Redlich, Phys. Rev. **98** (1955) 199
Re 55a Reynolds, Phys. Rev. **98** (1955) 1289
Re 55b Redlich, Phys. Rev. **99** (1955) 1427
Re 55e Reagan, Phys. Rev. **100** (1955) 113
Re 55f Reut, Korentchenko, Yurev and Pontecorvo, Dokl. Akad. Nauk **102** (1955) 723
Re 56 Reynolds and Standing, Phys. Rev. **101** (1956) 158
Re 56b Redmond, Phys. Rev. **101** (1956) 751
Re 56c Reich, Phillips and Russell, Phys. Rev. **104** (1956) 143
Re 57 Reiner, Physica **23** (1957) 338
Re 58 Redlich, Phys. Rev. **110** (1958) 468
Re 58b Retz-Schmidt, Zeits. für Natur. **13a** (1958) 833
Re 58c Remy and Winter, Nuovo Cimento **9** (1958) 664
Rh 58a Rhodes, Ph. D. Thesis, U. of Pennsylvania (1958)
Rh 58b Rhodes and Stephens, Phys. Rev. **110** (1958) 1415
Ri 41 Richards, Phys. Rev. **59** (1941) 796
Ri 50c Richardson, Phys. Rev. **80** (1950) 850
Ri 50d Ricamo, Zünti, Baldinger and Huber, Helv. Phys. Acta **23** (1950) 508
Ri 50e Richards, Smith and Browne, Phys. Rev. **80** (1950) 524
Ri 51c Ricamo and Zünti, Helv. Phys. Acta **24** (1951) 419

Ri 51d Ricamo and Zünti, Helv. Phys. Acta **24** (1951) 302
Ri 51e Ricamo, Nuovo Cimento **8** (1951) 893
Ri 54a Ribe and Seagrave, Phys. Rev. **94** (1954) 934
Ri 54b Rickard, Hudspeth and Clendenin, Phys. Rev. **96** (1954) 1272
Ri 55 Risser, Price and Class, Phys. Rev. **98** (1955) 1183A
Ri 55a Ribe, Phys. Rev. **100** (1955) 1254A
Ri 55b Riviere and Treacy, Australian J. Phys. **8** (1955) 408
Ri 56b Ribe, Phys. Rev. **103** (1956) 741
Ri 56d Riviere, Nuclear Physics **2** (1956) 81
Ri 57 Risser, Price and Class, Phys. Rev. **105** (1957) 1288
Ri 57a Ribe, Phys. Rev. **106** (1957) 767
Ri 57b Riviere and Treacy, Australian J. Phys. **10** (1957) 209
Ri 58 Risser, Miller and Kashy, Bull. Amer. Phys. Soc. **3** (1958) 27
Ri 58a Ridley, Nuclear Physics **6** (1958) 34
Ri 58b Riley, Warren and Griffiths, Bull. Amer. Phys. Soc. **3** (1958) 330
Ri 58c Richter and Ivash, Phys. Rev. **111** (1958) 245
Ro 50 Rose and Wilson, Phys. Rev. **78** (1950) 68
Ro 51g Roy, Phys. Rev. **82** (1951) 227
Ro 51h Roseborough, McCue, Preston and Goodman, Phys. Rev. **83** (1951) 1133
Ro 51j Rotblat, Nature **167** (1951) 1027
Ro 51k Rotblat, Phys. Rev. **83** (1951) 1271
Ro 55a Roy, Lagasse, Goes and Moerman, C. Rendus **241** (1955) 1567
Ro 56 Robbins, Phys. Rev. **101** (1956) 1373
Ro 56a Roclawski-Conjeaud and Cotton, Nuclear Physics **1** (1956) 603; J. Phys. Rad. **17** (1956) 552; Physica **22** (1956) 1155A
Ro 56b Roclawski-Conjeaud, Naggiar, Szteinsznaider and Thirion, Physica **22** (1956) 1158A
Ro 57a Roberts, Bull. Amer. Phys. Soc. **2** (1957) 234
Ro 57b Rosen and Stewart, Phys. Rev. **107** (1957) 824
Ro 57c Rosen and Brolley, Phys. Rev. **107** (1957) 1454
Ro 57d Rose and Warburton, Phil. Mag. **2** (1957) 1468
Ro 57e Roy, Lagasse, Goes, Achari and de Henau, C. Rendus **244** (1957) 2907
Ro 57f Roy, Goes and Pirson, C. Rendus **244** (1957) 3054
Ru 48 Russell, Sachs, Wattenberg and Fields, Phys. Rev. **73** (1948) 545
Ru 51 Ruby and Richardson, Phys. Rev. **83** (1951) 698
Ru 51a Rutherglen, Rae and Smith, Proc. Phys. Soc. A **64** (1951) 906
Ru 54 Ruhla, J. de Physique **15** (1954) 451
Ru 54a Rubin and Walter, Helv. Phys. Acta **27** (1954) 163
Ru 55 Rustad and Ruby, Phys. Rev. **97** (1955) 991
Ru 55a Rutherglen, Proc. of the Glasgow Conference (Pergamon Press, 1955)
Ru 56a Russell, Phillips and Reich, Phys. Rev. **104** (1956) 135
Ru 56c Rusbridge, Proc. Phys. Soc. A **69** (1956) 830
Ry 58 Rybka and Katz, Phys. Rev. **110** (1958) 1123

Sa 52 Sanders, Phil. Mag. **43** (1952) 630
Sa 53b Sawyer and Phillips, Los Alamos Report 1578 (1953)
Sa 53c Sanders, Phil. Mag. **44** (1953) 1302
Sa 54 Sack, Biedenharn and Breit, Phys. Rev. **93** (1954) 321
Sa 54a Savel and Nahmias, C. Rendus **238** (1954) 2155
Sa 55b Sawyer and Burkhardt, Phys. Rev. **98** (1955) 1305
Sa 55c Sattar, Morgan and Hudspeth, Phys. Rev. **100** (1955) 960A
Sa 55f Sample, Neilson, Chadwick and Warren, Canadian J. Phys. **33** (1955) 828
Sa 55h Sawicki, Acta Phys. Polon. **14** (1955) 135; **15** (1956) 358
Sa 55i Sawicki, Nuovo Cimento **1** (1955) 957
Sa 55j Santos, Goldemberg, Pieroni, Silva, Borelli, Villaça and Leite Lopes, Anais Acad. Brasil. Ciencias **27** (1955) 437
Sa 56 Sawicki, Acta Phys. Polon. **15** (1956) 71

Sa 56a Sachs, Phys. Rev. **103** (1956) 671
Sa 56d Sanders, Phys. Rev. **104** (1956) 1434
Sa 56e Samman, C. Rendus **242** (1956) 2232
Sa 56f Samman, C. Rendus **242** (1956) 3062
Sa 57 Sarma, Govindjee and Allan, Proc. Phys. Soc. A **70** (1957) 68
Sa 57a Sawicki, Phys. Rev. **106** (1957) 172
Sa 57c Salpeter, Phys. Rev. **107** (1957) 516
Sa 58 Sample, Dawson and Neilson, Bull. Amer. Phys. Soc. **3** (1958) 323
Sc 50 Schardt, Fowler and Lauritsen, Phys. Rev. **80** (1950) 136
Sc 52 Schardt, Fowler and Lauritsen, Phys. Rev. **86** (1952) 527
Sc 52a Schrank and Richardson, Phys. Rev. **86** (1952) 248
Sc 54b Scott, Thomson and Wright, Phys. Rev. **95** (1954) 582
Sc 54c Scherrer, Allison and Faust, Phys. Rev. **96** (1954) 386
Sc 55 Schmouker, Erdös, Jordan and Stoll, J. Phys. Rad. **16** (1955) 169
Sc 55a Schiff, Phys. Rev. **98** (1955) 1281
Sc 55b Scott and Segel, Phys. Rev. **100** (1955) 1244A
Sc 56 Schrank and O'Neill, Bull. Amer. Phys. Soc. **1** (1956) 29
Sc 56d Schneider, Helv. Phys. Acta **29** (1956) 55
Sc 56f Schiffer, Bonner, Davis and Prosser, Phys. Rev. **104** (1956) 1064
Sc 56g Schiffer, Kraus and Risser, Phys. Rev. **105** (1956) 1811
Sc 56h Schwartz and Gartenhaus, Bull. Amer. Phys. Soc. **1** (1956) 383
Sc 56i Schwarzschild, Rustad and Wu, Bull. Amer. Phys. Soc. **1** (1956) 336
Sc 57 Scobie and Lewis, Phil. Mag. **2** (1957) 1089
Sc 57a Scott, Bull. Amer. Phys. Soc. **2** (1957) 349
Sc 57b Schopper, Phil. Mag. **2** (1957) 710
Sc 57c Schrader, Benveniste and Zenger, Bull. Amer. Phys. Soc. **2** (1957) 309
Sc 58 Scott, Ph. D. Thesis, The Johns Hopkins U. (1958)
Sc 58a Scott, Phys. Rev. **110** (1958) 1398
Sc 59 Schwarzschild, Bull. Amer. Phys. Soc. **4** (1959) 79
Se 47 Seren, Friedlander and Turkel, Phys. Rev. **72** (1957) 888
Se 49 Segré and Wiegand, Phys. Rev. **75** (1949) 39
Se 49a Sexl, Acta Phys. Aust. **2** (1949) 377
Se 51b Seed, Phil. Mag. **42** (1951) 566
Se 51c Seagrave, Ph. D. Thesis, California Institute of Technology (1951)
Se 51e Seagrave, Phys. Rev. **84** (1951) 1219
Se 52 Seagrave, Phys. Rev. **85** (1952) 197
Se 52a Seed and French, Phil. Mag. **43** (1952) 1214
Se 52b Seed and French, Phys. Rev. **88** (1952) 1007
Se 53 Seagrave, Phys. Rev. **92** (1953) 1222
Se 53b Seed, Phil. Mag. **44** (1953) 921
Se 53c Seale, Phys. Rev. **92** (1953) 389
Se 54 Sempert, Schneider and Martin, Helv. Phys. Acta **27** (1954) 313
Se 54a Sempert, Ph. D. Thesis, Zürich ETH (1954)
Se 54c Sehr, Zeits. f. Physik **137** (1954) 523
Se 55 Seed, Phil. Mag. **46** (1955) 100
Se 55a Seitz and Huber, Helv. Phys. Acta **28** (1955) 227
Se 55c Selove, Phys. Rev. **98** (1955) 208
Se 56 Seidlitz, Bleuler and Tendam, Bull. Amer. Phys. Soc. **1** (1956) 29
Se 56a Selove, Phys. Rev. **101** (1956) 231
Se 56c Severiens and Hanna, Phys. Rev. **104** (1956) 1612
Se 57a Segel and Hanna, Phys. Rev. **106** (1957) 536
Se 57b Seward, Slaus, and Fulbright Phys. Rev. **107** (1957) 159
Se 57c Serdiokova, Khabakhpashev and Tsenter, Iszv. Akad. Nauk **21** (1957) 1017
Se 57d Senent, Villar and Bonet, An. Real. Soc. Espan. Fis. Quim. **53A** (1957) 109; Physics Abstracts 8264 (1958)
Se 58 Segel, Kane and Wilkinson, Phil. Mag. **3** (1958) 204

Se 58a Seidlitz, Bleuler and Tendam, Phys. Rev. **110** (1958) 682
Sh 49 Sherr, Muether and White, Phys. Rev. **75** (1949) 282
Sh 51a Shull, Phys. Rev. **83** (1951) 875
Sh 51c Sheline, Phys. Rev. **82** (1951) 954
Sh 51d Sher, Halpern and Mann, Phys. Rev. **84** (1951) 387
Sh 52 Sheline, Phys. Rev. **87** (1952) 557
Sh 53a Sherr and Gerhart, Phys. Rev. **91** (1953) 909
Sh 53b Shire, Wormald, Lindsay-Jones, Lundén and Stanley, Phil. Mag. **44** (1953) 1197
Sh 54a Shafroth and Hanna, Phys. Rev. **95** (1954) 86
Sh 54b Sherr and Miller, Phys. Rev. **93** (1954) 1076
Sh 54d Sheline, Johnson, Bell, Davis and McGowan, Phys. Rev. **94** (1954) 1642
Sh 54e Sherr, Li and Christy, Phys. Rev. **96** (1954) 1258
Sh 55 Shaw, Proc. Phys. Soc. A **68** (1955) 43
Sh 55b Sharp, Sperduto and Buechner, Phys. Rev. **99** (1955) 632A
Sh 55c Shire and Edge, Phil. Mag. **46** (1955) 640
Sh 55d Sherr, Gerhart, Horie and Hornyak, Phys. Rev. **100** (1955) 945
Sh 56 Sherr and Hornyak, Bull. Amer. Phys. Soc. **1** (1956) 197
Sh 56a Sher and Floyd, Phys. Rev. **102** (1956) 242
Sh 56b Shaw, Conzett, Slobodrian, and Summers-Gill, Bull. Amer. Phys. Soc. **1** (1956) 253
Sh 56d Sherman and Ravenhall, Phys. Rev. **103** (1956) 949
Sh 56e Shafroth and Hanna, Phys. Rev. **104** (1956) 399
Sh 56f Sherr, Hornyak and Yoshiki, Bull. Amer. Phys. Soc. **1** (1956) 231
Sh 57 Sherr and Rickey, Bull. Amer. Phys. Soc. **2** (1957) 29
Sh 57a Shpetnyi, Zh. Eksp. Teor. Fiz. **32** (1957) 423;
Zh. Eksp. Teor. Fiz. ("Soviet Physics") **5** (1957) 357
Sh 57b Sherr and Bennett, Proc. of the U. of Pittsburgh Conference on Nuclear Structure (1957)
Sh 58 Shapiro, Usp. Fiz. Nauk **65** (1958) 33
Sh 58a Shook, Bull. Amer. Phys. Soc. **3** (1958) 330
Si 50 Sikkema, Nature **165** (1950) 1016
Si 53 Simon and Welton, Phys. Rev. **90** (1953) 1036
Si 54 Sinclair, Phys. Rev. **93** (1954) 1082
Si 57 Sikkema, Nuclear Physics **3** (1957) 375
Si 57a Silver, UCRL 3887 (1957)
Si 57b Simons, Soc. Sci. Fennica, Commetationes Phys.-Math. **20** (1957) No. 3
Si 58 Sikkema, Pasma and Van Barneveld, Nuclear Physics **5** (1958) 351
Si 58a Siddig and Haslam, Canadian J. Phys. **36** (1958) 963
Sj 57 Sjögren, Arkiv f. Fysik **11** (1957) 383
Sk 58 Skyrme, Proc. of the Rehovoth Conf. (North-Holland Publishing Co., Amsterdam, 1958)
Sl 57 Slattery, Chapman and Bonner, Phys. Rev. **108** (1957) 809
Sm 54 Smith, Phys. Rev. **95** (1954) 730
Sm 55 Smorodinskii, Usp. Fiz. Nauk **56** (1955) 201
Sm 55a Smith and Aten, J. of Inorg. and Nuclear Chem. **1** (1955) 296
Sm 57a Smither, Phys. Rev. **107** (1957) 196
Sm 58 Smotrich, Jones, McDermott and Benenson, Bull. Amer. Phys. Soc. **3** (1958) 26
Sm 58a Smith and Baker, Bull. Amer. Phys. Soc. **3** (1958) 172
Sn 48 Snell, Science **108** (1948) 167
Sn 50a Snowdon, Phys. Rev. **78** (1950) 299
Sn 50e Snell, Barker and Sternberg, Phys. Rev. **80** (1950) 637
Sn 54 Snyder, Phys. Rev. **96** (1954) 1333
So 55 Softky, Phys. Rev. **98** (1955) 173
So 55a Sommers, Dash and Goldstein, Phys. Rev. **97** (1955) 855
So 56 Sokolov, Sulkovskaia, Karpushkina and Albitskaia, Zh. Eksp. Teor. Fiz. **30** (1956) 1007; Soviet Physics **3** (1956) 740
So 56a Sokolov, Sulkovskaia, Albitskaia and Karpushkina, Dokl. Akad. Nauk SSSR **111**

(1956) 1219
So 56b Sorokin and Taranov, Dokl. Akad. Nauk **111** (1956) 82
So 57 Soper, Phil. Mag. **2** (1957) 1219
So 57a Sorokin, Val'ter, Gavrilovskii, Karadshev, Man'ko and Taranov, Zh. Eksp. Teor. Fiz. **33** (1957) 606;
Zh. Eksp. Teor. Fiz. ("Soviet Physics") **6** (1958) 466
Sp 51a Sperduto, M.I.T. Progress Report (LNSE) (May, 1951)
Sp 53c Sperduto and Fader, M.I.T. Progress Report, May (1953)
Sp 54 Spearman, Hudspeth and Morgan, Phys. Rev. **94** (1954) 806A
Sp 54c Speiser and Fierz, Helv. Phys. Acta **27** (1954) 159
Sp 54d Speiser, Helv. Phys. Acta **27** (1954) 427
Sp 54e Sperduto, Buechner, Bockelman and Browne, Phys. Rev. **96** (1954) 1316
Sp 55 Spicer, Phys. Rev. **99** (1955) **33**
Sp 55a Spicer and Penfold, Phys. Rev. **100** (1955) 1375
Sp 57 Spicer, Australian J. Phys. **10** (1957) 326
Sp 58 Spear, Australian J. Phys. **11** (1958)
Sp 58a Spear, Australian J. Phys. (1958)
Sp 59 Spicer, (1959)
Sp 59a Spencen and Phillips, Bull. Amer. Phys. Soc. **4** (1959) 95
Sq 56 Squires, Bockelman and Buechner, Phys. Rev. **104** (1956) 413
Sq 58 Squires, Nuclear Physics **6** (1958) 504
St 50d Stebler, Bichsel and Huber, Helv. Phys. Acta **23** (1950) 511
St 51 Strait, Van Patter, Sperduto and Buechner, Phys. Rev. **81** (1951) 747
St 51a Stephens, Halpern and Sher, Phys. Rev. **82** (1951) 511
St 51b Stetter and Bothe, Zeits. für Natur. **6a** (1951) 61
St 51e Stelson and Preston, Phys. Rev. **83** (1951) 469
St 51h Stevenson and Deutsch, Phys. Rev. **83** (1951) 1202
St 52e Stratton, Freier, Keepin, Rankin and Stratton, Phys. Rev. **88** (1952) 257
St 53 Steigert and Sampson, Phys. Rev. **92** (1953) 660
St 53a Stoll and Wächter, Nuovo Cimento **10** (1953) 347
St 54a Standing, Phys. Rev. **94** (1954) 731
St 54c Stanley, Phil. Mag. **45** (1954) 430
St 54e Stelson and Preston, Phys. Rev. **95** (1954) 974
St 54f Stanley, Phil. Mag. **45** (1954) 807
St 54h Stoll, Helv. Phys. Acta **27** (1954) 395
St 54j Stelson, Phys. Rev. **96** (1954) 1584
St 55a Stephens, Mann, Patton and Winhold, Phys. Rev. **98** (1955) 839
St 55b Stewart, Phys. Rev. **98** (1955) 740
St 55c Stratton, Blair, Famularo and Stuart, Phys. Rev. **98** (1955) 629
St 55e Streib, Phys. Rev. **100** (1955) 1797A
St 56 Standing, Phys. Rev. **101** (1956) 152
St 56a Strauch and Titus, Phys. Rev. **103** (1956) 200
St 56b Steffen, Hinrichs and Neuert, Zeits. f. Physik **145** (1956) 156
St 56c Strauch and Titus, Phys. Rev. **104** (1956) 191
St 56d Stoltzfus, Friichtenicht and Nelson, Bull. Amer. Phys. Soc. **1** (1956) 329
St 56f Steffen and Neuert, Zeits. f. Physik **147** (1956) 125
St 57 Stewart and Rosen, Bull. Amer. Phys. Soc. **2** (1957) 33
St 57b Starik, Arslanov and Protopopov, Seventh Int. Conf. on Nuclear Spectroscopy in Leningrad, January 25–31 (1957)
St 57c Striebel and Huber, Helv. Phys. Acta **30** (1957) 67
St 57d Stelson and Campbell, Phys. Rev. **106** (1957) 1252
St 57e Stafford, Tornabene and Whitehead, Phys. Rev. **106** (1957) 831
St 57f Strizhak, Soviet J. of Atomic Energy **2** (1957) 72
St 57g Steffen and Neuert, Zeits. f. Physik **147** (1957) 125
St 58 Striebel, Darden and Haeberli, Nuclear Physics **6** (1958) 188
St 58a Stewart, Conference on Photonuclear Reactions, National Bureau of Standards (1958)

St 58b Strominger, Hollander and Seaborg, Revs. Mod. Phys. **30** (1958) 585
St 58c Strassenburg, Hubert, Krone and Prosser, Bull. Amer. Phys. Soc. **3** (1958) 372
Su 51b Sun, Jennings, Shoupp and Allen, Phys. Rev. **82** (1951) 267
Su 55a Summers-Gill, Phys. Rev. **100** (1955) 1795A
Su 56 Summers-Gill, Bull. Amer. Phys. Soc. **1** (1956) 253
Su 56a Sugimoto and Mizobuchi, Phys. Rev. **103** (1956) 739
Su 56b Summers-Gill, UCRL **3388** (1956)
Su 58 Sucher and Ferrell, Bull. Amer. Phys. Soc. **3** (1958) 49
Su 58a Summers-Gill, Phys. Rev. **109** (1958) 1591
Sv 57 Svantesson, Nuclear Physics **3** (1957) 273
Sw 55 Swann, Rothman, Porter and Mandeville, Phys. Rev. **98** (1955) 1183A
Sw 56a Swami, Schneps and Fry, Phys. Rev. **103** (1956) 1134
Sw 57a Swann and Metzger, Phys. Rev. **108** (1957) 982
Sw 58 Swann, Metzger and Rasmussen, Bull. Amer. Phys. Soc. **3** (1958) 187
Sw 58a Sweetman, Bull. Amer. Phys. Soc. **3** (1958) 186
Sw 59 Swann, Metzger and Rasmussen, Phys. Rev. (1959)
Sz 57 Szteinsznaider, Roclawski-Conjeaud and Naggiar, C. Rendus **244** (1957) 445

Ta 48 Taschek and Hemmendinger, Phys. Rev. **74** (1948) 373
Ta 53 Talbott and Heydenburg, Phys. Rev. **90** (1953) 186
Ta 54 Taylor, Robinson and Haslam, Canadian J. Phys. **32** (1954) 238
Ta 54c Takemoto, Dazai, Chiba, Ito, Suganomata and Watanabe, J. Phys. Soc. Japan **9** (1954) 447
Ta 55 Taylor, Lönsjö and Bonner, Phys. Rev. **100** (1955) 174
Ta 55b Tanner, Proc. Phys. Soc. A **68** (1955) 1195
Ta 56 Takemoto, Dazai, Chiba Suganomata and Ito, Phys. Rev. **101** (1956) 772
Ta 56a Tautfest and Rubin, Phys. Rev. **103** (1956) 196
Ta 56c Tanner, Phil. Mag. **1** (1956) 47
Ta 56d Tassie, Australian J. Phys. **9** (1956) 407
Ta 57 Tamura, Phys. Rev. **105** (1957) 1808
Ta 57a Tauber and Wu, Phys. Rev. **105** (1957) 1772
Ta 57b Tanner, Phys. Rev. **107** (1957) 1203
Ta 57c Tassie, Nuovo Cimento **5** (1957) 1497
Ta 58 Tautfest, Bull. Amer. Phys. Soc. **3** (1958) 25
Ta 58a Tai, Millburn, Kaplan and Moyer, Phys. Rev. **109** (1958) 2086
Ta 58b Tautfest, Phys. Rev. **110** (1958) 708
Ta 58c Tautfest, Phys. Rev. **111** (1958) 1162
Ta 58d Tanner, Proc. Phys. Soc. A **72** (1958) 457
Ta 59 Tanner, Phys. Rev. (1959)
Te 47 Templeton, Howland and Perlman, Phys. Rev. **72** (1947) 758
Te 51a Terrell and Phillips, Phys. Rev. **83** (1951) 703
Te 51b Telegdi, Phys. Rev. **84** (1951) 600
Te 54b Temmer and Heydenburg, Phys. Rev. **96** (1954) 426
Te 54c Telegdi, Physics in Canada, **10** (1954) 44
Te 55 Teem, Selove and Kruse, Phys. Rev. **98** (1955) 259A
Te 56 Temmer and Heydenburg, Phys. Rev. **104** (1956) 989
Th 49 Thomas, Rubin, Fowler and Lauritsen, Phys. Rev. **75** (1949) 1612
Th 51f Thirion, C. Rendus **233** (1951) 37
Th 52 Thomas and Lauritsen, Phys. Rev. **88** (1952) 969
Th 52b Thomas, Phys. Rev. **88** (1952) 1109
Th 52c Thomson, Cohen, French and Hutchinson, Proc. Phys. Soc. A **65** (1952) 745
Th 53 Thirion, Ann. de Physique **8** (1953) 489
Th 53a Thirion and Telegdi, Phys. Rev. **92** (1953) 1253
Th 54 Thirion, Barnes and Lauritsen, Phys. Rev. **94** (1954) 1076
Th 54a Thirion, Cohen and Whaling, Phys. Rev. **96** (1954) 850A

Th 54b Thompson and Risser, Phys. Rev. **94** (1954) 941
Th 54d Thompson, Phys. Rev. **96** (1954) 369
Th 55b Thirion and Barloutaud, C. Rendus **240** (1955) 2136
Th 56 Thomas, Walt, Walton and Allen, Phys. Rev. **101** (1956) 759
Th 56a Thieberger and Talmi, Phys. Rev. **102** (1956) 923
Ti 51 Titterton and Brinkley, Proc. Phys. Soc. A **64** (1951) 212
Ti 52 Titterton and Brinkley, Proc. Phys. Soc. A **65** (1952) 1052
Ti 53 Titterton and Brinkley, Proc. Phys. Soc. A **66** (1953) 579
Ti 53a Titterton, Aust. J. of Science **15** (1953) 174
Ti 53b Titterton and Brinkley, Proc. Phys. Soc. A **66** (1953) 194
Ti 54 Titterton, Phys. Rev. **94** (1954) 206
Ti 54a Titterton and Brinkley, Proc. Phys. Soc. A **67** (1954) 469
Ti 54b Titterton and Brinkley, Australian J. Phys. **7** (1954) 350
Ti 55 Titterton, Proc. of the Glasgow Conference (Pergamon Press 1955)
Ti 55a Titterton, Prog. in Nuclear Physics **4** (1955) 1
Ti 57 Titterton and Brinkley, Nature **179** (1957) 369
Ti 58 Titterton, Conference on Photonuclear Reactions, National Bureau of Standards (1958)
To 55c Toledo and Watanabe, Anais. Acad. Brasil. Ciencias **27** (1955) 471
To 56 Toppel, Wilkinson and Alburger, Phys. Rev. **101** (1956) 1485
To 56a Tobocman, Phys. Rev. **102** (1956) 588
To 56b Toppel, Phys. Rev. **103** (1956) 141
To 57 Toppel, Bloom and Wilkinson, Phil. Mag. **2** (1957) 61
To 57a Touchard, C. Rendus **244** (1957) 2499
To 58 Torki, Winter and Rémy, C. Rendus **246** (1958) 3047
Tr 53 Treacy, Phil. Mag. **44** (1953) 325
Tr 53a Trumpy, Grotdal and Graue, Univ. Bergen Arbok, No. 8 (1953); Physics Abstracts 2736 (1954)
Tr 54 Trumble, Phys. Rev. **94** (1954) 748A
Tr 54b Trail and Johnson, Phys. Rev. **95** (1954) 1363
Tr 55 Treacy, Proc. Phys. Soc. A **68** (1955) 204
Tr 55a Trail and Johnson, Phys. Rev. **98** (1955) 249A
Tr 55b Treacy, Nature **176** (1955) 923
Tr 56 Treacy, Nuclear Physics **2** (1956) 239
Tr 57 Treacy, Australian J. Phys. **10** (1957) 373
Tr 57a Treacy and Bowkett, Nuclear Instruments **1** (1957) 86
Ts 56 Tsai, Bull. Amer. Phys. Soc. **1** (1956) 327
Tu 53 Tucker and Gregg, Phys. Rev. **91** (1953) 1579
Tu 54 Tucker and Gregg, Phys. Rev. **93** (1954) 362A
Tu 56 Tulinov, Zh. Eksp. Teor. Fiz. **31** (1956) 698; Zh. Eksp. Teor. Fiz. ("Soviet Physics") **4** (1957) 596
Ty 57 Tyrén, Hillman and Johansson, Nuclear Physics **3** (1957) 336
Ty 57a Tyrén, Tibell and Maris, Nuclear Physics **4** (1957) 277
Ty 57b Tyrén and Maris, Nuclear Physics **4** (1957) 637
Ty 57c Tyrén, Maris and Hillman, Nuovo Cimento **6** (1957) 1507
Ty 58 Tyrén and Maris, Nuclear Physics **6** (1958) 82
Ty 58a Tyrén and Maris, Nuclear Physics **6** (1958) 446
Ty 58b Tyrén, Hillman and Maris, Nuclear Physics **7** (1958) 10
Ty 58c Tyrén, Tibell and Maris, Nuclear Physics **7** (1958) 281
Tz 56 Tzara, C. Rendus **242** (1956) 2340

Ue 53 Uebergang and Tanner, Australian J. Phys. **6** (1953) 53
Ue 54 Uebergang, Australian J. Phys. **7** (1954) 279
Um 58 Umezawa, Proc. of the Rehovoth Conf. (North-Holland Publishing Co., Amsterdam, 1958)

Va 49 Van Patter, Phys. Rev. **76** (1949) 1264
Va 51 Van Patter, Sperduto, Huang, Strait and Buechner, Phys. Rev. **81** (1951) 233
Va 51a Van Patter, Buechner and Sperduto, Phys. Rev. **82** (1951) 248
Va 52 Van Patter, Sperduto, Endt, Buechner and Enge, Phys. Rev. **85** (1952) 142
Va 54 Van Patter and Whaling, Revs. Mod. Phys. **26** (1954) 402
Va 54c Vashakidze and Chilashvili, Zh. Eksp. Teor. Fiz. **26** (1954) 254
Va 55a Van Loef, Ph. D. Thesis, U. of Utrecht (1955)
Va 55b Vaughn, UCRL **3174** (1955)
Va 56 Van Loef and Lind, Phys. Rev. **101** (1956) 103
Va 56a Van der Spuy, Nuclear Physics **1** (1956) 381
Va 56b Vanetsian and Fedchenko, Physica **22** (1956) 1124A
Va 56c Valckx, Ph. D. Thesis, U. of Utrecht (1956)
Va 57 Van Patter and Whaling, Revs. Mod. Phys. **29** (1957) 757
Va 57a Vasil'ev, Komarov and Popova, Zh. Eksp. Teor. Fiz. **33** (1957) 527; Zh. Eksp. Teor. Fiz. ("Soviet Physics") **6** (1958) 411
Va 57b Vanetsian and Fedchenko, Soviet J. of Atomic Energy **2** (1957) 141
Va 57c Vasil'ev, Komarov and Popova, Soviet J. of Atomic Energy, Suppt. 5 (1957) 69
Va 58 Van Heerden, Nuclear Physics **6** (1958) 55
Va 58a Vaughn, Imhof, Johnson and Walt, Bull. Amer. Phys. Soc. **3** (1958) 165
Va 58c Van der Spuy and Pienaar, Nuclear Physics **7** (1958) 397
Va 58d Vasil'ev, Komarov, and Popova, Soviet Physics (JETP) **6** (1958) 1016
Ve 56 Veeraraghavan, Proc. Ind. Acad. of Sciences **43A** (1956) 319
Ve 58 Vervier and Martegani, Phys. Rev. **109** (1958) 947; Nuclear Physics **6** (1958) 260
Ve 58a Vedder, UCRL 8324 (1958)
Vi 56 Visscher and Ferrell, Bull. Amer. Phys. Soc. **1** (1956) 16
Vi 57 Visscher and Ferrell, Phys. Rev. **107** (1957) 781
Vo 57 Von Herrmann and Pieper, Phys. Rev. **105** (1957) 1556
Vo 58 Vogelsang and McGruer, Phys. Rev. **109** (1958) 1663

Wa 52b Watson and Buechner, Phys. Rev. **88** (1952) 1324
Wa 52c Walker, Link and Smith, Proc. Phys. Soc. A **65** (1952) 861
Wa 53 Warters, Fowler and Lauritsen, Phys. Rev. **91** (1953) 917
Wa 54 Warren, Laurie, James and Erdman, Canadian J. Phys. **32** (1954) 563
Wa 55a Walt and Beyster, Phys. Rev. **98** (1955) 677
Wa 55c Wapstra, Physica **21** (1955) 367
Wa 55e Ward and Grant, Proc. Phys. Soc. A **68** (1955) 637
Wa 56a Warren, Alexander and Chadwick, Phys. Rev. **101** (1956) 242
Wa 56e Warburton, Ph. D. Thesis, U. of Pittsburgh (1956)
Wa 56f Watters, Phys. Rev. **103** (1956) 1763
Wa 57 Warburton and McGruer, Phys. Rev. **105** (1957) 639
Wa 57a Warren and Hay, Bull. Amer. Phys. Soc. **2** (1957) 178
Wa 57b Waddell, Adelson, Moyer and Shaw, Bull. Amer. Phys. Soc. **2** (1957) 181
Wa 57c Walton, Clement and Boreli, Phys. Rev. **107** (1957) 1065
Wa 57d Warhanek, Phil. Mag. **2** (1957) 1085
Wa 57e Waddell, Ph. D. Thesis, U. of California, UCRL **3901** (1957)
Wa 57f Wakatsuki, Hirao, Okada and Miura, J. Phys. Soc. Japan **12** (1957) 1178
Wa 58 Warburton and Rose, Phys. Rev. **109** (1958) 1199
Wa 58a Warner and Alford, Bull. Amer. Phys. Soc. **3** (1958) 204
Wa 58b Wagner and Huber, Helv. Phys. Acta **31** (1958) 89
Wa 58c Way, Nuclear Data Cards, National Research Council, Washington, D. C. (1958)
Wa 58d Warner and Alford, Bull. Amer. Phys. Soc. **3** (1958) 364
Wa 58e Watanabe, Nuclear Physics **8** (1958) 484
Wa 59 Warburton, Phys. Rev. (1959)
Wa 59a Warburton, Rose and Hatch, Phys. Rev. (1959)
We 54 Weddell and Roberts, Phys. Rev. **95** (1954) 117
We 54b Wetherill, Phys. Rev. **96** (1954) 679

We 55 Webb, Hagedorn, Fowler and Lauritsen, Phys. Rev. **99** (1955) 138
We 56 Wegner and Igo, Bull. Amer. Phys. Soc. **1** (1956) 21
We 56a Werner, Nuclear Physics **1** (1956) 9
We 56c Weber, Davis and Marion, Phys. Rev. **104** (1956) 1307
We 57a Weinman and Silverstein, Bull. Amer. Phys. Soc. **2** (1957) 34
We 57b Weil, Jones and Lidofsky, Phys. Rev. **108** (1957) 800
We 58 Weinman and Silverstein, Phys. Rev. **111** (1958) 277
We 58a Weber, Phys. Rev. **110** (1958) 529
We 58b Welch and Wallace, Bull. Amer. Phys. Soc. **3** (1958) 206
We 58c Wegner and Hall, Bull. Amer. Phys. Soc. **3** (1958) 338
We 58d Weil and Jones, Phys. Rev. **112** (1958) 1975
Wh 39 White, Delsasso, Fox and Creutz, Phys. Rev. **56** (1939) 512
Wh 50c Whitehead, Phys. Rev. **79** (1950) 393
Wh 50d Whaling and Bonner, Phys. Rev. **79** (1950) 258
Wh 51b Whitehead, Phys. Rev. **82** (1951) 553
Wh 53 Whitmore, Phys. Rev. **92** (1953) 654
Wh 56 Whetstone, Yergin and Halpern, Bull. Amer. Phys. Soc. **1** (1956) 192
Wh 57a White and Farley, Nuclear Physics **3** (1957) 476
Wh 58 Whitehead, Murray, Aitken, Middlemas and Collie, Phys. Rev. **110** (1958) 941
Wh 58a Whitehead and Foster, Can. J. Phys. **36** (1958) 1276
Wi 37e Wilhelmy, Zeits. f. Physik **107** (1937) 769
Wi 51 Willard, Preston and Goodman, Phys. Rev. **81** (1951) 329A
Wi 52a Willard, Bair, Kington, Hahn, Snyder and Green, Phys. Rev. **85** (1952) 849
Wi 53 Wilkinson and Jones, Phil. Mag. **44** (1953) 542
Wi 53a Wilkinson, Phys. Rev. **90** (1953) 721
Wi 53c Wilkinson, Phil. Mag. **44** (1953) 450
Wi 53f Wilkinson, Phil. Mag. **44** (1953) 1019
Wi 53g Wilkinson and Clegg, Phil. Mag. **44** (1953) 1322
Wi 53h Wilkinson and Jones, Phys. Rev. **91** (1953) 1575
Wi 54a Wilkinson, Phil. Mag. **45** (1954) 259
Wi 54c Willard, Bair and Kington, Phys. Rev. **95** (1954) 1359
Wi 54f Winn, Proc. Phys. Soc. A **67** (1954) 946
Wi 55c Williams and Rasmussen, Phys. Rev. **98** (1955) 56
Wi 55d Willard, Bair and Kington, Phys. Rev. **98** (1955) 669
Wi 55f Wilkinson, Phys. Rev. **99** (1955) 1347
Wi 55g Williamson and Jones, Phys. Rev. **100** (1955) 960A
Wi 55h Wilkinson, Phys. Rev. **100** (1955) 32
Wi 55i Wignall, Australian J. Phys. **8** (1955) 310
Wi 56 Wilkinson, Toppel and Alburger, Phys. Rev. **101** (1956) 673
Wi 56a Willard, Bair, Kington and Cohn, Phys. Rev. **101** (1956) 765
Wi 56b Willard, Bair, Cohn and Kington, Bull. Amer. Phys. Soc. **1** (1956) 54
Wi 56c Wilkinson, Phil. Mag. **1** (1956) 379
Wi 56d Wilkinson, Phil. Mag. **1** (1956) 1031
Wi 56e Wilkinson, Phil. Mag. **1** (1956) 127
Wi 56g Wilkinson and Clegg, Phil. Mag. **1** (1956) 291
Wi 56k Wilson, Phys. Rev. **104** (1956) 1424
Wi 57 Wilkinson, Phil. Mag. **2** (1957) 83
Wi 57a Wilkinson and Bloom, Phys. Rev. **105** (1957) 683
Wi 57b Wilkinson and Bloom, Phil. Mag. **2** (1957) 63
Wi 57c Wilkinson, Phys. Rev. **105** (1957) 666
Wi 57d Wilkinson, Phys. Rev. **105** (1957) 686
Wi 57e Willard, Bair, Cohn and Kington, Phys. Rev. **105** (1957) 202
Wi 57f Wickersham, Phys. Rev. **107** (1957) 1050
Wi 57g Wilhelmsson and Nilsson, Nuclear Physics **4** (1957) 234
Wi 58 Wills, Bair, Cohn and Willard, Phys. Rev. **109** (1958) 891
Wi 58a Willard, Bair and Cohn, Bull. Amer. Phys. Soc. **3** (1958) 18

Wi 58b Wilkinson, Phys. Rev. **109** (1958) 1603
Wi 58c Wilkinson, Phys. Rev. **109** (1958) 1610
Wi 58d Wilkinson, Phys. Rev. **109** (1958) 1614
Wi 58f Williamson, Hudspeth, Morgan and Moore, Phys. Rev. **110** (1958) 139
Wi 58g Wildermuth and Kanellopoulos, Nuclear Physics **7** (1958) 150
Wi 59 Wilkinson and Alburger, Phys. Rev. (1959)
Wo 53c Woodbury, Day and Tollestrup, Phys. Rev. **92** (1953) 1199
Wo 54 Woodbury, Tollestrup and Day, Phys. Rev. **93** (1954) 1311
Wo 54a Wong, Phys. Rev. **95** (1954) 761
Wo 54b Wong, Phys. Rev. **95** (1954) 765
Wo 56 Wolicki, Geer, Holmgren and Johnston, Bull. Amer. Phys. Soc. **1** (1956) 196
Wo 56a Wood and Singletary, Bull. Amer. Phys. Soc. **1** (1956) 246
Wo 56b Wolicki, Holmgren, Johnston and Geer, Bull. Amer. Phys. Soc. **1** (1956) 325
Wo 58 Wolff, Winhold, Stephens and Carroll, see Halpern in Conference on Photonuclear Reactions, National Bureau of Standards (1958); Bull.Amer. Phys. Soc. **3** (1958) 173
Wo 58a Wolff, U. of Pennsylvania, Tech. Report 4 (1958) and Phys. Rev. Lett. **1** (1958) 354
Wr 53 Wright, Phys. Rev. **90** (1953) 159
Wr 53a Wright, UCRL 2422 (1953)
Wr 56 Wright, Morrison, Reid and Atkinson, Proc. Phys. Soc. A **69** (1956) 77
Wr 57 Wright, Wyatt, Reynolds, Lyon and Handley, Nuclear Science and Engineering **2** (1957) 427
Wu 50 Wu, Revs. Mod. Phys. **22** (1950) 386
Wu 52 Wu, Rustad, Perez-Mendez and Lidofsky, Phys. Rev. **87** (1952) 1140
Wu 58 Wu and Schwarzschild, CU-173 (1958)
Wy 58 Wyman, Bull. Amer. Phys. Soc. **3** (1958) 187
Wy 58a Wyman, Fryer and Thorpe, Phys. Rev. **112** (1958) 1264

Ya 51 Yaffe and Stevens, Canadian J. Phys. **29** (1951) 186; Phys. Rev. **79** (1950) 893
Ya 53 Yarnell, Lovberg and Stratton, Phys. Rev. **90** (1953) 292
Yo 57a Young, Phillips and Spencer, Phys. Rev. **108** (1957) 72

Za 57 Zabel, WASH 192 (1957)
Ze 56 Zeidman and Fowler, Bull. Amer. Phys. Soc. **1** (1956) 325
Ze 57 Zeidman and Fowler, Bull. Amer. Phys. Soc. **2** (1957) 351
Zh 54 Zhpinel, Iszv. Akad. Nauk **18** (1954) 65
Zi 56a Zimmermann, Phys. Rev. **104** (1956) 387
Zi 57 Zipoy, Freier and Famularo, Phys. Rev. **106** (1957) 93
Zi 58 Zipoy, Phys. Rev. **110** (1958) 995
Zi 59 Zimmermann, Phys. Rev. (1959)
Zi 59a Zimmermann Phys. Rev. (1959)
Zu 50a Zucker and Watson, Phys. Rev. **78** (1950) 14

4.A:8.A *Nuclear Physics* **11** (1959) 341—348; ©*North-Holland Publishing Co., Amsterdam*
Not to be reproduced by photoprint or microfilm without written permission from the publisher

β—ν CORRELATION IN Ne^{23} WITH RESONANCE FLUORESCENCE

N. E. BOOTH †, G. W. HUTCHINSON, A. M. SEGAR, G. G. SHUTE †† and D. H. WHITE †††
Department of Physics, The University, Birmingham, England

Received 26 January 1959

Abstract: The correlation between the β-rays and those γ-rays Doppler-shifted by nuclear recoil to the energy needed for resonance scattering, has been measured for Ne^{23}. This correlation is directly related to the β—ν correlation for Gamow-Teller negaton emission.

The correlation expected depends on the M1, E2 mixing in the gamma transition. With the best estimate of this, the ratio of coincidences at 90° to those at 180° should be 0.87 for axial vector and 1.17 for tensor interaction. The experimental result, obtained in about 100 hours of running time, 0.56 ± 0.24, supports axial vector interaction. The results also give a value for the lifetime of the 436 keV level in Na^{23} of $(1.5 \pm 0.3) \times 10^{-10}$ sec.

1. Introduction

The measurement, by some indirect means, of the β—ν correlation has been used in many experiments to determine the nature of the interaction in β-decay. All experiments so far have involved direct observation of the momenta of the recoil nuclei. A number of authors have suggested the use of resonance fluorescence as an alternative to this method.

The knowledge that a γ-ray has been Doppler-shifted by the nuclear recoil velocity up to the resonance energy means that the nuclear recoil momentum along the γ-ray direction has been defined. Thus a β-resonant γ-correlation is related to the β-recoil nucleus correlation and hence to the β—ν correlation.

The β-resonant γ-correlation function has been calculated by Lewis and Curtis [1]), and by Morita, Morita and Yamada [2]).

There is now a great deal of evidence (given for example by Feynman and Gell-Mann [3]) both from β—ν correlation experiments and from experiments making use of parity violation, that supports a universal vector—axial-vector weak interaction.

However, in the Gamow-Teller β-decay of Ne^{23}, Ridley [4]) measured the spectrum of recoil nuclei and coincident electrons and obtained a result intermediate between that for axial vector and tensor interaction. Therefore, it was felt desirable to examine the Ne^{23} decay by another method. Since our

† Now at the Radiation Laboratory, University of California, Berkeley, California, U.S.A.
†† Now at the Physics Department, University of Melbourne, Melbourne, Australia.
††† Now at the Physics Department, University of Pennsylvania, Philadelphia, Pa., U.S.A.

May (3) 1959

work was completed, the recoil experiment of the Illinois group [5]) has supported axial vector interaction for this decay.

Ne^{23} satisfies very well the practical requirements for resonance fluorescence. It is gaseous, so that the probability of a collision within the γ-decay lifetime is small. The recoil momentum available is ample to shift the γ-ray energy up to the resonance energy, and the daughter isotope is abundant.

2. Experimental Method

2.1. GAS FLOW SYSTEM

The Ne^{23} was produced by the reaction $Na^{23}(n, p)Ne^{23}$, the fast neutron flux arising from deuteron bombardment of a beryllium target in the Nuffield cyclotron.

The target and the acetone flow system were similar to those used by Ridley [4]). However, the pumping system was much simpler in our case because of the different source requirement. Dry-ice and liquid air acetone traps were followed by a charcoal-liquid air trap, and then by a mercury diffusion pump. The latter pumped the neon to the source volume, a glass bulb 2 cm diameter of wall thickness about 0.1 mm. The rise of pressure in the source was so slow that connection to a backing pump was needed only at about hourly intervals. Thus, during a run all available neon, excepting small amounts in the traps, collected in the source. Decay curves and spectra showed no evidence of any contaminant activities.

Optimum source strength was about 30 μC, and this could be obtained with a few μA of cyclotron beam on the beryllium target.

2.2. COUNTERS AND ELECTRONICS

Fig. 1 is a plan of the source and counter geometry used. There were two gamma counters, 1 and 2. These were 3.8 cm dia. $\times$ 5 cm sodium iodide scintillation counters, each shielded from the source and viewing scatterer blocks 5 cm $\times$ 5 cm $\times$ 7.5 cm. The two beta counters used 7.5 cm dia. discs of plastic scintillator of a thickness sufficient to stop full energy electrons.

The sodium scatterers were blocks of pure sodium cast to size and sealed with paraffin in perspex containers. Background measurements were made with scatterers of aluminium powder, compressed into identical perspex containers to a density such that Compton scattering from both types of scatterer was the same to a few percent.

Fig. 1 shows a typical β-fluorescent γ-coincidence event of angle near 90°. The electron entered counter 4, and the gamma ray was resonantly scattered in the sodium and was then detected in the sodium iodide crystal of counter 1. Coincidences (1—3) and (2—4) were for β—γ angles near 180°, while coincidences (1—4) and (2—3) were for angles near 90°.

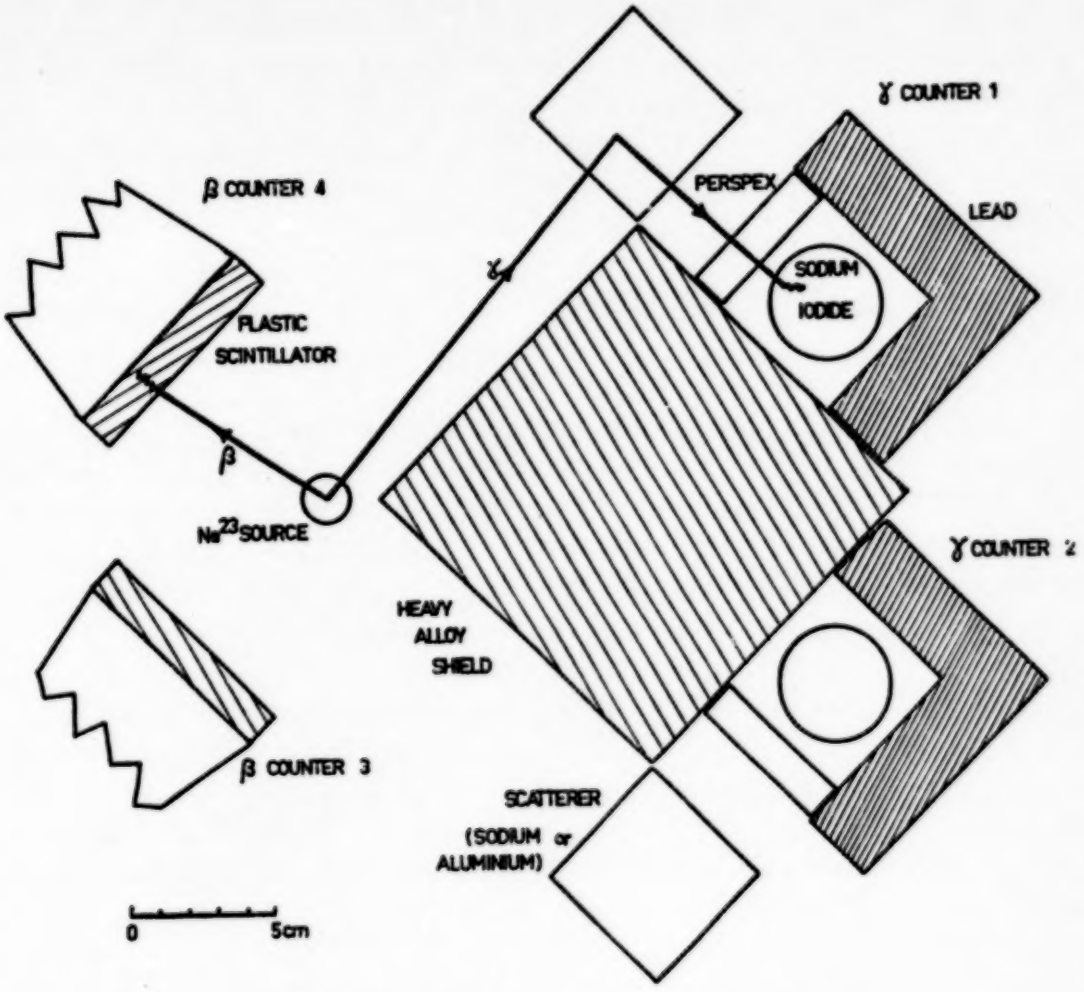

Fig. 1. Plan of the source and counter geometry.

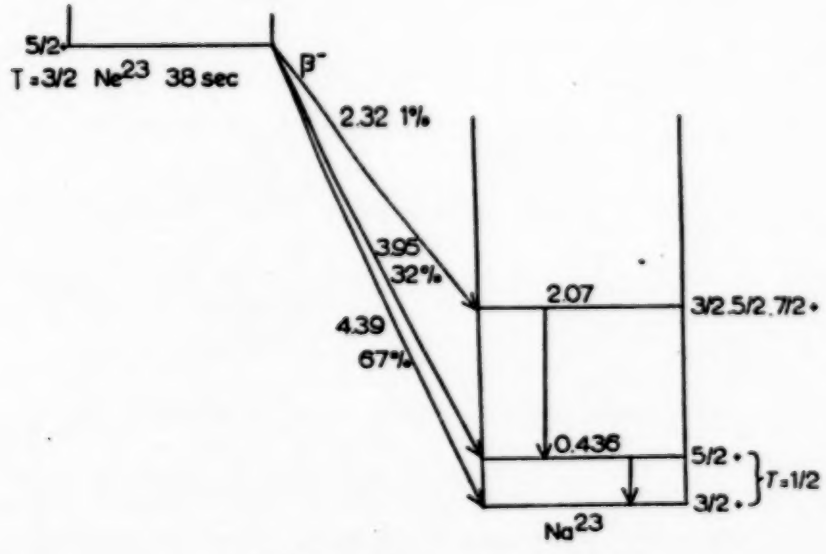

Fig. 2. Decay scheme of Ne^{23}.

In the geometry used, only about 5×10^{-5} of all gamma rays entering a sodium scattering block were resonantly scattered into the gamma counter. Consequently, the coincidence counting rate at optimum source strength was very low, in fact about 2 per hour of running time. The circuits and counting method used had therefore to be designed to make maximum use of this very meagre data.

Two coincidence circuits of resolving time 10^{-8} sec, produced true and random coincidence signals. The inputs to the circuits were mixed in such a way that all four sets of β—γ coincidences produced a coincidence output, but β—β and γ—γ combinations did not.

These outputs generated brightening pulses for two Tektronix type 545 oscilloscopes. The oscilloscope plates were connected in such a way that signals 1 and 2 produced deflections $\pm X$ on the screen, while signals 3 and 4 produced deflections $\pm Y$. Delays were inserted in signals 3 and 4 and in the coincidence signals such that the β-signal coincided with the peak of the relatively slow γ-signals, and such that the brightening pulse occurred at the peak of the β-signal, both in the real and the random displays.

Thus the display consisted of brightened dots on the screen occurring in 4 quadrants, two corresponding to $\beta\gamma$ angles near 90° and two to angles near 180°. The γ-pulse heights were given by the horizontal deflection of the spot from the origin, and the β-pulse height by the vertical deflection. The arrangement is like that described by Maeder [6]), though the overall resolving time is much shorter. The effective time of brightening was about 2×10^{-8} sec.

The oscilloscope displays were photographed, and the films scanned over appropriate ranges of β and γ-pulse heights. The results obtained occupied about 100 hours of cyclotron time, and about twice that time in scanning the films. The method of display ensured that the 90°/180° asymmetry was independent of effects of scanning loss. The fact that each counter was making measurements at both angles made the result independent of any differences in counter efficiencies.

3. Results

3.1. CORRELATION

In the γ-pulse height region at 436 keV, the main contributions to coincidences were:

(a) resonantly scattered true coincidences,

(b) Compton scattered true coincidences from the 1.63 MeV γ,

(c) random coincidences.

The β counters detected mainly β- and γ-rays from the source, at a counting rate of $\approx 10^5$ counts per sec. The main contribution to the counting rate of the γ-counters was room background radiation penetrating their shielding.

Contribution (a) was separated from (b) and (c) by subtraction of the counting rates with sodium and aluminium scatterers, with a small correction for the mismatch of the Compton scattering.

The result from 265 such resonantly-scattered counts, was that the ratio of counts of all β-energies at 90° to those at 180° was 0.56 ± 0.24.

As can be seen from the graph of fig. 3, which has been calculated from the results of Lewis and Curtis [1]), the interpretation of the result for the symmetry depends very much on the magnetic dipole-electric quadrupole

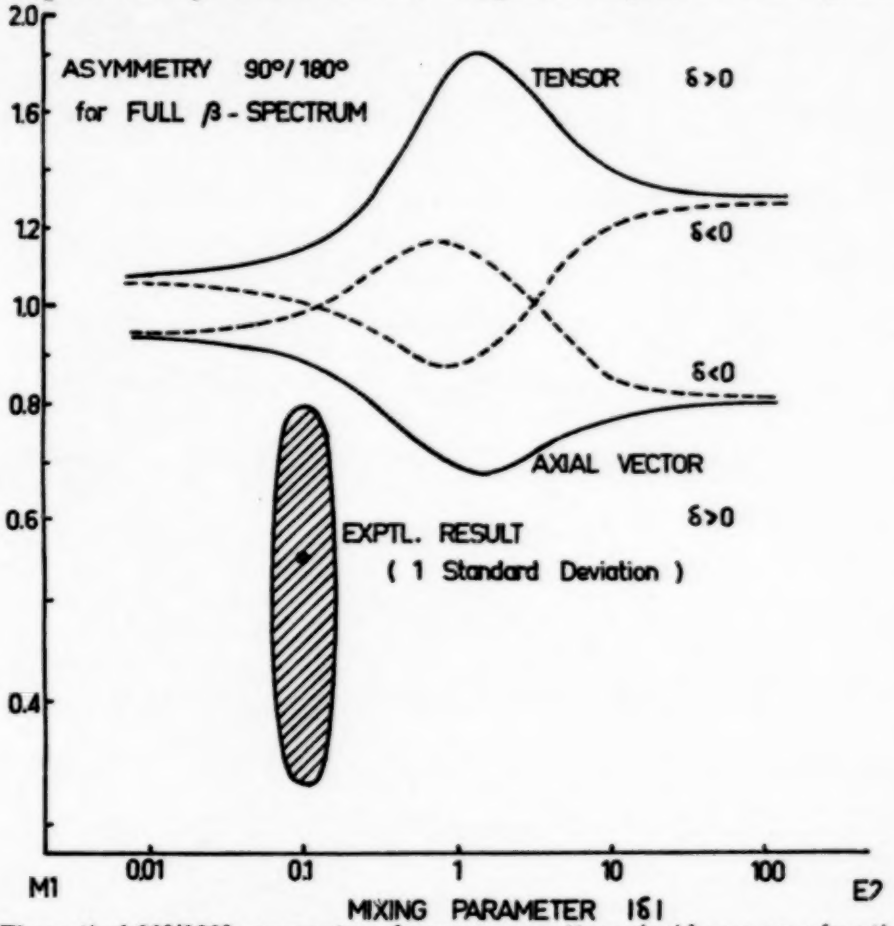

Fig. 3. Theoretical 90°/180° asymmetry of resonance scatter coincidences as a function of the M1—E2 mixing in the γ-transition. Shaded area is the experimental result.

mixing in the γ-transition. Berenbaum, Towle and Matthews [7]) have measured the K-shell internal conversion coefficient of the transition, and find $\Gamma_{E2}/\Gamma_{M1} < 0.05$ (or < 0.02 for one standard deviation). In order to determine the mixing, and in particular the phase of the mixing, we have measured the angular correlation of the gamma cascade. The result † was

$$W(\theta) = 1 - (0.009 \pm 0.026) \cos^2\theta.$$

† Note that $\cos^4\theta$ need not be considered since this can only occur in a term corresponding to an E2—E2 transition, and this must be small since the second transition is mainly M1.

The spin of the 2.07 MeV level in Na^{23} may be $\frac{7}{2}$, $\frac{5}{2}$ or $\frac{3}{2}$, and its parity is positive (Penning and Schmidt [8])). Thus both γ transitions can be M1—E2 mixtures. The graphs of fig. 4 show, for each of the spin values, the predicted

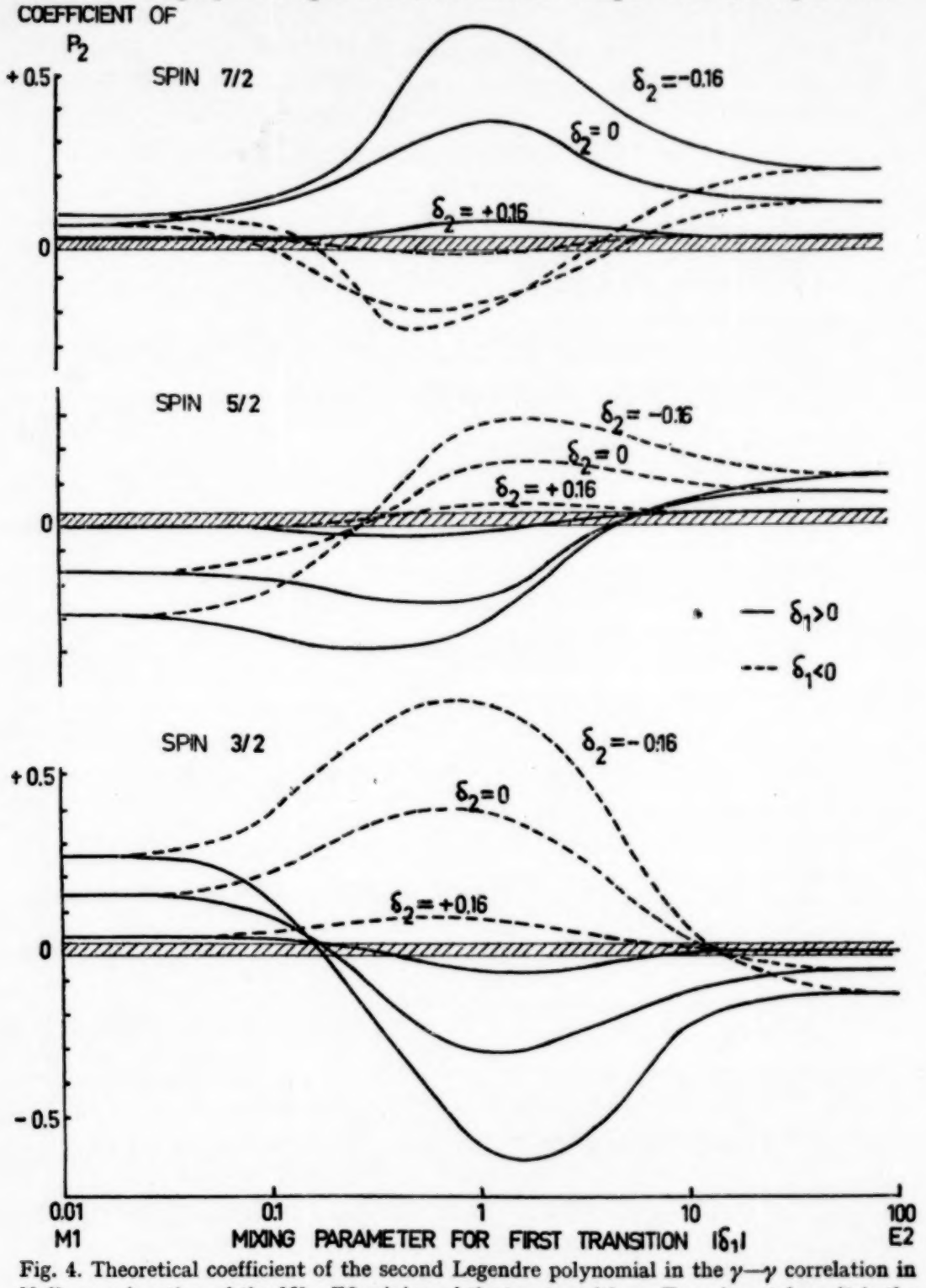

Fig. 4. Theoretical coefficient of the second Legendre polynomial in the γ—γ correlation in Na^{23}, as a function of the M1—E2 mixing of the two transitions. Experimental result is the shaded area.

coefficient of the second Legendre polynomial of the correlation as a function of the two mixing parameters, δ_1 and δ_2. Subscript 1 refers to the first and 2 to the second transition. Only the values $\delta_2 = 0$ and ± 0.16 are shown, corresponding to mixing ratios Γ_{E2}/Γ_{M1} of 0 and 0.026.

Each of the sets of graphs is similar in that large asymmetries are obtained over most of the range of δ_1 unless δ_2 is positive. In fact, the curves for $\delta_2 = +0.16$ fit the experimental correlation result reasonably well for all three spins and for any δ_1, while those for $\delta_2 = 0$ and -0.16 fit the result only over narrow ranges of values of δ_1.

It can be concluded that probably $\delta_2 > +0.08$, and from the experiment of Berenbaum *et al.*, $|\delta_2| < +0.15$.

The result for the mixing ratio and the 90°/180° asymmetry is plotted on fig. 3 together with the theoretical predictions. The axial vector prediction is in much better agreement with the experiment than is the tensor.

3.2. LIFETIME OF THE 436 keV STATE

Any measurement of a resonance scattering cross-section can be used to estimate the lifetime of the state concerned (Moon [9])).

In order to obtain an absolute measure of the resonance cross-section independent of scanning loss and any errors inherent in geometrical calculations, the resonance counts per monitor count were compared with Compton scatter counts per monitor. A comparison of the latter measurement with an absolute calibration of the monitor in terms of a Na^{22} source suggested that there was an appreciable scanning loss.

Since coincident resonant scattering was measured, it was necessary to integrate over the β-spectrum and the β-angular correlation, and for the latter the theoretical correlation was used. For the gamma spectrum, an approximate function (Moon and Ilakovac, unpublished) was assumed. Since the Doppler shift E_d required for resonance is 8.8 eV, and both level width and thermal broadening (0.9 eV) are small compared with the available recoil Doppler shift (± 89 eV) the effective cross section is

$$\sigma_{eff} = \left(f(E_d) / \int_0^\infty f(E)\mathrm{d}E \right) g \frac{\lambda^2}{8\pi} \int_0^\infty \frac{\Gamma^2}{(E-E_0)^2 + \frac{1}{4}\Gamma^2} \mathrm{d}E$$

where g allows for the spin multiplicity of ground and excited states, λ is the wavelength corresponding to the level energy E_0, Γ the level width, and $f(E)$ the gamma spectrum function. Hence the result for the lifetime of the 436 keV state in Na^{23}:

$$\tau = (1.5 \pm 0.3) \times 10^{-10} \text{ sec.}$$

This is much longer than the result of Krone, Everett and Hanna [10])

$$10^{-13} < \tau < 10^{-12} \text{ sec.}$$

It is a large but not unreasonable value for an M1 transition of this energy.

The authors wish to thank Dr. B. W. Ridley for his advice, particularly regarding the gas flow system, Professors P. B. Moon and W. E. Burcham for their encouragement and cooperation, and Professor F. L. Hereford for his valued assistance.

N.E.B. wishes to thank I.C.I. Ltd. for his research fellowship, and A.M.S. the Royal Society for his Rutherford Scholarship.

References

1) R. R. Lewis and R. B. Curtis, Phys. Rev. **110** (1958) 910
2) M. Morita, R. S. Morita and M. Yamada, Phys. Rev. **111** (1958) 237
3) R. P. Feynman and M. Gell-Mann, Phys. Rev. **109** (1958) 193
4) B. W. Ridley, Nuclear Physics **6** (1958) 34
5) R. L. Burman, W. B. Herrmannsfeldt, J. S. Allen and T. H. Braid, Phys. Rev. Letters **2** (1959) 9
6) D. Maeder, Nuclear Instruments **2** (1958) 299
7) R. Berenbaum, J. H. Towle and J. H. Matthews, Proc. Phys. Soc. A **69** (1956) 858
8) J. R. Penning and F. H. Schmidt, Phys. Rev. **105** (1957) 647
9) P. B. Moon, Proc. Phys. Soc. A **64** (1951) 76
10) R. W. Krone, A. Everett and S. S. Hanna, Bull. Am. Phys. Soc. **1** (1956) 329

2.L *Nuclear Physics* **11** (1959) 349—356; ©*North-Holland Publishing Co., Amsterdam*
Not to be reproduced by photoprint or microfilm without written permission from the publisher

INELASTIC SCATTERING OF HIGH ENERGY PROTONS BY B^{11} AND O^{16}

L. EGARDT

Institute for Theoretical Physics, University of Uppsala

Received 30 January 1959

Abstract: The differential cross-sections for the inelastic scattering to the 4.46-MeV level of B^{11} and to the 6.06- and 6.14-MeV levels of O^{16} are calculated in the extreme L-S coupling picture. The transition to the excited state is described by the free nucleon-nucleon scattering matrix. Only the absorption part of the optical potential is taken into account. Good agreement with experiment is obtained.

1. Introduction

During the last two years several measurements have been made by Tyrén *et al.* [1]) of the differential cross-sections in the inelastic scattering of 160—185 MeV protons by light nuclei. Theoretically the angular distribution for the scattering to the 4.43-MeV level of C^{12} has been extensively studied by many authors, among others by Squires [2]), whose calculation is based on known facts about free nucleon-nucleon scattering. Quite a similar method of approach is used in this paper for the scattering to the 4.46-MeV level of B^{11} and to the 6.06- and 6.14-MeV levels of O^{16}. Since the L-S coupling picture seems to reproduce the experimental data for the light nuclei better than the jj-coupling picture [2]) no attempt is made to consider the latter case. Only the absorption part of the optical potential is taken into account, as the inclusion of the additional terms in this potential do not appreciably alter the results obtained by Squires for C^{12}, as has recently been pointed out by McCauley [3]).

2. The Transition Matrix and the Differential Cross-Section

We expect the transition from the ground state ψ_1 to an excited state ψ_t to be the result of a single energetic collision between the incoming high energy proton and one nuclear particle. This process is assumed to be described by the t-matrix for free nucleon-nucleon scattering in a short-range approximation. The t-matrix is given by [4])

$$t_{1t} = a+c(\boldsymbol{\sigma}_1+\boldsymbol{\sigma}_k)\cdot\hat{\mathbf{n}}+b(\boldsymbol{\sigma}_1\cdot\hat{\mathbf{n}})(\boldsymbol{\sigma}_k\cdot\hat{\mathbf{n}})+d(\boldsymbol{\sigma}_1\cdot\hat{\mathbf{K}})(\boldsymbol{\sigma}_k\cdot\hat{\mathbf{K}}) \\ +e(\boldsymbol{\sigma}_1\cdot\hat{\mathbf{P}})(\boldsymbol{\sigma}_k\cdot\hat{\mathbf{P}}), \quad (1)$$

$\hat{\mathbf{n}}$, $\hat{\mathbf{P}}$, $\hat{\mathbf{K}}$ being mutually orthogonal unit vectors: $\hat{\mathbf{n}}$ is perpendicular to the momenta $\mathbf{k}_i$ and $\mathbf{k}_f$ of the incoming and outgoing protons respectively and $\hat{\mathbf{K}}$ is the unit vector in the direction of the momentum transfer to the excited particle,

$$\mathbf{K} = \mathbf{k}_i - \mathbf{k}_f, \tag{2}$$

neglecting nuclear recoil. The values of the angle-depending parameters $a, \ldots, e$ have been calculated by Squires for p—p and p—n scattering at 180 MeV from the phase-shifts of Gammel and Thaler [5]). In the present calculations these values are used.

The coherent attenuation of the proton beam due to the presence of other nucleons than the scattering one is described by the imaginary part of the central optical potential. If we denote the distorted incoming and outgoing waves by $\chi^+_{\mathbf{k}_i}(\mathbf{x})$ and $\chi^-_{\mathbf{k}_f}(\mathbf{x})$ respectively, we have the following expression for the transition matrix:

$$T_{fi}(\theta) = \langle \psi_f \chi^-_{\mathbf{k}_f}(\mathbf{x}) | \sum_k t_{ik} \delta(\mathbf{x} - \mathbf{x}_k) | \chi^+_{\mathbf{k}_i}(\mathbf{x}) \psi_i \rangle \tag{3}$$

where the sum is over the nuclear particles in the shell to be excited, and θ is the angle between the directions of the in- and outgoing wave vectors $\mathbf{k}_i$ and $\mathbf{k}_f$. The symbols i and f include the projection quantum numbers of both spin and orbital angular momentum. After transforming from the centre-of-mass system of the colliding particles to the laboratory system the inelastic differential cross-section is given by

$$\frac{\mathrm{d}\sigma}{\mathrm{d}\Omega} = 2 \, \S \, \mathrm{tr} \, [T^\dagger_{fi} T_{fi}]. \tag{4}$$

The symbol $\S$ stands for averaging over initial states and summing over final states. The factor $2 = 4 \cdot \frac{1}{2}$ is a product of the transformation-coefficient 4 for small angles and $\frac{1}{2}$ from the fact that the trace is to be taken in the two-dimensional spin-space of the incident and final proton. In the case of spin-zero nuclei eq. (4) reduces to that of Squires' and if the final state has $S = 0$ only the first two terms of the t-matrix contribute.

3. The Absorption and the Nuclear States

We assume a Gaussian shape for the density distribution of the nucleus. Recent calculations performed by Bjorklund and Fernbach [6]) give at 180 MeV a value about 20 MeV for the strength parameter of the imaginary part of the central optical potential, assumed to be of the Woods-Saxon form. Therefore it should be quite reasonable to take the value 30 MeV using the Gaussian distribution. The exponential parameter β is chosen to give the same root-mean-square radius for the potential as for the nuclear charge

distribution. These values are taken from a review article by Hofstadter [7]) giving us the r.m.s. radii 2.35 and 2.64 in units of 10^{-13} cm for B^{11} and O^{16} respectively.

The W.K.B. approximated incoming and outgoing proton-waves appear as a factor

$$e^{i\mathbf{K}\cdot\mathbf{x}} f(r) \tag{5a}$$

in the transition matrix elements, where r is the perpendicular distance from the straight-line integration paths to the parallel along $\mathbf{k}_i+\mathbf{k}_f$ passing through the centre of the nucleus. The use of straight-line paths in this manner [2]) does not introduce any serious errors for the angles considered in this work. The function $f(r)$ is of the form

$$f(r) = \exp\{-\delta e^{-\beta r^2}\} \tag{5b}$$

where δ is a constant.

It is convenient for the final integrations to expand the exponential, taking two terms and then adjusting the second one so as to get the best approximation of the original function in the region of absorption. This gives

$$f(r) \approx 1-0.60\, e^{-0.88\beta r^2} \qquad \text{for } B^{11}, \tag{6a}$$

$$f(r) \approx 1-0.62\, e^{-0.81\beta r^2} \qquad \text{for } O^{16}. \tag{6b}$$

The error introduced by this procedure is negligible. We next consider the nuclear states, treating the two nuclei separately.

B^{11}. According to Rasmussen *et al.* [8]) the ground state of this nucleus has spin $\frac{3}{2}$, parity—. The second excited state at 4.46 MeV, which is to be considered here, corresponds to the 4.43 MeV level of C^{12} and has spin $\frac{5}{2}$, parity—. The L-S coupling assignments for these states are ^{22}P and ^{22}D respectively, adopting the usual notation $^{2T+1,2S+1}L$. The orbital symmetry is in both cases (p^7 [43]).

O^{16}. The ground state is a ^{11}S-state and has space-symmetry [444] in the p-shell. The two adjacent levels at 6.06 and 6.14 MeV have spins and parities 0^+, 3^- respectively. The 3^--state has the L-S-assignment ^{11}F, the excited particle being in the d-shell. Regarding the nature of the 0^+-state there is some uncertainty. Unfortunately, the 3^- level is very close to the 0^+-level and on account of the limited energy resolution of the experimental set up, accurate measurements of the individual cross-sections are very difficult. Comparison between the theoretical differential cross-section for scattering to the 6.14 MeV level [10]) and experiment seems to rule out the alternative of simple two-particle excitation in the direct interaction picture; the 3^- theoretical cross-section being too small, In this paper a model proposed by Redmond [11]) is used, partly for reasons of simplicity. His interpretation of the 0^+-state as the result of a single particle excitation from the 1s- to the 2s-

shell gives excellent agreement with experiment as regards electric monopole transitions.

4. Details of the Calculation and Results

4.1. B^{11}

A convenient way of evaluating the matrix element (3) is to decouple the wave-function of particle 7, say, from the rest of the nuclear wave-function using the fractional parentage technique developed by Jahn *et al.* [9]). Thus we obtain the following scheme:

Ground-state:

$$\psi_1(p^7\,[43]\,{}^{22}P) = \sqrt{\tfrac{9}{14}}\,[\sqrt{\tfrac{16}{54}}(p^6\,[42]\,S)+\sqrt{\tfrac{3}{54}}\,(p^6\,[42]\,D_I)+\sqrt{\tfrac{35}{54}}(p^6\,[42]\,D_{II})]$$
$$\times\Big[\frac{1}{\sqrt{2}}\,{}^{13}\Gamma[\widetilde{42}]-\frac{1}{\sqrt{2}}\,{}^{31}\Gamma[\widetilde{42}]\Big] \qquad (7)$$
$$+\sqrt{\tfrac{5}{14}}[-(p^6\,[33]\,P)]\times[\sqrt{\tfrac{1}{10}}\,{}^{11}\Gamma[\widetilde{33}]+\sqrt{\tfrac{9}{10}}\,{}^{33}\Gamma[\widetilde{33}]].$$

Excited state:

$$\psi_1(p^7\,[43]\,{}^{22}D) = \sqrt{\tfrac{9}{14}}\,[\sqrt{\tfrac{35}{54}}(p^6\,[42]D_I)+\sqrt{\tfrac{3}{54}}(p^6\,[42]\,D_{II})-\sqrt{\tfrac{16}{54}}(p^6\,[42]\,F)]$$
$$\times\Big[\frac{1}{\sqrt{2}}\,{}^{13}\Gamma[\widetilde{42}]-\frac{1}{\sqrt{2}}\,{}^{31}\Gamma[\widetilde{42}] \qquad (8)$$
$$+\sqrt{\tfrac{5}{14}}[\sqrt{\tfrac{21}{25}}(p^6\,[33]\,P)-\sqrt{\tfrac{4}{25}}(p^6\,[33]\,F)]\times[\sqrt{\tfrac{1}{10}}\,{}^{11}\Gamma[\widetilde{33}]+\sqrt{\tfrac{9}{10}}\,{}^{33}\Gamma[\widetilde{33}]].$$

Here the Γ's denote charge-spin functions and D_I, D_{II} are the well-known D-states in the middle of the p-shell.

We now insert the expressions (7) and (8) into (3) and get, on account of the antisymmetry of the nuclear wave-function †,

$$T_{\substack{M'_S M_S\\ M'_L M_L}} = \frac{\sqrt{105}}{12}\langle p^6\,[42]\,{}^{13}D;\,{}^{22}p,\,{}^{22}D\,\tfrac{1}{2}M'_S M'_L|\chi^-\chi^+ t_7|p^6\,[42]\,{}^{13}D;\,{}^{22}p,\,{}^{22}P\,\tfrac{1}{2}M_S M_L\rangle$$
$$+\frac{\sqrt{105}}{12}\langle p^6\,[42]\,{}^{31}D;\,{}^{22}p,\,{}^{22}D\,\tfrac{1}{2}M'_S M'_L|\chi^-\chi^+ t_7|p^6\,[42]\,{}^{31}D;\,{}^{22}p,\,{}^{22}P\,\tfrac{1}{2}M_S M_L\rangle \qquad (9)$$
$$-\frac{\sqrt{21}}{20}\langle p^6\,[33]\,{}^{11}P;\,{}^{22}p,\,{}^{22}D\,\tfrac{1}{2}M'_S M'_L|\chi^-\chi^+ t_7|p^6\,[33]\,{}^{11}P;\,{}^{22}p,\,{}^{22}P\,\tfrac{1}{2}M_S M_L\rangle$$
$$-\frac{9\sqrt{21}}{20}\langle p^6\,[33]\,{}^{33}P;\,{}^{22}p,\,{}^{22}D\,\tfrac{1}{2}M'_S M'_L|\chi^-\chi^+ t_7|p^6\,[33]\,{}^{33}P;\,{}^{22}p,\,{}^{22}P\,\tfrac{1}{2}M_S M_L\rangle$$

where the quantum numbers of the state-vectors symbolise, e.g. for the ket-vector in the first term: "a ^{13}D-state of 6 particles is coupled to a p-particle with spin $\frac{1}{2}$ and iso-spin $\frac{1}{2}$ to form a ^{22}P state with projection quantum numbers $M_T = \frac{1}{2}$ (neutron), M_S and M_L". The t-matrix operates on the p-particle and the product $\chi^-\chi^+$ equals $e^{i\mathbf{K}\cdot\mathbf{x}}f(r)$. The evaluation of the

† Part of the antisymmetrization between the incoming proton and the nuclear particle is automatically taken into account by the use of the t-matrix.

T-matrix is now a lengthy but straightforward standard procedure in the theory of angular momentum. It is convenient to collect terms describing spin flip and spin-conserving processes separately both in the expressions (4) and (9) and to take care of symmetry properties of the t-matrix and of the integrals. Only integrals describing a change of the component of angular momentum by 0 or 2 units along the quantization axis, which is taken along the K-axis, will contribute. This fact depends on odd or even functions as integrands. Now it is simple to systematize the calculation and we finally obtain the following expression for the differential cross-section:

$$\frac{d\sigma}{d\Omega} = \frac{7.32}{45^2}\{3I_{11}^2+(I_{00}-I_{11})^2\}\{|7a+\tfrac{1}{2}a_{pp}|^2+|7c+\tfrac{1}{2}c_{pp}|^2+|\tfrac{1}{2}d_{pp}|^2+|c_{pp}|^2+|b_{pp}|^2+|e_{pp}|^2\} \quad (10)$$

with

$$I_{m'm} = \langle 1m'|e^{i\mathbf{K}\cdot\mathbf{x}}f(r)|1m\rangle. \quad (11)$$

In equation (10)

$$a = \tfrac{1}{2}(a_{pp}+a_{pn}), \qquad c = \tfrac{1}{2}(c_{pp}+c_{pn}), \quad (12)$$

where the indices pp and pn refer to proton-proton and proton-neutron scattering respectively. The matrix-element (11) is between 1p oscillator wave-functions with magnetic quantum numbers m' and m. The integrals can easily be solved exactly by introducing harmonic polynomials [12]), thus:

$$|1m\rangle = \sqrt{\frac{8\alpha^{\frac{5}{2}}}{3\pi^{\frac{3}{2}}}}\,e^{-\frac{1}{2}\alpha(x^2+y^2+z^2)}\times\mathscr{Y}_{1m}(\mathbf{x}) \quad (13)$$

where

$$\mathscr{Y}_{1\pm1}(\mathbf{x}) = \mp\tfrac{1}{2}\sqrt{\frac{3}{2\pi}}\,(x\pm iy), \qquad \mathscr{Y}_{10}(\mathbf{x}) = \tfrac{1}{2}\sqrt{\frac{3}{\pi}}\,z. \quad (14)$$

The oscillator well parameter α is fixed by the requirement that the r.m.s. radius of the nucleus should be equal to 2.35×10^{-13} cm [7]), which gives

$$\alpha = 0.381\times10^{26}\ \text{cm}^{-2}. \quad (15)$$

The computation of the integrals leads to the following expressions:

$$I_{00}-I_{11} = -\frac{K^2}{2\alpha}e^{-K^2/4\alpha}+0.60\,\frac{\alpha^2}{2(\alpha+\gamma)^2}\left[\frac{\gamma}{\alpha}+\frac{K^2}{(\alpha+\gamma)}\right]e^{-K^2/4(\alpha+\gamma)} \quad (16a)$$

$$I_{-11} = 0.60\,\frac{\alpha\gamma}{2(\alpha+\gamma)^2}\,e^{-K^2/4(\alpha+\gamma)} \quad (16b)$$

where

$$\gamma = 0.88\beta = 0.239\times10^{26}\ \text{cm}^{-2}. \quad (17)$$

From these expressions the effect of absorption is easily estimated. The theoretical differential cross-section is plotted in fig. 1, together with the experimental result.

4.2. O^{11}

In the case of O^{16} the calculations are much simpler than for B^{11} as O^{16} is a spin-zero nucleus. We first treat the scattering to the 3^--level.

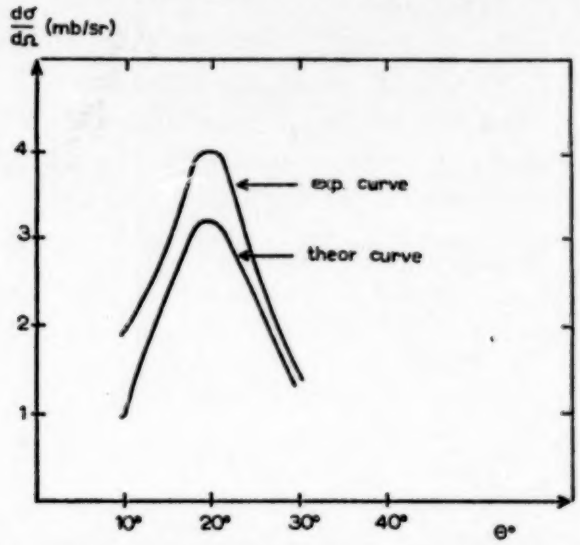

Fig. 1. The experimental and theoretical differential cross-sections for the inelastic scattering of 180 MeV protons by B^{11}.

A convenient way of evaluating the matrix (3) is to repeat the procedure of subsection 4.1, viz. to decouple the wave-function of particle 11, say, from the rest of the nuclear wave-function, lifting it to the d-shell, recoupling and finally antisymmetrizing. We get

$$T_{M0}=\sqrt{12}\langle p^{11}[443]^{22}P;\ ^{22}d,\ ^{11}F\,00M|\chi^-\chi^+t_{11}|p^{11}[443]^{22}P;\ ^{22}p,\ ^{11}S\,000\rangle, \quad (18)$$

which after some simple algebra reduces to

$$T_{M0}=2(a+c\sigma_1\cdot\hat{\mathbf{n}})\{2\sqrt{\tfrac{1}{5}}J_{11}-\sqrt{\tfrac{3}{5}}J_{00})\delta_{M,0}+(\sqrt{\tfrac{2}{3}}J_{11}-\sqrt{\tfrac{1}{3}}J_{20})(\delta_{M,2}+\delta_{M,-2})\} \quad (19)$$

with

$$J_{m'm}=\langle 2m'|e^{i\mathbf{K}\cdot\mathbf{x}}f(r)|1m\rangle. \quad (20)$$

The matrix element (20) is between harmonic oscillator functions with angular momenta 2 and 1 and projection quantum numbers m' and m respectively. Corresponding to (13) we have

$$|2m\rangle=\sqrt{\frac{16\alpha^{\frac{7}{2}}}{15\pi^{\frac{3}{2}}}}\,e^{-\frac{1}{2}\alpha(x^2+y^2+z^2)}\mathscr{Y}_{2m}(\mathbf{x}) \quad (21)$$

where $\mathscr{Y}_{2m}$ are the normalized harmonic polynomials for the d-shell. The r.m.s. radius 2.64×10^{-13} cm [7]) for O^{16} fixes the value of α to

$$\alpha=0.323\times10^{26}\ \text{cm}^{-2}. \quad (22)$$

Now the calculation of the integrals is easily done and we get

$$K_0=2\sqrt{\tfrac{1}{5}}J_{11}-\sqrt{\tfrac{3}{5}}J_{00}=i\tfrac{1}{4}\sqrt{\tfrac{2}{5}}\frac{K^3}{\alpha^{\frac{3}{2}}}e^{-K^2/4\alpha}-0.62i\tfrac{1}{2}\sqrt{\tfrac{1}{10}}\frac{K\alpha^{\frac{3}{2}}}{(\alpha+\gamma)^3}\left\{3\gamma+\frac{\alpha K^2}{(\alpha+\gamma)}\right\}e^{-K^2/4(\alpha+\gamma)}, \quad (23a)$$

$$K_1=\sqrt{\tfrac{2}{3}}J_{1-1}-\sqrt{\tfrac{1}{3}}J_{20}=-i0.62\frac{K\alpha^{\frac{3}{2}}\gamma}{(\alpha+\gamma)^3}\frac{1}{4\sqrt{3}}e^{-K^2/4(\alpha+\gamma)}, \quad (23b)$$

where

$$\gamma=0.81\beta=0.175\times10^{26}\ \text{cm}^{-2}. \quad (23c)$$

Introducing eq. (19) in (4) we obtain

$$\frac{d\sigma^{3-}}{d\Omega}=16\{|a|^2+|c|^2\}[|K_0|^2+2|K_1|^2] \quad (24)$$

for the scattering to the 3^--level.

For the scattering to the 0^+-level we easily get the following equations:

$$\begin{aligned}T&=4\langle 2s(1s)^3\,{}^{11}S000|e^{i\mathbf{K}\cdot\mathbf{x}}f(r)t_4|(1s)^4\,{}^{11}S000\rangle\\&=4(a+c\boldsymbol{\sigma}_1\cdot\hat{\mathbf{n}})\langle 2s|e^{i\mathbf{K}\cdot\mathbf{x}}f(r)|1s\rangle\end{aligned} \quad (25)$$

and

$$\frac{d\sigma^{0^+}}{d\Omega}=64\{|a|^2+|c|^2\}I^2_{2s,1s} \quad (26)$$

with

$$I_{2s,1s}=\sqrt{\tfrac{2}{3}}\left\{\frac{K^2}{4\alpha}e^{-K^2/4\alpha}-0.62\left(\frac{\alpha}{\alpha+\gamma}\right)^2\left[\frac{\gamma}{\alpha}+\frac{K^2}{4(\alpha+\gamma)}\right]e^{-K^2/4(\alpha+\gamma)}\right\}. \quad (27)$$

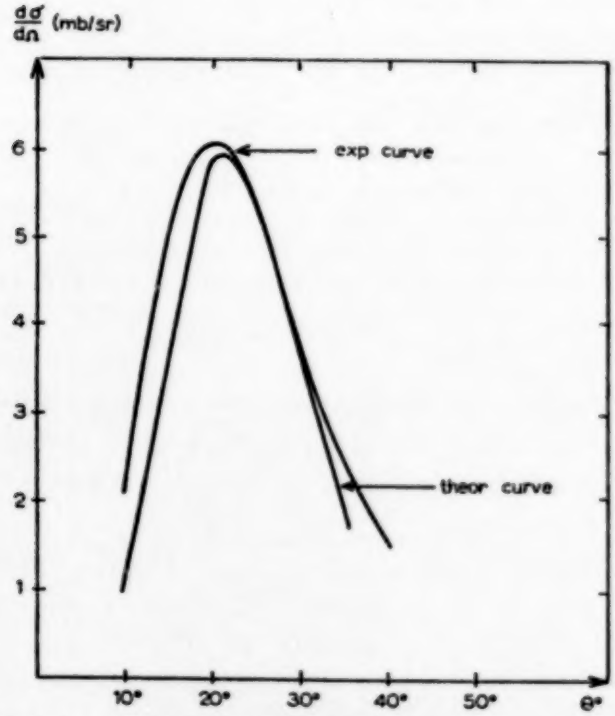

Fig. 2. The experimental and theoretical differential cross-sections for the inelastic scattering of 180 MeV protons by O^{16}.

Before comparing with experiment we must add the cross-sections associated with the 3^- and 0^+ levels. The result is shown in fig. 2.

5. Comparison with Experiments and Conclusions

It is seen from fig. 1 that the agreement with experiment is fairly good. It is interesting to note that the experimental differential cross-section for B^{11} is much smaller than that for C^{12} when we consider scattering to the 4.43 and 4.46 MeV levels respectively. This is not the case for the theoretical cross-sections in the direct interaction picture. The discrepancy between theory and experiment is probably due to a smaller amount of collective admixture into the excited state of B^{11} than into that of C^{12}, as discussed by Squires' [2]), assuming that a collective excitation really exists.

The calculated differential cross-section for O^{16}, as seen in fig. 2, shows nearly exact agreement with experiment, which should be expected since O^{16} is a closed-shell nucleus. The indirect success of the simple model used here for the description of the 0^+-state is notable [11]).

In conclusion I wish to thank Professor I. Waller and Dr. S. O. Lundqvist for suggesting the problem and for their interest in the work.

References

1) H. Tyrén and Th. A. J. Maris, Nuclear Physics **4** (1957) 637;
H. Tyrén and Th. A. J. Maris, Nuclear Physics **6** (1958) 82
2) E. J. Squires, Nuclear Physics **6** (1958) 504
3) G. P. McCauley, Proc. Phys. Soc. **73** (1959) 309
4) L. Wolfenstein and J. Ashkin, Phys. Rev. **85** (1952) 947
5) J. M. Gammel and P. M. Thaler, Phys. Rev. **107** (1957) 29
6) F. Bjorklund and S. Fernbach, Geneva Conference (Sept. 1958) A/Conf 15/P/649
7) R. Hofstadter, Annual Review of Nuclear Science **7** (1957)
8) V. K. Rasmussen, R. R. Metzger and C. P. Swann, Phys. Rev. **110** (1958) 154
9) H. A. Jahn and H. van Wieringen, Proc. Roy. Soc. A **209** (1951) 502
10) L. Egardt and S. O. Lundquist, Ark. f. Fysik, in press
11) P. J. Redmond, Phys. Rev. **101** (1956) 751
12) A. R. Edmonds, Angular Momentum in Quantum Mechanics (1957)

9.B *Nuclear Physics* **11** (1959) 357—367; © *North-Holland Publishing Co., Amsterdam*
Not to be reproduced by photoprint or microfilm without written permission from the publisher

SCATTERING OF μ-MESONS WITH MOMENTA OF ABOUT 100 MeV/c IN COPPER AND IRON

V. G. KIRILLOV-UGRYUMOV, B. A. DOLGOSHEIN, A. M. MOSKVICHOV and L. P. MOROZOVA

Moscow Engineering-Physical Institute, USSR

Received 18 October 1958

Abstract: Scattering of μ-mesons was studied in 4mm copper plates (μ-meson momenta between 85 and 144 MeV/c) and iron plates (μ-meson momenta between 81.2 and 135 MeV/c).

The μ-meson angular distribution derived from 2350 scattering events satisfactorily agrees with the distribution for a point nucleus.

1. Introduction

As is generally known, in a number of investigations on scattering of μ-mesons by nuclei, an excess of scattering events has been observed compared to what one would expect in the case of Coulomb interaction between the μ-mesons and the nuclei.

The most comprehensive survey of the data on μ-meson scattering has been presented by Fowler and Wolfendale [1]). In the opinion of these authors no anomalous scattering exists in the low energy region (below 600 MeV), the small excess observed in some investigations being conditioned by experimental errors. Three recent studies on slow μ-mesons confirm this opinion.

V. G. Kirillov-Ugryumov and A. M. Moskvichov [2]) investigated the scattering of μ-mesons with momenta of (130$\pm$16) MeV/c in 1 cm thick beryllium plates located in a cloud chamber. Not in one of the 2250 scattering events was scattering through an angle larger than 6° observed. The experimental angular distribution was found to be in satisfactory agreement with the distribution computed by the Molière theory.

A. I. Alikhanian and F. R. Arutyunian [3]) measured the scattering of μ-mesons in 7 mm lead plates with help of the Alagez mass spectrometer. The total μ-meson range was 19m. There is an agreement between the experiments and the theory which takes into account the finite size of the nucleus.

Chidley *et al.* [4]) who studied the scattering of 23 MeV μ-mesons in a 0.56 mm lead plate located in a propane bubble chamber also arrived at a negative result regarding the existence of anomalous scattering.

Fukui, Kitamura and Wataze [5]) did not observe any anomalous scattering of high energy ($\approx$ 1 GeV) μ-mesons; this result, however, contradicts to a certain degree other available experimental data as well as the theoretical predictions presented in ref. [1]). It is significant that agreement with the Coulomb interaction theory could be attained only if the μ-meson trajectories were chosen by recording μ—e decays of stopped μ-mesons.

In view of the importance of the problem regarding the absence or existence of anomalous scattering we undertook some measurements on scattering of μ-mesons with momenta of 81.2—144 MeV/c in 4 mm copper and iron plates.

In spite of the large number of nucleons in the nuclei of these elements the experimental data in the chosen energy and angle range can be compared with the exact Molière formula without making any assumptions regarding the distribution of the nuclear charge.

2. Experimental Arrangement

The measurements were performed with the arrangement depicted schematically in fig. 1. A large (55×40×14) cm^3 cloud chamber [6]) was

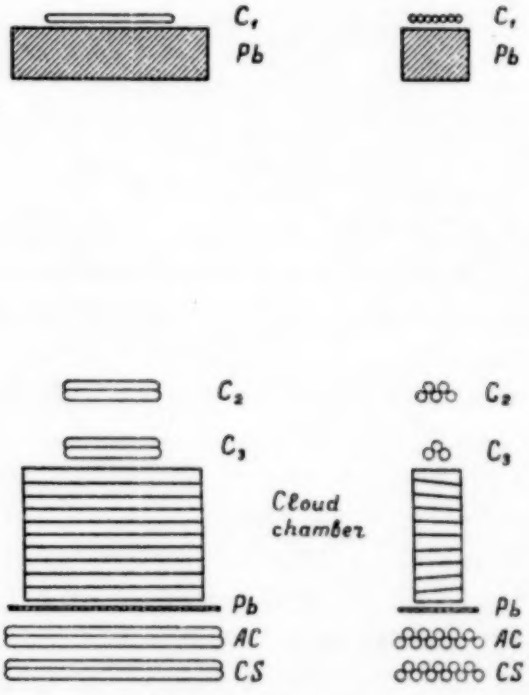

Fig. 1. Experimental arrangement.

controlled by a counter telescope. Counter sets C_1, C_2, C_3 were connected in coincidence and set AC in anticoincidence. In order to decrease anticoincidence losses a control set (CS) was placed below AC and was connected to a

duplicate anticoincidence circuit. Introduction of this set reduced the spurious anticoincidence rate to 0.5 %.

The apparatus was located at sea level. The 15 cm lead absorber above the cloud chamber served to absorb the electron component of cosmic rays.

In order to record μ-meson stoppings and measure scattering, nine 4mm copper (and in other experiments, iron) plates were placed in the cloud chamber. A 0.8 cm lead filter arranged beneath the chamber was employed to shield the anticoincidence row from μ-meson decay electrons.

Special measures were taken to minimize the distortions of the tracks in the chamber; thus temperature stabilization was incorporated and fast spark valves were used.

Photography was performed with a stereoscopic apparatus at a distance of 115 cm and base of 13.5 cm. Optical distortions of the angle projections were found to be negligible in this case.

From the amount of matter over the cloud chamber, including the thickness of the ceilings in the building in which the apparatus was located, the triggering rate of the cloud chamber was computed and found to be in good agreement with that observed experimentally.

3. Particle Identification; Measurement of μ-Meson Momenta and Scattering Angles

Particle identification was performed visually from the ionization density and multiple scattering of the particles in the chamber plates.

The scattering and density gradient of the tracks of μ-mesons stopped in the plates inside the chamber appreciably differed from electron and proton tracks. An estimation of the expected number of stopped protons indicated that it should not have exceeded 2 % of all recorded particles. The observed number of particles identified as protons was (1.5 ± 0.5) %. These particles were excluded from the scattering data.

It is significant that the number of stopped μ-mesons accompanied by decay electrons was in good agreement with the calculated value if the ratio between the positive and negative μ-mesons and also the geometry of the arrangement were taken into account.

The identification method described here was not suitable for separation of π- and μ-mesons. However, an analysis performed by us showed that under our conditions the π-meson admixture comprised not less than 1 % of the number of stopped μ-mesons. It can be shown that such a π-meson admixture should not change the expected theoretical μ-meson scattering angle distribution.

The mass of the particles identified by us as μ-mesons was computed on basis of the multiple scattering angles and ranges and found to equal $(209\pm10)m_e$.

Since the theoretical angular distributions are appreciably different for μ-mesons possessing even close momentum values, it was especially important in the scattering experiments to precisely measure the momenta and scattering angles of the μ-mesons. Because of this we used relatively thin plates to record the stopped particles and investigate scattering.

The μ-meson momenta were measured on basis of the residual range. Scattering and stopping of the μ-meson was assumed to take place in the middle of the plate. In the residual range computations account was made for deviation from the vertical of the angle of incidence of the μ-meson on the plate. For this purpose experimental distributions of the angles of entrance into the scattering plate were plotted (see table 1). It is easy to show that due to deviation from the vertical direction the effective thickness of the plates is sec $\sqrt{\overline{\vartheta^2_{\text{exp}}}}$ times larger than the true thickness ($\sqrt{\overline{\vartheta^2_{\text{exp}}}}$ is the mean square entrance angle).

TABLE 1

Mean square angles of entrance of μ-mesons in plates

No. of plate from stopping point	1	2	3	4	5	6	7	8	9
$\sqrt{\overline{\vartheta^2}}_{\text{exp}}$	14.5°	12.2°	10.5°	9°	8.5°	8°	7.5°	7°	6°

Momentum determination errors referring to the scattering point due to uncertainty in the residual range caused by the finite thickness of the plate and also by the change of the momentum in the scattering plate were computed and taken into account in plotting the scattering curves.

Since the momentum error was large in the plate directly above that in which the particles were stopped scattering was studied in all preceding plates excluding this one.

Projections of the scattering angles on a plane parallel to the front chamber window were measured; in general, this plane is different from that one passing through the initial direction of the particle for which the theoretical scattering angle distribution is computed. However, since the chamber was narrow (effective chamber depth 9.5 cm) and long (40 cm) the initial direction of the particles did not differ from the vertical by more than 4—5° and hence the difference between the projections of the angles on these two planes lies within the limits of accuracy of the angle measurements.

The μ-meson scattering angles were repeatedly measured by a number of observers; the mean square error in the angle did not exceed 30′.

An important factor in the angular distribution measurements were the geometrical dimensions of the recording device. Cousins *et al.* [7]) have shown that geometrical corrections connected with unequal probability of record-

ing different angles may lead to erroneous conclusions. Geometrical corrections were taken into account in the present work; they were introduced in the plot of the experimental angular distribution of scattered μ-mesons. A computation of the geometrical corrections (see appendix) shows, however, that they do not appreciably influence the shape of the curves. The reason of this is that the chamber width (55 cm) is sufficiently large compared with the comparatively narrow solid angle in which the μ-mesons enter the chamber. On the other hand the small depth of the chamber is of no importance because, as can be shown, scattering in a plane perpendicular to the plane of photography does not introduce any errors in the experimental angular distribution (this is true if the scattering angular distribution is approximated by a normal distribution).

4. Results of Measurements and Discussion

Two separate measurement sets were carried out with copper and iron plates.

475 μ-mesons stopped within the cloud chamber were recorded during a period of 3600 hours of operation of the apparatus with copper plates. For these 475 stopped μ-mesons 1460 scattering events in the plates were observed which involved momenta of at least 75 MeV/c. In the measurements with iron plates 890 scattering events were recorded.

Molière's theory can be applied to μ-mesons scattered in 4mm copper or iron plates since the final size of the nucleus becomes appreciable in the angular range beyond $\lambda\!\!\!^{-}/R$ ($\lambda\!\!\!^{-}$ is the μ-meson wave length and R the nuclear radius), which for our momentum values corresponds to angles $\approx 25-35°$.

Differential angular distributions were plotted separately for each μ-meson group with a given momentum. The experimental data were compared with the theoretical meson scattering curves plotted on basis of Molière's formula for a point nucleus.

Comparison of the theory for a finite nucleus with the experimental data yields satisfactory agreement between the observed and expected distribution for all angular intervals considered (see fig. 2).

In addition, the total differential distribution was plotted as a function of the dimensionless parameter φ_0 defined as

$$\varphi_0 = \frac{\theta_i}{B^{\frac{1}{2}}\,\xi}, \tag{1}$$

where θ_i is the scattering angle in radians and $B^{\frac{1}{2}}\,\xi$ the characteristic angle of multiple Coulomb scattering [8]; B being a slowly varying function of the plate thickness and particle momentum:

$$B = 2G, \tag{2}$$

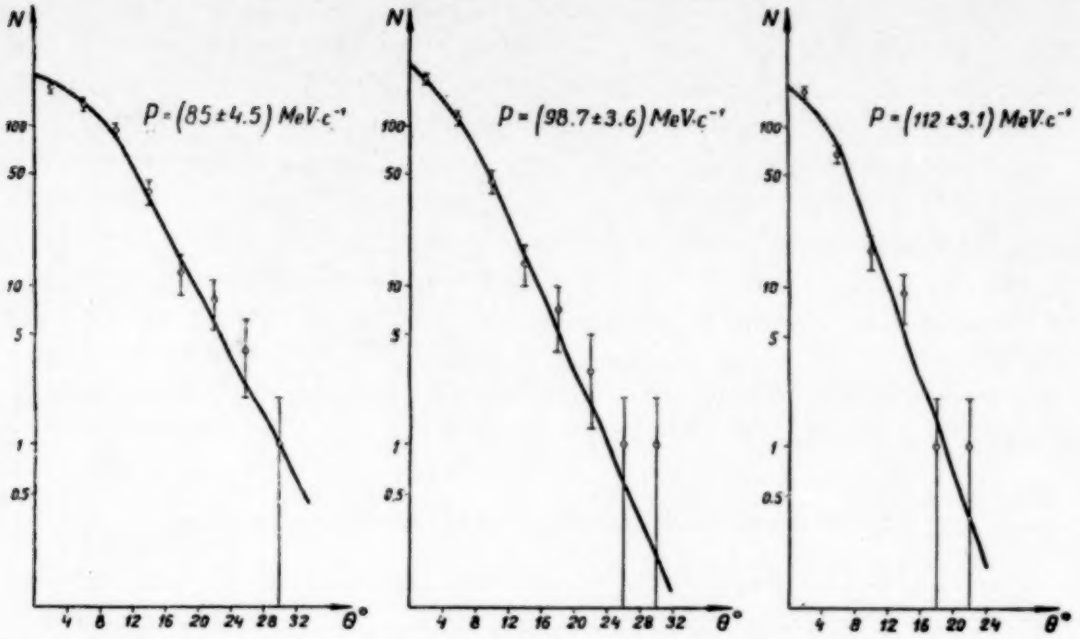

Fig. 2a. Differential angular cross-sections for three momentum intervals for copper.

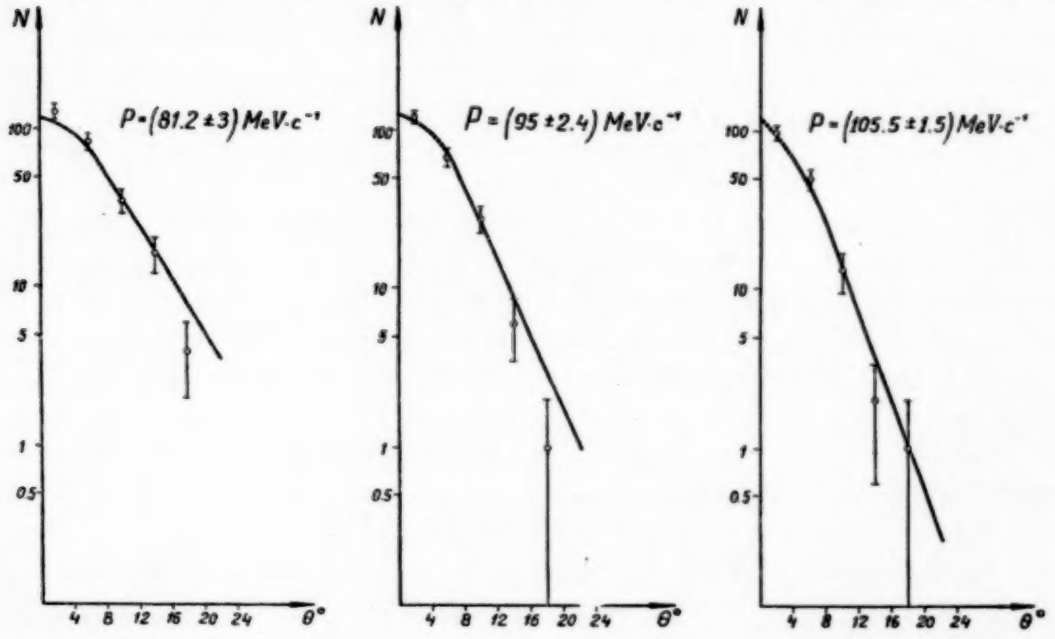

Fig. 2b. Differential angular cross sections for three momentum intervals for iron.

$$G = 5.66 + 1.24 \lg \frac{z^{\frac{1}{3}} A^{-1} t}{1.13\beta^2 + 3.76\left(\frac{z}{137}\right)^2}, \qquad (3)$$

β being the mean μ-meson velocity in the measured momentum interval (in our case $\beta = 0.6$, $G = 6.56$ and $B = 13.12$);

$$\xi = \frac{4\pi N e^4 t Z(Z+1)z^2}{(pV)^2} \tag{4}$$

where

N is the number of atoms per cm^3,

t the plate thickness in g/cm^2,

Z the charge of the scatterer nucleus,

z the particle charge,

p the particle momentum,

V the particle velocity.

The total angular distribution with respect to the dimensionless parameter φ_0 is presented in fig. 3 for copper and iron. It refers to scattering for momenta values lying between 81.2 and 144 MeV/c.

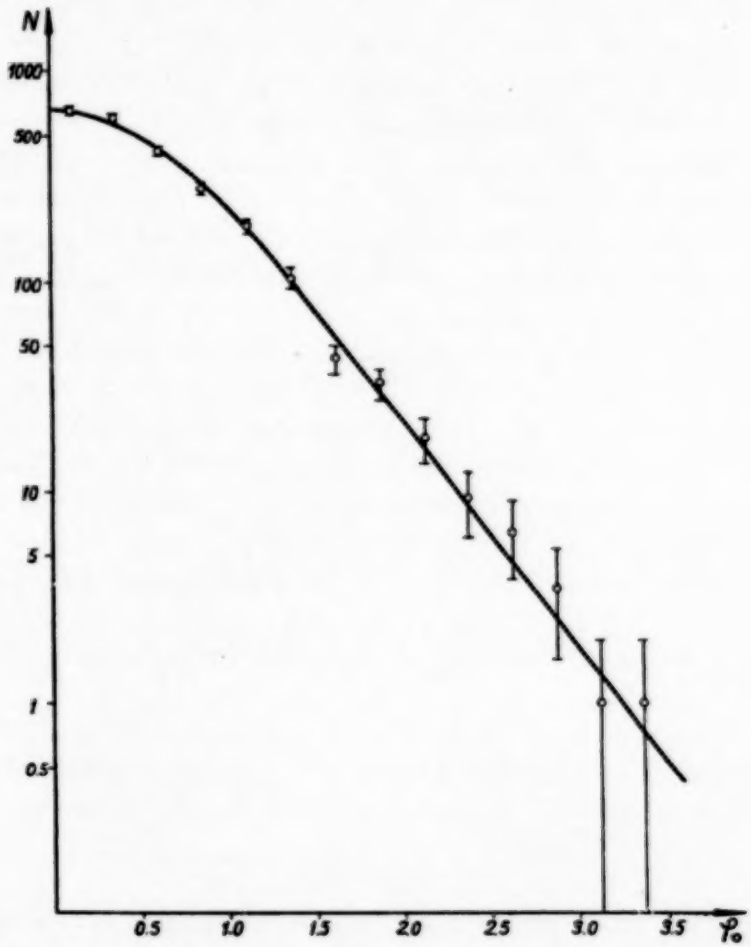

Fig. 3. Total differential distribution in dimensionless parameter φ_0 for copper and iron.

With the aid of the χ^2 criterion it was found that the agreement between experiment and theory is good ($P_{\chi^2} = 0.4$).

For comparison, the experimental and theoretical integral scattering angular distributions for momenta lying between 85 and 144 MeV/c (in copper) are presented in table 2.

TABLE 2

Integral number of observed and computed scattering events through an angle greater than a prescribed one in copper

$\theta° \geqq$	0	4	8	12	16	20	24	28
exp.	1460	678	279	107	42	20	7	2
theor.	1460	705	275	97.6	37.6	15.65	7.55	2.95

Thus an analysis of the results of the present investigation shows that satisfactory agreement between the experimental data and theoretical predictions can be obtained even if only Coulomb interaction between the μ-mesons and nuclei is taken into account.

Scattering of slow μ-mesons in copper was measured earlier on a mass spectrometer by A. I. Alikhanian and V. G. Kirillov-Ugryumov [9]). Good agreement between the experimental and theoretical distributions was observed in the small angle region, whereas for angles larger than 15° a small excess of scattering events was observed (23 events observed instead of the expected 15.67). This may possibly be due to the fact that the entrance angle of the μ-mesons in the cloud chamber of the mass spectrometer was relatively large and a geometrical correction calculated by the method described in ref. [7]) may yield complete agreement between the theoretical and experimental data. It is important that for π-mesons the entrance angle should deviate by a smaller degree from the vertical than in the case of μ-mesons and the geometrical correction should be correspondingly smaller. As a matter of fact, in the above mentioned work the agreement between the theoretical and experimental data is better for π-mesons than for μ-mesons.

Thus in ref. [2,3,4,9]) as well as in our work the facts do not point to the existence of anomalous scattering of mesons in the low energy region.

We take the opportunity to thank A. I. Alikhanian for continuous interest in this work and discussions, to B. I. Luchkov for great help in the work and F. R. Arutyunian and M. J. Ter-Mikayelian for discussions.

Appendix

COMPUTATION OF GEOMETRICAL CORRECTIONS TO THE ANGLE MEASUREMENTS

Consider a point X in plate m in which a μ-meson stopping in plate n is scattered (fig. 4). Owing to the finite dimensions of the telescope, mesons in a restricted entrance angle α interval arrive at point X.

If scattering in the plates preceding plate m is neglected this angle interval can be characterized by the diagram shown in fig. 5. In view of the

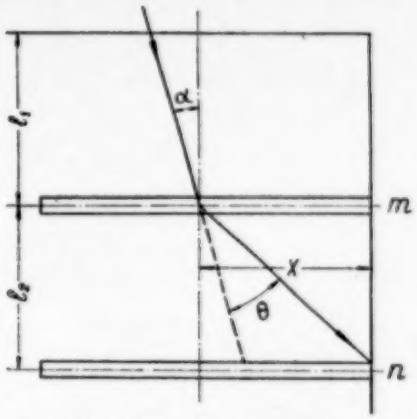

Fig. 4. Scattering of μ-meson (see text).

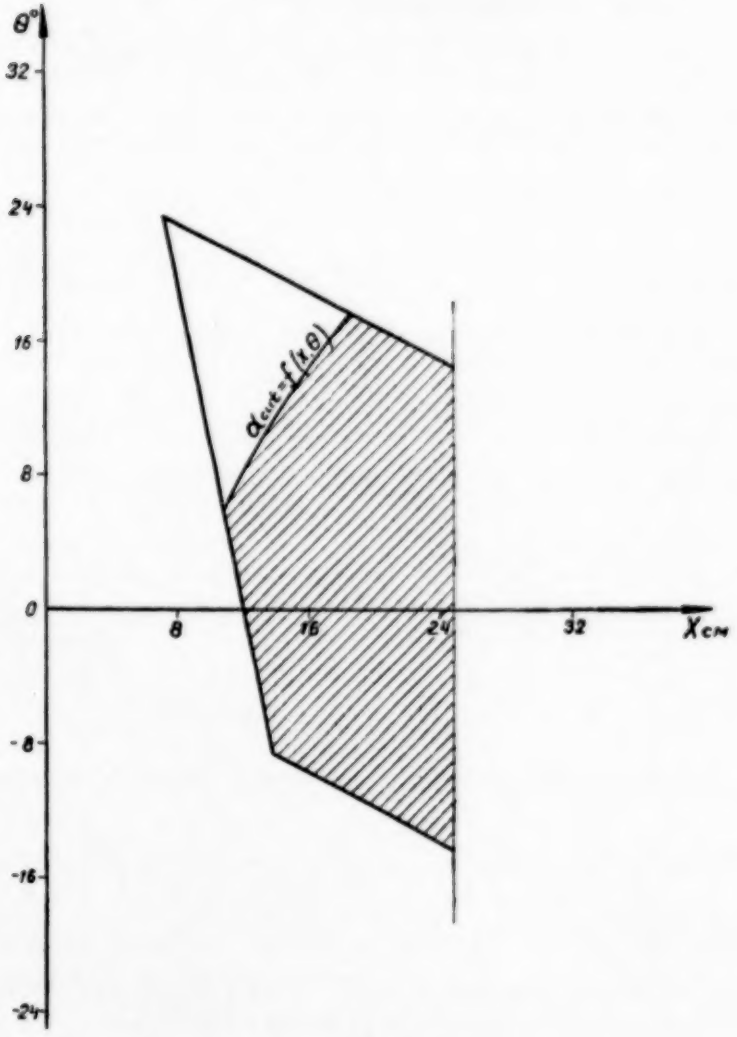

Fig. 5. Angle diagram.

symmetry of the arrangement only a half of the chamber, 25.5 cm $\geqq X \geqq 0$ will be considered.

Since for any X the entrance angle interval is sufficiently small ($\approx 10°$) we may assume that within this interval the μ-meson angular distribution is isotropic. Thus the area of diagram S is proportional to the probability of the μ-meson striking plate m.

If the scattering occurs in plates preceding plate m the diagram should "smear out" along each of the axes X and θ.

It can be demonstrated with sufficient accuracy that scattering leads to a diffuseness along the θ axis of $\sigma_1 = 0.35\,\sigma$, and along the X axis of $l_1 \operatorname{tg} \sigma_1$.

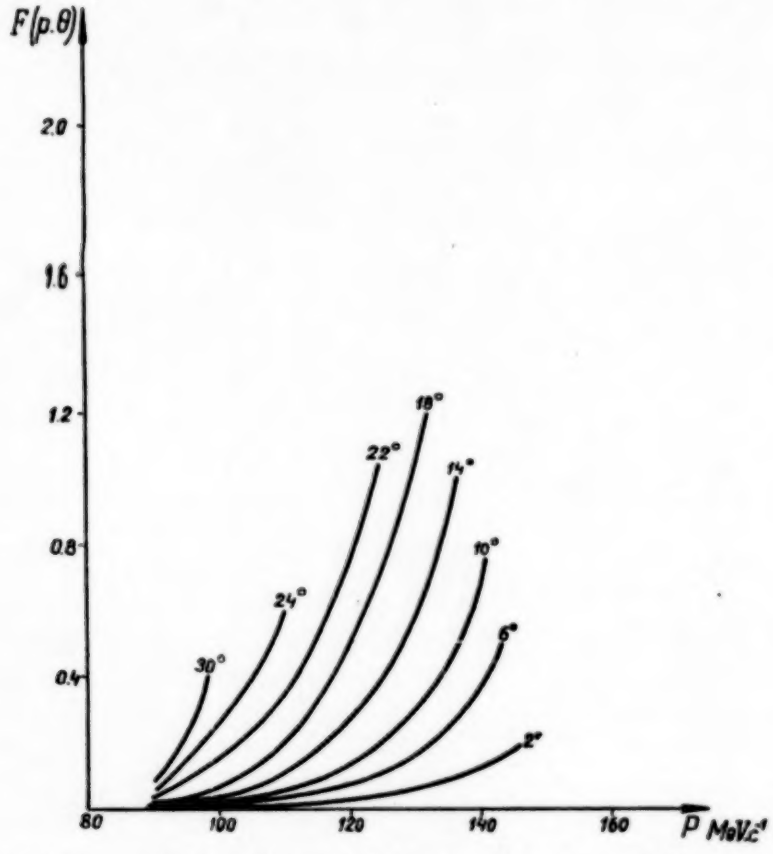

Fig. 6. Curve of geometrical corrections for measurements of angle θ as a function of the μ-meson momentum at the scattering point.

where σ is the mean square scattering angle of a μ-meson possessing a momentum equal to that of a μ-meson stopped in plate n, in a thickness equal to that of all the plates preceding plate m; l_1 is the distance from the top of the chamber to plate m.

Any meson which enters plate m at point X and possesses a momentum corresponding to a stopping in plate n can leave the plate either immediately as a result of scattering in plate m or as a result of scattering in plates located between m and n.

In order to take into account those μ-mesons which leave the chamber as a result of any of the possibilities mentioned above we shall assume (at any rate without underestimating the geometrical corrections) that scattering at point X in plate m through an angle θ is equivalent to scattering in $n-m$ plates through an angle $\theta_1 = \theta\sqrt{(n-m)}$. The probability of a particle remaining inside the chamber will then depend on a cut-off entrance angle defined by the relation

$$X = l_2 \operatorname{tg} (\theta\sqrt{n-m}+\alpha_{\text{cut}}).$$

The curve $\alpha_{\text{cut}} = f(X, \theta)$ cuts off on the diagram, which is proportional to the number of mesons entering plate m, a part which is proportional to the number of μ-mesons leaving the chamber as a result of scattering. The probability of registration of a meson which possesses a momentum corresponding to a stopping in plate n and which is scattered in plate m through an angle θ will then equal the ratio of the shaded area of the diagram to the total area S.

If the fraction of scattering events in plates $m = 1, 2, \ldots, 7$ is known from the experimental angular distributions for a given momentum (i.e., for $n-m = \text{const}$), one can determine $F(p, \theta)$ i.e., the correction for registration of an angle θ (fig. 6). Therefore in plotting the experimental angular distributions the quantity $N = N_{\text{exp}}(p, \theta)[1+F(p, \theta)]$ should be employed. Here $N_{\text{exp}}(p, \theta)$ is the experimental number of cases in which mesons with a momentum p are scattered through an angle θ.

References

1) G. N. Fowler and A. W. Wolfendale, Progress in elementary particle and cosmic rays physics (North-Holland Publ. Co., Amsterdam, 1958) pp. 123–153
2) V. G. Kirillov-Ugryumov and A. M. Moskvichov, JETP **34** (1958) 322
3) A. I. Alikhanian and F. R. Arutyunian, JETP (in press)
4) B. Chidley, G. Hinman, P. Goldstein, R. Summers and R. Adler, Can. Journ. Phys. **36** (1958) 801
5) Fukui, Kitamura and Wataze, private communication
6) V. G. Kirillov-Ugryumov, B. N. Deryagin and G. I. Merzon, Prib. Tekh. Eksp. no. 3 (1957) 15
7) J. E. Cousins, W. F. Nash and A. J. Pointon, Nuovo Cimento **6** (1957) 1113
8) G. Molière, Zs. f. Naturforsch. **3a** (1948) 78
9) A. I. Alikhanian and V. G. Kirillov-Ugryumov, Izv. Akad. Nauk. SSSR, ser. fiz. **19** (1955) 737

1.C *Nuclear Physics* **11** (1959) 368—386; © *North-Holland Publishing Co., Amsterdam*
Not to be reproduced by photoprint or microfilm without written permission from the publisher

DOUBLET SPLITTINGS IN NUCLEI AND THE STRONGLY CORRELATED NUCLEAR WAVE FUNCTIONS

J. SAWICKI and R. FOLK
Palmer Physical Laboratory, Princeton University †

Received 11 December 1958

Abstract: The nucleon-nucleus *LS* coupling is calculated using the Brueckner type of theory and the strongly correlated nuclear core density obtained from Jastrow's theory applied to the finite nucleus. The two-body potentials are replaced by the two-body scattering operators calculated from the potentials of Gammel and Thaler and of Signell and Marshak. It was possible to avoid many approximations often made in calculations of this type and thus some important correction to the leading Thomas-like term are included. The general theory is applied to the O^{17} problem with Dąbrowski variational trial functions of O^{16} to calculate the core density. Both the correct sign and the correct order of magnitude of the doublet splitting of O^{17} are obtained for both two-body potentials, and so this theory provides no clear distinction between these potentials.

1. Introduction

Many authors have attempted the explanation of the large nuclear spin-orbit coupling in terms of a) relativistic interactions, b) nucleon-nucleon tensor forces, c) nucleon-nucleon spin-orbit interactions. Keilson [1]), Kisslinger [2]), Jankovici [3,4]), and Nigam and Sundaresan [5]) use two-body tensor forces in second Born approximation in their calculations ††. Keilson obtains the wrong sign for the splitting; Kisslinger's paper involves questionable approximations (for some of them see Jankovici [3,4])), and his numerical results are therefore in doubt; Jankovici [3,4]) calculates doublet splittings that are not only too small, but also have the wrong sign; and finally, Nigam and Sundaresan [5]) find doublet splittings that are too small by a factor of 5 to 20 for the Yamagouchi separable potential. All these papers use the Born approximation (in ref. [5]) the effective mass correction is introduced), the Fermi model of the nucleus (or the Fermi model combined with the assumption of Swiatecki's [6]) "mixed density"), and various approximations such as the "forward scattering" approximation in the momentum space. Although many of these assumptions seem dubious, the inability to explain the *LS* coupling in terms of two-body tensor forces is not due to these approximations, but it seems to be established rather well on the basis of

† This work was supported by the U. S. Atomic Energy Commission and the Higgins Scientific Trust Fund.

†† The same problem was attacked for He^5 and the Li isotopes by Feingold and Wigner [35]).

the argument given by Brueckner, Gammel and Weitzner [7]) that the tensor force is not adequate to explain the spin-orbit splittings. Blanchard and Avery [8]), Hughes and Le Couteur [9]), Talmi [10]), Elliott and Lane [11]), and Blin-Stoyle [12]) derive the LS coupling in nuclei using two-body spin-orbit forces in Born approximation and assuming various nuclear densities. They had a certain amount of success for the Case and Pais [13]) two-body force which is involved in the recent Signell-Marshak [14, 15]) potentials.

The substitution of the Brueckner two-body "scattering operator" for the two-body potential as transition operator was first used by Kisslinger [2]) (in his part IV) and by Bell and Skyrme [16]). Unfortunately, many of Kisslinger's assumptions seem rather hard to justify (e.g., his matrix $A_2(k)$ is unrealistic). Bell and Skyrme obtain rather nice numerical results for the doublet splittings even though they use the doubtful Feshbach and Lomon[17]) phase shifts in their phase shift approximation of the scattering operator, a parabolic density distribution, and the forward scattering approximation.

While the present work was in progress, two new publications on the problem appeared. Nigam and Sundaresan [18]) calculated the doublet splittings for Ca^{41} and O^{17} using the spin-orbit part of the Signell-Marshak potential in first Born approximation together with the same assumptions for the nuclear model as in their previous paper [5]). Their numerical results differ from the experimental value by a factor of about 5. However, the sign of the last term in the square brackets of their $v_{s0}(0)$, eq. (3), should be reversed (compare e.g., $v_{s0}(0) = (-\frac{4}{3}\pi i)I_1$ with Moshinsky's [19]) I_1 for the Signell-Marshak potential given in his eq. (39)). This misprint is very serious since it changes the sign of $v_{s0}(0)$ and of the most important term $F_D(k)$ of eq. (8) of ref. [18]). In addition, the coefficient $\frac{1}{2}$ before the exchange term in ref. [18]) is missing.

In the second new publication referred to above, Moshinsky [19]) calculated the first order strength coefficient of the spin-orbit coupling (I_1 = the first moment of the two-body potential) in Born approximation using both the Signell-Marshak (S-M) and Gammel-Thaler (G-T) spin-orbit two-body potentials. He finds that neither of the two potentials can reproduce the experimental value of I_1 for heavy nuclei †; in particular the G-T potential cannot reproduce even the right order of magnitude of I_1. We believe that this conclusion is not justified; and that it is due partly to his treatment of the triplet even forces for which, as we shall see, the Born approximation is not valid even for the quantitative evaluation of the doublet splitting, and partly to the neglect of the strong correlations in the core.

The success of using the S-M and G-T potentials to explain the nucleon-nucleon scattering data indicates that these elementary static potentials are probably very realistic. In particular they contain the strong short range

† Provided the density distribution of heavy nuclei proposed by Blin-Stoyle [12]) is realistic.

spin-orbit potentials so important in the calculations of the nuclear doublet splittings. On the other hand, the Born approximation seems to be very poor for these forces; e.g., fig. 5 of ref. [7]) shows how much the "scattering operator" $K_{LS}\,\mathbf{L}\cdot\mathbf{S}$ differs from the potential $V_{LS}\,\mathbf{L}\cdot\mathbf{S}$ for the G-T case. As we shall see below, the doublet splittings are rather sensitive to the properties of these interaction operators at small distances.

In addition to dependence on the two-body potentials, the doublet splittings are sensitive to the properties of the nuclear densities (in particular to the shape of the derivatives of the density) of the strongly correlated nuclear core. It is the aim of the present paper to take into account the effects of $K_{LS}-V_{LS}$ and the strong correlations of the nuclear core, and to discuss the example of the doublet splitting of the O^{17} nucleus in detail.

In section 2 the doublet splitting is calculated with the K_{LS} matrix given in ref. [7]). The core density is obtained by using the Jastrow theory applied to a finite nucleus. As an example the doublet splitting of O^{17} is evaluated using Dąbrowski's O^{16} function to calculate the core density.

In section 3 a similar theory is developed using the phase shift approximation to calculate the spin-orbit part of the K matrix from both the Gammel and Thaler and the Signell and Marshak potentials. This theory is again applied to the O^{17} problem.

2. The K_{LS} Matrix of Brueckner, Gammel and Weitzner

2.1. GENERAL THEORY

The case discussed in this paper is that of a doubly-closed strongly correlated core with one extra relatively loosely bound nucleon, such as is true for O^{17} and Ca^{41}. The extra nucleon, whose doublet splitting we wish to calculate, interacts with all the members of the core. This interaction is assumed to be characterized by Brueckner's bound state "scattering operator" (or "reaction matrix") K. Brueckner *et al.* [7]) develop a theory of the finite nucleus in terms of the non-local two-body K operators of the form

$$(\mathbf{r}'_{12}|K|\mathbf{r}_{12})\chi_s^{m_s}=\frac{1}{(2\pi)^3}\int \mathrm{d}^3\,\mathbf{k}\varphi_{\mathbf{k}}(\mathbf{r}'_{12})v_{12}\Psi_{\mathbf{k}sm_s}(\mathbf{r}_{12}), \tag{1}$$

where $\chi_s^{m_s}$ is a spin wave function, $\varphi_{\mathbf{k}}$ is a plane wave function of momentum $\mathbf{k}$, and Ψ is an exact solution of the scattering problem defined by the relation

$$\Psi=\varphi+Gv_{12}\Psi,$$

where G is the Green's function appropriate to the local density of nuclear matter, the exclusion principle being taken into account.

The K matrices are computed for the G-T potential. The "non-locality" effect of the spin-orbit part of K is not large, and therefore the following

approximation is suggested:

$$(\mathbf{r}'_{12}|K|\mathbf{r}_{12})_{LS} \approx K_{LS}(r_{12})\delta(\mathbf{r}_{12}-\mathbf{r}'_{12}), \tag{2}$$

where

$$K_{LS}(r_{12}) = \int \mathrm{d}^3\mathbf{r}'_{12}(\mathbf{r}'_{12}|K|\mathbf{r}_{12})_{LS}.$$

The function $K_{LS}(r_{12})$ is computed in ref. [7]) using the even-state scattering only (S and D states), which seems to be a good approximation in a bound state problem. It is normalized as if it were a potential to be used in Born approximation. As we shall see below, the Born approximation, with the corresponding pseudo-potential given by Moshinsky [19]), does not apply, however, to the interaction in the even states. In this case the Born approximation result is erroneous (too small) by a factor of about 7. The central and tensor odd potentials are much smaller than the corresponding even potentials and can be neglected. The only contribution to K_{LS} in odd states comes from the spin-orbit odd potential. In view of the smallness of the triplet P phase shifts in the energy range important here, this part of the K_{LS} matrix can be approximated by its potential. This Born approximation calculation for the odd states potential was done by Moshinsky [19]), and the result was found to be small. We drop, therefore, the odd-state part of K_{LS} in the following calculation, and consequently the exchange amplitude. This applies to the neutron-neutron pairs in the example of O^{17}. To see this, we can write the "effective" total interaction of the extra-core nucleon n_0 (neutron, say) with the $\frac{1}{2}(A-1)$ core protons and $\frac{1}{2}(A-1)$ core neutrons as $\frac{1}{2}(A-1)$ $(K_{LS}^{n_0p}+K_{LS}^{n_0n})$. The B-G-W approximation corresponds to $K_{LS}^{n_0n} \approx 0$, which follows from eq. (1) with $v_{12} = \frac{1}{2}(1-P_{12})v_{12}^{3-}$ and $\Psi_{\mathbf{k}}$ approximated by a plane wave. A discussion of the contributions of $K_{LS}^{n_0n}$ in Born approximation and of the corresponding exchange amplitudes will be given later in the text and in appendix 1.

According to the above approximations, we may write the expression for the spin-orbit energy shift in the form †

$$\begin{aligned}(\widehat{\Delta E})_{LS} = \tfrac{3}{4}\int \mathrm{d}(3)\ldots\mathrm{d}(A)\int \mathrm{d}^3\mathbf{k}_1\mathrm{d}^3\mathbf{k}_2\mathrm{d}^3\mathbf{k}'_1\mathrm{d}^3\mathbf{k}'_2\,\Psi_0^*(\mathbf{k}'_1)\Phi^*(\mathbf{k}'_2, 3\ldots A)\\ \times I(\mathbf{k}_1, \mathbf{k}_2; \mathbf{k}'_1, \mathbf{k}'_2)\Psi_0(\mathbf{k}_1)\Phi(\mathbf{k}_2, 3\ldots A),\end{aligned} \tag{3}$$

where $\Psi_0(\mathbf{k}_1)$ is the Fourier transform of the extra-core particle in question, $\Phi(2, 3\ldots A)$ is the complete wave function of the (strongly correlated) core, and $\Phi(\mathbf{k}_2, 3\ldots A)$ is its Fourier transform with respect to the particle 2; further,

$$\begin{aligned}I(\mathbf{k}_1; \mathbf{k}_2; \mathbf{k}'_1, \mathbf{k}'_2) \equiv I = -\tfrac{1}{2}(A-1)\frac{1}{(2\pi)^3}\delta(\mathbf{K}-\mathbf{K}')\int \mathrm{e}^{-i\mathbf{q}\cdot\mathbf{r}_{12}}K_{LS}(r_{12})\\ \times \mathbf{S}\cdot(\mathbf{r}_{12}\times\mathbf{k})\mathrm{d}^3\mathbf{r}_{12},\end{aligned} \tag{4}$$

† Eq. (3) corresponds, e.g., to eq. (112) of Eden and Francis [36]); their operator t_i, given by eq. (105), being replaced by K of B-G-W. This seems to be correct, at least qualitatively.

where

$$\mathbf{K}=\mathbf{k}_1+\mathbf{k}_2,\quad \mathbf{K}'=\mathbf{k}'_1+\mathbf{k}'_2,\quad \mathbf{q}=\mathbf{k}-\mathbf{k}',\quad \mathbf{k}=\tfrac{1}{2}(\mathbf{k}_1-\mathbf{k}_2),$$
$$\mathbf{k}'=\tfrac{1}{2}(\mathbf{k}'_1-\mathbf{k}'_2),\quad \mathbf{S}=\tfrac{1}{2}(\boldsymbol{\sigma}_1+\boldsymbol{\sigma}_2).$$

The factor $\frac{3}{4}$ in eq. (3) comes from the fact that interactions occur in triplet states only, and the factor $\frac{1}{2}(A-1)$ in eq. (4) corresponds to the interactions of the particle 1 with all the core particles of different charge (i.e., protons in the O^{17} case) since the others are zero in our approximation.

Owing to the δ function (momentum conservation, $\mathbf{q}=\mathbf{k}_1-\mathbf{k}'_1\equiv-\mathbf{p}$; and the function I of eq. (4) may be rewritten as

$$I=-\tfrac{1}{2}(A-1)\frac{1}{(2\pi)^3}\delta(\mathbf{K}-\mathbf{K}')\mathbf{S}\cdot(\mathbf{k}\times\mathbf{k}')f(p), \tag{5}$$

where

$$f(p)=\frac{4\pi i}{p}\frac{\mathrm{d}}{\mathrm{d}p}\int_0^\infty j_0(pr_{12})K_{LS}(r_{12})r_{12}^2\,\mathrm{d}r_{12}.$$

Writing now explicitly the Fourier transform of the core function $\phi(\mathbf{k}_2,\,3\ldots A)$, performing the summations over the spin of the particle 2, integrating over $\mathbf{k}'_2$, and making use of the relation $\mathbf{k}\times\mathbf{k}'=\frac{1}{2}(\mathbf{k}_1\times\mathbf{k}'_1)+\frac{1}{2}(\mathbf{k}_2\times\mathbf{p})$, we can write

$$\begin{aligned}(\widehat{\Delta E})_{LS}=&-\tfrac{1}{4}\cdot\tfrac{3}{4}\frac{1}{(2\pi)^3}\int\mathrm{d}^3\mathbf{r}_a\mathrm{d}^3\mathbf{r}_b\int\mathrm{d}(3)\ldots\mathrm{d}(A)\int\mathrm{d}^3\mathbf{k}_1\mathrm{d}^3\mathbf{k}'_1\frac{1}{(2\pi)^3}\\&\times\int\mathrm{d}^3\mathbf{k}_2\Psi_0^*(\mathbf{k}'_1)\Phi^*(\mathbf{r}_a,3\ldots A)\mathrm{e}^{-i(\mathbf{k}_2-\mathbf{p})\cdot\mathbf{r}_a}\tfrac{1}{2}(A-1)\boldsymbol{\sigma}_1\cdot[(\mathbf{k}_1\times\mathbf{k}'_1)\\&+(\mathbf{k}_2\times\mathbf{p})]f(p)\Psi_0(\mathbf{k}_1)\Phi(\mathbf{r}_b,3\ldots A)\mathrm{e}^{+i\mathbf{k}_2\cdot\mathbf{r}_b}.\end{aligned} \tag{7}$$

With the change of variables $\mathbf{r}_a=\mathbf{R}+\frac{1}{2}\mathbf{r}$ and $\mathbf{r}_b=\mathbf{R}-\frac{1}{2}\mathbf{r}$ we have

$$-(\mathbf{k}_2-\mathbf{p})\cdot\mathbf{r}_a+\mathbf{k}_2\cdot\mathbf{r}_b=\mathbf{p}\cdot\mathbf{R}-(\mathbf{k}-\tfrac{1}{2}\mathbf{p})\cdot\mathbf{r}.$$

We next derive the expression for the mixed density function of the core particles:

$$\hat{\varrho}(\mathbf{r}_a,\mathbf{r}_b)\equiv\rho(\mathbf{R},\mathbf{r})=\int\Phi^*(\mathbf{r}_a,3\ldots A)\Phi(\mathbf{r}_b,3\ldots A)\mathrm{d}(3)\ldots\mathrm{d}(A). \tag{8}$$

Dąbrowski [22]) extended Jastrow's [23]) theory of strong correlations in nuclear matter to finite nuclei. His assumption is to take the nuclear wave function in the form

$$\Phi(1,\ldots A')=D^{-\frac{1}{2}}\prod_{i<j}^{A'}f(r_{ij})\Phi_0(1,\ldots A'),$$

where $D^{-\frac{1}{2}}$ is a normalization factor and

$$f(r_{ij})=\begin{cases}0 & \text{for } r_{ij}<r_c\\ 1 & \text{for } r_{ij}\to\infty\end{cases} \tag{9}$$

are the correlation functions taking care of the singular repulsive core nucleon-nucleon potentials and $\Phi_0(1, \ldots A') = (A'!)^{-\frac{1}{2}} \det\{\phi_k(1)\}$, with the $\Phi_k(1)$'s chosen as single particle orbitals. This imitation of the actual core wave function is rough. A more self-consistent approximation in the case of K of B-G-W would be to compute the core density of eq. (8) using the self-consistent Hartree-Fock wave functions corresponding to this K, if these were available. For the particular case of the O^{16} nucleus, a wave function of the type of eq. (9) was applied as a variational trial function to calculate the binding energy. A satisfactory agreement with experiment was obtained. In the example of O^{17} we shall use Dąbrowski's wave function explicitly for the O^{16}-core.

Let us define

$$h_i(\mathrm{a}, \mathrm{b}) = f(r_{\mathrm{a}i})f(r_{\mathrm{b}i}) - 1, \quad h(r_{ij}) = f(r_{ij})^2 - 1, \tag{10}$$

where

$$r_{\mathrm{a}i} = |\mathbf{r}_{\mathrm{a}} - \mathbf{r}_i|, \quad r_{\mathrm{b}i} = |\mathbf{r}_{\mathrm{b}} - \mathbf{r}_i|.$$

Using the Ursell-Mayer-Jastrow cluster development method (reviewed e.g., by Iwamoto and Yamada [24]) we can write

$$\prod_{i=3}^{A} f(r_{\mathrm{a}i})f(r_{\mathrm{b}i}) \prod_{i>j=3}^{A} f(r_{ij})^2 = 1 + \sum_{i=3}^{A} h_i(\mathrm{a}, \mathrm{b}) + \sum_{i>j=3}^{A} h(r_{ij}) + \sum_{k>l=3}^{A} h_k(\mathrm{a}, \mathrm{b})h_l(\mathrm{a}, \mathrm{b}) + \text{higher order terms}. \tag{11}$$

One can show that the most important correction in our problem of the doublet splitting comes from the second term. A contribution to ρ from the normalization denominator D cancels most of the contribution from the second correction term $\sum_{i>j=3}^{A} h(r_{ij})$. Using this approximation we obtain as a final result for an even nucleus

$$\hat{\varrho}(\mathbf{r}_{\mathrm{a}}, \mathbf{r}_{\mathrm{b}}) = \rho(\mathbf{R}, \mathbf{r}) = \rho_0(\mathbf{r}_{\mathrm{a}}, \mathbf{r}_{\mathrm{b}}) + \Delta\rho(\mathbf{r}_{\mathrm{a}}, \mathbf{r}_{\mathrm{b}}),$$

where ρ_0 is the uncorrelated density

$$\rho_0(\mathbf{r}_{\mathrm{a}}, \mathbf{r}_{\mathrm{b}}) = 4\sum_{\mathrm{c}} \phi_{\mathrm{c}}^*(\mathbf{r}_{\mathrm{a}})\phi_{\mathrm{c}}(\mathbf{r}_{\mathrm{b}}), \quad \rho_0(\mathbf{r}) = 4\sum_{\mathrm{c}} |\phi_{\mathrm{c}}(\mathbf{r})|^2 = \rho_0(\mathbf{r}, \mathbf{r}), \tag{12a}$$

and $\Delta\rho$ is the correction

$$\Delta\rho(\mathbf{r}_{\mathrm{a}}, \mathbf{r}_{\mathrm{b}}) = \int \mathrm{d}^3\mathbf{r}_3 h_3(\mathrm{a}, \mathrm{b})[\rho_0(\mathbf{r}_{\mathrm{a}}, \mathbf{r}_{\mathrm{b}})\rho_0(\mathbf{r}_3) - \tfrac{1}{4}\rho_0(\mathbf{r}_{\mathrm{a}}, \mathbf{r}_3)\rho_0(\mathbf{r}_3, \mathbf{r}_{\mathrm{b}})]. \tag{12b}$$

In the following we shall see that for the particular case of harmonic oscillator wave functions, the separation of the coordinates $\mathbf{R}$ and $\mathbf{r}$ can be performed in a simple form.

Going back to our eq. (7), we observe that since

$$\int \mathrm{d}^3\mathbf{k}_2\, \mathrm{e}^{-i\mathbf{k}_2\cdot\mathbf{r}} = (2\pi)^3\delta(\mathbf{r}) \quad \text{and} \quad \int \mathrm{d}^3\mathbf{k}_2(\mathbf{k}_2\times\mathbf{p})\mathrm{e}^{-i\mathbf{k}_2\cdot\mathbf{r}} = -i\mathbf{p}\times\nabla_{\mathbf{r}}\delta(\mathbf{r}),$$

and for any density satisfying the condition $\nabla_{\mathbf{r}}\rho(\mathbf{R}, \mathbf{r})|_{\mathbf{r}=0} = 0$

$$\int d^3\mathbf{r} e^{i\mathbf{p}\cdot\mathbf{r}} \rho(\mathbf{R}, \mathbf{r}) \nabla_{\mathbf{r}} \delta(\mathbf{r}) = -\tfrac{1}{2} i \mathbf{p} \rho(\mathbf{R}, 0),$$

we can rewrite eq. (7) in the form

$$(\widehat{\Delta E})_{LS} = -\tfrac{1}{8} \cdot \tfrac{3}{4} \frac{1}{(2\pi)^3} \int d^3\mathbf{k}_1 d^3\mathbf{k}'_1 \Psi_0^*(\mathbf{k}'_1) \int d^3\mathbf{R} e^{i\mathbf{p}\cdot\mathbf{R}} \rho(R, 0) \times \boldsymbol{\sigma}_1 \cdot (\mathbf{k}_1 \times \mathbf{k}'_1) f(p) \Psi_0(\mathbf{k}_1). \tag{13}$$

From eq. (13) we see that the contribution to $(\widehat{\Delta E})_{LS}$ will be small for large values of $\mathbf{p} = \mathbf{k}'_1 - \mathbf{k}_1$ because of the rapid oscillations of the wave function. Therefore, we can expand our $f(p)$ in powers of p and retain the two first terms:

$$f(p) = 4\pi i(\alpha + \delta p^2). \tag{14}$$

α and δ are constants characteristic for a given matrix $K_{LS}(r')$. The terms proportional to odd powers of p are zero (see eq. (5)). The first (leading) term is the usual (Thomas) term which contributes to the first derivative of the density; the second term contributes to the higher derivatives of the density. Going back to the configuration space we obtain as a final result

$$(\widehat{\Delta E})_{LS} = \tfrac{3}{8}\pi \int d^3\mathbf{R} \Psi_0^*(\mathbf{R}) \left[\frac{\alpha}{R} \frac{d\rho(R)}{dR} - \frac{\delta}{R} \frac{d}{dR} (\nabla^2 \rho(R)) \right] (\boldsymbol{\sigma}_1 \cdot \mathbf{L}) \Psi_0(\mathbf{R}), \tag{15}$$

where

$$\rho(R) = \rho(R, 0) = \rho_0(R, R) + \Delta\rho(R, R).$$

2.2. APPLICATION TO THE O^{17} PROBLEM

If harmonic oscillator functions are used, the zero order part of the mixed density of the O^{16} core can be shown to be

$$\rho_0(R, r) = N[1 + r_0^{-2}(R^2 - \tfrac{1}{4} r^2)] e^{-R^2/2r_0^2} e^{-r^2/8r_0^2}, \tag{16}$$

where $N = 4/(r_0\sqrt{2\pi})^3$ and r_0 is related to Dąbrowski's ν by $r_0 = 1/\sqrt{2\nu}$. The main correction to the density which has a noticeable effect on the doublet splitting can be written

$$\Delta\rho(\mathbf{r}_a, \mathbf{r}_b) = \int d^3\mathbf{r}_3 h_3(a, b)[\rho_0(\mathbf{r}_a, \mathbf{r}_b)\rho_0(\mathbf{r}_3) - \rho_0(\mathbf{r}_a, \mathbf{r}_3)\rho_0(\mathbf{r}_3, \mathbf{r}_b)] \equiv \int d^3\mathbf{r}_3 \mathscr{F}_{\mathbf{r}_3}(\mathbf{r}_a, \mathbf{r}_b). \tag{17}$$

Introducing the new coordinates $\mathbf{x}_a = \mathbf{r}_a - \mathbf{r}_3$ and $\mathbf{x}_b = \mathbf{r}_b - \mathbf{r}_3$ and using the symmetry property of $\mathscr{F}(\mathbf{x}_a, \mathbf{x}_b) \equiv \mathscr{F}_{\mathbf{r}_3}(\mathbf{r}_a, \mathbf{r}_b)$:

$$\nabla_{\mathbf{x}_a} \mathscr{F}(\mathbf{x}_a, \mathbf{x}_b) \equiv \nabla_{\mathbf{x}_b} \mathscr{F}(\mathbf{x}_a, \mathbf{x}_b) \quad \text{at} \quad \mathbf{x}_a \equiv \mathbf{x}_b,$$

we can show, without approximations, that the correction of $\Delta\rho$ to $(\widehat{\Delta E})_{LS}$ following from eq. (7) can be exactly contained in the form of eqs. (13) and (15). This correction can be written explicitly

$$\Delta(\widehat{\Delta E})_{LS} = \tfrac{3}{8}\pi \int \mathrm{d}^3\mathbf{R}\Psi_0^*(\mathbf{R}) \left\{ \frac{\alpha}{R}\frac{\mathrm{d}}{\mathrm{d}R}(\Delta\rho(R)) - \frac{\delta}{R}\frac{\mathrm{d}}{\mathrm{d}R}(\nabla^2\Delta\rho(R)) \right\} \times (\boldsymbol{\sigma}_1 \cdot \mathbf{L})\Psi_0(\mathbf{R}), \tag{18}$$

where

$$\Delta\rho(R) \equiv \Delta\rho(R, R) = \int \mathrm{d}^3\mathbf{r}_3 [f(r_{R3})^2 - 1]\{\rho_0(\mathbf{R})\rho_0(\mathbf{r}_3) - \tfrac{1}{4}[\rho_0(\mathbf{R}, \mathbf{r}_3)]^2\}, \tag{19}$$

with $r_{R3} = |\mathbf{R} - \mathbf{r}_3|$.

Dąbrowski's variational trial function giving a rather satisfactory fit to the experimental binding energy of O^{16} is formed from

$$f(r) = \begin{cases} 0 & \text{for } r < r_c \equiv 0.2\times 10^{-13}\ \mathrm{cm}, \\ 1 - \mathrm{e}^{-\beta[(r/r_c)^2 - 1]} & \text{for } r \geqq r_c, \end{cases} \tag{20}$$

where $\beta = 0.75$, together with $\sqrt{\nu} = 0.9\times 10^{13}\ \mathrm{cm}^{-1}$ for the oscillator wave functions †. This value of the parameter $\sqrt{\nu}$ differs rather much from the shell model of the uncorrelated O^{16} nucleus (according to Heisenberg [25]) $\sqrt{\tilde{\nu}} = 0.4045 \times 10^{13}\ \mathrm{cm}^{-1}$) or from $\sqrt{\nu'}$ corresponding to the ds-shell particles ($\sqrt{\nu'} = 0.6098\times 10^{13}\ \mathrm{cm}^{-1}$ according to Elliott and Flowers [26])). In the following we shall see that the greatest effect of the correlation on the doublet splitting comes from the change of $\sqrt{\nu}$. It follows from eq. (20) that

$$\Delta\rho(R) = 4\pi N^2 \mathrm{e}^{-R^2/r_0^2} \int_{r_c}^{\infty} x^2\{-2\mathrm{e}^{\beta}\mathrm{e}^{-\zeta_1 x^2} + \mathrm{e}^{2\beta}\mathrm{e}^{-\zeta_2 x^2}\} \times \left[\left(\frac{7r_0^2}{4Rx} + \frac{x}{R} + \frac{3R}{x} + \frac{3Rx}{4r_0^2} + \frac{3R^3}{xr_0^2} \right) \mathrm{sh}\frac{xR}{r_0^2} - \left(1 + \frac{3R^2}{2r_0^2} \right) \mathrm{ch}\frac{xR}{r_0^2} \right] \mathrm{d}x, \tag{21}$$

where $\zeta_1 = \beta/r_c^2 + 1/2r_0^2$, $\zeta_2 = 2\beta/r_c^2 + 1/2r_0^2$. To a good approximation we can write

$$\Delta\rho(R) \approx 4\pi N^2 \mathrm{e}^{-R^2/r_0^2} \tfrac{3}{4}\left(1 + 2\frac{R^2}{r_0^2}\right)\phi_1, \tag{22}$$

where

$$\phi_1 = \int_{r_c}^{\infty} x^2\{-2\mathrm{e}^{\beta}\mathrm{e}^{-\zeta_1 x^2} + \mathrm{e}^{2\beta}\mathrm{e}^{-\zeta_2 x^2}\}\mathrm{d}x.$$

The spin-orbit single particle potential from eq. (15) can be written as

$$V_{LS}(R)(\boldsymbol{\sigma}_1 \cdot \mathbf{L}) = \tfrac{3}{8}\pi \left\{ \alpha \left[r_0^{-2} N \mathrm{e}^{-R^2/2r_0^2} \left(1 - \frac{R^2}{r_0^2} \right) + \frac{1}{R}\frac{\mathrm{d}}{\mathrm{d}R}\Delta\rho(R) \right], - \frac{\delta}{R}\frac{\mathrm{d}}{\mathrm{d}R}[\nabla^2\rho(R)] \right\} (\boldsymbol{\sigma}_1 \cdot \mathbf{L}) \tag{23}$$

with the leading term written explicitly. The doublet splitting, given by

† A set of parameters corresponding to a larger value of r_c (e.g. $r_c = 0.4\times 10^{-13}$ cm) would be more realistic and still consistent with the binding energy of O^{16}. This would correspond to a larger radius of the O^{16} nucleus.

$$\Delta(\Delta E)_{LS} = -\tfrac{1}{2}(2l+1)\langle V_{LS}(R)\rangle, \tag{24}$$

is now evaluated for the 17-th particle in O^{17} with $l = 2$:

$$\Delta(\Delta E)_{LS} = -\tfrac{5}{2}\int_0^\infty |R_2(R)|^2 V_{LS}(R) R^2 \mathrm{d}R, \tag{25}$$

where

$$R_2(R) = N_2 \mathrm{e}^{-\frac{1}{2}\nu' R^2} R^2 \quad \text{and} \quad N_2^2 = \frac{\sqrt{\nu'}\,\nu'^3 2^4}{15\sqrt{\pi}}.$$

All the integrals involved are elementary (for some of them see Talmi [10]). $K_{LS}(r')$ is given in ref. [7]), fig. 5. To a good approximation this function can be taken as

$$K_{LS}(r') = \begin{cases} -K_0 & \text{for } r' \leqq r_K, \\ -V_0 \mathrm{e}^{-\mu r'/\mu r'} & \text{for } r' > r_K, \end{cases} \tag{26}$$

where $K_0 = 359$ MeV, $V_0 = 5000$ MeV, $r_K = 0.53\times 10^{-13}$ cm and $\mu = 3.7\times 10^{13}$ cm^{-1}. Then

$$f(p) = 4\pi i \left\{ K_0 r_K^5 \frac{j_2(pr_K)}{(pr_K)^2} + V_0 r_K^5 \mathrm{e}^{-\mu r_K} \left[\frac{2}{(\mu r_K)^2+(pr_K)^2} \left(j_0(pr_K) + \frac{\cos pr_K}{\mu r_K} \right) + \frac{1}{pr_K((\mu r_K)^2+(pr_K)^2)} \left(j_1(pr_K) + \frac{\sin pr_K}{\mu r_K} \right) \right] \right\}. \tag{27}$$

Therefore

$$\alpha = r_K^5 [\tfrac{1}{15} K_0 + \tfrac{1}{3} V_0 (\mathrm{e}^{-y}/y^2)(1+3/y+6/y^2+6/y^3)] \tag{28}$$

and

$$\delta = -\tfrac{1}{2} r_K^7 \left[\frac{1}{7\times 15} K_0 + V_0 (\mathrm{e}^{-y}/y^2)(\tfrac{1}{15}+1/(3y)+4/(3y^2)+4/y^3+8/y^4+8/y^5) \right],$$

where $y = \mu r_K$. We find $\alpha \approx 14 f^5$ MeV and $\delta \approx -2.0 f^7$ MeV ($f = 10^{-13}$ cm).

Using $\sqrt{\nu'} = 0.6098\ f^{-1}$ as given by Elliott and Flowers [26]) (i.e., $\lambda' = \sqrt{2\nu' r_0} \approx 0.678$), we find as a final result: $\Delta(\Delta E)_{LS} \approx (2.375-0.525)$ MeV $= 1.85$ MeV. The first number in the brackets corresponds to the α-part of $V_{LS}(R)$, the "Thomas term", and the second (negative) contribution comes from the $\delta(\propto p^2)$ term. The contribution of $\Delta\rho(R)$ is negative and amounts to about 2 % of that of $\rho_0(R)$ in the α term. The experimental $\Delta(\Delta E)_{LS\ \mathrm{exper.}} = 5.08$ MeV. However, our $\Delta(\Delta E)_{LS}$ is rather sensitive to the choice of the parameter $\sqrt{\nu'}$ of the 17-th particle. If we take $\sqrt{\nu'} = \sqrt{\nu}$, i.e. $\lambda' = 1$ rather than 0.678, our result becomes $\Delta(\Delta E)_{LS} = 4.69$ MeV.

In Born approximation, using the "equivalent pseudopotential" of Moshinsky [19]), given by his eq. (33) with the G-T parameters corresponding to even states, we get $\alpha^{\mathrm{Born}} = 2.28 f^5$ MeV and $\delta^{\mathrm{Born}} = -0.37 f^7$ MeV. α^{Born} and δ^{Born} are then 6 times too small (with respect to α and δ, respectively). $\Delta(\Delta E)_{LS}^{\mathrm{Born}}$ is then 6 times too small for $\lambda' = 0.678$, and thus one sees why Moshinsky's result was much too small (even of the wrong order of magnitude).

It is interesting to consider the Born approximation result for the Signell-Marshak potential [15]). For this case the approximation of eq. (14) is invalid, i.e., the usual Thomas type term is not an approximation for $(\Delta E)_{LS}$. Namely, in Born approximation we get $\alpha_{S-M}^{Born} = 42f^5$ MeV and $\delta_{S-M}^{Born} = -50f^7$ MeV, which, with the rejection of the terms containing the remaining part of $f(p)$, gives even the wrong sign of $\Delta(\Delta E)_{LS}$. This, however, applies to the Born approximation only.

The contribution of $K_{LS}^{n_0 n}$, as it was pointed out at the beginning of this section, is zero if one sets all the triplet odd states phase shifts equal to zero. If we do not make this approximation, but want to find the contribution of $K_{LS}^{n_0 n}$ more accurately, we can use the Born approximation since the phase shifts are small. Using Moshinsky's pseudopotential, we find $\alpha_{odd}^{Born} = 3.15f^5$ MeV and $\delta_{odd}^{Born} = 0.519f^7$ MeV, which yields a contribution from the direct amplitude of $V_{LS}^{n_0 n}$ to $\Delta(\Delta E)_{LS}$ of 0.40 MeV for $\lambda' = 0.678$ and 0.91 MeV for $\lambda' = 1$. The contribution of the n_0—n exchange amplitude is usually still smaller (compare e.g., ref. [18])). This amplitude is discussed in appendix I. In a very crude approximation presented there, the contribution of this term equals that of α_{odd}^{Born}. Adding all these corrections to the even part of $\Delta(\Delta E)_{LS}$, we obtain 2.78 MeV for $\lambda' = 0.678$ and 7.07 MeV for $\lambda' = 1$. ($\Delta\rho$ is neglected in the latter case.)

From the above results we see that the use of K_{LS} rather than V_{LS} is important for the magnitude of $\Delta(\Delta E)_{LS}$, i.e., that the Born approximation gives poor results. Furthermore, we see that $\Delta(\Delta E)_{LS}$ is sensitive to the parameter λ', depending on both the parameter $\sqrt{\nu'}$ of the 17-th particle, and r_0, characteristic of the O^{16} core. Dąbrowski's r_0 is much smaller than the usual "uncorrelated" r_0 owing to the strong correlations in the core. The increase in λ' would correspond to correlating the 17-th particle with the core particle. We see that even for an uncorrelated λ', we can obtain the right order of magnitude of $\Delta(\Delta E)_{LS}$. For a very reasonable λ' we can obtain a good agreement with the experimental number 5.08 MeV. The first correction to the Thomas term (δp^2) always gives a negative contribution and is important for the strongly correlated core only. The contribution of $\Delta\rho(R)$ is not large and amounts to about 2 % of the contribution of $\rho_0(R)$ in the leading α-term. The effect of the strong correlation of the core on the parameter r_0 is much more important. The leading term of $\Delta(\Delta E)_{LS}$ is smaller by a factor $(r_0/r_{0\,\text{uncorrel.}})^5$, which means that it is about 7 times smaller in the O^{17} case if the uncorrelated r_0 is used. The δ term is much less important (it decreases as r_0^{-2}) for this case.

3. Phase Shift Approximation of the K_{LS}-Matrix

In the momentum space the K_{LS} scattering operator, which describes the scattering of two nucleons, is a scalar function of the initial and final

relative momenta $\mathbf{k}$ and $\mathbf{k}'$, and the spins. The K matrix in momentum space was first given by Wolfenstein and Ashkin [27]) and by Dalitz [28]), and was related to the phase shifts by Wright [29]) and Stapp [30]). The spin-orbit part of K is the only part relevant to this problem.

In our problem the complete antisymmetrized interaction operator in question can be written in the form of eq. (5), where $\frac{1}{2}(A-1)f(p)$ has to be replaced by $-2i(A-1)(4\pi\hbar^2)/(M^*)F_0(\mathbf{k}, \mathbf{k}')$, where M^* is the nucleon effective mass and

$$\begin{aligned} F_0(\mathbf{k}, \mathbf{k}') &= \tfrac{1}{2}\{F_{np}(\mathbf{k}, \mathbf{k}')+F_{nn}(\mathbf{k}, \mathbf{k}')+F_{nn}^{ex}(\mathbf{k}, -\mathbf{k}')\}, \\ F_{np}(\mathbf{k}, \mathbf{k}') &= F_{nn}(\mathbf{k}, \mathbf{k}') = F_{nn}^{ex}(\mathbf{k}, \mathbf{k}'), \end{aligned} \tag{29}$$

where F_{np} refers to a neutron-proton pair, and F_{nn} and F_{nn}^{ex} are the neutron-neutron direct and exchange amplitudes respectively. We assume that the most important contribution to the scattering corresponds to elastic processes, where $k^2 = k'^2$ (the so-called "on-the-energy-shell approximation"). In the notation of Stapp [30]) we can write

$$k^2 \sin\theta_{(\mathbf{k},\mathbf{k}')} F_{np}(\mathbf{k}, \mathbf{k}') = -\tfrac{1}{4}\sqrt{2}(M_{10}-M_{01}); \tag{30}$$

M_{10} and M_{01} as given by Bell and Skyrme [16]) in their eq. (3) contain only the first two terms of their expansion in Legendre polynomials. Our explicit calculations indeed showed the next term to be small. We used the usual "reactance matrix" components of the Brueckner theory, i.e., replaced (exp $2i\delta-1$) by $2i$ tan δ in Stapp's expressions. This leads to the well-known singularity of tan $\delta_{1\alpha}$ as the $^3S_1$ phase shift passes through $\frac{1}{2}\pi$. Brueckner [31]) proposes to avoid this singularity by taking the principal values of the relevant integrals. He argues that this singularity is physically irrelevant for the many-body nuclear problems. On the other hand, Fukuda and Newton [32]) and de Witt [33]) recently pointed out that the phase shifts themselves rather than their tangents should be used. One should remark, however, that the use of either the free scattering phase shifts or their tangents is very dubious in general. Neither of them takes complete account of the exclusion principle in a high density fermion system. Fukuda and Newton [34]) point out that it is just a matter of notation whether we use tan δ or δ if we approximately take the exclusion principle into account by suitably modifying the phase shifts. However, the effect of the exclusion principle on the phase shifts used to calculate the K matrix for our case of a single nucleon outside of a doubly closed core (such as O^{17} or Ca^{41}) should be small because the extra-core particle belongs to another energy shell.

In the following calculations we used the phase shifts themselves rather than their tangents. We found, however, that the results for the earlier case differ little from those of the latter case except for the removal of the singularity.

In analogy to eq. (7) we can write the doublet splitting operator as

$$(\widehat{\Delta E})_{LS} = \tfrac{3}{8}i\frac{4\pi\hbar^2}{M^*}\frac{1}{(2\pi)^3}\int d^3\mathbf{r}_a d^3\mathbf{r}_b \int d^3\mathbf{k}_1 d^3\mathbf{k}'_1 \frac{1}{(2\pi)^3}\int d^3\mathbf{k}_2 \Psi_0^*(\mathbf{k}'_1) \times\rho(\mathbf{r}_a, \mathbf{r}_b)e^{i\mathbf{p}\cdot\mathbf{R}}e^{-i(\mathbf{k}_2-\mathbf{k}_1)\cdot\mathbf{r}}F_0(\mathbf{k},\mathbf{k}')\boldsymbol{\sigma}_1\cdot(\mathbf{k}_1\times\mathbf{k}'_1+\mathbf{k}_2\times\mathbf{p})\Psi_0(\mathbf{k}_1). \tag{31}$$

Let us first assume the approximation to $F_{np}(\mathbf{k},\mathbf{k}')$ of the form

$$F_{np}(\mathbf{k},\mathbf{k}') = \bar{a}+\bar{b}k^2+8c\mathbf{k}\cdot\mathbf{k}', \tag{32}$$

where $\bar{a}$, $\bar{b}$ and c are constants. It follows that

$$F_0(\mathbf{k},\mathbf{k}') = a+4bk^2+4c\mathbf{k}\cdot\mathbf{k}' \tag{33}$$

where $a = \frac{3}{2}\bar{a}$, $4b = \frac{3}{2}\bar{b}$.

As an example let us concentrate on the O^{17} problem with the O^{16} density $\hat{\varrho}(\mathbf{r}_a, \mathbf{r}_b) \approx \rho_0(R, r)$, where $\rho_0(R, r)$ is given by eq. (16). As before, in the following we shall use Dąbrowski's parameter r_0 corresponding to the correlated core, and we shall neglect $\Delta\rho(\mathbf{R},\mathbf{r})$. With this approximation the integrations over $\mathbf{k}_2$ and $\mathbf{r}$ can be performed and without any further approximations we find

$$(\widehat{\Delta E})_{LS} = \tfrac{3}{8}i\left(\frac{4\pi\hbar^2}{M^*}\right)\frac{1}{(2\pi)^3}\int d^3\mathbf{k}_1,\ d^3\mathbf{k}'_1\int d^3\mathbf{R}\Psi_0^*(\mathbf{k}'_1)e^{i\mathbf{p}\cdot\mathbf{R}}\boldsymbol{\sigma}_1\cdot(\mathbf{k}_1\times\mathbf{k}'_1) \{Z(R)+\rho_0(R)[\nu k_1^2+\nu' k_1'^2+2\mu\mathbf{k}_1\cdot\mathbf{k}_1]\}\Psi_0(\mathbf{k}_1), \tag{34}$$

where

$$Z(R) = a\rho_0(R)+(N/(2r_0^2))\tau(3+R^2/r_0^2)e^{-R^2/(2r_0^2)},$$

$$\tau = \tfrac{1}{2}(b+c), \qquad \nu = \tfrac{1}{4}(9b-3c), \qquad \nu' = \tfrac{1}{4}(b-3c), \qquad 2\mu = \tfrac{1}{2}(5c-3b).$$

Going back to the configuration space we find as the final result

$$(\widehat{\Delta E})_{LS} = -\tfrac{3}{8}\left(\frac{4\pi\hbar^2}{M^*}\right)\int d^3\mathbf{R}\Psi_0^*(\mathbf{R})\left[\frac{1}{R}\frac{d}{dR}Z(R)+\frac{\mu}{R}\frac{d}{dR}(\nabla^2\rho_0(R)) -(\nu+\nu'+2\mu)\frac{1}{R}\frac{d}{dR}\rho_0(R)\nabla^2\right](\boldsymbol{\sigma}_1\cdot\mathbf{L})\Psi_0(\mathbf{R}) \equiv \langle V_{LS}(R)\mathbf{L}\cdot\mathbf{S}\rangle, \tag{35}$$

where

$$\frac{1}{R}\frac{d}{dR}Z(R) = (N/r_0^2)e^{-R^2/2r_0^2}\left[\left(a-\frac{b+c}{4r_0^2}\right)-\left(a+\frac{b+c}{4r_0^2}\right)\frac{R^2}{r_0^2}\right]$$

and $\nu+\nu'+2\mu = b+c$. The quantity $\nabla^2\Psi_0(\mathbf{R})$ may be replaced by $(2M/\hbar^2)(V-E)\Psi_0$ from the appropriate Schroedinger equation.

We observe that eq. (15) of section 2 follows from (35) automatically by setting $\Delta\rho \equiv 0$, $a = -\alpha M^*/4\hbar^2$, $\nu+\nu'+2\mu = b+c = 0$, $\nu = \nu' = -\mu = -\delta M^*/4\hbar^2$. Indeed, if we set, in addition, $-\delta M^*/4\hbar^2 = 2b = -2c$, we have

$$-4i\frac{4\pi\hbar^2}{M^*}F_0(\mathbf{k},\mathbf{k}') \equiv f(p).$$

As in section 2 the doublet splitting of O^{17} is $\Delta(\Delta E)_{LS} = -\frac{5}{2}\langle V_{LS}(R)\rangle$. All the **R** integrations involved in eq. (35) are elementary as they were in section 2. The term proportional to a is the usual Thomas term; the terms involving b and c are the most important corrections to it.

Let us now consider in detail $F_0(\mathbf{k}, \mathbf{k}')$ for the sets of phase shifts obtained from the Signell-Marshak (S-M) potentials and the Gammel-Thaler (G-T) potentials. We first evaluate the "isotropic part" of $F_{np}(\mathbf{k}, \mathbf{k}')$ from the expression $(1/16k^3i)(2R^0_{11}+3R^1_{11}-5R^2_{11})$ in the notation of Bell and Skyrme [16]) and the "cosine part" of $F_{np}(\mathbf{k}, \mathbf{k}')$ from $\cos\theta_{(\mathbf{k},\mathbf{k}')}(1/16\ k^3i)\cdot(9R^1_{21}+5R^2_{21}-14R^3_{21})$. The "isotropic part" involves triplet odd phase shifts only; the "cosine part" depends on the triplet even phase shifts only.

For the Signell and Marshak case† the "isotropic part" of $F_{np}(\mathbf{k}, \mathbf{k}')$ is

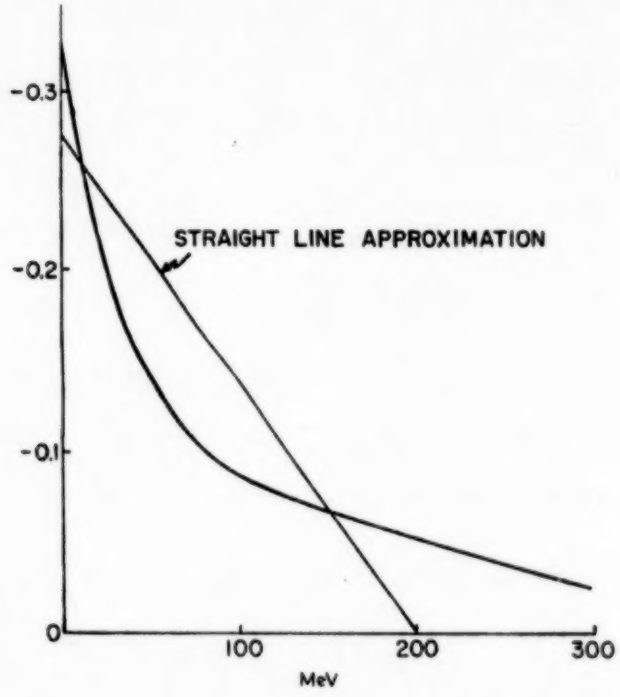

Fig. 1

plotted in fig. 1 as a function of energy $E = 2\hbar^2k^2/M$. This curve is fitted by the function

$$F^{\text{isotr.}} = -0.330(1+0.80\times10^{-6}E^3)e^{-0.01916E}f^3, \tag{36}$$

where E is expressed in MeV. The approximation of expanding this function in powers of k^2 with retention of only the two first terms is very poor. Indeed, the higher powers of k^2 are still important for $\Delta(\Delta E)_{LS}$, since, as it can be shown, the energies at least up to about 100 MeV are important.

† However, it is not easy to justify the use of Dąbrowski's wave function for the S-M case, because his calculations are based largely on the G-T potentials.

There is much arbitrariness in approximating $F^{\text{isotr.}}$ by a straight line of the form $\bar{a}+\bar{b}k^2$. However, the line with $\bar{a} = \frac{2}{3}a = -(\frac{2}{3}\times 0.413\ f^3$, $\bar{b} = \frac{8}{3}b = \frac{8}{3}\times 0.0428\ f^5$ seems to reproduce $F^{\text{isotr.}}$ to a reasonable extent. The "cosine term" $F^{\cos}$ is given in fig. 2. This term, due to the smallness of its coefficient in $\Delta(\Delta E)_{LS}$, when overestimated by $8c\mathbf{k}\cdot\mathbf{k}'$ with $c = -0.036f^5$, contributes only 1 % as much as $F^{\text{isotr.}}$. It should be noted that our resultant $F_0(\mathbf{k}, \mathbf{k}')$ is in qualitative disagreement with Bell and Skyrme's [16])

$$F_0 \equiv F_{\text{np}}(\theta_{(\mathbf{k},\mathbf{k}')} = 0)+\tfrac{1}{2}F_{\text{np}}(\theta_{(\mathbf{k},\mathbf{k}')} = \pi)$$

of their fig. 1. In addition it should also be noted that their F_0 corresponds to the "forward scattering approximation" which is avoided in the present paper. With the above numbers for a, b and c, and the same parameters as

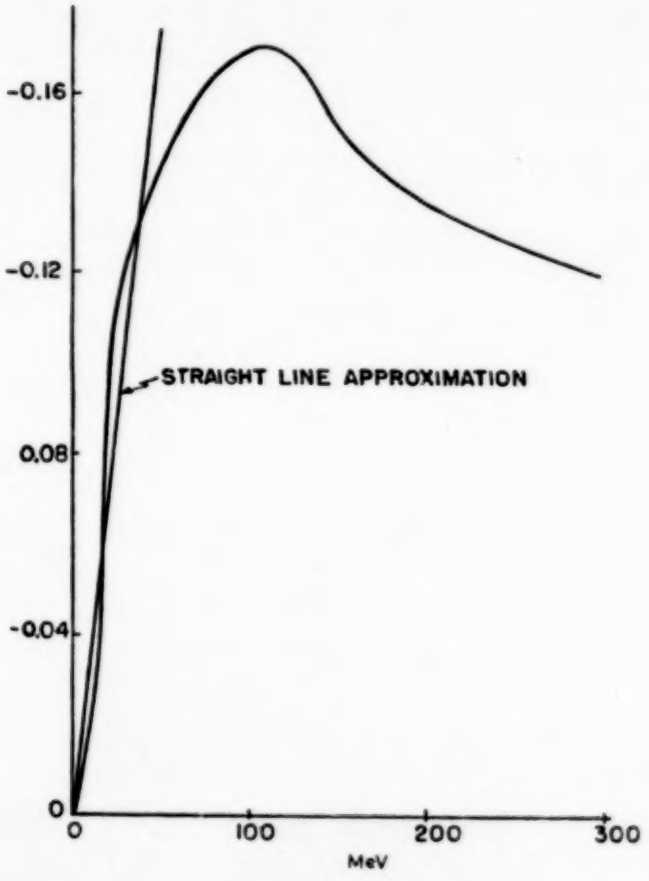

Fig. 2

in section 2, Dąbrowski's $r_0 \approx 0.786\ f$ and $\sqrt{\nu'}$ of ref. [26]), we find $\Delta(\Delta E)_{LS} = 8.12\ M/M^*$ MeV. With $M^* = 0.67\ M$ of ref. [34]) the doublet splitting is thus too large by a factor of about two. Any "decorrelation" of r_0 decreases this number; e.g., for $\lambda' = 1$ with $r_0'^2 = \frac{1}{2}\nu'$ we would have $\Delta(\Delta E)_{LS} = 3.96\ M/M^*$ MeV. In view of the crudeness of the approximations involved this result suggests at least that the S-M potentials yield a reasonable splitting

For the G-T case, $F^{\text{isotr.}}$ is plotted in fig. 3. We choose the straight line with $\bar{a} = \frac{2}{3}a = -\frac{2}{3} \times 0.21 f^3$ and $\bar{b} = \frac{8}{3}b = \frac{8}{3} \times 0.0084\ f^5$. The function $F^{\cos}$ is overestimated by $8c\mathbf{k} \cdot \mathbf{k}'$ with $c = -0.011\ f^5$ and is again negligible. The resulting doublet splitting in O^{17} is $\Delta(\Delta E)_{LS} = 5.3 M/M^*$ MeV with Dąbrowski's r_0 and $\sqrt{\nu'}$ of ref. [26]). The conclusion is: although the G-T case provides a better numerical result, no clear-cut distinction between this case and the S-M case can be obtained from this theory. From the last number ($5.3\ M/M^*$ MeV) we see that the phase shift approximation together with our straight line fit produces a result several times larger than that of section 2 for the same G-T potentials. In the phase shift approximation both the cases produce

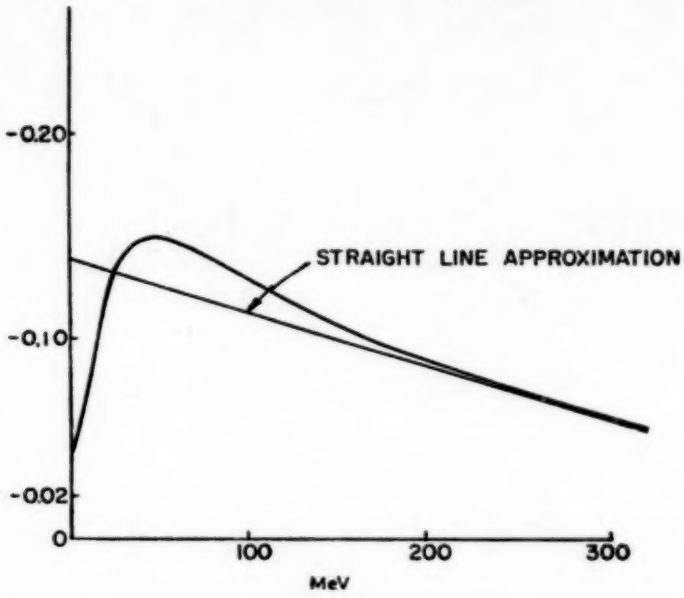

Fig. 3

similar spin-orbit splittings with the correct sign and correct order of magnitude.

We hope to develop this theory further and to extend its applications to other nuclei.

A more detailed discussion of $F^{\text{isotr.}}$ and of the straight line approximation are given in appendix 2.

We are indebted to J. D. Talman for calling our attention to the paper by Fukuda and Newton and to J. J. de Swart for providing us with unpublished phase shifts calculated from the most recently modified Signell-Marshak potentials. We thank Dr. C. A. Levinson for helpful criticism of the manuscript.

Appendix 1

THE EXCHANGE AMPLITUDE OF $V_{LS}^{\mathrm{n\cdot n}}$

Following a calculation similar to that of Nigam and Sundaresan [18]) with the same approximation of retaining the lowest order in p only, we obtain for the exchange amplitude, provided that $\Delta\rho(R, r)$ is neglected

$$(\widehat{\Delta E})_{LS}^{\mathrm{ex}} = \tfrac{1}{2}\cdot\tfrac{3}{4}\frac{(4\pi)^2}{(2\pi)^6}\int \mathrm{d}^3\mathbf{k}_1\mathrm{d}^3\mathbf{k}'_1\int \mathrm{d}^3\mathbf{R}\Psi_0^*(\mathbf{k}'_1)\mathrm{e}^{i\mathbf{p}\cdot\mathbf{R}}\boldsymbol{\sigma}_1\cdot(\mathbf{k}_1\times\mathbf{k}'_1)$$
$$\times\int_0^\infty r^2\mathrm{d}r\rho_0(R, r)\frac{j_1(k_1r)}{k_1}\int_0^\infty k^2kj_1(2kr)f_{\mathrm{X}}(2k)\Psi_0(\mathbf{k}_1)\,\mathrm{d}k, \qquad (\mathrm{A}_1 1)$$

where

$$f_{\mathrm{X}}(2k) = \frac{4\pi i}{2k}\frac{\mathrm{d}}{\mathrm{d}2k}\int_0^\infty r'^2\mathrm{d}r' j_0(2kr')V_{LS}^{\mathrm{n\cdot n}}(r'). \qquad (\mathrm{A}_1 2)$$

The lowest order term in $f_{\mathrm{X}}(2k)$ is equal to $4\pi i(-\frac{1}{3}I_1)$ where I_1 is Moshinsky's first moment of $V_{LS}^{\mathrm{n\cdot n}}(r')$. Since

$$\int_0^\infty k^3\mathrm{d}kj_1(2kr) = \frac{\pi}{4r}[\delta'(r)/2r+\delta''(r)],$$

we find for this term

$$(\widehat{\Delta E})_{LS}^{\mathrm{ex}} \approx \tfrac{1}{2}\cdot\tfrac{3}{4}\frac{(4\pi)^2}{(2\pi)^6}\tfrac{1}{8}\pi\int \mathrm{d}^3\mathbf{k}_1\mathrm{d}^3\mathbf{k}'_1\Psi_0^*(\mathbf{k}'_1)\int \mathrm{d}^3\mathbf{R}\mathrm{e}^{i\mathbf{p}\cdot\mathbf{R}}\boldsymbol{\sigma}_1\cdot(\mathbf{k}_1\times\mathbf{k}'_1)$$
$$\times(-\tfrac{4}{3}\pi i)I_1\rho_0(R)\Psi_0(\mathbf{k}_1). \qquad (\mathrm{A}_1 3)$$

This quantity is exactly equal to $(\widehat{\Delta E})_{LS}$ of eq. (13) with the coefficient α, occurring in eq. (14), replaced by $\frac{1}{3}I_1$.

Appendix 2

ALTERNATIVE CALCULATION OF $\Delta(\Delta E)_{LS}$ IN PHASE SHIFT APPROXIMATION OF THE K_{LS}-OPERATOR

As was pointed out in the discussion following eq. (36) there is considerable arbitrariness in approximating $F^{\mathrm{isotr.}}$ by a straight line of the form: $\bar{a}+\bar{b}k^2$. There is also the same arbitrariness in fitting F^{cos} with a straight line, but as it is stated in the same discussion, its contribution to the doublet splitting is negligible.

Of course, it would be desirable to evaluate the doublet splitting using eq. (36) exactly and without any further approximations. A less ambitious procedure is presented in this appendix where eq. (36) is used, but to simplify the involved calculations an approximation (forward scattering approximation) is made. Although it is not easy to estimate the effect of this approximation, we believe that the result of this calculation supports an earlier

claim that a "straight line" fit of $F^{\text{isotr.}}$ is not unreasonable. Since we again obtain the right order for the doublet splitting, we expect that with no approximation eq. (36) would lead to a reasonable result.

We put $F_0(\mathbf{k}, \mathbf{k}') = \frac{3}{2}F^{\text{isotr.}}$ in eq. (31) where $F^{\text{isotr.}} = -\zeta(1+\zeta' k^6)e^{-\zeta'' k^2}$ with ζ, ζ' and ζ'' following from eq. (36); and after changing the variables from $\mathbf{k}_2$ to $\mathbf{k}$, we can perform the angular integrations of $\mathbf{r}$ and $\mathbf{k}$, resulting in

$$(\widehat{\Delta E})_{LS} = -\frac{9\hbar^2 i}{4\pi^3 M^*}\int d^3\mathbf{k}_1 d^3\mathbf{k}'_1 \Psi_0^*(\mathbf{k}'_1)\int d^3\mathbf{R} e^{i\mathbf{p}\cdot\mathbf{R}}\boldsymbol{\sigma}_1\cdot(\mathbf{k}_1\times\mathbf{k}'_1) \tag{A$_2$1}$$
$$\times\int_0^\infty dr r^2\rho_0(R,r)\left[j_1(|\mathbf{k}_1-\tfrac{1}{2}\mathbf{p}|r)/|\mathbf{k}_1-\tfrac{1}{2}\mathbf{p}|\right]\int_0^\infty k^3\zeta(1+\zeta' k^6)e^{-\zeta'' k^2}j_1(2kr)$$
$$\times\Psi_0(\mathbf{k}_1)dk.$$

Using the same argument as given in the discussion following eq. (13), we set $|\mathbf{k}_1-\frac{1}{2}\mathbf{p}| \approx k_1$. This is the only approximation applied in the present calculation. We can now carry out the k and r integrations using $\rho_0(R, r)$ given by eq. (16). The result can be put into the form

$$(\widehat{\Delta E})_{LS} = \int d^3\mathbf{k}_1 d^3\mathbf{k}'_1\int d^3\mathbf{R}\Psi_0^*(\mathbf{k}'_1)e^{i\mathbf{k}'_1\cdot\mathbf{R}}\boldsymbol{\sigma}_1\cdot(\mathbf{k}_1\times\mathbf{k}'_1) \tag{A$_2$2}$$
$$\times\sum_{n=0}^{4}\Lambda_n^{(R)}k_1^{2n}e^{-k_1^2/(4/\zeta''+1/2r_0^2)}\Psi_0(\mathbf{k}_1)e^{-i\mathbf{k}_1\cdot\mathbf{R}},$$

where $\Lambda_n(R) = (A_n+B_nR^2)e^{-R^2/2r_0^2}$ with the A_n and B_n given by complicated functions of the parameters ζ, ζ', ζ'', and r_0 which are not presented here. We define

$$\varphi(R) = (2\pi)^{-\frac{3}{2}}\int d^3\mathbf{k}_1 e^{-i\mathbf{k}_1\cdot\mathbf{R}}e^{-k_1^2/(4/\zeta''+1/2r_0^2)}\Psi_0(\mathbf{k}_1). \tag{A$_2$3}$$

Going back to the configuration space, i.e., performing the $\mathbf{k}_1$ and $\mathbf{k}'_1$ integrations in eq. (A$_2$2), the spin-orbit energy becomes

$$(\widehat{\Delta E})_{LS} = i(2\pi)^3\int d^3\mathbf{R}(\boldsymbol{\sigma}_1\cdot\mathbf{L})\Psi_0^*(\mathbf{R})\frac{1}{R}\sum_{n=0}^{4}\frac{d\Lambda_n(R)}{dR}(-)^n\nabla^{2n}\varphi(\mathbf{R}). \tag{A$_2$4}$$

Again for the O^{17} problem we use the wave function $\Psi_0(\mathbf{R})$ given by eq. (25). For this case the radial part of $\varphi(\mathbf{R})$ is

$$\varphi(R) = N_2\gamma^{\frac{7}{2}}e^{-(\frac{1}{4}\nu')R^2\gamma}R^2, \tag{A$_2$5}$$

where

$$\gamma = [1+\nu'/(2/\zeta''+1/4r_0^2)]^{-1}.$$

For Dąbrowski's $r_0 \approx 0.786$ *f* and $\sqrt{\nu'}$ of ref. [26]), we obtain for the doublet splitting of O^{17}

$$\Delta(\Delta E)_{LS} \approx 2.15\, M/M^* \text{ MeV}. \tag{A$_2$6}$$

If, as before, we choose $M^* = 0.67\,M$ of ref. [34]), the doublet splitting is 3.2 MeV. The number $2.15\,M/M^*$ MeV differs significantly from our previous result $8.12\,M/M^*$ MeV obtained from the straight line fit of fig. 1. It is not easy to determine how much of this discrepancy is due to the straight line approximation on the one hand and to the forward scattering approximation made in this appendix on the other.

Notes added in proof:

1) Signell, Zinn and Marshak have modified their V_{LS} potential in a recent publication [37]). The change in the phase shifts is only slight in the energy region important here, but the Born approximation result is very different. We find $\alpha_{S-M}^{Born} = 0.85\,f^5$ MeV and $\delta_{S-M}^{Born} = -0.11\,f^7$ MeV for the new V_0 and μ and $r_c = 0.21\,f$. These produce a $\Delta(\Delta E)_{LS}$ about 17 times smaller than that of § 2. This differs very much from the phase shift approximation result. The computation of the K-matrix for the S-M case would be desirable to examine the effect of the difference $K_{LS}-V_{LS}$.

2) Dąbrowski's parameters r_c, β and r_0 used in the text correspond to a radius which is smaller than the O^{16} nucleus. We have examined the "phenomenological" density $\rho_0(R)$ corresponding to the harmonic oscillator wave functions. Feingold in a recent paper (preprint) computes the appropriate $\alpha = \frac{1}{2}r_0$ using the most recent Coulomb energies given by Kofoed-Hansen [38]). We get $\Delta(\Delta E)_{LS} = 0.82$ MeV for $\lambda' = 1$ and for K_{LS} of B-G-W against 4.69 MeV obtained in section 2.2.

Feingold's value of r_0 is $1.18f$ as compared to Dąbrowski's $r = 0.786f$. Pearse [39]), dealing with the same problem of doublet splittings, uses a value of $r_c = 0.60f$ which is much too small to account for the experimental radius of O^{16}.

References

1) J. Keilson, Phys. Rev. **82** (1951) 759
2) L. S. Kisslinger, Phys. Rev. **104** (1956) 1077
3) B. Jankovici, Phys. Rev. **107** (1957) 631
4) B. Jankovici, Nuovo Cimento **7** (1958) 290
5) B. P. Nigam and M. K. Sundaresan, Can. J. Phys. **36** (1958) 571
6) W. J. Swiatecki, Proc. Phys. Soc. A **64** (1951) 226
7) K. A. Brueckner, J. L. Gammell and H. Weitzner, Phys. Rev. **110** (1958) 431
8) C. H. Blanchard and R. Avery, Phys. Rev. **81** (1951) 35
9) J. Hughes and K. J. Le Couteur, Proc. Phys. Soc. A **63** (1950) 1219
10) I. Talmi, Helv. Phys. Acta **25** (1952) 185
11) J. P. Elliott and A. M. Lane, Phys. Rev. **96** (1954) 1160
12) R. J. Blin-Stoyle, Phil. Mag. **46** (1955) 973
13) K. M. Case and A. Pais, Phys. Rev. **80** (1950) 203
14) P. S. Signell and R. E. Marshak, Phys. Rev. **106** (1957) 832
15) P. S. Signell and R. E. Marshak, Phys. Rev. **109** (1958) 1229
16) J. S. Bell and T. H. R. Skyrme, Phil. Mag. **1** (1956) 1055

17) H. Feshbach and E. Lomon, Phys. Rev. **102** (1956) 891
18) B. P. Nigam and M. K. Sundaresan, Phys. Rev. **111** (1958) 284
19) M. Moshinsky, Revista Mexicana de Fisica **7** (1958) 95
20) J. L. Gammel and R. M. Thaler, Phys. Rev. **107** (1957) 291
21) J. L. Gammel and R. M. Thaler, Phys. Rev. **107** (1957) 1337
22) J. Dąbrowski, Proc. Phys. Soc. A **71** (1958) 658
23) R. Jastrow, Phys. Rev. **98** (1955) 1479
24) F. Iwamoto and M. Yamada, Progr. Theor. Phys. (Japan) **17** (1957) 543
25) W. Heisenberg, Theorie des Atomkerns (Goettingen, 1951)
26) J. P. Elliott and B. H. Flowers, Proc. Roy. Soc. A **229** (1955) 536
27) L. Wolfenstein and J. Ashkin, Phys. Rev. **85** (1952) 947
28) R. H. Dalitz, Proc. Phys. Soc. A **65** (1952) 175
29) S. C. Wright, Phys. Rev. **99** (1955) 996
30) H. P. Stapp, T. J. Ypsilantis and N. Metropolis, Phys. Rev. **105** (1957) 302
31) K. A. Brueckner, Phys. Rev. **96** (1954) 508
32) N. Fukuda and R. G. Newton, Phys. Rev. **103** (1956) 1558
33) B. S. de Witt, Phys. Rev. **103** (1956) 1565
34) T. H. R. Skyrme, Phil. Mag. **1** (1956) 1043
35) A. M. Feingold and E. P. Wigner, Phys. Rev. **79** (1950) 221(A);
A. M. Feingold, Phys. Rev. **101** (1956) 258
36) Eden and Francis, Phys. Rev. **97** (1955) 1366
37) Signell, Zinn and Marshak, Phys. Rev. Letters **1** (1958) 416
38) Kofoed-Hansen, Revs. Mod. Phys. **30** (1958) 449
39) Pearse, Phys. Rev. **106** (1957) 545

3A.: 6.D *Nuclear Physics* **11** (1959) 387—399: © *North-Holland Publishing Co., Amsterdam*
Not to be reproduced by photoprint or microfilm without written permission from the publisher

SIGN OF THE NUCLEAR QUADRUPOLE INTERACTION BY OBSERVATION OF POLARIZED GAMMA-GAMMA ANGULAR CORRELATIONS

SAMUEL M. HARRIS
Physics Department, University of Illinois, Urbana, Illinois †

Received 18 December 1958

Abstract: The sign of the nuclear quadrupole interaction cannot be determined by measurement of unpolarized γ—γ angular correlations. It can, however, be found by measuring the circular polarization of one of the radiations. Appropriate formulae are given to enable the reader to easily calculate the correlation function as a function of crystal orientation in the cases where the two radiations make angles of 90° and 180° with each other, are of multipole order $L \leqq 2$, and involve an intermediate state with spin $I \leqq \frac{7}{2}$. For the 90° case, in general, terms enter which are dependent on the sign of the interaction. The application of this technique to unpolarized β—γ correlations is also considered.

1. Introduction

Previous calculations have been performed which yield the angular correlation function when the intermediate state is subjected to perturbations due to magnetic dipole and electric quadrupole interactions [1]). These calculations are limited to the case of unpolarized γ—γ correlations, and verify the well-known fact that the correlation is independent of the sign of the quadrupole interaction. To this author's knowledge, only one calculation has been published that considers the measurement of the polarization of one of the radiations (in the cascade decay of Cd^{111}) [2]), with the result that quadrupole interaction sign-dependent terms do appear. The present paper is an attempt at the generalization of these results to the case where the intermediate state spin $I \leqq \frac{7}{2}$ and the radiations are of multipole orders $L \leqq 2$. Also, only quadrupole interactions are considered here. The notation and formalism used follows that of ref. [1]) as closely as possible.

The measurement of γ-polarization, at the present time, introduces attenuation of the order of 10^3 in the detector efficiency. If the polarizations of both of the radiations are detected, the coincidence efficiency is reduced by at least 10^6, making the experiment extremely difficult. The present calculation has, because of this, been performed considering detector 1 sensitive only to γ_1 of a particular polarization, whereas detector 2 detects

† This work was supported by the United States Office of Naval Research.

all γ_2. Note here that each detector is therefore assumed to be sensitive to only one of the radiations.

2. General Theory

Consider the cascade shown diagramatically in fig. 1. γ_1 and γ_2 are the first and second radiations of multipole orders L_1, L'_1 and L_2, L'_2 respectively, thus allowing for the possibility of mixed transitions; I_1, I, I_2 are the spins of the initial, intermediate, and final states.

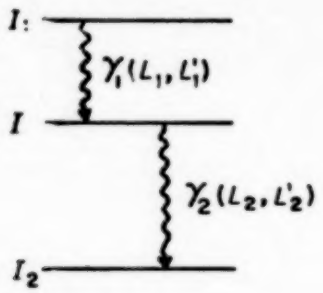

Fig. 1

The relative probability for the emission of two photons of momenta $\mathbf{k}_1$ and $\mathbf{k}_2$ separated by a time t can be written as

$$\begin{aligned} W(\mathbf{k}_1, \mathbf{k}_2, t) &= \sum_{m_1 m_t} |\sum_{m} \langle I_2 m_t|H_2(\mathbf{k}_2)|Im\, t\rangle\langle Im|H_1(\mathbf{k}_1)|I_1 m_1\rangle|^2 \\ &= \sum_{m_1 m_t m m'} \langle I_2 m_t|H_2|Imt\rangle\langle Im|H_1|I_1 m_1\rangle \\ &\times \langle I_2 m_t|H_2|Im'\, t\rangle^*\langle Im'|H_1|I_1 m_1\rangle^* \end{aligned} \tag{1}$$

where $H_j(\mathbf{k}_j)$ is the interaction Hamiltonian for the emission of $\mathbf{k}_j$.

If the nucleus is in the intermediate state $|Im\rangle$ immediately following the first transition, at a time t later it will be in a state

$$|Im\, t\rangle = |Im\rangle \exp\left[-i\,\frac{E_m}{\hbar}t - \frac{1}{2\tau}t\right]$$

where E_m is the quadrupole interaction energy when the intermediate state is in a magnetic substate m and τ is the lifetime of the intermediate state. In the above expression, no mixture of m states occurs because the quantization axis is taken to be the symmetry direction of the axially symmetric electric field gradient which is assumed to be present and causing the quadrupolar perturbation. The time dependent correlation function then becomes

$$\begin{aligned} W(\mathbf{k}_1, \mathbf{k}_2, t) &= \sum_{m_1 m_t m m'} \langle I_2 m_t|H_2|Im\rangle\langle Im|H_1|I_1 m_1\rangle\langle I_2 m_t|H_2|Im'\rangle^* \\ &\times \langle Im'|H_1|I_1 m_1\rangle \exp\left[-\frac{t}{\tau} - i\left(\frac{E_m - E_{m'}}{\hbar}\right)t\right]^{(2)}. \end{aligned} \tag{2}$$

If one introduces a coincidence function $\zeta(t)$, which is the coincidence circuit sensitivity when the delay time between the two radiations is t, eq. (2) becomes upon integrating over dt and dividing by $\int_0^\infty \zeta(t)\exp(-t/\tau)\mathrm{d}t$.

$$W(\mathbf{k}_1, \mathbf{k}_2) = \sum_{m_1 m_t m m'} \langle I_2 m_t | H_2 | I m\rangle \langle I m | H_1 | I_1 m_1\rangle \langle I_2 m_t | H_2 | I m'\rangle^* \times \langle I m' | H_1 | I_1 m_1\rangle^* \frac{\mathscr{H}_\zeta(x_{mm'})}{1+ix_{mm'}} \tag{3}$$

where

$$\frac{\mathscr{H}_\zeta(x_{mm'})}{1+ix_{mm'}} \equiv \frac{\int_0^\infty \zeta(t)\exp\left[-\frac{t}{\tau} - i\left(\frac{E_m - E_{m'}}{\hbar}\right)t\right]\mathrm{d}t}{\int_0^\infty \zeta(t)\exp(-t/\tau)\mathrm{d}t}. \tag{4}$$

and

$$x_{mm'} = (E_m - E_{m'})\tau/\hbar. \tag{5}$$

The factor $\int_0^\infty \zeta(t)\exp(-t/\tau)\mathrm{d}t$ is introduced for normalization so that in the absence of the quadrupole interaction ($x_{mm'} = 0$), (4) goes to unity. The $\mathscr{H}_\zeta$ will be given later for various experimental arrangements. At this point, the multipole expansions of H_1 and H_2 are introduced and utilizing the properties of angular momenta and Racah algebra in the usual manner (e.g., see ref. [3])), one obtains

$$W(\theta, \varphi, \Theta) \propto \sum_{k_1 k_2 \mu} \sum_{L_1 L'_1 L_2 L'_2} \langle I||L_1||I_1\rangle \langle I||L'_1||I_1\rangle^* \langle I||L_2||I_2\rangle \langle I||L'_2||I_2\rangle^* \times (-1)^{L'_1+L'_2+k_1} W(IIL_1L'_1; k_1 I_1) W(IIL_2L'_2; k_2 I_2) \times C_{k_1 0}(L_1 L'_1) C_{k_2 0}(L_2 L'_2) \mathscr{G}_\mu^{k_1 k_2} N_\mu^{k_1 k_2} P_{k_1}^\mu(\cos\alpha) P_{k_2}^\mu(\cos\beta) e^{i\mu\psi}; \tag{6}$$

$\langle I||L_i||I_j\rangle$ are the reduced nuclear matrix elements, $W(abcd; ef)$ Racah coefficients, $C_{k0}(LL')$ radiation parameters given by

$$C_{k0}(LL') = \sum_M (-1)^{L-M}[(2L+1)(2L'+1)]^{\frac{1}{2}} C(LL'k; M, -M), \tag{7}$$

where $\sum_M$ is a summation over polarizations of the emitted photon; $M = -1$ corresponds to right-hand circular polarization (RC), and $M = 1$ corresponds to left-hand circular polarization (LC); $C(abc; de)$ are the usual Clebsch-Gordan coefficients; $\mathscr{G}_\mu^{k_1 k_2}$ are the attenuation factors due to the perturbation and given by

$$\mathscr{G}_\mu^{k_1 k_2} = \frac{[(2k_1+1)(2k_2+1)]^{\frac{1}{2}}}{(2I+1)} \sum_{mm'} \frac{C(Ik_1I; m\mu m') C(Ik_2I; m\mu m')}{(1-ix_{mm'})} \mathscr{H}_\zeta(x_{mm'}); \tag{8}$$

$N_\mu^{k_1 k_2}$ are normalization factors given by

$$N_\mu^{k_1 k_2} = \left[\frac{(k_1-|\mu|)!(k_2-|\mu|)!}{(k_1+|\mu|)!(k_2+|\mu|)!}\right]^{\frac{1}{2}}; \tag{9}$$

P_k^μ are the Legendre polynomials. The expression (6) has been evaluated in the coordinate system shown in fig. 2, where

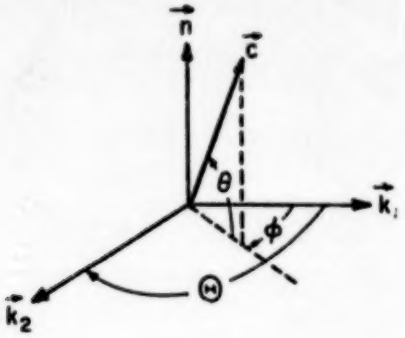

Fig. 2

$$\begin{aligned} \alpha &= \sphericalangle(\mathbf{c}, \mathbf{k}_1) & \cos\alpha &= \cos\theta\cos\varphi \\ \beta &= \sphericalangle(\mathbf{c}, \mathbf{k}_2) & \cos\beta &= \cos\theta\cos(\Theta-\varphi) \\ \psi &= \sphericalangle[(\mathbf{c}\times\mathbf{k}_1), (\mathbf{c}\times\mathbf{k}_2)] & \cos\psi &= \frac{\cos\Theta-\cos\alpha\cos\beta}{\sin\alpha\sin\beta}; \end{aligned} \tag{10}$$

c is the direction of symmetry of the electric field gradient.

If the direction but not the polarization of the emitted photon is measured, the radiation parameter becomes

$$\begin{aligned} C_{k0}^{\mathrm{dir}} &= (-1)^{L-1}[(2L+1)(2L'+1)]^{\frac{1}{2}}C(LL'k;\,1,\,-1) && \text{for } k \text{ even}, \\ C_{k0}^{\mathrm{dir}} &= 0 && \text{for } k \text{ odd}. \end{aligned} \tag{11}$$

For circularly polarized photons †, the sum in (7) degenerates to one term:

$$\begin{aligned} C_{k0}^{\mathrm{RC}} &= (-1)^{L-1+k}[(2L+1)(2L'+1)]^{\frac{1}{2}}C(LL'k;\,1,\,-1), \\ C_{k0}^{\mathrm{LC}} &= (-1)^{L-1}[(2L+1)(2L'+1)]^{\frac{1}{2}}C(LL'k;\,1,\,-1). \end{aligned} \tag{12}$$

Note here, however, that these radiation parameters are defined for both even and odd k. For even k, all three C's are equal. A more uniform notation is available if one introduces a polarization parameter ρ which is $\{^{+1}_{-1}\}$ for $\{^{\mathrm{RC}}_{\mathrm{LC}}\}$ polarized photons. Then (12) can be written in a combined form:

$$C_{k0}(\rho) = (-\rho)^k(-1)^{L-1}[(2L+1)(2L'+1)]^{\frac{1}{2}}C(LL'k;\,1,\,-1). \tag{12'}$$

At this point it is usual to introduce the F-functions of angular correlation theory, defined by

$$\begin{aligned} &F_k(LL'I'I) \\ &=(-1)^{I'-I-1}[(2I+1)(2L+1)(2L'+1)]^{\frac{1}{2}}C(LL'k;\,1,\,-1)W(IILL';\,kI'). \end{aligned} \tag{13}$$

Eq. (6) can then be rewritten as

† The unperturbed γ_c—γ_c correlation has recently been considered [4]).

$$W(\theta, \varphi, \Theta) \propto \sum_{k_1 k_2 \mu} \sum_{L_1 L'_1 L_2 L'_2} \langle I||L_1||I_1\rangle\langle I||L'_1||I_1\rangle^*\langle I||L_2||I_2\rangle\langle I||L'_2||I_2\rangle^* \times (\rho_1)^{k_1}(-\rho_2)^{k_2} F_{k_1}(L_1 L'_1 I_1 I) F_{k_2}(L_2 L'_2 I_2 I) \mathscr{G}_\mu^{k_1 k_2} \times N_\mu^{k_1 k_2} P^\mu_{k_1}(\cos\alpha) P^\mu_{k_2}(\cos\beta) e^{i\mu\psi}. \quad (14)$$

As previously mentioned, it will be assumed that only the polarization of the first photon is measured so that k_2 will be restricted to take on even integral values. Although the result of (14) is valid for mixed multipole transitions, it will now be assumed that both radiations are pure so that the sums over L_1, L'_1, L_2, and L'_2 all degenerate to one term. Furthermore, the reduced matrix elements now form a constant factor common to all terms in the expansion for the correlation function so that they may be ignored. Letting

$$A_{k_1 k_2} = F_{k_1}(L_1 L_1 I_1 I) F_{k_2}(L_2 L_2 I_2 I), \quad (15)$$

(14) becomes

$$W(\theta, \varphi, \Theta) = \sum_{k_1 k_2 \mu} (\rho_1)^{k_1} A_{k_1 k_2} \mathscr{G}_\mu^{k_1 k_2} N_\mu^{k_1 k_2} P^\mu_{k_1}(\cos\alpha) P^\mu_{k_2}(\cos\beta) e^{i\mu\psi}. \quad (16)$$

Tables for the various F-functions of general interest are published [3, 5, 6]. From the triangular conditions on the arguments of the Racah coefficients, it can easily be seen that

$$0 \leqq k_i \leqq \text{Min}\,(2I, 2L_i). \quad (17)$$

The quadrupole interaction energy can be written as [7]

$$E_m = -eQ \frac{\partial E_z}{\partial z} \frac{3m^2 - I(I+1)}{4I(2I-1)} \quad (18)$$

where Q is the quadrupole moment and $\partial E_z/\partial z$ is the field gradient along the c direction. It is seen from (18) that the interaction energy depends only upon the magnitude of m. Using this fact along with (4, 5, 8, 17), one is led to

$$\mathscr{G}_\mu^{k_1 k_2} = (-1)^{k_1+k_2} \mathscr{G}_{-\mu}^{k_1 k_2} = (-1)^{k_1} \mathscr{G}_{-\mu}^{k_1 k_2}; \quad (19)$$

the second relation follows immediately since k_2 is always even. The symmetry properties of the Clebsch-Gordan coefficients have been used in obtaining the above result. The relation

$$\mathscr{G}_0^{k_1 k_2} = \delta_{k_1, k_2} \quad (20)$$

follows directly from (8).

Using (19), the expression (16) can now be reduced to a sum over $\mu \geqq 0$ only:

$$W(\theta,\varphi,\Theta)=\sum_{k_1 k_2 \mu \geq 0}(1-\tfrac{1}{2}\delta_{\mu 0})(\rho_1)^{k_1}A_{k_1 k_2}\mathscr{G}_{\mu}{}^{k_1 k_2}N_{\mu}{}^{k_1 k_2}P^{\mu}_{k_1}(\cos\alpha)$$
$$\times P^{\mu}_{k_2}(\cos\beta)[e^{i\mu\psi}+(-1)^{k_1}e^{-i\mu\psi}]$$
$$=\sum_{\substack{k_1\ (\text{even})\\ k_2,\ \mu\geq 0}}(2-\delta_{\mu 0})A_{k_1 k_2}\mathscr{G}_{\mu}{}^{k_1 k_2}N_{\mu}{}^{k_1 k_2}P^{\mu}_{k_1}(\cos\alpha)P^{\mu}_{k_2}(\cos\beta)\cos\mu\psi \quad (21)$$
$$+2i\rho_1\sum_{\substack{k_1\ (\text{odd})\\ k_2,\ \mu>0}}A_{k_1 k_2}\mathscr{G}_{\mu}{}^{k_1 k_2}N_{\mu}{}^{k_1 k_2}P^{\mu}_{k_1}(\cos\alpha)P^{\mu}_{k_2}(\cos\beta)\sin\mu\psi.$$

From (4, 5, 8, 18), it can be seen that $\mathscr{G}$ is real for even k_1 and imaginary for odd k_1 so that the correlation function is a purely real function, as it must be. The second term in (21) can be regrouped to yield

$$W(\theta,\varphi,\Theta)$$
$$=\sum_{k_1\ (\text{even}),\ k_2,\ \mu\geq 0}(2-\delta_{\mu 0})A_{k_1 k_2}\mathscr{G}_{\mu}{}^{k_1 k_2}N_{\mu}{}^{k_1 k_2}P^{\mu}_{k_1}(\cos\alpha)P^{\mu}_{k_2}(\cos\beta)\cos\mu\psi \quad (22)$$
$$-2\rho_1\sum_{k_1(\text{odd}),\ k_2,\ \mu>0}A_{k_1 k_2}(-i\mathscr{G}_{\mu}{}^{k_1 k_2})N_{\mu}{}^{k_1 k_2}P^{\mu}_{k_1}(\cos\alpha)P^{\mu}_{k_2}(\cos\beta)\sin\mu\psi.$$

The first term above is exactly the correlation function of ref. [1]) if no polarization is measured and will be denoted by W_0. The polarization-dependent term is the second of these and will be called $\Delta W(\rho)$. It is linear in ρ_1 so that altering the sense of the polarization measurement merely changes the sign of ΔW. Thus, if both polarizations of γ_1 are equally detected (corresponding to no polarization measurement), no polarization effect results, as must be the case. The sign of the quadrupole interaction enters only through $\mathrm{Im}(\mathscr{G})$ as is apparent from (4, 8, 18). Thus it only produces an effect via $\Delta W(\rho)$.

An extremely useful and commonly made measurement is the anisotropy, defined as

$$\varepsilon=\frac{W(\theta,\varphi,\pi)-W(\theta,\varphi,\tfrac{1}{2}\pi)}{W(\theta,\varphi,\tfrac{1}{2}\pi)}. \quad (23)$$

From (22), W can be obtained for the special cases of $\Theta=\pi$, and $\Theta=\frac{1}{2}\pi$. It is assumed in the following that the radiations are of no higher order than quadrupole:

$$W_0(\theta,\varphi,\pi)=a_0+a_2\cos^2\theta\cos^2\varphi+a_4\cos^4\theta\cos^4\varphi$$
$$+a_6\cos^6\theta\cos^6\varphi+a_8\cos^8\theta\cos^8\varphi, \quad (24)$$
$$\Delta W(\theta,\varphi,\pi)=0;$$

$$W_0(\theta,\varphi,\tfrac{1}{2}\pi)=b_0+b_2\cos^2\theta+b_4\cos^4\theta+b'_4\cos^2\theta\sin^2\varphi$$
$$+b_6\cos^4\theta\sin^2\varphi+b_8\cos^4\theta\cos^2\varphi\sin^2\varphi$$
$$+b'_8\cos^4\theta\sin^4\varphi+b_{10}\cos^6\theta\cos^2\varphi\sin^2\varphi$$
$$+b_{12}\cos^6\theta\sin^4\varphi\cos^2\varphi+b_{16}\cos^8\theta\cos^4\varphi\sin^4\varphi, \quad (25)$$
$$\Delta W(\theta,\varphi,\tfrac{1}{2}\pi)=\rho_1\sin\theta\cos\theta\sin\varphi[b_3+b_5\sin^2\theta+b_7\cos^2\theta\sin^2\varphi$$
$$+b_9\sin^2\theta\cos^2\theta\sin^2\varphi+b_{11}\cos^4\theta\sin^4\varphi],$$

where the a's and b's are listed in tables 1 and 2.

TABLE 1

The functions a_i which enter into $W(\theta, \varphi, \pi)$

$$a_0 = 1+A_{22}\left(\tfrac{1}{4}+\tfrac{3}{4}G_2^{22}\right)+(A_{24}+A_{42})\left(-\tfrac{1}{8}\sqrt{15}G_2^{24}\right)+A_{44}\left(\tfrac{9}{64}+\tfrac{5}{16}G_2^{44}+\tfrac{35}{64}G_4^{44}\right)$$

$$a_2 = A_{22}\left(-\tfrac{3}{2}+3G_1^{22}-\tfrac{3}{2}G_2^{22}\right)+(A_{24}+A_{42})\left(-\tfrac{9}{2}\sqrt{\tfrac{5}{6}}G_1^{24}+\tfrac{9}{8}\sqrt{15}G_2^{24}\right)$$
$$+A_{44}\left(-\tfrac{45}{16}+\tfrac{45}{8}G_1^{44}-5G_2^{44}+\tfrac{35}{8}G_3^{44}-\tfrac{35}{16}G_4^{44}\right)$$

$$a_4 = A_{22}\left(\tfrac{9}{4}-3G_1^{22}+\tfrac{3}{4}G_2^{22}\right)+(A_{24}+A_{42})\left(15\sqrt{\tfrac{5}{6}}G_1^{24}-\tfrac{15}{8}\sqrt{15}G_2^{24}\right)$$
$$+A_{44}\left(\tfrac{555}{32}-\tfrac{255}{8}G_1^{44}+\tfrac{195}{8}G_2^{44}-\tfrac{105}{8}G_3^{44}+\tfrac{105}{32}G_4^{44}\right)$$

$$a_6 = (A_{24}+A_{42})\left(-\tfrac{21}{2}\sqrt{\tfrac{5}{6}}G_1^{24}+\tfrac{7}{8}\sqrt{15}G_2^{24}\right)$$
$$+A_{44}\left(-\tfrac{525}{16}+\tfrac{455}{8}G_1^{44}-35G_2^{44}+\tfrac{105}{8}G_3^{44}-\tfrac{35}{16}G_4^{44}\right)$$

$$a_8 = A_{44}\left(\tfrac{1225}{64}-\tfrac{245}{8}G_1^{44}+\tfrac{245}{16}G_2^{44}-\tfrac{35}{8}G_3^{44}+\tfrac{35}{64}G_4^{44}\right)$$

TABLE 2

The functions b_i which enter into $W(\theta, \varphi, \tfrac{1}{2}\pi)$

$$b_0 = 1+A_{22}\left(\tfrac{1}{4}-\tfrac{3}{4}G_2^{22}\right)+(A_{24}+A_{42})\left(\tfrac{1}{8}\sqrt{15}G_2^{24}\right)+A_{44}\left(\tfrac{9}{64}-\tfrac{5}{16}G_2^{44}+\tfrac{35}{64}G_4^{44}\right)$$

$$b_2 = A_{22}\left(-\tfrac{3}{4}+\tfrac{3}{4}G_2^{22}\right)+A_{24}\left(-\tfrac{1}{8}\sqrt{15}G_2^{24}\right)+A_{42}\left(-\sqrt{15}G_2^{24}\right)$$
$$+A_{44}\left(-\tfrac{45}{32}+\tfrac{5}{2}G_2^{44}-\tfrac{35}{32}G_4^{44}\right)$$

$$b_4 = A_{42}\left(\tfrac{7}{8}\sqrt{15}G_2^{24}\right)+A_{44}\left(\tfrac{105}{64}-\tfrac{35}{16}G_2^{44}+\tfrac{35}{64}G_4^{44}\right)$$

$$b'_4 = (A_{42}-A_{24})\left(\tfrac{7}{8}\sqrt{15}G_2^{24}\right)$$

$$b_6 = A_{24}\left(\tfrac{3}{4}\sqrt{15}G_2^{24}\right)+A_{42}\left(-\sqrt{15}G_2^{24}\right)$$

$$b_8 = A_{22}\left(\tfrac{9}{4}-3G_1^{22}+\tfrac{3}{4}G_2^{22}\right)+(A_{24}+A_{42})\left(\tfrac{9}{2}\sqrt{\tfrac{5}{6}}G_1^{24}\right)$$
$$+A_{44}\left(\tfrac{345}{32}-\tfrac{45}{8}G_1^{44}-15G_2^{44}+\tfrac{105}{8}G_3^{44}-\tfrac{105}{32}G_4^{44}\right)$$

$$b'_8 = (A_{24}+A_{42})\left(\tfrac{1}{8}\sqrt{15}G_2^{24}\right)$$

$$b_{10} = A_{42}\left(-\tfrac{21}{2}\sqrt{\tfrac{5}{6}}G_1^{24}+\tfrac{7}{8}\sqrt{15}G_2^{24}\right)$$
$$+A_{44}\left(-\tfrac{525}{32}+\tfrac{105}{8}G_1^{44}+\tfrac{105}{8}G_2^{44}-\tfrac{105}{8}G_3^{44}+\tfrac{105}{32}G_4^{44}\right)$$

$$b_{12} = (A_{24}-A_{42})\left(-\tfrac{21}{2}\sqrt{\tfrac{5}{6}}G_1^{24}+\tfrac{7}{8}\sqrt{15}G_2^{24}\right)$$

$$b_{16} = A_{44}\left(\tfrac{1225}{64}-\tfrac{245}{8}G_1^{44}+\tfrac{245}{16}G_2^{44}-\tfrac{35}{8}G_3^{44}+\tfrac{35}{64}G_4^{44}\right)$$

$$b_3 = -\sqrt{3}A_{12}g_1^{12}+\tfrac{3}{4}\sqrt{10}A_{14}g_1^{14}-A_{32}\left(3\sqrt{2}g_1^{23}-\tfrac{3}{2}\sqrt{5}g_2^{23}\right)$$
$$-A_{34}\left(-\tfrac{3}{2}\sqrt{15}g_1^{34}+\tfrac{5}{4}\sqrt{3}g_2^{34}\right)$$

$$b_5 = -A_{32}\left(-\tfrac{15}{4}\sqrt{2}g_1^{23}+\tfrac{3}{2}\sqrt{5}g_2^{23}\right)-A_{34}\left(\tfrac{15}{8}\sqrt{15}g_1^{34}-\tfrac{5}{4}\sqrt{3}g_2^{34}-\tfrac{5}{8}\sqrt{7}g_3^{34}\right)$$

$$b_7 = -\tfrac{7}{4}\sqrt{10}A_{14}g_1^{14}-A_{32}\left(-\tfrac{15}{4}\sqrt{2}g_1^{23}+\tfrac{3}{2}\sqrt{5}g_2^{23}\right)$$
$$-A_{34}\left(\tfrac{43}{8}\sqrt{15}g_1^{34}-10\sqrt{3}g_2^{34}+\tfrac{15}{8}\sqrt{7}g_3^{34}\right)$$

$$b_9 = -A_{34}\left(-\tfrac{35}{8}\sqrt{15}g_1^{34}+\tfrac{35}{4}\sqrt{3}g_2^{34}-\tfrac{15}{8}\sqrt{7}g_3^{34}\right)$$

$$b_{11} = -A_{34}\left(-\tfrac{35}{8}\sqrt{15}g_1^{34}+\tfrac{35}{4}\sqrt{3}g_2^{34}-\tfrac{15}{8}\sqrt{7}g_3^{34}\right) = b_9$$

In ref. [1]), five simple experimental arrangements are considered in detail:

Arrangement 1: $\varphi = 0$. The symmetry axis **c** lies in the $(\mathbf{k}_1, \mathbf{n})$ plane; **n** is the unit normal to the $(\mathbf{k}_1, \mathbf{k}_2)$ plane.

Arrangement 2: $\theta = 0$. The symmetry axis **c** lies in the $(\mathbf{k}_1, \mathbf{k}_2)$ plane.

Arrangement 3: $\theta = \frac{1}{2}\pi$. The symmetry axis **c** is parallel to **n**.

Arrangement 4: $\Theta = \pi$. Only radiations emitted in opposite directions are measured.

Arrangement 5: A crystalline powder is considered where the orientation of the c-axis is statistically distributed. Thus $W(\theta, \varphi, \Theta)$ is merely integrated over $\mathrm{d}\Omega(\theta, \varphi)$ to obtain some $W(\Theta)$.

In arrangements 1 and 2, there is no polarization contribution to the anisotropy. Furthermore, there is no polarization term entering into the general correlation function in arrangements 2, 3, 4 and 5.

Another arrangement which yields a simple result and does show polariza-

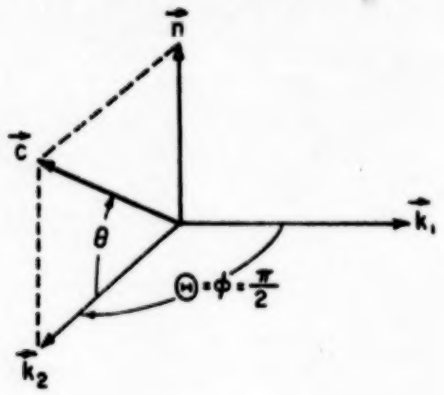

Fig. 3

tion effects is the case where $\varphi = \frac{1}{2}\pi$ (fig. 3). Then the correlation function simplifies to

$$\begin{aligned} W_0(\theta, \tfrac{1}{2}\pi, \tfrac{1}{2}\pi) &= b_0 + (b_2 + b'_4)\cos^2\theta + (b_4 + b_6 + b'_8)\cos^4\theta, \\ \Delta W(\theta, \tfrac{1}{2}\pi, \tfrac{1}{2}\pi) &= \rho_1 \sin\theta\cos\theta[(b_3 + b_5) + (b_7 - b_5 + b_9)\cos^2\theta \\ &\quad + (b_{11} - b_9)\cos^4\theta]. \end{aligned} \tag{26}$$

3. Calculation of the Attenuation Factors

From (8) one may write

$$\begin{aligned} G_\mu^{k_1 k_2} &= \mathrm{Re}(\mathscr{G}_\mu^{k_1 k_2}) \\ &= \frac{[(2k_1+1)(2k_2+1)]^{\frac{1}{2}}}{(2I+1)} \sum_{mm'} \frac{C(Ik_1I; m\mu m')C(Ik_2I; m\mu m')}{1+x_{mm'}^2} H_\zeta(mx), \\ g_\mu^{k_1 k_2} &= \mathrm{Im}(\mathscr{G}_\mu^{k_1 k_2}) \\ &= \frac{[(2k_1+1)(2k_2+1)]^{\frac{1}{2}}}{(2I+1)} \sum_{mm'} \frac{C(Ik_1I; m\mu m')C(Ik_2I; m\mu m')}{1+x_{mm'}^2} h_\zeta(mx) \end{aligned} \tag{27}$$

where

$$\frac{H_\zeta(mx)}{1+x_{mm'}^2} = \mathrm{Re}\left(\frac{\mathscr{H}_\zeta(mx)}{1-ix_{mm'}}\right), \qquad \frac{h_\zeta(mx)}{1+x_{mm'}^2} = \mathrm{Im}\left(\frac{\mathscr{H}_\zeta(mx)}{1-ix_{mm'}}\right). \tag{28}$$

If one defines

$$\begin{aligned} x &= -\frac{3}{4I(2I-1)}\frac{eQ}{\hbar}\frac{\partial E_z}{\partial z}\tau \qquad \text{for integral } I, \\ x &= -\frac{6}{4I(2I-1)}\frac{eQ}{\hbar}\frac{\partial E_z}{\partial z}\tau \qquad \text{for half-integral } I, \end{aligned} \tag{29}$$

the attenuation factors can be written as

$$\begin{aligned} G_\mu^{k_1 k_2} &= \sum_m S_{m\mu}^{k_1 k_2} H_\zeta(mx) \\ g_\mu^{k_1 k_2} &= \sum_m S_{m\mu}^{k_1 k_2} h_\zeta(mx) \end{aligned} \tag{30}$$

where m only takes on positive integral values or zero. The $S_{m\mu}^{k_1 k_2}$ are given in table 3.

The forms of H_ξ and h_ζ must now be investigated. If τ_d is defined as the delay time and τ_r as the resolving time of the coincidence circuit, then using

$$\xi = \tau_r/\tau, \qquad \eta = \tau_d/\tau,$$

H_ζ and h_ζ can easily be derived for certain simple cases:

A. *No delay, infinite resolving time*: $\eta = 0$, $\xi = \infty$.

$$H(mx) = 1, \qquad h(mx) = mx. \tag{31}$$

B. *No delay, finite resolving time*: $\eta = 0$, $\xi \neq \infty$.

$$\begin{aligned} H(mx) &= \frac{1-e^{-\xi}(\cos mx\xi - mx \sin mx\xi)}{1-e^{-\xi}}, \\ h(mx) &= \frac{mx-e^{-\xi}(\sin mx\xi + mx \cos mx\xi)}{1-e^{-\xi}}. \end{aligned} \tag{32}$$

C. *Delay, finite resolving time*: $0 < \xi \leqq \eta$.

$$\begin{aligned} H(mx) &= \frac{[\cos mx(\eta-\xi) - mx \sin mx(\eta-\xi)] - e^{-2\xi}[\cos mx(\eta+\xi) - mx \sin mx\,(\eta+\xi)]}{1-e^{-2\xi}} \\ h(mx) &= \frac{[\sin mx(\eta-\xi) + mx \cos mx(\eta-\xi)] - e^{-2\xi}[\sin mx(\eta+\xi) + mx \cos mx(\eta+\xi)]}{1-e^{-2\xi}}. \end{aligned} \tag{33}$$

D. *Delay, very short resolving time*: $\xi \ll 1$, $\xi \ll \eta$.

$$\begin{aligned} H(mx) &= [1+(mx)^2] \cos mx, \\ h(mx) &= [1+(mx)^2] \sin mx. \end{aligned} \tag{34}$$

TABLE 3

$S_{m\mu}^{k_1 k_2}$ functions used to calculate $G_{\mu}^{k_1 k_2}$ and $g_{\mu}^{k_1 k_2}$ from eq. (30)

	I \ m	0	1	2	3	4	5	6	7	8	9
S_{m1}^{22}	1		1								
	3/2		1								
	2		0.1429		0.8571						
	5/2		0.2857	0.7143							
	3		0.0476		0.3571		0.5952				
	7/2		0.1191	0.3809	0.5000						
S_{m2}^{22}	1	1									
	3/2		1								
	2	0.4286				0.5714					
	5/2		0.6429		0.3571						
	3	0.2857				0.4762				0.2381	
	7/2		0.4762		0.3571		0.1667				
S_{m1}^{44}	2		0.8571		0.1429						
	5/2		0.7143	0.2857							
	3		0.1948		0.4156		0.3896				
	7/2		0.3507	0.1948	0.4545						
S_{m2}^{44}	2	0.5714				0.4286					
	5/2		0.3571		0.6429						
	3	0.2597				0.0390				0.7013	
	7/2		0.3117		0.0065		0.6818				
S_{m3}^{44}	2				1						
	5/2				1						
	3				0.1818						0.8182
	7/2				0.3636			0.6364			
S_{m4}^{44}	2	1									
	5/2			1							
	3	0.4545								0.5455	
	7/2			0.6818				0.3182			
S_{m1}^{24}	2		−0.3499		0.3499						
	5/2		−0.4518	0.4518							
	3		−0.0963		−0.3853		0.4816				
	7/2		−0.2043	−0.2724	0.4767						
S_{m2}^{24}	2	−0.4949				0.4949					
	5/2		−0.4792		0.4792						
	3	−0.2724				−0.1362				0.4086	
	7/2		−0.3853		0.0482		0.3371				

TABLE 3 (continued)

	I \ m	0	1	2	3	4	5	6	7	8	9
S^{12}_{m1}	1		1								
	$\frac{3}{2}$		0.7746								
	2		0.2928		0.5855						
	$\frac{5}{2}$		0.3614	0.4517							
	3		0.1429		0.3571		0.3571				
	$\frac{7}{2}$		0.2061	0.3299	0.2887						
S^{14}_{m1}	2		−0.7171		0.2390						
	$\frac{5}{2}$		−0.5714	0.2857							
	3		−0.2889		−0.3853		0.2897				
	$\frac{7}{2}$		−0.3539	−0.2359	0.2752						
S^{23}_{m1}	$\frac{3}{2}$		0.6324								
	2		−0.2390		0.7171						
	$\frac{5}{2}$		−0.1380	0.6901							
	3		−0.1260				0.6300				
	$\frac{7}{2}$		−0.1343	0.1074	0.5641						
S^{23}_{m2}	$\frac{3}{2}$		1								
	2					0.7559					
	$\frac{5}{2}$		0.3273		0.5456						
	3					0.3984				0.3984	
	$\frac{7}{2}$		0.1699		0.3822		0.2973				
S^{34}_{m1}	2		0.5855		0.2928						
	$\frac{5}{2}$		0.2182	0.4364							
	3		0.2548				0.5096				
	$\frac{7}{2}$		0.2305	−0.0768	0.5378						
S^{34}_{m2}	2					0.6546					
	$\frac{5}{2}$		−0.2440		0.7319						
	3					−0.1140				0.6838	
	$\frac{7}{2}$		−0.1374		0.0515		0.6013				
S^{34}_{m3}	2				1						
	$\frac{5}{2}$				0.7454						
	3				0.3482						0.5222
	$\frac{7}{2}$				0.4199			0.3674			

Finally, it should be noted that $H(mx)$, corresponding to the polarization insensitive part of the correlation function, always involves even powers of x; $h(mx)$, the polarization sensitive part, involves odd powers and therefore the sign of x.

4. Mixed Transitions

If the first of the two radiations is of mixed multipole character (L_1 and L'_1), the result of (16) still applies providing that one uses

$$A_{k_1 k_2} = [F_{k_1}(L_1 L_1 I_1 I) + \delta^2 F_{k_1}(L'_1 L'_1 I_1 I) + 2\delta F_{k_1}(L_1 L'_1 I_1 I)] \times F_{k_2}(L_2 L_2 I_2 I) \quad (15')$$

in place of (15); δ^2 is the relative intensity of radiation L_1 with respect to radiation L'_1. A similar relation holds for the case of mixed γ_2. For any arbitrary mixture of radiation multipolarities, (14) can always be used to yield the correct result.

5. Application to Beta Decay

The polarization of the emitted electron in the β-decay process is now an experimentally verified fact. This polarization is given by

$$P^{\pm} = \pm \frac{cp}{E} = \pm \frac{v}{c} \quad (35)$$

where the $(\pm)$ refers to positon or negaton decay, and v, p and E are the electron's velocity, momentum and energy. Thus, in the extreme relativistic case, the measurement of the direction of the emitted electron is sufficient to also specify its polarization. Because of this, no polarization measuring devices are required to perform an experiment analogous to those previously discussed. In this case, the direction-direction correlation actually becomes

TABLE 4

Particle parameters, $e_k(L, L')$, for β—γ correlations

L	L'	e_k
0	0	$e_0 = \frac{1}{2}\lvert C_V\rvert^2 \cdot \lvert M_F\rvert^2$
1	1	$e_0 = \frac{1}{2}\lvert C_A\rvert^2 \cdot \lvert M_{GT}\rvert^2$ $e_1 = \frac{1}{3}\lvert C_A\rvert^2 \cdot \lvert M_{GT}\rvert^2 p/E$
0	1	$e_0 = 0$ $e_1 = \frac{1}{3}\mathrm{Re}\{C_V C_A^*\} M_F \cdot M_{GT}\, p/E$

In the above C' (the parity non-conserving part of the Hamiltonian) has been set equal to C, which is consistent with the concept of time reversal invariance.

a polarization correlation. The β—γ correlation function can be obtained from the corresponding γ_c—γ function simply by multiplying each $A_{k_1 k_2}$ by the appropriate particle parameter $e_{k_1}(L_1 L'_1)$ [5]; $\rho_1 = 1$ corresponds to positon decay, $\rho_1 = -1$ to negaton decay. These parameters for the case of allowed β-decay appear in table 4. Particle parameters for forbidden transitions have also been published [3]). As may be seen from table 4, only e_0 exists for pure Fermi transitions. Thus, Fermi transitions lead to complete isotropy even in this perturbed case. When G-T transitions are considered, it is seen that e_1 also exists so that, at most, only the two values 0 and 1 of k_1 need ever be considered. Thus, (25) becomes

$$W(\theta, \varphi, \tfrac{1}{2}\pi) = b_0 + \rho_1[b_3 \sin\theta \cos\theta \sin\varphi + b_7 \sin\theta \cos^3\theta \sin^3\varphi] \quad (36)$$

where the b's are given in table 2 and each $A_{k_1 k_2}$ entering into their calculation is multiplied by the appropriate e_{k_1}.

The author wishes to express his gratitude to Professor Hans Frauenfelder for originally bringing this problem to his attention. He also wishes to thank Professors J. D. Jackson and H. J. Lipkin for many illuminating discussions and especially for the latter's suggestion of considering β-decay in this connection.

References

1) Alder, Albers-Schoenberg, Heer and Novey, Helv. Phys. Acta **26** (1953) 761
2) R. Omnès, J. Phys. et Radium **17** (1957) 528
3) L. C. Biedenharn and M. E. Rose, Revs. Mod. Phys. **25** (1953) 729
4) E. G. Beltrametti, Nuovo Cimento **8** (1958) 445
5) Alder, Stech and Winther, Phys. Rev. **107** (1957) 728
6) M. Ferentz and N. Rosenzweig, AEC Report ANL-5324
7) H. G. Dehmelt, Am. J. Phys. **22** (1954) 110

2.A.1: 2.D

Nuclear Physics **11** (1959) 400—410; © *North-Holland Publishing Co., Amsterdam*

Not to be reproduced by photoprint or microfilm without written permission from the publisher

RADIATIVE DEUTERON CAPTURE $Zn^{64}(d, \gamma)Ga^{66}$

J. H. CARVER † and G. A. JONES

Atomic Energy Research Establishment, Harwell, Didcot, Berks.

Received 16 February 1959

Abstract: Induced radioactivity methods have been used to observe radiative deuteron capture in Zn^{64} for deuteron energies of 3.5—4.5 MeV. Observations were made with NaI(Tl) gamma-ray spectrometers used singly and in coincidence and the 9.5 hour Ga^{66} activity was identified in the presence of an intense 245 day Zn^{65} activity resulting from the Zn^{64} (d, p) and (d, n) reactions. At a deuteron energy of 4.5 MeV, $\sigma(d, \gamma) = 80 \pm 12$ μb and $\sigma(d, n+d, p) = 0.16 \pm 0.02$ b. The cross section ratio, $\sigma(d, \gamma)/\sigma(d, n+d, p) = 0.50 \pm 0.08 \times 10^{-3}$, is constant for 3.5—4.5 MeV deuterons. The magnitudes of the cross sections and their variation with energy are consistent with an interpreation in terms of the statistical decay of a compound nucleus, the radiative probability being calculated from photodisintegration data.

1. Introduction

There is only one well-known example of radiative deuteron capture, namely the reaction $He^3(d, \gamma)$ observed by Blair, Hintz and Van Patter [1]. This is somewhat surprising since the inverse reaction of photodisintegration with deuteron emission is well established [2, 3, 4, 5]. Several workers have looked for radiative deuteron capture in other nuclei. Sinclair [6] has set upper limits of 0.05 mb, 0.1 mb and 0.5 mb for the $H^2(d, \gamma)$, $He^4(d, \gamma)$ and $O^{16}(d, \gamma)$ reactions at deuteron energies of ≈ 1 MeV; Allan and Sarma [7] have set upper limits of 1.8 μb, 1 μb and 0.4 μb for the $Be^9(d, \gamma)$, $C^{12}(d, \gamma)$ and $Ne^{22}(d, \gamma)$ reactions at deuteron energies of 0.9—1.5 MeV.

Theoretically one expects radiative capture to make only small contribution to the total deuteron cross section as can be seen by considering two extreme models for the process. If, in the first case, it is assumed that a compound nucleus is formed, the radiative capture cross section can be calculated by means of the statistical theory. Since typical positive Q-values for (d, γ) reactions range from 10 to 15 MeV, there will, on this model, be strong competition from (d, n), (d, p) and (d, α) reactions, which will account for most of the total cross section. The second case, that of a direct radiative interaction without the formation of a compound nucleus, is forbidden for electric dipole emission from a nucleus with $N = Z$ since the nuclear charge-to-mass

† On leave from Research School of Physical Sciences, Australian National University, Canberra.

ratio is the same as that of the deuteron. This prohibition of electric dipole emission in direct interactions will be relaxed if the nucleus has sufficient neutron excess or if there is appreciable electric polarization of the incident deuteron. It follows that direct radiative capture is expected to be less important for deuteron capture than for proton or neutron capture.

The method of induced radioactivity was used in the present investigation since it leads to a more positive identification of the reaction and is capable of greater sensitivity than the detection of the capture gamma-rays. It is important when using this method to select a target nucleide (N, Z) for which the isotope $(N+1, Z)$ is unstable, since even with isotopically separated targets any small impurity of the $(N+1, Z)$ isotope will give a prolific (d, n) yield identical with the desired (d, γ) product. For a similar reason it is desirable, though not so essential, that the neighbouring $(Z+1)$-element should have no stable isotope of $(Z+1, N)$ composition, as otherwise elemental impurities in the target material will lead to confusion through the $(Z+1, N)$ (d, p) reaction. Both these criteria are satisfied by Zn^{64} since Zn^{65} and Ga^{65} are unstable.

2. Experimental Method and Results

The targets, which consisted of isotopically separated Zn^{64} enriched to 96.6 %, were 7 mg/cm^2 thick and were electroplated onto 0.010″ gold backing. These targets were bombarded with deuteron beams of ≈ 4 μA from the Harwell Van de Graaff and the activities induced were observed with NaI(Tl) scintillation spectrometers. A number of separate bombardments were made varying in duration from $\frac{1}{2}$ to 7 hours. Bombardments were made at deuteron energies of 3.5, 4 and 4.5 MeV.

Ga^{66} decays by K-capture and positon emission with a half-life of 9.4 hours; the gamma-ray spectrum is complex and extends to an energy of 4.83 MeV [8]). The two strongest gamma-rays are of 1.04 and 2.75 MeV and are emitted in coincidence. This activity must be observed in the presence of an intense yield of positons and 1.1 MeV radiation from 245 day Zn^{65} produced directly by the Zn^{64}(d, p) reaction and indirectly as the daughter of 15 and 8 min Ga^{65} produced by the Zn^{64}(d, n) reaction. A further complication arises from sodium impurity in the target material which produces 15 hour Na^{24} by means of the Na^{23}(d, p)Na^{24} reaction. Na^{24} decays by negaton emission and produces 1.38 and 2.75 MeV gamma-rays in coincidence.

Other, short-lived, activities from, for example, light element impurities in the target and from 15 and 8 min Ga^{65} were allowed to decay before commencing to count the activity.

The complicated gamma-ray spectrum shown in fig. 1 was observed with a NaI spectrometer about 20 hours after bombarding a separated Zn^{64}

target with 4.5 MeV deuterons. Observations made with a number of different gain and bias settings have been combined in fig. 1. The peak at 511 keV arises mainly from 245 day Zn^{65} which obscures the comparatively weak 9.4 hour Ga^{66} component. The strongest gamma-ray line in the Ga^{66} spectrum is that at 1.04 MeV but this is also obscured in the observed spectrum by the intense 1.11 MeV Zn^{65} gamma-ray. Na^{24} produces the small peak observed at 1.38 MeV and also contributes to the peak at 2.75 MeV. It was not possible to resolve the 2.75 MeV peak accurately into 15 hour and 9.4 hour components corresponding to Na^{24} and Ga^{66} activities.

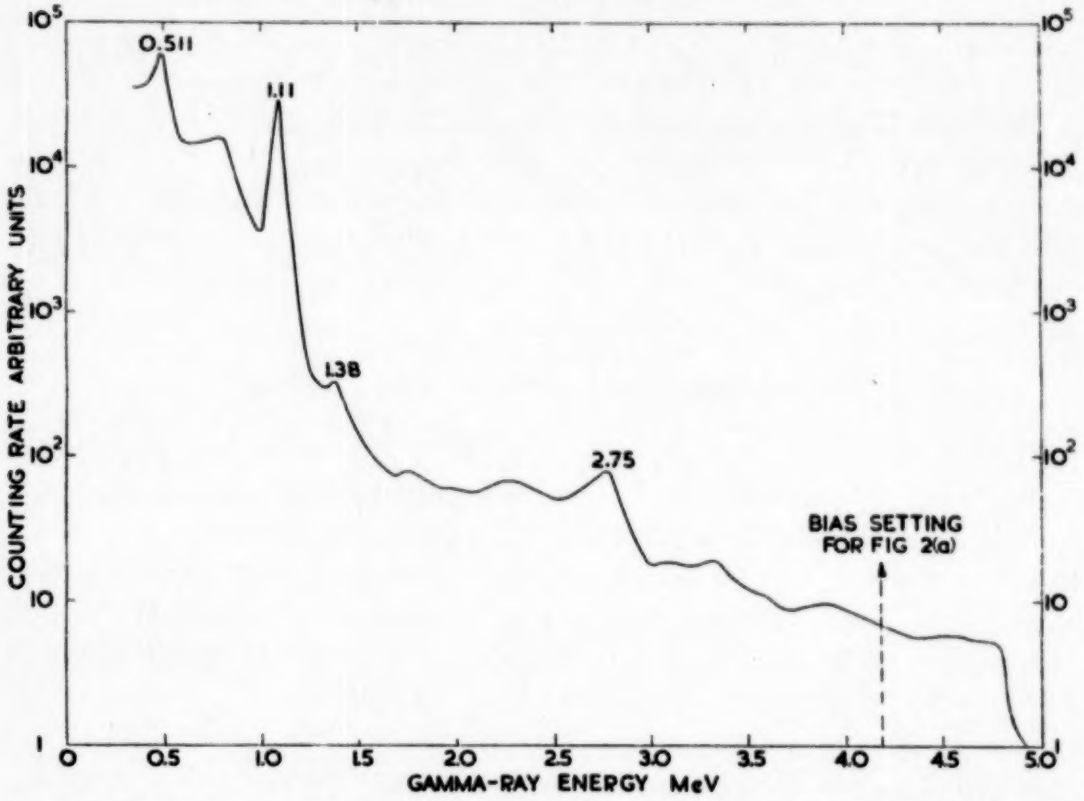

Fig. 1. Gamma-ray spectrum observed with a single NaI(Tl) crystal approximately 20 hours after deuteron bombardment of Zn^{64}. The spectrum has been composed from several observations with different gain and bias settings. The radiation is produced by Zn^{65}, Ga^{66} and Na^{24} impurity.

Apart from the Ga^{66} gamma-rays the highest energy line to be expected in the spectrum of fig. 1 is a 4.13 MeV and arises from summation of the 1.38 and 2.75 MeV Na^{24} gamma-rays. Thus, the higher energy components of fig. 1 may be identified with the known 4.3 and 4.8 MeV lines of Ga^{66} [8]). The decay of the high-energy component, $E_\gamma > 4.2$ MeV, is shown in fig. 2(a) and the observed half-life of (9.5 ± 0.1) confirms the identification of this radiation with Ga^{66}.

While observation of the high energy component of the singles spectrum provides evidence for the occurrence of the reaction $Zn^{64}(d, \gamma)Ga^{66}$, a more

clear-cut interpretation, and a more accurate estimate of the reaction cross section, can be obtained by coincidence techniques. Conventional electronic equipment was used to observe the gamma-ray spectrum from a $1\frac{1}{2}''$ dia. $\times 1''$ long NaI(Tl) crystal (counter A) in coincidence with the 2.75 MeV gamma-ray line observed in a $4\frac{1}{2}''$ dia. $\times 3''$ long NaI(Tl) crystal (counter

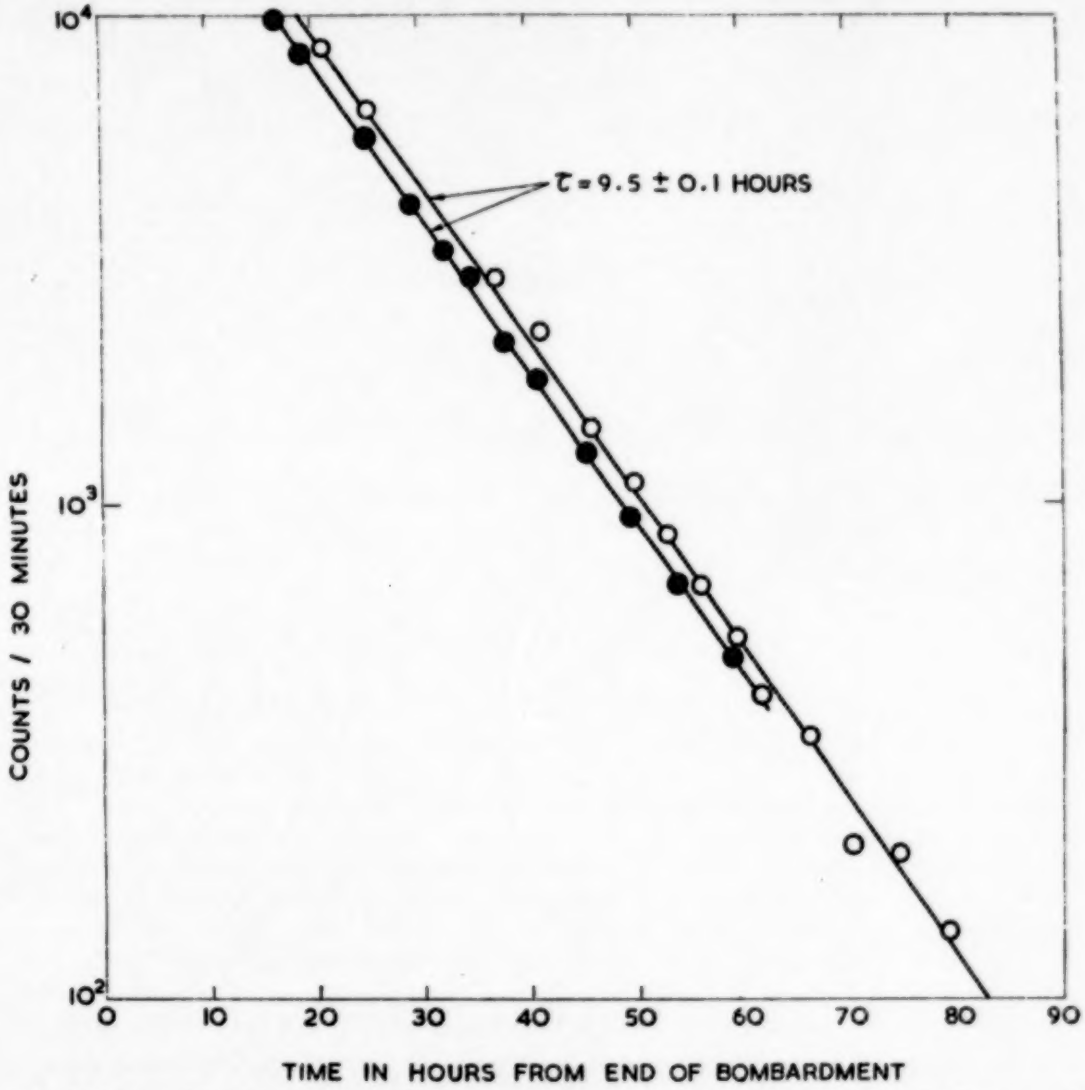

Fig. 2. Decay of Ga^{66} activity. (a) Decay of the high energy gamma-rays (> 4.2 MeV) measured with a single NaI(Tl) counter (solid circles, ●). (b) Decay of the 1.04—2.75 MeV gamma ray cascade measured in coincidence (open circles, ○).

B). This arrangement was designed to select the strong 1.04—2.75 MeV gamma-ray cascade of Ga^{66} from the observed complex singles spectrum of fig. 1. It very effectively discriminates against the 1.11 MeV gamma-ray of 245 day Zn^{65} which predominates in the singles spectrum at this energy. This is shown by comparing the observed true coincidence spectrum (fig. 3a full line) with the random coincidence spectrum (fig. 3a dotted line) obtained with a fast input of random pulses replacing the 2.75 MeV pulses from count-

er B. The displacement between the 1.04 MeV Ga^{66} and 1.11 MeV Zn^{65} gamma-rays is clearly seen.

The true coincidence spectrum (fig. 3a full curve) shows the 1.04 MeV gamma-ray line in coincidence with the 2.75 MeV gamma rays of Ga^{66} and, in addition, the 1.38 MeV line arising from the 1.38—2.75 MeV coincident

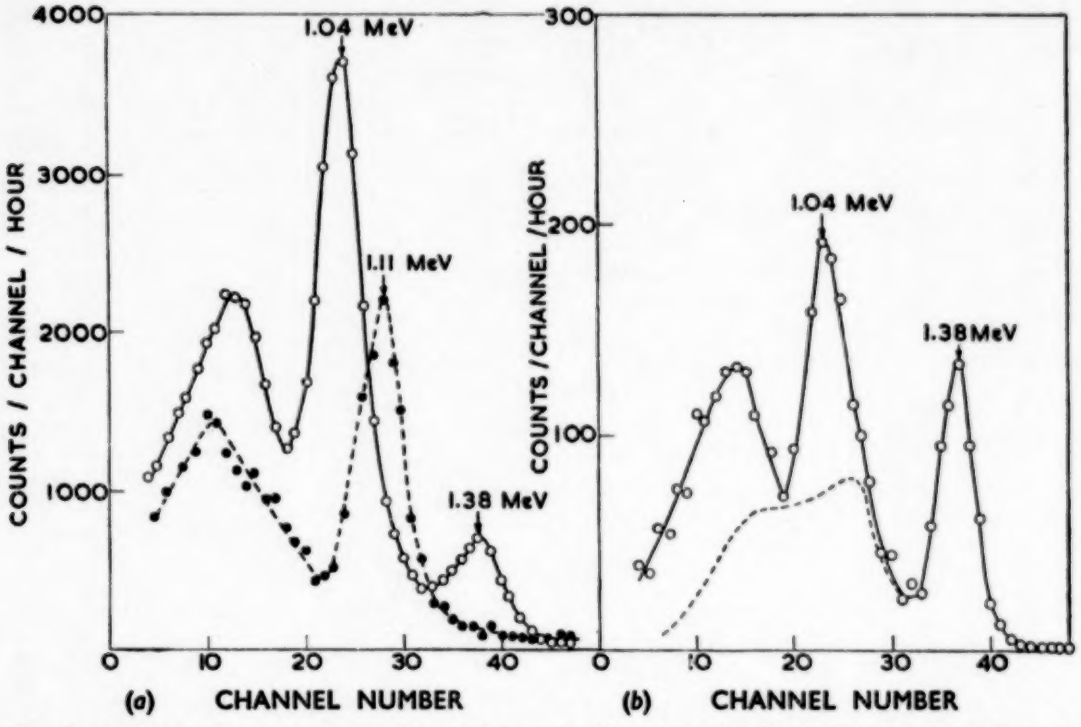

Fig. 3. Ga^{66} gamma-ray spectra observed in coincidence with 2.75 MeV radiation. There is a bias of 400 keV and the spectra below channel 14 are distorted by the gate giving the spurious peaks in the Compton distribution. (a) Coincidence spectrum observed 21 hours after deuteron bombardment of Zn^{64} (full line). The peak at 1.04 MeV is produced by Ga^{66}, that at 1.38 MeV by Na^{24} impurity. The random coincidence spectrum (dotted line, arbitrary count rate) is dominated by the 1.11 MeV gamma-ray of Zn^{65}. (b) Coincidence spectrum 70 hours after bombardment showing increased ratio of Na^{24} to Ga^{66}. The dotted line indicates the shape of a pure Na^{24} spectrum normalized to the 1.38 MeV peak.

gamma-rays of 15 hour Na^{24}. Comparison of the spectra of figs. 3(a) and 3(b), which were separated by 49 hours indicates the different half-lives of the 1.04 and 1.38 MeV lines in the coincidence spectra. The measured decay of the 1.04 MeV line is shown in fig. 2b; the half-life of 9.5 ± 0.1 is in good agreement with other determinations of the Ga^{66} half-life [10]). The 1.38 MeV line was found to decay with the 15 hour half-life of Na^{24}.

The absolute efficiencies of the apparatus for detecting 2.75 and 1.38 MeV gamma-rays were determined by measuring the coincidence counting rate and the single counting rates in both arms with a pure Na^{24} source placed in the same geometry as the Ga^{66} sample. The relative efficiency of the $1\frac{1}{2}'' \times 1''$ NaI(Tl) crystal for 1.38 and 1.04 MeV gamma-rays was obtained from the compilation of Mott and Sutton [9]).

With this estimate of the counting efficiencies the cross section for the $Zn^{64}(d, \gamma)Ga^{66}$ reaction was determined from the counting rate of the 1.04 MeV gamma-ray in coincidence with the 2.75 MeV gamma-ray. The Ga^{66} decay scheme proposed by Mann *et al.* [8]) was used. The capture cross sections corrected for effective target thickness are shown in fig. 4 for deuteron energies of 3.5, 4.0 and 4.5 MeV.

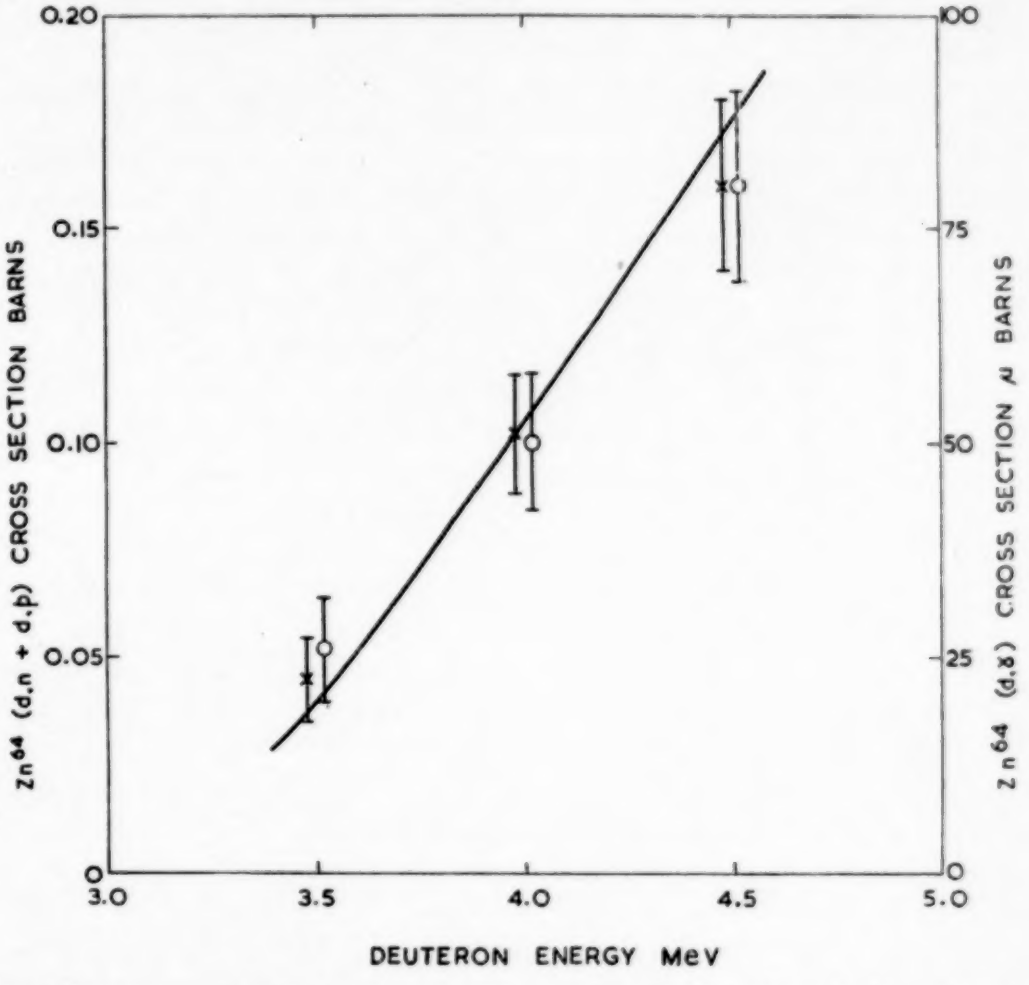

Fig. 4. The measured Zn^{64} (d, γ) cross section (circles ○) and (d, n+d, p) cross section (crosses ×) both corrected for target thickness and, for clarity, slightly separated in energy. The errors arise mainly from the estimation of the counting efficiencies. The ratio of the two cross section scales equals the calculated σ(d, γ)/σ(d, n+d, p) ratio at 4.5 MeV for $T = 7$ MeV and the curve, drawn to the σ(d, n+d, p) scale, is the calculated total cross section for compound nucleus formation (see text).

The Zn^{64}(d, n)+(d, p) cross section was determined from the strength of the 245 day Zn^{65} activity using the decay scheme given in ref. [10]). This activity was measured some three weeks after the bombardment when it was the only activity remaining, and the 15 min and 8 min Ga^{65} produced in the Zn^{64}(d, n) reaction had decayed to Zn^{65}. The results of these measurements are also shown in fig. 4.

At a deuteron energy of 4.5 MeV,

$$\sigma(\mathrm{d},\gamma) = 80\pm12\ \mu\mathrm{b},$$
$$\sigma(\mathrm{d},\mathrm{n+d},\mathrm{p}) = 0.16\pm0.02\ \mathrm{b}$$
$$\sigma(\mathrm{d},\gamma)/\sigma(\mathrm{d},\mathrm{n+d},\mathrm{p}) = (0.50\pm0.08)\times10^{-3}.$$

This ratio is nearly constant over the measured range of deuteron energies (3.5—4.5 MeV).

3. Calculation of the Radiation Width from Statistical Theory

The measured cross sections can be compared with the predictions of the compound nucleus statistical theory of nuclear reactions according to which the cross sections are related to the corresponding widths by

$$\sigma(\mathrm{d},\mathrm{x})/\sigma(\mathrm{total}) = \Gamma_x/\Gamma(\mathrm{total}). \tag{1}$$

We first calculate the radiation width Γ, considering only electric dipole transitions. From the principle of detailed balance [11, 12]), the width $\Gamma(\varepsilon)$ for the electric dipole emission of a gamma-ray of energy ε is given by

$$\Gamma(\varepsilon)\omega_J(E) = \tfrac{1}{3}\frac{\varepsilon^2}{\pi^2\hbar^2c^2}\sigma_\gamma(\varepsilon), \tag{2}$$

where E is the excitation energy of the capturing state, $\omega_J(E)$ is the density at E of states of the same spin J as the capturing state and $\sigma_\gamma(\varepsilon)$ is the cross section for the inverse process of gamma-ray excitation. In the present case the transitions are, mainly, between two excited states but we shall assume that σ_γ has the same giant resonance shape as the cross section for photodisintegration of nuclei in their ground states. Following Brink [13]) we use the giant resonance shape proposed by Steinwedel and Jensen [14]), and write

$$\sigma_\gamma(\varepsilon) = 4\pi\frac{NZ}{A}\frac{e^2\hbar}{Mc}(1+0.8x)\frac{\Gamma_g\varepsilon^2}{(\varepsilon^2-E_\mathrm{m}^2)^2+(\Gamma_g\varepsilon)^2}, \tag{3}$$

where x is the fraction of the neutron-proton force which has an exchange character, E_m is the peak energy, Γ_g the width of the photonuclear giant resonance, and the other symbols have their usual significance. Eq. (3) satisfies the dipole sum rule, since

$$\int_0^\infty \sigma_\gamma\,\mathrm{d}\varepsilon = 2\pi^2\frac{NZ}{A}\frac{e^2\hbar}{Mc}(1+0.8x).$$

With suitable choice of the parameters E_m and Γ_g eq. (3) can be made to fit the observed photonuclear cross sections in the region of the giant resonance. For the present calculations it is important to know the behaviour of σ_γ at lower energies (< 10 MeV), where experimental evidence from photodisintegration studies is scanty. However, Brink (1955) has shown that the

use of eq. (3), suitably fitted to the observed giant resonance, accounts quantitatively for the neutron capture radiative widths [15]), indicating that the expression can still be used at these lower energies.

The radiative capture cross section, as measured by induced radioactivity, can be estimated by integrating eq. (2) over all energetically possible gamma-ray transitions, omitting those transitions in which the primary emission of a (low) energy gamma-ray is followed by particle emission. Let $R = E-\varepsilon$ denote the excitation energy of the residual nucleus and T the effective "threshold" for secondary particle emission following the primary gamma-ray, such that for $R > T$ particle emission dominates further gamma-ray emission. Strictly speaking, T is not a well-defined energy, but it suffices for the present purpose to neglect the small intermediate region in which the particle and radiation widths are comparable. T is $\approx$ 6—7 MeV in the present case (see below), so that only transitions from the capturing state, at $\approx$ 15 MeV excitation, to states within 6—7 MeV of the ground state contribute to the observed cross section. Since these comparatively low-lying states may retain some of the character of the ground state, the use of the ground state photodisintegration data to determine σ_γ is not such a poor assumption as it would be if all primary gamma-ray transitions contributed to the cross section.

It follows that the total gamma-ray width from the capturing state (E, J) as measured by induced radioactivity is given by

$$\Gamma_\gamma = \int_0^T \Gamma(\varepsilon)\omega_K(R)\mathrm{d}R, \tag{4}$$

where $\omega_K(R)$ is the level density at excitation R of those states which combine with the capturing state by electric dipole transitions (i.e. $K = J-1, J, J+1$). If we assume that $\omega_J = (2J+1)\omega_0$, where ω_0 is the density of states of spin zero, $\omega_K = 3(2J+1)\omega_0$ and from eqs. (2), (3) and (4)

$$\Gamma_\gamma = 4\frac{NZ}{A}\frac{e^2}{\hbar c}\frac{1+0.8x}{Mc^2}\frac{\Gamma_g}{\omega_0(E)}\int_0^T \frac{\omega_0(R)\varepsilon^4\mathrm{d}R}{(\varepsilon^2-E_m^2)^2+(\Gamma_g\varepsilon)^2}. \tag{5}$$

For the particular case of Ga^{66} we take $\Gamma_g = 5.5$ MeV, $E_m = 19$ MeV and obtain

$$\Gamma_\gamma = \frac{1.25\times 10^3}{\omega_0(E)}\int_0^T \frac{\omega_0(R)y^4}{(y^2-1)^2+0.084y^2}\mathrm{d}R \ \text{(eV)}, \tag{6}$$

where R is in MeV and $y = \varepsilon/E_m$.

4. Calculation of the Particle Widths

The widths Γ_p and Γ_n for proton and neutron emission are given by

$$\Gamma_p\omega(E) = \frac{2M}{\hbar^2\pi^2}\int_0^P \varepsilon\sigma_p(\varepsilon)\omega_R(P-\varepsilon)\mathrm{d}\varepsilon, \tag{7}$$

$$\Gamma_n \omega(E) = \frac{2M}{\hbar^2 \pi^2} \int_0^N \varepsilon \sigma_n(\varepsilon) \omega_{R'}(N-\varepsilon) d\varepsilon, \quad (8)$$

where ε is the energy of the emitted particle; P and N are the maximum energies with which protons and neutrons may be emited; ω is the level density of the compound nucleus; ω_R and $\omega_{R'}$ are the level densities of the residual nuclei. The cross sections σ_p and σ_n for the inverse reactions of proton and neutron capture into the compound nucleus have been obtained from Blatt and Weisskopf [16]) for a nuclear radius $R = 1.5A^{\frac{1}{3}} \times 10^{-13}$ cm.

These expressions neglect stripping so that the corresponding (d, p) and (d, n) cross sections may be underestimated by 10—15 %, an error which is not serious in a calculation of this sort.

5. Comparison of the Statistical Calculations with Experiment

The partial widths have been calculated from eqs. (6), (7) and (8) using the semi-empirical results of Cameron [17]), to determine the level densities of Ga^{66}, Zn^{65} and Ga^{65}. The Q-values for the reactions were taken from the compilation of ref. [10]), the values used being Zn^{64}+d: 10.7 MeV, Ga^{65}+n: 8.9 MeV and Zn^{65}+p: 5.0 MeV. Thus, proton emission determines the maximum residual excitation energy T above which competition from particle emission prevents the development of a gamma-ray cascade. It follows that T is greater than 5 MeV and it is estimated that $T = 6$—7 MeV.

For a deuteron energy of 4.5 MeV, the maximum used in these experiments, the calculated ratio of the Zn^{64}(d, γ) and (d, n)+(d, p) cross sections is

$$\sigma(d, \gamma)/\sigma(d, n+d, p) = 0.40 \times 10^{-3} \quad \text{for } T = 6 \text{ MeV}$$
$$= 0.49 \times 10^{-3} \quad \text{for } T = 7 \text{ MeV}.$$

The measured ratio is $0.50 \pm 0.08 \times 10^{-3}$.

The calculations predict an increase of 15 % in this ratio for 3.5 MeV deuterons but the experimental data of fig. 4 are not sufficiently accurate to establish such an effect and are consistent with a constant ratio over the measured energy range.

Since other competing reactions are likely to have small cross sections it is fairly safe to assume that the (d, n)+(d, p) cross section is equal to the total cross section. The total cross section has been calculated using the penetrability tables of Sharp, Gove and Paul [18]) assuming a nuclear radius of $(1.5A^{\frac{1}{3}}+1.0) \times 10^{-13}$ cm. The result for 4.5 MeV deuterons is

$$\sigma(\text{total}) = 0.175 \text{ b},$$

which may be compared with the experimental value for 4.5 MeV deuterons,

$$\sigma(d, n+d, p) = 0.16 \pm 0.02 \text{ b}.$$

The calculated variation of the total cross section with deuteron energy is shown in fig. 4 and is seen to compare well with the measured variation of the (d, n)+(d, p) cross section.

From the calculated (d, γ) to (d, n)+(d, p) ratio and the calculated total cross section, assumed equal to the (d, n)+(d, p) cross section, the calculated (d, γ) cross section for 4.5 MeV deuterons is 86 μb for $T = 7$ MeV. This is to be compared with an experimental value of 80 ± 12 μb.

6. Conclusions

Radiative deuteron capture has been observed by measurements of the induced radioactivity in the reaction $Zn^{64}(d, \gamma)Ga^{66}$ for deuteron energies from 3.5 to 4.5 MeV.

These observations can be interpreted in terms of the statistical decay of a compound nucleus. The cross section for the inverse reaction of gamma-ray excitation between excited states has been assumed to have the same magnitude and the same giant resonance shape as that deduced from photodisintegration studies of nuclei in their ground states. Semi-empirical formulae [17]) have been used to estimate the level densities, and in order to calculate the cross section as measured by induced radioactivity only those radiative transitions are included which are not followed by particle emission. The calculation is subject to uncertainties on all these grounds but, with these limitations, this simple theory accounts for the absolute magnitude of the cross section, its variation with energy and the ratio of the radiative capture cross section to the total cross section.

The present data are, however, severely limited both because they are restricted to one nucleide and because the spectrum of the capture gamma-rays is not known. Other mechanisms may contribute to the process, for example direct electric dipole capture which would imply a strong dependence of the cross section upon the $(N-Z)$ of the capturing nucleide. Further experiments to extend these observations are in progress.

We are indebted to Dr. A. M. Lane for discussion of several points arising in the analysis of these experiments. One of us (J. H. Carver) wishes to thank Dr. E. Bretscher and Dr. E. B. Paul for the facilities made available to him at Harwell.

References

1) J. M. Blair, N. M. Hintz and D. M. Van Patter, Phys. Rev. **96** (1954) 1023
2) P. R. Byerly and W. E. Stephens, Phys. Rev. **83** (1951) 54
3) L. Katz and A. S. Penfold, Phys. Rev. **81** (1951) 815; ibid **83** (1951) 169
4) L. S. Ring, Phys. Rev. **99** (1955) 137

5) E. W. Titterton, Prog. in Nuclear Physics (O. Frisch ed.) **4** (1955) 1
6) R. M. Sinclair, Phys. Rev. **93** (1954) 1082
7) H. R. Allan and N. Sarma, Proc. Phys. Soc. A **68** (1955) 535
8) L. G. Mann, W. E. Meyerhof and H. I. West, Phys. Rev. **92** (1953) 1481
9) W. E. Mott and R. B. Sutton, Encyclopedia of Physics (S. Flügge, ed.) **45** (1958) 86
10) K. Way, R. W. King, C. L. McGinnis and R. van Lieshout, Nuclear Level Schemes $A = 40$—92, USAEC report No. TID-5300 (1955)
11) V. F. Weisskopf, Phys. Rev. **52** (1937) 295
12) V. F. Weisskopf and D. H. Ewing, Phys. Rev. **57** (1940) 472
13) D. M. Brink, Thesis (1955) Oxford; quoted by Kinsey [15])
14) H. Steinwedel and J. H. D. Jensen, Z. f. Naturforsch **5a** (1950) 413
15) B. B. Kinsey, Encyclopedia of Physics (S. Flügge, ed.) **40** (1957) 202
16) J. B. Blatt and V. Weisskopf, Theoretical Nuclear Physics (John Wiley, New York, 1953)
17) A. G. W. Cameron, Can. J. Phys. **36** (1958) 1040
18) W. T. Sharp, H. E. Gove and E. B. Paul, Chalk River Report No. TPI-70 (1953)

1.E.1:
3.A

Nuclear Physics **11** (1959) 411—418; © *North-Holland Publishing Co., Amsterdam*
Not to be reproduced by photoprint or microfilm without written permission from the publisher

THE LEVEL STRUCTURE OF Dy^{160}

R. G. ARNS, R. E. SUND and M. L. WIEDENBECK

The Harrison M. Randall Laboratory of Physics, University of Michigan, Ann Arbor, Mich. †

Received 24 January 1959

Abstract: Gamma rays in Dy^{160} following beta decay of the 72 day Tb^{160} have been studied using coincidence and angular correlation methods. The relative intensity and coincidence measurements confirm the principal features of the decay scheme proposed by Nathan [1]). Angular correlation measurements were made on six cascades. The spin and parity of the 0.087 MeV, 0.964 MeV, and 1.262 MeV levels were found to be 2+, 2+, and 2− respectively. The measurements favour spins of 4 and 3 for the 0.283 MeV and 1.359 MeV levels. These assignments are in agreement with previous assignments by Ofer [2]). The multipolarities of the main gamma transitions are given.

1. Introduction

The level structure of Dy^{160} following beta decay of the 72 day Tb^{160} has been the subject of several investigations [1–8]). The more recent of these studies have been in agreement on several features of the level structure. However, conflicts still exist in regard to the relative intensities and multipolarities of certain strong gamma transitions. The angular correlation of the 1.076 MeV—0.196 MeV cascade reported by Ofer [2]) was considerably different from that observed by Nathan [1]). In addition, Ofer found it necessary to postulate an attenuation [2, 9]) in interpreting three of his angular correlation measurements (those involving the 0.087 MeV level). Under the circumstances an attenuation is difficult to understand and further study of this aspect would seem to be of value. Thus the present coincidence and angular correlation measurements were undertaken in the hope of resolving some of the incompatible aspects of previous research on this decay.

2. Experimental Procedure

Qualitative coincidence measurements were carried out using a fast-slow coincidence circuit with multichannel recording of the "gray wedge" type (modified Beva Lab 210). The detectors were $1\frac{1}{2}'' \times 1''$ NaI(Tl) crystals mounted on RCA type 6342 phototubes.

The quantitative coincidence measurements and angular correlation

† Supported in part by the Michigan Memorial Phoenix Project and the United States Atomic Energy Commission.

measurements employed a conventional fast-slow coincidence circuit [10]) with an effective resolving time of 20 ns. The scintillation counters consisted of 2″ × 2″ NaI(Tl) crystals mounted on RCA type 6342 phototubes. Differential analyzers were used to provide energy selection. Lateral lead shielding was used to prevent counter-to-counter scattering.

Angular correlation data were taken in a double quadrant sequence. A least-squares fit of the data was made to the function

$$W'(\theta) = \alpha_0 + \alpha_2 P_2(\cos\theta) + \alpha_4 P_4(\cos\theta).$$

The resultant expansion coefficients were then normalized and corrected for finite angular resolution by a collimated beam method [11]). This yielded a correlation function of the form

$$W(\theta) = 1 + (A_2 \pm \sigma_2) P_2(\cos\theta) + (A_4 \pm \sigma_4) P_4(\cos\theta).$$

The σ_2 and σ_4 are the root-mean-square errors as defined by Rose (ref.[12]), eq. (30)).

High purity Tb_2O_3 powder was irradiated for 24 hour periods in The University of Michigan Ford Nuclear Reactor. The activated powder was then dissolved in HCl and the solution was diluted. No impurity activities were found to be present in the source material.

3. Results

3.1. COINCIDENCE MEASUREMENTS

In order to determine the position of the various gamma rays in the decay scheme, measurements were made of the gamma rays coincident with the following energy regions:

$$0.080 \text{ MeV} \leqq E \leqq 0.100 \text{ MeV}, \quad 0.160 \text{ MeV} \leqq E \leqq 0.240 \text{ MeV},$$
$$0.250 \text{ MeV} \leqq E \leqq 0.350 \text{ MeV}, \quad \text{and} \quad 0.830 \text{ MeV} \leqq E \leqq 1.00 \text{ MeV}.$$

The qualitative results are summarized in table 1.

A knowledge of the relative intensities of the 0.877, 0.960 and 0.964 MeV lines is necessary in order to interpret the angular correlation data. Hence a careful measurement was made by means of the 0.298 MeV coincidence spectrum. After correction for detector efficiency and the slight overlap of the lines, the intensity ratio 0.877: 0.964 : 0.960 was found to be $1 : 0.73 \pm 0.06 : 0.29 \pm 0.06$. This ratio was confirmed by measurements in the 0.087 MeV coincidence spectrum although the presence of interfering cascades prevented reliable quantitative results. The present results are in good agreement with the ratio $1 : 0.68 \pm 0.10 : 0.35 \pm 0.10$ found by Nathan. A ratio of $1 : 0.90 \pm 0.18 : 0.05 \pm 0.01$ has been quoted by Ofer.

TABLE 1

Gamma-gamma coincidence measurements

Energy Region (MeV)	Transitions Selected (MeV)	Coincident Transitions (MeV)	Remarks
$0.080 \leqq E \leqq 0.100$	0.087	0.196+0.215, 0.298, 0.877, 0.960, 1.175, 1.272	The photopeak at 0.960 MeV was found to be about $\frac{1}{3}$ as strong as the 0.876 MeV photopeak after subtraction of interfering cascades.
$0.160 \leqq E \leqq 0.240$	0.196, 0.215	0.087, 0.196+0.215, 0.298, 0.681, 0.764, 0.960, 1.076	The 0.681 MeV transition was found to be about $\frac{1}{2}$ as strong as the 0.764 MeV transition. No gamma ray was found at 1.047 MeV thus ruling out the presence of a strong ground state transition from the 1.047 MeV level.
$0.250 \leqq E \leqq 0.350$	0.298	0.087, 0.196, 0.877, 0.964	The 0.964 MeV transition was found to be about $\frac{2}{3}$ as strong as the 0.877 MeV transition.
$0.830 \leqq E \leqq 1.00$	0.877, 0.960, 0.964	0.087, 0.159, 0.215, 0.298	

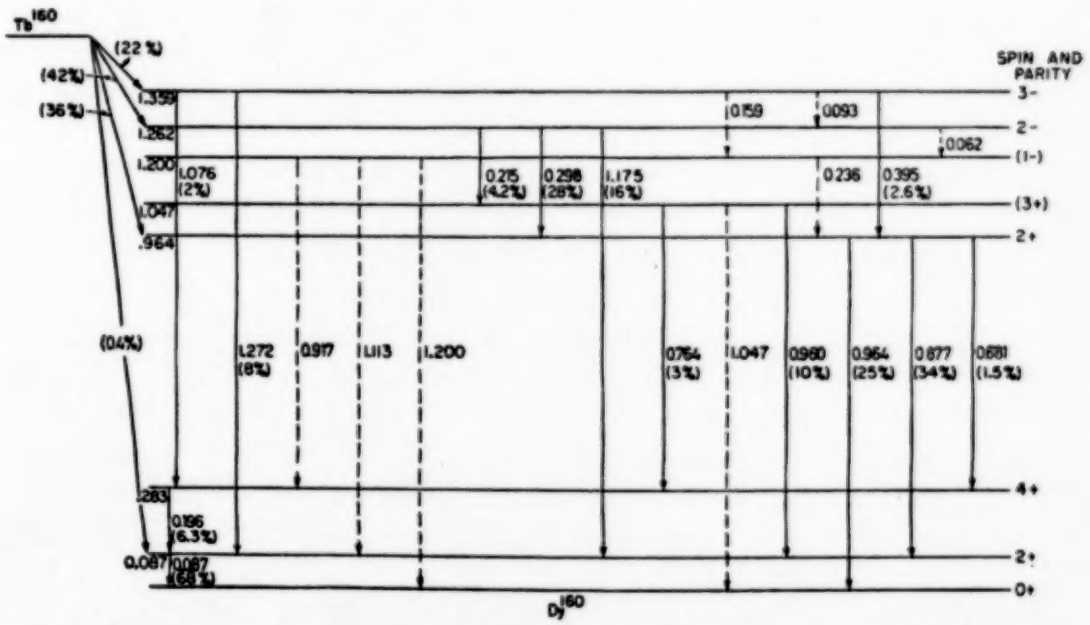

Fig. 1. Decay scheme of Tb^{160}. The beta decay data and gamma ray energies (in MeV) are according to Nathan. The relative intensities are due to Nathan except where directly measured in the present research. A number of weak transitions observed by Gregor'ev *et al.* [7]) (relative intensities unknown) have been included.

The decay scheme shown in fig. 1 is due to Nathan [1]). The relative intensities of some transitions have been modified to agree with the present measurements. An additional level at 1.200 MeV and several weak transitions have been added to the scheme on the basis of internal conversion measurements by Grigor'ev *et al.* [7]).

3.2. ANGULAR CORRELATION OF THE 0.298 MeV—0.877 MeV and 0.298 MeV—0.964 MeV CASCADES

Although the 0.877 MeV photopeak and the 0.960 MeV and 0.964 MeV combined photopeak were easily resolved by the scintillation counters, there remains a small overlap of these lines which must be considered in analyzing the angular correlation data. Two angular correlation measurements were made. In each measurement one of the differential analyzers was set to accept the upper half of the photopeak of the 0.298 MeV gamma ray. In one case the second differential analyzer was set to accept a narrow range of pulses in the upper half of the 0.964 MeV photopeak. In the other measurement, the second differential analyzer selected a narrow range of energies centered on the 0.877 MeV photopeak.

Using the measured relative intensities (without the detector efficiency correction), the 0.877 MeV and 0.964 MeV photopeaks were constructed from known shapes of single gamma rays in this energy region. The integrated contribution of both gamma rays to each correlation function was then determined. The two correlation functions were combined with special attention to the errors in the relative intensities, channel settings, and the correlation functions themselves. In this manner the 0.298 MeV—0.964 MeV angular correlation yielded expansion coefficients $A_2 = +0.259 \pm 0.042$ and $A_4 = -0.031 \pm 0.030$. These are in good agreement with the theoretical coefficients for a pure 2(D)2(Q)0 cascade, i.e., $A_2 = +0.250$, $A_4 = 0$. If the cascade is of the form 2(D, Q)2(Q)0, the limits of error will allow a maximum of 0.5 % quadrupole content in the 0.298 MeV transition. This assignment is supported by the measured K-conversion coefficients [1,7]) which indicate an E1 multipolarity for the 0.298 MeV gamma ray and E2 for the 0.964 MeV transition. It seems safe to assign a spin and parity of 2+ to the 0.964 MeV level on the basis of the conversion data. The expansion coefficients for this sequence are also consistent with a 3(D, Q)2(Q)0 cascade with a quadrupole content Q_1 for the first transition of $0.21 \leqq Q_1 \leqq 0.65$. An M2 content of this magnitude is inconsistent with experience and with the measured K-conversion coefficients. Thus a spin assignment of 3 must be ruled out for the 1.262 MeV level.

In the manner described above the corrected expansion coefficients for the 0.298 MeV—0.877 MeV sequence were found to be $A_2 = -0.126 \pm 0.026$ and $A_4 = +0.015 \pm 0.020$. The first excited state (at 0.087 MeV) can almost

certainly be characterized as 2+. If the 0.298 MeV transition is assumed to be pure dipole, the data are then consistent with a 2(D)2(D, Q)2 sequence with $0.95 \leqq Q_2 \leqq 0.99$ or $0.25 \leqq Q_2 \leqq 0.35$. The latter possibility can be ruled out by the angular correlation data from the 0.877 MeV—0.087 MeV cascade which is given below. The possibility of a small M2 admixture in the 0.298 MeV transition cannot be ruled out. The graphical analysis [13]) of the data for a doubly mixed cascade is shown in fig. 2 in which the range of

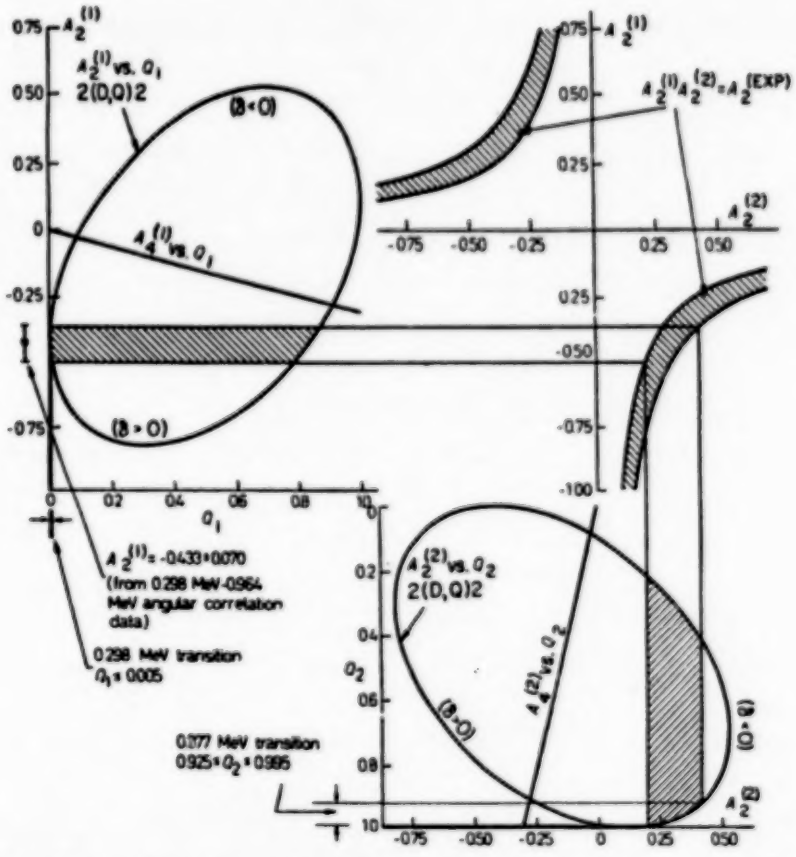

Fig. 2. Analysis of the 0.298 MeV—0.877 MeV angular correlation in terms of a 2(D, Q)2(D, $\acute{Q}$)2 sequence. The limits of quadrupole content for the first step of the cascade are known from the 0.298 MeV—0.964 MeV angular correlation.

E1+M2 mixture for the 0.298 MeV transition is assumed from the results of the 0.298 MeV—0.964 MeV correlation. Again in accord with the results of the 0.877 MeV—0.087 MeV angular correlation, the data still require a quadrupole content of $0.925 \leqq Q_2 \leqq 0.995$ for the 0.877 MeV transition.

In summary, it has been shown that the 0.298 MeV gamma ray proceeds from a 2— level at 1.262 MeV to a 2+ level at 0.964 MeV by radiation which is predominantly electric dipole ($\leqq 0.5$ % M2). The 0.964 MeV level decays by pure E2 radiation to the 0+ ground state and by 96 ± 3.5 % E2 and 4 ∓ 3.5 % M1 radiation (0.877 MeV gamma ray) to the 2+ first excited state at 0.087 MeV.

3.3. ANGULAR CORRELATION OF THE 0.877 MeV—0.087 MeV CASCADE

The 0.877 MeV gamma ray is a transition from the 2+ level at 0.964 MeV to the first excited state (spin and parity of 2+) at 0.087 MeV. Angular correlation measurements on this cascade can provide information on the multipolarity of the 0.877 MeV transition, assuming that the 0.087 MeV transition is pure E2. An accurate measurement is not possible, however, due to the presence of the Compton distributions of interfering cascades. The chief contributions to this background, i.e., the 1.272 MeV—0.087 MeV, 1.175 MeV—0.087 MeV, 0.960 MeV—0.087 MeV and 0.298 MeV—0.877 MeV cascades, comprise nearly 50 % of the real coincidences measured by accepting a small portion of the 0.087 MeV and 0.877 MeV photopeaks in alternate differential analyzers. However, the range of multipolarities possible for the 0.877 MeV gamma ray is already known from the 0.298 MeV—0.877 MeV angular correlation measurement. Thus, despite the large errors introduced by the interference subtraction, the 0.877 MeV—0.087 MeV data can be used to distinguish between the two allowable ranges. The corrected data showed the negative A_2 and large positive A_4 characteristic of a 2(D, Q)2(Q)0 sequence with a large (> 90 %) quadrupole content in the first transition.

The angular correlation of this cascade was also measured by Ofer [2]). In that measurement the experimental data were corrected for interference from the 1.272 MeV—0.087 MeV and 1.175 MeV—0.087 MeV cascades and the resultant coefficients were considerably smaller than would be expected for the large quadrupole admixture present in the 0.877 MeV transition. The present measurements indicate that it is not necessary to postulate an attenuation if all interference is considered. However, the presence of some attenuation cannot be ruled out. Ofer and Cohen [9]) were unable to achieve a completely satisfactory explanation for the large attenuation proposed. It will be seen below that the results of the 1.272 MeV—0.087 MeV and 1.175 MeV—0.087 MeV angular correlations can be more readily understood if no attenuation is present.

3.4. ANGULAR CORRELATION OF THE 1.272 MeV—0.087 MeV AND 1.175 MeV—0.087 MeV CASCADES

The 1.175 MeV and 1.272 MeV photopeaks are barely resolved in the scintillation spectrum, and an analysis similar to that outlined in section 3.2 must be applied in order to obtain the corrected angular correlation functions. The errors involved are large due to a poor knowledge of the relative intensities and are reflected in the increased error limits of the expansion coefficients. The corrected expansion coefficients for the 1.175 MeV—0.087 MeV angular correlation were found to be $A_2 = +0.133 \pm 0.041$ and $A_4 = +0.008 \pm 0.083$. Similarly the 1.272 MeV—0.087 MeV cascade yielded $A_2 = +0.148 \pm 0.065$ and $A_4 = -0.09 \pm 0.14$.

The 1.175 MeV gamma ray proceeds from the 2− level at 1.262 MeV to the first excited state. The cascade is certainly of the form 2(D, Q)2(Q)0. The expansion coefficients are then consistent with an E1+M2 mixture for the 1.175 MeV gamma ray with 97.5 ± 1.5 % E1 and 2.5 ∓ 1.5 % M2. This is in agreement with the K-conversion coefficient measurements of Nathan and of Grigor'ev *et al.* If a perturbation were present, a larger M2 content could not be ruled out. Assuming an attenuation, Ofer's data [2]) would require an M2 content of about 65 %. This would contradict the conversion measurements and also constitute a much larger M2 admixture than is normally encountered. Hence the results tend to favor the present interpretation.

The 1.272 MeV gamma ray is a transition from a level at 1.359 MeV to the first excited state. Of the spin assignments logically available for the 1.359 MeV level, the angular correlation data is consistent only with 2 or 3. As will be shown below, the 1.076 MeV—0.196 MeV angular correlation rules out a spin assignment of 2 for the 1.359 MeV level. For a 3(D, Q)2(Q)0 sequence the data require $0.04 \leqq Q_0 \leqq 0.18$ or $0.66 \leqq Q_1 \leqq 0.86$. The K-conversion coefficient measured by Nathan favors an E1 multipolarity for the 1.272 MeV transition. Hence the 1.359 MeV level is most naturally characterized as 3− and the 1.272 MeV gamma ray is an E1+M2 mixture with 89 ± 7 % E1 and 11 ∓ 7 % M2. Ofer, assuming a perturbation, found a quadrupole content of between 27 % and 50 % for the 1.272 MeV transition.

3.5. ANGULAR CORRELATION OF THE 1.076 MeV—0.196 MeV CASCADE

The 1.076 MeV gamma ray is a transition from the 1.359 MeV level to the second excited state at 0.283 MeV. The 0.196 MeV gamma ray is a transition between the second and first excited states. Both gamma rays involved are very weak. The window of one differential analyzer was set to accept the 0.205 MeV photopeak and the other was set with a narrow window in the region where the 1.076 MeV gamma ray should occur. It was found that interference was present due to the high energy tails of the 0.960 MeV and 0.964 MeV gamma rays as the 0.215 MeV—0.960 MeV and the 0.298 MeV—0.964 MeV cascades. No adequate method could be found for subtracting out this interference.

It seems highly probable that the second excited state can be characterized as 4+. Of the possible sequences 4(D, Q)4(Q)2, 2(Q)4(Q)2, and 3(D, Q)4(Q)2, the first two require a positive A_4 coefficient. The present data, even with the large interference, require an A_4 which is negative or at worst vanishing. Thus a spin of 3 must be assigned to the 1.359 MeV level but the multipolarity of the 1.076 MeV transition remains undetermined.

4. Discussion

Nathan [1]) has discussed the level structure of Dy^{160} in terms of the unified model. His spin and multipolarity assignments were based on internal conversion and relative intensity measurements. The present angular correlation measurements confirm his assignments when interpreted in accord with the internal conversion data.

References

1) O. Nathan, Nuclear Physics **4** (1957) 125
2) S. Ofer, Nuclear Physics **5** (1958) 331
3) Burson, Jordan and LeBlanc, Phys. Rev. **94** (1954) 103
4) Keshishian, Kruse, Klotz and Fowler, Phys. Rev. **96** (1954) 1050
5) Bertolini, Bettoni and Lazzarini, Nuovo Cimento **3** (1956) 754; and Nuovo Cimento **3** (1956) 1162
6) M. A. Clark and J. W. Knowles, Bull. Am. Phys. Soc. **4** (1957) 231
7) Grigor'ev, Dželepov, Zolotavin, Kraft, Kratsik and Peker, Izv. Akad. Nauk SSSR, Ser. Fiz. **22** (1958) 101
8) Avotina, Grigor'ev, Zolotavin and Kratsik, Doklady Akad. Nauk SSSR, **119** (1958) 1127
9) S. Ofer and S. G. Cohen, Proc. Rehovoth Conf. Nucl. Structure (North Holland Publishing Co. 1958) p. 479
10) Stewart, Scharenberg and Wiedenbeck, Phys. Rev. **99** (1955) 691
11) Arns, Sund and Wiedenbeck, University of Michigan Research Institute Technical Report 2375-4-T (January, 1959)
12) M. E. Rose, Phys. Rev. **91** (1953) 610
13) R. G. Arns and M. L. Wiedenbeck, Phys. Rev. **111** (1958) 1631

8.B *Nuclear Physics* **11** (1959) 419—431; © *North-Holland Publishing Co., Amsterdam*
Not to be reproduced by photoprint or microfilm without written permission from the publisher

DEPOLARIZATION OF μ^--MESONS IN μ-MESIC ATOM FORMATION

I. M. SHMUSHKEVICH

Physico-Technical Institute of the U.S.S.R. Academy of Sciences, Leningrad

Received 15 October 1958

Abstract: For not very highly excited states the level width in μ-mesic atoms is considerably smaller than the distance between fine structure levels. Spin-orbit interaction should therefore lead to considerable depolarization of μ^--mesons involved in the formation of μ-mesic atoms. The magnitude of this effect is estimated. The influence of hyperfine splitting of the μ-mesic atom ground state on the angular distribution of neutrons created in the capture of μ^--mesons by nuclei is also considered.

1. Introduction

It is well known that the formation of μ-mesic atoms precedes the decay and nuclear capture of negative μ-mesons in matter. It will be shown below that if the μ-mesons were initially polarized their degree of polarization should significantly diminish when the mesic atom undergoes a transition to the ground state from the highly excited states. Radiative and Auger transitions † are mainly of a dipole nature. Since the dipole moment operator does not act on the spin variables it would seem at first glance that the polarization of the μ-mesons should not change up to the moment the mesons enter the K-orbit. This surmise would be true if the width of the μ-mesic atom excited state levels were much larger than the fine structure splitting of the levels. In this case the spin-orbit interaction would not noticeably affect the spin state of the μ-meson during the short time the mesic atom remains in an excited state. In reality, however, the ratio of the radiative width of the levels to the distance between the fine structure levels in mesic atoms (and in general in hydrogen-like systems) is of the order of $e^2/\hbar c$, i.e., much less than unity. This ratio can be determined with greater precision. Denoting the distance between levels with the same values of n and l but different $j (j = l \pm \frac{1}{2})$ by Δ_{nl} we have

$$\Delta_{nl} = m_\mu c^2 \left(\frac{Ze^2}{\hbar c}\right)^4 \frac{1}{2n^3 l(l+1)}. \qquad (1)$$

† The relative probability of transitions for which the orbital angular momentum l changes by more than one or does not change at all is small not only for radiative but for Auger transitions as well [1, 2]). An exception is the 2s → 1s transition which occurs as a consequence of the Auger effect.

The radiative level width Γ_{nl} is also proportional to $m_\mu Z^4$ (the total width of a level with given values of n and l does not depend on j). Thus by using the tables for transition probabilities in hydrogen [3]) it is not difficult to find that for n lying between 2 and 6 and any value of l, the ratio Γ_{nl}/Δ_{nl} varies between 0.0091 and 0.0097 (the approximate constancy of Γ_{nl}/Δ_{nl} is connected with the fact that for a given l, Γ_{nl} is proportional to $1/n^3$ and decreases with increase of l [3]). The smallness of Γ_{nl}/Δ_{nl} means that the excited states which the μ-mesic atom passes through play an important role in depolarization of the μ-mesons. It should be noted, however, that the total width of the mesic atom levels is the sum of the radiative width and Auger transition width. Auger transitions, however, are important for highly excited states and small Z [1, 2]). The value of Z below which Auger transitions practically play a very small role (excluding $2s \to 1s$ transitions) increases with growth of Z. Thus, at least in the last stage of formation of μ-mesic atoms on a nucleus with a sufficiently large Z radiative transitions play the main role. Therefore, for the mesic atom levels which are significant under these conditions the following condition holds:

$$\Gamma_{nl} \ll \Delta_{nl}. \tag{2}$$

Here Γ_{nl} denotes the total width which is equal to the sum of the radiative width and Auger transition width.

In accord with the foregoing we shall divide the μ^--meson depolarization problem into two parts. The first part encompasses capture of the μ^--meson from the continuous spectrum and the subsequent cascade transition to an orbit with a sufficiently large value of n which we denote by n_0. Transition of the μ^--meson from this level to the ground state comprises the second part. In this case we choose n_0 so that condition (2) will hold in the second part.

2. Transition of Captured μ-Meson to Ground State

2.1. THEORY OF DEPOLARIZATION FOR SPIN-ZERO NUCLEI

Let us first consider the second part. In order to avoid complications connected with the necessity of taking into account the hyperfine structure (some remarks concerning this point are made in subsection 4.2) we shall restrict our consideration to μ-mesic atoms produced on zero spin nuclei. Moreover, we shall temporarily neglect the Auger transition probabilities (excluding the $2s \to 1s$ transition). It will be seen from the following that this neglection is immaterial.

From a state with a principal quantum number n_0, orbital angular momentum l_0, total angular momentum j_0 and projection of the latter, μ_0, the mesic atom can go over to the ground state in various ways. Thus, from

the $6s_{\frac{1}{2}}$ state this transition can occur in the following ways:

$$6s_{\frac{1}{2}} \to 2p_{\frac{1}{2}} \to 1s_{\frac{1}{2}},\ 6s_{\frac{1}{2}} \to 2p_{\frac{3}{2}} \to 1s_{\frac{1}{2}},\ 6s_{\frac{1}{2}} \to 5p_{\frac{1}{2}} \to 3d_{\frac{3}{2}} \to 2p_{\frac{3}{2}} \to 1s_{\frac{1}{2}}$$

and in many others as well. Inasmuch as under the conditions considered here the level widths are even smaller than the distances between the fine structure levels, a different set of quanta will correspond to each transition path. Various transition paths therefore do not interfere and the resultant probability for transition from a given state to the ground state is the sum of the transition probabilities over various paths. Let $A^{\alpha}_{\mu_f\mu_i}(\mathbf{k}_1, \mathbf{e}_1; \mathbf{k}_2, \mathbf{e}_2; \ldots \mathbf{k}_f, \mathbf{e}_f)$ be the mesic atom transition amplitude (in the second part of the process) from a state with quantum numbers n_0, l_0, j_0, μ_0 to a state n_f, l_f, j_f, μ_f, a definite set of quanta with momenta and polarizations $\mathbf{k}_1, \mathbf{e}_1; \mathbf{k}_2, \mathbf{e}_2; \ldots \mathbf{k}_f, \mathbf{e}_f$ being emitted. Index α indicates a definite transition path, i.e., a definite sequence of states which the mesic atom passes in transition from the initial and final states:

$$A^{\alpha}_{\mu_f\mu_0} = C_{\alpha} \sum_{\mu_1, \mu_2, \ldots \mu_f} \prod_{i=1}^{f} \langle n_i, l_i, j_i, \mu_i | H(\mathbf{k}_i, \mathbf{e}_i) | n_{i-1}, l_{i-1}, j_{i-1}, \mu_{i-1} \rangle; \quad (3)$$

$H(\mathbf{k}_i, \mathbf{e}_i)$ is an operator corresponding to emission of a quantum with a momentum $\mathbf{k}_i$ and polarization $\mathbf{e}_i$.

The modulus of constant C_{α} (which is precisely the quantity required) is defined by the condition

$$\sum_{\mu_f} \int_{\mathbf{e}_1, \mathbf{e}_2, \ldots \mathbf{e}_f} |A^{\alpha}_{\mu_f\mu_0}|^2 \rho_1 \mathrm{d}\Omega_1 \rho_2 \mathrm{d}\Omega_2 \ldots \rho_f \mathrm{d}\Omega_f = \prod_{i=0}^{f-1} \frac{\gamma_i^{i+1}}{\Gamma_i}. \quad (4)$$

Here γ_i^{i+1} is the partial width of the i^{th} level and corresponds to a radiative transition to the $i+1$ level; Γ_i is the total width of the i^{th} level. Summation in the left hand side in (4) is carried out over the magnetic quantum numbers of the final state and over the polarizations of all emitted quanta. ρ_i is the state density of the i^{th} quantum per unit energy interval. Introducing for the initial state specified by quantum numbers, $n_0\ l_0\ j_0$, a density matrix expressed in terms of the magnetic quantum numbers, $P_{\mu_0\mu'_0}$, we obtain for a similar density matrix $P_{\mu_f\mu'_f}$ of the final state specified by $n_f l_f j_f$ the expression

$$P'_{\mu_f\mu'_f} = B_f \sum_{\alpha} \int_{\mathbf{e}_1, \mathbf{e}_2, \ldots \mathbf{e}_f} \sum_{\mu_0\mu'_0} P_{\mu_0\mu'_0} A^{\alpha}_{\mu_f\mu_0} A^{\alpha *}_{\mu'_f\mu'_0} \cdot \rho_1 \mathrm{d}\Omega_1 \ldots \rho_f \mathrm{d}\Omega_f. \quad (5)$$

The constant B_f is defined by the condition

$$\mathrm{tr}\, P' = 1. \quad (6)$$

In the integrand or sum in (4) there are no terms containing the product of the amplitudes $A^{\alpha}_{\mu_f\mu_0}$ and $A^{\alpha *}_{\mu'_f\mu'_0}$ with $\alpha \neq \alpha'$ because of the above-mentioned non-coherency of quanta emitted in various transition paths α.

The mean value of the spin in the f^{th} level, $\bar{s}_f$, can be written down with help of matrix P' as follows:

$$\bar{\mathbf{s}}_f = \sum P'_{\mu_f\mu'_f} \langle n_f l_f j_f \mu'_f | \bar{\mathbf{s}} | n_f l_f j_f \mu_f \rangle. \tag{7}$$

Since for dipole transitions the dependence of the matrix elements encountered in (7) on the magnetic quantum numbers is known, all required summations can be performed by first substituting (3) in (5) and then in (7). This yields the formula

$$\bar{\mathbf{s}}_f = \beta_f \bar{\mathbf{s}}_0 \tag{8}$$

which relates $\bar{\mathbf{s}}_f$ to the mean spin value $\bar{\mathbf{s}}_0$ in the initial state. However, this result can be obtained, and β_f computed, in a simpler way. As is well known, for a state with definite values of nl and j there is a relation between the mean values of the total angular momentum vector $\bar{\mathbf{j}}$ and mean spin vector $\bar{\mathbf{s}}$ which follows from the operator equality $\mathbf{j} = \mathbf{l}+\mathbf{s}$ and from the fact that $\bar{\mathbf{j}}$ and $\bar{\mathbf{s}}$ are parallel. This relation is

$$\bar{\mathbf{s}} = \frac{\langle \mathbf{sj} \rangle}{j(j+1)} \bar{\mathbf{j}} = \frac{j(j+1) - l(l+1) + \frac{3}{4}}{2j(j+1).} \bar{\mathbf{j}}. \tag{9}$$

In a similar manner one can obtain a relation between the mean values of the total mesic atom angular momentum vectors $\bar{\mathbf{j}}_i$ and $\bar{\mathbf{j}}_{i+1}$ for the i^{th} and $i+1^{\text{th}}$ levels corresponding to a dipole transition of the mesic atom from one level to another. In such a transition the radiation carries off an angular momentum f equal to unity. Hence from the equality

$$\mathbf{j}_i = \mathbf{j}_{i+1} + \mathbf{f} \tag{10}$$

(which is to be understood in the sense of a relation between the matrix elements of the corresponding quantities) and parallelism between vectors $\bar{\mathbf{j}}_i$ and $\bar{\mathbf{j}}_{i+1}$ we obtain in analogy to (9)

$$\begin{aligned} \bar{\mathbf{j}}_{i+1} = \frac{\langle \mathbf{j}_i \mathbf{j}_{i+1} \rangle}{j_i(j_i+1)} \bar{j}_i &= \frac{j_i(j_i+1) + j_{i+1}(j_{i+1}+1) - f(f+1)}{2j_i(j_i+1)} \bar{\mathbf{j}}_i \\ &= \frac{j_i(j_i+1) + j_{i+1}(j_{i+1}+1) - 2}{2j_i(j_i+1)} \bar{\mathbf{j}}_i. \end{aligned} \tag{11}$$

Hence, taking into account (9) we get

$$\bar{\mathbf{s}}_{i+1} = \beta \bar{\mathbf{s}}_i \tag{12}$$

where

$$\beta = \frac{j_{i+1}(j_{i+1}+1) - l_{i+1}(l_{i+1}+1) + \frac{3}{4}}{j_i(j_i+1) - l_i(l_i+1) + \frac{3}{4}} \frac{j_i(j_i+1) + j_{i+1}(j_{i+1}+1) - 2}{2j_{i+1}(j_{i+1}+1)}. \tag{13}$$

Therefore, for a cascade transition of a mesic atom from a level with quantum numbers $n_0 l_0 j_0$ to a level with numbers $n_1 l_1 j_1$, then to level

$n_2 l_2 j_2$, etc., and finally, to level $n_f l_f j_f$ we have

$$\bar{\mathbf{s}}_f = \frac{j_f(j_f+1)-l_f(l_f+1)+\frac{3}{4}}{j_0(j_0+1)-l_0(l_0+1)+\frac{3}{4}} \prod_{i=0}^{f-1} \frac{j_i(j_i+1)+j_{i+1}(j_{i+1}+1)-2}{2j_{i+1}(j_{i+1}+1)} \bar{\mathbf{s}}_0. \tag{14}$$

This formula yields the change in the polarization of a μ^--meson when the mesic atom makes a transition in a definite way from the initial level to the final level, the transition probability being $\Pi_{i=0}^{f-1}(\gamma_i^{i+1}/\Gamma_i)$. Averaging over all possible paths we obtain

$$\begin{aligned}\bar{\mathbf{s}}_f = &\left(\sum_\alpha \prod_{i=0}^{f-1} \frac{\gamma_i^{i+1}}{\Gamma_i}\right)^{-1} \frac{j_f(j_{f+1})-l_f(l_f+1)+\frac{3}{4}}{j_0(j_0+1)-l_0(l_0+1)+\frac{3}{4}} \\ &\cdot \sum_\alpha \prod_{i=0}^{f-1} \frac{\gamma_i^{i+1}}{\Gamma_1} \frac{j_i(j_i+1)+j_{i+1}(j_{i+1}+1)-2}{2j_{i+1}(j_{i+1}+1)} \bar{\mathbf{s}}_0.\end{aligned} \tag{15}$$

One other circumstance should be kept in mind when employing this formula to determine the polarization of μ-mesons in the $1s_{\frac{1}{2}}$ ground state. A mesic atom in a level $n_0 l_0 j_0$ will finally pass over via a radiative transition to one of the two states, $1s_{\frac{1}{2}}$ or $2s_{\frac{1}{2}}$. The mesic atom undergoes with a probability of unity an Auger transition from the $2s_{\frac{1}{2}}$ to the $1s_{\frac{1}{2}}$ state providing that various effects, and in particular those connected with the finite size of the nucleus [4]), do not lead to a significant shift in the 2s and 2p levels. During such a transition the polarization of the μ^--meson will not change as the spin projection has a definite value in s states and the perturbation which causes the Auger transition is due to spin-independent Coulomb interaction between the μ-meson and electron of the atomic shell. Therefore, for the mean value of the spin in the K-shell, $\bar{\mathbf{s}}_K$, we obtain

$$\bar{\mathbf{s}}_K = \beta_K \bar{\mathbf{s}}_0 \tag{16}$$

where

$$\beta_K = \frac{3}{2} \frac{1}{j_0(j_0+1)-l_0(l_0+1)+\frac{3}{4}} \sum_\alpha \prod_{i=0}^{f-1} \frac{\gamma_i^{i+1}}{\Gamma_i} \frac{j_i(j_i+1)+j_{i+1}(j_{i+1}+1)-2}{2j_{i+1}(j_{i+1}+1)}. \tag{17}$$

In this formula the sum is taken over all paths leading to state $1s_{\frac{1}{2}}$ as well as state $2s_{\frac{1}{2}}$; the sum of the transition probabilities to these two states is equal to unity and therefore the first factor in (15) is absent in formula (17). Due to the finite size of the nucleus the energy of the s levels appreciably increases at sufficiently large values of Z. As mentioned in ref.[5]) a consequence of this is that instead of the $2s \to 1s$ Auger transition the $2s \to 2p$ transition may become dominant. This leads to a certain decrease of the μ-meson polarization in the K-shell compared to that which formula (17) yields (since an additional depolarization appears in $2s \to 2p \to 1s$ transitions). However, this decrease is very small as the probability for transition to the $2s_{\frac{1}{2}}$ level is much smaller than that for transition to the $1s_{\frac{1}{2}}$ level.

In the further calculations this circumstance will not be taken into account and formula (17) will be employed.

2.2. COMPUTATIONS AND DISCUSSION

In order to estimate the polarization occurring in the second part of the process coefficient β_K was computed for transitions from states with a principal quantum number $n_0 = 5$ and various values of l_0 and j_0. The calculations were performed with aid of formula (17) and the table of radiative transition probabilities given in ref.[1]). This table contains the values of the probabilities $W(n_1, l_1; n_2, l_2)$ for transition from a state with quantum numbers $n_1 l_1$ to a state with quantum numbers $n_2 l_2$, the probabilities being summed over all possible values of j_2. In order to obtain from here the transition probabilities $W(n_1, l_1, j_1; n_2, l_2, j_2)$ from states with quantum numbers n_1, l_1, j_1 to the state n_2, l_2, j_2 calculations should be carried out according to the formulas

$$
\begin{aligned}
&W(n_1, l_1, l_1+\tfrac{1}{2}; n_2, l_1-1, l_1-\tfrac{1}{2}) \\
&\qquad = W(n_1, l_1; n_2, l_1-1) \\
&W(n_1, l_1, l_1-\tfrac{1}{2}; n_2, l_1-1, l_1-\tfrac{1}{2}) \\
&= \frac{1}{l_1(2l_1-1)} W(n_1, l_1; n_2, l_1-1), \\
&W(n_1, l_1, l_1-\tfrac{1}{2}; n_2, l_1-1, l_1-\tfrac{3}{2}) \\
&= \frac{(l_1-1)(2l_1+1)}{l_1(2l_1-1)} W(n_1, l_1; n_2, l_1-1),
\end{aligned}
\qquad
\begin{aligned}
&W(n_1, l_1, l_1-\tfrac{1}{2}; n_2, l_1+1, l_1+\tfrac{1}{2}) \\
&\qquad = W(n_1, l_1; n_2, l_1+1) \\
&W(n_1, l_1, l_1+\tfrac{1}{2}; n_2, l_1+1, l_1+\tfrac{1}{2}) \\
&= \frac{1}{(l_1+1)(2l_1+3)} W(n_1, l_1; n_2, l_2), \\
&W(n_1, l_1, l_1+\tfrac{1}{2}; n_2, l_1+1, l_1+\tfrac{3}{2}) \\
&= \frac{(2l_1+1)(l_1+2)}{(l_1+1)(2l_1+3)} W(n_1, l_1; n_2, l_2).
\end{aligned}
\qquad (18)
$$

Results of the calculations of β_K for various initial states with a principal quantum number 5 are presented in table 1. The absence of depolarization

TABLE 1

Initial state	$5s_{\frac{1}{2}}$	$5p_{\frac{1}{2}}$	$5p_{\frac{3}{2}}$	$5d_{\frac{3}{2}}$	$5d_{\frac{5}{2}}$	$5f_{\frac{5}{2}}$	$5f_{\frac{7}{2}}$	$5g_{\frac{7}{2}}$	$5g_{\frac{9}{2}}$
β_K	0.39	≈ 1	≈ 1	0.24	≈ 1	0.12	1	0.06	1

for initial states which are p states ($5p_{\frac{3}{2}}$ or $5p_{\frac{1}{2}}$) is natural, as from p states the mesic atom predominantly goes over directly to the 1s or 2s state and for such transitions, as formula (13) shows, $\beta = 1$. It can moreover be seen from table 1 that for $l_0 > 1$ and $j_0 = l_0 - \frac{1}{2}$ one has $\beta_K \ll 1$ which becomes more pronounced with growth of l_0. When $j_0 = l_0 + \frac{1}{2}$, β_K is practically equal to unity. This latter circumstance can easily be understood qualitatively. To demonstrate this let us first consider a $5g_{\frac{9}{2}}$ initial state, that is, a state with the highest possible values of l_0 and j_0 for a given n_0. Assume, moreover,

that $\mu_0 = j_0 = \frac{9}{2}$, i.e., that μ_0 is also maximal. Dipole transitions from this state to the K-shell will occur in the following order:

$$(5g_{\frac{9}{2}}, \mu = \tfrac{9}{2}) \to (4f_{\frac{7}{2}}, \mu = \tfrac{7}{2}) \to (3d_{\frac{5}{2}}, \mu = \tfrac{5}{2}) \to (2p_{\frac{3}{2}}, \mu = \tfrac{3}{2}) \to (1s_{\frac{1}{2}}, \mu = \tfrac{1}{2}).$$

States for which $\mu = j = l + \frac{1}{2}$ are involved in this sequence and hence the spin projection possesses a definite value equal to $\frac{1}{2}$. This means that no depolarization will occur in the transition under consideration, i.e., $\beta_K = 1$ and this result does not depend on the assumption made above that $\mu_0 = j_0$ since β_K is in general independent of μ_0. The same result obtains when the initial state is $5f_{\frac{7}{2}}$ (i.e., a state with l_0 smaller than the highest possible value by unity). Indeed, if we again assume that $\mu_0 = j_0 = \frac{7}{2}$ it can easily be verified that when the mesic atom changes from the state under consideration to the K shell it will pass only through those states in which the spin projection remains constant and equal to $+\frac{1}{2}$. If the initial state is $5d_{\frac{5}{2}}$, besides the transitions

$$5d_{\frac{5}{2}} \to 2p_{\frac{3}{2}} \to 1s_{\frac{1}{2}}, \quad 5d_{\frac{5}{2}} \to 3p_{\frac{3}{2}} \to 1s_{\frac{1}{2}}, \quad 5d_{\frac{5}{2}} \to 3p_{\frac{3}{2}} \to 2s_{\frac{1}{2}}$$

in which the mean value of the spin does not change, sequences of other types should also be possible, such as $5d_{\frac{5}{2}} \to 4f_{\frac{5}{2}} \to 3d_{\frac{3}{2}} \to 2p_{\frac{3}{2}} \to 1s_{\frac{1}{2}}$ etc., in which some depolarization occurs. However, the contribution of these depolarizing transitions are vanishingly small since they are all connected with the transitions $5d_{\frac{5}{2}} \to 4f_{\frac{5}{2}}$ and $5d_{\frac{5}{2}} \to 4p_{\frac{3}{2}}$, the probability of which is very small compared with that for transitions to lower states. If, however, l_0 is large and $j_0 = l_0 - \frac{1}{2}$ then in the initial as well as in the subsequent intermediate states the spin projection, generally speaking, does not have a definite value and every transition from one level to another is accompanied by a certain degree of depolarization. Since, however, l_0 is large the mesic atom must pass through a large number of intermediate states before it reaches the K-level. As a result accumulation occurs and β_K turns out to be very small.

Thus, when l_0 is large and $j_0 = l_0 + \frac{1}{2}$ in the initial state, depolarization practically does not occur whereas for initial states with a large l_0 but $j_0 = l_0 - \frac{1}{2}$ the depolarization is almost complete. It is evident that these results are valid for any initial state and do not rest on the assumption that $n_0 = 5$. What is more, it may be asserted that the conclusions drawn above will also be true if Auger transitions are taken into account, since these transitions are also mostly of a dipole nature (see the note on p. 419). Thus formulas (13), (14) and (15) are valid when the Auger effect is taken into account, providing that γ_i^{i+1} and Γ_i are regarded as the sum of the corresponding radiative width and width with respect to Auger transitions and providing that the formulas are applied to transitions in the region in which condition (2) is valid.

3. Capture of the μ-Meson

A complete solution of the depolarization problem would require a quantitative analysis of the first part of the μ-mesic atom formation process. This is a very difficult problem which essentially has not been solved up to the present. What we really need is the probability of the μ-meson going over to levels with different values of n_0, l_0 and j_0 (when these numbers are sufficiently large) and also the mean values of the spin $\bar{\mathfrak{s}}_0$ on these levels. As regards the first point, i.e., the probability of a μ-meson occupying various highly excited levels, one may, in accord with ref. [6]), make various assumptions and compare them with the results obtained. On basis of some arguments given in ref. [6]) and [7]) it may be assumed that for a given n_0 the μ-mesons predominantly go over to levels with very large values of l_0 which are close to the highest possible value. Furthermore, for a sufficiently large n_0 the level width, due to Auger transitions, begins to exceed the fine structure splitting. Assuming that the μ^--mesons in these levels are still completely polarized one can in principle by employing the technique developed in ref. [8]) determine the μ-meson polarization in the ground state. Referring this to the future, at the present we shall confine ourselves to a rough estimate of the mean values $\bar{\boldsymbol{\sigma}}_0 = 2\bar{\mathfrak{s}}_0$ †. In order to do this we shall assume that during the first moment after the polarized μ-meson reaches a shell with quantum numbers n_0, l_0 the wave function has the form

$$\Psi_0 = \sum_m a_m \varphi_{n_0 l_0 m} \chi_{\frac{1}{2}} = \sum_{j_0 m} a_m C^{j_0 m+\frac{1}{2}}_{l_0 m, \frac{1}{2}\frac{1}{2}} \Phi_{n_0, l_0, j_0, m+\frac{1}{2}}. \tag{19}$$

Here $\varphi_{n_0 l_0 m}$ is the mesic atom wave function without account of the spin, m is the projection of the orbital angular momentum, $\chi_{\frac{1}{2}}$ is the μ-meson spin function with a spin projection of $\frac{1}{2}$, $j_0 = l_0 \pm \frac{1}{2}$,

$$\Phi_{n_0 l_0 j_0 m+\frac{1}{2}} = \sum_{r\lambda} C^{j_0 m+\frac{1}{2}}_{l_0 r, \frac{1}{2}\lambda} \varphi_{n_0 l_0 r} \chi_\lambda$$

is the mesic atomic wave function with quantum numbers n_0, l_0, j_0 and $\mu_0 = m + \frac{1}{2}$. For $t > 0$ we get for the wave function

$$\Psi = \sum_{j_0 m} a_m C^{j_0 m+\frac{1}{2}}_{l_0 m, \frac{1}{2}\frac{1}{2}} \Phi_{n_0 l_0 j_0 m+\frac{1}{2}} e^{-(i/\hbar) E_{n_0 l_0 j_0} t}. \tag{20}$$

States with $j_0 = l_0 + \frac{1}{2}$ and $j_0 = l_0 - \frac{1}{2}$ can be considered independently if condition (2) is satisfied for the levels under consideration. Assuming furthermore that all values of m are equally probable, we obtain for the probability p_{j_0} of a given value of j_0 the expression

$$p_{j_0} = \sum_m |a_m|^2 (C^{j_0 m+\frac{1}{2}}_{l_0 m, \frac{1}{2}\frac{1}{2}})^2 = \frac{1}{2l_0+1} \sum_m (C^{j_0 m+\frac{1}{2}}_{l_0 m, \frac{1}{2}\frac{1}{2}})^2 = \frac{2j_0+1}{2(2l_0+1)}. \tag{21}$$

† Here $\bar{\boldsymbol{\sigma}}_0$ has been introduced instead of $\bar{\mathfrak{s}}_0$ since it is precisely the vector $\xi = \bar{\sigma}$ which is usually employed to characterize the polarization state.

For the mean value σ_z in a state with a definite value of j_0 we get

$$\overline{(\sigma_z)}_{n_0 l_0 j_0} = \frac{1}{p_{j_0}} \sum_{\substack{mm' \\ rr' \nu\nu'}} a_m a^*_{m'} C^{jm+\frac{1}{2}}_{lm,\frac{1}{2}\frac{1}{2}} C^{jm'+\frac{1}{2}}_{lm',\frac{1}{2}\frac{1}{2}} C^{jm+\frac{1}{2}}_{lr,\frac{1}{2}\nu} C^{jm'+\frac{1}{2}}_{lr',\frac{1}{2}\nu'} (\nu'|\sigma_z|\ \nu\rangle. \tag{22}$$

Summation over the magnetic quantum numbers can be carried out in this expression by the well-known technique [9]) which yields

$$\overline{(\sigma_z)}_{n_0 l_0 j_0} = \frac{[\frac{3}{4}+j_0(j_0+1)-l_0(l_0+1)]^2}{3j_0(j_0+1)} = \begin{cases} \dfrac{2l_0+3}{3(2l_0+1)} & \text{for } j_0 = l_0+\frac{1}{2} \\ \dfrac{2l_0-1}{3(2l_0+1)} & \text{for } j_0 = l_0-\frac{1}{2}. \end{cases} \tag{23}$$

According to ref. [6]) and [7]), μ-meson capture originally takes place in a state with a large l. However, for large values of l

$$p_{j_0} \cong \tfrac{1}{2} \quad \text{and} \quad \overline{(\sigma_z)}_{n_0 l_0 j_0} = \tfrac{1}{3}. \tag{24}$$

Therefore, polarized μ-mesons are captured into highly excited orbits of the mesic atom with $j_0 = l_0+\frac{1}{2}$ with a probability of $\frac{1}{2}$ and with an equal probability into states with $j_0 = l_0-\frac{1}{2}$. On basis of the conclusions reached above (subsection 2.2), in descending from states with $j = l+\frac{1}{2}$ to the K-shell the μ-mesons retain their polarization (equal to $\frac{1}{3}$), whereas when proceeding from the $j = l-\frac{1}{2}$ state they reach the ground state almost completely depolarized. Thus on the average the μ^--meson polarization in K shell should equal $\frac{1}{6}$ or about 17 %. This is approximately what is observed experimentally [10, 11]).

4. Special Problems

4.1. REVERSAL OF SPIN DIRECTION

In conclusion we shall consider some problems related to depolarization in μ-mesic atoms. The first question concerns the sign of β in formula (7). The point here is to ascertain whether the mean spin can reverse its direction in some certain level. Consider a level with $j_r = l_r+\frac{1}{2}$. Transitions from higher levels to the one under consideration can occur from three types of states: 1) $l = l_r+1$, $j = l+\frac{1}{2}$, 2) $l = l_r+1$, $j = l-\frac{1}{2}$, 3) $l = l_r-1$, $j = l+\frac{1}{2}$. According to (13), $\beta = 1$ in transitions from states of the first type and $\beta = -(1+(j_r-1)/j_r^2)$ for transitions of the second type, i.e., β is negative (excluding the case $j_r = \frac{1}{2}$). However, for states of the second type the depolarization is quite noticeable (if the r^{th} level under consideration is not very strongly excited) and, moreover, for equal values of n and l the probability for transitions from states of the second type is $(l_r+1)(2l_r+1)$ times smaller than that for states of the first type. Thus, as a result of transitions of the

first and second type it may be expected that the spin direction will remain unchanged, that is, it will be the same as the initial direction. Transitions of the third type will not affect this result as their probability is small and for them $\beta = 1-(1/j_r^2) > 0$.

It is more difficult to draw any conclusions regarding the possibility of reversal of the spin direction for a level with $j_r = l_r-\frac{1}{2}$. In this case too transitions from three types of states are possible: 1) $l = l_r-1$, $j = l-\frac{1}{2}$, 2) $l = l_r-1$, $j = l+\frac{1}{2}$, 3) $l = l_r+1$, $j = l-\frac{1}{2}$. For these states β is equal respectively to

$$1, \quad -\left[1-\frac{j_r+2}{(j_r+1)^2}\right], \quad \left[1-\frac{1}{(j_r+1)^2}\right].$$

A consideration of transitions of the first and second type from levels with identical values of n and l reveals the following. Transition from type 2 states involve spin reversal (with the exception of $s_{\frac{1}{2}} \to p_{\frac{1}{2}}$); however, these transitions are $l_r(2l_r+1)$ times less probable than transitions from states of the first type in which the spin direction does not change. Nevertheless in states of the first and also third type the mean value of the spin may be very small (significant depolarization in states with $j = l-\frac{1}{2}$) and hence it is difficult to draw any definite conclusions regarding the possibility of spin reversal when the μ^--meson reaches a level with $j = l-\frac{1}{2}$. Possibly this circumstance may be of importance for interpretation of the experiments suggested in ref. [12]) to determine the helicity of μ^--mesons emitted in π^--meson decay.

4.2. POLARIZATION OF NUCLEI BY CAPTURE OF POLARIZED μ-MESONS ON K-SHELL OF μ-MESIC ATOM

In determining the depolarization in the case of μ-mesic atoms produced on nuclei with spins I not equal to zero not only the fine but also the hyperfine structure of the mesic atom levels should be taken into account. This problem requires a special analysis. However, in analyzing experiments on polarized μ-meson capture by nuclei with $I \neq 0$ besides μ-meson depolarization, the nuclear polarization which arises in the ground state of the mesic atom at various values of the total angular momentum $F = I \pm \frac{1}{2}$ should also be taken into account. As an example, we shall take the case of μ-mesic hydrogen formation from an initially polarized μ^--meson and unpolarized proton. It is well known that the hyperfine splitting of the ground state levels in μ-mesic hydrogen is much larger than $\hbar/\tau$ where τ is the μ-meson half-life. The spin states of the μ^-—p system in the K shell should therefore be considered separately for $F = 1$ and $F = 0$ (these states form an incoherent mixture). The spin density matrix ρ_t in the triplet state should have the form

$$\rho_t = \tfrac{1}{4}[1+\lambda \mathbf{j}(\sigma_p+\sigma_\mu)+\tfrac{1}{3}\sigma_p \cdot \sigma_\mu] \qquad (25)$$

where $\mathbf{j}$ is a unit vector in the direction of the initial μ^--meson polarization.

In writing down (25) we made use of the invariance and Hermitian conditions imposed on ρ_t and also of the fact that ρ_t should be linear with respect to $\mathbf{j}$ and symmetrical (triplet state) with respect to the proton and μ^--meson spin variables. The coefficients before the first and third terms in (25) have been chosen so that the conditions

$$\mathrm{tr}\,\rho_t = 1 \quad \text{and} \quad \mathrm{tr}\,(\rho_t S^2) = 2 \tag{26}$$

be fulfilled, where

$$S^2 = \left(\frac{\boldsymbol{\sigma}_p + \boldsymbol{\sigma}_\mu}{2}\right)^2. \tag{27}$$

It can be seen from formula (25) that in the triplet state the proton and neutron polarization vectors are identical and equal to $\lambda\mathbf{j}$. In the singlet state we have for the density matrix

$$\rho_s = \tfrac{1}{4}(1 - \boldsymbol{\sigma}_p \cdot \boldsymbol{\sigma}_\mu). \tag{28}$$

We now determine the angular distribution of neutrons created in the capture of the μ^--meson by a proton in the reaction

$$\mu^- + p \to n + \nu. \tag{29}$$

For this purpose we shall employ an interaction Hamiltonian in the form given in ref. [13]) but in which the electron wave functions ψ_e are replaced by the μ^--meson functions ψ_μ. Taking into consideration eq. (25) we obtain for the neutron angular distribution in the case of capture from triplet states, the expression

$$\begin{aligned} dW_t = \frac{1}{8\pi^3 a_\mu^{\,3}} p_n^{\,2}\{&|C_S + C_V|^2 + |C'_S + C'_V|^2 + |C_T + C_A|^2 + |C'_T + C'_A|^2 \\ &+ 2\,\mathrm{Re}[(C_S + C_V)(C_T^* + C_A^*) + (C'_S + C'_V)(C'^*_T + C'^*_A) \\ &+ 2\lambda\,\mathrm{Re}[(C_S + C_V)(C'^*_S + C'^*_V) + (C_T + C_A)(C'^*_T + C'^*_A) \\ &+ (C_S + C_V)(C'^*_T + C'^*_A) + (C'_S + C'_V)(C_T^* + C_A^*)]\cos\vartheta\}\,d\Omega. \end{aligned} \tag{30}$$

Here ϑ is the angle between the $\mathbf{j}$ vector and direction of neutron emission, $p_n \approx m_\mu c$ is the neutron momentum, a_μ is the radius of the μ-meson Bohr orbit. For capture from singlet states we obtain with the aid of (28)

$$\begin{aligned} dW_s = \frac{1}{8\pi^3 a_\mu^{\,3}} p_n^{\,2}\{&|C_S + C_V|^2 + |C'_S + C'_V|^2 + 9|C_T + C_A|^2 + 9|C'_T + C'_A|^2 \\ &- 6\,\mathrm{Re}[(C_S + C_V)(C_T^* + C_A^*) + (C'_S + C'_V)(C'^*_T + C'^*_A)]\}\,d\Omega. \end{aligned} \tag{31}$$

For the resulting angular distribution dW we get

$$dW = p_t\,dW_t + p_s\,dW_s \tag{32}$$

where p_t and p_s are respectively the probabilities for the μ-meson making a transition to a triplet or singlet state in the K shell. If one assumes that

these probabilities are proportional to the statistical weights of the triplet and singlet states, i.e., $p_t = \frac{3}{4}$ and $p_s = \frac{1}{4}$ we obtain for the angular distribution

$$dW = \frac{1}{8\pi^3 a_\mu^3} p_n^2 (|C_S+C_V|^2+|C'_S+C'_V|^2+3|C_T+C_A|^2+3|C'_T+C'_A|^2) \\ (1+\alpha \cos\vartheta) d\Omega, \tag{33}$$

$$\alpha = \tfrac{3}{4}\lambda \frac{2\,\mathrm{Re}[(C_S+C_V)(C'^*_S+C'^*_V)+(C_T+C_A)(C'^*_T+C'^*_A) \\ +(C_S+C_V)(C'^*_T+C'^*_A)+(C'_S+C'_V)(C^*_T+C^*_A)]}{|C_S+C_V|^2+|C'_S+C'_V|^2+3|C_T+C_A|^2+3|C'_T+C'_A|^2}. \tag{34}$$

Expression (34) for the neutron angular distribution asymmetry constant differs significantly from that given in ref. [14]) and [15]). Thus, the combination of the constants in the numerator in (34) differs from the corresponding expression in ref. [14]) and [15]). In particular in the Gell-Mann and Feynman scheme (A—V interactions) (34) yields $\alpha = 0$. Secondly, the factor $\frac{3}{4}\lambda$ is smaller than unity even when μ meson polarization is maximum, $\lambda = 1$. This difference is due to the fact that in the aforementioned papers [14, 15]) (see also ref.[16])) the capture probability was calculated under the assumption that the proton prior to capture could be considered to be unpolarized despite the polarization of the μ^--meson in the K-shell. This assumption corresponds to a density matrix of the form

$$\rho = \tfrac{1}{2}(1+\lambda \mathbf{j}\cdot\boldsymbol{\sigma}_\mu) \tag{35}$$

and appears to be incorrect.

It should be mentioned that due to a mechanism proposed and investigated in ref. [17]) an especially pronounced depolarization occurs during the capture of μ-mesons in hydrogen and deuterium (at sufficient densities). Hence the reaction $\mu^- + p \to n + \nu$ discussed here primarily serves an illustrative purpose. In principle, however, polarization of the nucleus (for $I \neq 0$) should always be taken into consideration in capture process studies.

It will not be difficult to extend formulas (25) and (28) to the case of nucleus possessing an arbitrary spin. For $F = I+\frac{1}{2}$ the formulas have the form

$$\rho_+ = \frac{1}{2(2I+1)}\left\{1+\frac{2}{I+1}\mathbf{I}\cdot\mathbf{s}+\lambda_+\mathbf{j}\cdot\left(\frac{3}{I+1}\mathbf{I}+2\mathbf{s}\right)\right. \\ \left. +\frac{3\lambda_+}{(I+1)(I+\frac{3}{2})}[(\mathbf{j}\cdot\mathbf{I})(\mathbf{s}\cdot\mathbf{I})+(\mathbf{s}\cdot\mathbf{I})(\mathbf{j}\cdot\mathbf{I})-\tfrac{2}{3}I(I+1)\mathbf{j}\cdot\mathbf{s}]\right\}. \tag{36}$$

For $F = I-\frac{1}{2}$,

$$\rho_- = \frac{1}{2(2I+1)}\left\{1-\frac{2}{I}\mathbf{I}\cdot\mathbf{s}+\lambda_-\mathbf{j}\cdot\left(\frac{3}{I}\mathbf{I}-2\mathbf{s}\right)\right.$$
$$\left.-\frac{3\lambda_-}{I(I+\frac{1}{2})}[(\mathbf{j}\cdot\mathbf{I})(\mathbf{s}\cdot\mathbf{I})+(\mathbf{s}\cdot\mathbf{I})(\mathbf{j}\cdot\mathbf{I})-\tfrac{2}{3}I(I+1)\mathbf{j}\cdot\mathbf{s}]\right\}. \quad (37)$$

Here $\mathbf{s}$ and $\mathbf{I}$ are the μ-meson and nuclear spin operators; the absolute values of λ_+ and λ_- are smaller than unity.

Depolarization of μ^+-mesons will also occur when muonium is formed from polarized μ^+-mesons and unpolarized electrons. However, this effect should be weaker in muonium as it is due to a weaker interaction which leads to hyperfine splitting. It is not difficult to verify that in muonium the level widths are of the same order as the hyperfine splitting. There does not appear to be much sense in considering this problem quantitatively because even if muonium formation were possible it could occur only in condensed medium in which other factors could be more important for depolarization, such as the interaction of the muonium electron with other electrons in matter.

In conclusion I would like to express my sincere appreciation to S. S. Gershtein, V. N. Gribov and A. Z. Dolginov for interest in this work and profitable discussions.

References

1) G. R. Burbridge and A. H. de Borde, Phys. Rev. **89** (1953) 189
2) A. H. de Borde, Proc. Roy. Phys. Soc. **67** (1954) 57
3) H. A. Bethe, Quantum Mechanics of Simplest Systems (Russ. ed.) (ONTI, 1935) p. 238
4) L. L. Foldy and E. Eriksen, Phys. Rev. **95** (1954) 1048
5) B. L. Ioffe and I. Ya. Pomeranchuk, JETF **23** (1952) 123
6) M. B. Stearns and M. Stearns, Phys. Rev. **105** (1957) 1573
7) N. Bohr, Quoted by B. Bruno, Arkiv Mat. Astronom. Fysik **36A**, no. 8 (1948) 44
8) G. Goertzel, Phys. Rev. **70** (1946) 897
9) G. Racah, Phys. Rev. **62** (1942) 438; **63** (1943) 367
10) R. L. Garwin, L. M. Lederman and M. Weinrich, Phys. Rev. **105** (1957) 1415
11) A. E. Ignatenko, L. B. Yegorov, B. Khalupa and D. Chultem, JETP (in press)
12) A. Z. Dolginov, Nuclear Physics **7** (1958) 569
13) T. D. Lee and C. N. Yang, Phys. Rev. **104** (1956) 254
14) Kerson Huang, C. N. Yang and T. D. Lee, Phys. Rev. **108** (1957) 1340
15) I. S. Shapiro, E. I. Dolinsky and L. D. Blokhintsev, Doklady AN SSSR **116** (1957) 946
16) B. L. Ioffe, JETP **22** (1957) 308
17) S. S. Gerstein, JETP **34** (1958) 463; **34** (1958) 993

1.B:2.L *Nuclear Physics* **11** (1959) 432—443; © *North-Holland Publishing Co., Amsterdam*
Not to be reproduced by photoprint or microfilm without written permission from the publisher

THE THEORY OF n—d SCATTERING WITH TENSOR FORCES

L. M. DELVES† and D. BROWN††
Physics Department, Auckland University, Auckland, N.Z.

Received 8 January 1959

Abstract: The scattering of neutrons by deuterons at energies below 3.5 MeV has been investigated in an approximation including the effects of both the tensor force and the distortion of the deuteron by the neutron. The distortion is found to be small at these energies in the doublet state, but not in the quartet state. Angular distribution and polarization curves for the neutron are given as a function of energy, and the second order spin moment of the deuteron calculated at 3.25 MeV neutron energy. Agreement with experiments where these exist is reasonable. Polarizations of the order of 10 % are predicted.

1. Introduction

The scattering of nucleons by deuterons is perhaps the simplest example of a problem involving forces between more than two nucleons, and thus might be hoped to yield more information on these forces than the two-body data. However, at low energies progress has been hindered by lack of suitable approximation methods. Previous calculations [1, 2, 3]) have assumed that the deuteron is not distorted by the incoming neutron, and have neglected all effects of spin-orbit coupling in the nucleon-nucleon force. It is hard to estimate the validity of these approximations, so that conclusions on the nucleon-nucleon force based on these calculations can only be tentative. The reasonable agreement with experimental angular distributions found at energies greater than a few MeV gives hope that the errors introduced are small in this region; but there is some evidence [4]) that at lower energies this is not so. Moreover a calculation of the neutron polarization induced by the scattering would be of great interest; and this involves introducing explicitly a nucleon-nucleon spin-orbit coupling force. These have been introduced [5, 6]) in Born approximation, which leads to zero polarization with real potentials; and a recent paper by Bransden *et al.* [7]) sets up the problem including tensor forces, in a form suitable for calculation, but neglecting the distortion of the deuteron. It would seem useful to have available a simple method which will give an estimate of this distortion at low energies, and of the characteristic effects of including the tensor force such as the polarization of the neutron. We give such a method here, based on a semi-classical picture of the scatter-

† Now at the Clarendon Laboratory, Oxford, England.
†† Present address: AERE, Harwell, England.

ing which is expected to be reasonable at energies less than a few MeV. This picture leads to an effective two-body neutron-deuteron potential, the wave equation for which can be solved numerically.

2. Equivalent n—d potential

Labelling the incoming neutron and the two particles in the deuteron 1, 2, 3 respectively, and writing

$$\begin{aligned} \mathbf{r}_{12} = \mathbf{r}_1, \quad \mathbf{r}_{13} = \mathbf{r}_2, \quad \mathbf{r}_{23} = 2\mathbf{R}, \\ \mathbf{r} = \mathbf{r}_1 + \mathbf{R} = \mathbf{r}_2 - \mathbf{R}, \end{aligned} \tag{1}$$

those parts of the interaction containing 1 are

$$V_{12} + V_{13}, \tag{2}$$

where V_{ij} will in general contain spin and exchange operators in addition to $\mathbf{r}_{ij}$. At low neutron energies we expect physically an adiabatic approximation to hold: for a given $\mathbf{r}$ the neutron sees an effective potential

$$V_{nd} = \langle \phi_d | V_{12} + V_{13} | \phi_d \rangle \tag{3}$$

where ϕ_d is the wave-function of the deuteron in the presence of a neutron at distance $\mathbf{r}$ from its centre of mass. This is not known. The usual approximation made is to set ϕ_d equal to the free-state wave-function of the deuteron, which is thus not distorted by the presence of the neutron. This is only expected to be good at high energies, where one can reasonably expect some sort of impulse approximation to be valid. We here assume a form for ϕ_d containing an adjustable parameter which is a measure of the average distortion experienced over the collision, and we shall fit this parameter by requiring a fit to the zero-energy scattering lengths. We neglect the small d-state probability of the deuteron and take

$$\begin{aligned} \phi_d = \beta^{\frac{3}{2}}[0.04893 \exp(-0.0170\beta^2 r^2) + 0.1968 \exp(-0.0911\beta^2 r^2) \\ + 0.41555 \exp(-0.4323\beta^2 r^2)] \end{aligned} \tag{4}$$

where $r = 2R$ is measured in units of 10^{-13} cm. This wave-function with $\beta = 1$ represents the free state wave-function of the deuteron to within 5 % to several deuteron radii [1]). The nucleon-nucleon potential assumed has the form

$$V_{ij} = -V_0[\tfrac{1}{2}(1 + P_{ij}^M) + \alpha \mathbf{s}_i \cdot \mathbf{s}_j + \gamma S_{ij}] \exp(-ar^2). \tag{5}$$

Such a potential differs from recent fits to the two-body data in having no repulsive core and no term of the form $\mathbf{L} \cdot \mathbf{S}$. The effects of such features on the results is discussed later. A potential of the form (5) can give a reasonable fit to the low energy two-body data for a range of parameters V_0, α, a, γ [11]).

With this form for V_{ij} we have

$$\langle e^{-bR^2}|e^{-ar_1^2}+e^{-ar_2^2}|e^{-bR^2}\rangle = \frac{\pi^{\frac{1}{2}}}{2(a+2b)^{\frac{3}{2}}}\exp\left(-\frac{2abr^2}{a+2b}\right) \tag{6}$$

and

$$\langle e^{-bR^2}|\mathbf{s}_1\cdot\mathbf{s}_2\, e^{-ar_1^2}+\mathbf{s}_1\cdot\mathbf{s}_3 e^{-ar_2^2}|e^{bR^2}\rangle = \frac{\pi^{\frac{1}{2}}\mathbf{s}_1\cdot\mathbf{s}_d}{4(a+2b)^{\frac{3}{2}}}\exp-\left(\frac{2abr^2}{a+2b}\right). \tag{7}$$

The exchange terms can be evaluated approximately by expanding $P_{ij}^{M} = \exp(i\pi\mathbf{r}_{ij}\times\mathbf{p}_{ij})/\hbar$ as a power series in $\mathbf{r}_{ij}\times\mathbf{p}_{ij}$ [12]), rewriting $\mathbf{r}_{ij}$ and $\mathbf{p}_{ij}$ in terms of $\mathbf{r}$ and $\mathbf{p}$ relative to the deuteron centre of mass, regrouping the terms, and neglecting terms in $\mathbf{R}\times\mathbf{P}$ higher than the first. Such terms contribute nothing at zero energy; at higher energies they are small owing to the spherical symmetry of the deuteron.

The result, valid at low energies, is

$$\langle e^{-bR^2}|P_{12}^{M}e^{-ar_1^2}+P_{13}^{M}e^{-ar_2^2}|e^{-bR^2}\rangle = \frac{\pi^{\frac{1}{2}}P_{1d}^{M}}{2(a+2b)^{\frac{3}{2}}}\exp\left[-\frac{2ab}{a+2b}r^2\right]. \tag{8}$$

The tensor terms can be evaluated by expanding

$$S_{12} = \frac{3}{r_1^2}(\mathbf{s}_1\cdot\mathbf{r}_1)(\mathbf{s}_2\cdot\mathbf{r}_1)-\mathbf{s}_1\cdot\mathbf{s}_2 \tag{9}$$

and noticing that the averages over $\mathbf{s}_2$ and $\mathbf{R}$ are independent. This gives

$$\langle e^{-bR^2}|S_{12}e^{-ar_1^2}+S_{13}e^{-ar_2^2}|e^{-bR^2}\rangle$$
$$= S_{1d}r^2\int_0^\infty \frac{R^2}{r^2+R^2}[e^{-a(r-R)^2}-e^{-a(r+R)^2}]e^{-2bR^2}\,dR \tag{10}$$

where S_{1d} has the same form as (9) with $\mathbf{s}_2$ replaced by the deuteron spin $\mathbf{s}_d$. The expression (10) is zero for $r = 0$, as would be expected from considerations of symmetry. For large $r \gg b$ it is

$$\frac{S_{1d}[\pi(a+2b)]^{\frac{1}{2}}}{4[(a+2b)^2+a^2]}\exp\left[-\frac{2abr^2}{a+2b}\right] \tag{10a}$$

and for small $r \ll b$ it is

$$\frac{S_{1d}\pi^{\frac{1}{2}}r^2}{2(a+2b)^{\frac{1}{2}}}\exp(-ar^2). \tag{10b}$$

For intermediate values of r, (10) must be integrated numerically.

The limit of a point deuteron ($b \to \infty$) is of interest; in this case we have at once

$$\langle\phi_d|S_{12}e^{-ar_1^2}+S_{13}e^{-ar_2^2}|\phi_d\rangle = S_{1d}e^{-ar^2}. \tag{10c}$$

3. Numerical Calculations

The effective neutron deuteron potential derived in the previous section contains non-zero matrix elements between the quartet and doublet states of the system, as well as between states of different angular momenta. Thus $\mathbf{S}^2$ is not a good quantum number in n—d collisions with tensor forces, in contrast to nucleon-nucleon scattering. Nevertheless we shall neglect terms leading to a change in channel spin; the remaining matrix elements of S_{1d} are then given by

$$
\begin{aligned}
S_{1d}\mathscr{Y}^M_{J,\frac{1}{2}} &= 0,\\
S_{1d}\mathscr{Y}^M_{J,J-\frac{1}{2},\frac{1}{2}} &= -[(2J-3)/4J]\mathscr{Y}^M_{J,J-\frac{1}{2},\frac{1}{2}}+\{3(2J-1)(2J+3)\}^{\frac{1}{2}}/4J\mathscr{Y}^M_{J,J+\frac{1}{2},\frac{1}{2}},\\
S_{1d}\mathscr{Y}^M_{J,J+\frac{1}{2},\frac{1}{2}} &= [(2J-3)/4J]\mathscr{Y}^M_{J,J+\frac{1}{2},\frac{1}{2}}+\{3(2J-1)(2J+3)\}^{\frac{1}{2}}/4J\mathscr{Y}^M_{J,J-\frac{1}{2},\frac{1}{2}} \qquad (11)\\
S_{1d}\mathscr{Y}^M_{J,J-\frac{1}{2},\frac{1}{2}} &= [(2J+5)/4(J+1)]\mathscr{Y}^M_{J,J-\frac{1}{2},\frac{1}{2}}+\{3(2J-1)(2J+3)\}^{\frac{1}{2}}/4(J+1)\mathscr{Y}^M_{J,J+\frac{1}{2},\frac{1}{2}},\\
S_{1d}\mathscr{Y}^M_{J,J+\frac{1}{2},\frac{1}{2}} &= -[(2J+5)/4(J+1)]\mathscr{Y}^M_{J,J+\frac{1}{2},\frac{1}{2}}+\{3(2J-1)(2J+3)\}^{\frac{1}{2}}/4(J+1)\mathscr{Y}^M_{J,J-\frac{1}{2},\frac{1}{2}},
\end{aligned}
$$

where $\mathscr{Y}^M_{J,l,s}$ is the usual normalized spin-angle function. Note that the nucleon spin operators used in the definition of S_{ij} differ in normalization from the Pauli spin matrices by a factor $\frac{1}{2}$.

The constants of the motion are then $\mathbf{S}^2$, J, π, and the doublet states of the system are single channel states; the Schrödinger equation for these can be integrated without trouble to give the (real) channel phase-shifts. The quartet states for $J \neq \frac{1}{2}$ are two-channel states in which channels with orbital angular momenta l and $l+2$, say, are coupled together. Two such channels are characterized by two real eigenphase-shifts ${}^4\delta_{\alpha J\pi}$ and ${}^4\delta_{\beta J\pi}$ and a mixture parameter ${}^4\varepsilon_{J\pi}$, in the notation of Blatt and Biedenharn [13,14]). We shall usually drop the suffixes J, π and the spin index. The functions $\cot\delta_\alpha$, $\cot\delta_\beta$ and $\tan\varepsilon$ can be expanded in terms of the wave-number k as follows [13,14]):

$$
\begin{aligned}
k^{2l+1}\cot\delta_\alpha &= [(2l+1)!!]^2/a_\alpha^{2l}\left[-\frac{1}{a_\alpha}+\tfrac{1}{2}r_\alpha k^2+\ldots\right],\\
k^{2l+5}\cot\delta_\beta &= [(2l+5)!!]^2/a_\beta^{2l+4}\left[-\frac{1}{a_\beta}+\tfrac{1}{2}r_\beta k^2+\ldots\right], \qquad (12)\\
\tan\varepsilon &= q_0k^2+q_1k^4+\ldots,
\end{aligned}
$$

and the coefficients $q_0, q_1, a_\alpha, a_\beta, r_\alpha, r_\beta$ can be calculated from a knowledge of the wave-functions at zero energy. The necessary relations are given in ref. [14]) for the state with $l = 0$, which is here the $J = \frac{3}{2}$, $\pi = +1$ quartet state.

The extension to states with $l \neq 0$ is straightforward; the results are

$$
\begin{aligned}
r_\alpha &= 2/a_\alpha^{2l+2}\int_0^\infty \{{}_0U_\alpha^{\infty 2} - {}_0U_\alpha{}^2 - {}_0W_\alpha{}^2 - a_\alpha^{4l+2}(2l+1)^{-2}r^{-2l}\}\mathrm{d}r,\\
r_\beta &= 2/a_\beta^{2l+6}\int_0^\infty \{{}_0U_\beta^{\infty 2} + {}_0W_\beta^{\infty 2} - {}_0U_\beta{}^2 - {}_0W_\beta{}^2 - a_\beta^{4l+10}(2l+)5^{-2}r^{-(2l+4)}\}\mathrm{d}r,\\
q_1 &= \frac{(2l+1)!!}{(2l+5)!!a_\alpha^{2l+1}}\int_0^\infty \{{}_0U_\alpha^\infty {}_0U_\beta^\infty + {}_0W_\alpha^\infty {}_0W_\beta^\infty - {}_0U_\alpha {}_0U_\beta - {}_0W_\alpha {}_0W_\beta\\
&\qquad - a_\alpha^{2l+1}a_\beta^{2l+5}(2l+3)(2l+5)^{-1}r^{-(2l+4)}q_0\}\mathrm{d}r;
\end{aligned}
\tag{13}
$$

${}_0U_\alpha$, ${}_0W_\alpha$ and ${}_0U_\beta$, ${}_0W_\beta$ are particular sets of solutions of the coupled equations for the state at zero energy. Their definitions, together with those of the other terms in (13) and the results for a_α, a_β and q_0 are given in refs. [13]) and [14]). The single channel states can be included uniformly with the two-channel states by defining for them a second phase-shift δ_β and a mixture parameter ε which are both identically zero; the eigenphase-shift δ_α is then the phase-shift for the channel as usually defined.

The parameter ${}^4a_{\alpha J\pi}$ for $J = \frac{3}{2}$, $\pi = +1$ is the quartet scattering length; and there is similarly a doublet scattering length ${}^2a_{\alpha\frac{1}{2}+}$. Experimentally these are not known uniquely, the two sets

$$
\begin{aligned}
&\text{(A)}\ {}^2a = (0.8\pm0.3)\times10^{-13}\ \text{cm}, \quad {}^4a = (8.3\pm0.3)\times10^{-13}\ \text{cm};\\
&\text{(B)}\ {}^2a = (6.2\pm0.1)\times10^{-13}\ \text{cm}, \quad {}^4a = (2.4\pm0.2)\times10^{-13}\ \text{cm}
\end{aligned}
\tag{14}
$$

both fitting the available data; and there has been some discussion theoretically as to which of these sets is correct [1,15–18]).

The scattering lengths ${}^2a$ and ${}^4a$ have been calculated numerically for nucleon-nucleon potentials of the form (5) of intrinsic ranges from 1.6 to 3.3×10^{-13} cm, and values of the deuteron distortion parameter β from 1 (no distortion) to ∞ (point deuteron). Note that the picture of the collision used does not allow values of β less than one for attractive potentials; the distorting neutron will always tend to compress the deuteron. It was not possible to get agreement with set (A) for any values of β and force constants. This is due to the very small doublet scattering length for this set, which corresponds to a partial well more than twice as deep as is required for the two-body data. Thus, set (A) may be ruled out. It was possible, however, to fit set (B) for all nucleon-nucleon potentials in the range tried; the calculated deuteron distortions are not very sensitive to this range, and are given in table 1 for representative nucleon intrinsic ranges. These results indicate that neglect of the distortion of the deuteron is a good approximation even at very low energies in the doublet state, but is not valid in the quartet state. The value 0.8 for β in the doublet state with intrinsic range 2.6×10^{-13} cm is probably not significantly different from 1; however, the results would seem to rule out a nucleon-nucleon force of range as long as 3.3×10^{-13} cm; such a range is already in disagreement with other data [11]).

To estimate the polarization of the neutron in the scattering, the elements of the scattering matrix have been calculated for neutron energies from 0 to 3.25 MeV assuming a nucleon-nucleon force with an intrinsic range of 2.6 $\times 10^{-13}$ cm and parameters

$$V_0 = 31.58 \text{ MeV}, \quad \alpha = 0, \quad \gamma = 3.93. \tag{15}$$

TABLE 1

Deuteron distortion parameter β

Nucleon-nucleon intrinsic range	β_d	β_q
1.6	1.05	1.9
2.6	0.8	2.13
3.3	0.67	2.08

A neutron distortion as given in table 1 was assumed, independent of energy. For the one-channel states the calculation is straightforward; for the two-channel states the effective n—d force has been replaced by a square well giving the same scattering lengths and the coupled equations integrated numerically at zero energy to give the first two terms in the expansions (12) of the δ_α, δ_β, ε. States up to $J = \frac{5}{2}$ have been included; the numerical results are given in table 2, together with those for the single-channel states.

TABLE 2

Expansion coefficients for the scattering matrix

S	J	π	$a_\alpha \times 10^{13}$	$a_\beta \times 10^{13}$	$r_\alpha \times 10^{13}$	$r_\beta \times 10^{13}$	$q_0 \times 10^{25}$	$q_1 \times 10^{50}$
$\frac{1}{2}$	$\frac{1}{2}$	+	7.52	0	2.28	0	0	0
$\frac{1}{2}$	$\frac{1}{2}$	−	0	0	0	0	0	0
$\frac{1}{2}$	$\frac{3}{2}$	+	4.21	0	0.772	0	0	0
$\frac{1}{2}$	$\frac{3}{2}$	−	0	0	0	0	0	0
$\frac{3}{2}$	$\frac{1}{2}$	+	−5.419	0	− 2.217	0	0	0
$\frac{3}{2}$	$\frac{1}{2}$	−	−0.767	0	−35.7	0	0	0
$\frac{3}{2}$	$\frac{3}{2}$	+	2.55	2.45	1.09	−1.33	0.0219	1.477
$\frac{3}{2}$	$\frac{3}{2}$	−	-9.78	2.62	−12.04	1.145	0.0663	0.000403
$\frac{3}{2}$	$\frac{5}{2}$	+	−4.73	2.41	− 0.351	−0.686	0.00399	0.0000195
$\frac{3}{2}$	$\frac{5}{2}$	−	−1.77	3.58	− 2.04	−0.857	0.114	0.986

These results have been used to calculate the angular distribution and polarization of the neutron over this range of energies. The angular distribution may be written

$$\mathrm{d}\sigma/\mathrm{d}\Omega = \sum_L a_L P_L (\cos\theta). \tag{16}$$

Figs. 1 to 4 give plots of $4\pi a_0 = \sigma_{tot}$, a_1/a_0, a_2/a_0 and a_3/a_0 against neutron energy in the laboratory system. The experimental points have been calculated from the experimental angular distributions [19–23]); the full line drawn through the experimental points for σ_{tot} is taken from ref. [24]), while for a_1/a_0, a_2/a_0 the smooth curve labelled "experimental" has been drawn through the experimental points by eye for comparison purposes. There is also plotted the theoretical results for a nucleon-nucleon force of the same intrinsic range but with no tensor force, i.e. $\gamma = 0$, which gives the same n–d scattering lengths; the amount of tensor force is not determined

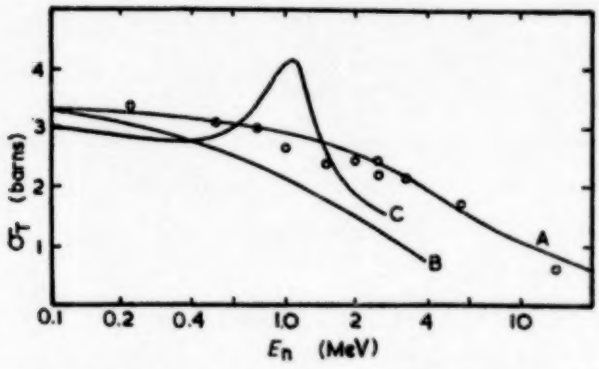

Fig. 1. A graph of the total n—d cross-section against neutron energy in the laboratory system.
Curve A: experimental from ref. [24]);
B: theory, no tensor force;
C: theory, including tensor force.
The open circles are experimental points from refs. [19–23]).

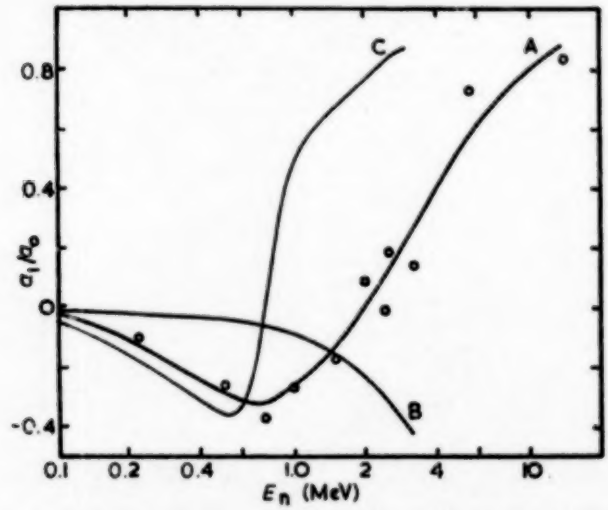

Fig. 2. A graph of a_1/a_0 against neutron energy in the laboratory system.
Curve A: experimental;
B: theory, no tensor force;
C: theory including tensor force.
The open circles are experimental points from refs. [19–23]).

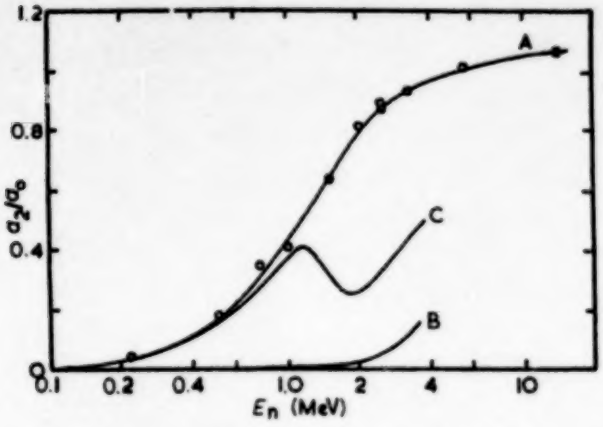

Fig. 3. A graph of a_2/a_0 against neutron energy in the laboratory system.
Curve A: experimental;
B: theory, no tensor force;
C: theory, including tensor force.
The open circles are experimental points from refs. [19–23]).

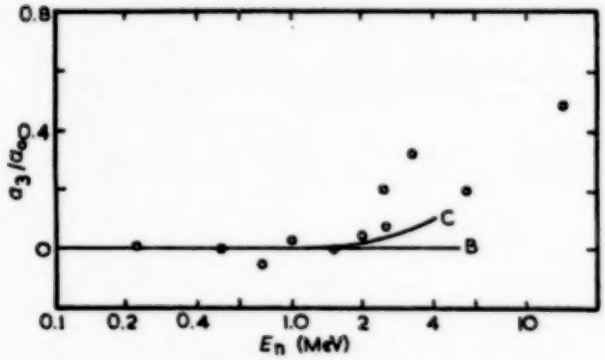

Fig. 4. A graph of a_3/a_0 against neutron energy in the laboratory system.
Curve B: theory, no tensor force;
C: theory, including tensor force.
The open circles are experimental points from refs. [19–23]).

uniquely by the two-body data but lies between $\gamma = 0$ and $\gamma = 3.93$ [11]).

Figs. 5 and 6 give angular distributions and the energy variation at 90° c.m. of the neutron polarization, measured along $\mathbf{r}_{\text{inc}} \times \mathbf{r}_{\text{scattered}}$. The variation with energy is rather rapid. Polarization measurements have been carried out by Brüllman *et al.* [25]) at 3 MeV, and by White, Chisholm and Brown [26]) in this laboratory at 2.26 and 3.1 MeV. The two results are not consistent, that of Brüllman being $(+3\pm6)$ % and that of White $(+48\pm5)$ % at 2.26 MeV and $(+40\pm20)$% at 3.1 MeV. Note figs. 5 and 6 differ from the results quoted in ref. [26]) owing to the correction of a numerical error.

A recent measurement at 2 MeV by Cranberg [28]) also indicates a small (< 7 %) polarization. Segel [27]) has carried out measurements of the

polarization of protons scattered from deuterium at 3 MeV, and obtained (-12 ± 7) %. The results of Brüllman and Segel are in agreement with the theoretical predictions; those of White *et al.* are not. The experiment is being repeated with neutrons in this laboratory†.

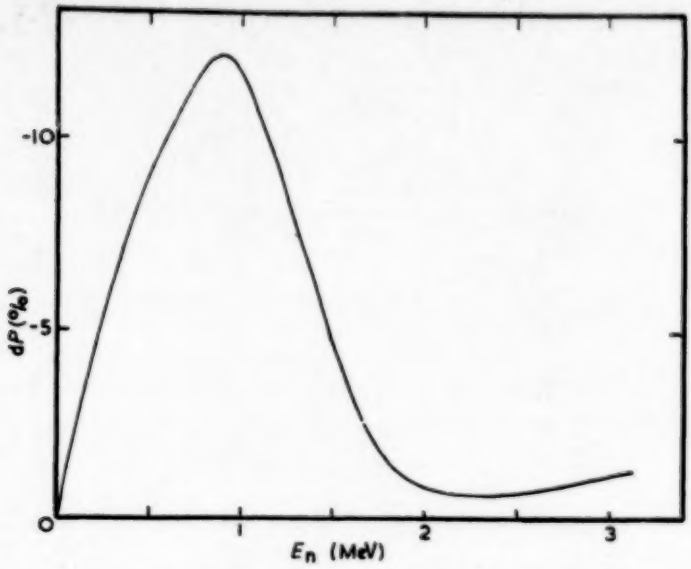

Fig. 5. A graph of neutron polarization at $\theta = 90°$ c.m., $\phi = 0$, against neutron energy in the laboratory system. The polarization is measured in the direction of $\mathbf{r}_{inc} \times \mathbf{r}_{scattered}$.

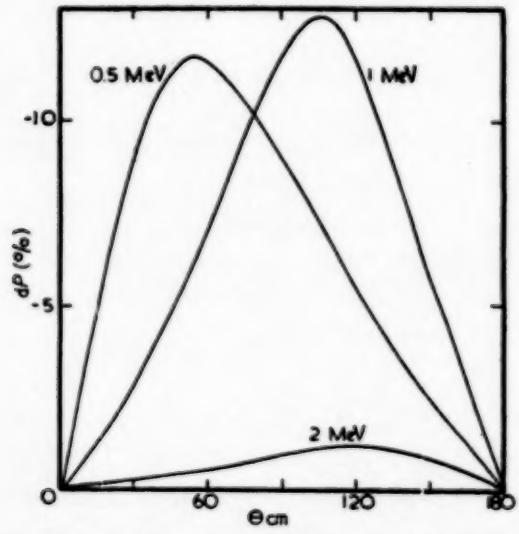

Fig. 6. Angular distributions of neutron polarization at $\phi = 0$.

The second spin moments of the recoil deuteron are plotted in fig. 7 at 3.25 MeV neutron lab energy. It is seen that the effects are large, but this does not seem a practicable way of preparing aligned deuterons owing to the low intensities available.

† *Note added in proof:* Brüllman *et al.* have recently [30]) remeasured the polarization at 53° c.m., obtaining $(+15\pm8)$ %.

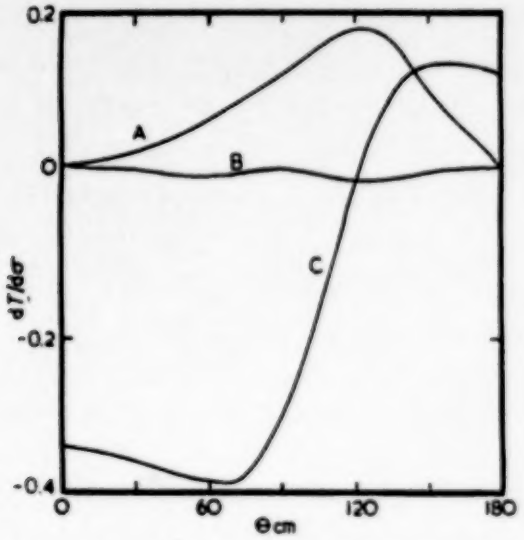

Fig. 7. A graph of the second order spin moments of the deuteron at 3.25 MeV neutron energy in the laboratory system. The z-axis is taken along the angle of scattering of the deuteron.
Curve A: $\langle T_2^1 \rangle / d\sigma$;
B: $\langle T_2^2 \rangle / d\sigma$;
C: $\langle T_2^0 \rangle / d\sigma$.

4. Discussion

The theory of n—d scattering with tensor forces presented here has been rather severely simplified. In fitting the distortion of the deuteron at zero energy to the observed scattering lengths we have neglected the effects of the Pauli principle, the coupling between the doublet and quartet states, and the D-state probability of the deuteron. The last effect is expected to be small for the energies we are interested in; the neutron will see only the gross structure of the deuteron.

At higher energies further simplifications have been made. The effective range expansion for the coupled channels is valid only so long as higher terms in the series are not important. For nucleon-nucleon collisions this is not until an energy of 10—15 MeV, but for n—d scattering they are already appreciable at less than 1 MeV. Above this energy the results become increasingly unreliable owing to this case. Moreover, we have implicitly assumed that the distortion of the deuteron is independent of energy and of angular momentum. This is unlikely to be so; the distortion is expected to tend to zero at high enough energies, and to do so more quickly with increasing angular momentum. Inclusion of this effect, and of momentum-dependent terms omitted from the Majorana exchange integrals, leads to an explicitly energy-dependent effective potential; it is then no longer valid to use effective range expansions in the form (12) [29]).

Nonetheless it would appear from the measure of agreement with experimental angular distributions that the most important features of the problem have been retained. In particular, the results for the angular distribution

show that in the absence of any tensor force the contributions from angular momenta greater than zero are far too small, while the nucleon-nucleon potential parameters (15) reproduce the observed curves of a_1/a_0 fairly well. The main discrepancy is in the prediction of too large an effective range parameter r_a for the quartet $J = \frac{3}{2}, \pi = -1$ state, giving an $l = 1$ resonance in the total cross-section and too sharp a rise in the curve for a_1/a_0.

Polarization calculations are more sensitive to changes in the scattering matrix, and the results shown are not expected to give more than a qualitative account of the polarization to be expected. The angular distribution of polarization is less sensitive than the total magnitude to small changes in the force parameters, and measurements for a range of angles and energies would be of great interest. It would also be of interest to repeat the calculations for a more realistic nucleon-nucleon potential, including a term of the type $\mathbf{L} \cdot \mathbf{S}$, and a repulsive core. A spin orbit force of this nature will not change the fit to the scattering lengths, but will contribute to the calculated asymmetry and polarization. Inclusion of a repulsive core on the other hand may change the calculated distortion significantly. The major contribution to the effective n—d potential comes from the region of the deuteron wave-function near the origin; with a repulsive core the wave-function is zero in this region. On the other hand the nucleon-nucleon potential is then much deeper outside the core to fit the two-body data. It is therefore likely that calculated distortions will be smaller than found with a smoothly varying potential, but the scattering matrix will be more sensitive to the distortion than with a smoothly varying potential such as that assumed here. The effect of distorting the deuteron is to make the equivalent n—d potential deeper and of a shorter range than for an undistorted deuteron; these two effects partially cancel.

5. Conclusions

The methods used give a reasonable account of the angular distribution and absolute cross-section of neutrons scattered from deuterium at low energies, and enable the scattering lengths to be determined uniquely. Neglect of the distortion of the deuteron by the neutron is a good approximation in the doublet state, but in the quartet state the deuteron is strongly distorted at low energies. The polarization of the neutron in the scattering is expected to be of the order of -2 % at 3 MeV.

References

1) R. A. Christian and J. L. Gammel, Phys. Rev. **91** (1953) 100
2) R. A. Buckingham and H. S. W. Massey, Proc. Roy. Soc. A **179** (1941) 123
3) R. A. Buckingham, S. J. Hubbard and H. S. W. Massey, Proc. Roy. Soc. A **211** (1952) 183

4) A. Werner, Nuclear Physics **1** (1956) 9
5) T. Y. Wu and J. Ashkin, Phys. Rev. **73** (1948) 973
6) B. H. Bransden, Proc. Roy. Soc. A **209** (1951) 380
7) B. H. Bransden, K. Smith and C. Tate, Proc. Roy. Soc. A **247** (1958) 73
8) L. C. Biedenharn and J. M. Blatt, Nuclear Physics **6** (1958) 359
9) J. L. Gammel and R. M. Thaler, Phys. Rev. **107** (1957) 1337
10) P. S. Signell and R. E. Marshak, Phys. Rev. **106** (1957) 832
11) J. M. Blatt and V. Weisskopf, Theoretical Nuclear Physics (J. Wiley and Sons, 1952) Chapters II and IV
12) J. Wheeler, Phys. Rev. **50** (1936) 643
13) J. M. Blatt and L. C. Biedenharn, Phys. Rev. **86** (1952) 399
14) L. C. Biedenharn and J. M. Blatt, Phys. Rev. **93** (1954) 1387
15) A. Troesche and M. Verde, Helv. Phys. Acta **24** (1951) 39
16) M. M. Gordon, Phys. Rev. **80** (1950) 111
17) F. G. Prohammer and T. A. Welton, Quarterly Report ORNL 1005
18) As. Davidov and G. T. Filippov, J.E.T.P. (USSR) **4** (1957) 267
19) R. K. Adair, A. Okazaki and M. Walt, Phys. Rev. **89** (1953) 1165
20) J. D. Seagrave, Phys. Rev. **97** (1955) 1757
21) J. C. Allred, A. H. Armstrong and L. Rosen, Phys. Rev. **91** (1953) 1165
22) J. D. Seagrave and L. Cranberg, Phys. Rev. **105** (1957) 1816
23) I. Hamouda and G. de Montmoullin, Helv. Phys. Acta **25** (1952) 107
24) D. J. Hughes and J. A. Harvey, Neutron Cross-sections BNL 325 (1955)
25) M. Brüllman, H. J. Gerber and D. Meier, Helv. Phys. Acta **31** (1958) 318
26) R. E. White, A. Chisholm and D. Brown, Nuclear Physics **7** (1958) 233
27) R. Segel, private communication
28) L. Cranberg, Bull. Am. Phys. Soc. **3** (1958) 365
29) L. M. Delves, Nuclear Physics **8** (1958) 358
30) M. Brüllman *et al.*, Helv. Phys. Acta **31** (1958) 580

4.C:7.C *Nuclear Physics* **11** (1959) 444—453; © *North-Holland Publishing Co., Amsterdam*
Not to be reproduced by photoprint or microfilm without written permission from the publisher

MESONIC "EXCHANGE" EFFECTS IN BETA-DECAY

R. J. BLIN-STOYLE and V. GUPTA
Clarendon Laboratory, Oxford, England
and
H. PRIMAKOFF
Washington University, St. Louis, U.S.A.

Received 11 March 1959

Abstract: An estimate is made, using no-recoil meson theory, of the π-mesonic exchange contributions to the beta-decay of nuclei assuming that such effects only contribute to the axial vector part of the beta-decay interaction. A few percent enhancement in the matrix element for the $H^3 \rightarrow He^3$ decay is obtained which is sufficient to account for the discrepancy between the decays of H^3 and n. A similar effect is found for heavier nuclei.

1. Introduction

It was recently pointed out by Bell and Blin-Stoyle [1]) that it is extremely difficult to give a consistent account of the beta-decay of nuclei having *LS*-closed cores plus or minus one particle within the framework of conventional beta-decay theory and with use of shell-model nuclear wave functions. Improvements of the nuclear wave functions seemed unlikely to rectify the inconsistencies and the situation was not relieved to any great extent by taking account of possible Fierz interference terms, relativistic effects or Coulomb effects. It was therefore concluded that the only way of resolving the inconsistencies was to appeal to mesonic effects of an "exchange" character. Since the publication of the above paper, however, more accurate values have been obtained for the *ft*-values [2]) for the decay of the neutron and H^3, namely $(ft)_n = 1180 \pm 35$ s and $(ft)_{H^3} = 1135 \pm 20$ s and these values are such that the inconsistencies are now no longer so striking. In particular, comparing theoretical predictions with the above *ft*-values we have for the V—A interaction

$$\varepsilon = \frac{\left[|M_F|^2 + \frac{g_A'^2}{g_V'^2}|M_{GT}|^2\right]_{H^3}}{\left[|M_F|^2 + \frac{g_A'^2}{g_V'^2}|M_{GT}|^2\right]_n} = \frac{1180 \pm 35}{1135 \pm 20} = 1.04 \pm 0.04 \qquad (1)$$

with an obvious notation. But $g_A'^2/g_V'^2 \approx 1.5$ with sufficient accuracy for our purposes, and $|M_F|_n^2$, $|M_{GT}|_n^2$, $|M_F|_{H^3}^2$, $|M_{GT}|_{H^3}$ are 1, 3, 1, 2.85 (Blatt [3])) respectively. Thus, according to ordinary theory, $\varepsilon = 0.96$ so that the

neutron-tritium discrepancy is $8\pm4\,\%$ which may not be significant. Nevertheless, it is still to be expected that many-body terms of mesonic exchange origin appear in the effective nucleon-lepton beta-decay interaction and it is the object of the present paper to make some estimate of the magnitude and form of these terms.

Mesonic effects for an isolated nucleon have been discussed by various authors [4–7]) and the indications are that, because of the interaction between the nucleon and pi-meson fields, the effective or renormalized beta-decay interaction for a physical nucleon differs from that for a bare nucleon. However, in order to retain the idea of a universal V—A Fermi interaction and to account for the agreement between the theoretical and experimental values for the half-lives of the muon and O^{14}, such renormalization (at least for the V-part of the interaction) appears undesirable. Thus, Feynman and Gell-Mann [8]) proposed a scheme whereby the polar vector interaction is, in the limit of zero momentum transfer, neither renormalized nor adjoined by many-body terms. This scheme is very satisfactory except that it now becomes difficult to understand the renormalized value (g'_A) of the axial vector coupling constant g_A. For example, the pion-nucleon interaction theory with neglect of nucleon recoil (no-recoil theory) predicts that $|g'_A| < |g_A|$, which, assuming that $|g_A| = |g_V| = |g'_V|$, contradicts experiment (which indicates that $|g'_A| \approx 1.25|g'_V|$). The explanation may lie in the (strong) interaction of the nucleon field with fields other than the pion [9]), or we may have here an example of the inadequacy of the no-recoil theory. Nevertheless, in spite of this unsatisfactory feature of the problem, it might still be expected that the no-recoil theory will give a fair description of the nature of mesonic exchange effects in beta-decay. Accordingly, a calculation is made on the basis of this theory, adopting the Feynman—Gell-Mann philosophy that such effects will appear only in the case of the axial vector interaction.

One final point has to be discussed before embarking on the calculation, namely that of taking over the no-recoil theory of Chew [10]) and Chew and Low [11]), which in its original form only dealt with problems involving a single static nucleon, to treat the case of two nucleons. This problem has, in fact, been discussed by Frantz [12]) and his work shows that a perturbation approximation of the usual kind can be used with the unrenormalized pion-nucleon coupling constant f_0 replaced by the corresponding renormalized coupling constant f. Further, since the nucleon-lepton vertex operator for the axial vector interaction behaves like $\boldsymbol{\sigma\tau}$, it can be treated in the same way as the pion-nucleon vertex operator. However, since the nucleon-lepton vertex operator does not contain an f_0, a factor f/f_0 will occur in transition matrix elements linear in this vertex operator. The quantity f/f_0 has been evaluated by Miyazawa [13]), who found $f/f_0 \approx 0.65$.

In using a perturbation expansion with the renormalized coupling constant we must, of course, not consider diagrams which just correspond to a modified vertex, since these are already included insofar as f rather than f_0 is used. However, in the following calculations it has been found more convenient to use the method of successive canonical transformations in order to obtain the effective beta-decay interaction Hamiltonian. In general this could lead to ambiguities since all diagrams are then included and the corresponding expansion should properly be in terms of f_0. In the present case, however, it transpires that there are no pion exchange contributions to the effective beta-decay interaction Hamiltonian which are second order in f_0 so that, carrying the calculation to fourth order, all vertex modifications to second order diagrams will also vanish. On the other hand there will be one pion exchange contributions from diagrams of the type illustrated in fig. 1 which appear in the final result for the effective beta-decay interaction Hamiltonian. Thus in this particular case it is perfectly consistent to use the canonical transformation method and to replace f_0 by f as in the perturbation expansion.

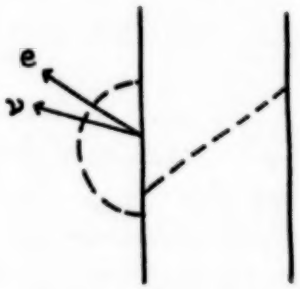

Fig. 1. Diagram for single pion exchange.

In section 2 the canonical transformation is briefly discussed. The deduction of the effective beta-decay interaction Hamiltonian is given in section 3 and application of the results to actual nuclei in section 4.

2. The Canonical Transformations

The total Hamiltonian $\mathscr{H}$ for the nucleon-pion-lepton systems is taken to be, remembering the discussion above, as

$$\mathscr{H} = H_\pi + H_{N\pi} + H_\beta \tag{2}$$

where

$$\begin{aligned} H_\pi &= \tfrac{1}{2}\sum_\alpha \int \mathrm{d}^3k\{p_\alpha(\mathbf{k})p_\alpha(-\mathbf{k}) + \omega_k^2 q_\alpha(\mathbf{k})q_\alpha(-\mathbf{k})\}, \\ H_{N\pi} &= \frac{i}{\pi\sqrt{2}}\frac{f}{\mu}\sum_{i,\alpha}\int \mathrm{d}^3k v(k)\tau_\alpha^{(i)} e^{i\mathbf{k}\cdot\mathbf{r}_i}(\boldsymbol{\sigma}^{(i)}\cdot\mathbf{k})q_\alpha(\mathbf{k}), \\ H_\beta &= g_A \sum_i \tau_\nu^{(i)}\boldsymbol{\sigma}^{(i)}\cdot\mathbf{L}(\mathbf{r}_i); \end{aligned} \tag{3}$$

H_π is the free field Hamiltonian for the pions, $H_{N\pi}$ is the Hamiltonian representing the pion-nucleon interaction and H_β represents the axial vector nucleon-lepton beta-decay interaction Hamiltonian. In equations (2) and (3) units of $\hbar = c = 1$ have been used and the following notation has been adopted:

$$q_\alpha(\mathbf{k}) = \sqrt{\frac{1}{2\omega_k}}\,(a_\alpha(\mathbf{k})+a_\alpha^*(-\mathbf{k})); \quad p_\alpha(\mathbf{k}) = i\sqrt{\tfrac{1}{2}\omega_k}(a_\alpha^*(\mathbf{k})-a_\alpha(-\mathbf{k})) \quad (4)$$

where $a_\alpha(\mathbf{k})$ and $a_\alpha^*(\mathbf{k})$ are annihilation and creation operators, respectively, for pions of momentum $\mathbf{k}$ and isobaric spin component α; $\omega_k = \sqrt{\mu^2+k^2}$, where μ is the mass of the pion; $v(k)$ is an appropriate cut-off function; $\tau_\alpha^{(i)}$ is the α^{th} component of the isobaric spin operator of the i^{th} nucleon and $\boldsymbol{\sigma}^{(i)}$ is the Pauli spin operator for the i^{th} nucleon; $\mathbf{L}(\mathbf{r}_i)$ is the lepton functional arising in a Gamow-Teller transition evaluated at the position of the i^{th} nucleon; g_A is the axial vector (unrenormalized) coupling constant for a bare nucleon.

In the original Schrödinger equation

$$\mathcal{H}\Psi = (H_\pi+H_{N\pi}+H_\beta)\Psi = i\hbar\frac{\partial\Psi}{\partial t}, \quad (5)$$

we treat H_β as a small perturbation and in the first instance we are concerned with the Hamiltonian $H = H_\pi+H_{N\pi}$. We now transform this Hamiltonian by a sequence of canonical transformations to remove non-diagonal parts with respect to the pion occupation numbers, each such transformation being characterized by a successively increasing power of f. The appropriate transformations have been given by Hatano and Kaneno [14]) and we are in agreement with their results. In their notation the successive transformations are denoted by $e^{iS_i}(i = 1, \cdots, 5)$ so that the transformed Hamiltonian finally obtained is $H' = U^\dagger HU$ where $U = e^{iS_1}e^{iS_2}e^{iS_3}e^{iS_4}e^{iS_5}$.

3. The Effective Beta-Decay Interaction Hamiltonian

The transformed Hamiltonian H' now contains coupling terms between the pion and nucleon fields that can contribute to beta-decay processes only to an order greater than f^4 and all such coupling terms are neglected in the following calculations. An eigenstate of the original Hamiltonian H can be written as $\Psi = U\Psi'$, where Ψ' is an eigenstate of H', and since, to the approximation just mentioned, H' has no pion-nucleon coupling terms, it follows that we can write $\Psi' = \Psi\phi_0$ where Ψ is a nuclear wave function involving only nucleon variables, and ϕ_0 is the pion vacuum state. It then follows that, treating H_β as a perturbation, a beta-decay transition matrix element between the states Ψ_1 and Ψ_f can be written

$$\begin{aligned}\langle\Psi_f|H_\beta|\Psi_1\rangle &= \langle\Psi'_f|U^\dagger H_\beta U|\Psi'_1\rangle \\ &= \langle\psi_f\phi_0|U^\dagger H_\beta U|\psi_1\phi_0\rangle \\ &= \langle\psi_f|H'_\beta|\psi_1\rangle\end{aligned} \quad (6)$$

where

$$H'_\beta = \langle\phi_0|U^\dagger H_\beta U|\phi_0\rangle$$
$$= H_\beta + \langle\phi_0|(U^\dagger-1)H_\beta + H_\beta(U-1) + (U^\dagger-1)H_\beta(U-1)|\phi_0\rangle. \tag{7}$$

Thus the transition matrix element appears as that of a transformed beta-decay interaction Hamiltonian involving only nucleon coordinates, H'_β, taken with respect to conventional nuclear wave functions. We call H'_β the *effective beta-decay interaction Hamiltonian.*

Expressing H'_β in terms of the S_i and retaining only those terms having the nature of two-body exchange operators, we find that only one term remains, namely $[iS_3, [iS_1, H_\beta]]$. It is then a straightforward but laborious matter to simplify the spin and isobaric spin dependence of this term and obtain the pion exchange contribution to the effective beta-decay interaction Hamiltonian in the case of an allowed (axial vector) transition:

$$H_\beta^{\text{exch.}} = g_A \sum_{i\neq j} \left\{ \left[g_I(r)\boldsymbol{\sigma}^{(i)}\times\boldsymbol{\sigma}^{(j)} + g_{II}(r)\frac{\mathbf{r}\cdot(\boldsymbol{\sigma}^{(i)}\times\boldsymbol{\sigma}^{(j)})\mathbf{r}}{r^2}\right](\boldsymbol{\tau}^{(i)}\times\boldsymbol{\tau}^{(j)})_v \right.$$
$$+ \left[h_I(r)(\boldsymbol{\sigma}^{(i)}-\boldsymbol{\sigma}^{(j)}) + h_{II}(r)\frac{\mathbf{r}\cdot(\boldsymbol{\sigma}^{(i)}-\boldsymbol{\sigma}^{(j)})\mathbf{r}}{r^2}\right](\tau_v^{(i)}-\tau_v^{(j)}) \tag{8}$$
$$\left. + \left[j_I(r)(\boldsymbol{\sigma}^{(i)}+\boldsymbol{\sigma}^{(j)}) + j_{II}(r)\frac{\mathbf{r}\cdot(\boldsymbol{\sigma}^{(i)}+\boldsymbol{\sigma}^{(j)})\mathbf{r}}{r^2}\right](\tau_v^{(i)}+\tau_v^{(j)}) \right\}$$

where

$$\begin{aligned}
g_I(r) &= -\tfrac{4}{3}\lambda M_6(2M_2+M_3)\\
g_{II}(r) &= \tfrac{4}{3}\lambda M_6(2M_2-M_3)\\
h_I(r) &= \tfrac{1}{2}\lambda(M_2M_4+M_3M_5+M_3M_4+\tfrac{8}{3}M_6M_3)\\
h_{II}(r) &= \tfrac{1}{2}\lambda(4M_5M_2-M_5M_3-M_2M_4-\tfrac{8}{3}M_6(2M_2-M_3))\\
j_I(r) &= -\tfrac{1}{2}\lambda(M_2M_4+M_3M_5+M_3M_4-\tfrac{8}{3}M_6M_3)\\
j_{II}(r) &= -\tfrac{1}{2}\lambda(4M_5M_2-M_5M_3-M_2M_4+\tfrac{8}{3}M_6(2M_2-M_3))
\end{aligned} \tag{9}$$

and

$$M_1 = 2\int_0^\infty \frac{k^3\,\mathrm{d}k v^2(k)}{(\mu^2+k^2)}\left(\frac{\sin kr}{k^2r^2}-\frac{\cos kr}{kr}\right)$$
$$M_2 = 2\int_0^\infty \frac{k^4\,\mathrm{d}k v^2(k)}{(\mu^2+k^2)}\left(\frac{\sin kr}{kr}+\frac{2\cos kr}{k^2r^2}-\frac{2\sin kr}{k^3r^3}\right)$$
$$M_3 = 4\int_0^\infty \frac{k^4\,\mathrm{d}k v^2(k)}{(\mu^2+k^2)}\left(\frac{\sin kr}{k^3r^3}-\frac{\cos kr}{k^2r^2}\right) \tag{10}$$
$$M_4 = -\frac{1}{2\mu}\frac{\partial M_3}{\partial\mu},\quad M_5 = -\frac{1}{2\mu}\frac{\partial M_2}{\partial\mu},\quad M_6 = \int_0^\infty \frac{k^4\,\mathrm{d}k v^2(k)}{(\mu^2+k^2)^2};$$
$$r \equiv r_{ij} \equiv |\mathbf{r}_i-\mathbf{r}_j|;\quad \lambda = \frac{f}{f_0}\frac{f^4}{\pi^2\mu^4}.$$

Apart from M_6 all of the above integrals are finite (provided convergence factors are introduced in the usual way) even if $v(k)$ is replaced by unity. They can therefore be evaluated exactly and an algebraic form for the radial dependence of $H_\beta^{\text{exch.}}$ can be obtained in this approximation. However, bearing in mind that the conventional procedure is to cut off the momentum at $k_{\max} \approx M$ (the nucleon mass), it follows that the explicit radial dependence obtained in the "no cut-off" approximation will not be reliable for small values of r. The forms obtained from eqs. (9), (10) for the functions g, h and j are as follows:

$$\begin{aligned}
g_{\mathrm{I}}(r) &= \tfrac{8}{3}f^4 \frac{f}{f_0}\left(\frac{1}{x}+\frac{1}{x^2}+\frac{1}{x^3}\right)\frac{M_6}{\pi\mu}\,\mathrm{e}^{-x} \\
g_{\mathrm{II}}(r) &= -\tfrac{8}{3}f^4 \frac{f}{f_0}\left(\frac{1}{x}+\frac{3}{x^2}+\frac{3}{x^3}\right)\frac{M_6}{\pi\mu}\,\mathrm{e}^{-x} \\
h_{\mathrm{I}}(r) &= -\tfrac{1}{2}f^4 \frac{f}{f_0}\left[\left(\frac{2}{x^2}+\frac{1}{x^3}\right)\mathrm{e}^{-2x} - \tfrac{16}{3}\frac{M_6}{\pi\mu}\left(\frac{1}{x^2}+\frac{1}{x^3}\right)\mathrm{e}^{-x}\right] \\
h_{\mathrm{II}}(r) &= \tfrac{1}{2}f^4 \frac{f}{f_0}\left[\frac{2}{x}+\frac{6}{x^2}+\frac{7}{x^3}+\frac{2}{x^4}\right]\mathrm{e}^{-2x} - g_{\mathrm{II}} \\
j_{\mathrm{I}}(r) &= \tfrac{1}{2}f^4 \frac{f}{f_0}\left[\left(\frac{2}{x^2}+\frac{1}{x^3}\right)\mathrm{e}^{-2x} + \tfrac{16}{3}\frac{M_6}{\pi\mu}\left(\frac{1}{x^2}+\frac{1}{x^3}\right)\mathrm{e}^{-x}\right] \\
j_{\mathrm{II}}(r) &= -\tfrac{1}{2}f^4 \frac{f}{f_0}\left[\frac{2}{x}+\frac{6}{x^2}+\frac{7}{x^3}+\frac{2}{x^4}\right]\mathrm{e}^{-2x} - g_{\mathrm{II}}
\end{aligned} \tag{11}$$

where, using a square cut-off,

$$M_6 = \mu\left[\frac{k_{\max}}{\mu} - \tfrac{3}{2}\tan^{-1}\left(\frac{k_{\max}}{\mu}\right) + \frac{(k_{\max}/\mu)}{2[(k_{\max}/\mu)^2+1]}\right] \tag{12}$$

and $x = \mu r$.

The functions g, h, j all diverge for $r = 0$; this is because no cut-off factor was used in evaluating $M_1 \cdots, M_5$. However, any nuclear wave funtions $\psi_{\mathrm{I}}, \psi_{\mathrm{f}}$ used in conjunction with $H_\beta^{\text{exch.}}$ should be eigenfunctions of the nuclear part of the transformed Hamiltonian H' which includes the no-recoil theory internucleon potential. Such an internucleon potential has been evaluated, for example, by Gartenhaus [15]), using $k_{\max} \approx M$ and is characterized by a strongly repulsive core of radius r_{c} lying between $0.5/\mu$ and $0.6/\mu$. This means that the nuclear wave functions vanish whenever two nucleons are closer than r_{c}. Thus there is no contribution to $\langle\psi_{\mathrm{f}}|H_\beta^{\text{exch.}}|\psi_{\mathrm{I}}\rangle$ from the divergent parts of $H_\beta^{\text{exch.}}$ and it is only necessary to know its form for $r > r_{\mathrm{c}}$ where the no cut-off approximation is more reliable. This point will be discussed further in the next section.

4. Applications

We now evaluate the contribution of $H_\beta^{\text{exch.}}$: (1) to the beta-decay of the triton, using a simple form for the H^3 and the He^3 wave functions; (2) to the decay of heavier nuclei of the type LS-closed core plus or minus one particle in the approximation that $H_\beta^{\text{exch.}}$ has zero range. The latter approximation is discussed in the paper by Bell and Blin-Stoyle [1]).

In the case of the triton we have to calculate the transition matrix element

$$M_A = \langle \psi_f | H'_\beta | \psi_i \rangle = \frac{g'_A}{g_A} \langle \psi_f | g_A \sum_{i=1}^{3} \tau_v^{(i)} \sigma^{(i)} | \psi_i \rangle + \langle \psi_f | H_\beta^{\text{exch.}} | \psi_i \rangle. \tag{13}$$

Here, in the first term, allowance has been made for the experimentally observed renormalization of g_A; also ψ_i and ψ_f represent the ground state wave functions for H^3 and He^3 respectively and $H_\beta^{\text{exch.}}$ is given by eqs. (8), (11), and (12). For ψ_i and ψ_f we take the expressions given by Villars [16]), namely:

$$\begin{aligned} \psi_i^{\pm} &= N(\phi_a^{\pm}\eta_b^{-} - \phi_b^{\pm}\eta_a^{-}) f_r(r_{12}, r_{13}, r_{23}) \\ \psi_f^{\pm} &= N(\phi_a^{\pm}\eta_b^{+} - \phi_b^{\pm}\eta_a^{+}) f_r(r_{12}, r_{13}, r_{23}) \end{aligned} \tag{14}$$

where N is a normalization factor and f_r is a radial function, which is assumed to have the form

$$f_r(r_{12}, r_{13}, r_{23}) = e^{-\frac{1}{2}\alpha(r_{12}^2 + r_{13}^2 + r_{23}^2)} p(r_{12}, r_{13}, r_{23}), \tag{15}$$

α denoting a size parameter and $p(r_{12}, r_{13}, r_{23})$ a correlation function which reflects the repulsive core nature of the internucleon potential, i.e.

$$p(r_{12}, r_{13}, r_{23}) = \begin{cases} 1 & \text{for } r_{12}, r_{13}, r_{23} > r_c \\ 0 & \text{otherwise.} \end{cases} \tag{16}$$

The $\phi_{a,b}^{\pm}$ are spin functions given by

$$\begin{aligned} \phi_a^{\pm} &= \frac{1}{\sqrt{2}} \chi_0(1, 2) \chi_{\pm}(3), \\ \phi_b^{\pm} &= \frac{1}{\sqrt{6}} \{\chi_0(2, 3)\chi_{\pm}(1) + \chi_0(1, 3)\chi_{\pm}(2)\}, \end{aligned} \tag{17}$$

where $\chi_0(i, j) = (\chi_+(i)\chi_-(j) - \chi_-(i)\chi_+(j))$; $\chi_{\pm}(i)$ is a spin function for the i^{th} nucleon and the plus and minus signs refer to the two possible spin orientations. Similarly, the isobaric spin functions $\eta_{a,b}^{\pm}$ are defined in a completely analogous manner to the spin functions $\phi_{a,b}^{\pm}$ with the functions $\chi_{\pm}(i)$ replaced by isobaric spin functions $\xi_{\pm}(i)$.

By the Wigner-Eckart theorem the form of the matrix elements between states corresponding to different initial and final nuclear spin orientations is determined purely from angular momentum considerations so that it is only necessary to calculate the matrix elements for one particular choice of these orientations. We therefore choose to calculate $\langle \psi_f^{+} | H_\beta^{\text{exch.}} | \psi_i^{+} \rangle$. Writing

$$M_A = \frac{g'_A}{g_A} \langle \psi_f^+ | g_A \sum_{i=1}^{3} \tau_v^{(i)} \sigma^{(i)} | \psi_i^+ \rangle [1+C], \tag{18}$$

where

$$C = \frac{g_A}{g'_A} \left[\langle \psi_f^+ | H_\beta^{\text{exch.}} | \psi_i^+ \rangle / \langle \psi_f^+ | g_A \sum_{i=1}^{3} \tau_v^{(i)} \sigma^{(i)} | \psi_i^+ \rangle \right], \tag{19}$$

shows that we can interpret C as a pion exchange correction factor to the usual Gamow-Teller transition matrix element. After some tedious evaluation of matrix elements of the spin and isobaric spin operators, we obtain

$$C = 16 \frac{g_A}{g'_A} |N|^2 \langle f_r | g_I(r_{12}) + \tfrac{1}{3} g_{II}(r_{12}) + h_I(r_{12}) + \tfrac{1}{3} h_{II}(r_{12}) | f_r \rangle \tag{20}$$

where the fact has been used that, because of the symmetry of f_r under the permutation of any two nucleons,

$$\langle f_r | g_I(r_{12}) | f_r \rangle = \langle f_r | g_I(r_{13}) | f_r \rangle = \langle f_r | g_I(r_{23}) | f_r \rangle$$

and similarly for h.

In the above expression for C two parameters appear, α and r_c. We investigate the value of C for two reasonable values of α, namely μ^2 and $\frac{3}{2}\mu^2$; it turns out that the results are not very sensitive to this parameter. On the other hand, the value of C depends critically on r_c. The values obtained for C for different values of r_c are shown in table 1. It is seen that corrections are

TABLE 1

Values of C and D for different values of r_c, and with $f^2 = 0.08$ and $h_{\max} = M$

μr_c	0.25	0.4	0.5	0.6	0.7
$C(\alpha = \mu^2)$	0.087	0.036	0.022	0.018	0.010
$C(\alpha = \frac{3}{2}\mu^2)$	0.072	0.031	0.020	0.013	0.009
D	0.33	0.026	0.023	0.021	0.020

obtained in the right direction and of the right order of magnitude to resolve the discrepancy discussed in section 1, viz. $\approx 4\,\%$ for $\mu r_c = 0.5$, remembering that the squares of transition matrix elements are involved in the evaluation of *ft*-values.

For heavier nuclei an estimate of the magnitude of the pion exchange effects can be made by using the procedure indicated in the paper by Bell and Blin-Stoyle [1]). There it is shown that for a nucleus of the type *LS*-closed core plus or minus one particle the pion exchange terms (in the zero range approximation) contribute an additional effective one-body operator given by

$$(H_\beta^{\text{exch.}})_{\text{one body}} = g_A [G_I + \tfrac{1}{3} G_{II} + H_I + \tfrac{1}{3} H_{II}] \rho(r) \sigma \tau_v \tag{21}$$

where $\rho(r)$ is the density of the core nucleons at the position r of the odd particle,

$$G_{\mathrm{I}} = 4\pi \int_{r_c}^{\infty} g_{\mathrm{I}}(r')(r')^2 \mathrm{d}r' \quad \text{etc.}, \tag{22}$$

and where it has again been assumed that because of the repulsive core in the internucleon potential there are contributions from $g_{\mathrm{I}}(r')$ etc. only for values of $r' > r_c$. Assuming a constant density $\rho = A/\frac{4}{3}\pi R^3$ for a nucleus of atomic number A and radius $R(R = r_0 A^{\frac{1}{3}}$ with $r_0 = 1.2\times 10^{-13}$ cm) we obtain $H'_\beta = g'_{\mathrm{A}}[1+D]\sigma\tau_\nu$ with

$$D = \frac{g_{\mathrm{A}}}{g'_{\mathrm{A}}}\frac{f}{f_0} f^4 \left[\left(\tfrac{1}{2}\mu r_c + \tfrac{1}{4} + \frac{1}{\mu r_c}\right)\mathrm{e}^{-2\mu r_c} + \frac{8}{3}\frac{M_6}{\pi\mu}(\mu r_c + 1)\mathrm{e}^{-\mu r_c}\right] \tag{23}$$

where M_6 is given by eq. (12) and D can again be interpreted as a pion exchange correction factor to the usual Gamow-Teller interaction Hamiltonian. The values obtained for D for different values of r_c are given in table 1. Again the corrections are such as to enhance the transition matrix element and are moreover of the same order of magnitude as for the triton decay.

5. Discussion

The foregoing calculations indicate that the small discrepancy between the *ft*-values for the neutron and the triton beta-decays can be resolved by appeal to pion exchange effects. However, a discrepancy still remains between the neutron decay data and the data for the decays of Ca^{39}, Sc^{41} and F^{17}, though not for O^{15}. These discrepancies are of the order of magnitude 5—10 % in the Gamow Teller matrix elements; or, if both the Gamow-Teller and the Fermi matrix elements are decreased by about the same proportion, a modification of 3—5 % in each is required. It is not unreasonable [1]) to suppose that modifications of this order of magnitude might arise from wave function "impurities," relativistic effects, etc.

Calculations aimed at deducing the one pion exchange contribution to $H_\beta^{\mathrm{exch.}}$ have also been carried out by Fujita *et al.*[17]) by relating the relevant diagram (fig. 1 gives the appropriate 4th order diagram) to the corresponding diagrams involved in the case of electromagnetic interactions and then using the dispersion-theory results of Kurobashi and Hara [18]). To fourth order the corresponding terms in our calculations are those $\propto M_6 \mathrm{e}^{-x}$ (eq. (11)). We are in agreement with the form of the results of Fujita *et al.* as far as the terms $\propto M_6 \mathrm{e}^{-x}$ appearing in h_{I}, h_{II}, j_{I} and j_{II} are concerned, but we disagree in the case of g_{I} and g_{II}. As a consequence, whereas our results give a small enhancement of the Gamow-Teller matrix elements, theirs give a reduction. In addition we have a further small enhancing contribution from two pion exchange terms ($\propto \mathrm{e}^{-2x}$: eq. (11)).

One of the authors (H.P.) wishes to thank the physicists at the Clarendon Laboratory for making his stay there a most interesting and enjoyable one and to acknowledge the support of the research programme at Washington University by the U.S.A.F. Research and Development Command.

References

1) J. S. Bell and R. J. Blin-Stoyle, Nuclear Physics **6** (1958) 87
2) Sosnovskii, Spivak, Prokofiev, Kutikov and Dobrinin, Jour. Exper. Theor. Phys. **35** (1958) 1059 (n);
F. T. Porter, Phys. Rev., to be published (H_1^3)
3) J. M. Blatt, Phys. Rev. **89** (1953) 86
4) R. J. Finkelstein and S. A. Moszkowski, Phys. Rev. **95** (1954) 1695
5) S. S. Gershtein and Ia. B. Zeldovich, Soviet Physics (J.E.T.P.) **2** (1956) 576
6) B. Stech, Z. Physik **145** (1956) 319
7) M. Ross, Phys. Rev. **104** (1956) 1736
8) R. P. Feynman and M. Gell-Mann, Phys. Rev. **109** (1958) 193
9) R. J. Blin-Stoyle, Nuovo Cimento **10** (1958) 132
10) G. F. Chew, Phys. Rev. **94** (1954) 1755
11) G. F. Chew and F. E. Low, Phys. Rev. **101** (1956) 1570, 1579
12) L. M. Frantz, Phys. Rev. **111** (1958) 346
13) H. Miyazawa, Phys. Rev. **101** (1956) 1564
14) S. Hatano and T. Kaneno, Prog. Theor. Phys. **15** (1956) 63
15) S. Gartenhaus, Phys. Rev. **100** (1955) 900
16) F. Villars, Helv. Phys. Acta **20** (1947) 476
17) J. Fujita, Z. Matumoto, E. Kurobashi and H. Miyazawa, Prog. Theor. Phys. **20** (1958) 308
18) E. Kurobashi and Y. Hara, Prog. Theor. Phys. **20** (1958) 163

1.D.2 *Nuclear Physics* **11** (1959) 454—458; © *North-Holland Publishing Co., Amsterdam*
Not to be reproduced by photoprint or microfilm without written permission from the publisher

ON THE DEFORMABILITY OF NUCLEAR CORES

ZDZISŁAW SZYMAŃSKI
University of Warsaw
and
Institute for Nuclear Research, Warsaw

Received 29 December 1958

Abstract: The self-consistent deformation of the nuclear core induced by an outside nucleon has been calculated. It is shown that this can account for the weak collective effects of heavy nuclei near closed shells.

1. Introduction

Nuclei which contain one single nucleon outside a doubly closed shell core are probably one of the best tests for the shell model. It is well known that the ground-state spins and the first few excited levels of such nuclei are in good agreement with shell model predictions. There are, however, some discrepancies [1]) even for such simple nuclei, which cannot be explained in the frame-work of the shell model. For instance the quadrupole moment of the O^{17} nucleus with single external neutron is large ($Q \approx -0.04 \times 10^{-24}$ cm^2) and its half-life is relatively low ($T_{\frac{1}{2}} \approx 2.5 \times 10^{-10}$ sec). Both these facts are incompatible with the shell model, if only simple configuration of one neutron moving in the spherical rigid potential well is introduced. Similar discrepancies were observed for several other nuclei of the kind mentioned above, for instance F^{17}, Pb^{207} etc. In order to explain these facts various additional assumptions were introduced, such as nucleon-surface coupling [2–4]), interconfigurational mixing [5–8]), or both these effects simultaneously [9]). Another explanation of the effects mentioned above is the assumption of deformability of the nuclear core by the external nucleon [1]). According to this assumption the contribution to the total mass-quadrupole moment is supplied not only by the single nucleon, but also by the core deformation induced by the orbital motion of the single nucleon. Let us assume that the core deformation is very weak, so that it can be treated as a perturbational parameter. For nuclei of this kind, we may hope that this is a good approximation. Then, writing the total mass-quadrupole moment in the form of a sum:

$$Q_M = Q_{core} + Q_p \qquad (1)$$

(where Q_p is the quadrupole moment of the odd particle), we may assume that

$$Q_{\text{core}} = \gamma Q_p. \tag{2}$$

The coefficient γ so defined may be called the deformability of the nuclear core.

The charge-quadrupole moment can then be expressed by the formula

$$Q_e = e_p Q_p + \frac{eZ}{A}\gamma Q_p,$$

where e_p denotes the charge of the last nucleon ($e_p = 0$ for a neutron, e for a proton). Thus the effect of the deformability of the core can be expressed by introducing the concept of the effective charge:

$$e_{\text{eff}} = e_p + \frac{eZ}{A}\gamma.$$

Assuming the nuclear potential in the harmonic oscillator form, it can be shown [1]) that the resulting deformability equals 1. Such a value corresponds well with the experimental data for light nuclei. For instance the effective charge for F^{17} and O^{17} is $\frac{3}{2}e$ and $\frac{1}{2}e$, respectively. For heavy nuclei, however, the value $\gamma = 1$ is not in agreement with experimental data. For example, in the neighbourhood of the Pb^{207} nucleus the effective charge which can be computed from the observed [10]) lifetimes is [9]) $e_{\text{eff}} \approx 1.15\, e$, which corresponds to the value

$$\gamma \approx 1.15 \frac{A}{Z} = 2.91. \tag{3}$$

This discrepancy, however, may be expected, for it is well known that the real nuclear potential is essentially different from the harmonic oscillator potential in the domain of heavy nuclei. The present paper is concerned with the calculation of the deformability γ when the other extreme, the square well potential, is assumed. Since the real potential is probably intermediate between the harmonic oscillator and the square well it may be presumed that the numerical values obtained for γ will be overestimated.

The problem of the deformability of the nuclear core may also have some relevance to the recent calculations on the influence of pairing interactions on the collective properties of nuclei [11]).

2. Calculations and Results

It is assumed that the nuclear core is deformed in a self-consistent manner, i.e. that the nuclear shape determined by the wave function coincides with the potential well shape. For weak spheroidal deformations it may be

hoped that the assumption of the infinite depth of the potential well and the neglect of nucleon spins will not effect too great a change on the results [12]).

The single-nucleon wave functions for the spheroidal infinite potential well can be obtained using the Moszkowski method [12]) of the transformation of the coordinate system ($\mathbf{r}$) into a new system ($\mathbf{r}'$) in such a way as to obtain a spherically symmetric potential. Then the perturbational part of the total hamiltonian is derived only from the kinetic energy and has the form

$$\frac{T_{20}(\mathbf{p}')}{m} d = \frac{d}{2m} (3p_z'^2 - \mathbf{p}'^2) \tag{4}$$

where the deformation parameter d is defined by the formula for the well shape

$$R = R_0(1+dP_2(\cos\theta)); \tag{5}$$

one has $d = \sqrt{5/4\pi}\beta$, where β is the deformation used by Bohr and Mottelson [13]). The deformation parameter d will be used as a parameter of expansion in the perturbation theory.

Let $\Phi_{nlm}(\mathbf{r})$ denote a complete set of wave functions for infinitely deep spherical square well. Then the wave function $\Psi_{(nlm)}(\mathbf{r}')$ of the spheroidal well can be developed in the neighbourhood of Φ_{nlm}:

$$\Psi_{(nlm)}(\mathbf{r}') = \Phi_{nlm}(\mathbf{r}') + d \sum_{n'l'} C_{n'l'} \Phi_{n'l'm}(\mathbf{r}') \tag{6}$$

where the coefficients

$$C_{n'l'} = - \frac{\left(\Phi_{n'l'm} \frac{T_{20}}{m} \Phi_{nlm}\right)}{E_{nl} - E_{n'l'}} \tag{7}$$

have been given by Moszkowski [12]).

Making use of the functions (6), the ratio $\langle r_{\|}^2 \rangle / \langle r_{\perp}^2 \rangle$ (where $r_{\|} = r\cos\theta$, $r_{\perp} = r\sin\theta\cos\varphi$) of the expectation values summed over closed shells plus the last odd nucleon may be calculated. This ratio may be made equal to the analogous ratio $R^2(\theta = \frac{1}{2}\pi)/R^2(\theta = 0)$ characterizing the shape of the well. The resulting self-consistent deformation is then

$$d = \frac{\frac{1}{2}Q_p}{\sum\limits_{\text{occ. shells}} \sum\limits_{n'l'} \{C_{n'l'}(\Phi_{nlm}(\mathbf{r}')|r_{\perp}'^2 - r_{\|}'^2|\Phi_{n'l'm}(\mathbf{r}')) + \text{c.c.}\}}. \tag{8}$$

If Q_{core} is calculated as the quantity $\langle (r_{\|}^2 - r_{\perp}^2) \rangle$ summed over occupied shells, we obtain for the deformability γ defined by the equation (2) the following expression (making use of (8)):

$$\gamma = 3 \frac{\sum\limits_{\text{occ. shells}} (\Phi_{nlm}(\mathbf{r}')|r_{\perp}'^2|\Phi_{nlm}(\mathbf{r}'))}{\sum\limits_{\text{occ. shells}} \sum\limits_{n'l'} \{C_{n'l'}(\Phi_{nlm}|r_{\perp}'^2 - r_{\|}'^2|\Phi_{n'l'm}) + \text{c.c.}\}} - 1. \tag{9}$$

It may easily be verified that this formula gives the value $\gamma = 1$ for the harmonic oscillator potential.

The vector addition rules of angular momenta lead to the familiar selection rule $l' = l \pm 2$. Furthermore we may hope that the intershell matrix elements (with $n \neq n$). can be neglected in comparison with the elements with $n' = n$. Indeed, for example, a numerical computation of the coupling (1d)—(2s) showed that the neglect of this term led to an error of less than 2 %. Making use of the explicit expressions for $C_{n'l'}$ (see ref. [12])) and summing over the closed shells according to standard methods (see for instance ref. [14])), a final expression for the deformability can be obtained in the form

$$\gamma = -1 + \frac{5}{12} \frac{\sum_{nl} (2l+1) \mathscr{R}_{nl}^{nl}}{\sum_{nl} \sum_{l'=l\pm 2} a_{l'} \frac{\omega_{nl}\omega_{nl'}}{(\omega_{nl}^2 - \omega_{nl'}^2)^2} \mathscr{R}_{nl}^{nl'}}, \tag{10}$$

where $\sum_{nl}$ denotes the sum over quantum numbers n, l for closed shells, ω_{nl} is an n-th node of $j_l(x)$, and the coefficients $a_{l'}$ are

$$a_{l'} = \begin{cases} -(l'+1)(l'+2) & \text{for } l' = l-2 \\ l'(l'-1) & \text{for } l' = l+2; \end{cases}$$

finally, the radial integrals are defined by the following expressions:

$$\mathscr{R}_{nl}^{n'l'} = (R_{nl} r^2 R_{n'l'}). \tag{11}$$

TABLE 1

Configuration	Number of particles in given shell	Total number of particles	γ
1s	4	4	5.26
1p	12	16	4.65
1d	20	36	4.14
2s	4	40	4.26
1f	28	68	3.93
2p	12	80	4.09
1g	36	116	3.85
2d	20	136	3.95
1h	44	180	3.63
3s	4	184	3.64
2f (neutrons only)	14	198	3.70
1i (neutrons only)	26	224	3.63
3p (neutrons only)	6	230	3.58

For the numerical estimation of the formula (10) the radial integrals were assumed to be all equal. In this case the results of the numerical computations are given in table 1.

3. Discussion

It is seen from table 1 that the deformability γ calculated for the square-well potential is larger than that for the harmonic oscillator; the latter is more resistant to deformation. The square-well deformability γ decreases on the average with increasing nucleon number. For heavy nuclei ($A \approx 200$) the calculated deformability γ (see table 1) is somewhat larger than the experimental value given by (3). This is connected with the fact that the real nuclear potential deviates from the pure square-well-shape.

The author wishes to express his sincere thanks to Dr B. Mottelson for suggesting this problem and for his many valuable remarks. He is also indebted to Dr D. Bès for a helpful discussion.

This calculation was partly carried out during the author's stay at the Summer School of Theoretical Physics in Les Houches and he takes this opportunity to acknowledge his gratitude to the School Board for making his stay possible.

References

1) B. Mottelson, Lectures on the collective motion of nuclei given at Les Houches (1958) (to be published)
2) F. C. Barker, Phil. Mag. **1** (1956) 329
3) W. W. True, Phys. Rev. **101** (1956) 1342
4) B. J. Raz, Phys. Rev. **107** (1957) 1201
5) M. A. Perks, Proc. Phys. Soc. A **68** (1955) 1083
6) H. Horie and A. Arima, Phys. Rev. **99** (1955) 778
7) R. D. Amado and R. J. Blin-Stoyle, Proc. Phys. Soc. A **70** (1957) 532
8) R. D. Amado, Phys. Rev. **108** (1957) 1462
9) W. W. True and K. Ford, Phys. Rev. **109** (1958) 1675
10) N. H. Lazar and E. D. Klema, Phys. Rev. **98** (1955) 710
11) S. T. Beliaew, Mat. Fys. Medd. Dan. Vid. Selsk. **31** (1959) no. 11
12) S. Moszkowski, Phys. Rev. **99** (1955) 803
13) A. Bohr and B. Mottelson, Mat. Fys. Medd. Dan. Vid. Selsk. **27** (1953) no. 16
14) E. V. Condon and G. H. Shortley, The Theory of Atomic Spectra (Cambridge, 1951)

7.A

Nuclear Physics **11** (1959) 459—465; © *North-Holland Publishing Co., Amsterdam*

Not to be reproduced by photoprint or microfilm without written permission from the publisher

SOME RESULTS ON ANALYTIC FUNCTIONS IN LOCAL FIELD THEORY

DANIEL J. KLEITMAN †

Institute for Theoretical Physics, Copenhagen

Received 17 February 1959

Abstract: Lorentz invariance, local commutativity, and the absence of negative mass states imply that the vacuum expectation value and the Fourier transform of the retarded commutator of a product of field operators are boundary values of analytic functions. The cases of four and five local scalar fields are investigated in the spirit of the approach of Källén and Wightman. It is shown that the domain of analyticity of the vacuum expectation value in x-space contains that of the retarded commutator in p-space. A computation of the real points of these domains is discussed in an appendix.

1. Introduction

Implications of the principles of Lorentz invariance, the existence of a lowest energy vacuum state, and local commutativity on the structure of general functions of field theory have lately been subject to considerable investigation [1,2]).

Källén and Wightman [1]) have determined the analyticity properties of three point vacuum expectation values and retarded commutators required by these general principles. They find that the first two requirements insure that the three-point vacuum expectation value can be continued to a function regular in a certain domain M_3 in scalar product space, while local commutativity leads to analyticity in a region containing the union of such domains formed with each of the various permutations of the three operators within the expectation value. They find the same analyticity region for the retarded commutator in terms of suitable momentum-space variables.

The present work is part [2]) of an attempt to generalize the results obtained by Källén and Wightman to more involved functions. It consists of an extension of their argument leading to analyticity in the union of permuted M-domains to the cases of products of four and five local fields, and a discussion of the properties of such regions both for vacuum expectation values and retarded commutators. The discussion indicates that the domain of analyticity in momentum space is contained in the corresponding position-space domain.

† National Science Foundation Postdoctoral Fellow.

In an appendix, a calculation of the real points of M_4, capable of being generalized to the case of M_5, is described.

2. The Position Space Function

We consider first the four-point vacuum expectation value P_{ABCD} which is defined according to

$$P_{ABCD}(x_2-x_1, x_3-x_2, x_4-x_3) = (0|A(x_1)B(x_2)C(x_3)D(x_4)|0). \quad (2.1)$$

That the vacuum state is the lowest energy state of the system requires that the Fourier transform of this expectation value vanishes outside the forward light cone, in the variables conjugate to x_2-x_1, x_3-x_2, and x_4-x_3.

Such behaviour of the Fourier transform is equivalent to the condition that the expectation value itself can be extended to a function of the scalar products of the $(x_{i+1}-x_i)$ which is regular within the domain M_{4ABCD} of points (z_{ij}) that are representable in the form

$$z_{ij} = -(x_{i+1}-x_i-i\eta_i)(x_{j+1}-x_j-i\eta_j), \quad (2.2)$$

where η_i are real four-vectors lying within the forward light cone.

Local commutativity of the operators A, B, C and D implies a set of equalities of the form

$$P_{ABCD}(x_2-x_1, x_3-x_2, x_4-x_3) = P_{BACD}(x_1-x_2, x_3-x_1, x_4-x_3) \quad (2.3)$$

which hold whenever the relevant arguments $(x_{i+1}-x_i)$ are real and space-like. If a six-dimensional manifold of scalar products corresponding to such sets of vectors lies in the interior of both M_{4ABCD} and M_{4BACD}, the equality (2.3) extends to the union of these two regions.

In four-dimensional space time, the set of points for which the vectors $(x_{i+1}-x_i)$ are real, space-like and further form a space-like hypersurface, give rise to scalar products that are interior to the domains M_4 for all permutations among the operators A, B, C, D. The four-point position space function is therefore analytic in the region U_{12}, the union of the M_4 formed domains with all permutations of A, B, C and D.

This region is symmetric among the four-vector variables x_1, x_2, x_3, and x_4, and has therefore the symmetry corresponding to the twenty four-element permutation group on four objects. Since six complex scalar products are required in the description of U_{12}, there is no choice of scalar product variables in terms of which the region is completely symmetrical.

In terms of vector arguments $x_{i+1}-x_i$ which we relabel as v_i, the twelve permutations appear as follows. The cyclic permutations give rise, in the definition (2.2) of the corresponding M_4, to the arguments

$$\begin{array}{lll} 1. & v_1, v_2, v_3 & (ABCD) \\ 2. & v_2, v_3, -v_1-v_2-v_3 & (BCDA) \\ 3. & v_1, v_3, -v_1-v_2-v_3 & (CDAB) \\ 4. & v_1, v_2, -v_1-v_2-v_3 & (DABC). \end{array} \tag{2.4}$$

The remaining permutations lead to arguments

$$\begin{array}{lll} 5. & v_1+v_2, -v_2, v_2+v_3 & (ACBD) \\ 6. & -v_2, v_2+v_3, -v_1-v_2-v_3 & (CBDA) \\ 7. & v_2+v_3, -v_1-v_2-v_3, v_1+v_2 & (BDAC) \\ 8. & -v_1-v_2-v_3, v_1+v_2, -v_2 & (DACB) \\ 9. & v_1, v_2+v_3, -v_3 & (ABDC) \\ 10. & v_2+v_3, -v_3, -v_1-v_2 & (BDCA) \\ 11. & -v_3, -v_1-v_2, v_1 & (DCAB) \\ 12. & -v_1-v_2, v_1, v_2+v_3 & (CABD). \end{array} \tag{2.5}$$

The forms of these permutations in terms of the (z_{ij}) may be obtained from this list by application of (2.2).

The union U_{12} displays symmetry under the group of permutations among the four vector elements

$$\begin{array}{l} 3v_1+2v_2+v_3 \\ -v_1+2v_2+v_3 \\ -v_1-2v_2+v_3 \\ -v_1-2v_2-3v_3. \end{array} \tag{2.6}$$

Three elements of this group, which suffice to generate it, are

$$\begin{array}{llll} 1. & v_1 \to -v_2-v_3, & v_2 \to v_2, & v_3 \to -v_1-v_2; \\ 2. & v_1 \to v_1, & v_2 \to v_2+v_3, & v_3 \to -v_3; \\ 3. & v_1 \to -v_1, & v_2 \to v_1+v_2, & v_3 \to v_3. \end{array} \tag{2.7}$$

In terms of scalar products z_{ij} these generating elements of the symmetry group of the union of permuted domains take the form

$$\begin{array}{lll} 1. & z_{11} \to z_{22}+z_{33}+2z_{23} & z_{12} \to -z_{23}-z_{22} \\ & z_{22} \to z_{22} & z_{13} \to -z_{12}-z_{22} \\ & z_{33} \to z_{11}+z_{22}+2z_{12} & z_{23} \to z_{22}+z_{13}+z_{12}+z_{23}; \\ 2. & z_{11} \to z_{11} & z_{12} \to z_{12}+z_{13} \\ & z_{22} \to z_{22}+z_{33}+2z_{23} & z_{13} \to -z_{13} \\ & z_{33} \to z_{33} & z_{23} \to -z_{23}-z_{33}; \\ 3. & z_{11} \to z_{11} & z_{12} \to -z_{11}-z_{12} \\ & z_{22} \to z_{11}+z_{22}+2z_{12} & z_{13} \to -z_{13} \\ & z_{33} \to z_{33} & z_{23} \to z_{13}+z_{23}. \end{array} \tag{2.8}$$

The five-point vacuum expectation value may be treated in a similar manner. There is, in that case, no longer a sufficiently large region in which the domains of analyticity overlap for all permutations of the operators (now A, B, C, D and E), and for which the corresponding vector arguments

can be chosen real and space-like. However, the permuted domains do all overlap together † and do overlap at least in pairs in five-dimensional regions corresponding to real space-like vector arguments, so that conclusions of the type deduced above for the four-point function again follow in this case.

3. The Retarded Commutator

The retarded commutator $R_4^{O_1;O_2O_3O_4}$ of four local field operators O_1, O_2, O_3, O_4, may be defined according to

$$R_4^{O_1;O_2O_3O_4} = \sum_{\substack{j,k,l=2\\ j\neq k\neq l\neq j}}^{4} \theta(x_1-x_j)\theta(x_j-x_k)\theta(x_k-x_l) \cdot \langle 0|[O_l(x_l),[O_k(x_k),[O_j(x_j)O_1(x_1),]]]|0\rangle \tag{3.1}$$

where we use the notation

$$\theta(x) = \tfrac{1}{2}(1+\varepsilon(x)) = \begin{cases} 0 & (x_0 < 0) \\ 1 & (x_0 > 0). \end{cases} \tag{3.2}$$

Such a function, by construction, vanishes unless x_1-x_2, x_1-x_3 and x_1-x_4 are all in the forward light cone. Its Fourier transform thus must be the boundary value of a function that is analytic in an M_4 domain whose arguments are the scalar products of the momentum variables conjugate to these.

In addition, the retarded commutator satisfies the following identity:

$$\begin{aligned}
R_4^{O_1;O_2O_3O_4} &= \tfrac{1}{8}\sum_{\substack{j,k,l,m=1\\ l\neq j\neq m\neq k}}^{4} \varepsilon(x_j-x_k)\varepsilon(x_k-x_l)\varepsilon(x_l-x_m)\langle 0|O_mO_lO_kO_j|0\rangle \\
&+ \tfrac{1}{8}\sum_{\substack{j,k,l,=2\\ k\neq j\neq l\neq k}}^{4} \varepsilon(x_1-x_j)[\varepsilon(x_k-x_l)\langle 0|[[O_l,O_k],[O_j,O_1]]|0\rangle \\
&\qquad +\varepsilon(x_j-x_k)\langle 0|[O_l,[O_k[O_j,O_1]]]|0\rangle] \\
&+ \tfrac{1}{8}\sum_{\substack{j,k,l=2\\ j\neq k\neq l\neq j}}^{4} \varepsilon(x_j-x_k)\langle 0|O_1\{O_k,O_j\}O_l+O_l\{O_k,O_j\}O_1 \\
&\qquad +[[O_l,O_1],\{O_j,O_k\}]|0\rangle \\
&+ \tfrac{1}{8}\sum_{\substack{j,k,l=2\\ j\neq k\neq l\neq j}}^{4} \varepsilon(x_1-x_j)\langle 0|\{\{O_k,O_l\},[O_j,O_1]\}+O_k[O_1,O_j]O_l|0\rangle \\
&+ \tfrac{1}{8}\sum_{\substack{j,k,l=2\\ j\neq k\neq l\neq j}}^{4} \langle 0|[O_l,[O_k,[O_j,O_1]]]|0\rangle \\
&+ \tfrac{1}{8}\varepsilon(x_2-x_4)\varepsilon(x_4-x_3)\langle 0|[O_1,[O_2,[O_3,O_4]]]|0\rangle \\
&+ \tfrac{1}{8}\varepsilon(x_2-x_3)\varepsilon(x_2-x_4)\langle 0|[O_1,[O_4,[O_3,O_2]]]|0\rangle \\
&- \tfrac{1}{8}\langle 0|[O_4,[O_3,[O_2,O_1]]]|+[O_2,[O_3,[O_4,O_1]]]|0\rangle.
\end{aligned} \tag{3.3}$$

† The domain M_8 would be the same as defined above if space were four-dimensional in a five-dimensional space time, that is, if an additional space axis were introduced. This follows from the characterization of the domains M_n given in the second appendix of ref. [1]). In five dimensions, all four vectors can be chosen real and on a space-like hypersurface. Their scalar products then trivially lie in the interior of all of the permuted domains of analyticity.

The first term on the right hand side of this equation is symmetric in the four operators O_1, O_2, O_3, O_4. The remaining terms vanish so long as the conjugate momenta and their sums and differences are all space-like, since by the nature of the mass spectrum all states of the system must have momenta within a light cone. The connection between the condition and its implication here can be seen from the following treatment of a typical term in (3.3).

We consider

$$I = \int e^{i(p_1(x_2-x_1)+p_2(x_3-x_1)+p_3(x_4-x_1))}\varepsilon(x_1-x_2)\varepsilon(x_3-x_4) \cdot \langle 0|O_1(x_1)O_2(x_2)O_3(x_3)O_4(x_4)|0\rangle (dx_1)(dx_2)(dx_3). \tag{3.4}$$

By Lorentz invariance, with $r_1 = x_2-x_1$, $r_2 = x_3-x_1$ and $r_3 = x_4-x_3$, we have

$$I = \int e^{i(p_1r_1+p_2r_2+p_3(r_3+r_3))}\,\varepsilon(r_1)\varepsilon(r_3)(dr_1)(dr_2)(dr_3) \cdot \langle 0|O_1(0)O_2(r_1)O_3(r_2)O_4(r_2+r_3)|0\rangle. \tag{3.5}$$

Upon expanding in terms of a complete set of intermediate states we obtain

$$\begin{aligned} I &= \sum_n \int e^{i(p_1r_1+p_2r_2+p_3(r_3+r_3))}(dr_1)(dr_2)(dr_3)\varepsilon(r_1)\varepsilon(r_3) \\ &\qquad \cdot \langle 0|O_1(0)O_2(r_1)|n\rangle\langle n|O_3(r_2)O_4(r_1+r_3)|0\rangle \\ &= \sum_n \Big[\int (dr_2)e^{ir_2(p_2+p_3-p_n)}\Big]\Big[\int (dr_1)(dr_3)\varepsilon(r_1)\varepsilon(r_3) \\ &\qquad \cdot \langle 0|O_1(0)O_2(r_1)|n\rangle\langle n|O_3(0)O_4(r_3)|0\rangle\Big]. \end{aligned} \tag{3.6}$$

This integral vanishes for p_2+p_3 space-like, since p_n must be time-like.

As a consequence of these remarks, the four retarded commutators $R^{O_1;O_2O_3O_4}$, $R^{O_2;O_1O_3O_4}$, $R^{O_3;\cdots}$ and $R^{O_4;\cdots}$, may be identified within their domains of analyticity so long as the interiors of these regions can be shown to overlap one another and the surface of points corresponding to real space-like vector arguments in a 6-dimensional region.

In terms of the vectors p_1, p_2 and p_3, conjugate to x_1-x_2, x_1-x_3, x_1-x_4, the corresponding variables that are related to R^{O_2}, R^{O_3} and R^{O_4} as these are to R^{O_1} take the form

$$\begin{aligned} &p_1, p_2, -p_1-p_2-p_3 \\ &p_2, p_3, -p_1-p_2-p_3 \\ &p_3, p_1, -p_1-p_2-p_3. \end{aligned} \tag{3.7}$$

These are precisely the permutations of vector arguments (2.4) that arise from cyclic permutation of the operators in the position-space function. Thus, the arguments described in the last section regarding questions of overlap for the position space function apply as well here.

The resulting "union of permuted domains" U_4 that is obtained in this

manner as the momentum space analyticity domain is, from (3.7), completely symmetric in the four vectors p_1, p_2, p_3 and $-p_1-p_2-p_3$.

The results of this section can be extended without modification, in principle, to the five-fold momentum space function.

From permutation of the real points of M_4 which are given in the appendix, one can show that there are real scalar products in the interior of the x-space domain of analyticity U_{12} that are not in the interior of U_4.

Thus U_{12}, the position space domain, is non-trivially larger than U_4; though this relationship need not be maintained between the holomorphy envelopes of these domains, at this stage the general principles here discussed involve more stringent requirements on the singularities of the vacuum expectation value than on those of the retarded commutator.

These remarks also may be extended to the expectation value and commutators of five local field operators — again in this case the position-space domain of analyticity is the wider one.

The work described in the appendix was performed in collaboration with N. Burgoyne.

I would like to thank Professor Källén for suggesting this investigation and for helpful comments during its progress, and Mr. N. Burgoyne for several stimulating conversations.

Finally, I would like to thank Professor Niels Bohr for the hospitality extended to me at this institute.

Appendix

THE REAL POINTS OF M_4.

Jost [3]) has shown that a set of $n-1$ real vectors gives rise to scalar products lying in the interior of M_n if, and only if, all linear combinations of these vectors with positive coefficients are space-like.

For two vectors, v_1 and v_2, this condition becomes

$$(v_1+\lambda v_2)^2 > 0 \tag{A.1}$$

for non-negative λ. In terms of scalar products (A.1) takes the form

$$z_1+2\lambda z_{12}+\lambda^2 z_2 < 0. \tag{A.2}$$

The parameter may be eliminated by elementary algebraic procedure. Jost's condition is then found to be equivalent to the inequality

$$z_{12}-\sqrt{z_1 z_2} < 0 \tag{A.3}$$

for M_3. The corresponding condition on M_4, that any linear combination of all three vectors with positive coefficients be space-like, may be replaced by the condition that any linear combination of two of the vectors should

form a Jost point in M_3 with the third. This condition may be written in any of the forms

$$\begin{aligned} &v_1(v_2+\lambda v_3)+\sqrt{v_1^2(v_2+\lambda v^3)^2}>0 \\ &v_2(v_1+\lambda v_3)+\sqrt{v_2^2(v_1+\lambda v_3)^2}>0 \\ &v_3(v_1+\lambda v_2)+\sqrt{v_3^2(v_1+\lambda v_2)^2}>0 \end{aligned} \tag{A.4}$$

for λ greater than zero. If two of the non-diagonal z_{ij} are less than zero, at least one of the equivalent scalar product inequalities

$$\begin{aligned} &z_{12}+\lambda z_{13}-\sqrt{z_1(z_2+2\lambda z_{23}+\lambda^2 z_3)}<0 \\ &z_{13}+\lambda z_{23}-\sqrt{z_3(z_1+2\lambda z_{12}+\lambda^2 z_2)}<0 \\ &z_{12}+\lambda z_{23}-\sqrt{z_2(z_1+\lambda z_{13}+\lambda^2 z_3)}<0 \end{aligned} \tag{A.5}$$

will hold trivially for all positive λ. Such points are therefore automatically Jost points.

If z_{12} and z_{13} are both greater than zero, (A.5a) may be rearranged and squared; it becomes

$$(z_1 z_2-z_{12}^2)+2\lambda(z_1 z_{23}-z_{12}z_{13})+\lambda^2(z_1 z_3-z_{13}^2)>0. \tag{A.6}$$

The parameter appearing in (A.6) may be eliminated. With the notation

$$A_{ij}=(-1)^{i+j}(z^{-1})_{ij}\det z \tag{A.7}$$

(A.6) becomes

$$A_{33}+2\lambda A_{23}+\lambda^2 A_{22}>0 \tag{A.6'}$$

or

$$A_{23}+\sqrt{A_{22}A_{33}}>0. \tag{A.8}$$

Thus, the real symmetric matrix (z_{ij}) is contained in the interior of M_4 if $z_{ii}<0$ for $i=1,2,3$ and one of the conditions below is satisfied:

$$\begin{aligned} &1.\quad \text{Two of } z_{12},\ z_{13},\ z_{23} \text{ are less than zero,} \\ &2.\quad z_{12},\ z_{23}>0, \qquad A_{13}+\sqrt{A_{11}A_{33}}>0, \\ &3.\quad z_{12},\ z_{13}>0, \qquad A_{23}+\sqrt{A_{22}A_{33}}>0, \\ &4.\quad z_{23},\ z_{13}>0, \qquad A_{12}+\sqrt{A_{11}A_{22}}>0. \end{aligned} \tag{A.9}$$

The procedure here used to obtain the real points of M_4 using condition (A.3) can be extended to M_5 through analogous use of (A.9).

The real points of U_4 and U_{12}, the domains of analyticity in momentum and position space implied by our general requirements, may be obtained directly from the conditions given here. Determination of the real points of the holomorphy envelopes of these domains, on the other hand, involve additional non-trivial steps.

References

1) Källén and Wightman, Dan. Vid. Selsk. Mat. Fys. Skr. **1** (1958) no. 6 (earlier references are given in this paper)
2) Källén and Wilhelmson, Dan. Vid. Selsk. Mat. Fys. Skr. **1** (1959) no. 9
3) R. Jost, Helv. Phys. Acta **30** (1958) 409

1.D.1:
3.A

Nuclear Physics **11** (1959) 466—474; © *North-Holland Publishing Co., Amsterdam*
Not to be reproduced by photoprint or microfilm without written permission from the publisher

ELECTRIC QUADRUPOLE ENHANCEMENT NEAR O^{16}

G. BARTON

Clarendon Laboratory, Oxford

Received 2 February 1959

Abstract: The core enhancement of E2 effects near O^{16} is calculated on the shell model with configuration mixing. The physical basis of the method is clarified by tracing its connection with Hartree-Fock theory and it is shown that it allows only for the static distortion of the core, but not for the genuine dynamic correlations between the odd particle and the core protons. The calculations cannot correlate, let alone explain the data, which are therefore interpreted as evidence for the importance of long range correlations in the nucleus.

1. Introduction

On the simplest version of the shell model, the electric multipole matrix elements between low-lying states in the odd-neutron nucleus O^{17} are zero. Experimentally, however, O^{17} is found to have a quadrupole moment [1]) of $(-2.65\pm0.3)f^2$ ($f = 10^{-13}$ cm) while the $2s_{\frac{1}{2}}$ to $1d_{\frac{5}{2}}$ (first excited to ground state) E2 reduced matrix element calculated from the observed lifetime [2]) is $(-2.6\pm1)f^2$. It is clear, therefore, that the odd particle is distorting the core; since only a small fractional distortion is indicated one may hope that a perturbation treatment will be adequate. Such calculations have been made on the Bohr-Mottelson collective model by Raz [3]) and on the shell model by Amado [4]).

The purpose of the present paper is to generalise the shell model calculation so that it can be extended to the mirror nucleus F^{17} and at the same time to investigate what physical effects this procedure allows for. We also reopen the question whether the parameters needed to fit the O^{17} data are in fact acceptable.

We shall consider in some detail the zero order wave functions entering the calculation, and also examine the basic nucleon-nucleon interaction used. Finally we report a parallel calculation performed with the Skyrme pseudopotential [5]). The results confirm those obtained with a conventional shell model interaction.

The preliminary conclusions published previously by the writer [6]) have been found to rest on a numerical error in a less compact form of calculation and are now revised.

2. The Zero-Order Wave Functions

We describe the O^{16} ground state by a single Slater determinant

$$\begin{aligned} \Psi &= \det \prod_i \psi_i, \\ \psi_i &= \phi_{nlm}(\mathbf{r}) \times (\text{spin function}) \times (\text{iso-spin function}). \end{aligned} \tag{1}$$

Our central simplification is to interpret the single particle functions $\phi_{nlm}(\mathbf{r}) = R_{nl}(r)Y_{lm}(\Omega)$ as solutions of the sixteen-body Hartree-Fock equations, while approximating in practice by using oscillator functions corresponding to a range parameter b and level spacing $\hbar\omega$, with

$$\hbar\omega = 13 \text{ MeV}, \qquad b^2 = \hbar/m\omega = (1.77f)^2. \tag{2}$$

These values are so chosen that the charge distribution given by Ψ fits the Stanford electron scattering data [7]) on O^{16}. The oscillator functions are a reasonable approximation only if they are already small at radial distances where the actual Hartree-Fock potential drops to zero; in view of the large separation energies calculated with these functions in O^{16} this condition will certainly be satisfied.

It is not at all obvious that one can use oscillator functions for the last particles in the $A = 17$ nuclei. These functions enter in two distinct ways: once for calculating the single proton (zero-order) matrix element in F^{17} and again in calculating the core contributions. Amado [4]) has examined in very great detail the latter types of expressions and finds that they, and their ratios even more, are insensitive to the range parameters of the single particle functions involved. Since we shall have one adjustable parameter prefacing these contributions in any case it is quite safe to evaluate them with oscillator functions for all seventeen particles.

Much greater care is of course necessary in calculating the F^{17} single particle 2s—1d radial matrix element (this being the only one of experimental interest). Using oscillator functions one gets the radial integral

$$\int_0^\infty R_{1d} R_{2s} r^4 dr = -9.9f^2.$$

Using functions calculated for a finite square well with the radius $3.4f$ suggested by the Stanford experiments, and with depth adjusted to give the observed separation energies for O^{17}, this is increased to $-11.7f^2$. Lastly, we have solved the radial equations for the two F^{17} states, using the observed separation energies and the same well radius as before, by the following numerical method: the equations are integrated inwards from a point chosen arbitrarily at $r =$ (11 well radii) to the well edge, in the Coulomb field of the core. Inside the well the Coulomb field is neglected and the depth adjusted to give smooth continuation across the edge. The functions thus obtained give a radial integral of $-10f^2$, practically the oscillator value. The decrease on

introducing the Coulomb repulsion happens to agree with the result obtained by treating it as a perturbation modifying the oscillator functions when, in first order, it again lowers the absolute value of the matrix element.

In view of these results we shall proceed to use the oscillator functions for calculating both the core and the zero-order single particle contributions.

3. Perturbation Method and Closure

Let $|0J\rangle$ denote the zero order Slater determinant with the odd particle in state $|J\rangle$. We use J, J' for the 1d and 2s orbits respectively. Let $V = \sum_{i>j} V_{ij}$ be the interaction energy and $U = \sum_i U_i$ the Hartree-Fock potential corresponding to O^{16} in its ground state. In the spirit of the last section $|J\rangle$ and $|J'\rangle$ are interpreted as solutions of the single-particle Schroedinger equation in this potential.

Working to first order in the perturbation $V-U$ no normalisation terms enter and we write the corrected function, denoted by $|\rangle_J$, as

$$|\rangle_J = |0J\rangle + \sum_{n\neq 0J}{}' |n\rangle \frac{\langle n|V-U|0J\rangle}{E_{0J}-E_n} \tag{3}$$

with a similar equation for $|\rangle_{J'}$. The energy difference $E_{0J}-E_{0J'}$ is negligible compared with the typical denominators in (3). Neglecting this difference we introduce a mean energy denominator E formally defined by

$$\begin{aligned} {}_{J'}\langle|Q|\rangle_J - \langle 0J'|Q|0J\rangle \\ = \frac{1}{E}\sum_n{}'\{\langle 0J'|V-U|n\rangle\langle n|Q|0J\rangle + \langle 0J'|Q|n\rangle\langle n|V-U|0J\rangle\}. \end{aligned} \tag{4}$$

Here Q is the electric quadrupole operator

$$Q = \sum_i \tfrac{1}{2}\{1+\tau_3(i)\} r_i^2 Y_{20}(\Omega_i).$$

Introduce the abbreviated notation

$$\langle aJ'|V_{12}|aJ\rangle = \int d\mathbf{q}_1 \int d\mathbf{q}_2 \psi_a^*(\mathbf{q}_1)\psi_{J'}^*(\mathbf{q}_2) V_{12} \psi_a(\mathbf{q}_1)\psi_J(\mathbf{q}_2) \tag{5}$$

where the $\mathbf{q}$'s contain spatial, spin, and iso-spin coordinates, and where the symbol standing first in the bra or ket denotes the orbit of the particle with coordinate labelled 1. Further, let

$$\langle aJ'|V'|aJ\rangle = \langle aJ'|V|aJ\rangle - \langle aJ'|V|Ja\rangle. \tag{6}$$

By using the definition of U,

$$\langle i|U|j\rangle = \sum_a \langle ai|V'|aj\rangle, \tag{7}$$

where the sum runs over all orbits occupied in the O^{16} core, we can express

the right hand side of (4) in terms of sums of integrals over single particle orbits. It becomes

$$\frac{1}{E}\sum_a \{\langle J'a|Q_2 V'_{12}+V'_{12}Q_2|Ja\rangle-2\langle a|Q|a\rangle\langle J'a|V'|Ja\rangle\} \tag{8}$$

with a parallel equation for the diagonal element. The summation is as in (7), and we have used the completeness property of the single particle functions.

For the two-body interaction we take first of all a conventional shell model expression

$$V_{12} = B\exp(-r^2/a^2)\{\alpha+\beta P^{\mathrm{M}}+\gamma P^{\sigma}+\delta P^{\mathrm{M}}P^{\sigma}\} \tag{9}$$

where [8]) $a = 1.9f$. Noting that

$$\begin{aligned} V'_{12} = V_{12}(1-P^{\sigma}P^{\mathrm{M}}P^{\tau}) = B\exp(-r^2/a^2)\{\alpha+\beta P^{\mathrm{M}}+\gamma P^{\sigma} \\ -\delta P^{\tau}-\alpha P^{\sigma}P^{\mathrm{M}}P^{\tau}-\beta P^{\sigma}P^{\tau}-\gamma P^{\mathrm{M}}P^{\tau}+\delta P^{\sigma}P^{\mathrm{M}}\} \end{aligned} \tag{10}$$

we perform the sums over the spin and iso-spin coordinates; the right hand side of (8) becomes

$$\frac{1}{E}\{\mathbf{A}\times(\text{direct})+\mathbf{B}\times(\text{exchange})\}$$

where the expressions (direct) and (exchange) now consist, respectively, of sums of direct and exchange integrals over the spatial coordinates only, and where the coefficients **A**, **B**, involving the exchange parameters, depend on whether the odd particle is a proton (**A**(p), **B**(p)) or a neutron (**A**(n), **B**(n)).

Thus,

$$\mathbf{A}(\mathrm{p}) = 2\alpha-\beta+\gamma-2\delta, \qquad \mathbf{B}(\mathrm{p}) = -\alpha+2\beta-2\gamma+\delta, \tag{11}$$

and

$$\mathbf{A}(\mathrm{n}) = 2\alpha+\gamma, \qquad \mathbf{B}(\mathrm{n}) = 2\beta+\delta. \tag{12}$$

On evaluating the spatial integrals it is found that for each matrix element the terms (direct) and (exchange) are equal to within 10 %. To this accuracy, then, our expressions are proportional to the coefficient

$$\mathbf{C} = \mathbf{A}+\mathbf{B}.$$

In table 1 we give the parameters of four exchange mixtures: the Rosenfeld mixture, used by Elliott and Flowers [9,10]), the simplified mixture used by Kurath [11]), the Serber mixture, and a mixture used with great success in the p-shell by Soper [12]). In table 2 we give the corresponding values of **A**, **B**, **C**, and of **C**(n)/**C**(p). Inspection of table 2 makes it clear that the enhancement is between 2 and 4 times greater for the odd neutron than for the odd proton. This differentiation is the most marked and the most interesting feature of

the present type of calculation; it is in sharp contrast to the prediction of the collective model which makes the two enhancements identically equal.

TABLE 1
Exchange Mixtures

	Rosenfeld	Simplified	Soper	Serber
α	$-\frac{2}{15}$	0	0.4	0.5
β	$\frac{14}{15}$	0.8	0.3	0.5
γ	$\frac{7}{15}$	0.2	0.2	0
δ	$-\frac{4}{15}$	0	0.1	0

TABLE 2
The coefficients A, B and C

	Rosenfeld	Simplified	Soper	Serber
$A(n) = 2\alpha+\gamma$	0.2	0.2	1.0	1.0
$B(n) = 2\beta+\delta$	1.6	1.6	0.7	1.0
$A(p) = 2\alpha-\beta+\gamma-2\delta$	−0.2	−0.6	0.5	0.5
$B(p) = -\alpha+2\beta-2\gamma+\delta$	0.8	1.2	−0.1	0.5
C(n)	1.8	1.8	1.7	2.0
C(p)	0.6	0.6	0.4	1.0
C(n)/C(p)	3	3	4	2

4. Comparison with the Data

Adjusting the value of B/E to reproduce the observed O^{17} quadrupole moment with the Serber mixture (cf. section 6) we find

$$B/E = 2.5.$$

Defining the additional charge η as

$$\eta = \{_J\langle|Q|\rangle_J - \langle J'|Q|J\rangle\}/\{(\langle J'|Q|J\rangle)_{\text{for proton}}\},$$

this leads to $\eta = 0.55$ and 0.27 for odd neutron and proton respectively in both 1d—1d and 2s—1d matrix elements. The single proton $2s_{\frac{1}{2}}-1d_{\frac{5}{2}}$ reduced matrix element is $-4/^2$ so that the predicted F^{17} matrix element is $(1.0+0.27)\times(-4/^2) = -5.1/^2$. Experimentally [13]) the extreme limits on the matrix element are

$$8.45/^2 \leqq |\langle||Q||\rangle| \leqq 11/^2.$$

Thus, although the odd-neutron data can be correlated by this type of calculation [4]) the odd-proton and odd-neutron results are in very definite disagreement. (Note that this disagreement would persist even if the calculated additional charges were the same, as on the collective model.)

5. Connection with Hartree-Fock Theory

In view of the strong disagreement noted above, we are led to enquire what physical effects our calculation includes. To find out, we must enumerate the types of admixture that occur in (3). Recalling the selection rules on two- and one-body operators (V and U, Q, respectively), we see that $|n\rangle$ can represent states with

(i) one core particle excited;

(ii) one core particle and the odd particle excited.

The definition of U precludes the excitation by $V-U$ of the odd particle alone.

States with two core particles excited also occur in (3), but then $|n\rangle$ and $|0J'\rangle$ differ by two occupation numbers and the matrix element $\langle 0J'|Q|n\rangle$ in (4) vanishes. Similarly, excitations of type (ii) contribute only if one of the excited states is the same as J'. Except for this special case (which because of the Pauli principle cannot occur in diagonal elements) the only contributions to η come from single excitations of the core which, essentially, amount to modifying the single-particle orbits in the core. But in principle the Hartree-Fock method would provide, for the *seventeen-body* problem, a Slater determinant into which the residual interaction $V-U_{17}$ does not mix any single-particle excitations, U_{17} being defined analogously to (7) but for the 17-body, not the 16-body core. U_{17} would not be spherically symmetric, whence the single particle orbits even of the first 16 particles would be automatically distorted, thus contributing to the E2 matrix elements.

Thus, the perturbation procedure is a first step taken to correct the deviation of our zero-order function from the 17-body Hartree-Fock solution. Because of the exceptional stability of the O^{16} core we are fairly confident that this first step does cover an appreciable portion of the distance. But even the true 17-body Hartree-Fock solution neglects all genuine dynamical correlations between the particles; a fortiori, therefore, these have been left completely out of account. Our inability to correlate the data merely points to the importance of such correlations in the nuclei considered.

6. The Mean Excitation Energy

The results of the last section certainly cast doubts on the relevance of fitting even the odd neutron data separately [4]) by a suitable adjustment of B/E. We therefore examine whether the value of B/E needed is theoretically

acceptable. The question has been considered by Amado [4]) whose arguments on this particular point have failed to convince the present writer. First we need a reliable estimate for B. Since we are concerned with the interaction of the odd nucleon with the core, it is reasonable to require that the value of B corresponding to a particular exchange mixture in (9) lead to the correct separation energy for the last particle. This requirement puts the Rosenfeld and simplified mixtures out of court since they would require $B = -134$ MeV and $B = -320$ MeV respectively. But since nowadays one no longer demands that the saturation property follow from the explicit appearance of the interaction (which must be interpreted as some kind of approximation to the t-matrix), we are at liberty to use, as we have done, the Serber and Soper mixtures which lead to -39 MeV and -44 MeV respectively, in good agreement with the values used in conventional shell model calculations. Adopting $B = -40$ MeV, B/E leads to

$$|E| = 16 \text{ MeV}.$$

We saw above that our perturbation expansion was made in terms of eigenstates of the Schroedinger equation with the self-consistent Hartree-Fock potential of the O^{16} ground state, whence the energy denominators are determined by the eigenvalues of this equation. In practice we approximated the low-lying solutions by the oscillator *functions*; but this does not imply that the oscillator *potential* has any relevance whatever to the highly excited states over which the perturbation series is taken.

What we require are the empirical energies of states that can be identified as containing a single odd particle moving in the field of the O^{16} core.

The low-lying positive parity levels of O^{16} are notorious teazers and will certainly not provide relevant information.

Rather discouraging information is derived from the giant resonance which in O^{16} centres around 25 MeV. This energy should on the shell model correspond to the excitation of one particle into the next orbit of opposite parity. Since we are looking for the energy difference between orbits of the same parity (selection rule on Q in (4)) we would expect $|E|$ to be higher still. However, Elliott and Flowers [10]) have calculated the positions of the 1^- levels; it appears from their results that once their mutual repulsion is allowed for, these would come to lie near 16 MeV, providing this as a rather lenient lower limit to $|E|$.

We note at this point that 16 MeV is close to the separation energy in O^{16} whence our single particle levels almost certainly will lie in the continuum. Now Baldinger *et al.* [14]) have in fact observed several resonances in the elastic scattering of neutrons on O^{16} at energies between 1.9 MeV ad 4.4 MeV; the presence of these resonances and their analysis makes it extremely plausible to look for $|E|$ in the corresponding region of 22 to 26 MeV, which makes the value of 16 MeV unacceptable.

7. The Skyrme Pseudo-Potential

We have noted above that the interaction V must be interpreted as an approximation to the t-matrix. Now Skyrme [5]) has proposed a pseudo-potential to be used in this sense, but incorporating more of the main features that the t-matrix is expected to possess, and has fitted its parameters empirically. The pseudo-potential has considerable success in correlating data in the p-shell. We have used it in a calculation exactly parallel to that carried out with the Gaussian above. The result for the 2s—1d additional charge is

$$\eta \text{ (neutron)} = 6.4 \text{ MeV}/|E|,$$
$$\eta \text{ (proton)} = 3.5 \text{ MeV}/|E|.$$

Again the additional charge is roughly twice as great for neutron as for proton; the value of $|E|$ required to fit the O^{17} data is even lower than before.

8. Short Range Correlations

We have estimated the effects of the short range correlations introduced into the nuclear wave function by the hard core in the internucleon potential, using the analytic approximation to the correlation function proposed by Amado [15]), and working to first order in the cluster expansion. The effect is of the order of 3 % and is therefore completely negligible. The writer is indebted to Dr. J. S. Bell for pointing out an error in the writer's original calculation of this effect.

9. Conclusions

It is impossible to correlate the odd neutron and odd proton data using only the static distortion of the O^{16} core by the odd particle. Furthermore this distortion cannot even account for the magnitude of either of the data considered separately. We conclude therefore that effects other than those taken into account by our calculation are important in determining E2 enhancement; in particular we suspect that genuine two-particle correlations contribute essentially.

This paper is based on a doctoral thesis currently submitted at Oxford. It is a great pleasure to thank Dr. R. J. Blin-Stoyle, under whose supervision the work was done, for his guidance. A maintenance grant from the Department of Scientific and Industrial Research is gratefully acknowledged.

References

1) Kamper, Lea and Lustig, Proc. Phys. Soc. B **70** (1957) 897
2) Thirion and Telegdi, Phys. Rev. **92** (1953) 1253
3) B. J. Raz, Phys. Rev. **107** (1957) 1201

4) R. Amado, Phys. Rev. **108** (1957) 1462; and Oxford thesis, unpublished
5) T. H. R. Skyrme, Nuclear Physics **9** (1959) 615
6) G. Barton, Nuclear Physics **6** (1958) 100
7) R. Hofstadter, Annual Review of Nuclear Science (1957)
8) L. Rosenfeld, Nuclear Forces (North Holland, 1948) p. 153
9) Elliott and Flowers, Proc. Roy. Soc. A **229** (1955) 536
10) Elliott and Flowers, Proc. Roy. Soc. A **242** (1957) 57
11) D. Kurath, Phys. Rev. **101** (1956) 216; and *ibid.* **106** (1957) 975
12) J. M. Soper, Phil. Mag. **2** (1957) 1219; cf. also report by B. H. Flowers in Proceedings of the Rehovoth Conference (1958)
13) Lehmann, Lévêque, Grjebine, Picou and Barloutaud, Compt. Rend. **245** (1957) 2259
14) Baldinger, Huber and Proctor, Helv. Phys. Acta **25** (1952) 142
15) R. Amado, Phys. Rev. **111** (1958) 548

7.A *Nuclear Physics* 11 (1959) 475—478; © *North-Holland Publishing Co., Amsterdam*
Not to be reproduced by photoprint or microfilm without written permission from the publisher

ON THE ORDERED-EXPONENTIAL SOLUTIONS FOR THE THIRRING MODEL

F. L. SCARF †
CERN, *Theoretical Study Division, Geneva*

Received 16 February 1959

Abstract: The explicit solutions for the Thirring model obtained by Glaser and Pradhan are shown to be equivalent when the latter is defined by a suitable limiting process. It is found that they lead to identical expressions for the wave function renormalization constant and for the invariant Green's functions.

Glaser has constructed an explicit solution [1]) for Thirring's spinor field theory [2]) ($\gamma^\mu \partial_\mu \psi + g(\bar{\psi}\psi)\psi = 0$, one space dimension) by expressing the bare particle operators ψ_τ ($\tau = 1, 2$) as explicit functionals of the incoming fields ϕ. He uses the identities $\rho_\tau = \psi_\tau^* \psi_\tau = \phi_\tau^* \phi_\tau$, and $\phi_1 = \phi_1(v)$, $\phi_2 = \phi_2(u)$, $u = x+t$, $v = x-t$. Then, if ϕ and ϕ^* obey conventional free field commutation relations,

$$\{\phi_\tau(a), \phi_{\tau'}^*(b)\} = \delta_{\tau\tau'}\delta(a-b), \qquad \{\phi_\tau(a), \phi_{\tau'}(b)\} = 0,$$

Glaser asserts that $[\rho_\tau(a), \rho_{\tau'}(b)] = 0$ everywhere. Accordingly, the ρ_τ are treated as c-numbers with respect to each other ($[\rho_\tau, \phi_{\tau'}]$ is not zero for $\tau = \tau'$) and ψ is constructed using the classical solutions of the equations of motion ($\psi_1 = \phi_1 \exp ig \int du\, \rho_2(u)$, etc.).

Recently, Pradhan [3]) has examined several features of the Glaser and Thirring solutions and has obtained results similar in many respects to Glaser's by treating the ρ_τ as operators. This study was motivated by the observation that

$$[\rho_2(u), \rho_2(u')] = \delta(u-u')\phi_2^*(u)\phi_2(u') - \delta(u-u')\phi_2^*(u')\phi_2(u), \qquad (1)$$

so that the commutator has an indeterminate form at $u = u'$. While this new technique is of interest, we wish to point out here that it is completely consistent to take the right hand side of eq. (1) equal to zero for *all* u, u'. This is so because all matrix elements of $[\rho, \rho]$ between physical states either vanish identically or are zero when defined by an appropriate limiting process.

† U.S. National Science Foundation Postdoctoral Fellow on leave from the University of Washington, Seattle, Washington.

Let $c_2(p)$ be the Fourier transform of $\phi_2(u)$. Then $c_2(p) = \theta(-p)a(p) + \theta(p)b^*(-p)$, and the physical vacuum has $a|0\rangle = b|0\rangle = 0$. States with N physical particles, N' antiparticles, are represented by $(a^*)^N(b^*)^{N'}|0\rangle$. If we examine

$$M_{N,N'} = \langle N|\phi_2^*(u)\phi_2(u')|N'\rangle = (2\pi)^{-1}\int dp \int dq e^{i(qu'-pu)}\langle N|c_2^*(p)c_2(q)|N'\rangle \tag{2}$$

we find that the most general matrix element is a sum of contributions of two distinct types. The first form resembles M with $|N'\rangle = a^*(K_1)|0\rangle$, $\langle N| = \langle 0|b(-K_2)$ and behaves like exp $(-iK_1u + iK_2u')$. Clearly, for these terms, $\delta(u-u')[M(u,u') - M(u',u)] = 0$ since $\delta(x)f(x) \equiv \delta(x)f(0)$ if $f(x)$ is regular.

The spatial dependence of the other terms is typified by that of $M_{0,0}$. This has $\langle 0|c_2^*(p)c_2(q)|0\rangle = \theta(p)\delta(p-q)$ and

$$M_{0,0}(u,u') = (2\pi)^{-1}\int_0^\infty dp\, e^{-ip(u-u')} = [2\pi i(u'-u-i\varepsilon)]^{-1}, \tag{3}$$

so that

$$\langle 0|[\rho_2(u), \rho_2(u')]|0\rangle = -i\delta(u-u')\mathrm{P}[1/\pi(u-u')]. \tag{4}$$

Using $x\delta(x) \equiv 0$, $x\delta'(x) + \delta(x) = 0$, Pradhan replaces the right hand side of eq. (4) by a δ' function. If this replacement were unique, it certainly would be wrong to treat the ρ_τ as c-numbers. However, it is necessary to note that the δ-function in (4) is *strictly* even about the point $u = u'$ (i.e., it is not $\lim_{\varepsilon\to 0}\delta(u-u'-\varepsilon)$) since it arises from the canonical commutation relations for ϕ, ϕ^*. Furthermore, eq. (4) contains the Cauchy principal value of x^{-1}, and $\mathrm{P}(x^{-1}) \equiv \lim_{\varepsilon\to 0} x/(x^2+\varepsilon^2)$. In other words, when $x = 0$, $\mathrm{P}(x^{-1}) = 0$, and $\delta(x)\mathrm{P}(x^{-1})$ should be set equal to zero, not to a δ' function. [There is actually no unique and rigorous specification for $\delta(x)\mathrm{P}(x^{-1})$. If one regards the quantity as a product of two distinct limiting sequences, then $\delta(x)\mathrm{P}(x^{-1}) = 0$; however, if one defines it using the limit of the products, then

$$\delta(x)\mathrm{P}(x^{-1}) = \lim_{\varepsilon\to 0}\frac{\varepsilon x}{(x^2+\varepsilon^2)^2},$$

which behaves like a δ' function. The formal result is ambiguous, but a choice may be made on the following grounds: $\int_{-\infty}^{\infty} du'[\rho_2(u), \rho_2(u')] = [\rho_2(u), Q_2] = 0$, for all u (Q_2 is a constant of the motion), and therefore $[\rho_2(u), \rho_2(u')]$ should be defined to be zero. In quantum electrodynamics an equivalent ambiguity concerning the integrability condition is resolved in the same way.] The result is seen more clearly if one imposes periodic boundary conditions, $\phi(0) = \phi(L)$. Then, eq. (4) becomes

$$\langle 0|[\rho_2(u), \rho_2(u')]|0\rangle = 2i\delta(u-u')L^{-1}\sum_{n>0}\sin[2\pi n(u-u')/L] \equiv 0. \tag{5}$$

Thus, we conclude that all matrix elements of $[\rho_\tau, \rho_{\tau'}]$ are zero, and that Glaser's solution is correct.

In view of the equivalence between the two methods, it is of interest to understand the assertion that the operator formalism and "c-number" technique give different values for $Z^{\frac{1}{2}}$, the wave function renormalization constant ($Z^{\frac{1}{2}} = \langle U_1 \rangle_0$ where $\psi_1(x, t) = \phi_1(v)U_1(u, -\infty)$). Pradhan's calculation of U_1 is based on the differential equation (ref. [3]), eqs. (47), (53)):

$$\frac{\partial U_1}{\partial c^*} = \sum_{p'} R_{pp'}[c^{(-)}(p')U_1 + U_1 c^{(+)}(p')]. \tag{6}$$

Although the general solution of eq. (6) is $U_1 = f_0(u)\overline{\mathrm{N}}\,[\exp \sum_{pp'} R_{pp'} c^*(p)c(p')]$ where $\overline{\mathrm{N}}$ means anti-ordered product, only the value $f_0(u) = 1$ was considered. However, since an unknown function $f_0(u)$ is actually contained in the expression, the value of $Z^{\frac{1}{2}}$ cannot be determined by simply taking expectation values of this solution. The renormalization constant must be computed by other means, such as Glaser's and identical results are obtained.

Another interesting point involves properties of the bare particle causal functions, such as

$$S_{12}^{(+)'}(x, t; x', t') = i\langle 0|\psi_1(x, t)\psi_1^*(x', t')|0\rangle = S_{12}^{(+)}(v - v')\langle 0|(U_1(u, u')|0\rangle. \tag{7}$$

Upon expanding Glaser's classical solution for $U_1(u, u')$, Pradhan was able to show that $\langle 0|U_1(u, u')|0\rangle = B(g)$, $u \neq u'$, and unity for $u = u'$. This is to be compared with the expression given by Thirring:

$$S_{12}^{(+)'}(x_i, x'_i) = \int_{-\infty}^{\infty} \mathrm{d}m\,[a(g)\delta(m) + b(g)|m|^{-1}]S_{12}^{(+)}(x_i, x'_i, m) \tag{8}$$

where expansion over intermediate states leads to $a(g) \approx 1$, $b(g) \approx g \tan \frac{1}{2}g/2\pi^2$ and second-order perturbation theory gives $a(g) \approx 1$, $b(g) \approx (g/2\pi)^2$. The integral in (8) may be evaluated using

$$S_{12}^{(+)}(x, t, m) = -\frac{2}{(2\pi)^2}[\gamma^\mu \partial_\mu + m]_{12}\mathrm{P}\int_{-\infty}^{\infty} \mathrm{d}k \int_0^{\infty} \mathrm{d}k_0 \frac{\varepsilon(t)\mathrm{e}^{i(kx - k_0 t)}}{k^2 + m^2 - k_0^2} \tag{9}$$

and one finds $S_{12}^{(+)'}(x, t) = S_{12}^{(+)}(v)[a(g) + b(g)I]$, $I = \mathrm{P}\int_0^\infty \mathrm{d}x/x(1-x)$. Thus, $S^{(+)'}$ is simply $S^{(+)}$ multiplied by an infinite constant. This conclusion is, in fact, rigorously true for the exact function; eq. (8) is merely a modified form of Lehmann's representation [4]), and $\rho(m) = a\delta(m) + b\varepsilon(m)m^{-1}$ is the most general function which has the dimension m^{-1} †. [There is no other length in the theory since g is dimensionless and the rest mass is zero. A contribution to $\rho(m)$ such as $c(g)m^{-1}$ is eliminated because it does not lead to the form $S_{12}^{(+)'} = S_{12}^{(+)}(v)f(u)$.] The same result may be established using covariance

† This fact was pointed out by W. Thirring (private communication).

arguments †; $\langle 0|U_1(u, u')|0\rangle$ must be an invariant function of $(u-u')$, and hence a constant ††.

The difference between Pradhan's value and the above (i.e. $\langle 0|U_1(u, u)|0\rangle = 1$ or ∞) is simply that the exact expression involves renormalized operators, $(\psi_r \psi_r^*)_R$, while Glaser's unordered classical solution describes unrenormalized fields. Thus, the two results should differ by an infinite multiplicative constant, $(Z\,Z^*)^{-\frac{1}{2}}$, and there is no discrepancy.

I am grateful to Professors V. Glaser and W. Thirring for valuable discussions. I also wish to thank Professor B. Ferretti and CERN for their hospitality.

References

1) V. Glaser, Nuovo Cimento **9** (1958) 990
2) W. Thirring, Ann. Phys. **9** (1958) 91
3) T. Pradhan, Nuclear Physics **9** (1958/59) 124
4) H. Lehmann, Nuovo Cimento **11** (1954) 342

† V. Glaser (private communication).

†† Both these arguments fail if a cut-off length is introduced in order to eliminate the infra-red divergence. We have carried out the exact calculation of $S^{(+)'}$ by ordering $\psi\psi^*$ so that matrix elements can be taken and a covariant cut-off inserted. An account of this work is in preparation.

10.D *Nuclear Physics* **11** (1959) 479—480; © *North-Holland Publishing Co., Amsterdam*

BOOK REVIEW

H. ETHERINGTON (Editor), *Nuclear engineering handbook* (McGraw Hill Book Co., New York-Toronto-London 1958. xv—1847 pages. £ 9.14.0)

The amount and variety of information laid down on these 1850 India paper pages are truly amazing. This handbook is not just a compilation of tables and recipes: it is a whole encyclopedia of nuclear engineering and its ancillary sciences in their theoretical and practical aspects. Random reading (more cannot be demanded of the reviewer of such a book) has conveyed a favourable impression of the conception and composition of the various sections; even for such eminent specialists as are the authors and editor, the selection of the material to be included and of the way in which to present it must have been an exacting job, which they appear to have mastered very successfully. The nuclear engineer sunbathing with this book in his hand may confidently declare: *omnia mea mecum porto.*

L. R.

Physics and heat technology of reactors (Supplement no. 1 of the Soviet Journal of Atomic Energy, Moscow 1958) (Consultants Bureau, New York 1958. v—174 pages. $ 22.50)

Translation of a collection of Russian papers. The offset printing of the formulae and diagrams is very clear; the solid binding and neat jacket are a great improvement in the presentation. The price is still much too high.

L. R.

P. M. ENDT and M. DEMEUR (Editors), *Nuclear Reactions*, Vol. I (North-Holland Publishing Co., Amsterdam, 1959. xii—502 p., Fl. 43)

The 1956 Amsterdam Conference on Nuclear Reactions demonstrated that there has been considerable recent progress in this field of nuclear physics. This book, a product of this meeting, might more appropriately be titled "Recent Advances in Nuclear Physics". Four of its ten chapters concern nuclear models.

Each chapter is written by a leading expert of the subject under discussion. As is to be expected when many authors contribute to a text, the presentations vary from excellent reviews of our knowledge to relatively poor ones. Overall, the articles are well written and make lively reading. This reviewer was particularly impressed by the summaries of R. J. Eden on the "Nucleus as a Many-Body System" and of J. H. Fremlin on "Heavy Ion Reactions". Both give exciting accounts of subjects still under development and make clear how much work remains to be done. A large part of the book is devoted to up-to-date summaries of resonance reactions (E. Vogt, H. E. Gove, K. J. Le Couteur, D. J. Hughes, and R. L. Zimmermann) and the detailed information that has been obtained from them. By contrast P. C. Gugelot's survey on nucleon and alpha-particle induced reaction experiments is the only chapter which touches on the direct reaction mechanism, and there is no detailed theoretical discussion of this subject. Perhaps this will appear in the second volume of the series.

The subject material of several of the articles has previously appeared in other texts. An example is A. K. Kerman's treatise on "Nuclear Rotational Motion", which, however, includes recent advances not described elsewhere. Further, J. P. Elliott and L. J. B. Goldfarb, who here write on the "Shell Model" and on "Angular Correlations and Polarizations" respectively, have contributed to similar articles in the new edition of the Handbuch der Physik. One might wonder whether it is advisable to have the same subjects expounded by the same authors in several books. Since the Handbuch is monetarily out of reach of most physicists, the coverage

of these articles in a standard-sized text does appear to this reviewer to be worth while. Furthermore, the emphasis here is not on completeness, but rather on a concise presentation of the present state of the art.

The book is primarily directed to the research worker and is obviously not meant to serve as a graduate student's first introduction to nuclear physics. However, it could be a useful supplement to a text such as Blatt and Weisskopf's.

In some instances inadequate editing is apparent, and whereas it may preserve some of the "personal flavour" (as stated in the Introduction) it does not add to the readability. In the Table of Contents, two chapter headings were interchanged. Aside from these minor criticisms, the high standard of most of the articles makes this work a valuable, but perhaps quickly outdated, addition to a researcher's library.

Ernest M. Henley

G. N. WALTON, *Glove Boxes and Shielded Cells* (Butterworths Scientific Publications, London, 1958. 473 pages. 95s.) (Academic Press Inc., New York, 1958. $ 6.80)

The book is a record of the Proceedings of the Symposium on Glove Box Design and Operation held in the Cockroft Hall, A. E. R. E., Harwell, on February 19th to 21 st, 1957.

The first Glove Box Symposium was held at Harwell in September 1951, and during the six years, experience in the use of glove-boxes has grown enormously. Also the number of people using these techniques has been steadily increasing in a large number of countries. The needs for a contemporary record of existing methods and techniques are therefore quite obvious.

In view of the growing use of glove-box techniques also when handling multicurie α, β, and γ-sources, the scope of the symposium has been extended to comprise heavily shielded cells. The future will call for glove-box handling of spontaneously fissile isotopes with new complications arising from protection against neutrons.

The papers are presented under 20 chapter headings, 12 dealing with Unshielded Boxes, the rest with Shielded Cells. Existing design and operation experience with unshielded boxes is most comprehensively treated, whereas the papers on shielded cells are of a more casual form. However, the editor has done an excellent job in arranging the papers so as to form an agreeable and readable whole.

The papers give not only a number of solutions to different problems in the handling of radioactive materials. They also give the reader, through a number of survey articles, an idea of how to choose the proper equipment for his own particular work. One of the commonest mistakes in this field is overelaboration of handling equipment — mistakes which are easily understood, but cost a lot of money.

Fortunately, much of the equipment is to-day commercially available, and in Appendix IV are listed names and addresses of firms manufacturing components described in the text. This is a good idea, but the list is, I am afraid, rather incomplete. However, buying glove-box equipment commercially is an immensely difficult and tedious job, and any help is heartily welcome.

Many useful references are found at the end of each chapter, and a thoroughly prepared index makes the whole work an invaluable reference book.

The book is neatly printed on white glossy paper (which shines a bit) and bound in the usual dark green binding.

K. Heydorn

2.D *Nuclear Physics* 11 (1959) 481—491; © *North-Holland Publishing Co., Amsterdam*
Not to be reproduced by photoprint or microfilm without written permission from the publisher

A STATISTICAL ANALYSIS OF EXCITED NUCLEAR STATES

TORLEIF ERICSON †
NORDITA (*Nordisk Institut for Teoretisk Atomfysik*), *Copenhagen*

Received 13 March 1959

Abstract: The many known excited states of some medium-weight nucleides are analysed in terms of the total number of states as a function of the excitation energy. Low-energy nuclear temperatures can be determined and are found to agree well with those obtained from evaporation spectra. There is a marked odd-even difference in the number of states of odd and even nuclei, appearing as a displacement of the curves with respect to each other by the pairing energy. Information on the spin distribution among the excited states is obtained and is related to a nuclear moment of inertia. The theoretical interpretation of the odd-even effect and a constant temperature is discussed in terms of an energy-gap model.

1. Introduction

The individual properties of excited nuclear states have been intensively studied for a number of years. It has always been recognized that the highly excited states seen in neutron or proton resonances can be analysed in terms of their statistical properties. However, at lower excitation the level spectra are now in many cases so well known and contain so many states that, parallel to the individual level analysis, a statistical analysis may be applied. At present, (pp′) and (dp) experiments permit the study of 50 to 100 levels in a single nucleus, and it should be possible to raise the number even further. Nuclear temperatures are ordinarily determined from evaporation spectra. We can now determine the temperatures directly and thus obtain a long-needed check on the evaporation temperatures. The fact that the data from the low-energy experiments can be directly connected with the neutron resonance data is very important in that it considerably extends the region in which the average spectrum can be studied. In this paper we shall present a method of analysing the data of nuclear level densities, with an application to some of the best-studied medium-weight nuclei. As we now study the real level density, it is easy to make a direct comparison between the level densities of different nuclei and investigate the influence of the individuality of the nuclei.

The level densities from neutron resonances refer to only a few spin states. Together with the total level density which we find here, the distribution of spins among the nuclear states is easily derived.

† On leave from the Institute for Theoretical Physics, Lund, Sweden.
Present address: Massachusetts Institute of Technology, Cambridge, Mass.

2. Method of Statistical Analysis

In the following we shall confine our statistical study to an analysis of the level density and spin distribution for particular nuclei. As we are dealing with the individual nuclear states, we shall obtain the level density $\tilde{\rho}(E)$ not as a smooth function of the excitation energy E, but rather as a sum of δ-functions, each corresponding to one state. A level density $\rho(E)$ which is a smooth function of energy is obtained by averaging over a suitable energy interval. The averaging is most easily performed on the step function $N(E)$, the total number of states with excitation energies less than E. For this function, the averaging is in practice obvious for $N(E) > 10$ (see figures), and in the following we shall assume it to have been carried out.

By plotting the quantity $\log N(E)$ as a function of E we can obtain a kind of nuclear temperature τ which is somewhat different from the ordinary nuclear temperature T defined by the level density †. We have the relations

$$\frac{\mathrm{d}}{\mathrm{d}E}\log N(E) = \frac{1}{\tau} = \frac{\rho(E)}{N(E)} \tag{1}$$

so that

$$N(E) = \tau\rho(E). \tag{2}$$

Therefore, if we know $\rho(E)$ and τ, we also know $N(E)$. This relation is important because it permits us to relate a level density determined from, say, neutron resonances to the known level-number curve $N(E)$ at lower energy, obtained directly from a knowledge of the nuclear states.

The temperature τ is related to the ordinary nuclear temperature T by

$$\frac{\mathrm{d}}{\mathrm{d}E}\log \rho(E) = \frac{1}{T} = \frac{1}{\tau}\left(1 - \frac{\mathrm{d}\tau}{\mathrm{d}E}\right). \tag{3}$$

It is well known that $\rho(E)$ has an essentially exponential behaviour. Therefore we expect the two temperatures to be nearly equal. If $N(E)$ depends upon the excitation energy like a pure exponential, they are indeed equal.

Though in principle we can determine $N(E)$ from a known level density $\rho(E)$ with the aid of eq. (2), the situation is usually complicated because only level densities for certain spin values and parities are known. We have therefore to correct for such effects before applying eq. (2). Theoretically, we expect on very general grounds that the density of states of definite parity and spin j can to a good approximation be expressed by

$$\rho_j(E) = (2j+1)\mathrm{e}^{-\frac{j(j+1)}{2\sigma^2}}\rho_0(E). \tag{4}$$

† Here and in the following we shall call $\{(\mathrm{d}/\mathrm{d}E)\log\rho(E)\}^{-1}$ the nuclear temperature T, as this is the quantity ordinarily determined by experiment.

This form of the spin distribution assumes only that the spins associated with the excited degrees of freedom are coupled at random. For further details we refer the reader to appendix A of ref. [1]). Thus, from the density of states of spin 0, $\rho_0(E)$, we obtain for the total level density $\rho(E)$ (with the assumption of an equal probability of either parity)

$$\begin{aligned}\rho(E) &= 2\rho_0(E)\times\sum_j (2j+1)\mathrm{e}^{-\frac{j(j+1)}{2\sigma^2}} \\ &\approx 4\rho_0(E)\times\int_0^\infty x\mathrm{e}^{-\frac{x^2}{2\sigma^2}}\,\mathrm{d}x = 4\sigma^2\rho_0(E).\end{aligned} \tag{5}$$

The dispersion σ is directly connected with the number n of spin-carrying elementary excitations through the relation

$$\sigma^2 = n\sigma_0^2, \tag{6}$$

where σ_0 is the spin dispersion for a single elementary excitation. A knowledge of the variation of σ^2 with energy is therefore equivalent to a knowledge of the variation of the number of elementary excitations with energy. We can always express σ in terms of a nuclear moment of inertia $\mathcal{I}$ by the relation

$$\sigma^2 = \frac{\mathcal{I}T}{\hbar^2}, \tag{7}$$

which formally indicates that a part $\hbar^2 j(j+1)/2\mathcal{I}$ of the excitation energy is used to rotate the nucleus. If the system has a classical analogue, we have, at sufficiently high excitation,

$$\mathcal{I} = \mathcal{I}_{\text{rigid}}. \tag{8}$$

This relation has been shown explicitly for certain models [2,3]).

Little is known about the actual value of σ. It is theoretically expected that the moment of inertia will be smaller than its rigid-body value as it approaches this limit at high excitation [4]). At low excitation, deviations in either direction can be expected. Angular distributions in compound nucleus processes in the iron region indicate a reduced moment of inertia [1,5]) (cf. also ref. [6])).

3. Examples

In the following we shall analyse experimental data from (pp') and (dp) reactions for the low-energy region and data from neutron resonances for the high-energy region according to the method outlined in the preceding section. Limitations of the analysis may be brought about by

1) selection rules which lead to such a weak population of some states that they are not observed;

2) finite resolution, which may lead to underestimation of $N(E)$ when

adjoining states are not resolved. This effect becomes increasingly important with increasing excitation.

A calculation of the l-values of the ingoing particles shows that levels with a wide range of spin values of both parities should be excited. For target nuclei of spin 0 or $\frac{1}{2}$ it is possible, however, that some high-spin states are not populated. That selection rules are unimportant is further confirmed by the fact that the same states are populated in both (pp') and (dp) reactions up to quite high excitations [7,8]).

The second limitation has a considerably greater influence. The number of unresolved levels is a function of the spacing between the levels. At present, up to 40—70 levels, with very few unresolved levels among them, can be assigned to a nucleide in the iron region.

The number of unresolved levels has been estimated from the resolution given in the experimental papers and is indicated in the figures by arrows. The values thus obtained are only approximate and must not be taken too literally.

The following analysis is chiefly based on the high-precision (dp)-measurements of the ONR-Generator group at MIT, level-densities from neutron resonances being also included when available.

For the calculation of the value of $N(E)$ corresponding to the neutron-resonance level density we have used the temperature τ from the $N(E)$-curve at lower energy. This extrapolation is justifiable because, whenever it has been possible to compare, τ has been found to agree closely with the temperatures from evaporation spectra, and furthermore, minor uncertainties in the temperature introduce only small changes in the calculated value for $N(E)$.

Because the quantity σ (which determines the cut-off for the distribution of spins) is practically unknown, we have marked in the figures the calculated number of levels corresponding to different values of σ.

3.1. Al^{28} AND S^{33}

Al^{28} (fig. 1). This nucleus has been studied by (dp)-reactions up to the neutron binding energy [9]). Up to 4.5 MeV, practically all levels should be resolved, but even at neutron binding energy about one half of the states seem to be observed according to fig. 1. In this nucleus, the neutron resonances have been very intensively studied by Hibdon [6]), who has resolved no less than 66 resonances in the first half MeV. We have determined the level density in the energy range 175 keV $< E_n <$ 375 keV for the incident neutron, where s, p and d waves give important contributions to the cross section. The spin $\frac{5}{2}$ of Al^{27} together with these l-values assures that most resonances in this energy range are excited. This is also clearly indicated by the value of $N(E)$ calculated from the level density with the use of the value

of the temperature determined at lower excitation. The level density has been determined over an appreciable energy region, and the local fluctu-

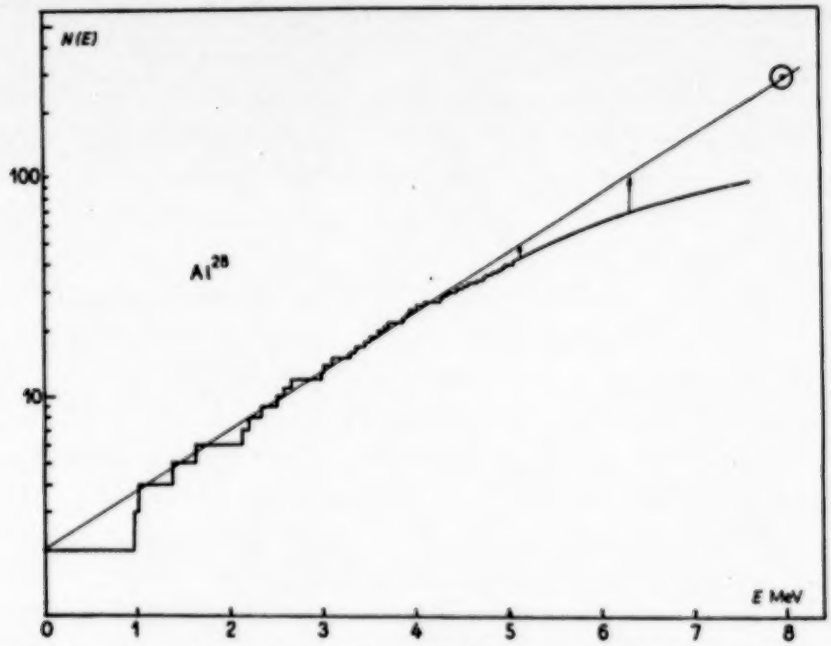

Fig. 1. The total number of states up to the excitation energy E in Al^{28} vs. E as obtained by (dp)-reaction [9]). The arrows indicate the number of unresolved levels estimated from the resolution. The point from the neutron-resonance level density [9]) has been calculated by means of eq. (2). The curve corresponds to a nuclear temperature τ of 1.6 MeV.

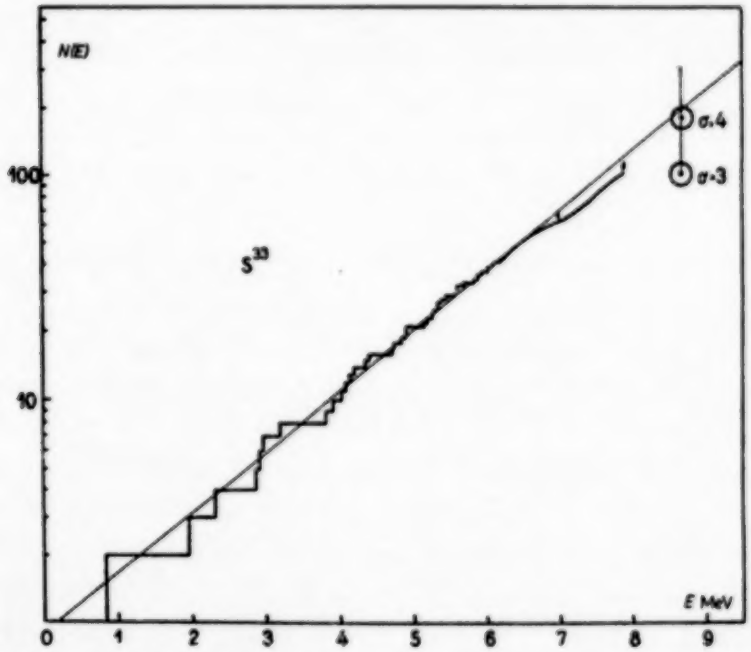

Fig. 2. The total number of states up to the excitation energy E in S^{33} vs. E as obtained by (dp)-reaction [10]). The arrows indicate the estimated number of unresolved levels. The point from the neutron-resonance level density [11]) has been calculated by means of eq. (2) with the spin distribution of eq. (4). Its value for two different σ and its estimated uncertainty are indicated. The curve corresponds to a nuclear temperature τ of 1.6 MeV and to σ 4.

ations in the temperature should therefore be negligible. Corrections to the calculated point for unresolved levels and for a temperature increasing with energy tend to increase its value but are probably negligible. This must therefore be considered independent confirmation that Hibdon observes most neutron resonances in this energy range for the incident neutrons. We can furthermore conclude that the nuclear temperature is practically constant up to about 8 MeV for this nucleus. This is also indicated by its high value, $\tau = 1.6$ MeV, in the low-energy part of the curve.

S^{33} (fig. 2). Also in the case of sulphur the levels have been studied by (dp)-reaction up to the neighbourhood of the neutron binding energy [10]). The neutron-resonance level density has been estimated from the three known s-wave resonances [11]), but the few resonances lead to a rather large uncertainty. The data are consistent with the curve obtained from the (dp)-reaction and give an approximately constant nuclear temperature of 1.6 MeV (equal to that for Al^{28}) and a value for σ of about 4. As in the case of Al^{28}, it would be of considerable interest to have also a study by (dp)-reaction of the neutron resonant states.

3.2. Mn AND Fe ISOTOPES

For the heavier nucleides now to be discussed, the present experimental resolution is not sufficient to study all the nuclear levels up to the neutron binding energy. Consequently, the directly determined part of the $N(E)$-curve and the point calculated from neutron resonances are separated by several MeV, and we must extrapolate over this region. It is fortunate that the nuclear temperatures from the evaporation spectra of α-particles have been very carefully studied in this region (Ni—Zn) [5, 12]).

The temperatures τ obtained below for Mn and Fe are 1.15—1.2 MeV, while the evaporation temperatures range from 0.94 to 1.16 MeV. The differences in the temperatures are of the order to be expected from the fact that different nuclei are studied and from the influence on the evaporation spectrum of the spin distribution among the excited states. We can therefore conclude that the temperature is nearly constant up to 10 MeV, and can also rather safely carry out the extrapolations.

Mn^{56} (fig. 3). The estimates of the number of unresolved levels are based on this nucleus. At 2.4 MeV excitation, there was an indication of a break in the $N(E)$-curve and an appreciable increase of the temperature [13]) to a value above that determined from α-particle evaporation [12]). This effect appeared just in the region where resolution effects should start to become important. A special investigation showed that this was indeed a resolution effect and that the true curve is in very good agreement with the expected curve [14]) †. The temperature is 1.15 MeV. The point at neutron binding energy is based on

† I am indebted to P. R. Christensen, O. Elbek and M. C. Olesen for these unpublished data.

6 resonances [15]) and indicates a value for σ of 4.5. This value is somewhat uncertain owing to a rather large uncertainty in the level density.

Fe^{57} (fig. 4). The $N(E)$-curve is obtained from (pp') and (dp) data [7,8]). The level density is based on 8 neutron resonances [16]). The temperature is 1.2 MeV, σ is approximately 3.7.

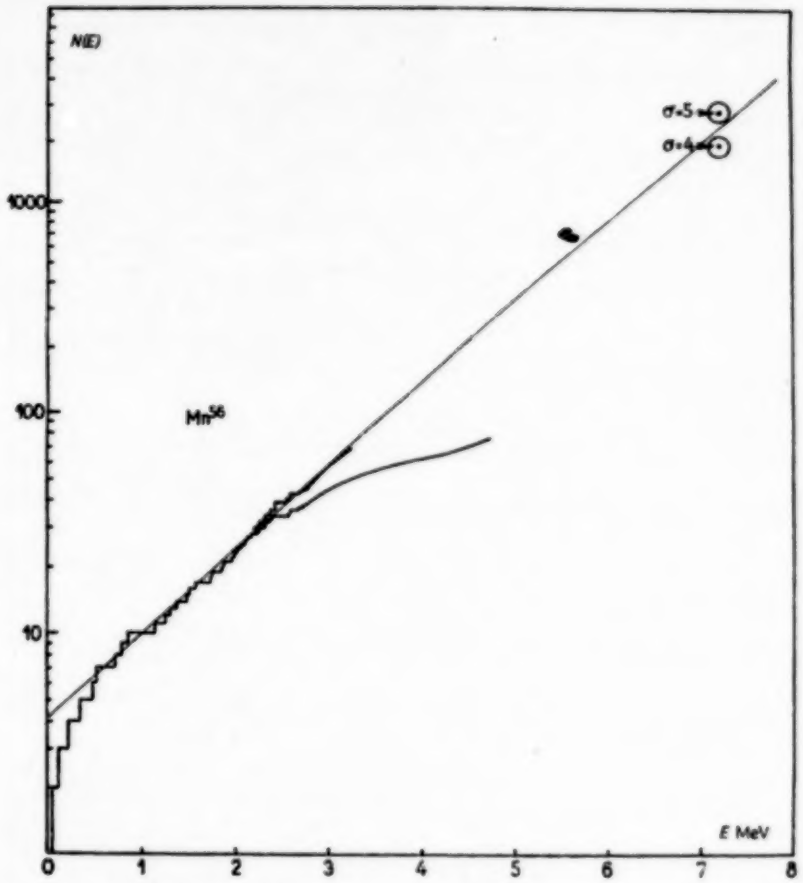

Fig. 3. The total number of states up to the excitation energy E in Mn^{56} vs. E as obtained from (dp)-reaction [13]). The higher curve for $2 < E < 3$ MeV has been obtained from a special investigation of the influence of the resolution [14]). The point from the neutron-resonance level density [15]) has been calculated by means of eq. (2) with the spin distribution of eq. (4). The curve corresponds to a nuclear temperature τ of 1.15 MeV and to σ 4.5.

Mn^{56}, Fe^{55}, Fe^{57}, Fe^{58} (fig. 5). We have plotted the $N(E)$-curves for these nuclei in the same figure in order to compare even, odd, and odd-mass nuclei. The difference is striking. For $N(E) > 10$ we obtain three groups of rather parallel curves, displaced with respect to each other by roughly 1 MeV. The energy difference between the extreme curves, 2.2 MeV, is quite close to the pairing energy for these nuclei.

4. Discussion

The analysis of the preceding section brings up several interesting properties of the nuclear level density in the low-energy region.

The outstanding feature is the displacement of the curves for odd and

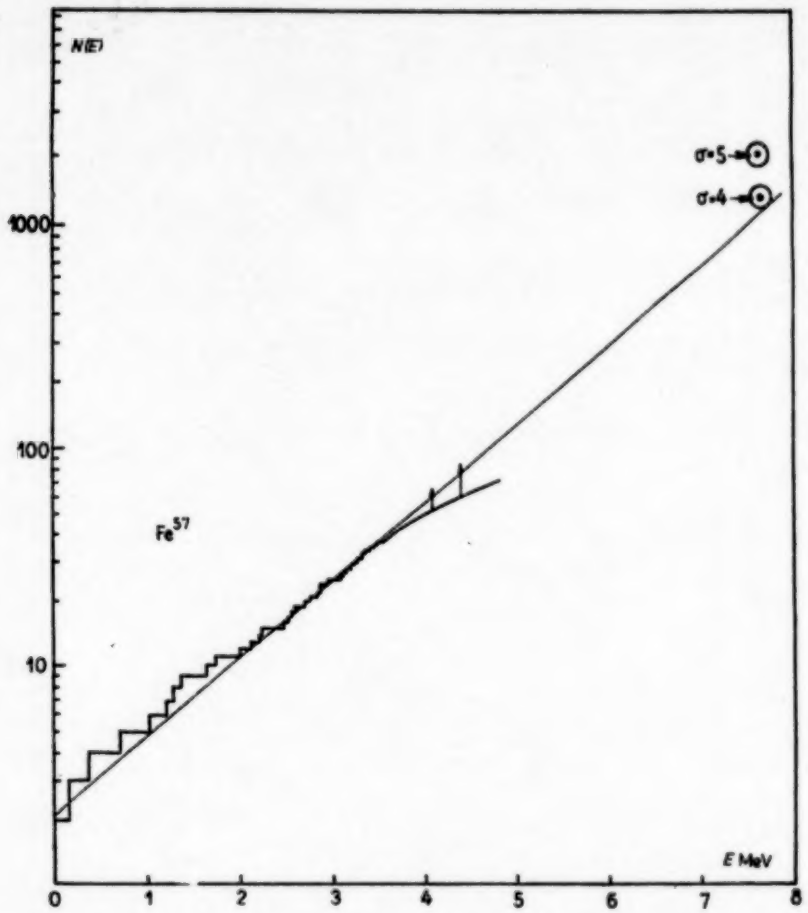

Fig. 4. The total number of states up to the excitation energy E in Fe^{57} vs. E as obtained from (pp′) and (dp)-reactions [7,8]). The arrows correspond to the number of unresolved levels estimated from the resolution. The point from the neutron-resonance level density [16]) has been calculated by means of eq. (2) with the spin distribution of eq. (4). The curve corresponds to a nuclear temperature τ of 1.2 MeV and to σ 3.7.

even nuclei with respect to each other (fig. 5). A similar odd-even difference is suggested by the level densities determined from neutron resonances [17–19]). This effect indicates the existence of an energy gap in the nuclear spectrum[20]) similarly as for a system of interacting electrons in a superconductor [21,22]). That such displacements of the level-density curves occur even at low excitation energy has been predicted for a system with an energy gap for the elementary excitations [19]). The energy gap is expected to be of the order of half the pairing energy. The displacement is for the Mn—Fe group 2.2 MeV,

while the pairing energy of Fe^{58} is 2.3 MeV, which shows the close agreement between these quantities.

It is also seen from the $N(E)$-curves that the nuclear temperature is nearly constant as a function of energy for the nuclei and energy intervals considered. Attempts are often made to fit nuclear level densities, using a

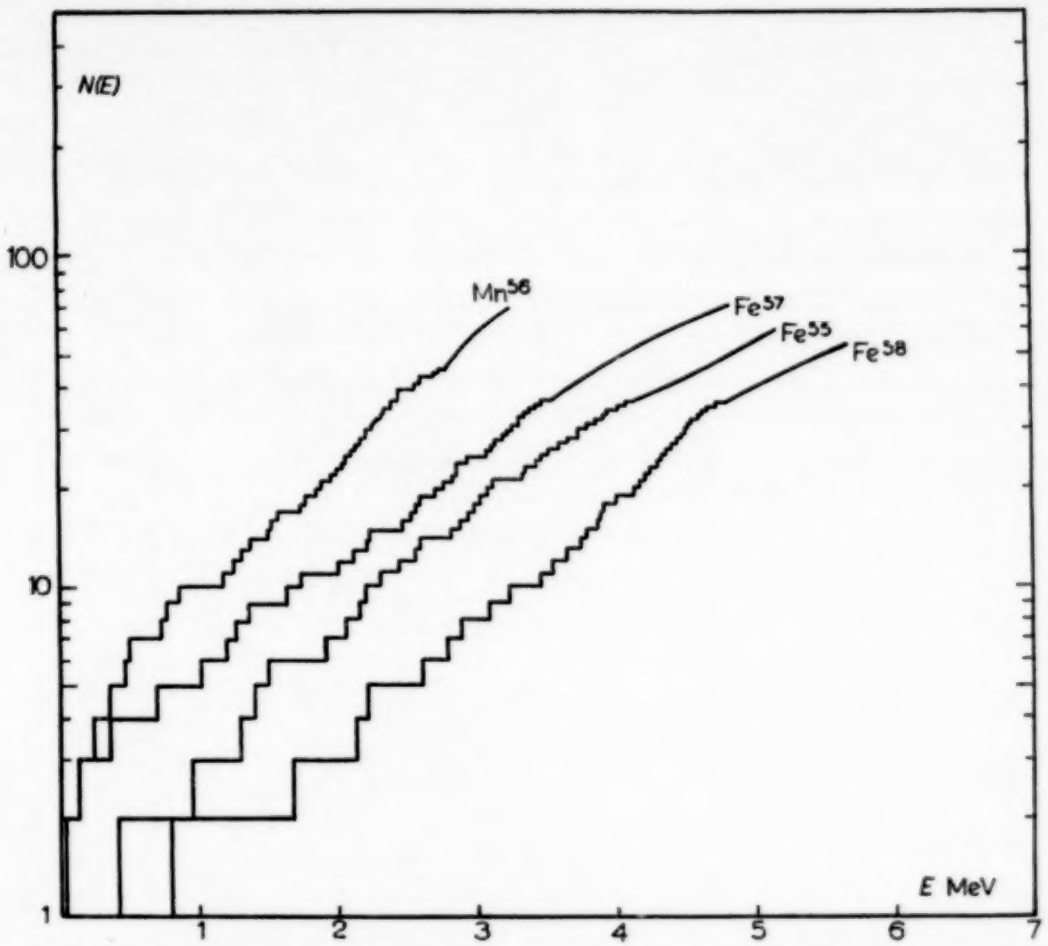

Fig. 5. The total number of states up to the excitation energy E for Mn^{56}, Fe^{55}, Fe^{57}, and Fe^{58} vs. E. The resolution is somewhat higher in the case of Mn^{56} than for the rest. The figure compares the total numbers of states for even, odd, and odd-mass nuclei.

square-root law for the temperature as a function of energy [2, 23]). However, this law is the high-energy asymptotic form, and there is no reason for it to be valid at low excitation. A constant temperature might be qualitatively understood as follows [19]). An energy gap introduces a certain ordering in the nucleus. With increasing excitation this ordering is gradually overcome as in a melting system [24]). The temperature therefore tends to be constant. When the ordering disappears, we might possibly expect a second-order phase transition [25]) when the system goes into a state that can be described as an ordinary Fermi gas. The energy at which such a phase transition might occur is unknown, and there is so far no experimental evidence of it.

Nuclear temperatures have not previously been obtained directly from the excited nuclear states, and thus it was hitherto impossible to verify that the nuclear temperatures from evaporation spectra are the same as those from level densities. It is therefore gratifying to observe the agreement of the nuclear temperatures from α-particle evaporation spectra in the Ni—Cu region with those determined here [12]). This is strongly in support of the evaporation approximation giving a good description of a certain class of nuclear reactions.

The value of σ obtained from the extrapolated $N(E)$-curves for Mn^{56} and Fe^{57} agrees roughly with the value obtained from the angular distribution of α-particles evaporated from nickel ($\sigma \approx 3.6$) [1]). It is still impossible, however, to draw any definite conclusion about a reduction, due to pairing interactions, of the rigid moment of inertia of these nuclei. The values so far obtained for σ correspond to moments of inertia reduced by 0—30 %, but the uncertainty is still of the same order as the expected effect [4]).

For Al^{28} the value of σ has been determined from the spin assignments to the neutron resonances to be 1.7 [6]), corresponding to a reduction of the moment of inertia to about one third of its rigid-body value, or in a shell-model picture corresponding to an average number of about 2 excited particles. This value is rather surprising when compared with the large value in S^{33}, $\sigma = 4$, which we have obtained. The latter value seems rather well established because of the obvious need for a large number of additional states with spins higher than $\frac{1}{2}$. The error in σ for sulphur is hardly more than 33 %. The sulphur value corresponds to a moment of inertia 50 % higher than the rigid-body value, which, however, falls within the limits of uncertainty. The origin of the discrepancy between the Al^{28} and the S^{33} value must be further investigated. It cannot be explained as a shell effect, but it might partly be due to the difficulty of assigning spins and higher l-values to neutron resonances.

It is seen in fig. 5 that the $N(E)$-curve for Fe^{57} lies higher than that for Fe^{55}. We associate this with a shell effect, as Fe^{55} has only one neutron outside the $f_{\frac{7}{2}}$ shell, while Fe^{57} has three. There is therefore a greater number of recombination possibilities in Fe^{57} than in Fe^{55} at the same energy [26, 27]). The effect is smaller than expected on the basis of an independent particle estimate, presumably owing to pairing effects.

It is interesting to compare our results with the very detailed semi-phenomenological calculation of level densities made by Cameron [28]). His calculation is based on an independent-particle shell model. The interparticle interactions which give rise to the odd-even shift are only taken into account phenomenologically, by introduction of a "true" ground state for the non-interacting system corresponding to that of an odd nucleus. In fitting his data to the experimental level densities he has to adjust his parameters in

such a way that they implicitly correspond to a moment of inertia two orders of magnitude larger than the rigid-body value. According to our eq. (6) this would imply a very large number of excited particles, and as Cameron's formula has been adjusted to the low-spin neutron resonances, it also implies a total level density about two orders of magnitude larger than the one we obtain (cf. our eq. (5)). While Cameron's expression should therefore still provide an excellent practical guide for estimates of neutron level densities, care must be taken when spin distributions are calculated from it. His large value of the moment of inertia is not surprising. The pairing interactions should reduce the level density predicted by the independent-particle model, and this reduction can phenomenologically be achieved also be assuming a large moment of inertia. In the present case the independent-particle result has thus been decreased by several orders of magnitude.

It is a pleasure to thank Dr. B. R. Mottelson for several stimulating discussions.

References

1) T. Ericson and V. Strutinski, Nuclear Physics **8** (1958) 284; **9** (1958/9) 689
2) H. Bethe, Revs. Mod. Phys. **9** (1937) 69
3) C. Bloch, Phys. Rev. **93** (1954) 1094
4) V. Strutinski, Congrès International de Physique Nucléaire, Paris (1958)
5) N. O. Lassen and N. O. Roy Poulsen, Congrès International de Physique Nucléaire, Paris (1958)
6) C. T. Hibdon, Bull. Am. Phys. Soc. **3** (1958) 48
7) A. Sperduto, MIT LNS Progr. Rep. May 1957
8) A. Sperduto, MIT LNS Progr. Rep. May 1958
9) W. W. Buechner *et al.*, Phys. Rev. **101** (1956) 188
10) P. M. Endt and C. H. Paris, Phys. Rev. **110** (1958) 89
11) R. E. Peterson *et al.*, Phys. Rev. **79** (1950) 593
12) N. O. Lassen *et al.*, Mat. Fys. Medd. Dan. Vid. Selsk., to appear
13) J. W. Green *et al.*, Phys. Rev. **108** (1957) 841
14) P. R. Christensen, O. Elbek and M. C. Olesen, private communication
15) H. Marshak and H. W. Newson, Phys. Rev. **106** (1957) 110
16) C. T. Hibdon, Phys. Rev. **108** (1957) 414
17) T. D. Newton, Can. J. Phys. **34** (1956) 804
18) T. Ericson, Nuclear Physics **6** (1958) 62
19) T. Ericson, Nuclear Physics **8** (1958) 265; and **9** (1958/9) 697
20) A. Bohr, B. R. Mottelson and D. Pines, Phys. Rev. **110** (1958) 936
21) J. Bardeen, L. N. Cooper and J. R. Schrieffer, Phys. Rev. **108** (1957) 1175
22) N. N. Bogolyubov, JETP **34** (1958) 58
23) J. Blatt and V. Weisskopf, Theoretical Nuclear Physics (John Wiley and Sons, New York, 1952)
24) L. E. H. Trainor and W. R. Dixon, Can. J. Phys. **34** (1956) 229
25) V. G. Soloviev, Nuclear Physics **9** (1958/9) 655
26) N. Rosenzweig, Phys. Rev. **108** (1957) 817
27) M. L. Bollinger *et al.*, (submitted to Phys. Rev.)
28) A. G. W. Cameron, Can. J. Phys. **36** (1958) 1040

4.E *Nuclear Physics* 11 (1959) 492—498; © *North-Holland Publishing Co., Amsterdam*
Not to be reproduced by photoprint or microfilm without written permission from the publisher

THE BETA DECAY OF K^{40}

W. H. KELLY, G. B. BEARD and R. A. PETERS
Department of Physics and Astronomy, Michigan State University, East Lansing, Michigan †

Received 17 February 1959

Abstract: The beta decay of K^{40} has been studied using a 1 inch diameter × 1 inch high KI(Tl) scintillation crystal. The Kurie plot of the beta spectrum was made linear down to less than 200 keV by the use of the exact third forbidden correction factor. The uncertainty in the correction for electron escape is suggested as the main source of non-linearity below this energy. The extrapolated end point energy was 1.35 ± 0.02 MeV. A specific activity of 27.2 ± 0.5 betas per second per g of natural potassium was obtained. This corresponds to a decay constant $\lambda(\beta) = (4.72 \pm 0.09) \times 10^{-10} y^{-1}$ and a half-life $t(\beta) = (1.47 \pm 0.03) \times 10^{9} y$.

1. Introduction

According to beta decay theory, the beta spectrum of K^{40} should be of the unique third forbidden type [1,2]). In recent years various measurements of the spectrum have been made. These can be divided into two groups; those in which the K^{40} source was external to the detector [3,4,5]) and those in which the source was a part of the detector [6,7,8]). Of the first group, the best results were obtained using enriched K^{40} sources in magnetic spectrometers. These results showed that the allowed Kurie plot was indeed non-linear and that it could be made linear in the region above 500 keV by applying the appropriate correction factor. The deviations from linearity of the corrected Kurie plots at the lower energies could readily be explained by the distortion introduced by the excessive source thicknesses needed to obtain reasonable counting rates.

The second group used KI(Tl) crystals and measured the self-scintillations of the naturally occurring K^{40} in the crystals. The first work by Smaller *et al.* [8]) gave a very crude spectrum, but later work by Good [6]) and Kono [7]) showed the corrected Kurie plot to be linear above 300 keV. Good used a rather small crystal (5.26 grams) and, because of the subsequent rather large correction necessary for those electrons reaching the surface before losing all their energy, it is not surprising that the Kurie plot becomes non-linear at fairly high energy. Kono used crystals from 2 to 8 times as large as Good.

† This research was supported in part by the United States Air Force under contract No. AF49(638)-10 monitored by the Air Force Office of Scientific Research of the Air Research and Development Command.

For the larger crystals the surface escape correction would be considerably smaller. One might therefore expect the Kurie plot to be linear to lower energies. Kono attributes the deviation at low energies to spurious pulses caused by the known delayed phosphorescence of the crystal [8]). However, as Good has pointed out, for pulse widths of the order of a few microseconds the delayed pulses would be essentially of single electron size and thus too small to affect the experiments.

In testing the uniqueness of the K^{40} spectrum shape, Alburger [3]) found that both the unique second and third forbidden correction factors gave linear Kurie plots above 500 keV. Consequently, either correction was equally acceptable when judged only by the experimental results.

Considering the above, a further investigation of the K^{40} beta spectrum was undertaken with special interest in the low energy end of the spectrum. It was anticipated that a Kurie plot linear to lower energy could be obtained, thus allowing an experimental differentiation to be made among the shape correction factors.

2. Experimental Procedure and Results

2.1. K^{40} BETA SPECTRUM

A 1 inch by 1 inch cylindrical KI(Tl) crystal † was mounted on an RCA 6342 photomultiplier as part of a conventional single channel scintillation spectrometer. Preliminary measurements were made using a type A-1 linear amplifier. In observing the pulses with an oscilloscope it appeared that some of the low lying pulses were due to spurious counts introduced by overloading of the amplifier. The very large pulses causing blocking occurred with a frequency consistent with the expected cosmic ray background. The A-1 amplifier was replaced by one of good non-overload properties ††. Comparison of the two spectra showed that the non-overloading amplifier did have the expected smaller relative counting rates at low energies. Since non-overloading amplifiers have only been in general use in the last few years, it is possible that both the spectra of Good and Kono contained some spurious pulses at low energy caused by amplifier overload.

As a further test, the integral pulse height selector of the non-overloading amplifier was set at 1.5 MeV and the output used to trigger a univibrator which produced an 80 microsecond blanking pulse. The blanking pulse was then applied in anticoincidence with the single channel analyzer output. In this way any counts due to possible spurious pulses produced by amplifier overloading would have been eliminated. The observed low energy counting rates were unaffected by this addition.

† Obtained from Harshaw Chemical Co.

†† Baird Atomic Model 215.

The spectrometer linearity was found to be within 1 % when checked using gamma rays from external sources of Ba^{133}, Se^{75}, Au^{198}, Cs^{137}, Zn^{65} and Na^{22}. The resolution of the Cs^{137} 662 keV gamma ray photopeak was about 14 % and varied inversely with the square root of the energy. The experimental beta spectrum including the minor corrections for background, absorption of the K^{40} 1.46 MeV gamma ray and the finite resolution of the spectrometer is shown in fig. 1. The statistical errors in the original data were all less than 1 % except for a few points at the high energy end of the spectrum. Also shown in fig. 1 is the beta spectrum after the correction for the escape of electrons through the crystal surface.

Sufficient lead, iron and copper shielding was used to reduce the background to an almost negligible value. Using a 1″×1″ comparison NaI(Tl) crystal the differential background was measured to be never more than $\frac{1}{3}$ % at any point.

By considering the absorption coefficient of KI and the energy and emission rate of the K^{40} gamma rays as well as the size and geometry of the

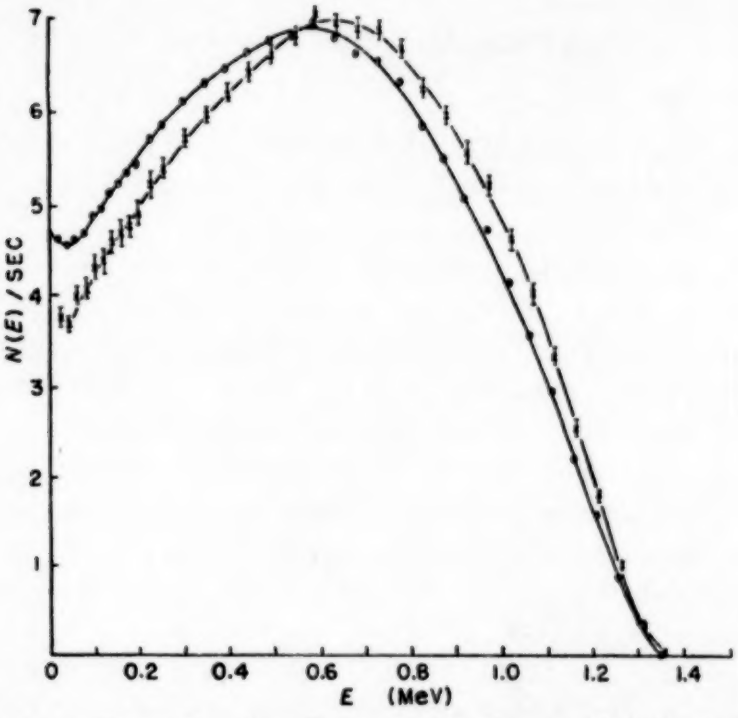

Fig. 1. K^{40} spectrum. The circles show the measured spectrum including background, 1.46 MeV gamma and finite resolution corrections. The ×-s show the spectrum after the electron escape correction. The flags represent total estimated error at each point, due mostly to the uncertainty in the electron escape correction.

crystal, one can readily estimate the gamma ray count to comprise about 2 % of the total measured activity. The pulse height distribution was estimated using the observed pulse height distributions of external gamma

sources of Cs^{137}, Zn^{65}, and Na^{22} (1.28 MeV). Although this is a rough approximation, the correction is so small that the errors in it have little effect.

The resolution correction was made using the results of Palmer and Laslett [9]). This correction was appreciable only at the high energy end of the spectrum.

The correction for the escape of electrons from the surface of the crystal was by far the most important and caused the major part of the difference between the experimental and corrected curves, especially in the low energy region. The method given by Mateosian and Smith [10]) was used to compute this correction. This calculation is based on the assumption that in the crystal an electron travels in a straight line a distance equal to its range. For this reason the uncertainty in the correction is believed to be quite large (estimated here as ± 50 %). The error flags on the corrected beta spectrum in fig. 1 are due mostly to this large uncertainty.

2.2. TOTAL K^{40} BETA ACTIVITY

To measure the total beta activity of the KI(Tl) crystal the integral count was recorded at various input pulse height settings. The resulting integral

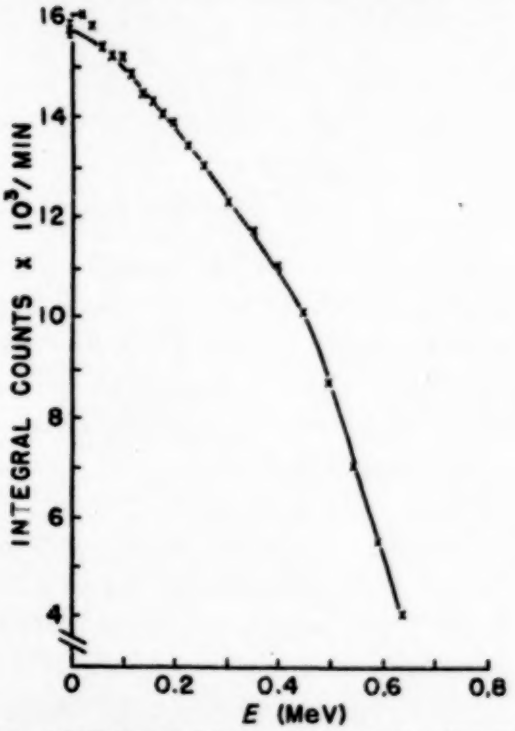

Fig. 2. Low energy region of K^{40} integral beta spectrum showing the extrapolation to zero energy. The statistical error of each point is smaller than the size of the points. The error flag at zero energy represents the uncertainty in the extrapolation.

count curve behaved well down to an energy of about 70 keV. Below 70 keV the electronic noise background became appreciable and so these points were discarded and the integral curve was extrapolated to zero energy. As can be

seen from fig. 2, which shows the low energy end of the integral curve, the activity added by this extrapolation amounts to only about 3 % of the total. Therefore, the uncertainty in the extrapolation has small effect on the total measured activity. The statistical error of each point is smaller than the size of the points and the corresponding background count was less than $\frac{1}{2}$ % for energies above 70 keV.

When the background and total K^{40} gamma ray counts were subtracted an activity of $15\,400 \pm 200$ counts per minute remained. The error was estimated by considering the uncertainties in the extrapolation, background correction and the total gamma ray activity. This value is equivalent to an activity of 27.2 ± 0.5 beta particles per second per gram of natural potassium. This value agrees well with that of Good [6]) but is somewhat lower than that obtained by Kono [7]).

3. Discussion

Kurie plots were made of the corrected beta spectrum using the following shape factors corresponding to allowed, and first, second, and third unique forbidden spectra. The shape factors are included as a_n, where [11])

$a_0 = 1$	allowed
$a_1 = p^2+q^2$	1st forbidden
$a_2 = p^4+q^4+\frac{10}{3}p^2q^2$	2nd forbidden
$a_3 = p^6+q^6+7p^2q^2(p^2+q^2)$	3rd forbidden

(p = electron momentum, q = neutrino momentum).

Fig. 3 shows the Kurie plots for $n = 0$, 1 and 2, while the plot for $n = 3$ is practically identical with that of fig. 4. The allowed plot is definitely non-linear and the a_3 correction factor appears to make it linear over the greatest range. It is interesting to note that all three forbidden shape factors linearize the curve above 500 keV, and it is only at energies below 300 keV that one can distinguish between the $n = 2$ and $n = 3$ factors.

The Kurie plot containing the a_3 shape factor still deviates from linearity at energies somewhat higher than expected. These shape factors, however, are an approximation and ignore the Coulomb effect on the electron, although they are expected to be fairly accurate for low Z. Since K^{40} has a low Z, it was not anticipated that the use of the exact shape correction factor would have an appreciable effect, but it was still felt worth while to see what the effect would be on the third forbidden plot. The exact expression for the general shape factor is [11])

$$a'_n = \sum_{\nu=0}^{n} \frac{(2n+1)!(2\nu+1)!}{2^{2\nu}(\nu!)^2(2n-2\nu+1)!}\, q^{2(2n-\nu)} L_\nu(P \mp Z).$$

The L_ν function has been tabulated by Rose *et al.* [12]).

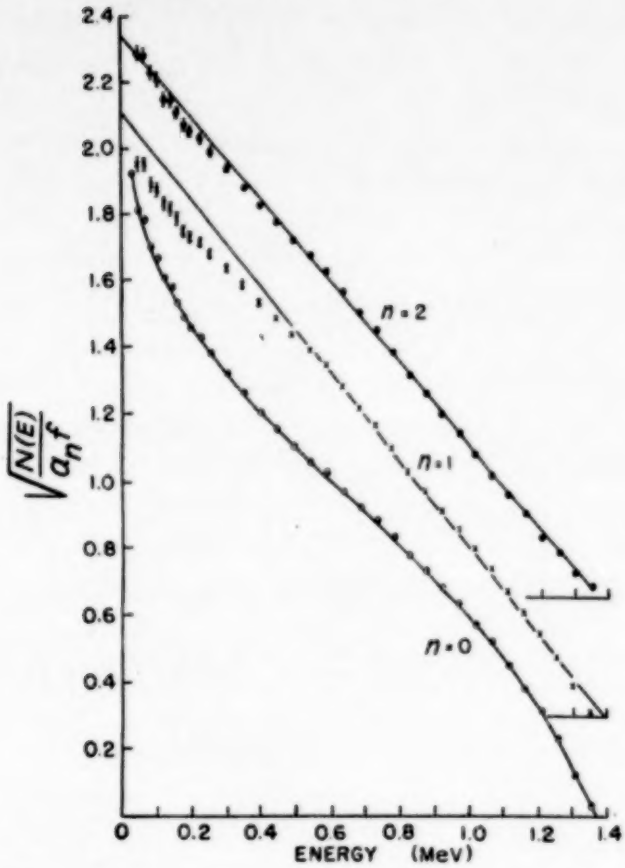

Fig. 3. Allowed, and unique first and second forbidden corrected Kurie plots. The ordinates are normalized to the same scale for convenience. The first and second forbidden corrected plots are displaced upward by arbitrary amounts.

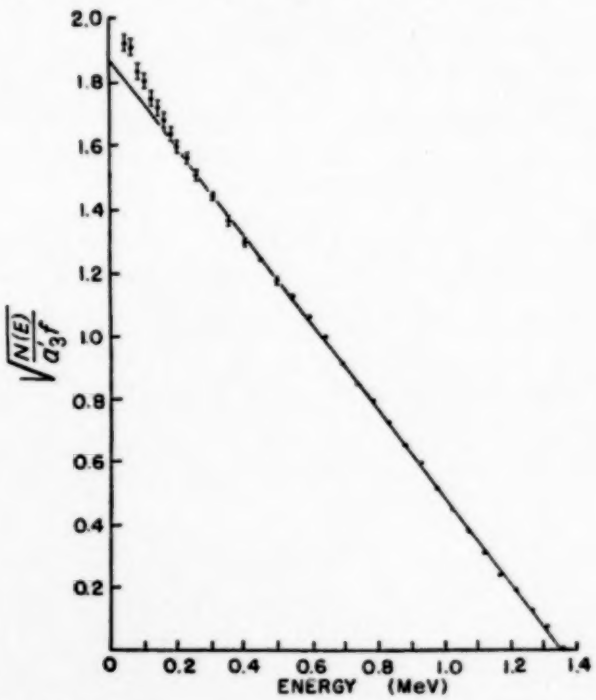

Fig. 4. K^{40} unique third forbidden corrected Kurie plot. The exact correction factor taking into account the Coulomb effect on the electron was used.

When the a'_3 shape factor was used the only change in the Kurie plot was a barely perceptible improvement at low energy. Fig. 4 shows this Kurie plot.

To determine its effect on the beta spectrum, the escape correction was arbitrarily changed by ± 50 % and new Kurie plots made. The 50 % decrease caused the Kurie plot to deviate from linearity at around 250 keV, while the 50 % increase made the low energy end linear down to well below 100 keV. However, in the latter case the deviations from linearity in the mid-energy region of the plot were increased somewhat. Since an exact calculation of the electron escape would be difficult, one might be able to use several crystals of quite different surface to volume ratios to determine this correction empirically with greater accuracy.

When the integral count above 200 keV was added to the count obtained by extrapolating the Kurie plot of fig. 4 to zero energy, the total count differed by about $\frac{1}{2}$ % from the extrapolated value of the integral curve of fig. 2. The integral curve result was judged to be the more accurate. Assuming the relative abundance of K^{40} to be 0.0118 %, the value of 27.2 ± 0.5 betas per gram per sec corresponds to a decay constant $\lambda(\beta) = (4.72 \pm 0.09) \times 10^{-10} y^{-1}$ and a beta half-life of $(1.47 \pm 0.03) \times 10^9 y$.

The Kurie plot end point gives a maximum beta energy of 1.35 ± 0.02 MeV. This value agrees with the results of the majority of previous investigations [3, 4, 5, 7]).

References

1) R. E. Marshak, Phys. Rev. **70** (1946) 980
2) E. Greuling, Phys. Rev. **61** (1942) 568
3) D. E. Alburger, Phys. Rev. **78** (1950) 629
4) L. Feldman and C. S. Wu, Phys. Rev. **87** (1952) 1091
5) Bell, Weaver and Cassidy, Phys. Rev. **77** (1950) 399
6) M. L. Good, Phys. Rev. **83** (1951) 1054
7) S. Kono, J. Phys. Soc. Japan **10** (1955) 495
8) B. Smaller, J. May and M. Freedman, Phys. Rev. **79** (1950) 940
9) T. P. Palmer and L. J. Laslett, AEC Report AECU-1220 (March 14, 1951) unpublished
10) E. der Mateosian and A. Smith, Phys. Rev. **88** (1952) 1186
11) E. Konopinski, in Beta- and Gamma-Ray Spectroscopy, edited by K. Siegbahn (North Holland Publishing Company, Amsterdam, 1955) Ch. 10, p. 292
12) M. E. Rose, C. L. Perry and N. M. Dismuke, Oak Ridge National Laboratory Report 1459 (1953)

2.L:7.A *Nuclear Physics* **11** (1959) 499—521; © *North-Holland Publishing Co., Amsterdam*
Not to be reproduced by photoprint or microfilm without written permission from the publisher

THE POLES OF THE *S*-MATRIX OF A RECTANGULAR POTENTIAL WELL OR BARRIER

H. M. NUSSENZVEIG †
Centro Brasileiro de Pesquisas Físicas, Rio de Janeiro

Received 26 January 1959

Abstract: To test the validity of current ideas on the poles of the *S*-matrix, a simple example is treated: non-relativistic scattering by a spherically symmetric rectangular potential well (or barrier). The poles of the *S*-matrix associated with this problem, in the case of zero angular momentum, are determined, and their behaviour as a function of the well depth (barrier height) is discussed. Some results for higher angular momenta are also given. The usual physical interpretation may be applied only to a very restricted class of poles. Difficulties appear in the case of "short-lived decaying states". However, the present model leads to a connection between the limiting cases of strongly bound states in a deep well and of certain characteristic states attached to a "hard sphere" or to a perfect conductor (antenna). It is shown that some poles, previously described as "meaningless", give rise to important physical effects.

1. Introduction

The general properties of the poles of the *S*-matrix have been the object of a great number of papers. However, few attempts have been made to test and to illustrate these properties by determining all the poles of the *S*-matrix in concrete physical examples. This has been done for the Coulomb potential; in this case, however, there are only purely imaginary poles, which correspond to bound states: no complex †† poles exist. To our knowledge, no example where complex poles occur has ever been completely treated.

A simple example of this kind is the scattering of non-relativistic particles by a spherically symmetric rectangular potential well (or barrier). This example was considered in 1930 by Beck [1]), who observed that, when the well depth decreases, the bound levels are "pushed" into the continuous spectrum, giving rise to "virtual" levels. After the introduction of the *S*-matrix, the rectangular potential well was mentioned as an example in a paper by Møller [2]), where it is stated (incorrectly) that there are no complex poles in this case. Complex poles were also disregarded in a later treatment of the problem by Schützer [3]).

As will be shown in sect. 3, the poles of the *S*-matrix associated with this

† Fellow of the National Research Council of Brazil; present address: Institute for theoretical Physics, University of Utrecht.

†† We call a number complex if it has non-vanishing real and imaginary parts.

problem, for angular momentum $l = 0$, may be completely determined. Some results for higher angular momenta will be given in sect. 4. The interest of this example is that it allows us to test the usual point of view on the poles of the S-matrix. We have found several inexact statements in the literature; in fact, the whole problem of the physical interpretation of the poles of the S-matrix should be dealt with much more carefully than has usually been done hitherto.

Let us summarize the usual point of view. We shall restrict ourselves to the case of non-relativistic scattering by a central potential of finite radius. In this case, as is well known, the S-matrix is a diagonal matrix, with elements

$$S_l(k) = \exp\,[2i\eta_l(k)], \tag{1}$$

where $\eta_l(k)$ is the phase-shift corresponding to the angular momentum l and wave number k. In the cases in which we are interested, the analytic continuation of $S_l(k)$ in the complex k-plane is a meromorphic function. The following properties are generally ascribed to the poles of this function:

(A) The poles are located either on the positive imaginary axis or in the lower half-plane [4, 5]).

(B) A pole on the positive imaginary axis, $k = i\kappa_n (\kappa_n > 0)$, corresponds to a bound state with energy $E_n = -(\hbar\kappa_n)^2/2m$, where m is the mass of the particle †.

(C) Complex poles are usually interpreted either by means of so-called "quasi-stationary" or "virtual" states [8, 9]) or in terms of resonance scattering [10]). The first interpretation involves the analytic continuation of Schrödinger's wave function to "complex energies". A pole at the point $k = k' - i\kappa (\kappa > 0)$ is associated with the "complex energy"

$$W = E - \tfrac{1}{2}i\Gamma = (\hbar^2/2m)(k' - i\kappa)^2. \tag{2}$$

If $k' > 0$, the corresponding "wave function" is said to represent a "decaying state", with decay constant $\Gamma/\hbar$ and "energy" E (defined with an uncertainty given by Γ). Poles with $k' < 0$ are associated with "capture" processes. It is assumed, in both cases, that $E > 0$ (cf. sect. 5.2).

It is well known that a "complex-energy wave function" cannot be normalized, owing to its exponential increase with the distance (this is attributed to emission that took place "a long time ago" [9])). This difficulty is usually circumvented by interpreting a "complex-energy wave function" as an approximation to a wave packet that is a proper solution of Schrödinger's equation [11, 12]). It must be emphasized, however, that this approxima-

† If the scattering potential does not vanish rapidly enough at infinity, there may also exist "spurious" poles on the positive imaginary axis, which do not correspond to bound states [6, 7]).

tion rests upon the following assumptions: (a) $|\Gamma| \ll E$; (b) $|\Gamma| \ll$ level spacing. If these conditions are not fulfilled, it is very doubtful whether such an interpretation is possible (cf. sect. 5.2).

The interpretation of complex poles by means of resonance scattering associates (2) with a "Breit-Wigner peak" in the scattering cross-section; E gives the resonance energy and Γ is the half-width of the peak. Besides conditions (a) and (b), it is assumed that the pole in question is a simple pole. According to Hu [10]), this is always so if the scattering potential has a short range, i.e., if $k'a \ll 1$, where a is the radius of the potential.

2. Formulation of the Problem

We shall consider the potential

$$V(r) = -V_0, \quad r < a, \quad V(r) = 0, \quad r > a,$$

where $V_0 > 0$ in the case of a well, and $V_0 < 0$ in the case of a barrier. It is convenient to introduce the following dimensionless parameters:

$$\alpha = [2m(E+V_0)]^{\frac{1}{2}} a/\hbar, \tag{3}$$

$$\beta = ka = (2mE)^{\frac{1}{2}} a/\hbar, \tag{4}$$

$$\pm A^2 = V_0/\mathscr{E} \qquad (+ \text{ for a well, } - \text{ for a barrier}), \tag{5}$$

where E is the energy (taken, for the moment, to be real), and

$$\mathscr{E} = \hbar^2/(2ma^2) = E/\beta^2. \tag{6}$$

The parameters α and β correspond to the wave number inside and outside of the potential, respectively; $\mathscr{E}$ is the energy of a particle for which $ka = 1$; A^2 is a well-depth (barrier-height) parameter. It follows from the above equations that

$$\alpha^2 = \beta^2 \pm A^2 \qquad (+\text{for a well, } - \text{ for a barrier}). \tag{7}$$

It follows from (1) and from the well-known expression for the phase-shift [13]) that †

$$S_l(\beta) = -\frac{\beta j_l(\alpha) h_l'^{(2)}(\beta) - \alpha j'_l(\alpha) h_l^{(2)}(\beta)}{\beta j_l(\alpha) h_l'^{(1)}(\beta) - \alpha j'_l(\alpha) h_l^{(1)}(\beta)}, \tag{8}$$

where $j_l(z)$ is the spherical Bessel function of the first kind, and $h_l^{(1)}(z)$, $h_l^{(2)}(z)$ are spherical Hankel functions of the first and second kinds, respectively [14]).

To obtain the analytic continuation of $S_l(\beta)$, it suffices to consider (8) as a function of the complex variable $\beta = u+iv$. It follows from the properties of

† It is assumed in (8), as well as in subsequent expressions (unless otherwise stated), that, in accordance with (7), α has been replaced by $\pm(\beta^2 \pm A^2)^{\frac{1}{2}}$ (the sign of the square root is irrelevant).

the spherical Bessel functions that (8) is a meromorphic function of β, which satisfies the well-known relations

$$S_l(\beta)S_l(-\beta) = S_l(\beta)S_l^*(\beta^*) = 1. \tag{9}$$

According to (9), if β is a pole of $S_l(\beta)$, so is $-\beta^*$, while $-\beta$ and β^* are zeros. Therefore, it suffices to determine the poles on the imaginary axis and in the right half-plane.

3. The Case of Zero Angular Momentum

For $l = 0$, (8) becomes

$$S_0(\beta) = \exp(-2i\beta)(\alpha \cot \alpha + i\beta)(\alpha \cot \alpha - i\beta)^{-1}. \tag{10}$$

The poles of $S_0(\beta)$ are the roots of the complex transcendental equation

$$\alpha \cot \alpha = i\beta. \tag{11}$$

It can be shown, by considering the real and imaginary parts of (7) and (11), that property (A) of sect. 1 is satisfied: $S_0(\beta)$ cannot have any poles in the upper half-plane, except on the imaginary axis.

3.1. THE POTENTIAL WELL

To determine the roots of (11), it is more convenient to work with the variable $\alpha = x+iy$ than with β. Eliminating β from (7) and (11), we find

$$\alpha^{-1} \sin \alpha = \pm A^{-1}. \tag{12}$$

The corresponding values of β are given by

$$\beta = \pm(\alpha^2 - A^2)^{\frac{1}{2}}, \tag{13}$$

where the sign must be chosen in such a way that (11) is satisfied.

The problem is now reduced to the determination of the roots of (12) as a function of the parameter A. This is carried out in appendix A. Making use of (13) and of the results derived in appendix A, it is a simple matter to determine the poles of $S_0(\beta)$ in the β-plane. Some of these poles, together with the corresponding values of A, are shown in fig. 1.

For each given value of A, there exists an infinite number of poles. When A varies, the poles describe certain paths in the β-plane (the curves in full line in fig. 1). The poles corresponding to a given A may be numbered according to their limiting positions for $A \to 0$; thus, $\beta_n = u_n + iv_n$, where

$$\lim_{A \to 0} \beta_n = n\pi - i\infty \qquad (n = 0, \pm 1, \pm 2, \ldots). \tag{14}$$

The following abbreviations will be introduced for describing the poles: a-poles (a = anti), for poles with $u_n = 0$, $v_n < 0$; b-poles (b = bound),

for poles with $u_n = 0$, $v_n > 0$, and c-poles (c = complex), for poles with $u_n \neq 0$, $v_n \neq 0$. The denomination "anti-pole" will be justified in sect. 5.2.

Let us describe the behaviour of the poles when A increases from 0 (free particles) to ∞ (infinitely deep well), beginning with the pole β_0 on the

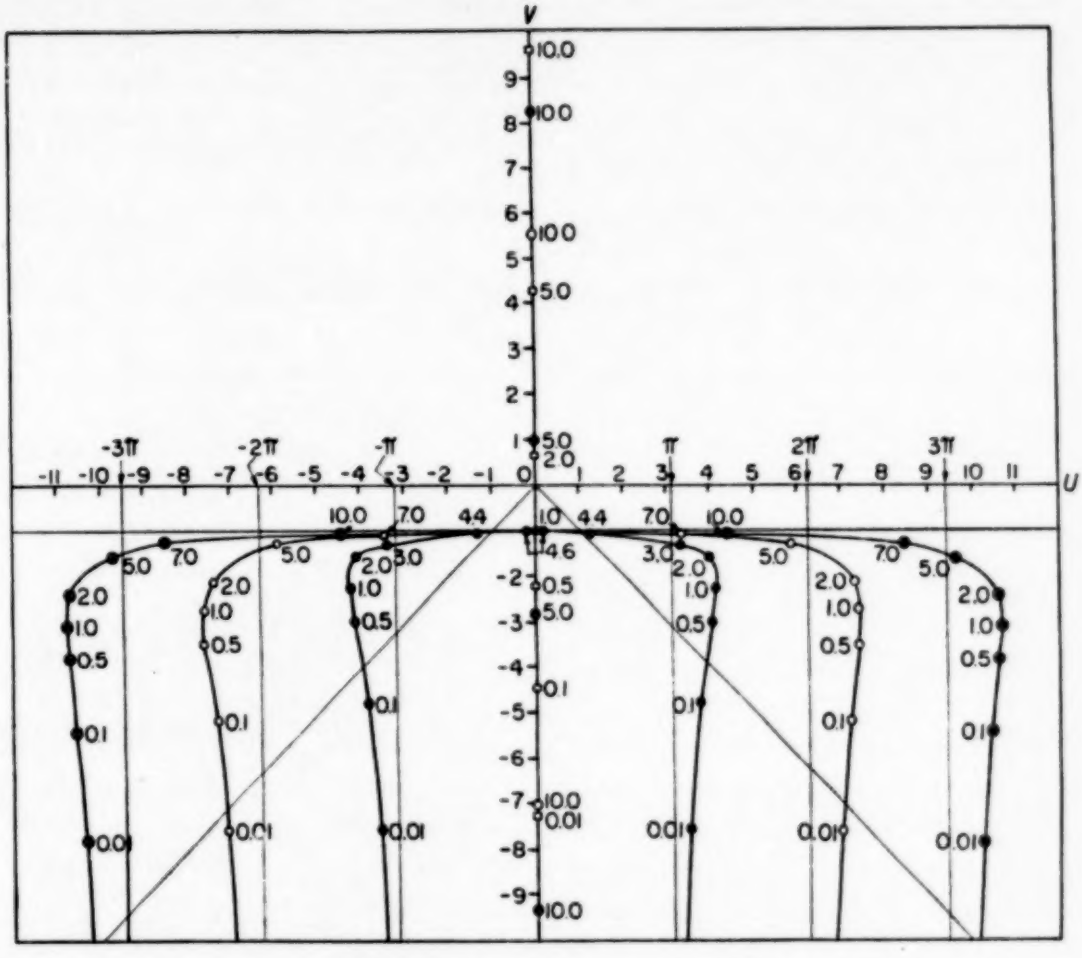

Fig. 1. The poles β_n of $S_0(\beta)$ for a potential well.
□ $n = 0$; ● $n = \pm 1$; ○ $n = \pm 2$; ◉ $n = \pm 3$.
The numbers beside the poles give the corresponding values of A. The curves in full line are the paths described by the poles. The bisectors of the third and fourth quadrants are also indicated.

imaginary axis. For $0 < A < 1$, β_0 corresponds to a root of (A3) (see appendix A); it is an a-pole, and it moves from $-i\infty$ to $-i$ when A increases from 0 to 1. For $A > 1$, β_0 arises from a root of (A2) in the interval $0 < x < \pi$. According to (A4), when A increases from 1 to $\frac{1}{2}\pi$, β_0 is an a-pole, which moves from $-i$ to the origin. For $A > \frac{1}{2}\pi$, β_0 becomes a b-pole (first bound state), and it moves upwards from the origin to $i\infty$ when A increases from $\frac{1}{2}\pi$ to ∞.

It must be pointed out that the origin itself is never a pole of $S_0(\beta)$, since

this would violate the unitarity condition. In the present case, for $A = \frac{1}{2}\pi - \varepsilon$, $|\varepsilon| \ll 1$, we have, in the neighbourhood of the origin,

$$S_0(\beta) \approx -(\beta+\beta_0)(\beta-\beta_0)^{-1} \approx -(\beta-\tfrac{1}{2}i\pi\varepsilon)(\beta+\tfrac{1}{2}i\pi\varepsilon)^{-1} = -1+i\pi\varepsilon(\beta+\tfrac{1}{2}i\pi\varepsilon)^{-1}, \quad (15)$$

so that the residue at $\beta = \beta_0$ vanishes when $\varepsilon \to 0$. This is due to the fact that $\beta_0^* = -\beta_0$, which is a zero of $S_0(\beta)$, approaches the origin simultaneously with β_0. Thus, the "conservation of the number of poles" fails to hold at the origin.

Let us consider next a pair of poles, $\beta_{\pm n}$, with $n \geqq 1$. For $0 < A < A_n$, where A_n is defined by (A7), β_n is a c-pole, which corresponds to the root α_n of (A1), and β_{-n} is the mirror image of β_n with respect to the imaginary axis. The paths described by the first few pairs of poles are shown in fig. 1. For $A \to 0$, β_n approaches asymptotically the straight line $u = n\pi$. When A increases, β_n moves upwards, until it approaches the straight line $v = -1$, and then it moves towards the imaginary axis. When $A \to A_n$, β_n and β_{-n} approach, from opposite sides, the point $\beta = -i$, where they coalesce for $A = A_n$. The paths described by $\beta_{\pm n}$ are tangent to the straight line $v = -1$ at this point.

Thus, for $A = A_n$, $S_0(\beta)$ has a double pole at the point $\beta = -i$. It may be easily verified that all other poles are simple poles. However, the existence of double poles $k = k' - i\kappa$, with $k'a = 0$, $\kappa a = 1$, contradicts Hu's statement, quoted at the end of sect. 1. To explain this discrepancy, we notice that it is implicitly assumed in Hu's paper [10]) (see his eqs. (32)—(33)) that $\kappa a \ll 1$, but, as shown by the present example, this need not be true.

For $A > A_n$, the double pole at $\beta = -i$ splits into a pair of poles, which move in opposite directions along the imaginary axis. We shall call the one which moves upwards β_n, and the one which moves downwards β_{-n} (this choice is, of course, entirely a matter of convention). Thus, β_{-n} is an a-pole, which moves from $-i$ to $-i\infty$ when A increases from A_n to ∞. On the other hand, for $A_n < A < c_n$, where c_n is defined by (A6), β_n is an a-pole, which moves from $-i$ to the origin. For $A > c_n$, β_n becomes a b-pole, which moves from the origin to $i\infty$ when A increases from c_n to ∞. Thus, *every pair of* c-*poles ultimately gives rise to an* a-*pole and a* b-*pole.*

An approximate analytical representation of the poles for $1 < A < A_n$ may easily be derived from (13), (A8) and (A11)—(A12). Let us notice, in particular, that, for $1 < A \ll A_n$, we have: $\beta_n \approx x_n - iy_n$, where x_n, y_n are given by (A13) and (A14). The case $A \ll 1$ will be considered in sect. 4.1.

3.2. THE POTENTIAL BARRIER

To carry out the transition from the potential well to the potential barrier, it suffices to replace A by iA in (12) and (13):

$$\alpha^{-1} \sin \alpha = \pm iA^{-1}, \tag{16}$$

$$\beta = \pm(\alpha^2 + A^2)^{\frac{1}{2}}. \tag{17}$$

The roots of (16) are determined in appendix B; the poles of $S_0(\beta)$ in the β-plane then follow from (17). All of them are c-poles. For each value of A, there is an infinite number of poles, $\beta_{\pm n} = \pm u_n + iv_n$, corresponding to the roots α_n of (16).

It suffices to consider the behaviour of the poles in the lower right quadrant. The paths described by the first few poles as a function of A are shown in fig. 2. We find that $\beta_n \to c_{n-1} - i\infty$ for $A \to 0$. When A increases,

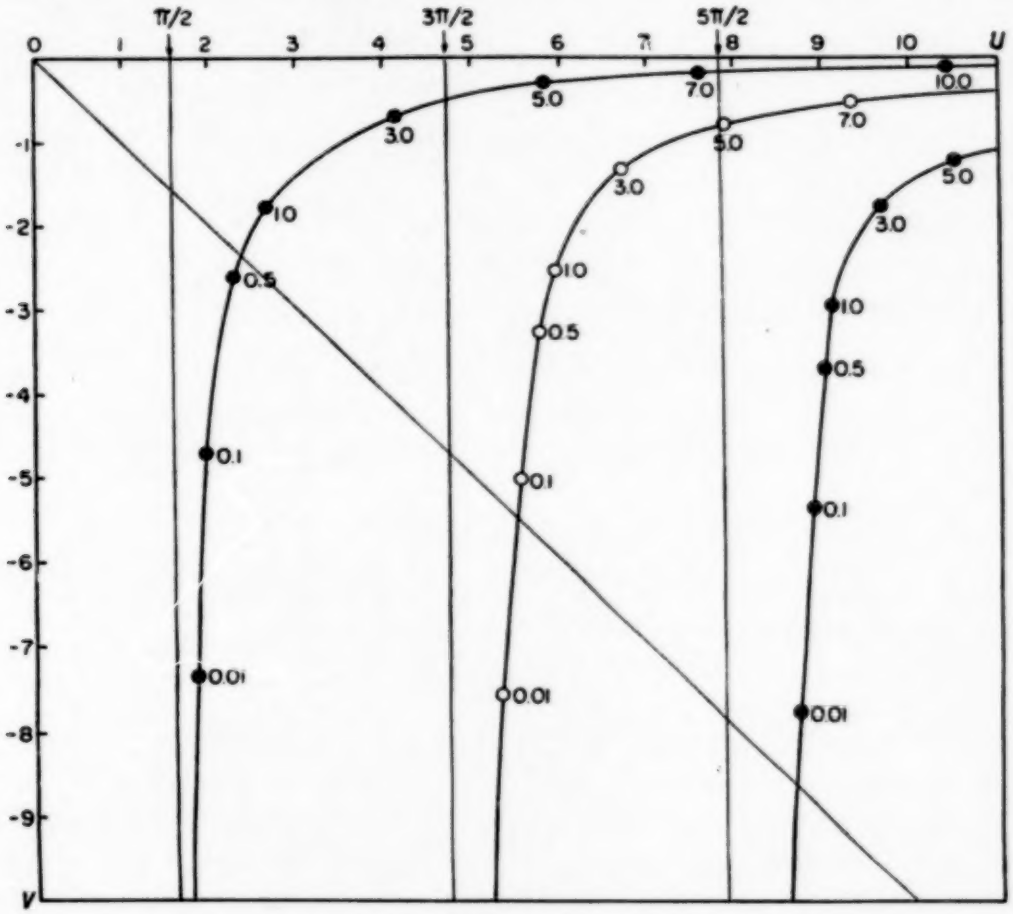

Fig. 2. The poles β_n of $S_0(\beta)$ for a potential barrier.
● $n = 1$; ○ $n = 2$; ◉ $n = 3$.
The numbers beside the poles give the corresponding values of A. The curves in full line are the paths described by the poles. The bisector of the fourth quadrant is also indicated.

β_n moves upwards and away from the imaginary axis, tending to approach the real axis when A becomes very large. In fact, when $A \gg \xi'_n$ (cf. appendix B), we have, according to (17), (B9) and (B10),

$$\beta_n \approx A[1+\tfrac{1}{2}(n\pi/A)^2]-iz_n(n\pi/A)[1+\tfrac{1}{2}(n\pi)^{-2}]. \tag{18}$$

Thus, $u_n \to \infty$ and $v_n \to 0$ for $A \to \infty$. This means that $S_0(\beta)$ has no poles (at finite distance) in the limiting case of an impenetrable barrier ("hard sphere").

Notice that, for $1 < A \ll \xi'_n$, we have $\beta_n \approx x_n - iy_n$, where x_n, y_n are given by (B7) and (B8). The case $A \ll 1$ will be treated in sect. 4.1.

4. The Case of Higher Angular Momenta

The complete determination of the poles of $S_l(\beta)$ is more difficult for $l > 0$ than for $l = 0$. We shall restrict ourselves to a discussion of the general behaviour of "large" poles and to some special results for $l = 1$.

4.1. GENERAL BEHAVIOUR OF "LARGE" POLES

A pole of $S_l(\beta)$ at $\beta = \beta_n = u_n - iw_n$, where $w_n = -v_n > 0$ (it suffices to consider $u_n \geqq 0$), will be called a "large" pole if it fulfils the following conditions:

$$\text{(i)}|\beta_n| \gg A;\ \text{(ii)}|\beta_n| \gg A^2;\ \text{(iii)}|\beta_n| \gg l+1;\ \text{(iv)}\ \exp(w_n) \gg 1. \tag{19}$$

According to (5) and (6), (19) implies that $|E_n| \gg |V_0|$ and

$$|E_n| \gg l(l+1)\hbar^2/2ma^2$$

the height of the "centrifugal barrier". It is not surprising that, under these conditions, we find common features in the behaviour of the poles, as will be shown below.

It follows from (8) and from the relationship

$$j_l(\beta)h_l'^{(1)}(\beta) - j'_l(\beta)h_l^{(1)}(\beta) = i\beta^{-2} \tag{20}$$

that, in the free-particle limit ($A \to 0$) we have, as it should be,

$$\lim_{A\to 0} S_l(\beta) = 1. \tag{21}$$

It may be expected, therefore, that the poles of $S_l(\beta)$ are rejected to infinity when $A \to 0$, so that there are only large poles for very small A.

To determine the large poles of (8), we may, according to (i) and (ii), make the following approximations: $\alpha \approx \beta \pm A^2/(2\beta)$; $|A^2/\beta| \ll 1$. On the other hand, according to (iii) and (iv), we may replace the spherical Bessel functions by their asymptotic expansions, neglecting terms in $\exp(-i\beta)$ in comparison with $\exp(i\beta)$. If this is done, we find that the large poles are approximately given by the equation

$$1 \pm (-1)^l\,[\tfrac{1}{2}A\beta^{-1}\exp(i\beta)]^2 = 0 \quad (+ \text{ for a well, } - \text{ for a barrier}). \tag{22}$$

In this approximation, therefore, the large poles of $S_l(\beta)$ for a potential well (barrier) with even l coincide with those for a potential barrier (well) with odd l.

If we put

$$u_n = U_n + \varepsilon_n \qquad (0 \leqq \varepsilon_n < \tfrac{1}{2}\pi), \tag{23}$$

where

$$U_n = \begin{cases} n\pi & \text{for a well with even } l \text{ or a barrier with odd } l, \\ (n-\frac{1}{2})\pi & \text{for a well with odd } l \text{ or a barrier with even } l, \end{cases} \tag{24}$$

we find that (22) may be replaced, in both cases, by the pair of equations

$$\tan \varepsilon_n = u_n/w_n, \tag{25}$$

$$\exp w_n = (2/A)(u_n^2 + w_n^2)^{\frac{1}{2}}. \tag{26}$$

Neglecting ε_n in comparison with U_n, we get

$$\varepsilon_n = \tan^{-1}(U_n/w_n), \tag{27}$$

$$w_n = \tfrac{1}{2}\log[(2U_n/A)^2 + (2w_n/A)^2] = f(w_n). \tag{28}$$

Eq. (28) may be solved by iteration †, taking

$$w_n^{(1)} = \log(2U_n/A) \qquad (U_n \neq 0), \tag{29}$$

$$w_n^{(r+1)} = f(w_n^{(r)}) \qquad (r = 1, 2, \ldots). \tag{30}$$

In general, the third or fourth iteration already gives a very good approximation.

In particular, if $w_n^{(1)} \ll U_n$, which is certainly the case for $A > 1$,

$$w_n \approx \log(2U_n/A) + \tfrac{1}{2}U_n^{-2}[\log(2U_n/A)]^2 + \ldots, \tag{31}$$

$$u_n \approx U_n + \tfrac{1}{2}\pi - U_n^{-1}w_n + \ldots. \tag{32}$$

Equations (A13)—(A14) and (B7)—(B8) are particular cases of these results.

On the other hand, if $w_n^{(1)} \gg U_n$, which is the case for very small A, we find

$$w_n \approx L_1 + L_2 + L_2L_1^{-1} + (L_2 - \tfrac{1}{2}L_2^2 + \tfrac{1}{2}U_n^2)L_1^{-2} + \ldots, \tag{33}$$

$$u_n \approx U_n + U_n w_n^{-1} + \ldots, \tag{34}$$

where

$$L_1 = \log(2/A); \qquad L_2 = \log\log(2/A). \tag{35}$$

Notice that (33) remains valid if $u_n = U_n = 0$.

It follows from (33) and (34) that

$$\lim_{A \to 0} \beta_n = U_n - i\infty,$$

which generalizes the results obtained for $l = 0$. Notice, in particular, that there is always an isolated (unpaired) pole on the imaginary axis in the first case of (24), but not in the second one.

† A very similar equation has been discussed by de Bruijn [18]).

4.2. THE CASE $l = 1$

For $l = 1$, (8) becomes

$$S_1(\beta) = \exp(-2i\beta)(\alpha^{-1}\cot\alpha - \alpha^{-2} + \beta^{-2} + i\beta^{-1})(\alpha^{-1}\cot\alpha - \alpha^{-2} + \beta^{-2} - i\beta^{-1})^{-1}. \tag{36}$$

The poles of $S_1(\beta)$ are the roots of

$$\alpha^{-1}\cot\alpha - \alpha^{-2} + \beta^{-2} - i\beta^{-1} = 0. \tag{37}$$

(a) *The potential well*

Let us consider first the poles on the imaginary axis, $\beta = iv$. No such poles exist for $|v| > A$. For $|v| < A$, according to (7) and (37), they are given by the points of intersection of the curve

$$x^{-1}\cot x - x^{-2} = v^{-1} + v^{-2}, \tag{38}$$

which has been drawn in full line in fig. 3, with the family of circles

$$x^2 + v^2 = A^2, \tag{39}$$

some of which have been drawn in dashed line in fig. 3.

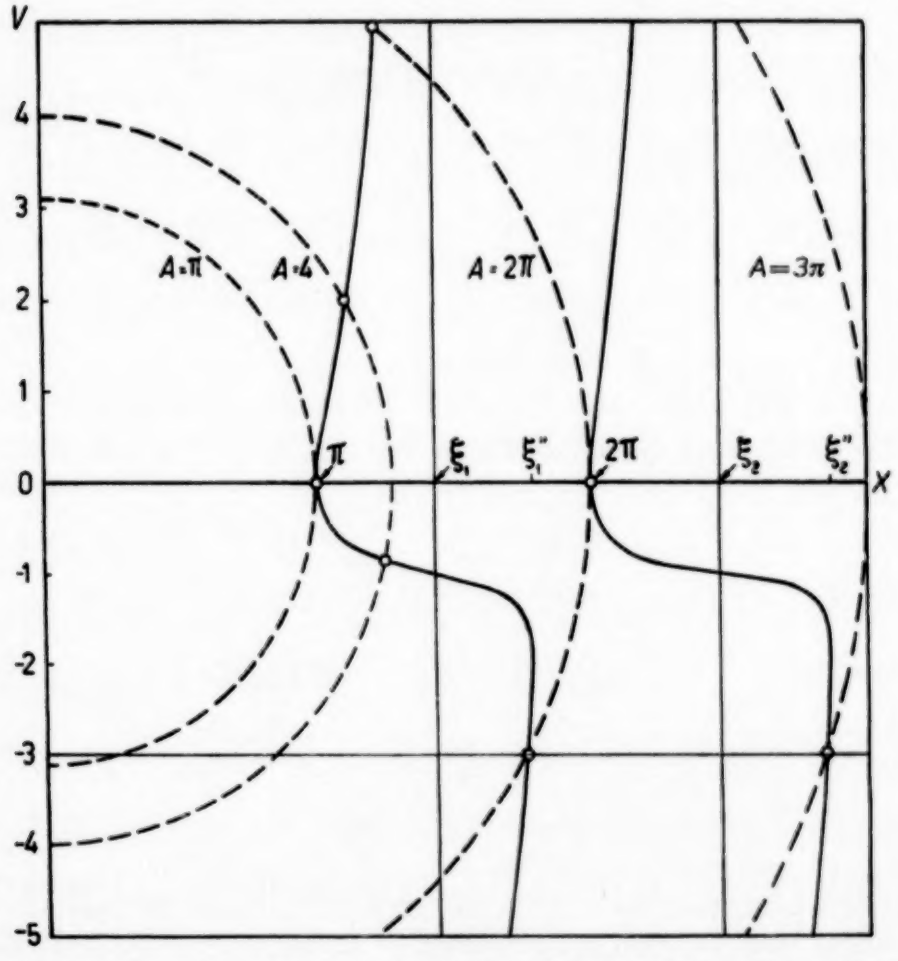

Fig. 3. Determination of the purely imaginary poles of $S_1(\beta)$ for a potential well.
——— $x^{-1}\cot x - x^{-2} = v^{-1} + v^{-2}$; – – – – $x^2 + v^2 = A^2$.
Notice that the intersections occur close to the straight line $v = -3$ for $A = 2\pi$ and $A = 3\pi$.

The curve (38) is defined in the intervals: $n\pi \leqq x \leqq \xi''_n (n = 1, 2, \ldots)$, where ξ''_n is the nth positive root of the equation: $x^{-1}\cot x - x^{-2} = -\frac{1}{4}$. The straight lines $x = \xi_n$, where ξ_n is given by (A5), are vertical asymptotes.

There are no poles on the imaginary axis for $A < \pi$. For $A = \pi$, (38)—(39) have a double root at $v = 0$. However, this is not a pole of $S_1(\beta)$ (cf. sect. 3.1). For $A > \pi$, this double root splits into a pair of roots, giving rise to an a-pole, which moves downwards for increasing A, and a b-pole (first bound p-state), which moves upwards when A increases. A similar process takes place each time that A goes through an integral multiple of π.

How do these poles appear on the imaginary axis? A comparison with the case $l = 0$ suggests that they must arise from the confluence of pairs of c-poles. If this is true, there must be a pair of c-poles close to the origin whenever A approaches an integral multiple of π. In order to determine these poles, we shall make the following assumptions in (37):

$$0 < A(n\pi - A) = \delta_n \ll 1 \quad (n = 1, 2, \ldots), \tag{40}$$

$$|\beta| \ll A, \qquad |\beta|^2 \ll 2A. \tag{41}$$

Under these conditions, (37) may be approximated by

$$\delta_n - i\delta_n\beta - \tfrac{3}{2}\beta^2 + \tfrac{1}{2}i\beta^3 = 0, \tag{42}$$

neglecting terms of the order of $A^{-2}\beta^4$.

The roots of (42) are

$$\begin{aligned} \beta_{\pm n} &= \pm(\tfrac{2}{3}\delta_n)^{\frac{1}{2}} - i(\tfrac{2}{9}\delta_n) + O(\delta_n{}^{\frac{3}{2}}), \\ \beta' &= -3i + \tfrac{4}{9}i\delta_n + O(\delta_n{}^2). \end{aligned} \tag{43}$$

Notice that β_n and β_{-n} are approximate roots of (37), but this is only true for β' if it fulfils condition (41). Thus, β' is not an approximate root of (37) for $n = 1$. However, it may be shown that, for $n \geqq 2$, there exists indeed an a-pole close to the point $-3i$. For $n = 2$ and $n = 3$, this may be clearly seen in fig. 3.

For $A \to n\pi$, the c-poles $\beta_{\pm n}$ approach the origin along a parabolic arc (with vertex at the origin). For $A > n\pi$, they dissociate into an a-pole and a b-pole.

The behaviour of the poles differs from the behaviour for $l = 0$ in the following respects: (1) according to sect. 4.1, $\beta_n \to c_{n-1} - i\infty$ as $A \to 0$; therefore, there is no isolated pole on the imaginary axis; (2) the "joining-point" of the c-poles is at the origin (instead of the point $\beta = -i$).

(b) *The potential barrier*

In this case, according to sect. 4.1, $\beta_n \to n\pi - i\infty$ as $A \to 0$, so that there is an isolated pole on the imaginary axis, $\beta_0 = iv_0$. When A increases from 0 to ∞, β_0 moves upwards from $-i\infty$ to $-i$.

As was the case for $l = 0$, the c-poles $\beta_{\pm n} = \pm u_n + iv_n$ ($n \geqq 1$) tend to approach the real axis for large values of A. However, in contrast with the case $l = 0$, one pole remains at finite distance as $A \to \infty$, namely, the a-pole $\beta_0 = -i$.

Generally, for any angular momentum l, l poles remain at finite distance in the limiting case of a "hard sphere". These poles are the roots of the equation

$$h_l^{(1)}(\beta) = 0. \tag{44}$$

The poles corresponding to the first few values of l are given in table 1 [16]).

TABLE 1

The poles of $S_l(\beta)$ for a "hard sphere"

$l =$	0	1	2	3
$\beta =$	$-$	$-i$	$\pm\frac{1}{2}\sqrt{3}-\frac{1}{2}i$	$-2.26i$ $\pm 1.75-1.87i$

Notice that, in agreement with the results of sect. 4.1, there are only pairs of c-poles for even l, whereas, for odd l, there is also an isolated a-pole.

By comparing the "hard sphere" with its electromagnetic counterpart, a perfect conductor, we find an interesting connection with antenna theory †. In fact, the roots of (44), for $l \geqq 1$, are also the characteristic values associated with the so-called magnetic modes of oscillation of a perfectly conducting sphere [16]). These characteristic values are the poles of the S-matrix of the associated scattering problem.

5. Discussion

5.1. GENERAL PROPERTIES OF THE POLE DISTRIBUTION

The results obtained in the previous sections allow us to verify, in the present example, some general properties of the pole distribution for non-relativistic scattering by a central potential of finite range ††:

(1) There is an infinite number of poles, but only a finite number of them lie on the imaginary axis [17, 18]).

(2) For large n, the distance $|\beta_{n+1}-\beta_n|$ between two consecutive c-poles approaches the value π (see ref.[18])). This follows from sect. 4.1.

(3) The distance of the c-poles to the real axis increases logarithmically with n (see ref. [18])). If we put: $\beta_n = |\beta_n| \exp(-i\theta_n)$, we find, according to

† The author is indebted to Prof. G. Beck for pointing out the connection between the antenna problem and the S-matrix. We expect to treat this point more fully in a future paper, in collaboration.

†† Properties (2) and (3) have been derived for the case of s-scattering [18]).

sect. 4.1 †,

$$\sin \theta_n \approx (n\pi)^{-1} \log n \ (n \to \infty). \tag{45}$$

5.2. ON THE PHYSICAL INTERPRETATION OF THE POLES

According to Heitler and Hu [9]), almost all the poles of the S-matrix have a simple physical interpretation (namely, the interpretation that we have outlined in sect. 1). In the non-relativistic case, the only "meaningless" poles would be those which are located in the region of the complex k-plane where the real part E of the "complex energy" (2) is negative, i.e., below the bisectors of the third and fourth quadrants (cf. fig. 1 and fig. 2).

Besides the fact that a continuous transition from these so-called meaningless poles to the so-called meaningful ones is possible (as shown by the present example), it must be pointed out that the interpretation of E as the approximate energy of a "decaying state" is certainly not valid if $|\Gamma/E| \gg 1$. Therefore, there seem to be no grounds for accepting the above criterion.

As we have mentioned in the introduction, the approximations involved in the usual interpretation of c-poles are based upon conditions (a) and (b) of sect. 1. In the present example, these conditions are fulfilled only in a few cases (cf. fig. 1 and fig. 2). One of them is the case of the lowest-order poles for a very high barrier (which are given by (18) for $l = 0$). These poles correspond to virtual energy levels lying above the top of the barrier. The well-known analogy with optical interference phenomena in thin plates may be applied to them. The "level width" may be estimated by the usual formula[19])

$$\Gamma = \hbar T v_i/(2a), \tag{46}$$

where v_i is the "velocity" inside the potential and T is the "transmissivity" of the potential step.

Eq. (46) may also be applied to the lowest-order c-poles for a very deep potential well, provided $|\Gamma| \ll E$. In this case, it gives $\Gamma/\mathscr{E} \approx 4(E/\mathscr{E})^{\frac{1}{2}}$. This result is equivalent to the fact that the c-poles tend to approach the straight line $v = -1$ in the β-plane (cf. fig. 2 and sect. 3.1). The virtual levels of a well are much broader than those of a barrier of comparable range and transmissivity; this is due to the much larger value of v_i in the case of a well.

One runs into serious difficulties as soon as one tries to apply the usual interpretation in cases when the above-mentioned conditions are not fulfilled. As the poles get farther away from the real axis, the corresponding resonance peaks in the scattering cross-section become broader and broader, tending to overlap in an inextricable way, until they merge into a slowly-

† Eq. (45) should be compared with eq. (19) of Regge's paper [18]) ($\lambda = 0$ in our example). There are some errors in eqs. (16)—(19) of that paper; in particular, a factor $2/\pi$ is missing in the second member of eqs. (18) and (19). Notice that Regge's way of numbering the poles is different from ours, so that his n (in eq. (19)) is equivalent to our $\frac{1}{2}n$.

varying background, which is usually included in the so-called potential scattering.

On the other hand, it is exceedingly doubtful whether these poles can be interpreted in terms of "decaying states". This is clearly seen when we consider the case of a very shallow well (or a very low barrier), in which all the poles are large poles (sect. 4.1). If we build up a wave packet that is initially concentrated within the potential, in this case, it will propagate and spread practically in the same way as it would do in the case of free particles, and this process has nothing to do with exponential decay †.

It has been shown by Regge [18, 21]) that the asymptotic behaviour of the large poles depends very critically on the asymptotic behaviour of the potential. Physically unimportant changes in the potential may completely modify the behaviour of the large poles, so that these poles cannot have much physical significance [21]). This "hypersensitiveness" of the poles with respect to asymptotic conditions, which had previously been noticed in the case of "spurious" poles, is a very unwelcome feature of the S-matrix formalism.

Let us now consider the poles on the negative imaginary axis (a-poles). The "energies" that formally correspond to them, according to (2), are real negative energies, just as in the case of bound states (b-poles). However, while the energy levels of the bound states are determined by the condition that the wave function at $r = a$ may be smoothly joined to a *purely decreasing* exponential for $r > a$, the energies associated to a-poles are those for which the wave function at $r = a$ may be smoothly joined to a *purely increasing* exponential for $r > a$. For this reason, we propose to call them *anti-levels* ††, and to call the associated poles *anti-poles*.

In the case of a potential well with $l = 0$, the anti-level associated to the a-pole β_0(sect. 3.1) lies below the bottom of the well for $0 < A < 1$, and within the well for $1 < A < \frac{1}{2}\pi$. All other anti-levels lie within the well; as may readily be verified, there is one anti-level between every pair of bound states.

Let us sum up. It is convenient to classify the poles of the S-matrix into several (not sharply separated) groups. They range all the way from those which are associated with well-defined physical concepts to those which seem to be no more than mathematical properties of the formalism. The bound states belong to the first category. The usual interpretation of c-poles may be applied to "long-lived decaying states", either for an attractive or for a repulsive potential. However, it seems to be very difficult to give a precise and general formulation of the scattering problem in the case of "short-lived decaying states".

† A discussion of the exponential decay law has recently been given in a paper by Höhler [20]).

†† They are sometimes called "virtual levels" (cf. sect. 5.3), but it seems to us that this is a most unfortunate terminology, since it is apt to suggest the idea of quasi-stationary states.

The limiting case of a "hard sphere" is specially interesting. In the related case of a perfect conductor, it is known that there exist certain characteristic states of the field, which are more or less strongly damped by radiation according to the shape of the conductor. Our model indicates the existence of a connection between these "antenna states" and the other limiting case of strongly bound states in a deep well (cf. the end of sect. 4.2).

The large poles seem to have very little physical significance. It might be expected that the a-poles, which are "meaningless" in the usual interpretation, cannot have any physical importance. However, this is not true, as will be shown in the next section.

5.3. THE LOW-ENERGY SCATTERING CROSS-SECTION

It will be shown in this section that some poles of the S-matrix that would be considered to be "meaningless" according to the usual interpretation (in particular, a-poles) may give rise to important physical effects in the low-energy scattering cross-section.

The scattering cross-section σ_l for angular momentum l is given by the well-known expression

$$\sigma_l = (2l+1)\pi a^2 \beta^{-2} |1-S_l(\beta)|^2. \tag{47}$$

(a) *The case* $l = 0$

Let us consider a potential well that is almost deep enough for the appearance of the first bound state, so that $A = \frac{1}{2}\pi - \varepsilon$, $0 < \varepsilon \ll 1$. According to (15), this implies the existence of an a-pole at $\beta = \beta_0 \approx -\frac{1}{2}i\pi\varepsilon$, and, according to (15) and (47),

$$\sigma_0 \approx 4\pi a^2 [\beta^2 + (\tfrac{1}{2}\pi\varepsilon)^2]^{-1}, \tag{48}$$

so that the cross-section becomes very large as $\beta \to 0$. *An* a-*pole very close to the origin gives rise to an anomalously large scattering cross-section at low energies.*

This behaviour is well known in the case of neutron-proton scattering. It is usually interpreted in terms of a so-called virtual singlet state of the deuteron, the definition of which has occasioned some confusion in the literature. There have been several attempts to define a "virtual level" at a small positive energy. It must be stressed, in this connection, that, in the present example, all c-poles are far away from the origin for $A \approx \frac{1}{2}\pi$, as may readily be verified from fig. 1. The definition by means of an a-pole of the S-matrix has been considered by several authors [22, 23, 24]).

Let us follow the behaviour of the low-energy cross-section during the process which leads to the appearance of the next bound s-state ($A \to \frac{3}{2}\pi$). In S-matrix language, this process corresponds to the transformation of the pair of c-poles $\beta_{\pm 1}$ into an a-pole and a b-pole (cf. sect. 3.1 and fig. 1).

It may be verified without difficulty that, as β_1 approaches the bisector of the fourth quadrant, the low-energy cross-section becomes very small ($\ll \pi a^2$). The value of A for which β_1 crosses the bisector practically coincides with the value $A = \pi\sqrt{2} \approx 4.44$, which marks the appearance of the first zero in the cross-section. This zero appears at the point $\beta = \frac{1}{2}\pi$; when A increases, it splits into a pair of zeros, one of which moves towards lower energies, while the other one moves towards higher energies. In fig. 4, the

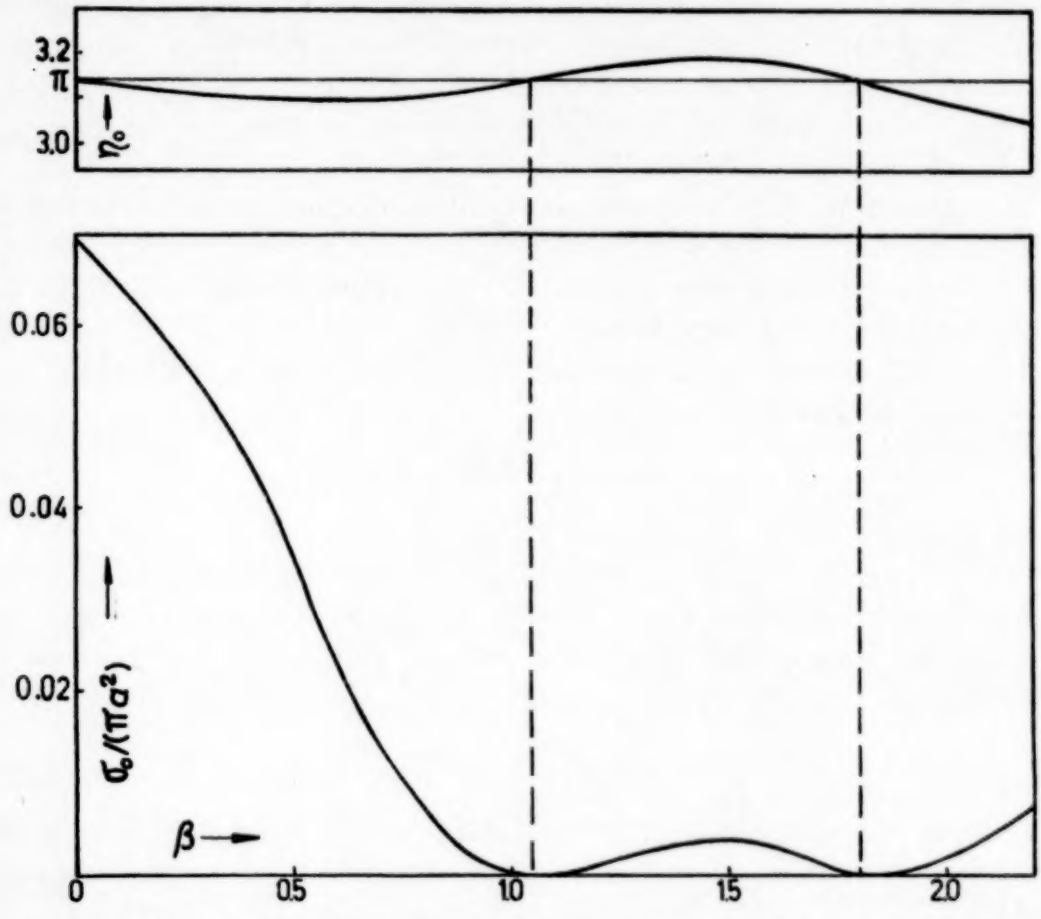

Fig. 4. The ratio $\sigma_0/(\pi a^2)$ and the phase-shift η_0 as a function of β for a potential well with $A = 4.46$.

ratio $\sigma_0/(\pi a^2)$ has been plotted as a function of β, for $A = 4.46$, together with the corresponding values of the phase-shift $\eta_0 (\eta_0 = \pi$ at the zeros of the cross-section). A vanishing cross-section at low energy is well known in the theory of the Ramsauer-Townsend effect.

For $A = \xi_1 \approx 4.49$, the zero-energy cross-section vanishes. For $A > \xi_1$, the low-energy cross-section begins to increase. For $A = A_1 \approx 4.61$, β_1 and β_{-1} coalesce at the point $\beta = -i$, giving rise to a pair of a-poles. The low-energy cross-section keeps increasing while one of these a-poles moves towards the origin, and it attains again very large values when the a-pole is very close to the origin ($A \to \frac{3}{2}\pi \approx 4.71$).

A similar process takes place before the appearance of other bound states. Thus, *the typically quantal anomalies (very small or very large values) of the low-energy cross-section, which precede the appearance of a new bound state, are related to poles of the S-matrix that would be considered to be "meaningless" according to the usual interpretation.*

(b) *The case* $l = 1$

Let us consider a potential well that is almost deep enough for the appearance of a new bound p-state, so that (40) is satisfied. In this case, as we have seen in sect. 4.2, there exists a pair of c-poles, $\beta_{\pm n}$, given by (43), very close to the origin.

To obtain the low-energy p-wave cross-section, we may employ (36) and (47), replacing the denominator of (36) by the first member of (42), and expanding $\exp(-2i\beta)$ in powers of β. The result is †

$$\sigma_1/(12\pi a^2) \approx \beta^4[(\tfrac{3}{2}\beta^2-\delta_n)^2+\beta^2(\tfrac{1}{2}\beta^2-\delta_n)^2]^{-1}. \tag{49}$$

In the region

$$|\beta^2-\tfrac{2}{3}\delta_n| \ll \tfrac{2}{3}\delta_n, \tag{50}$$

eq. (49) gives rise to a "Breit-Wigner peak" of half-width $(\frac{4}{3})(\frac{2}{3}\delta_n)^{\frac{1}{2}}$, centered at $\beta^2 = \frac{2}{3}\delta_n$. This agrees with the usual interpretation. The existence of a sharp resonance in this case may be attributed to the "centrifugal barrier".

It might be expected that only the poles (and corresponding zeros) that are close to the origin would determine the behaviour of the low-energy cross-section. If this were so, (36) could be replaced by

$$S_1(\beta) \approx \exp(-2i\beta)(\beta+\beta_n)(\beta+\beta_{-n})(\beta-\beta_n)^{-1}(\beta-\beta_{-n})^{-1}. \tag{51}$$

Replacing (51) in (47), and taking into account (43), we get

$$\sigma_1/(12\pi a^2) \approx [(\beta^2-\tfrac{2}{9}\delta_n)^2+(\tfrac{2}{9}\delta_n)^2\beta^2][(\beta^2-\tfrac{2}{3}\delta_n)^2+\tfrac{4}{9}(\tfrac{2}{3}\delta_n)^3]^{-1}. \tag{52}$$

Although this agrees with (49) in the region (50), it is by no means a good approximation outside of this region. In particular, (52) would give

$$\lim_{\beta\to 0}[\sigma_1/(12\pi a^2)] = \begin{cases} \frac{1}{9} & \text{for } \delta_n \neq 0, \\ 1 & \text{for } \delta_n = 0, \end{cases} \tag{53}$$

whereas, according to (49) ††,

$$\lim_{\beta\to 0}[\sigma_1/(12\pi a^2)] = \begin{cases} 0 & \text{for } \delta_n \neq 0, \\ \frac{4}{9} & \text{for } \delta_n = 0. \end{cases} \tag{54}$$

† This differs from the result given by Schiff in eq. (19.30) of his book [25]). The discrepancy is due to the fact that Schiff fails to take into account terms of the order of $(ka)^2$ and $(ka)^4$ in the denominator of his eq. (19.27).

†† For $\delta_n = 0$, (54) does not agree with the result given in p. 36 of Mott and Massey's book [13]). This is due to an error in their eq. (39): a factor $2/(2n+1)$ should be inserted in the second member of that equation.

The difference between (52) and (49) is due to the omission of the root $\beta' \approx -3i$ of (43) from $S_1(\beta)$. According to sect. 4.2, β' is an a-pole for $n \geqq 2$. In this case, therefore, the correct behaviour of the low-energy cross-section may only be obtained by taking into account the a-pole β' (together with the corresponding zero), even though it is far away from the origin. This is another example of the physical effects that may be produced by an a-pole.

The author is greatly indebted to Prof. G. Beck for suggesting this problem and for many helpful discussions. He is also grateful for the hospitality of the Technische Hogeschool at Eindhoven, where this work was written.

Appendix

A. THE ROOTS OF EQUATION (12)

Replacing $\alpha = x+iy$ in (12), and separating real and imaginary parts, we find the following three possibilities:

$$\begin{aligned} &x^{-1}\tan x = y^{-1}\tanh y \quad \text{(I)}, \\ &y = \cosh^{-1}|x/(A\sin x)| \quad \text{(II)}, \end{aligned} \qquad (x \neq 0, \quad y \neq 0), \tag{A1}$$

$$\begin{aligned} &x^{-1}\sin x = \pm A^{-1}, \\ &y = 0, \end{aligned} \tag{A2}$$

$$\begin{aligned} &x = 0, \\ &y^{-1}\sinh y = A^{-1} \quad (A > 0). \end{aligned} \tag{A3}$$

The corresponding choice of sign in (13), in order to satisfy (11), is such that $v < 0$, in the case of (A1) and (A3), and such that

$$\operatorname{sgn} v = -\operatorname{sgn}(x \sin 2x) \tag{A4}$$

in the case of (A2), as may be easily proved.

Since the roots of (12) are symmetrical with respect to the x and y axes, we shall restrict ourselves to the first quadrant ($x \geqq 0$, $y \geqq 0$) in the following discussion.

There are no roots of (A3) for $A > 1$. For each value of A belonging to the interval 0—1, (A3) has one root; when A increases from 0 to 1, y decreases from ∞ to 0.

The roots of (A1) and (A2) may be found by graphical means. Equation (II) defines a family of curves depending on the parameter A. For each value of A, the roots of (A1) are given by the points of intersection of curves (II) and (I), whereas the roots of (A2) are given by the intersections of (II) with the real axis.

Curve (I) has been drawn in full line in fig. 5. It is defined for $n\pi < x \leqq \xi_n$ $(n = 1, 2, 3, \ldots)$, where ξ_n is the nth positive root of the equation $\tan x = x$. For large n, we have

$$\xi_n \approx c_n - c_n^{-1} - \tfrac{2}{3}c_n^{-3} - \ldots, \tag{A5}$$

where

$$c_n = (n+\tfrac{1}{2})\pi. \tag{A6}$$

Portions of curves (II) have been drawn in dashed line in fig. 5; the corresponding values of A are also indicated.

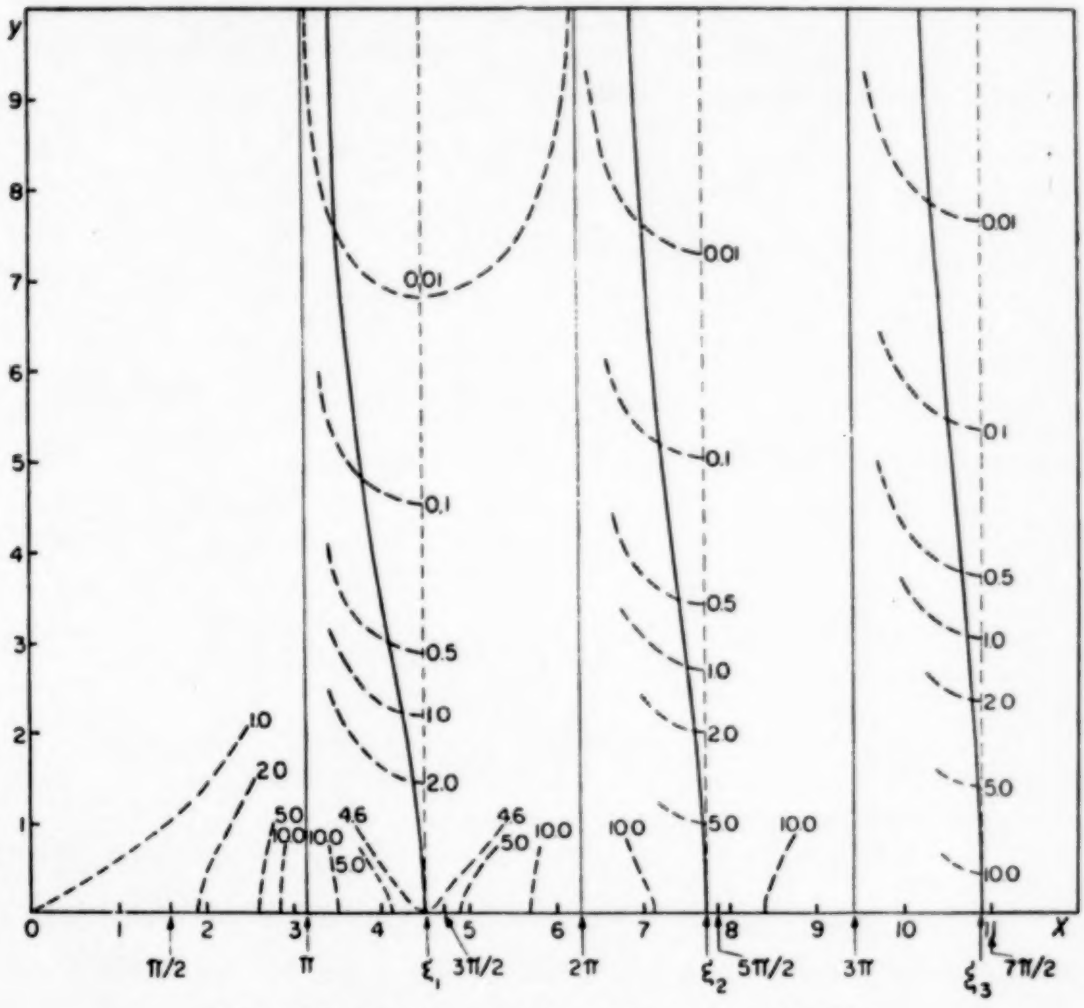

Fig. 5. Determination of the roots of (A1) and (A2).
——— Curve (I); - - - - Curves (II) (the corresponding values of A are indicated beside the curves).

Let I_n be the interval $n\pi \leqq x < (n+1)\pi$. In I_0, curves (II) intersect the real axis only for $A \geqq 1$. The corresponding root of (A2) increases from 0 to π when A increases from 1 to ∞.

The following discussion applies to all the intervals I_n with $n \geqq 1$. To illustrate the behaviour of curves (II) in I_n, a typical curve ($A = 0.01$

in I_1) has been drawn in fig. 5. Each curve (II) goes through a single minimum in I_n. This point is located on the straight line $x = \xi_n$. When A increases, it moves downwards along this line, reaching the real axis for $A = A_n$, where

$$A_n = |\xi_n/\sin \xi_n| \approx c_n - \tfrac{1}{2}c_n^{-1} - \tfrac{7}{24}c_n^{-3} - \ldots . \tag{A7}$$

It can easily be shown that, for every value of A between 0 and A_n, curves (I) and (II) intersect at one and only one point in I_n. The corresponding root, $\alpha_n = x_n + iy_n$, moves downwards when A increases. Notice that $\alpha_n \to n\pi + i\infty$ for $A \to 0$, and $\alpha_n \to \xi_n$ for $A \to A_n$.

For $A > 1$, an approximate analytical representation of α_n may be derived. Under this condition, the intersection occurs close to the minimum of (II), so that (II) may be approximated by

$$y_n \approx Y_n + \tfrac{1}{2}b_n(\xi_n - x_n)^2, \tag{A8}$$

where

$$Y_n = \cosh^{-1}|A_n/A|, \tag{A9}$$

$$b_n = y''(\xi_n) = [1-(A/A_n)^2]^{-\frac{1}{2}}. \tag{A10}$$

On the other hand, if we put $x_n = c_n - \delta_n$, (I) may be replaced by

$$(c_n\delta_n)^{-1} + c_n^{-2} + (c_n^{-2} - \tfrac{1}{3})c_n^{-1}\delta_n \approx Y_n^{-1} \tanh Y_n = (b_n Y_n)^{-1},$$

from which we find, by iteration,

$$x_n \approx c_n\left\{1 - \left[\left(\frac{c_n^2}{b_n Y_n} - 1\right) + \left(\frac{c_n^2}{3} - 1\right)\left(\frac{c_n^2}{b_n Y_n} - 1\right)^{-1}\right]^{-1}\right\}. \tag{A11}$$

In the immediate neighbourhood of $A = A_n$, this may be replaced by

$$x_n \approx \xi_n - [1-(b_n Y_n)^{-1}]\xi_n^{-1}. \tag{A12}$$

Equations (A8) and (A11)–(A12) give a very good approximation to the roots of (A1) when $1 < A < A_n$. In particular, for large n, i.e., for $1 < A \ll A_n$, we find

$$x_n \approx c_n - c_n^{-1}\log(2c_n/A) + \ldots , \tag{A13}$$

$$y_n \approx \log(2c_n/A) + \tfrac{1}{2}c_n^{-2}\{[\log(2c_n/A)-1]^2 - \tfrac{1}{2}A^2 - 1\} + \ldots . \tag{A14}$$

For $A = A_n$, we have $\alpha_n = \xi_n$. This is a double root of (12), which arises from the confluence of a root in the upper half-plane with a root in the lower half-plane. For $A > A_n$, it splits into a pair of roots of (A2), which move in opposite directions when A increases, approaching the end-points of I_n when $A \to \infty$.

B. THE ROOTS OF EQUATION (16)

Replacing $\alpha = x + iy$ in (16), and separating real and imaginary parts, we find that there are no solutions with $x = 0$ or $y = 0$. For $x \neq 0$, $y \neq 0$, we obtain

$$x \tan x = -y \tanh y \quad (I'),$$
$$y = \sinh^{-1}|x/(A \cos x)| \quad (II'). \tag{B1}$$

The curve (I'), which is defined for $c_{n-1} < x \leqq n\pi$ $(n \geqq 1)$, has been drawn in full line in fig. 6. Portions of curves (II') have been drawn in

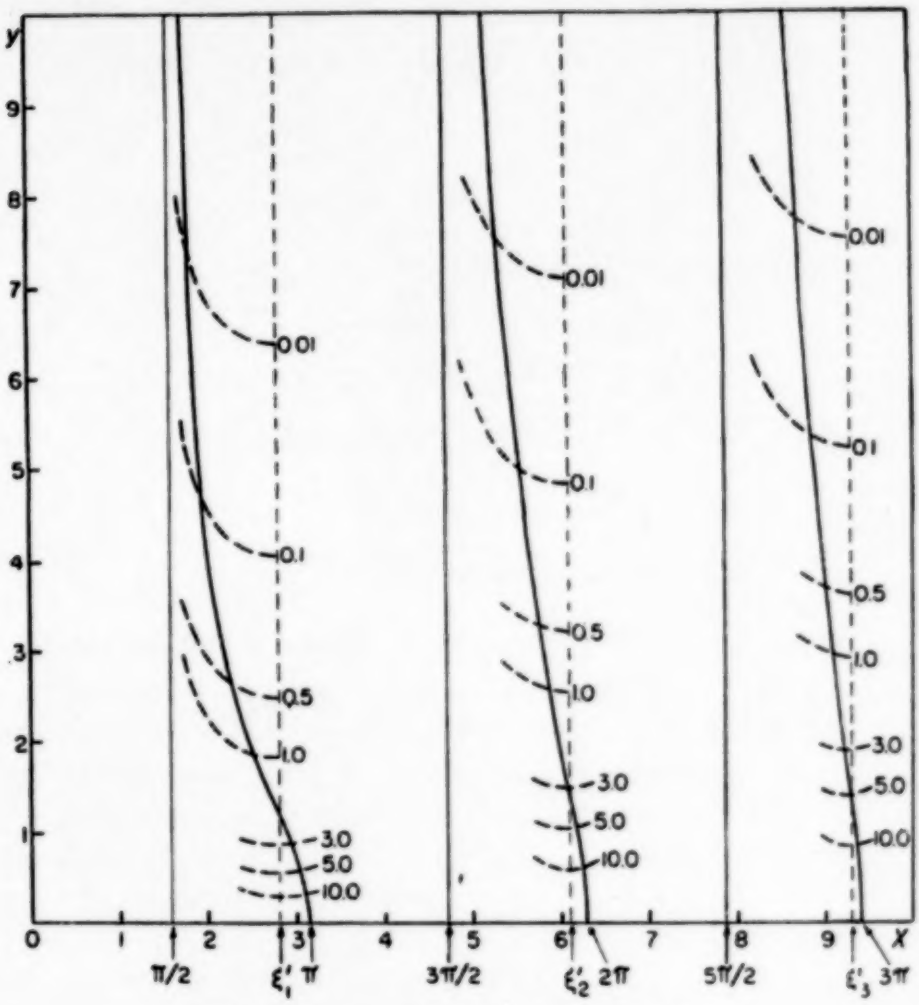

Fig. 6. Determination of the roots of (B1).
——— Curve (I'); - - - - Curves (II') (the corresponding values of A are indicated beside the curves).

dashed line; the corresponding values of A are indicated. In each interval $I'_n : c_{n-1} \leqq x < c_n$, each curve (II') goes through a single minimum, located on the straight line $x = \xi'_n$, where ξ'_n is the nth positive root of the equation $\cot x = -x$. For large n,

$$\xi'_n \approx n\pi - (n\pi)^{-1} - \tfrac{2}{3}(n\pi)^{-3} - \ldots. \tag{B2}$$

When A increases, the minimum of (II') moves downwards, approaching the real axis for $A \to \infty$.

For every value of A, (I') and (II') intersect at one and only one point in

I'_n. The corresponding root of (16), $\alpha_n = x_n + iy_n$, moves downwards when A increases. We find that $\alpha_n \to c_{n-1} + i\infty$ for $A \to 0$, and $\alpha_n \to n\pi$ for $A \to \infty$.

The following formulae, the derivation of which is similar to that of (A8)—(A11), give a very good approximation to the roots when $A > 1$:

$$x_n \approx n\pi - (n\pi)^{-1} b'_n Y'_n - (n\pi)^{-3}(b'_n Y'_n)^2(1 - \tfrac{1}{3} b'_n Y'_n), \tag{B3}$$

$$y_n \approx Y'_n + \tfrac{1}{2} b'_n (\xi'_n - x_n)^2, \tag{B4}$$

where

$$Y'_n = \sinh^{-1} z_n, \quad b'_n = (1 + z_n^{-2})^{-\frac{1}{2}}, \tag{B5}$$

$$z_n = (1 + \xi'^2_n)^{\frac{1}{2}}/A. \tag{B6}$$

In particular, for $1 < A \ll \xi'_n$, we have

$$x_n \approx n\pi - (n\pi)^{-1} \log(2n\pi/A) + \ldots, \tag{B7}$$

$$y_n \approx \log(2n\pi/A) + \tfrac{1}{2}(n\pi)^{-2}\{[\log(2n\pi/A) - 1]^2 + \tfrac{1}{2}A^2 - 1\} + \ldots. \tag{B8}$$

On the other hand, for $A \gg \xi'_n (z_n \ll 1)$, we find

$$x_n \approx n\pi - (n\pi)^{-1} z_n^2 + \ldots, \tag{B9}$$

$$y_n \approx z_n + \tfrac{1}{2}(n\pi)^{-2} z_n + \ldots. \tag{B10}$$

Note added in proof: It has been shown by Humblet (Mém. in-8° Soc. Roy. Sc. Liège **12** (1952) no. 4) that the properties of the pole distribution which are mentioned in sect. 5.1 are valid for a very general class of potentials of finite range and for arbitrary values of the angular momentum. Humblet has also given a thorough discussion of the asymptotic behaviour of large poles. The results given in sect. 4.1 of the present paper are in complete agreement with his results. The author wishes to thank Prof. L. Rosenfeld for bringing Humblet's paper to his attention.

References

1) G. Beck, Z. Phys. **62** (1930) 331;
See also G. Beck and L. H. Horsley, Nature **135** (1935) 430
2) C. Møller, Mat. Fys. Medd. Dan. Vid. Selsk. **22** (1946) no. 19
3) W. Schützer, An. da Acad. Brasileira de Ciências **19** (1947) 283
4) W. Schützer and J. Tiomno, Phys. Rev. **83** (1951) 249
5) N. G. van Kampen, Phys. Rev. **89** (1953) 1072; and **91** (1953) 1267
6) S. T. Ma, Phys. Rev. **71** (1947) 195
7) R. Jost, Helv. Phys. Acta **20** (1947) 256
8) C. Møller, Nature **158** (1946) 403; and ref. [2])
9) W. Heitler and N. Hu, Nature **159** (1947) 776
10) N. Hu, Phys. Rev. **74** (1948) 131
11) G. Breit and F. L. Yost, Phys. Rev. **48** (1935) 203
12) A. M. Lane and R. G. Thomas, Revs. Mod. Phys. **30** (1958) 257, 343 (following a suggestion by N. G. van Kampen)

13) N. F. Mott and H. S. W. Massey, The theory of atomic collisions, 2nd ed. (Clarendon Press, Oxford, 1949) p. 35
14) P. M. Morse and H. Feshbach, Methods of theoretical physics (McGraw-Hill Book Company, New York, 1953) p. 1573
15) N. G. de Bruijn, Asymptotic methods in analysis (North-Holland Publishing Company, Amsterdam, 1958) p. 25
16) J. A. Stratton, Electromagnetic theory (McGraw-Hill Book Company, New York, 1941) p. 559
17) H. Rollnik, Z. Phys. **145** (1956) 654
18) T. Regge, Nuovo Cimento **8** (1958) 671
19) J. M. Blatt and V. F. Weisskopf, Theoretical nuclear physics (John Wiley & Sons, New York, 1952) p. 389
20) G. Höhler, Z. Phys. **152** (1958) 546
21) T. Regge, Nuovo Cimento **9** (1958) 491
22) W. Heisenberg, Theorie des Atomkerns (Göttingen, 1951)
23) S. T. Ma, Rev. Mod. Phys. **25** (1953) 853
24) J. Humblet, Phys. Rev. **97** (1955) 1145
25) L. I. Schiff, Quantum mechanics (McGraw-Hill Book Company, New York, 1949) p. 113

2.J *Nuclear Physics* 11 (1959) 522—530; © *North-Holland Publishing Co., Amsterdam*
Not to be reproduced by photoprint or microfilm without written permission from the publisher

A SUGGESTED EXPLANATION FOR THE ANOMALOUS ANISOTROPIES IN HIGH ENERGY FISSION

I. HALPERN

Physics Department, University of Washington, Seattle, Washington

Received 9 March 1959

Abstract: Recent experiments on fission induced by high energy protons have shown that the angular distributions of fragments are peaked at right angles to the beam. The fission fragments thus come off mainly with oribital angular momenta oriented along the beam axis despite the fact that the angular momenta of the incident protons with respect to the nuclear centre are oriented perpendicular to this direction. This "anomaly" is attributed to the cooperation of two effects: (1) There are relatively many collisions of an incident proton with individual nucleons in a nucleus which result in angular momentum transfers to the nucleus along the beam axis. This is due to the nature of the nucleon-nucleon differential cross section at high energy. (2) The collisions just described generally leave relatively small amounts of excitation energy in the nucleus. It has been shown that small excitation energies are particularly favourable for the production of large anisotropies.

1. Introduction

The fragments in fission induced by moderate energy particles are emitted with greatest probability forward and backward along the beam[1–3]). In two recent studies of fission induced in U^{238} by high energy protons [4, 5]), it was found, on the other hand, that more fission fragments are emitted at right angles to the beam than in other directions (fig. 1). The results at

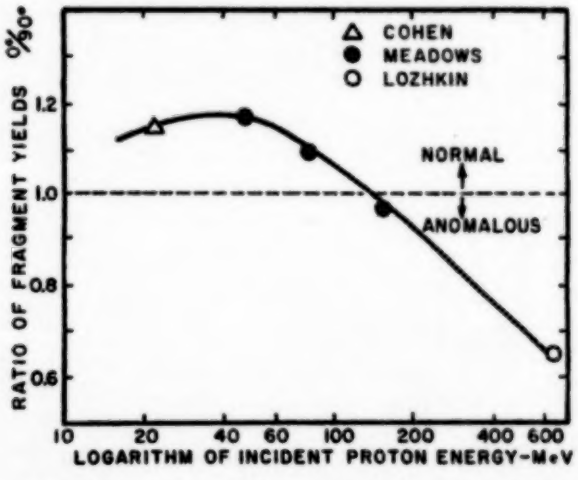

Fig. 1. The anisotropy in proton induced fission as a function of bombarding energy. This figure is adapted from ref. [5]). The data come from refs. [1, 4, 5]).

moderate energy have been consistently explained in terms of fairly general considerations [6]). The reason that fragments tend to come off mainly along the beam appears to be fundamentally a consequence of the requirements of angular momentum conservation. It is the purpose of this paper to suggest a possible explanation for the reversal in anisotropy observed at the higher energies.

The basic elements of the proposed explanation are these:

(1) *Nuclear Transparency.* Protons with energies of over 100 MeV find even a heavy nucleus somewhat transparent because of the reduced nucleon-nucleon cross sections which are effective at these energies. As a result high energy protons are generally not completely absorbed in a reaction and they deposit neither their full energy nor momentum in the nucleus.

(2) *Importance of Transverse Collisions.* Of the relatively many events where the incident proton collides with only one or two nucleons in the nucleus, a large fraction result in momentum transfers nearly at right angles to the incident proton. This comes about because the differential nucleon-nucleon cross section at high energy favours "transverse collisions". Such collisions correspond to glancing or nearly head-on collisions between billiard balls. They are characterized by the fact that after the collision one of the nucleons is moving with relatively little energy in a direction almost perpendicular to the incident direction. This nucleon is almost always absorbed in the nucleus. The second nucleon is fast and it continues essentially in the original direction. It (or one of its descendants in further collisions) has a very good chance to escape from the nucleus. Thus, the momentum and angular momentum deposited in a nucleus are often perpendicular to the directions they would have if the incident particle were absorbed. Angular distributions from nuclei produced in this way are "perpendicular" to the usual distributions.

(3) *Importance of Small Energy Deposits.* The fact that the transverse momentum deposits are associated with the lowest excitation energy deposits enhances their relative importance as regards the angular distributions. It has been shown [6]) that large fission anisotropies occur only at very low excitation energies even for large angular momentum deposits.

2. Discussion

Each of these three points will now be examined in sufficient detail to show, semi-quantitatively, what role it may play in determining the fission fragment distributions. It is convenient to begin with a consideration of the second point. The upper curve in fig. 2 shows the measured differential proton-nucleon cross sections at 600 MeV [7]). If one assumes that these cross sections apply within nuclear matter, it is possible to compute the

angular distribution of nucleons after collisions of a 600 MeV proton with an internal nucleon in, say, U^{238}. The bottom part of fig. 2 shows this probability distribution. We assume, provisionally, that the struck nucleon was originally at rest. Then if a nucleon leaves the scene of collision at an angle θ_L in the laboratory, its partner must be leaving at an angle only slightly less than $90°-\theta_L$. The relativistic decrease of the angle between the nucleons is

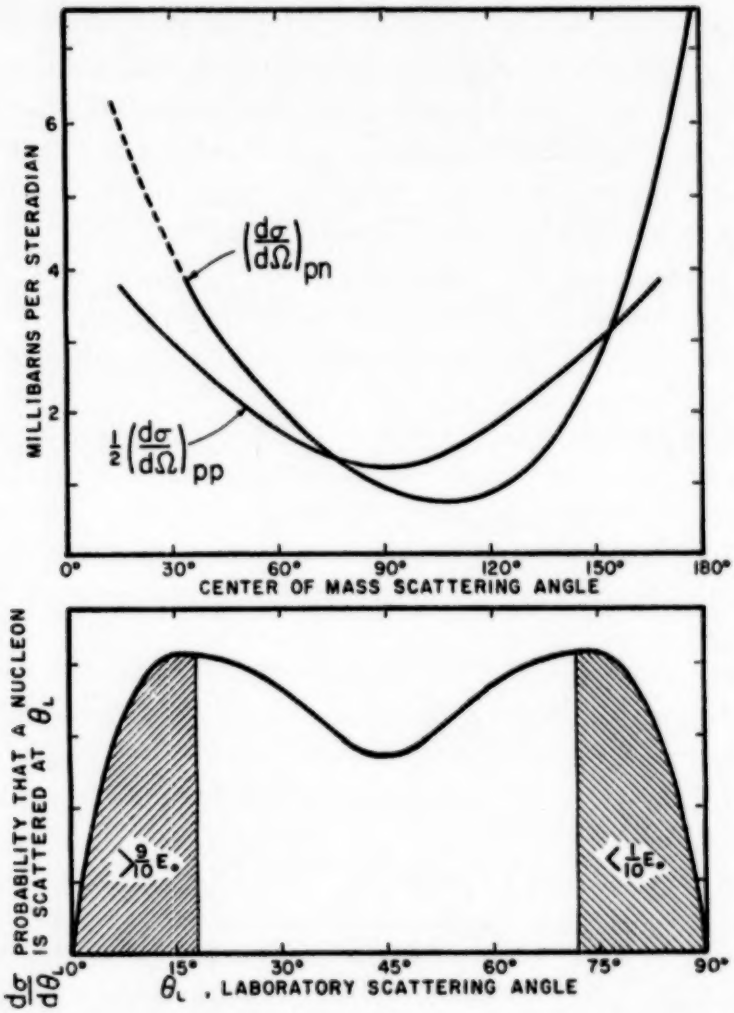

Fig. 2. (Top) The proton-nucleon differential cross section for 600 MeV protons. (Bottom) The probability that one of the nucleons leaves the scene of a collision at the angle θ_L when 600 MeV protons collide with nucleons inside a uranium nucleus. θ_L is the laboratory angle between the nucleon direction and the original proton direction. The shaded area represents those events where one of the collision partners receives less than 10 % of the incident energy.

especially small for the transverse collisions. The depression in the distribution curve that appears near $\theta_L = 45°$ in fig. 2 reflects the rareness of 90° collisions in the centre-of-mass system. As a result, in more than $\frac{1}{3}$ of the collisions one nucleon leaves the collision at an angle less than 18° to the

original direction. It has more than 90 % of the energy of the incident nucleon. Its partner leaves at a wide angle with less than 10 % of the energy. This is illustrated by the shaded areas in the figure.

Let us consider for the moment only those events where the incident nucleon makes but a single collision in the nucleus. Of these events we consider only the fraction, $\frac{1}{3}$, corresponding to the shaded region in fig. 2. It is not difficult to see what sort of distribution of fission fragments arises from these particular interactions. The momentum deposited in the nucleus is that belonging to the soft collision partners. They leave the collision at an average angle $\theta_0 \approx 80°$ to the original beam. If these collisions are imagined to take place with equal probability throughout the nuclear volume, the fission fragment angular distribution produced by the events in question will resemble that due to a *set* of beams incident on the nucleus at the same angle θ_0 to the original proton direction and uniformly distributed in the azimuthal direction. The relationship of this family of beams to the original beam is illustrated in fig. 3.

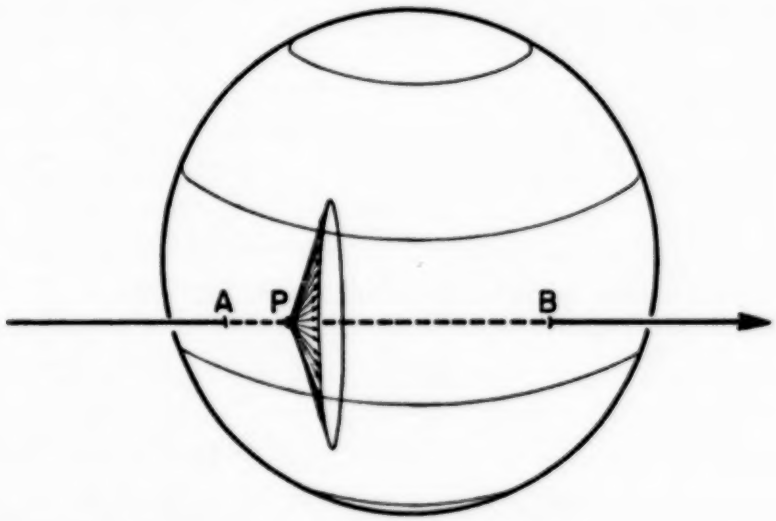

Fig. 3. A fast proton enters the nucleus at A. It collides with a nucleon at P and one of the collision partners leaves the nucleus with considerable energy at some small angle to AB. The other nucleon has little energy and is absorbed in the nucleus. It leaves from point P at an angle θ_0 (close to $\frac{1}{2}\pi$) to the line AB and all azimuthal angles about AB are equally probable. If the collision point P has an equal chance of being anywhere within the nucleus, the momentum deposited in the nucleus by a beam of fast protons incident in the direction AB, resembles that due to a set of lower energy beams uniformly distributed in azimuth about AB but all making an angle θ_0 with that direction.

The "equivalent" beams differ from the original beam in an important way. They consist of *low energy* nucleons. There have been many measurements of fission angular distributions with low energy particles and the general features are by now well-established. The distributions have maxima

back and forth along the beam. When the angular momentum deposits are relatively large or when the excitation energies are very small, these maxima can be rather sharp requiring high powers of $\cos^2\theta$ for their description. Here θ refers to the angle between the fission fragments and the beam. For purposes of illustration, it is simplest to assume that the low energy angular distributions have the form $1+A\cos^2\theta$. Then the angular distribution due to the set of beams in fig. 3 can be shown to be $1+A\cos^2\theta_0+\frac{1}{2}A(1-3\cos^2\theta_0)\sin^2\beta$ where β is the angle between the fission fragments and the direction of the original high energy proton beam. For $\theta_0 = 80°$, this distribution is very nearly $1+0.45\,A\sin^2\beta$ provided that A is not many times larger than unity. It is seen here how the transverse collisions can give rise to angular distributions peaking at right angles to the original beam. It is also seen that the azimuthal averaging over the equivalent low energy beams reduces the size of the anisotropy coefficient only by a factor of about 2.

To compare the effects of the absorption of the internally produced collision partners with those of an "equivalent" set of externally incident beams more closely it is convenient to assume that the two sets of nucleons have the same kinetic energies, say 30 MeV. The coefficient A is proportional to the average of the square of angular momentum deposited by a beam [6]). It can easily be shown that a uniformly distributed "internal beam" of collision partners deposits only $\frac{4}{5}$ as much of this quantity as an external beam of particles with the same speed. (This factor is simply the ratio of moments of inertia of a sphere to a disc.) This implies that we would slightly overestimate the anisotropy if we used measured (external beam) anisotropies to estimate those due to our collision-produced internal beams. This small difference is, however, largely compensated by the fact that the single collisions of the original high energy protons are not really uniformly distributed through the nucleus. It can be shown that these collisions occur mostly near the surface of the nucleus. This correction to the assumed uniform distribution of the collision partners corresponds to an increase in the average angular momentum deposit. All in all, the actual internal beams of struck nucleons deposit about as much angular momentum as a set of true external beams with the same velocity.

A much more important difference between the effects of the internal and external beams is that the nuclear excitation energy associated with the internal projectiles is much smaller than that brought in by external particles which have the same velocity *outside* the nucleus that the struck particles have inside. The coefficient A increases rapidly as the nuclear excitation energy decreases [6]). In fact, for excitation energies near the fission threshold the anisotropy, i.e., the 0°/90° cross section ratio, can become as large as 10 or even larger [8]). Nuclei with such low excitation energies can be produced in bombardments at moderate energies as a result

of neutron evaporation. The point is that the observed anomalous anisotropy can be due to a relatively small number of interactions that have an effect out of proportion to their number. This is possible because the excitation energy enters in expressions for the angular distribution in an extremely non-linear way. The fissions occurring at the lowest excitation energies tend to dominate in an angular distribution. We have tried to show here how it may come about that in high energy proton bombardments these important low energy fissions are connected with *transverse* momentum deposits.

The foregoing discussion is not meant to imply that the anisotropy is altogether due to $\frac{1}{3}$ of the relatively rare events in which only a single collision occurs within the nucleus. In a sizeable fraction of the events in which two or three collisions occur, the fission fragments will also tend to come off at right angles to the incident beam. For rough orientation let us imagine that the incident proton (or its fast descendants) move through the nucleus in a straight line with a constant mean free path, λ. From the fact that the chance for having exactly n collisions in the length L is $1/n!\,(L/\lambda)^n e^{-L/\lambda}$ one can find the probability that a fast proton will have exactly n collisions in passing through a sphere whose diameter is $x\lambda$. It is

$$P_n(x) = \frac{2}{n!x^2}\left[(n+1)! - e^{-x}\sum_{i=0}^{n+1}\frac{d^i}{dx^i}x^{n+1}\right].$$

For 600 MeV protons incident on uranium, x is about 4.5. According to the expression for $P_n(x)$, there is a 10 % chance that a proton will pass through a uranium nucleus without any collisions. In about $\frac{1}{5}$ of the interactions, the proton will collide with only one nucleon. In another fifth it will collide with just two nucleons. In events involving a small number of collisions, the momentum deposits along the beam add constructively, those transverse to the beam add incoherently, that is, with random azimuthal orientations. Since the "parallel" momentum deposits tend to be small, their effects do not predominate (despite the constructive way in which they add) in interactions where there are only a few nucleon-nucleon collisions. It is likely, nevertheless, that 2 and 3 collision events are not as influential in determining the angular distribution as the single collision events because they tend to deposit larger excitation energies in the nucleus.

It has been assumed that the nucleons struck by the fast proton are originally at rest. If their actual motion is taken into account it will produce a smearing of the distributions estimated along the foregoing lines. An examination of the kinematics of the situation indicates, however, that this smearing is not too severe as long as the momentum of the incoming proton remains large compared to that of nuclear nucleons. In particular, for 600 MeV protons, this effect should not be very serious.

One can probably develop the "equivalent-transverse beam" model to

the point where it can be used, together with measured low energy fission distributions for the quantitative prediction of high energy results. It would be necessary to include a number of "corrections" to the simple model, some of which were already mentioned. It is, of course, much easier to make only rough estimates on the basis of the model and these are in close enough accord with the high energy results to suggest that the basic assumptions in the model truly reflect the physical origin of the anomalous anisotropy. The model does not really lend itself to extensive quantitative refinement. When many distribution functions must be folded together, it is generally best to proceed with Monte Carlo methods where, one by one, a large number of typical events can be constructed in a statistical way. Although such calculations have already been made for high energy proton bombardments[9]), they unfortunately do not provide any information about the deposition of angular momentum and the angular distributions of the particles which are emitted from the compound nuclei formed in the bombardments. It should not be too difficult to extend these calculations to provide the desired information. Two remarks are in order about the relationship of the present treatment of the fission problem to a detailed Monte Carlo calculation. First, it is easier to see the physical basis of the anomalous anisotropy in an analysis that begins by singling out the relevant physical processes. The relative importance for a particular problem of the different pieces of input information tend to be somewhat obscured in a Monte Carlo calculation. The second point is that our analysis has shown that the most important effects, as regards the fission anisotropy, arise from collisions in which very little excitation energy is left in the nucleus. This serves to emphasize that one must be careful in a Monte Carlo calculation how one takes into account the internal nucleon motions and the Pauli principle. Some of the most important events, as far as the angular distributions are concerned, are those which are "almost forbidden" by the Pauli Principle.

3. Comparison with Experimental Data

In conclusion we shall briefly review the experimental information on high energy fission distributions to see to what extent it is consistent with the implications of the foregoing discussion.

The fact that high energy nucleons are not completely absorbed when they hit a nucleus is well known. It is perhaps worth citing the work of Ivanova in particular. She finds that almost all of the fissions induced in U^{238} by 660 MeV protons are accompanied by fast forward particles[10]).

One of the implications of the present analysis is that the large anomalous anisotropy observed with 660 MeV protons is due to a relatively small number of events. That is, the peak at 90° to the beam should be rather narrow. This is supported by the statement of Lozhkin *et al.*[4]) that their

angular distribution is of the form $a+b\sin^n\theta$ where n is at least four.

Perhaps the most definite implication of the foregoing model is that the anomalous anisotropy should be connected with events in which the nuclear excitation energy is abnormally small. Here the evidence is mixed. Lozhkin and his co-workers have developed a criterion for use with photographic emulsions to establish the amounts of excitation energy deposited in high energy events. Within their errors they find that the anisotropy *increases* with excitation energy [4]). On the other hand the work of Meadows [5]), involving radiochemical techniques, seems to be quite consistent with the expected correlation between excitation energy and anisotropy. At a bombarding energy of 155 MeV he finds that only the asymmetric mass pairs among the fragments show the anomalous anisotropy. The anisotropy of symmetric pairs is normal. In view of the fact that asymmetric fission occurs at low excitation energy and symmetric fission is more probable at higher energies [11, 12]), Meadows' observations seem to fit the expectations.

He also finds that the anomalous anisotropy of asymmetric pairs is larger for Th^{232} than for U^{238}. This too is what one might expect. Because of their moderately high fissility, the species made in the U^{238} bombardments tend to fission before many neutrons are evaporated. Relatively few nuclei survive against fission until the very low excitation energies are reached. In the Th^{232} bombardments, a larger fraction of the nuclei formed will undergo fission at low excitation energies and consequently one may expect to see a larger anisotropy. This refers of course to the asymmetric mass pairs since the symmetric ones come, in any case, only from fissions at higher excitation energies.

In this connection it should be noted that in the fission of bismuth with 450 MeV protons [13]), Wolke finds that the anisotropy is small but "normal." This is to be explained by the fact that in the lighter fissile targets, like bismuth, virtually no fission takes place at low excitation energy [14, 15]). The events responsible for the anomalous anisotropies in uranium and thorium produce essentially no fission in bismuth. The observed fissions in bismuth are due to symmetric mass pairs and Wolke's results are consistent with Meadows' findings for the symmetric mass pairs in uranium fission.

Incidentally, Meadows points out that by comparing the angular distributions in the forward and backward hemispheres one can hope to learn about the forward component of the linear momentum deposit in those events which give rise to the observed fissions. According to our ideas, this momentum deposit should be very small for events connected with the anomalous anisotropy. It should be possible to look into this question with a slight extension of Meadows' techniques, or perhaps more directly with photographic plates, where the momentum deposit should be directly measurable from the angle between fission fragments.

Finally, it should be mentioned that the nature of the angular momentum deposit in high energy reactions can be examined through angular distributions of emitted particles other than fission fragments. This general problem has recently been discussed by Ericson and Strutinski [16]). An interesting experimental result is that of D. Skyrme. She finds that neutrons are evaporated most often back and forth along the beam when wolfram is bombarded with 147 MeV protons [17]). Thus, neutrons from wolfram show a "normal" anisotropy at the same bombarding energy that fission fragments from uranium show an "anomalous" one. This difference in distributions must in part be due to the fact that the low energy excitations are not nearly so important for neutrons as for fission fragments. At low excitation energies, the neutrons evaporate in $l = 0$ or $l = 1$ states and the anisotropies are neither as sharp nor as large as they apparently are for fission fragments. Although the anisotropies of neutrons are presumably also "anomalous" at the lower energies, they are simply not large enough to influence the average in their favour when they are considered together with the angular distributions associated with the deposits of larger excitation energies.

I would like to thank Drs. V. M. Strutinski and J. S. Blair for a number of helpful discussions of some of the points which have have been considered here.

References

1) Cohen, Ferrell-Bryan, Coombe and Hullings, Phys. Rev. **98** (1955) 685
2) R. L. Henkel and J. E. Brolley, Jr., Phys. Rev. **94** (1956) 640
3) C. T. Coffin and I. Halpern, Phys. Rev. **112** (1958) 536
4) Lozhkin, Perfilov and Shamov, JETP, USSR **29** (1955) 292
5) J. W. Meadows, Phys. Rev. **110** (1958) 1109
6) I. Halpern and V. M. Strutinski, Second U.N. International Conference on the Peaceful Uses of Atomic Energy, paper no. 1513
7) W. N. Hess, Revs. Mod. Phys. **30** (1958) 368
8) Katz, Baerg and Brown, Second U.N. International Conference on the Peaceful Uses of Atomic Energy, paper no. 200
9) N. Metropolis *et al.*, Phys. Rev. **110** (1958) 185
10) N. S. Ivanova and I. I. P'ianov, JETP, USSR **31** (1956) 416
11) Bowles, Brown and Butler, Phys. Rev. **107** (1957) 751
12) A. W. Fairhall and R. C. Jensen, Bull. Am. Phys. Soc., **2** (1957) 378
13) R. L. Wolke and J. R. Gutman, Phys. Rev. **107** (1956) 850
14) Fairhall, Jensen and Neuzil, Second U.N. International Conference on the Peaceful Uses of Atomic Energy, paper no. 677
15) I. Halpern and C. T. Coffin. Second U.N. International Conference on the Peaceful Uses of Atomic Energy, paper no. 642
16) T. Ericson and V. M. Strutinski, Nuclear Physics **8** (1958) 284
17) D. Skyrme, to be published

9.B *Nuclear Physics* 11 (1959) 531—539; © *North-Holland Publishing Co., Amsterdam*
Not to be reproduced by photoprint or microfilm without written permission from the publisher

MEASUREMENT OF THE ABSORPTION LENGTH OF PENETRATING SHOWER PRODUCING COSMIC RAY PARTICLES IN LEAD

G. BOZÓKI, E. FENYVES and L. JÁNOSSY
Central Research Institute of Physics, Department for Cosmic Rays, Budapest

Received 16 February 1959

Abstract: The absorption length of penetrating shower producing particles was measured in lead under great absorber thicknesses by means of a penetrating shower detector. In order to select single nuclear active particles, local penetrating showers were detected, and the coincidence rates measured were corrected for spurious effects. The absorption length was found to be 414 ± 17 g/cm², in good agreement with the results of other experiments. The mean energy of the recorded penetrating shower producing particles was estimated to be between 30 and 60 GeV.

1. Introduction

The absorption length of penetrating shower producing cosmic ray particles has been measured by several authors in the atmosphere and also in dense absorbers. The absorption was found to obey to good approximation an exponential law:

$$N(x) = N_0 e^{-x/\lambda_a}, \tag{1}$$

where $N(x)$ is the number of penetrating shower producing particles at a depth of x g/cm² and λ_a a constant called the absorption length. The absorption lengths found were in general two or three times larger than the collision mean free paths (λ_c) of high energy nuclear active particles for the same absorber.

The absorption of penetrating shower producing particles in successive collisions in nuclear matter was first investigated theoretically by Heitler and Jánossy [1]). They have shown that with a primary spectrum following a power law, the absorption is strictly exponential, in good agreement with the experimental results †. The physical importance of the determination of the absorption length for the investigation of nuclear cascade processes in high energy interactions was discussed by Asimov, Dobrotin *et al.* [2]). The latter authors have shown that the ratio of the absorption length to the

† In the derivation of this result it was assumed that the probability $w(\varepsilon, E)\mathrm{d}\varepsilon$ for an energy loss ε by a nuclear active particle with energy E hitting a nucleon at rest, has the form $w(\varepsilon, E)\mathrm{d}\varepsilon = w(\varepsilon/E)\mathrm{d}\varepsilon/E$.

collision mean free path has a constant value of about 3 for carbon, iron and lead absorbers. From this experimental result they have concluded — assuming that a nuclear active particle hitting a nucleus interacts in successive collisions with the nucleons inside the nucleus — that a) the absorption † of penetrating shower producing particles takes place on average after about three interactions, in light as well as in heavy materials and b) neutral π-mesons also contribute to the nuclear cascade processes inside the nucleus It was also shown by Dobrotin *et al.* [3]) that experimental data on the absorption length of high energy nuclear active particles permit approach of the problem as to the degree of energy partition among secondary particles of nuclear interactions. Theoretical investigation concerning the nature of secondary particles having energies close to that of the primary was carried out recently by Friedländer and Ruckenstein [4]).

Stimulated by the above results we have worked out a program for the investigation of the absorption length and collision mean free path of penetrating shower producing particles in different absorbers. The measured value of the absorption length and also that of the collision mean free path depend, however, on the experimental arrangement used [5]). It is necessary, therefore, to measure the absorption length as well as the collision mean free path with the same penetrating shower detector using different absorber materials.

In the present paper we give the description of the apparatus used and the results of measurements of the absorption length with a lead absorber.

2. Experimental Arrangement

The penetrating shower detector (N) consisted of four counter sets A, B, C and D embedded in a lead block (fig. 1). Each counter set consisted of

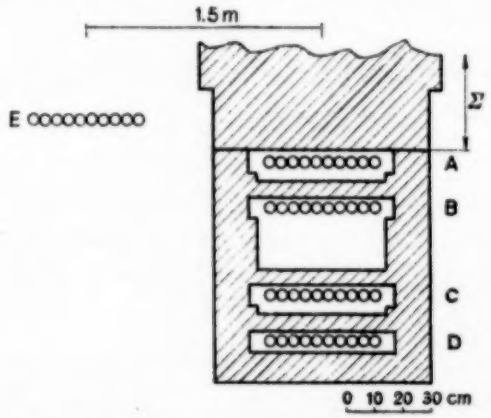

Fig. 1. The experimental arrangement.

† Absorption of penetrating shower producing particles means that they become inefficient to produce penetrating showers.

10 counters, each counter having a diameter of 4 cm and an effective length of 40 cm. The total amount of lead between the counter trays A and D was 170 g/cm² and was subdivided into three layers of equal thickness, separating the individual counter sets from each other. The thickness of the lead absorber Σ placed above the top counters A, in which the absorption of the penetrating shower producing particles was measured, was varied from 0 to 900 g/cm².

We have selected by means of discriminators the events by which at least two or three counters, respectively, of each of the sets A, B, C and D were discharged. Coincidences of the type ($A_{\geq 2}$, $B_{\geq 2}$, $C_{\geq 2}$, $D_{\geq 2}$) and ($A_{\geq 3}$, $B_{\geq 3}$, $C_{\geq 3}$, $D_{\geq 3}$) are denoted by N_2 and N_3, respectively.

At a distance 1.5 m from the penetrating shower detector N was placed an unshielded set of counters (E) having a total sensitive surface of 3 200 cm²; it served for the discrimination between local and extensive penetrating showers †.

We have measured simultaneously the coincidences and anticoincidences (N_2), (N_2, E), (N_2, −E) or (N_3), (N_3, E), (N_3, −E) ††.

Coincidences of the type ($A_{\geq 2}$, $B_{\geq 1}$, $C_{\geq 1}$, $D_{\geq 1}$), ($A_{\geq 1}$, $B_{\geq 2}$, $C_{\geq 1}$, $D_{\geq 1}$) etc. and ($A_{\geq 3}$, $B_{\geq 1}$, $C_{\geq 1}$, $D_{\geq 1}$), ($A_{\geq 1}$, $B_{\geq 3}$, $C_{\geq 1}$, $D_{\geq 1}$) etc. as well as ($A_{\geq 1}$, $B_{\geq 1}$, $C_{\geq 1}$, $D_{\geq 1}$) were measured for each absorber thickness to allow estimation of the μ-meson flux falling on the penetrating shower detector and the single and double knock-on probabilities for the different counter trays A, B, C and D. The results of these measurements were used in the correction for spurious events and served also for checking the operation of the apparatus. The measurements were carried out at Csillebérc, Budapest, 410 m above sea level.

3. Results

The rates of coincidences and anticoincidences (N_2), (N_2, −E) and (N_3), (N_3, −E) measured as functions of the thickness of the lead absorber Σ are plotted in fig. 2. The curves show between 0 and about 450 g/cm² thicknesses of lead the well-known transition effect and have flat maxima at about 150 g/cm², which corresponds to about one geometrical collision mean free path $\lambda_c^{(\text{geom.})} = 160$ g/cm². The shape of the curves between 450 and 900 g/cm² does not deviate significantly from an exponential and thus we have supposed that the influence of the transition effect can be neglected at these absorber thicknesses [8]). This is also supported by the results of Asimov *et al.* [9]) who found, that the influence of the transition effect disappears at

† The whole arrangement was identical with that used for the detection of nuclear active particles when investigating extensive air showers [6,7]).

†† For part of the measuring time the penetrating shower detector N was connected in coincidence with the extensive air shower apparatus described in ref. [6]).

absorber thicknesses of about 2—3 times the geometrical collision mean free path.

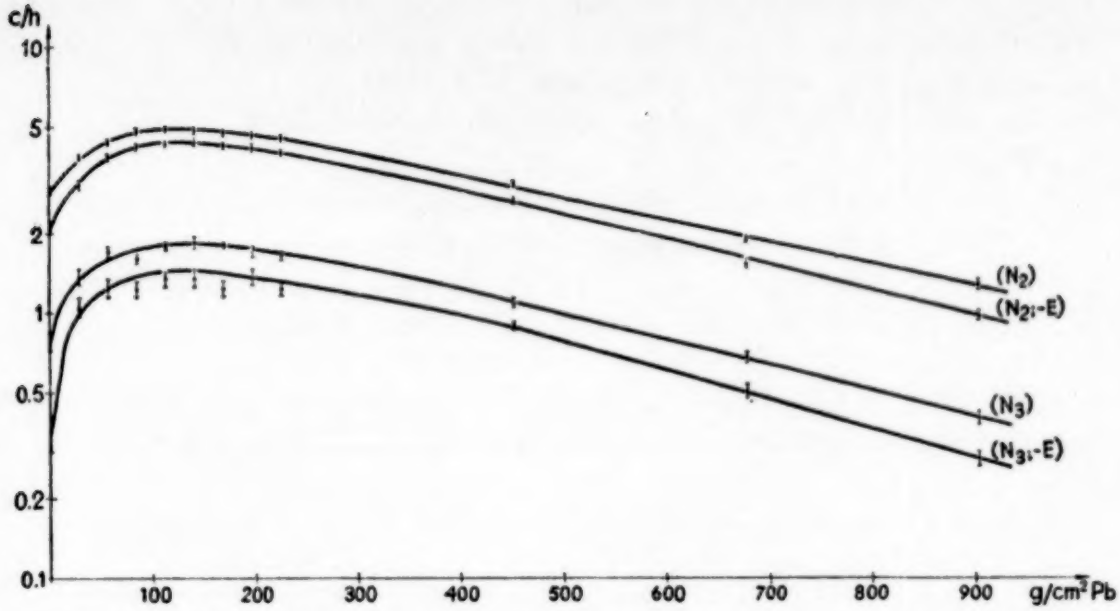

Fig. 2. The rate (c/h) of coincidences and anticoincidences (N_2), (N_3), (N_2, $-E$) and (N_3, $-E$) vs. the thickness of the lead absorber.

Using this part of the absorption curves, i.e. the points corresponding to 450, 680 and 900 g/cm² thicknesses, we have calculated the values of the absorption length λ_a by the method of least squares (table 1). The values of λ_a given in the table are corrected for the effect, that particles passing the absorber Σ in directions inclined to the vertical traverse more absorber than the vertical thickness given. For this calculation it was assumed, that the differential angular distribution of penetrating shower producing particles is proportional to $\cos^7\theta$, where θ is the angle of the direction to the vertical [10]).

TABLE 1

Type of coincidence	λ_a(g/cm²)
(N_2)	534 ± 24
(N_3)	443 ± 27
(N_2, $-E$)	455 ± 21
(N_3, $-E$)	394 ± 25
(N_2, E)	673 ± 117
(N_3, E)	598 ± 99

The rates of coincidences (N_2, E) and (N_3, E) as functions of the thickness of the lead absorber are plotted in fig. 3. It can be seen from fig. 3 that these curves are quite different from those plotted in fig. 2 and do not show any pronounced maximum. The values of λ_a were calculated for these curves also,

using the points corresponding to the same thicknesses (450, 680 and 900 g/cm²) and applying the same correction as used for the curves of fig. 2. The values of λ_a obtained are given in table 1.

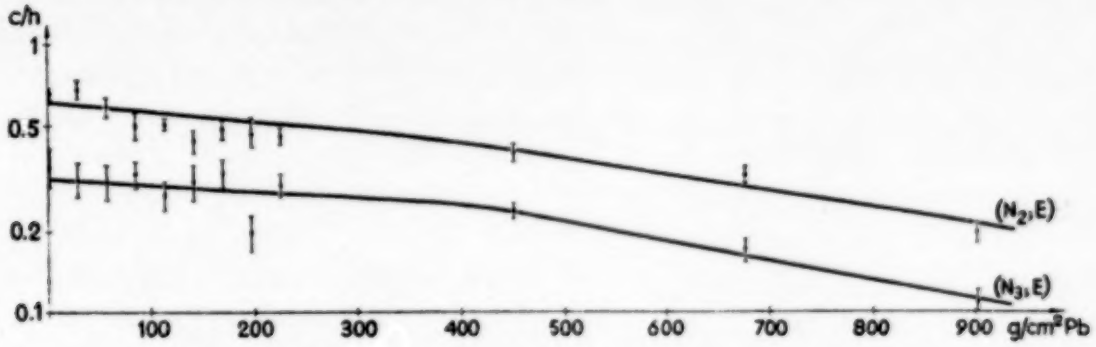

Fig. 3. The rate (c/h) of coincidences (N_2, E) and (N_3, E) vs. the thickness of the lead absorber.

4. Discussion

4.1. ESTIMATION OF THE ABSORPTION LENGTH OF PENETRATING SHOWER PRODUCING PARTICLES

Events corresponding to coincidences of the type (N_2, −E), (N_3, −E) and (N_2, E), (N_3, E) are commonly called local and extensive penetrating showers, respectively. The striking difference between the transition curves of local and extensive penetrating showers as well as the near-significant difference between their absorption lengths shows that they represent two different physical phenomena. It seems obvious that local penetrating showers are produced mainly by single high energy nuclear active particles, while extensive penetrating showers are produced not only by single nuclear active particles but also by associated penetrating particles (μ-mesons and nuclear active particles). Accordingly the latter events do not show any transition effect with a pronounced maximum and have greater absorption lengths than the local penetrating showers. Events corresponding to coincidences (N_2) and (N_3) consist of local as well as extensive penetrating showers, thus representing mixed physical phenomena.

It is quite clear from the above considerations that for the estimation of the absorption length of high energy nuclear active particles the absorption curve of local penetrating showers must be used. The efficiency of selection for local penetrating showers is, however, strongly dependent on the experimental arrangement used, in particular on the size of the surface of the electron detector E and the distance between E and the penetrating shower detector N.

We must consider also another effect. Several authors [11, 12, 13]) have found that the energy spectra of nuclear active particles which are associated, as

well as those which are not associated, with air showers can be represented in the form of a power law, having lower exponent for particles associated with air showers ($\gamma \approx 0.9$) than for those not associated with such showers ($\gamma \approx 1.5$). This means that the measurement of extensive penetrating showers gives a bias against lower energies, and inversely selection of local penetrating showers means bias against higher energies of nuclear active particles. This may cause — taking into account the constancy of the threshold energy of the penetrating shower detector — an increase (or decrease) of the measured absorption length for extensive (or local) penetrating showers.

The effects considered above depend in opposite ways on the size of the surface of the electron detector E. A larger surface secures better selection for local penetrating showers, but causes stronger bias against higher energies for the single nuclear active particles detected by coincidences (N_2, $-E$) and (N_3, $-E$). Preliminary measurements carried out in our laboratory have shown, however, that the choice of the size of the surface of E is not very critical. Therefore we have used an electron detector, the size of which, as conventional, has the same order of magnitude as that of the penetrating shower detector.

Coincidences of the type (N_2, $-E$) and (N_3, $-E$) can be caused also by spurious events for which the data have to be corrected. These spurious events are [14]):

a) production of knock-on showers in the individual counter trays by μ-mesons,

b) random coincidences of two or more incident penetrating particles (μ-mesons),

c) nuclear interaction initiated by μ-mesons.

From the measured value of the probability of discharge of two or three counters in each individual counter tray by single and double knock-on processes, the measured intensity of the μ-meson flux and the value of the resolving time of the coincidence apparatus, it was possible to calculate the corrections for knock-on showers and random coincidences of μ-mesons (events a) and b)). In consequence of the very poor information available on the cross section for the production of penetrating showers by μ-mesons of the size detected by our apparatus, no correction was made for this latter effect (events c)). This was justified by a very rough estimation of the higher limit of this effect which showed that the possible correction in the value of λ_a does not exceed the statistical error. For the rates of (N_2, $-E$) the value of the correction for knock-on processes was negligible. Thus these rates were corrected only for randomly coincident μ-mesons and from these values the corrected absorption length was estimated. The correction was negligible for the rates of (N_3, $-E$). Corrected values of the absorption length for (N_2, $-E$) and (N_3, $-E$) are collected in table 2.

TABLE 2

Type of coincidence	λ_a corrected (g/cm²)
(N_2, −E)	429±22
(N_3, −E)	394±25

It can be seen that the corrected values of λ_a for (N_2, −E) and (N_3, −E) are in very good agreement and their weighted mean value is found to be

$$(414\pm17)\ \text{g/cm}^2. \tag{2}$$

This value is slightly influenced by the imperfect selection of local penetrating showers, by the bias against particles of higher energies and by the neglect of the effect of penetrating showers produced by μ-mesons.

4.2. ESTIMATION OF THE ENERGY OF THE PENETRATING SHOWER PRODUCING PARTICLES

The mean energy of the penetrating shower producing particles can be evaluated approximately from the observed and calculated rate of coincidences assuming a power law for the energy spectrum of nuclear active particles [15]). For the efficiency (w) of the penetrating shower apparatus, i.e. for the probability that a nuclear active particle of energy E incident on the top absorber will be detected, we have assumed

$$w(E) = 0, \quad \text{when } E < E_{\text{th}},$$
$$w(E) = a, \quad \text{when } E \geqq E_{\text{th}},$$

where a is a constant and E_{th} the threshold energy of the apparatus. We have estimated the value of a for 150 g/cm² absorber thickness (near the maximum of the transition curve) to be about 0.4. Using the energy spectrum of nuclear active particles determined by Bridge and Rediker [16]) the threshold energy and the mean energy of detected particles was estimated for different types of coincidence as

$$E_{\text{th}} = 10\ \text{GeV}, \quad \langle E\rangle = 30\ \text{GeV} \quad \text{for } (N_2), \tag{3}$$

$$E_{\text{th}} = 18\ \text{GeV}, \quad \langle E\rangle = 54\ \text{GeV} \quad \text{for } (N_3). \tag{4}$$

Thus the mean energy value of penetrating shower producing particles detected with our apparatus by means of coincidences (N_2) and (N_3) is between 30 and 60 GeV and the absorption length obtained, (414±17) g/cm², corresponds to this energy region.

4.3. COMPARISON WITH OTHER EXPERIMENTS

Similar experiments concerning the absorption length of high energy nuclear active particles (10^{10}—10^{11} eV) in lead were carried out by several

authors [2,12,16–20]). The values of the absorption length obtained for lead in these measurements are collected in table 3.

TABLE 3

Experiment	Technique used	Absorption length in lead λ_a(g/cm²)
Fahy and Schein [17])	ion. chamber	434
Stinchcomb [18])	ion. chamber	350±40
Zacepin *et al.*[12])	ion. chamber	340±60
Bridge and Rossi [19])	ion. ch. and GM counters	430±90
Bridge and Rediker [16])	ion. ch. and GM counters	440±50
Rosser and Swift [20])	emulsion (showers with $n_s \geqq 2$)	380±65
Asimov, Dobrotin *et al.*[2])	GM counters	482±31
present exp.	GM counters	414±17

It can be seen clearly from table 3 that the measured values do not deviate significantly from one another in spite of the different techniques used. The weighted mean value of all data published before the present experiment is $\langle\lambda_a\rangle = (420\pm19)$ g/cm² in good agreement with the value found by us.

The absorption length of high energy nuclear active particles associated with extensive air showers was determined by Zacepin *et al.* [12]) as (570±120) g/cm². This value is not in disagreement with our values of λ_a obtained from coincidences (N_2, E) and (N_3, E) (see table 1).

5. Conclusions

It is quite clear from the above discussion that the absorption length of penetrating shower producing nuclear active particles can be measured directly by the absorption of local penetrating showers at great absorber thicknesses. The value of the absorption length for nuclear active particles having mean energy between 30 and 60 GeV was determined as (414±17) g/cm². This value, although influenced by several effects, which have been discussed above, seems to be a good approximation of the real absorption length.

References

1) W. Heitler and L. Jánossy, Proc. Phys. Soc. A **62** (1949) 374
2) S. A. Asimov, N. A. Dobrotin, A. L. Ljubimov and K. P. Ryshkova, Izv. A. N. SSSR. **17** (1953) 80
3) N. A. Dobrotin, G. T. Zacepin, S. I. Nikol'skij and G. B. Kristiansen, Nuovo Cimento Suppl. **10** (1956) 635
4) E. Friedländer and E. Ruckenstein, JETP **35** (1958) 104
5) G. Bozóki, E. Fenyves and L. Jánossy, Nuclear Physics **1** (1956) 501
6) G. Bozóki, E. Fenyves, T. Sándor and A. Somogyi, Nuclear Physics **7** (1958) 677
7) G. Bozóki, E. Fenyves, T. Sándor and A. Somogyi, Acta Phys. Hung. **9** (1959) 347

8) M. I. Podgoretzkij, JETP **21** (1951) 1097
9) S. A. Asimov, V. F. Vishnevskij and N. I. Chil'ko DAN **78** (1951) 231
10) M. Cervasi Fidecaro, G. Fidecaro, G. Marini and L. Mezzetti, Nuovo Cimento **9** (1958) 38
11) Y. Watase, S. Fukui, I. Higashimo, K. Suga, K. Hinotai, S. Mitani, Y. Murata, Y. Tanaka and S. Miyamoto, Ann. Rep. Scient. Works, Fac. Sci. Osaka Univ. **5** (1957) 1
12) G. T. Zacepin, V. V. Krugovüh, E. A. Murzina and S. I. Nikol'skij, JETP **34** (1958) 298
13) O. I. Dovzhenko, O. A. Kozhevnikov, S. I. Nikol'skij and I. V. Rakobolskaya, JETP **34** (1958) 1637
14) F. E. Froehlich and K. Sitte, Phys. Rev. **97** (1955) 151
15) R. W. Williams, Phys. Rev. **98** (1955) 1393
16) H. S. Bridge and R. H. Rediker, Phys. Rev. **88** (1952) 206
17) E. F. Fahy and M. Schein, Phys. Rev. **75** (1949) 207
18) T. G. Stinchcomb, Phys. Rev. **83** (1951) 422
19) H. S. Bridge and B. Rossi, Phys. Rev. **75** (1949) 810
20) W. G. V. Rosser and M. W. Swift, Phil. Mag. **42** (1951) 856

2.B:2.L *Nuclear Physics* **11** (1959) 540—553; © *North-Holland Publishing Co., Amsterdam*
Not to be reproduced by photoprint or microfilm without written permission from the publisher

POLARIZATION OF HIGH ENERGY PROTONS IN ELASTIC AND INELASTIC SCATTERING

ARNE JOHANSSON, GUNNAR TIBELL † and PETER HILLMAN ††
The Gustaf Werner Institute for Nuclear Chemistry, University of Uppsala

Received 9 March 1959

Abstract: The polarizations of 180 MeV protons elastically and inelastically scattered by lithium, beryllium, boron, iron and bismuth have been measured with an energy resolution of 2—2.5 MeV full width at half height. The polarizations of scattered protons corresponding to the low-lying levels closely resemble each other and previous results for carbon, oxygen and calcium. Good agreement is found when the data are compared with existing theoretical calculations. The elastic polarizations agree fairly well with measured asymmetries at those points where a comparison can be made.

1. Introduction

The polarization of high energy protons inelastically scattered by nuclei has been calculated by several authors. One approach to the problem has been to treat the excitation of the target nucleus in terms of the collective model. In that model Maris [1]) and Ruderman [2]) have shown that the Born approximation gives the same result for elastic and inelastic polarization:

$$P(\vartheta) = \frac{\alpha(\gamma+\beta)k^2 \sin\vartheta}{1+\beta^2+\frac{1}{4}\alpha^2k^4(1+\gamma^2)\sin^2\vartheta} \tag{1}$$

where ϑ is the scattering angle and the potential is written as

$$\mathscr{V} = V(\mathbf{r}\alpha_\mu)(1+i\beta)+\frac{\alpha}{2\hbar}(1-i\gamma)\nabla V(\mathbf{r}\alpha_\mu)\times\mathbf{p}\cdot\boldsymbol{\sigma}. \tag{2}$$

Köhler [3]) obtained the same formula, but in a better approximation that included the distortion of the scattered wave by the optical model potential of the nucleus. Nishimura and Ruderman [4]), using different approximation methods, got significant deviations from the Born approximation values at angles where the scattering amplitudes are small.

A number of authors have calculated the polarization of inelastically scattered protons from nucleon-nucleon phase shifts, treating the particular level as being excited through a single particle collision. Squires [5]) studied

† Now at SC Division, CERN, Geneva.
†† CERN (European Organisation for Nuclear Research), Theoretical Study Division. Now at SC Division, CERN.

the 4.43 MeV state of C^{12} using shell model wave functions and a nucleon-nucleon t matrix of the form

$$t_i = a_i + c_i(\boldsymbol{\sigma}_i + \boldsymbol{\sigma}) \cdot \mathbf{n} + b_i(\boldsymbol{\sigma}_i \cdot \mathbf{n})(\boldsymbol{\sigma} \cdot \mathbf{n}) + d_i(\boldsymbol{\sigma}_i \cdot \mathbf{k})(\boldsymbol{\sigma} \cdot \mathbf{k}) + e_i(\boldsymbol{\sigma}_i \cdot \mathbf{P})(\boldsymbol{\sigma} \cdot \mathbf{P}), \tag{3}$$

where the index i means the i^{th} particle of the nucleus and $\mathbf{n}$, $\mathbf{k}$ and $\mathbf{P}$ are mutually orthogonal unit vectors, $\mathbf{n}$ being orthogonal to the scattering plane. He took into account only the imaginary central part of the optical model potential, a reasonable approximation as can be seen from the work of McCauley and Brown [6, 7]). In the L-S coupling extreme Squires got

$$P(\vartheta) = \frac{2 \operatorname{Re}(a^* c)}{|a|^2 + |c|^2} \tag{4}$$

where a and c are mean values of $a_i(\vartheta)$ and $c_i(\vartheta)$ for p—n and p—p scattering. He also pointed out that in L-S coupling eq. (4) will always result if the target nucleus has $S = 0$ in the ground and final states. Calculating a and c from the Gammel and Thaler [8]) phase shifts, Squires got very good agreement with experiment. The j-j coupling extreme predicted polarizations that were too small around 20° scattering angle. Köhler [3]) showed that eq. (4) is a reasonable approximation even when the distortion due to the complex optical potential is taken into account. He also pointed out that (1) and (4) are identical if the potential parameters are allowed to vary slowly with angle according to

$$\frac{1 - i\gamma}{1 + i\beta} \alpha k^2 = \frac{-2i}{\sin \vartheta} \frac{c}{a}. \tag{5}$$

From these theoretical considerations one observes that the polarization of inelastically scattered protons to a large extent is independent of the mass of the target nucleus and also of the excitation energy. This was pointed out by Squires on the basis of eq. (4) and more strongly stressed by Köhler.

Experimental determinations of the polarization of inelastically scattered protons and of the asymmetry in the inelastic scattering of polarized protons have been made at Rochester [9, 10]), Harwell [11]), Harvard [12]) and Uppsala [13, 14]). All elements studied have been rather light, calcium being the heaviest, and they have all had ground state spin zero, except Be^9, studied at Rochester. From existing theories one would expect these experimental results to show striking similarities, which indeed they do.

The reduction of the expression for the polarization to the form (4) which contains only the parameters a and c of the t matrix will not in general occur in j-j coupling, or in L-S coupling if $S \neq 0$ in the ground or final states. One might, therefore, among other things, hope to gain information on nuclear structure from the results of polarization measurements of inelasti-

cally scattered protons by nuclei that are not purely L-S coupled or of "spin-saturated" or α-structure. The present work reports on such measurements with the target nuclei Li, Be, B, Fe and Bi.

2. Experiment

2.1. LEVELS STUDIED

The selection of inelastic levels to be studied was made on the basis of the measurements performed by Tyrén and Maris [15, 16]) of the differential cross sections for exciting these levels by high energy protons. The polarizations have been determined for protons scattered from the following levels with forward-dipped cross sections:

4.6 MeV in lithium,
2.4 and 6.5 MeV in beryllium,
4.5 and 6.6 MeV in boron,
4.4 and 6.7 MeV in iron and
4.5 MeV in bismuth.

There has been no attempt in this work to measure the excitation energies accurately. The uncertainty is about ± 0.3 MeV. In a few cases, however, only one level is possible and its excitation energy known from other sources. For bismuth the results of Tyrén and Maris are not published: a peak structure of somewhat irregular shape is seen at about 4.5 MeV excitation energy for 20° scattering angle. The "continuum" on both sides of this peak is about half the total peak height and the width at $\frac{3}{4}$ height above zero is roughly 3 MeV.

A few additional levels have been studied: 8.5 (with strongly forward-peaked cross section), 12 and 17 MeV in boron, and 16 MeV in iron.

The work of Tyrén and Maris shows that the cross section spectra for most elements have little or no structure above about 10 MeV excitation energy i.e. in the continuum region, except for a persistent broad peak near 20 MeV. The polarization may, however, vary markedly along the spectrum, e.g. corresponding to the excitation of particles from different shells in the nucleus. To investigate this point the polarizations of the inelastically scattered protons have been measured at 20° lab as a function of the excitation energy for Li, Be, Fe and Bi.

The elastic polarization was measured for all five elements: Li, Be, B, Fe and Bi.

2.2. METHOD AND APPARATUS

The method and the apparatus used have been described in detail in an earlier publication [14]), and are unchanged except that an additional counter has been inserted in front of the old counter array in order to reduce the

background and accidental counting rates. The different target thicknesses used and the corresponding angular resolutions are given in table 1. The energy resolution varies somewhat with target thickness and scattering angle (due to the varying width of the object for the magnetic analyser) but

TABLE 1

Element	Target thickness (MeV)	Mean energy (MeV)	Root mean square angular spread	
			Multiple scattering	Total
Li	9	181	0.3°	0.6°
Be	11	181	0.4°	0.7°
B	10	182	0.4°	0.7°
Fe	16	179	1.3°	1.4°
Bi	17	179	2.6°	2.7°

is always between 2 and 2.5 MeV full width at half height. In some cases this resolution is sufficient to ensure clean separation of protons leaving the nucleus in different states, but in other cases the level density is so great that the measured polarizations must be considered as averages over many levels. For beryllium a correction has been applied for the overlap between the elastic and the 2.4 MeV inelastic peaks, using separately measured spectra and assuming that there is no contribution from the possible 1.7 MeV and the 3.1 MeV states [17]). In the other cases no corrections have been applied for the finite energy resolution. An idea of the cleanness of the separation can be obtained from the spectrum measurements by Tyrén and Maris [15, 16]).

3. Results

The results for lithium, beryllium, boron, iron and bismuth are shown in figs. 1—5. The errors given are of a purely statistical origin, except that in the case of Be they also include errors from the procedure of correcting for the overlap between the elastically scattered protons and those scattered from the 2.4 MeV level. Both the corrections and the errors are quite small, however.

Figs. 6—9 show the variations of the polarization along the spectra for lithium, beryllium, iron and bismuth. The scattering angle is 20° in all four cases.

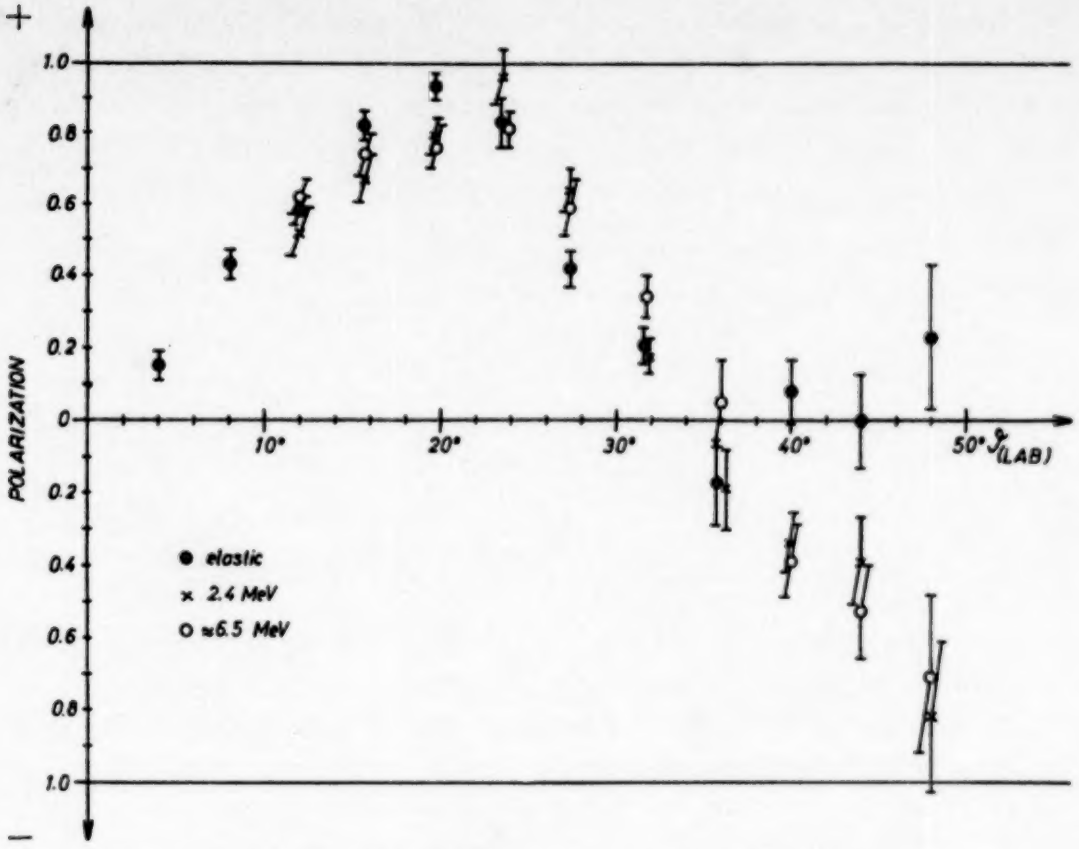

Fig. 1. Polarizations of 181 MeV protons scattered from lithium.

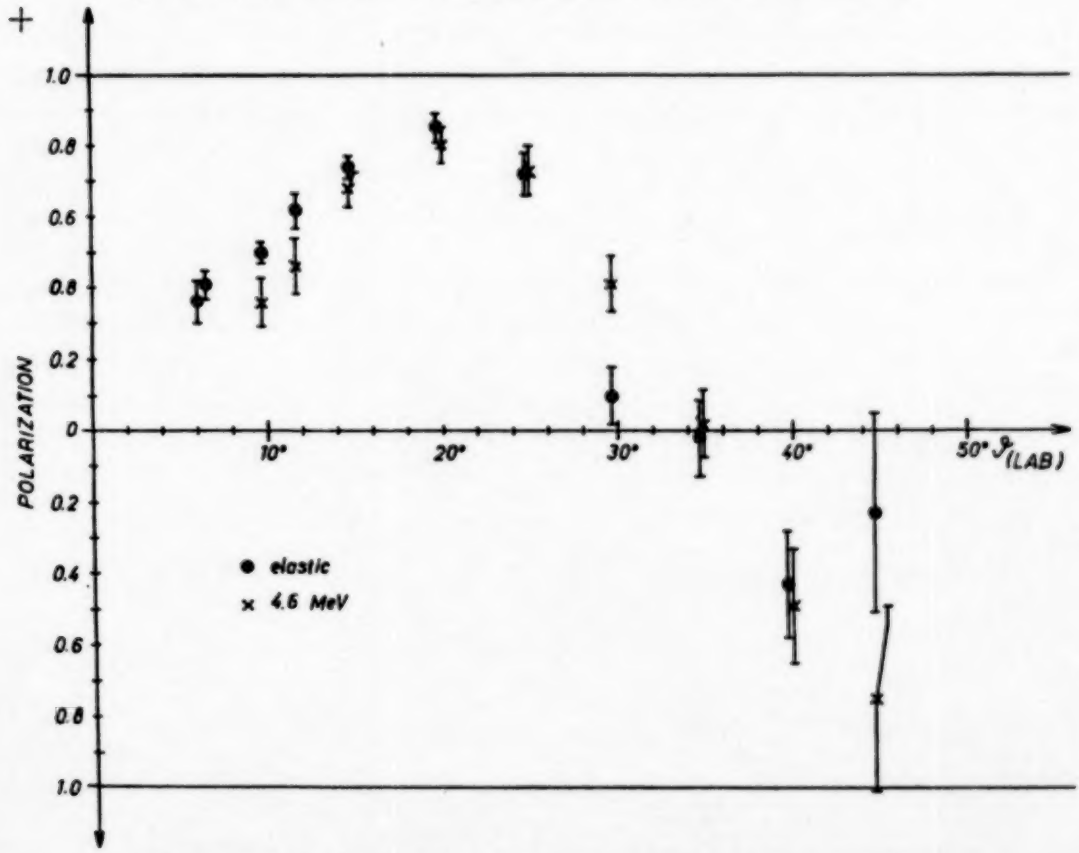

Fig. 2. Polarizations of 181 MeV protons scattered from beryllium.

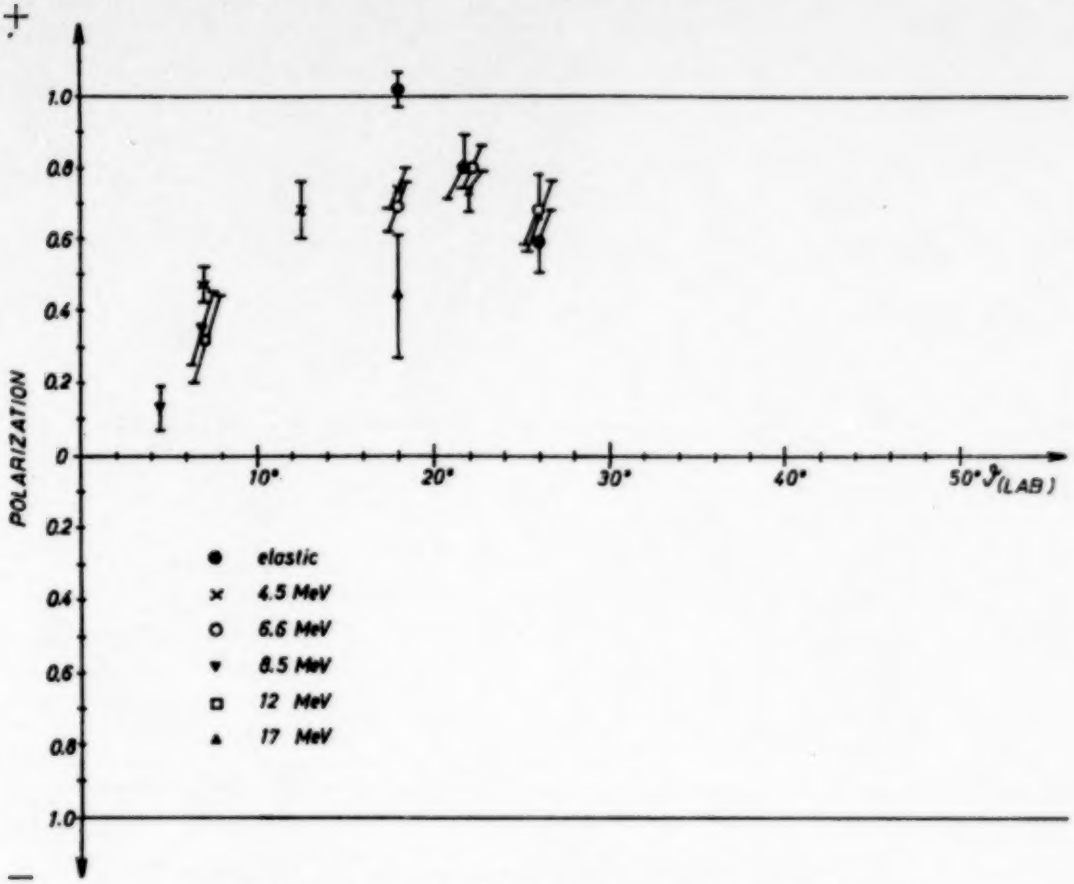

Fig. 3. Polarizations of 182 MeV protons scattered from boron.

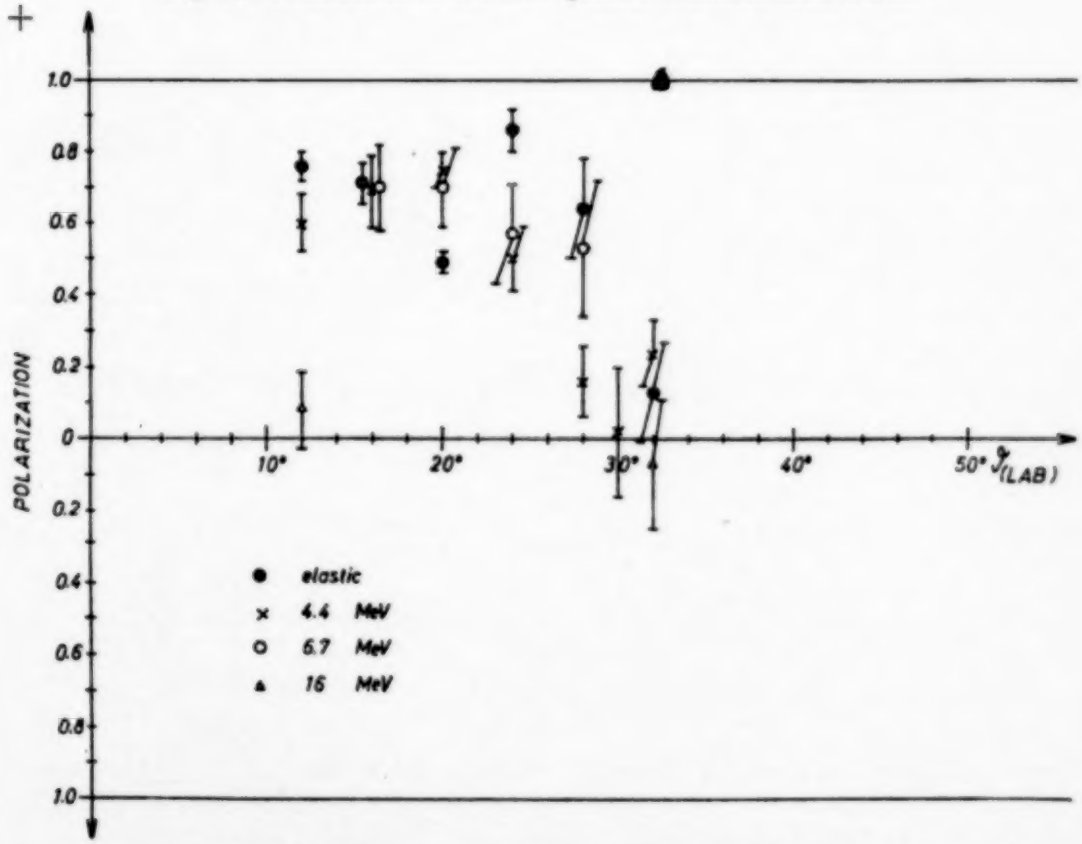

Fig. 4. Polarizations of 179 MeV protons scattered from iron.

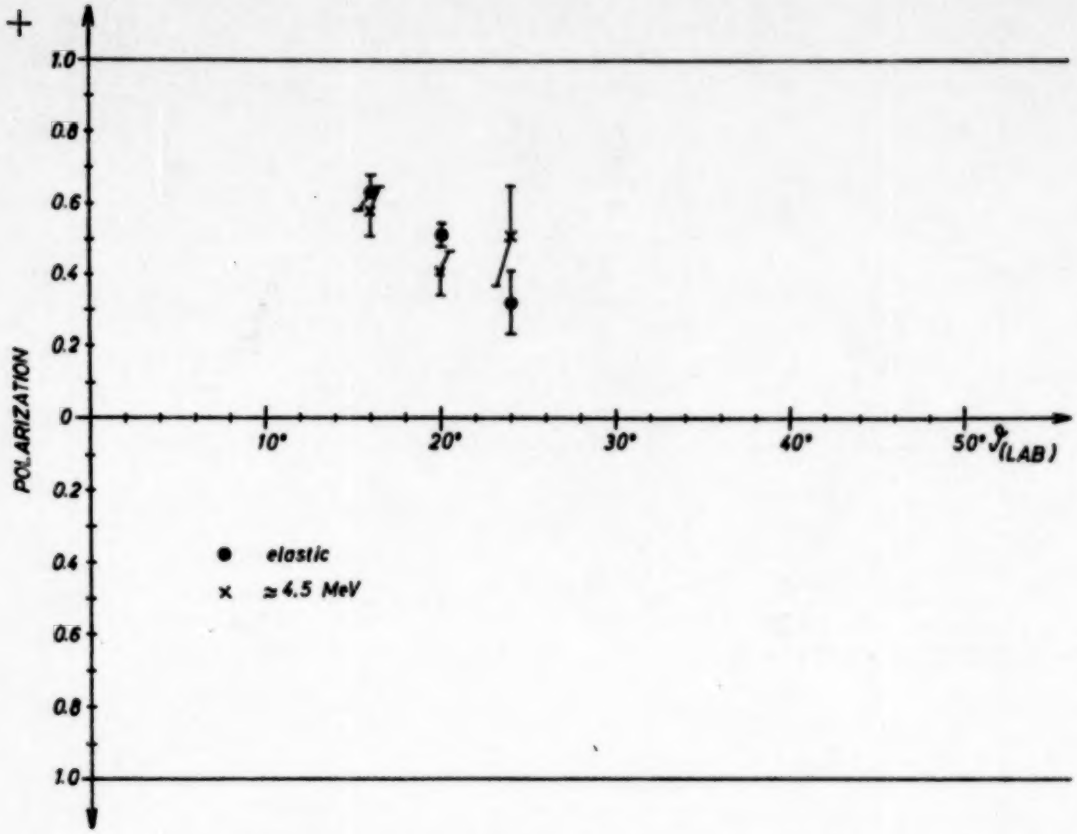

Fig. 5. Polarizations of 179 MeV protons scattered from bismuth.

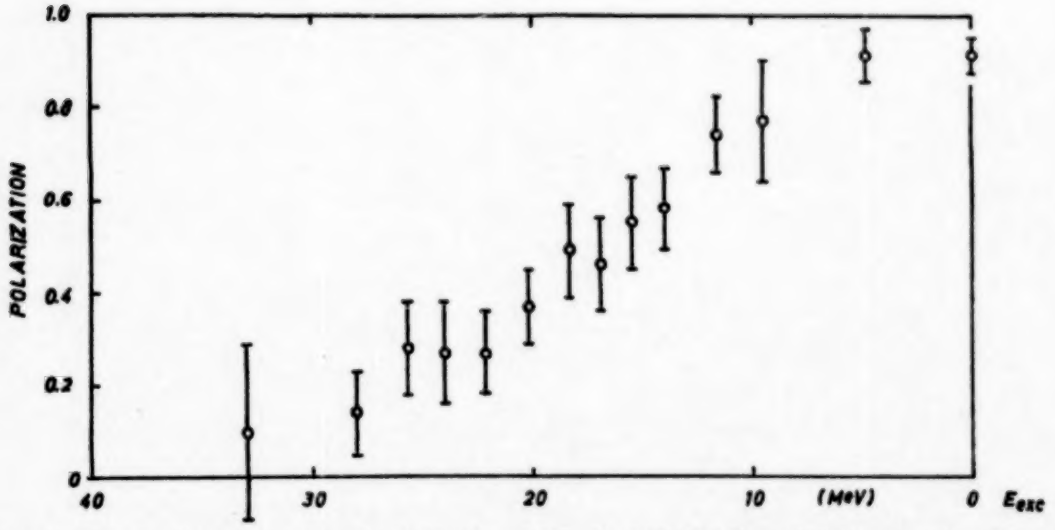

Fig. 6. Polarizations of protons inelastically scattered at 20° lab from lithium as a function of excitation energy.

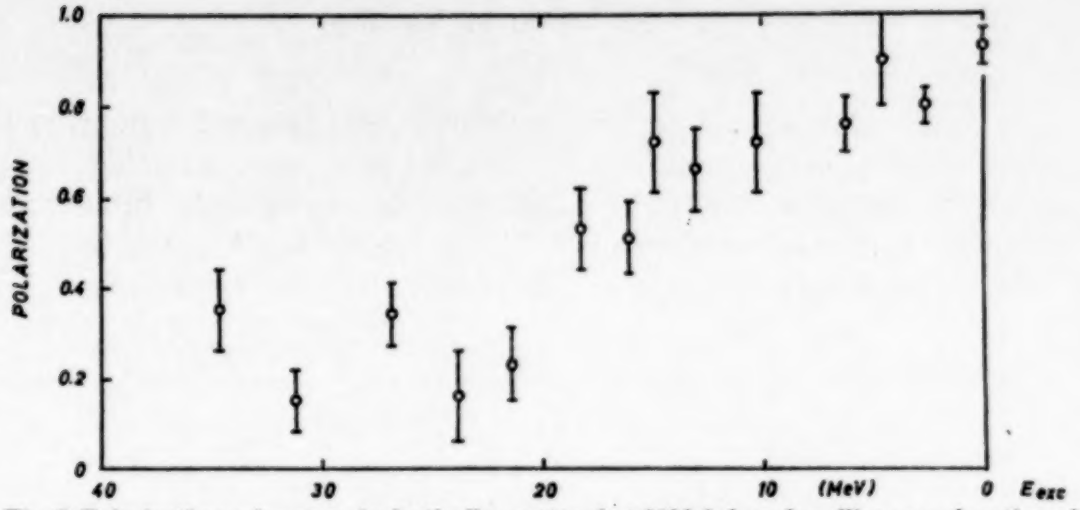

Fig. 7. Polarizations of protons inelastically scattered at 20° lab from beryllium as a function of excitation energy.

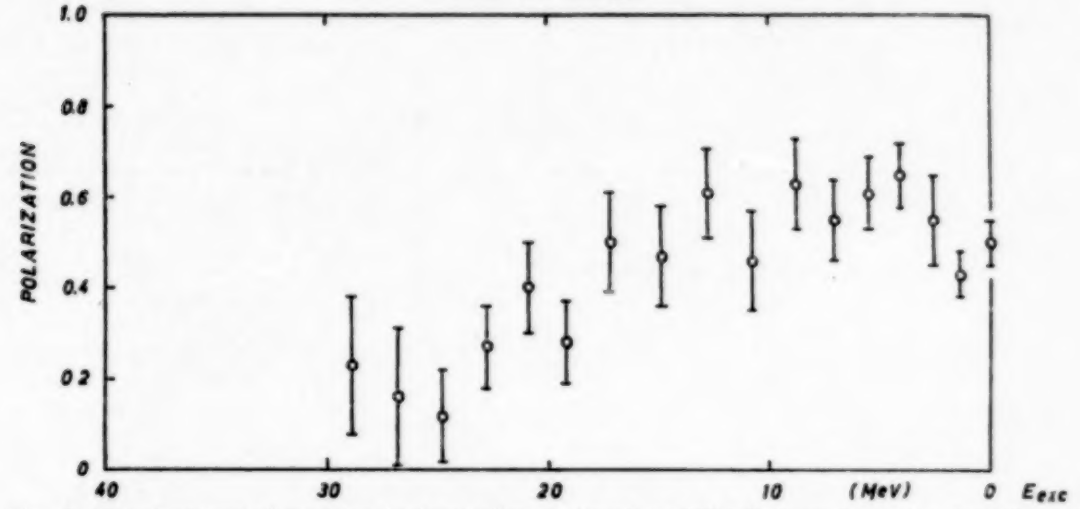

Fig. 8. Polarizations of protons inelastically scattered at 20° lab from iron as a function of excitation energy.

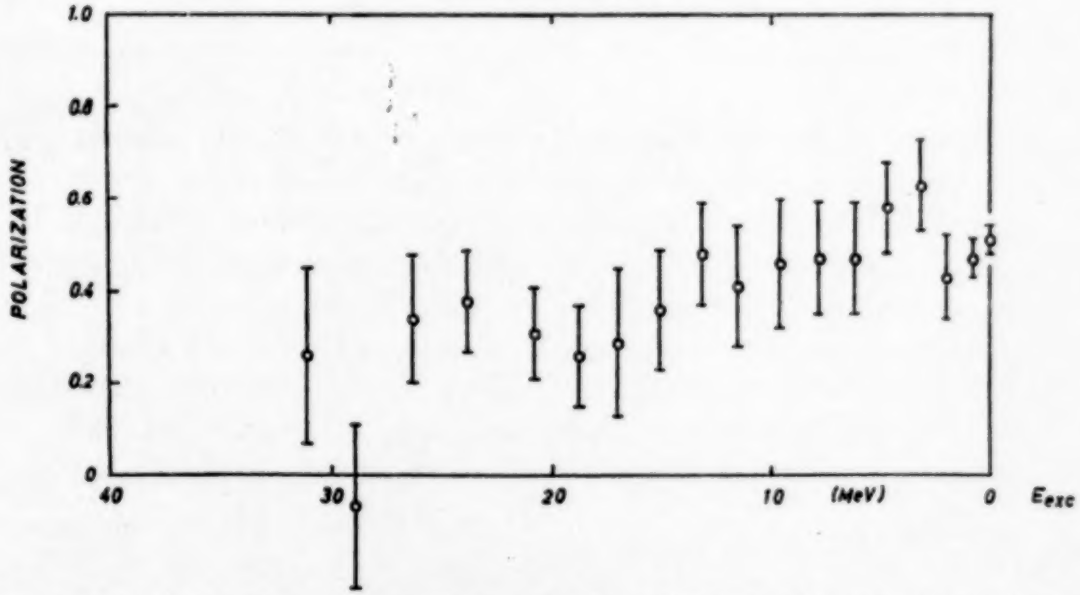

Fig. 9. Polarizations of protons inelastically scattered at 20° lab from bismuth as a function of excitation energy.

4. Discussion of Results

4.1. ELASTIC SCATTERING

In elastic scattering the equality between polarization and asymmetry is required by symmetry principles [18]). This has been discussed earlier in an article [19]) where also the elastic polarization data of fig. 1 for lithium are compared with asymmetry results †. The agreement was found to be good. In fig. 10 the same comparison is made between the iron elastic polarization

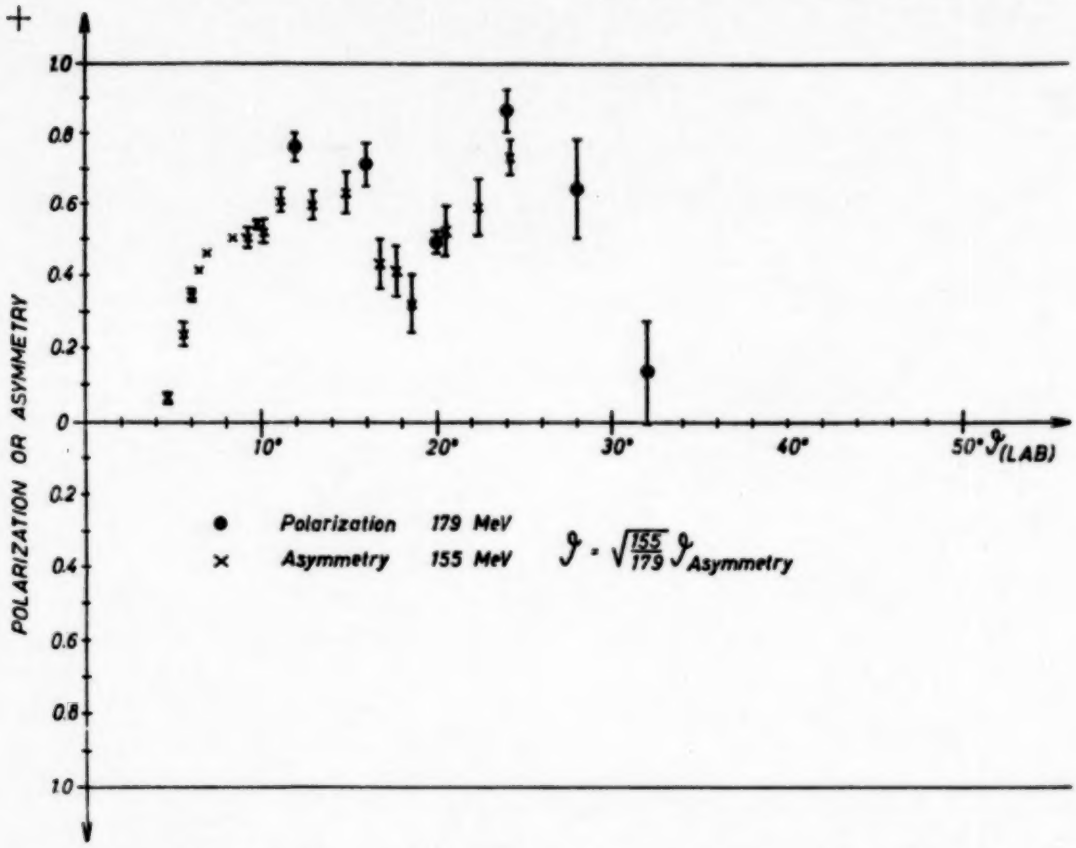

Fig. 10. Elastic polarizations of iron compared with asymmetries of Alphonce *et al.* [21]).

and the iron asymmetry, obtained by Alphonce *et al.* [20]). The angular scale has been transformed in figs. 10—12 by the square root of the energy ratio to correct for the different energies of the protons in the two cases. In the limited angular region that is covered by both measurements, the agreement is fair. There has been no determination of the elastic asymmetry for Be at Uppsala, but at a slightly higher energy this quantity has been measured by Hafner in Rochester [10]). In fig. 11 his data are compared with the elastic polarization from fig. 2. There are two regions of disagreement. Between 7° and 15° the difference between the two sets of results is very small and

† The polarization data shown in ref. [19]) for lithium and aluminium have been corrected slightly; the conclusions of that article are not affected.

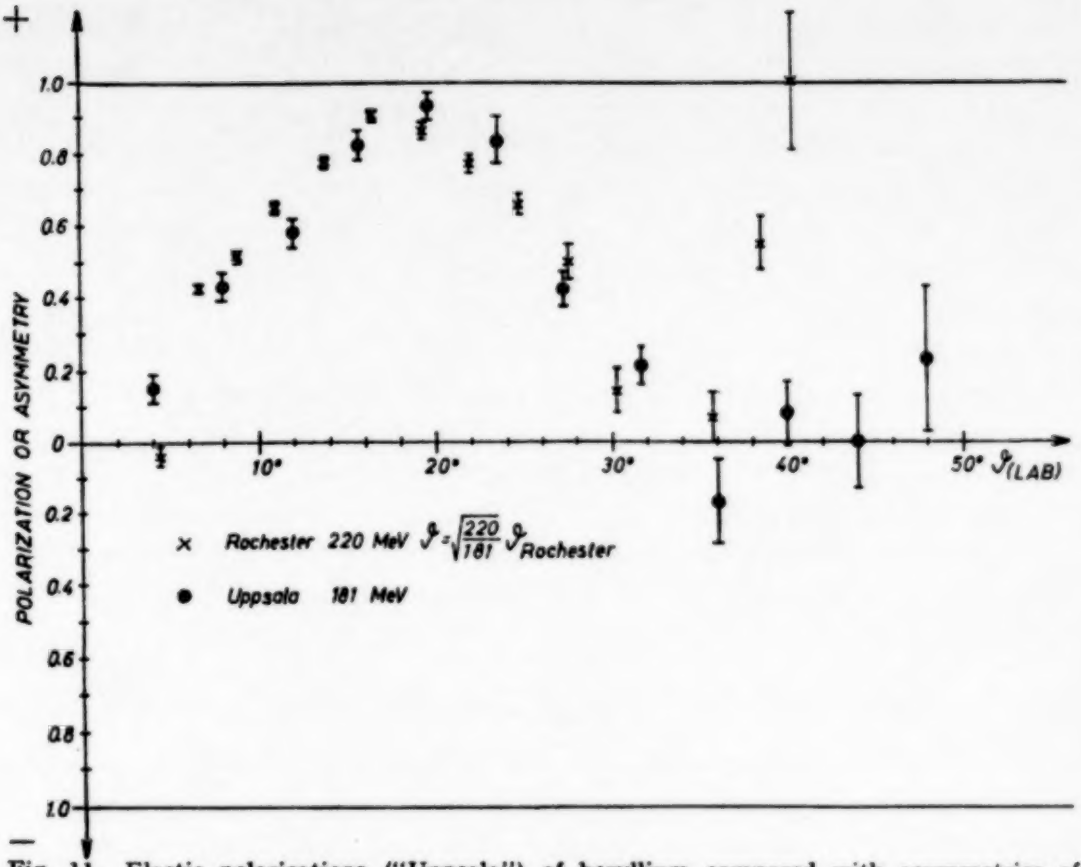

Fig. 11. Elastic polarizations ("Uppsala") of beryllium compared with asymmetries of Hafner [10]) ("Rochester").

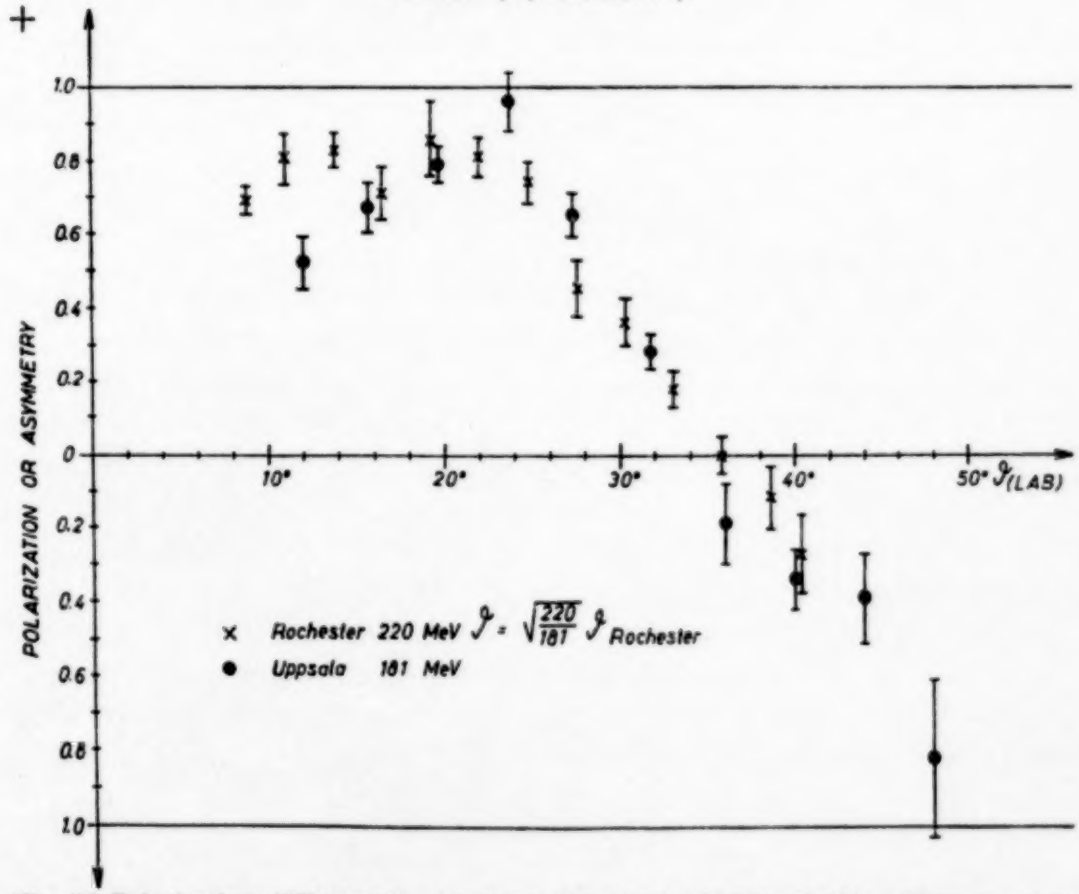

Fig. 12. Polarizations ("Uppsala") of protons from the 2.4 MeV level of beryllium compared with asymmetries of Hafner [10]) ("Rochester").

not statistically significant but, nevertheless, probably real, because the same tendency is also seen in carbon [21]) and aluminium [10,19]). The effect may be due to the fact that while the positions of the minima should vary with energy as $E^{\frac{1}{2}}$ as we have assumed, the smaller angle region should really be corrected by a factor proportional to E, as may be seen from eq. (1). Around 40° the discrepancy is more serious. While Hafner obtains about 100 % asymmetry, the polarization measured here is close to zero. This difference is probably too great to be explained by the different proton energies. It may be that the difficulty of separating the elastic peak from the inelastic level at 2.4 MeV is the cause of error. There is also a large difference between the ratios of elastic to 2.4 MeV inelastic cross sections. Hafner obtained about twice as many elastically scattered protons as protons exciting the 2.4 MeV level, whereas the elastic peak is about 30 % less than the inelastic at Uppsala. It is also interesting to note that the measurements of polarization and asymmetry of protons exciting the 2.4 MeV level give results that agree very well at large angles, as is seen from fig. 12.

4.2. INELASTIC SCATTERING

There is no immediate reason to believe that the asymmetry e and the polarization P of inelastically scattered protons should be identical. Of the theoretical treatments to date, only Squires [5]) has differentiated between these two quantities, and he concluded that $|P-e|$ is likely to be very small. The only asymmetry measurement made with a target nucleus that is also studied in this work was reported by Hafner [10]) and concerns the 2.4 MeV level of Be^9. In fig. 12 the polarization and the asymmetry for inelastically scattered protons from this level are compared. The agreement is seen to be very good except at small angles where the differences may well be due to difficulties in separating the inelastic events from the elastic as the elastic scattering is much stronger.

In fig. 13 all measured polarizations of inelastically scattered protons from low-lying levels are plotted together with a curve fitted through the 4.4 MeV carbon results of the earlier report [14]). This curve also represents the theoretical calculations very well [3]). The Li, Be and B results are seen to follow the curve closely. These nuclei do not have ground state spin zero and the reduction of the expression for the polarization P to formula (4) does not occur even in L-S coupling. However, an explicit calculation by Egardt [22]) for the 4.46 MeV level of B^{11} has shown that the additional terms that enter into (4) are quite small and do not alter the values appreciably. His results are shown as a curve in fig. 14 together with the measured polarizations of the 4.5 MeV level in boron. The agreement is seen to be reasonably good. It is likely that j-j coupling would decrease the amount of polarization and thus worsen the fit in the same way as it did for C^{12} according to Squires [5]).

Fig. 13 also shows that the polarization pattern for the 4.4 MeV level of iron seems to be contracted in angle. The same tendency was noticeable in the calcium data of the earlier report [14]). The contraction is, however, far less than that which occurs for elastic scattering. The maximum value of the

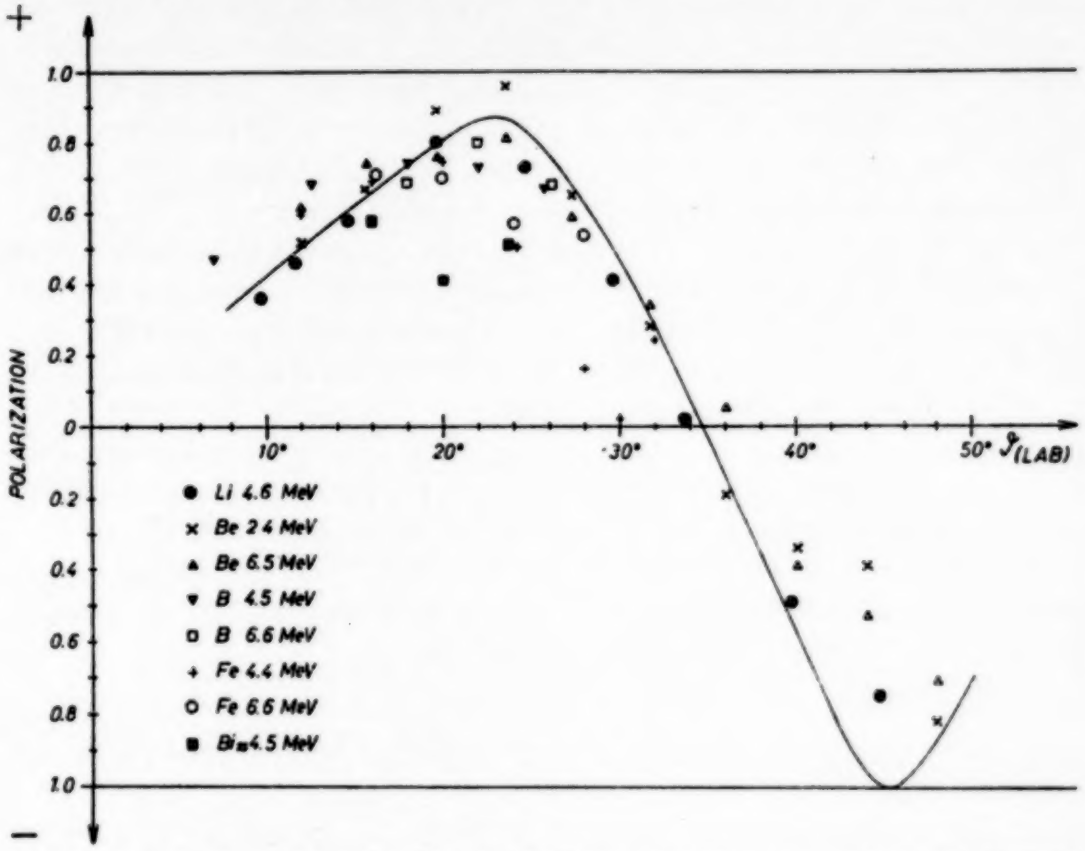

Fig. 13. Polarizations of low-lying levels of lithium, beryllium, boron, iron and bismuth.

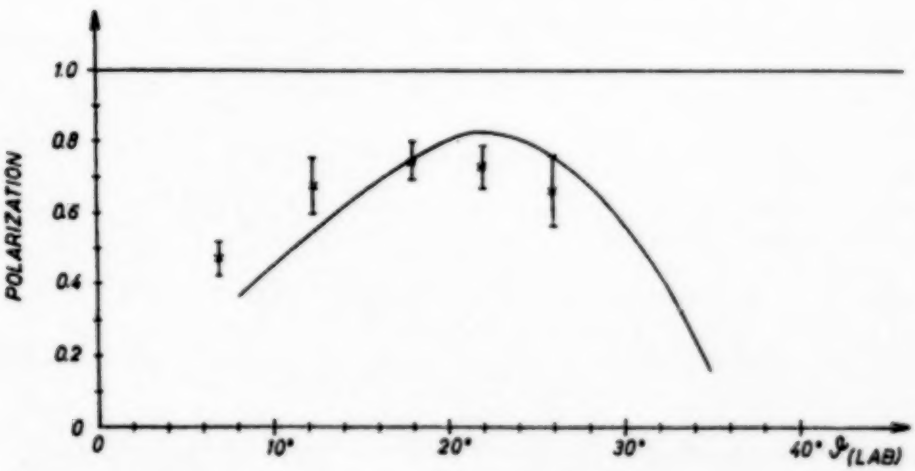

Fig. 14. Polarization of protons from the 4.5 MeV level of boron compared with theoretical curve of Egardt [23]).

polarization is still quite high for a nucleus as heavy as iron, which might indicate an appreciable amount of L-S coupling in the nuclear wave function. The bismuth polarization at 20° is somewhat smaller than 50 %. It is difficult to say if this is due to further contraction of the angular scale or to other reasons because the experimental points are too few and uncertain.

From the variations in the polarization with excitation energy shown in figs. 6—9, one can see two clear trends. The first is that in all elements there is a steady decrease in polarization with increasing excitation energy, with little reflection of the cross section structure. This is understandable for instance on the model of Köhler [3]) for inelastic scattering, in which, independent of the specific level involved (though dependent on the nature of the coupling and to some extent on the final state spin) the polarization is enhanced above the free nucleon-nucleon value for all bound final states. Thus one would expect a decrease in polarization towards the free nucleon-nucleon value with increasing excitation energy as more and more of the final states are unbound; and, for instance, rapid falls in the polarization are noticeable in lithium and beryllium near 20 MeV, where it becomes energetically possible to extract s-state nucleons from the nucleus [23]).

The other trend is the decrease in polarization at small excitation energies with increasing atomic number. This may be understandable on the grounds of increasing j-j coupling as discussed above.

We are grateful to Prof. The Svedberg for encouragement. Discussions and correspondence with Prof. D. R. Inglis and especially Mr. S. Köhler have been very stimulating. We thank Dr. H. Tyrén and Dr. Th. A. J. Maris for making available to us the unpublished bismuth data, and we also thank Mr. L. Egardt for letting us use his results before publication. As always the cyclotron crew under Mr. Å. Svanheden has been most helpful. The work was supported by the Swedish Atomic Energy Commission.

References

1) Th. A. J. Maris, Nuclear Physics **3** (1957) 213
2) M. Ruderman, Phys. Rev. **98** (1955) 267
3) S. Köhler, Nuclear Physics **9** (1958) 49
4) K. Nishimura and M. Ruderman, Phys. Rev. **106** (1957) 558
5) E. J. Squires, Nuclear Physics **6** (1958) 504
6) G. P. McCauley and G. E. Brown, Proc. Phys. Soc. **71** (1958) 893
7) G. P. McCauley, Proc. Phys. Soc. **73** (1959) 309
8) J. M. Gammel and R. M. Thaler, Phys. Rev. **107** (1957) 291, 1337
9) W. G. Chesnut, E. M. Hafner and A. Roberts, Phys. Rev. **104** (1956) 449
10) E. M. Hafner, Phys. Rev. **111** (1958) 297
11) J. M. Dickson and D. C. Salter, Nuovo Cimento **2** (1955) 907
12) Private communication

13) R. Alphonce, A. Johansson and G. Tibell, Nuclear Physics **4** (1957) 672
14) P. Hillman, A. Johansson and H. Tyrèn, Nuclear Physics **4** (1957) 648
15) H. Tyrén and Th. A. J. Maris, Nuclear Physics **6** (1957) 82
16) H. Tyrén and Th. A. J. Maris, Nuclear Physics **7** (1958) 24
17) C. K. Bockelman, A. Leveque and W. W. Buechner, Phys. Rev. **104** (1956) 456
18) L. Wolfenstein, Ann. Rev. Nucl. Sci. **6** (1956) 43
19) P. Hillman, A. Johansson and G. Tibell, Phys. Rev. **110** (1958) 1218
20) R. Alphonce, A. Johansson and G. Tibell, Nuclear Physics **3** (1957) 185
21) R. Alphonce, A. Johansson and G. Tibell, Nuclear Physics **4** (1957) 643
22) L. Egardt, private communication
23) H. Tyrén, P. Hillman and Th. A. J. Maris, Nuclear Physics **7** (1958) 10

8.B

Nuclear Physics **11** (1959) 554—568; © *North-Holland Publishing Co., Amsterdam*

Not to be reproduced by photoprint or microfilm without written permission from the publisher

ENERGY AND ANGULAR DISTRIBUTIONS OF MESONIC HYPERFRAGMENT DECAYS

N. BYERS † and W. N. COTTINGHAM

Department of Mathematical Physics, University of Birmingham, England

Received 16 February 1959

Abstract: The distribution in energy and angle for the decay ${}_{\Lambda}He^5 \rightarrow \pi^- + p + He^4$ has been investigated. It is shown that the angular asymmetry observed in three-pronged hyperfragment decays of this type can result from low-energy nuclear resonances (compound nucleus formation). Angular and energy distributions for the decay ${}_{\Lambda}He^5 \rightarrow \pi^- + p + He^4$ are presented which have been calculated neglecting pion interactions. The form of these curves is largely determined by the fact that there is a low-energy $P_{\frac{3}{2}}$ resonance in proton-He^4 scattering. Effects due to parity violation and pion interactions are discussed and it is found that they will not produce any significant qualitative effects.

1. Introduction

In a world survey of hypernuclei [1]), a marked angular anisotropy in the decays of hypernuclei into a π^-, proton, and residual nucleus was reported

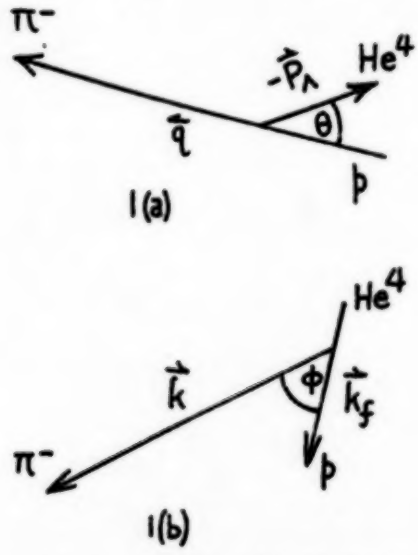

Fig. 1. Variables which designate the final state in the decay ${}_{\Lambda}He^5 \rightarrow \pi^- + p + He^4$; in fig. 1(a) **q** is the momentum conjugate to the displacement of the pion from the proton, $-\mathbf{P}_{\Lambda}$ is momentum conjugate to displacement of He^4 from centre of mass of pion-proton system (similarly, in fig. (1b) $\mathbf{k}_f$ is the relative momentum of proton-He^4 system, and **k** is momentum conjugate to displacement of pion from centre of mass of proton-He^4 system). Experimental observations[1]) indicate a preference for small θ.

† Now at the Institute of Theoretical Physics, Department of Physics, Stanford University.

(see fig. 1). It is plausible to consider these decays as Λ^0's having a distribution of momenta P_Λ (because they are bound to the residual nucleus) decaying as if they were free. The reported anisotropy seemed to contradict this simple model. However, as Dalitz [2]) suggested, this apparent contradiction may be due to interactions between the particles in the final state. The interaction of the proton with the residual nucleus is strong and, in many cases included in the survey, gives rise to low-energy resonant states [3]). Since the angular anisotropy shows that the proton emission tends to be in the same direction as the nuclear recoil, it is likely that these resonances are responsible for the observed effect. To confirm this, we have calculated the angular and P_Λ distribution for the decay ${}_\Lambda\mathrm{He}^5 \rightarrow \pi^- + \mathrm{p} + \mathrm{He}^4$. This process is particularly amenable to quantitative analysis because there are extensive data available on the p-He^4 interaction from scattering and polarization measurements [4]). Since a preliminary investigation (see sec. 4) showed that the effects of pion interactions would be small compared to those due to purely nuclear interactions, we calculated the transition probability for this process taking into account only the proton-He^4 interaction in the final state. We find a very strong angular correlation of the observed type. It is primarily due to the formation of the ground state of Li^5, a sharp $\mathrm{P}_{\frac{3}{2}}$ resonant state in proton-He^4 scattering at about 2 MeV. This disagrees with the results of Hill's phenomenological analysis [5]). He concluded that the proton-He^4 system is produced largely in the first excited state of Li^5, a broad $\mathrm{P}_{\frac{1}{2}}$ resonance which lies 5—10 MeV above the ground state [3]). We find that decays into the $\mathrm{P}_{\frac{1}{2}}$ resonance region are not strongly favoured because of the poor overlap between the initial and final state wave functions. The $\mathrm{P}_{\frac{1}{2}}$ wave functions which contain the large experimental $\mathrm{P}_{\frac{1}{2}}$ phase shifts have their first node near the nuclear surface. The initial state wave function is appreciable (and always positive) out to distances of the order of three times the nuclear radius because the Λ^0 is loosely bound. As a result, there is strong cancellation in the transition matrix element and comparatively few transitions can take place into this resonance region.

Our results are to a very large extent dictated by the proton-He^4 scattering data. However, it was necessary to postulate a model for the nuclear interactions. For simplicity, we neglected the internal structure of the He^4 and represented its nuclear interactions with the Λ^0 and the proton by square well potentials. (The extent to which our results are model dependent is discussed in sec. 3.) Since, in the main, the qualitative features of the ${}_\Lambda\mathrm{He}^5$ decay are determined by low-energy proton-He^4 interactions, any quantitative estimate must take the Coulomb repulsion into account. In this calculation it was possible to do this adequately (see sec. 2). The effect of parity violation is discussed in sec. 2 and at the end of sec. 3. In sec. 5 we discuss some other hyperfragment decays.

2. Method of Calculation

Treating the decay interaction in first-order perturbation theory, the transition matrix element for the decay ${}_{\Lambda}\mathrm{He}^5 \rightarrow \mathrm{He}^4+\mathrm{p}+\pi^-$ is given by

$$T = \sum \langle \Psi_f | \mathbf{k}_p \mathbf{k}_\pi \mathbf{k}_\alpha \rangle \langle \mathbf{k}_p \mathbf{k}_\pi | H | \mathbf{k}_\Lambda \rangle \langle \mathbf{k}_\Lambda \mathbf{k}_\alpha | \Psi_i \rangle, \tag{1}$$

where $\langle \mathbf{k}_p \mathbf{k}_\pi | H | \mathbf{k}_\Lambda \rangle$ is the matrix element for the decay of a free Λ^0 of momentum $\mathbf{k}_\Lambda$ into a pion and a proton of momenta $\mathbf{k}_\pi$ and $\mathbf{k}_p$, respectively; and $\langle \mathbf{k}_\Lambda \mathbf{k}_\alpha | \Psi_i \rangle$ and $\langle \mathbf{k}_p \mathbf{k}_\pi \mathbf{k}_\alpha | \Psi_f \rangle$ are the Fourier transforms of the initial and final state wave functions. The spin dependence of these quantities is to be understood and the sum taken over all momentum and spin variables. Allowing for parity non-conservation, the most general decay Hamiltonian in non-relativistic approximation is

$$\langle \mathbf{k}_\pi \mathbf{k}_p | H | \mathbf{k}_\Lambda \rangle = (2\pi)^2 \left(\frac{1+\mu}{\mu}\right)^{\frac{1}{2}} (s + p\boldsymbol{\sigma} \cdot \mathbf{q}) \delta(\mathbf{k}_\Lambda - \mathbf{k}_p - \mathbf{k}_\pi) \left(\frac{2\pi}{V}\right)^{\frac{3}{2}} \tag{2}$$

where $\mathbf{q} = (\mathbf{k}_\pi - \mu \mathbf{k}_p)/(1+\mu)$ (μ is the ratio of pion to proton mass), V is the normalization volume, and the components of $\boldsymbol{\sigma}$ are the Pauli spin matrices. Measuring q in units of q_Λ, its value for free Λ^0 decay, $|s|^2$ and $|p|^2$ are the relative probabilities for free Λ^0 decay into pion-proton states with $l = 0$ and $l = 1$, respectively. The free decay lifetime τ, neglecting pion-proton interactions, is given by the equation

$$\frac{1}{\tau} = 2q_\Lambda(|s|^2 + |p|^2). \tag{3}$$

Assuming the Λ^0 is bound in an $S_{\frac{1}{2}}$ state and evaluating (1) in the rest frame of the ${}_{\Lambda}\mathrm{He}^5$, one can easily verify if pion interactions are neglected that, aside from a small correction to be discussed below, the sum over initial and final spin states yields

$$\sum_{\text{spins}} |T|^2 = (2\pi) \left(\frac{1+\mu}{\mu}\right) \frac{1}{V^2} (|s|^2 + q^2|p|^2) \sum_{\text{spins}} |M|^2 \tag{4}$$

where, suppressing spin indices,

$$M = \langle \Psi_f | \Psi_i \rangle = \int \psi_f^*(\mathbf{r}) \exp(-\tfrac{4}{5} i \mathbf{k} \cdot \mathbf{r}) \psi_\Lambda(\mathbf{r}) \mathrm{d}^3\mathbf{r} \tag{5}$$

and q is the relative momentum of the pion-proton system in the final state. In (5) ψ_Λ is the (normalized wave function for the Λ^0—He^4 bound state, $\mathbf{k}$ is the momentum of the pion, and ψ_f is the proton-He^4 wave function with incoming scattered waves, which asymptotically is a plane wave of momentum $\mathbf{k}_f$ (normalized) to one particle per unit volume). To obtain the expression (4) we have taken the term linear in q in (2) outside the integral

(1). This amounts to neglecting a term in (4) of the form

$$\mu p\sigma \cdot \int \frac{(\nabla \psi_l^s(\mathbf{r}))^*}{q_\Lambda} \exp(-\tfrac{4}{5} i\mathbf{k}\cdot\mathbf{r})\psi_\Lambda(\mathbf{r})\mathrm{d}^3\mathbf{r}, \tag{6}$$

where ψ_l^s is the scattered wave part of ψ_l. This correction is, if $|p/s| \approx 1$, of the order of magnitude of the ratio of the pion to proton mass μ. Since $|p/s|$ is not yet known (Dalitz [6]) finds that $0.45 \leqq |p/s| \leqq 1$), we have not taken this term into account. In eq. (4) interference between the $l = 0$ and $l = 1$ decay channels do not appear because parity-violating terms cannot survive the spin sums. If spins are not observed, the decay is completely characterized by two momenta, and therefore the transition probability cannot depend on a pseudoscalar quantity. As energy and momentum are conserved, the transition probability depends on just two non-trivial kinematic variables, and one can choose these to be k_l and ϕ, or P_Λ and θ (see fig. 1). The former choice is the most convenient one for the study of effects arising from proton-He^4 interaction, since k_l is the relative proton-He^4 momentum. However, the latter choice is more convenient for the study of the Λ^0-He^4 interaction and effects due to parity violation, since P_Λ and q are the relative momenta of the Λ^0-He^4 system and pion-proton system, respectively. Experimental data have been reported in terms of P_Λ and θ. Therefore, our results for the transition probability are given as a function of these variables. The probability for an event in an interval $\mathrm{d}P_\Lambda\,\mathrm{d}\cos\theta$ is given by

$$2q_\Lambda(|s|^2+|p|^2q^2)|M(p_\Lambda,\cos\theta)|^2\frac{qP_\Lambda^2}{(2\pi)^2}\mathrm{d}P_\Lambda\mathrm{d}\cos\theta. \tag{7}$$

All effects of parity violation, aside from the relatively minor effects arising from (6), are contained in the factor $(|s|^2+q^2|p|^2)$. Since q is a function of P_Λ only (see appendix), this factor has no angular dependence. Its dependence on P_Λ is important only in the region of large P_Λ, because q^2 is a slowly-varying function of P_Λ for all but the largest values of P_Λ. (Unfortunately in this region of large P_Λ, proton-He^4 interactions are important and cannot be taken into account sufficiently accurately (see sec. 3) to enable one to obtain an estimate of $|p|^2/|s|^2$ from this effect.)

To evaluate the overlap integral (5), it is necessary to assume a model for the nuclear interactions. We assume that the Λ^0 is bound in an s-state. The probability of finding it inside the He^4 is of the order of $\frac{1}{2}$. Therefore, the contribution to the overlap integral M from the region where r is less than the radius a of the He^4 cannot be neglected and must be calculated on the basis of some model. The contribution to M for $r > a$ is model independent and determined by the experimental proton-He^4 phase shifts. Scattering and polarization measurements [4]) show that there is a sharp $P_{\frac{3}{2}}$ and a

broad $P_{\frac{1}{2}}$ resonance in proton-He^4 scattering (see fig. 2). Ajzenberg and Lauritsen [3]) identify the $P_{\frac{3}{2}}$ resonance as the formation of the ground state of Li^5, a state lying 1.8 MeV above the zero of kinetic energy for the proton-He^4 system. They interpret the behaviour of the $P_{\frac{1}{2}}$ phase shift as corresponding to the formation of a very broad excited state of Li^5 located 5—10 MeV above the ground state. Reliable quantitative estimates of the effects of these resonances should follow from the use of the very extensive low-energy scattering data and a simple model consistent with the data. To obtain such estimates for energies less than 9 MeV we assumed that the proton-He^4 interaction occurs only in the $S_{\frac{1}{2}}$, $P_{\frac{1}{2}}$ and $P_{\frac{3}{2}}$ states, neglected the internal structure of the He^4, and represented the interaction in these states by three square well potentials. We also represented the Λ^0—He^4 interaction by a square well potential. A sharp low-energy resonance determines rather precisely the effective range of the corresponding interaction. Sack, Biedenharn and Breit [7]) found that the behaviour of the $P_{\frac{3}{2}}$ phase shift in the region 0—14 MeV would arise if the interaction energy was given by a square well potential of radius 3.15×10^{-13} cm. Important computational simplifications follow from the assumption that the radii of the potentials are all equal. Therefore, we took all wells to be of this radius. This is larger than the radius of He^4 as determined by electron scattering measurements [8]). However, neutron scattering experiments indicate that the effective radius of nuclei for nuclear interactions is larger than for electromagnetic interactions.

The assumption of a nuclear radius of 3.15×10^{-13} cm limits the accuracy with which we can take the $P_{\frac{1}{2}}$ resonance into account. The experimental data indicate a larger effective range than we can obtain with this assumption (see fig. 2). However, the $P_{\frac{1}{2}}$ resonance is very broad and located in an energy range where shape-dependent effects are likely to be important. Therefore, if we had taken a range for the $P_{\frac{1}{2}}$ interaction which yielded a better fit, it is doubtful that results so obtained would be much more reliable. With our choice of radius, we found that the binding energy† of ${}_\Lambda He^5$($B_\Lambda = 3.1$ MeV) corresponds to a well depth of 13.0 MeV for the Λ^0—He^4 potential††. Fits to the $S_{\frac{1}{2}}$, $P_{\frac{1}{2}}$, and $P_{\frac{3}{2}}$ experimental proton-He^4 phase shifts were obtained using wells of depths 37.5, 14.6 and 22.22 MeV, respectively. These well depths were obtained by matching square well wave functions to Coulomb wave functions at the nuclear surface. The fit to the experimental phase shifts is shown in fig. 2. As can be seen in fig. 2, the $S_{\frac{1}{2}}$ phase shift is negative, and therefore could also be fitted by a repulsive

† This value was obtained by averaging the observed Q values for seven ${}_\Lambda He^5$ decay events reported in ref. [1]), using $M_\Lambda = 1\,115.2$ MeV as given by Barkas, Giles, Heckman, Inman, Mason and Smith, Padua-Venice Conference (September 1957).

†† A range of 3.15×10^{-13} cm is probably an overestimate for the Λ^0—He^4 interaction. As a result, we may have underestimated somewhat the relative contribution to M from the region $r < a$.

potential. However, we believe that a more natural interpretation is that the phase shift has the value π at zero kinetic energy and decreases from this value with increasing energy giving rise to an apparent negative phase shift. This latter interpretation implies that the effective potential in the $S_{\frac{1}{2}}$ state is attractive and deep enough to produce a bound state. Indeed, if it were not for the Pauli principle, one would expect that a nucleon could be bound to He^4 in an $l = 0$ state. Therefore, we have taken the interaction in the $S_{\frac{1}{2}}$ state to be attractive and strong enough to produce one bound state.

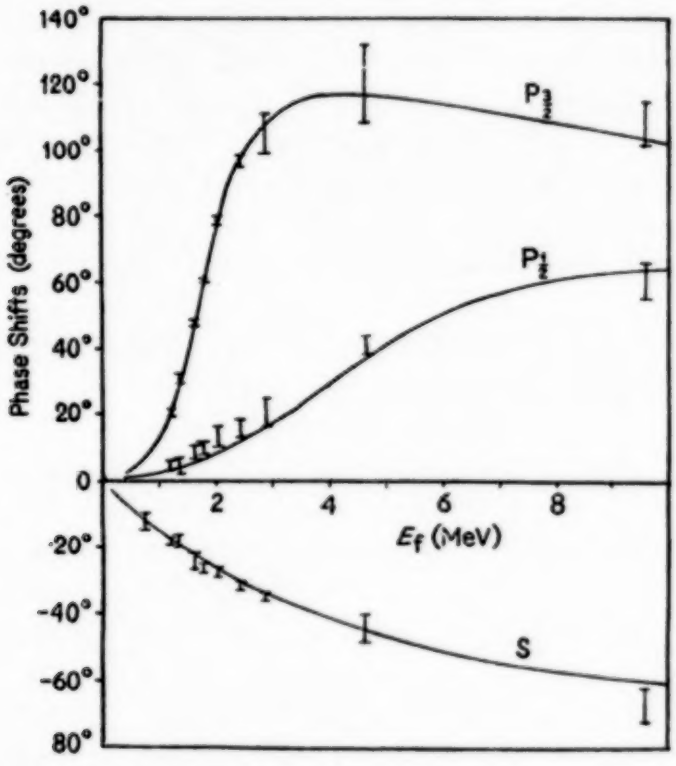

Fig. 2. Proton-He^4 $S_{\frac{1}{2}}$, $P_{\frac{1}{2}}$, and $P_{\frac{3}{2}}$ phase shifts from 0—10 MeV centre-of-mass energy. The curves show the phase shifts calculated from the model (see sec. 2). The experimental points below 3 MeV were obtained from C. L. Critchfield and D. C. Dodder, Phys. Rev. **76** (1949) 602; the point at 4.65 MeV is from D. C. Dodder and J. L. Gammel, Phys. Rev. **88** (1952) 520; and the point at 9.6 MeV is from K. W. Brockmann, Phys. Rev. **108** (1957) 1000.

As can be seen in fig. 2, the phase shifts predicted by our model begin to show definite disagreement with the experimental phase shifts in the region of 9 MeV. Therefore, the quoted well depths have been used only for events in which the kinetic energy of relative motion of the proton and He^4, E_f, is less than or equal to 9 MeV. For calculating M for higher E_f values, at each energy well depths determined by the experimental phase shifts [4]) were used (radii always taken as 3.15×10^{-13} cm).

The Coulomb repulsion between the proton and He^4 is easily taken into account in our square well approximation. At the energies where Coulomb

effects must be included ($E_t \leqq 5$ MeV), the partial waves in ψ_t with $l \geqq 2$ can be neglected and Coulomb effects need to be included only in the s and p partial waves of ψ_t. To do this, we observe that the potentials obtained from proton-He^4 scattering data differ from those that would apply for neutron-He^4 scattering by 0.92 MeV, the Coulomb potential at $r = a$ (the variation of this potential for $r < a$ is small and can be neglected compared to the depth of the wells). Therefore, apart from normalization, the wave function for a neutron-He^4 system of energy $E_t - 0.92$ MeV is just that for a proton-He^4 system of energy E_t when $r \leqq a$. For $r > a$, these functions differ somewhat due to the variation of the Coulomb potential; however, this variation is not sufficient to alter the wave function appreciably in the region of interest ($a < r < 3a$) since we are here concerned with wavelengths greater than $6a$. (The overlap integral (5) contains appreciable contributions only from within the sphere $r \leqq 3a$.) Therefore, the proton-He^4 wave function of energy E_t may be approximated by the neutron-He^4 wave function of energy $E_t - 0.92$ MeV provided this simple square-well wave function is normalized so that it is equal to the exact proton-He^4 wave function at $r = a$. Using this approximation, one calculates distributions for the decay ${}_\Lambda He^5 \rightarrow \pi^0 + n + He^4$ along with the distributions for the π^- decay mode. In the next section, our results for the π^- decay mode are presented and the comparison with the π^0 decay mode is discussed (see footnote on p. 563). Though it would have been simpler to have determined our nuclear potentials from neutron-He^4 scattering data, we used the proton scattering data because it is far more complete. As a check, we used our potentials and the above approximation to calculate neutron-He^4 phase shifts and found good agreement with those deduced from experiment [9]).

3. Discussion of Results

Using the wave functions described above, the integral M was evaluated as a function of k_t and ϕ. Converting to the variables P_Λ and θ, we found that the angular correlation as a function of θ is given by the function shown in fig. 3, aside from some small corrections due to the availability of the $l = 1$ channel for free Λ^0 decay (see below). The pronounced preference for angles less than 50° ($\cos\theta > 0.65$) is the kinematic result of the strong enhancement of transitions to final states with $E_t \approx 2$ MeV (see appendix, eq. (A3)). The sharp fall of the function shown in fig. 3, as θ increases from zero, is due to the fact that this resonance enhancement is occurring in a proton-He^4 $J = \frac{3}{2}$ state. (If the enhancement had been due to a resonance in a $J = \frac{1}{2}$ state, the angular distribution function would not vary much in the region $0.7 \leqq \cos\theta \leqq 1$.) The characteristic $J = \frac{3}{2}$ state angular correlation between $\mathbf{k}_t$ and $\mathbf{k}$ allows the full enhancement to be evident only when $\cos\theta$ is close to unity ($\cos\phi = \pm 1$).

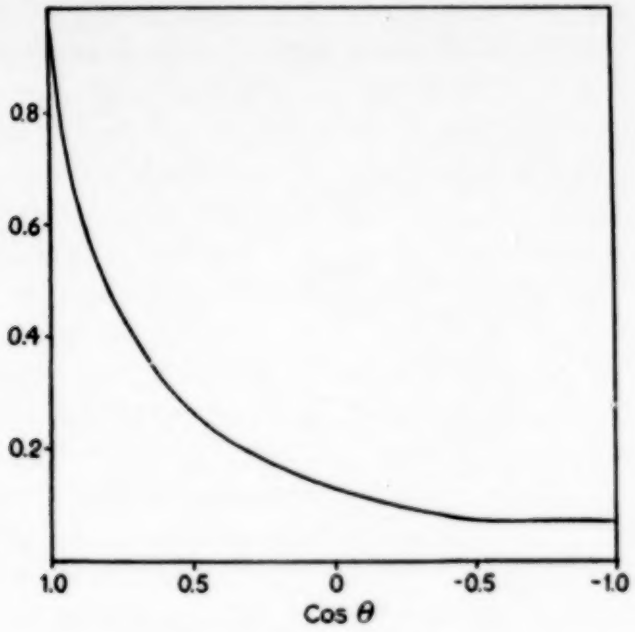

Fig. 3. Angular distribution function $\frac{1}{(2\pi)^2}\sum_{\text{spins}}\int_0^{P_{\Lambda\max.}}|M(P_\Lambda,\cos\theta)|^2\,qP_\Lambda^2\,\mathrm{d}P_\Lambda$.

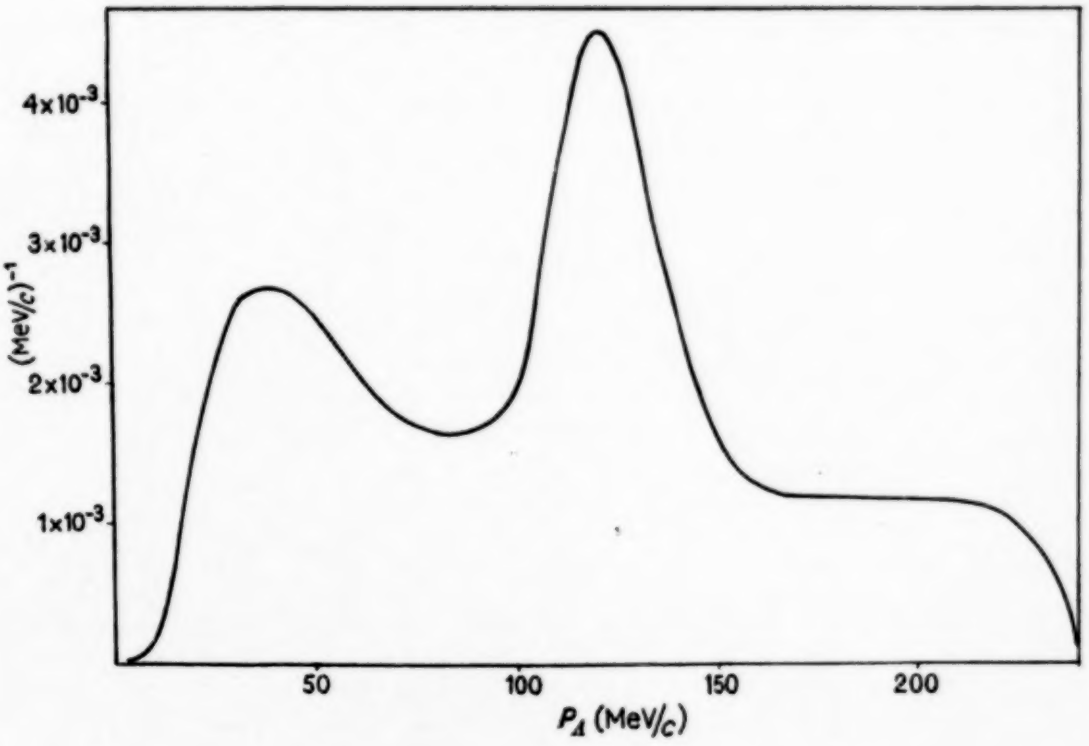

Fig. 4. The P_Λ distribution function $\frac{1}{(2\pi)^2}\sum_{\text{spins}}\int_{-1}^{1}|M(P_\Lambda,\cos\theta)|^2\,qP_\Lambda^2\,\mathrm{d}(\cos\theta)$ (maxima occur at $P_\Lambda = 41$ and 120 MeV/c).

The P_Λ distribution shown in fig. 4 shows clearly the dominant effect of the $P_{\frac{3}{2}}$ resonance. The pronounced maximum at $P_\Lambda = 120$ MeV/c arises because events for which $E_t = 1.8$ MeV and $\cos\phi = 1$ are very strongly favoured (see fig. 6). If the phase space factor were not included in this distribution function, another strong maximum would be evident near $P_\Lambda = 20$ MeV/c corresponding to events for which $E_t = 1.8$ MeV and $\cos\phi = -1$. The structure in the curve shown in fig. 4 is characteristic of a $J = \frac{3}{2}$ resonance enhancement. If the resonance had occurred in a $J = \frac{1}{2}$ state, all events for which $40 < P_\Lambda < 130$ MeV/c would be more nearly equally favoured.

The transition probabilities corresponding to fig. 3 and to fig. 4 for $P_\Lambda < 165$ MeV/c are considerably suppressed by the strong nuclear s-state interaction. That such suppression will take place is indicated by the negative values of the experimental $S_{\frac{1}{2}}$ phase shifts. We interpreted these as indicating an attractive interaction strong enough to bind (see sec. 2). As a result, the s-wave part of the low energy continuum wave functions ψ_t are nearly orthogonal to ψ_Λ since these radial $S_{\frac{1}{2}}$ wave functions must have a node inside the nuclear surface. Therefore, strong cancellation occurs in the term in M which corresponds to transitions to $S_{\frac{1}{2}}$ proton-He^4 final states. The smallness of this term is not a very model-dependent effect since it would also be small (though probably not as small) if the nuclear interaction in the $S_{\frac{1}{2}}$ state had been represented by a repulsive potential. A more detailed discussion of the model dependence of our calculations is given below.

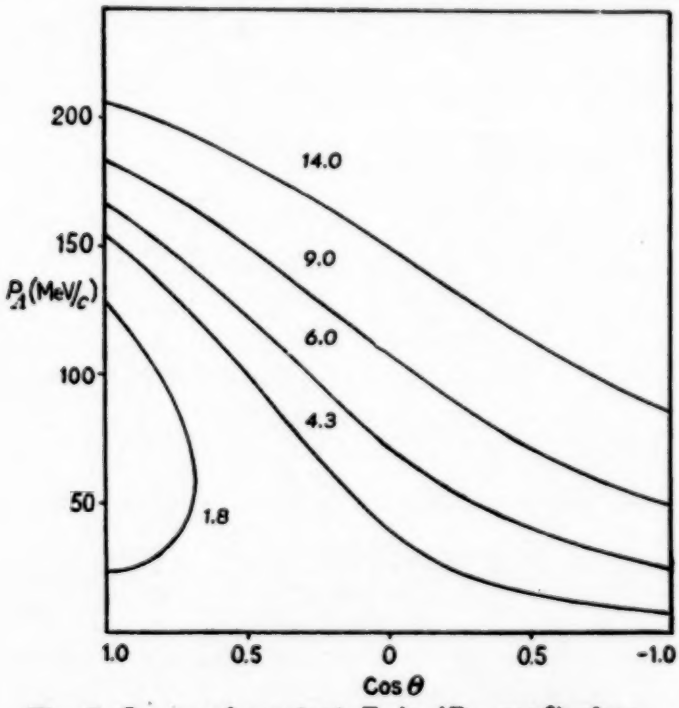

Fig. 5. Curves of constant E_t in (P_Λ, $\cos\theta$) plane. The numbers give the values of E_t in MeV.

For a more detailed understanding of the distributions shown in figs. 3 and 4, one must look at the surface $|M|^2$ over the $(P_\Lambda, \cos\theta)$ plane. The curves of constant E_t in the $(P_\Lambda, \cos\theta)$ plane are shown in fig. 5. The surface $|M(P_\Lambda, \cos\theta)|^2$ has a very steep high ridge located above the curve $E_t = 1.8$ MeV. Here the contribution to $|M|^2$ from the $P_{\frac{1}{2}}$ partial wave in ψ_t dominates completely. An idea of the steepness of the ridge can be obtained from a glance at fig. 6. The large P_Λ peak in fig. 6 indicates the behaviour of $|M|^2$

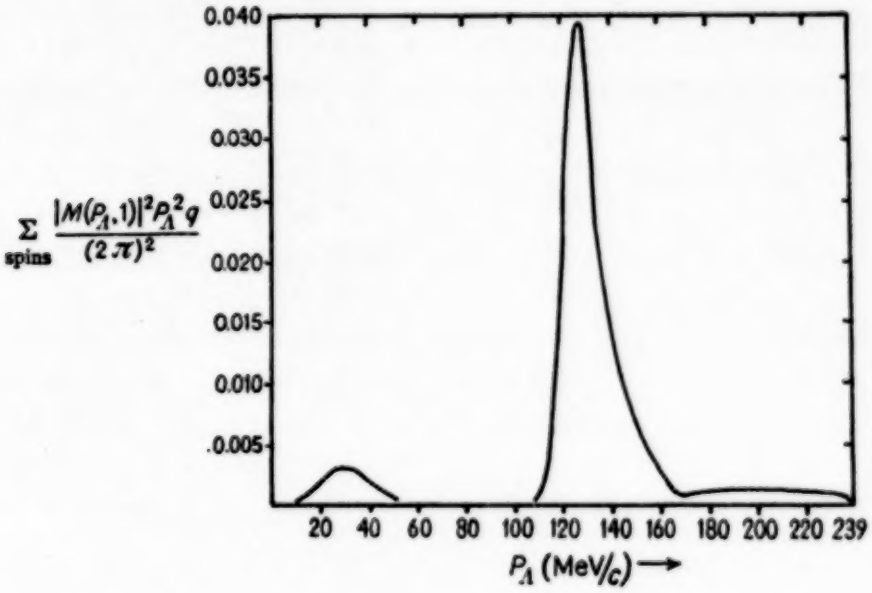

Fig. 6. The P_Λ distribution for events with $\cos\theta = 1$, i.e., $\frac{1}{(2\pi)^2} \sum_{\text{spins}} |M(P_\Lambda, 1)|^2 q P_\Lambda^2$.

in the resonance region (the phase space factor has almost wiped out the lower peak). At $E_t = 0$, $|M|^2 = 0$ because of the Coulomb repulsion †. It remains very small until E_t is very near the resonance energy because the proton-He^4 final states are suppressed by the strong cancellation mentioned above. When $E_t > 1.8$ MeV, $|M|^2$ falls less steeply because Coulomb effects are becoming less important and because the $P_{\frac{1}{2}}$ resonance is beginning to enhance the transition probability. The $P_{\frac{1}{2}}$ resonance enhancement ceases when $E_t = 4$ MeV. The enhancement due to the $P_{\frac{1}{2}}$ resonance is largest when E_t is between 3 and 4 MeV and ceases altogether at 8 MeV. For $E_t > 8$ MeV, the $P_{\frac{1}{2}}$ contribution to $|M|^2$ falls off quite rapidly because the first radial node in the $P_{\frac{1}{2}}$ part of ψ_t moves in close to the nuclear surface and

† Our method of taking the Coulomb repulsion into account also gives $|M|^2$ for the decay ${}_\Lambda He^5 \to \pi^0 + n + He^4$. This function differs significantly from that discussed in the text only for $E_t < 5$ MeV. The difference is primarily that the ridge due to the $P_{\frac{1}{2}}$ resonance is higher and occurs at a lower E_t value. The neutron-He^4 $P_{\frac{1}{2}}$ resonance (see ref. [3])) occurs at 1.15 MeV. As a result there is an even more pronounced preference for small angles in the $\cos\theta$ distribution and the two peaks in the P_Λ distribution are more sharply defined and lie closer together, the maximum of the higher P_Λ peak lies at $P_\Lambda \approx 105$ MeV/c.

strong cancellation takes place in the corresponding term in M. The similar cancellation that takes place in the $S_{\frac{1}{2}}$ transition amplitude becomes complete between 5 and 6 MeV, and as E_t rises from 6 to 14 MeV the magnitude of the $S_{\frac{1}{2}}$ transition amplitude rises steeply. Therefore, in the region 6 MeV $< E_t <$ < 14 MeV, $|M|^2$ has a rapidly increasing $S_{\frac{1}{2}}$ term and a rapidly decreasing $P_{\frac{1}{2}}$ term. The variation with energy of these contributions is very model dependent. Therefore, our values of $|M|^2$ in this region are not quantitatively reliable. The curves $E_t = 6$ and 14 MeV in fig. 5 show the values of P_A and $\cos\theta$ for which our calculation has this strong model dependence. For $E_t > 14$ MeV, the various contributions $|M|^2$ no longer have rapid variations, Their order of magnitude is dictated by the effect of the centrifugal barrier and the scattering phase shifts. We calculated $|M|^2$ as a function of $\cos\phi$ at only three E_t values greater than 14 MeV. We feel that the results obtained by interpolating between these are reasonable order-of-magnitude estimates.

To show the extent to which figs. 3 and 4 are quantitatively reliable, we shall designate as region I, $0 < E_t < 6$ MeV; region II, $6 < E_t < 14$ MeV; and region III, $E_t > 14$ MeV. Within the framework of the effective range approximation, our calculations in region I can be expected to be model independent. Our calculations in region II are strongly model dependent. As order-of-magnitude estimates, our calculated results in region III are not expected to be model dependent. Table 1 shows the relative contributions

TABLE 1

The percentage contributions to the function shown in fig. 3 from region II ($6 < E_t < 14$ MeV) where our calculation depends sensitively on the model we have chosen for the nuclear interaction and region III ($E_t > 14$ MeV) where our results are reliable only as order-of-magnitude estimates

$\cos\theta$	Contribution from region II (%)	Contribution from region III (%)
1.0	4	3
0.8	5	8
0.6	10	13
0.3	30	28
0.0	36	36
−0.5	38	49
−1.0	43	57

from these regions to the angular distribution function shown in fig. 3. From this table one can see that the predicted values are likely to be quantitatively reliable for $\cos\theta > 0.6$. At larger angles the contribution from the model-dependent region II becomes significant; however, since this contribution never dominates, our results are probably reliable as order of

magnitude estimates at the larger angles. The relative contributions from regions II and III to the P_Λ distribution (fig. 4) vary considerably with P_Λ. Region I accounts for 93 % of the total at the lower maximum, 88 % at the other, and 71 % at the minimum between them. However, for $P_\Lambda > 165$ MeV/c, contributions come only from regions II and III. For this reason, the P_Λ distribution given in fig. 4 was calculated at only two P_Λ values greater than 165 MeV/c. The curve in this region was obtained by interpolating between these two points and taking the vanishing of the phase space factor into account. For $P_\Lambda > 165$ MeV/c, fig. 4 is only valid as an order of magnitude estimate.

The actual transition probability (given by eq. (7)) differs from the functions we have calculated by the factor $(|s|^2+q^2|p|^2)$. To estimate the effect of this factor (remembering q must be taken in units for which its value for the free decay is unity), one can use Dalitz's estimates [6]) of the upper and lower limits for $|p/s|$, namely $0.45 < |p/s| < 1$. If $|p/s| = 1$, multiplication by the factor $(|s|^2+q^2|p|^2)/(|s|^2+|p|^2)$ would reduce the peak at $P_\Lambda = 120$ MeV/c in fig. 4 by 14 %; the corresponding reduction at $P_\Lambda = 200$ MeV/c is 36 %. As is indicated by fig. 6, the resulting correction to the angular distribution function arising from the availability of the $l = 1$ decay channel for free Λ^0 decay is small and certainly not appreciable for forward angles. Therefore, the only significant effect of Λ^0 decay in the $l = 1$ channel is to decrease the number of events with large P_Λ.

4. Pion Interactions

Pion interactions may be expected to produce corrections. That these are not likely to give rise to any qualitative changes can be seen from the following considerations. Consider first the pion-He^4 interaction. Pi-mesic atom level shifts are small, indicating that a strong cancellation takes place in the low energy s-wave interaction of pions with light nuclei. Therefore, the pion-He^4 s-wave interaction cannot be expected to produce any significant corrections; however, their p-wave interaction may produce appreciable effects. These effects are not likely to change our results in any qualitative way because when the pion is in a p-state with respect to the He^4 the proton-He^4 system is mostly in a p-state. Since the pions emitted in ${}_\Lambda He^5$ decay do not have sufficient energy for the pion-nucleon $\frac{3}{2}, \frac{3}{2}$ resonance to be effective, the nuclear $P_{\frac{3}{2}}$ and $P_{\frac{1}{2}}$ resonances will certainly dominate when $E_t < 6$ MeV. When E_t is in the range 6—14 MeV, appreciable effects due to pion-He^4 interaction may arise. However, the main effects we have found are not sensitive to the behaviour of the transition matrix element in this energy range.

As regards the pion-proton interaction, it is convenient to separate it into

two parts: (a) its behaviour at small distances to which the pion-proton wave function $\phi(\mathbf{r})$ at small $\mathbf{r}$ is sensitive, and (b) its behaviour at larger distances which determines the low energy pion-nucleon scattering phase shifts. Part (a) will affect the free and bound Λ^0 decays similarly, yielding factors like $\phi(0)$ and $\nabla\phi(0)$ in the effective coupling constants s and p of eq. (2). As a result, these quantities will vary somewhat with q. However, since the pion-proton kinetic energy is small compared to their interaction energy, they are likely to be slowly varying functions of q. Part (b) will not affect free Λ^0 decays but will affect bound Λ^0 decays. However, the pion-proton scattering phase shifts are not large at the energies with which we are concerned and, therefore, the effect of part (b) cannot be expected to be large. We have made some crude estimates and find that the effect of part (b) of the pion-proton interaction will be to produce some smearing of the peaks shown in fig. 4. Correspondingly, the pronounced forward angle preference may be diminished somewhat but will not be qualitatively changed. Since our predictions for backward angles cannot be more accurate than order-of-magnitude estimates, corrections in this region due to pion interactions are of little consequence. We can see no reason to expect them to change the order of magnitude of our results.

5. Remarks Concerning other Hyperfragment Decays

If our analysis is correct, one would not expect to see a pronounced angular asymmetry favouring small θ in the decay ${}_{\Lambda}H^3 \rightarrow \pi^- + p + D$ since the p-D phase shifts in the low energy region do not show resonant behaviour [10]). However, referring to the compilations of Ajzenberg and Lauritsen [3,11]), one sees that in other hyperfragment decays of this type the proton and residual nucleus can be emitted in resonance (e.g., ${}_{\Lambda}Li^7$ and ${}_{\Lambda}Li^8$). If many-body effects do not significantly reduce the overlap integral M, those decays may be expected to display an angular correlation of the type found here, provided the resonance energies are sufficiently low. If the proton-residual nucleus system has energy less than a certain value (see appendix, eqs. (A2) and (A3)) $\mathbf{q}$ must lie within a cone of half-angle θ_{max} about $\mathbf{P}_{\Lambda}$, and therefore, if the resonance energy is below that value it will only enchance the probability for events with θ less than θ_{max}. The resonance energy must also be low to yield effective enhancement in decays of loosely bound Λ^0's because, as we have seen, in the approximation in which the structure of the residual nucleus is neglected, the wave function of the proton-residual-nucleus system must have its first radial node in the region where ψ_{Λ} falls off rapidly; for light hypernuclei this region is well outside the nuclear surface.

The level structure of Be^7 indicates that there are two low-energy resonan-

ces which can occur in the decay ${}_{\Lambda}\mathrm{Li}^7 \rightarrow \pi^- + \mathrm{p} + \mathrm{Li}^6$ (corresponding to the formation of the $\frac{3}{2}^+$ and $\frac{5}{2}^-$ states of Be^7) [11]). The formation of the $\frac{3}{2}^+$ state of Be^7 is seen as a very broad resonance in proton-Li^6 scattering at energies which are below the proton-Li^6 Coulomb barrier. Its broadness, therefore, indicates the many-body nature of this resonance. The state decays primarily into He^3 and He^4 and by γ-ray transitions to lower levels. Therefore, it is not likely to have an important effect on the process ${}_{\Lambda}\mathrm{Li}^7 \rightarrow \pi^- + \mathrm{p} + \mathrm{Li}^6$. The $\frac{5}{2}^-$ state of Be^7, however, is seen as a sharp maximum in the proton-Li^6 elastic scattering cross-section at about 1.83 MeV [11]). It should be noted that if ${}_{\Lambda}\mathrm{Li}^7$ is a $J = \frac{1}{2}$ state, angular momentum conservation prevents the formation of the $\frac{5}{2}^-$ state of Be^7 when the Λ° decays into the s-wave channel. Therefore, if $|p/s|^2 \ll 1$ this resonance will not play a significant role in the decay of ${}_{\Lambda}\mathrm{Li}^7$'s with total angular momentum equal to $\frac{1}{2}$. For ${}_{\Lambda}\mathrm{Li}^7$'s decaying from a $J = \frac{3}{2}$ state, however, a $\cos\theta$ probability distribution that favours events with $\cos\theta > 0.7$ and a P_Λ distribution that has a maximum in the neighbourhood of 125 MeV/c can be expected if the $\frac{5}{2}^-$ state of Be^7 decays primarily into the elastic scattering channel (i.e., if the elastic scattering provides the main contribution to the absolute proton-Li^6 cross section) and can be treated in terms of a proton-Li^6 two-body interaction. However, the structure of the curves will differ somewhat from fig. 3 and 4 because resonance enhancement arises due to the formation of a $J = \frac{5}{2}$ instead of a $J = \frac{3}{2}$ compound nuclear state. A preliminary investigation indicates that the preference for forward angles will be less strong and that the P_Λ distribution may not have a minimum.

In the decay ${}_{\Lambda}\mathrm{Li}^8 \rightarrow \pi^- + \mathrm{p} + \mathrm{Li}^7$, there are many excited states of Be^8 that can be formed. The behaviour of the proton-Li^7 elastic scattering cross section [3, 11]) shows four pronounced maxima for energies less than 2 MeV. Assuming that all of the corresponding states of Be^8 produce enhancement, we can infer that the angular distribution will show that angles θ less than 49° are favoured (see appendix, eq. (A3)). Little can be said about the shapes of the angular and P_Λ distribution without more detailed consideration of the nature of these resonances. These states can contribute to the P_Λ distribution in the region 30 MeV/c $< P_\Lambda <$ 150 MeV/c.

The authors are grateful to Professor R. E. Peierls for many helpful comments and suggestions and to both Professor Peierls and Professor R. H. Dalitz for suggesting this problem. We wish also to express our gratitude to Mrs. P. Truscott and Mr. J. Stuttard for their help with the computations.

Appendix

In the rest frame of a hyperfragment ${}_{\Lambda}\mathrm{X}^A$, the final state of the decay ${}_{\Lambda}\mathrm{X}^A \rightarrow \pi^- + \mathrm{p} + \mathrm{X}^{A-1}$ may be specified by the vectors $\mathbf{P}_\Lambda$ and $\mathbf{q}$ or $\mathbf{k}_f$ and $\mathbf{k}$, where

$-\mathbf{P}_A$ = momentum of residual nucleus X^{A-1},
$\mathbf{q}$ = relative pion-proton momentum,
$\mathbf{k}_f$ = relative proton-residual nucleus momentum,
$\mathbf{k}$ = pion momentum.

It follows from these definitions and conservation of energy that these vectors are related by the equations

$$\mathbf{P}_A = \mathbf{k}_f + \frac{A-1}{A}\mathbf{k}$$

$$\mathbf{q} = \frac{\mu+A}{A(\mu+1)}\mathbf{k} - \frac{\mu}{\mu+1}\mathbf{k}_f \tag{A1}$$

$$2Q = \frac{\mu+1}{\mu}q^2 + \frac{\mu+A}{(\mu+1)(A-1)}P_A^2 = \frac{A}{A-1}k_f^2 + \frac{\mu+A}{\mu A}k^2,$$

where, in units in which the proton mass is one,

Q = energy release of the decay,
$A-1$ = mass of residual nucleus,
μ = pion mass.

It follows from these relations that when the kinetic energy of the proton-residual-nucleus system E_f satisfies

$$E_f < [\mu(A-1)/(\mu+1)A]Q, \tag{A2}$$

there is a maximum angle $\theta_{\max}$ between $\mathbf{P}_A$ and $\mathbf{q}$ which can occur. It is given by the equation

$$\cos\theta_{\max} = [(1-y)(1-xy)]^{\frac{1}{2}}, \tag{A3}$$

where

$$y = \frac{A(1+\mu)}{\mu(A-1)}\frac{E_f}{Q} \quad \text{and} \quad x = \frac{\mu(A-1)}{\mu+A}.$$

References

1) Levi-Setti, Slater and Telegdi, Proceedings of the Seventh Annual Rochester Conference (Interscience Publishers, 1957)
2) R. H. Dalitz, Proceedings of the Seventh Annual Rochester Conference (Interscience Publishers, 1957)
3) F. Ajzenberg and T. Lauritsen, Revs. Mod. Phys. **27** (1955) 77
4) J. L. Gammel and R. M. Thaler, Phys. Rev. **109** (1958) 2041
5) R. D. Hill, Nuovo Cimento **8** (1958) 459
6) R. H. Dalitz, Phys. Rev. **112** (1958) 605
7) Sack, Biedenharn and Breit, Phys. Rev. **93** (1954) 321
8) R. Hofstadter, Revs. Mod. Phys. **28** (1956) 214
9) E. van der Spuy, Nuclear Physics **1** (1956) 381
10) R. S. Christian and J. L. Gammel, Phys. Rev. **91** (1953) 100
11) F. Ajzenberg and T. Lauritsen, Energy Levels of Light Nuclei (VI), Nuclear Physics **11** (1959) 1

8.B *Nuclear Physics* **11** (1959) 569—573; © *North-Holland Publishing Co., Amsterdam*

Not to be reproduced by photoprint or microfilm without written permission from the publisher

ON THE ELECTRON-MUON MASS DIFFERENCE

I. SAAVEDRA

Department of Theoretical Physics, University of Manchester †

Received 19 February 1959

Abstract: On the basis of a previously developed formalism it is shown that a hypothetical (uncharged) boson isoscalar would remove the electron-muon mass degeneracy.

1. Introduction

In a recent paper [1]) we have proposed a modification of the isospace-formalism developed in ref. [2,3,4]), in an attempt to incorporate leptons into the scheme in a more natural and unique way. Weak leptonic interactions were described by using two-component spinors in M-space. Up to this point, no assumptions on the bare masses of leptons had been introduced. However, if we define electromagnetic interactions as those conserving j_3^+, j_3^- and m_3 (in the nomenclature of ref. [1])) a [4]-description of charged leptons is unavoidable. On giving it, we ignored the electron-muon mass difference and defined the four-spinor

$$\Psi \equiv \begin{pmatrix} \mu^+ \\ \mu^- \\ e^+ \\ e^- \end{pmatrix} \tag{1}$$

This definition implies the assumption that electrons and muons have the same bare mass. Consequently, the observed mass difference must be understood purely as a self-mass effect. If the formalism is self-consistent, we would expect, therefore, the prediction of an interaction able to select between muons and electrons, being effective only for the former.

But the search for such an interaction seems to be unsuccessful. Just one of the most attractive features of our scheme is that *leptons cannot take part in strong interactions with the rest of the known particles* ††, if these are defined as fully invariant in [4]-space and only Yukawa-type interactions are considered. It also turns out that intermediate interactions (i.e. interactions less symmetric than the strong ones — see, for example, ref. [3])) cannot be constructed either.

† On leave of absence from Laboratorio de Fisica Nuclear, Universidad de Chile, Santiago.

†† In this connection it is perhaps interesting to point out that the π-meson, introduced in isospace as an antisymmetric self-dual tensor, provides an interaction that picks out the muon components of Ψ, but which must be rejected because it violates conservation of electric charge.

However, some other possibilities still remain open, namely, those furnished by the hypothetical particles that can be included in the scheme. The purpose of this note is to show that one of these (as yet unobserved) new particles does provide the required interaction. This is the boson isoscalar corresponding to the D_{00} representation of the [4]-rotation group. Some of the properties of this particle — the existence of which has been suggested, for instance, by Schwinger [5]) (and called by him σ-particle) — as well as some of its interactions are reviewed.

2. New Particles and Muon Self-Mass

As is well-known, any successful attempt at classifying elementary particles (excluding leptons) is based on the fact that strong interactions can be described with two unrelated quantum numbers, e.g. the isobaric spin and the strangeness. The formalism we are dealing with uses the further fact that irreducible representations of the [4]-rotation group can also be labelled with two independent quantum numbers. *For baryons and mesons* the electric charge is defined by

$$q = j_3^+ + j_3^-, \tag{2}$$

and the restriction is made that it can only take the values $q = 0, \pm 1$. Then, the only integer (single-valued) representations of the rotation group that come into consideration are D_{00}, $D_{\frac{1}{2}\frac{1}{2}}$, D_{10} and D_{01}, and the particles can be classified as shown in table 1.

TABLE 1

Baryons		Mesons	
Particle	Representation	Particle	Representation
Λ^0	D_{00}	—	D_{00}
N, Ξ	$D_{\frac{1}{2}\frac{1}{2}}$	K, $\bar{\mathrm{K}}$	$D_{\frac{1}{2}\frac{1}{2}}$
Σ	D_{10}	π	D_{10}
—	D_{01}	—	D_{01}

When definition (2) is generalized [1]) for leptons as

$$q = j_3^+ + j_3^- + \tfrac{1}{2}n, \tag{2'}$$

n being the neutrino charge, leptons are attributed half-integer (double-valued) representations of the rotation group †. In particular, charged leptons are associated with the representation $D_{\frac{1}{2}0} + D_{0\frac{1}{2}}$.

Table 1 shows that three representations seem not to be realized in nature. These are a baryon triplet D_{01}, a boson triplet D_{01} and a boson singlet D_{00}.

† In this sense, the formalism splits the family of fermions, providing a distinction between baryons and leptons.

We want to consider them in connection with an interaction effective only for the muon-components of the four-spinor Ψ.

If strong interactions are considered to be only of the Yukawa-type, the baryon corresponding to the representation D_{01} must obviously be excluded. The double-strange boson corresponding to D_{01} is described in isospace by an anti-selfdual tensor, $\omega_{\mu\nu}$, say. The corresponding strong interaction is then (omitting the space-time factors)

$$\frac{1}{i} G\Psi^*\Gamma_\mu\Gamma_\nu\Psi\omega_{\mu\nu}, \qquad (\mu, \nu = 1, \ldots, 4) \tag{3}$$

where the Γ_μ are 4×4 Dirac matrices in isospace, and $\omega_{\mu\nu}$ is given, for instance, by

$$\omega_{\mu\nu} = \begin{cases} \omega_{12} = -\omega_{34} = \omega_0 \\ \omega_{23} = -\omega_{14} = \frac{1}{\sqrt{2}}(-\omega^+ - \omega^-) \\ \omega_{31} = -\omega_{24} = \frac{1}{i\sqrt{2}}(\omega^+ - \omega^-). \end{cases}$$

Writing (3) explicitly, it turns out that this interaction violates electric charge conservation and thus must be rejected, even though it succeeds in selecting two components of Ψ. Finally, it is easy to show that the isoscalar of D_{00} provides the desired interaction.

To prove this, let us recall first that the [4]-isospace we are considering is *Euclidean*. From this follows that $\Psi^*\Psi$ *is a scalar* (i.e. no Γ_4 factor is required). Remembering next that *only rotations* are allowed in the formalism, it is seen that $\Psi^*\Gamma_5\Psi$ *is also a scalar*. If the isoscalar is denoted by σ_0, the corresponding interactions are, in an obvious notation,

$$\begin{aligned} L_S &= G_S\Psi^*(I\times\gamma_4)\Psi\sigma_0 \\ &= G_S(\overline{\mu^+}\mu^+ + \overline{\mu^-}\mu^- + \overline{e^+}e^+ + \overline{e^-}e)\sigma_0, \end{aligned} \tag{4}$$

and

$$\begin{aligned} L_P &= G_P\Psi^* I\times\gamma_4\Gamma_5\Psi\sigma_0 \\ &= G_P(-\overline{\mu^+}\mu^+ - \overline{\mu^-}\mu^- + \overline{e^+}e^+ + \overline{e^-}e^-)\sigma_0. \end{aligned} \tag{5}$$

Here the representation

$$\Gamma_j = \begin{pmatrix} 0 & -i\sigma_j \\ i\sigma_j & 0 \end{pmatrix}, \qquad \Gamma_4 = \begin{pmatrix} 0 & -\underline{1} \\ -\underline{1} & 0 \end{pmatrix}, \qquad \Gamma_5 = \begin{pmatrix} -\underline{1} & 0 \\ 0 & +\underline{1} \end{pmatrix}, \tag{6}$$

has been used, I being the 4×4 unit matrix. The general interaction will then be of the form

$$L = \tfrac{1}{2}(L_S \pm L_P). \tag{7}$$

In expression (7) the factor $\frac{1}{2}$ is introduced for convenience and the $\pm$ sign simply emphasizes the fact that the positions of muons and electrons in the spinor are arbitrary, because Ψ is defined with respect to electromagnetic interactions, which do not distinguish between both particles.

Moreover, the Lagrangians L_S and L_P describe the same interactions,

between the same particles, and with the same symmetries in isospace. The strength of these interactions cannot depend on the fact of coming either from L_S or from L_P. Therefore, G_S must be equal to G_P, up to a sign † which is already arbitrary, as remarked above. Putting $G_S = G_P = G$, it is easily seen that the interaction (7) is effective only for two components of the four-spinor Ψ, *these two components being, therefore, the particle we have called muon (positive and negative)*. Keeping definition (1), this interaction is then written

$$\tfrac{1}{2}G\Psi^* I \times \gamma_4 (I - \Gamma_5)\Psi\sigma_0, \tag{8}$$

or, explicitly,

$$G(\overline{\mu^+}\mu^+ + \overline{\mu^-}\mu^-)\sigma_0, \tag{9}$$

if σ_0 is considered to be a scalar in space-time.

Finally, we remark that if uncharged leptons are introduced in [4]-space by the spinor (for notation see ref. [1]))

$$\Psi_0 \equiv \begin{pmatrix} \nu_L \\ \nu_L{}^c \\ \nu_R{}^c \\ \nu_R \end{pmatrix},$$

an interaction like (8) would not produce a $\nu_L - \nu_R$ mass difference. This follows from the definitions $\nu_L = a\nu$, $\nu_L{}^c = \bar{a}\nu^c$, $\nu_R = \bar{a}\nu$, $\nu_R{}^c = a\nu^c$, which make the interaction

$$\tfrac{1}{2}G\Psi_0^* I \times \gamma_4 (I - \Gamma_5)\Psi_0\sigma_0$$

vanish identically††. As in the case of Ψ, it is easily shown that neutrinos would not interact strongly with the rest of the particles either. Thus, the introduction of Ψ_0 would not contradict any experimental data and, on the other hand, would enable us to develop the whole formalism given in ref. [1]) starting from considerations in the [4]-isospace. This latter procedure was considered unnecessary in our previous work.

We proceed now to investigate the possible interactions of σ_0 with the rest of the particles. It turns out that it can interact strongly with the known strongly-interacting particles, the corresponding interactions (in the notation of ref. [1])) being:

$$(N, \Xi, \sigma_0): \quad G_1 \overline{B}_\alpha B_\alpha \sigma_0 = G_1(\bar{p}p + \bar{n}n + \overline{\Xi^-}\Xi^- + \overline{\Xi^0}\Xi^0)\sigma_0, \tag{10}$$

$$(\Sigma, \sigma_0): \quad G_2 \overline{\Sigma}_{\alpha\beta} \Sigma_{\alpha\beta} \sigma_0 = 4G_2(\overline{\Sigma^0}\Sigma^0 + \overline{\Sigma^+}\Sigma^+ + \overline{\Sigma^-}\Sigma^-)\sigma_0, \tag{11}$$

$$(\Lambda^0, \sigma_0): \quad G_3 \overline{\Lambda^0}\Lambda^0 \sigma_0. \tag{12}$$

† Even if G_S is assumed to be different from G_P, the fact that the interactions L_S and L_P are both of the same symmetry type makes it natural that both should be of the same order of magnitude. Interaction (7) would then be much stronger for the muon components of Ψ than for the electron ones (the corresponding squares of the coupling constants would be $(G_S + G_P)^2$ and $(G_S - G_P)^2$, respectively), which is all that we need.

†† This result is independent of the space-time properties of σ_0, as long as this is spinless. However, it would not follow, if, for instance, σ_0 were a vector in space-time.

Since the interactions have the same degree of symmetry, we may expect the different coupling constants in (10), (11) and (12) to be of the same order of magnitude, but not necessarily equal to each other. These interactions would give rise to some self-mass contributions to the baryon spectra. They would not, however, give any contribution tending to remove the nucleon-cascade particle mass degeneracy.

To summarize, the σ_0 particle would be a scalar or pseudoscalar in space-time and a scalar in isospace, with zero isobaric spin, zero strangeness and therefore no electric charge. It would interact strongly with all known baryons, and with only two components of the lepton four-spinor Ψ, thus providing a way to understand the electron-muon mass difference. (In this respect, it may be remarked that the form of the interaction (8) is not *ad hoc*, not arbitrarily defined, but, on the contrary, it follows as a natural consequence of the formalism.) Finally, if the σ_0 particle were sufficiently massive it would decay very quickly into pions (or photons), which would explain the fact that it has never been observed †.

Recently some theoretical work has been done regarding the possible existence of this particle. For instance, it has been shown [6]) that a *scalar* particle with a mass of about three nucleon-masses would give rise to the muon self-mass with a reasonable value of the $\mu-\sigma_0$ coupling constant and in a way compatible with the observed muon magnetic moment. The σ_0-meson interactions would also be compatible with the experimental data on muon-nucleon scattering, anomalous magnetic moment of the proton and pion production in high-energy processes. In the latter cases the existence of the particle would tend to bring the theoretical values closer to the experimental ones.

It is a pleasure to thank Professor L. Rosenfeld and Professor B. Flowers for helpful comments; I also thank Dr. P. Roman for valuable discussions about this problem. This work was performed during the tenure of a British Council Scholarship.

† The interactions (10), (11) and (12) show that the decay of σ_0 into a pair of leptons would be forbidden if the principle that weak interactions are to be constructed with charged-uncharged fermion bilinears holds.

References

1) I. Saavedra, Nuclear Physics **10** (1959) 6
2) A. Salam and J. C. Polkinghorne, Nuovo Cimento **2** (1955) 685
3) J. C. Polkinghorne, Nuovo Cimento **6** (1957) 864
4) B. d'Espagnat, J. Prentki and A. Salam, Nuclear Physics **5** (1958) 447
5) J. Schwinger, Ann. Physics **2** (1957) 407
6) W. S. Cowland, Nuclear Physics **8** (1958) 397;
I. R. Gatland, Nuclear Physics **9** (1958/59) 267;
S. N. Gupta, Phys. Rev. **111** (1958) 1436, 1698

2.E *Nuclear Physics* **11** (1959) 574—583; © *North-Holland Publishing Co., Amsterdam*
Not to be reproduced by photoprint or microfilm without written permission from the publisher

FOCUSING OF PARTICLES IN THE OPTICAL MODEL

IAN E. McCARTHY †
School of Physics, University of Minnesota, Minneapolis, Minnesota

Received 9 March 1959

Abstract: The behaviour of the quantal flux of neutrons in a typical optical model potential is examined as the energy is increased from 5 MeV to 30 MeV. At the higher energies the behaviour can be described quite well by geometrical optics using the classical trajectories of the neutrons. The classical focus is reproduced quantally both in its general shape and its behaviour with varying energy and potentials. There are also standing wave effects near the far edge of the nucleus which cannot be understood classically. The relative probability of reactions occurring in different angular regions and in different radial regions is estimated by integrating the divergence of the flux over these regions.

1. Introduction

Although the optical model has so far only been used quantitatively to describe elastic scattering and reaction cross sections which involve a knowledge of the wave functions at infinity, it is widely believed that it also describes the motion of particles in the nucleus. Elastic scattering calculations are incapable of giving an unambiguous description of the potential, but there are some general properties of particles in a potential which hold for a wide range of potentials. The quantal flux and its divergence give a complete description of entrance channel phenomena and it is interesting to examine their behaviour in some typical potentials.

In previous publications [1, 2]) the quantal flux of particles in the optical model has been discussed and compared with the flux calculated in a classical approximation. It was noticed that there was a region of very concentrated flux in the far side (i.e. the shadow side) of the nucleus which corresponded roughly to a focus. In the part of the nucleus where the classical trajectories do not intersect, it was found that for energies of the order of 40 MeV the classical flux vector and its divergence, which can be derived from the classical trajectories, was quite similar to the corresponding quantal quantities. In this paper it is proposed to discuss the far side of the nucleus in more detail and, in particular, to examine the properties of the quantal focus.

Assuming that nuclear reactions are initiated by a two-body collision [3]) it is reasonable from the classical point of view to say that the probability of

† Present address: Department of Physics, University of California, Los Angeles 24, California.

a collision occurring at a point is proportional to the divergence of the flux at the point. This neglects coherent effects between outgoing waves arising from different points in the nucleus. The relative importance of different parts of the nucleus from the point of view of reactions will be discussed for 30 MeV neutrons in a reasonable potential for strontium.

The quantal flux vector $\mathbf{S}(\mathbf{x})$ is given by

$$\mathbf{S}(\mathbf{x}) = \frac{\hbar}{2im}[\bar{\psi}(\mathbf{x})\nabla\psi(\mathbf{x}) - \psi(\mathbf{x})\nabla\bar{\psi}(\mathbf{x})]. \tag{1}$$

The wave function ψ is normalized to unit incident flux. The classical trajectory is calculated in an equivalent real potential V', which is constructed to make the wave number k at the point $\mathbf{x}$ equal to the one obtained from the Schrödinger equation for a plane wave in a constant complex potential V_c+iW_c (V_c and W_c are the values of the real and imaginary parts of the optical potential at $\mathbf{x}$):

$$V' = -\tfrac{1}{2}\{[(E-V_c)^2+W_c^2]^{\frac{1}{2}}-E-V_c\}, \tag{2}$$

where E is the incident energy.

The optical model potential is $(V+iW)f(r)$, where

$$f(r) = 1/\{1+\exp[(r-R)/a]\}. \tag{3}$$

The polar coordinates of $\mathbf{x}$ are r, θ and ϕ; the azimuth ϕ does not enter the calculation since the flux is axially symmetric about the incident direction ($\theta = 0$).

In section 2 we shall examine the behaviour of the focus in a fixed potential as the energy is increased, and its behaviour for fixed energy and different values of V and W. The behaviour is qualitatively the same as would be expected classically. In section 3 the focusing effects will be examined in more detail and compared with the classical effects. In section 4 the divergence of the flux will be integrated over different volumes in the nucleus in order to investigate the relative probability of collisions occurring in these volumes.

2. Variation of the Focus with Energy and Potential

Let us first consider the behaviour of the flux pattern as the energy is increased. Most of the interesting features will be contained in a knowledge of the magnitude of the flux vector along the nuclear diameter parallel to the incident direction. This quantity is plotted in fig. 1 for incident neutron energies of 5, 10, 15, 20, 30 MeV and for the potential defined by $V = -45$ MeV, $W = -8$ MeV, $R = 5.7\times10^{-13}$ cm, $a = 0.5\times10^{-13}$ cm for strontium 88. This will be called potential I.

It is interesting to notice the transition from the low energy limit to the energy range where the classical flux is a good approximation. In the low

energy limit, only the s-wave flux is present. This is spherically symmetric and so should build up to a peak at the centre of the nucleus. This can be easily seen by considering the wave functions for a complex square well. As the energy is increased, the peak appears to move toward the far side of the nucleus and to decrease in size. In the near side of the nucleus at the lower energies there are violent fluctuations in the magnitude of the flux which are obviously wave effects and in which it is difficult to observe any regular trend, except that their wave-length shortens with increasing energy.

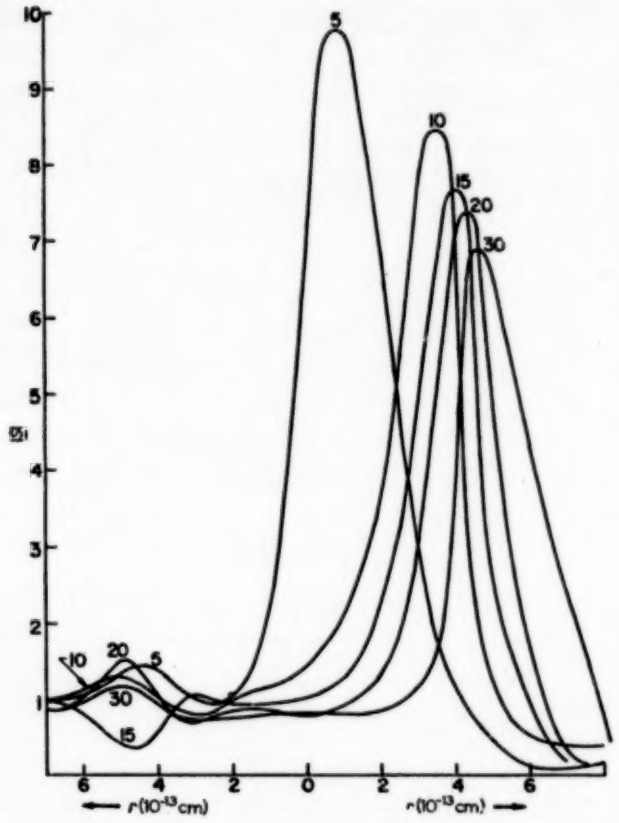

Fig. 1. The magnitude of the flux on the nuclear axis for particles incident from left to right. Potential I is used, and the curves are labelled according to the incident neutron energy in MeV.

At 30 MeV these fluctuations have become less violent and the behaviour is more like what we would expect classically, that is a falling off of flux towards the centre and a large increase on the far side due to focusing of the particles in the potential.

It will be noticed that the width of the peak (the length of the focus) decreases with increasing energy up to 20 MeV. At 30 MeV it has increased and we begin to see an elongated focus as we would expect from spherical aberration in the classical sence. There is no doubt that, in the low energy limit, the focus is most easily understood as a wave effect due to constructive interference of the waves reflected from the nuclear surface. In some of the

potentials examined the reflected wave is actually stronger than the incident wave at some points so that the flux has zeros and reverses in direction. In potential I, the imaginary potential is rather too strong to allow violent fluctuations, but if W is reduced to -2 MeV, there are two zeros on the near side of the centre for 0.5 MeV neutrons. As the energy is increased, the fluctuations move back, but in some potentials, even for wave numbers k corresponding to energies of 60 MeV or more, $\mathbf{S}$ has zeros on the axis between the focus and the far edge of the nucleus, in any case $|\mathbf{S}|$ fluctuates strongly

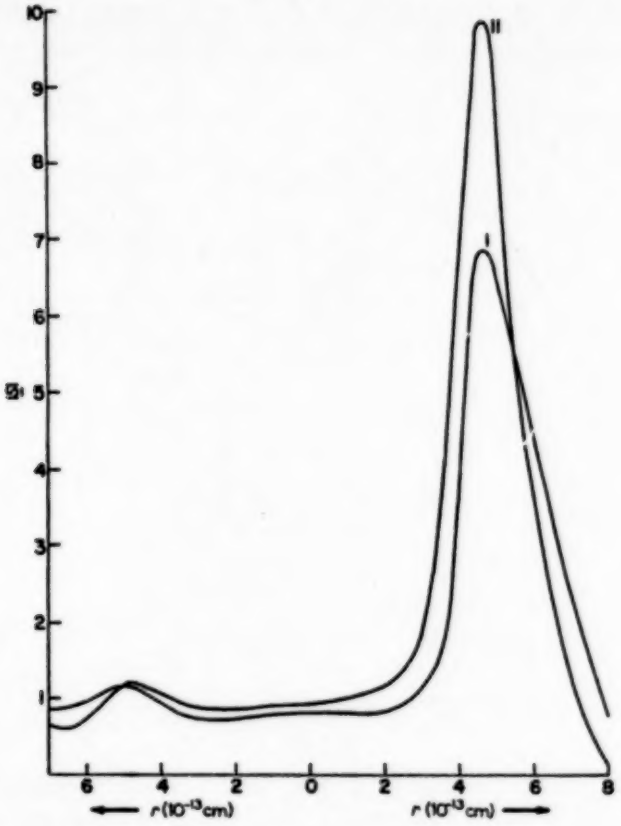

Fig. 2. The magnitude of the flux on the nuclear axis for 30 MeV neutrons in potentials I and II. Particles are incident from left to right.

in this region away from the axis. In the next section this region will be examined in more detail, from the point of view of seeing how well the focus can be described by geometrical optics.

It seems from fig. 1 that at 30 MeV the flux pattern can begin to be understood by geometrical optics. In fig. 2 the flux on the axis is plotted for 30 MeV neutrons in potential I and potential II (i.e. the same potential except that $V = -55$ MeV). Classically the stronger potential bends the trajectories more and causes them to focus more strongly. This is also the case quantally. Changing W from -8 MeV to -6 MeV does not move the peak noticeably and causes an almost imperceptible change in its width.

In this section we have seen how, as the wave number increases, there is a gradual transition from the spherically symmetric standing wave pattern of the s-state flux to a pattern that has properties that can be described by geometrical optics. In the next section we shall see that some detailed features of the pattern are well reproduced by geometrical optics.

3. Comparison of the Focal Region with Geometrical Optics

Figs. 3 and 4 show the classical trajectories for 30 MeV neutrons in the potentials I and II. A trajectory is drawn for each value of the angular momentum quantum number l. Since the diagram is a section of a three

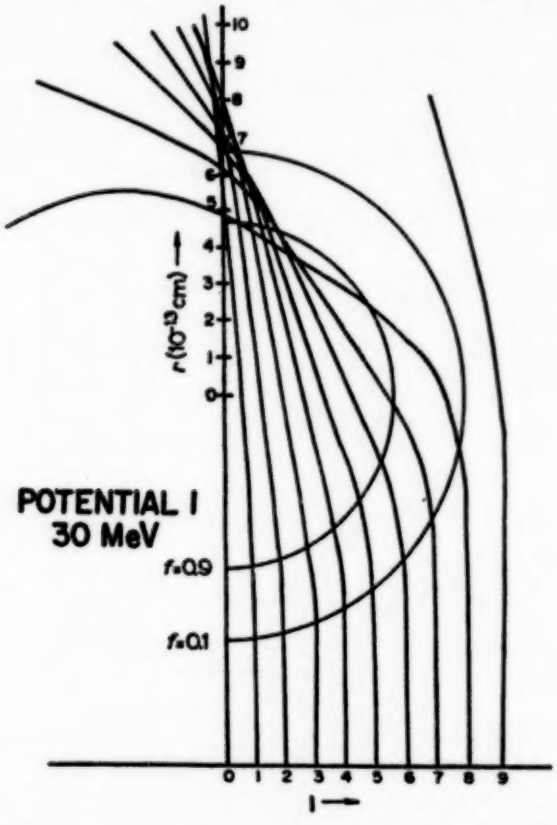

Fig. 3. Classical trajectories of 30 MeV neutrons in potential I †.

dimensional diagram it is clear that more flux comes from higher values of l because the area on which the flux is incident is proportional to l. Consider the flux on the axis. In the cases illustrated the peak in the flux diagram should occur at about $l = 8$. This corresponds to $r \approx 4.8 \times 10^{-13}$ cm in both cases, which agrees very well with the peaks in fig. 2. In potential I the rays for $l = 7$ and 8 are further apart when they reach the axis, so we should expect the peak for potential I in fig. 2 to be lower than for potential II.

† In figs. 3—7, the circular arcs marked $f = 0.9$ and $f = 0.1$ represent the parts of the nuclear surface where the form factor f is 90 % and 10 %, respectively, of its central value.

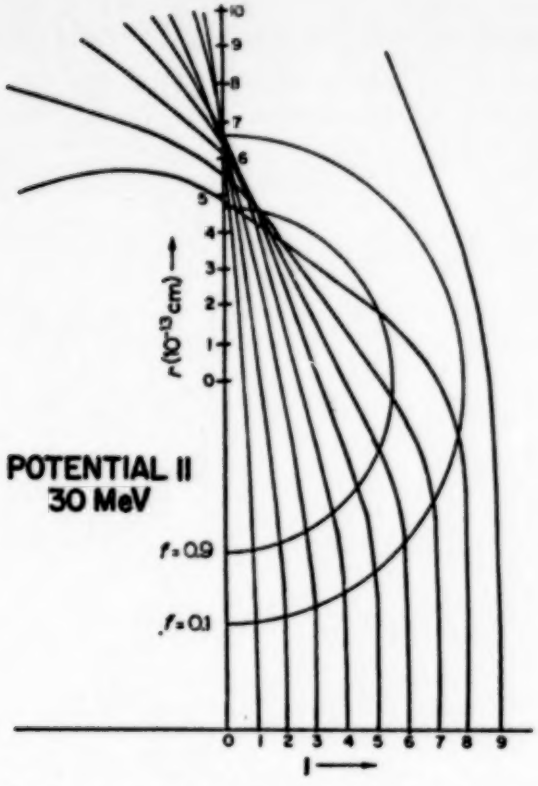

Fig. 4. Classical trajectories of 30 MeV neutrons in potential II.

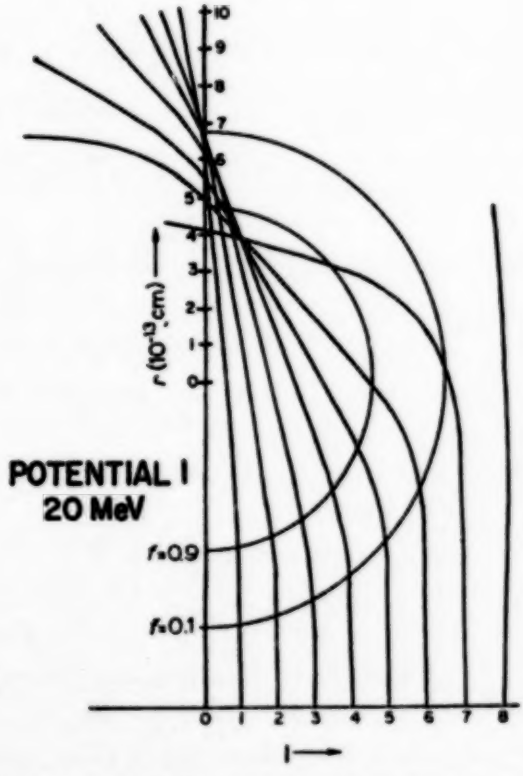

Fig. 5. Classical trajectories of 20 MeV neutrons in potential I.

This is confirmed, and the ratio is clearly of the right order of magnitude, although the accuracy of the classical calculation does not warrant an estimate of the ratio. The widths of the peaks are also seen to be closely estimated by the classical calculation.

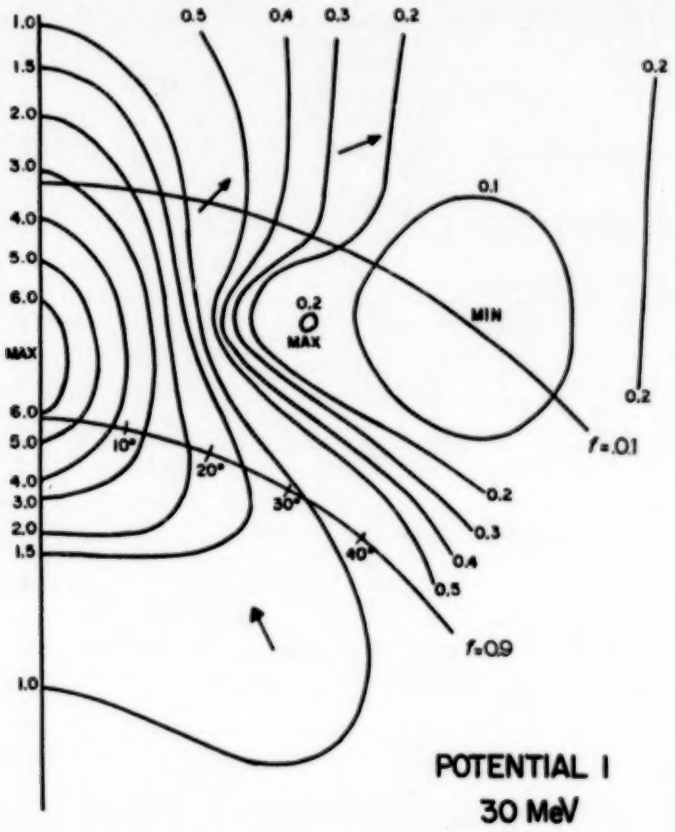

Fig. 6. Contour map of the magnitude of the quantal flux in the far side of the nucleus for 30 MeV neutrons in potential I. The arrows indicate the direction of the flux.

Fig. 5 shows the classical trajectories for 20 MeV neutrons in the potential I. The focus on the axis again seems to be a good estimate of the peak in the flux. In this case there appears to be a strong focusing of the classical rays about 14° off the axis. This represents a ring of focus around the axis. This focus is not reproduced in the quantal calculation which is shown in fig. 7. Similar, but not so strong, effects at 30 MeV are not reproduced in the quantal calculation for potential I illustrated in fig. 6.

The flux diagrams of figs. 6 and 7 can be qualitatively understood from the classical pictures. It must be realised that the quantal picture includes flux from the other side of the nucleus which has crossed the axis. This appears to account for the bulge in the flux peak at the top of the diagram in both figs. 6 and 7. The bulge at the bottom of the diagram is due to flux from the side of the nucleus which is illustrated. In both classical cases there is a region of very small flux density from about 30° to 40°, which is reproduced

in the quantal pictures. However, in figs. 6 and 7 there are small maxima and minima in this region which have no classical analogue and must be purely standing wave effects, caused by reflections from the far edge of the nucleus which are not included in the classical approximation.

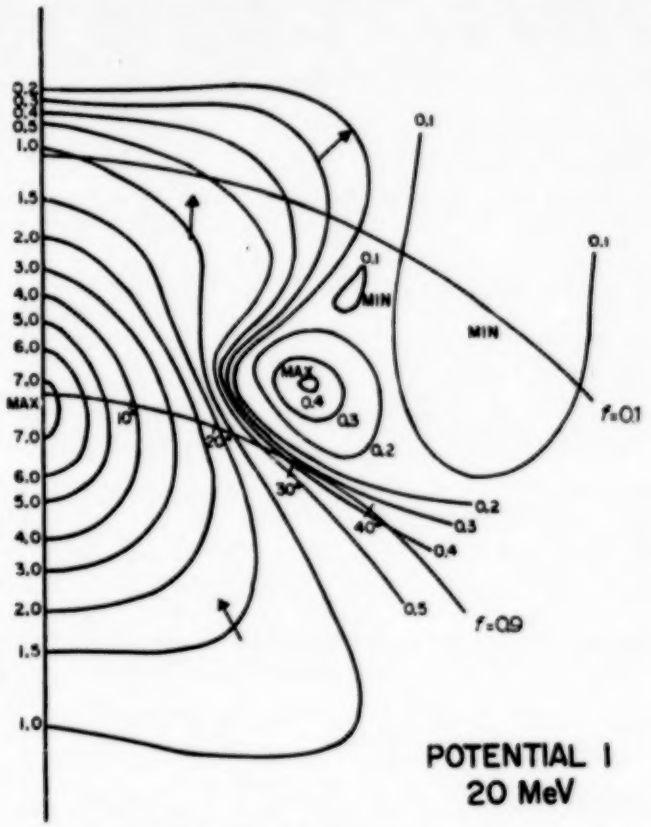

Fig. 7. Contour map of the magnitude of the quantal flux in the far side of the nucleus for 20 MeV neutrons in potential I. The arrows indicate the direction of the flux.

It should be pointed out that there are some classical effects which are not included in the classical calculation [4]). The most important of these is the fact that the gradient of W contributes a term to V'.

4. Divergence of the Flux in Various Nuclear Regions

The divergence of the flux of 30 MeV neutrons in potential I was integrated over different regions of the nucleus. The integral of eq. (4) was evaluated numerically, by integrating first with respect to r and then with respect to θ.

$$\sigma_R = 2\pi \int_0^\infty dr \int_0^\pi d\theta \, r^2 \sin\theta \, \mathrm{div}\, \mathbf{S}(r, \theta) \tag{4}$$

Fig. 8 shows

$$2\pi \int_0^\infty dr \, r^2 \sin\theta \, \mathrm{div}\, \mathbf{S}(r, \theta)$$

plotted against θ, and in fig. 9,

$$2\pi \int_0^{\pi} d\theta \, r^2 \sin\theta \, \mathrm{div}\, \mathbf{S}(r, \theta)$$

is plotted against r.

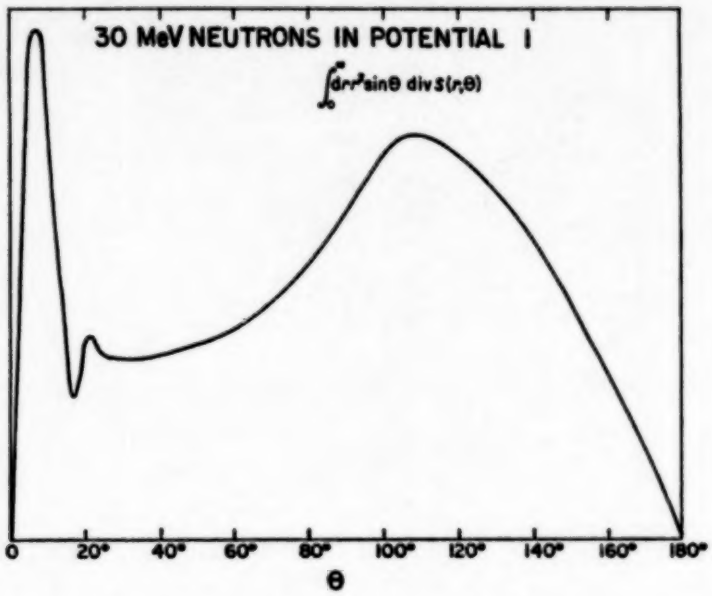

Fig. 8. $\int_0^{\infty} dr \, r^2 \sin\theta \, \mathrm{div}\, \mathbf{S}(r, \theta)$ plotted in arbitrary units against θ for 30 MeV neutrons in potential I.

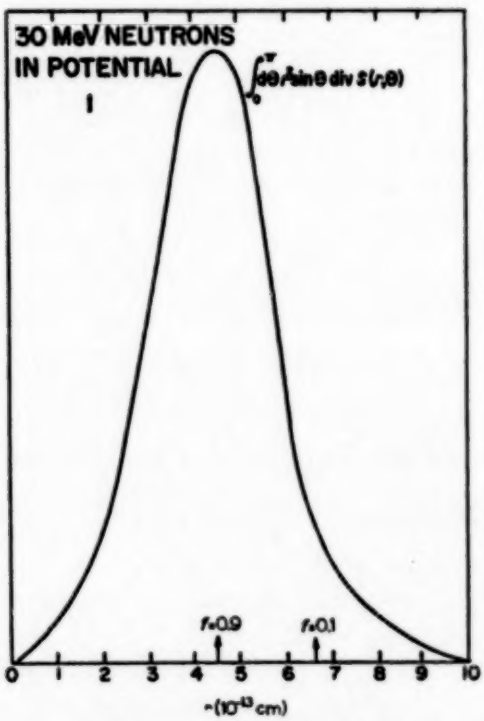

Fig. 9. $\int_0^{\pi} d\theta \, r^2 \sin\theta \, \mathrm{div}\, \mathbf{S}(r, \theta)$ plotted in arbitrary units against r for 30 MeV neutrons in potential I.

The most interesting number obtained from fig. 8 is an estimate of the relative number of two-body collisions occurring in the focal region. About 15 % of the double integral in eq. (4) lies between $\theta = 0°$ and $\theta = 20°$. At higher energies, the divergence peak is not so large, since the focus occurs further out in the nuclear surface where the imaginary potential is small. Hence, it is a reasonable estimate that in medium energy reactions, not more than 20 % of the initial reactions occur in the focus.

From fig. 9 it is possible to estimate the relative number of initial reactions occurring in the surface. In this case 49 % of all initial reactions occur outside the 90 % density radius. In optical models in which the imaginary potential is peaked in the surface [5]), the proportion would be much higher since the divergence is proportional to $W|\psi|^2$. However, it seems that this number is fairly typical of potentials in which both V and W are of the Saxon type.

The author would like to thank Mr. R. Spurrier for computing the classical trajectories and Dr. C. E. Porter for many discussions.

References

1) I. E. McCarthy, Nuclear Physics **10** (1959) 583
2) R. M. Eisberg, I. E. McCarthy and R. A. Spurrier, Nuclear Physics **10** (1959) 571
3) I. E. McCarthy, E. V. Jezak and A. Kromminga, to be published
4) D. R. Yennie, private communication
5) F. Bjorklund and S. Fernbach, Phys. Rev. **109** (1958) 1295

1.E.1:
1.E.3:
3.A

Nuclear Physics 11 (1959) 584—598; © *North-Holland Publishing Co., Amsterdam*
Not to be reproduced by photoprint or microfilm without written permission from the publisher

ANGULAR CORRELATION MEASUREMENTS ON Cs^{133} AND THE MAGNETIC MOMENT OF THE 81 keV-LEVEL

E. BODENSTEDT, H. J. KÖRNER and E. MATTHIAS
Physikalisches Staatsinstitut Hamburg

Received 25 February 1959

Abstract: The directional correlation of the 355 keV—81 keV γ—γ-cascade has been measured as

$$W(\theta) = 1 + (0.042 \pm 0.005)\ P_2(\cos\theta) - (0.004 \pm 0.007)\ P_4(\cos\theta).$$

The determination of the anisotropy as a function of the time delay between the two gamma rays showed no measurable perturbations by internal fields.

The directional correlation of the 276 keV—160 keV γ—γ-cascade is found as

$$W(\theta) = 1 - (0.442 \pm 0.009)\ P_2(\cos\theta) - (0.040 \pm 0.012)\ P_4(\cos\theta).$$

The angular correlation data are in agreement with the proposed spin and parity assignments for the 81 keV-level and the 436 keV-level and yield $\frac{1}{2}+$ for the 160 keV-level as the most probable value. A reinvestigation of the half life of the 81 keV-level confirmed the known value. The result is

$$T_{\frac{1}{2}} = (6.31 \pm 0.05) \times 10^{-9} \text{ sec}.$$

Upper limits for the half lifes of the 160 keV-level and the 436 keV-level are

$$T_{\frac{1}{2}}(160 \text{ keV}) \leqq 5 \times 10^{-10} \text{ sec and } T_{\frac{1}{2}}(436 \text{ keV}) \leqq 1.5 \times 10^{-9} \text{ sec}.$$

The gyromagnetic ratio of the 81 keV-level has been obtained by two different methods: a) The rotation and attenuation of the directional correlation pattern of the 355 keV-81 keV γ—γ-cascade is observed in a constant external magnetic field. b) The anisotropy of the same directional correlation is measured as a function of the external magnetic field. The result is

$$g = +1.23 \pm 0.12,$$

which yields a magnetic moment

$$\mu = 3.1 \pm 0.3 \quad \text{nuclear magnetons}.$$

A lower limit for the gyromagnetic ratio of the 160 keV-level can be given:

$$g \geqq +0.25.$$

This result has been obtained by observing the rotation of the 276 keV—160 keV directional correlation in an external magnetic field of 24 200 gauss. This field yields a rotation

$$\omega_L \cdot \tau = +1.20° \pm 0.35°$$

(ω_L = Larmor frequency, τ = mean life of the 160 keV-level).

1. Introduction

The decay of 7.2 y Ba^{133} has been investigated by many authors [1, 2, 3, 4]). In addition to the intense gamma rays of 355 keV, 302 keV and 81 keV,

weak transitions of 436 keV, 383 keV, 276 keV, 223 keV, 160 keV and 53 keV have been reported [3,4]). Fig. 1 shows the pulse height spectrum of Ba^{133} obtained with a $1\frac{1}{2}'' \times 1''$ NaI(Tl) crystal. The source was located at a distance of 70 mm from the crystal to avoid summing peaks of the intense gamma lines.

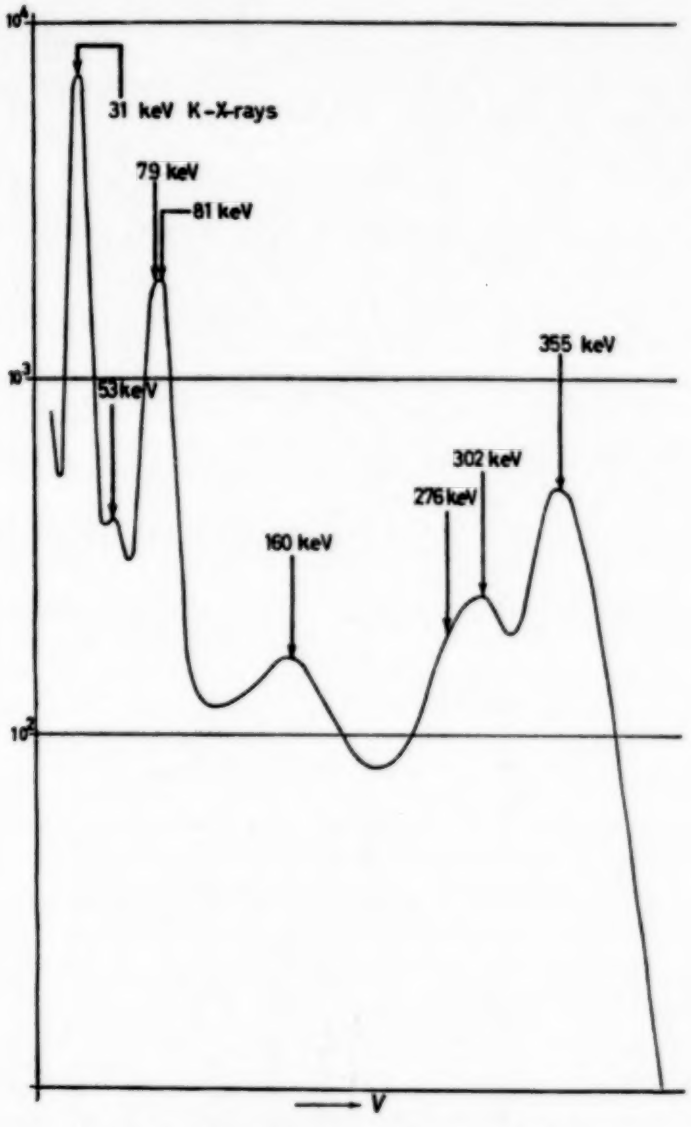

Fig. 1. Pulse height spectrum of Ba^{133}.

The small peak at 53 keV has been attributed to secondary processes by B. Craseman *et al.* [2]). Careful coincidence studies by S. Koicki *et al.* [3]), however, proved the existence of a 53 keV gamma ray. Furthermore, the intense photopeak in the 80 keV region was shown by them to consist of two gamma rays with energies of 79 keV and 81 keV respectively.

The decay scheme of Ba^{133} is shown in fig. 2. It was proposed by R. W. Hayward *et al.* [1]), Gupta *et al.* [4]), and B. Craseman *et al.* [2]) and was con-

firmed by the extensive coincidence measurements of S. Koicki *et al.* [3]). Most of the transitions in Cs^{133} have been found in Coulomb excitation too [5]).

The spin of the ground state of Cs^{133} is $\frac{7}{2}+$. This spin has been measured by the atomic beam method [6]). The spin assignments for the 81 keV-level, the 383 keV-level and the 436 keV-level are $\frac{5}{2}+$, $\frac{3}{2}+$ and $\frac{1}{2}+$ respectively. They have been derived from considerations about conversion coefficients, gamma ray transition probabilities in the decay of Cs^{133}, beta ray transition probabilities, and the directional correlation measurements of the 355 keV-81 keV γ—γ-cascade by M. G. Stewart [7]).

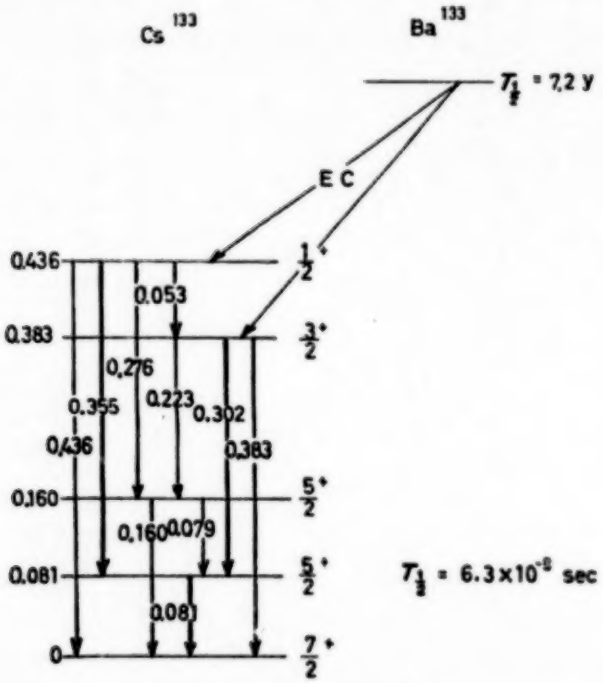

Fig. 2. Decay scheme of Ba^{133}.

These four levels can be explained by the shell model as single particle levels, the ground state being $g_{\frac{7}{2}}$, the 81 keV-level $d_{\frac{5}{2}}$, the 383 keV-level $d_{\frac{3}{2}}$, and the 436 keV-level $s_{\frac{1}{2}}$. [1])

There are different proposals for the spin of the 160 keV-level. B. Craseman *et al.*[2]) give arguments for the assignment $\frac{7}{2}+$, $\frac{9}{2}+$, or $\frac{11}{2}+$. On the other hand S. Koicki *et al.*[3]) propose $\frac{3}{2}+$, but this value still leads to difficulties. Our assignment is $\frac{5}{2}+$ as discussed in section 6.

The half life of 6×10^{-9} sec for the 81 keV-level has been determined by several authors [8, 9, 10]).

2. The Directional Correlation of the 355 keV-81 keV γ—γ-Cascade

As already mentioned this directional correlation has been measured first by M. G. Stewart [7]). The author used a solid source of $BaCl_2$. In his paper he

makes no remarks about perturbations by internal fields. These might exist because the half life of the intermediate state is long and because the source decays by K-capture [11]).

Perturbations by internal fields are minimized in liquid sources [11, 12]). Therefore, we prepared our source as $BaCl_2$ in aqueous solution. The radioactive Ba^{133} was produced in Oakridge by neutron irridation. Unfortunately, this isotope can be delivered only in rather low specific activity. Therefore, angular correlation measurements could be done only by using rather large source volumes. We used a 8 mm long cylindric lucite container of 4 mm diameter. Both gamma rays were detected by NaI(Tl) scintillation crystals

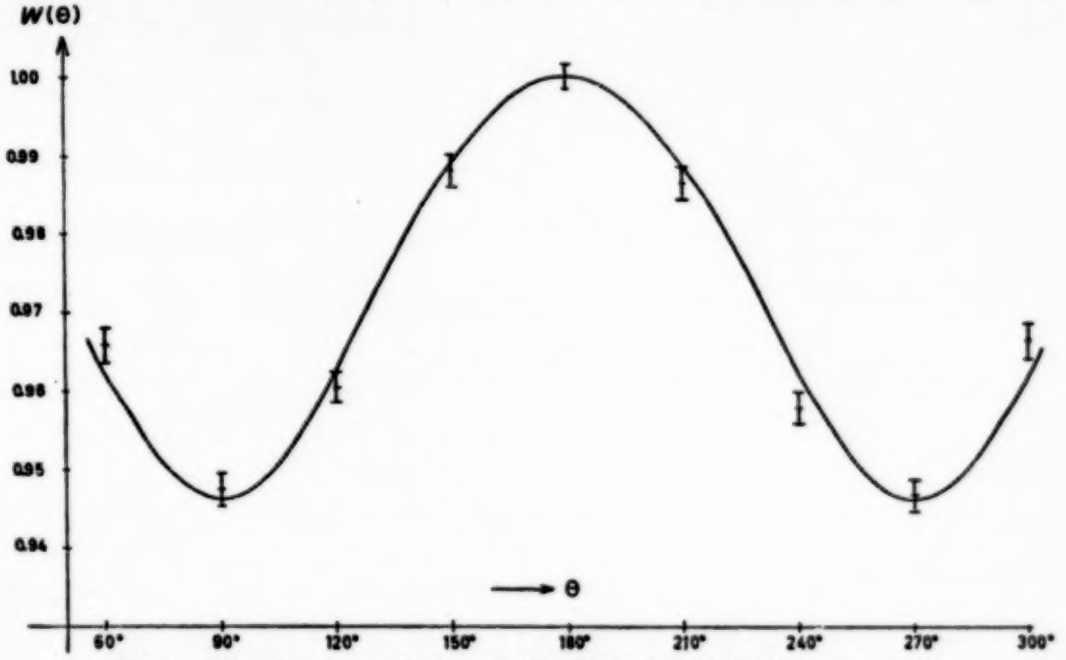

Fig. 3. Directional correlation of the 355 keV—81 keV γ—γ-cascade.

($1\frac{1}{2}$" diameter, 1" long). Our electronic equipment is a fast-slow coincidence spectrometer with two single-channel analyzers. The distance between the source and the crystals was 70 mm. The crystals were surrounded by conical lead shields. The single-channel analyzer for the 355 keV line was set on the right side of the 355 keV photopeak in order to make admixtures of the 302 keV line negligible. The window of the other analyzer was set on the top of the 79 keV—81 keV photopeak. Thus contributions of other cascades were excluded. The position of the channels was controlled continuously during the measurement. The data were accumulated in 50 runs. Each run included 10 minutes measurements of the coincidence counting rates at 10 different angles. The result is shown in fig. 3. It contains a correction for selfabsorption of the two gamma rays in the source. It is interesting to note that this correction is angular dependent †. This can be understood in the

† We are indebted to Prof. H. Frauenfelder who pointed out this problem to us.

following way: At small angles there is a large region where both gamma rays traverse only a small part of the source. On the other hand at 180° at least one gamma ray has to cross a large fraction of the source diameter. The result is that the coincidence counting rate at small angles is less attenuated by selfabsorption than at large angles. For a quantitative calculation the absorption coefficients of the two gamma rays in the source have been determined experimentally. Then the integrals which describe the total attenuation of the coincidence counting rate have been evaluated numerically for the different angles.

To investigate whether the angular correlation is attenuated by internal fields we have measured the anisotropy of the angular correlation for various time delays between the two gamma rays. Even with time delays up to four half lifes, no attenuation of the anisotropy has been observed (fig. 4).

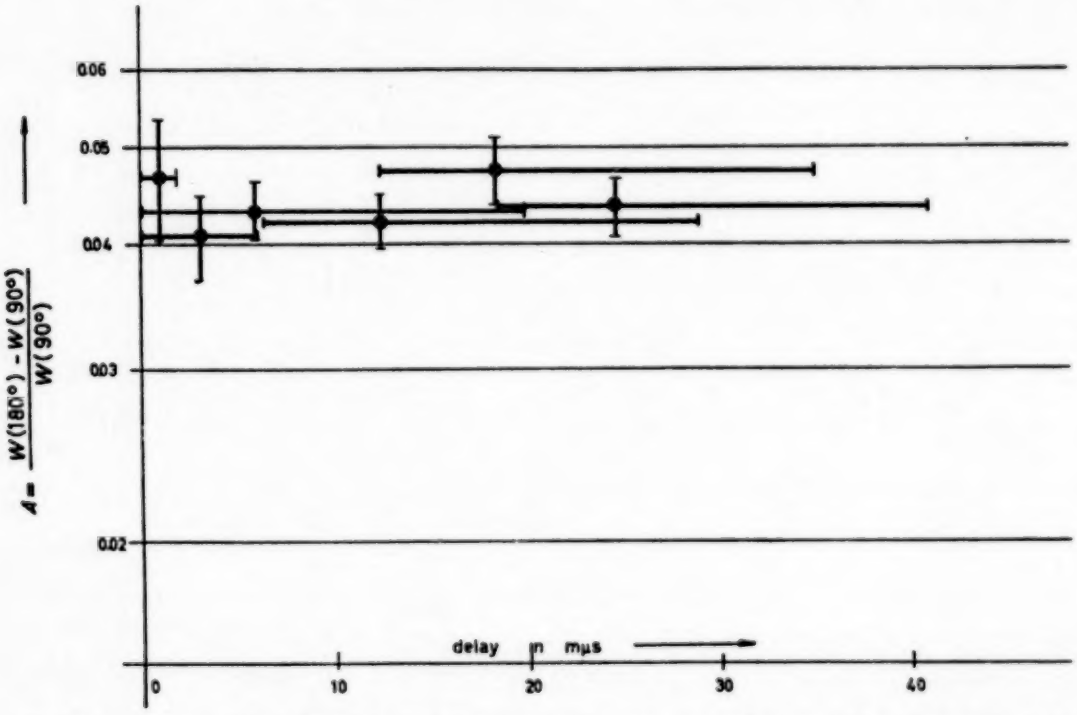

Fig. 4. Measurement of the anisotropy of the 355 keV—81 keV directional correlation as a function of delay.

Therefore no corrections are necessary for perturbations by internal fields.

After correction for the finite solid angles of the detectors we get the result for the angular correlation function of the 355 keV—81 keV cascade:

$$W(\theta) = 1 + (0.042 \pm 0.005)\, P_2(\cos\theta) - (0.004 \pm 0.007)\, P_4(\cos\theta).$$

This function agrees quite well with the measurement of M. G. Stewart [7]).

The coefficient of P_4 is so small that we have not been able to assure its sign. This has the consequence that our result contributes no strong argu-

ment for the spin assignments of the 81 keV- and 355 keV-level. We have shown, however, that we get agreement with the theoretical angular correlation for the proposed spin assignments only if the 81 keV gamma transition is a mixture of M1 with 2.5 % E2 ($\delta = -0.16 \pm 0.01$).

3. The Directional Correlation of the 276 keV—160 keV γ—γ-Cascade

A measurement of the directional correlation of the 276 keV—160 keV γ—γ-cascade is especially interesting because it might settle the question of the spin assignment for the 160 keV-level.

Fortunately, the directional correlation of this cascade can be measured without admixtures of other cascades if the two single-channel analyzers are set on the photopeaks of the two lines. One cannot avoid that gamma rays of

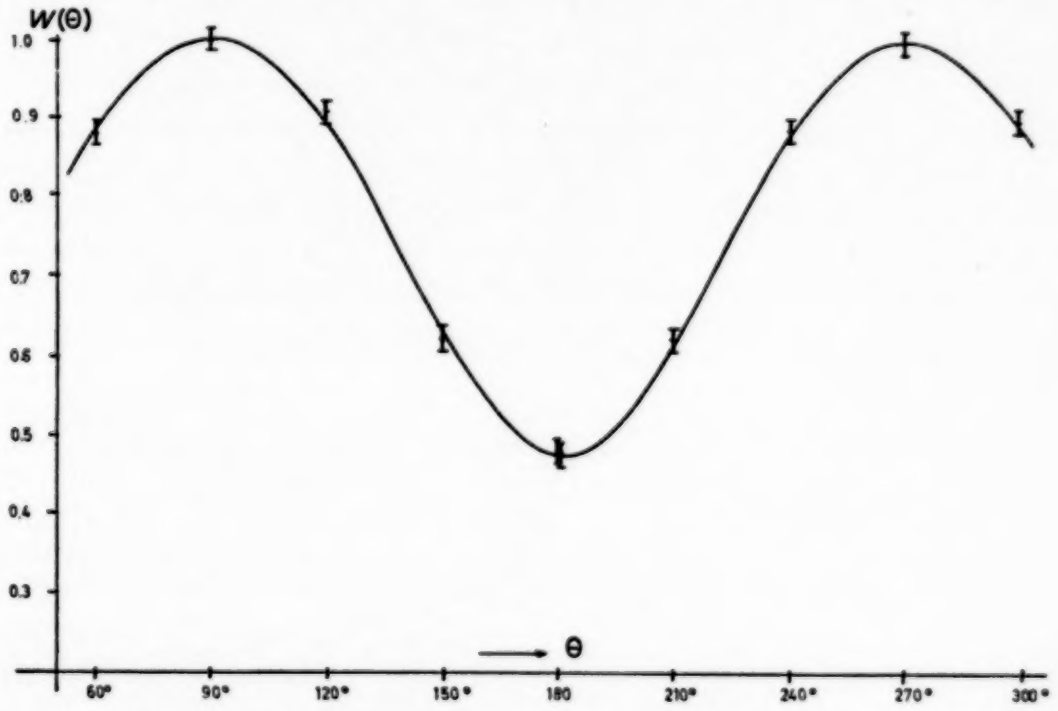

Fig. 5. Directional correlation of the 276 keV—160 keV γ—γ-cascade.

higher energy contribute to the single-channel counting rates by means of their Compton background. On the other hand there is no coincident pair of gamma rays of higher energy in the decay of Ba^{133}. Therefore, the admixtures of higher energy gamma lines in the single-channels only contribute to the chance but not to the true coincidences †.

The right settings of the single-channel analyzers were found by a measurement of the coincidence spectrum for both lines. The distance between

† Contributions of the 81 keV—79 keV summing peak to the 160 keV channel were eliminated by using a tantalum absorber in front of the scintillation crystal.

source and crystals was 70 mm. A solid source of $BaCl_2$ was used because liquid sources of even rather large volumes supply too low counting rates. An attenuation of the directional correlation can be excluded by the following consideration: The 160 keV-level has a shorter half life than the 81 keV-level (section 4) for which we have shown experimentally that no measurable attenuation occurs (section 2). This measurement has been done, however, with a liquid source. On the other hand, the directional correlation pattern of the 355 keV—81 keV cascade obtained by M. G. Stewart [7]) by means of a solid source of $BaCl_2$ agrees with our result (section 2). This shows that even solid sources of this isotope give no observable attenuation.

The result of the directional correlation measurement of the 276 keV—160 keV cascade is shown in fig. 5.

After correction for the solid angles of the detectors we get

$$W(\theta) = 1-(0.442\pm0.009)\ P_2(\cos\theta)-(0.040\pm0.012)\ P_4(\cos\theta).$$

We have investigated which spin assignments for the 160 keV, and 436 keV-levels yield a directional correlation which is in agreement with this result. The spin of the ground state has been assumed to be $\frac{7}{2}$ as determined by the atomic beam resonance method [6]). For the 436 keV-level we tried the values $\frac{1}{2}$ and $\frac{3}{2}$. Larger values can be excluded because the gamma transition to the ground state has a very low intensity. For the intermediate level all values between $\frac{1}{2}$ and $\frac{13}{2}$ have been admitted. Quadrupole admixtures to all dipole

TABLE 1

Attempts to fit the directional correlation result for the 276 keV—160 keV gamma-gamma cascade by different spin assignments for the levels involved

Spin for the 160 keV level	Spin for the 436 keV level	Multipolarity for the 276 keV transition	Multipolarity for the 160 keV transition	Solution	Arguments and remarks
$\frac{1}{2}$	$\frac{1}{2}$	dipole + quadr.	octupole	no	$A_2 = A_4 = 0$
	$\frac{3}{2}$	dipole + quadr.	octupole	no	$A_2 = A_4 = 0$
$\frac{3}{2}$	$\frac{1}{2}$	dipole + quadr.	quadr.	no	$A_4 = 0$
	$\frac{3}{2}$	dipole + quadr.	quadr.	no	$A_4 = 0$
$\frac{5}{2}$	$\frac{1}{2}$	quadr.	dipole + quadr.	yes	mixing parameter $\delta_2 = +0.68$ or $\delta_2 = +2.25$
	$\frac{3}{2}$	dipole + quadr.	dipole + quadr.	no	$A_4 > 0$
$\frac{7}{2}$	$\frac{1}{2}$	octupole	dipole + quadr.	no	$A_2 \gtrless -0.34$
	$\frac{3}{2}$	quadr.	dipole + quadr.	no	$A_4 > 0$
$\frac{9}{2}$	$\frac{1}{2}$	2^4-pole	dipole + quadr.	no	$A_4 > 0$
	$\frac{3}{2}$	octupole	dipole + quadr.	no	$A_4 > 0$
$\frac{11}{2}$	$\frac{1}{2}$	2^5-pole	quadr.	no	$A_2 > 0$
	$\frac{3}{2}$	2^4-pole	quadr.	no	$A_2 > 0$
$\frac{13}{2}$	$\frac{1}{2}$	2^6-pole	octupole	no	$A_2 > 0$
	$\frac{3}{2}$	2^5-pole	octupole	no	$A_2 > 0$

transitions have been taken into account and all transitions of higher multipolarity have been assumed to be pure. With this assumption the only solution is $\frac{5}{2}$ for the 160 keV-level and $\frac{1}{2}$ for the 436 keV-level as shown in table 1.

The 160 keV transition must be a mixture of dipole and quadrupole radiation. There are still two solutions for the mixing parameter which agree with the measured correlation function:

$$\delta = +0.68 \text{ or } +2.25.$$

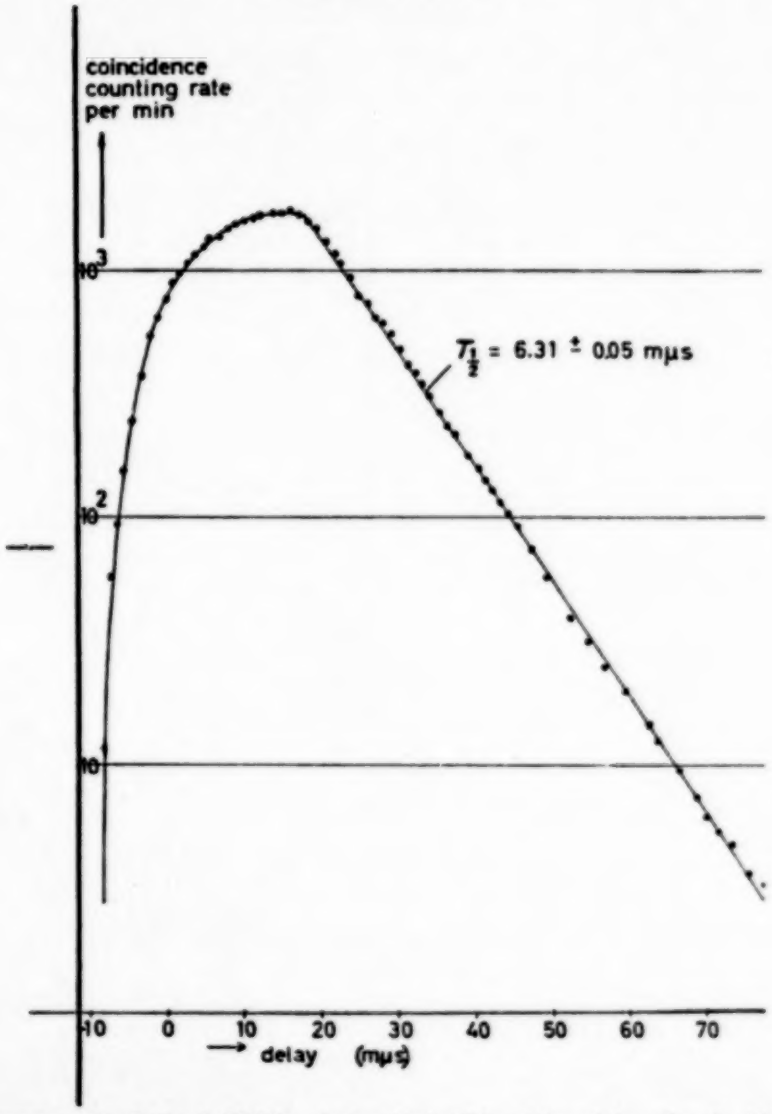

Fig. 6. Measurement of the half life of the 81 keV-level by delayed coincidences between the 355 keV-line and the 81 keV-line.

4. Life Time Measurements on the 81 keV, 160 keV and 436 keV Level

4.1. 81 keV-LEVEL

The half life of the 81 keV-level has been determined by R. L. Graham and R. E. Bell [8]):

$$T_{\frac{1}{2}} = (6.0 \pm 0.4) \times 10^{-9} \text{ sec.}$$

This value has been verified by P. Lehmann *et al.*[9]) and T. Alvaeger *et al.*[10]) who obtain

$T_{\frac{1}{2}} = (6.0 \pm 0.4) \times 10^{-9}$ sec and $T_{\frac{1}{2}} = (6.3 \pm 0.2) \times 10^{-9}$ sec, respectively.

For a determination of the nuclear g-factor a precise knowledge of the half

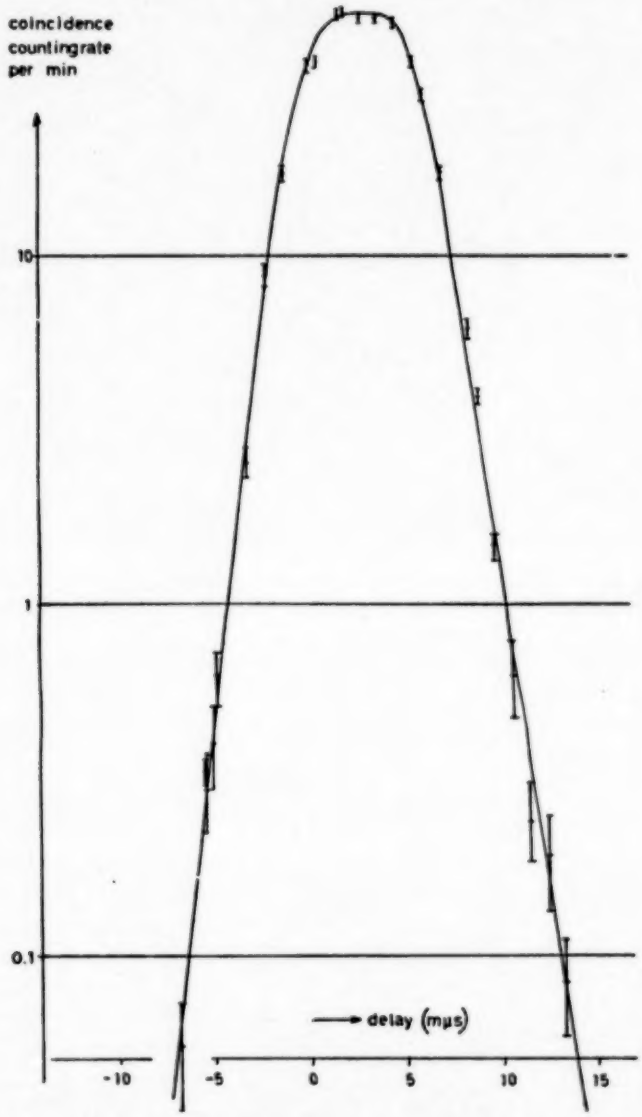

Fig. 7. Investigation of the half life of the 160 keV-level by delayed coincidences between the 276 keV-line and the 160 keV-line.

life is necessary. Therefore we tried to reduce the limits of error. We applied the method of delayed coincidences between the 355 keV and 81 keV gamma rays. The different time delays between the two gamma rays were obtained by using cables of various lengths. The resolving time of the fast coincidence

unit was set to $2\tau = 18.5\times10^{-9}$ sec. The result (fig. 6) is

$$T_{\frac{1}{2}} = (6.31\pm0.05)\times10^{-9}\text{ sec.}$$

4.2. 160 keV-LEVEL

The knowledge of this half life gives an additional argument for the spin assignment of the 160 keV-level. Furthermore, it should be possible to measure the g-factor of this level if the half life is of the order of 10^{-9} sec.

The measurement has been performed by the same method as mentioned above. Difficulties arise from admixtures of gamma rays with higher energy to the single-channel counting rate which increase the chance coincidence rate. Therefore, the activity of the source must be kept very small. For the same reason the resolving time of the fast coincidence unit has been reduced

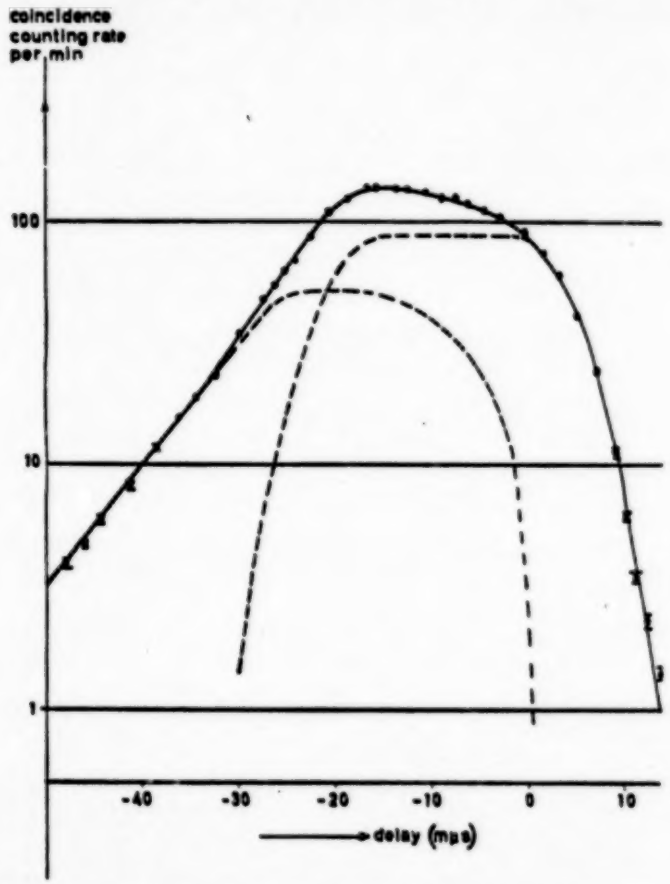

Fig. 8. Investigation of the half life of the 436 keV-level (delayed coincidences between the 31 keV K—X-rays and the 355 keV gamma rays have been measured. The analysis yields a superposition of a 6.3×10^{-9} sec decay with a prompt decay).

to $2\tau = 6.5\times10^{-9}$ sec. The result of the measurement (fig. 7) yields an upper limit for the half life:

$$T_{\frac{1}{2}} \leqq 5\times10^{-10}\text{ sec.}$$

4.3. 436 keV-LEVEL

For the interpretation of the delay experiment described in section 2 it is useful to know the half life of the 436 keV-level. B. Craseman *et al.*[2]) have shown that this half life cannot be much longer than 2 μsec.

This half life can be determined by measuring delayed coincidences between the 31 keV-K-X-rays of Ba^{133} and the 355 keV gamma rays. The deexcitation time of the K-shell is short enough to be neglected.

The result (fig. 8) shows the superposition of a 6.3×10^{-9} sec decay and a prompt decay. 6.3×10^{-9} sec is the half life of the 81 keV-level. This contribution results from the fact that the 81 keV transition is strongly converted and thus detected by its K-X-rays in the low energy channel. The prompt decay must be attributed to the 436 keV-level. Other possible admixtures are negligible.

The analysis delivered an upper limit for the half life of the 436 keV-level:

$$T_{\frac{1}{2}} \leqq 1.5\times10^{-9} \text{ sec.}$$

5. The Magnetic Moments of the 81 keV, and the 160 keV Level

The gyromagnetic ratio of the intermediate level in a gamma-gamma cascade can be determined by measuring the rotation and attenuation of the directional correlation pattern in an external magnetic field [11]).

This method is applicable if the following assumptions are fulfilled:

1) The directional correlation of the gamma-gamma cascade must have a measurable anisotropy.

2) The order of magnitude of the half life of the intermediate level has to be between 10^{-7} sec $\geqq T_{\frac{1}{2}} \geqq 10^{-9}$ sec. The upper limit is set by the ratio of chance to true coincidences. The lower limit is determined by the available magnetic field strength.

3) The results of the measurements are influenced by internal fields, which disturb the directional correlation. Corrections can be made, however, if the magnitude of these perturbations is known. Furthermore, the radioactive isotope should not be paramagnetic; otherwise difficult corrections for the effective magnetic field are necessary.

The magnetic moment of the 81 keV-level of Cs^{133} has been obtained by two different methods:

a) The directional correlation of the 355 keV—81 keV γ—γ-cascade is observed in a constant magnetic field applied perpendicular to the plane of the two counters.

b) The anisotropy of the directional correlation of the same cascade is measured for various magnetic fields.

The experimental arrangement has been described in detail earlier [13]). The distance between the source and the NaI(Tl) crystals was 5 cm. We

used the same liquid source as described in section 2 but with a diameter of 5 mm.

The result of the measurements of method a) is shown in fig. 9. The data contain corrections for the finite source diameter (section 2) but no correc-

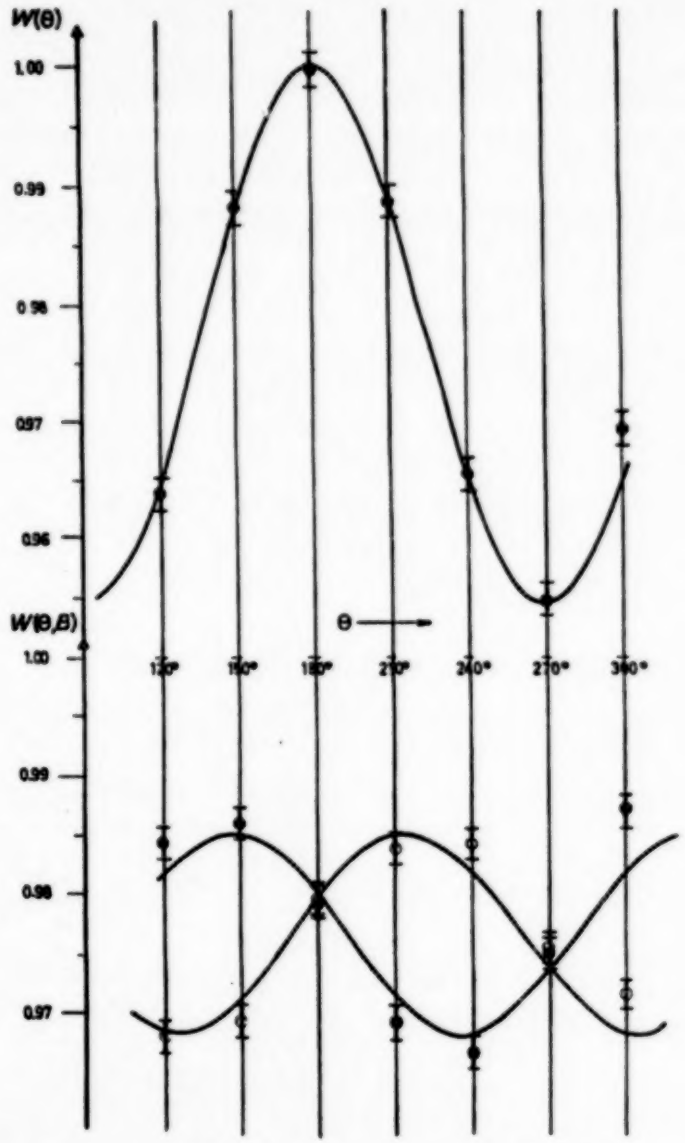

Fig. 9. Measurement of the nuclear g-factor of the 81 keV-level $W(\theta)$ = Directional correlation of the 355 keV—81 keV γ—γ-cascade without magnetic field. $W(\theta, B)$ = Directional correlation of the same cascade in a magnetic field of 22 400 gauss. The data were taken for both field directions. ($\overline{\phi}$ = magnetic field up, $\underline{\phi}$ = magnetic field down.)

tions for the finite solid angle of the counters. There seems to be still a small perturbation at 300°. The counting rates of all three measurements are too large at this angle. This might be explained by Compton scattering from one crystal into the other through the conical lead shields because at

300° the crystals are closest to each other. To investigate this effect one crystal was shielded against the direct radiation by a thick lead absorber. The remaining coincidence counting rate in this arrangement can arise only from scattering effects; but the observed intensity was too small to explain the deviation. On the other hand one has to take into account that the absolute magnitude of the perturbation is only about 0.5 % which is a region where the prevention of systematic errors in directional correlation measurements becomes rather difficult. The nuclear gyromagnetic ratio g has been evaluated by a least square fit which omitted the 300° values.

To assure the result a second determination by method b) has been made (fig. 10). From the result of the measurements by method a) one might

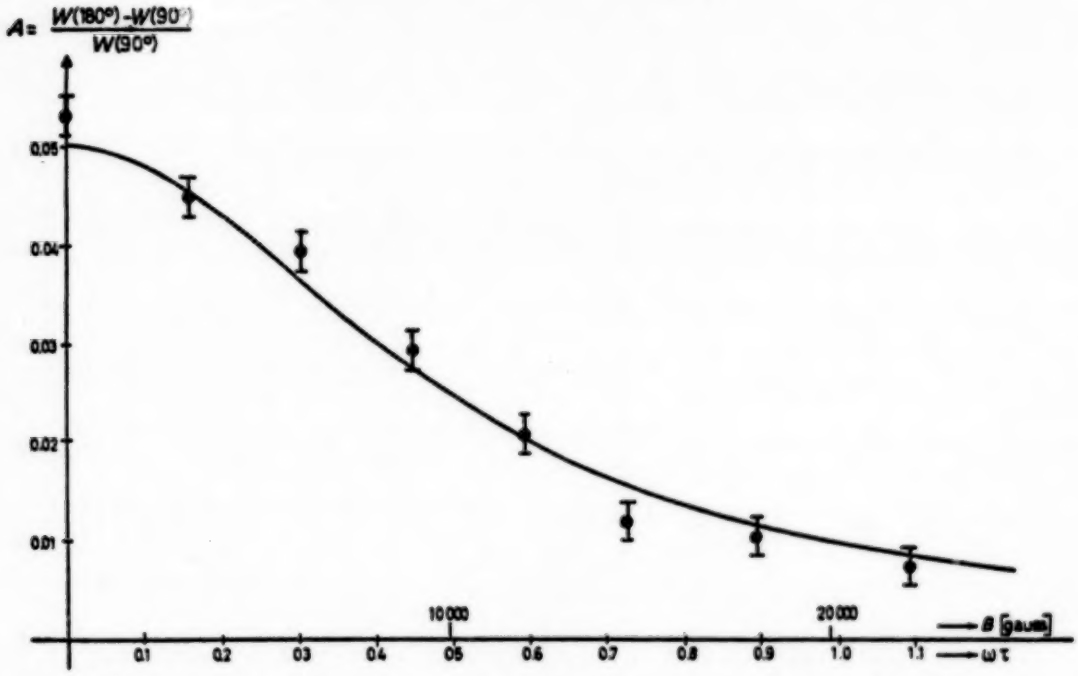

Fig. 10. Measurement of the nuclear g-factor of the 81 keV-level. The anisotropy of the 355 keV—81 keV directional correlation is observed as a function of the applied magnetic field.

expect small perturbations even at 270°. By method b), however, magnetic field independent perturbations can be eliminated by a suitable least square calculation. The results of both measurements agree within their limits of error. The average value is

$$g = +1.23 \pm 0.12.$$

Using the spin assignment $\frac{5}{2}$ for the 81 keV-level one gets a magnetic moment

$$\mu = +3.1 \pm 0.3 \text{ nuclear magnetons.}$$

The 276 keV—160 keV directional correlation has been observed in an

external magetic field of 24 200 gauss. We restricted this measurement on the two angles 135° and 225°. The difference of the coincidence counting rate for both field directions has been determined. We find

$$\omega_L \tau = +0.021 \pm 0.006$$

which corresponds to a rotation of $+1.20° \pm 0.35°$. As we only know an upper limit for the half life of the 160 keV-level we get for the nuclear g-factor

$$g \geqq +0.25.$$

The sign of the g-factor follows from the direction of the rotation.

6. Conclusions

The ground state and the levels at 81 keV, 383 keV and 436 keV have been interpreted as the single particle levels $g_{\frac{7}{2}}$, $d_{\frac{5}{2}}$, $d_{\frac{3}{2}}$ and $s_{\frac{1}{2}}$ according to the shell model [1]). Our angular correlation measurements are in agreement with these spin assignments. The magnetic moment of the 81 keV-level, $\mu = +3.1$ n.m. lies between the two Schmidt-lines but nearer to the upper one, thus confirming the interpretation of the 81 keV-state as a single particle level.

The interpretation of the 160 keV-level seems to be rather difficult. Our angular correlation measurement of the 276 keV—160 keV cascade makes the spin assignment $\frac{5}{2}$ most probable. In this case the 160 keV transition must be a mixture of dipole with quadrupole ($\delta = +0.68$ or $\delta = +2.25$). The following facts favour this assignment:

a) The conversion coefficient identifies the 160 keV radiation as mainly E2. This agrees with the result of our directional correlation measurement favouring even parity for the 160 keV-level and the mixing parameter $\delta = +2.25$.

b) Smaller spin values may be excluded because this level is not fed by a β-transition from Ba^{133} and the β-transition from Xe^{133} is of very small intensity [14]).

c) Spin values larger than $\frac{7}{2}$ are improbable because they would yield a high multipolarity of the 276 keV radiation. This would be inconsistent with the short half life of the 436 keV-level since the intensity of the 276 keV radiation is not negligible small compared with the 355 keV and 53 keV transition.

d) The short half life of the 160 keV-level excludes a higher multipolarity than quadrupole for the 160 keV and 79 keV transitions.

However, there are still some facts which are not well understood:

a) The gamma transition from the 383 keV-level to the 160 keV-level is of much smaller intensity than to the 81 keV-level.

b) The β-transition from the $\frac{3}{2}+$ level of Xe^{133} to the 160 keV-level is of much smaller intensity than to the 81 keV-level.

These difficulties might be solved by assuming a higher spin than $\frac{5}{2}$ for the 160 keV-level. But we would like to reject these solutions because our directional correlation measurement then demands mixtures of higher multipolarities † which are very improbable from theoretical points of view.

The absence of an attenuation of the directional correlation of the 355 keV—81 keV cascade is astonishing because the proceeding K-capture leaves the atomic shell highly excited thus causing strong internal fields. The short half life of the 436 keV-level excludes that the atomic shell de-excites completely before the intermediate state at 81 keV is formed. The explanation is probably the extremely small quadrupole moment of the Cs^{133} nucleus.

The authors wish to thank Prof. W. Jentschke for many helpful discussions and his continuous interest in this work. Mr. E. Gerdau and Miss G. I. v. Wredenhagen assisted in taking the data. The support given by the Bundesministerium für Atomkernergie und Wasserwirtschaft is gratefully acknowledged.

† We have tried a fit for the spins $\frac{7}{2}$ and $\frac{9}{2}$ allowing admixtures also to the gamma transitions of higher multipolarity. We got the following result: No fit is possible for the spin $\frac{7}{2}$, but there are two solutions for $\frac{9}{2}$. Both solutions yield the spin $\frac{9}{2}$ for the 436 keV-level. The mixing parameters for the two solutions are $\delta_1 = -0.135$; $\delta_2 = -2.6$ and $\delta_1 = -0.56$; $\delta_2 = 0.38$. The first solution is favoured with regard to the conversion coefficient of the 160 keV gamma ray.

References

1) R. W. Hayward, D. D. Hoppes and H. Ernst, Phys. Rev. **93** (1954) 916
2) B. Craseman, J. G. Pengra and I. E. Lindstrom, Phys. Rev. **108** (1958) 1500
3) Stevan Koicki, Anka Mijatowic and Jowan Simic, Bull. Inst. Nucl. Sci., Boris Kidrich, Belgrade **8** (1958) 1
4) R. K. Gupta, S. Jha, M. C. Joshi and B. K. Madan, Nuovo Cimento **8** (1958) 48
5) L. W. Fagg, Phys. Rev. **109** (1958) 100
6) J. E. Mack, Revs. of Mod. Phys. **22** (1950) 64
7) M. G. Stewart, Ames Laboratory, Iowa State College Semi-Annual Summary Research Report (January-June 1957)
8) R. L. Graham and R. E. Bell, Can. Journ. of Phys. **31** (1953) 377
9) P. Lehmann and J. Miller, Compt. rend. **240** (1955) 1525
10) T. Alvaeger, B. Johansson and W. Zuk, Arkiv för Fysik **14** (1958) 373
11) H. Frauenfelder, in Beta- and Gamma-Ray Spectroscopy, Ed. K. Siegbahn (North-Holland Publicity Co., Amsterdam, 1955) Ch. XIX (I) § 13
12) A. Abragam and R. V. Pound, Phys. Rev. **92** (1953) 943
13) E. Bodenstedt, E. Matthias und H. J. Körner, Zs. f. Phys. **153** (1959) 423
14) A. H. Snell and F. Pleasonton, Phys. Rev. **111** (1958) 1338

8.B *Nuclear Physics* 11 (1959) 599—603; © *North-Holland Publishing Co., Amsterdam*
Not to be reproduced by photoprint or microfilm without written permission from the publisher

PAIS DOUBLETS AND THE UNIVERSAL FERMI INTERACTION

J. C. POLKINGHORNE
Trinity College, Cambridge, England

Received 25 February 1959

Abstract: A universal Fermi interaction responsible for all weak decays is investigated in terms of Pais's doublet representation of baryons. Some understanding may be gained of the apparently anomalous hyperon-leptonic decays and some of the consequences of the $\Delta I = \frac{1}{2}$ rule are simulated. One of the two alternative schemes proposed would lead to a direct decay mode for Ξ particles into nucleons and pions.

1. Introduction

Pais [1]) has discussed a symmetrical form of baryon-meson interactions in which the baryons are described by four doublets †: N_1(nucleon), N_2 and N_3 (composed of combinations of Σ and Λ particles), and N_4 (cascades). There are two separately conserved strangenesses, S_1 and S_2, and this implies selection rules that are not in accord with experiment. Accordingly this symmetrical theory cannot describe the whole of the strong interaction effects, as one might indeed expect from the triplet-singlet mass structure of the Σ—Λ system. However if, as Pais [2, 3]) has suggested may be the case, K^+ and K^0 have opposite parities, the apparent success of conventional charge independence is best understood by supposing that this symmetrical doublet scheme (DS) represents an important element of structure in the strong interactions.

The purpose of this paper is to see if any understanding of weak interactions may be obtained by expressing them in terms of a universal Fermi interaction (UFI) framed in terms of DS. The recent revived success of UFI in explaining weak interaction of non-strange particles makes the suggestion of its extension to strangeness violating interactions attractive [4]). There is a degree of arbitrariness in doing so, but this is reduced in DS by its symmetrical treatment of baryons. In particular a scheme will be constructed that has universal features and which may provide an understanding of the unexpected weakness of hyperon leptonic decays [5]) and simulate some of the more successful predictions of the $\Delta I = \frac{1}{2}$ rule for non-leptonic decays.

It may be objected that a picture so approximate as DS should not be expected to be used to understand *weak* interactions. The philosophy of this approach is the same as that of the $\Delta I = \frac{1}{2}$ rule or other more detailed

† Throughout the paper we use the notation of ref. [1]).

assumptions [6]) about the isobaric nature of weak interaction currents. These latter approaches have utility and meaning even though the much stronger electromagnetic interactions violate isobaric spin conservation. Of course the violations of DS are more violent and important than those of the conventional isobaric scheme and so the predictions of the theory are fraught with greater ambiguity. However, if K^+ and K^0 do have opposite parity, conventional isobaric spin assignments are no longer possible and we are only left with the modified I'-spin defined by DS†. This paper indicates a successor to the $\Delta I = \frac{1}{2}$ rule in that case.

The most significant violations of DS arise from the actual triplet-singlet particle nature of the supposed pair of doublets N_2 and N_3. The ultimate understanding of this seems far off. Some phenomenological account can be taken of it, however. Pais [3]) has pointed out that a mixing parameter could appear in the distribution of Σ^0 and Λ^0 between the neutral members, N_2^0 and N_3^0, of the doublets. It would be nice to get some idea of this parameter from associated production data, but since the DS forbidden process

$$\pi^+ + p \to \Sigma^+ + K^+ \tag{1}$$

has a cross-section comparable with the DS allowed modes near threshold this does not seem to be possible. We shall see that the data on hyperon leptonic decays might indicate something about this parameter.

The strength of the interaction (1) is a warning against supposing that DS allowed interactions will always predominate over those not allowed. The precise circumstances in which this might happen cannot be formulated without solving the strong interaction problem but we shall see that some coherence can be brought into the pattern of weak decays through a UFI framed in terms of DS by supposing that there at least the rule gives a rough indication of strength. This supposition rather resembles those in which the medium strong K-meson interactions are taken not to alter too greatly conclusions reached about the form of weak decays in their absence [8]). Indeed, it should be better because global symmetry [9]) supposes DS to be exact for pion-baryon interactions and DS also takes into account what may be the major factors in the K-meson-baryon interaction.

2. Universal Fermi Interaction

The doublets divide into two groups: N_1 and N_2 with positive and neutral members; N_3 and N_4 with neutral and negative members. If the UFI is thought of as arising from the combinations of two currents (Lorentz space factors are omitted in what follows) it is natural to generalize the nucleon β-decay current into a contribution

$$\bar{N}_1 \tau^+ N_1 + \bar{N}_2 \tau^+ N_2 + \bar{N}_1 \tau^+ N_2 \tag{2}$$

† A different approach to this problem has been made by Takeda and Kato [7]).

from the first group and to add to this the corresponding combination

$$\overline{N}_3\tau^+N_3+\overline{N}_4\tau^+N_4+\overline{N}_3\tau^+N_4 \tag{3}$$

from the second group. Combination of the last members of (2) and (3) with the other baryon currents or with the lepton currents will give strangeness-violating weak decays and the form of these cross term currents has been chosen to give the rule

$$\frac{\Delta S_1}{\Delta Q} = +1. \tag{4}$$

This prevents the coupling with leptons giving the decay

$$\Sigma^+ \to N^0+e^++\nu \tag{5}$$

but does permit the decay

$$\Lambda^0 \to P+e^-+\bar{\nu} \tag{6}$$

with a partial lifetime larger by a factor 10 than the current experimental limit [5]). This is calculated on the basis of a universal coupling constant and the assumption that

$$N_2^0 = (1/\sqrt{2})(\Lambda^0-\Sigma^0). \tag{7}$$

The strange story of pion β-decay makes one hesitant to assume the final existence of a contradiction. If, however, the results on hyperon leptonic decays remain unchanged, it is possible to reconcile them with UFI by abandoning the (certainly not accurate) equation (7). The weakness of the β-decay is then to be interpreted in terms of the mixing parameter as showing that the N_2^0 state is principally Σ^0, and so the N_3^0 state must be principally Λ^0. The β-decay of the Σ^0 would, of course, form an unobservable fraction ($\approx 10^{-12}$) of the fast Σ^0 decays.

The extension of UFI so far considered is certainly not adequate to describe all weak interactions, for it does not cause any S_2-non-conserving decays. Since these decays have strengths comparable to the S_1-non-conserving decays, it is contrary to our philosophy to suppose that they arise solely from the failure of DS. One must therefore add to the currents a cross-term between the two doublet groups such as

$$\overline{N}_1N_3+\overline{N}_2N_4. \tag{8}$$

This satisfies the rule

$$\frac{\Delta S_2}{\Delta Q} = +1 \tag{9}$$

and may be combined with the other baryon currents to give all the observed decays. Rules (4) and (9) together ensure that the cascade cannot decay directly to a nucleon. However, the absence of hyperon leptonic decays means that (8) cannot be coupled to the lepton currents. This introduces an

asymmetry into the couplings. The currents would be supposed to fall into three classes: (i) leptons, (ii) within baryon groups, (iii) cross terms between baryon groups; with couplings between (i) and (ii), and (ii) and (iii) only.

This scheme is inimical to the idea that the exchange of a heavy boson is the medium of UFI. An alternative scheme which is in accord with this latter idea is to take the cross terms as

$$\overline{N}_1 N_4 + \overline{N}_2 N_3. \tag{10}$$

These change both S_1 and S_2 and coupling with the S_1-violating currents gives S_2-violating decays into strongly interacting particles. Such decays into leptons are, however, forbidden and so a completely symmetrical coupling scheme can be constructed. A consequence of this scheme would, however, be that the cascade could decay directly into a nucleon. It would be interesting to know more about the properties of Ξ. It may be that the very small number of known Ξ's [10]) is due to failure to recognize them when they do not have a cascading decay.

Certainly this second scheme seems an otherwise more attractive way of systematizing the weak decays.

3. Decay Rules

The $\Delta I = \frac{1}{2}$ rule provided some insight into features of the weak decays into strongly-interacting particles. If Pais' suggestion about opposite $K^+ - K^0$ parity is correct, conventional isobaric spin has no meaning but DS defines a different I'-spin, conserved by strong interactions, which is $\frac{1}{2}$ for each baryon doublet, 1 for the pions, and 0 for the K-mesons. Some features of the old $\Delta I = \frac{1}{2}$ rule are simulated by the present formulation of UFI. In particular we can explain the long lifetime of K^+.

Its decay takes place through S_2-violating interactions containing such terms as

$$\overline{N}_1 \tau^+ N_2 \cdot \overline{N}_4 N_1. \tag{11}$$

The total effect is to produce a change of I'-spin:

$$|\Delta I'| \leqq 1, \tag{12}$$

a result which is independent of the choice of cross-group couplings. However, the state of two pions into which a charged spinless meson can decay has I'-spin 2 and so (12) forbids this decay of K^+ in the DS approximation. (We note that the K^+ leptonic decays also appear to be unexpectedly weak [11]), as one would expect in terms of the picture presented in this paper.)

In a similar manner the rule (12) produces the same consequences for $K^+_{3\pi}$ decay as those which follow from the conventional $\Delta I = \frac{1}{2}$ rule.

The decay of K^0 takes place through terms such as

$$\bar{N}_1 \tau^+ N_1 \cdot N_2 \tau^- N_1 \tag{13}$$

which gives

$$|\Delta I'| \leqq 2. \tag{14}$$

In this theory there is no simple connection between K^+ and K^0 decays and so no problem arises about fitting the K_1^0 decay branching ratio [12]).

The other most successful prediction of the $\Delta I = \frac{1}{2}$ rule was the branching ratio of Λ decay. This is a more difficult matter to discuss in terms if this theory. However, Okubo, Marshak and Sudarshan [13]) have pointed out that another type of interaction can simulate the $\Delta I = \frac{1}{2}$ result and their arguments can be adopted in similar form in the present theory if the first of the two alternative schemes is chosen.

References

1) A. Pais, Phys. Rev. **110** (1958) 574
2) A. Pais, Phys. Rev. **112** (1958) 624
3) A. Pais, Phys. Rev., to be published
4) R. P. Feynman and M. Gell-Mann, Phys. Rev. **109** (1958) 193
5) Eisler, Plano, Prodell, Samios, Schwartz, Steinberger, Conversi, Franzini, Manelli, Santangelo and Silvestrini, Phys. Rev. **112** (1958) 979
6) S. Okubo, R. E. Marshak, E. C. G. Sudarshan, W. B. Teutsch and S. Weinberg, Phys. Rev. **112** (1958) 665
7) G. Takeda and M. Kato, Progr. Theor. Phys., to be published
8) B. D'Espagnat, J. Prentki and A. Salam, Nuclear Physics **5** (1957) 447
9) M. Gell-Mann, Phys. Rev. **106** (1957) 1296;
   J. Schwinger, Ann. of Phys. **2** (1957) 407
10) cf. J. R. Oppenheimer, Proceedings of CERN Conference on High Energy Nuclear Physics (1958) 288
11) S. Oneda, Nuclear Physics **9** (1959) 426
12) M. Gell-Mann, Nuovo Cimento **5** (1957) 758
13) S. Okubo, R. E. Marshak and E. C. G. Sudarshan, to be published

8.B *Nuclear Physics* **11** (1959) 604—614; © *North-Holland Publishing Co., Amsterdam*
Not to be reproduced by photoprint or microfilm without written permission from the publisher

PARITY NON-CONSERVATION AND THE ALGEBRA OF ELEMENTARY PARTICLES

KATSUHIKO SEKINE
Department of Physics, University of Tokyo

Received 19 February 1959

Abstract: An attempt is made to incorporate the phenomenological expression (1.2) for the observed non-conservation of parity into the property of the algebra of elementary particles, and to reconstruct the theory on the basis of the new algebra, which is now characterized by the non-unitarity of representation for the improper Lorentz group.

1. Introduction

Recent experimental results have established the fact that parity in the usual sense is not conserved in weak interactions [1]). As is well known, the observed right and left asymmetry can be explained if and only if one takes a Hamiltonian which is non-invariant under space inversion as well as charge conjugation [2]). Take the β-decay, for instance; the interaction Hamiltonian is of the form

$$H = \sum (\bar{\psi}_{\mathrm{p}} \Omega \psi_{\mathrm{n}})(C\bar{\psi}_{\mathrm{e}} \Omega \psi_{\nu} + C' \bar{\psi}_{\mathrm{e}} \Omega \gamma_5 \psi_{\nu}) + \mathrm{h.c.} \tag{1.1}$$

where, it should be remembered, the condition

$$\mathrm{Re}(C^* C') \neq 0 \tag{1.2}$$

is essential for reproducing the asymmetry.

As an important criterion for the observed non-conservation of parity, the expression (1.2) has been extensively used in the phenomenological analyses. However, it seems that the theoretical basis of the formula is still missing; in other words, it seems to be necessary to add something like d'Espagnat and Prentki's theory of the isobaric group to the phenomenological expression of Nishijima-Gellmann's selection rules [3]).

The main purpose of this paper is to reinvestigate the group structure of elementary particles and throw light on some remarkable mathematical facts, which seem to be intimately connected with the non-conservation of parity. It will be shown that the characteristic relation (1.2) can be incorporated into the underlying algebra under some restrictions which will be specified. The main feature of the new algebra is the non-unitarity of representation for the improper Lorentz group. This is a rather remarkable conclusion, contrasting with the usual postulate that all the elementary

particles are to be described by unitary representations of the full group of Lorentz transformations.

In section 2 we examine the definition and assumptions under which the non-invariance of (1.1) is usually asserted. We propose to modify some features of the underlying algebra in such a way that the invariance of the interaction Hamiltonian together with that of the free field equations is again established. The theory is now to be reconstructed on the basis of the new algebra, the properties of which will be described in section 3. The fundamental equations of motion in the interaction representation are introduced in the next section from the requirement of invariance under the full Lorentz group. On the other hand, owing to the non-unitarity of the representation, special consideration is needed regarding the canonical form of commutation relations: this will be discussed in some detail. The last section contains some remarks on the extension of the formalism to strange particle interactions.

2. Preliminary Considerations

The aim of this section is to find the new algebra which leaves invariant the interaction Hamiltonian (1.1) together with the free field equations. Bearing this in mind, we shall begin our discussion by reviewing the usual definition of space inversion.

Suppose that the four-dimensional Minkowski space x_μ ($\mu = 1, 2, 3, 4$) be given. According to the method of Brauer and Weyl [4]), we first consider the linearization of the quadratic form

$$\delta_{\mu\nu} x_\mu x_\nu = (\gamma_\mu x_\mu)^2 \tag{2.1}$$

and obtain the well-known γ-algebra

$$\gamma_\mu \gamma_\nu + \gamma_\nu \gamma_\mu = 2\delta_{\mu\nu}. \tag{2.2}$$

Next comes the relation which implies the mapping of the Lorentz transformations $x'_\mu = a_{\mu\nu} x_\nu$ onto their spinor representations S:

$$S \gamma_\mu S^{-1} = a_{\mu\nu} \gamma_\nu. \tag{2.3}$$

Then, the wave function of the fermion field is transformed as

$$\psi \to S\psi \tag{2.4}$$

and its adjoint is to be suitably defined such that

$$\bar{\psi} \to \bar{\psi} S^{-1}. \tag{2.4a}$$

Take space inversion, in particular: $\mathbf{x}' = -\mathbf{x}$, $t' = t$. Then, eqs. (2.2) and (2.3) imply $S = \gamma_4$ uniquely, apart from a factor of modulus one. And the transformation (2.4) in this case reads

$$\psi(\mathbf{x}, t) \to \gamma_4 \psi(-\mathbf{x}, t). \tag{2.5}$$

Now, we reformulate the expression (1.1) in the following way: Regarding the proton and the neutron as two different states of the nucleon, we describe this by the use of the conventional τ-formalism. Quite similarly, we can treat the electron and the neutrino as the lepton, and we shall introduce a new set of Pauli operators ω_k specifying the two kinds of leptons. The Hamiltonian (1.1) can be brought into the form

$$\begin{aligned} H = \sum\, & (\bar{\psi}_N \Omega \tau_+ \psi_N)(\bar{\psi}_L \Omega (C + C'\gamma_5)\omega_+ \psi_L) \\ & + (\bar{\psi}_N \Omega \tau_- \psi_N)(\bar{\psi}_L \Omega (C^* - C'^*\gamma_5)\omega_- \psi_L) \end{aligned} \tag{2.6}$$

where ψ_N and ψ_L denote the wave functions of the nucleon and the lepton, respectively. They are transformed under space inversion, according to (2.5), as

$$\begin{aligned} \psi_N(\mathbf{x}, t) &\to \gamma_4 \psi_N(-\mathbf{x}, t) \\ \psi_L(\mathbf{x}, t) &\to \gamma_4 \psi_L(-\mathbf{x}, t). \end{aligned} \tag{2.7}$$

As is well known, it is usually believed that the Hamiltonian (2.6) is not invariant under the transformation (2.7). However, we must here note that one makes the implicit assumption that γ_μ are to be quite independent of τ_j and ω_k, and commutable with one another:

$$[\gamma_\mu, \tau_j] = 0, \tag{2.8}$$

$$[\gamma_\mu, \omega_k] = 0, \tag{2.9}$$

$$[\tau_j, \omega_k] = 0, \tag{2.10}$$

where τ_j and ω_k are the usual Pauli operators, satisfying

$$\{\tau_j, \tau_k\} = 2\delta_{jk}, \qquad \tau_1 = i\tau_2\tau_3 \quad \text{etc.} \tag{2.11}$$

$$\{\omega_j, \omega_k\} = 2\delta_{jk}, \qquad \omega_1 = i\omega_2\omega_3 \quad \text{etc.} \tag{2.12}$$

It is clear that the algebra consisting of γ_μ, τ_j and ω_k is well defined by the above relations (2.2) (2.8—10) and (2.11—12).

We now note that the nucleon and the lepton wave functions are transformed quite independently. It will therefore be possible to modify the relation (2.9) and leave (2.8) unchanged. Let us now assume that γ_μ and τ_j as usual commute with each other, while γ_μ and ω_k no longer do, and introduce the non-commutativity in such a way that

$$[(C + C'\gamma_5)\omega_+, \gamma_\mu] = 0, \tag{2.13}$$

$$[(C^* - C'^*\gamma_5)\omega_-, \gamma_\mu] = 0. \tag{2.14}$$

If the algebraic relation between γ_μ and ω_k is changed in this way, it is clear that the invariance of the Hamiltonian under (2.7) will again be established.

Needless to say, the equations (2.13—14) alone are not sufficient to determine the full relation between the two kinds of operators. It is necessary to define the relations between their other components. For this purpose, we

further assume that the free equation of the lepton,

$$[\gamma_\mu \partial_\mu + \tfrac{1}{2}m(1+\omega_3)]\psi_L = 0, \tag{2.15}$$

or

$$[i\gamma_4(\boldsymbol{\gamma}\cdot\mathbf{p}) + \tfrac{1}{2}m\gamma_4(1+\omega_3)]\psi_L = E\psi_L, \tag{2.15a}$$

is also invariant. This requirement of invariance implies

$$[\omega_3, \gamma_\mu] = 0. \tag{2.16}$$

Finally, we add one more condition:

$$[\omega_k, \gamma_{\mu\nu}] = 0 \tag{2.17}$$

where

$$\gamma_{\mu\nu} = \frac{1}{2i}(\gamma_\mu\gamma_\nu - \gamma_\nu\gamma_\mu)$$

are, as is well known, the infinitesimal operators of the proper Lorentz transformations. According to this condition (2.17), the theory will remain essentially unchanged as far as the proper Lorentz transformations are concerned, and the conservation laws associated with them, such as the conservation of energy, momentum and angular momentum, will be valid as before without any alteration.

By the above, the main features of the new algebra are outlined. Rigorously speaking, however, it may still be an open question whether the conditions above enumerated are internally consistent with one another, and whether they permit a solution or not. This question will be answered in the next section by constructing explicitly the matrix representation of the algebra.

3. Underlying Algebra and its Representations

The relations defining the algebra are summarized as follows:

$$\{\gamma_\mu, \gamma_\nu\} = 2\delta_{\mu\nu}, \tag{3.1}$$

$$\{\tau_j, \tau_k\} = 2\delta_{jk}, \qquad \tau_1 = i\tau_2\tau_3 \quad \text{etc.}, \tag{3.2}$$

$$\{\omega_j, \omega_k\} = 2\delta_{jk}, \qquad \omega_1 = i\omega_2\omega_3 \quad \text{etc.}, \tag{3.3}$$

$$[\gamma_\mu, \tau_k] = 0, \tag{3.4}$$

$$[\gamma_\mu, \omega_3] = 0, \tag{3.5}$$

$$[\gamma_\mu, (C+C'\gamma_5)\omega_+] = 0, \tag{3.6}$$

$$[\gamma_\mu, (C^*-C'^*\gamma_5)\omega_-] = 0, \tag{3.7}$$

$$[\gamma_{\mu\nu}, \omega_k] = 0, \tag{3.8}$$

$$[\tau_j, \omega_k] = 0. \tag{3.9}$$

In the above Greek letters range from 1 to 4, and Roman indices from 1 to 3.

Since the nucleon and the lepton wave functions are transformed quite

independently, it will be possible to construct the representations separately for the $\gamma-\tau$ and for the $\gamma-\omega$ algebras. As to the former, being exactly the same as in the conventional theory, the matrix representation is given by

$$\tau_1 \leftrightarrow \begin{pmatrix} 0 & 1 \\ 1 & 0 \end{pmatrix}, \qquad \tau_2 \leftrightarrow \begin{pmatrix} 0 & -i \\ i & 0 \end{pmatrix}, \qquad \tau_3 \leftrightarrow \begin{pmatrix} 1 & 0 \\ 0 & -1 \end{pmatrix} \tag{3.10}$$

and

$$\gamma_\mu \leftrightarrow \begin{pmatrix} \underline{\gamma_\mu} & 0 \\ 0 & \underline{\gamma_\mu} \end{pmatrix} \tag{3.11}$$

where the underlined γ_μ's denote the usual 4×4 matrices.

On the other hand, the $\gamma-\omega$ algebra cannot be represented in such a form as the above because of the non-commutativity introduced by (3.6—7). Even when we fix the representative matrix for ω_3 as

$$\omega_3 \leftrightarrow \begin{pmatrix} 1 & 0 \\ 0 & -1 \end{pmatrix} \tag{3.12}$$

those for the other components are not uniquely determined. A special representation is that in which γ_μ are represented by

$$\gamma_\mu \leftrightarrow \begin{pmatrix} \underline{\gamma_\mu} & 0 \\ 0 & \underline{\gamma_\mu} \end{pmatrix} \tag{3.13}$$

as in the nucleon case, while the transition operators $\omega_\pm \equiv \frac{1}{2}(\omega_1 \pm i\omega_2)$ are to be of the following form

$$\omega_+ \propto \begin{pmatrix} 0 & C+C'\underline{\gamma_5} \\ 0 & 0 \end{pmatrix}, \qquad \omega_- \propto \begin{pmatrix} 0 & 0 \\ C^*-C'^*\underline{\gamma_5} & 0 \end{pmatrix}. \tag{3.14}$$

Now, it can be verified that these matrices do satisfy all the algebraic relations above listed, if and only if the condition

$$\mathrm{Im}\,(C^*C') = 0 \tag{3.15}$$

is fulfilled. It is to be noted that this is the very condition of invariance under time reversal.

There exists another possibility of representing the algebra, in which, in turn, all ω_k are represented by the usual Pauli matrices

$$\omega_+ \leftrightarrow \begin{pmatrix} 0 & 1 \\ 0 & 0 \end{pmatrix}, \qquad \omega_- \leftrightarrow \begin{pmatrix} 0 & 0 \\ 1 & 0 \end{pmatrix} \tag{3.16}$$

while γ_μ are now given by

$$\gamma_\mu \leftrightarrow \begin{pmatrix} \underline{\gamma_\mu} & 0 \\ 0 & \underline{\gamma'_\mu} \end{pmatrix} \tag{3.17}$$

where

$$\underline{\gamma'_\mu} = \mathrm{e}^{-f^*\underline{\gamma_5}}\underline{\gamma_\mu}\mathrm{e}^{+f\underline{\gamma_5}} \tag{3.18}$$

and

$$f = \tanh^{-1}(-C'/C). \tag{3.19}$$

Other representations are also possible which are characterized as intermediate between the above two, but we do not go into details because their physical meaning is not so clear. It may, however, be mentioned that it is common to all of them that only $\omega_\pm$ have nondiagonal elements, while γ_μ have the form of direct sums consisting of electron and neutrino factors. Therefore, it turns out that the two kinds of leptons do not mix in their unperturbed states, and they go into each other only through an interaction involving $\omega_\pm$. That is to say, the concept of free electron and of free neutrino are valid as before separately.

This can be easily seen when we take the representation (3.13—14) in which γ_μ are represented in exactly the same way as in the nucleon case, while the unusual character of lepton transitions is expressed in the fact that $\omega_\pm$ are not simply represented by the usual Pauli matrices. However, the second representation (3.16—17), in which $\omega_\pm$ are described by the well-known matrices, is more convenient in order to see the connection between the usual formalism and ours.

It should here be noted that the condition (1.2) for reproducing the observed asymmetry, together with (3.15) obtained above, implies the reality of both C and C', and hence

$$f \neq 0, \text{ real}, \tag{3.20}$$

which means, in view of the relation (3.18), that it is impossible to give both γ_μ and γ'_μ unitary representations at the same time. If we now take the unitary one for the electron, the neutrino is to be transformed according to a non-unitary representation of the Dirac ring.

To understand the transformation character of the primed representation, we note the following theorem (we shall from now on drop the underlining denoting a 4×4 matrix):

In the product of any odd number of γ_μ's, there exists a difference by a factor $\exp(2f\gamma_5)$ between the expressions with and without prime:

$$\gamma'_\mu = e^{-2f\gamma_5}\gamma_\mu = \gamma_\mu e^{+2f\gamma_5}, \tag{3.21}$$

while in the product of an even number of γ_μ's, both expressions are equal. For instance,

$$\gamma'_\mu\gamma'_\nu = \gamma_\mu\gamma_\nu \tag{3.22}$$

and

$$\gamma'_5 = \gamma_5 \tag{3.23}$$

which are immediately derived from (3.18), together with $f^* = f$.

According to this theorem, we can conclude that, although one takes an unusual representation for the neutrino, the theory remains unchanged as far as the proper Lorentz transformations are concerned, because any rotation can be expressed as a product of an even number of reflections, and

hence the corresponding S is a product of an even number of γ_μ's [5]). Differences occur only for improper Lorentz transformations, which are expressed as products of an odd number of reflections, and hence of an odd number of γ_μ's. Thus, in particular, the revised definition of space inversion is to be

$$\psi_e(\mathbf{x}, t) \to \gamma_4 \psi_e(-\mathbf{x}, t) \tag{3.24}$$

for the electron, but

$$\psi_\nu(\mathbf{x}, t) \to \gamma'_4 \psi_\nu(-\mathbf{x}, t) = e^{-2f\gamma_5} \gamma_4 \psi_\nu(-\mathbf{x}, t) \tag{3.25}$$

for the neutrino †.

That is to say, the parity operator for the neutrino is different from that of the electron. They do not commute with each other, and therefore cannot be diagonalized simultaneously. This means that parity is not a good quantum number for the process concerned.

Finally, it is interesting to note that, as can be seen from (3.19), one of the parity operators becomes singular when $C = \pm C'$, which corresponds to the case of the two-component neutrino [8]).

The algebra described here may be considered rather artificial at first sight. However, it should be mentioned that the same result can be obtained also in a more familiar way, viz., as a consequence of a renormalization carried out consistently for partity non-conserving interactions. The detail of this problem has been discussed in a separate paper [9]), and will not be given here.

4. Fundamental Equations of Motion and Canonical Commutation Relations

The theory is now to be reconstructed on the basis of the new algebra.

We first introduce, in the interaction representation, the fundamental equations of motion from the requirement of invariance under the full group of Lorentz transformations. The field equations are to be

$$[i\gamma_4(\boldsymbol{\gamma} \cdot \mathbf{p}) + m\gamma_4]\psi_e = E_e \psi_e \tag{4.1}$$

and

$$i\gamma'_4(\boldsymbol{\gamma}' \cdot \mathbf{p})\psi_\nu = i\gamma_4(\boldsymbol{\gamma} \cdot \mathbf{p})\psi_\nu = E_\nu \psi_\nu \tag{4.2}$$

where the primed γ'_μ's are eliminated by making use of the identity (3.22). It is clear that these equations are quite equivalent to the conventional ones as far as we take the usual unitary representation for the γ_μ's without prime.

The equation for the state vector is given by

$$i\frac{\delta \Psi[\sigma]}{\delta \sigma(x)} = H(x)\Psi[\sigma] \tag{4.3}$$

† Such a transformation was proposed by Wouthuysen [6]) and independently by the present author [7]).

where

$$H(x) = \sum (\bar{\psi}_p \Omega \psi_n)(C\bar{\psi}_e \Omega \psi_\nu + C'\bar{\psi}_e \Omega \gamma_5 \psi_\nu) + \text{h.c.} \tag{4.4}$$

It should be mentioned that $H(x)$ is now uniquely determined on the basis of the new algebra from the requirement of invariance under the full Lorentz group (including inversions).

By using the conventional method of calculation in perturbation theory, we can derive from the above system of equations the observed asymmetry and the polarization of particles.

On the other hand, special consideration is needed of the canonical form of the commutation relations. Clearly, the expression

$$\{\psi_\nu(\mathbf{x}, t), \psi_\nu^\dagger(\mathbf{x}', t)\} = \delta^3(\mathbf{x}-\mathbf{x}') \tag{4.5}$$

is not invariant under the improper transformations because of the non-unitarity of the primed algebra, that is, $\gamma'_\mu \gamma'^\dagger_\mu \neq 1$. Nevertheless, all the proper transformations leave (4.5) invariant as in the conventional theory, which is easily proved by making use of the theorem previously mentioned.

Here may be raised an argument against taking the non-unitary representation which, as a matter of fact, violates the invariance of the canonical commutation relations. However, now that the parity non-conservation is experimentally established, there is no a priori reason for requiring the invariance under space inversion for any part of the theory. Hence it is not unreasonable to consider that the invariance is violated, not in the fundamental equations, but in the canonical commutation relations †. It is further to be noted that, in our reformulation, the invariance of the latter can be derived as a consequence of the non-unitarity of representation.

Now, to construct bilinear covariants, we review the definition of the adjoint field. In order that $\bar{\psi}$ transforms into $\bar{\psi}S'^{-1}$ when $\psi \to S'\psi$, the adjoint must be defined as

$$\bar{\psi} \equiv \psi^\dagger A \tag{4.6}$$

with A satisfying

$$\gamma_\mu'^\dagger = \pm A\gamma'_\mu A^{-1}. \tag{4.7}$$

As is known, this implies the property [10])

$$S'^+ A = AS'^{-1}. \tag{4.8}$$

On the other hand, solving the equation (4.7) gives, apart from a numerical factor,

$$A = \gamma_4, \tag{4.9}$$

from which we can see that A defining the adjoint is always the usual, unitary γ_4 (without prime), even when the underlying algebra is modified

† Indeed, the invariance of the canonical commutation relations is violated in the two-component theory of the neutrino (see ref. [8])).

into the primed one. (Remember that the quantities with and without prime are related by the formula (3.18), now with $f^* = f$.)

By making use of (4.8) we can prove

$$\bar{\psi}\Omega'\psi = (\bar{\psi}\Omega'\psi)^\dagger, \tag{4.10}$$

that is, the bilinear covariants are always real despite the non-unitarity of representation †. Therefore, the expectation values of the energy-momentum, for instance, are real, and the unitarity of the S-matrix is assured.

In constructing the Lagrangian which leads to the equation (4.2), we have two possibilities: The first is the expression written in terms of γ'_μ with prime

$$\mathscr{L}_1 = -\bar{\psi}\gamma'_\mu\partial_\mu\psi, \tag{4.11}$$

which is real according to (4.10). The reality in this case is necessary in order that the equation for ψ and that for $\bar{\psi}$ be consistent with each other. An alternative possibility is to construct the similar expression in terms of γ_μ without prime:

$$\mathscr{L}_2 = -\bar{\psi}\gamma_\mu\partial_\mu\psi. \tag{4.11a}$$

Making use of the conventional procedure we obtain the commutation relations

$$\{\psi(\mathbf{x}, t),\ \psi^\dagger(\mathbf{x}', t)\} = \mathrm{e}^{2f\gamma_5}\delta^3(\mathbf{x}-\mathbf{x}') \tag{4.12}$$

and

$$\{\psi(\mathbf{x}, t),\ \psi^\dagger(\mathbf{x}', t)\} = \delta^3(\mathbf{x}-\mathbf{x}'), \tag{4.12a}$$

respectively. Both are compatible, in the usual sense, with the equation of motion (4.2). It should, however, be remarked that only the latter, together with the Hamiltonian (4.4), is able to reproduce the observed asymmetry and polarization. To see this, it is only necessary to rewrite the relations in terms of canonical variables. Put $\exp(f\gamma_5)\psi \equiv \underset{\sim}{\psi}$; then the commutation relation (4.12) is brought into the canonical form

$$\{\underset{\sim}{\psi}(\mathbf{x}, t),\ \underset{\sim}{\psi}^\dagger(\mathbf{x}', t)\} = \delta^3(\mathbf{x}-\mathbf{x}')$$

and, at the same time, the Hamiltonian (4.4) reduces to the expression

$$H(x) = \sum (\bar{\psi}_\mathrm{p}\Omega\psi_\mathrm{n})(\bar{\psi}_\mathrm{e}\Omega\underset{\sim}{\psi}_\nu) + \mathrm{h.c.}$$

As can be seen, the parity non-conserving terms have disappeared.

Here, it should be mentioned that we have just utilized the so-called Lagrangian formalism only to prove the consistency between the equations and the commutation relations. This could, however, be proved more directly without any reference to the Lagrangian. In view of the fact that $\mathscr{L}_2$ is not

† Shirokov called such a representation real non-unitary [11].

invariant, or what is the same, is not constructed on the basis of its own algebra, it might be possible to consider that the conventional Lagrangian formalism is not satisfactory as a fundamental framework of future theory.

Summarizing, the fundamental equations of motion (4.1—4) and the commutation relations (4.5) form a consistent system of equations, which is in fact the minimum requirement for reproducing the observed asymmetries and polarizations. These expressions are exactly the same in our reformulated theory as in the conventionally accepted one. However, the transformation character is different owing to the modification of the underlying algebra. In the conventional theory, the commutation relations are invariant while the equations of motion are not. In our reformulation, on the contrary, the latter are invariant while the former are not. It may be worthwhile to note that the fundamental equations of motion are invariant under a wider range of transformations (viz., the proper and the improper Lorentz group) than the canonical commutation relations (under the proper subgroup only).

Finally it should be added that, although the equations of motion in the interaction representation are quite equivalent to the conventional ones, bilinear covariants in general are different in the usual and in our reformulated theory.

5. Concluding Remarks

Although our discussion has so far been restricted to the β-decay interaction, extension of the formalism developed above to the other lepton processes, such as $\pi-\mu$, $\mu-$e and $K_{\mu 2}$ decay, is straight-forward. In all these cases, we can take advantage of the fact that the neutrino mass is exactly zero.

As to the hyperon decays, however, some remarks are to be added. Owing to the finiteness of the masses we cannot eliminate completely the primed γ'_μ from the equations of motion. Accordingly, the field equation for at least one of the associated fermions, say for the Λ-particle, becomes different from the conventional Dirac equation. It is to be further remarked that in this case the question is quite open whether the modified field equation is consistent with the canonical form of commutation relations. It seems, nevertheless, to be promising to explore the possibility; as was once stated by Lee and Yang [12]), the strange particles belong to strange representations of the Lorentz group.

It is a pleasure to thank Prof. T. Yamanouchi for his kind interest and continuous encouragement. The author is also grateful to Prof. H. Umezawa, Dr. T. Okabayashi and Dr. H. Miyazawa for helpful discussions and criticisms. He is indebted to the Yomiuri Yukawa Fellowship for financial aid.

References

1) C. S. Wu *et al.*, Phys. Rev. **105** (1957) 1413; **106** (1957) 1361;
R. L. Garwin *et al.*, Phys. Rev. **105** (1957) 1415;
J. I. Friedman and V. L. Telegdi, Phys. Rev. **105** (1957) 1681;
F. S. Crawford *et al.*, Phys. Rev. **108** (1957) 1102;
F. Eisler *et al.*, Phys. Rev. **108** (1957) 1353
2) T. D. Lee and C. N. Yang, Phys. Rev. **104** (1957) 254;
T. D. Lee, R. Oehme and C. N. Yang, Phys. Rev. **106** (1957) 340;
B. L. Ioffe, L. B. Okun and A. P. Rudik, JETP **32** (1957) 396
3) B. d'Espagnat and J. Prentki, Nuclear Physics **1** (1956) 33
4) R. Brauer and H. Weyl, Amer. Journ. Math. **57** (1935) 425
5) E. Cartan, La Théorie des Spineurs (Hermann et Cie, Paris, 1938)
6) S. A. Wouthuysen, Proc. Kon. Ned. Akad. Wetens. B **61** (1958) 54
7) K. Sekine, Progr. Theor. Phys. **19** (1958) 740
8) T. D. Lee and C. N. Yang, Phys. Rev. **105** (1957) 1671;
L. D. Landau, Nuclear Physics **3** (1957) 127;
A. Salam, Nuovo Cimento **5** (1957) 299
9) K. Sekine, Nuovo Cimento **11** (1959) 87
10) J. M. Jauch and F. Rohrlich, The Theory of Photons and Electrons (Addison-Wesley, Cambridge, Mass. 1955) Appendix ii
11) Yu. M. Shirokov, JETP **33** (1957) 861
12) T. D. Lee and C. N. Yang, ref. [8])

1.C:
1.D.3

Nuclear Physics **11** (1959) 615—624; © *North-Holland Publishing Co., Amsterdam*
Not to be reproduced by photoprint or microfilm without written permission from the publisher

THE α, α INTERACTION

E. VAN DER SPUY

Physics Department, University, Stellenbosch †

Received 23 January 1959

Abstract: The 8-body problem of the (α, α) scattering interaction is formulated by using the group resonance formalism, with two unpolarized α groups, and with the central nucleon-nucleon exchange force and α wave-function both having a gaussian radial dependence. Choosing parameters as far as possible the same as required by the low energy nucleon-nucleon data, the α binding energy, and the (α, n) scattering interaction, it was attempted to explain the S and D phases for low energy (α, α) scattering which was previously found to require a velocity-dependent interaction. The (α, α) scattering requires slightly different values of $y = 4w+2b-2h-m$, both of which are lower than required by the (α, n) problem. It is shown that the S wave interaction essentially behaves as a potential at low energies. For low energies this potential effectively has a repulsive core with an attractive outside well—features which also emerged from a previous purely phenomenological analysis.

1. Introduction

In a previous publication [1]) the (α—α) interaction was subjected to a phenomenological analysis to see whether the (α, α) scattering data at low energy could be represented by a velocity-independent interaction, common to the S and D waves. This was found impossible, and in fact velocity or l-dependence of the interaction was indicated even below laboratory energies of 6 MeV. The simplest velocity dependence with some support from fundamental considerations was for a common outer attractive well with an inner repulsive core, with an l-dependent radius. It was decided to try and see whether the velocity-dependent integral interaction which normally comes from a many-body problem would not naturally fulfil these demands. Thus, it is now proposed to set up the corresponding 8-body problem by the group resonance formalism [2]), with an assumed form for the nuclear force: a central exchange force of gaussian radial dependence. The discussion will be limited to low energies as before [1]).

2. The 8-Body Problem

It is again assumed that, since the α particle is tightly bound, for the consideration of the α—α interaction below the centre of mass energies $E \approx 3$ MeV, one may consider only unpolarized α groups. Such α groups are

† Now at Max-Planck-Institut für Physik, München.

in the normal $^1S_0$ state and since they are spin-saturated, one may neglect all spin-orbit couplings between nucleons in this approximation.

The overall antisymmetrized wave-function Ψ is thus given as follows, where 1, 2, 5, 6 are neutrons and 3, 4, 7, 8 are protons:

$$\begin{aligned}\Psi = &\{1-H(25)-H(26)-H(15)-H(16)+H(15)H(26)\}\\ &\cdot\{1-H(47)-H(48)-H(37)-H(38)+H(37)H(48)\\ &\cdot\psi_a(\widetilde{12},\widetilde{34})\psi_b(\widetilde{56},\widetilde{78})\mathcal{J}(\mathbf{r}_{a,b}),\end{aligned} \tag{1}$$

where $H(25)$, for example, is the Heisenberg exchange operator, exchanging both space and spin coordinates of particles 2 and 5;

$$\psi_a(\widetilde{12},\widetilde{34}) = \chi(\widetilde{12},\widetilde{34})\phi(1234) \tag{2}$$

is the normal $^1S_0$ unpolarized α wave-function,

$$\chi(\widetilde{12},\widetilde{34}) = \tfrac{1}{2}(\alpha(1)\beta(2)-\beta(1)\alpha(2))(\alpha(3)\beta(4)-\beta(3)\alpha(4))$$

being the antisymmetric spin wave-function, with α and β corresponding to $+$ and $-$ spin, respectively, and ϕ (1234) the symmetric, spatial part of the α wave-function; and finally $\mathcal{J}(\mathbf{r}_{a,b})$ is the wave-function for the relative motion of α particles a, b, with

$$\mathbf{r}_{a,b} = \mathbf{r} = \tfrac{1}{4}(\mathbf{r}_1+\mathbf{r}_2+\mathbf{r}_3+\mathbf{r}_4)-\tfrac{1}{4}(\mathbf{r}_5+\mathbf{r}_6+\mathbf{r}_7+\mathbf{r}_8)$$

denoting the vector between the centres of mass of the α particles a, b. The α particle, having zero spin, $\mathcal{J}(\mathbf{r}_{a,b})$ is symmetrical for spatial inversions.

The hamiltonian is taken as

$$\mathcal{H} = -\frac{\hbar^2}{2M}\sum_{i=1}^{8}\nabla_i^2+\sum_{(1\ldots8)}\mathcal{V}(ij), \tag{3}$$

where M is the nucleon mass, and $\sum(1\ldots8)$ denotes a summation over all i, j combinations for $i, j = 1$ to 8, but with $i \neq j$; and where

$$\mathcal{V}(ij) = \{w+mP_x(ij)+bP_\sigma(ij)+hH(ij)\}V(ij), \tag{4}$$

with the exchange coefficients normalized: $w+m+b+h = 1$; the operators $P_x(ij)$, $P_\sigma(ij)$ being, respectively, the space and spin exchange operators for particles i, j, and $V(ij)$ the common radial dependence of the central exchange type nucleon-nucleon force law. For simplicity, the gaussian form of $V(ij)$ is assumed:

$$V(ij) = A\exp(-\beta r_{ij}^2). \tag{5}$$

Now

$$\mathcal{H}\Psi = E'\Psi \tag{6}$$

is the 8-body Schrödinger equation; by simple elimination one constrains the equation to refer to the centre of mass system. To get the equation of relative motion of a, b or the wave equation for $\mathscr{I}(\mathbf{r}_{a,b})$ one must integrate out all the nucleon-nucleon coordinates. In the process the variational form of the α wave equation is used for some constraints on the parameters of $\phi(1234)$ and $\mathscr{V}(ij)$, by requiring the variational treatment to predict the α binding energy $-E_\alpha = 28.20$ MeV. A typical case of this variational equation is

$$\int_{SS}^{a} \chi(\widetilde{12}, \widetilde{34})\phi^*(1234)\{K_a - E_\alpha + \sum_{(1234)} \mathscr{V}(ij)\}\chi(\widetilde{12}, \widetilde{34})\phi(1234) = 0, \quad (7)$$

where as usual K_a is the α kinetic energy operator [4]) in the centre of mass system of α particle a:

$$K_a = -\frac{\hbar^2}{M}\{\tfrac{2}{3}\nabla^2_{1,234} + \tfrac{3}{4}\nabla^2_{2,34} + \nabla^2_{3,4}\},$$

and where $\int_{SS}^{a}$ effects the integrations over all the spin and space coordinates of α particle a.

For simplicity the following form is assumed for the symmetrical spatial part of the α wave-function:

$$\phi(1234) = N \exp -\alpha(r_{12}^2 + r_{13}^2 + r_{14}^2 + r_{23}^2 + r_{24}^2 + r_{34}^2), \quad (8)$$

with $N^2 = (2)^{21/2}(\alpha/\pi)^{\frac{3}{2}}$ by normalization.

Multiplying (6) by $\psi_a^*(\widetilde{12}, \widetilde{34})\psi_b^*(\widetilde{56}, \widetilde{78})$ and integrating over the space and spin variables of all the nucleons, keeping $\mathbf{r}$ constant, the use of eq. (7), and the above force law and α wave-function, leads with the symmetries to the following wave equation for $\mathscr{I}(\mathbf{r})$:

$$\left\{\frac{\hbar^2}{4M}\nabla^2 + (E' - 2E_\alpha) - V_D(r)\right\}\mathscr{I}(\mathbf{r}) = \int d\mathbf{r}' K(\mathbf{r}, \mathbf{r}')\mathscr{I}(\mathbf{r}'), \quad (9)$$

where $E' - 2E_\alpha$ is the relative energy E of the two α particles, in the centre of mass system, and the direct interaction

$$V_D(r) = 4(4w + 2b - 2h - m)A\left(\frac{16\alpha}{16\alpha + 3\beta}\right)^{\frac{3}{2}} \exp -\frac{16\alpha\beta}{16\alpha + 3\beta} r^2, \quad (10)$$

with $y = 4w + 2b - 2h - m$, the usual factor which also appears in the α—n direct interaction. The symmetrical kernel $K(\mathbf{r}, \mathbf{r}')$ of the velocity-dependent integral interaction term is given by

$$K(\mathbf{r},\mathbf{r}') = 2^{11}\left(\frac{\alpha}{3\pi}\right)^{\frac{3}{2}}\exp\{-\tfrac{8}{3}\alpha(5r^2+5r'^2-8\mathbf{r}\cdot\mathbf{r}')\}$$
$$\times\left[\frac{\alpha\hbar^2}{M}\{\tfrac{256}{9}\alpha(7r^2+7r'^2-13\mathbf{r}\cdot\mathbf{r}')-62\}+E'-6A(w+m)\left(\frac{4\alpha}{4\alpha+\beta}\right)^{\frac{3}{2}}\right.$$
$$+(4m+2h-2b-w)A\exp\{-4\beta(r^2+r'^2-2\mathbf{r}\cdot\mathbf{r}')\}$$
$$-3(2b+3w-2m-2h)A\left(\frac{6\alpha}{6\alpha+\beta}\right)^{\frac{3}{2}}\exp\left\{-\frac{8\alpha\beta}{18\alpha+3\beta}(r^2+r'^2+2\mathbf{r}\cdot\mathbf{r}')\right\}$$
$$-6(w+m)A\left(\frac{6\alpha}{6\alpha+\beta}\right)^{\frac{3}{2}}\exp\left\{-\frac{8\alpha\beta}{18\alpha+3\beta}(r^2+r'^2-4\mathbf{r}\cdot\mathbf{r}')\right\}$$
$$\left.\times\exp\left\{-\frac{8\alpha\beta}{6\alpha+\beta}r^2\right\}+\exp\left\{-\frac{8\alpha\beta}{6\alpha+\beta}r'^2\right\}\right] \qquad (11)$$
$$+3\times 2^9\left(\frac{\alpha}{4\pi}\right)^{\frac{3}{2}}\exp\{-8\alpha(r^2+r'^2)\}$$
$$\times\left[-\left\{\frac{\alpha\hbar^2}{M}[64\alpha(r^2+r'^2)-54]+E'-4(w+m)A\left(\frac{4\alpha}{4\alpha+\beta}\right)^{\frac{3}{2}}\right\}\right.$$
$$+4(2b+2w-3m-2h)A\left(\frac{8\alpha}{8\alpha+\beta}\right)^{\frac{3}{2}}\exp\left\{-\frac{8\alpha\beta}{8\alpha+\beta}(r^2+r'^2-2\mathbf{r}\cdot\mathbf{r}')\right\}$$
$$\left.+8(w+m)A\left(\frac{16\alpha}{16\alpha+3\beta}\right)^{\frac{3}{2}}\exp\left\{-\frac{16\alpha\beta}{16\alpha+3\beta}r'^2\right\}+\exp\left\{-\frac{16\alpha\beta}{16\alpha+3\beta}r^2\right\}\right].$$

The kernel $K(\mathbf{r},\mathbf{r}')$ depends only on the parameters α, β, A, y, E and $x = w+m$. The other coefficients simplify:

$$4m+2h-2b-w = 3x-y,$$
$$2b+3w-2m-2h = y-x,$$
$$2b+2w-3m-2h = y-2x.$$

To separate out the partial waves one puts

$$\mathscr{F}(\mathbf{r}) = \frac{1}{r}\sum_l f_l(r)P_l(\cos\theta), \qquad (12)$$

with l only having even values on account of symmetry. Then (9) simplifies to

$$\left\{\frac{\hbar^2}{4M}\left(\frac{\mathrm{d}^2}{\mathrm{d}r^2}-\frac{l(l+1)}{r^2}\right)+E-V_{\mathrm{D}}(r)\right\}f_l(r) = \int_0^\infty k_l(r,r')f_l(r')\mathrm{d}r', \qquad (13)$$

where

$$k_l(r,r') = 2\pi rr'\int_{-1}^{+1}K(\mathbf{r},\mathbf{r}')P_l(\cos\theta)\mathrm{d}(\cos\theta), \qquad (14)$$

θ in eq. (14) being the angle between $\mathbf{r}$ and $\mathbf{r}'$.

There are only three types of terms in $K(\mathbf{r}, \mathbf{r}')$ as far as dependence on θ is concerned: they are of the forms

$$\text{(a) } B, \qquad \text{(b) } B \exp(b\cos\theta), \qquad \text{(c) } B\cos\theta \exp(b\cos\theta),$$

where B is a function of r, r' in general and b is proportional to rr', the proportionality factor depending on α, β. Eq. (14) then gives for the $k_l(r, r')$ terms:

(a) $4\pi rr' B\delta_{l0}$, with $\delta_{l0} = 0$ for $l \neq 0$, $\delta_{00} = 1$;

(b) $$4\pi rr' B \frac{n_l(b)}{b};$$

(c) $$4\pi rr' B \frac{\mathrm{d}}{\mathrm{d}b}\left(\frac{n_l(b)}{b}\right),$$

with

$$n_l(b) = i^{l-1} j_l(ib), \qquad j_l(\theta) = \sqrt{\tfrac{1}{2}\pi\theta}\, J_{l+\frac{1}{2}}(\theta);$$

$n_l(b)$ is proportional to b^{l+1}, or $(rr')^{l+1}$ for small b and increases sharply for higher b. Since B is a function which in general eventually decreases sharply as a gaussian with increasing r^2 and r'^2, $k_l(r, r')$ is effective over a finite domain — it turns out that it has an effective range smaller than $V_D(r)$.

Eq. (9) and in fact (13) for $l = 0$ has a trivial solution which corresponds to an excluded bound S state for which Ψ vanishes. It is easy to show that Ψ vanishes for $\mathscr{S}(\mathbf{r}) = \exp -8\alpha r^2$, a purely S wave corresponding to the choice (8) of the α spatial wave-function. Any solution of (13) for $l = 0$, has an arbitrary proportion of this wave-function. On account of its finite range (as it turns out, about half of that of $V_D(r)$) it has no effect on accurately calculated scattering phases. Iterative approximation methods have, however, to recognize the possibility of error arising from solutions having a large proportion of this function.

The contribution of the Coulomb force between protons has still to be calculated. Since it is a weak force it will only be taken into account in its contribution to the direct interaction, $V_c(r)$. One easily finds

$$V_c(r) = 4\frac{e^2}{r}\,\mathrm{erf}\,(4r\sqrt{\tfrac{1}{3}\alpha}). \tag{15}$$

Thus, one has $V'_D(r) = V_D(r) + V_c(r)$ as the direct potential so far.

Even with $k_l(r, r')$ known numerically, eq. (13) is a very difficult equation to interpret physically, except in the most general terms. To tie up with a previous phenomenological analysis [1]), and to state the results if possible in a form which may readily be interpreted in terms of the structure of the α particle, and which may be some pointer to the interaction of α groups, the following further treatment is required.

The right-hand side of (13), by the Taylor expansion of $f_l(r')$, becomes

$$\int_0^\infty k_l(r, r')f_l(r')\mathrm{d}r' = \sum_n \left[\int_0^\infty k_l(r, r') \frac{(r'-r)^n}{n!}\mathrm{d}r'\right] \frac{\mathrm{d}^n}{\mathrm{d}r^n} f_l(r)$$
$$= \sum_n V_{nl}(r) \frac{\mathrm{d}^n}{\mathrm{d}r^n} f_l(r). \tag{16}$$

The "potential" $V_{nl}(r)$ is $1/n!$ of the n-th moment of the kernel $k_l(r, r')$ around the point $r' = r$. The n-th moment is limited in value owing to the small range of $k_l(r, r')$, and $V_{nl}(r)$ is further limited by the $1/n!$ weighting. One may hence hope that the first few terms in (16) are the only important ones:

(a) $n = 0$: $V_{0l}(r)f_l(r)$ gives an l-dependent direct interaction potential. One has thus a total direct interaction potential

$$V_T(r) = V_{0l}(r) + V'_D(r). \tag{17}$$

(b) $n = 1$: $V_{1l}(r)(\mathrm{d}/\mathrm{d}r)f_l(r)$ has a less direct physical interpretation (similar to that of the following term (c)). For a $k_l(r, r')$ which has only one sign for all r, r' combinations and has its main values distributed roughly symmetrically around $r = r'$, this and other odd moments will tend to cancel out.

(c) $n = 2$: $V_{2l}(r)$ $(\mathrm{d}^2/\mathrm{d}r^2)f_l(r)$ has the obvious effect of leading to a correction to the α mass in interaction, as for nucleons in nuclear matter [3]). If $V_{2l}(r)$ is positive, the exchange interaction increases the effective α mass.

Concerning units, a useful way to read eq. (13) is with r in units of $f = 10^{-13}$ cm; then $\hbar^2/4Mf^2$, E, $V_D(r)$ and $k_l(r, r')f$, which enter in eq. (13), may all be worked in MeV. Similarly, the $V_{nl}(r)$ will then all be in MeV.

3. The Numerical Analysis

To test the predictions of (13) for scattering, for the full range of parameters and with good accuracy for $f_l(r)$, by an iterative process, with due regard to the excluded bound state solution for $l = 0$, really requires an electronic computer. The latter was not available and in any case one prefers here to find parameters which also satisfy other nuclear problems. In an analysis of the (α, n) results [4]) using $x = 0.8$, a set of values of α, β, A and y were found which gave the correct value of the α binding energy $-E_\alpha = 28.20$ MeV by a variational calculation from (7), represented the S, $^2P_{\frac{1}{2}}$, $^2P_{\frac{3}{2}}$ results for the (α, n) scattering, and were close to the best values for the low energy nucleon-nucleon results. In this way α, β and A are fixed by E_α and the range of the phenomenological α—n potential [4]); and y by the magnitude of this potential. It was hence investigated, first of all, whether the same parameters would yield the (α, α) scattering S and D phases at low energy. To anticipate, one should mention that this was not successful,

but using the above values of α, β, A (i.e. the correct E_α, nucleon-nucleon parameters, and α—n interaction range) different values of y were required. A different y may perhaps be considered to correspond to phases with the same general trend as the experimental (α, n) phases, but of a different magnitude. There is just a possibility (see later) that a fully self-consistent set of parameters may emerge from a proper account of a repulsive core in $V(ij)$ (eq. (5)), and more complicated and refined forms for ϕ and $f_l(r)$ to recognize nucleon-nucleon correlation effects. In principle, the calculations would be the same, but the numerical program would be a major project.

Thus, the calculations started with

$$\alpha = 0.08387\, f^{-2}, \qquad \beta = 0.2853\, f^{-2},$$
$$A = -47.62 \text{ MeV} \qquad y = 1.620, \quad x = 0.8,$$
$$\hbar^2/M = 0.4147 \times 10^{-24} \text{ cm}^2 \cdot \text{MeV}.$$

Table 1 gives the values of the interaction potentials, and $k_l(r, r')f$ in MeV, for these parameters. The kernels are for $E = 0$, with the $E = 3$ MeV value in brackets.

TABLE 1

r	0	1	2	3	4	5
$V_C(r)$	4.3	3.8	2.7	1.9	1.4	1.2
$V_D(r)$	−147.2	−123.7	−73.3	−30.7	−9.1	−1.9
$V'_D(r)$	−142.9	−119.9	−70.6	−28.8	−7.6	−0.7
$k_0(r, \frac{1}{2})f$	0	86.6	−11.6	−4.0	−0.2	
$k_0(r, 1)f$	0	86.3 (89.0)	24.5 (24.7)	−1.4 (−1.4)	−0.1 (−0.1)	
$k_0(r, 2)f$	0	24.5 (24.7)	35.3 (37.8)	12.9 (13.3)	0.5 (0.5)	
$k_0(r, 3)f$	0	−1.4 (−1.4)	12.9 (13.3)	3.8 (4.1)	1.1 (1.1)	
$k_0(r, 4)f$	0	−0.1 (−0.1)	0.5 (0.5)	1.1 (1.1)	0.2 (0.2)	
$k_2(r, 1)f$	0	11.8 (13.7)	27.0 (27.9)	2.2 (2.3)	0.0 (0.0)	
$k_2(r, 2)f$	0	27.0 (27.9)	21.4 (23.4)	9.5 (9.8)	0.4 (0.4)	
$k_2(r, 3)f$	0	2.2 (2.3)	9.5 (9.8)	2.2 (2.5)	0.9 (0.9)	
$k_2(r, 4)f$	0	0.0 (0.0)	0.4 (0.4)	0.9 (0.9)	0.2 (0.2)	
$V_{00}(r)$	0	130.4	67.4	15.3	1.7	
$V_{10}(r)$	0	1.4	3.9	−5.4	−1.6	
$V_{20}(r)$	0	15.9	8.1	0.0	0.7	
$V_T(r)$, $l = 0$	−142.9	10.5	−3.2	−13.5	−5.9	−0.7
$V_{02}(r)$	0	42.4	58.5	14.9	1.5	
$V_{12}(r)$	0	31.9	−13.6	−12.7	−1.8	
$V_{22}(r)$	0	18.0	18.6	10.1	1.4	
$V_T(r)$, $l = 2$	−142.9	−77.5	−12.2	−13.9	−6.1	−0.7

The range of $V'_D(r)$ the direct potential is up to $5f$, and that of the kernels is some $1f$ smaller. Therefore, it was decided to cut the potentials off at $5f$ and see whether they can give the logarithmic derivatives corresponding to

the experimental phases, at $5f$. It is clear that E has only a noticeable, though small, effect on the kernels for very small radii, when the wave-functions are small. It was hence decided to neglect this effect in the low energy domain (or put $E = 0$ in the kernel). For the S waves one notices that $V_{00}(r)$ is the predominant $V_{n0}(r)$ term. It was decided to undertake the fitting as if it were the only one. In this way the S wave interaction is velocity-independent and the analysis gives a good representation of the integral term itself; insistence on better accuracy for the integral term (or its kernel) will probably be equivalent to demanding an account of polarization effects also, which may account for a similar order of correction to this term. It must be stated, however, that the difficulty of the α—α problem is clearly illustrated for the S wave, for which (except for $r = 0$) $|V_T(r)|$ is small compared with $|V'_D(r)|$ or $V_{00}(r)$ up to 2—$3f$. The accuracy of $V_T(r)$ (the same may be true of the overall interaction in (13)) is thus likely to be worse than that of either of the latter two, especially for smaller radii. Note that for the S wave the $V_{20}(r)$ term indicates increase of α mass due to interaction (eventually reversing sign for low r) — quite appreciably so at $r < 3f(\hbar^2/4Mf^2 = 10.4$ MeV should be compared with 8.1 MeV at $r = 2f$).

For the D wave one sees that, although $V_{02}(r)$ is still usually larger in magnitude than the other $V_{n2}(r)$, it does not predominate and this partial wave has a fully velocity-dependent interaction. Nevertheless, insofar as the $V_{02}(r)$ is the larger, one notices, by comparing $V_T(r)$ for the S and D waves, that the S wave potential has an essentially repulsive core (it has a pith which is negative, but at low energies the wave-function is likely to be so low there that its effect is probably negligible) whereas the D wave potential has none. This agrees with the phenomenological requirements, and since $V_T(r)$ for $l = 2$ is generally deeper the calculation tends to be in the right direction.

While looking at these potentials one notices that $V_T(r)$ for $l = 0$ provides a repulsive core — a feature demanded for the α—α interaction, if α groups with an interaction near to that of two α particles are to be the basic constituents of low mass $4n$-nuclei [5]). The low magnitude of the core potential, its degree of velocity-dependence, and its absence from the $l = 2$ wave (which will be important for a number of α groups bound together, owing to the exclusion principle) may, however, spell trouble for an α model.

For the S wave, taking $V_T(r)$ as the full interaction, and using an analysis developed previously [1,4]), with 4 harmonics, it was found that the above parameters do not fit the results. In fact, keeping the other parameters the same, it was found possible to get a reasonable representation of the logarithmic derivative in the range $E = 0$ to 3 MeV (especially for the lower energy part) with $y = 1.00$. This value is thus appreciably different from that found to be the best [4]) for the α—n problem. The latter does, however,

allow some latitude — an analysis of the α—n problem by Massey *et al.* [6]) from a somewhat different viewpoint gave $y = 1.143$ with α, β and A not very different from the present values. The nucleon-nucleon force is still unsaturated. In the sense explained already one may consider $V_{00}(r)$ to represent the integral interaction for the present purposes except perhaps near $r = 3f$. Table 2 gives the first few orders of $V_{n0}(r)$, for $y = 1.00$.

TABLE 2

r	0	1	2	3	4	5
$V_{00}(r)$	0	84.0	44.2	12.7	1.6	
$V_{10}(r)$	0	−2.5	1.4	−6.0	−1.9	
$V_{20}(r)$	0	14.2	12.9	0.0	1.4	
$V'_{D}(r)$	−86.5	−72.6	−42.6	−17.0	−4.2	−0.0
$V_{T}(r)$, $l = 0$	−86.5	11.4	1.7	−4.4	−2.5	−0.0

The above parameters will represent (α, α) scattering up to $E = 1.5$ MeV, when the S wave practically appears alone. Above this energy, one must investigate the requirements of the D wave as well. For the latter, the integral interaction cannot be simplified. To enable the calculation to be made on a desk machine it was decided to select a suitable y, using as first approximation for $f_2(r)$ in the integral term the $f_2(r)$ obtaining for the square well (depth 4 MeV) which was found [1]) to represent the D wave results best (for the present outer radius $5f$) up to $E = 3$ MeV. In this way the integral term is assessed by numerical integration and the logarithmic derivative at $5f$ calculated as for the S waves [1,4]). The calculations also give the second approximation to $f_2(r)$ which may be used to gauge its effect on the integral term and hence on the choice of y. On the first approximation to the integral term, $y = 0.88$ is near the best value up to $E = 3$ MeV. The second approximation will necessitate the choice of a lower value of y. A unique choice for the S and D waves is thus impossible on the above calculation and using the present values for α, β, A. The difference in the value of y for the S and D waves is not large, however, and the former represents the results up to $E = 1.5$ MeV, or up to laboratory energies of 3 MeV. A compromise of the S and D waves on the basis of the present type of calculation may arise with the following refinements:

The lower choice of y for the D waves arises because the "openness" of, for example, $V_T(r)$ for the D wave subjects this partial wave to its very deep, attractive, central core. This eventuality is avoided, by repulsive effects, for the S wave. It may hence be that a repulsive core to the nucleon-nucleon potential, $V(ij)$ in (5), and consequent correlation effects in ϕ and $f_1(r)$ may work for a compromise of S and D wave demands by "filling up" the cores of the interactions.

The present analysis of the α—α problem is of a preliminary nature, and points to its difficulties. With an electronic calculator one may attempt a higher accuracy in the analysis, with a more detailed selection of parameters, and possibly with the introduction of the above refinements. The present analysis demonstrates that, for the final set of parameters it will be useful for the physical interpretation of the kernel, for the S wave especially, to calculate $V_{n0}(r)$ and $V_T(r)$.

References

1) E. van der Spuy and H. J. Pienaar, Nuclear Physics **7** (1958) 397
2) J. Wheeler, Phys. Rev. **52** (1937) 1083, 1107
3) H. A. Bethe, Phys. Rev. **103** (1956) 1353
4) E. van der Spuy, Nuclear Physics **1** (1956) 381
5) A. Herzenberg, Nuclear Physics **3** (1957) 1
6) Massey, Hochberg, Robertson and Underhill, Proc. Phys. Soc A **68** (1955) 746

Nuclear Physics 11 (1959) 625—645; © *North-Holland Publishing Co., Amsterdam*
Not to be reproduced by photoprint or microfilm without written permission from the publisher

THEORY OF RADIATIVE CAPTURE REACTIONS

A. M. LANE

U.K.A.E.A. *Research Group, Atomic Energy Research Establishment, Harwell, Didcot, Berks.*

Received 2 February 1959

Abstract: Starting from an exact dispersion theory, it is shown how cross-sections for capture by various mechanisms may be extracted by appropriate specialisations of the theory. The cross-section for "compound nucleus" capture is derived by the usual assumption of random signs for matrix elements (reduced width amplitudes). It is pointed out that this cross-section reduces to the Weisskopf-Ewing formula that is commonly used only after a second assumption is made, viz. that the density of energy levels of spin I in the final nucleus is proportional to $(2I+1)$. The cross-section for "direct" capture, which has previously been derived phenomenologically, is extracted from the exact formalism by techniques developed by Bloch and by Brown and de Dominicis for treating other kinds of direct reactions. Attention is drawn to the fact that the integrals in the matrix elements of the electromagnetic interaction should be taken to infinity, thereby incorporating a contribution from the channels besides the usual one from the nuclear interior. In the following paper, this channel contribution is shown to be very important in practice.

1. Introduction

Previous discussions of radiative capture have been based upon the compound nucleus model. At low energies (below 4 MeV, say) it is certainly true that most capture reactions proceed through the formation and decay of the compound nucleus. The large cross-sections observed at resonances in low-energy neutron capture are adequate testimony to this. At higher energies, the cross-sections for compound nucleus capture are predicted to be very much reduced by competition from other modes of decay of the compound nucleus. Consequently, at these energies, we must be prepared to find that the cross-sections are dominated by new mechanisms not subject to competition.

The main purpose of this paper is to describe one such mechanism which has been suggested previously on a phenomenological basis by other authors [1–3]). Cohen [1]) remarked that the complex potential model [4]) implies the existence of a new capture mechanism. According to this model, an incident particle moves some appreciable way through a target nucleus before a compound nucleus is formed. During the initial period of free motion in the mean nuclear potential field, the particle may radiate energy in the form of a photon and drop into a bound particle orbit. This process has been termed "direct" or "one-stage" capture, to distinguish it from the

compound nucleus process which is "delayed" or "two-stage". Since no feature of the direct process depends strongly on energy or mass-number, the cross-sections for the process should not vary strongly with these quantities, at least, not below 30 MeV or so. In contrast, the cross-sections for the compound nucleus process are predicted to decrease sharply with increase in either quantity because of the competition. In the experimental results of Cohen [1]) on (p, γ) reactions above 5 MeV, no such decreases were found.

Beck [2]) has set up a quantitative expression to represent the direct capture cross-section on the basis of phenomelogical considerations, and has made some quantitative comparison with experiment. Kursunoğlu [3]) has studied the case when the final orbit is unbound (nuclear bremsstrahlung).

In section 2, a description is given of the essential features of the formalisms used for discussing nuclear reactions. In section 3, expressions are presented for averaged cross-sections for compound nucleus capture ("averaged" signifies averaged over an energy interval containing many levels of the compound nucleus). Most emphasis is on the cases when so many particle channels are open that they can be treated statistically, i.e. cases when the incident energy is greater than a few MeV. (The case when the incident energy is low and only a few particle channels are open has been discussed in a previous paper [5]).)

The compound nucleus contribution to the total capture cross-section is extracted from exact reaction theories by making the customary assumption that nuclear matrix elements (reduced width amplitudes) have random signs. This assumption means that the cross-sections are determined by levels of the compound nucleus near the incident energy, and that other levels do not contribute. The existence of other reaction mechanisms must be associated with partial breakdown in the assumption; thus the problem of extracting the cross-section for direct capture from the exact theories is essentially that of summing over far-away levels. Bloch [6]), and also Brown and de Dominicis [7]) have developed a method for doing this in the case of direct inelastic scattering reactions and, in section 4, we apply their method to the case of direct capture reactions.

2. Formalisms for Discussing Nuclear Reactions

The cross-section for production of final particles α'' and β'' in bombardment of target β' by projectile α' may be written in the form

$$\sigma_{\alpha'\beta',\alpha''\beta''} = \frac{\pi}{k'^2} \sum_{Jl's'l''s''} \frac{2J+1}{(2i_{\alpha'}+1)(2i_{\beta'}+1)} |S^J_{c'',c'}|^2; \qquad (1)$$

k' is the wave-number of relative motion of the initial pair (α', β'), $i_{\alpha'}$ and $i_{\beta'}$

are their spins, s' labels their channel spin: $\mathbf{s}' = \mathbf{i}_{\alpha'} + \mathbf{i}_{\beta'}$, and l' labels their relative angular momentum. The set of quantities $(\alpha'\beta's'l')$ specifying a "channel" is denoted by c'. Similar quantities for the final pair (α'', β'') are denoted with double primes, and those for a general pair (α, β) will be denoted without primes. J labels the total spin of the complete system and $S^J_{c'',c'}$ is the scattering matrix element. The exact reaction theories of Kapur and Peierls [8]) and of Wigner and Eisenbud [9]) prescribe forms for the scattering matrix.

2.1. THE KAPUR-PEIERLS THEORY

These authors give the form

$$S^J_{c'',c'} = \sum_\lambda \frac{A_{\lambda c''} A_{\lambda c'}}{(E_\lambda - \frac{1}{2}i\Gamma_\lambda) - E}. \tag{2}$$

For given spin J, λ labels a set of states of the complete system. The wave-functions of the states will be written $X_{\lambda(JM)}$ where M is the component of the spin J. The states are defined by the conditions:

(i) In each channel c, $X_{\lambda(JM)}$ has the form of outgoing waves at the channel energy ε_c corresponding to the total energy E of the system. If E_α, E_β are the internal energies of α and β,

$$\varepsilon_c = E - E_\alpha - E_\beta. \tag{3}$$

(ii) The $X_{\lambda(JM)}$ are eigenfunctions of the Schrödinger equation of the complete system. If H is the Hamiltonian,

$$HX_{\lambda(JM)} = (E_\lambda - \tfrac{1}{2}i\Gamma_\lambda)X_{\lambda(JM)}, \tag{4}$$

where $E_\lambda - \frac{1}{2}i\Gamma_\lambda$ is the eigenvalue.

(iii) the normalisation of the $X_{\lambda(JM)}$ is

$$(\lambda JM|\lambda JM) = 1 \tag{5}$$

where the left-hand side stands for

$$\int_I [(-)^{J-M} X_{\lambda(J-M)}] X_{\lambda(JM)} \, d\tau,$$

the integration being over the internal region I of configuration space bounded by the channel surfaces. Notice that $(-)^{J-M} X_{\lambda(J-M)}$ is not the same as $(X_{\lambda(JM)})^*$, the time-reversed solution which is obtained from $X_{\lambda(JM)}$ by taking the complex conjugate and multiplying by $-i\sigma_y$ for each particle. This is because of the fact that $X_{\lambda(JM)}$ satisfies complex boundary conditions and is therefore *intrinsically* complex. The first two properties of the $X_{\lambda(JM)}$ imply that

$$(\lambda JM|\lambda' J' M') = 0 \tag{6}$$

if one or more of λ, J, M is not equal to λ', J', M' respectively.

The quantities $A_{\lambda c}$ in (2) are "width-amplitudes", one for each channel c

and level λ. They are defined by

$$A_{\lambda c} = (2P_c)^{\frac{1}{2}}\gamma_{\lambda c} \tag{7}$$

where the "reduced width amplitude" $\gamma_{\lambda c}$ is

$$\gamma_{\lambda c} = (cJM|\left(\frac{\hbar^2}{2M_c a_c}\right)^{\frac{1}{2}}\delta(r_c - a_c)|\lambda JM) \tag{8}$$

and P_c is the barrier penetration factor, whose precise form need not be specified here, and M_c is the reduced channel mass. a_c is the interaction radius for the channel c; i.e. the minimum value of the separation distance r_c of α and β at which they do not interact strongly. $|cJM)$ is the "channel wave-function" for channel $c \equiv (\alpha\beta sl)$; it will also be written as $\chi_{c(JM)}$ when appropriate. It consists of the wave-functions of α and β vector-coupled to spin s, and this in turn vector-coupled to the angular wave functions Y_{lm} of relative motion of α and β to give total spin J, component M.

Finally we remark that the width Γ_λ occurring in (2) and (4) is expressible as a sum over channels c of partial widths $\Gamma_{\lambda c}$:

$$\Gamma_\lambda = \sum_c \Gamma_{\lambda c}. \tag{9}$$

The partial width $\Gamma_{\lambda c}$ is related to the amplitude $A_{\lambda c}$ by

$$\Gamma_{\lambda c} = |A_{\lambda c}|^2 / \int_I |X_{\lambda(JM)}|^2 \mathrm{d}\tau. \tag{10}$$

2.2. THE WIGNER-EISENBUD THEORY

The Wigner-Eisenbud theory is quite equivalent to that of Kapur and Peierls since both are exact. At the same time, each of the two theories has its own merits for certain applications. The Kapur-Peierls theory lends itself especially to the extraction of direct components of reactions; as we shall see in section 4, the equations in the extraction are simpler than with the other theory. On the other hand, it is not clear how the compound nucleus cross-sections may be extracted from the Kapur-Peierls theory, except at low energies where resonance levels are isolated. Using the Wigner-Eisenbud theory and making certain specific assumptions Thomas [10]) has extracted cross-sections of the compound nucleus form. In order to use his results, we shall now give an outline of Wigner-Eisenbud theory.

The set of functions $X^0_{\lambda(JM)}$ in the Wigner-Eisenbud theory corresponding to $X_{\lambda(JM)}$ of Kapur-Peierls are defined by a different boundary condition, namely

$$\left(\frac{\mathrm{d}X^0_{\lambda(JM)}}{\mathrm{d}r_c}\right)_{r_c=a_c} = b_c\left(X^0_{\lambda(JM)}\right)_{r_c=a_c} \tag{11}$$

where the quantities b_c are energy-independent and real, but otherwise arbitrary. It follows that the energy eigenvalue $E_\lambda{}^0$ of $X^0_{\lambda(JM)}$ is real and

energy-independent, as is the amplitude defined by (7). We shall distinguish the various quantities of Wigner-Eisenbud theory by a superscript zero: E_λ^0, $A_{\lambda c}^0$. We note that the fact that the $X_{\lambda(JM)}^0$ and $A_{\lambda c}^0$ are essentially real implies that (10) becomes

$$\Gamma_{\lambda c}^0 = (A_{\lambda c}^0)^2. \tag{12}$$

The disadvantage of Wigner-Eisenbud theory is that the expression for the matrix element corresponding to (2) is complicated, involving some matrix inversion. However, Thomas has shown that, if there is sufficient randomness in the signs of the amplitudes $\gamma_{\lambda c}^0$ to make the non-diagonal elements of the matrix

$$R_{c''c'} = \sum_\lambda \frac{\gamma_{\lambda c''}^0 \gamma_{\lambda c'}^0}{E_\lambda^0 - E} \tag{13}$$

small compared with the diagonal ones, then in this approximation, for $c' \neq c''$,

$$S_{c'',c'}^J = \sum_\lambda \frac{\tilde{A}_{\lambda c''} \tilde{A}_{\lambda c'}}{E_\lambda^0 - E - \frac{1}{2}i\tilde{\Gamma}_\lambda} \tag{14}$$

irrespective of whether the widths $\tilde{\Gamma}_\lambda$ are greater or smaller than the level spacings. In this expression,

$$\tilde{\Gamma}_\lambda = \sum_c \tilde{\Gamma}_{\lambda c} \tag{15}$$

$$\tilde{\Gamma}_{\lambda c} = |\tilde{A}_{\lambda c}|^2 \tag{16}$$

$$\tilde{A}_{\lambda c} = A_{\lambda c}^0/(1 - iP_c\tilde{R}_c) \tag{17}$$

$$\tilde{R}_c = R_c^\infty + i\pi s_c \tag{18}$$

$$R_c^\infty(E) = \int \frac{s_c(E')}{E' - E}\,\mathrm{d}E' \tag{19}$$

$$s_c = \rho\langle(\gamma_{\lambda c}^0)^2\rangle; \tag{20}$$

s_c is the "strength-function" for channel c and $\langle\rangle$ denotes average over levels λ near energy E, ρ is the density of levels λ (always for a given spin J). The above equations have been simplified by setting the parameter b_c in (11) equal to S_c, the shift factor [10]) corresponding to the penetration factor P_c:

$$b_c = S_c. \tag{21}$$

The diagonal elements of the scattering matrix in the same approximation as (14) are, according to Thomas [10]),

$$S_{c,c}^J = \mathrm{e}^{2i\phi_c}\left[-1 + 2\left(1 - \tfrac{1}{2}i\sum_\lambda \frac{\Gamma_{\lambda c}^0}{E_\lambda^0 - E - \frac{1}{2}i\tilde{\Gamma}''_\lambda}\right)^{-1}\right] \tag{22}$$

where ϕ_c is the "hard-sphere phase" and where $\tilde{\Gamma}''_\lambda$ denotes the quantity (15)

minus the contribution from channel c. Wigner [11]) has shown that the average of this quantity over levels λ near E is

$$\langle S^J_{c,c}\rangle = e^{2i\phi_c}[-1+2(1-iP_c\tilde{R}_c)^{-1}]. \tag{23}$$

We notice that

$$1-|\langle S^J_{c,c}\rangle|^2 = 2\pi\langle\tilde{\Gamma}_{\lambda c}\rangle\rho. \tag{24}$$

According to Feshbach, Porter and Weisskopf [4]), the left-hand side of this is essentially the cross-section for compound nucleus formation $\sigma_{c(J)}$ for total spin J in channel c. Specifically,

$$\sigma_{c(J)} = \frac{\pi}{k^2}\,\frac{2J+1}{(2i_\alpha+1)(2i_\beta+1)}\,(1-|\langle S^J_{c,c}\rangle|^2). \tag{25}$$

3. Compound Nucleus Capture Cross-Sections

3.1. GENERAL COMPOUND NUCLEUS CROSS-SECTION

Inserting Thomas' scattering matrix (14) in (1) and averaging over levels λ near energy E with the assumption of random signs for the $A^0_{\lambda c}$ we find

$$\langle\sigma_{\alpha'\beta',\alpha''\beta''}\rangle = \frac{\pi}{k'^2}\sum_J \frac{(2J+1)}{(2i_{\alpha'}+1)(2i_{\beta'}+1)}\,\frac{(\sum_{s'l'} T_{c'(J)})(\sum_{s''l''} T_{c''(J)})}{(\sum_c T_{c(J)})}. \tag{26}$$

This is just the result obtained by Bethe using the same assumption and a scattering matrix of the same form as (14). The quantities $T_{c(J)}$ are transmission factors defined by

$$T_{c(J)} = 2\pi\langle\tilde{\Gamma}_{\lambda c(J)}\rangle\rho_J \tag{27}$$

where we have inserted subscripts J to stress the dependence on the total spin. From (24) and (25) the average cross-section may be expressed in terms of compound-nucleus formation cross-sections by using the relation

$$T_{c(J)} = \sigma_{c(J)}\left(\frac{\pi}{k^2}\,\frac{2J+1}{(2i_\alpha+1)(2i_\beta+1)}\right)^{-1}. \tag{28}$$

In fact, the expression (26) with (28) is essentially that deduced by Weisskopf and Ewing [12]) for compound nucleus cross-sections by starting directly from qualitative properties expected for compound nucleus processes. The fact that the Weisskopf-Ewing formula can be extracted from Wigner-Eisenbud theory as described above was first noted by Thomas [10]).

We are interested in the case when many channels are open so that for each emerging particle α the sum in the denominator of (26) can be written as a sum over integrals over states of the final nuclei β:

$$\sum_{\beta sl} T_{c(J)} = \sum_{sli_\beta}\int_0^{E_{\beta m}^*} dE_\beta^*\,\rho_{i_\beta}(E_\beta^*)\,T_{c(J)} \tag{29}$$

where $\rho_{i\beta}(E_\beta^*)$ is the density of states of the nucleus β at excitation energy E_β^* with spin i_β. The integral is over the range of energies from zero to the maximum allowed energy $E_{\beta m}^* = E - E_\alpha - E_{\beta 0}$, where $E_{\beta 0}$ is the ground state energy of nucleus β.

Usually one observes cross-sections averaged over states β'' in an energy region containing many such states. For the cross-section averaged over final states in this way we write

$$\frac{\mathrm{d}}{\mathrm{d}E_{\beta''}} \langle \sigma_{\alpha'\beta',\alpha''\beta''} \rangle = \sum_{i_{\beta''}} \langle \sigma_{\alpha'\beta',\alpha''\beta''(i_{\beta''})} \rangle \rho_{i_{\beta''}}(E_{\beta''}^*). \tag{30}$$

The only way that has been discovered to eliminate explicitly sums over channel spins and J when (26) is inserted in (30) is on the basis of the assumptions:

(i) $\rho_{i\beta}$ depends on i_β as $\rho_{i\beta} = (2i_\beta+1)\rho_0$ for all β;

(ii) $T_{c(J)}$ is the same for all channel spins s allowed for given l and J by $\mathbf{s}+\mathbf{l} = \mathbf{J}$. Further, $T_{c(J)}$ is independent of all J allowed for given l and i_α, i_β by $\mathbf{l}+\mathbf{i}_\alpha+\mathbf{i}_\beta = \mathbf{J}$.

With these assumptions it is straightforward to show that

$$\frac{\mathrm{d}}{\mathrm{d}E_{\beta''}} \langle \sigma_{\alpha'\beta',\alpha''\beta''} \rangle = \sigma_{\alpha'\beta'} \left(\frac{\dfrac{k''^2}{\pi}(2i_{\alpha''}+1)\sigma_{\alpha''\beta''}\rho_0(E_{\beta''}{}^*)}{\displaystyle\sum_{\alpha\beta}\int \mathrm{d}E_\beta{}^* \frac{k^2}{\pi}(2i_\alpha+1)\sigma_{\alpha\beta}\rho_0(E_\beta{}^*)} \right). \tag{31}$$

In this expression $\sigma_{\alpha\beta}(\varepsilon)$ is the total cross-section for compound nucleus formation when α bombards β with energy ε:

$$\sigma_{\alpha\beta}(\varepsilon) = \frac{\pi}{k^2}\sum_l (2l+1)T_c(\varepsilon). \tag{32}$$

Formula (31) is exactly the result of Weisskopf and Ewing.

3.2. SPECIALISATION TO RADIATION CHANNELS

It can be shown [13]) that the exact reaction theory described in section 2 is applicable to radiation channels. The only difference is that channels are labelled rather differently. If the final nuclear state is μ with spin I, one would normally label channel states by the channel spin defined as the vector sum of I and the intrinsic spin (unity) of the photon. However, a more appropriate label for the photon channels is the total photon spin, i.e. the vector sum $\mathscr{L}$ of the photon intrinsic spin and orbital angular momentum l. The parity $(-)^l$ is also a significant label, but we need not draw attention to this explicitly in the following.

Equation (14) applies when c'' represents a photon channel $(\gamma\mu\mathscr{L})$. The expression for the width amplitude corresponding to (7) and (8) is

$$\tilde{A}_{\lambda c''} = A^0_{\lambda c''} = (2P_{\mathscr{L}}(\varepsilon_\gamma))^{\frac{1}{2}}(\mu I||\mathscr{H}^{(\mathscr{L})}||\lambda J)(2J+1)^{-\frac{1}{2}} \tag{33}$$

where the reduced matrix element on the right is defined by

$$(\mu I||\mathscr{H}^{(\mathscr{L})}||\lambda J) = (2J+1)^{\frac{1}{2}} \sum_{M+\mathscr{M}=i} (JM\mathscr{L}\mathscr{M}|Ii)(\mu Ii|\mathscr{H}^{(\mathscr{L})}_{\mathscr{M}}|\lambda JM). \tag{34}$$

$P_{c''} = P_{\mathscr{L}}$ is a penetration-type factor for photons which need not be specified here, and $\mathscr{H}^{(\mathscr{L})}_{\mathscr{M}}$ is the operator corresponding to photons of multipole order $\mathscr{L}$, component $\mathscr{M}$. We note that, according to (16), the difference between $\tilde{A}_{\lambda c}$ and $A^0_{\lambda c}$ is $O(\Gamma_{\lambda c}\rho)$. For photon channels, this quantity is very small, so one can equate $\tilde{A}_{\lambda c''}$ and $A^0_{\lambda c''}$. The photon width is

$$\Gamma^0_{\lambda c''} = (A^0_{\lambda c''})^2 \tag{35}$$

and we define a transmission factor for photon channels by analogy with (27):

$$T_{c''(J)} = 2\pi\langle\Gamma^0_{\lambda c''(J)}\rangle\rho_J. \tag{36}$$

Making assumptions (i), (ii) above, formula (31) for compound nucleus cross-sections applies to capture reactions. For the production of photons of multipolarity $\mathscr{L}$, one uses (31) with the photon absorption cross-section

$$\sigma_{\alpha''\beta''} = \frac{\pi}{k_\gamma{}^2} \sum_{\mathscr{L}} \tfrac{1}{2}(2\mathscr{L}+1)T_{c''} \tag{37}$$

and with $(2i_{\alpha''}+1)$ replaced by the photon spin multiplicity 2.

For particle channels, assumption (ii) is believed to be quite well founded. In the absence of any arguments to the contrary, the assumption can also be made for photon channels on the basis of analogy. The assumption can be partially justified by the following observations:

(1) The reduced matrix element in (33) is symmetric in states μ and λ; therefore, if it is assumed that $\rho_J = (2J+1)\rho_0$, the transmission factors clearly cannot depend on J for states μ near states λ.

(2) The assumption has the merit of predicting the experimental fact that total capture widths of resonance levels do not depend on J (again assuming that $\rho_J = (2J+1)\rho_0$). This was pointed out by Brink [14]).

The observed data on radiative capture are in the form of measurements of induced activity. These give the cross-sections for capture to all the bound states of the total system by the emission of any number of photons. In order to compare the present theory with these results, one must therefore increase cross-sections computed for capture by single photon emission by the cross-sections for processes in which there are cascades through intermediate unbound states.

4. Direct Capture Cross-Sections

4.1. DIRECT CAPTURE TO INDIVIDUAL FINAL STATES

We may proceed from either the Kapur-Peierls expression (2) or the Wigner-Eisenbud-Thomas expression (14) for the scattering matrix elements. Let us choose the former, and specialise the bombarding particle α' to be a heavy particle and the emerging particle α'' to be a photon.

In order to extract the direct component from the scattering matrix element (2), it is convenient to change the basic set in (2) from the $X_{\lambda(JM)}$ to a new set of functions

$$u_{Nl}(r_c)\chi_{c(JM)} \equiv |NcJM) \tag{38}$$

where c labels states of the *incident* particles α', β' (these form a complete set in themselves), and the single particle functions $u_{Nl}(r_c)$ have the properties:

(i) they satisfy the boundary condition of outgoing waves in all channels like the X_λ;

(ii) they are solutions of the Schrödinger equation in a potential $u_c(r_c)$ which will be specified just below;

(iii) they are normalised by

$$\int_0^{a_c} (u_{Nl})^2 r_c^2 \mathrm{d}r_c = 1. \tag{39}$$

Expanding the $X_{\lambda(JM)}$ in this set:

$$X_{\lambda(JM)} = \sum_{N_c} (\lambda|Nc) u_{Nl}\chi_{c(JM)}, \tag{40}$$

and substituting in the width amplitudes (7) and (33),

$$A_{\lambda c'} = (2P_{c'})^{\frac{1}{2}} \left(\frac{\hbar^2}{2M'a'}\right)^{\frac{1}{2}} \sum_{N'l'} u_{N'l'}(a')(\lambda|N'c'), \tag{41}$$

$$A_{\lambda c''} = (2P_{c''}/(2J+1)^{\frac{1}{2}} \sum_{Nc} (\lambda|Nc)(\mu I||\mathscr{H}^{(\mathscr{L})}||NcJ). \tag{42}$$

Substituting these expressions in the scattering matrix element (2) and using closure to remove the sum over λ,

$$S^J_{c'',c'} = \left(\frac{\hbar^2}{2M'a'}\right)^{\frac{1}{2}} \left(\frac{4P_{c''}P_{c'}}{2J+1}\right)^{\frac{1}{2}} \sum_{NcN'} (\mu I||\mathscr{H}^{(\mathscr{L})}||NcJ) \left(NcJ\left|\frac{1}{H-E}\right|N'c'J\right) u_{N'l'}(a'). \tag{43}$$

It may appear that the development so far is exact. In fact, it is not because we have ignored questions of anti-symmetrisation which arise in connection with the change to the set (38). To avoid a digression at this stage, we give a discussion of this matter in appendix 1. It suffices for the subsequent discussion to quote the result of the discussion, namely that the set (38) should be understood as being anti-symmetrised between the particle state u_{Nl} and the "core" state $\chi_{c(JM)}$.

The basic problem remaining is that of expressing the matrix element of

in $(H-E)^{-1}$ in more suitable form. Both Bloch [6]) and Brown and de Dominicis [7]) suggest procedures for doing this. If H_0 is the Hamiltonian of the product states (38), and V defined as $H-H_0$, then we have the identity

$$\left(Nc\left|\frac{1}{H-E}\right|N'c'\right)=\frac{\delta_{Nc,N'c'}}{E_{Nc}-E}$$
$$-\frac{1}{(E_{Nc}-E)(E_{N'c'}-E)}\left[(Nc|V|N'c')-\left(Nc\left|V\frac{1}{H-E}V\right|N'c'\right)\right]. \quad (44)$$

Following Brown and de Dominicis, for each given c' we may choose the potential $U_{c'}$ to be such that, when $Nc=N'c'$, the last term vanishes for all N when averaged over resonances. Thus a diagonal element averaged over energy is

$$\left\langle\left(N'c'\left|\frac{1}{H-E}\right|N'c'\right)\right\rangle=\frac{1}{E_{N'c'}-E}, \quad (45)$$

and, if we assume that the phases of the matrix elements of V are fairly random, the last term in the square bracket may be neglected in non-diagonal elements which will have the form

$$\left\langle\left(Nc\left|\frac{1}{H-E}\right|N'c'\right)\right\rangle=-\frac{(Nc|V|N'c')}{(E_{Nc}-E)(E_{N'c'}-E)}. \quad (46)$$

Thus the average of (43) is

$$\langle S^J_{c'',c'}\rangle=\left(\frac{\hbar^2}{2M'a'}\right)^{\frac{1}{2}}\left(\frac{4P_{c''}P_{c'}}{2J+1}\right)^{\frac{1}{2}}(\mu I||\mathscr{H}(\mathscr{L})||\varepsilon'c'J) \quad (47)$$

where we have assumed that phase-randomness makes contributions from $Nc\neq N'c'$ negligible, and where $|\varepsilon'c'J)=u_{c'l'}\chi_{c'(J)}$, with the radial wave-function

$$u_{c'l'}(r')=\left(\frac{\hbar^2}{2M'a'}\right)^{\frac{1}{2}}(2P_{c'})^{\frac{1}{2}}\sum_{N'}\frac{u_{N'l'}(a')u_{N'l'}(r')}{\varepsilon_{N'l'}-\varepsilon'}. \quad (48)$$

This is just the solution for the potential $U_{c'}$ at channel energy ε' with normalisation such that the coefficient of the incoming exponential is $(\hbar v')^{-\frac{1}{2}}$ where v' is the bombarding velocity. Thus (47) is just the expression that one would set up phenomenologically to represent direct capture to a given final state.

We note that the expression for the complex potential $U_{c'}$ implied by the condition of Brown and de Dominicis is

$$U_{c'}(r')=(c'|\textstyle\sum v|c')+\left\langle\sum_\lambda\frac{|(c'|V|\lambda)|^2}{E_\lambda-E}\right\rangle \quad (49)$$

where $\sum v$ is the interaction between one particle and the rest. The imaginary (absorbing) part of this is

$$W = \pi\langle|(c'|V|\lambda)|^2\rangle\rho \tag{50}$$

where ρ is the density of levels λ.

Bloch's procedure is to develop the matrix element of $(H-E)^{-1}$ on the assumption that the matrix elements of V in the set (38) have random signs. He assumes that $U_{c'}$ is defined as the first term in (49), i.e. a real potential. The result of this approach can be written in the form (47) with $u_{c'l'}$ defined by (48) except for an energy shift in the denominators

$$\sum_{Nc} \frac{|(Nc|\sum v|N'c')|^2}{E_{Nc}-E_{N'c'}}.$$

This term is closely related to the expectation value of the second term in (49) in the state N', and this means that the results from the two approaches are essentially identical.

The above derivation has been given in the Kapur-Peierls formalism. It can also be given starting from the Wigner-Eisenbud-Thomas expression [13]). If the complete set (38) used in (40) and (43) now satisfy the Wigner-Eisenbud boundary condition (11) then all the subsequent equations follow with the only difference that one has to carry from (14) the factor $(1-iP_{c'}\tilde{R}_{c'})$ which occurs in $\tilde{A}_{\lambda c'}$ in (17). The inclusion of this factor on the right hand side of (48) with the newly defined u_{Nl} means that $u_{c'l'}$ as defined by (48) is again just the solution of the complex potential, at energy ε'.

In connection with (47) we note:

(i) If c' represents neutron channels then for all electric multipoles other than dipole (E1), the matrix element is essentially zero. As is well known, the effective neutron charge for E1 radiation is $-(Z/A+1)e$, where the target contains A nucleons, Z of them being protons.

(ii) If the final state is assumed to be a shell-model state of the form $u_{Nl}\chi_{c(JM)}$ where the orbit Nl is not contained in the target nucleus, the matrix element in (47) becomes $(Nl||\mathscr{H}^{(\mathscr{L})}||\varepsilon'l')$, a single particle matrix element. We notice that, for M1 radiation, this would be zero if $|Nl)$ and $|\varepsilon'l')$ were solutions of the same potential. In fact, their two potentials only differ by iW which is small at low energies so the direct M1 cross-sections may be expected to be correspondingly small.

(iii) if the target nucleus is a shell model state consisting of closed shells and n 'loose' particles in the Nl-orbit, the final nucleus has states of a similar type with $(n+1)$ particles in the Nl-orbit. The matrix element in (47) is then of the type $((Nl)^{n+1}||\mathscr{H}^{(\mathscr{L})}||Nl)^n(\varepsilon'l'))$. When $n = 0$, we have the above example (ii) and the transition is a single particle one. When $n = 2l$, the matrix element can be shown to be equal to the single particle value, when it is evaluated with properly anti-symmetrised wave-functions. (A factor $(2l+1)^{\frac{1}{2}}$ from anti-symmetrisation is just compensated by a factor $(2l+1)^{-\frac{1}{2}}$ from vector-coupling.) When (47) is inserted in (1), the statistical weight

factor implies that the cross-section for $n = 2l$ is $(2l+1)$ times less than that for $n = 0$.

4.2. DIRECT CAPTURE TO ALL BOUND STATES

The most commonly measured experimental quantity is the capture cross-section summed over all bound final states. In order to perform the summation of the above cross-section over such states, it is convenient to expand each final state wave-function $\psi_{\mu(Ii)}$:

$$\psi_{\mu(Ii)} = \sum_{cN} (\mu|cN) u_{Nl} \chi_{c(Ii)}. \tag{51}$$

Inserting this in (47), and carrying out some Racah algebra,

$$\langle S^J_{c'',c'} \rangle = (2P_{c''})^{\frac{1}{2}} \left[\sum_{Nl} U(\mathscr{L} l J s', l' I)(\mu|c'N) \frac{(Nl||\mathscr{H}^{(\mathscr{L})}||\varepsilon' l')}{(2l'+1)^{\frac{1}{2}}} + \sum_{\beta N} (\ldots)(\mu|cN)(Nl|\varepsilon' l')(\beta i_\beta||\mathscr{H}^{(\mathscr{L})}||\beta' i_{\beta'}) \right]. \tag{52}$$

The first term represents direct capture due to a transition of the incident particle to bound single particle states; the second represents direct capture due to transitions of the target nucleus to excited states; (. . .) represents a vector-coupling factor which is of no interest.

Let us ignore the core term for the moment. Inserting the first term of (52) into (1) and summing over J gives

$$\sigma_{\alpha'\beta',\gamma\mu} = \frac{\pi}{k'^2} \sum_{\mathscr{L} l' N l} 2P_{\mathscr{L}} |(\mu|c'N)|^2 |(Nl||\mathscr{H}^{(\mathscr{L})}||\varepsilon' l')|^2 \frac{2I+1}{(2l+1)(2i_{\alpha'}+1)(2i_{\beta'}+1)} (\sum_s 1), \tag{53}$$

where the sum over s is restricted to those allowed by $\mathbf{i}_{\alpha'}+\mathbf{i}_{\beta'} = \mathbf{s}$, $\mathbf{I}+\mathbf{l} = \mathbf{s}$. We have dropped interference terms between different Nl on the grounds that each bound state μ may be assumed to involve an appreciable amount of only one single particle state Nl for each c in (52). This situation is expected because the product states in (52) are expected to be shared out amongst only those states μ in an energy region of the order of the absorption potential $W \approx 2$ MeV †.

Summing (53) over bound states μ and assuming that the function $s_{c'N'}(E_\mu) \equiv |(\mu I|c'NI)|\rho_I$ which will be called the "strength function", is independent of I,

† Here we are implicitly assuming that α' is a nucleon. The absorption potential W is larger for alphas and deuterons and so this statement and others below in this subsection are probably incorrect for these particles. In any case, we note that, for a target nucleus of mass A, charge Z, the effective charges for E1 radiation by alphas and deuterons are

$$e\left(\frac{2Z-A}{A+2}\right), \quad 2e\left(\frac{2Z-A}{A+4}\right)$$

respectively, so that direct capture must be small in light nuclei.

$$\sigma_{\alpha'\beta',\gamma} = \frac{\pi}{k'^2} \sum_{\mathscr{L}l'Nl} |(Nl||\mathscr{H}^{(\mathscr{L})}||\varepsilon' l')|^2 \Big(\int 2P_{\mathscr{L}}(\varepsilon_\gamma) s_{c'N}(E_\mu) \mathrm{d}E_\mu \Big). \qquad (54)$$

From the definition of the above strength function, and the normalisation of states $|\mu I)$ and $|c'NI)$, it follows that

$$\int s_{c'N}(E_\mu) \mathrm{d}E_\mu = 1$$

where the integral is over all energies. In general, the form of $s_{c'N}(E_\mu)$ is a peak about the energy $E_\mu = E_{c'N}$ with a width of the order of twice the absorption potential W. For bound states Nl, $W \lesssim 2$ MeV and so, for states Nl that are not too lightly bound, we may assume that the last equation holds approximately when the integration is restricted to bound state energies. $P_{\mathscr{L}}$ in (54) depends on E_μ through the photon energy $\varepsilon_\gamma = E - E_\mu$. Defining an effective penetration factor $P_{\mathscr{L}N}$ by

$$P_{\mathscr{L}N} = \int P_{\mathscr{L}}(\varepsilon_\gamma) s_{c'N}(E_\mu) \mathrm{d}E_\mu,$$

eq. (54) can be written in the form

$$\sigma_{\alpha'\beta',\gamma} = \frac{\pi}{k'^2} \sum_{\mathscr{L}l'Nl} 2P_{\mathscr{L}N} |(Nl||\mathscr{H}^{(\mathscr{L})}||\varepsilon' l')|^2. \qquad (55)$$

To the approximation that $P_{\mathscr{L}N} = P_{\mathscr{L}}(\varepsilon' - \varepsilon_{Nl})$, this is just the phenomenological expression used by Beck [2]) to estimate direct capture, i.e. the cross-section for radiative capture from an incident wave scattered by a complex potential $U_{c'}$ to bound (unfilled) states of the real potential. It is also closely related to the expression deduced by Brown and Levinger [15]) for the direct photonuclear cross-section.

We now turn to the matter of the neglect of the core terms in (52). It is essential to neglect these to reproduce Beck's expression (55) and we now consider possible justifications for this.

First we notice that, for photon energies $\lesssim 30$ MeV (i.e. bombarding energies $\lesssim 25$ MeV) only E1 processes need be considered, the photon wavelength being larger than the nucleon radius. There are two kinds of argument that may justify neglect of core terms:

(i) The factor $(\mu|cN)(\varepsilon' l'|Nl)$ will decrease with increasing excitation of the final nucleus μ. Furthermore for any state μ, the factor decreases with bombarding energy (see appendix 2 for justification of these remarks). Thus this factor will be small except for transitions to near the ground state at low bombarding energies.

(ii) In all nuclei except certain light ones ($A < 20$), the E1 matrix elements between the ground state and bound excited states are known to be much smaller than the single particle value. One can infer from the extrapolation of the photon-nuclear cross-sections to low energies that the

sum of all transitions (perhaps thousands) from the ground state to bound states is only of the order of a single particle transition. Thus the second term in (52) consists of a sum of very many terms, each much smaller than the single particle value. There is no obvious reason why there should be any coherence in the phases of these terms, and so one may assume that their sum is much smaller than the first (single particle) term in (52).

This argument does not apply to certain light nuclei in which strong E1 transitions have been observed. However there is another argument that can be used in this case. It also applies to the above case as well. Suppose the target state is $\varphi_0(A)$ and the final state is $\varphi_0(A)\mu_{Nl}$ (anti-symmetrised). Now the members of the set of states in the expansion (51) should be considered as anti-symmetrised, according to appendix 1. Thus the expansion (51) applied to the final state $\varphi_0(A)u_{Nl}$ contains only one term, i.e. there is only one core state, $\varphi_0(A)$. There are no terms corresponding to core states $\varphi_0(A-1)u_{Nl}$, and so there are no core terms in (52). Thus the existence of strong observed E1 transitions of the type $\varphi_0(A-1)u_{Nl} \to \varphi_0(A)$ in light nuclei is quite compatible with the neglect of core terms in (52), since such core terms are already included in the first term.

As was mentioned at the end of the previous section, the observed capture cross-sections refer to all processes in which the bound states are produced. Thus the cross-sections computed with (54) for single photon capture should be augmented by those for cascades through intermediate unbound states. Since these states decay preferentially by neutron emission, such corrections will be small if the primary photon spectrum is fairly uniform.

4.3. INCLUSION OF "EXTERNAL" TRANSITIONS

Strictly, the integration in a matrix element $(\mu I||\mathscr{H}^{(\mathscr{L})}||\varepsilon' c' J)$ for capture from an initial free state $|\varepsilon' c' J)$ to a final bound state $|\mu I)$ should be over all space. Previously we have only considered the contribution from the internal region $r' < a'$. For instance, in expressions (47) and (54), the integration is confined to the internal region. In order to include the external or "channel" contribution, the matrix element in (47) must be augmented by a similar term in which the integration is in the external region i.e. through the incident channel. In the channel contribution, $u_{\varepsilon' l'}$ must be replaced by the actual channel wave-function of the bombarding particle. This has the essential asymptotic form:

$$\sim \frac{1}{r'}\left(e^{-i(k'r'-\frac{1}{2}l'\pi)} - S_{\varepsilon',\varepsilon'} e^{i(k'r'-\frac{1}{2}l'\pi)}\right). \tag{56}$$

When resonance levels overlap, which is so above 5 MeV bombarding energy in most nuclei, $S_{\varepsilon',\varepsilon'}$ is a smooth function and can be replaced by its average value. This means that (56) is equal to $u_{\varepsilon' l'}$, the solution of the complex potential which, by its definition, must reproduce the average nuclear scatter-

ing matrix element $\langle S_{c',c'} \rangle$. Thus it follows that, for energies > 5 MeV, the external contribution may be included in (47) simply by extending the range of integration to all space, and normalising the final state μ to unity over all space. When the external contribution is included in the matrix element of the total capture cross-section (54), it causes the matrix element to depend on the energy E_μ, and the new formula † is

$$\sigma_{\alpha'\beta',\gamma} = \frac{\pi}{k'^2} \sum_{\mathscr{L}'Nl} \int \mathrm{d}E_\mu 2P_{\mathscr{L}}(\varepsilon_\gamma) s_{c'N}(E_\mu) |(\widetilde{Nl}||\mathscr{H}^{(\mathscr{L})}||\varepsilon' l')|^2 \qquad (57)$$

where $|\widetilde{Nl}) \equiv \tilde{u}_{Nl} Y_l$ is a modified final particle state extended into the external region:

$$\tilde{u}_{Nl}(r') = \begin{cases} C^{\frac{1}{2}} u_{Nl}(r') & (r' < a') \\ C^{\frac{1}{2}} u_{Nl}(a') \dfrac{e_l(r', \varepsilon'_\mu)}{e_l(a', \varepsilon'_\mu)} & (r' > s'). \end{cases} \qquad (58)$$

Here C is the ratio of the square integral of $\tilde{u}_{N_l}$ in the internal region to that over all space; $e(r', \varepsilon'_\mu)$ is the radial part of the external wave-function of angular momentum l and (negative)energy ε'_μ, the binding energy of state μ. If the strength function $s_{c'N}(E_\mu)$ in (57) is sufficiently localised, then $\tilde{u}_{Nl}(r')$ as defined by (58) becomes essentially equal in all space to the normalised bound state wave-function for the (Nl) orbit.

Another situation in which the external contribution can be included in a simple way is when the bombarding energy is very low and in between resonances. In this case $S_{c',c'}$ in (56) is, from (22) given by

$$S_{c',c'} = \mathrm{e}^{2i\phi_{c'}}[-1+2(1-iP_c R_c^{\infty})^{-1}]. \qquad (59)$$

This is just the scattering matrix that is reproduced by the real part of the complex potential model wave function. Thus, in this case, one should calculate with (57) with the function $\tilde{u}_{c'l'}$ in the external contribution to the matrix element takes as the real part of the solution to the potential.

In the intermediate region between very low energies and the point where levels overlap, there is a correction to be applied to the cross-section computed with the $\langle S_{c',c'} \rangle$. This correction is proportional to $\langle |S_{c',c'} - \langle S_{c',c'} \rangle|^2$, the compound elastic scattering [4]). Fortunately it seems that capture in this intermediate region is always dominated by the compound nucleus process[17]) so that this correction is never of practical importance.

It seems likely that the external contribution to capture may be quite important, and perhaps dominant in some cases. Since neutron wave-functions are not attenuated in the external region by Coulomb barriers one may presume that the external contribution is largest in absolute value for

† In formula (57), the core contribution to the external direct capture is neglected for just these reasons for which it was neglected in the internal direct capture as discussed above.

neutrons. However, the value relative to the internal contribution may be larger for deuterons, since the internal part is very small if the mean free path of deuterons inside the nucleus is very small. In light nuclei, where $N \approx Z$, the effective deuteron charge for dipole radiation is small so that direct capture will be small. In very heavy nuclei, the Coulomb barrier will reduce the external capture. In medium nuclei, however, it seems possible that direct external processes could be dominant in deuteron capture. Verification of this can be achieved by computation and comparison with experimental results.

5. Conclusions

In this investigation, we have examined two types of mechanism for capture reactions. We have extracted the compound nucleus component from exact reaction theory and shown that, subject to certain explicit assumptions, one may use formulae of the Weisskopf-Ewing type for computing compound nucleus capture cross-sections averaged over resonances.

The second mechanism to be examined is that of direct capture which has previously been suggested on phenomenological grounds by Cohen [1]), Beck [2]) and Kurşunoglu [3]). We have shown that the component of the cross-section from this mechanism may be extracted from exact reaction theory using procedures set up by Bloch [6]) and by Brown and de Dominicis [7]) for discussing other types of direct reaction. Our work is closely related to study of the direct component in photo nuclear reactions by Brown and Levinger [15]).

We have presented explicit expressions for cross-sections arising from the two mechanisms. Further discussion can be given only after computations are made, and comparison made with experimental data. This is done in the following paper [17]). An especially interesting matter is the contribution from the external region as discussed in the last section. This contribution occurs even when the strong absorption model of nuclear reactions applies, just as in the case of other types of direct reactions. Since compound nucleus cross-sections decrease sharply with increasing energy, one may assume that, for every nucleus, there exists a critical energy at which the compound nucleus capture cross-section falls to a value below that for direct capture, either internal or external. Above this energy, direct capture dominates.

One expects at higher energies to find a second critical energy at which the type of direct capture we have considered falls off sharply and is succeeded by another type which we can call "two particle" direct capture. The single particle direct capture is appreciable only at energies where there are large amplitudes corresponding to the incident wave-number occurring in the Fourier transforms of the bound state wave-functions. At higher energies,

the process of capture can be considered as the inverse of Levinger's "quasi-deuteron model" of the high-energy nuclear photo-effect [18]). The necessary high momentum components in the final state are not provided by the single particle motion, but by the correlations between the incident particle and individual target particles.

Finally we remark that no mention has been made here of angular distributions of the photons in capture reactions. It is quite straightforward to give expressions for these distributions, but there are no data. In contrast to (pp') and other direct reactions that show forward peaks at moderate energies ≈ 10 MeV, we cannot expect such peaks for capture reactions because the dipole nature of the capture at such energies limits the type of angular pattern. Only when the incident energy rises above 30 MeV or so may interference with other multipoles produce forward peaks.

Appendix 1

THE CONSEQUENCES OF ANTI-SYMMETRISATION

The compound state wave-function X_λ must be anti-symmetrical. The correct definition (8) of the reduced width amplitude for a heavy particle, a proton (say), is

$$\gamma_{\lambda c} = \left(\frac{\hbar^2}{2Ma_c}\right)^{\frac{1}{2}} (\lambda | \sum_i \delta(r_i - a_c) | c) \tag{A1}$$

where i labels protons. The channel wave-function χ_c is (ignoring spins for simplicity)

$$\chi_c = Z^{-\frac{1}{2}} \sum_i (-)^i \varphi_\alpha(-i) \tag{A2}$$

where Z is the number of protons, and φ_α is the internal wave-function of the nucleus α.

The expansion (40) of X_λ in terms of the product wave-functions $u_N \chi_c$ may be understood in two ways:

$$X_\lambda = \sum_{cN} (\lambda | N\alpha)_1 \varphi_\alpha(-Z) u_N(Z), \tag{A3}$$

$$X_\lambda = \sum_{cN} (\lambda | N\alpha)_2 [Z^{-\frac{1}{2}} \sum_i (-)^i \varphi_\alpha(-i) u_N(i)]. \tag{A4}$$

The first of these is a "fractional parentage" expansion with a definite proton, the Z^{th}, in the single particle state and all the rest (denoted by $-Z$) in the core state. The product states are orthogonal, and therefore,

$$\sum_\lambda (\lambda | N\alpha)_1 (\lambda | N'\alpha')_1 = \delta_{N\alpha, N'\alpha'}; \qquad \sum_{N\alpha} (\lambda | N\alpha)_1 (\lambda' | N\alpha)_1 = \delta_{\lambda\lambda'}. \tag{A5}$$

However there is a disadvantage of (A3) that makes it useless for our purposes. This is that the core states α for which $(\lambda | N\alpha)$ are large are numerous

and occur spread over a large energy range. As an example, consider (A3) applied to the shell-model wave-function of F^{17} in its ground state, i.e. $(1s)^2(1p)^6(1d)$. The states α occurring in the sum (A3) arise from the configurations obtained by removing a particle from the closed shells besides that obtained by removing 1d. These configurations cover a large energy range in the core nucleus O^{16}. Correspondingly the particle states N in the sum in (A3) include all bound states. For actual wave-functions of excited states of heavier nuclei, the parent states α cover even larger ranges. The consequence is that in the width amplitude of (A1),

$$\gamma_{\lambda c} = \left(\frac{\hbar^2}{2M_c a_c}\right)^{\frac{1}{2}} Z^{-\frac{1}{2}} \left[\left[\sum_N (\lambda|N\alpha)_1 u_N + \sum_{\alpha' N} (\lambda|N\alpha')_1 \int \varphi_{\alpha'}(-Z)\varphi_\alpha(-i)u_N(Z)\delta(r_i - a_c)\mathrm{d}\tau \right] \right. \quad \text{(A6)}$$

(where $\int \mathrm{d}\tau$ signifies integration over all co-ordinates), the second term is the dominant one. In the example of F^{17}, $Z = 9$, $(\lambda|N\alpha)_1 = 9^{-\frac{1}{2}}$, and the second part of (A6) contributes 8 times the first term.

Now let us consider (A4) in which the product states are anti-symmetrical between the proton and the core. This has the disadvantage that the states are no longer orthogonal:

$$\int \varphi_\alpha(-i)\varphi_{\alpha'}(-j)u_N(i)u_N(j)\mathrm{d}\tau \begin{cases} = \delta_{N\alpha, N'\alpha'} & (i = j) \\ \neq 0 & (i \neq j). \end{cases} \quad \text{(A7)}$$

Therefore the relations

$$\sum_{N\alpha} (\lambda|N\alpha)_2(\lambda'|N\alpha)_2 = \delta_{\lambda\lambda'}, \qquad \sum_{\lambda} (\lambda|N\alpha)_2(\lambda|N'\alpha')_2 = \delta_{N\alpha, N'\alpha'} \quad \text{(A8)}$$

are, at best, only approximately valid, and their approximate justification depends on the extent to which the overlaps (A7) can be neglected when $i \neq j$. As we have seen the overlap terms in (A6) are dominant. However, there is an important difference in the expansion (A4) which makes (A8) a reasonable approximation, viz. the single particle states N which are occupied in the ground state φ_0 of the core nucleus do not contribute appreciably to the sum in (A4). The reason is that the anti-symmetrisation operation in the product states in (A4) effectively eliminates such states. In the example of F^{17}, (A4) becomes

$$X_\lambda = 9^{-\frac{1}{2}} \sum_i (-)^i \varphi_0(-i)u_{1d}(i) \quad \text{(A9)}$$

where φ_0 is the ground state of O^{16}, i.e. there is only one core state α and one particle state N in the sum in (A4). It should be noticed that the set of product states in (A4) is over-complete, a fact which is concommitant with their lack of orthogonality. This means that many such expansions are possible. In the example of F^{17}, one could write

$$X_\lambda = 9^{-\frac{1}{2}} \sum_i (-)^i \varphi_1(-i) u_{1p}(i) \qquad \text{(A10)}$$

where φ_1 is the state of O^{16} with the configuration $(1s)^2(1p)^5(1d)$. This wave-function is identical to (A9). Clearly there are others as well. Thus, in choosing to use (A9), we are adopting the convention that the single particle states in the sum in (A4) are restricted to those that are not filled in the ground state of the core. This convention may be expected to remove much of the ambiguity in the expansion (A4) due to over-completeness, and to justify (A8) approximately. No attempt has been made to estimate the residual corrections. This task appears to be far from easy.

Finally the expression for the width amplitude using (A1) and (A4) is

$$\gamma_{\lambda c} = \left(\frac{\hbar^2}{2M_c a_c}\right)^{\frac{1}{2}} \Big[\sum_N (\lambda|N\alpha)_2 u_N + (\tfrac{1}{2}(Z-1)) \sum_{N\alpha'} (\lambda|N\alpha')_2 \int \varphi_\alpha(-i)\varphi_{\alpha'}(-j) u_N(j) \delta(r_i - a_c) \mathrm{d}\tau\Big]. \qquad \text{(A1)}$$

The second term may be dropped for the same reason that the overlaps (A7) for $i \neq j$ are assumed negligible for product states that contribute significantly to the expansion (A4), i.e. for particle states N that are unfilled in the core, the overlap $\int \varphi_\alpha(-i) u_N(j) \mathrm{d}r_j$ is small.

The essential conclusion of the above considerations is that the expansion (40) in the text should be considered as an expansion in anti-symmetrised product states of type (A4). This is made necessary because the alternative interpretation (A3) leads to a useless expression (A6) for the width amplitude. The disadvantage of (A4) is that the use of closure leading to (43) and the expression

$$\gamma_{\lambda c} = \left(\frac{\hbar^2}{2M_c a_c}\right)^{\frac{1}{2}} \sum_N (\lambda|N\alpha)_2 u_N$$

for the width amplitude are subject to correction terms, which one hopes are small.

Appendix 2

THE MAGNITUDE OF $(\mu/cN)(\varepsilon' l'/Nl)$

From (49), one sees that the overlap $(\varepsilon' l'/Nl)$ decreases away from the energy $\varepsilon' = \mathrm{Re}(\varepsilon_{Nl})$ as $(\varepsilon_{Nl} - \varepsilon')^{-1}$. According to the fine structure interpretation of mountain resonances [16]), for any given product state $\chi_c u_{Nl}$, the "parentage coefficient" (μ/cN) has a maximum for states μ for which $E_\mu = E_\alpha + E_\beta + \mathrm{Re}(\varepsilon_{Nl})$ and falls off away from this value as $[E_\mu - (E_\alpha + E_\beta + \varepsilon_{Nl})]^{-1}$ or possibly even more quickly. Assuming that $\mathrm{Im}(\varepsilon_{Nl})$ has the form indicated by scattering experiments: 2 MeV + 0.5 ε', and that the

binding energies of the states Nl and μ are both ≈ 4 MeV, the overlap product behaves like

$$|(\mu/cN)(\varepsilon' l'/Nl)|^2 \approx [\{(4+\varepsilon')^2+(2+\tfrac{1}{2}\varepsilon')^2\}\{(E_\beta-E_{\beta'})^2+4\}]^{-1}. \quad \text{(A12)}$$

When $\varepsilon' = 10$ MeV, and $E_\beta - E_{\beta'} = 4$ MeV, the value of (A12) is $\frac{1}{5000}$, which is less than the maximum value $\frac{1}{80}$ achieved at $\varepsilon' = 0$, $E_\beta = E_{\beta'}$ by a factor 60. From (A12) one sees that, for a given bombarding energy, the size of contributions in (52) from various core states β drops off with increasing excitation energy. Also, for given core state β, the terms in (52) drops off with increasing bombarding energy.

The particle transition term in (52) contains the factors $[E_\mu-(E_{\alpha'}+$ $+E_{\beta'}+\varepsilon_{Nl})]^{-1}$ $[\varepsilon_{N'l'}-\varepsilon']^{-1}$ where $\varepsilon_{N'l'}$ is the nearest particle level to the energy ε'. Taking the binding of the states μ and Nl to be 4 MeV as above, this becomes $\sim[(\varepsilon_{N'l'}-\varepsilon')\,\mathrm{Im}\,(\varepsilon_{Nl})]^{-1}$. The amplitude fluctuates as the bombarding energy changes but, unlike the above case where Nl is bound, the bombarding energy ε' can coincide with $\varepsilon_{N'l'}$. If this occurs at $\varepsilon' = 0$, 10 MeV, the value of the intensities of the single-particle transition to be compared with the figures $\frac{1}{80}$ and $\frac{1}{5000}$ above are $\frac{1}{16}$ and $\frac{1}{200}$. One sees that at low energies, the factors multiplying the single particle transitions in (52) may be almost as small as those multiplying the core terms. As the energy increases however, they become considerably greater than those multiplying the core terms.

There is an effect which we have ignored so far that tends to reduce even further the factors multiplying the core terms relative to those multiplying the single particle terms. This is the external contribution to the overlap $(\varepsilon' l'/Nl)$. In the above, only the internal contribution is considered in the relation $(\varepsilon' l'/Nl) \propto (\varepsilon_{Nl}-\varepsilon')^{-1}$. If $u_{\varepsilon' l'}$ and u_{Nl} wave solutions of the same potential, and Nl is bound, the overlap $(\varepsilon' l'/Nl)$ taken over all space is zero. In fact, there is a difference in the potentials of the two wave-functions, namely the imaginary part W. Also, as mentioned in the text, when the external contribution is excluded, u_{Nl} should be taken in the external region at the free-wave solution at an energy which need not be the same as ε_{Nl}. However these energies can only differ by $\lesssim W$, so that one may say that the overlap goes to zero with W. Since W is, in fact quite small for bound states ($\lesssim 2$ MeV), the overlap factor $(\varepsilon' l'/Nl)$ that multiplies the core terms in (13) may be assumed to be smaller than estimated above. One may estimate that the reduction is by a factor $WC^{\frac{1}{2}}/[\varepsilon'-\mathrm{Re}(\varepsilon_{Nl})]$ where C is the normalisation factor mentioned in section 4d. It can be neglected except when $|\varepsilon'-\mathrm{Re}(\varepsilon_{Nl})| < 1$ MeV, when it decreases and ultimately cancels the infinity at $\varepsilon' = \mathrm{Re}(\varepsilon_{Nl})$.

References

1) B. L. Cohen, Phys. Rev. **100** (1955) 206
2) F. Beck, Physica **22** (1956) 1164
3) B. Kursunoglu, Phys. Rev. **105** (1957) 1846
4) Feshbach, Porter and Weisskopf, Phys. Rev. **96** (1954) 448
5) A. M. Lane and J. E. Lynn, Proc. Phys. Soc. A **70** (1957) 557
6) C. Bloch, Nuclear Physics **4** (1957) 503
7) G. E. Brown and C. T. de Dominicis, Proc. Phys. Soc. A **70** (1957) 686; *ibid.* 668
8) P. L. Kapur and R. E. Peierls, Proc. Roy. Soc. A **166** (1938) 277
9) E. P. Wigner and L. Eisenbud, Phys. Rev. **72** (1947) 29
10) R. G. Thomas, Phys. Rev. **97** (1955) 224
11) E. P. Wigner, Ann. Math. **53** (1951) 36
12) V. F. Weisskopf and D. H. Ewing, Phys. Rev. **57** (1940) 472
13) A. M. Lane and R. G. Thomas, Revs. Mod. Phys. **30** (1958) 257
14) D. M. Brink, Thesis Oxford (1955) unpublished
15) G. E. Brown and J. Levinger, Proc. Phys. Soc. A **71** (1958) 733
17) Lane, Thomas and Wigner, Phys. Rev. **98** (1955) 693
17) A. M. Lane and J. E. Lynn, Nuclear Physics **11** (1959) 646
18) J. Levinger, Phys. Rev. **84** (1951) 43

2.A.1:
2.E

Nuclear Physics **11** (1959) 646—669; © *North-Holland Publishing Co., Amsterdam*
Not to be reproduced by photoprint or microfilm without written permission from the publisher

ANALYSIS OF EXPERIMENTAL DATA ON NUCLEON CAPTURE REACTIONS

A. M. LANE and J. E. LYNN

U.K.A.E.A. *Research Group, Atomic Energy Research Establishment, Harwell, Didcot, Berks.*

Received 2 February 1959

Abstract: Using expressions derived in the previous paper, estimates are made of capture cross-sections with emphasis on those for capture of 14 MeV neutrons by heavy elements. It is found that the compound nucleus mechanism for capture predicts values several orders of magnitude less than those observed, even after account is taken of the important "photon cascade" contribution. The correct explanation of the data appears to be the "direct" mechanism, which gives order-of-magnitude agreement. Investigation of the structure of the direct E1 integrals shows that the contributions from inside the nucleus are dominated by those from outside. This suggests that direct capture is a "channel" phenomenon, not directly related to the optical model. The same appears to be true of the direct component of photonuclear cross-sections.

1. Introduction

In the preceding paper [1]) theoretical expressions are presented for capture cross-sections by processes of the "compound nucleus" and "direct" kinds. We have used these expressions to make numerical estimates, and the present paper is devoted to presenting these, and comparing them with the experimental data.

The "compound nucleus" process is examined in section 2, and graphs are given of quantities occurring in the evaluation of cross-sections for capture by this process. Comparison with experiment is made in section 3, and it is found that, although certain low-energy data are consistent with the theory, there is a discrepancy of several orders of magnitude in the cross-sections for 14 MeV neutrons on heavy nuclei.

In section 4, results are presented for the direct capture cross-sections, and special attention is given to the contribution to matrix elements coming from the channels. This "channel capture" appears to be the dominant mode of capture at higher energies, and it is in order-of-magnitude agreement with the data. Speculations on the removal of the comparatively small discrepancy that remains are given in section 5, and conclusions are drawn in section 6.

2. Estimates of Cross-Sections for Capture by the Compound Nucleus Process

It is a well-known fact [2]) that the cross-section for capture by the emission of single photons in the bombardment of target β' by projectile α' of energy ε' may be written as

$$\sigma_{\alpha'\beta',\gamma}(\varepsilon') = \sigma_{\alpha'\beta'}(\varepsilon')\frac{\Gamma_\gamma}{(1+x)\Gamma_n} \tag{1}$$

where $\sigma_{\alpha'\beta'}(\varepsilon')$ is the compound nucleus formation cross-section and Γ_γ, Γ_n are the total capture and neutron widths at the compound nucleus excitation energy E^*:

$$\Gamma_\gamma(E^*) = \frac{1}{2\pi\rho_0(E^*)}\int_0^{B_n}\frac{2k_\gamma^2}{\pi}\sigma_{\gamma\mu}(E^*-E_\mu^*)\rho_0(E_\mu^*)\mathrm{d}E_\mu^*, \tag{2}$$

$$\Gamma_n(E^*) = \frac{1}{2\pi\rho_0(E^*)}\int_0^{E^*-B_n}\frac{2k_n^2}{\pi}\sigma_{n\beta}(E^*-E_\beta^*)\rho_0^{(\beta)}(E_\beta^*)\mathrm{d}E_\beta^*. \tag{3}$$

In (1), x is a quantity, $\ll 1$ except in the lighter nuclei, to account for the presence of processes other than neutron emission that compete for the decay of the compound nucleus. We will always set it equal to zero in the following. In (2) and (3), k_γ and k_n are the photon and neutron wave-numbers, and E_μ^*, E_β^* are the excitation energies of the nuclei resulting from γ and n emission respectively. $\rho_0(E^*)$ is such that the level density of the compound nucleus at excitation E^* for levels of spin J is given by $\rho_J(E^*) = (2J+1)\rho_0(E^*)$. The quantity $\rho_0^{(\beta)}(E_\beta^*)$ is similarly defined for levels of spin i_β in the residual nucleus β: $\rho_{i_\beta}(E_\beta^*) = (2i_\beta+1)\rho_0^{(\beta)}(E_\beta^*)$. B_n is the neutron binding energy in the compound nucleus. In all but the lighter nuclei, any final state that is below the neutron threshold will almost invariably decay by photon emission rather than charged particle emission. This is why B_n is chosen as the upper limit in (2). (In the preceding paper, below equation (31), the assumptions underlying the above formulae are discussed.)

2.1. ESTIMATION OF NEUTRON WIDTH

In order to compute Γ_n from (3), the level density $\rho_0(E^*)$ and the absorption cross-section $\sigma_{n\beta}$ must be specified. For the former, one may assume the form [3])

$$\rho_0(E^*) = CU^{-2}\mathrm{e}^{(bU)^{\frac{1}{2}}} \tag{4}$$

where b, C are slowly varying functions of the effective excitation energy U. This is defined as $U \equiv E^*-P$ where P is the pairing energy [3]) of the nucleus. Near any prescribed energy $\bar{U}$, a convenient approximate form of (4) is

$$\rho_0(E^*) = \bar{C}\mathrm{e}^{U/T} \tag{5}$$

where $\bar{C}$, T depend on $\bar{U}$, but not U:

$$\frac{1}{T} = \left(\frac{b}{4\overline{U}}\right)^{\frac{1}{2}} - \frac{2}{\overline{U}}, \tag{6}$$

$$\bar{C} = C\overline{U}^{-2}e^{2+\frac{1}{2}(b\overline{U})^{\frac{1}{2}}}. \tag{7}$$

Eqs. (5), (6) and (7) reproduce the value and slope of (4) at the energy $\overline{U}$.

The neutron absorption cross-section for nuclear ground states $\beta = 0$ is found [4]) to equal the geometrical nuclear area πR^2 at high energies ($kR \gg 1$) and to equal $4\pi/k_n K$ at low energies ($kR \ll 1$) where K is a wave-number corresponding to the nuclear potential well $V = \hbar^2K^2/2M = 42$ MeV. An expression representing these facts to an adequate approximation is

$$\sigma_{n\beta} = \frac{4\pi}{k_n K} + \pi R^2. \tag{8}$$

We will assume that this expression also represents the absorption cross-section for excited states $\beta \neq 0$. (Thomas [5]) has suggested that the absorption cross-section must fall off for highly excited states β to satisfy the requirements of a sum-rule. We assume that this occurs at excitations higher than those considered here.)

Inserting expressions (5) and (8) in formula (3) the neutron width emerges as

$$\Gamma_n(E^*) = \frac{2T_\beta^2}{\pi}\left[\left(\frac{\pi}{T_\beta V}\right)^{\frac{1}{2}} + \frac{MR^2}{\hbar^2}\right]\frac{\rho_0^{(\beta)}(E^* - B_n)}{\rho_0(E^*)}. \tag{9}$$

Here M is the nucleon mass, T_β is the temperature, given by (6), of the nucleus β at energy $E_\beta^* \equiv E^* - B_n$, and the superscript β denotes that the level density $\rho_0^{(\beta)}$ is that of the residual nucleus β. The special case of low maximum neutron energy [6]) where the statistical treatment fails is discussed in appendix 1.

In deriving (3) and (9), it has not only been assumed [1]) that $\rho_{i_\beta}^{(\beta)} = (2i_\beta+1)\rho_0^{(\beta)}$ but also that $\rho_J = (2J+1)\rho_0$. If the former holds but the latter fails, the correct width $\Gamma_{n(J)}$ (say) depends on J; it is given by (9) with $1/\rho_0(E^*)$ replaced by $(2J+1)/\rho_J(E^*)$. The derivation of the basic formula (1) does not depend on ρ_J being proportional to $(2J+1)$ since $\Gamma_{\gamma(J)}/\Gamma_{n(J)}$ is independent of J even if the two widths separately are not.

As an example, in fig. 1, we plot the quantity $\Gamma_{n(J)}\rho_J/(2J+1)$ as a function of neutron energy for the compound nucleus U^{239}. The evaluation has been made using (9) for two choices of the level density parameters b, C occurring in (4). These choices both reproduce the observed level density in U^{239} at the neutron threshold. It is to be noticed that the curves do not depend on the value of B_n.

2.2. THE PHOTON WIDTH

For the level density in (2) one may use (4) or (5). The only factor remaining to be specified is the photon absorption cross-section $\sigma_{\gamma\mu}$. When μ is the ground state ($\mu = 0$), we know from experiment that $\sigma_{\gamma\mu}$ has the form of a peak with width $\gamma \approx 6$ MeV centered at the photon energy $\varepsilon_\gamma = \varepsilon_R$ (say) ≈ 15 MeV [7]). We also know that for $\varepsilon_\gamma < 25$ MeV, the absorption is mainly E1 and that the integrated cross-section for E1 absorption [7]) equals

$$\mathscr{S} = 2\pi^2\hbar e^2 NZ(1+0.8y)/McA \tag{10}$$

where y is the fraction of exchange forces, a quantity to which the value 0.5 is usually assigned. We will now assume that the absorption cross-section for any excited state ($\mu \neq 0$) has the same properties, which we can embody in the equation

$$\sigma_{\gamma\mu} = \mathscr{S}\varepsilon_\gamma f(\varepsilon_\gamma) \tag{11}$$

where the profile function $f(\varepsilon_\gamma)$ satisfies

$$\int_0^\infty \varepsilon_\gamma f(\varepsilon_\gamma)\mathrm{d}\varepsilon_\gamma = 1 \tag{12}$$

and has the form of a peak centred at energy ε_R and of width γ.

The simplest form for $f(\varepsilon_\gamma)$ is perhaps the Cauchy form

$$f(\varepsilon_\gamma) = \frac{\gamma/2\pi\varepsilon_R}{(\varepsilon_\gamma-\varepsilon_R)^2+\frac{1}{4}\gamma^2} \tag{13}$$

with the proviso that $f(\varepsilon_\gamma)$ falls off rather more steeply than (13) at large values of ε_γ, say $\varepsilon_\gamma \geqq 2\varepsilon_R$, in order to avoid a divergence in the integral (12). The observed photonuclear absorption cross-sections appear to be somewhat asymmetric with a sharper fall below the peak than above it. Furthermore the use of (13) with observed values of γ and ε_R leads to predicted values of the radiation widths of slow neutron resonance levels several times larger than those observed. Brink [7]) and Cameron [8]) have compared experimental and theoretical values of these widths. We can fit the observed widths by modifying (13) to the form

$$f(\varepsilon_\gamma) = \frac{\gamma/2\pi\varepsilon_R}{(\varepsilon_\gamma-\varepsilon_R)^2+\frac{1}{4}\gamma^2}\, \mathrm{e}^{a(\varepsilon_\gamma-\varepsilon_R)} \tag{14}$$

for energies $\varepsilon_\gamma \leqq \varepsilon_R$. (We can assume that the normalisation condition (12) is preserved by modification of $f(\varepsilon_\gamma)$ at high energies.) Using Cameron's results [8]), the choice $a \approx 0.3$ MeV^{-1} gives the best overall fit when values of γ and ε_R are chosen to be those observed.

It is debatable whether (13) and (14) constitute a close approximation to the correct function $f(\varepsilon_\gamma)$ for absorption of photons into excited states ($\mu \neq 0$). One might guess that the photonuclear peak tends to flatten out with increasing excitation of the target nucleus. In the absence of concrete

evidence or arguments to the contrary, we will assume that (13) and (14) *do* apply to excited states. Consequently the estimates below of capture cross-sections at higher energies may be in error if this assumption turns out to be wrong. This will be discussed in the next section.

If one could neglect the energy dependence of $f(\varepsilon_\gamma)$ in the range of integration in (2), the maximum value of the integrand will occur at an energy E_m^* (say) determined by the opposing trends of the ε_γ^3 factor and the level density. Referring to the temperature approximation (5), E_m^* will equal B_n, the neutron binding energy, if $E^*-B_n > 3T_m$ and will equal E^*-3T_m otherwise, T_m being the temperature evaluated from (6) at E_m^*. In either case

$$\Gamma_\gamma(E^*) = \frac{\mathscr{S}}{\hbar^2 c^2 \pi^2} \frac{\rho_0(E_m^*)}{\rho_0(E^*)} e^{\frac{1}{T_m}(B_n - E_m^*)} \cdot \left[f(\varepsilon_\gamma)\varepsilon_\gamma^4 \left\{ \left(\frac{T_m}{\varepsilon_\gamma}\right) + 3\left(\frac{T_m}{\varepsilon_\gamma}\right)^2 + 6\left(\frac{T_m}{\varepsilon_\gamma}\right)^3 + 6\left(\frac{T_m}{\varepsilon_\gamma}\right)^4 \right\} \right]_{\varepsilon_\gamma = E^* - E_m^*}. \quad (15)$$

If energies are expressed in MeV, the first factor equals $5.4A \times 10^{-6}$. The neglect of the energy dependence of $f(\varepsilon_\gamma)$ will not cause appreciable error, except possibly for lighter nuclei at excitation energies $E^* \approx \varepsilon_R$ when the energy dependence of $f(\varepsilon_\gamma)$ acts with the ε_γ^3 factor to neutralise the level density factor.

If ρ_J for the compound nucleus is not equal to $(2J+1)\rho_0$ then $\Gamma_{\gamma(J)}$ is given by (15) with $1/\rho_0(E^*)$ replaced by $(2J+1)/\rho_J(E^*)$. As mentioned in the discussion of the neutron width above, this possibility does not prevent the use of (1). More serious is the deviation of ρ_I from $(2I+1)\rho_0$ for the bound (final) states μ of spin I. According to theories of the level density [3], for values of I above a "cut-off" value σ, ρ_I falls below the value $(2I+1)\rho_0$ and is given by

$$\rho_I = (2I+1)e^{-I^2/2\sigma^2}\rho_0. \quad (16)$$

At high energies, the compound states have spins up to a value J_m (say). As we are considering only E1 radiation, we have implicitly assumed that ρ_I for bound states equals $(2I+1)\rho_0$ up to the value $I_m = J_m+1$. If the incident energy is increased, a point will be reached where J_m becomes greater than σ and, this assumption breaks down and the capture cross-section must fall below estimates based on (1). However, we shall see that these estimates are often already much smaller than the observed values, so this matter is not of much practical importance.

In fig. 1, we present results of computations using (9) and (15) for the case of the compound nucleus U^{239}. If the values of b and C in (4) are restricted to reproduce the same level density at the neutron threshold, the computed curves are essentially independent of b, C. The main dependence of the curve is on the binding energy, and this is illustrated by a second curve corresponding to a binding 2 MeV greater than the actual value (4.8 MeV).

2.3. "CASCADE" CAPTURE

So far we have considered the cross-section for capture in which the emission of one photon leads directly to a bound state. The observed cross-sections are based on activity measurements and will include contributions for processes in which two (or more) photons are emitted before a bound state is formed [10]). The cross-section for two photon capture $\sigma_{\alpha',\beta',2\gamma}$ is given by a formula like (1) with Γ_γ replaced by a quantity $\Gamma_{2\gamma}$. One determines $\Gamma_{2\gamma}$ by forming the product of the probability of formation of an unbound state of spin I and excitation $E^{*\prime}$, and the ratio Γ_γ/Γ_n for that state, and then integrating over $E^{*\prime}$ and summing over I. The dependence of the formation probability on I is a complicated one in general if one uses only the assumptions that we have made so far. The new assumption that the maximum angular momentum l_m (say) of the incident particles is much higher than the spin on the target, together with the assumption that $\rho_J = (2J+1)\rho_0$ for the compound nucleus, implies that the formation probability is independent

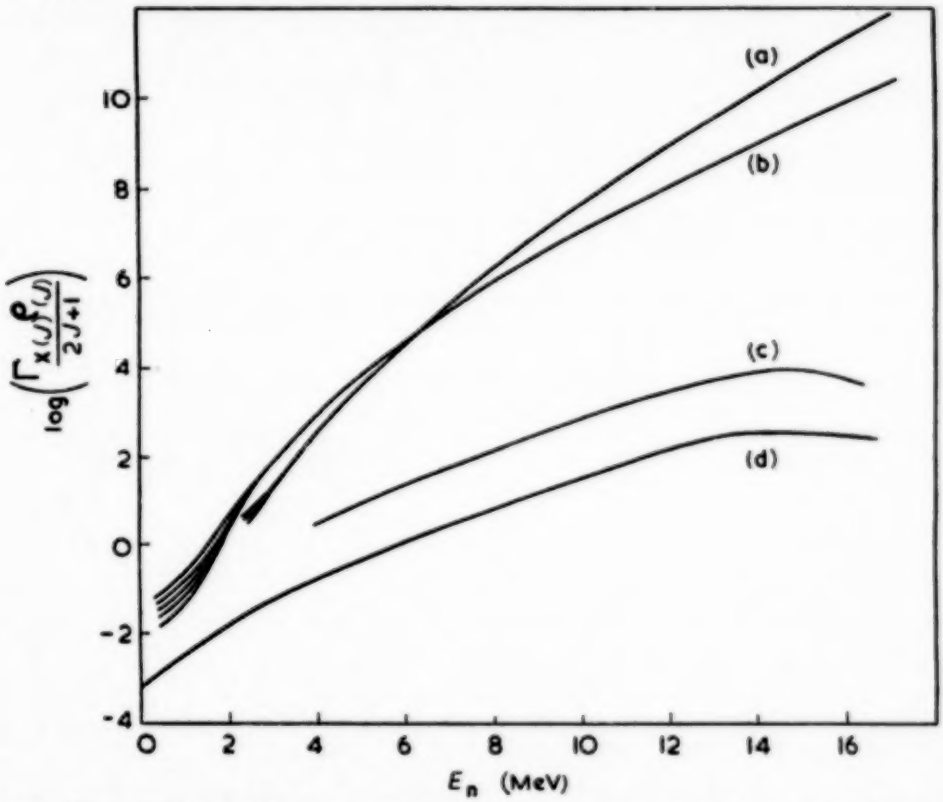

Fig. 1. $\log [\Gamma_{x(J)}\rho_J/(2J+1)]$ as a function of neutron energy. The upper pair of curves (a) and (b) refer to x = n (neutron) and are computed with the level density parameters (a) $b = 104$, $C = (1700)^{-1}$ (Newton [3])), (b) $b = 72$, $c = (64)^{-1}$ (Cameron [12])). These curves do not depend on B_n, the neutron binding. (Notice the dependence on spin J for low energies. From top to bottom the low-energy curves refer to $J = \frac{1}{2}, \frac{3}{2}, \frac{5}{2}, \frac{7}{2}, \frac{9}{2}$.) The lower pair of curves (c) and (d) refer to x = γ (photon). (c), (d) are computed with $B_n = 6$ MeV$+P$, 4 MeV$+P$ respectively where P is arbitrary pairing energy. There is very little dependence on level density parameters provided these give the same density at the neutron threshold and, on changing between the above sets (a) and (b), (c) and (d) are unchanged.

of I for $I \leqq l_m$, and is small for $I > l_m$. It follows that

$$\Gamma_{2\gamma}=\int_{B_n}^{E^*}\frac{d\Gamma_\gamma}{dE^{*\prime}}\left(\sum_{I\leq l_m}\rho_I(E^{*\prime})\frac{\Gamma_{\gamma(I)}(E^{*\prime})}{\Gamma_{n(I)}(E^{*\prime})+\Gamma_{\gamma(I)}(E^{*\prime})}\right)\left(\sum_{I\leq l_m}\rho_I(E^{*\prime})\right)^{-1}dE^{*\prime} \quad (17)$$

where $d\Gamma_\gamma/dE^{*\prime}$ is evaluated from (2) with the upper limit B_n replaced by $E^{*\prime}$. Use of (2) and (10) then give

$$\frac{\sigma_{\alpha'\beta',2\gamma}}{\sigma_{\alpha'\beta',\gamma}}=\frac{\Gamma_{2\gamma}}{\Gamma_\gamma}=\int_{B_n}^{E^*}Q(E^{*\prime})\frac{dE^{*\prime}}{T_m} \quad (18)$$

where this defines $Q(E^{*\prime})$ as a dimensionless quantity

$$Q(E^{*\prime})=\frac{(E^*-E^{*\prime})^3 f(E^*-E^{*\prime})\left[\rho_0(E^{*\prime})\sum_I\rho_I(E^{*\prime})\frac{\Gamma_{\gamma(I)}}{\Gamma_{\gamma(I)}+\Gamma_{n(I)}}\right](\sum_I\rho_I(E^{*\prime}))^{-1}}{\int_0^{B_n}(E^*-E^{*\prime\prime})^3 f(E^*-E^{*\prime\prime})\rho_0(E^{*\prime\prime})dE^{*\prime\prime}}. \quad (19)$$

At energies where $\Gamma_{\gamma(I)}/\Gamma_{n(I)}$ is independent of I (i.e. neutron energies more than a few MeV according to fig. 1), the quantity in square brackets sim-

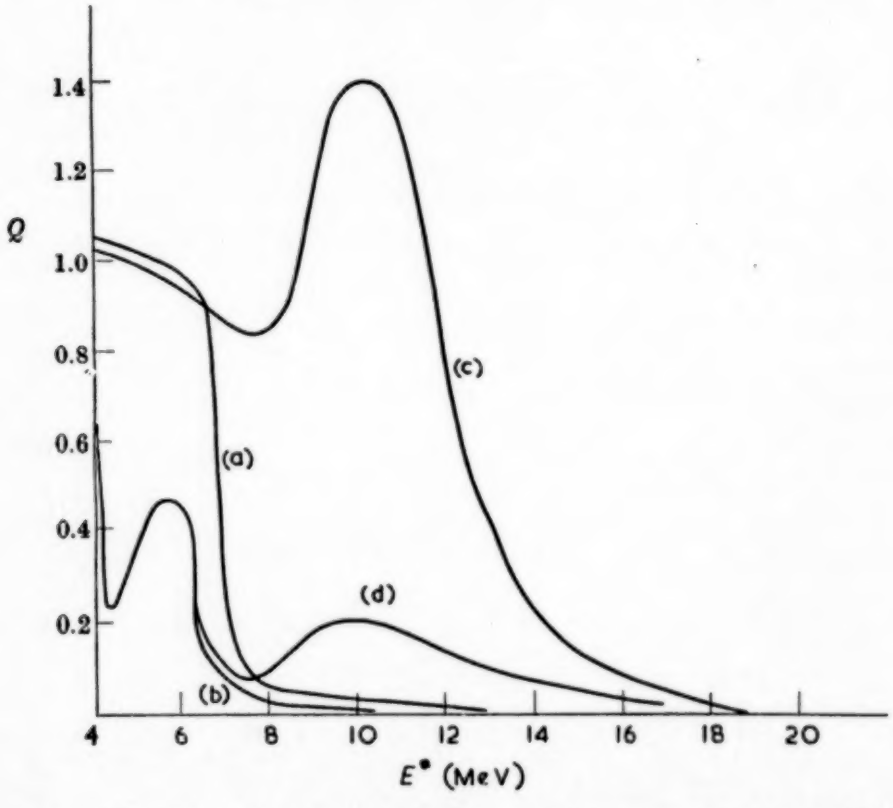

Fig. 2. Q defined by (19) as a function of $E^{*\prime}$, the excitation energy after the emission of the first photon. The area under a curve divided by the temperature T_m gives the ratio of two-photon to one-photon capture. All curves are computed for $B_n = 4$ MeV$+P$. (a) and (c) are computed for bombarding energy 14 and 19 MeV respectively and for level density parameters $b = 104$, $C = (1700)^{-1}$ (Newton [3])). (b) and (d) are the same for level density parameters $b = 72$, $C = (64)^{-1}$ (Cameron [12])).

plifies to $\rho_0 \Gamma_\gamma / \Gamma_n$. The most uncertain element in the evaluation of $Q(E^{*\prime})$ is the dependence of ρ_I on I for large I (i.e. the value of σ in (16)) in the low energy region where $\Gamma_{\gamma(I)}/[\Gamma_{n(I)}+\Gamma_{\gamma(I)}]$ depends on I. (This ratio increases with I to the asymptotic value unity for large I.) Fortunately the maximum error introduced into the estimates of $\sigma_{x'\beta',2\gamma}$ by this uncertainty is usually less than the amount by which the predicted cross-sections are less than the observed ones. In heavier nuclei, for 14 MeV bombarding neutrons the uncertainty is a factor of at most 5 or so. The predicted capture cross-sections are less than those observed by a factor of 10^4; see below.

As an illustration, in fig. 2, we plot Q for the case of neutron capture in U^{238} for two bombarding energies and two choices of the level density parameter b in (4). The value $b = 104$ is taken from the work of Newton [3]) and of Lang and le Couteur [11]); the corresponding cut-off at low energies is deduced from their work as $\sigma \approx 3.5$. The value $b = 71$ is taken from the work of Cameron [12]) with the cut-off value $\sigma \approx 2$. One can see exhibited the qualitative facts that the two-photon capture becomes relatively more important when the incident energy is raised and when the rate of increase of level density (i.e. b) is raised.

3. Comparison of Observed Cross-Sections with Predictions of the Compound Nucleus Theory

The data available † for purposes of the comparison are:

(i) Neutron capture cross-sections on 14 elements at 4 MeV [13]). The cross-sections are 10 mb to within a factor 3 apart from values of 1 mb at closed shells and in light nuclei.

(ii) Similar data at 14 MeV [14]) on 30 elements. For neutron number $N > 40$, the cross-sections are centred around 3 mb with a scatter of a factor of 3. For $N < 40$, they are centred around 0.3 mb (fig. 3).

(iii) The proton capture cross-section in Bi^{209} as a function of proton energy from 6 to 25 MeV [15]). This increases from 10^{-2} mb at 6 MeV to 0.8 mb at 16 MeV (the rise being due to barrier penetration), then it falls off slowly to 0.1 mb at 24 MeV (fig. 4).

We will not concern ourselves with various measurements on neutron capture below 2 MeV where the statistical theory of section 2 does not apply, and nuclei must be treated individually. Qualitatively, the observed values and trends are in accord with compound nucleus theory. In the cases of U^{238} and Th^{232}, quantitative agreement has been demonstrated [6]).

We have made a number of estimates of 4 MeV neutron capture cross-sections using (1), (9) and (14). Although there are differences with experimental values for some nuclei, the discrepancies are never as much as an

† There are also some Ni(p, γ) data that have been examined by Beck [16]).

order of magnitude. Furthermore there is rough agreement with the general trend of values with mass-number. The average predicted values are somewhat lower than those observed, but the inclusion of the cascade contribution $\sigma_{\alpha',\beta',2\gamma}$ will tend to remove this difference. It seems that the compound nucleus theory gives an adequate account of the 4 MeV data, and there is no call for a new reaction mechanism.

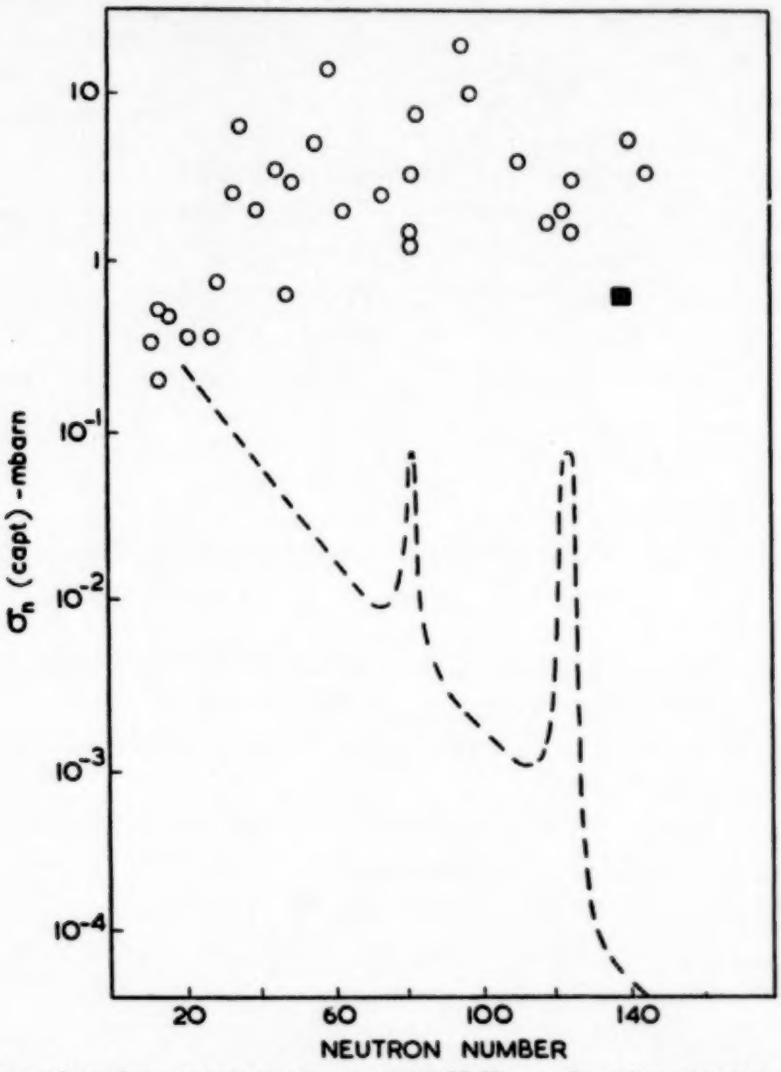

Fig. 3. Cross-sections for neutron capture at 14.5 MeV as a function of neutron number N. The curve is the prediction of compound nucleus theory as described in section 2 using Newton's [3]) level densities. The peaks at magic numbers are due to the anomalously low densities in these regions. The points are experimental values [14]). The point at $N = 135$ is the value predicted by the direct capture theory as described in section 4.

The situation is quite different in respect of the 14 MeV data; it is illustrated in fig. 3. Although the compound nucleus predictions agree with observed values for lighter nuclei ($A < 50$) in order of magnitude (0.5 mb), the observed values become progressively greater than the predicted ones with increasing mass number until, for $A \approx 240$, the discrepancy is about 5 orders of

magnitude. From fig. 2, we see that the inclusion of the cascade contribution may increase the predicted value by as much as an order of magnitude, but this still leaves an enormous discrepancy. Not only do the absolute values from theory and experiment disagree, but the trends with mass number are opposite. The observed values from $A = 50$ to 240 fluctuate in the range 1—10 mb with a slight mean increase with A. The predicted values decrease by 3 or 4 orders of magnitude in the same range.

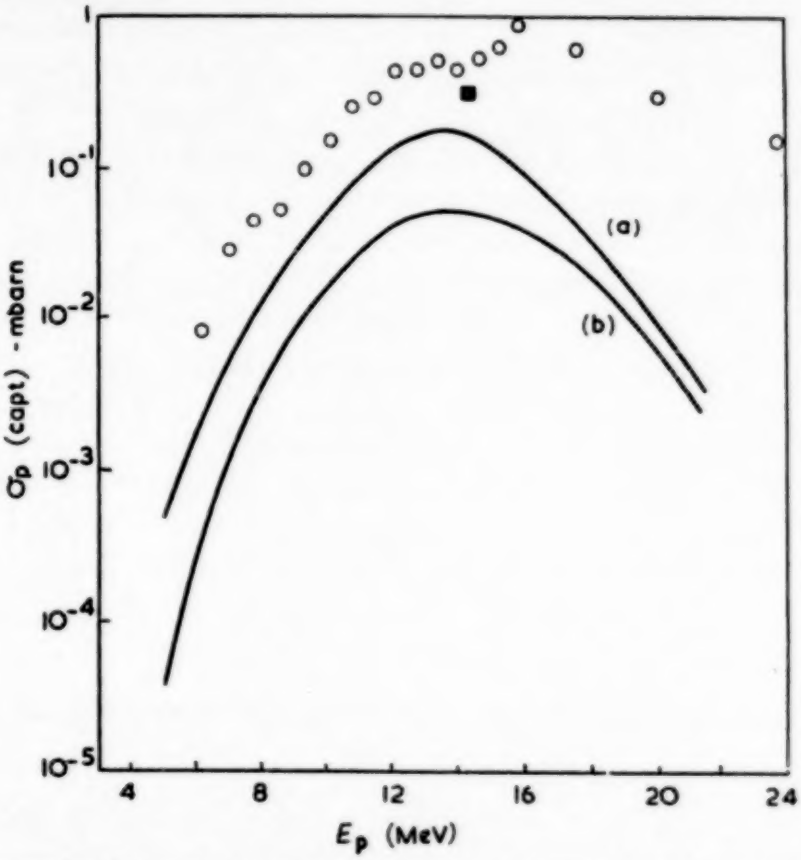

Fig. 4. Cross-section for proton capture in bismuth as a function of proton energy. Curves (a) and (b) are computed with compound nucleus theory using Newton's and Cameron's level density parameters respectively, and the observed proton reaction cross-section [28]). The point at 14 MeV is the prediction of direct capture theory for incident neutrons reduced by the proton penetration factor.

There are, of course, some sources of uncertainty in the theoretical values arising mainly from uncertainty in the level density parameters b, C in (4) and the form of $f(\varepsilon_\gamma)$. Changing b from 104 to 71 in the case of $U^{238}(n, \gamma)$ increases the predicted value by only one order of magnitude. Clearly no reasonable values of b, C can give an increase of the required 3 or 4 orders.

For the form of $f(\varepsilon_\gamma)$ for states near the neutron threshold, we have assumed the same form as is observed for the ground state with a peak at $\varepsilon_\gamma = \varepsilon_R \approx 15$ MeV. Presumably, a more realistic form is one in which the peak is smeared out to some extent. Thus the form that we have used for

$f(\varepsilon_\gamma)$ *over*-estimates the neutron capture cross-sections at 14 MeV bombarding energy.

It is of interest to know at what energy the compound nucleus theory ceases to be able to give a good account of the data. For the case of a heavy nucleus like uranium, one can estimate from fig. 1 that the compound nucleus cross-section falls to the observed 14 MeV value of 3 mb at about 4 MeV. Thus, in heavy nuclei, there is need for a new mechanism at energies greater than 4 MeV; in lighter nuclei, this critical energy is larger.

Referring now to the source (iii) of experimental information, that on the reaction $Bi^{209}(p, \gamma)$ from 6 to 25 MeV, we see in fig. 4 that compound nucleus theory is in order-of-magnitude agreement below 14 MeV, but falls off strongly above this energy whereas the observed cross-section is fairly constant. One can assume that, in a nucleus further from the closed shell Pb^{208}, the discrepancy would be worse since the compound nucleus cross-section is especially large for Bi because the level density is anomalously low.

To summarise, it seems to be established beyond doubt that the compound nucleus theory fails completely to explain high energy (> 10 MeV) capture cross-sections, especially in heavy elements. This is due to the great reduction in compound nucleus cross-sections caused by competition, and to the predominance of some other mechanism which does not involve competition. In the next section, we will investigate certain "direct" mechanisms, and compare with the data on heavy elements where the discrepancies with compound nucleus theories are largest.

4. Estimates of Cross-Sections for Direct Capture

4.1. THEORY

An incident nucleon α', moving in the complex potential field [17]) of the target nucleus β' can make a direct transition to one of the unfilled particle states in the nucleus. Restricting the discussion to electric dipole radiation and using the standard expressions for electromagnetic transition probabilities [18]), the cross-section for capture by such "direct" transitions appears in the form

$$\sigma_{\alpha'\beta',\gamma} = \frac{8\pi\bar{e}^2 M'}{3k'\hbar^2} \sum_{ll'} \left(\frac{\varepsilon_\gamma}{\hbar c}\right)^3 (l+l'+1)|R^{\frac{1}{2}} I_{l'l}|^2; \qquad (20)$$

l' and l label the relative orbital angular momenta before and after the transition, $\bar{e}$ is the effective charge ($-Ze/A$ for a neutron, Ne/A for a proton where Z, N and A are the charge, neutron and mass numbers of the target), M' is the reduced mass, k' is the incident wave-number, ε_γ is the photon energy equal to the difference $(\varepsilon' - \varepsilon_{Nl})$ between the initial and final nucleon energies, R is the nuclear radius and $I_{l'l}$ is the dimensionless dipole integral

$$I_{l'l} = R^{-\frac{1}{2}} \int_0^\infty \psi_{l'}(r) u_{Nl}(r) r^3 \, dr; \tag{21}$$

$u_{Nl}(r)$ is the radial part of the final particle wave-function, normalised by

$$\int_0^\infty (u_{Nl}(r))^2 r^2 \, dr = 1 \tag{22}$$

and satisfying

$$\left(\frac{\hbar^2}{2M} \frac{d^2}{dr^2} + \frac{\hbar^2}{2M} \frac{l(l+1)}{r^2} + V(r) - \varepsilon_{Nl} \right) r u_{Nl}(r) = 0 \tag{23}$$

where $V(r)$ is the real part of the nuclear potential. $\psi_{l'}(r)$ is the radial part of the component of the incident wave of angular momentum l' and satisfies †

$$\left(\frac{\hbar^2}{2M} \frac{d^2}{dr^2} + \frac{\hbar^2}{2M} \frac{l'(l'+1)}{r^2} + V + iW - \varepsilon' \right) r \psi_{l'}(r) = 0 \tag{24}$$

where $W(r)$ is the imaginary part of the nuclear potential; $\psi_{l'}$ has the asymptotic form for large r

$$\psi_{l'} \sim \frac{1}{2ik'r} \left(e^{-i(k'r - \frac{1}{2}l'\pi)} - S_{l',l'} e^{i(k'r - \frac{1}{2}l'\pi)} \right); \tag{25}$$

$S_{l',l'}$ is the scattering matrix element for the l' partial wave. Ignoring the effects of the spin orbit force on the incident wave, $S_{l',l'}$ can be written in the form

$$S_{l',l'} = e^{-2i\phi_{l'}} \left(\frac{f_{l'} - S_{l'} + iP_{l'}}{f_{l'} - S_{l'} - iP_{l'}} \right) \tag{26}$$

where $f_{l'}$ is R times the logarithmic derivative of $r\psi_{l'}$ taken at $r = R$, and $S_{l'}$, $P_{l'}$, $\phi_{l'}$ are the usual shift, penetration and phase factors. In terms of the regular and irregular spherical Bessel functions, $j_{l'}$ and $n_{l'}$, these functions are, for neutrons,

$$S_{l'} = 1 + \rho' \left(\frac{j_{l'} \frac{\partial j_{l'}}{\partial \rho'} + n_{l'} \frac{\partial n_{l'}}{\partial \rho'}}{j_{l'}^2 + n_{l'}^2} \right); \quad P_{l'} = \frac{1}{\rho' (j_{l'}^2 + n_{l'}^2)}; \quad \phi_{l'} = \tan^{-1} \left(\frac{j_{l'}}{-n_{l'}} \right) \tag{27}$$

where the argument of all functions is $\rho' \equiv k'R$.

† In equation (21) the E1 operator $\dot{\mathbf{r}}$ has been replaced by $(\varepsilon' - \varepsilon_{Nl})(i\hbar)^{-1}\mathbf{r}$. When the initial and final states belong to the same potential, the justification for this follows from the relation $[H, \mathbf{r}] = i\hbar\dot{\mathbf{r}}$. In the present problem however, the potentials differ by iW and this suggests that there is a correction to $I_{l'l}$ as given by (21). It is easily seen that the fractional amount of this correction is $(W/\varepsilon_\gamma)(I_{l'l}(r < R)/I_{l'l})$. Since $I_{l'l}(r < R)$ is usually $\ll I_{l'l}$ (see text below), and W is usually $\ll \varepsilon_\gamma$, this correction is unimportant in practice.

Furthermore, one may argue that the correction does not exist. If one derives (20) from dispersion theory [1,24]) instead of phenomenologically, one ends up with the operator $(\varepsilon' - \varepsilon_{Nl})(i\hbar^{-1})\mathbf{r}$. This is true whether one begins with the operator $\dot{\mathbf{r}}$ or $i\omega_{ll'}\mathbf{r}$.

Although formula (20) has been presented as phenomenological one, it can be derived more rigorously from nuclear dispersion theory [1]). In fig. 5, the unfilled orbits available as final states Nl are shown for a selection of nuclei (Schröder's work [19]) on single particle spectra was useful in this connection).

In order to make numerical predictions, the integrals $I_{l'l}$ defined by (21) must be computed. For 14 MeV neutron capture on a heavy nucleus, values

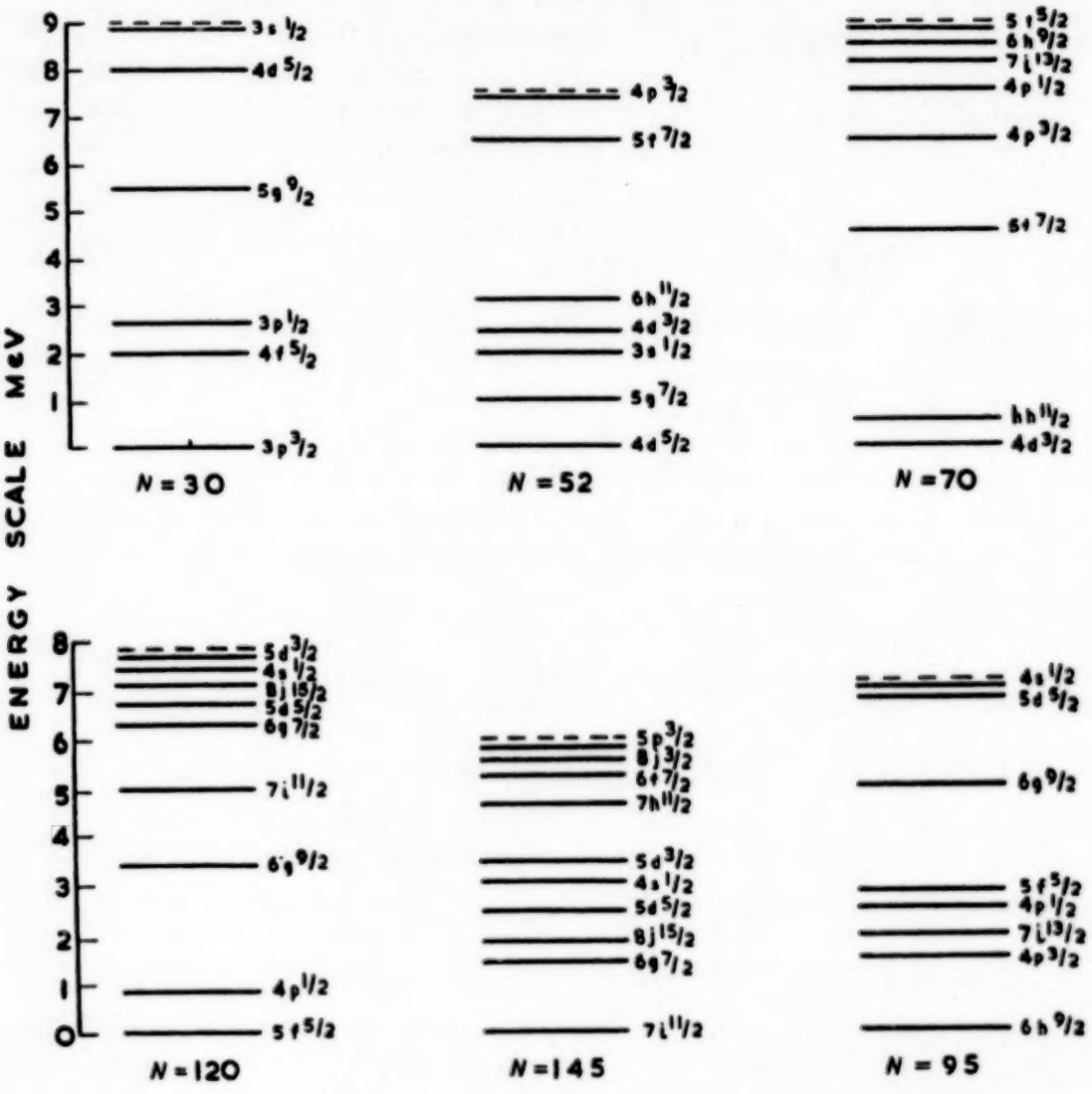

Fig. 5. Spectra of unfilled bound neutron levels in a representative set of nuclei. The dotted lines indicate the top of the potential well and the lowest state shown is the lowest unfilled one.

of l' up to 7 make appreciable contributions to the capture cross-section (20). Even with an automatic computing machine, the computation of all the $\bar{I}_{l'l}$ for a general shape of nuclear potential demands considerable time and expense. Therefore we have based our calculations on a square well. It is clear that, for such a well, the range of integration is naturally divided into

two parts, namely $r < R$ and $r > R$, where R is the radius of the well. The integral $I_{l'l}$ is corresponding composed of two parts:

$$I_{l'l} = I_{l'l}(r < R) + I_{l'l}(r > R) \tag{28}$$

and we now present formulae for these.

The incident wave-function $\psi_{l'}$ inside the nucleus is the solution of (24), and, in the case where the potential is constant for $r < R$, this solution is proportional to $j_{l'}(Kr)$, where K is the (complex) wave number corresponding to the energy $\varepsilon' + |V| + i|W|$. The constant of proportionality is easily found by joining the wave function (25) to $j_{l'}(Kr)$ at $r = R$, and the internal contribution to the integral $I_{l'l}$ emerges as

$$I_{l'l}(r < R) = \frac{-e^{-i\phi_{l'}}(P_{l'}/\rho' R^5)^{\frac{1}{2}} \int_0^R j_{l'}(Kr) u_{Nl}(r) r^3 \, dr}{KRj'_{l'}(KR) - (S_{l'} + iP_{l'} - 1) j_{l'}(KR)}. \tag{29}$$

The final state wave-function is the solution of (23) in $r < R$, and is proportional to $j_l(K_{Nl} r)$ where K_{Nl} is the wave number corresponding to the energy $(|V| + \varepsilon_{Nl})$. The normalisation is given by (22).

In the region $r > R$, u_{Nl} has the form

$$u_{Nl}(r) = \left(\frac{2}{R^3}\right)^{\frac{1}{2}} \theta_{Nl} \frac{h_l(ik_{Nl} r)}{h_l(ik_{Nl} R)} \tag{30}$$

where $h_l(x)$ is the spherical Hankel function and k_{Nl} is the wave-number corresponding to the binding energy $-\varepsilon_{Nl}$ of the state. θ_{Nl} is the dimensionless reduced width amplitude defined by

$$\theta_{Nl} = (\tfrac{1}{2} R^3)^{\frac{1}{2}} u_{Nl}(R). \tag{31}$$

From (25) and (21), it follows that the external contribution to $I_{l'l}$ is

$$I_{l'l}(r > R) = \frac{\theta_{Nl}}{2^{\frac{1}{2}}} [(S_{l',l} + 1) j_{l'l} + (S_{l',l} - 1) i n_{l'l}] \tag{32}$$

where we have introduced the integrals

$$\begin{aligned} j_{l'l} &= R^{-4} \int_R^\infty j_{l'}(k' r) \frac{h_l(ik_{Nl} r)}{h_l(ik_{Nl} R)} r^3 \, dr, \\ n_{l'l} &= R^{-4} \int_R^\infty n_{l'}(k' r) \frac{h_l(ik_{Nl} r)}{h_l(ik_{Nl} R)} r^3 \, dr. \end{aligned} \tag{33}$$

Details of the analytical development of these integrals for purposes of computation is given in appendix 2. One finds that their values fluctuate strongly with l', l and the arguments $k'R$ and $k_{Nl}R$. The combinations

$$\begin{aligned} H_{l'l} &= j_{l'l} \cos \phi_{l'} + n_{l'l} \sin \phi_{l'}, \\ R_{l'l} &= n_{l'l} \cos \phi_{l'} - j_{l'l} \sin \phi_{l'} \end{aligned} \tag{34}$$

do not fluctuate, but have smoothly varying values and are more physically significant: $H_{l'l}$ corresponds to neutrons being scattered by a hard sphere of radius $r = R$ (i.e. $f_{l'} = \infty$), and $R_{l'l}$ corresponds to resonance scattering (i.e. $f_{l'} = S_{l'}$). From (26) and (32),

$$I_{l'l}(r > R) = 2^{\frac{1}{2}}\theta_{Nl}e^{-i\phi_{l'}}\left[\frac{(f_{l'}-S_{l'})H_{l'l}-P_{l'}R_{l'l}}{f_{l'}-S_{l'}-iP_{l'}}\right]. \tag{35}$$

4.2. NUMERICAL EVALUATION OF INTEGRALS

We have considered the case of capture of 14 MeV neutrons by a nucleus rather heavier than lead with radius 8.8×10^{-13} cm, and with the available particle states listed in table 1. Using the above formulae (29) and (32), we computed $I_{l'l}(r < R)$ and $I_{l'l}(r > R)$ for various situations. In table 1, we give representative sets of values. Inserting these values in (20) gives a cross-section of 0.7 mb for the capture cross-section. This is only a factor of 3 or 4 less than the observed value (in contrast to the discrepancy of 10^4 in section 3 with compound nucleus theory). One sees from table 1 that the external region contributes most of the cross-section. (If the integrals $I_{l'l}(r > R)$ are neglected, the cross-section is only 0.1 mb.) We will now consider the assumptions underlying the entries in table 1 and the sources of variation in the numbers given.

TABLE 1

Final state lj	Binding (MeV)	l'	$\lvert I_{l'l}(r < R)\rvert^2\times10^4$	$\lvert I_{l'l}(r > R)\rvert^2\times10^4$
$d_{\frac{3}{2}}$	0.5	1	1.3	4.8
		3	2.1	7.4
$d_{\frac{5}{2}}$	1.5	1	1.3	4.4
		3	2.1	7.0
$j_{\frac{15}{2}}$	2	6	0.4	7.8
		8	1.3	6.0
$g_{\frac{7}{2}}$	3	3	0.9	5.5
		4	1.7	2.4
$i_{\frac{13}{2}}$	4.5	5	0.5	2.6
		7	0.3	9.6
$g_{\frac{9}{2}}$	5	3	0.9	4.8
		4	1.7	2.6

Considering first the integrals $I_{l'l}(r < R)$, these were computed using (26), assuming that the complex potential [17]) scattering the incident particle is:

$$V+iW = -42-i(2+\tfrac{1}{3}\varepsilon') \text{ MeV}. \tag{36}$$

With the square well model that we use, it is not possible to reproduce correctly all the particle binding energies as listed in table 1. In other words, the boundary conditions at $r = R$ for eigenfunctions of the square well cannot agree with all those implied by the binding energies in the table. How-

ever, it emerges from our calculations that, although individual integrals $I_{l'l}(r < R)$ do depend upon choice of boundary condition, the typical value does not. We have evaluated $I_{l'l}(r < R)$ for two extreme cases, namely, in which $u_{Nl}(r)$ and $\mathrm{d}u_{Nl}/\mathrm{d}r$ have zeros at $r = R$. The average values of $I_{l'l}$ and of the cross-section (neglecting the external contribution) are almost the same in the two cases. (The values quoted in table 1 correspond to the condition $u_{Nl}(R) = 0$.)

The magnitudes of the internal contributions in table 1 are surprisingly small. If one approximates the integral $I_{l'l}(r < R)$ by a sum over single particle resonance levels, and assigns conventional single particle radiative widths to these levels, one obtains a value nearly an order of magnitude larger than that obtained by the exact calculation. The reason for this is that there is severe cancellation in the exact dipole matrix elements. For lower l' values, this is expected because of the large number of nodes in the wavefunctions. The only transitions without nodes are of the type $1l' \to 1l$ with $l' = l+1$. For the nucleus we are considering, the values of l for nodeless orbits are 6, 7, so $l' = 7, 8$. Unfortunately, the energies at which these waves are near resonance (i.e. the dipole matrix elements are large) are below the angular momentum barrier. The fact that the potential contains an absorbing part means that no strong resonance effects can develop for energies below the barrier, so the nodeless transitions contribute little to the cross-section.

Turning now to the external integrals $I_{l'l}$ $(r > R)$ given by (35), we have investigated the dependence of these upon the boundary conditions satisfied by the incident waves $\psi_{l'}$ at the nuclear surface $r = R$ i.e. upon the values of $f_{l'}$ in (35). By appropriate choice of V and W, one can consider the following models:

(i) no interaction, $V = W = 0$, $f_{l'} = S_{l'}(k'R)+P_{l'}(k'R)\cot\phi_{l'}(k'R)$; $I_{l'l} = 2i\theta_{Nl}j_{l'l}$;
(ii) hard sphere reflection, $V = \infty$, $f_{l'} = 0$, $I_{l'l} = 2i\theta_{Nl}H_{l'l}$;
(iii) strong absorption [4]), V finite, W large, $f_{l'} = S_{l'}(KR)-iP_{l'}(KR)$;
(iv) weak absorption, V finite, W small, $f_{l'} = S_{l'}(KR)+P_{l'}(KR)\cot\phi_{l'}(KR)$;
(v) moderate absorption [17]), V, W finite.

If $l' > k'R$, the l'th partial wave does not reach the nucleus, and all models give about the same value for $I_{l'l}(r > R)$. It is interesting to observe that, when the integrals $I_{l'l}$ for such waves are inserted in (20), they account for almost half of the cross-section. (Notice the factor $(l+l'+1)$ in (20), which is vital in this respect.) In estimating more conventional cross-sections, one usually neglects these waves.

In table 1, the values of $I_{l'l}$ for waves that reach the nucleus are given for model (i). This may seem rather arbitrary, but the gratifying fact that has emerged from the computations of $I_{l'l}(r > R)$ is that the cross-section is

substantially model independent. Models (ii) and (iii) can be expected to give about the same values of $I_{l'l}(r > R)$ because model (iii) implies a near-node at $r = R$. We have checked that this is so, and found that cross-section for models (ii) (iii) is about 30 % less than that implied by the entries in table 1. Model (iv) gives about the same cross-section as model (i), although individual $I_{l'l}(r > R)$ are different. Clearly model (v) gives values between those of models (ii), (iii) and models (i), (iv).

In principle, values of θ_{Nl} for insertion in (35) can be obtained from the eigenfunctions u_{Nl} using (31). However, as we already saw, the square well that we are using does not give the correct binding energies of individual particle orbits. It will also give errors in individual θ_{Nl}. We have assumed $\theta_{Nl} = 1$ in calculating $I_{l'l}(r > R)$ (more precisely, we have assumed $\theta_{Nlj} = (2j+1)/2(2l+1)$ allowing for the fact that the particle states in table 1 are spin-orbit-coupled). It is known that this is true to within 20 % for all potential wells and binding energies of interest.

5. Further Considerations of Direct Capture

In the last section, we considered the direct capture of neutrons by a heavy nucleus in terms of transitions to discrete single particle states of a square well. The cross-section, which came mostly from the region $r > R$, was estimated as about 0.7 mb which is about 4 times smaller than the observed value. With this discrepancy in mind, we consider some necessary generalisations of the model.

5.1. "SMEARING" OF FINAL PARTICLE STATES

In nuclei the final particle states u_{Nl} do not exist as actual eigenstates of the system. Rather each state is shared between the actual eigenstates in an energy region about the energy ε_{Nl}. According to the fine structure interpretation of giant resonance phenomena [20]), this region has width $2W$, where W is the absorption potential. This smearing affects the estimates of section 4. The dipole phase space factor $\varepsilon_\gamma{}^3$ in (20) takes continuously varying values instead of discrete ones, and $I_{l'l}(r > R)$ must be evaluated for all binding energies up to some maximum value corresponding to the ground state. To estimate the effects of smearing, we have assumed that the energy smearing of state Nlj is given by a Cauchy (resonance) form centred on ε_{Nlj}. Repeating the calculations of section 4, with the single particle states listed in table 1. the new cross-section is about 40 % less than the previous one when W is taken as 2 MeV. This is due to serious fractions of the states being displaced upwards into the unbound region which does not contribute to observed capture. However, we must also consider the displacement of fractions of unbound levels downwards into the bound region. When this is done, the new cross-section is almost the same as the old one. (These remarks are still true when the external contributions are neglected.)

It is of considerable interest to enquire what happens when W is allowed to become large, and particle states are completely smeared out. (This corresponds to the "strong interaction" or "continuum" theory [4]).) Since the incident wave is strongly attenuated inside the point $r = R$, $I_{r'l}(r < R)$ becomes essentially zero. However, the external contribution $I_{r'l}(r > R)$ persists. It is easy to compute. For a given final bound state μ, the capture cross-section is given by (20), with $I_{r'l}(r > R)$ given by (32) or (35), θ_{Nl} being replaced by the width amplitude θ_μ for the state μ. The total capture follows on summing over μ, using the value for the strength function that is implied by the continuum theory:

$$\langle \theta_\mu^2 \rangle \rho_\mu = \frac{1}{\pi K R} \left(\frac{\hbar^2}{M R^2} \right)^{-1} \tag{37}$$

where ρ_μ is the density of states μ.

The result is that the value of the capture cross-section is almost the same as in the opposite extreme model of section 4 where it was assumed that no smearing occurs. Thus one can justifiably refer to direct capture cross-sections as *essentially independent of the nuclear absorption properties.* The reason for this is that the major contributions to the integrals $I_{r'l}$ come from $r > R$ where no absorption can occur, i.e. from the channels. We can refer to the direct capture as "channel capture". Although we introduced the discussion of direct capture in section 4 in terms of the complex potential model, *the existence of the channel contribution does not depend on the validity of this model, and must always be taken into account.* (This is clear from the formal introduction of the channel contribution in the preceding paper [1]).)

5.2. "ROUNDING" OF EDGE OF POTENTIAL

The "smearing" just discussed does not alter the value of the cross-section, so we still have a discrepancy of a factor 4 or so between the observed cross-sections (3 mb) and the predicted value (0.7 mb). We suggest that this may be due to our having used a square well instead of the more realistic "rounded" well in our calculations. It is fairly clear that rounding the edge of the well will increase the cross-section. First there is less reflection at $r = R$, so more incident particles enter the nucleus and the value of $I_{r'l}(r < R)$ rises. With the square well, the cross-section neglecting channel contributions is only 0.1 mb. It seems very unlikely that the decrease in reflection will raise this to the observed 3 mb, especially at 14 MeV where the reflection is not very strong anyway. (Also the absorption potential in the interior is fairly high at this energy.) A more important effect of rounding the potential is to increase the surface or channel contributions. Not only do the exponential tails of the bound states attenuate less rapidly when the potential is extended outwards, but also some partial wave components of the incident wave are

enhanced near $r = R$. For instance, those waves with impact parameters rather larger than R will be increased. (We have seen that these contribute about half of the cross-section.) A mean increase of 50 % in the wave-function amplitudes will be enough to increase the cross-section by the desired factor of 4.

Of course, when the potential is rounded, the value $R = r$ separating the "internal" and "external channel" regions becomes uncertain to the extent of the surface thickness. If R is taken at the outer edge of the potential, it will probably be no longer true that $I_{l'l}(r > R)$ is larger than $I_{l'l}(r < R)$ so it cannot be said that the major contribution comes from the channels. However, it seems very likely that the major contribution always comes from outside the mid-point of the potential and, in this sense, the direct capture is a "channel" phenomenon.

5.3. EFFECT OF CHARGE ON THE INCIDENT PARTICLE

In section 4, the incident particle was assumed to be a neutron. If it were a proton, the channel capture for a given partial wave l' will be reduced in proportion to the probability of finding the incident particle near the edge of the nucleus i.e. to the barrier penetration factor. The cross-sections for compound nucleus capture is decreased by the same factor, so the ratio between the two cross-sections is about the same as for incident neutrons exciting the same system at the same total energy. If we estimate the proton direct capture cross-section in Bi^{209} (fig. 4) at 14 MeV by multiplying the neutron cross-section by the penetration factor, the resulting value, 0.2 mb is in reasonable agreement with observation.

For deuterons and alphas, the direct capture is relatively smaller because of the smallness of their effective charges for E1 radiation. For these composite particles there may be special forms of direct capture involving partial break-up before capture occurs [21]).

5.4. EFFECT OF VARYING THE BOMBARDING ENERGY

Let us assume for the moment, that for each incident l' wave that reaches the nucleus (i.e. for $l' < k'R$) there are always final bound states of $l = l' \pm 1$ which can be produced by dipole radiation. From our calculations of $I_{l'l}$ $(r > R)$, we find that, in these conditions, $\sum_{ll'}(l+l'+1)|I_{l'l}|^2$ depends on incident energy as $1/\varepsilon'$. From (20), it follows that the direct capture cross-section tends to increase with energy as $(\varepsilon'+4)^3/\varepsilon'^{\frac{1}{2}}$, where we have replaced the photon energy ε_γ by the mean value $\varepsilon'+4$ MeV. In fact, such an increase is inhibited by the fact that the l-values of the bound orbits are restricted. For a well-depth of 42 MeV, this can be expressed roughly by $(l+1) \leqq R$ (in 10^{-13} cm). Thus, the cross-section will fall away from the above energy-dependence for energies above that at which the partial wave $l' = R$ (in 10^{-13} cm) reaches the nucleus. Using $l' \leqq k'R$, this energy is about 20 MeV

in all nuclei. Because of this effect, we find that the cross-section at 35 MeV is reduced by about 75 %. This overcompensates the above energy dependence between 20 and 35 MeV and causes a net decrease in this range.

5.5. EFFECT OF CHANGING THE TARGET NUCLEUS

From our calculations, we find that $\sum_{ll'}(l+l'+1)|I_{l'l}|^2$ depends on R as R^{-2}. Let us assume that the incident energy is less than the critical value of 20 MeV mentioned just above, then, from (20), since the effective neutron charge is $-Ze/A$, and $R \propto A^{\frac{1}{3}}$, the capture cross-section depends on the target nucleus like $\sigma \propto Z^2/A$. This dependence is in reasonable agreement with the observed trend at 14 MeV [14]). (The somewhat large values observed near $A = 60$ are probably due to the larger binding energies in this region which increase the $\varepsilon_\gamma{}^3$ factors and the number of final states.)

6. Conclusions

The only previous attempt to make a detailed fit to a high energy capture cross-section is that of Beck [16]), who has made estimates for the case of the $Ni^{60}(p, \gamma)$ Cu^{61} reaction up to 22 MeV. With compound nucleus theory, he found that the cross-section at 20 MeV was 100 times less than the observed value. However, Beck did not allow the photon strength function to vary in the way indicated by the photonuclear peak [8]), and also he did not consider the contribution from cascade processes. Both these effects tend to remove the discrepancy. In the case of the heavier elements that we have considered, the situation is more clear-cut and there is no doubt of the existence of a large discrepancy between compound nucleus theory and experiment.

In considering the direct capture cross-section Beck neglected the external contribution and found that the internal contribution gave a value of about 0.25 mb compared with the experimental one of about 0.8 mb. The theoretical value is larger than one would have guessed from our value of 0.1 mb from exact calculation for heavy nuclei, but it may be that there is less cancellation in matrix elements in lighter nuclei because the number of nodes is smaller. Another important point is that the nucleon binding energy is large in the region $A \approx 60$, so that the $\varepsilon_\gamma{}^3$-factors are larger and there are more final particle states available. These considerations should not affect the ratio of internal and external contributions and, from our work described above, it seems reasonable that the discrepancy between Beck's cross-section and the observed one is due to his neglect of the channel contribution. Attention was first drawn to the possible importance of this contribution by Thomas [22]) in the case of thermal neutron capture. The present paper shows it to be important for other situations as well.

At this point it is appropriate to repeat our most important result, that most of the observed nucleon capture cross-section at energies greater than a

few MeV is attributable to the contribution to direct capture † from the channels, and is essentially model independent, in particular independent of the validity or otherwise of the complex potential model in the internal region. In contrast, the contributions to the direct capture integrals from $r < R$ depend critically on the validity of the complex potential model; in fact, the formal extraction [1]) of this part of the direct capture integrals from dispersion theory is only possible if the complex potential model is valid in the sense of the intermediate coupling model [20]) being correct.

Brown and Levinger [21]) have considered the formal extraction of the direct photonuclear cross-section from dispersion theory, and they assumed implicitly without numerical checks that the internal direct contribution accounts for the experimental data. From our present calculations, we would disagree with this result and suggest that most of the observed direct photonuclear particles *can be explained in terms of the contributions to the dipole integrals from the channels, and have little to do with the complex potential model in the internal region.* For the case of Pb^{208}, we have computed the necessary channel matrix elements and found that the cross-section from the channels is about 5 % of the total absorption cross-section at the peak energy, while the internal direct contribution is about an order of magnitude less.

Another situation in which the present work has significance is that of the study of gamma-ray lines resulting from thermal neutron capture. It has been observed many times that individual transitions in various nuclei have properties quite unlike those expected on the compound nucleus picture. Use of the idea of direct capture enables these anomalies to be understood and will be the subject of a further paper [23]). We remark here just that the dominance of channel contribution is very pronounced in this situation because of the very strong reflection of low energy particles by the nucleus.

Finally we comment on capture cross-sections at very high energies (> 40 MeV). Just as the compound nucleus cross-section falls off above about 4 MeV to be dominated by the channel direct cross-section, so we expect that the channel direct cross-section will fall off (at energies above 40 MeV) to be dominated by other mechanisms. In this paper we have considered only dipole radiation, and this is probably reasonable up to 20 MeV or so. Above this energy quadrupoles and other multipoles become significant, and ultimately the multipole expansion ceases to be useful, and one must use the

† It is important to realise that the statement that the main contribution to direct capture comes from the channels is a mathematical statement about the properties of the integrals of the operator $\mathbf{r}$. It does *not* imply that the physical process of direct photon emission occurs mainly outside the nucleus, because such processes cannot be localised in the quantal description that we are using. The truth of this can be immediately exhibited by changing to the operators $\dot{\mathbf{r}}$ or $\ddot{\mathbf{r}}$, which are equally good E1 operators. The relative contribution from outside the nucleus is quite different with these operators; in fact, in the case of $\ddot{\mathbf{r}}$, which is equivalent to ∇V, there is no contribution. (We are indebted to Drs. G. E. Brown and J. S. Levinger for discussions on this point.)

operator $\mathbf{p}\exp(i\mathbf{k}_\gamma\cdot\mathbf{r})$ where $\mathbf{p}$ is the nucleon momentum and $\hbar\mathbf{k}_\gamma$ the photon momentum. It is clear that matrix elements of this operator between the initial states of free particle momentum $\hbar\mathbf{k}'$ and the final bound states of momentum $\hbar\mathbf{k}_{Nl}$ will fall off when $|\mathbf{k}'-\mathbf{k}_{Nl}-\mathbf{k}_\gamma|$ increases, i.e. when the incident energy becomes much larger than the bound state energies. When the direct capture falls off, the internal contribution will tend to dominate since the internal wave-functions have higher momentum components (corresponding to the nuclear well depth of 40 MeV). Above incident energies of 40 MeV this contribution will also fall off, and capture will only proceed by virtue of high momentum components in the bound state wave-function i.e. because of two-body correlations between particles. In other words, the capture cross-section will be dominated by processes which are just the time-reverse of those described by Levinger in his quasi-deuteron model [25]) of the high energy photo-effect.

We are grateful to Mr. E. B. Fossey for programming some of the integrals.

Appendix 1

THE NEUTRON WIDTH FOR LOW MAXIMUM NEUTRON ENERGIES

Formula (9) for the neutron width cannot be considered reliable at arbitrarily low energies because of the failure of the level density formulae (4) and (5) when applied to the residual nucleus. From (6), it can be seen that, below a certain critical energy $\overline{U}_\beta = 64/b$, the temperature T increases with decreasing energy. (At the critical energy, $T = 32/b$.) This illustrates the fact, which is also clear from the derivation [3]) of (4), that (4) is incorrect for $U_\beta < \overline{U}_\beta$. In any case, even if (4) were still reliable in this region, the above formulae will be unreliable because they depend on the assumption that the level density of the residual nucleus β as a function of spin i_β is proportional to $(2i_\beta+1)$. Actually it is proportional to $(2i_\beta+1)\mathrm{e}^{-i_\beta^2/2\sigma^2}$, where σ is a cut-off. As the energy U_β falls, so does σ, so that the assumption steadily breaks down. This means, amongst other things, that Γ_n begins to depend on J, the spin of the compound state. In this situation, the basic formula (1) is wrong since a summation over J has been performed to arrive at it. It must be replaced by one that contains a sum over J and factors $\Gamma_{\mathrm{n}(J)}$. For the estimation of $\Gamma_{\mathrm{n}(J)}$ at low energies we adopt the following procedure. Above the energy $U_\beta = 2\overline{U}_\beta$, chosen rather arbitrarily, we will assume that (9) is valid, with the implication that Γ_n does not depend on J. For the lowest energies, we will drop the statistical treatment of the nucleus β, and compute $\Gamma_{\mathrm{n}(J)}$ directly from the experimentally determined levels and spins. (This was the procedure adopted by Lane and Lynn [6]) is fitting capture cross-sections below 1 MeV.) Between the two energy regions, $\Gamma_{\mathrm{n}(J)}$ will

be computed by interpolating between the two computed values with an exponential law: $\Gamma_{n(J)}(E^*) = Ae^{E^*x}$, where A, x are constants.

Appendix 2

RECURRENCE RELATIONS FOR INTEGRALS

We are concerned with the evaluation of

$$J^{(n)}_{l'l} = i^{-l}\int_R^\infty j_{l'}(k'r)r^n h_l(ikr)r^2\mathrm{d}r,$$

$$N^{(n)}_{l'l} = i^{-l}\int_R^\infty n_{l'}(k'r)r^n h_l(ikr)r^2\,\mathrm{d}r$$

for the case $n = 1$ (dipole), $l' = l\pm 1$. These integrals are simply related to those defined by (33) in the text.

Use of the recurrence relations

$$j_{l-1}(\rho)+j_{l+1}(\rho) = \frac{2l+1}{\rho}\,j_l(\rho),$$

$$h_{l-1}(i\rho)+h_{l+1}(i\rho) = \frac{2l+1}{i\rho}\,h_l(i\rho)$$

leads to the results

$$J^{(1)}_{l+1,\,l} = \frac{2l+1}{k'}J^{(0)}_{l,\,l} - J^{(1)}_{l-1,\,l},$$

$$J^{(1)}_{l-1,\,l} = -\left(\frac{2l-1}{k}\right)J^{(0)}_{l-1,\,l-1} + \frac{2l-3}{k}J^{(0)}_{l-2,\,l-2} - J^{(1)}_{l-2,\,l-2}.$$

Also, on using the free wave differential equation satisfied by the spherical Bessel functions, the recurrence relation for $J^{(0)}_{l,l}$ emerges as

$$J^{(0)}_{l,\,l} = -(2l-1)\frac{R}{kk'}\,i^{-(l-1)}h_{l-1}(ikR)j_{l-1}(k'R) - J^{(0)}_{l-2,\,l-2}.$$

The integrals $J^{(0)}_{0,0}$, $J^{(0)}_{1,1}$, $J^{(1)}_{0,1}$ and $J^{(1)}_{1,2}$ must be computed directly, then these relations enable one to determine $J^{(1)}_{l\pm1,\,l}$, $J^{(0)}_{l,\,l}$ for any l. Precisely analogous relations apply to the integrals $N_{l'\,l}$. We have made machine computation of the various integrals. Since each integral depends on four variables, two discrete (l and l') and two continuous kR and $k'R$, the results cannot be presented in any simple way.

References

1) A. M. Lane, Nuclear Physics **11** (1959) 625
2) For example, J. M. Blatt and V. F. Weisskopf, Theoretical Nuclear Physics (John Wiley, New York, 1952) p. 340
3) T. D. Newton, Can. Jour. Phys. **34** (1956) 804
4) H. Feshbach and V. F. Weisskopf, Phys. Rev. **76** (1949) 1550

5) R. G. Thomas, Phys. Rev. **97** (1955) 224
6) A. M. Lane and J. E. Lynn, Proc. Phys. Soc. A **70** (1957) 557
7) J. S. Levinger and H. A. Bethe, Phys. Rev. **78** (1950) 115
8) D. M. Brink, Oxford Thesis (1955) unpublished;
H. Morinaga, Phys. Rev. **101** (1956) 100
9) A. G. W. Cameron, Can. Jour. Phys. **35** (1957) 1021
10) A. Zucker, Oak Ridge Conference on Heavy Ion Physics (May 1958)
11) J. M. B. Lang and R. J. Le Couteur, Proc. Phys. Soc. A **67** (1954) 585
12) A. G. W. Cameron, Can. Jour. Phys. **36** (1958) 1040
13) I. Hofman, Proceedings of the Moscow Conference on Nuclear Physics (November 1957)
14) M. Perkin, O'Connor and Coleman, Proc. Phys. Soc. A **72** (1958) 505
15) E. Kelly, UCRL-1044 (1950) unpublished
16) F. Beck, Nuclear Physics **9** (1958/59) 140
17) Feshbach, Porter and Weisskopf, Phys. Rev. **96** (1954) 448
18) Ref. [2]), page 583
19) A. Schröder, Nuovo Cimento **7** (1958) 461
20) Lane, Thomas and Wigner, Phys. Rev. **98** (1955) 693
21) E. Henley, private communication
22) R. G. Thomas, Phys. Rev. **84** (1951) 1061
23) A. M. Lane and J. E. Lynn, to be published
24) G. E. Brown and J. S. Levinger, Proc. Phys. Soc. A **71** (1958) 733
25) J. S. Levinger, Phys. Rev. **84** (1951) 43
26) Andre *et al.*, Phys. Rev. **101** (1956) 645

1.D.2:
3.C

Nuclear Physics **11** (1959) 670—674; © *North-Holland Publishing Co., Amsterdam*
Not to be reproduced by photoprint or microfilm without written permission from the publisher

EINE BEMERKUNG ZUR QUADRUPOLWECHSELWIRKUNGS-ENERGIE IN μ-MESONENATOMEN

J. VON BEHR und H. MARSCHALL
Physikalisches Institut der Universität Freiburg i. Br.

Eingegangen am 13. März 1959

Abstract: The calculation of the influence of a deformed nucleus on the fine structure of meson-atomic spectra requires a model of the charge distribution. The usual model involves an additional surface charge on a spherical nucleus. A more realistic, but still simplified model, represents the nucleus as a spheroid with constant charge density. It is pointed out that the differences between the two models are of the same order of magnitude as the relativistic corrections of the quadrupole-energy.

1. Einleitung

Bei der Berechnung der Quadrupol-Wechselwirkungsenergie in Mesonenatomen muß das von den Elektronenatomen übernommene Rechenschema im allgemeinen in zweifacher Hinsicht modifiziert werden:

1) Die Beschreibung eines zu festem F gehörigen Zustandes des Gesamtsystems Kern-Meson durch weitere Quantenzahlen I, j der Teilsysteme ist nicht mehr zulässig.

2) Die Schematisierung der Quadrupolwechselwirkung durch $Q_0/2r^3$, wo Q_0 das „intrinsic" Quadrupolmoment des Kerns bedeutet, ist nicht mehr statthaft.

Die gemeinsame Ursache für beide Behauptungen ist die bei den Mesonenatomen auftretende Verkleinerung der Bahnradien: Die nichtdiagonalen Elemente $\langle IK, j; F|H_Q|I'K, j'; F\rangle$ der „Quadrupoloperators" H_Q können so groß werden, daß sie bei der Diagonalisierung des Gesamtoperators

$$H = H_{\text{Kern}} + H_{\text{Meson}} + H_Q$$

nicht mehr vernachlässigt werden dürfen. Die Folge ist dann eine — unter Umständen sehr starke — Vermischung der zu verschiedenen I gehörigen Kernzustände einerseits und der zu verschiedenen j gehörigen Mesonenzustände andererseits [1, 2]). Überdies erfordert die Kernnähe des umlaufenden Mesons die Berücksichtigung des Quadrupolpotentials im Gesamtbereich $0 \leqq r \leqq \infty$. Nach dem Vorbild früherer von A. Wheeler durchgeführten Rechnungen [3]) geschieht dies durch die Schematisierung des Quadrupol-

potentials

$$W(r,\vartheta) = \tfrac{1}{2}eQ_0P_2(\vartheta)f(r) \quad \text{mit} \quad f(r) = \begin{cases} r^{-3} & \text{für } r \geqq R \\ r^2/R^5 & \text{für } r \leqq R, \end{cases} \tag{1}$$

wobei der *deformierte Kern* durch ein homogen geladenes Rotationsellipsoid mit dem (intrinsic) Quadrupolmoment Q_0 repräsentiert wird. Im kerneigenen Koordinatensystem sind r, ϑ die Koordinaten des Aufpunktes (vergl. auch Fig. 1). Die Beschreibung des Potentials durch (1) ist aber an die Voraus-

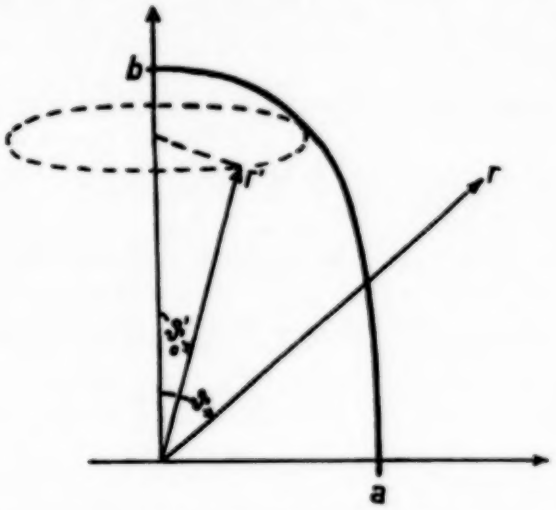

Fig. 1. Definition der Koordinaten r, ϑ und r', ϑ'. Liegt r' im Bereich $a \leqq r' \leqq b$, so existiert jeweils ein Schnittpunkt von r' mit dem Kernellipsoid, welcher den Winkel ϑ'_0 definiert.

setzung des *hinreichend schwach deformierten Kerns* geknüpft: Beschreibt man diesen nämlich durch die volumengleiche Kugel des Radius R, bei welcher Q_0 durch fiktive Oberflächenladungen erzeugt wird, so erhält man gerade (1) für den Quadrupolanteil des Potentials. Diese weitere Simplifizierung des bereits stark vereinfachten Kern-Ellipsoid-Modells ist für stark deformierte Kerne in Mesonenatomen nicht mehr zu rechtfertigen; anstelle von (1) muß der vollständige Potentialverlauf des Ellipsoids zur Darstellung der Wechselwirkung Kern-Meson benutzt werden. Sobald eine Spektroskopie der Quadrupoleffekte in den Spektren von Mesonenatomen möglich wird, ist es wichtig, die durch die Wheelersche Schematisierung bedingten Abweichungen von genaueren Rechnungen abzuschätzen. Dies soll im folgenden für die konkreten Fälle des $_{90}Th^{230}$- und $_{72}Hf^{176}$-Kerns geschehen.

2. Das Quadrupolpotential des stark deformierten Kerns

Ist $\rho(\mathbf{r}')$ die Protonendichte, so lautet der Quadrupolanteil des Potentials allgemein

$$\varphi(r,\vartheta) = eP_2(\vartheta)[r^2\int_r^\infty r'^{-3}\rho(\mathbf{r}')P_2(\vartheta')\mathrm{d}\tau' + r^{-3}\int_0^r r'^2\rho(\mathbf{r}')P_2(\vartheta')\mathrm{d}\tau'], \tag{2}$$

wo r, ϑ die Koordinaten des Aufpunktes, r', ϑ' diejenigen des Integrationspunktes sind †. Für $r \to \infty$ enthält (2) die wohlbekannte Definition des (intrinsic) Quadrupolmomentes

$$\varphi(r, \vartheta) \sim \frac{1}{r^3} P_2(\vartheta) \tfrac{1}{2} e Q_0, \quad Q_0 = 2 \int_0^\infty r'^2 \rho(\mathfrak{r}') P_2(\vartheta') \mathrm{d}\tau'. \tag{3}$$

Notieren wir anstelle von (2)

$$\varphi(r, \vartheta) = \tfrac{1}{2} e Q_0 P_2(\vartheta) F(r) \tag{4}$$

mit

$$Q_0 F(r) = 2[r^2 \int_r^\infty r'^{-3} \rho(\mathfrak{r}') P_2(\vartheta') \mathrm{d}\tau' + r^{-3} \int_0^r r'^2 \rho(\mathfrak{r}') P_2(\vartheta') \mathrm{d}\tau'], \tag{4a}$$

so werden (1) und (4) für $r \to \infty$ identisch : $F(r) \equiv f(r) = 1/r^3$, wie man unmittelbar mit (3) folgert.

Zur Berechnung von $\varphi(r, \vartheta)$ und Q_0 bemerken wir, daß bei dem homogen geladenen Kernellipsoid die Bereiche $r' < a$ und $r' > b$ keinen Beitrag liefern. In dem Zwischenbereich $a \leqq r' \leqq b$ existiert für festgehaltenes r' (vergl. Fig. 1) jeweils ein Winkel $\vartheta'(r') = \vartheta'_0$, bis zu welchem

$$\rho = \frac{Z}{\frac{4}{3}\pi a^2 b} = \text{const.} \quad (a \leqq b, a \leqq r' \leqq b) \tag{5}$$

gilt. Damit werden die Winkelintegrationen und anschließend die Radialintegrationen elementar durchführbar. Für Q_0 folgt unter Berücksichtigung von (5)

$$Q_0 = \tfrac{1}{15} 8\pi\rho a^2 b(b^2 - a^2) = \tfrac{2}{5} Z(b^2 - a^2). \tag{6}$$

Die Darstellung des Potentials geschieht ebenfalls durch elementare Funktionen, das Resultat wird jedoch recht unübersichtlich. Für das eingangsgenannte Beispiel des $_{90}\mathrm{Th}^{230}$-Kerns zeigt Fig. 2 den Verlauf von $F(r)$.

Unsere besondere Aufmerksamkeit gilt nun dem Einfluß des Vorzeichens von Q_0 auf das Quadrupolpotential: Als Folge der eingangs erwähnten Vermischung mehrerer Kernzustände ist die Bestimmung des intrinsic Quadrupolmomentes — ebenso wie bei der Coulombanregung — auch für solche Kerne möglich, welche im Grundzustand $I = 0$ haben. Im Gegensatz zur Coulombanregung erhält man aber überdies das Vorzeichen von Q_0, und für die quantitative Auswertung eines Mesonenatomspektrums wird daher der Vorzeicheneinfluß von Q_0 auf $F(r)$ von Interesse. Bei einem Kern des Volumens $V = \frac{4}{3}\pi a^2 b$ mit dem Quadrupolmoment Q_0 und der Protonenzahl Z, bedeutet ein Vorzeichenwechsel von Q_0 eine Abänderung der Halbachsen a, $a(< b)$ und b in die neuen Halbachsen a', $a'(> b')$ und b'. Setzt man nun,

† Eine strenge Behandlung des homogen geladenen Rotationsellipsoids in elliptischen Koordinaten gibt S. Flügge [6]).

wie dies gewöhnlich geschieht $a' = b$, $b' = a$, so verletzt man die Volumenkonstanz — nach (6) ändert Q_0 nicht nur sein Vorzeichen, sondern auch seinen Betrag — was bei schwach deformierten Kernen gerechtfertigt ist. Bei stark deformierten Kernen ist jedoch auf die Volumenkonstanz zu achten, d.h. bei der Vorzeichenumkehr von Q_0 ist auf die Nebenbedingung $a^2b = a'^2b'$ zu achten und als Folge wird dann $a' \neq b$ und $b' \neq a$. So ergeben sich für zwei Kerne, die abgesehen von dem Vorzeichen von Q_0 identisch sind, verschiedene Radialfunktionen $F_+(r)$ bezw. $F_-(r)$ des Quadrupolpotentials, im Gegensatz zu der vereinfachten Darstellung (1), wo $f(r)$ für $\pm Q_0$ dasselbe bleibt.

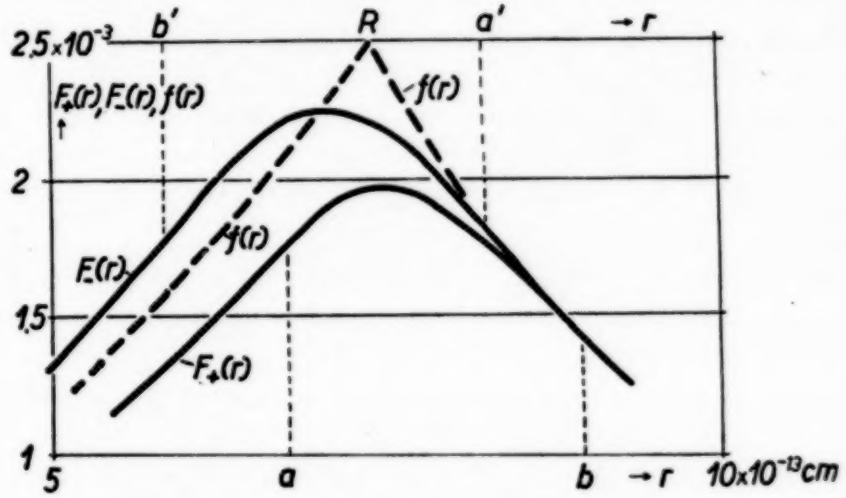

Fig. 2. Die Radialabhängigkeit des Quadrupolpotentials. Für $Q_0 > 0$ — Radialfunktion $F_+(r)$ — hat der Kern die Halbachsen a, a, b; für $Q_0 < 0$ — Radialfunktion $F_-(r)$ — die Halbachsen a', a', b'. Die Volumengleichheit beider Kerne ist durch $a^2b = a'^2b'$ garantiert. Die Wheelersche Schematisierung von Q_0 durch eine volumengleiche oberflächengeladene Kugel des Radius R wird durch $f(r)$ beschrieben. Im einzelnen ist für ${}_{90}\mathrm{Th}^{230}$, $|Q_0| = 12.2$b, $a = 6.7$, $b = 8.88$, $a' = 8.25$, $b' = 5.85$ jeweils in Einheiten von 10^{-13} cm.

Für ${}_{90}\mathrm{Th}^{230}$ mit $Q_0 = 12.2$ zeigt Fig. 2 die mit (4) gewonnenen Radialfunktionen $F_+(r)$ und $F_-(r)$. Für $Q_0 > 0$ sind die Halbachsen a, b aus (6) und mit Hilfe der volumengleichen Kernkugel $R^3 = r_0{}^3A = a^2b$, $r_0 = 1.2 \times \times 10^{-13}$ cm gewonnen. Die für $Q_0 < 0$ verbindlichen Halbachsen a', b' folgen unter Einhaltung der Volumenkonstanz. Die gestrichelte Kurve entspricht der Schematisierung (1). Asymptotisch verhalten sich alle drei Radialfunktionen definitionsgemäß wie r^{-3}. Für $r < a$ bezw. $r < b'$ erhält man Parabeln proportional r^2 mit verschiedenen Proportionalitätsfaktoren.

Für die quantitative Auswertung der Spektren benötigt man die Quadrupolaufspaltung, zu deren Berechnung man die eingangs erwähnten Matrixelemente $\langle IK, j;\ F|H_Q|I'K, j';\ F\rangle$ des Operators

$$H_Q = -e\varphi = -\tfrac{1}{2}e^2Q_0P_2(\vartheta)F(r) \qquad (7)$$

kennen muß. Den Arbeiten [1, 2]) von Wilets und Jacobsohn entnimmt man Proportionalität der Matrixelemente zu

$$\langle j|F(r)|j'\rangle = \int_0^\infty \chi_j(r)F(r)\chi_{j'}(r)\mathrm{d}\tau, \tag{8}$$

wo $\chi_j(r)$ den Radialanteil des Mesonenzustandes beschreibt. Geschieht die Berechnung der Integrale (8) mit den Wasserstoffeigenfunktionen (Ersetzung der Elektronen- durch die Mesonenmasse) des 2P-Zustandes, dann findet man für deren Verhältnis bei den durch $F_+(r)$ und $F_-(r)$ unterschiedenen Fällen von $Q_0 = \pm 12.2$ b für ${}_{90}\mathrm{Th}^{230}$ rund 1.06. Für den ${}_{72}\mathrm{Hf}^{176}$-Kern mit $Q_0 = +8.2$ b wurde (8) mit der Wheelerschen Radialfunktion $f(r)$ und mit $F_+(r)$ berechnet. Für das Verhältnis beider Integrale findet man wieder 1.06.

Für eine genauere Rechnung hat man natürlich — wie es Fitch und Rainwater [4]) sowie Flügge und Zickendraht [5]) getan haben — für die $\chi_j(r)$ relativistische Eigenfunktionen zu verwenden. Nach Wilets bringt dies gegenüber den Schrödingerfunktionen eine Reduktion des Integrals (8) um etwa 6 %. Etwa dieselbe Verkleinerung bringt aber nach den obigen Angaben für den ${}_{72}\mathrm{Hf}^{176}$-Kern gerade der Übergang von dem durch (1) dargestellten Quadrupolpotential zu dem hier benutzten Potential (4), so daß nur die gleichzeitige Benutzung beider Korrekturen sinnvoll erscheint.

Schließlich sei darauf hingewiesen, daß zwischen den Quadrupolpotentialen (1) und (4) auch ein begrifflicher Unterschied existiert: Bei der Wheelerschen Schematisierung kann das durch den Kernradius beschriebene Kernvolumen unabhängig von Q_0 geändert werden, bei der hier gewählten Beschreibung bringt eine Abänderung des durch a und b beschriebenen Kernvolumens im allgemeinen auch eine Veränderung von Q_0 mit sich, da dieses wegen (6) durch die geometrischen Größen a, b festgelegt ist. Während so im ersten Fall Kernvolumen- und Quadrupoleinfluß auf das Spektrum getrennt diskutiert werden können, darf dies bei stark deformierten Kernen ohne Abänderung der Ladungsdichte nicht mehr geschehen.

Literatur

1) L. Wilets, Mat. Fys. Medd. Dan. Vid. Selsk. **29**, No. 1 (1954)
2) B. A. Jacobsohn, Phys. Rev. **96** (1954) 1637
3) A. Wheeler, Phys. Rev. **92** (1953) 812
4) V. L. Fitch und J. Rainwater, Phys. Rev. **92** (1953) 789
5) S. Flügge und W. Zickendraht, Z. f. Phys. **143** (1953) 1
6) S. Flügge, Z. f. Phys. **130** (1951) 159

2.L *Nuclear Physics* 11 (1959) 675—686; © *North-Holland Publishing Co., Amsterdam*
Not to be reproduced by photoprint or microfilm without written permission from the publisher

POLARISATIONSEFFEKTE BEI DER MOTT-STREUUNG

H. SCHOPPER
Institut für Kernphysik, Mainz

Eingegangen am 16. Februar 1959

Abstract: A complete verification of the theory for electron scattering by nuclei can only be performed if at least three quantities are observed: the differential scattering cross section, the electron polarization *perpendicular* to the scattering plane and the change of an initial polarization *in* the scattering plane.

Only the first two experiments have been performed up to the present time. However, in the light of the parity experiments it seems now feasible to observe at the same time the polarization before and after the scattering. The effects to be expected were calculated for unscreened nuclei. In contrast to the well known polarization effects perpendicular to the scattering plane there is only a small Z-dependence for the change of polarization in the scattering plane. Thus polarization effects can be investigated also for low values of Z. Experimental arrangements are proposed.

1. Einleitung

In den letzten Jahren wurde die Streuung von Elektronen am Kern (Mott-Streuung) bei Paritätsexperimenten häufig als Analysator für die Elektronenpolarisation benutzt. Dadurch wurde das Interesse am Streuvorgang selbst von Neuem angeregt, insbesondere da es bisher nicht gelang, eine detaillierte Übereinstimmung zwischen Theorie und Experiment zu erzielen. Darüberhinaus ist es möglich, mit Hilfe der Mott-Streuung weitere Aussagen zu gewinnen, so z.B. ob das Elektron ein elektrisches Dipolmoment besitzt [1]).

Es wurde eine große Zahl von Messungen des differentiellen Streuquerschnittes ausgeführt, die qualitativ der Erwartung entsprechen [2, 3, 4]). Es bestehen aber immer noch Widersprüche zwischen den experimentellen Resultaten untereinander und besonders bei kleinen Elektronenenergien auch Abweichungen von der theoretischen Vorhersage.

Noch weniger geklärt waren bis vor kurzem die Verhältnisse bei der Beobachtung der Links-Rechts-Asymmetrie, die Auftritt, wenn transversal polarisierte Elektronen gestreut werden [2, 4]). Neueste Ergebnisse, die bei Doppelstreuexperimenten [5]) erhalten wurden, zeigen, daß auch hier Übereinstimmung mit den Rechnungen für Elektronenenergien oberhalb von etwa 150 keV besteht, daß aber für kleinere Elektronenenergien die gemessenen Asymmetrien zu klein sind. Diese Ergebnisse werden bestätigt durch Messungen, bei denen die auf Grund der Paritätsverletzung polari-

sierten Beta-Teilchen gestreut werden [6]). Dabei wird ihre longitudinale Polarisation durch Ablenkung in einem Zylinderkondensator in eine transversale umgewandelt. Auf diese Weise kommt man mit einer Mott-Streuung aus, wodurch die Intensität wesentlich erhöht wird.

Die gefundenen Abweichungen bei kleinen Energien dürften darauf zurückzuführen sein, daß sich der Einfluß der Abschirmung des Kernfeldes durch die Hüllenelektronen nur ungenau berechnen läßt. Vielleicht liegen aber bei den Experimenten auch noch systematische Fehler vor.

Tolhoek [4]) wies schon darauf hin, daß die Beobachtung des differentiellen Streuquerschnittes und Doppelstreuexperimente nicht ausreichen, um eine vollständige Bestätigung der Theorie zu erreichen. In der Amplitude der Streuwelle treten zwei komplexe Funktionen f und g auf. Zwischen ihren Real- und Imaginär-Teilen besteht eine Identität, so daß aber immer noch drei voneinander unabhängige Experimente erforderlich sind, um diese beiden Funktionen vollständig zu bestimmen. Ein drittes, von den beiden genannten unabhängiges Experiment liegt aber nur dann vor, wenn die Elektronenpolarisation vor ***und*** nach der Streuung gleichzeitig beobachtet wird. Dies schien bisher nur durch ein Dreifach-Streuexperiment möglich zu sein. Wegen der geringen dabei zu erwartenden Intensität dürfte ein solches Experiment aber undurchführbar sein. Aufgrund der in den letzten Jahren erzielten Fortschritte bei der Erzeugung und beim Nachweis der Elektronenpolarisation erscheinen jedoch andere Experimente als durchaus realisierbar, bei denen polarisierte Elektronen gestreut werden und außerdem die Polarisation nach der Streuung gemessen wird.

Intensive Strahlen von polarisierten Elektronen lassen sich mit Hilfe der Molekularstrahltechnik erzeugen [7]). Noch einfacher ist es, die beim Beta-Zerfall entstehenden longitudinal polarisierten Elektronen, deren Polarisationsgrad v/c ist (v Elektronengeschwindigkeit, c Lichtgeschwindigkeit) zu benutzen. Zum Nachweis der Polarisation nach der Streuung steht nunmehr eine Reihe von Methoden zur Verfügung, die sowohl die Messung der longitudinalen als auch der transversalen Polarisation gestatten [8]). Im letzten Abschnitt werden einige Meßanordnungen angegeben, die die Durchführung eines Experimentes möglich erscheinen lassen, das zu den bisher ausgeführten eine unabhängige Information liefert. Um die günstigste Versuchsanordnung zu finden, werden im folgenden die zu erwartenden Effekte als Funktion des Streuwinkels und der Elektronenenergie berechnet.

2. Berechnung der Polarisationsabhängigkeit der Mott-Streuung

Der differentielle Wirkungsquerschnitt für die Streuung von Elektronen am Coulomb-Feld des Kernes wurde unter Berücksichtigung der Polarisation vor und nach der Streuung von Tolhoek [4]) und später von Mühlschlegel und

Koppe [9]) berechnet. Der Streuquerschnitt für unpolarisierte Elektronen ist gegeben durch

$$\mathrm{d}\sigma/\mathrm{d}\Omega = (\lambda/2\pi)^2 I(\vartheta), \tag{1}$$

wobei ϑ der Streuwinkel und λ die de Broglie-Wellenlänge der Elektronen ist. Für den Polarisationsvektor der Elektronen nach der Streuung $\mathbf{P}'$ gilt, wenn $\mathbf{P}$ die Polarisation der Elektronen vor der Streuung ist †,

$$\mathbf{P}' = \frac{1}{1+\frac{D}{I}P_s}\left\{\left(P_s+\frac{D}{I}\right)\mathbf{n}_0 + \frac{C}{I}\mathbf{P}_p + \frac{B}{I}(\mathbf{n}_0\times\mathbf{P}_p)\right\}. \tag{2}$$

Dabei ist $\mathbf{n}_0$ ein Einheitsvektor senkrecht zur Streueben e: $\mathbf{n}_0 = (\mathbf{n}_1\times\mathbf{n}_2)/\sin\vartheta$, wobei $\mathbf{n}_1$ und $\mathbf{n}_2$ Einheitsvektoren in Richtung des Elektronenimpulses vor und nach der Streuung sind. Der Vektor $\mathbf{P}$ wurde zerlegt in einen Vektor $\mathbf{P}_s = P_s\mathbf{n}_0$, der senkrecht zur Streuebene steht und einen Vektor $\mathbf{P}_p$, der in der Streuebenene liegt: $\mathbf{P} = \mathbf{P}_s+\mathbf{P}_p$.

Da alle beobachtbaren Größen Produkte aus zwei Wellenfunktionen sind, treten die komplexen Streuamplituden f und g nur in quadratischen Termen auf und zwar in Form der Größen I, B, C und D, die definiert sind durch die Beziehungen ††

$$\begin{aligned} I(\vartheta) &= ff^* + gg^* \\ B(\vartheta) &= fg^* + f^*g = 2\ \mathrm{Re}\ fg^* \\ C(\vartheta) &= ff^* - gg^* \\ D(\vartheta) &= i(fg^*-f^*g) = -2\ \mathrm{Im}\ fg^*. \end{aligned} \tag{3}$$

Die Funktionen $f(\vartheta)$ und $g(\vartheta)$ lassen sich aus der Dirac-Gleichung berechnen. Daß hier zwei Funktionen auftreten, liegt daran, daß die Elektronen durch Spinoren mit 4 Komponenten, von denen aber nur zwei unabhängig sind, beschrieben werden.

Wie man leicht nachrechnen kann, besteht folgende Identität:

$$C^2+B^2+D^2 = I^2. \tag{4}$$

Wenn daher drei dieser Größen gemessen sind, dann läßt sich die vierte aus dieser Identität berechnen, allerdings ohne Vorzeichen. Durch diese Beziehung ist außerdem sichergestellt, daß $P' = 1$, wenn $P = 1$ war, d.h. eine vollständige Polarisation bleibt vollständig.

Aus (2) lassen sich einige charakteristische Eigenschaften der Polarisation $\mathbf{P}'$ ablesen. Besitzen die einfallenden Elektronen eine Polarisation senkrecht

† Die bei Tolhoek [4]) angegebene Formel (3.8) enthält einen Fehler.

†† Die hier definierte Größe C hängt mit dem bei Tolhoek eingeführten C_T in folgender Weise zusammen: $C = I-C_T$.

zur Streuebene ($\mathbf{P}_p = 0$), dann steht auch $\mathbf{P}'$ senkrecht zur Streuebene und es gilt

$$\mathbf{P}'_s = \frac{P_s + D/I}{1 + P_s \cdot D/I} \mathbf{n}_0. \tag{5}$$

Die Richtung der Polarisation bleibt unverändert, nur ihr Betrag ändert sich. Sind die einfallenden Elektronen unpolarisiert, dann erhält man das bekannte Ergebnis $\mathbf{P}' = (D/I)\mathbf{n}_0$. Streut man Elektronen mit der Polarisation $P\mathbf{n}_0$ dann erhält man eine links-rechts Asymmetrie $S = P \cdot (D/I)$. Die Asymmetrie bei einem Doppelstreuexperiment ergibt sich dann zu

$$\delta = \frac{D}{I}(\vartheta_1) \cdot \frac{D}{I}(\vartheta_2),$$

wobei ϑ_1 und ϑ_2 die beiden Streuwinkel bedeuten.

Aus dem differentiellen Wirkungsquerschnitt und der bisher gemessenen Polarisationsabhängigkeit [5]) lassen sich daher nur die beiden Größen I und D bestimmen. Wie man Gleichung (2) entnimmt, lassen sich B und C nur dann messen, wenn von $\mathbf{P}$ und $\mathbf{P}'$ gleichzeitig Komponenten *in* der Streuebene beobachtet werden. Dabei gibt es mehrere Möglichkeiten, je nachdem ob man longitudinale oder transversale Polarisationen herstellt und misst.

In (2) ist $\mathbf{P}'$ zerlegt in Komponenten parallel und senkrecht zu $\mathbf{P}_p$. Experimentell beobachtet man dagegen die Komponenten von $\mathbf{P}'$ parallel oder senkrecht zu $\mathbf{n}_2$, d.h. die longitudinale oder transversale Polarisation der gestreuten Elektronen. Es ist daher zweckmäßig, von dem Koordinatensystem mit den Achsenrichtungen $\{\mathbf{P}_p, \mathbf{n}_0 \times \mathbf{P}_p, \mathbf{n}_0\}$ überzugehen auf ein Koordinatensystem $\{\mathbf{n}_2, \mathbf{n}_0 \times \mathbf{n}_2, \mathbf{n}_0\}$. Dies bedeutet eine Drehung um den Winkel $(\eta - \vartheta)$ mit $\mathbf{n}_0$ als Drehachse (vgl. Fig. 1). Die senkrecht zur Streu-

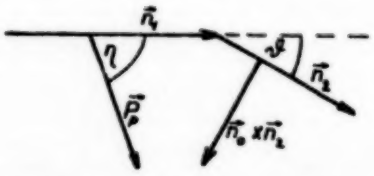

Fig. 1. $\mathbf{n}_1$, $\mathbf{n}_2$ Richtung des Elektronenimpulses vor und nach der Streuung, $\mathbf{P}_p$ in der Streuebene liegende Komponente der Elektronenpolarisation vor der Streuung, $\mathbf{n}_0 = (\mathbf{n}_1 \times \mathbf{n}_2)/\sin\vartheta$.

ebene liegende Komponente von $\mathbf{P}$ wird dabei nicht beeinflußt. Ihre Veränderung durch die Streuung wurde bereits in (5) angegeben.
Die Polarisation $\mathbf{P}'$ läßt sich dann schreiben

$$\mathbf{P}' = \frac{1}{1 + P_s \cdot (D/I)} \left\{ (P_s + D/I)\mathbf{n}_0 + (\tilde{\tilde{C}}/\tilde{\tilde{I}}) P_p \mathbf{n}_2 + (\tilde{\tilde{B}}/\tilde{\tilde{I}}) P_p (\mathbf{n}_0 \times \mathbf{n}_2) \right\}, \tag{6}$$

wobei die zweifach geschlängelten Größen aus den ungeschlängelten durch eine Drehung hervorgehen:

$$\{\tilde{\tilde{C}}/\tilde{\tilde{I}},\ \tilde{\tilde{B}}/\tilde{\tilde{I}}\} = \{C/I,\ B/I\} \cdot \begin{pmatrix} \cos(\eta-\vartheta) & \sin(\eta-\vartheta) \\ -\sin(\eta-\vartheta) & \cos(\eta-\vartheta) \end{pmatrix}. \tag{7}$$

Für die spätere Rechnung ist es zweckmäßig, einmal geschlängelte Größen einzuführen, die man durch Zerlegung der Gesamtdrehung in zwei Drehungen um die einzelnen Winkel erhält:

$$\{\tilde{\tilde{C}}/\tilde{\tilde{I}},\ \tilde{\tilde{B}}/\tilde{\tilde{I}}\} = \{\tilde{C}/\tilde{I},\ \tilde{B}/\tilde{I}\} \cdot \begin{pmatrix} \cos\eta & \sin\eta \\ -\sin\eta & \cos\eta \end{pmatrix}. \tag{8}$$

Betrachten wir nun Sonderfälle, die für die experimentelle Durchführung wichtig sind:

1) Die einfallenden Elektronen sollen longitudinal polarisiert sein, d.h. $\mathbf{P} = P_{\parallel}\mathbf{n}_1 (\eta = 0,\ P_s = 0,\ P_p = P_{\parallel})$.

a) Beobachtet wird die longitudinale Polarisation der gestreuten Elektronen $\mathbf{P}' = P'_{\parallel}\mathbf{n}_2$. Aus (6) und (8) erhält man

$$P'_{\parallel}/P_{\parallel} = \tilde{C}/\tilde{I}.$$

b) Man misst die transversale Polarisation der gestreuten Elektronen $\mathbf{P}' = \mathbf{P}'_{\perp}(\mathbf{n}_0 \times \mathbf{n}_2)$. Dann ist

$$P'_{\perp}/P_{\parallel} = \tilde{B}/\tilde{I}.$$

2) Die einfallenden Elektronen sind transversal polarisiert: $\mathbf{P} = P_{\perp}(\mathbf{n}_0 \times \mathbf{n}_2)(\eta = 90°,\ P_s = 0,\ P_p = P_{\perp})$.

a) Beobachtet man die longitudinale Polarisation $P'_{\parallel}$ der gestreuten Elektronen, dann gilt

$$P'_{\parallel}/P_{\perp} = -(\tilde{B}/\tilde{I}) = -P'_{\perp}/P_{\parallel}. \tag{9}$$

b) Bei Messung der transversalen Polarisation $P'_{\perp}$ erhält man

$$P'_{\perp}/P_{\perp} = \tilde{C}/\tilde{I} = P'_{\parallel}/P_{\parallel}. \tag{10}$$

Die Messung von $P'_{\parallel}/P_{\parallel}$ und $P'_{\perp}/P_{\perp}$ liefert also das gleiche Ergebnis und gestattet die Bestimmung der Größe $\tilde{C}$. Führt man dagegen eine "gemischte Messung" durch, d.h. wird $P'_{\parallel}/P_{\perp}$ oder $P'_{\perp}/P_{\parallel}$ beobachtet, dann kann die Größe $\tilde{B}$ bestimmt werden.

Um eine Aussage über die Größe der zu erwartenden Effekte zu bekommen, müssen die Ausdrücke $\tilde{B}/\tilde{I}$ und $\tilde{C}/\tilde{I}$ berechnet werden. Bei der Lösung der Dirac-Gleichung ist es zweckmäßig, anstelle von f und g zwei neue komplexe Funktionen F und G einzuführen durch die Beziehungen [1])

$$\begin{aligned} f &= -i\gamma F + G, \\ g &= i\gamma F \operatorname{cotg} \tfrac{1}{2}\vartheta + G \operatorname{tg} \tfrac{1}{2}\vartheta, \qquad \gamma = \sqrt{1-\beta^2}\,(Z\alpha/\beta). \end{aligned} \tag{11}$$

Dabei ist α die Feinstrukturkonstante, $\beta = v/c$ und Z die Ordnungszahl des streuenden Atoms. Drückt man die Größen I, B, C und D durch die Funktionen F und G aus, dann erhält man komplizierte Beziehungen. Für $\tilde{I}$, $\tilde{B}$, $\tilde{C}$ und $\tilde{D}$ dagegen erhält man verhältnismäßig einfache Ausdrücke, wodurch die Einführung dieser Größen gerechtfertigt wird:

$$\begin{aligned} \tilde{I} &= I = \gamma^2 \frac{|F|^2}{\sin^2 \tfrac{1}{2}\vartheta} + \frac{|G|^2}{\cos^2 \tfrac{1}{2}\vartheta} \\ \tilde{B} &= (4\gamma/\sin\vartheta)\{-\mathrm{Im}\, FG^*\} \\ \tilde{C} &= -\gamma^2 \frac{|F|^2}{\sin^2 \tfrac{1}{2}\vartheta} + \frac{|G|^2}{\cos^2 \tfrac{1}{2}\vartheta} \\ \tilde{D} &= D = (4\gamma/\sin\vartheta)\ \mathrm{Re}\, FG^*. \end{aligned} \tag{12}$$

Sherman [10]) hat die ausführlichsten Rechnungen für die Funktionen F und G durchgeführt, allerdings nur für das ungestörte Coulomb-Feld des Kerns. Mit Hilfe der von diesem Autor veröffentlichten Tabellen wurden die Größen $\tilde{I}$, $\tilde{B}$, $\tilde{C}$ und $\tilde{D}$ für verschiedene Streuwinkel und Elektronenenergien berechnet.

In Fig. 2 ist zunächst der Vollständigkeit halber die Größe $S = D/I$, die schon von Sherman berechnet wurde, für die Streuung an Hg-Kernen graphisch dargestellt. Oft wurde nur die Streuung bei $\vartheta = 90°$ mit einem Maximum bei etwa 130 keV betrachtet. Bei größeren Streuwinkeln wandert das Maximum zu höheren Energien. Bei Streuung an Kernen mit kleinem Z (z.B. Al) ist S sehr klein.

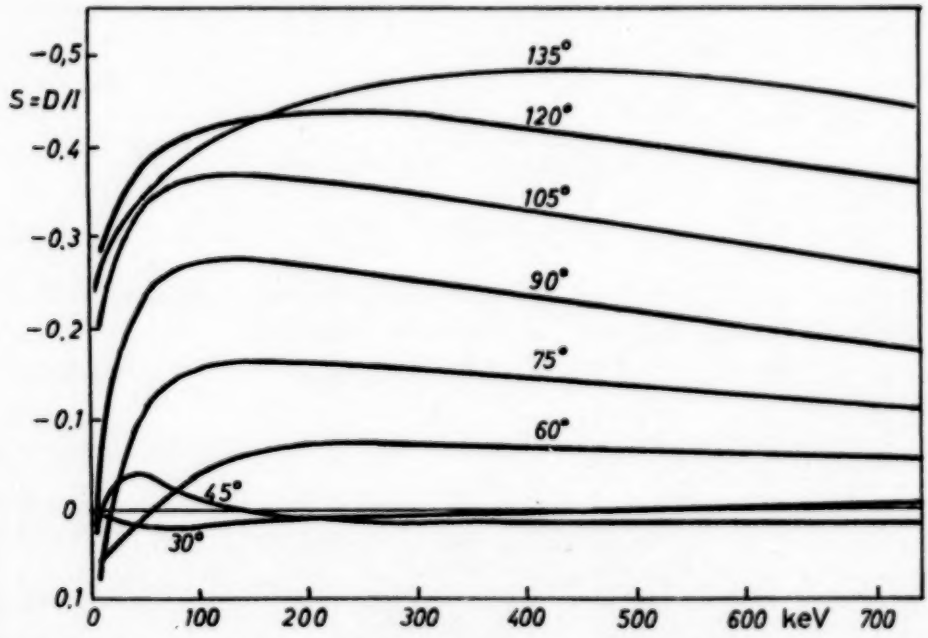

Fig. 2. $S = D/I$ als Funktion der Elektronenenergie für verschiedene Streuwinkel. Streuung an Hg ($Z = 80$).

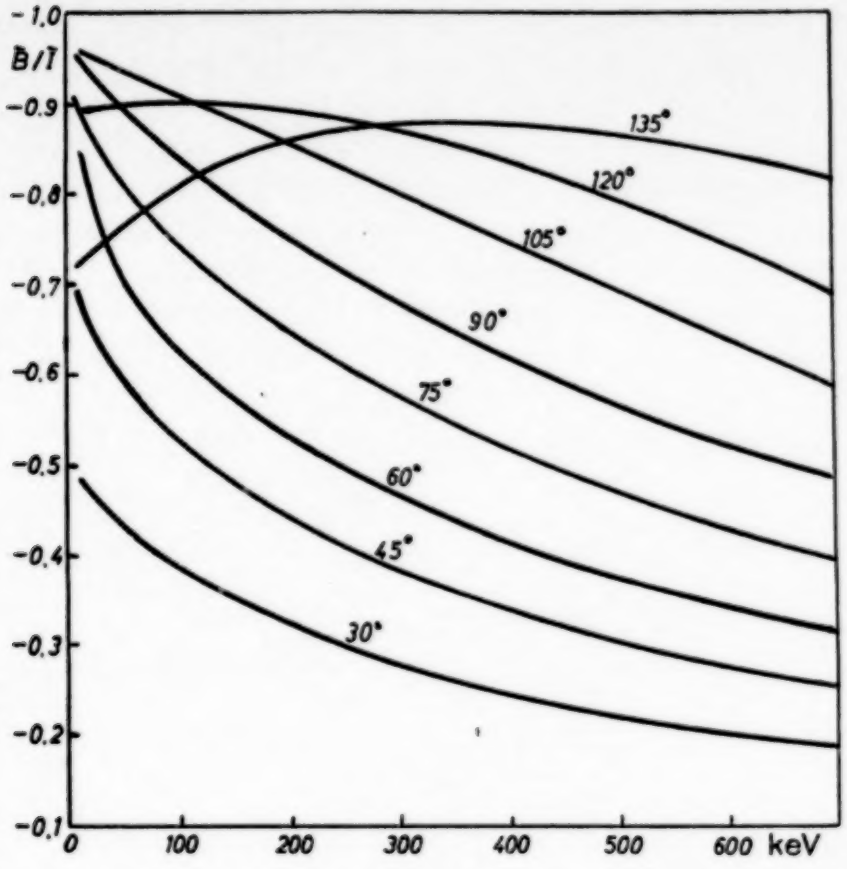

Fig. 3. $P'_{\perp}/P_{\parallel} = -P'_{\parallel}/P_{\perp} = \tilde{B}/\tilde{I}$ als Funktion der Elektronenenergie für die Streuung an Hg ($Z = 80$).

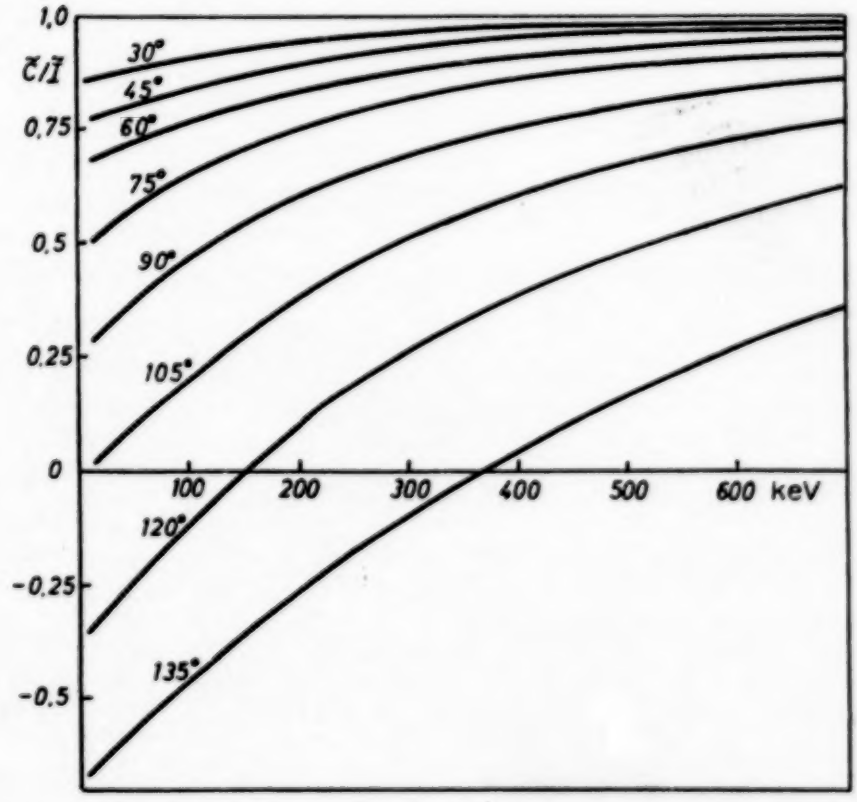

Fig. 4. $P'_{\parallel}/P_{\parallel} = P'_{\perp}/P_{\perp} = \tilde{C}/\tilde{I}$ als Funktion der Elektronenenergie für die Streuung an Hg ($Z = 80$).

In Fig. 3 und 4 sind die Größen $P'_{\parallel}/P_{\perp} = -P'_{\perp}/P_{\parallel} = -\tilde{B}/\tilde{I}$ und $P'_{\parallel}/P_{\parallel} = P'_{\perp}/P_{\perp} = \tilde{C}/\tilde{I}$ als Funktion der Elektronenenergie für verschiedene Streuwinkel für die Streuung an Hg aufgetragen. Es darf jedoch nicht vergessen werden, daß genauere Rechnungen (mit Abschirmung) bei kleinen Elektronenenergien etwas andere Kurven ergeben würden.

In Fig. 5 ist der Verlauf der gleichen Größen als Funktion des Streuwinkels für einige Elektronenenergien dargestellt. Diese Darstellung ist besonders geeignet um die Ergebnisse zu diskutieren. Man würde erwarten, daß sich der Spin der Elektronen bei der Streuung im Coulomb-Feld des

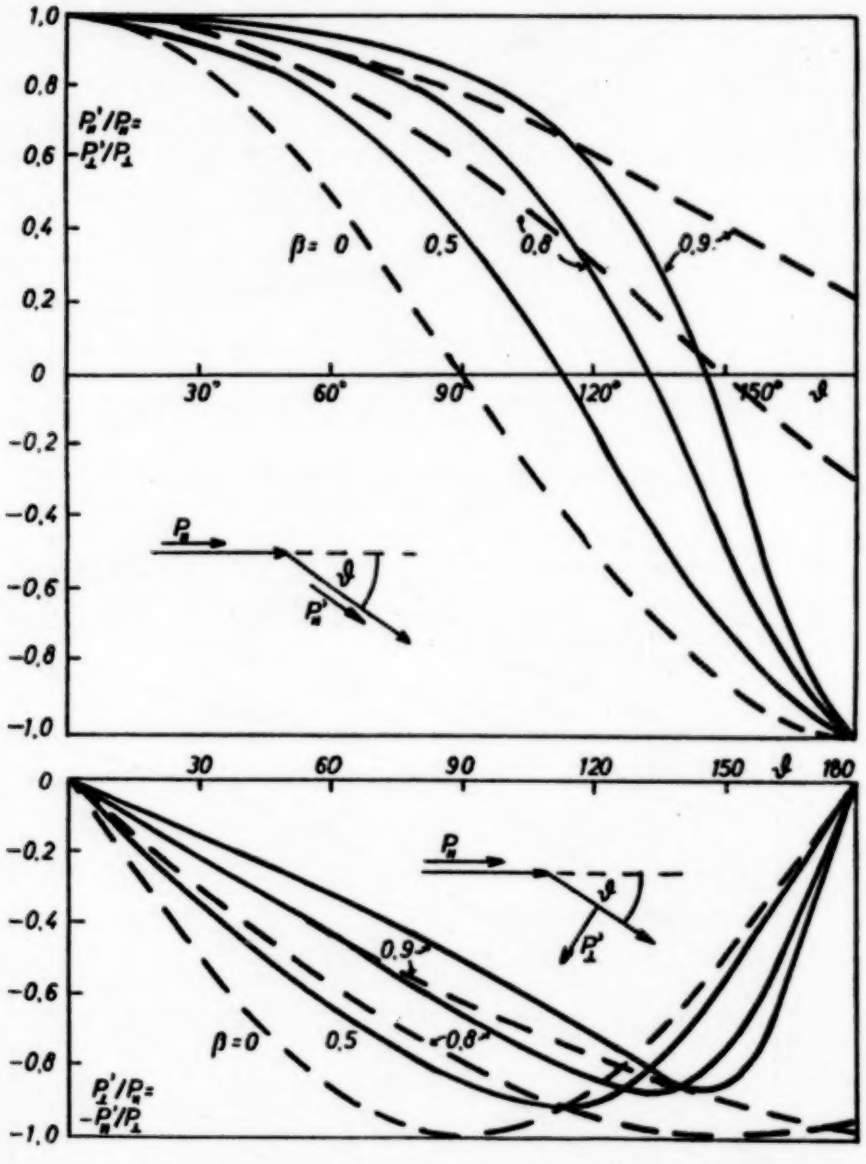

Fig. 5. $P'_{\parallel}/P_{\parallel}$ and $P'_{\perp}/P_{\perp}$ als Funktion des Streuwinkels ϑ für verschiedene Elektronengeschwindigkeiten (ausgezogene Kurven) für die Streuung an Hg ($Z = 80$). Die gestrichelten Kurven geben die entsprechenden Größen an, die man bei Ablenkung der Elektronen um den Winkel ϑ in einem Zylinderkondensator erhalten würde.

Kernes ähnlich verhält, wie bei der Ablenkung in einem makroskopischen elektrischen Feld. Dabei wird der Impuls der Elektronen gedreht, während der Spin im nichtrelativistischen Fall seine Lage im Raum beibehält. Bei relativistischen Elektronen erfolgt eine teilweise Mitdrehung des Spins mit dem Impuls. In Fig. 5 sind gestrichelte Kurven eingezeichnet, die einer solchen Ablenkung des Elektrons in einem Zylinderkondensator um den Winkel ϑ entsprechen. Man erkennt, daß bei kleinen Streuwinkeln der Verlauf der Kurven für die Mott-Streuung ähnlich ist demjenigen für die Ablenkung in einem Zylinderkondensator. Bei größeren Streuwinkeln dagegen bestehen erhebliche Abweichungen. Dies rührt insbesondere daher, daß bei der Mott-Streuung die Rückwärtsstreuung einen ausgezeichneten

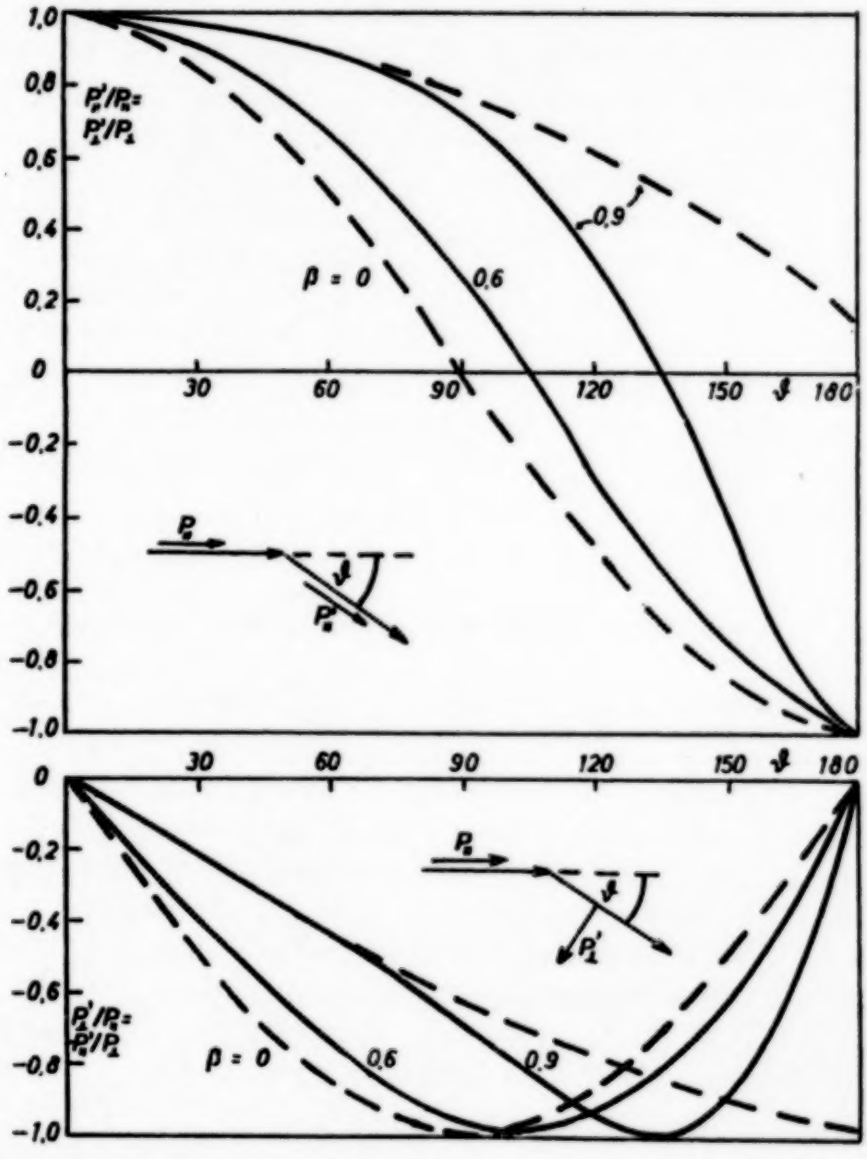

Fig. 6. Dasselbe wie Fig. 5 aber für die Streuung an Al ($Z = 13$).

Fall darstellt, während dies bei der Ablenkung in einem Zylinderkondensator nicht gilt. Bei Rückwärtsstreuung ist $P'_{\parallel}/P_{\parallel} = -1$, d.h. der Spin behält bei allen Elektronenenergien seine Lage im Raum bei, während der Impuls seine Richtung umkehrt. Als Folge davon gibt es für jede Elektronenenergie einen Winkel zwischen 90° und 180°, bei dem $P'_{\parallel}/P_{\parallel} = 0$ ist. Nach der Streuung ist die Polarisation dann rein transversal, was sich in einem Minimum in den $P'_{\perp}/P_{\parallel}$-Kurven ausdrückt. Daß dabei $|P'_{\perp}/P_{\parallel}|$ kleiner als 1 bleibt, liegt daran, daß bei diesen Streuwinkeln auch $P_s = D/I$ verhältnismäßig große Werte annimmt (vgl. Fig. 2) und andererseits $|P'|^2 = |P'_{\parallel}|^2 + |P'_{\perp}|^2 + |P_s|^2 \leqq 1$ sein muß.

In Fig. 6 sind die entsprechenden Kurven für die Streuung an Aluminium für 2 Elektronenenergien dargestellt. Ein Vergleich zeigt, daß sie sich von den Kurven für die Streuung am Quecksilber nicht wesentlich unterscheiden. Sie weichen nur insofern voneinander ab, als bei der Streuung an Aluminium die Mitdrehung des Spins etwas geringer ist. Außerdem liegen die Minima der $P'_{\perp}/P_{\parallel}$-Kurven sehr nahe bei 1. Dies liegt daran, daß bei der Streuung an Aluminium P'_s sehr klein ist.

Zunächst erscheint es erstaunlich, daß bei P_s eine starke Z-Abhängigkeit vorhanden ist, während bei P_p diese Abhängigkeit nur gering ist. Dieser Unterschied wird jedoch verständlich aus dem Umstand, daß für $\alpha Z \to 0$ die Funktion F imaginär und G reell wird [2]) und daher FG^* nahezu rein imaginär ist. Aus (12) folgt dann, daß für kleine Z die Große $\tilde{D}$ klein wird, $\tilde{B}$ dagegen groß bleibt. Infolge der großen Werte von $\tilde{B}/\tilde{I}$ kann die Polarisationsabhängigkeit der Mott-Streuung auch bei kleinem Z experimentell untersucht werden.

3. Vorschläge für experimentelle Anordnungen

In naher Zukunft ist zu erwarten, daß mit Hilfe eines Stern-Gerlach-Versuches und nachfolgender Photoionisation der Atome Strahlen von nahezu vollständig polarisierten Elektronen bis zu Stromstärken von etwa 10^{-8} A hergestellt werden können [7]). Solange diese Technik nicht erprobt ist, dürfte es aber am einfachsten sein, die beim Beta-Zerfall entstehenden longitudinal polarisierten Elektronen zu verwenden. Ihre Polarisation ist bekanntlich $P = -v/c$. Da die Umwandlung dieser longitudinalen in eine transversale Polarisation mit Intensitätsverlust verknüpft ist, wird die Beobachtung der Größen $P'_{\parallel}/P_{\parallel}$ und $P'_{\perp}/P_{\parallel}$ am einfachsten sein. Man hat also die von einem radioaktiven Präparat herkommenden Beta-Teilchen an einer Folie zu streuen, die so dünn ist, dass Mehrfachstreuung gegenüber Einzelstreuung zu vernachlässigen ist. Nach der Streuung muß dann die transversale oder longitudinale Polarisation der Elektronen gemessen werden.

Die Beobachtung der transversalen Polarisation könnte durch eine zweite Mott-Streuung erfolgen. Man käme also zu einer Anordnung wie sie z.B. von Heintze [11]) verwendet wurde †, nur müßte die erste Streufolie genügend dünn gemacht werden. Sie könnte aus einem Material mit kleinem oder großem Z bestehen, während für die zweite Streufolie nur ein hohes Z in Frage kommt. Intensitätsmässig scheint ein solches Experiment nicht undurchführbar zu sein, sodaß damit $P'_{\perp}/P_{\parallel} = \tilde{B}/\tilde{I}$ bestimmt werden könnte.

Die longitudinale Polarisation nach der Streuung könnte mit Hilfe eines Zylinderkondensators in eine transversale umgewandelt werden und dann wieder mit Hilfe einer zweiten Mott-Streuung nachgewiesen werden. Eine andere Möglichkeit bestünde in dem direkten Nachweis der longitudinalen Polarisation mit Hilfe der Møller-Streuung (Elektron-Elektron-Streuung). In beiden Fällen dürfte jedoch die erreichbare Intensität nur sehr gering sein. Günstiger ist es, wenn man die Elektronen nach der Streuung Bremsstrahlung erzeugen läßt (Fig. 7, Konvertor K), deren zirkulare Polarisation

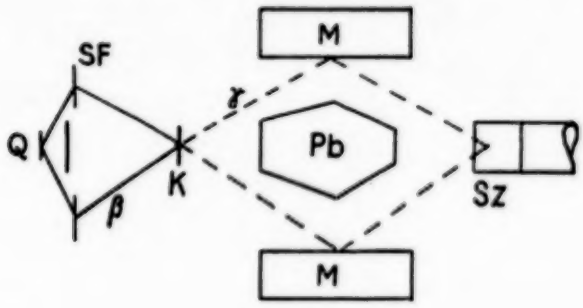

Fig. 7. Anordnung zur Messung von $P'_{||}/P_{||}$ mit Hilfe der zirkularen Polarisation der von den Elektronen erzeugten Bremsstrahlung. Q radioaktives Präparat, SF Streufolie, K Konvertor, M Streumagnet zur Messung der zirkularen Polarisation der Photonen, Sz Szintillationszähler.

der longitudinalen Elektronenpolarisation $P'_{||}$ proportional ist. Die Messung der zirkularen γ-Polarisation kann durch Streuung an magnetisiertem Eisen erfolgen [13]). Bei diesem Experiment wäre es möglich, eine rotationssymmetrische Anordnung zu benützen (Fig. 7), wodurch man große Raumwinkel erhält. Ein Nachteil besteht darin, daß man nur eine integrale Messung über die Elektronenenergie ausführen kann, sodaß man einen Mittelwert von $\tilde{C}/\tilde{I}$ erhält. Das erste und das letzte von den hier vorgeschlagenen Experimenten ist in Vorbereitung.

Herrn Dr. G. Kramer, Heidelberg, danke ich für viele klärende Diskussionen.

† Die von Lipkin u.a.[12]) benutzte Geometrie ist hier weniger geeignet, da dabei leicht Mehrfachstreuung auftreten kann.

Literatur

1) E. Sobolak und P. Stehle, Vorabdruck
2) vgl. N. F. Mott und Massey, The Theory of Atomic Collisions (Oxford, 1952)
3) R. D. Birkhoff, Handbuch der Physik, Bd. **24** (1958) Seite 101
4) H. A. Tolhoek, Revs. mod. Phys. **28** (1956) 277
5) H. Schneider und E. Barnad, Nuovo Cimento **8** (1958) 770;
   W. G. Pettus, Phys. Rev. **109** (1958) 1458;
   D. F. Nelson und R. W. Pidd, Bull. Am Phys. Soc. **4** (1959) 60
6) H. Bienlein, G. Felsner, K. Güthner, H. V. Issendorff und H. Wegener, Vorabdruck
7) H. Friedmann, Phys. Verhandlungen **9** (1958) 236; und private Mitteilungen
8) vgl. H. Schopper, Fortschritte der Physik **5** (1957) 581
9) B. Mühlschlegel und H. Koppe, Zeitschr. f. Phys. **150** (1958) 474
10) N. Sherman, Phys. Rev. **103** (56) 1601
11) J. Heintze, Zeitschr. f. Phys. **148** (1957) 560
12) H. J. Lipkin, S. Cuperman, T. Rothem und A. de Shalit, Phys. Rev. **107** (1957) 1459; und **109** (1958) 223
13) vgl. H. Schopper, Nuclear Instruments **3** (1958) 158

8.B *Nuclear Physics* **11** (1959) 687—690; © *North-Holland Publishing Co., Amsterdam*
Not to be reproduced by photoprint or microfilm without written permission from the publisher

ON THE UNIVERSAL FERMI INTERACTION

W. KRÓLIKOWSKI
Institute of Theoretical Physics, University of Warsaw
and
Institute for Nuclear Research, Polish Academy of Sciences, Warsaw

Received 9 March 1959

Abstract: A formalism proposed previously [1]) for elementary particles enables us to express the universal Fermi interaction between fermions in a concise form.

Recently, the V—A Fermi interaction [2–5]) was rather successful in explaining the β decay, μ decay, μ capture and π decays. It should be expected, in the spirit of the universality of the Fermi interaction, that this interaction also applies to mesonic and leptonic decays of hyperons and K mesons. The accurate measurements of branching ratios of leptonic and mesonic decays of hyperons should play a crucial role in further research on the universality of the Fermi interaction.

From the point of view of this universality it may be of considerable interest to search for a concise form of the Fermi interaction. In the present paper such a concise form of the Fermi interaction between fermions is written down by means of the formalism proposed for elementary particles in ref. [1]).

First, we observe that the total charges of the lepton field $L(x)$ and the baryon field $B(x)$ introduced in ref. [1]) may be rewritten in the forms (cf. (29) and (12) of ref. [1]))

$$\begin{aligned} Q^L &= e\int \mathrm{d}_3 x L^*[-\xi_\alpha^*(\tau_-^*\tau_-)_{\alpha\beta}\xi_\beta]L, \\ Q^B &= e\int \mathrm{d}_3 x B^*[\tau_+^*\tau_+ - \xi_\alpha^*(\tau_-^*\tau_-)_{\alpha\beta}\xi_\beta]B, \end{aligned} \tag{1}$$

where

$$\tau_+ = \tau_-^* = \tfrac{1}{2}(\tau_1 - i\tau_2) = \begin{pmatrix}0&0\\1&0\end{pmatrix}, \quad \tau_+^* = \tau_- = \tfrac{1}{2}(\tau_1 + i\tau_2) = \begin{pmatrix}0&1\\0&0\end{pmatrix}. \tag{2}$$

We have, of course, $\tau_+^*\tau_+ = \frac{1}{2}(\tau_3+1)$ and $-\tau_-^*\tau_- = \frac{1}{2}(\tau_3-1)$. For further explanation of the applied notation see ref. [1]). The operators ξ_α and ξ_α^* acting on the fields $L(x)$ and $B(x)$ annihilate and create the "strange parts" of elementary leptons and baryons ($\alpha = 1, 2$ correspond to the "strange parts" having charges 0, $-e$), while the operators $\tau_\pm$ and $\tau_\pm^*$ acting on the

field $B(x)$ change the charges of the "fundamental parts" of elementary baryons ($\pm$ correspond to charges $+e$, $-e$). A difference from ref.[1]) is that we here assume that the operators ξ_α and ξ_α^* act on all indices of the field $L(x)$, in other words that the leptons consist of the "strange parts" only, whereas the baryons contain the "strange parts" as well as the "fundamental parts".

The properties of the τ's and ξ's enable us to propose tentatively the universal Fermi interaction between fermions in the form

$$\mathscr{H}^{\mathrm{F}}(x) = g^{\mathrm{F}} J_\mu^*(x) J_\mu(x), \tag{3}$$

where

$$\begin{aligned} J_\mu(x) = {} & \bar{L}(x)\gamma_\mu(1+\gamma_5)(\xi_\alpha^*\tau_{-\alpha\beta}\xi_\beta+\xi_-)L(x) \\ & +\bar{B}(x)\gamma_\mu(1+\gamma_5)(\tau_-+\xi_\alpha^*\tau_{-\alpha\beta}\xi_\beta+\xi_-)B(x). \end{aligned} \tag{4}$$

Here $\xi_- = \xi_2$.

Using the results of ref.[1]) we obtain explicitly

$$\begin{aligned} J_\mu(x) = {} & \bar{\nu}\gamma_\mu(1+\gamma_5)\mathrm{e}^- \\ & +i\bar{\nu}\gamma_\mu(1+\gamma_5)\mu^- \\ & +\bar{\mathrm{p}}\gamma_\mu(1+\gamma_5)\mathrm{n}+2\sqrt{2}[\bar{\Sigma}^+\gamma_\mu(1+\gamma_5)\Sigma^0+\bar{\Sigma}^0\gamma_\mu(1+\gamma_5)\Sigma^-]+\Xi^0\gamma_\mu(1+\gamma_5)\Xi^- \\ & +\frac{1}{\sqrt{2}}[\bar{\mathrm{p}}\gamma_\mu(1+\gamma_5)(\Sigma^0+i\Lambda^0)+\sqrt{2}\bar{\mathrm{n}}\gamma_\mu(1+\gamma_5)\Sigma^-+i\sqrt{2}\bar{\Sigma}^+\gamma_\mu(1+\gamma_5)\Xi^0 \\ & +i(\bar{\Sigma}^0+i\bar{\Lambda}^0)\gamma_\mu(1+\gamma_5)\Xi^-]. \end{aligned} \tag{5}$$

We note that the terms $\bar{\Sigma}^+\Lambda^0$ and $\bar{\Lambda}^0\Sigma^-$ do not appear in the operator (4).

The connections between the fields $L(x)$ and $B(x)$ and the experimentally interpretable fields are as follows (cf. ref. [1]):

$$L = \begin{pmatrix} L_{\alpha_1} \\ L_{\alpha_1\alpha_2} \end{pmatrix}, \qquad B = \begin{pmatrix} B_\alpha \\ B_{\alpha\alpha_1} \\ B_{\alpha\alpha_1\alpha_2} \end{pmatrix}, \tag{6}$$

where

$$\begin{aligned} & L_\alpha = \begin{cases} \nu \\ \mathrm{e}^- \end{cases}; \quad \frac{1}{i\sqrt{2}}(L_{12}-L_{21}) = \frac{\sqrt{2}}{i}L_{12} = \mu^-, \qquad L_{11} = L_{22} = 0; \\ & B_\alpha = \begin{cases} \mathrm{p} \\ \mathrm{n} \end{cases}; \\ & \frac{1}{i\sqrt{2}}(B_{12}-B_{21}) = \Lambda^0, \quad B_{11} = \Sigma^+, \quad \frac{1}{\sqrt{2}}(B_{12}+B_{21}) = \Sigma^0, \quad B_{22} = \Sigma^-; \\ & \frac{1}{i\sqrt{2}}(B_{\alpha_{12}}-B_{\alpha_{21}}) = \frac{\sqrt{2}}{i}B_{\alpha_{12}} = \begin{cases} \Xi^0 \\ \Xi^- \end{cases}, \quad B_{\alpha_{11}} = 0 = B_{\alpha_{22}}. \end{aligned} \tag{7}$$

The interaction (3) with (4) gives directly the weak processes exemplified in table 1.

Some weak processes given indirectly (i.e. together with strong interactions) by the interaction (3) with (4) are listed in table 2.

TABLE 1

Part of interaction (3) of type	gives	does not give
$\tau_-{}^*\tau_-$	$n \to p+e^-+\bar{\nu}$	$p \to p+\left\{\begin{matrix}\nu+\bar{\nu}\\ e^-+e^+\end{matrix}\right\}$ in nuclei $n \to n+\left\{\begin{matrix}\nu+\bar{\nu}\\ e^-+e^+\end{matrix}\right\}$ $\Sigma^- \to \Lambda^0+e^-+\bar{\nu}$ (would appear if the term $\bar{\Lambda}^0\Sigma^-$ were present) $\Sigma^0 \to \Lambda^0+\left\{\begin{matrix}\nu+\bar{\nu}\\ e^-+e^+\end{matrix}\right.$ $\Lambda^0 \to \Lambda^0+\left\{\begin{matrix}\nu+\bar{\nu}\\ e^-+e^+\end{matrix}\right\}$ in nuclei
$\tau_-{}^*\xi_-$	$\mu^- \to \nu+e^-+\bar{\nu}$ $\Lambda^0 \to p+e^-+\bar{\nu}$ $\mu^-+p \to \nu+n$	$\mu^- \to e^-+e^-+e^+$ $\Lambda^0 \to n+\left\{\begin{matrix}\nu+\bar{\nu}\\ e^-+e^+\end{matrix}\right.$ $\mu^-+p \to e^-+p$
$\xi_-{}^*\xi_-$	$\Lambda^0 \to p+\mu^-+\bar{\nu}$	$\Lambda^0 \to n+\mu^-+e^+$

TABLE 2

Interaction (3)	
gives	does not give
$\pi^- \to n+\bar{p} \to \mu^-+\bar{\nu}$ (strong: $\uparrow$) $\quad e^-+\bar{\nu}$	$\pi^0 \to \mu^-+e^+$ e^-+e^+ $\nu+\bar{\nu}$
$\Lambda^0 \to p+n+\bar{p} \to p+\pi^-$ (strong: $\uparrow$) $\quad \uparrow n+\pi^0$	
$K^- \to \Lambda^0+\bar{p} \to \mu^-+\bar{\nu}$ (strong: $\uparrow$) $\quad e^-+\bar{\nu}$	$\bar{K}^0 \to \mu^-+e^+$ e^-+e^+ $\nu+\bar{\nu}$
$K^- \to \Lambda^0+\bar{p}+\pi^0 \to \mu^-+\bar{\nu}+\pi^0$ (strong: $\uparrow$) $\quad e^-+\bar{\nu}+\pi^0$	$K^- \to \mu^-+e^+ +\pi^-$ $e^-+e^+ +\pi^-$ $\nu+\bar{\nu}+\pi^-$
$\bar{K}^0 \to \Lambda^0+\bar{p}+\pi^+ \to \mu^-+\bar{\nu}+\pi^+$ (strong: $\uparrow$) $\quad e^-+\bar{\nu}+\pi^+$	$\bar{K}^0 \to \mu^-+e^+ +\pi^0$ $e^-+e^+ +\pi^0$ $\nu+\bar{\nu}+\pi^0$
$K^- \to \Lambda^0+\bar{p} \to p+\bar{n} \to 2\pi$ and 3π (strong: $\uparrow$ at K^- and at $\bar{n}$)	
$\bar{K}^0 \to \Lambda^0+\bar{n} \to p+\bar{p} \to 2\pi$ and 3π (strong: $\uparrow$ at $\bar{K}^0$ and at $\bar{p}$)	

We observe that in the interaction (3) with (5) the coupling constants for the processes $n \to p+e^-+\tilde{\nu}$, $\mu^- \to e^-+\nu+\tilde{\nu}$ and $\mu^-+p \to n+\nu$ are equal, as is expected experimentally.

Finally, let us remark that, if we assumed the operators ξ_α and ξ_α^* acting on all indices of the field $L(x)$, the lepton field $L(x)$ should contain an additional component $L_0(x)$ being a vacuum element with respect to the operators ξ_α and ξ_α^*:

$$L = \begin{pmatrix} L_0 \\ L_{\alpha_1} \\ L_{\alpha_1\alpha_2} \end{pmatrix}. \tag{8}$$

The component L_0 would represent a second neutrino ν_0, $L_0 = \nu_0$, experimentally undistinguishable from the previous neutrino ν. The formula (5) for the operator (4) would contain an additional term

$$\tilde{\nu}_0 \gamma_\mu (1+\gamma_5) e^-. \tag{9}$$

References

1) W. Królikowski, Nuclear Physics **8** (1958) 461
2) R. Marshak and G. Sudarshan, Venice Conference on Elementary Particles (September 1957); Phys. Rev. **10** (1958) 1860
3) R. P. Feynman and M. Gell-Mann, Phys. Rev. **109** (1958) 193
4) J. J. Sakurai, Nuovo Cimento **7** (1958) 649
5) M. Gell-Mann, Phys. Rev. **111** (1958) 362

1.D.2:
1.E.4

Nuclear Physics **11** (1959) 691—695; © *North-Holland Publishing Co., Amsterdam*
Not to be reproduced by photoprint or microfilm without written permission from the publisher

E2—M1 MIXING RATIOS IN $2' \rightarrow 2 \rightarrow 0$ TRANSITIONS

S. S. MALIK †, V. R. POTNIS †† and C. E. MANDEVILLE †††

Bartol Research Foundation of the Franklin Institute, Swarthmore, Penna *

Received 16 March 1959

Abstract: The results of twelve published angular correlation experiments have been analyzed, and the E2—M1 mixing ratios of the $2' \rightarrow 2$ transitions have been obtained for twelve different even nuclei. Particular attention has been given to evaluation of the errors in the measured values of the mixing ratios. The available data range from $A = 56$ to $A = 198$. When $(\delta/E_\gamma)^2$ is plotted against $Z^2A^{\frac{1}{3}}$, three of the experimentally observed points, those for Fe^{56}, Zr^{92} and Hg^{198}, deviate sharply from a curve calculated from the theoretical considerations of Davydov and Filippov.

1. Introduction

From spatial correlation functions of the cascade emissions, the mixing ratios, values of δ^2 of the $2' \rightarrow 2$ transition of the $2' \rightarrow 2 \rightarrow 0$ spin sequence of even nuclei can be obtained. The quantity δ is here defined as

$$\delta = \pm\sqrt{I(\mathrm{E2})/I(\mathrm{M1})}. \tag{1}$$

In the case of $2' \rightarrow 2 \rightarrow 0$ transitions,

$$A = \frac{3+8.782\delta+0.715\delta^2}{7-2.927\delta+9.286\delta^2} \tag{2}$$

where A, the anisotropy, is given by

$$A = \frac{1+A_2+A_4}{1-\frac{1}{2}A_2+\frac{3}{8}A_4} - 1. \tag{3}$$

In eq. (3), A_2 and A_4 are the coefficients of the Legendre polynomials of the correlation function which may be written

$$W(\theta) = 1+A_2P_2(\cos\theta)+A_4P_4(\cos\theta). \tag{4}$$

2. Results

Values of δ have been discussed and estimated in a number of recent publications [1–4]). More recently, values of δ have been calculated from theory by Davydov and Filippov [5]). In order to make proper comparisons with the

† Permanent address: Muzaffar Nagar (U.P.), India.

†† Permanent address: Gwalior (M.P.), India.

††† At present at the Dept. of Physics, University of Alabama, Tuscaloosa, Alabama.

* This research was supported by the U. S. Air Force through the Air Force Office of Scientific Research of the Air Research and Development Command.

theoretical predictions, a series of experiments wherein δ was obtained for $2' \rightarrow 2 \rightarrow 0$ transitions in even nuclei have been considered. In most instances δ has been re-evaluated from the data of the angular correlation measurements with emphasis upon proper estimation of error. In these cases, the independence and non-independence of errors in all quantities concerned was taken into account in combining errors to obtain the error in δ. The results of these calculations are summarized in table 1.

It will be noted that according to eq. (2), δ is a double-valued function of the asymmetry A. To determine which value of δ is applicable, the experimentally determined values of A_2 and A_4 are compared with theoretical values of these coefficients given by the following equations:

$$A_2 = \frac{1}{1+\delta^2}(0.250+0.732\delta-0.077\delta^2), \tag{5}$$

$$A_4 = \frac{0.326\delta^2}{1+\delta^2}. \tag{6}$$

In this manner, the value of δ which is compatible with the observed values of both A_2 and A_4 can be selected. Values of A_2 and A_4 are plotted along with eqs. (5) and (6) in fig. 1. The appropriate values of δ so obtained are indicated by an asterisk in table 1. Values of δ for Sn^{116} and Pt^{192} and their

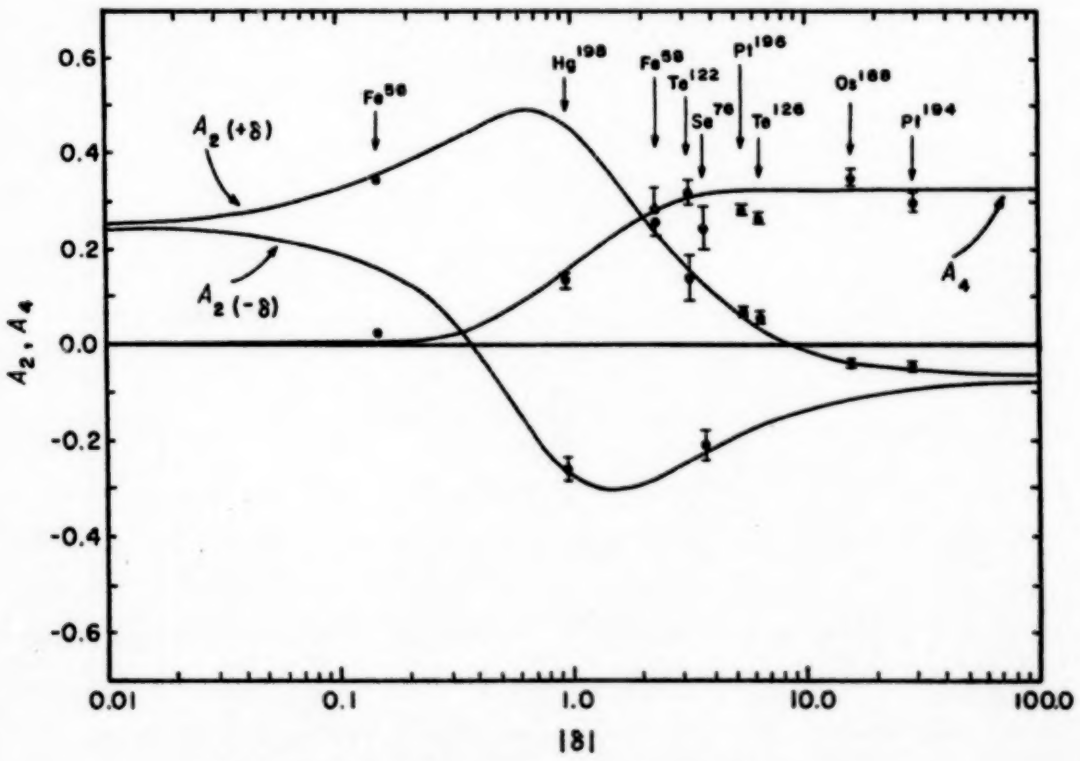

Fig. 1. Coefficients A_2 and A_4 plotted as a function of δ.

TABLE 1
Values of δ

Element and Isotope	E_γ (keV)	A_2	A_4	A	δ	Reference
$_{26}Fe^{56}$	1810	0.346	0.025	0.64 ± 0.1	0.15 ± 0.075* 1.89 ± 0.39	a)
$_{26}Fe^{58}$	805	0.26 ± 0.03	0.28 ± 0.05	0.58 ± 0.10	2.32 ± 0.47* 0.11 ± 0.07	b)
$_{34}Se^{76}$	643	-0.21 ± 0.03	0.246 ± 0.045	-0.13 ± 0.07	$(-3.71) \pm 1.86$* $(-0.53) \pm 0.13$	c)
$_{40}Zr^{92}$	900	0.236 ± 0.049	0.036 ± 0.068	0.42 ± 0.15	$(-0.0047) \pm 0.106$* 3.12 ± 1.63	c)
$_{50}Sn^{116}$	800				3.5 ± 1.5	d)
$_{52}Te^{122}$	693	0.14 ± 0.05	0.32 ± 0.025	0.39 ± 0.044	3.21 ± 0.48* $(-0.01) \pm 0.03$	e)
$_{52}Te^{126}$	740	0.06 ± 0.01	0.30 ± 0.03 0.27 ± 0.014	0.26 ± 0.05	6.37 ± 0.90* $(-0.14) \pm 0.02$	f)
$_{76}Os^{188}$	478	-0.040 ± 0.002	0.35 ± 0.02	0.14 ± 0.03	15.69 ± 7.01* $(-0.207) \pm 0.021$	g)
$_{78}Pt^{192}$	296				$(-6.5) \pm 1.5$	h)
$_{78}Pt^{194}$	293	-0.042 ± 0.002	0.30 ± 0.02	0.11 ± 0.02	29.1 ± 25.8* $(-0.24) \pm 0.02$	i)
$_{78}Pt^{196}$	331	0.073 ± 0.004	0.286 ± 0.015	0.27 ± 0.02	5.43 ± 0.53* $(-0.112) \pm 0.015$	j)
$_{80}Hg^{198}$	675	-0.261 ± 0.023	0.137 ± 0.012	-0.26 ± 0.03	$(-0.96) \pm 0.22$* $(-1.60) \pm 0.42$	k)

a) F. R. Metzger and W. B. Todd, Phys. Rev. **92** (1953) 905
b) H. Frauenfelder *et al.*, Phys. Rev. **103** (1956) 352
c) C. F. Coleman, Nuclear Physics **7** (1958) 488
d) R. Scharenberg *et al.*, Phys. Rev. **101** (1956) 689
e) T. Lindquist and I. Marklund, Nuclear Physics **4** (1957) 189
f) M. Sakai, private communication
g) V. R. Potnis *et al.*, Phys. Rev. **102** (1956) 459
h) J. Mraz, Nuclear Physics **4** (1957) 457
i) C. E. Mandeville *et al.*, Phys. Rev. **98** (1955) 94
j) V. R. Potnis, Indian J. Phys. **30** (1956) 375
k) C. D. Shrader, Phys. Rev. **92** (1953) 928

respective errors have been taken arbitrarily as quoted by the authors of the indicated references. Because of insufficient data concerning A_2 and A_4 in these two cases, no critical evaluation of δ was attempted.

3. Discussion

In their theory of axially asymmetrical nuclei, Davydov and Filippov [5]) have given the expression for δ^2 as

$$\delta^2 = \tfrac{2}{3} E_\gamma^2 Z^2 A^{\frac{4}{3}} \times 10^{-10} \tag{7}$$

with E_γ in keV. A log-log plot of this expression appears in fig. 2. Experimentally determined values of $(\delta/E_\gamma)^2$ have been calculated from the data

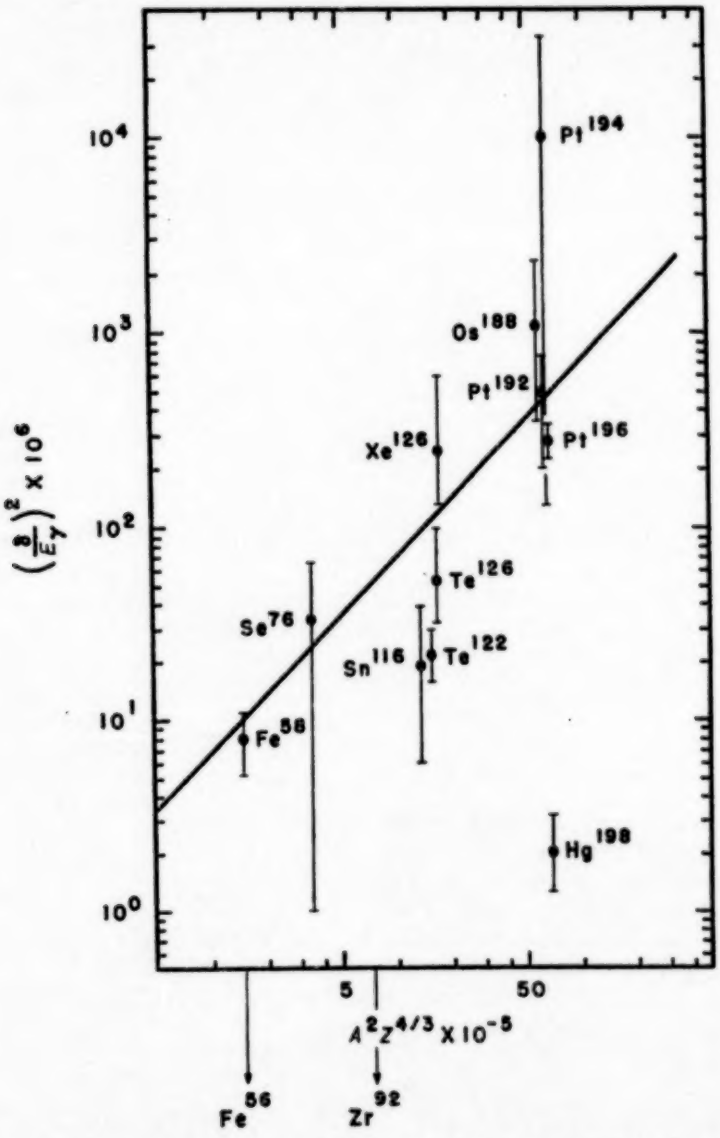

Fig. 2. Comparison of measured values of $(\delta/E_\gamma)^2$ with the theory of Davydov and Filippov. Values or the ordinate are decades smaller for $Fe^{56}(7\times10^{-3}\pm7\times10^{-3})$ and $Zr^{92}(2\times10^{-5}\pm1.3\times10^{-2})$.

table 1 and are shown in fig. 2 along with their associated probable errors.

It is evident from fig. 2 that with certain exceptions, there appears to be a general trend of agreement between experiment and theory. The extreme variations from the theory evidenced by Hg^{198}, Zr^{92} and Fe^{56} are perhaps related to shell effects. In the case of Zr^{92}, there is not absolute certainty that the level from which the mixed transition occurs is the $2'$ (second $2+$) level.

References

1) I. Bergström and G. Andersson, Arkiv f. Fys. **12** (1957) 415
2) T. Lindquist and I. Marklund, Nuclear Physics **4** (1957) 189
3) Mitsuo Sakai, Report on Even-Even Nuclei, Institute for Nuclear Study, University of Tokyo, Japan. INS-J-6 (February 24, 1958)
4) V. R. Potnis and C. E. Mandeville, J. Franklin Inst. **266** (1958) 226
5) A. S. Davydov and G. P. Filippov, Nuclear Physics **8** (1958) 237

7.A *Nuclear Physics* **11** (1959) 696—699; © *North-Holland Publishing Co., Amsterdam*
Not to be reproduced by photoprint or microfilm without written permission from the publisher

CAUSALITY IN QUANTUM FIELD THEORY

S. T. MA

The F.B.S. Falkiner Nuclear Research and Adolph Basser Computing Laboratories, School of Physics, University of Sydney †

Received 16 March 1959

Abstract: A recent work dealing with the relation between the causal function and the causality condition was confined to the virtual bosons taking part in the scattering of fermions. It is here extended to cover all the virtual particles of any scattering process.

1. Introduction

In a recent note on local quantum field theory[1]) †† it has been shown that the S-matrix calculated by covariant perturbation method for the scattering of fermions through exchange of bosons may be mathematically expressed so that the causality condition for the exchange of bosons is fulfilled for all distances. This is made possible by separating the boson field into retarded and advanced components, and the fermion distribution into sources and sinks. It is the object of the present note to extend our previous work to cover all the virtual particles taking part in any scattering process, i.e. particles which exist in the intermediate states and are represented by internal lines in a Feynman diagram †††.

It is of importance to mention that we lay no claim to having established that the local quantum field theory of the present time is a completely causal theory. As numerous discussions of long standing show, the question whether non-relativistic quantum mechanics is a causal theory is a very subtle one, and its answer depends largely on how causality is expressed in mathematical language. The situation is similar in quantum field theory. The implications of causality in our articles are somewhat the same as in the great number of recent papers on the dispersion relations. In either case, the scattering amplitudes are transformed so that the integrands contain factors which fulfil the causality condition—commutators and anticommutators in the papers on dispersion relations, and propagators for retarded and advanced potentials in ours. It will be in this sense that we regard our results as causal representations of the S-matrix.

† Also supported by the Nuclear Research Foundation within the University of Sydney.

†† This article will be quoted as I, and its equations as (I.1), etc.

††† We use the term virtual particle in its modern sense, so that both energy and momentum obey the conservation law, but the relation between energy and momentum for a real particle is usually violated.

2. Fermion Propagation Functions

As only mathematical relations for the boson propagation functions were given in I, we give here, in preparation for later discussion, a few analogous relations for the fermion case.

We define the fermion propagation functions S_R, S_A, S_C by the relation

$$S_i(x) = (\nabla - im)\Delta_i(x), \tag{1}$$

where $\nabla = \beta(\boldsymbol{\alpha}\cdot\boldsymbol{\nabla} + \partial/\partial t)$, $\boldsymbol{\alpha}$ and β being the Dirac matrices. The functions S_i satisfy the equation

$$(\nabla + im)S_i(x) = \delta(x), \tag{2}$$

so that, for a given spinor function $\xi(x)$, the differential equation

$$(\nabla + im)\psi(x) = \xi(x) \tag{3}$$

has the solutions

$$\psi_i(x) = \int S_i(x-x')\xi(x')\mathrm{d}^4x'. \tag{4}$$

In analogy with eqs. (I.12), (I.19), (I.20) we have

$$S_{C+}(x) = S_{R+}(x), \qquad S_{C-}(x) = S_{A-}(x), \tag{5}$$

$$\int S_C(x-x')\xi(x')\mathrm{d}^4x' = \int S_R(x-x')\xi_+(x')\mathrm{d}^4x' + \int S_A(x-x')\xi_-(x')\mathrm{d}^4x', \tag{6}$$

$$\int \bar{\xi}(x)S_C(x-x')\mathrm{d}^4x = \int \bar{\xi}_-(x)S_R(x-x')\mathrm{d}^4x + \int \bar{\xi}_+(x)S_A(x-x')\mathrm{d}^4x. \tag{7}$$

In eq. (7) $\bar{\xi}$ denotes the adjoint of ξ.

3. Causal Representations of the S-matrix

As has already been mentioned in I, the scattering matrix element of any scattering process which involves virtual bosons may be written in the form

$$I = \int \Delta_C(1, 2)s(1, 2)\mathrm{dV}_1\mathrm{dV}_2. \tag{8}$$

This is the same as (I.26) except that a subscript has been omitted. If there are several internal boson lines in a Feynman diagram, there is an integral of the form (8) for each. It was shown in I that the integral may be converted into the form

$$I = \int [\Delta_R(1, 2)s_{+-}(1, 2) + \Delta_A(1, 2)s_{-+}(1, 2)]\mathrm{dV}_1\mathrm{dV}_2. \tag{9}$$

Likewise, the scattering matrix element of any scattering process which involves virtual fermions may be written in the form

$$J = \int \mathrm{Tr}\, S_C(1, 2)\xi(1, 2)\mathrm{dV}_1\mathrm{dV}_2, \tag{10}$$

where $\xi(1, 2)$ is a 4×4 matrix at any two world points 1 and 2. In the same

way as in deriving (6) and (7) we obtain

$$J = \int \mathrm{Tr}[S_{\mathrm{R}}(1, 2)\xi_{+-}(1, 2)+S_{\mathrm{A}}(1, 2)\xi_{-+}(1, 2)]\mathrm{d}V_1\mathrm{d}V_2. \tag{11}$$

Eqs. (9) and (11) may be interpreted, in conformity with the requirement of relativistic causality, in the following manner: (i) The propagation functions $\Delta_{\mathrm{R}}(1, 2)$ and $S_{\mathrm{R}}(1, 2)$ describe virtual particles emitted at 1 and travelling from 1 to 2, whereas $\Delta_{\mathrm{A}}(1, 2)$ and $S_{\mathrm{A}}(1, 2)$ describe those absorbed at 1 after travelling from 2 to 1, with $t_1 < t_2$ in the first case and $t_2 < t_1$ in the second case. (ii) A plus sign attached to the functions $s(1, 2)$ and $\xi(1, 2)$ indicates a source, and a minus sign indicates a sink.

According to this interpretation, retarded and advanced potentials have equal status with respect to causality. We changed $\Delta_{\mathrm{A}}(1, 2)$ into $\Delta_{\mathrm{R}}(2, 1)$ in I in order to express the final result in terms of retarded propagation alone, but such a change is not indispensable for the discussion.

The situation has so far been the same for bosons and fermions. A special feature for the fermions is the distinction between the fermions travelling from 1 to 2 and those from 2 to 1, demanded by the hole theory. For example, if the fermions travelling from 1 to 2 are negatons, then, on account of the conservation of charge at a vertex, the fermions from 2 to 1 should be identified with positons. No such distinction is necessary for the photons, or the π-mesons of the neutral and symmetric theories.

The work of this section may be summarized by saying that any scattering matrix element has a causal representation for each of its internal, boson or fermion lines. These causal representations seem to fit in with the ideas of the Stueckelberg-Feynman theory, discussions of which may be found in ref.[1–5]) of I and ref. [2–4]) of this article.

4. Causal Representation in Momentum Space

The S-matrix has also a causal representation in momentum space, which treats all the internal lines on the same footing.

It will be sufficient to consider all the internal lines meeting at a vertex. Take, for example, the typical case of one boson line and two fermion lines. They make the following contribution to the S-matrix:

$$\Lambda = \int \Delta_{\mathrm{C}}(x_1-x)S_{\mathrm{C}}(x_2-x)\gamma S_{\mathrm{C}}(x-x_3)\mathrm{d}^4x. \tag{12}$$

Let $S_i(p)$ denote the Fourier transform of $S_i(x)$, so that

$$S_i(x) = \int S_i(p) \exp(ip \cdot x)\mathrm{d}^4p. \tag{13}$$

Eq. (12) becomes then

$$\Lambda = (2\pi)^4 \int \Delta_C(p_1) S_C(p_2) \gamma S_C(-p_3) \delta(p_1+p_2+p_3) \cdot \exp\,[i(p_1 \cdot x_1 + p_2 \cdot x_2 + p_3 \cdot x_3)] \mathrm{d}^4 p_1 \mathrm{d}^4 p_2 \mathrm{d}^4 p_3. \quad (14)$$

In terms of the 4-vector p, the decomposition formulas (I.12) and (5) may be put in the form

$$\Delta_C(p) = \Delta_R(p)\eta(p) + \Delta_A(p)\eta(-p), \quad (15)$$

$$S_C(p) = S_R(p)\eta(p) + S_A(p)\eta(-p), \quad (16)$$

where $\eta(p) = 1$ or 0 according as the time component of p is positive or negative. Applying (15) and (16) to the integrand (14) gives rise to eight terms. Owing to the δ-function, however, there is only one term different from zero for any values of the energy-momentum variables which satisfy the conservation law. Thus the propagation of the boson and fermion fields is either retarded or advanced.

We have assumed in the above that the functions $\Delta_C(p)$ and $S_C(p)$ have no singularities at points where the time component of p is zero, so that these points may be left out of the discussion of the integral (14). This assumption is justified for particles of finite mass, and for particles of vanishing mass too, if they are given an infinitesimal mass which is to be put equal to zero after integration.

References

1) S. T. Ma, Nuclear Physics **7** (1958) 163
2) R. P. Feynman, Phys. Rev. **76** (1949) 749
3) N. N. Bogolyubov and D. V. Shirkov, Introduction to the Theory of Quantized Fields (English translation by National Research Council, Ottawa, Canada, 1958)
4) T. Okabayashi, Supplemento al Nuovo Cimento **9** (1958) 599

8.B *Nuclear Physics* **11** (1959) 700—705; © *North-Holland Publishing Co., Amsterdam*
Not to be reproduced by photoprint or microfilm without written permission from the publisher

ON NON-LEPTONIC DECAYS OF HYPERONS

B. D'ESPAGNAT and J. PRENTKI
CERN, *Geneva*

Received 23 March 1959

Abstract: Some numerical estimates are made of various parameters entering in Σ and Λ decays. These are based on the assumptions of an earlier paper, which, using the global symmetry formalism, lead to a general Hamiltonian for weak interactions relating non-leptonic decays of hyperons between each other.

1. Introduction

The new results on up-down asymmetries in Σ decays, obtained by Cool *et al.*[1]) are, as is well-known, compatible with the $|\Delta \mathbf{I}| = \frac{1}{2}$ rule. In order to establish some theoretical connection between these results and the decay rate and asymmetry parameter of Λ decay some hypothesis has clearly to be made. Two different and mutually exclusive hypotheses have lately been suggested for that purpose: one of them [1,2]) is essentially to carry over to Λ decay the $I = \frac{1}{2}$ amplitudes found in Σ decay; the other one is to use, for establishing the $\Lambda-\Sigma$ connection, a principle very similar to that used in global symmetry [3]). In the present paper a comparison of the results of these two approaches is made, and it is shown that they lead to essentially different predictions. Moreover, assuming the second approach to be the correct one, a principle of "modified mass reversal" will be given, which leads unambiguously to the appropriate strangeness non-conserving current.

For the sake of completeness the analysis of the Σ decay using the $|\Delta \mathbf{I}| = \frac{1}{2}$ rule should first be very briefly recalled.

2. Σ Decay Analysis

Expressing the $|\Delta \mathbf{I}| = \frac{1}{2}$ rule by means of the spurion formulation the most general wave function for the products of Σ decay is †,

$$(C_s Y_s + C_p Y_p)\tfrac{1}{i}\mathbf{x}^* \boldsymbol{\tau} \mathbf{N} \times \boldsymbol{\pi} + (D_s Y_s + D_p Y_p)\mathbf{x}^* \mathbf{N} \boldsymbol{\pi}, \qquad (1)$$

where Y_s and Y_p are normalized s and p wave functions and where C_s, C_p, D_s, D_p are arbitrary amplitudes which, if PC is conserved and if Σ has spin $\frac{1}{2}$, should be almost real numbers. The approximation of treating them as real

† Notations : $\mathbf{N} = \begin{pmatrix} p \\ n \end{pmatrix}$, $\mathbf{x} = \begin{pmatrix} 0 \\ 1 \end{pmatrix}$ (spurion), $\boldsymbol{\tau}$ = Pauli matrices, $\boldsymbol{\pi} = (\pi_1, \pi_2, \pi_3)$.

numbers is quite sufficient for our purpose and will be used throughout the paper.

The expression (1) gives

$$(C_s Y_s + C_p Y_p)(\sqrt{2}p\pi^0 + n\pi^+) + (D_s Y_s + D_p Y_p)n\pi^+ \tag{2}$$

for Σ^+ decay and

$$(C_s Y_s + C_p Y_p)(-n\pi^-) + (D_s Y_s + D_p Y_p)n\pi^- \tag{3}$$

for Σ^- decay.

It is then immediately checked that the choices

$$C_s = \quad C_p = \quad D_s = -D_p \tag{4a}$$
$$C_s = \quad C_p = -D_s = \quad D_p \tag{4b}$$
$$C_s = -C_p = \quad D_s = \quad D_p \tag{4c}$$
$$-C_s = \quad C_p = \quad D_s = \quad D_p \tag{4d}$$

give the correct Σ^+ branching ratio, the correct Σ^+/Σ^- lifetime ratio and the correct asymmetry parameters (i.e. 0 for $n\pi^\pm$ and 1 for $p\pi^0$).

An equivalent method of analysis [1]) is of course to write the final state wave function as

$$(A_1 Y_s + B_1 Y_p)F_{\frac{1}{2}} + \sqrt{2}(A_3 Y_s + B_3 Y_p)F_{\frac{3}{2}} \tag{5}$$

where $F_{\frac{1}{2}}$ and $F_{\frac{3}{2}}$ are the isospin wave functions for $I = \frac{1}{2}$ and $I = \frac{3}{2}$ respectively (the $\sqrt{2}$ is introduced only for convenience). There is of course a linear correspondence between A_1, B_1, A_3, B_3 and C_s, C_p, D_s, D_p which turns out to be

$$\begin{aligned} A_1 &= -\sqrt{\tfrac{2}{3}}(2C_s - D_s), \quad A_3 = -\sqrt{\tfrac{2}{3}}(C_s + D_s), \\ B_1 &= -\sqrt{\tfrac{2}{3}}(2C_p - D_p), \quad B_3 = -\sqrt{\tfrac{2}{3}}(C_p + D_p). \end{aligned} \tag{6}$$

The solutions (4a, b, c, d) correspond therefore to

$$A_1 : B_1 : A_3 : B_3 = \begin{cases} 1 : \quad 3 : 2 : 0 & (7a) \\ 3 : \quad 1 : 0 : 2 & (7b) \\ 1 : -3 : 2 : 0 & (7c) \\ -3 : \quad 1 : 0 : 2. & (7d) \end{cases}$$

For a Hamiltonian formulation of the decay process it is necessary to assume that the corrections due to strong interactions (e.g. corrections to weak interaction vertex, etc.) are not extremely important (as is seemingly the case in β decay). If such corrections are neglected the derivation of the Hamiltonian from the final state wave function (1) or (5) implies, generally speaking, the replacement of any form

$$EY_s + FY_p \quad \text{by} \dagger \quad Ei\gamma_\mu + F\rho_\Sigma i\gamma_\mu\gamma_5,$$

† If, of course, a (V, A) form of coupling is desired.

where

$$\rho_\Sigma = (m_\Sigma - m_N)[(m_\Sigma - m_N)^2 - \mu^2]^{-\frac{1}{2}} \approx 1.2 \tag{8}$$

makes a compensation for a dynamical factor. Solution (4a) for instance, then implies that the Hamiltonian has a form

$$\bar{\Sigma} i\gamma_\mu (1+\rho\gamma_5) \frac{1}{i} x^* \tau N \times \partial_\mu \pi + \bar{\Sigma} i\gamma_\mu (1-\rho\gamma_5) x^* N \partial_\mu \pi + \text{h.c.} \tag{9}$$

Alternatively one may of course assume that $\rho = 1$ and that the renormalizations of the V and A couplings differ by 20 %. The interaction Hamiltonian written in terms of bare fields would then be simply

$$g\bar{\Sigma} i\gamma_\mu (1+\gamma_5) \frac{1}{i} x^* \tau N \times \partial_\mu \pi + g\bar{\Sigma} i\gamma_\mu (1-\gamma_5) x^* N \partial_\mu \pi + \text{h.c.} \tag{9'}$$

3. Connection with Λ Decay

One has here to study the consequences of two alternative assumptions hereafter denoted by "$\frac{1}{2}$" and "GS".

3.1. "$\frac{1}{2}$" ASSUMPTION [4])

The Hamiltonian is proportional to

$$\bar{\Lambda} i\gamma_\mu (A_1 + \rho_\Sigma B_1 \gamma_5)(\sqrt{2} p\pi^- - n\pi^0) + \text{h.c.}, \tag{10}$$

A_1 and B_1 being the same as in Σ decay. The motivation for this assumption is of course the fact that $|\Delta \mathbf{I}| = \frac{1}{2}$ implies that Λ decays into a pure $I = \frac{1}{2}$ channel. Neglecting strong interaction corrections the final state wave function is then proportional to

$$A_1 y_s + \rho_\Sigma v_\Lambda B_1 y_p \tag{11}$$

where

$$v_\Lambda = (m_\Lambda - m_N)^{-1}[(m_\Lambda - m_N)^2 - \mu^2]^{+\frac{1}{2}} \approx 0.61. \tag{8'}$$

This leads to an asymmetry parameter $\alpha(\Lambda)$ which is related to $\alpha^0 = \alpha(\Sigma^+ \to p\pi^0) = \pm 1$ through

$$\alpha(\Lambda) = \pm 0.75 \text{ for solutions (7a, c)}, \tag{12}$$

$$\alpha(\Lambda) = \pm 0.46 \text{ for solutions (7b, a)}, \tag{12'}$$

i.e. which has *the same sign* as α^0.

3.2. "GS" ASSUMPTION [3])

This assumption is very similar to global symmetry. Let us introduce the notations

$$\begin{gathered} \Sigma_\alpha{}^\beta = \frac{1}{\sqrt{2}} \Sigma \cdot \tau_\alpha{}^\beta, \quad \pi_\alpha{}^\beta = \frac{1}{\sqrt{2}} \pi \cdot \tau_\alpha{}^\beta; \\ \bar{\Sigma}_\alpha{}^\beta = \frac{1}{\sqrt{2}} \bar{\Sigma} \cdot \tau_\beta{}^\alpha; \quad N_1 = p, \quad N_2 = n; \quad x^1 = 0, \quad x^2 = 1, \end{gathered} \tag{13}$$

i.e., in a more explicit writing,

$$\begin{pmatrix} \Sigma_1^1 & \Sigma_1^2 \\ \Sigma_2^1 & \Sigma_2^2 \end{pmatrix} = \begin{pmatrix} \frac{1}{\sqrt{2}}\Sigma^0, & \Sigma^+ \\ \Sigma^-, & -\frac{1}{\sqrt{2}}\Sigma^0 \end{pmatrix} \quad \text{etc.} \tag{14}$$

Then the following identities are easily proved:

$$\bar{\Sigma}_\alpha{}^\beta \pi_\alpha{}^\gamma = \bar{\boldsymbol{\Sigma}} \cdot \boldsymbol{\pi} \delta_\beta{}^\gamma + i\bar{\boldsymbol{\Sigma}} \times \boldsymbol{\pi} \cdot \boldsymbol{\tau}_\beta{}^\gamma, \tag{15}$$

$$\bar{\Sigma}_\alpha{}^\beta \pi_\gamma{}^\beta = \bar{\boldsymbol{\Sigma}} \cdot \boldsymbol{\pi} \delta_\gamma{}^\alpha - i\bar{\boldsymbol{\Sigma}} \times \boldsymbol{\pi} \cdot \boldsymbol{\tau}_\gamma{}^\alpha, \tag{15'}$$

and using (15) and (15'), the Hamiltonian (9') for Σ decay takes the compact form

$$\bar{\Sigma}_\alpha{}^\beta i\gamma_\mu \partial_\mu \pi_\alpha{}^\gamma N_\gamma x^\beta - \bar{\Sigma}_\alpha{}^\beta i\gamma_\mu \gamma_5 \partial_\mu \pi_\gamma{}^\beta N_\alpha x^\gamma + \text{h.c.} \tag{16}$$

The Λ decay Hamiltonian can now be introduced in a very natural way into the picture by simply redefining $\Sigma_\alpha{}^\beta$ as

$$\begin{pmatrix} \Sigma_1^1 & \Sigma_1^2 \\ \Sigma_2^1 & \Sigma_2^2 \end{pmatrix} = \begin{pmatrix} \frac{1}{\sqrt{2}}(\Lambda + \Sigma^0) & \Sigma^+ \\ \Sigma^- & \frac{1}{\sqrt{2}}(\Lambda - \Sigma^0) \end{pmatrix} = \begin{pmatrix} Z & \Sigma^+ \\ \Sigma^- & Y \end{pmatrix}. \tag{17}$$

This corresponds to the hypothesis of global symmetry .The Hamiltonian (16) then describes both Λ and Σ decays and the part corresponding to Λ decay is

$$g\bar{\Lambda} i\gamma_\mu (1-\gamma_5) x^* \boldsymbol{\tau} \cdot N \partial_\mu \boldsymbol{\pi} + \text{h.c.}, \tag{18}$$

to be added to (9'). The complete phenomenological Hamiltonian is therefore

$$\begin{aligned} & g_\Sigma \frac{1}{i} \bar{\boldsymbol{\Sigma}} i\gamma_\mu (1+\rho_\Sigma \gamma_5) \times x^* \boldsymbol{\tau} N \cdot \partial_\mu \boldsymbol{\pi} \\ & + g'_\Sigma \bar{\boldsymbol{\Sigma}} i\gamma_\mu (1-\rho'_\Sigma \gamma_5) \cdot x^* N \partial_\mu \boldsymbol{\pi} \\ & + g_\Lambda \bar{\Lambda} i\gamma_\mu (1-\rho_\Lambda \gamma_5) x^* \boldsymbol{\tau} \cdot N \partial_\mu \boldsymbol{\pi} + \text{h.c.}, \end{aligned} \tag{19}$$

where $g_\Sigma = g'_\Sigma = g_\Lambda$; $\rho_\Sigma = \rho'_\Sigma = \rho_\Lambda = 1$ if (19) is written in terms of bare fields ($m_\Sigma = m_\Lambda$). If (19) is written in terms of physical fields the considerations of section 2 show that, to a rather good approximation,

$$\rho'_\Sigma \approx \rho_\Sigma \approx 1.2, \quad g'_\Sigma \approx g_\Sigma. \tag{20}$$

It seems, however, rather likely that the same strong interactions that split the Λ and Σ masses will also differentiate between g_Λ and g_Σ. One has then (assuming that strong interactions do not destroy completely the picture of weak interactions presented here)

$$g_\Lambda \sim g_\Sigma; \quad \rho_\Lambda \sim \rho_\Sigma \approx 1.2 \tag{21}$$

the symbol $\sim$ meaning a rough, approximate equality to within, say, 20 or 30 %. Under these conditions one has for the asymmetry parameter α_Λ

$$|\alpha_\Lambda| = \frac{2\rho_\Lambda v_\Lambda}{1+\rho_\Lambda{}^2 v_\Lambda{}^2} \tag{22}$$

which yields

$$|\alpha_\Lambda| = 0.89\ ;\ 0.95\ ;\ 0.99 \tag{23}$$

for

$$\rho_\Lambda = \quad 1 \quad ;\ 1.2 \quad ;\ 1.4.$$

This shows that the sensitivity of α_Λ to the precise value of ρ_Λ is quite small and that for any reasonable value of ρ_Λ, α_Λ is predicted to be quite large. This is a rather significant difference between the predictions derived from the "GS" and the "$\frac{1}{2}$" assumptions. A much more crucial difference, however, lies in the relative signs of α_Λ and α^0 (asymmetry parameter of $\Sigma^+ \to p + \pi^0$ decay): whereas *the "$\frac{1}{2}$" assumption predicts these signs to be the same, the "GS" assumption*, as is easily seen from (19), *predicts them to be opposite* † viz.

$$\text{for } \alpha^0 \sim \pm 1, \quad \alpha_\Lambda \sim \mp 1. \tag{23'}$$

Concerning the ratio of Σ^- to Λ lifetimes it is unfortunately difficult to make any reliable comparison of the theory with the experimental values: this comes from the fact that this ratio is essentially proportional to

$$\frac{1+\rho_\Lambda{}^2 v_\Lambda{}^2}{1+\rho_\Sigma{}^2 v_\Sigma{}^2} \cdot \frac{g_\Lambda{}^2}{g_\Sigma{}^2} \tag{24}$$

and that this expression is fairly sensitive to the relative values of the quantities ρ_Σ, ρ_Λ and g_Λ, g_Σ. All that one can say on this subject is that if one takes into account the uncertainties expressed by (21) this ratio of lifetimes is not in contradiction with the experimental values.

4. A Modified Mass-Reversal

By introducing the notation

$$\begin{pmatrix} B_1{}^1 & B_1{}^2 \\ B_2{}^1 & B_2{}^2 \end{pmatrix} = \begin{pmatrix} \Xi^0 & p \\ \Xi^- & n \end{pmatrix} \tag{25}$$

the expression (16) can be generalized in a natural way to include the Ξ weak interactions: this is done by simply replacing $N_i x^j$ by $B_i{}^j$. The new expression (16) can then be written down in the more conventional notation ††
$\boldsymbol{\Sigma}$, Λ, $\mathbf{B}$, B_8 as

$$\mathbf{J}_\mu \cdot \partial_\mu \boldsymbol{\pi} + \text{h.c.} \tag{26}$$

with

$$\mathbf{J}_\mu = \tfrac{1}{i}\,\bar{\boldsymbol{\Sigma}} i\gamma_\mu(1+\gamma_5) \times \mathbf{B} + \bar{\boldsymbol{\Sigma}} i\gamma_\mu(1-\gamma_5) B_8 + \bar{\Lambda} i\gamma_\mu(1-\gamma_5)\mathbf{B}. \tag{27}$$

† The $p\pi^0$ term comes only from the first term in (19); it occurs therefore essentially with $1 \pm \gamma_5$ if the Λ decay occurs with $1 \mp \gamma_5$.

†† $\mathbf{B}$, B_8 play in $B_i{}^j$ the same role as $\boldsymbol{\Sigma}$, Λ in $\Sigma_i{}^j$, i.e.

$$B^+ = p, \quad B_3 = \frac{1}{\sqrt{2}}(\Xi^0 - n), \quad B^- = \Xi^-; \quad B_8 = \frac{1}{\sqrt{2}}(\Xi^0 + n).$$

The form $\mathbf{J}_\mu$ of the strangeness non-conserving current can in turn be derived from a modified mass-reversal principle [5]) which states that $\mathbf{J}_\mu$ should be invariant under the two separate transformations

$$\text{(I)}\quad \begin{aligned} \Sigma &\to -\gamma_5\Sigma \\ \mathbf{B} &\to -\mathbf{B} \\ \Lambda &\to \gamma_5\Lambda \\ \mathrm{B}_s &\to \mathrm{B}_s \end{aligned} \qquad \text{(II)}\quad \begin{aligned} \Sigma &\to -\Sigma \\ \mathbf{B} &\to -\gamma_5\mathbf{B} \\ \Lambda &\to \Lambda \\ \mathrm{B}_s &\to \gamma_5\mathrm{B}_s. \end{aligned} \tag{28}$$

Together with the $|\Delta\mathbf{I}| = \frac{1}{2}$ rule, the assumption that $\mathbf{J}_\mu$ is separately invariant under (I) and (II) unambiguously determines the structure of each of the three terms in (27). The same assumption, however, is not as efficient as regards the strangeness conserving current.

5. Conclusions

As the situation now stands, it seems not unlikely that the non-leptonic and leptonic decay interactions are rather more different than was previously believed. It would seem for instance that the leptonic interactions are of the general V−A form while the non-leptonic interactions are not (indeed in (27) a very special mixture of V−A and V+A occurs).

Further it would seem that the $|\Delta\mathbf{I}| = \frac{1}{2}$ rule, or, better, the invariance in M space [6]), is a property of non-leptonic interactions which can hardly be extended to leptonic interactions (where such facts as the large μ-meson mass and the appearance of neutral currents in M space raise a number of serious difficulties). This might perhaps be put in comparison with the fact that the strangeness non-conserving leptonic decays appear abnormally slow. If non-leptonic interactions are studied without any preconceived ideas emerging from what we know or believe about leptonic interactions, it seems that a non-leptonic Hamiltonian of the form (26) with (27) is the one which best fits both present experimental knowledge and current ideas about the description of the Λ, Σ system. Relation (23′) will of course provide a rather crucial test for such ideas.

References

1) R. L. Cool, B. Cork, J. W. Cronin and W. A. Wenzel, to be published
2) S. B. Bludman, Bull. Am. Phys. Soc. **4** (1959) 83
3) B. d'Espagnat and J. Prentki, to be published
4) Y. Yamaguchi, Prog. Theor. Physics **19** (1958) 485
5) J. Tiomno, Nuovo Cimento **1** (1955) 226
6) B. d'Espagnat, J. Prentki and A. Salam, Nuclear Physics **5** (1958) 447

10.D *Nuclear Physics* **11** (1959) 706; © *North-Holland Publishing Co., Amsterdam*

BOOK REVIEWS

F. A. ROUGH and A. A. BAUER, Constitutional Diagrams of Uranium and Thorium (Addison-Wesley Publishing Company, Reading, Mass. 1958. vi—153 p., $ 5.00).

This book supersedes the Batelle Memorial Institute publication "Compilation of US and UK Uranium and Thorium Constitutional Diagrams" by H. A. Saller and F. A. Rough (BMI 1000).

Like BMI 1000 this book is divided into two sections, on uranium alloys and thorium alloys; both sections include binary and ternary systems. For each system the constitutional diagram is described if it is known, otherwise the data available for the system are mentioned. Besides the constitutional diagrams, the crystallography of the intermetallic compounds for each system is summarized in tabulations.

In comparison with BMI 1000 this book is enlarged with much new information, for instance descriptions of new binary and ternary alloys (spec. uranium — rare earths) and recently found constitutional diagrams e.g. U/Pu and Th/Pu.

The description of each system is supplied with an explicit list of references, which are generally unclassified; for several systems, however, the unclassified literature is incomplete and the classified references are given.

This book can be recommended as a useful reference piece for each laboratory occupied with development of uranium and thorium alloys.

Niels Hansen

G. JOOS and E. SCHOPPER, *Grundriss der Photographie und ihrer Anwendungen, besonders in der Atomphysik* (Akademische Verlagsgesellschaft, 1958. xii—408 pages. DM 48)

As the authors remark in their preface, this book is not intended to be a photographic handbook. Rather, it is a description of photographic phenomena, effects, materials and applications. It is intended especially for those who use photography as part of their work, and who therefore wish to acquire a more professional knowledge of the technique. Of the six sections, the last, dealing with nuclear emulsions, is the most elaborate, though it does not give as detailed a survey of the field as might have been wished. However, the gap in the literature in this respect has recently been filled by Demers' excellent book (P. Demers, Ionographie, Montréal, 1958).

The first part (110 pages) provides an outline of the elementary principles of photography, followed by an excellent account of the modern theories of the elementary photographic process. The second part (64 pages) deals with the theoretical and practical aspects of the optical and mechanical techniques used in conjunction with photography. Light sources, illumination, the spectral composition of light, colour temperature, energy of light and the spectral qualities of filters etc. are discussed in the third section (28 pages).

The fourth section (82 pages) is a discussion of the optical application of photography, the sensitizing of emulsions, and their use in the measurement of distances, light intensities and various spectra. In addition, astrophotographical applications and the photography of cloud chamber tracks are treated. This section is followed by a short discussion of X-ray photography (12 pages).

The last section (95 pages) begins with an historical preface, which is followed by discussions of the electron microscope, the mass spectrograph, autoradiography and finally nuclear emulsion. This last part deals first with the composition of nuclear emulsions, followed by a description of the techniques used for processing exposed emulsions and the qualities of the processed emulsion. Problems of microscopy associated with the scrutiny of the emulsions are then discussed briefly, and the various measurements which can be made on the particle tracks (blob-count, residual range, scattering, etc.) are discussed in relation to the information they can yield about the particle which made the track. Finally, there is a short survey of the applications of nuclear emulsions.

The book is richly illustrated (271 illustrations and one colour plate) and includes many references to original work. It provides an excellent introduction to theoretical photography. On the other hand, it is not very useful as a reference book, in so far as many practical details are not discussed sufficiently thoroughly.

Erik Dahl Jensen

AUTHOR INDEX

AJZENBERG-SELOVE, F. and T. LAURITSEN, Energy levels of light nuclei. VI 1

ARNS, R. G., R. E. SUND and M. L. WIEDENBECK, The level structure of Dy^{160} 411

BARTON, G., Electric quadrupole enhancement near O^{16} 466

BEARD, G. B., *see* KELLY

BLIN-STOYLE, R. J., V. GUPTA and H. PRIMAKOFF, Mesonic "exchange" effects in beta-decay 444

BODENSTEDT, E., H. J. KÖRNER and E. MATTHIAS, Angular correlation measurements on Cs^{133} and the magnetic moment of the 81 keV-level 584

BOOTH, N. E., G. W. HUTCHINSON, A. M. SEGAR, G. G. SHUTE and D. H. WHITE, β—ν correlation in Ne^{23} with resonance fluorescence 341

BOZÓKI, G., E. FENYVES and L. JÁNOSSY, Measurement of the absorption length of penetrating shower producing cosmic ray particles in lead 531

BROWN, D., *see* DELVES

BYERS, N. and W. N. COTTINGHAM, Energy and angular distributions of mesonic hyperfragment decays 554

CARVER, J. H. and J. A. JONES, Radiative deuteron capture $Zn^{64}(d, \gamma)Ga^{66}$ 400

COTTINGHAM, W. N., *see* BYERS

DELVES, L. M. and D. BROWN, The theory of n—d scattering with tensor forces 432

D'ESPAGNAT, B. and J. PRENTKI, On non-leptonic decays of hyperons 700

DOLGOSHEIN, B. A., *see* KIRILLOV-UGRYUMOV

EGARDT, L., Inelastic scattering of high energy protons by B^{11} and O^{16} 349

ERICSON, TORLEIF, A statistical analysis of excited nuclear states . . 481

FENYVES, E., *see* BOZÓKI

FOLK, R., *see* SAWICKI

GUPTA, V., *see* BLIN-STOYLE

HALPERN, I., A suggested explanation for the anomalous anisotropies in high energy fission 522

HARRIS, SAMUEL M., Sign of the nuclear quadrupole interaction by observation of polarized gamma-gamma angular correlations . . 387

HILLMAN, PETER, *see* JOHANSSON

HUTCHINSON, G. W., *see* BOOTH

JÁNNOSSY, L., *see* BOZÓKI
JOHANSSON, ARNE, GUNNAR TIBELL and PETER HILLMAN, Polarization of high energy protons in elastic and inelastic scattering 540
JONES, G. A., *see* CARVER
KELLY, W. H., G. B. BEARD and R. A. PETERS, The beta decay of K^{40} 492
KIRILLOV-UGRYUMOV, V. G., B. A. DOLGOSHEIN, A. M. MOSKVICHOV and L. P. MOROZOVA, Scattering of μ-mesons with momenta of about 100 MeV/c in copper and iron 357
KLEITMAN, DANIEL J., Some results on analytic functions in local field theory 459
KÖRNER, H. J., *see* BODENSTEDT
KRÓLIKOWSKI, W., On the universal Fermi interaction 687
LANE, A. M., Theory of radiative capture reactions 625
LANE, A. M. and J. E. LYNN, Analysis of experimental data on nucleon capture reactions 646
LAURITSEN, T., *see* AJZENBERG-SELOVE
LYNN, J. E., *see* LANE
MA, S. T., Causality in quantum field theory 696
MALIK, S. S., V. R. POTNIS and C. E. MANDEVILLE, E2—M1 mixing ratios in $2' \rightarrow 2 \rightarrow 0$ transitions 691
MANDEVILLE, C. E., *see* MALIK
MARSCHALL, H., *see* VON BEHR
MATTHIAS, E., *see* BODENSTEDT
MCCARTHY, IAN E., Focusing of particles in the optical model 574
MOROZOVA, L. P., *see* KIRILLOV-UGRYUMOV
MOSKVICHOV, A. M., *see* KIRILLOV-UGRYUMOV
NUSSENZVEIG, H. M., The poles of the S-matrix of a rectangular potential well or barrier 499
PETERS, R. A., *see* KELLY
POLKINGHORNE, J. C., Pais doublets and the universal Fermi interaction 599
POTNIS, V. R., *see* MALIK
PRENTKI, J., *see* D'ESPAGNAT
PRIMAKOFF, H., *see* BLIN-STOYLE
SAAVEDRA, I., On the electron-muon mass difference 569
SAWICKI, J. and R. FOLK, Doublet splittings in nuclei and the strongly correlated nuclear wave functions 368
SCARF, F. L., On the ordered-exponential solutions for the Thirring model 475
SCHOPPER, H., Polarisationseffekte bei der Mott-Streuung 675
SEGAR, A. M., *see* BOOTH
SEKINE, KATSUHIKO, Parity non-conservation and the algebra of

elementary particles 604
SHMUSHKEVICH, I. M., Depolarization of μ^--mesons in μ-mesic atom formation 419
SHUTE, G. G., *see* BOOTH
SUND, R. E., *see* ARNS
SZYMANSKI, ZDZISŁAW, On the deformability of nuclear cores 454
TIBELL, GUNNAR, *see* JOHANSSON
VAN DER SPUY, E., The α, α interaction 615
VON BEHR, J. und H. MARSCHALL, Eine Bemerkung zur Quadrupolwechselwirkungsenergie in μ-Mesonenatomen 670
WHITE, D. H., *see* BOOTH
WIEDENBECK. M. L., *see* ARNS

SUBJECT INDEX

1. Nuclear Structure

1.B *Two- and three-body problems*

The theory of n—d scattering with tensor forces, L. M. Delves and D. Brown 432

1.C *Many-particle systems*

Doublet splittings in nuclei and the strongly correlated nuclear wave functions, J. Sawicki and R. Folk 368
The α, α interaction, E. van der Spuy 615

1.D *Nuclear models*

1.D.1 *Shell model*

Electric quadrupole enhancement near O^{16}, G. Barton 466

1.D.2 *Collective model*

On the deformability of nuclear cores, Zdzisław Szymański 454
Eine Bemerkung zur Quadrupolwechselwirkungsenergie in μ-Mesonenatomen, J. von Behr und H. Marschall 670
E2—M1 mixing ratios in $2' \to 2 \to 0$ transitions, S. S. Malik, V. R. Potnis and C. E. Mandeville 691

1.D.3 *Other models*

The α, α interaction, E. van der Spuy 615

1.E *Properties of nuclei*

1.E.1 *Energy levels*

Energy levels of light nuclei. VI, F. Ajzenberg-Selove and T. Lauritsen 1
The level structure of Dy^{160}, R. G. Arns, R. E. Sund and M. L. Wiedenbeck 411
Angular correlation measurements on Cs^{133} and the magnetic moment of the 81 keV-level, E. Bodenstedt, H. J. Körner and E. Matthias 584

1.E.3 *Electric and magnetic moments*

Angular correlation measurements on Cs^{133} and the magnetic moment of the 81 keV-level, E. Bodenstedt, H. J. Körner and E. Matthias 584

1.E.4 *Transition probabilities; Cross sections*

E2—M1 mixing ratios in $2' \to 2 \to 0$ transitions, S. S. Malik, V. R. Potnis and C. E. Mandeville 691

2. Nuclear Reactions

2.A *General properties*

2.A.1 *Cross-sections, energy relations*

Radiative deuteron capture $Zn^{64}(d, \gamma)Ga^{66}$, J. H. Carver and G. A. Jones 400

Theory of radiative capture reactions, A. M. Lane 625
Analysis of experimental data on nucleon capture reactions, A. M. Lane and J. E. Lynn 646

2.B *Angular distributions, Correlations; Polarization*

Polarization of high energy protons in elastic and inelastic scattering, Arne Johansson, Gunnar Tibell and Peter Hillman. 540

2.D *Statistical model*

Radiative deuteron capture $Zn^{64}(d, \gamma)Ga^{66}$, J. H. Carver and G. A. Jones . 400
A statistical analysis of excited nuclear states, Torleif Ericson 481

2.E *Optical model*

Focusing of particles in the optical model, Ian E. McCarthy 574
Theory of radiative capture reactions, A. M. Lane 625
Analysis of experimental data on nucleon capture reactions, A. M. Lane and J. E. Lynn. 646

2.J *Fission and spallation*

A suggested explanation for the anomalous anisotropies in high energy fission, I. Halpern 522

2.L *Scattering processes (except two-nucleon system and meson scattering)*

Inelastic scattering of high energy protons by B^{11} and O^{16}, L. Egardt . . . 349
The theory of n—d scattering with tensor forces, L. M. Delves and D. Brown 432
The poles of the *S*-matrix of a rectangular potential well or barrier, H. M. Nussenzveig 499
Polarization of high energy protons in elastic and inelastic scattering, Arne Johansson, Gunnar Tibell and Peter Hillman. 540
Polarisationseffekte bei der Mott-Streuung, H. Schopper 675

3. Electromagnetic Radiation

3.A *Gamma radiation*

Sing of the nuclear quadrupole interaction by observation of polarized gamma-gamma angular correlations, Samuel M. Harris 387
The level structure of Dy^{160}, R. G. Arns, R. E. Sund and M. L. Wiedenbeck 411
Electric quadrupole enhancement near O^{16}, G. Barton 466
Angular correlation measurements on Cs^{133} and the magnetic moment of the 81 keV-level, E. Bodenstedt, H. J. Körner and E. Matthias 584

3.C *Extranuclear effects*

Eine Bemerkung zur Quadrupolwechselwirkungsenergie in μ-Mesonenatomen, J. von Behr und H. Marschall 670

4. Beta decay; Parity

4.A *General theory*

β—ν correlation in Ne^{23} with resonance fluorescence, N. E. Booth, G. W. Hutchinson, A. M. Segar, G. G. Shute and D. H. White. 341

4.C *Evaluation of matrix elements*

Mesonic "exchange "effects in beta-decay, R. J. Blin-Stoyle, V. Gupta and H. Primakoff 444

4.E *Analysis of data*

The beta decay of K^{40}, W. H. Kelly, G. B. Beard and R. A. Peters 492

6 Methods and Instruments

6.D *Tables and computational aids*

Sign of the nuclear quadrupole interaction by observation of polarized gamma-gamma angular correlations, Samuel M. Harris 387

7. Quantum Field Theory

7.A *General*

Some results on analytic functions in local field theory, Daniel J. Kleitman 459
On the ordered-exponential solutions for the Thirring model, F. L. Scarf . 475
The poles of the *S*-matrix of a rectangular potential well or barrier, H. M. Nussenzveig. 499
Causality in quantum field theory, S. T. Ma 696

7.C *π-meson field (scattering and nuclear forces)*

Mesonic "exchange" effects in beta-decay, R. J. Blin-Stoyle, V. Gupta and H. Primakoff 444

7. Elementary Particles

8.A *Experimental*

β—ν correlation in Ne^{23} with resonance fluorescence, N. E. Booth, G. W. Hutchinson, A. M. Segar, G. G. Shute and D. H. White. 341

8.B *Theory; interactions, transformations properties*

Depolarization of μ^--mesons in μ-mesic atom formation, I. M. Shmushkevich 419
Energy and angular distributions of mesonic hyperfragment decays, N. Byers and W. N. Cottingham 554
On the electron-muon mass difference, I. Saavedra 569
Pais doublets and the universal Fermi interaction, J. C. Polkinghorne . . 599
Parity non-conservation and the algebra of elementary particles, Katsuhiko Sekine 604
On the universal Fermi interaction, W. Królikowski 687
On non-leptonic decays of hyperons, B. D'Espagnat and J. Prentki 700

9. Cosmic Radiation

9.B *Passage of particles through matter*

Scattering of μ-mesons with momenta of about 100 MeV/c in copper and iron, V. G. Kirillov-Ugryumov, B. A. Dolgoshein, A. M. Moskvichov and L. P. Morozova 357
Measurement of the absorption length of penetrating shower producing cosmic ray particles in lead, G. Bozóki, E. Fenyves and L. Jánossy . . . 531

10. News Items

10.D *Book Reviews*

ENDT, P. M. and M. DEMEUR, editors, Nuclear Reactions, Vol. I (Ernest M. Henley) 479
ETHERINGTON, H., editor, Nuclear engineering handbook (L. R.) 479
Physics and heat technology of reactors (Supplement no. 1 of the Soviet Journal of Atomic Energy), (L. R.) 479
G. N. WALTON, Glove boxes and shielded cells (K. Heydorn). 480